



Vulnerability, Uncertainty, and Risk

ANALYSIS, MODELING, AND MANAGEMENT

Proceedings of the
ICVRAM 2011 and ISUMA 2011 Conferences

Edited by
Bilal M. Ayyub, Ph.D., P.E.

ASCE

VULNERABILITY, UNCERTAINTY, AND RISK

ANALYSIS, MODELING, AND MANAGEMENT

PROCEEDINGS OF THE FIRST INTERNATIONAL CONFERENCE ON
VULNERABILITY AND RISK ANALYSIS AND MANAGEMENT (ICVRAM 2011)
AND THE FIFTH INTERNATIONAL SYMPOSIUM ON UNCERTAINTY MODELING
AND ANALYSIS (ISUMA 2011)

April 11–13, 2011
Hyattsville, Maryland

SPONSORED BY
The Council on Disaster Risk Management (CDRM)
of the American Society of Civil Engineers

EDITED BY
Bilal M. Ayyub, Ph.D., P.E., F. ASCE

ASCE AMERICAN SOCIETY
OF CIVIL ENGINEERS

1801 ALEXANDER BELL DRIVE
RESTON, VIRGINIA 20191-4400

Cataloging-in-Publication Data on file with the Library of Congress.

American Society of Civil Engineers
1801 Alexander Bell Drive
Reston, Virginia, 20191-4400

www.pubs.asce.org

Any statements expressed in these materials are those of the individual authors and do not necessarily represent the views of ASCE, which takes no responsibility for any statement made herein. No reference made in this publication to any specific method, product, process, or service constitutes or implies an endorsement, recommendation, or warranty thereof by ASCE. The materials are for general information only and do not represent a standard of ASCE, nor are they intended as a reference in purchase specifications, contracts, regulations, statutes, or any other legal document. ASCE makes no representation or warranty of any kind, whether express or implied, concerning the accuracy, completeness, suitability, or utility of any information, apparatus, product, or process discussed in this publication, and assumes no liability therefore. This information should not be used without first securing competent advice with respect to its suitability for any general or specific application. Anyone utilizing this information assumes all liability arising from such use, including but not limited to infringement of any patent or patents.

ASCE and American Society of Civil Engineers—Registered in U.S. Patent and Trademark Office.

Photocopies and permissions. Permission to photocopy or reproduce material from ASCE publications can be obtained by sending an e-mail to permissions@asce.org or by locating a title in ASCE's online database (<http://cedb.asce.org>) and using the "Permission to Reuse" link. *Bulk reprints.* Information regarding reprints of 100 or more copies is available at <http://www.asce.org/reprints>.

Copyright © 2011 by the American Society of Civil Engineers.
All Rights Reserved.
ISBN 978-0-7844-1170-4
Manufactured in the United States of America.

Preface

In recent years, significant advances have been made in the areas of risk, vulnerability and uncertainty modeling, analysis and management. The joint International Conference on Vulnerability and Risk Analysis and Management (ICVRAM) and International Symposium on Uncertainty Modeling and Analysis (ISUMA) provided a forum for experts and decision makers involved in vulnerability and risk analysis and management to share information on current and emerging hazards and research results affecting the built environment with means for an appropriate consideration of uncertainty. ISUMA complemented ICVRAM by providing in-depth coverage on uncertainty modeling and analysis that would offer opportunities for cross-pollination. As we make advancements in technology, exploit resources, and step into new realms of human endeavors, we are exposed to new hazards. The novelty of the situation with its attendant uncertainties can pose a challenging situation for experts and decision makers charged with providing technical assistance and policy recommendations. The proceedings of this joint conference contribute towards the transitioning of intellectual discussions into robust frameworks for handling emerging vulnerabilities and risks, and providing analytical bases to prepare for national and international disasters.

The first International Conference on Vulnerability and Risk Analysis and Management was initiated and sponsored by the Council on Disaster Risk Management (CDRM) of the American Society of Civil Engineers (ASCE). This conference was held April 11-13, 2011 at the Marriott Inn & Conference Center of the University of Maryland University College, Hyattsville, Maryland, USA.

All papers in the proceedings were subjected to peer review by qualified engineers or academics working or teaching in fields relating to the paper. This effort by the many reviewers is truly appreciated. Hundreds of hours were volunteered to produce the proceedings. The work of the International Program Committee is indeed noteworthy for its excellence and support throughout the development of the program and the proceedings, particularly Professor Nii Attoh-Okine, Professor William McGill, Professor Qingbin Cui, and Dr. Scott Ferson.

The efforts of the Conference Department and Technical Activities Committee of ASCE, particularly Ms. Barbara Hickman and Ms. Catherine Tehan, are acknowledged for providing much of the conference preparation including scheduling, accommodations, local tours, and the conference program. The University of Maryland, College Park campus provided student helpers for the paper presentations. Special thanks to Ms. Che-yu Chang for her help and support in making this conference successful.

Bilal M. Ayyub, Ph.D., P.E., F.ASCE
Proceedings Editor
Professor and Director, Center for Technology & Systems Management
University of Maryland, College Park, Maryland, USA

This page intentionally left blank

Acknowledgments

Organizing Institutions

Council on Disaster Risk Management, ASCE
University of Maryland at College Park, USA Center for Technology and Systems
Management
University of Delaware, USA

Collaborating Institutions

Society for Risk Analysis

General Chair

Bilal M. Ayyub (USA)

Conference Co-Chairs

Nii O. Attoh-Okine (USA)
M. Gupta (Canada)

Publications Chair

William L. McGill (USA)

Honorary Co-Chairs

Alfredo Ang (USA)
George Klir (USA)
Lotfi Zadeh (USA)

International Program Committee

L. Achenie (USA)	I. Elishakoff (USA)	M. Kearney (USA)
J. Agarwal (UK)	B. Ellingwood (USA)	S. Kikuchi (USA)
T. Aven (Norway)	B. Ezell (USA)	S.-H. Kim (Korea)
F. Awadallah (Palestine)	M. Faber (Switzerland)	G. Klir (USA)
A. Badiru (USA)	S. Fan (USA)	R. Kohout (USA)
M. Beer (Singapore)	S. Ferson (USA)	S. Labi (USA)
Y. Ben-Haim (Israel)	D. Frangopol (USA)	J. Lambert (USA)
D. Bental (USA)	H. Furuta (Japan)	J. Li (China)
D. Blockley (UK)	G. Gavardashvili (Georgia)	D. Linzell (USA)
D. Bowles (USA)	S. Guikema (USA)	S. Liu (China)
R.-H. Cheng (Taiwan)	Y. Haimes (USA)	Y. Lin (USA)
K. Cogger (USA)	J. Hall (UK)	C. Loh (Taiwan)
K. Crowther (USA)	A. Harkness (USA)	M. Maes (Canada)
Q. Cui (USA)	A. Haldar (USA)	C. Menches (USA)
G. de Souza (Brazil)	P. Johnson (USA)	A. Mosleh (USA)
A. Der Kiureghian (USA)	J. Kacprzyk (Poland)	V. Mujumdar (USA)
D. Dubois (France)	H. Kamal (Kuwait)	Y. Najjar (USA)
		T. Norton (USA)

B. Ogunnaike (USA)
L. Parker (USA)
G. Parnell (USA)
M. Pecht (UMD)
J. Peerenboom (USA)
K.-K. Phoon (Singapore)
S. Prakash (USA)
M. Popescu (USA)
A. Ruedin (Argentina)
Y. Seda-Sanabria (USA)

E. Simui (USA)
I. Smith (Switzerland)
A. Sorensen (USA)
J. Sørensen (Denmark)
P. Spanos (USA)
S. Tabsh (UAE)
W. Tang (Hong Kong)
B. Tansel (USA)
S. Timashev (Russia)
N. Uddin (USA)

E. VanMarcke (USA)
W. Wallace (USA)
G. Woo (UK)
G. Wyss (USA)
R. Yager (USA)
L. Zadeh (USA)
Y. Zhao (Japan)
M. Ziara (Palestine)

Contents

Keynote Papers

Application of Evolutionary Computing to Disaster Restoration and Prevention Problems	1
Hitoshi Furuta and Koichiro Nakatsu	
Quantitative Risk Analysis of Damage to Structures during Windstorms: Random Field and System Reliability Aspects	11
Erik Vanmarcke and Ning Lin	

Imprecision, Statistics, and Simulation Method

Statistical Decisions with Random Fuzzy Data—A Possibilistic Approach	21
Olgierd Hryniewicz	
Statistic Inference under Two Structurally Different Approaches to Interval Data	29
Scott Ferson and Jack Siegrist	
Independence in Generalized Interval Probability	37
Yan Wang	
Embodied Knowledge of Gesture Motion Acquired by Singular Spectrum Analysis	45
I. Hayashi, Y. Jiang, and S. Wang	
Fuzzy Probability in Engineering Analyses	53
M. Beer and S. Ferson	
A Process for the Estimation of the Duration of Activities in Fuzzy Project Scheduling	62
A. Maravas and J. P. Pantouvakis	
Uncertainty Arithmetic on Excel Spreadsheets: Add-In for Intervals, Probability Distributions, and Probability Boxes	70
Scott Ferson, James Mickley, and William McGill	
Extended Uniform Distribution Accounting for Uncertainty of Uncertainty	78
James-A. Goulet and Ian F. C. Smith	
Efficiency Comparison of Markov Chain Monte Carlo Simulation with Subset Simulation (MCMC/ss) to Standard Monte Carlo Simulation (sMC) for Extreme Event Scenarios	86
Duzgun Agdas, Michael T. Davidson, and Ralph D. Ellis	
Multi-Agent Simulation Considering the Influence of Leader during Flood Disaster	96
Michiyuki Hirokane, Yusuke Miyawaki, and Yuhei Inoue	

Multi-Agent Simulation to Uncertain Civilian Return Trips during a Hypothetical Earthquake.....	104
Seiichi Kagaya, Yukako Ishiguro, and Ken-etsu Uchida	
Statistical Characterization and Prediction of Sea Waves Based on Buoy Data	113
Che-Yu Chang and Bilal M. Ayyub	
Measuring Validity of Reasoning Process for Transportation Planning Using Bayesian Inference and Dempster-Shafer Theory.....	121
Nopadon Kronprasert and Shinya Kikuchi	
A Simulation Framework for the Path Planning of Unmanned Autonomous Systems	129
M.-W. Kang, S. Wang, M. K. Jha, C.-C. Chen, and P. Schonfeld	
Development of Gap Acceptance Fuzzy Models Using Data from Driving Simulator Experiments.....	138
R. Rossi, M. Gastaldi, and G. Gecchele	
<i>Infrastructure Risk, Management, and Protection</i>	
Entropy Approach to Risk-Analysis of Critical Infrastructure Systems	147
S. A. Timashev and A. N. Tyrnin	
A Survey of Network Theoretic Approaches for Risk Analysis of Complex Infrastructure Systems	155
Sarah LaRocca and Seth Guikema	
Regional Social and Economic Risks As Conditions of Formation of Critical Infrastructure.....	163
Alexander V. Shibin, Julia L. Shibina, and Alexander A. Kuklin	
Decomposition Methods for Restoring Infrastructure Systems.....	171
Burak Cavdaroglu, Sarah G. Nurre, John E. Mitchell, Thomas C. Sharkey, and William A. Wallace	
Strategic Planning for Power System Restoration	180
Carleton Coffrin, Pascal Van Hentenryck, and Russell Bent	
Preparedness of Finnish Electricity Users against Major Disturbances in Supply of Electric Power	188
J. Sarsama, R. Molarius, P. Verho, J. Strandén, and H. Krohns	
Development of Spatial Risk Profiles of Cargo Rail Systems	197
Bilal M. Ayyub, Kristen Markham, and Che-yu Chang	
Probabilistic Study of Cascading Failures in Complex Interdependent Lifeline Systems.....	205
Isaac Hernandez-Fajardo and Leonardo Dueñas-Osorio	
Vulnerability Assessment of Infrastructure Networks by Using Hierarchical Decomposition Methods	214
C. Gómez, J. Buriticá, M. Sánchez-Silva, and L. Dueñas-Osorio	
Sustainability: Complexity, Regulations, and Decisions.....	222
Tonatiuh Rodriguez-Nikl and Colin B. Brown	
A Systems Approach to Vulnerability Assessment	230
Jitendra Agarwal, Mei Liu, and David Blockley	

System Reliability Analysis of Fatigue-Induced Sequential Failure	238
Young-Joo Lee and Junho Song	
Sample Treatment of Uncertainties in Earthquake Portfolio Risk Analysis	246
Craig Taylor, William Graf, Yajie (Jerry) Lee, Charles Huyck, and Zhenghui Hu	
Probabilistic Application in Seismic Vulnerability Assessment of Structures	252
Mohsen Javanpour and Panam Zarfam	
Options for the Treatment of Uncertainty in Seismic Probabilistic Safety Assessment of Nuclear Power Plants	260
Tamas J. Katona	
Seismic Investigation for the Temple of Antioch Reconstruction	268
Ece Erdogmus, Terri Norton, Cody M. Buckley, Kyle Kauzlarich, and Brad Petersen	
<i>Risk Issues, Management, and Decision Making</i>	
Multicriteria Optimization under Uncertainty: Average Criteria Method	276
L. E. K. Achenie, I. V. Datskov, and G. M. Ostrovsky	
National-Level Infrastructure Risk Evaluation Framework and Best Practices	284
Yujie Lu, Qingbin Cui, Longquan Mao, and Liang Chen	
Probabilistic Performance Risk Evaluation of Infrastructure Projects	292
Byung-Cheol Kim	
Optimal Planning of Public Works Using Improved Genetic Algorithm	300
Koichiro Nakatsu, Hitoshi Furuta, and Ken Ishibashi	
Quantitative Risk Assessment, Public Policy, and Decision-Making	308
Vilas Mujumdar	
Research on the Establishment of Mega Public Building Safety Risk Assessment System in China	316
Liang Chen, Longquan Mao, Ye Feng, and Hu Cheng	
A New Model of Supervision of Chinese Government over Building Safety: Based on the Third-Party Assessment Mechanism	326
Hu Cheng, Longquan Mao, Youliang Huang, and Xin Zhao	
Development of Spatial Risk Profiles Resulting from Sea Level Rise	334
Bilal M. Ayyub, Michael Kearney, Josue Ramirez, Kristen Markham, and Che-Yu Chang	
Evaluating the Source of the Risks Associated with Natural Events	342
P. Gardoni and C. Murphy	
Florida International University’s Wall of Wind: A Tool for Improving Construction Materials and Methods for Hurricane-Prone Regions	352
Aly Mousaad Aly, Girma Bitsuamlak, and Arindam Gan Chowdhury	
Risk Management of Long Term Infrastructure Projects “PPP-BOT Projects” by Using Uncertainty, Probabilistic and Stochastic Methods, and Models	360
Meghdad Attarzadeh, David Kim Huat Chua, and Michael Beer	

Mixing Good Data with Bad: How to Do It and When You Should Not	368
J. Siegrist	
Study on the Method Selection for Building Safety Risk Assessment in China	374
Longquan Mao, Youliang Huang, Liang Chen, and Wu Yang	
Decision-Making Model for Offshore Offloading Operations Based on Probabilistic Risk Assessment	385
C. E. Patiño Rodríguez and G. F. M. Souza	
Preliminary Risk Analysis of a Liquefied Natural Gas Regasification System in an Offshore Unit	394
Adriana Miralles Schleder, Marcelo Ramos Martins, and Gilberto Francisco Martha Souza	
Seismic Risk Assessment and Sensitivity Analysis in Terms of Life-Cycle Repair Cost	402
Alexandros A. Taflanidis	
Influence of Socio-Economic Consequences of World Economic Crisis on a Shadow Economy	410
A. S. Naydenov	
<i>Risk Methodologies and Management</i>	
Classification and Moral Evaluation of Uncertainties in Engineering Modeling	417
C. Murphy, P. Gardoni, and C. E. Harris, Jr.	
Making Urban Territories More Resilient to Flooding by Improving the Resilience of Their Waste Management Network: A Methodology for Analysing Dysfunctions in Waste Management Networks during and after Flooding	425
Hélène Beraud, Bruno Barroca, Damien Serre, and Gilles Hubert	
A Polynomial Chaos Approach for Uncertainty Analysis of Chloride-Induced Corrosion in Concrete Structures	433
B. Saassouh and Z. Lounis	
Method of Assessment of Human-Induced Area Risks and Creation of Risk Map Using Geoinformation Systems	442
Yu I. Shokin, V. V. Moskvichev, and V. V. Nicheporchuk	
Closed-Form Approximation to Annual Failure Probabilities	450
Ramesh Kumar and Paolo Gardoni	
Use of Quantitative Risk Assessment in Structural Design	458
Nasim Uddin and Mohammed A. Mousa	
Statistical Tools for Populating/Predicting Input Data of Risk Analysis Models	468
G. L. Pita, R. Francis, Z. Liu, J. Mitrani-Reiser, S. Guikema, and J.-P. Pinelli	
Integrating Risk Management within the Project Delivery Process at Caltrans: A Transportation Project Case Study	477
Pedro Maria-Sanchez, Ross Cather, Lou Melendez, and Robert Lowrie	
The Relationship between Hazards Vulnerability and Stage of Economic Development in Haiti and Chile	485
Lan Nguyen and Ross B. Corotis	

Applying Heuristics to Civil Engineering	493
X. J. Irias	
Probabilistic and Optimization Considerations in Multihazard Engineering	501
Dat Duthinh and Florian Potra	
Asset Management of Structures Using Hybrid Structural Health Monitoring and Structural Uncertainty Analysis Procedure	510
M. Modares and J. Mohammadi	
Structural Health Assessment Using Only Noise-Contaminated Responses	518
Ajoy Kumar Das and Achintya Haldar	
Statistically Detecting Clustering for Rare Events	526
J. Siegrist, S. Ferson, J. Goode, and R. Grimson	
A Bayesian Framework to Predict Deformations during Supported Excavations Based on a Semi-Empirical Method	533
J. K. Park, P. Gardoni, and G. Biscontin	
A Bayesian Network Approach for Identification of Critical Components of a System	541
M. Bensi and A. Der Kiureghian	
Damage Detection in Water Distribution Pipe Network Using Bayesian Framework and System Reliability Analysis	549
Won-Hee Kang and Junho Song	
Bayesian Network for Post-Earthquake Decision on Monitored Structures	561
S. Broglio and A. Der Kiureghian	
<i>Climate and Wind Engineering</i>	
Risk-Based Framework for Stream Repair Projects	570
Peggy A. Johnson	
Managing Climate Change Uncertainty in Water Supply Planning	578
X. J. Irias and A. R. Coate	
Improvements in Hurricane Surge Response Functions: Incorporating the Effects of Forward Speed, Approach Angle, and Sea Level Rise	587
I. E. Udoh and J. L. Irish	
A Comparison of Top-Down Statistical Models with Bottom-Up Methods for Power System Reliability Estimation in High Wind Events	594
Roshanak Nateghi and Seth D. Guikema	
Classification of Current Building Stock for Hurricane Risk Analysis	602
Boback Bob Torkian, Jean-Paul Pinelli, and Kurt Gurley	
Probabilistic Hurricane Surge Risk Estimation through High-Fidelity Numerical Simulation and Response Surface Approximations	610
Alexandros A. Taflanidis, Andrew B. Kennedy, Joannes J. Westerink, Jane Smith, Kwok F. Cheung, Mark Hope, and Seizo Tanaka	
Wind Vulnerability Curves for Low-Rise Commercial-Residential Buildings in the Florida Public Hurricane Loss Model	618
G. L. Pita, J.-P. Pinelli, K. Gurley, J. Weekes, and J. Mitrani-Reiser	

Database-Assisted Design: Why and How?	626
E. Simiu	
Probabilistic Demand Models and Fragility Estimates for Offshore Wind Turbine Support Structures	633
M. Mardfekri, P. Gardoni, and J. M. Roesset	
The Use of Aerodynamic and Wind Climatological Databases for High-Rise Reinforced Concrete Structure Design.....	641
DongHun Yeo	
Development of Large Directional Wind Speed Databases.....	650
DongHun Yeo	

Geotechnical Hazards Analysis

Dynamic Displacement Analysis of a Shallow Landslide in Norwood Tuff	659
Keith E. Beisner, Aurelian C. Trandafir, and Ronald L. Bruhn	
Intra- and Inter-Event Uncertainties of Ground Motion Attenuation Relations	667
Swagata Banerjee	
Effective Shear Strengths of Isotopic Spatially Variable Soil Masses.....	675
Jianye Ching and Kok-Kwang Phoon	
Transportation Risk Analysis (TRA) of Bosphorus Suspended Bridge Using Probabilistic Approach	683
H. Aslan, H. S. Kuyuk, and M. Aktas	
Effects of Spatial Variability of Soil Property on Slope Stability.....	691
K. Kasama and K. Zen	
Interval Reliability Analysis for Gravity Retaining System of Deep Excavation.....	699
Jingchun Wang, Pengfei Xu, and Weihong Hou	
Methodology for Risk Analysis of Ground Surface Subsidence	708
H. A. Kamal and B. M. Ayyub	

Security Risk and Vulnerability Analysis

A Methodology of Constructing Dynamic Risk Maps for Large Metropolitan Areas	716
E. Guryev, L. Poluyan, and S. Timashev	
A Methodology to Produce Interdependent Networks Disturbance Scenarios	724
Serge Lhomme, Damien Serre, Youssef Diab, and Richard Laganier	
Automated Security Risk Analysis Tool for USAF Installation Security	732
Kenneth J. Knox	
Risk-Based Cost-Benefit Analysis for Security Assessment Problems	738
Gregory D. Wyss, John P. Hinton, Katherine Dunphy-Guzman, John Clem, John Darby, Consuelo Silva, and Kim Mitchiner	
Assessing Vulnerability to Floods of the Built Environment—Integrating Urban Networks and Buildings	746
Damien Serre, Serge Lhomme, Kristina Heilemann, Leif Sigurd Hafskjold, Andrew Tagg, Nicholas Walliman, and Youssef Diab	

Quantifying System Vulnerability As a Performance Measure for Systems Investment Evaluation and Decision-Making	754
S. Labi, Q. Bai, I. Kumar, A. Ahmed, and P. Anastasopoulos	
Resilience and Preparedness of Critical Infrastructure	764
S. A. Timashev	
Development of Spatial Risk Profiles Resulting from Sea Level Rise: What Predictions of Future Sea Level Rise Mean for the Built Coast.....	772
Michael S. Kearney and Bilal M. Ayyub	
Defining and Assessing Vulnerability of Infrastructure to Terrorist Attack.....	782
Geoffrey S. French and David Gootzit	
Integrating Flood Defence Fragility to Measure Built Environment Vulnerability—A GIS Based Approach.....	790
Damien Serre, Serge Lhomme, Brunno Barroca, and Youssef Diab	
<i>Water Resource Analysis and Management</i>	
Many-Objective Risk-Based Planning within Complex Engineering Systems: An Urban Water Planning Example.....	798
Patrick M. Reed, Joseph R. Kasprzyk, and Gregory W. Characklis	
Risk Management of Asalouye Desalination Project	805
Meghdad Attarzadeh, David Kim Huat Chua, and Michael Beer	
Forecasting of Erosion and Debris Flow Processes for the Energy Supply and Transport Corridors of Georgia Using the Theory of Reliability and Risk	813
G. V. Gavardashvili	
Probabilistic Dominance Application to the Sacramento-San Joaquin Delta	821
Jay R. Lund	
Capacity Planning under Nonstationary Uncertainties.....	829
Neela P. Babu, Jan Kuakkal, Daniel P. Loucks, and Warren E. Walker	
A Hybrid Approach of Uncertainty Analysis for Performance Measurement of Water Distribution System.....	836
Krishna Khatri and Kalanithy Vairavamoorthy	
A New Approach of Risk Analysis for Complex Infrastructure Systems under Future Uncertainties: A Case of Urban Water Systems	846
Krishna Khatri and Kalanithy Vairavamoorthy	
<i>Performance Analysis and Measurement</i>	
Toward Guidance for Identifying and Measuring Structural Damage Following a Blast Event	857
Andrew D. Sorensen and William McGill	
Expected Building Damage Using Stratified Systematic Sampling of Failure Triggering Events.....	865
Stefan T. Szyniszewski	
Design of Supplemental Dampers for Seismic Risk Reduction of Isolated Bridges.....	873
Alexandros A. Taflanidis	

Evaluating the Efficiency of Current Nonlinear Static Pushover Procedures on Estimating Torsion Effect for Asymmetric High-Rise Buildings.....	881
Q. W. Zhang, Kusnowidjaja Megawati, L. P. Huang, and T. C. Pan	
Analysis of Bridge Performance under the Combined Effect of Earthquake and Flood-Induced Scour	889
Swagata Banerjee and Gautham G. Prasad	
Uncertainty Modeling in Bridge Network Maintenance Optimization.....	897
Paolo Bocchini and Dan M. Frangopol	
Overcoming the Limitations of Traditional Model-Updating Approaches.....	905
James-A. Goulet and Ian F. C. Smith	
Reliability Analysis of Mooring Dolphin Structures	914
Reda Farag, Mahmoud El-Meligy, and Achintya Haldar	
Adaptive Reliability Analysis of Reinforced Concrete Bridges Using Nondestructive Testing	922
Q. Huang, P. Gardoni, and S. Hurlbaas	
Modeling Long-Term Reliability of Vertical Barriers	930
Arthur S. Kurzydlo and Jamshid Mohammadi	
<i>Info-Gap Methods in Risk and Uncertainty Analysis</i>	
Managing Biological Invasions under Severe Uncertainty: Light Brown Apple Moth in California	938
Craig D. Osteen and L. Joe Moffitt	
Robust Conservation Decision-Making.....	945
Eve McDonald-Madden, Peter W. J. Baxter, and Hugh P. Possingham	
A New Approach of Decision Making under Uncertainty for Selecting a Robust Strategy: A Case of Water Pipes Failure.....	953
Krishna Khatri and Kalanithy Vairavamoorthy	
Robust Satisficing and the Probability of Survival.....	963
Yakov Ben-Haim	
An Info-Gap Model to Examine the Robustness of Cost-Efficient Budget Allocations.....	971
Vanessa M. Adams and Robert L. Pressey	
Info-Gap Approach to Regression	980
Miriam Zacksenhouse and Simona Nemets	
Robust Resource Allocation: An Info-Gap Approach.....	988
Lior Davidovitch and Yakov Ben-Haim	
<i>Indexes</i>	
Author Index	997
Subject Index	1001

Application of Evolutionary Computing to Disaster Restoration and Prevention Problems

Hitoshi Furuta¹ and Koichiro Nakatsu²

¹Department of Informatics, Kansai University, 2-1-1 Ryozenji-cho, Takatsuki, Osaka, 569-1095, Japan; Tel & Fax: +81-72-690-2348; e-mail: furuta@res.kutc.kansai-u.ac.jp

²Department of Informatics, Kansai University, 2-1-1 Ryozenji-cho, Takatsuki, Osaka, 569-1095, Japan; Tel & Fax: +81-72-690-2348; e-mail: inside2@sc.kutc.kansai-u.ac.jp

ABSTRACT

In this paper, an attempt is made to apply evolutionary computing for earthquake disaster restoration and prevention problems. The relationships among early restoration, minimization of life-cycle cost and target safety level of road network are discussed by using multi-objective genetic algorithm. A comprehensive disaster prevention program is developed based on the recognition that road networks may be unavoidably damaged when very strong earthquakes occur. By introducing the concept of multi-objective optimization into the restoration and prevention scheduling for earthquake disasters, it is possible to find out several near-optimal restoration and prevention scheduling plans.

INTRODUCTION

Japan has been exposed to many natural hazards such as typhoons, tsunamis and earthquakes. After earthquake disaster, road networks play important roles in rescue, evacuation activities, extinguishing fires, and disaster-relief activities. In this study, an attempt is made to apply evolutionary computing for earthquake disaster restoration and prevention problems. First, the early restoration of road networks after the earthquake disasters is discussed, in which two issues are dealt with, the first one is an allocation problem which groups restore which disaster places and the second is a scheduling problem what order is the best for the restoration. In order to solve the two problems simultaneously, Genetic Algorithm (GA), which is a representative method of evolutionary computing, is applied, because it has been proven to be very powerful in solving combinatorial problems.

The relationships among early restoration, minimization of LCC, and target

safety level of road network are discussed by using Multi-Objective Genetic Algorithm (MOGA). Moreover, it is intended to introduce various uncertainties involved in the disaster restoration scheduling.

Next, a comprehensive disaster prevention program is developed because road networks may be unavoidably damaged when very strong earthquakes occur. The damage to the road network is associated with severe effects on the daily life and economic activities of people. The seismic performance of road network is evaluated based on the following three factors: (a) the characteristics of road network such as existence or non-existence of detour, (b) importance of bridge such as existence or non-existence of a medical center near a particular bridge of the network, and (c) road traffic condition. The purpose of this study is to provide a framework for optimal allocation of strengthening cost for increasing the seismic performance of road networks. The relationship between strengthening cost of an entire road network and safety level of this network is discussed by using MOGA. Namely, the following two objective functions are considered: (a) strengthening cost of the road network is minimized and (b) safety level of road network is maximized. By introducing the concept of multi-objective optimization into the restoration and prevention scheduling for earthquake disasters, it is possible to find out several near-optimal restoration and prevention scheduling plans.

OPTIMAL RESTORATION SCHEDULING BY GENETIC ALGORITHM CONSIDERING UNCERTAINTY

The purpose of this research is to propose an early restoration for road networks after earthquake disasters. In general, road networks after earthquake disasters have an uncertain environment, that is, the actual restoring process should be performed by considering various uncertainties simultaneously. Genetic Algorithm Considering Uncertainty (GACU) [Tamaki et al., 1999] can treat various uncertainties involved, but it is difficult to obtain the schedule which has robustness. In this study, an attempt is made to develop a decision support system of the optimal restoration scheduling by using the improved GACU [Furuta and Nakatsu, 2010].

Here, it is assumed that a road network is damaged, in which multiple portions are suffered from damage so that it can not function well. The objective of this study is the realization of quick restoration of the road networks. It is intended to determine the optimal allocation of restoring teams and optimal scheduling of restoring process. Then, the following conditions should be taken into account [Furuta and Nakatsu and ., 2004]:

1. The optimal allocation of restoring team, optimal scheduling of restoring process, and optimal allocation of restoring method must be determined simultaneously.
2. A portion of the road network is suffered from several kinds of damage that have a hierarchical relation in time.

At a devastated area after an earthquake disaster, the circumstances are changing with aftershock, fire and bad weather. The devastated area may have another damage and the circumstances may not be constant. This is due to the uncertainty of a damage which occurs from the followings:

1. **Delay:** Delay induces the increase of restoring days of a work. The delay of the work influences the whole restoring schedule.
2. **Impossibility to restore:** Impossibility to restore is such a situation that a team without sufficient restoring equipment and facility is assigned to large damage work. Such a team cannot restore the large damage work. Impossibility of work to restore causes failure of restoring schedule.

In order to obtain the restoration schedule which has robustness to the uncertainty of damage, it is necessary to implement sampling many times. In GACU, objective function is defined as the expected value of $F'(x)$ to consider the search process as the sampling.

$$F'(x) = F(x) \text{ with Uncertainty} \quad (1)$$

$F(x)$ contains a variable element, that is, uncertainty, so that $F'(x)$ is changing according to the uncertainty. It is assumed that the number of sampling is the age of individual. This sampling is performed by considering the evolution mechanism of inheritance, that is, gene of parents is resembled to that of children. The procedure of

GACU is applied to obtain the optimal robust restoration schedule. The effects of increasing the damage obtained by 1000 simulations are shown in Table 1. Table 2 presents the effects of the delay obtained by 1000 simulations. It is considered that teams without restoring equipment are not assigned to large damage works and medium damage works which are changeable to large damage, and waiting time is properly assured to avoid the effects of delay. In addition, most of larger damage works are assigned to restoration team with high ability. The schedule is not only robust but also optimum for the early restoring.

Table 1: Effects of increasing the damage obtained by 1000 simulations

Probability changed	Average of evaluation	Impossible to restore
5%	6.87	0/1000
10%	7.00	0/1000
20%	7.27	0/1000

Table 2 Effects of the delay obtained by 1000 simulation

Probability changed	Evaluation	SimpleGA	GACU
5%	Evaluation(Ave)	7.52	7.88
	Evaluation(Max)	8.80	7.97
	Evaluation(Min)	7.11	7.18
	Standard deviation	0.52	0.47
10%	Evaluation(Ave)	9.12	7.91
	Evaluation(Max)	17.22	8.31
	Evaluation(Min)	7.11	7.18
	Standard deviation	2.12	0.57
20%	Evaluation(Ave)	15.04	8.01
	Evaluation(Max)	17.56	8.41
	Evaluation(Min)	14.35	7.20
	Standard deviation	3.22	1.29

OPTIMAL COST ALLOCATION FOR IMPROVING SEISMIC PERFORMANCE OF ROAD NETWORKS

The seismic performance of road network is evaluated based on the following three factors: (a) the characteristics of road network such as existence or non-existence of detour, (b) importance of bridge such as existence or non-existence of a medical center near a particular bridge of the network, and (c) road traffic condition. The purpose of this study is to provide a framework for optimal allocation of strengthening cost for increasing the seismic performance of road networks. Here, an attempt is made to discuss the relationship between strengthening cost of an entire road network and safety level of this network by using Multi-Objective Genetic Algorithm (MOGA) [Furuta, Kameda and Frangopol, 2004].

As an example, an existing road network in Osaka, Japan is considered. As indicated in Figure 1, this network has 10 bridges, 27 nodes, 4 hospitals, and 4 emergency evacuation centers.

The user cost (UC) associated with the road network in Figure 1, is calculated as a function of the relation between vehicle speed and traffic density and considering an average cost of 82 yen/minutes/car.

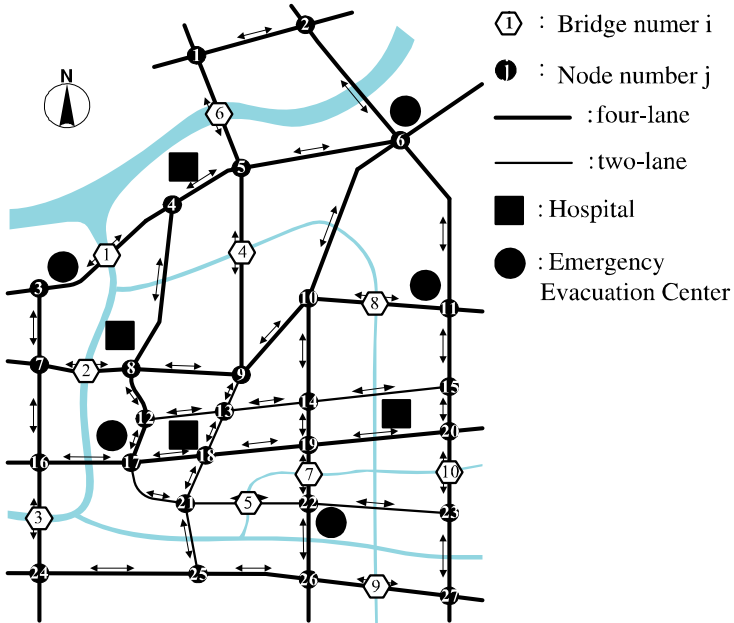


Figure 1. Road network in Osaka, Japan

In addition to the user cost, the importance of a bridge depends on the access to a hospital and/or an emergency evacuation center.

The total effect of bridge closing on the number of detours is defined by the following relation

$$C_i = (1 - H_i) + (1 - E_i) \quad (2)$$

where H_i is the ratio of total number of detours due to the closing of bridge i to arrive at a hospital and total number of nodes in the network, and E_i is the ratio of total number of detours due to the closing of bridge i to arrive at a emergency evacuation center and total number of nodes in the network.

The importance of bridge i to the road network is defined as follows:

$$B_i = \frac{UC_i / C_i}{\sum_{j=1}^{10} (UC_j / C_j)} \quad (3)$$

where UC_i is the user cost associated with the i -th bridge and C_i is defined in (2).

In this study, strengthening cost and safety level are used as objective functions. Strengthening cost is minimized and safety level is maximized. There are trade-off relations among these two objective functions. For example, safety level decreases when strengthening cost decreases. Therefore, multi-objective optimization can provide a set of Pareto solutions that can not improve an objective function without making other objective functions worse.

The strengthening cost of each bridge depends on the strengthening method. The four strengthening methods considered, denoted as α , β , γ and δ , are defined in Table 3. It is assumed that all bridges in the network have the same safety level (i.e., 0.5) before strengthening is applied.

The objective function is defined as

$$SC = \sum_{i=1}^{10} SC_i \quad (4)$$

where SC is the strengthening cost of the road network, and SC_i is the strengthening cost of the i -th bridge of the network. The bridge strengthening cost is a function of the safety level after strengthening as indicated in Table 3.

Safety level depends on the traffic volume and the condition of bridge. In this study, bridge, and S_i is the safety level of the i -th bridge.

Table 3. Safety level and strengthening cost

Strengthening method	Bridge safety level after strengthening	Bridge strengthening cost (thousand yen)
Strengthening method α	0.6	10000
Strengthening method β	0.7	20000
Strengthening method γ	0.8	27000
Strengthening method δ	0.9	33000

the safety level (SL) of the road network is maximized, as follows

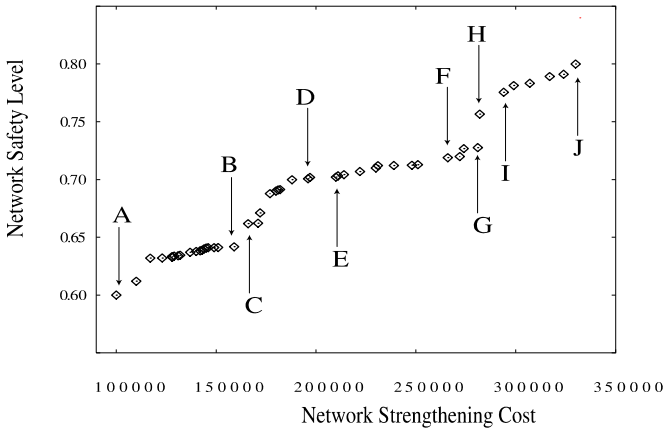
$$SL = \sum_{i=1}^{10} B_i \times S_i \rightarrow \max \quad (5)$$

where SL is the safety level of the road network, B_i is the importance of the i -th

In the implementation of MOGA, the GA parameters considered are as follows: number of individuals = 200, crossover rate = 0.60, mutation rate = 0.05, and number of generations = 5000. Figure 2 shows the results obtained by MOGA. Table 4 shows the values of the two objectives of each Pareto solution. Comparing the Pareto solutions D and E with respect to safety level, there is no significant difference. However, considering strengthening cost, solution E is more expensive than solution D. Conversely, the Pareto solutions G and H are similar with respect to the associated strengthening cost, but they are very different with respect to their associated safety level. Regarding safety level, the Pareto solutions D and F are similar. However, there is a significant difference between the strengthening cost associated with these two solutions. Table 5 shows the allocation of network strengthening cost of the Pareto solutions in Figure 2. Figure 3 shows the detailed allocation of earthquake strengthening cost associated with the solution D shown in Figure 2. Therefore, when selecting a strengthening program, the proposed method enables to compare feasible optimal solutions associated with different values of the objectives.

Table 4. The values of each Pareto solution

Pareto solution	Network strengthening cost (thousand yen)	Network safety Level
A	100000	0.600
B	160000	0.641
C	166000	0.661
D	194000	0.702
E	214000	0.704
F	267000	0.706
G	274000	0.712
H	276000	0.757
I	292000	0.775
J	330000	0.800

**Figure 2. Pareto solutions obtained by MOGA**

CONCLUSIONS

In this paper an attempt was made to apply evolutionary computing, especially genetic algorithms, for disaster restoration and prevention problems. Introducing the genetic algorithm considering uncertainty, it is possible to obtain a restoration schedule which can take into account various uncertainties involved in the restoration process. Furthermore, it was attempted to formulate the optimal allocation of seismic strengthening cost of a road network as a multi-objective optimization problem. By considering network strengthening cost and network safety level as objective functions, it is possible to obtain the relationships between these two performance indicators. This paper provided of a framework for optimal allocation of strengthening cost for improving the seismic performance of road networks.

REFERENCES

- Furuta, H. and Nakatsu, K. (2004). "Optimal restoration scheduling for earthquake disaster by emergent computing", Reliability and Optimization of Structural Systems.
- Furuta, H., Kameda, T. and Frangopol, D. M. (2004). "Balance of structural performance measures", Proc. of Structures Congress, Nashville, Tennessee, ASCE, May, CD-ROM.
- Furuta, H. and Nakatsu, K. (2010). "Life cycle performance of infrastructure networks considering seismic risk, J. Li et al. eds.: Proceedings of International Symposium on Reliability Engineering and Risk Management, 45-56, Tongji University Press, Shanghai, China.
- Tamaki, H., Arai, T. and Abe, S. (1999). "A Genetic algorithm approach to optimization problems with uncertainties", Institute of Systems, Control and Information Engineers Journal, 12(5), 297-303. (in Japanese).

Quantitative Risk Analysis of Damage to Structures During Windstorms: Random Field and System Reliability Aspects

Erik Vanmarcke¹ and Ning Lin²

¹ Department of Civil and Environmental Engineering, Princeton University, Princeton, NJ; M. ASCE; PH (609) 751-0221; email: evm@princeton.edu

² Department of Earth and Planetary Sciences, Massachusetts Institute of Technology, Cambridge, MA, U.S.A.; email: ninglin@mit.edu

ABSTRACT

Quantitative risk analysis (QRA) enables rational accounting for the effect of spatial scale on estimates of damage to individual (multi-component) structures or to groups of closely spaced structures during severe windstorms. The case of the window breakage on the facade of Boston's John Hancock Tower, which motivated a series of such risk-based studies, is summarized. We further describe and illustrate an integrated vulnerability model to estimate structural damage in clusters of residential buildings due to tropical-cyclone winds, accounting for the "chain reaction" of events involving wind pressure damage and wind-borne debris damage, amplifying aggregate losses. The last part of the paper provides relevant background information on new methodology to analyze multi-scale random fields, presented in the second (2010) edition of the first author's book *Random Fields*.

1 THE CASE OF BOSTON'S HANCOCK BUILDING WINDOW BREAKAGE: RISK-RELATED STUDIES

Estimating economic losses resulting from damage to structures during severe windstorms has become a topic of considerable research interest in scientific fields such as meteorology, structural engineering and actuarial sciences. Of particular interest herein is the dependence of estimates of overall damage and economic loss on spatial scale, i.e., on the number of vulnerable components in a single structure or on the number (and density and variability of characteristics) of structures in a residential neighborhood. The senior author gained much related experience, while on the faculty at M.I.T., in connection with the problems, widely reported in the local press, of window



Figure 1: **Window breakage on the facade of Boston’s John Hancock Tower in the mid-1970’s**

breakage at the site of the John Hancock Tower in Boston, Massachusetts in the mid-1970’s (see Figure 1), soon after the building’s completion and initial occupancy. When an individual pane of glass failed on a high floor of this 62-story building during a moderate windstorm, as happened several times during the first few months of occupancy, it often caused a cascade of damage and failure of windows on lower floors. Consisting of more than 10,000 window panes, the building’s facade exhibited disastrous weakest-link vulnerability, as many possible combinations of high local pressure and low window-specific resistance made the chance of failure of a window somewhere on the building’s facade highly likely, with severe “system-wide” consequences. In addition, some windows, damaged during one storm, had reduced resistance to breakage during subsequent events or at a later time during the same windstorm, exemplifying critical time-dependence of the risks.

Conventional component-focused and static-load-based deterministic building codes, like those still in force in Boston in the early 1970’s, considered

neither the reality of occasional extremely high (random time-varying and spatially correlated) local pressures on a building's facade during windstorms nor the probability distribution of breakage strength of individual glass panes. Within the code framework, designers did not consider that, given a "design criterion" (as recommended in the glass manufacturer's guide) of eight-tenths of one percent (or 0.008) probability of failure for single glass-panes, approximately $10,000 \times 0.008 = 80$ windows are expected to fail during a design-intensity windstorm (not counting "secondary failures"). It was therefore no surprise that some windows did fail during several first-year modest-intensity windstorms. Extensive subsequent analytical and experimental research (funded by the then-owner and unpublished owing to only-recently-relaxed legal constraints) demonstrated the need for quantitative risk analysis (QRA). This eventually resulted, after several years during which the building was known as the "plywood palace", in the replacement of all exterior windows in the building with panes of glass having resistance-to-breakage roughly 4 times the original. A number of consulting reports (heretofore not made public) on the first author's risk assessment research related to the case of the John Hancock Tower (Vanmarcke, 1972, 1973, 1974a & b, 1975, 1976 & 1978; and a summary of the above in Vanmarcke, 1983) provide much detail on the methodological breakthroughs and their application to the case.

2 PREDICTING DAMAGE TO DWELLINGS DUE TO TROPICAL CYCLONES

2.1 Background and Scope of the Study. An integrated vulnerability model developed by Lin, Vanmarcke and Yau (2010) for predicting damage to low-rise structures during strong windstorms, and especially tropical cyclones, explicitly accounts for the interaction between pressure damage and debris damage by fully coupling a debris risk model (Lin and Vanmarcke 2008 & 2010) and a component-based pressure damage model. This integrated methodology can be applied to general site- and storm-specific analyses for residential developments consisting of large numbers of houses, or it can be combined with a "windstorm-event simulator" so as to yield estimates of probability distributions of aggregate annual (or multi-year) economic losses.

A cluster of buildings is defined by specifying the location, orientation and (significant) structural details of each building in a study area. Building types

considered include one-story concrete and wood-frame houses with gable roof or hip roof, of arbitrary overall dimensions, roof slope, number of openings, and other features (as illustrated in Figure 2). Statistics on relevant house characteristics, such as layouts and dimensions, structural components, and component resistances, as well as types and characteristics of potential debris sources (mainly on the house roof), are obtainable from information about the local building stock, as in many cases building-specific data will not be (readily) available. Specification of resistance, wind pressure coefficient, and wind pressure zone distribution for each building component parallels that in the Florida Public Hurricane Loss Projection (FPHLP) model (Gurley et al. 2005) and the ASCE 7 standard (ASCE 2003). Various uncertain quantities characterizing the structures, such as the component resistances, are represented by (joint) probability distributions. The model implements Monte Carlo simulation, with structural parameter values randomly assigned to every building in each simulation run.

2.2 Tropical-Cyclone-Wind Characteristics. An appropriate, tractable description of wind conditions is necessary to evaluate the structural damage to (a cluster of) buildings. During a tropical cyclone event, a structure is exposed to winds from different directions as the cyclone moves along its track. After initial structural damage is incurred to a building component, a change in wind direction may significantly affect the subsequent occurrences of damage. This interdependence among component failures cannot be quantified reliably without considering the incremental changes in wind speed and wind direction over time within individual strong-wind events.

Currently, two ways of specifying wind characteristics are commonly used in different vulnerability models. In the first method, used in damage estimation models such as HAZUS-MH, the structural loading and performance are evaluated at a series of steps in time at which wind speed and direction are specified (Vickery et al. 2006); the structural damage at a particular time step depends on the damage accumulated during previous time steps. The second method, used in the FPHLP model, evaluates the structural performance at a given wind speed and direction (Gurley et al. 2005, Li and Ellingwood 2006). We considered both methods of analysis to assess damage from windstorm events to clusters of buildings.

Due to the lack of historical tropical cyclone records, many advanced meteorological models have been developed to simulate wind data for various

geographical regions (e.g., Powell et al. 2005, Vickery et al. 2000). Their solutions, typically in the form of a time-dependent field having two spatial dimensions, provide much more information than was needed for the purpose of structural damage estimation. We adopted, instead, a simpler, geographically non-specific, parametric model (Lin et al. 2010, Yau 2011) that fairly approximates the temporal features of the wind field at a single location.

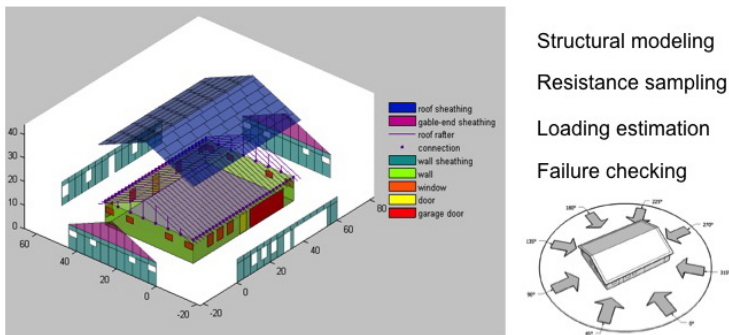


Figure 2: **Analysis of an idealized multi-component structure.**

2.3 Integrated Vulnerability Model. The wind-borne debris risk model developed by Lin and Vanmarcke (2008 & 2010) evaluates the risk of damage to vulnerable components (e.g. windows and doors) on a building envelope from the impact of roof-originated debris (e.g. covers and sheathing). This then enables the coupling of the debris model with a component-based pressure damage model, in an iterative mode of analysis.

Wind loads on structural components are calculated based on the specified wind condition and designated load paths. By comparing the sample component resistance to the load, the pressure damage model assesses wind-pressure damage to each building component. The structural system being analyzed comprises roof cover, roof sheathing panels, roof-to-wall connections, walls, wall sheathing panels, doors, windows and garage doors. The levels of damage to these building components are highly correlated in most cases. When

opening damage (for instance, to windows, doors, or garage doors) occurs due to pressure or debris damage, the internal pressure is adjusted (see Gurley et al. 2005) in a way that affects the damage conditions of almost all the components. After the adjustment, further damage to openings may again change the internal pressure. An iterative algorithm is applied to obtain the equilibrium between the internal pressure and the damage condition.

2.4 Case Study: Damage due to Hurricane Charley (2004) to a Residential Development in Sarasota County, FL. A residential development of 358 single-story houses in Sarasota County, Florida (see Figure 3) was selected to illustrate how the integrated vulnerability model can be applied. The locations of the residences are known, while the structural characteristics of each house are estimated based on information about the building stock in central Florida (Gurley et al. 2005). We estimate wind damage from Hurricane Charley (2004), which passed to the left of the study area. Hurricane Charley was numerically simulated using the Weather Research and Forecasting (WRF) model (Skamarock et al. 2005), which yields a simulated wind-velocity time history at a representative location within the study region.

Unlike other vulnerability models (Gurley et al. 2005, Vickery et al. 2005) that evaluate individual prototype buildings, the integrated vulnerability



Figure 3: Study area of a residential development of 358 houses in Sarasota County, Florida (left) and simulated storm track (middle) and wind field (right) of Hurricane Charley of 2004.

model analyzes a cluster of buildings as a whole, seeking to account for the (time-varying) interaction between building damage levels due to wind-borne debris. Evaluating building performance only at the maximum wind speed (and the corresponding direction) has the advantage of reduced computational effort, but may significantly underestimate damage, compared to results based on (multi-structure) cumulative damage analysis, when pressure-and-debris damage is estimated, in increments, over a time series of wind speed and wind direction. Debris damage is found to contribute greatly to overall average damage ratios, especially during high-intensity windstorms, and its explicit consideration (in a multi-structure setting) tends to add greatly to the *uncertainty* in estimates of overall damage ratios. Also, the more variation there is in resistances and in quality of construction within a residential neighborhood, the greater the overall mean damage ratio.

3 NEW RANDOM FIELD CONCEPTS AND METHODS

Random field concepts and methods have been applied in many areas of science and engineering, as the need to account for the reality of complex random variation and quantify risks in natural environments and complex engineered systems is ever more widely recognized, and fast-growing computing power and sizes of databases provide further motivation and empirical support for high-level probabilistic modeling.

In the recent 2nd edition of *Random Fields: Analysis and Synthesis* (Vanmarcke 2010), the treatment of the correlation structure of one-dimensional (single-scale) random processes – in terms of the variance function and the scale of fluctuation – is extended to multi-scale random processes, based on the concept of the “scale spectrum”. Specifically, “multi-scale” random variation in space and/or time can be modeled, in many applications (e.g., in order to represent random time-varying and spatially correlated local pressures on a building’s facade during windstorms), as a summation of statistically independent single-scale random processes. The composite model’s “scale spectrum” depicts the variances of the component processes as a function of their respective scales of fluctuation. The scale spectrum of any “single-scale process” is a Dirac-delta function, while natural phenomena are typically characterized by a wide, band-limited scale spectrum (that also happens to be indicative of fractal or self-similar behavior).

Another principal focus of *Random Fields*, essential to system reliability analysis, concerns threshold excursions and extreme values (and, related, conditions for stable level-exursion statistics to exist). Lastly, new results are presented for a family of quantum-physics-based probability density functions that express the inherent randomness of single energy quanta associated with local thermal equilibrium (blackbody radiation – at any temperature). The distributions have a simple analytical form and tractable statistical properties, and promise to be very useful in applications of random fields.

4 CONCLUSIONS

We present and illustrate improved methodology to assess structural vulnerability and wind-related economic losses in residential neighborhoods during tropical cyclones or other severe windstorms. Involving the interaction between a pressure damage model and a debris risk model, the method is capable of estimating cumulative damage to the overall structural system and the interior of buildings in a residential development. It also accounts for the linkage, as to damage, between buildings that can be both sources and recipients of debris. By means of a numerical example, it is shown that wind-borne debris tends to contribute significantly to total damage and resulting economic loss, and that the cumulative wind-related damage during the passage of a storm may be much greater than would be estimated by considering only the maximum wind speed during the storm. The methodology, in broad outline, is also applicable to the assessment and management of risk and vulnerability of tall buildings and clusters of tall buildings (as in a mega-city core) during severe windstorms.

The window breakage problems of Boston's John Hancock building exemplify the importance of accounting for weakest-link and cascading-damage phenomena related to debris during windstorms. Only quantitative risk analysis (QRA) is capable of accounting for important effects of "spatial scale" – when a system has increasingly many interacting components or "subsystems" – and providing a rational basis for wind-hazard-related risk management. The temporal evolution of "systemic risk", whether it relates, in the case of civil infrastructure, to slowly deteriorating resistances or potential long-term changes in windstorm frequencies and intensities (as a consequence of global change), is likewise made tractable by means of QRA.

ACKNOWLEDGEMENTS

We gratefully acknowledge support for this research, partly through a grant to Princeton University from Baseline Management Company and partly under a project entitled "Improved Hurricane Risk Assessment with Links to Earth System Models", funded through the Cooperative Institute for Climate Science (CICS) by the National Oceanographic and Atmospheric Administration (NOAA).

REFERENCES

- American Society of Civil Engineers (2003). *Minimum design loads for buildings and other structures*. ASCE Standard 7-02, ASCE.
- Gurley, K., Pinelli, J.-P., Subramanian, C., Cope, A., Zhang, L., Murphree, J., Artiles, A., Misra, P., Culati, S. and Simiu, E. (2005). "Florida Public Hurricane Loss Projection Model engineering team final report." International Hurricane Research Center, Florida Internat'l University.
- Li, Y. and Ellingwood, B.R. (2005). "Hurricane damage to residential construction in the US: Importance of uncertainty modeling in risk assessment." *Engineering Structures*, 28(7): 1009-1018.
- Lin, N. and Vanmarcke, E. (2008). "Windborne debris risk assessment." *Probabilistic Engineering Mechanics*, 23(4): 523-530.
- Lin, N. and Vanmarcke, E. (2010). "Windborne debris risk analysis - Part I. Introduction and methodology." *Wind and Structures*, 13(2): 191-206.
- Lin, N., Vanmarcke, E. and Yau, S.C. (2010). "Windborne debris risk analysis - Part II. Application to structural vulnerability modeling." *Wind and Structures*, 13(2): 207-220.
- Powell, M.D., Soukup, G., Cocke, S., Gulati, S., Morisseau-Leroy, N., Hamid, S. Dorst, N., and Axe L. (2005). "State of Florida Hurricane Loss Projection Model: Atmospheric science component." *J Wind Eng. and Ind. Aerodynamics*, 93(8): 651674.
- Skamarock, W.C., Klemp J.B., Dudhia, J., Gill D.O., Barker, D.M. Wang, W. and Powers, J.G. (2005). "A description of the advanced research WRF version 2." Technical report, Mesoscale and Microscale Meteorology Division, National Center for Atmospheric Research (NCAR).
- Twisdale, L.A., Vickery, P.J. and Steckley, A.C. (1996). "Analysis of hurricane windborne debris risk for residential structures." Technical report, Raleigh (NC): Applied Research Associates, Inc.

- Vanmarcke, E. (1972). "Relationship between peak factors for wind velocity and pressure." Consulting Report to Hansen, Holley and Biggs.
- Vanmarcke, E. (1973). "Determination of probability of window breakage during windstorms." Consulting Report to Hansen, Holley and Biggs.
- Vanmarcke, E. (1974a). "Estimates of damping coefficients from building motion records." Consulting Report to Hansen, Holley and Biggs.
- Vanmarcke, E. (1974b). "Statistical analysis of airport-to-top-of-tower wind speed conversion factors." Consulting Report to Hansen, Holley and Biggs.
- Vanmarcke, E. (1975). "Prediction of the likelihood of wind-induced permanent distortion of a tall building." Consulting Report to Hansen, Holley and Biggs.
- Vanmarcke, E. (1976). "Risk of occupant ejection associated with window failures in a tall building." Consulting Report to Hansen, Holley and Biggs.
- Vanmarcke, E. (1978). "Mechanisms of glass failure: a statistical question." Consulting Report to Hansen, Holley and Biggs.
- Vanmarcke, E. (1983). "Risk analysis and structural safety." *Proc. of the M.I.T. Symposium on Struct. Eng.: Research, Education and Practice*, in Tribute to Professors Emeriti John M. Biggs, Robert J. Hansen and Myle J. Holley, M.I.T. Department of Civil Engineering, 228-233.
- Vanmarcke, E. (2010). *Random Fields: Analysis and Synthesis*, 2nd Edition, World Scientific Publishing Company (1st Edition, The MIT Press, 1983).
- Vickery, P.J., Skerlj, P.F., Steckley, A.C., and Twisdale, L.A. (2000). "Hurricane wind field model for use in hurricane simulations." *J. of Struct. Eng.*, 126(10): 12031221.
- Vickery, P.J., Skerlj, P.F., Lin, J., Twisdale, L.A., Young, M.A. and Lavelle, F.M. (2006). "HAZUS-MH Hurricane Model methodology. II: Damage and loss estimation." *Natural Hazards Review*, 7(2): 94-103.
- Yau, S.C. (2011). "Wind Hazard Risk Assessment and Management for Structures." Ph.D. Thesis, Princeton University.

Statistical decisions with random fuzzy data - a possibilistic approach

Olgierd Hryniewicz¹

¹Systems Research Institute, Newelska 6, 01-447 Warsaw, Poland, PH: +48 22 3810 120; email: hryniewi@ibspan.waw.pl

ABSTRACT

In the majority of decision models used in practice all input data are assumed to be precise. This assumption is made both for random results of measurements, and for constant parameters such as, e.g. costs related to decisions. In reality many of these values are reported in an imprecise way. When this imprecision cannot be related to randomness the fuzzy set theory yields tools for its description. It seems to be important to retain both types of uncertainty, random and fuzzy, while building mathematical models for making decisions. In the paper we propose a fuzzy-Bayesian model for making statistical decisions. In the proposed model the randomness of data is reflected in related risks, and fuzziness is described by possibility measures of dominance such as PSD (Possibility of Strict Dominance) and NSD (Necessity of Strict Dominance). The proposed model allows a decision-maker to reflect in his/hers decisions different types of uncertainty.

INTRODUCTION

Testing statistical hypotheses is one of the most important parts of statistical inference. On the other hand it can be regarded as a part of the decision theory. In the decision theory we assume that decisions (actions belonging to a certain action space) should depend upon a certain state which is uncontrollable and unknown for a decision maker. We usually assume that unknown states are generated by random mechanisms. However, all we could know about these mechanisms is their description in terms of the probability distribution P_θ that belongs to a family of distributions $\{P_\theta: \theta \in \Theta\}$ indexed by a parameter θ (one or multidimensional). In such a case a state space is often understood as equivalent to the parameter space Θ . If we knew the true value of θ we would be able to take a correct decision. The choice of an appropriate decision depends upon a value of a certain utility function that has to be defined on the product of the action space and the state space. If we had known the unknown state we would have been able to choose the most preferred action looking for the action with the highest value of the assigned utility. In practice, we define the expected reward (or the loss) associated with the given action for the given state $\theta \in \Theta$, and then we define the utility $u \in U$ that 'measures' the preference the decision maker assigns to that reward (loss).

In the Bayesian setting of the decision theory we assume that there exists the prior information about the true state, and that this information is expressed in terms of the probability distribution $\pi(\theta)$ defined on the parameter space Θ . By doing this we identify each action with probability distribution on a set of possible utilities U . According to the Bayesian decisions paradigm we choose the action with the highest

value of the *expected* utility, where expectation is calculated with respect to the probability distribution defined on U .

When a decision maker has an opportunity to observe a random variable (or a random vector) X that is related to the state θ , such an observation provides him with additional information which may be helpful in making proper decisions. In such a case the decision problem is called the statistical decision problem. Comprehensive presentation of the Bayesian decision theory is presented in a classical textbook of Raiffa and Schleifer (1961), and the Bayesian approach to statistical decision problems may be found in DeGroot (1970).

In the statistical decision theory we deal with many quantities which may be vague and imprecise. First, our observation may be imprecise, described in linguistic terms. In such a case we deal with imprecise (fuzzy) statistical data. Many books and papers have been written on the statistical analysis of fuzzy data. Classical problems of statistical decisions with fuzzy data have been discussed, e.g., in the paper of Grzegorzewski and Hryniewicz (2001). More general approaches, referring to different concepts of fuzzy randomness, are presented in an overview paper by Gil and Hryniewicz (2008). First results presenting the Bayesian decision analysis for imprecise data were given in papers published in the 1980th and the 1990th by such authors like Casals, Delgado, Gil, Hryniewicz, Lopez-Diaz, Taheri and Behboodian, and Viertl. The references to these early works can be found in Hryniewicz (2002).

The crucial problem of the fuzzy approach to the Bayes statistical decision analysis is to compare fuzzy risks related to considered decisions. This problem arises from the fact that fuzzy numbers that describe fuzzy risks are not naturally ordered. Thus, the decisions depend upon the method used for such an ordering. In this paper we propose to use the Necessity of Strict Dominance Index (*NSDI*) introduced by Dubois and Prade (1983). We claim that in specific situations this approach is preferable to the others.

CALCULATION OF THE BAYES RISKS IN CRISP ENVIRONMENT

In the Bayesian approach to statistical decisions we take into consideration potential losses and rewards associated with each considered decision. Let $\theta \in \Theta$ be a parameter describing an element of the state space, and $\delta \in \Delta$ be a decision (action) from a space of possible (admissible) decisions. Usually we define an utility function $u(\theta, \delta)$ which assigns a certain utility $u \in U$ to the decision δ which describes a decision maker's level of preference for the decision δ if the true state is described by θ .

Assume now that the decision maker knows the likelihood function $L(\mathbf{x}|\theta) = L(x_1, \dots, x_n|\theta)$ that summarizes the observations of a random sample (X_1, \dots, X_n) . Moreover, we assume that the decision maker has some prior information about possible values of θ . This information, according to the Bayes decision theory, is represented by the prior probability distribution $\pi(\theta)$. This information is merged with the information yielded by the random sample. The updated information about the true value of the state θ is calculated using the Bayes theorem, and expressed in the form of the posterior probability distribution

$$g(\theta|\mathbf{x}) = \frac{L(\mathbf{x}|\theta)\pi(\theta)}{\int_{\Theta} L(\mathbf{x}|\theta)d\pi(\theta)} = \frac{g_n(\theta|\mathbf{x})}{n(\mathbf{x})} \tag{1}$$

where $\mathbf{x} = (x_1, \dots, x_n)$, and $g_n(\theta|\mathbf{x})$ is the non-normalised posterior distribution. Further analysis is performed in exactly the same way with the posterior probability distribution $g(\theta|\mathbf{x})$ replacing the prior probability distribution $\pi(\theta)$.

Let $\delta(\mathbf{x}) = \delta(x_1, \dots, x_n)$ be a decision function which is used for choosing an appropriate decision for given sample values (x_1, \dots, x_n) . The risk function, interpreted as an expected loss incurred by the decision δ , is calculated as

$$\rho(\delta) = \int_{\Theta} \int_X u(\theta, \delta(x_1, \dots, x_n))f(x_1, \dots, x_n|\theta)\pi(\theta)d\mathbf{x}d\theta \tag{2}$$

Let Δ be the space of possible decision functions. Function δ^* that fulfils the following condition

$$\rho(\delta^*) = \inf_{\delta \in \Delta} \rho(\delta) \tag{3}$$

we call the Bayes decision function, and the corresponding risk $\rho(\delta^*)$ we call *the Bayes risk*. Statistical decisions with the risk equal to the Bayes risk are called optimal. In this paper we present a particular problem of the Bayes decisions, namely to the Bayes test of statistical hypothesis $H_0 : \theta \in \Theta_0$ against the alternative hypothesis $H_1 : \theta \in \Theta_1$, where Θ_0 and Θ_1 are the subsets of the state space Θ such that $\Theta_0 \cap \Theta_1 = \emptyset$. Moreover, we show how this general approach can be used for solving a particular problem of Bayes decisions - estimation of the parameter of the Weibull distribution.

Let us define two functions:

$$H_0(\theta) = \begin{cases} 1, & \theta \in \Theta_0 \\ 0, & \theta \in \Theta_1 \end{cases} \text{ and } H_1(\theta) = \begin{cases} 0, & \theta \in \Theta_0 \\ 1, & \theta \in \Theta_1 \end{cases} \tag{4}$$

Now, let us define utility functions:

$$u(\theta, a_0) = a(\theta)[1 - H_0(\theta)] \tag{5}$$

that describes the utility related to the acceptance of H_0 , and

$$L(\theta, a_1) = b(\theta)[1 - H_1(\theta)] \tag{6}$$

that describes the utility related to the acceptance of H_1 . Functions $a(\theta)$ and $b(\theta)$ are two arbitrary nonnegative functions. In such a case we may consider only two risks: the risk of accepting H_1 when H_0 is true given by

$$R_1 = \int_{\Theta_1} u(\theta, a_1)g(\theta|\mathbf{x})d\theta \tag{7}$$

and the risk of accepting H_0 when H_1 is true given by

$$R_0 = \int_{\Theta_0} u(\theta, a_0)g(\theta|\mathbf{x})d\theta \tag{8}$$

In the following section we present methods for the computation of such a risk in different cases representing situations when different parts of the decision model are described in an imprecise way.

BAYES RISKS FOR FUZZY STATISTICAL DATA AND FUZZY PRIOR INFORMATION

Let us consider situation when available statistical data are vague and are described by fuzzy random variables. The notion of a fuzzy random variable has been defined by many authors in a different way. One of these definitions, attributed to Kwakernaak and – independently – to Kruse (see, e.g. Kruse and Meyer (1986) for

more information), considers the fuzzy random variable \tilde{X} as a fuzzy (vague) perception of an unknown ordinary random variable $X: \Omega \rightarrow R$, called an original of \tilde{X} . In the presence of fuzzy statistical data the posterior distribution of the state variable θ can be obtained by the application of Zadeh's extension principle to (1). Let $\tilde{x}_i^\alpha = (\tilde{x}_{i,L}^\alpha, \tilde{x}_{i,U}^\alpha)$, $i=1, \dots, n$ be the α -cuts of the fuzzy observations $\tilde{x}_1, \dots, \tilde{x}_n$. Following Frühwirth-Schnatter (1993) let's denote by $C(\tilde{\mathbf{x}})_\alpha$ the α -cut of the fuzzy sample which is equal to the Cartesian product of the α -cuts $\tilde{x}_1^\alpha, \dots, \tilde{x}_n^\alpha$. Frühwirth-Schnatter (1993) also proposed a generalization of the fuzzy risk model by allowing fuzziness in the description of the prior information. In such case the probability density function $\pi(\theta, \boldsymbol{\eta})$ that describes the prior knowledge about the values of the state variable θ may be described as the function of fuzzy parameters $\tilde{\boldsymbol{\eta}}$ denoted by $\pi(\theta, \tilde{\boldsymbol{\eta}})$. Let us denote α -cut of the fuzzy vector $\tilde{\boldsymbol{\eta}}$ by $C(\tilde{\boldsymbol{\eta}})_\alpha$. Thus, the α -contours of the fuzzy posterior probability density are now given by (see Frühwirth-Schnatter (1993))

$$g_\alpha^L(\theta) = \min_{\mathbf{x}, \boldsymbol{\eta} \in C(\tilde{\mathbf{x}})_\alpha \times C(\tilde{\boldsymbol{\eta}})_\alpha} \frac{f(\mathbf{x} | \theta) \pi(\theta, \boldsymbol{\eta})}{n(\theta, \boldsymbol{\eta})} \quad (9)$$

$$g_\alpha^U(\theta) = \max_{\mathbf{x}, \boldsymbol{\eta} \in C(\tilde{\mathbf{x}})_\alpha \times C(\tilde{\boldsymbol{\eta}})_\alpha} \frac{f(\mathbf{x} | \theta) \pi(\theta, \boldsymbol{\eta})}{n(\theta, \boldsymbol{\eta})} \quad (10)$$

where $n(\theta, \boldsymbol{\eta})$ is a normalizing constant. Having these α -contours we can use the general methodology for integrating fuzzy functions presented in Dubois and Prade (1980) and compute the membership functions of fuzzy risks $\tilde{\mathbf{R}}_0$ and $\tilde{\mathbf{R}}_1$. Let us denote by $C(\tilde{R}_h)_\alpha = (\tilde{R}_h^{\alpha,L}, \tilde{R}_h^{\alpha,U})$ the α -cuts of the fuzzy risks \tilde{R}_h , $h=0,1$. The lower and upper bounds of these α -cuts are now calculated from the following formulae:

$$R_h^{\alpha,L} = \int_{\Theta_h} L(\theta, a_h) g_\alpha^L(\theta) d\theta, h=0,1 \quad (11)$$

$$R_h^{\alpha,U} = \int_{\Theta_h} L(\theta, a_h) g_\alpha^U(\theta) d\theta, h=0,1 \quad (12)$$

The knowledge of these α -cuts is thus equivalent to the knowledge of the membership functions of fuzzy risks \tilde{R}_0 and \tilde{R}_1 , respectively. Further generalization may be achieved by assuming a vague character of utilities (losses). The procedure for finding the α -cuts of $\tilde{\mathbf{R}}_0$ and $\tilde{\mathbf{R}}_1$ is similar, and described in Hryniewicz (2002).

BAYES RISKS IN CASE OF FUZZY STATISTICAL HYPOTHESES

In this subsection we present a method proposed in Hryniewicz (2002) for the computation of fuzzy risks related to the test of the fuzzy hypothesis \tilde{H}_0 against a fuzzy alternative \tilde{H}_1 . First, let us suppose that all remaining information (i.e. statistical data, prior information, and loss functions) are crisp.

Let $\tilde{H}_h : \theta \in \tilde{\Theta}_h, h=0,1$ be considered fuzzy statistical hypotheses, where $\tilde{\Theta}_h, h=0,1$ are the fuzzy sets described by their membership functions $\mu_{\Theta_h}(\theta)$. To simplify the problem let us assume that each fuzzy set $\tilde{\Theta}_h$ may be presented in a form of a fuzzy interval $(\tilde{\Theta}_{L,h}, \tilde{\Theta}_{U,h})$, where fuzzy sets $\tilde{\Theta}_{L,h}$ and $\tilde{\Theta}_{U,h}$ have the α -cuts $(\Theta_{L,h}^{\alpha,L}, \Theta_{L,h}^{\alpha,U})$ and $(\Theta_{U,h}^{\alpha,L}, \Theta_{U,h}^{\alpha,U})$ such that $\Theta_{L,h}^{\alpha,L} \leq \Theta_{U,h}^{\alpha,L}$, and $\Theta_{L,h}^{\alpha,U} \leq \Theta_{U,h}^{\alpha,U}$. Denote the membership functions of $\tilde{\Theta}_{L,h}$ and $\tilde{\Theta}_{U,h}$ as $\mu_{L,h}$ and $\mu_{U,h}$, respectively. Using the notation of Dubois and Prade (1980) we may write the membership functions of the fuzzy risks $\tilde{\mathbf{R}}_h, h=0,1$ as

$$\mu_{\tilde{\mathbf{R}}_h}(t) = \sup_{y,z:t = \int_{\tilde{\Theta}_h} u(\theta, a_h) g(\theta|x) d\theta} \min[\mu_{L,h}(y), \mu_{U,h}(z)] \tag{13}$$

Finally, let us consider the most general case when we deal with fuzzy statistical data, fuzzy prior information, fuzzy loss function, and fuzzy statistical hypotheses. In this case the fuzzy risks $\tilde{\mathbf{R}}_h, h=0,1$ are given as integrals over fuzzy sets from fuzzy functions, i.e.

$$\tilde{\mathbf{R}}_h = \int_{\tilde{\Theta}_h} \tilde{u}(\theta, a_h) \tilde{g}(\theta | \tilde{x}) d\theta. \tag{14}$$

Such a fuzzy integral is practically impossible to calculate. However, Hryniewicz (2002) proposed its reasonable approximation form above using the following formulae

$$\mathbf{R}_h^{\alpha,L} = \int_{\Theta_{L,h}^{\alpha,L}}^{\Theta_{U,h}^{\alpha,L}} L_{\alpha}^L(\theta, a_h) g_{\alpha}^L(\theta | \mathbf{x}) d\theta, \tag{15}$$

$$\mathbf{R}_h^{\alpha,U} = \int_{\Theta_{L,h}^{\alpha,U}}^{\Theta_{U,h}^{\alpha,U}} L_{\alpha}^U(\theta, a_h) g_{\alpha}^U(\theta | \mathbf{x}) d\theta. \tag{16}$$

When only two hypotheses are considered we have to deal with a relatively simple problem of comparing two fuzzy numbers $\tilde{\mathbf{R}}_0$ and $\tilde{\mathbf{R}}_1$. For doing such comparison Hryniewicz (2002) proposed to use a possibilistic approach introduced by Dubois and Prade (1983). To compare these fuzzy risks he proposed to use the concept of the Necessity of Strict Dominance Index (*NSD*) and Possibility of Dominance Index (*PD*). The *PD* index is defined for two fuzzy sets \tilde{A} and \tilde{B} as

$$PD = Poss(\tilde{A} \succ \tilde{B}) = \sup_{x,y:x \geq y} \min\{\mu_{\tilde{A}}(x), \mu_{\tilde{B}}(y)\}, \tag{17}$$

where $\mu_{\tilde{A}}(x)$ and $\mu_{\tilde{B}}(y)$ are the membership functions of \tilde{A} and \tilde{B} , respectively. *PD* is the measure for possibility that the set \tilde{A} is not dominated by the set \tilde{B} . The *NSD* index is defined as

$$NSD = Ness(\tilde{A} > \tilde{B}) = 1 - \sup_{x,y:x \leq y} \min\{\mu_{\tilde{A}}(x), \mu_{\tilde{B}}(y)\}. \tag{18}$$

NSD represents necessity that the set \tilde{A} dominates the set \tilde{B} . If *NSD*>0 there exists a strong indication of the acceptance of one hypothesis (say \tilde{A}) over another one (say \tilde{B}).

In the next section we show a simple example of this methodology for the case of the lifetime data described by the Weibull distribution.

TESTING HYPOTHESES FOR THE WEIBULL DISTRIBUTION USING IMPRECISE INFORMATION

Let X be the random variable describing lifetime data. The Weibull distribution, defined by the probability density function (pdf)

$$f(x|\gamma, s) = \frac{sx^{s-1}}{\gamma \exp(x^s/\gamma)}, x > 0, s > 0, \gamma > 0 \quad (19)$$

is frequently used for modeling such data. The parameter s determines the shape of the pdf function, and the parameter γ determines the spread of variability of X . Because of its great applicability in the analysis of reliability (or survival, in a more general setting) classical (non-Bayesian) methods of statistical analysis for the Weibull distribution have been developed by many authors. For more detailed information the reader can be directed to many textbooks, such as e.g. the book by Lawless (1982). The number of papers devoted to the problem of the Bayesian analysis of the lifetime data described by the Weibull distribution is not so high because of difficulties with finding analytical solutions. Comprehensive bibliography of the problem together can be found in the recent paper by Fernández (2009). The reason of these problems stems from the fact that the bivariate conjugate prior distribution for both parameters of the Weibull distribution does not exist. Therefore, indirect methods, such as the method proposed by Kaminskiy and Krivtsov (2005), have to be used.

The problem of the statistical analysis of data described by the Weibull distribution becomes much easier if the value of the shape parameter is s known. In such case the random variable $Y = X^s$ is distributed exponentially with the scale parameter equal to γ . Statistical analysis of lifetime data described by the exponential distribution is well developed, both in classical (non-Bayesian) and Bayesian sense. For example, in the case of Bayesian approach there exists the conjugate prior probability distribution for the scale parameter γ . This is the inverted gamma distribution defined by the following pdf function

$$g(\gamma) = \frac{a^b \exp^{-a/\gamma}}{\Gamma(b)\gamma^{b+1}}, \gamma > 0, a > 0, b > 0 \quad (20)$$

Note, that the prior distribution for the inverse of the scale distribution $\lambda = 1/\gamma$ is the well known gamma distribution. Moreover, in case of the exponential distribution there exists sufficient statistic that summarizes available statistical data. For example in case of type-II censoring this statistic is given by $(w(y), r)$, where $w(y) = \sum_{i=1}^r y_{(i)} + (n-r)y_{(r)}$, and $y_{(1)} \leq y_{(2)} \leq \dots \leq y_{(r)}$. The posterior distribution of γ is also the inverted gamma distribution with parameters $a' = a + w(y)$ and $b' = b + r$

Now let's consider the case that we have only *partial knowledge* about the value of the shape parameter s . Formal description of partial knowledge is still the subject of controversies. Some researchers claim that classical probabilities are sufficient in this case. However, many other researchers present counterexamples showing that some other methods, like imprecise probabilities, Dempster-Shafer

belief functions, p-boxes, possibility distributions etc., should be used in order to capture the essence of partial knowledge. In this paper we assume that our knowledge about the value of s is described by a *possibility distribution*, which from a formal point of view is equivalent to the *membership function* $\mu(s)$ of a fuzzy number \tilde{s} . Thus, we assume that we analyze a *fuzzy random variable* defined as

$$\tilde{Y} = X^{\tilde{s}}, \tag{21}$$

and the sample information is presented as the *fuzzy number*

$$\tilde{w}(y) = \sum_{i=1}^r \tilde{y}_{(i)} + (n-r)\tilde{y}_{(r)}. \tag{22}$$

Therefore, all results of statistical analyses, either Bayesian or non-Bayesian, will be presented using terms related to fuzzy sets.

Let us consider the problem of the Bayesian estimation of the parameter γ in case of type-II censored lifetime data. As natural Bayesian estimators can be considered such statistics like the mode of the posterior distribution or its median. In case of the known s it can be done by solving nonlinear equations (see Fernández (2009)). However, when we have fuzzy data in the form of $\tilde{w}(y)$ this task is rather difficult to do. Much simpler result can be obtained when we use a decision-theoretic approach. When the losses due to erroneous estimation are proportional to $(\gamma_B - \gamma)^2$ then the optimal estimator that minimizes the Bayesian risk is equal to the expected value in the posterior distribution, and in the case of fuzzy data is given by a very simple formula

$$\tilde{\gamma}_B = \frac{a + \tilde{w}(y)}{b + r + 1}. \tag{23}$$

The membership function of $\tilde{\gamma}_B$ is similar to the membership function of $\tilde{w}(y)$, except for a linear transformation of the x -axis.

Acquisition of the parameters of the prior distribution is the most important practical problem of the Bayesian approach to statistics. Usually, an expert proposes his/hers evaluations of the moments of the prior distribution, and these values are set equal to their theoretical counterparts, forming equations the parameters of the prior distribution are calculated from. Implementation of this practice in the considered case is rather questionable, as the parameter γ does not have any direct interpretation. Therefore such equations should be constructed using information that is directly related to observed lifetimes or other reliability indices.

Let h_t be the value of the reliability function at time t . Fernández (2009) shows that the expected value of the prior distribution of this index is given by $E = E[h_t] = sbt^{s-1}/a$, and its variance is given by $V = V[h_t] = s^2bt^{2s-2}/a^2$. These two equations can be used for the calculation of a and b . However, in the considered case of the fuzzy information about the value of s these equations have fuzzy solutions.

$$\tilde{a} = \left(\frac{V}{E\tilde{s}t^{\tilde{s}-1}} \right)^{1/2} \quad \text{and} \quad \tilde{b} = \frac{E}{\tilde{s}t^{\tilde{s}-1}} \tag{24}$$

Let (s_L^α, s_U^α) be the α -cut of the fuzzy variable \tilde{s} that represents imprecise information about the value of the shape parameter s . The α -cut of the Bayesian estimator of the parameter γ can be calculated as follows

$$\gamma_{B,L}^\alpha = \inf_{s \in (s_L^\alpha, s_U^\alpha)} \frac{\left(\frac{V}{E\tilde{s}t^{\tilde{s}-1}} \right)^{1/2} + \sum_{i=1}^r x_{(i)}^s + (n-r)x_{(i)}^s}{\frac{E}{st^{\tilde{s}-1} + r + 1}}$$

$$\gamma_{B,U}^\alpha = \sup_{s \in (s_L^\alpha, s_U^\alpha)} \frac{\left(\frac{V}{Est^{s-1}}\right)^{1/2} + \sum_{i=1}^r x_{(i)}^s + (n-r)x_{(i)}^s}{\frac{E}{st^{s-1}} + r + 1}$$

In a similar, but more complicated, way one can calculate fuzzy risks related to statistical hypotheses about γ and its different functions such as reliability function or hazard rate.

REFERENCES

- De Groot M.H (1970). "Optimal Statistical Decisions." McGraw Hill, New York.
- Dubois D., Prade H. (1980). "Fuzzy Sets and Systems. Theory and Applications." Academic Press, New York.
- Dubois D., Prade H. (1983). "Ranking fuzzy numbers in the setting of possibility theory." *Information Sciences*, 30, 184-244.
- Fernández A.J. (2009). "Weibull inference using trimmed samples and prior information." *Statistical Papers*, 50, 119-136.
- Frühwirth-Schnatter S. (1993). "Fuzzy Bayesian inference." *Fuzzy Sets and Systems*, 60, 41-58.
- Gil M., Hryniewicz O. (2009). "Statistics with Imprecise Data." In: Robert A. Meyers (Ed.): *Encyclopedia of Complexity and Systems Science*. Springer, Heidelberg, 8679-8690.
- Grzegorzewski P., Hryniewicz O. (2001). "Soft Methods in Hypotheses Testing." In: D. Ruan, J. Kacprzyk and M. Fedrizzi (Eds.), *Soft computing for risk evaluation and management*. Physica Verlag, Heidelberg, 55-72.
- Hryniewicz O. (2002). "Possibilistic approach to Bayes statistical decisions." In: Grzegorzewski P., Hryniewicz O., Gil M.A. (Eds.): *Soft methods in probability. Statistics and data analysis*. Physica-Verlag, Heidelberg, 207-218.
- Hryniewicz O. (2007). "Fuzzy sets in the evaluation of reliability." In: Levitin G. (Ed.): *Computational intelligence in reliability engineering*. Springer-Verlag, Berlin, 363-386.
- Kaminskiy M.P., Krivtsov V.V. (2005). "A Simple procedure for Bayesian Estimation of the Weibull Distribution." *IEEE TR*, 54, 612-616.
- Kruse R., Meyer K.D. (1987). "Statistics with Vague Data." Riedel, Dordrecht.
- Lawless J.F. (1982). "Statistical models and methods for lifetime data." J.Wiley, New York (2nd edition in 2003).
- Raiffa H., Schleifer R. (1961). "Applied Statistical Decision Theory." The M.I.T. Press, Cambridge.

Statistical inference under two structurally different approaches to interval data

Scott Ferson and Jack Siegrist

Applied Biomathematics, 100 North Country Road, Setauket, New York 11733-1300;
phone: 1-631-751-4350; fax: -3425; email: scott@ramas.com

ABSTRACT

Two broadly different approaches have been proposed for handling data that contain non-negligible interval uncertainty from censoring, plus-minus digital readouts, and other sources of measurement imprecision or incertitude. Modeling interval data with uniform distributions over their ranges allows relatively straightforward calculation of sample statistics, but does not guarantee these estimates will approach the parameters of the actual distribution, even for asymptotically many random samples. In contrast, modeling interval data as bounds on possible values yields corresponding bounds on sample statistics that are easier to interpret although often more difficult to calculate. We illustrate the approaches in estimating descriptive statistics, empirical distribution functions, and best-fit distributions. Statistical inference under the bounding approach generally yields a class of decisions under the theory of imprecise probabilities. In contrast, the uniforms approach will yield a unique decision (up to indifference), although this decision cannot be said to be implied by the data alone because it depends on ancillary assumptions that may not be tenable.

INTRODUCTION

Epistemic uncertainty in sample data that has the form of intervals about imprecisely measured values can arise from many sources, including intermittent observations or coarse measurements, the plus-minus intervals implied by digital readouts, non-detects and data censoring of various kinds, missing values, post-hoc data blurring for privacy or security reasons, and data binning to condense data when capacity for information storage or transmission bandwidth is limited.

This kind of uncertainty is often neglected in statistical analyses, which is probably reasonable when variance among the samples is relatively large compared to the imprecision of the individual measurements. It is perhaps also reasonable when the uncertainty due to measurement imprecision is swamped by other sources of uncertainty such as sampling uncertainty because of small sample sizes. However, there can be cases in which measurement incertitude should not be neglected. There is a large statistical literature on handling data with interval uncertainty, which are sometimes called “censored” data (Helsel 1990; 2005; Meeker and Escobar 1995). There is also a growing literature on “symbolic” data (Bertrand and Groupil 2000; Bock and Diday 2000), of which interval data are a special case. In this literature,

different values within each data interval are presumed to be equally likely and therefore modeled as uniform distributions, in an extension of Laplace's principle of insufficient reason. We consider all of these approaches to be with the current tradition of statistical analysis.

An alternative approach, outside of the current tradition, arises from the theory of imprecise probabilities (Walley 1991). This approach models each interval as a *set* of possible values rather than a probability distribution of any shape (Manski 2003; Ferson et al. 2007). As a result it creates imprecisely specified probability distributions, which can be characterized by p-boxes (Ferson et al. 2003) which are interval-like bounds about a cumulative distribution function. A p-box may be identified with a set or class of probability distributions in the same way that an interval can be identified with a set of real numbers. We call this approach to handling incertitude in data the interval statistics approach.

DESCRIPTIVE STATISTICS FOR INTERVAL DATA

The differences between the two approaches can be illustrated by considering the following two measured data sets consisting of intervals:

Skinny	Puffy
[3.99, 4.99]	[5.5, 8.4]
[8.11, 8.41]	[3.8, 5.7]
[1.34, 1.49]	[1.2, 3.5]
[6.85, 7.47]	[0.0, 3.5]
[5.02, 5.57]	[4.5, 10.7]
[0.55, 1.47]	[0.0, 3.1]
	[2.0, 5.6]
	[4.4, 4.8]
	[7.9, 8.7]

The data set Skinny has 6 interval values, but they are fairly narrow, representing good measurement precision. The data set Puffy has fifty percent larger sample size of 9 interval values, but they are generally wider, representing poorer precision. Skinny and Puffy are graphically displayed in Figure 1, in which the vertical displacements are for the ease of visualization and don't mean anything. In this and other figures in this paper, Skinny is depicted in the left graph, and Puffy on the right graph.

The interval statistics approach to characterizing data sets consisting of intervals assumes that the measurands' true values are somewhere in the reported intervals (Manski 2003; Ferson et al. 2007). This approach can bound the empirical distribution functions for the two data sets with the p-boxes depicted in Figure 2, which were computed by cumulating the left and right endpoints of the intervals in the respective data sets. These p-boxes clearly enclose the actual empirical distribution functions wherever the actual values are within the intervals. They capture both the variability of the sample data as well as their imprecision.

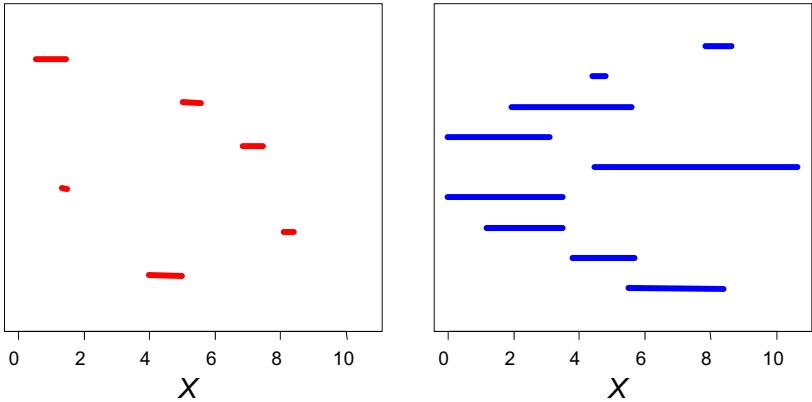


Figure 1. Skinny data set (left) and Puffy data set (right).

The interval statistics approach can also bound the moments for the data sets. For example, the mean of Skinny is the interval $[4.31, 4.90]$. The left endpoint of this interval is the mean of the left endpoints of the underlying 6 intervals, and the right endpoint is similarly the mean of the right endpoints. The mean of Puffy is the less precise interval $[3.25, 6.00]$. The range of possible sample variances for Skinny is $[7.40, 10.22]$. The configuration of values inside each of the six intervals of Skinny that leads to the smallest possible variance is $\{4.586, 8.11, 1.49, 6.85, 5.02, 1.47\}$. The configuration that leads to the largest possible variance is $\{3.99, 8.41, 1.34, 7.47, 5.57, 0.55\}$. The range of possible sample variances for Puffy is $[2.04, 16.29]$, which is many times wider than that for Skinny. Ferson et al. (2008) reviewed algorithms to compute a variety of univariate descriptive and inferential statistics for interval data sets. Several of these statistics can be computationally challenging for large data sets, although efficient algorithms are known for several special cases depending on the nature of the interval data.

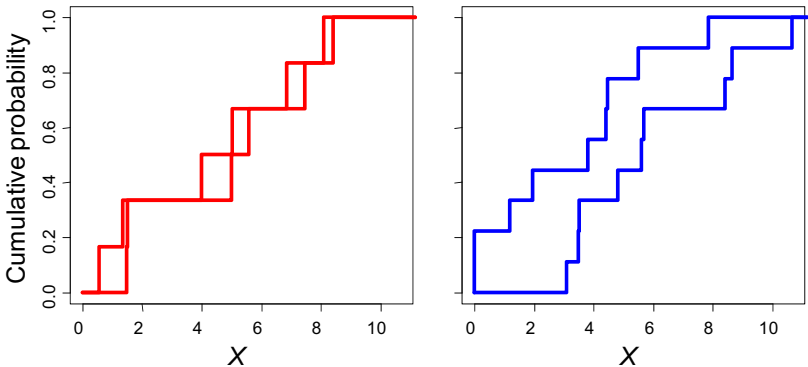


Figure 2. Bounds on empirical distribution functions for the two datasets.

Several analysts have suggested an alternative treatment for interval data based on modeling each interval as a *uniform distribution* (e.g., Bertrand and Groupil 2000; Billard and Diday 2000; Billard and Diday n.d.; Bock and Diday 2000; cf. Gioia and Lauro 2005). Bertrand and Groupil (2000) call this the “equidistribution hypothesis” and it represents the idea that each possible value in an interval is equally likely. Billard and Diday (n.d.) survey some of the descriptive statistics that can be computed from interval data under this model.

An empirical distribution under the equidistribution hypothesis would be formed as an equal-weight mixture of the uniform distributions representing the respective intervals. Figure 3 displays such empirical distributions for Skinny and Puffy, which are superimposed over the p-boxes (gray) from using the interval statistics approach previously depicted in Figure 2. As can be seen in the graphs, this approach is a way to split the difference, as it were, in estimating the empirical distribution. They capture the variability of the sample data, but seem to understate their imprecision, at least as compared to the p-box summaries. Because this approach yields ordinary, precise distributions, their summary statistics are fairly easy to compute.

For instance, under the equidistribution hypothesis of interval uncertainty, the estimated means are 4.605 for Skinny and 4.63 for Puffy. These means are simply the averages of the midpoints of the respective intervals. The corresponding estimates of variances are 7.283 for Skinny and 6.55 for Puffy, which are the variances of the distributions formed from mixtures of uniform distributions having the same supports as the respective intervals. Note that these moment estimates are very similar between the two data sets, despite the considerable disparity between the data sets.

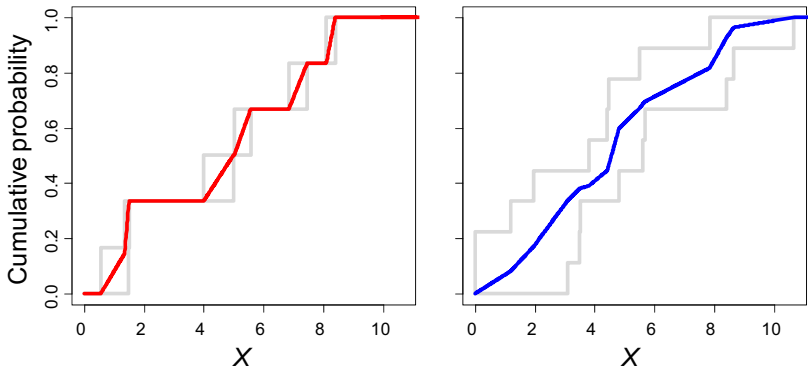


Figure 3. Distribution functions under the ‘uniforms’ model.

FITTING DISTRIBUTIONS WITH SHAPE ASSUMPTIONS TO DATA

An empirical distribution summarizes the data themselves and makes no assumption about the distribution shape or family. In many problems, however,

analysts desire to make such distributional assumptions. The interval statistics approach to fitting distributions to data via the maximum likelihood criterion creates a *class* of maximum likelihood solutions. Every one of these solves a maximum likelihood problem for some configuration of possible measurement values within the respective intervals.

As an example, consider fitting exponential distributions to the two data sets. The likelihood function for an interval datum $\mathbf{x} = [\underline{x}, \bar{x}]$ is $L(\lambda) = f(\mathbf{x}; \lambda)$ where f denotes the probability density function, which is $\lambda \exp(-\lambda x)$ for an exponential distribution with mean $1/\lambda$. Assuming samples are independent, these likelihoods for each datum are multiplied to get the likelihoods for the overall data set. The set of parameter values λ that maximize any of these likelihood functions form an interval, so the result is a p-box or class of exponential distributions, each of which are best-fit to some possible configuration of measurement values. Figure 4 shows exponential p-boxes fitted to the data via maximum likelihood, superimposed over the respective bounds on the empirical distribution functions.

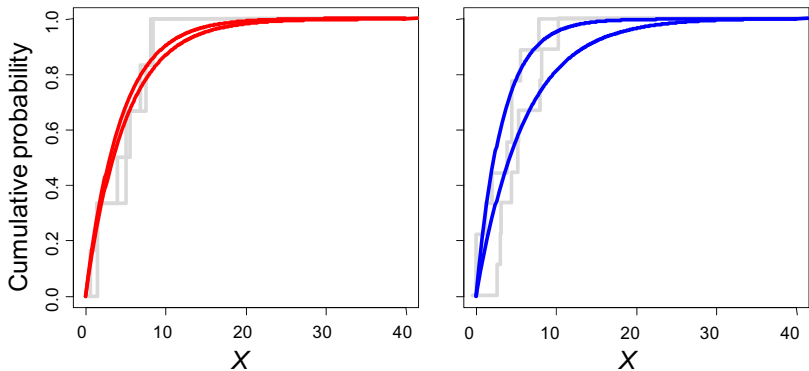


Figure 4. P-boxes fitted by maximum likelihood.

In contrast, the traditional approach (Meeker and Escobar 1995) to fitting distributions by maximum likelihood to data sets with interval censoring computes the likelihood for an interval datum $\mathbf{x} = [\underline{x}, \bar{x}]$ as

$$\begin{aligned} L(\lambda) &= \Pr(\underline{x} \leq X \leq \bar{x}) \\ &= \Pr(\bar{x} \leq X) - \Pr(\underline{x} \leq X) \\ &= F(\bar{x}; \lambda) - F(\underline{x}; \lambda) \end{aligned}$$

where F denotes the cumulative distribution function, which is $F(x; \lambda) = 1 - \exp(-\lambda x)$ for an exponential distribution with mean $1/\lambda$. Assuming samples are independent, these likelihoods for each datum are multiplied to get the likelihood for the overall data set. The best fitting parameter λ is found by maximizing this function for λ . Figure 5 shows exponential distributions fitted in this traditional way, superimposed on the p-boxes (gray) previously depicted in Figure 4.

Are the results from the traditional method reasonable? It picks a single precise exponential to fit interval data, no matter how wide those intervals might be.

This seems counterintuitive. In this example, as was true for the moments computed under the equidistribution hypothesis, the best-fit distributions for the two data sets are very similar. In fact, if they were superimposed on a single graph, it would be almost impossible to distinguish them visually. This is decidedly different from the best-fit p-boxes in Figure 4 whose differences embody the disparity between the two data sets. There is no guarantee that an answer computed by the traditional method approaches the true distribution *even if asymptotically many data are collected*. Such convergence depends on other implicit assumptions. For instance, it depends on the measurement errors being independent among samples (which is different from the assumption that samples are independent of each other).

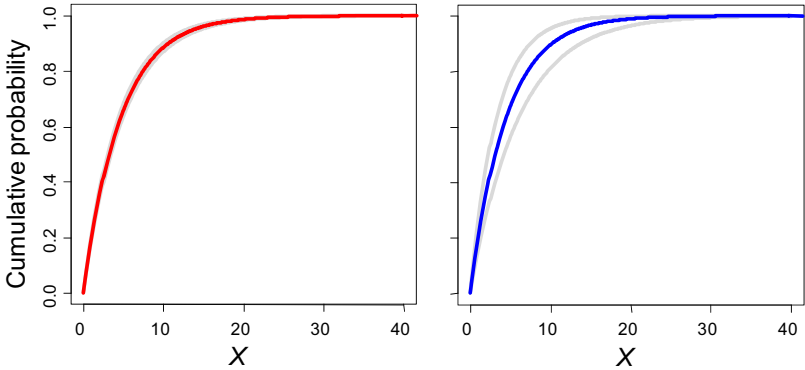


Figure 5. Precise distributions fitted by traditional maximum likelihood.

One might look to confidence procedures to express the uncertainty about the best-fit distribution, but it turns out that confidence procedures cannot recapture the imprecision once it has been lost by the traditional method. Confidence or credibility intervals around λ can be directly translated to confidence or credibility bands around the exponential distribution. Confidence bands computed with the traditional method are actually substantially *smaller* for Puffy than they are for Skinny. Of course, this outcome is due to the fact that the confidence procedure is sensitive to sampling uncertainty and neglects the imprecision of the individual measurements. It turns out that analogous confidence bands computed about the best-fit p-boxes happen to be fairly similar between the two data sets, which implies that, in this numerical example, the imprecision in Puffy has roughly the same effect on overall uncertainty as the smaller sample size in Skinny.

CONCLUSIONS

Data sets whose values contain interval uncertainty arise from various kinds of censoring, intermittent measurements, missing data, plus-or-minus digital readouts, data binning, and intentional data blurring for privacy and security reasons. Two broadly different approaches to such data have been proposed for situations in which

the uncertainty about the values cannot reasonably be neglected. The differences between the two approaches have been illustrated in the paper with numerical examples including the calculation of descriptive statistics, empirical distribution functions, and distributions with known shape fitted by maximum likelihood.

The first approach, which can trace its roots to Laplace's principle of insufficient reason, models the interval uncertainty of each datum with a uniform distribution over its range. It allows relatively straightforward calculation of sample statistics. However, it does not necessarily have good statistical properties. In particular, it cannot guarantee that estimates computed from such models will approach the parameters of the actual distribution from which the data were drawn even when there are asymptotically many random samples. This is related to the fact that the resulting single distribution conflates the imprecision and variability of sample data.

The second approach is completely different from the first and models the interval uncertainty of each datum solely in terms of the bounds on the possible value, which corresponds not to any single distribution but rather to a class of distributions all having support over the interval's range. This approach is motivated under the theory of imprecise probabilities (Walley 1991) so it has a much more recent heritage. Although calculation of even basic descriptive sample statistics such as the variance is generally computationally difficult under this approach, it nevertheless has several interpretational advantages. Its results are expressed as intervals or p-boxes (bounds on cumulative distributions) that manifest measurement incertitude as well as sampling uncertainty in ways that point estimates and precise distributions, or even confidence limits thereon, cannot.

Under the interval statistics approach, calculations usually result in a class of values or distributions, and, likewise, statistical inference under this approach generally yields a class of decisions. In contrast, the traditional approaches will yield a unique decision (up to indifference), although this decision *cannot be said to be implied* by the data alone because it depends on ancillary assumptions that may not be tenable for the analyst. However, if those assumptions such as the equidistribution hypothesis or ancillary independence assumptions in censoring are correct, then the traditional approach can be much more powerful and determinative than the interval statistics approach. The choice between the two approaches will perhaps always be a modeling decision beyond empirical justification because the data that would distinguish between the two approaches is exactly the data that is absent (Manski 2003).

ACKNOWLEDGMENTS

We thank Bill Huber from Quantitative Decisions, Floyd Spencer from Sandia National Laboratories, Lynne Billard from the University of Georgia, Vladik Kreinovick from University of Texas at El Paso, and Lev Ginzburg of Stony Brook University for engaging reviews and discussions. This work was supported by the National Library of Medicine, a component of the National Institutes of Health, under Award Number RC3LM010794, and by Sandia National Laboratories under Contract Number 19094 in the Epistemic Uncertainty project directed by William Oberkampf.

The content is solely the responsibility of the authors and does not necessarily represent the official views of the National Library of Medicine, the National Institutes of Health, or Sandia National Laboratories.

REFERENCES

- Bertrand, P., and Groupil, F. (2000). Descriptive statistics for symbolic data. Pages 107-124 in *Analysis of Symbolic Data*, H.-H. Bock and E. Diday (eds.), Springer, Berlin.
- Billard, L., and Diday, E. (2000). Regression analysis for interval-valued data. Pages 369-374 in *Data Analysis, Classification and Related Methods*, H.A.L. Kiers, J.-P. Rassoon, P.J.F. Groenen and M. Schader (eds.), Springer, Berlin.
<http://www.stat.uga.edu/faculty/LYNNE/ifcs2.ps>
- Billard, L., and Diday, E. (n.d.). Symbolic data analysis: definitions and examples. [manuscript]. http://www.stat.uga.edu/faculty/LYNNE/tr_symbolic.pdf
- Bock, H.-H., and Diday, E. (2000). *Analysis of Symbolic Data*. Springer, Berlin.
- Ferson, S., Kreinovich, V., Ginzburg, L., Myers, D.S., and Sentz, K. (2003). *Constructing Probability Boxes and Dempster-Shafer Structures*. SAND2002-4015. Sandia National Laboratories, Albuquerque, NM.
<http://www.ramas.com/unabridged.zip>.
- Ferson, S., Kreinovich, V., Hajagos, J., Oberkampf, W., and Ginzburg, L. (2007). *Experimental Uncertainty Estimation and Statistics for Data Having Interval Uncertainty*. SAND2007-0939, Sandia National Laboratories, Albuquerque, NM.
<http://prod.sandia.gov/techlib/access-control.cgi/2007/070939.pdf>
- Gioia, F., and Lauro, C.N. (2005). Basic statistical methods for interval data. *Statistica Applicata [Italian Journal of Applied Statistics]* 17(1): 75-104.
- Helsel, D.R. (1990). Less than obvious: Statistical treatment of data below the detection limit. *Environmental Science and Technology* 24: 1766-1774.
- Helsel, D.R. (2005). *Nondetects and Data Analysis: Statistics for Censored Environmental Data*. Wiley, New York.
- Manski, C.F. (2003). *Partial Identification of Probability Distributions*, Springer Series in Statistics, Springer, New York.
- Meeker, W.Q., and Escobar, L.A. (1995). *Statistical Methods for Reliability Data*. John Wiley and Sons, New York.
- Walley, P. (1991). *Statistical Reasoning with Imprecise Probabilities*. Chapman & Hall, London.

Independence in Generalized Interval Probability

Yan Wang

Woodruff School of Mechanical Engineering, Georgia Institute of Technology, Atlanta, GA 30332-0405; PH (404)894-4714; FAX (404)894-9342; email: yan.wang@me.gatech.edu

ABSTRACT

Recently we proposed a new form of imprecise probability based on the generalized interval, where the probabilistic calculus structure resembles the traditional one in the precise probability because of the Kaucher arithmetic. In this paper, we study the independence properties of the generalized interval probability. It resembles the stochastic independence with proper and improper intervals and supports logic interpretation. The graphoid properties of the independence are investigated.

INTRODUCTION

Probability theory provides the common ground to quantify uncertainty. However, it has limitations in representing epistemic uncertainty that is due to lack of knowledge. It does not differentiate the total ignorance from other probability distributions, which leads to the Bertrand-style paradoxes such as the Van Fraassen's cube factory (van Fraassen 1989). Probability theory with precise measure also has limitation in capturing indeterminacy and inconsistency. When beliefs from different people are inconsistent, a range of opinions or estimations cannot be represented adequately without assuming some consensus of precise values on the distribution of opinions. Therefore imprecise probabilities have been proposed to quantify aleatory and epistemic uncertainty simultaneously. Instead of a precise value of the probability $P(E) = p$ associated with an event E , a pair of lower and upper probabilities $P(E) = [\underline{p}, \bar{p}]$ are used to include a set of probabilities and quantify epistemic uncertainty. The range of the interval $[\underline{p}, \bar{p}]$ captures the epistemic uncertainty component and indeterminacy. $P = [0, 1]$ accurately represents the total ignorance. When $\underline{p} = \bar{p}$, the degenerated interval probability becomes a precise one. In a general sense, imprecise probability is a generalization of precise probability.

Many representations of imprecise probabilities have been developed. For example, the Dempster-Shafer evidence theory (Dempster 1967; Shafer 1990) characterizes evidence with discrete probability masses associated with a power set of values, where Belief-Plausibility pairs are used to measure uncertainties. The behavioral imprecise probability theory (Walley 1991) models uncertainties with the *lower prevision* (supremum acceptable buying price) and the *upper prevision* (infimum acceptable selling price) following the notations of de Finetti's subjective probability theory. The possibility theory (Dubois and Prade 1988) represents

uncertainties with Necessity-Possibility pairs. Probability bound analysis (Ferson et al. 2003) captures uncertain information with pairs of lower and upper distribution functions. F-probability (Weichselberger 2000) represents interval probability as a set of probabilities which maintain the Kolmogorov properties. A random set (Malchanov 2005) is a multi-valued mapping from the probability space to the value space. Fuzzy probability (Möller and Beer 2004) considers probability distributions with fuzzy parameters. A cloud (Neumaier 2004) is a combination of fuzzy sets, intervals, and probability distributions.

Recently we proposed a new form of imprecise probability based on the generalized interval (Wang 2008; 2010), where the probabilistic calculus structure is simplified based on the Kaucher arithmetic (Kaucher 1980). The generalized interval is an extension of the classical set-based interval with enhanced algebraic and semantic properties. Proper and improper interval probabilities are used. In this paper, we study the independence properties of the generalized interval probability.

The concept of independence is essential for the probability theory to decompose a complex problem into simpler and manageable components. Similarly, it is fundamental for imprecise probability theories. Various definitions of independence have been developed, such as epistemic irrelevance and independence (Walley 1991), conformational irrelevance (Levi 1980), mutual independence (Weichselberger 2000), and interval independence (Kuznetsov 1995).

In the remainder of the paper, we first give a brief review of generalized interval. Then the generalized interval probability is introduced. The conditional probability and independence in the generalized interval probability are defined and discussed.

GENERALIZED INTERVAL

In the interval arithmetic, it is guaranteed that the output intervals calculated from the arithmetic include all possible combinations of real values within the respective input intervals. That is, if $[x, \bar{x}]$ and $[y, \bar{y}]$ are two real intervals (i.e., $x, \bar{x}, y, \bar{y} \in \mathbb{R}$) and let $\circ \in \{+, -, \times, /\}$, then we have $\forall x \in [x, \bar{x}], \forall y \in [y, \bar{y}], \exists z \in [x, \bar{x}] \circ [y, \bar{y}], x \circ y = z$. For example, $[1, 3] + [2, 4] = [3, 7]$ guarantees that $\forall x \in [1, 3], \forall y \in [2, 4], \exists z \in [3, 7], x + y = z$. Similarly, $[3, 7] - [1, 3] = [0, 6]$ guarantees that $\forall x \in [3, 7], \forall y \in [1, 3], \exists z \in [0, 6], x - y = z$. This is an important property that ensures the completeness of range estimations. When input variables are not independent, the output results will over-estimate the actual ranges. This only affects the soundness of estimations, not completeness. Some special techniques also have been developed to avoid over-estimations based on monotonicity properties of functions.

Generalized interval (Gardeñes et al. 2001; Dimitrova et al. 1994) is an extension of the set-based classical interval (Moore 1966) with better algebraic and semantic properties based on the Kaucher arithmetic (Kaucher 1980). A generalized interval $x := [x, \bar{x}] (x, \bar{x} \in \mathbb{R})$ is not constrained by $x \leq \bar{x}$ any more. Therefore, $[4, 2]$ is also a valid interval and called *improper*, while the traditional interval is called *proper*. Based on the Theorems of Interpretability (Gardeñes et al. 2001), generalized interval provides more semantic power to help verify completeness and soundness of range estimations by logic interpretations.

The four examples in Table 1 illustrate the interpretations for operator “+”, where the range estimation $[\underline{z}, \bar{z}] = [4, 7]$ in the 1st row is *complete* and the estimation $[\underline{z}, \bar{z}] = [7, 4]$ in the 4th row is *sound*. $-, \times, /$ have the similar semantic properties.

Table 1. Illustrations of the semantic extension of generalized interval.

Algebraic Relation: $[\underline{x}, \bar{x}] + [\underline{y}, \bar{y}] = [\underline{z}, \bar{z}]$	Corresponding Logic Interpretation	Quantifier of $[\underline{z}, \bar{z}]$	Range Estimation of $[\underline{z}, \bar{z}]$
$[2, 3] + [2, 4] = [4, 7]$	$(\forall x \in [2, 3])(\forall y \in [2, 4])(\exists z \in [4, 7])(x + y = z)$	\exists	$[4, 7]$ <i>complete</i>
$[2, 3] + [4, 2] = [6, 5]$	$(\forall x \in [2, 3])(\forall z \in [5, 6])(\exists y \in [2, 4])(x + y = z)$	\forall	$[5, 6]$ <i>sound</i>
$[3, 2] + [2, 4] = [5, 6]$	$(\forall y \in [2, 4])(\exists x \in [2, 3])(\exists z \in [5, 6])(x + y = z)$	\exists	$[5, 6]$ <i>complete</i>
$[3, 2] + [4, 2] = [7, 4]$	$(\forall z \in [4, 7])(\exists x \in [2, 3])(\exists y \in [2, 4])(x + y = z)$	\forall	$[4, 7]$ <i>sound</i>

Compared to the *semi-group* formed by the classical set-based intervals, generalized intervals form a *group*. Therefore, arithmetic operations of generalized intervals are simpler. The set of generalized intervals is denoted by $\mathbb{KR} = \{[\underline{x}, \bar{x}] \mid \underline{x}, \bar{x} \in \mathbb{R}\}$. The set of proper intervals is $\mathbb{IR} = \{[\underline{x}, \bar{x}] \mid \underline{x} \leq \bar{x}\}$, and the set of improper interval is $\overline{\mathbb{IR}} = \{[\underline{x}, \bar{x}] \mid \underline{x} \geq \bar{x}\}$. The relationship between proper and improper intervals is established with the operator *dual* as $\text{dual}[\underline{x}, \bar{x}] := [\bar{x}, \underline{x}]$.

The *less than or equal to* partial order relationship between two generalized intervals is defined as

$$[\underline{x}, \bar{x}] \leq [\underline{y}, \bar{y}] \Leftrightarrow \underline{x} \leq \underline{y} \wedge \bar{x} \leq \bar{y} \quad (1)$$

The *inclusion* relationship is defined as

$$[\underline{x}, \bar{x}] \subseteq [\underline{y}, \bar{y}] \Leftrightarrow \underline{y} \leq \underline{x} \wedge \bar{x} \leq \bar{y} \quad (2)$$

With the Kaucher arithmetic, generalized intervals form a lattice structure similar to real arithmetic, which is not available in the classical interval arithmetic. This property significantly simplifies the computational requirement. For instance, in classical interval arithmetic, $[0.2, 0.3] + [0.2, 0.4] = [0.4, 0.7]$. However, $[0.4, 0.7] - [0.2, 0.3] = [0.1, 0.5] \neq [0.2, 0.4]$. Furthermore, $[0.1, 0.2] - [0.1, 0.2] = [-0.1, 0.1] \neq 0$. In the Kaucher arithmetic, if a *dual* is associated with “ $-$ ”, then $[0.4, 0.7] - \text{dual}[0.2, 0.3] = [0.4, 0.7] - [0.3, 0.2] = [0.2, 0.4]$. $[0.1, 0.2] - \text{dual}[0.1, 0.2] = 0$. “ \times ” and “ \div ” are similar.

GENERALIZED INTERVAL PROBABILITY

Definition 1. Given a sample space Ω and a σ -algebra \mathcal{A} of random events over Ω , the generalized interval probability $\mathbf{p} \in \mathbb{KR}$ is defined as $\mathbf{p}: \mathcal{A} \rightarrow [0, 1] \times [0, 1]$ which obeys the axioms of Kolmogorov: (1) $\mathbf{p}(\Omega) = [1, 1]$; (2) $[0, 0] \leq \mathbf{p}(E) \leq [1, 1]$ ($\forall E \in \mathcal{A}$); and (3) for any countable mutually disjoint events $E_i \cap E_j = \emptyset$ ($i \neq j$), $\mathbf{p}(\bigcup_{i=1}^n E_i) = \sum_{i=1}^n \mathbf{p}(E_i)$. Here “ \leq ” is defined as in Eq.(1).

Definition 2 (union). $\mathbf{p}(A) := \sum_{S \subseteq A} (-\text{dual})^{|A|-|S|} \mathbf{p}(S)$ for $A \subseteq \Omega$.

Definition 3 (*logic coherence constraint*). For a mutually disjoint event partition $\bigcup_{i=1}^n E_i = \Omega$, $\sum_{i=1}^n \mathbf{p}(E_i) = 1$.

The logic coherent constraint ensures that the imprecise probabilities are logically coherent with precise probabilities. For instance, given that $\mathbf{p}(\text{down}) = [0.2, 0.3]$, $\mathbf{p}(\text{idle}) = [0.3, 0.5]$, $\mathbf{p}(\text{busy}) = [0.5, 0.2]$ for a system's working status, we can interpret it as $(\forall p_1 \in [0.2, 0.3])(\forall p_2 \in [0.3, 0.5])(\exists p_3 \in [0.2, 0.5])(p_1 + p_2 + p_3 = 1)$.

With semantics, we differentiate *non-focal* events (“*busy*” in this example) from *focal* events (“*down*”, “*idle*”). An event E is focal if the associated semantics for $\mathbf{p}(E)$ is universal. Otherwise, it is a non-focal if the semantics is existential. While the uncertainties associated with focal events are critical to the analyst, those associated non-focal events are not.

CONDITIONAL PROBABILITY AND CONDITIONAL INDEPENDENCE

The concepts of conditional probability and independence are essential for the classical probability theory. With them, we can decompose a complex problem into simpler and manageable components. Similarly, they are critical for imprecise probabilities. However, there is no agreement on how to define them yet.

Different from all other forms of imprecise probabilities, which are based on convex probability sets, our conditional probability is defined directly from the marginal ones.

Definition 4 (*conditional probability*). $\mathbf{p}(E | C) := \mathbf{p}(E \cap C) / \text{dual } \mathbf{p}(C) = [\underline{\mathbf{p}}(E \cap C) / \underline{\mathbf{p}}(C), \bar{\mathbf{p}}(E \cap C) / \bar{\mathbf{p}}(C)]$ for all $E, C \in \mathcal{A}$ and $\mathbf{p}(C) > 0$.

Thanks to the algebraic properties of generalized intervals, this definition can greatly simplify computation in applications. In traditional imprecise probabilities, linear and nonlinear programming procedures are heavily dependent upon to compute convex hulls of probability sets. In our definition, only algebraic computation is necessary.

Definition 5. For $A, B, C \in \mathcal{A}$, A is said to be *conditionally independent* with B on C if and only if $\mathbf{p}(A \cap B | C) = \mathbf{p}(A | C)\mathbf{p}(B | C)$.

Definition 6. For $A, B \in \mathcal{A}$, A is said to be *independent* with B if and only if $\mathbf{p}(A \cap B) = \mathbf{p}(A)\mathbf{p}(B)$.

The independence in Definition 5 is a special case of conditional independence in Definition 4, where C is the complete sample space Ω . In addition to computational simplification, our approach also allows for logic interpretation of conditional independence in Definition 4 is interpreted as

$$(\forall p_1 \in \mathbf{p}'(A|C))(\forall p_2 \in \mathbf{p}'(B|C))(\exists p_3 \in \mathbf{p}'(A \cap B|C))(p_1, p_2 = p_3)$$

This is useful to verify the completeness and soundness of interval bound estimations. The conditional independence in Definition 4 also has a second form, as shown in Theorem 3.1.

Theorem 3.1. For $A, B, C \in \mathcal{A}$, $\mathbf{p}(A \cap B|C) = \mathbf{p}(A|C)\mathbf{p}(B|C) \Leftrightarrow \mathbf{p}(A|B \cap C) = \mathbf{p}(A|C)$.

Proof. $\mathbf{p}(A \cap B|C) = \mathbf{p}(A|C)\mathbf{p}(B|C) \Leftrightarrow \mathbf{p}(A \cap B \cap C) / \text{dual } \mathbf{p}(C) = \mathbf{p}(A|C) \cdot \mathbf{p}(B \cap C) / \text{dual } \mathbf{p}(C) \Leftrightarrow \mathbf{p}(A \cap B \cap C) / \text{dual } \mathbf{p}(B \cap C) = \mathbf{p}(A|C) \Leftrightarrow \mathbf{p}(A|B \cap C) = \mathbf{p}(A|C)$. \square

Corollary 3.2 For $A, B, C, D \in \mathcal{A}$ and $A \cap D = \emptyset$, the conditional independence between A and B given C and between A and D given C infers the independence between $A \cup D$ and B given C .

Proof. $\mathbf{p}(A \cup D|B \cap C) = \mathbf{p}((A \cup D) \cap B \cap C) / \text{dual } \mathbf{p}(B \cap C) = [\mathbf{p}(A \cap B \cap C) + \mathbf{p}(D \cap B \cap C)] / \text{dual } \mathbf{p}(B \cap C) = \mathbf{p}(A \cap B \cap C) / \text{dual } \mathbf{p}(B \cap C) + \mathbf{p}(D \cap B \cap C) / \text{dual } \mathbf{p}(B \cap C) = \mathbf{p}(A|B \cap C) + \mathbf{p}(D|B \cap C) = \mathbf{p}(A|C) + \mathbf{p}(D|C) = \mathbf{p}(A \cup D|C)$. \square

The most intuitive meaning of “independence” is that an independence relationship satisfies several *graphoid* properties. With X, Y, Z, W as sets of disjoint random variables and “ \perp ” denoting independence, the axioms of graphoid are

(A1) Symmetry: $X \perp Y | Z \Rightarrow Y \perp X | Z$

(A2) Decomposition: $X \perp (W, Y) | Z \Rightarrow X \perp Y | Z$

(A3) Weak union: $X \perp (W, Y) | Z \Rightarrow X \perp W | (Y, Z)$

(A4) Contraction: $(X \perp Y | Z) \wedge (X \perp W | (Y, Z)) \Rightarrow X \perp (W, Y) | Z$

(A5) Intersection: $(X \perp W | (Y, Z)) \wedge (X \perp Y | (W, Z)) \Rightarrow X \perp (W, Y) | Z$

The stochastic independence in precise probability is semi-graphoid satisfying symmetry, decomposition, weak union and contraction. When the probability distributions are strictly positive, intersection is also satisfied. Then, it becomes graphoid. Here, we show that conditional independence in generalized interval probability has these graphoid properties.

Corollary 3.3 (Symmetry) For random variables X, Y, Z , $X \perp Y | Z \Rightarrow Y \perp X | Z$.

Proof. $X \perp Y | Z \Rightarrow \mathbf{p}(X = x \cap Y = y | Z = z) = \mathbf{p}(X = x | Z = z)\mathbf{p}(Y = y | Z = z)$ for any values of $x, y, z \Rightarrow \mathbf{p}(Y = y \cap X = x | Z = z) = \mathbf{p}(Y = y | Z = z)\mathbf{p}(X = x | Z = z) \Rightarrow Y \perp X | Z$. \square

Remark. If knowing Y does not tell us more about X , then similarly knowing X does not tell us more about Y .

Corollary 3.4 (Decomposition) For random variables X, Y, Z, W , $X \perp (W, Y) | Z \Rightarrow X \perp Y | Z$.

Proof. $X \perp (W, Y) | Z \Rightarrow \mathbf{p}(X = x \cap W = w \cap Y = y | Z = z) = \mathbf{p}(X = x | Z = z)$ for any values of x, y, z . Since $Y = y$ is equivalent to (W has all possible values, $Y = y$), $\mathbf{p}(X = x \cap Y = y | Z = z) = \mathbf{p}(X = x \cap W = \text{all values} \cap Y = y | Z = z) = \mathbf{p}(X = x | Z = z) \Rightarrow X \perp Y | Z$. \square

Remark. If combined two pieces of information is irrelevant to X , either individual one is also irrelevant to X .

Corollary 3.5 (Composition) For random variables X, Y, Z, W , $(X \perp Y | Z) \wedge (X \perp W | Z) \Rightarrow X \perp (W, Y) | Z$.

Proof. Because $X \perp Y | Z \Rightarrow \mathbf{p}(X = x \cap Y = y | Z = z) = \mathbf{p}(X = x | Z = z)$ and $X \perp W | Z \Rightarrow \mathbf{p}(X = x \cap W = w | Z = z) = \mathbf{p}(X = x | Z = z)$, the combination of the above two gives us $\mathbf{p}(X = x \cap W = w \cap Y = y | Z = z) = \mathbf{p}(X = x | Z = z)$, which is $X \perp (W, Y) | Z$. \square

Remark. The combined two pieces of information that are individually irrelevant to X is also irrelevant to X .

Corollary 3.6 (Contraction) For random variables X, Y, Z, W , $(X \perp Y | Z) \wedge (X \perp W | (Y, Z)) \Rightarrow X \perp (W, Y) | Z$.

Proof. $X \perp W | (Y, Z)$ and $X \perp Y | Z \Rightarrow \mathbf{p}(X | W \cap (Y \cap Z)) = \mathbf{p}(X | Y \cap Z) = \mathbf{p}(X | Z) \Rightarrow X \perp (W, Y) | Z$. \square

Remark. If two pieces of information X and Y are irrelevant with prior knowledge of Z and X is also irrelevant to a third piece of information W after knowing Y , then X is irrelevant to both W and Y before knowing Y .

Corollary 3.7 (Reduction) For random variables X, Y, Z, W , $(X \perp Y | Z) \wedge (X \perp (W, Y) | Z) \Rightarrow X \perp W | (Y, Z)$.

Proof. $X \perp Y | Z$ and $X \perp (W, Y) | Z \Rightarrow \mathbf{p}(X | Y \cap Z) = \mathbf{p}(X | Z) = \mathbf{p}(X | (W \cap Y) \cap Z) = \mathbf{p}(X | W \cap (Y \cap Z)) \Rightarrow X \perp W | (Y, Z)$. \square

Remark. If two pieces of information X and Y are irrelevant with prior knowledge of Z and at the same time X is also irrelevant to both W and Y , then X is irrelevant to the

third piece of information W even after knowing Y .

Corollary 3.8 (Weak union) For random variables X, Y, Z, W , $X \perp (W, Y) | Z \Rightarrow X \perp W | (Y, Z)$

Proof. From the decomposition property in Corollary 3.4, $X \perp (W, Y) | Z \Rightarrow X \perp Y | Z$.

Then from the reduction property in Corollary 3.7, $(X \perp Y | Z) \wedge (X \perp (W, Y) | Z) \Rightarrow (X \perp W | (Y, Z))$. \square

Remark. Gaining more information about irrelevant Y does not affect the irrelevance between X and W .

Corollary 3.9 (Redundancy) For random variables For random variables X and Y , $X \perp Y | X$.

Proof. $\mathbf{p}(Y | X \cap X) = \mathbf{p}(Y | X) \Rightarrow Y \perp X | X \Rightarrow X \perp Y | X$ because of symmetry property in Corollary 3.3. \square

Corollary 3.10 (Intersection) For random variables X, Y, Z, W , $(X \perp W | (Y, Z)) \wedge (X \perp Y | (W, Z)) \Rightarrow X \perp (W, Y) | Z$.

Proof. $X \perp W | (Y, Z) \Rightarrow \mathbf{p}(X | W \cap Y = y \cap Z) = \mathbf{p}(X | Y = y \cap Z)$ for any y . Therefore, $\mathbf{p}(X | W \cap Y = \text{all values} \cap Z) = \mathbf{p}(X | Y = \text{all values} \cap Z)$. That is, $\mathbf{p}(X | W \cap Z) = \mathbf{p}(X | Z)$.

Then $X \perp Y | (W, Z) \Rightarrow \mathbf{p}(X | W \cap Y \cap Z) = \mathbf{p}(X | W \cap Z) = \mathbf{p}(X | Z) \Rightarrow X \perp (W, Y) | Z$ \square

Remark. If combined information W and Y is relevant to X , then at least either W or Y is relevant to X after learning the other.

Compared to other definitions of independence in imprecise probabilities, the independence defined in generalized interval probability has the most of graphoid properties. Walley's *epistemic irrelevance* (Cozman and Walley 2005) does not have symmetry, whereas the *epistemic independence* as well as Kuznetsov's interval independence (Cozman 2008) do not have the contraction property. Among three possibilistic conditional independence (de Campos and Huete 1999), the two with *not modifying information* comparison operation and with *default conditioning* are not symmetric, whereas the one with *not gaining information* satisfies all.

SUMMARY

In this paper, the conditional independence in a new form of imprecise probability, generalized interval probability, is defined and studied. The generalized interval probability is a generalization of traditional precise probability that considers variability and incertitude simultaneously, in which proper and improper intervals capture epistemic uncertainty. With an algebraic structure similar to the precise probability, generalize interval probability has a simpler calculus structure than other forms of imprecise probabilities. It is shown that the definition of independence in generalized interval probability has graphoid properties similar to the stochastic

independence in the precise probability.

REFERENCES

- Cozman F.G. and Walley P. (2005) Graphoid properties of epistemic irrelevance and independence. *Annals of Mathematics & Artificial Intelligence*, **45**(1-2): 173-195
- Cozman F.G. (2008) Sets of probability distributions and independence. *SIPTA Summer School Tutorials, July 2-8, Montpellier, France*
- de Campos L.M. and Huete J.F. (1999) Independence concepts in possibility theory: Part I. *Fuzzy Sets & Systems*, **103**: 127-152
- Dempster A. (1967) Upper and lower probabilities induced by a multi-valued mapping. *Annals of Mathematical Statistics*, **38**(2):325-339
- Dimitrova N.S., Markov S.M., and Popova E.D. (1992) Extended Interval Arithmetic: New Results and Applications. In L. Atanassova and J. Herzberger (Eds.) *Computer Arithmetic and Enclosure Methods*, pp.225-232
- Dubois D. and Prade H. (1988) Possibility Theory: An Approach to Computerized Processing of Uncertainty. Plenum, New York.
- Ferson S., Kreinovich V. Ginzburg L., Myers D.S., and Sentz K. (2003) Constructing probability boxes and Dempster-shafer structures. *Sandia National Laboratories Technical report SAND2002-4015*, Albuquerque, NM.
- Gardeñes E., Sainz M.Á., Jorba L., Calm R., Estela R., Mielgo H., and Trepát A. (2001) Modal intervals. *Reliable Computing*, **7**(2): 77-111
- Levi I. (1980) *The Enterprise of Knowledge*. MIT Press, Cambridge, MA.
- Molchanov I. (2005) *Theory of Random Sets*. London: Springer.
- Möller B. and Beer M. (2004) Fuzzy Randomness: Uncertainty in Civil Engineering and Computational Mechanics. Springer, Berlin.
- Moore R.E. (1966) *Interval Analysis*. Prentice-Hall, Englewood Cliffs, NJ.
- Neumaier A. (2004) Clouds, fuzzy sets, and probability intervals. *Reliable Computing*, **10**(4):249-272.
- Kuznetsov V.P. (1995) Interval methods for processing statistical characteristics. *Proc. 1995 Int. Workshop on Applications of Interval Computations, El Paso, TX*
- Shafer G.A. (1990) *Mathematical Theory of Evidence*, Princeton University Press, NJ
- van Fraassen B. (1989) *Laws and Symmetry*. Clarendon Press, Oxford.
- Walley P. (1991) *Statistical Reasoning with Imprecise Probabilities*. Chapman & Hall, London
- Wang Y. (2008) Imprecise probabilities with a generalized interval form. *Proc. 3rd Int. Workshop on Reliability Engineering Computing, Savannah, GA*
- Wang Y. (2010) Imprecise probabilities based on generalized intervals for system reliability assessment. *International Journal of Reliability & Safety*, **4**(4): 319-342
- Weichselberger K. (2000) The theory of interval-probability as a unifying concept for uncertainty. *International Journal of Approximate Reasoning*, **24**(2-3): 149-170

Embodied Knowledge of Gesture Motion Acquired by Singular Spectrum Analysis

I. Hayashi¹, Y. Jiang², and S. Wang²

1. Faculty of Informatics, Kansai University, 2-1-1, Ryozenji-cho, Takatsuki, Osaka 569-1095, Japan; PH (072) 690-2448; FAX (072) 690-2491; email: ihaya@cbii.kutc.kansai-u.ac.jp
2. School of Systems Engineering, Kochi University of Technology, 185 Miyanokuti, Tosayamada, Kami, Kochi 782-8502, Japan; PH (088) 757-2013; FAX (088) 757-2013; email: {jiang.yinlai, wang.shuoyu}@kochi-tech.ac.jp

ABSTRACT

Whenever a disaster occurs, it's of utmost importance that the rescue system recognizes accurately human behavior and evacuation command in the fire and its black smoke. However, we have infinite pattern for movement instructions by our personality. On the other hand, the singular spectrum analysis method has proposed as analytical method for time-series data. In this paper, we propose a method for acquiring embodied knowledge of human behavior from time-series gesture data using singular spectrum analysis. A behavior is distinguished in terms of gesture characteristic with similarity criteria by interval time-series data. We discuss the usefulness of the proposed method using an example of gesture motion.

I. INTRODUCTION

In order to assure safety and security in the occurrence of a natural disaster or a large-scale accident, it is important to communicate with each other in the disaster, and such how to communicate can allow us to detect and avoid more dangers. For the communication tool, we need a development of monitoring system which records human behavior in the disaster, and distinguishes the gesture motion and informs people a safety escape route automatically adding safety intelligence, e.g., disaster information, criminal information. Especially, it's of utmost importance for evacuees to recognize commands of inducer accurately to find an escape route under fire and black smoke in the disaster. However, it is difficult to recognize an evacuation command from inducer's infinite gesture motion, and so we need a system which can recognize human behavior automatically [1].

In this paper, we aim a development of rescue robot which sense a movement of evacuation command and acquire embodied knowledge of the movement [2, 3]. A gesture recognition method [4] is proposed to enable the rescue robot to communicate with humans. Gesture recognition has been studied extensively and there have been varied approaches to handle gesture recognition, ranging from mathematical models based on hidden Markov chains to tools or approaches based on soft computing [5]. We discuss a new gesture recognition method to identify 3-dimensional gesture motions using singular value decomposition (SVD). Applications which employ the SVD include computing the pseudoinverse, least squares fitting of data, matrix approximation, and determining the rank, range and null space of a matrix [6]. Recently, the SVD have been utilized in time-series data analysis for knowledge discovery [7] and motion analysis to extract similarities and differences in human behavior [8]. In our proposed model, we measure the similarity criteria between the gesture of evacuation command and the instruction we learned before using left singular vectors and singular values decomposition, and distinguish the gestures. We proposed two kinds of methods, first method to measure the similarity between the gesture distances and the second method to measure the similarity of the gesture vector. We discuss the usefulness of the proposed methods using an example of five kinds of 3-dimensional gesture motions.

II. MEASUREMENT OF 3-DIMENSIONAL EVACUATION GESTURE

The motions of the hand gestures are measured with Movetr/3D and GE60/W (Library, Tokyo, Japan). Subjects are two males, SW and ST, in twenties. Five markers, M_1 on the tip of the thumb, M_2 on the tip of the middle finger, M_3 on the tip of the little finger, M_4 on the thumb-side of the wrist and M_5 on the little finger side of the wrist, were measured. The gestures were performed in a 50cm×50cm×50cm cubic space shown in Figure 1. In the experiment, five kinds of hand gestures, CH (Come here), GA (Go away), GR (Go right), GL (Go left), and CD (Calm down), were performed by subjects. One gesture was executed 9 times by each subject. Data of the first 5 times execution were used as patterns of the gesture. Data of last 4 times were used to be distinguished.

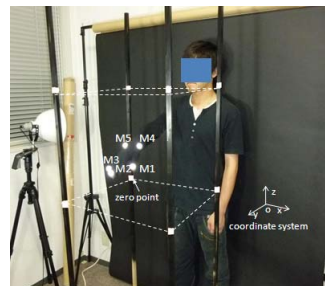


Figure 1: Experiment

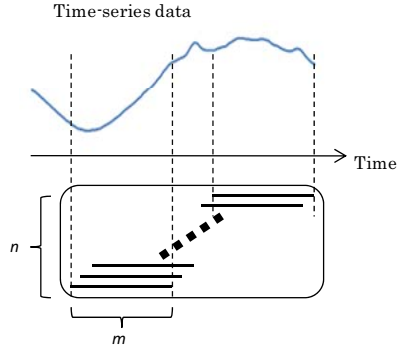
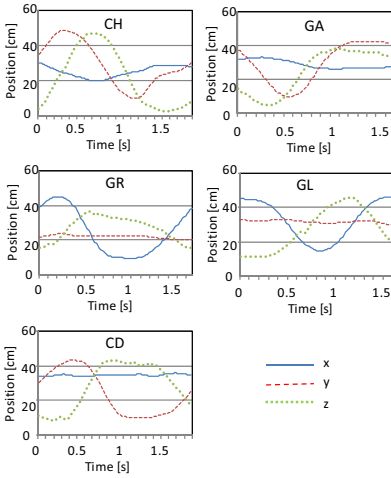


Figure 3: Design of Matrix $M_X^{i,G}$

Figure 2: Gesture of Examples (M2 of SW)

The measurement time-series data of M_2 when subject SW performed the five kinds of gestures are shown in Figure 2. A movement change as for GA, CH, and CD is big in the top and bottom direction (onto z -axis) and in the front and back direction (onto y -axis), and as for GR and GL, the movement change is big in the right and left direction (onto x -axis).

III. GESTURE ANALYSIS USING SINGULAR VALUE DECOMPOSITION

Suppose M is an m -by- n matrix. Then there exists a factorization of the form: $M = U \Sigma V^T$, where $U = (u_1, u_2, \dots, u_m)$, $V = (v_1, v_2, \dots, v_m)$, and the matrix Σ is m -by- n diagonal matrix with nonnegative real numbers on the diagonal. The matrix U contains the left singular vectors of M and the matrix V contains the right singular vectors of M . Suppose that there are w measurement points (P_1, P_2, \dots, P_w). On point P_i , the measured data series of gesture G is denoted as $\tau^{i,R}$, which consists of 3-dimensional data ($X^{i,G}, Y^{i,G}, Z^{i,G}$). We detect the time series $X_X^{i,G} = (x_1^{i,G}, x_2^{i,G}, \dots, x_n^{i,G})^T$ contains the x coordinate values of the P_i point. Then matrix $M_X^{i,G}$ is defined as a collective of the change of x coordinate values of the gesture, $M_X^{i,G} = (X_1^{i,G}, X_2^{i,G}, \dots, X_n^{i,G})$.

The matrix $M_X^{i,G}$ can be decomposed into a product of $U_X^{i,G}$, $\Sigma_X^{i,G}$ and $V_X^{i,G}$. The design of matrix $M_X^{i,G}$ is shown in Figure 3. Let us denote the singular values

and the left singular vectors as $((\delta_{1,X}^{i,G}, u_{1,X}^{i,G}), (\delta_{2,X}^{i,G}, u_{2,X}^{i,G}), \dots, (\delta_{l,X}^{i,G}, u_{l,X}^{i,G}))$, for $u_{j,X}^{i,G} = (u_{1j,X}^{i,G}, u_{2j,X}^{i,G}, \dots, u_{hj,X}^{i,G}, \dots, u_{qj,X}^{i,G})$ in descending order of the singular values. The parameter l represents the number of representative patterns under consideration, and the parameter q represents the number of elements of the singular vector. The left singular vectors, $u_{1,X}^{i,G}$, $u_{2,X}^{i,G}$, ..., $u_{l,X}^{i,G}$ of $M_X^{i,G}$, represent the change patterns of the x coordinate values on this point of the hand gesture. We proposed two kinds of motion analysis methods for gesture recognition using SVD.

1) Method for Similarity between Gesture Distances

Suppose that the measured data series are divided into $\tau_{TRD}^{i,G}$ as reference data series and $\tau_{CHD}^{i,G}$ as data series to be recognized. Let us denote the left singular vectors of $\tau_{X,TRD}^{i,G}$ related to the x coordinate values of the P_i point on the hand while a hand gesture G as $u_{X,TRD}^{i,G} = (u_{1,X,TRD}^{i,G}, u_{2,X,TRD}^{i,G}, \dots, u_{l,X,TRD}^{i,G})$, for $u_{j,X,TRD}^{i,G} = (u_{1j,X,TRD}^{i,G}, u_{2j,X,TRD}^{i,G}, \dots, u_{hj,X,TRD}^{i,G}, \dots, u_{qj,X,TRD}^{i,G})$, and the left singular vectors of $\tau_{X,CHD}^i$ as $u_{X,CHD}^i = (u_{1,X,CHD}^i, u_{2,X,CHD}^i, \dots, u_{l,X,CHD}^i)$, for $u_{j,X,CHD}^{i,G} = (u_{1j,X,CHD}^{i,G}, u_{2j,X,CHD}^{i,G}, \dots, u_{hj,X,CHD}^{i,G}, \dots, u_{qj,X,CHD}^{i,G})$. Three kinds of similarity criteria between gestures related to data series of 3-dimensional data $(X^{i,G}, Y^{i,G}, Z^{i,G})$ are defined as follows;

$$S_1: r_i(u_{TRD}^{i,G}, u_{CHD}^i) = \frac{1}{3} \sum_{k=1}^3 \sum_{j=1}^l \left| \sum_{h=1}^q u_{hj,k,TRD}^{i,G} - \sum_{h=1}^q u_{hj,k,CHD}^i \right| \quad (1)$$

$$S_2: r_i(u_{TRD}^{i,G}, u_{CHD}^i) = \frac{1}{3} \sum_{k=1}^3 \sum_{j=1}^l \sum_{h=1}^q \left| u_{hj,k,TRD}^{i,G} - u_{hj,k,CHD}^i \right| \quad (2)$$

$$S_3: r_i(u_{TRD}^{i,G}, u_{CHD}^i) = \frac{1}{3} \sum_{k=1}^3 \sqrt{\sum_{j=1}^l \sum_{h=1}^q (u_{hj,k,TRD}^{i,G} - u_{hj,k,CHD}^i)^2}. \quad (3)$$

Since there are w measurement points (P_1, P_2, \dots, P_w) , the estimated gesture G^*

is identified by the following two kinds of estimations;

$$E_1 : G^* = \left\{ G_f \mid \max_f \sum_{i=1}^w n(G_f^i), \text{ for } G_f^i = \{G_f \mid \min_f r_i(u_{TRD}^{i,G_f}, u_{CHD}^i)\} \right\} \quad (4)$$

$$E_2 : G^* = \left\{ G_f \mid \min_f \sum_{i=1}^w r_i(u_{TRD}^{i,G_f}, u_{CHD}^i) \right\} \quad (5)$$

where, G_f is the f -th gesture among five hand gestures, and $n(G_f^i)$ is a counting function which is $n(G_f^i) = 1$ if the condition G_f^i is satisfied at the P_i point.

2) Method for Similarity between Gesture Vectors

If one of the data series $X_p^{i,G}$ in $M_X^{i,G}$ is replaced by another data series X_{CHD}^i , the singular values and left singular vectors of $M_{X,CHD}^i$ will be different from those of $M_X^{i,G}$.

$$M_{X,CHD}^i = [X_1^{i,G}, X_2^{i,G}, \dots, X_{p-1}^{i,G}, X_{CHD}^i, X_{p+1}^{i,G}, \dots, X_n^{i,G}] \quad (6)$$

The difference between the left singular vectors of $X M_X^{i,G}$ and $M_{X,CHD}^i$ is determined by how X_{CHD}^i is different from the other $p-1$ data series. Therefore, if X_{CHD}^i comes from another kind of hand gesture, the difference can be utilized as a criterion for judging whether X_{CHD}^i comes from the same kind of hand gesture as the other data series. In our method, the location of X_{CHD}^i is fixed in the end of data series, and three kinds of similarity between gestures related to data series of 3-dimensional data ($X^{i,G}$, $Y^{i,G}$, $Z^{i,G}$) are defined as follows;

$$S_4 : r_i(u_{TRD}^{i,G}, u_{CHD}^i) = \frac{1}{3l^2} \sum_{k=1}^3 \sum_{j=1}^l \left| \sum_{h=1}^q u_{hj,k,TRD}^{i,G} - \sum_{h=1}^q u_{hj,k,CHD}^i \right| \quad (7)$$

$$S_5 : r_i(u_{TRD}^{i,G}, u_{CHD}^i) = \frac{1}{3l^2} \sum_{k=1}^3 \sum_{j=1}^l \sum_{h=1}^q \left| u_{hj,k,TRD}^{i,G} - u_{hj,k,CHD}^i \right| \quad (8)$$

$$S_6 : r_i(u_{TRD}^{i,G}, u_{CHD}^i) = \frac{1}{3l^2} \sum_{k=1}^3 \sqrt{\sum_{j=1}^l \sum_{h=1}^q (u_{hj,k,TRD}^{i,G} - u_{hj,k,CHD}^i)^2}. \quad (9)$$

Since there are w measurement points (P_1, P_2, \dots, P_w), the estimated gesture G^* is identified by the following estimation;

$$E_3 : G^* = \left\{ G_f \left| \min_f \sum_{i=1}^w r_i(u_{TRD}^{i,G_f}, u_{CHD}^i) \right. \right\}.$$

IV. RESULTS AND DISCUSSIONS

In order to show the usefulness of the proposed methods, we distinguished gestures of two subjects, SW and ST using two kinds of methods. Since the average number of SW and ST's gestures is 125.2 (SD: 29.0), the number of data m is set to be 125. We also set $n=5, q=125, l=1$, and $w=5$.

1) Method for Similarity between Gesture Distances

Table I shows the recognition results. The pair of the similarity S_2 and the estimation E_1 is 90.0 %. The recognition results suggest that the pair of S_2 and E_1 is more feasible in gesture recognition. Table 2 and Table 3 show the counting number of measurement points for two

Table 1: Recognition of Gestures

	Similarity (S ₁)	Similarity (S ₂)	Similarity (S ₃)
Estimation (E ₁)	70.0%	90.0%	80.0%
Estimation (E ₂)	60.0%	80.0%	80.0%

subjects with the pair of S_2 and E_1 . The recognition results suggest that the gestures of CH, GA, and CD are distinguished well, but it is not so well for two gestures of GR and GL of SW. However, in general it is hard to distinguish between a gesture of GR (Go right) and GL (Go left), and so the results are understandable.

2) Method for Similarity between Gesture Vectors

Table 4 shows the recognition results based on the three kinds of similarity definitions of S_4, S_5 , and S_6 . The recognition results suggest that similarity definitions of S_5 and S_6 led to relatively higher correct recognition rates while the correct rate of the recognition based on S_4 was very low. Therefore, S_5 and S_6 are more feasible in gesture recognition.

Table 2: Result of Subject SW Gestures

Estimated Gesture	Gesture of SW				
	CH	GA	GR	GL	CD
CH	12	1	4	4	4
GA	0	10	2	2	4
GR	0	0	0	4	0
GL	2	1	9	5	0
CD	1	3	0	0	7
Result	CH	GA	GL	GL	CD

Table 3: Result of Subject ST Gestures

Estimated Gesture	Gesture of ST				
	CH	GA	GR	GL	CD
CH	8	2	3	2	0
GA	1	9	1	0	2
GR	0	0	11	1	0
GL	3	2	0	10	2
CD	3	2	0	2	11
Result	CH	GA	GR	GL	CD

Table 4: Results of Method for Similarity between Gesture

Estimated Gesture	Similarity (S_4)		Similarity (S_5)		Similarity (S_6)	
	Correct	Others	Correct	Others	Correct	Others
SW_CH	1	3	2	2	1	3
SW_GA	3	1	4	0	4	0
SW_GR	2	2	3	1	3	1
SW_GL	1	3	3	1	3	1
SW_CD	0	4	3	1	3	1
ST_CH	2	2	2	2	2	2
ST_GA	1	3	4	0	4	0
ST_GR	3	1	4	0	4	0
ST_GL	0	4	3	1	2	2
ST_CD	0	4	4	0	4	0
Correct Rate	30.3%		80.0%		75.0%	

3) Discussions

Similar to speech and handwriting, gestures vary between individuals, even for the same individual between different instances. However, as shown in Table 1 to Table 4, the recognition results based on S_2 and S_5 illustrated high recognition rate among several similarity measures. Since the formulation of S_2 and S_5 are same, the absolute differential of the left singular vectors at the same order is suitable for gesture recognition as similarity definition. As for the incorrect recognitions, for example, the gestures GR and GL have completely different meanings, but their

motions are very similar in that the hand waves left and right. Their difference lies in whether the hand moves faster from left to right, or from right to left. Sometimes even humans make mistakes in distinguishing them from each other.

V. CONCLUSIONS

In this paper, a novel 3D motion analysis algorithm using singular value decomposition (SVD) is proposed for gesture recognition. We applied the proposed method to gesture recognition, and the experiment results verified the effectiveness of the algorithm. This work was partially supported by the Ministry of Education, Culture, Sports, Science, and Technology of Japan under Strategic Project to Support the Formation of Research Bases at Private Universities, 2008-2012.

REFERENCES

- [1] D.Tsuda, S.Wang, N.Miura, and Y.Jiang: Development and safety validation of lead for a guidance robot, *Journal of Biomedical Fuzzy Systems Association*, Vol.11, No.1, pp.43-48 (2009) [in Japanese].
- [2] Y.Jiang, I.Hayashi, M.Hara, and S.Wang: Three-dimensional Motion Analysis for Gesture Recognition Using Singular Value Decomposition, *Proc of 2010 IEEE International Conference on Information and Automation*, pp.805-810 (2010).
- [3] I.Hayashi, Y.Jiang, M.Hara, and S.Wang: Knowledge Acquisition from Motion of Evacuation Instruction Using Singular Value Decomposition, *Proc. of the 26th Fuzzy System Symposium*, pp.824-829 (2010) [in Japanese]
- [4] A. Kendon, *Gesture: Visible Action as Utterance*. Cambridge University Press, Cambridge (2004).
- [5] S. Mitra and T. Acharya: Gesture recognition: a survey, *IEEE Transactions on Systems, Man, and Cybernetics, Part C: Applications and Reviews*, Vol.37, issue 3, pp.311- 324 (2007)
- [6] M.E. Wall, A. Rechtsteiner, and L.M. Rocha. "Singular value decomposition and principal component analysis". in *A Practical Approach to Microarray Data Analysis*. D.P. Berrar, W. Dubitzky, M.Granzow, eds. pp.91-109, Kluwer: Norwell, MA (2003).
- [7] T. Ide and K. Inoue: Knowledge discovery from heterogeneous dynamic systems using change-point correlations, *Proc. 2005 SIAM International Conference on Data Mining (SDM 05)*, pp.571-576 (2005).
- [8] K. Mishima, S. Kanata, H. Nakanishi, Y. Horiguchi, and T. Sawaragi: Extraction of similarities and differences in human behavior using singular value decomposition, *Proc of the 53rd annual conference of the Institute of Systems, Control and Information Engineers (SCI'09)*, pp.409-410, (2009) [in Japanese].

Fuzzy probability in engineering analyses

M. Beer¹ and S. Ferson²

¹Department of Civil Engineering, National University of Singapore, BLK E1A #07-03, 1 Engineering Drive 2, Singapore 117576, Singapore; phone (65) 6516-4913; fax (65) 6779-1635; email: cvebm@nus.edu.sg

²Applied Biomathematics, 100 North Country Road, Setauket, NY 11733, USA; phone (1) 631-751-4350; fax (1) 631-751-3435; email: scott@ramas.com

ABSTRACT

Predicting the behavior and reliability of engineering structures and systems is often plagued by uncertainty and imprecision caused by sparse data, poor measurements and subjective information. Accounting for such limitations complicates the mathematical modeling required to obtain realistic results in engineering analyses. The framework of imprecise probabilities provides a mathematical basis to deal with these problems which involve both probabilistic and non-probabilistic sources of uncertainty. A common feature of the various concepts of imprecise probabilities is the consideration of an entire set of probabilistic models in one analysis. But there are differences between the concepts in the mathematical description of this set and in the theoretical connection to the probabilistic models involved. This study is focused on fuzzy probabilities, which combine a probabilistic characterization of variability with a fuzzy characterization of imprecision. We discuss how fuzzy modeling can allow a more nuanced approach than interval-based concepts. The application in an engineering analysis is demonstrated by means of an example.

INTRODUCTION

The analysis and reliability assessment of engineering structures and systems involves uncertainty and imprecision in parameters and models of different type. In order to derive predictions regarding structural behavior and reliability, it is crucial to represent the uncertainty and imprecision appropriately according to the underlying real-world information which is available. To capture variation of structural parameters, established probabilistic models and powerful simulation techniques are available for engineers, which are widely applicable to real-world problems; for example, see (Schenk and Schuëller 2005). The required probabilistic modeling can be realized via classical mathematical statistics if data of a suitable quality are available to a sufficient extent.

In civil engineering practice, however, the available data are frequently quite limited and of poor quality. These limitations create epistemic uncertainty, which can sometimes be substantial. It is frequently argued that expert knowledge can compen-

sate for the limitations through the use of Bayesian methods based on subjective probabilities. If a subjective perception regarding a probabilistic model exists and some data for a model update can be made available, a Bayesian approach can be very powerful, and meaningful results with maximal information content can be derived. Bayesian approaches have attracted increasing attention in the recent past and considerable advancements have been reported for the solution of various engineering problems (Papadimitriou et al. 2001, Igusa et al. 2002, Der Kiureghian and Ditlevsen 2009). An important feature of Bayesian updating is that the subjective influence in the model assumption decays quickly with growing amount of data. It is then reasonable practice to estimate probabilistic model parameters based on the posterior distribution, for example, as the expected value thereof.

When less information and experience are available, greater difficulties will be faced. If the available information is very scarce and is of an imprecise nature rather than of a stochastic nature, a subjective probabilistic model description may be quite arbitrary. For example, a distribution parameter may be known merely in the form of bounds. Any prior distribution which is limited to these bounds would then be an option for modeling. But the selection of a particular model would introduce unwarranted information that cannot be justified sufficiently. Even the assumption of a uniform distribution, which is commonly used in those cases, ascribes more information than is actually given by the bounds. This situation may become critical if no or only very limited data are available for a model update. The initial subjectivity is then dominant in the posterior distribution and in the final result. If these results, such as failure probabilities, determine critical decisions, one may wish to consider the problem from the following angle.

If several probabilistic models are plausible for the description of a problem, and no information is available to assess the suitability of the individual models or to relate their suitability with respect to one another, then it may be of interest to identify the worst case for the modeling rather than to average over all plausible model options with arbitrary weighting. The probabilistic analysis is carried out conditional on each of many particular probabilistic models out of the set of plausible models. In reliability assessment, this implies the calculation of an upper bound for the failure probability as the worst case. This perspective can be extended to explore the sensitivity of results with respect to the variety of plausible models, that is, with respect to a subjective model choice. A mathematical framework for an analysis of this type has been established with imprecise probabilities (see Walley 1991). Applications to reliability analysis (Kozine and Filimonov 2000, Möller et al. 2003, Utkin 2004) and to sensitivity analysis (Ferson and Tucker 2006, Hall 2006) have been reported. This intuitive view, however, is by far not the entire motivation for imprecise probabilities (see Klir 2006). Imprecise probabilities are not limited to a consideration of imprecise distribution parameters. They are also capable of dealing with imprecise conditions and dependencies between random variables and with imprecise structural parameters and model descriptions. They allow statistical estimations and tests with imprecise sample elements. Results from robust statistics in form of solution domains of statistical estimators can be considered directly and appropriately (Augustin and Hable 2010).

In this paper, the implementation of intervals and fuzzy sets as parameters of probabilistic models is discussed in the context of proposed concepts of imprecise probabilities. A structural reliability analysis is employed to illustrate the effects in an example.

PROBABILISTIC MODELS WITH IMPRECISE PARAMETERS

In engineering analyses, parameters of probabilistic models are frequently limited in precision and are only known in a coarse manner. This situation can be approached with different mathematical concepts. First, the parameter can be considered as uncertain with random characteristics, which complies with the Bayesian approach. Subjective probability distributions for the parameters are updated by means of objective information in form of data. The result is a mix of objective and subjective information – both expressed with probability. Second, the parameter can be considered as imprecise but bounded within a certain domain, where the domain is described as a set. In this manner, only the limitation to some domain and no further specific characteristics are ascribed to the parameter, which introduces significantly less information in comparison with a distribution function as used in the Bayesian approach. Imprecision in the form of a set for a parameter does not migrate into probabilities, but it is reflected in the result as a set of probabilities which contains the true probability. Intervals and fuzzy sets can thus be considered as models for parameters of probability distributions.

An interval is an appropriate model in cases where only a possible range between crisp bounds x_l and x_r is known for the parameter x , and no additional information concerning value frequencies, preference, etc. between interval bounds is available nor any clues on how to specify such information. Interval modeling of a parameter of a probabilistic model connotes the consideration of a set of probabilistic models, which are captured by the set of parameter values

$$X_I = \{x \mid x \in [x_l, x_r]\} . \quad (1)$$

This modeling corresponds to p-box approach (Ferson and Hajagos 2004) and to the theory of interval probabilities (Weichselberger 2000). Events E_i are assessed with a range of probability, $[P_l(E_i), P_r(E_i)] \subseteq [0,1]$, which is directly used for the definition of interval probability, denoted as IP , as follows,

$$IP: E_\Omega \rightarrow I \text{ with} \\ E_\Omega = \mathbf{P}(\Omega), I = \{[a,b] \mid \forall a,b \mid 0 \leq a \leq b \leq 1\} . \quad (2)$$

In Eq. (2), $\mathbf{P}(\Omega)$ is the power set on the set Ω of elementary events ω . This definition complies with traditional probability theory. Kolmogorov's axioms and the generation scheme of events are retained as defined in traditional probability theory (see also Yamauchi and Mukaidono 1999). Traditional mathematical statistics are applicable for quantification purposes. In reliability analysis with interval probabilities, the parameter interval X_I is mapped to an interval of the failure probability,

$$X_l \rightarrow P_{f_l} = \left\{ P_f \mid P_f \in [P_{f_l}, P_{f_r}] \right\}. \quad (3)$$

Scrutinizing the modeling of parameters as intervals shows that an interval is a quite crude expression of imprecision. The specification of an interval for a parameter implies that, although a number's value is not known exactly, exact bounds on the number can be provided. This may be criticized because the specification of precise numbers is just transferred to the bounds. Fuzzy set theory provides a suitable basis for relaxing the need for precise values or bounds. It allows the specification of a smooth transition for elements from belonging to a set to not belonging to a set. Fuzzy numbers are a generalization and refinement of intervals for representing imprecise parameters. The essence of an approach using fuzzy numbers that distinguishes it from more traditional approaches is that it does not require the analyst to circumscribe the imprecision all in one fell swoop with finite characterizations having known bounds. The analyst can now express the available information in form of a series of plausible intervals, the bounds of which may grow, including the case of infinite limits. This allows a more nuanced approach compared to interval modeling.

Fuzzy sets provide an extension to interval modeling that considers variants of interval models, in a nested fashion, in one analysis. A fuzzy set \tilde{X} of parameter values can be represented as a set of intervals X_l ,

$$\tilde{X} = \left\{ (X_\alpha, \mu(X_\alpha)) \mid \begin{array}{l} X_\alpha = X_l, \\ \mu(X_\alpha) = \alpha \\ \forall \alpha \in (0, 1] \end{array} \right\}, \quad (4)$$

which is referred to as α -discretization; see Figure 1 (Zimmermann 1992). In Eq. (4), X_α denotes an α -level set of the fuzzy set \tilde{X} , and $\mu(\cdot)$ is the membership function. This modeling applied to parameters of a probabilistic model corresponds to the theory of fuzzy random variables and to fuzzy probability theory. Detailed discussions are provided, for example, in (Kruse and Meyer 1987, Li et al. 2002, Gil et al. 2006, Beer 2009). The definition of a fuzzy random variable refers to imprecise observations as outcome of a random experiment. A fuzzy random variable \tilde{Y} is the mapping

$$\tilde{Y}: \Omega \rightarrow F(\mathbf{Y}) \quad (5)$$

with $F(\mathbf{Y})$ being the set of all fuzzy sets on the fundamental set \mathbf{Y} , whereby the standard case is $\mathbf{Y} = \mathbb{R}^n$. The pre-images of the imprecise events described by $F(\mathbf{Y})$ are elements of a traditional probability space $[\Omega, \mathcal{S}, P]$. This complies with traditional probability theory and allows statistics with imprecise data (Kruse and Meyer 1987, Bandemer and Näther 1992, Viertl 1996). As a consequence of Eq. (5), parameters of probabilistic models, including descriptions of the dependencies and distribution type, and probabilities are obtained as fuzzy sets. This builds the relationship

to the p-box approach and to the theory of interval probabilities. A representation of a fuzzy probability distribution function of a fuzzy random variable \tilde{Y} with aid of α -discretization leads to interval probabilities $[F_{al}(y), F_{ar}(y)]$ for each α -level as one plausible model variant,

$$\tilde{F}(y) = \left\{ (F_{\alpha}(y), \mu(F_{\alpha}(y))) \mid \begin{array}{l} F_{\alpha}(y) = [F_{al}(y), F_{ar}(y)] \\ \mu(F_{\alpha}(y)) = \alpha \forall \alpha \in (0, 1] \end{array} \right\}. \quad (6)$$

As depicted in Figure 1, in a reliability analysis, the fuzzy set \tilde{X} of parameter values is mapped to a fuzzy set of the failure probability,

$$\tilde{X} \rightarrow \tilde{P}_f. \quad (7)$$

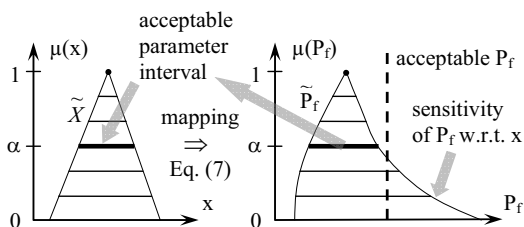


Figure 1. Relationship between fuzzy parameters and failure probability.

The membership function serves only instrumentally to summarize various plausible interval models in one embracing scheme. The interpretation of the membership value μ as epistemic possibility, which is sometimes proposed may be useful for ranking purposes, but not for making critical decisions. The importance of fuzzy modeling lies in the simultaneous consideration of various magnitudes of imprecision at once in the same analysis.

The features of a fuzzy probabilistic analysis can be utilized to identify sensitivities of the failure probability with respect to the imprecision in the probabilistic model specification; see Figure 1. Sensitivities of P_f are indicated when the interval size of $P_{f\alpha}$ grows strongly with a moderate increase of the interval size of X_{α} of the parameters. If this is the case, the membership function of \tilde{P}_f shows outreaching or long and flat tails. An engineering consequence would be to pay particular attention to those model options X_{α} , which cause large intervals $P_{f\alpha}$ and to further investigate to verify the reasoning for these options and to possibly exclude these critical cases.

A fuzzy probabilistic analysis also provides interesting features for design purposes. The analysis can be performed with coarse specifications for design parameters and for probabilistic model parameters. From the results of this analysis, acceptable intervals for both design parameters and probabilistic model parameters can be determined directly without a repetition of the analysis; see Figure 1. Indications are

provided in a quantitative manner to collect additional specific information or to apply certain design measures to reduce the input imprecision to an acceptable magnitude. This implies a limitation of imprecision only to those acceptable magnitudes and so also caters for an optimum economic effort. For example, a minimum sample size or a minimum measurement quality associated with the acceptable magnitude of imprecision can be directly identified. Further, revealed sensitivities may be taken as a trigger to change the design of the system under consideration to make it more robust. Beer and Liebscher (2008) describe a related method for designing robust structures in a pure fuzzy environment. These methods can also be used for the analysis of aged and damaged structures to generate a rough first picture of the structural integrity and to indicate further detailed investigations to an economically reasonable extent—expressed in form of an acceptable magnitude of input imprecision according to some α -level.

EXAMPLE

To illustrate this approach, we use an example reliability analysis for a reinforced concrete frame (Möller et al. 2003) shown in Figure 2. The structure is loaded by its dead weight, a small horizontal load P_H , and the vertical loads P_{V0} and p_0 which are increased with the factor v until global structural failure is attained. For the purpose of demonstration, only the load factor v is introduced as a random variable with an extreme value distribution of Ex-Max Type I with mean \tilde{m}_v and standard deviation $\tilde{\sigma}_v$. Imprecision of the probabilistic model is modeled with triangular fuzzy numbers $\tilde{m}_v = \langle 5.7, 5.9, 6.0 \rangle$ and $\tilde{\sigma}_v = \langle 0.08, 0.11, 0.12 \rangle$. In addition, the rotational stiffness of the springs at the column bases is modeled as a triangular fuzzy number $\tilde{k}_\phi = \langle 5, 9, 13 \rangle$ MNm/rad to take account of the only vaguely known soil properties. Based on this input information, the fuzzy reliability index $\tilde{\beta}$ shown in Figure 3 is calculated.

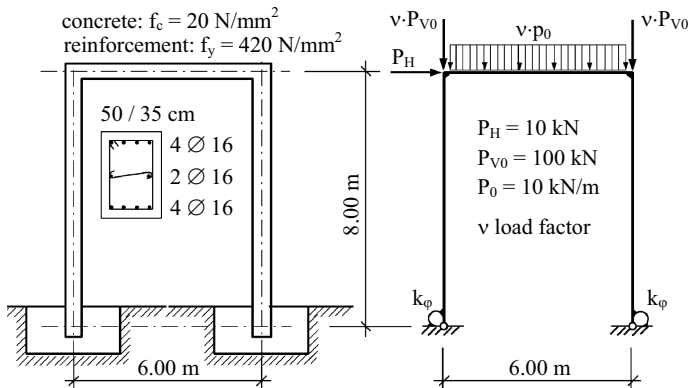


Figure 2. Reinforced concrete frame, structural model, and loading.

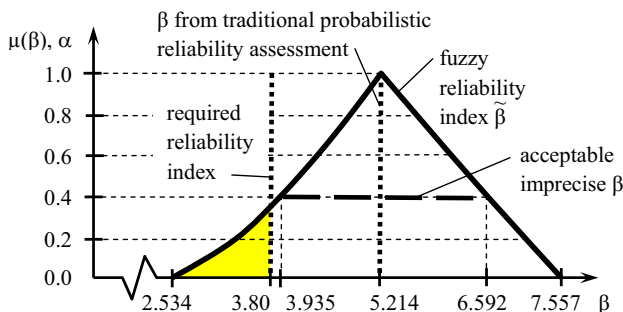


Figure 3. Fuzzy reliability index and evaluation against safety requirement.

The result spreads over a large range of possible values for β . The shaded part of $\tilde{\beta}$ does not comply with the safety requirements. This means that a sufficient structural reliability is not ensured when the parameters are limited to the plausible ranges for $\alpha = 0$. In a traditional reliability analysis, using crisp assumptions for the parameters out of their plausible range such as the values associated with the membership $\mu = 1$, this critical situation is not revealed. So far, the results from p-box approach or from interval probabilities would lead to the same conclusions. As an additional feature of fuzzy probabilities, it can be observed that the left tail of the membership function of β slightly tends to flatten towards small values. This indicates a slight sensitivity of β with respect to imprecision of the fuzzy input when this grows in magnitude. So one may wish to reduce the input imprecision to a magnitude which is associated with the steeper part of the membership function of β . In Figure 3, the part $\mu(\beta) \geq 0.4$ is a reasonable choice in this regard. Further, the result $\beta_{\alpha=0.4} = [3.935, 6.592]$ for $\mu(\beta) \geq 0.4 = \alpha$ (according to the definition of α -level sets) satisfies the safety requirement $\beta_{\alpha=0.4} \geq 3.8$. That is, a reduction of the imprecision of the fuzzy input parameters to the magnitude on α -level $\alpha = 0.4$ would lead to an acceptable reliability of the structure despite the remaining imprecision in the input. For example, a collection of additional information can be pursued to achieve the requirements $k_{\phi} \in [6.6, 11.4]$ MNm/rad = $k_{\phi, \alpha=0.4}$, $m_v \in [5.78, 5.96] = m_{v, \alpha=0.4}$, and $\sigma_v \in [0.092, 0.116] = \sigma_{v, \alpha=0.4}$. If this cannot be achieved for one or more parameters, the fuzzy analysis can be repeated with intervals for the parameters with non-reducible imprecision and with fuzzy sets for the parameters with reducible imprecision to separate the effects. The evaluation of the results then leads to a solution with proposed reduction of the imprecision only of those parameters for which this is possible. In this manner, it is also possible to explore sensitivities of the result β with respect to the imprecision of certain groups of input parameters or of individual input parameters. The repetition of the fuzzy analysis for these purposes can be avoided largely when a global optimization technique is used for the fuzzy analysis. This type of fuzzy analysis leads to a set of points distributed over the value ranges of the fuzzy input parameters and associated with results $\beta \in \tilde{\beta}$. For each construc-

tion of membership functions for the fuzzy input parameters, it is then immediately known which points belong to which α -level so that a discrete approximation of a result can be obtained directly without a repeated analysis. Repetition of the analysis is then only required for a detailed verification.

REFERENCES

- Augustin, Th. and Hable, R. (2010). On the impact of robust statistics on imprecise probability models: a review, *Structural Safety*, 32(6): 358–365.
- Bandemer, H. and Näther, W. (1992). *Fuzzy Data Analysis*, Kluwer Academic Publishers, Dordrecht.
- Beer, M. (2009). Fuzzy probability theory, in: R. Meyers (Ed.), *Encyclopedia of Complexity and Systems Science*, Vol 6, Springer, New York, 4047–4059.
- Beer, M. and Liebscher, M. (2008). Designing robust structures – a nonlinear simulation based approach, *Computers and Structures*, 86(10), 1102–1122.
- Der Kiureghian, A. and Ditlevsen, O. (2009). Aleatory or epistemic? Does it matter?, *Structural Safety*, 31(2), 105–112.
- Ferson, S. and Tucker, W. T. (2006). Sensitivity analysis using probability bounding, *Reliability Engineering & System Safety*, 91(10–11), 1435–1442.
- Ferson, S. and Hajagos, J. G. (2004). Arithmetic with uncertain numbers: rigorous and (often) best possible answers, *Reliability Engineering & System Safety*, 85(1–3), 135–152.
- Gil, M. A., López-Díaz, M. and Ralescu, D. A. (2006). Overview on the development of fuzzy random variables, *Fuzzy Sets and Systems*, 157(19), 2546–2557.
- Hall, J. W. (2006). Uncertainty-based sensitivity indices for imprecise probability distributions, *Reliability Engineering & System Safety*, 91(10–11), 1443–1451.
- Igusa, T., Buonopane, S. G., and Ellingwood, B. R. (2002). Bayesian analysis of uncertainty for structural engineering applications, *Structural Safety*, 24(2–4), 165–186.
- Klir, G.J. (2006). *Uncertainty and Information: Foundations of Generalized Information Theory*, Wiley-Interscience, Hoboken.
- Kozine, I. and Filimonov, Y. (2000). Imprecise reliabilities: experiences and advances, *Reliability Engineering and System Safety*, 67, 75–83.
- Kruse, R. and Meyer, K. (1987). *Statistics with Vague Data*, Reidel, Dordrecht.
- Li, S., Ogura, Y. and Kreinovich, V. (2002). *Limit Theorems and Applications of Set Valued and Fuzzy Valued Random Variables*, Kluwer Academic Publishers, Dordrecht.
- Möller, B., Graf, W. and Beer, M. (2003). Safety assessment of structures in view of fuzzy randomness, *Computers and Structures*, 81(15), 1567–1582.
- Papadimitriou, C., Beck, J. L. and Katfygiotis, L. S. (2001). Updating robust reliability structural test data, *Probabilistic Engineering Mechanics*, 16, 103–113.
- Schenk, C. A. and Schuëller, G. I. (2005). *Uncertainty Assessment of Large Finite Element Systems*, Springer, Berlin, Heidelberg.
- Utkin, L. V. (2004). An uncertainty model of structural reliability with imprecise parameters of probability distributions, *ZAMM - Zeitschrift für Angewandte Mathematik und Mechanik*, 84(10–11), 688–699.

- Viertl, R. (1996). *Statistical Methods for Non-Precise Data*, CRC Press, Boca Raton New York London Tokyo.
- Walley, P. (1991). *Statistical Reasoning with Imprecise Probabilities*, Chapman & Hall, London.
- Weichselberger, K. (2000). The theory of interval-probability as a unifying concept for uncertainty, *International Journal Approximate Reasoning*, 24(2–3), 149–170.
- Yamauchi, Y. and Mukaidono, M. (1999). Interval and paired probabilities for treating uncertain events, *IEICE Transactions on Information and Systems*, E82_D(5), 955–961.
- Zimmermann, H. J. (1992). *Fuzzy Set Theory and Its Applications*, Kluwer Academic Publishers, Boston London.

A Process for the Estimation of the Duration of Activities in Fuzzy Project Scheduling

A. Maravas¹ and J.P. Pantouvakis²

¹Centre for Construction Innovation, Dept. of Construction Engineering and Management, Bldg. of Strength of Materials—Annex A, National Technical University of Athens, Iroon Polytechniou 9 st, 15770, Athens, Greece email: amaravas@mail.ntua.gr

²Centre for Construction Innovation, Tel. +302107721268, email: jpp@central.ntua.gr

ABSTRACT

In dealing with uncertainty and imprecision Fuzzy Project Scheduling (FPS) has been presented as an alternative to well established traditional scheduling methods. The aim of this paper is to propose a process for the estimation of the duration of activities that are to be used in a FPS system. Initially, the sources of uncertainty are distinguished into the project and activity level. Then, the work focuses primarily on the calculation of the duration of activities based on the productivity of resources and the fuzzy parameters that define it. Thereafter, a specific example is presented from earthworks in a motorway project. Finally, the estimated duration can be adjusted based on the perceived risks at the project level. Overall, the paper presents a means for encoding a project manager's perception of uncertainty in the duration of activities that are to be used in FPS.

INTRODUCTION

The management of projects in an uncertain environment requires decisions that are based on inconsistent, vague and imprecise data. The shortcomings of traditional scheduling methods such as CPM and PERT, that employ deterministic or basic probabilistic views mandate to the formulation of a methodology capable of satisfying the real-world requirements for project scheduling. It should be noted that probability theory and fuzzy set theory are two distinct approaches; the former deals with random events by assigning probability distributions to the data whereas the latter deals with the imprecision of the data. Fuzzy Project Scheduling (FPS) is based on fuzzy set theory and is useful in dealing with circumstances involving uncertainty, imprecision, vagueness and incomplete data (Herroelen and Leus, 2005).

In terms of FPS, Prade (1979) was the first researcher to propose the application of fuzzy set theory in scheduling problems. Chanas and Kamburowski (1981) presented a fuzzy version of PERT which they named FPert. Important research in FPS has been conducted by McCahon and Lee (1988), Chang et al. (1995), Hapke et al.

(1994), Lorterapong and Moselhi (1996), Dubois et al. (2003), Bonnal et al. (2004), Chen and Huang (2007). Guiffrida and Nagi (1998) provide a review of FPS.

The modeling of uncertainty in construction productivity with Fuzzy Set Theory has been addressed by several researchers. Zhang et al. (2003) described the application of a fuzzy logic rule-based model in dealing with uncertainties in the quantity of resources involved in construction operations. Marzouk and Moselhi (2004) developed a fuzzy clustering model for estimating haulers' travel time in earthmoving production. Fayek et al. (2005) illustrated the application of fuzzy expert systems on predicting construction labor productivity in pipe rigging and welding. Karimi et al. (2007) presented a fuzzy optimization model for earthwork allocations with imprecise parameters that were modeled as fuzzy numbers. Castro-Lacouture et al. (2009) used fuzzy mathematical models for examining the impact of unexpected material shortages on project completion time.

A fundamental issue in the application of FPS is the selection of an appropriate membership function of the fuzzy numbers that encode the estimation or perception of uncertainty in the activity duration. However, the setting of guidelines for the selection of the most appropriate membership function as well as the limits of the fuzzy numbers remains an under-researched domain. In a real-world project a project manager will receive estimates from many professionals from various disciplines and different degrees of experience. Hence, a unified approach is required to homogenize estimates and to ensure that uncertainty is not under or over estimated. At the same time whereas significant research has been conducted in the modeling of construction productivity with fuzzy set theory, the research results have not been integrated with FPS. To this extent, this paper aims at presenting a methodology for the calculation of the duration of activities based on the productivity of resources and the specific fuzzy parameters that affect it. The ultimate goal is to view uncertainty in construction productivity and FPS in a unified approach.

FUZZY SET THEORY – MEMBERSHIP FUNCTIONS

Fuzzy set theory is used to characterize and quantify uncertainty and imprecision in data and functional relationships. It permits the gradual assessment of the membership of elements in a set in the real unit interval $[0, 1]$. Hence, a fuzzy set A of a universe X is characterized by a membership function $\mu_A: X [0, 1]$ which associates with each element x of X a number $\mu_A(x)$ in the interval $[0, 1]$ representing the grade of membership of x in A . In fuzzy set theory the triangular membership function which is defined by three numbers a, b, c is encountered very often. At b membership is 1, while a and c are the limits between zero and partial membership. The triangular fuzzy number $\tilde{x} = \langle a, b, c \rangle$ has the following membership function:

$$\mu_A(x) = \begin{cases} 0 & x < a \\ (x-a)/(b-a) & a \leq x \leq b \\ (c-x)/(c-b) & b \leq x \leq c \\ 0 & x > c \end{cases} \quad (1)$$

There are several ways to develop and assign membership functions to fuzzy variables. The assignment process can be intuitive or it can be based on some algorithmic or logical operations. Some straightforward methods are: intuition, inference, rank ordering, neural networks, genetic algorithms, inductive reasoning and statistics. (Ross, 2004). The choice of the method depends entirely on the problem size and problem type. Triangular, trapezoidal and LR type are the most common fuzzy numbers used in engineering problems.

The specific rules that govern the way in which the operators of summation, subtraction, multiplication and division are applied on fuzzy arithmetic are termed fuzzy arithmetic. It should be noted that the multiplication and division of fuzzy numbers changes the shape of their membership functions. Overall, for triangular fuzzy numbers, the operators are defined as follows:

$$\tilde{x} + \tilde{y} = \langle a, b, c \rangle + \langle d, e, f \rangle = \langle a + d, b + e, c + f \rangle \quad (2)$$

$$\tilde{x} - \tilde{y} = \langle a, b, c \rangle - \langle d, e, f \rangle = \langle a - f, b - e, c - d \rangle \quad (3)$$

$$\tilde{x} \otimes \tilde{y} = \langle a, b, c \rangle \otimes \langle d, e, f \rangle = \langle a \cdot d, b \cdot e, c \cdot f \rangle \quad (4)$$

$$\tilde{x} \div \tilde{y} = \langle a, b, c \rangle \div \langle d, e, f \rangle = \langle a / f, b / e, c / d \rangle \quad (5)$$

FRAMEWORK FOR ACTIVITY DURATION ESTIMATION

The first step in estimating the duration of activities in FPS is to distinguish the sources of uncertainty and imprecision into those of the project level and that of the activity level (see Figure 1). Project level uncertainty can be influenced by contractual issues, site conditions, weather, financial environment, building regulations, health and environment legislation, exchange rate volatility, funding restrictions etc. Activity level uncertainty is pertinent to the construction methodology and the specific labor, machinery and materials that are selected. Thereby, a specific construction activity may have different uncertainties if executed in a different location with a different project context.

A serious pitfall in FPS is the use of fuzzy activity durations with an obscure convolution of uncertainty from many sources. Thus, an uncertainty classification process is important in controlling the quality of duration estimates and consequently that of the FPS schedule. In terms of assessing uncertainty at the activity level it is possible to distinguish three sub-levels. At level 1, direct estimates of the activity durations are made. At level 2, the initial focus is on estimating the unit production rates of labor and machinery. Thereafter, the activity duration is calculated from the production rates. At level 3, uncertainty is entered at the level of the parameters that affect production rates. Definitely, level 2 and 3 are more thorough than level 1, but they require better knowledge of the project and a higher amount of effort in the estimation process. In assessing level 3 uncertainties, because of the peculiarities of fuzzy arithmetic, the processing of fuzzy parameters may create complex fuzzy membership functions which are difficult to manipulate in FPS.

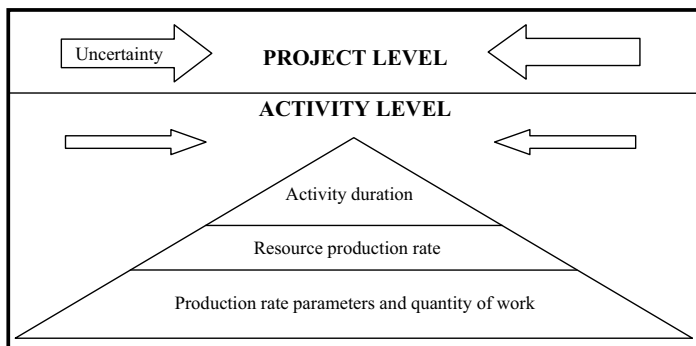


Figure 1. Uncertainty in construction.

Overall, uncertainties can be also classified into controllable and non-controllable risks. Examples of controllable risks (internal factors) are project characteristics, service providers influences and client organizational influences. Uncontrollable risks (external factors) can consist of socio-economic issues, unforeseen circumstances, economic and global dynamics, governmental/statutory controls (Mbachu and Nkado, 2007). In many cases, activity level risks are controllable whereas project level ones may be uncontrollable. The differentiation of the source of uncertainty between the project and activity level is crucial in determining the degree of controllability of risks.

NUMERICAL EXAMPLE OF PRODUCTION RATE CALCULATION

Road and motorway projects are often characterized by many uncertainties and require dedicated machinery and labor resources for their completion. For many years various performance handbooks have assisted project managers in estimating productivity and thereby project completion times. In particular, the Caterpillar Performance Handbook (2004) includes productivity estimations for tractors, graders, loaders, excavators, backhoe loaders, forest machines, pipelayers, scrapers, trucks, landfill compactors, pavers and asphalt pavers. Factors bearing directly on productivity include such things as weight to horsepower ratio, capacity, type of transmission, speeds and operating costs and are considered in detail. There are other less direct machine performance factors such as serviceability, parts availability and operator convenience. The Performance Handbook serves as an aid which, when coupled with experience and a good knowledge of local conditions, can assist in estimating true machine performance. Although, the data is based on field testing, computer analysis, laboratory research and experience it is sometimes necessary to correct the results indicated in the handbook tables by appropriate factors. Provisions are made for actual job efficiency, operator efficiency, material characteristics, haul

road conditions, altitude and other factors which may reduce performance or production on a particular job. More specifically, the production rate of a mass excavator is given by the following formula.

$$Q_e = \frac{60 \cdot V_e \cdot f}{t_s} \cdot \eta_e \quad (6)$$

Where Q_e : the production rate of an excavator in m^3/h , V_e : the bucket capacity in m^3 , f : the bucket fill factor, t_s : the cycle time in min and η_e : operational efficiency.

The above formula can be augmented with additional factors concerning operator skill/efficiency and machine availability. However, the key issue is that in the deterministic approach crisp numbers are utilized to calculate the excavator production rate. In Table 1, the specific crisp parameters yield a production rate of $352.75 \text{ m}^3/\text{h}$ for a 365B Series II excavator with a 4.0 m^3 rock bucket, an average bucket fill factor of 85 % which is reasonable for blasted rock and an estimated cycle time of 0.48 minutes. A general operational efficiency of 83 % is assumed.

Table 1. Excavator production rate

		Deterministic parameters	Fuzzy parameters
bucket capacity	$V_e (\text{m}^3)$	4	4
bucket fill factor	f	0.85	$\langle 0.75, 0.85, 0.90 \rangle$
cycle time	$t_s (\text{min})$	0.48	$\langle 0.43, 0.48, 0.52 \rangle$
operational efficiency	η_e	0.83	$\langle 0.80, 0.83, 0.86 \rangle$
production rate	$Q_e (\text{m}^3/\text{h})$	352.75	

An interesting alternative is to consider that the production rate parameters are uncertain and thereby they can be modeled with triangular fuzzy numbers. Table 1 shows how the bucket fill factor varies from 75-90 % for blasted rock. The fill factor depends on the type of soil/rock and can even attain values close to 100 % in good soil or 120 % in sand. The possible limits of uncertainty can be set by referring to the Performance Handbook or other recorded statistical data. Similarly, the cycle time is from 0.43-0.52 minutes for hard rock digging whereas the operational efficiency can vary from 80-86 %. It is noted that the bucket capacity still has a crisp value.

In this case the calculation of the production rate requires the use of a fuzzy calculator that performs the mathematical operations on these parameters. Because of the non-linearity of the multiplication and division operations the resulting membership function of the production rate depicted in Figure 2 is not a triangular fuzzy number. Unlike the deterministic evaluation the production rate varies from 276.9 to $432 \text{ m}^3/\text{h}$. Furthermore, it is possible to estimate the duration D of the activity by dividing the total amount of work W with the production rate Q .

$$\tilde{D} = \tilde{W} / \tilde{Q}_e \quad (7)$$

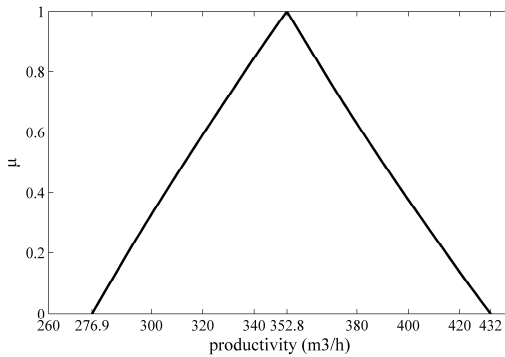


Figure 2. Membership function of excavator production rate.

In the specific example the total amount of work (9800, 10000, 10200) m³ is also a fuzzy number indicating that there is uncertainty in the initial total work quantity estimation. Since the derived duration membership function (see Figure 3) is not a triangular fuzzy number it may be difficult to manipulate in FPS and therefore an approximation with a triangular fuzzy number may alternatively be considered with a small degree of error. Here, the activity duration varies from 22.6 to 36.8 hrs. Additionally, in the event that an activity is realized by different resources an analysis is required to determine which one is driving the completion date.

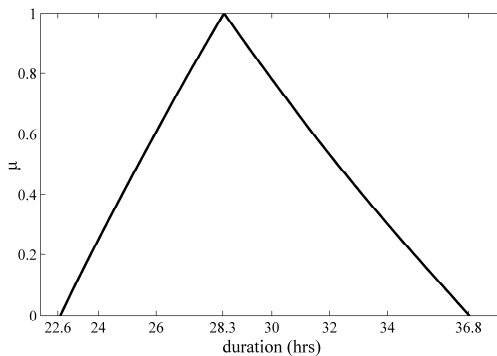


Figure 3. Membership function of activity duration.

Finally, the uncertainty in the calculated duration can be increased or decreased by considering the risk stemming from the project level. Thus, a factor of 1 can be considered in an average environment, a factor of 0.8 in an exceptionally favorable location or a factor of 1.2 in an adverse project execution environment. Figure 4

shows the inflation and deflation of project duration uncertainty of the initial fuzzy duration which is noted with the bold line. Understandably, the precise values of these inflation and deflation factors as well as the characteristics than define different locations are a subject of future research.

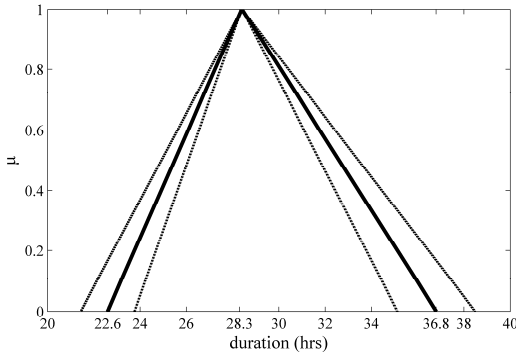


Figure 4. Inflation and deflation of duration uncertainty.

CONCLUSIONS

FPS is a very promising alternative to traditional scheduling methods. However, the current lack of transparency in the estimation of activity durations may hinder the validity of FPS. Therefore, the setting of guidelines for the estimation of the uncertainty of activities in FPS is crucial in avoiding certain pitfalls created by inaccurate and ill-supported uncertainty estimates. The in-depth analysis and calculation of productivity provides project managers with extra confidence about the accuracy and sources of uncertainties in the project schedule. In the specific example activity level uncertainty was identified from the type of soil, the total amount of work, the cycle time and the operational efficiency whereas project level uncertainty can be incorporated if deemed necessary. Furthermore, in large projects a similar process can assist in achieving homogeneous duration estimates in all activities. Obviously, there is a lot of hard work in moving from a vague perception and estimation of uncertainty to a very thorough calculation process. Compared to other approaches although this methodology involves fuzzy arithmetic, it is closer to practitioners knowledge domain than neural networks, genetic algorithms, etc. A software application including the parameters of the Caterpillar Performance Handbook that generates membership functions for different types of machinery could be an ideal starting point for this new approach and a means for performing uncertainty sensitivity analysis. Finally, it is acknowledged that the estimations of fuzzy productivity must be integrated with FPS in order to achieve widespread application in the construction industry.

REFERENCES

- Bonnal, P., Gourc, K., and Lacoste, G. (2004). "Where do we stand with Fuzzy Project Scheduling?" *J. of Constr. Eng. Manage.*, 130(1), 114-123.
- Castro-Lacouture, D., Süer, G. A., Gonzalez-Joaqui, J., and Yates, J. K. (2009). "Construction project scheduling with time, cost, and material restrictions using fuzzy mathematical models and Critical Path Method", *J. of Constr. Eng. Manage.*, 135(10), 1096-1104.
- Caterpillar (2004). *Caterpillar Performance Handbook (Edition 35)*, Illinois, U.S.A.
- Chanas, S., and Kamburowski, J. (1981). "The use of fuzzy variables in PERT." *Fuzzy Sets Syst.*, 5(1), 11-19.
- Chang, S., Tsujimura, Y., Gen, M., and Tozawa, T. (1995). "An efficient approach for large scale project planning based on fuzzy Delphi method." *Fuzzy Sets Syst.*, 76, 227-288.
- Chen, C. T., and Huang, S. F. (2007). "Applying fuzzy method for measuring criticality in project network." *Inform. Sciences*, 177, 2448-2458.
- Dubois, D., Fargier, H., and Galvagnon, V. (2003). "On latest starting times and floats in activity networks with ill-known durations." *Eur. J. Oper. Res.*, 147, 266-280.
- Fayek, A.R., and Oduba, A. (2005). "Predicting industrial construction labor productivity using fuzzy expert systems." *J. of Constr. Eng. Manage.*, 131(8), 938-941.
- Guiffrida, A. L., and Nagi, R. (1998). "Fuzzy Set Theory applications in production management research: A literature survey." *J. Intel. Manuf.*, 9(1), 39-56.
- Hapke, M., Jaskiewicz, A., and Slowinski, R. (1994). "Fuzzy Project Scheduling for software development." *Fuzzy Sets Syst.*, 67, 101-117.
- Herroelen, W., and Leus, R. (2005). "Project scheduling under uncertainty: Survey and research potentials." *Eur. J. Oper. Res.*, 165, 289-306.
- Karimi, S. M., Mousavi, S. J., Kaveh, A., and Afshar, A. (2007). "Fuzzy optimization model for earthwork allocations with imprecise parameters." *J. of Constr. Eng. Manage.*, 133(2), 181-190.
- Lorterapong, P., and Moselhi, O. (1996). "Project-network analysis using fuzzy sets theory." *J. of Constr. Eng. Manage.*, 122(4), 301-318.
- Marzouk, M., and Moselhi, O. (2004). "Fuzzy clustering model for estimating haulers' travel time." *J. of Constr. Eng. Manage.*, 130(6), 878-886.
- Mbachu, J., and Nkado, R. (2007). "Factors constraining successful building project implementation in South Africa." *Const. Manage. Econom.*, 25(1), 39-54.
- McCahon, C. S., and Lee, E. S. (1988). "Project network analysis with fuzzy activity times." *Comput. Math. Applicat.*, 15(10), 829-838.
- Prade, H. (1979). "Using Fuzzy Set Theory in a scheduling problem: A case study." *Fuzzy Sets Syst.*, 2, 153-165.
- Ross, T. J. (2004). *Fuzzy Logic with Engineering Applications (2nd Edition)*, John Wiley, Chichester, England.
- Zhang, H., Tam, C. M., and Shi, J. J. (2003). "Application of fuzzy logic to simulation for construction operations." *J. Comput. Civ. Eng.*, 17(1), 38-45.

Uncertainty Arithmetic on Excel Spreadsheets: Add-in for Intervals, Probability Distributions and Probability Boxes

Scott Ferson¹, James Mickley², and William McGill³

¹Applied Biomathematics, 100 North Country Road, Setauket, New York 11733 USA; phone 1-631-751-4350; fax -3425; email: scott@ramas.com

²Department of Ecology and Evolutionary Biology, University of Connecticut, Storrs, Connecticut 06269-3043; email: james.mickley@uconn.edu

³College of Information Sciences and Technology, Pennsylvania State University, 102L IST Building, University Park, Pennsylvania 16802; email wmcgill@ist.psu.edu

ABSTRACT

Despite their limitations as a platform for calculations, Microsoft Excel spreadsheets enjoy widespread use throughout much of engineering and science, and they have emerged as a lingua franca for computations in some quarters. Given their ubiquity, it would be useful if Excel spreadsheets could express uncertainty in inputs and propagate uncertainty through calculations. We describe an add-in for Microsoft Excel that supports arithmetic on uncertain numbers, which include intervals, probability distributions, and p-boxes (i.e., bounds on probability distributions). The software enables native calculations in Excel with these objects and ordinary scalar (real) numbers. The add-in supports basic arithmetic operations (+, -, ×, ÷, ^, min, max), standard mathematical functions (exp, sqrt, atan, etc.), and Excel-style cell referencing for both function arguments and uncertain number results. Graphical depictions of uncertain numbers are created automatically. Using function overloading, the standard Excel syntax is extended for uncertain numbers so that the software conducts uncertainty analyses almost automatically and does not require users to learn entirely new conventions or special-purpose techniques.

INTRODUCTION

Engineering is about numerical calculation. Engineers need to make calculations even when there is uncertainty about the quantities involved. Some uncertainty comes from the intrinsic variability in fluctuating performance environments, variation in materials, or small inconsistencies in manufacturing or realization of systems. These sources produce ‘aleatory’ uncertainty. Another kind of uncertainty, called ‘epistemic’ uncertainty, arises from measurement imprecision or lack of perfect knowledge about a system. For instance, in the early phases of engineering design, full specification of the intended system may not yet be available. Even after design specifications have been settled, there may be uncertainty about the future conditions in which the system will perform, or imperfect scientific understanding about the underlying physics or biology involved. In some cases, these uncertainties are small enough that they can be neglected, or swept away with a simple worst-case analysis. But when the uncertainties are large, this may not be possible, or will at least be suboptimal. Instead, a comprehensive strategy for accounting for the two kinds of uncertainty is needed that can propagate imprecise and variable numerical information through calculations.

Although modern risk analyses comprehensively treat stochastic variation using Monte Carlo simulation and other methods of probability, they often neglect arguably more fundamental kinds of uncertainty that arise from measurement error. Because all empirical measurements are unavoidably subject to some error, methods are needed to propagate the effect of such uncertainty through mathematical calculations. Dwyer (1951) introduced “range arithmetic” as a generalization of the arithmetic of significant digits which had been traditionally used to estimate the precision of calculations based on measured quantities. This approach is known today as interval arithmetic or interval analysis (Moore 1966; Adams and Kulisch 1993). The approach is broadly useful for epistemic uncertainty. Along with uncertainties from measurements, there is often considerable model uncertainty about the correct form of the mathematical expression that should be used, the appropriate family of probability distributions, and the true nature of dependencies among variables (Lambert et al. 1994; Haas 1997; 1999). Interval methods can be broadly useful in characterizing and propagating these structural uncertainties as well (Ferson and Ginzburg 1996). Although widely known, interval analysis is rarely formally used in science and engineering, and it has been almost completely ignored in probabilistic risk analysis. This is because intervals bounds are a rather crude encapsulation of uncertainty that is associated with the old worst-case paradigm of risk analysis.

A more practical approach to wrangling the two forms of uncertainty is to integrate interval analysis with probability theory. This combination can take many forms including interval probability, imprecise probabilities (Walley 1991), Dempster-Shafer theory, robust Bayes analysis, or probability bounds analysis (Yager 1986; Williamson and Downs 1990; Ferson 2002; Ferson et al. 2003), which is the method implemented in the Excel add-in described in this paper.

UNCERTAIN NUMBERS AND THEIR ARITHMETIC

The add-in enables Excel to do arithmetic with numbers of four kinds:

- **scalar** (known or mathematically defined integer or real value),
- **interval** (unknown value or values for which sure bounds are known),
- **probability distribution** (random values varying according to specified law such as normal, lognormal, Weibull, etc., with known parameters),
- **p-box** (random values for which the probability distribution cannot be specified exactly but can be bounded).

The software allows these four types of numbers to be freely mixed together in mathematical expressions to reflect what is known about each quantity. An interval is an uncertain number representing values obeying an unknown distribution over a specified range, or perhaps a single value that is imprecisely known even though it may in fact be fixed and unchanging. Intervals thus embody epistemic uncertainty. Uncertain numbers also include probability distributions which express aleatory uncertainty (i.e., variability), and p-boxes which express both aleatory and epistemic uncertainty (Ferson 2002; Ferson et al. 2003). Scalars in contrast may be called certain numbers. A user can specify scalars using any of the traditional computer representations such as 5 or 2.6 or $-4.7e-3$. Intervals can be specified by a pair of scalars corresponding to the lower and upper bounds of the interval. When entering an interval, the bounds are ordered, separated by a comma and enclosed by square

brackets, e.g., [2, 3] or [13.8, 22.2]. Intervals may also be given in plus-or-minus notation within square brackets, e.g., [2.5 +- 0.5] to represent 2.5 ± 0.5 which is equivalent to [2, 3]. Enclosing a single scalar in square brackets creates an interval implied by the significant digits the scalar has, e.g., [4.8] is equivalent to [4.75, 4.85]. Probability distributions are specified by their shape and parameters, such as **gaussian(5,1)**, **uniform(0,9)**, or **weibull(3,6)**. Over forty named distributions are supported. P-boxes can be specified as probability distributions with intervals for one or more of their parameters. If the shape of the underlying distribution is not known, but some parameters such as the mean, mode, variance, etc. can be specified (or given as intervals), the software will construct distribution-free p-boxes whose bounds are guaranteed to enclose the unknown distribution subject to constraints specified.

Interval arithmetic computes with ranges of possible values, as if many separate calculations were made under different scenarios. However, the actual computations the software does are made all at once, so they are very efficient. Probability bounds analysis integrates interval analysis and probabilistic convolutions which are often implemented with Monte Carlo simulations. It uses p-boxes, which are bounds around probability distributions, to simultaneously represent the aleatory uncertainty about a quantity and the epistemic uncertainty about the nature of that variability. Probability distributions are special cases of p-boxes, so one can do a traditional probabilistic analysis with the add-in as well. The calculations the software does are very efficient and do not require Monte Carlo replications.

Several example inputs for the add-in are listed in Figure 1. The add-in is currently set to summarize results graphically and to give the range of the calculated uncertain number, and, if determinable, its mean and variance (which may be known only to within bounds), and the shape of its distribution. The summary numerical and textual information is given on the cell in which the quantity was defined, as shown in Figure 2. As with ordinary Excel input, the user can edit the cell by pressing F2 or double-clicking on it. This restores the input originally entered by the user for modification. The graphical displays corresponding to the six uncertain inputs and calculations in the sample spreadsheet are shown in Figure 3. Intervals appear as rectangles, and probability distributions and p-boxes are depicted in terms of cumulative probability (which makes them graphically comparable to the intervals). These graphs appear in a special window devoted to the current calculation beside the worksheet, or on a separate tabbed worksheet. The detailed numerical information used to create these graphs is also accessible to the user in a separate tabbed worksheet. Whenever the user changes the current cell in the spreadsheet to one containing an uncertain number, the graphs and numerical values in these two worksheets are redisplayed.

```

1 [1,4]
2 [5,6]
3 uniform(5,12)
4 gaussian(C2,1)
5 =weibull(10,2)+weibull(8,12)
6 =C1+C3/C4+C5

```

Figure 1. Sample input for the Excel add-in.

	B	C	D	E	F	G	H
1		[1, 4]					
2		[5, 6]					
3		~uniform(range=[5,12], mean=8.5, var=4.083)					
4		~normal(range=[2.424,8.576], mean=[5,6], var=1)					
5		~(range=[0,32.211], mean=16.529, var=22.062)					
6		~(range=[1.583,41.161], mean=[18.9,22.4], var=[22.21,24.76])					
7							

Figure 2. Excel spreadsheet with summary numerical output.

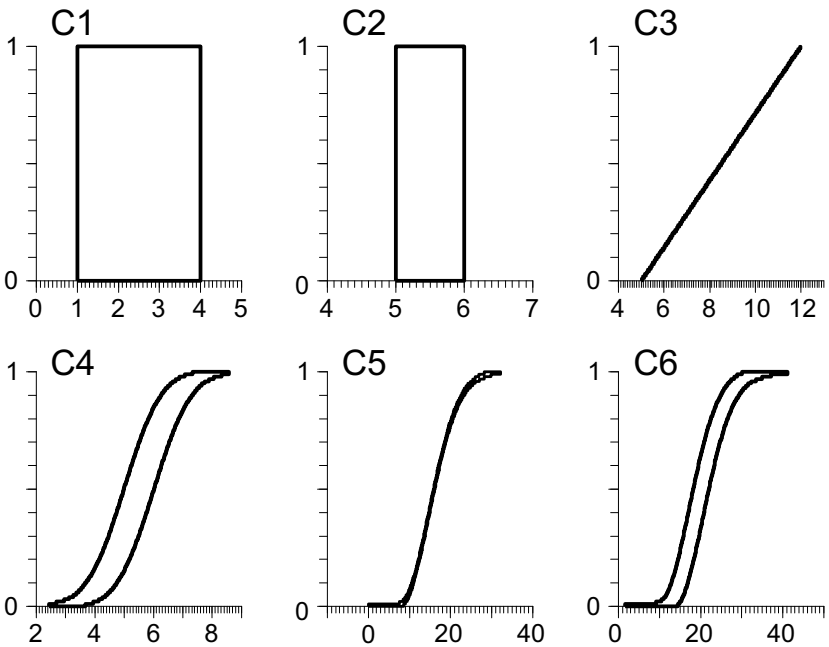


Figure 3. Graphical displays for the outputs of the sample spreadsheet.

The calculations in the first three rows of the example spreadsheet created two intervals and a uniform distribution, as depicted in the first row of graphs in Figure 3. The fourth calculation was specified as a Gaussian (normal) distribution with unit standard deviation but with mean given by the previously entered interval [5,6]. The imprecision of the mean makes this structure a p-box, as depicted in the lower, left graph of Figure 3. The lower, middle graph shows the convolution of two Weibull distributions, and the lower, right graph shows the p-box that results from combining an interval, a precise probability distribution, a p-box, and the sum-of-Weibulls distribution according to a particular formula. From this result, we can infer bounds on various statistics such as its range, mean, variance, median, and tail risks. For instance, the probability that the quantity is larger than 25 is between 0.1 and 0.29.

In principle, an existing Excel spreadsheet can be enriched by uncertainty analysis simply by altering one or more of the inputs to reflect the analyst's uncertainty. This might be as simple as placing square brackets around measured inputs to propagate the uncertainties implied by reported significant digits. Or it might be considerably more elaborate by expressing some uncertainty with distributions or intervals or combinations of both. The user would not have to alter the spreadsheet formulas used to compute results, nor specifically direct the uncertainty analysis itself.

Dependence assumptions. By default, the add-in assumes that each newly specified probability distribution or p-box is stochastically independent of every other. Users can change this assumption by specifying cells containing uncertain numbers on which the new distribution depends, and the nature of the dependence (perfect, opposite, positive, negative, or unknown). In addition, the add-in automatically tracks calculations that were used to compute uncertain numbers and will modify the default assumption of independence if appropriate. For instance, an increasing monotone function (such as log, exp, and sqrt) of a distribution creates an uncertain number that is perfectly dependent on the original distribution. Reciprocation creates an uncertain number that is oppositely dependent on the original distribution. When the function that transforms an uncertain number is complex and the relationship between the original distribution and the result cannot be deduced, the two are assigned the unknown dependence. If the two later are used in a calculation, Fréchet convolution, which makes no assumption about the dependence between the arguments, is used to combine them. Fréchet convolution must be used because an assumption of independence would be untenable, because one argument is a direct function of the other. Generally, Fréchet convolution creates p-boxes from precise probability distributions, or widens the results from p-boxes relative to convolutions that assume independence or some other precise dependence function. The extra width represents the additional uncertainty arising from not knowing the dependence function. Users can countermand the add-in's automatic tracking of dependence and specify the assumption to be used in any particular convolution.

EXCEL IS A POOR ENVIRONMENT FOR STATISTICAL COMPUTING

One might expect that the ergonomic disadvantages of spreadsheets generally (Panko 1998; Powell et al. 2008) and the well-documented inconsistencies sported by

the Microsoft Excel implementation particularly (Knüsel 1998; McCullough and Wilson 2002; McCullough and Heiser 2008; Yalta 2008) might be sufficient argument to dissuade a would-be user from adopting Excel spreadsheets as a platform for professional calculations. McCullough and Heiser (2008) have railed against Excel because of Microsoft's inability or unwillingness to correct serious statistical computing errors in the software, even many years after they have been documented. But as constant as Microsoft's failure to fix Excel is the public's continued use of the software and its expansion into error-critical domains. NASA even uses Excel as an integration platform for collaborative design of spacecraft (Parkin et al. 2003).

Accepting the Chinese proverb "better to light a candle than to curse the darkness" (or perhaps the English proverb "if you can't beat 'em, join 'em"), our goal in developing the add-in for Excel was to improve its usefulness in handling uncertainty so that users who might not have facility with the theory of imprecise probabilities can nevertheless benefit from uncertainty analyses. It surely does not seem reasonable to ignore these uncertainties or pretend they are always negligible. In fact, both epistemic and aleatory uncertainties are commonly quite large in many engineering problems. Therefore, they ought to be incorporated into any calculations. Making these analyses and their advantages widely available in a familiar and popular platform should, we expect, increase the demand for them in all fields where calculations are essential.

REPEATED UNCERTAIN NUMBERS

The main limitation to the routine use of the Excel add-in for risk and uncertainty analyses is the numerical complication arising from multiple occurrences of an uncertain variable in a mathematical expression. Consider the estimation of the quantity $ab + ac$ where a , b and c are all uncertain numbers. In some situations, its evaluation will differ from the evaluation of $a(b + c)$. The reason is that the uncertain number a appears twice in the first formulation and, in effect, the uncertainty it represents is entered twice into the resulting calculation. This is a result of the fact that the distributive law of real numbers $ab + ac = a(b + c)$ does not generally hold for uncertain numbers. This problem arises in most uncertainty calculi. Although the signal advantage of Monte Carlo methods is that they can escape this problem, it can also occur in a simulation conducted in multiple steps. For instance, if the first term ab in the example above is estimated with one simulation and then the second term ac and the final sum are estimated in a second, independent simulation, the uncertainty of a will have been introduced into the result twice.

Repeated occurrences of uncertain numbers in an expression should be canceled and reduced algebraically whenever possible to avoid possible distortion of the uncertainty. This guideline applies whether the uncertain numbers are intervals, probability distributions or p-boxes. Unfortunately, it is not always possible to reduce all multiple occurrences. For example, the expression $(a+b)/(a+c)$ cannot be reduced to a single instance of a . In such cases, special and often *ad hoc* strategies must be devised. In the context of interval analysis, at least we are guaranteed that multiple introduction of a quantity's uncertainty will yield a final result with a width *no smaller* than the correct answer. Thus, even if multiple occurrences of the variable cannot be eliminated, we can always compute a conservative estimate, which may

satisfy the practical needs of risk analyses. A similar guarantee accompanies Fréchet convolutions of probability distributions and p-boxes, but does not extend to convolutions that assume independence or other precise dependencies among the arguments. The magnitude of the consequence of failing to correct for a multiple occurrence of some quantity will depend on the details of the mathematical expression and the particular quantities involved.

CONCLUSION

The new add-in for Microsoft Excel spreadsheets supports interval arithmetic, probabilistic convolutions and their generalization probability bounds analysis. The add-in enables Excel users to account for the uncertainties in their calculations with a minimum of fuss and without having to learn a new software environment. The software observes Excel conventions and permits calculations that are less expensive computationally than alternative sampling-based approaches. It allows users to make calculations involving uncertain numbers (i.e., intervals, probability distributions, and p-boxes) which can be specified interactively according to what empirical information is available. The add-in supports standard operators and functions, including +, -, *, /, ^, max, min, exp, logs, sqrt, atan, etc. Binary operations are computed according to what can be assumed about the stochastic dependence between the operands. The add-in supports operations assuming the operands are independent, perfect, opposite, positive, negatively dependent, or without any assumption whatever about the dependence between the operands. The software chooses the appropriate dependence assumption automatically, but the choice may be overridden by the user. Operations and functions are transparently supported for pure or mixed expressions involving scalars, intervals, probability distributions and p-boxes. Expressions are evaluated as they are entered and the resulting values automatically displayed graphically.

There have been attempts to introduce interval methods to spreadsheets before, including the commercially unsuccessful Interval Solver from DeliSoft, which have led to improvements in Excel's Solver add-in (Fylstra et al. 1998). Add-ins for Excel that support probabilistic risk analysis have also been developed, prominently including the commercially successful Monte Carlo simulation software tools @Risk (Salmento et al. 1989) and Crystal Ball (Burmester and Udell 1990). Other stand-alone software packages have supported probability bounds analysis, including RAMAS Risk Calc (Ferson 2002) and DEnv (Berleant and Cheng 1998). The present implementation seems to be the first time the methods of probability bounds analysis have been made available for Excel spreadsheets.

ACKNOWLEDGMENTS

We thank Yan Bulgak for his indefatigable programming efforts. We also thank Troy Tucker, Jimmie Goode, Jack Siegrist, and Lev Ginzburg for their many contributions. This work was funded by a SBIR grant from NASA to Applied Biomathematics (contract NNL07AA06C). Lawrence Green from the Langley Research Center served as the Contracting Officer's Technical Representative. We thank him especially for his interest, patience and guidance.

REFERENCES

- Adams, E., and Kulisch, U. (1993). *Scientific Computing with Automatic Result Verification*. Academic Press, San Diego.
- Berleant, D., and Cheng, H. (1998). A software tool for automatically verified operations on intervals and probability distributions. *Reliable Computing* 4:71-82.
- Burmaster, D.E. and Udell, E.C. (1990). Crystal Ball. *Risk Analysis* 10: 343-345.
- Dwyer, P. (1951). *Linear Computations*. John Wiley, New York.
- Ferson, S. (2002). *RAMAS Risk Calc 4.0 Software: Risk Assessment with Uncertain Numbers*. Lewis Publishers, Boca Raton, Florida.
- Ferson, S., and Ginzburg, L.R. (1996). Different methods are needed to propagate ignorance and variability. *Reliability Engineering & Systems Safety* 54: 133-144.
- Ferson, S., Kreinovich, V., Ginzburg, L., Myers, D.S., and Sentz, K. (2003). *Constructing Probability Boxes and Dempster-Shafer Structures*. SAND2002-4015. Sandia National Laboratories.
- Fylstra, D., Lasdon, L., Watson, J., and Waren, A. (1998). Design and use of the Microsoft Excel solver. *Interfaces* 28(5): 29-55. www.solver.com/press200202.htm.
- Haas, C.N. (1997). Importance of distributional form in characterizing inputs to Monte Carlo risk assessments. *Risk Analysis* 17: 107-113.
- Haas, C.N. (1999). On modeling correlated random variables in risk assessment. *Risk Analysis* 19: 1205-1214.
- Knüsel, L. (1998). On the accuracy of statistical distributions in Microsoft Excel 97. *Computational Statistics and Data Analysis*, 26, 375-377.
- Lambert, J.H., Matalas, N.C., Ling, C.W., Haines, Y.Y., and Li, D. (1994). Selection of probability distributions in characterizing risk of extreme events. *Risk Analysis* 14: 731-742.
- McCullough, B.D., and Heiser, D.A. (2008). On the accuracy of statistical procedures in Microsoft Excel 2007. *Computational Statistics & Data Analysis* 52: 4570-8.
- McCullough, B.D., and Wilson, B. (2002). On the accuracy of statistical procedures in Microsoft Excel 2000 and Excel XP. *Computational Statistics & Data Analysis* 40(4): 713-721.
- Moore, R.E. (1966). *Interval Analysis*. Prentice Hall, Englewood Cliffs, New Jersey.
- Panko, R. (1998). What we know about spreadsheet errors. *Journal of End-User Computing* 10: 15-21. <http://panko.shidler.hawaii.edu/SSR/Mypapers/whatknow.htm>
- Parkin, K.L.G., Sercel, J.C., Liu, M.J., and Thunnissen, D.P. (2003). ICEMaker™: An Excel-based Environment for Collaborative Design. IEEEAC paper #1564.
- Powell, S.G., Baker, K.R., and Lawson, B. (2008). A critical review of the literature on spreadsheet errors. *Decision Support Systems* 46: 128-138.
- Salmento, J.S., Rubin, E.S., and Finkel, A.M. 1989. @Risk. *Risk Analysis* 9: 255-257.
- Walley, P. (1991). *Statistical Reasoning with Imprecise Probabilities*. Chapman & Hall.
- Williamson, R.C., and Downs, T. (1990). Probabilistic arithmetic I: Numerical methods for calculating convolutions and dependency bounds. *International Journal of Approximate Reasoning* 4:89-158.
- Yager, R.R. (1986). Arithmetic and other operations on Dempster-Shafer structures. *International Journal of Man-machine Studies* 25: 357-366.
- Yalta, A.T. (2008). The accuracy of statistical distributions in Microsoft Excel 2007. *Computational Statistics & Data Analysis* 52(10): 4579-4586.

Extended Uniform Distribution Accounting for Uncertainty of Uncertainty

James-A. Goulet¹, Ian F.C. Smith²

¹Swiss Federal Institute of Technology (EPFL), IMAC Laboratory, EPFL ENAC IS IMAC, Station 18, CH-1015, Lausanne, Switzerland; James.A.Goulet@gmail.com

²Swiss Federal Institute of Technology (EPFL), IMAC Laboratory, EPFL ENAC IS IMAC, Station 18, CH-1015, Lausanne, Switzerland; Ian.Smith@epfl.ch

ABSTRACT

Increasingly, uncertainties are explicitly considered for important engineering tasks. Often, little case-specific information is available for characterizing these uncertainties. Uniform distributions are an easy way to describe errors in absence of more precise information. In many situations, the bounds are fixed based on user experience. The extended uniform distribution (EUD) provides a probability density function that accounts for higher orders of uncertainty (uncertainty of uncertainty) when using a uniform distribution to describe errors. Since the EUD accounts for several orders of uncertainty it is more representative than uniform and curvilinear distributions. The extended uniform distribution helps increase the reliability and robustness of tasks requiring uncertainty combination through better representing incomplete knowledge of parameters.

KEYWORDS

Uncertainties, Extended uniform distribution, System Identification, CMS4SI

Uncertainty is a fundamental part of applied science research. Uncertainty is usually used to describe the distribution of an error through its probability density function (PDF). An error PDF may either be used as itself or it may be combined with other sources of uncertainties. This is called propagation of uncertainties. Several methods are available to propagate uncertainties through models (JCGM 2008a; JCGM 2008b). These methods involve a combination of model-parameter uncertainties into a single probability density function describing the overall uncertainty of model predictions. Propagation methods assume that the uncertainties are adequate representations of the error. In many cases, little information is available for characterizing uncertainties. In absence of knowledge other than the position of minimal and maximal error bounds, the uniform distribution is often chosen according to the principle of maximum entropy (Jaynes 1957). Bounds are usually

defined based on user experience. Therefore, an uncertainty can be assigned to the position of minimal and maximal bounds. These three distributions can be combined (the main uncertainty plus the two uncertainties on the minimal and maximal bound position) into a curvilinear probability distribution function (Lira 2008; Raghu and James 2007; Raghu and James 2010). Figure 1 shows an example of this function.

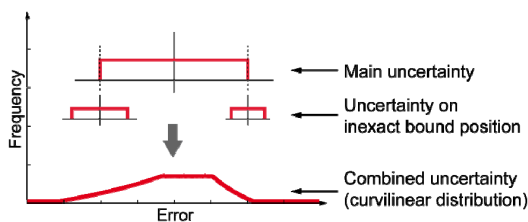


Figure 1 – Example of a Curvilinear Probability Distribution Function

This distribution was adopted in a metrology guideline for expression of uncertainty in measurements as the probability density function to use when the upper and lower limit of an uniform distribution are not known exactly (JCGM 2008a).

The curvilinear distribution represents a more robust representation of uncertainty when compared with the uniform distribution. However, one question remains; are the bounds of the uncertainty on bound positions exactly known? Since the answer is rarely positive, the concept behind the curvilinear distribution needs to be extended in order to account for the inexact position of bounds for higher orders.

This paper introduces the extended uniform distribution (EUD) which overcomes the limitation mentioned above. The first part presents the concepts behind EUD. The second section explains how samples can be drawn from the extended uniform distribution. The third section presents the result of a comparative study between uniform, EUD and the curvilinear distribution and shows how curvilinear distribution is a special case of EUD. In this section, the impact of the number of orders of uncertainty accounted for is studied. Finally, the last section provides a discussion of the results obtained and the use of the extended uniform distribution.

EXTENDED UNIFORM DISTRIBUTION

The Extended Uniform Distribution (EUD) accounts for the uncertainty over the bound position for multiple orders of uniform distributions. Figure 2 shows the resulting probability density function obtained using EUD.

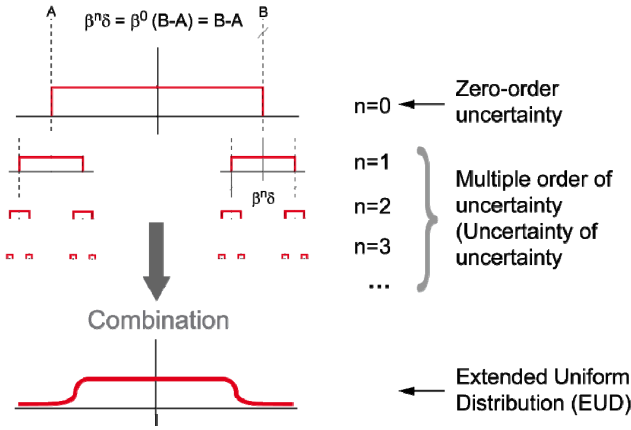


Figure 2 - Extended Uniform Distribution

In this figure, the main uncertainty ($n=0$) on a given quantity is expressed by a uniform distribution. For illustration purposes, assume that it represents the probability that a modelling error has a certain value. Since errors are never known exactly, the position of the lower and higher bounds ($A, B, A \leq B$) of this distribution are fixed based upon engineering experience. A constant β expresses the uncertainty on the bound positions as a fraction of the zero-order uncertainty varying between zero and one. For the zero-order uncertainty: $\beta^0 \delta = \beta^0 (B-A) = B-A$. The first order of uncertainty ($n=1$) accounts for incomplete knowledge of the exact position of each bound. For the purpose of illustration, it is assumed that the uncertainty on the lower and upper bounds are the same. The width of the uniform distributions representing the uncertainty on the position of bound A and B is: $\beta^1 \delta = \beta \delta = \beta (B-A)$. The combination of these uncertainties would lead to a curvilinear distribution. However, as mentioned above, the knowledge on the position of the bounds for the order one ($n=1$) is also incomplete. Therefore, the second order of uncertainty ($n=2$) accounts for incomplete knowledge of order one. The width of the uniform distributions representing the uncertainty on the position of bound of the first order is: $\beta^2 \delta = \beta^2 \delta = \beta^2 (B-A)$. Combining general uncertainty orders leads to the extended uniform distribution (EUD). Compared with the uniform distribution, the EUD better represents the lack of knowledge related to the upper and lower-bound positions when user experience is used to fix uncertainties.

SAMPLING FROM AN EXTENDED UNIFORM DISTRIBUTION

The extended uniform distribution may be used in a Monte-Carlo uncertainty combination process as described in the Supplement 1 of JCGM (2008b). In this section a sampling procedure is presented for the case where the uncertainties on the lower and higher bounds are equal (a single value of β is required). These guidelines also allow for unequal uncertainties.

The number of orders of uncertainty has to be fixed initially in order to obtain a stable EUD probability density function. This step is required since it is not possible to sample over an infinite number of uniform PDF in a numerical process. It is possible to obtain a good approximation using a limited number of orders since the influence of each order decreases exponentially. A study of the number of orders is presented in Section 0. The sum of the maximal bound position for an infinite number of orders, as shown in Equation 1, converge to a finite limit. As n becomes larger, the contribution of each order tends to zero

$$\sum_{n=0}^{\infty} \frac{\beta^n (B-A)}{2} \quad (1)$$

In this equation, A and B are respectively the lower and upper bound of the main uncertainty described by a uniform distribution and where β varies between zero and one.

To generate EUD samples, a sparse matrix M of size $[NBO, 2^{NBO}]$ is created, where NBO is the number of orders. For each row $i=1..NBO$, the columns 1 to 2^i are filled with uniformly distributed number between 0 and 1. For one sample, the uncertainty propagation process starts with the last row (highest uncertainty order number) and propagates up to the main uniform distribution (first row). The algorithm that propagates uncertainties is presented below.

```
for i=[NBO:-1:2]
  for j=1:2:(2^i)
    beta_loop=( (beta/2) ^ (i-1) ) * (B-A)
    M(i,j)=M(i,j)-beta_loop
    M(i,j+1)=M(i,j+1)+beta_loop
    M(i-1, (j-1)/2+1)=M(i,j)+ (M(i,j+1)-M(i,j)) * rand(1)
  end
end
```

Logically, the upper bound for the error must always remain larger than its lower bound. In the stochastic process for sampling in the EUD, it could be possible to generate uncertainty of uncertainty that do not respect that criterion. Therefore, the second part of the code verifies that at zero-order the upper bound (B) is larger or

equal to the lower bound (A). If the condition is fulfilled, it generates a sample for the extended uniform distribution, if falsified, it discards the generation.

```

if M(2,1) >= M(1,1)
    EUD_sample = M(1,1) + M(2,1) - M(1,1) * rand(1)
end

```

Note that for β values smaller or equal to 0.5 the inequality is always satisfied. During Monte-Carlo analysis, the procedure presented above is often repeated several thousand times in order to achieve a target reliability.

A COMPARISON BETWEEN UNIFORM, EUD AND CURVILINEAR DISTRIBUTION

This section presents a comparative study between the uniform, the EUD and the curvilinear distribution. Figure 3 show the EUD distribution obtained using only one level of uncertainty ($n=1$). This case is equivalent to the curvilinear distribution. In this figure, the horizontal axis represents the error and the vertical axis is the normalized probability at which each error value should be obtained. The different curves are computed from a Monte-Carlo analysis over 10,000,000 samples by varying the value for β between zero and one. When β is equal to zero, the result obtained is a uniform distribution having lower and upper bounds of -1 and 1.

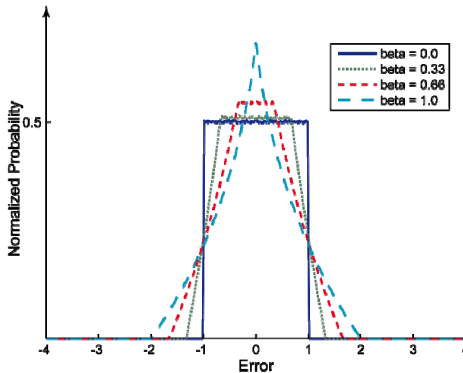


Figure 3 - Extended Uniform Distribution with one Order of Uncertainty ($N=1$)

The PDF shapes diverge from the uniformly distributed shape as the β value increases; all curves have an integral equivalent to unity. Apart from the small variations due to numerical sampling, the distribution shows sharp edges at their extremities and at the intersection with the constant central portion. Figure 4 shows the PDFs for the same conditions as in Figure 3, except that this time, several order of uncertainty are used.

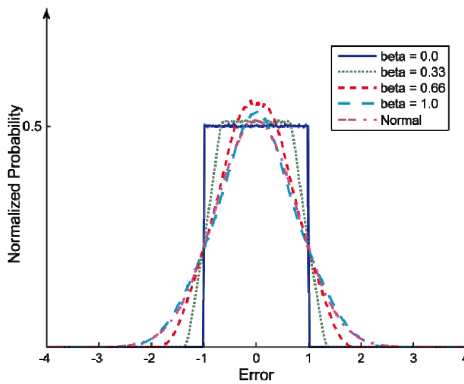


Figure 4 - Extended Uniform Distribution with Several Orders of Uncertainty ($N > 1$)

Again, when β is equal to zero, the result obtained is a uniform distribution having lower and upper bounds of -1 and 1. For values of $\beta > 0$, the EUD curves shows smoother transitions than the curvilinear distribution. When $\beta = 1$ the shape obtained is close to a normal distribution (also shown in Figure 4) having the same standard deviation (as $EUD(\beta = 1)$).

Figure 5 presents the evolution of the 95% reliability bounds as a function of the β value and the number of orders taken into account in EUD distribution for zero-order distribution of -1 to 1. In this figure, the β value is plotted on horizontal axis and the bound defining a coverage interval of 95% for each PDF is plotted on the vertical axis. In addition to the EUD distribution using one to four levels of uncertainty, the results obtained with a uniform and a normal distribution (having the same standard deviation as “EUD – 4 orders”) are shown. In the case of the uniform distribution and when $\beta = 0$ the 95% reliability bound has a value of 0.95. For EUD using any number of uncertainty level, the reliability bound increases when the uncertainty over the exact bound position increases. For small values of β (< 0.5) there is no significant change between a curvilinear and EUD distributions. For $\beta \geq 0.5$, the discrepancy between the two distributions types (curvilinear and EUD) increases. For $\beta = 1$, EUD shows a reliability bound almost equal to a normal distribution having the same standard deviation.

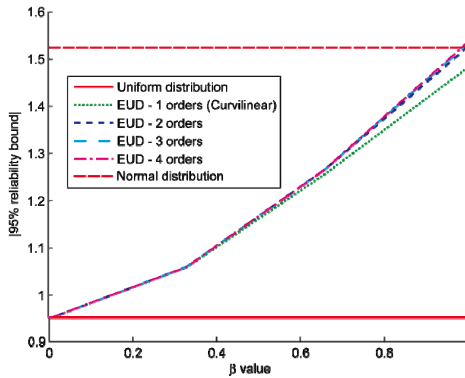


Figure 5 - Evolution of 95% reliability bounds in relation with uncertainty order and beta value for a zero-order distribution from -1 to 1

For $0 \leq \beta \leq 1$ the reliability bounds obtained from extended uniform distributions using a number of levels of uncertainty larger than one for these distributions can all be considered as equivalent for engineering purposes and the PDFs obtained are all similar to the one showed in Figure 4.

DISCUSSION

For engineering applications, two or three orders of uncertainties (as shown in Figure 5) may be sufficient to obtain a close approximation of the extended uniform distribution. Also, in every situation, the EUD distributions provide equal or conservative reliability bounds compared with the curvilinear distributions.

Uniform distributions are often used to describe an error distribution. If the knowledge related to the position of the bounds defining the distribution is incomplete, the extended uniform distribution can be used. For practical applications, when the uncertainty on the exact position of the bounds describing the distribution is large (for instance $\beta = 1$), the EUD distribution can be replaced by a normal distribution having the same mean as the main uniform distribution and a standard deviation equal to 0.39 times the zero-order interval width. This value was determined numerically from $1E7$ samples.

The concept of higher order uncertainty and EUD can be used to define the probability density function of errors in system identification tasks. A methodology proposed by Goulet and Smith (2010) explicitly accounts for uncertainty coming from model and measurements in order to identify the behaviour of systems. In such a case, modelling uncertainties may only be quantified through relying on

engineering experience. Therefore, the EUD may increase the utility the identification outcome.

CONCLUSIONS

1. The extended uniform distribution (EUD) provides a probability density function that accounts for uncertainty of uncertainty when using uniform distributions to describe errors. EUD accounts for several orders of uncertainty making it more representative than uniform and curvilinear distribution.
2. The extended uniform distribution has the potential to increase the reliability and robustness of decision making that requires the combination of uncertainties through better representing incomplete knowledge of parameters such as modelling uncertainty.

ACKNOWLEDGEMENTS

This research is funded by the Swiss National Science Foundation under contract no. 200020-117670/1.

REFERENCES

- Goulet, J.-A., and Smith, I. F. C. (2010). "Structural Identification with Correlated Uncertainties." *Engineering Structures (Submitted for publication)*.
- Jaynes, E. T. (1957). "Information Theory and Statistical Mechanics. II." *Physical Review*, 108(2), 171.
- JCGM. (2008a). "Evaluation of measurement data - Guide to the expression of uncertainty in measurement." Bureau international des poids et mesures, Paris, France.
- JCGM. (2008b). "Evaluation of measurement data - Supplement 1 to the "Guide to the expression of uncertainty in measurement" - Propagation of distributions using a Monte Carlo method." Paris, France.
- Lira, I. (2008). "The generalized maximum entropy trapezoidal probability density function." *Metrologia*, 45(4), L17.
- Raghu, N. K., and James, F. L. (2007). "Trapezoidal and triangular distributions for Type B evaluation of standard uncertainty." *Metrologia*, 44(2), 117.
- Raghu, N. K., and James, F. L. (2010). "Rectangular distribution whose end points are not exactly known: curvilinear trapezoidal distribution." *Metrologia*, 47(3), 120.

Efficiency Comparison of Markov Chain Monte Carlo Simulation with Subset Simulation (MCMC/ss) to Standard Monte Carlo Simulation (sMC) for Extreme Event Scenarios

Duzgun Agdas¹, Michael T. Davidson², Ralph D. Ellis¹

¹Department of Civil and Coastal Engineering, University of Florida. P.O. Box 116580, Gainesville, FL 32611; PH (352) 392 9537; e-mail: duzgun@ufl.edu, relli@ce.ufl.edu.

²Civil Engineering Department, University of Kentucky, 382 O. H. Raymond Bldg, Lexington, KY 40503; PH (352) 562 1404; email: michael.davidson@uky.edu.

ABSTRACT

Standard Monte Carlo (sMC) simulation models have been widely used in AEC industry research to address system uncertainties. Although the benefits of probabilistic simulation analyses over deterministic methods are well documented, the sMC simulation technique is quite sensitive to the probability distributions of the input variables. This phenomenon becomes highly pronounced when the region of interest within the joint probability distribution (a function of the input variables) is small. In such cases, the standard Monte Carlo approach is often impractical from a computational standpoint. In this paper, a comparative analysis of standard Monte Carlo simulation to Markov Chain Monte Carlo with subset simulation (MCMC/ss) is presented. The MCMC/ss technique constitutes a more complex simulation method (relative to sMC), wherein a structured sampling algorithm is employed in place of completely randomized sampling. Consequently, gains in computational efficiency can be made. The two simulation methods are compared via theoretical case studies.

INTRODUCTION

Although inherent to most of the AEC industry business activities, incorporating uncertainty into process analysis has been a somewhat recent development, most likely due to recent increases in personal computing power. The most prolific and commonly used method in addressing the uncertainty in AEC industry has been the Standard Monte Carlo Simulation (sMC) technique, which consists of a simple, yet extremely robust algorithm. The sMC technique has been used in various aspects of the AEC research from, risk analysis (Akintoye and McLeod 1997), to scheduling (Lee, 2005) and cost engineering (Chau 1995).

The standard Monte Carlo simulation technique consists of repeatedly, independently sampling values of random variables within a system and evaluating performance functions of interest for each set of sampled values, if necessary. Each set of sampled random variable values is considered to be one possible (simulated) state for a physical system or process of interest. A certain number of repeated simulations are carried out to obtain a probabilistic outcome for the process of

interest. The effectiveness and pervasiveness of the sMC approach as a probabilistic simulation technique is well documented in the literature (e.g., Melchers 1999).

OVERVIEW OF THE sMC

The sMC simulation technique is used in conjunction with the inverse CDF method of random variable value generation. The inverse CDF method begins with the generation of a random number, Y_i , which is obtained from a uniform probability distribution function (PDF), q_Y . Given Y_i , a CDF value (or cumulative probability), Q_{Y_i} is determined according to the governing CDF, Q_Y . A CDF value, Q_{U_i} , is then defined subject to the constraint:

$$Q_{U_i} = Q_{Y_i} \quad \text{Equation 1}$$

Using Q_{U_i} and the CDF, Q_U (which corresponds to the random variable U), a sample U_i is then obtained. A random number is drawn for each variable within the physical model, a value which is later used in order to obtain the value of the parameter of interest using the probability distribution of the variable. By doing so, randomization of the parameters that consist of the physical model, within their respective distributions, is accomplished. Thus, the sMC simulation technique has a clear edge over the deterministic approaches because of its ability to incorporate uncertainty to physical models developed without imposing any bias.

A PROBLEMATIC CASE: JOINT PROBABILITY DISTRIBUTION

One possible shortcoming of the sMC approach results from its biggest strength, the completely randomized sampling of the variables within the physical model. A common assumption in using sMC in physical models is that the parameters within the models are independent and only discretely related. When the main parameter of the interest is dependent on the joint probability of the multiple variables, especially when this area of interest is rather small, the completely randomized sampling will, as a result, suffer from computational inefficiencies.

To illustrate this problem more accurately a hypothetical case scenario has been devised (Davidson 2010), in which the reliability of a structural component is assumed to be based on two factors only, load (S) and resistance (R). In this context, structural failure will take place for any simulated state in which the load (S) exceeds the design resistance (R). Four different case scenarios were designed in order to assess the computation requirements to achieve meaningful solutions using sMC. In each case the systems load is assumed to be normally distributed with a mean of 60 kips and a standard deviation of 10. Different resistance values were devised in order to vary the joint probability of the load and resistance (Table 1). Note that the resistance values were chosen to make the joint probability of two variables 0.1, 0.01, 0.001 and 0.0001 for different cases. As both S and R variables are assumed to be normally distributed probability of load exceeding the resistance can be explicitly calculated (The explicit calculation steps can be found in Field 2009).

Table 1. Different Case Scenarios

	S	R ₁	R ₂	R ₃	R ₄
Mean, μ	60	74.3	86	94.5	101.5
St. Dev., σ	10	5	5	5	5
P(R<S)		0.1	0.01	0.001	0.0001

OVERVIEW OF THE sMC ALGORITHM

An overview of the sMC algorithm, as it pertains to the two parameter demonstration case, is shown in Table 1. Given statistical descriptions of the system random variables R and S ; the applicable limit state function ($R<S$); and, the corresponding limit state exceedance probabilities (0.1, 0.01, 0.001, 0.0001), the approximate number of simulations, n , required to obtain a meaningful sMC estimate of the limit state exceedance rate, p_{sMC} , may be determined using the required level of reliability of the sMCS. Because of the unbiased random number generation, a sufficient number of simulation cycles are necessary to confirm that the results are consistent. i.e. the failure probability plane defined in this paper is, theoretically, a normally distributed joint probability. Thus, provided enough sMCS were to be run, the resulting failure plane would have to be normally distributed. Although it is not critical in this case as the focus is point failure estimates rather than a distribution, if a failure distribution were to be developed a substantial number of simulation runs would have been necessary to achieve the failure probability distribution convergence. The number of simulations run, thus, becomes highly influential in determining the reliability of the estimates obtained from sMCS. In structural reliability literature the sample size has been of great interest and using an empirical formula and a predetermined standard dispersion measure, the sample size for a probability failure can be determined.

A meaningful estimate is defined as—in the context of the two-parameter demonstration case—a p_{sMC} value with a coefficient of variation (COV) less than or equal to 0.1, such that:

$$n = \frac{1 - p_{sMC}}{\delta_{sMC}^2 \cdot p_{sMC}} \quad \text{Equation 2}$$

where δ_{sMC}^2 is the COV associated with p_{sMC} . Note that COV is a measure that is used to standardize the spread of the data points for a given set of points. In this case, the COV has been selected to assess the reliability of different simulation results and the rather conservative value 0.1 was chosen to signify the importance of the accuracy of different simulation runs related to the structural reliability. Using the explicit solution for the failure probability for the given R and S values and the COV value of 0.1, the number of simulations necessary was determined. For probability of failure values of 0.1, 0.01, 0.001 and 0.0001, the required number of simulations has been determined to be 900, 9900, 99900 and 999900 respectively.

LIMITATIONS OF THE sMC APPROACH

It should be noted that the joint probability cases devised for this paper are overly simplified interpretation of a real-world problem. More realistic modeling will not only include more variables and more complex distributions, but also it might be

more beneficial to obtain an outcome distribution instead of a point prediction which was the case in this example. Thus, the number of necessary sMC simulations is likely to be much greater when additional complexities are incorporated. An innovative approach, “Subset Simulation”, originally proposed by Au and Beck (2001) is used to maximize the efficiency of the computational efforts. The authors (Au and Beck) suggested use of the subset simulation for cases in which the joint probability of the interest region is too small to efficiently utilize more traditional sMC.

OVERVIEW OF THE MCMC/ss

For a given target reliability level for different batches of simulation sets (e.g., failure probability estimate COV), the computational requirement associated with the sMC approach increases inversely proportional to size of the probability region of interest. In contrast, the corresponding computational requirement associated with the MCMC/ss approach increases in an approximately logarithmic manner (Au et al. 2007). Hence, the relative efficiency of the MCMC/ss approach increases slowly (relative to the sMC approach) as the probability of interest approaches zero making MCMC/ss a viable candidate for the extreme event simulation cases. Unlike sMC, the MCMC/ss procedure is divided into sequential stages of simulation (subsets), where selected data from one subset is supplied to the next subset until the probability estimate of the area of interest is obtained. For each subset, the simulation parameters are constrained to the results at or below a prescribed probability of a specific threshold value. For systems with small probability regions of interest, therefore, the process of estimating these probabilities is divided into a series of generating simulated states that satisfy prescribed, decreasing probability thresholds. As a result, high levels of efficiency can be achieved through the use of MCMC/ss.

GENERAL OVERVIEW OF THE MCMC/ss ALGORITHM

The MCMC/ss process begins with sMC simulation, which is referred to as subset 0 . For subset 0 , the minimum probability of exceedance threshold is initialized to 1 (no constraint is placed on the generation of simulated states). Using the results from subset 0 , however, a probability of exceedance threshold is determined for the next stage of simulation, subset 1 . Specifically, a pre-determined number of the subset 0 simulation results (points) are selected as subset 1 seed values that would be evaluated as candidates for the next subset. Simultaneously, the selected points define the probability of exceedance threshold for subset 1 , and furthermore, initialize (or seed) the subset 1 simulations.

It has been recommended in the literature that, for all subsets, values at the 90th percentile and greater (in terms of proximity to failure) are carried over from one subset to the next (Au and Beck 2001). This selection dictates the permissible region that can be explored within a given subset. For example, a selection of simulation results (from the pool of subset 0 simulations) at the 90th percentile is tantamount to identifying those simulations with a probability of exceedance less than or equal to 0.1. The point among the subset 1 seed values that is farthest from the limit state boundary has a probability of exceedance of 0.1 (in an empirical sense), and is used to define a minimum demand boundary, which is referred to as the subset 1 threshold.

The subset l threshold is simply a mapping of the probability of exceedance (i.e., 0.1) in the plane (space) of the limit state.

Given the subset l seed values and the subset l threshold, the next stage of simulation (subset l) can be carried out. In this stage, random variables are sampled using a modified Metropolis-Hastings Sampling (MHS) scheme, rather than the inverse CDF method (associated with the sMC approach). For a given simulated state (e.g., a seed value), the modified MHS technique perturbs the present state in order to produce the next state (rather than independently sampling the next simulated state). Samples formed in this way “step” from one simulation point to the next, producing a chain of simulations (referred to as a Markov Chain). Specific to the MCMC/ss approach is the constraint that all simulations conducted in subset l are constrained such that simulation results cannot fall below the subset l threshold (Fig. 1).

The subset l Markov Chain steps are continued until the total number of simulations conducted in subset l becomes equal to the number of simulations, n , conducted in subset 0 . Then, the process of selecting subset 2 seed values and the subset 2 threshold is carried out in a manner that is analogous to that used for the previous subset. Consequently, given that a 90th percentile selection process is carried out using the pool of subset l simulation results, then the probability of exceedance threshold associated with the subset 2 seed values corresponds to a probability of exceedance that is one-tenth of the corresponding subset l probability of exceedance level (0.1). Consequently, the probability of exceedance threshold associated with the subset 2 seed values is 0.01. The process of carrying out subsets of Markov Chain simulations, selecting seed values, and determining a minimum threshold for the next subset is repeated until all of the seed values for subset t correspond to values that reach or exceed the limit state boundary. Subsequently, the failure probability can be estimated as (Au and Beck 2001):

$$p_{\text{MCMC/ss}} = f_{\text{exc}}^t \cdot NF / n_{\text{sub}} \quad \text{Equation 3}$$

where $p_{\text{MCMC/ss}}$ is the MCMC/ss probability of failure estimate; t , as an exponent, is the final subset number; f_{exc} is the probability of exceedance threshold factor (e.g., a 90th percentile selection process corresponds to a f_{exc} value equal to 0.1); NF is the number of simulation values in subset t that exceed the limit state boundary; and, n_{sub} is the number of simulations carried out in subset t .

RANDOM VARIABLE VALUE GENERATION FOR MCMC/ss

For all subsets beyond subset 0 , the MCMC/ss simulation technique requires the use of the modified Metropolis-Hastings Sampling (MHS) (and starting seed values of random variables) for random variable value generation as part of the Markov Chain steps. The purpose of modified MHS is to facilitate the generation of “candidate” random variable values. Candidate values of random variables are, in turn, used to evaluate a limit state function of interest, and if the candidate values constitute an acceptable simulated state (i.e., if the simulation results satisfy the applicable probability of exceedance threshold), then the candidate random variable values are

retained as seed values for the next step in the Markov Chain. Otherwise, the Markov Chain remains in place (the step length is zero), and the sampling process is repeated.

The process of generating candidate random variable values is illustrated in Fig. 2 for the random variable U of arbitrary distribution, q_U . Given a previously obtained seed value, U_j^{seed} , for simulation j , a uniform PDF, $q_{U_j^{pre}}$, is formed such that the mean value is U_j^{seed} and the standard deviation is equal to that associated with the random variable U . The PDF $q_{U_j^{pre}}$ is then used to generate a “pre-candidate” sample value, U_j^{pre} . An acceptance ratio, r_j , is then calculated as:

$$r_j = \min\left(1, \frac{q_U(U_j^{pre})}{q_U(U_j^{seed})}\right) \quad \text{Equation 4}$$

where $q_U()$ indicates the evaluation of the PDF frequency. The acceptance ratio, r_j , is then compared to Y_j , which is a randomly sampled number between 0 and 1 in accordance with q_Y . If r_j is greater than Y_j , U_j^{seed} is retained as the candidate sample. Otherwise, the pre-candidate sample, U_j^{pre} , is accepted as the candidate sample.

DEMONSTRATION CASE SOLUTION USING MCMC/ss ALGORITHM: SUBSET 0

Given values of n_{sub} , f_{exc} , and statistical descriptions for R and S , the sMC method is employed. For each simulation i , values of R_i , S_i , and Z_i are stored in arrays $\{R_i\}_0$, $\{S_i\}_0$, and $\{Z_i\}_0$, respectively; additionally, for any instances where Z_i is less than or equal to zero (recall Equation 2), the failure tabulation parameter, NF , is incremented. After n_{sub} sMC simulations have been carried out, the entries of $\{Z\}_0$ are ranked in increasing order, and the ranked values are stored in $\{Z^{sort}\}_0$. Arrays for the R and S parameters are then formed ($\{R^{sort}\}_0$ and $\{S^{sort}\}_0$, respectively) to maintain consistency with the ranked entries in $\{Z^{sort}\}_0$. Then, a threshold entry parameter, j_{TH} , is calculated:

$$j_{TH} = \lfloor n_{sub} \cdot f_{exc} \rfloor \quad \text{Equation 5}$$

DEMONSTRATION CASE SOLUTION USING MCMC/ss ALGORITHM: SUBSET 1

Given values of n_{sub} ; f_{exc} ; the subset I seed values; and, the subset I threshold value, Markov Chains are formed, where one Markov Chain is initialized at each subset I seed value. The length (number of steps) of each Markov Chain, n_{step} , is dictated by:

$$n_{step} = \lfloor n_{sub} / \text{length}(\{Z^{seed}\}_1) \rfloor \quad \text{Equation 6}$$

where $\text{length}()$ indicates the evaluation of the number of entries in an array. Then, for each subset I seed, a Markov Chain consisting of n_{step} simulation points is formed using modified MH sampling (Fig. 3, middle). During formation of the Markov Chains, if any values stored $\{Z\}_1$ are found to be less than or equal to zero, then the failure tabulation parameter, NF , is incremented. When the total number of simulations conducted becomes equal to n_{sub} , the ranked $\{Z^{\text{sort}}\}_1$ array, and the corresponding arrays $\{R^{\text{sort}}\}_1$ and $\{S^{\text{sort}}\}_1$, are formed in the same manner as that described for subset 0 . Then, the threshold entry parameter, j_{TH} , is calculated for subset I using Eq. 5. Analogous to that of subset 0 , if the entry $\{Z^{\text{sort}}_{j_{\text{TH}}}\}_1$ is less than or equal to zero, then no additional simulation conduction is required and the failure probability estimate, $p_{\text{MCMC/SS}}$, can be calculated (recall Eq. 3). If, however, the entry $\{Z^{\text{sort}}_{j_{\text{TH}}}\}_1$ is greater than zero, then the subset 2 seed values and the subset 2 threshold value are formed (Fig. 4, bottom left), where the formation process is identical to that described for the corresponding subset I quantities. Subsequently, the subset 2 simulations can be carried out.

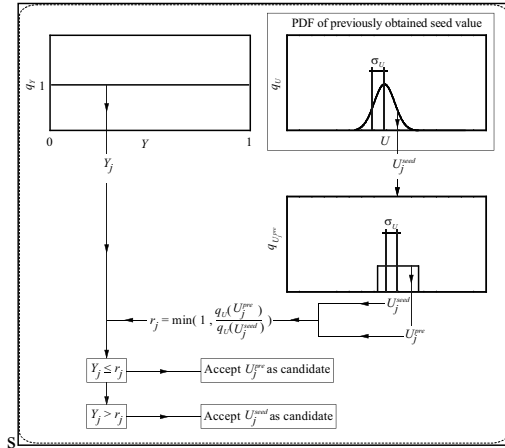
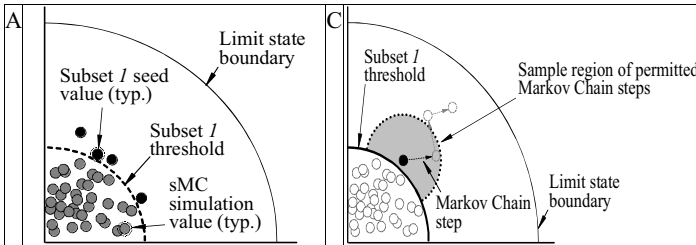


Figure 1. MHS algorithm



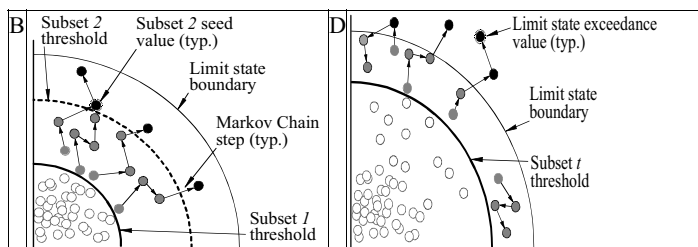


Figure 2. Overview of MCMC/ss

DEMONSTRATION CASE SOLUTION USING MCMC/SS ALGORITHM: SUMMARY

The MCMC/ss algorithm, as it applies to the demonstration case, is summarized in Fig. 3. For subset t —using results from the simulations conducted for subset t —the quantities NF , j_{TH} , and $\{Z_{j_{TH}}^{sort}\}_t$ are calculated. Then, if the value of $\{Z_{j_{TH}}^{sort}\}_t$ is calculated to be greater than zero, the quantities necessary to begin subset $t+1$ (the subset $t+1$ seed values and the subset $t+1$ threshold) can be formed. Otherwise, the $p_{MCMC/ss}$ failure probability can be estimated using Eq. 3.

Using the random variables defined in Table 1 and the limit state function ($R < S$) twenty samples were generated using the MCMC/ss approach. Each sample consisted of four subsets, where each subset consisted of 500 simulations (Au et al. 2007). Also, a probability of exceedance threshold factor, f_{exc} , of 0.1 was employed. The mean-valued estimate of the failure probability, $p_{MCMC/ss}$ is presented in Table 2.

Table 2. MCMC/ss Simulation Analysis Results

Discrete $P(R < S)$	$P_{MCMC/ss}$	St. Dev.	COV	Average Sample Size
0.1	9.83E-02	7.91E-03	0.092	725
0.01	9.91E-03	2.05E-03	0.207	1,325
0.001	1.18E-03	4.79E-04	0.405	1,725
0.0001	1.07E-04	4.36E-05	0.407	2,200

Table 2 clearly indicates the computational advantages of MCMC/ss over sMC, as discussed by Au and Beck (2001). However, the improved computational efficiency seems to have been reached with the expense of reduced consistency (i.e. the COV values are all greater than benchmark of 0.1 used in the sMC analysis). The COV values also seem to inflate as the joint probability of interest gets smaller. In order to achieve consistent MCMC/ss results, the subset sample size needs to be adjusted depending on the size of the joint probability plane. For the scenarios in this study, a second batch of simulations was run while varying the subset sample size to approximate the failure plane and also keeping the dispersion of the results below the benchmark value of 0.1.

This process was carried out by generating twenty samples using the MCMC/ss approach with an arbitrary number of simulations per subset (i.e., 1000 simulations per subset, held constant for each of the twenty samples). Then, the COV

associated with the point estimate (failure probability) from the twenty samples was calculated. If the COV value was found to be greater than the benchmark value (0.1), then the number of simulations per subset was increased. The subset size necessary to maintain a COV below 0.1, for each of the theoretical, is shown in Table 3. While substantial efficiencies are gained through use of MCMC/ss, the subset size must increase by a significant amount as the failure probability approaches zero.

Table 3. MCMC/ss Simulation Analysis Results with Subset Sample Size Adjustment

Discrete P(R<S)	$P_{MCMC/ss}$	St. Dev.	COV	Average Sample Size	Subset Sample Size
0.1	1.02E-01	9.38E-03	0.092	1,350	900
0.01	1.03E-02	1.01E-03	0.099	7,050	3,000
0.001	1.02E-03	9.57E-05	0.094	34,000	10,000
0.0001	1.02E-04	9.88E-06	0.097	65,250	15,000

CONCLUSIONS

MCMC/ss can be a viable alternative to the sMC in cases where the joint probability of the variables of interest is small. As the analysis indicated, in a simple two-parameters system when the joint probability is around 0.1 and for a COV of 0.1, sMC analysis requires a sample size of 900, whereas the MCMC/ss requires, on average, 1,350 simulations with a subset sample size of 900. Under the same conditions with a joint probability of 0.0001, sMC requires 999,900 simulations whereas MCMC/ss require only 65,250 simulations. In the case of extreme events, i.e. rare scenarios, MCMC/ss will have a distinct computational advantage over the sMC technique; however, attention needs to be paid to the subset sample size. As illustrated in this study, the consistency of the MCMC/ss is not insensitive to the subset sample size. Furthermore, the suggested subset simulation size of 500 might not be suitable in all cases, and therefore, analysts must remain cognizant of the reliability levels associated with MCMC/ss failure probability estimates.

REFERENCES

- Akintoye, A.S., and MacLeod M.J. (1997). "Risk analysis and management in Construction." *Int. J. of Proj. Man.*, 15(1), 31-38.
- Au, S.K., and Beck, J.L. (2001). "Estimation of small failure probabilities in high dimensions by subset simulation." *Prob. Engrg. Mech.*, 16, 263-277.
- Au, S.K., Ching, J., and Beck, J.L. (2007). "Application of subset simulation methods to reliability benchmark problems". *Struc. Safety*, 29, 183-193.
- Chau K.W. (1995). "Monte Carlo simulation of construction costs using subjective data." *Cons. Man. and Econ.*, 13(5), 369-383.
- Davidson, M.T. (2010). "Simplified dynamic barge collision analysis for bridge pier design barge impact." PhD Dissertation, Gainesville, Florida.
- Field, A. (2009). "Discovering statistics using SPSS." Sage Publications, London.
- Lee, D. (2005). "Probability of Project Completion Using Stochastic Project Scheduling Simulation." *J. of Cons. Engrg. and Man.*, 131 (3), 310-318.
- Martinez, J.C. (2010). "Methodology for Conducting Discrete-Event Simulation

Studies in Construction Engineering and Management,” *J. of Cons. Engrg. and Man.*, 136(1), 3-16.

Melchers, R. (1999). “Uncertainties in reliability assessment.” *Structural Reliability Analysis and Prediction*, 2nd Ed., John Wiley & Sons, Chichester, United Kingdom.

Shannon, R. E. (1998). “Introduction to the art and science of simulation.” Proc., 1999 Winter Simulation Conf., IEEE, Piscataway, N.J.

Multi-Agent Simulation Considering the Influence of Leader During Flood Disaster

Michiyuki Hirokane¹ and Yusuke Miyawaki² and Yuhei Inoue³

¹ Faculty of Informatics, Kansai University, 1-1-2 Ryozenji-cho Takatuki-shi Osaka-Fu 569-1095 Japan; PH81-72-690-2601; FAX81-72-690-2601; e-mail: hirokane@res.kutc.kansai-u.ac.jp

²Graduate School of Informatics, Kansai University Graduate School, 1-1-2 Ryozenji-cho Takatuki-shi Osaka-Fu 569-1095 Japan;PH81-72-262-1889; e-mail:wakki1028@yahoo.co.jp

³Graduate School of Informatics, Kansai University Graduate School, 1-1-2 Ryozenji-cho Takatuki-shi Osaka-Fu 569-1095 Japan;PH81-66-933-4916; e-mail: fa82005@edu.kutc.kansai-u.ac.jp

ABSTRACT

Recent natural disasters such as typhoons and heavy rains have frequently occurred in Japan. Moreover, people have failed to escape because of improper evacuation activities and a lack of post-disaster risk awareness; this includes fire or tsunamis caused by earthquakes. Almost all of the victims evacuate using a hazard map, evacuation signs, or with assistance from local residents. However, the local community tends to rarely than before. Therefore, hazard maps and evacuation signs are more important than ever. In our research, we studied the influence of leaders during evacuation using a multi-agent model based on flood evacuation system for decreasing the number of victims who failed to get out in time by the indication of the leader during evacuation to the escaping residence. Through our implementation of this multi-agent model based on flood evacuation simulation, we discuss the requisite number of leaders during evacuation and the arrangement of such leaders in the city of Takatsuki.

1. Introduction

Natural disasters such as earthquakes, typhoons, and tsunamis have recently occurred in many parts of the world, causing terrible damage. In particular, we recall

the Sumatra earthquake and the resulting tsunami of 2004, as well as China's Sichuan earthquake of 2008. In Japan, similar large-scale seismic disasters have occurred, including the Iwate-Miyagi inland earthquake of 2008 and the Nomi peninsula earthquake of 2007 [1]. Other natural disasters involving typhoons and heavy rainfall include the heavy rains in the northern regions of Chugoku-Kyushu in 2009 and heavy rainfall throughout Japan at the end of August 2008. In these disasters, damage is widespread and many fail to escape due to improper evacuation activities and a lack of risk awareness in the aftermath of a disaster, including such dangers as fire and tsunamis resulting from large-scale earthquakes [2][3].

Almost all of the victims evacuate by depending on a hazard map, evacuation signs, and on the local residents. Recently, the community in the local area has been tending to rarefy than before. Therefore, hazard maps and evacuation signs are more important than ever. Hazard maps are generally available on the Web, but it is difficult to obtain such maps after a disaster occurs. Evacuation signs may show the correct course to an evacuation center, but in some places, such signs are outdated or show routes that are impassable because of the disaster itself. Furthermore, disaster victims likely do not ensure that evacuation signs are directing them in the correct direction.

In our research, we considered the influence of leaders during evacuation using a multi-agent model based on a flood evacuation system for decreasing the number of victims during evacuation to the escaping residence. Through our implementation and experimentation, we study the requisite number of leaders during evacuation and the actual arrangement of such leaders in the city of Takatsuki.

2. Agents and their Behavior

In our research, we defined two types of agents: leaders and victims. Leader agents model the leaders of an evacuation and know the shortest path from a local point to refuge. After the onset of a flood, they stay at the local point to teach the shortest path to the victim agents; after a certain period of time, they move to refuge. Victim agents model local members of the community and are unaware of the path to refuge. They escape from the water flow and when picked up by a leader agent, they learn the correct path of evacuation and move to refuge. After the victim agents have this evacuation information, they in turn can pick up other victim agents without the information, teach them, and together move to refuge.

Other agents defined include road and overflow agents. Road agents model

ordinary roads, while overflow agents model flooded roads. As time ticks away, overflow agents overtake road agents. Leader and victim agents cannot pass overflow agents.

In our research, we supposed the emergency evacuation simulation, agent migration speed is configured as 2 m/s. Leader and victim agents move one cell forward per step; one cell is configured as 20 m. Therefore, one step is configured to take ten seconds. Thus, time taken to walk 60 and 180 steps was 10 min and 30 min in actual time, respectively.

3. Experimentation

3.1 Setup

The experimental space in our research was Takatsuki's maritime region. If a flood was to occur in this area, people would actively evacuate. Figure 1 shows the model of Takatsuki's maritime area used in our experimentation. This region has a center road, sixteen prefectural roads, and three refuges.

Because this region is a maritime area, after 10 min, some parts of the area are flooded; after 30 min, the entire area is flooded [3]. In our system, evacuation is successful if agents in some parts arrive at a refuge within 10 min and from other areas within 30 min. Default positions of both leader and victim agents were assigned randomly on road agents.

3.2 Experiment 1

In Experiment 1, we changed the number of leaders to validate the effectiveness of leaders during evacuation and determine the most effective number of leaders. Figure 2 shows our results, showing the ratio of leaders to victims versus the evacuation success rate.

Compared with a leader ratio of 0% in which the evacuation success rate is only 36%, the evacuation success rate substantially increases when leaders are present, confirming the effectiveness of leaders in such situations. As shown in the figure, a leader ratio of 15% results in an evacuation success rate of 86%; furthermore, a leader ratio of 20% results in an evacuation success rate of 88% and a leader ratio of 25% results in an evacuation success rate of 90%. Note that when the leader ratio is more than 15%, the evacuation success rate does not increase very rapidly. This is likely due to the pervasiveness of information sharing by both leader and victim agents. From our results, we identify 15% as an effective ratio.

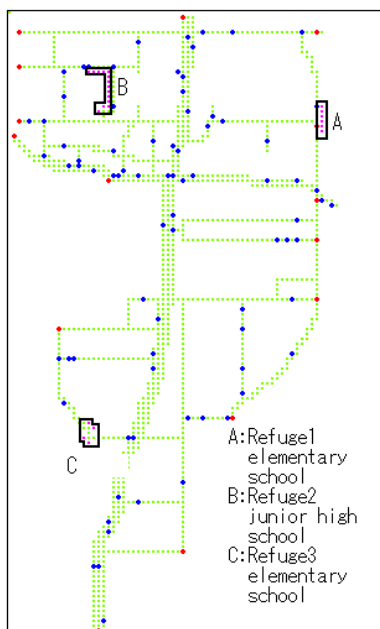


Figure 1. Model map of the city of Takatsuki

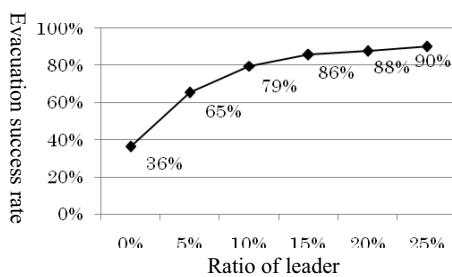


Figure 2. Ratio of leader and evacuation

3.3 Experiment 2

In Experiment 2, using effective leader ratios from Experiment 1, we changed the arrangement of these leader agents to determine the most effective arrangement in terms of evacuation success rate.

3.3.1 Experiment 2-1

In Experiment 2-1, arrangement of leader agents is circumambient to the space, as shown in Figure 3. Figure 4 shows our results in which the evacuation success rate was high. After 10 min, the evacuation success rate was only 51%. This may be because the leader agents were arranged in a limited space, and thus it took a long time for the other agents to identify the leader agent.

3.3.2 Experiment 2-2

In Experiment 2-2, leader agents were placed at crossroads of the center road, as shown in Figure 5. There is prefectural road 16 suitable for evacuation from Takatsuki's maritime area.

Figure 6 shows the results of Experiment 2-2. As shown in the figure, evacuation success rates increase rapidly during the 30-min period. We believe that victim agents easily identify leader agents early and therefore evacuate quickly.

3.3.3 Experiment 2-3

In Experiment 2-3, leader agents are arranged uniformly in the given space, as shown in Figure 7. In this area, Modeled map was wide, leader arranged uniformly for people agent picked out leader agent averagely.

Figure 8 shows the results of Experiment 2-3, revealing an evacuation success rate similar to that of Experiment 2-2. We believe that victim agents easily identified the leader agents because of the uniformity. People agent in the blind lane vicinity easily picked up leader agent, but people agent in the center road vicinity take time picking up leader agent.

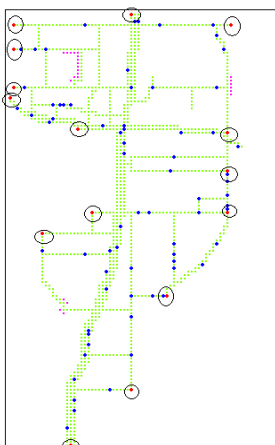


Figure 3. Arrangement of leader agents in Experiment 2-1

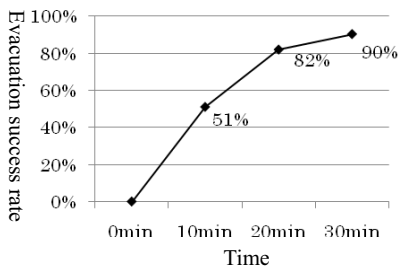


Figure 4. Results of Experiment 2-1

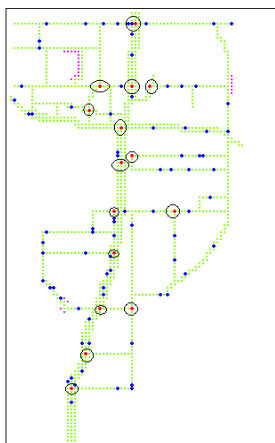


Figure 5. Arrangement of leader agents in Experiment 2-2

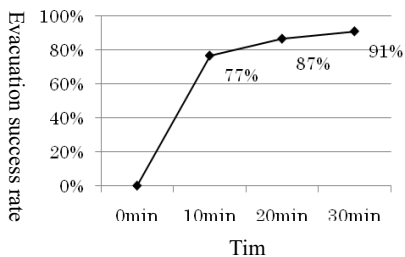


Figure 6. Results of Experiment 2-2

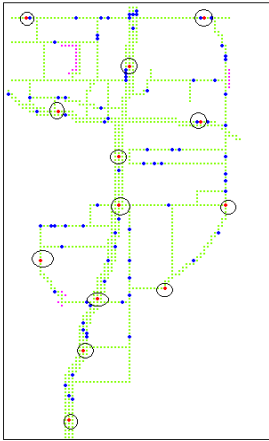


Figure 7 Arrangement of these leaders in the experience 2-3

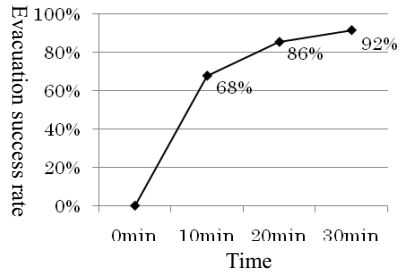


Figure 8 Results of Experiment 2-3

3.4 Result and consideration

Table 1 summarizes all Experiment 2 results. After 30 min, evacuation success rates for Experiments 2-1, 2-2, and 2-3 were 90%, 91%, and 92%, respectively. All results were similar after 30 min; however, after 10 min, evacuation success rates for Experiments 2-1, 2-2, and 2-3 were only 51%, 77%, and 68%, respectively. Note that Experiment 2-2 had the top evacuation success rate at the 20-min mark. Victim agents easily identified leader agents at the crossroads of the wide center road.

Experiment 2-2 had the highest ratios, except for a slight 1% difference with Experiment 2-3. The arrangement of uniformity in the space because of people agent having information effectively giving information people agent. In the simulated flood event that required prompt action, our results verify that this arrangement was the most effective.

Table 1. Results

Elapsed time	Experiment2-1	Experiment2-2	Experiment2-3
10min	51%	77%	68%
20min	82%	87%	86%
30min	90%	91%	92%

4. Conclusion

In our research, we considered the influence of leaders during disaster-based evacuation by applying a multi-agent model of flood evacuation to the city of Takatsuki. We studied the effectiveness of the number of leaders and their respective positions by conducting simulations using this model.

We determined the ideal ratio of leaders versus victims to be 15%, after which the rate of increase in the evacuation success rate decreased, showing only marginal improvements. Regarding the arrangement of these leaders, our experimental results were similar, but placing leaders at crossroads of a center road (Experiment 2-2) had the best overall evacuation success rates. Based on our findings, we conclude that a more effective evacuation can be achieved by instructing people to evacuate toward center roads as their first response to a disaster. This evidently depends on the layout and organization of the affected area.

In our current work, agents were given evacuation route information by leader and victim agents; such information was assumed to be correct, but in reality, information may change because of factors such as modifications in the surrounding, misinterpretation, or human error. A probabilistic model or prospect theory would be an improvement over our current approach. Furthermore, in our current experiment, victim agents were randomly arranged; in reality, more populated areas exist, which should be considered and modeled for more realistic simulations. Using genetic algorithms or enforced learning could also provide more useful results.

References

- [1] Japan Meteorological Agency. Japan Meteorological Agency statistical information < <http://www.seisvol.kishou.go.jp/eq/higai/higai1996-new.html>>
- [2] Ministry of Land, Infrastructure, Transport and Tourism. Sikoku Regional Development Bureau < http://www.skr.mlit.go.jp/bosai/jishin/tounankai/kisochishiki/damage/02damage_history.html#top>
- [3] Disaster Prevention System Institute. <<http://www.bo-sai.co.jp/TounankaiNankai.htm>>
- [4] Yodogawa River Office. < http://www.yodogawa.kkr.mlit.go.jp/activity/MainTenance/possess/sim/bosai_sonae_010201.html>

Multi-Agent Simulation to Uncertain Civilian Return Trips during a Hypothetical Earthquake

Seiichi Kagaya¹ Yukako Ishiguro² and Ken-etsu Uchida¹

¹Graduate School of Engineering, Hokkaido University, N13, W8, North-ward, Sapporo, 060-8628, JAPAN, PH+81-11-706-6210, FAX+81-11-706-6211, email:kagayas@eng.hokudai.ac.jp, ²NTT DATA Corporation, Toyosu Center Building, Toyosu 3-3-3, Koto-ward, Tokyo, 135-6033, JAPAN, PH+81-3-5546-8202

ABSTRACT

After Hanshin-Awaji huge earthquake disaster in 1994, it has been important for Japanese local Government to build a comprehensive evacuation program of a large earthquake occurrence. In this program, it is substantial to give appropriate information on human behavior for the evacuation time. Thus, a new methodology based on behavior-oriented agent system should be developed. In this study, the production rules of the attributive groups were constructed in terms of the questionnaire survey for civilian return-trips from the working or the shopping places during earthquake disaster. Next, using the set of production rules composed of the questionnaire data, a multi-agent system model for return trips in a hypothetical large-scaled earthquake was built by a MAS method. It comes to the conclusion that the human behaviors during the earthquake impact were constructed by multi-agent system model and the possibility of the return-home was found in view of the conditions of the roads and the human attributes.

INTRODUCTION

In Japan, after Hanshin-Awaji huge earthquake disaster, it has been an important role of the society to build a comprehensive measure against natural disaster. In particular, in the case of earthquake disaster, it is substantial to establish the evacuation system including both public organization and communities synthetically. Considering the emergent evacuation system, it is difficult to grasp the characteristics of human behavior towards the disaster [Batty, 2001]. In most of large cities people gather from their home into the city center to work or to enjoy shopping in daytime. If a large natural disaster like an earthquake is occurred around the area, some of them think how to evacuate for a safe area and the rest of them worry about their families existing in different area. Then, they want to return to their home and a large number of people choose similar behavior to return home. As a result, a panic breaks out in the city center. It is because human behavior is various in terms of unusual state of psychology. In other words, when many people refuge or return home simultaneously due to the large earthquake occurrence in a city, they may think

and judge how to act independently, and then behave by themselves differently. Moreover, they also give influences to each other. Therefore, it is difficult to know the whole evacuation or returning behavior stochastically due to a simple individual activity [Ulieru, *et al.*2000].

Here the method of multi-agent simulation is discussed as a new technology examining such an emergence or return trip during a hypothetical earthquake disaster. A multi-agent system is constructed to apply the return trips with an occurrence of earthquake. We also studied to apply such a technique to evacuating behavior by means of walking or car use [Negishi, *et al.* 2004].

In view of this background, the objectives of this study is to build the return-trips simulation model based on the rules of human behavior and to execute some alternatives by use of the model. Using the return-trips simulation model, it is also to grasp the characteristics of human traffic behavior during the earthquake occurrence.

Multi-Agent Simulation and GIS

Human behavior and intelligent agents. An agent is anything that can be viewed as perceiving its environment through sensors and acting on that environment through effectors. A human generally has five senses for sensors, and hands, legs, mouth and other body parts for effectors [Horvitz, *et al.* 1988]. Thus, the acts of an agent substitute for human behavior including both sensors and effectors. Rational activity depends on the performance measure, the percept sequence, the knowledge of the environment and the performance of action. In other words, an agent should do whatever action is expected to maximize its performance measure based on the evidence provided by the percept sequence and whatever built-in knowledge the agent has.

We should decide how to build a real program to implement the mapping from percepts to action. Thus, four types of agent programs will be considered like simple reflex agent, agents keeping track of the world, goal-based agents and utility-based agents. Humans have many connections such as a condition-action rule written as “if the order of evacuation is announced then evacuation is initiated”.

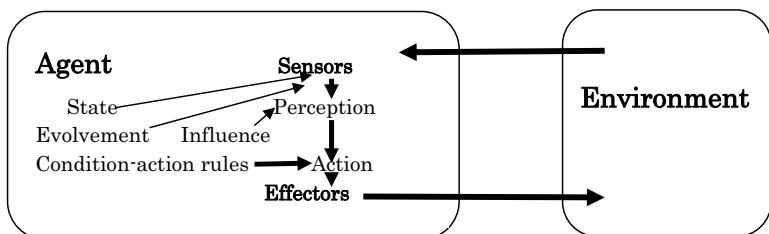


Figure 1. Diagram of a Reflex Agent with Internal State

Figure 1 shows a structure of a reflex agent system with internal state. This model illustrates how the condition-action rules make the agent to connect from perception to action [Russell, *et al.* 1995]. It also shows how the current perception

is combined with the old internal state to generate the updated description of the current state. The some options for perception are added. In the goal-based agent model, we discuss goals in the stage of action. On the other hand, the utility-based agent model adds an evaluation stage due to utility after the percept stage. This study adopts a reflex type with internal state.

Here, the rule-based system is defined as a combination between perceptions and action in terms of data base, production rule bases and an interpreter, and the inference engine. The multi-agent system is applied to a system comprising the following elements, that is, an environment, a set of objects, an assembly of agents, an assembly of relations, an assembly of operations and operators. The technology of multi-agent simulation contributes to the construction of evacuation behavior model and its simulation. Multi-agent is generally composed of a set of agents that act for themselves beneficially in terms of their strategies. It has also some two-way relationships among them. Multi-agent simulation (MAS) is to simulate the system which is established in terms of computer program [Kagaya, *et al.* 2007].

Application of digital map and GIS. In this study, the emergent traffic roads are used for the civilian return trips from the center of city to their houses. The roads are based on the map of disaster prevention by a municipality. The agents who want to return home in an earthquake occurrence act on the roads. They are called as return trip agents. A return trip agent acts from the center of city to his/ her home. The geographical information is composed of the location of node, the length of link between different two nodes, the vulnerable of link against earthquake, and so on.

PROCEDURE OF SIMULATION

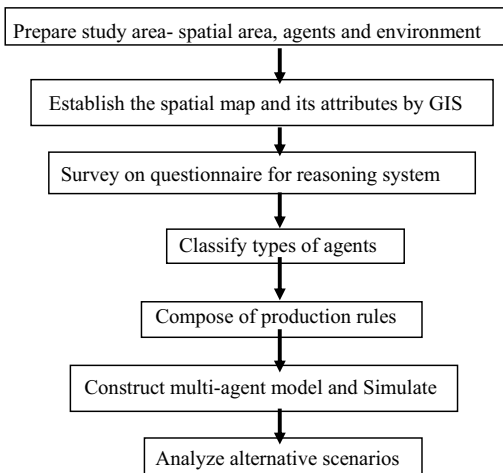


Figure 2 Procedure of Multi-Agent Simulation Analysis

First of all, we suppose such a condition and evoke the evacuation behavior in terms of creating each agent. Each agent is included in a family and a community simultaneously. The agents usually act on the multi-agent system interacting with the other agents. The interactions here are characterized by three conditions of mobility such as i) following the other agents, ii) leading to the other agents and iii) the inhibition of travel with congestion. Figure 2 illustrates the procedure of multi-agent simulation analysis which is constructed by us. Here, first of all, the space, the agents and the environment in a study area is prepared. Next, a digital map of space in terms of GIS is established. Then, the questionnaire is surveyed to make the reasoning system and to classify several types of agents using the results due to cluster analysis. The production rules are combined to simulate multi-agent system. After that, the multi-agent model is constructed and simulation is promoted by Monte Carlo method. Finally, some alternative scenarios are analyzed by the recreated model.

SURVEY ON RETURN TRIP BEHAVIORS

Objective of Survey. The action rule bases depend on the standard of judgment due to individual characteristics such as the age, the experiences on earthquake disaster etc. So it is necessary to survey a questionnaire in order to construct the return trip behavioral rules. It is also important to execute the precise survey, because the accuracy of estimating the agent behavior depends on it. Specifically, the survey was carried out for the inhabitants in Sapporo City, Hokkaido. They have experienced comparatively several earthquake disasters. The features of the evacuation behavior can be grasped in terms of the data obtained by the questionnaire survey. The objective of this analysis is to clarify the relationship between the behavior of return home and the personal attributes and experiences in the earthquake disaster.

Several results were obtained by analyzing responses as follows:

- 1) The average time when respondents have experienced to walk continuously was 1.72 hours and 2.93 hours was the time when they can walk continuously. As a result, 3 hours can be determined as a maximum time for a return trip.
- 2) The decision on returning trip can be affected by the age of a traveler, the distance of returning and the location for a trip objective. Here, the distance of returning was classified into three divisions, namely, the distance of 0-5.4km, 5.5-9.4km and greater than 9.5km due to the survey. The districts where travelers return exist in such three ranges of distance. The eight districts in the northern east part of Sapporo City were selected as the districts of case study.
- 3) Using the cross tabulation, the statistical significance of Chi square was reasonable in the data of the returning distance and the location. Based on this result, travelers were classified by the returning distance and the location and the contents of attributes such as the rate of return, the preference of road, the knowledge of the return road by walk and the conditions of circumstances were obtained by the survey. Table 1 shows the rate of each attribute for the agents.
- 4) In table 2, the actions of agents to the surrounding agents are defined as four characteristics, namely, leading, following, cooperative and independent.

The selection of evacuation road is decided due to five conditions, that is, the minimum distance, the high density, low density, many numbers of shelters and no road selected. The characteristics of each agent are composed of the above whole attributes. And then, the agents' actions are decided by such characteristics. Therefore, the agents with different characteristics act due to their own thinking, when an earthquake occurs.

Table 1 Rate of the agents' attribute for the multi-agents simulation model

Distance (km)	Aim	Rate of return trips (%)	Relation to the surrounding travelers (%)			
			leading	following	cooperative	independent
0.0-5.4	working	38.7	13.9	16.7	22.2	47.2
	shopping	72.7	9.4	18.8	21.8	50.0
	traveling	57.4	6.5	16.1	25.8	51.6
5.5-9.4	working	41.5	13.6	22.8	13.6	50.0
	shopping	55.6	0.0	20.0	40.0	40.0
	traveling	62.8	7.4	7.4	25.9	59.3
9.5-	working	15.5	36.4	9.1	9.1	45.4
	shopping	43.8	28.6	14.3	42.8	14.3
	traveling	37.2	23.1	15.4	38.4	23.1

Table 2 Rate of selection and knowledge of evacuation roads

Distance (km)	Aim	Selection of the evacuation road (%)					Knowledge of the evacuation road (%)	
		Minimum distance	high density	low density	no traffic	shelter	Yes	No
0.0-5.5	working	47.2	11.1	0.0	30.6	11.1	77.8	22.2
	shopping	56.3	12.5	0.0	21.9	9.3	81.3	18.8
	traveling	58.1	6.5	3.2	22.6	9.7	54.8	45.2
5.5-9.5	working	68.2	18.2	0.0	13.6	0.0	54.5	45.5
	shopping	20.0	0.0	0.0	80.0	0.0	20.0	80.0
	traveling	51.9	3.7	11.1	11.1	22.2	48.1	51.9
9.5-	working	63.6	9.1	0.0	27.3	0.0	36.4	63.6
	shopping	85.7	0.0	0.0	0.0	14.3	57.1	42.9
	traveling	84.6	0.0	0.0	15.4	0.0	30.8	69.2

CONSTRUCTION OF SIMULATION MODEL OF EVACUATION BEHAVIOR

Establishment of the Simulation Space. Figure 3 represents a conceptual map used for simulation. This is also made of the actual map in Sapporo City. The evacuation place is displayed by the deep color part in the center of the map. The scale of simulation space is 12km in length and 10km in width by the real distance. The designated emergent roads by the municipality are introduced in the simulation. The points in the map represent the location of returning. In this case the return home indicates a concentrated mark of a district. A node agent is distributed at an intersection. Thus, a return agent selects some links acquiring the road information on the route condition. When a return agent arrive at his/her house (the mark of district), the goal agent acts to eliminate the return agent from the map.

Number of Agents Used with Simulation and Their Attributes. In this analysis, the experimental agents are obtained with the past person trip survey. Table 3 indicates the result in calculation of return agents in each destination with three aims

in the city center. This data was surveyed at six o'clock in the evening. The downtown area (the city center) is congested by commuters and shoppers at that time.

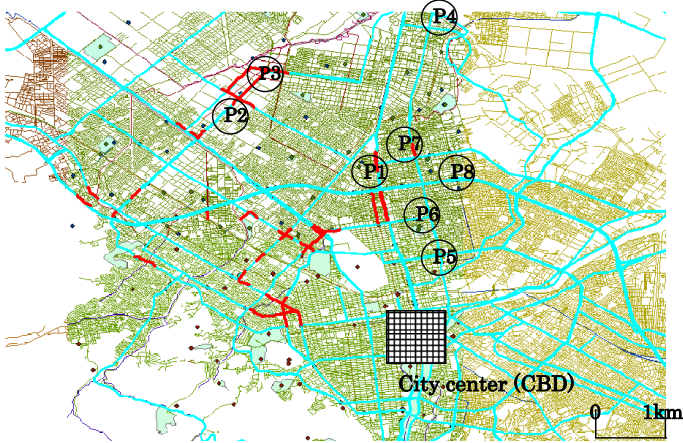


Figure 3 Simulation space and return points

Table 3 Number of return agents in every destination with three aims

Aim	Point1	Point2	Point3	Point4	Point5	Point6	Point7	Point8
work	4220	4325	1010	1484	2365	4557	3519	2865
shopping	2046	346	222	459	848	1533	973	670
travel	985	686	371	363	428	768	570	567

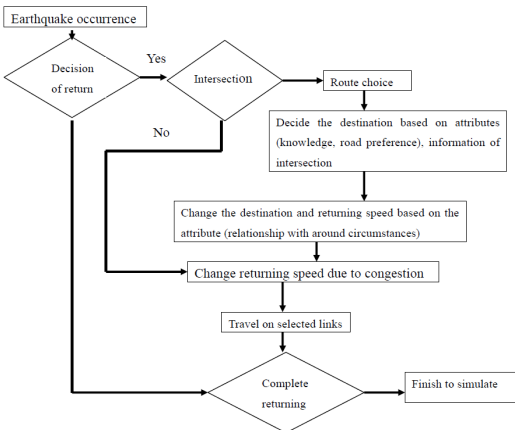


Figure 4 Behavior decision process of a returning agent

Flow Diagram of Behavioral Simulation Model of Returning Agents.

The behavior of a return agent in simulation model is represented as the process in Figure 4. In simulation the agents are introduced as the people who decide to return home. The return agent chooses the route at every crossroad (a node), and it goes out of the map. Furthermore, it also removes itself changing the walking speed in terms of the congestion level in each time. The route choice is promoted at other two stages. Three kinds of agents are prepared, namely, the return people agents, the node agents and the goal agents with simulation in the multi-agent system. The return people agents are consisted of their existing coordinates, personal attributes, walking speed, the information on nodes and links and intersection information. The node agents are distributed on intersections. The return people agents acquire the information of routes from the node agents with route choice information. They include the information of the node location, intersection attributes and the shelters. The goal agents are also located at the returning points and are used to recognize their arrivals. Using the agents, the multi-agent simulation model is built by the software MAS.

RESULTS AND CONSIDERATION

Reconstruction of Behavior under the Existing Condition Due to Simulation. The existing condition and state were reconstructed due to the supposed environment and the data obtained by questionnaire.

Figure 5 represent dynamic change of proportion of return agents on the way to home. The rates of agents that finished walking are only 15% of all agents within 180 minutes. This indicates the possible continuous walking time. In particular, most of agents who should walk in long distance wandered on the way to home.

Here the behaviors of aged people more than 60 years old were discussed. Most of them could not approach to their home. However, a half of agents who would return in short distance such as less than 5km reached to their home.

Moreover, the agent with knowledge of the routes could return to the home earlier than the one without knowledge of the routes.

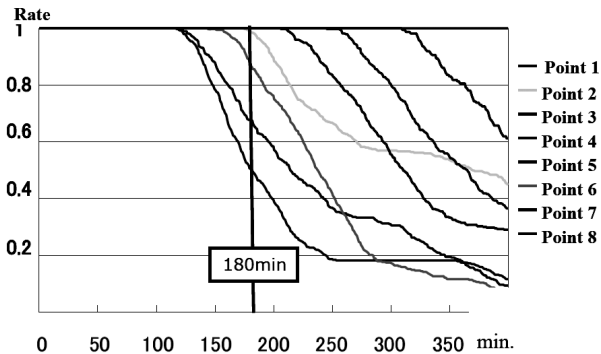


Figure 5 Proportion of return agents on the way to home in process of time

CONCLUSION AND REMARKS

In most of large cities, many people commute into the center business district (CBD). On the other hand, many people concentrate there for shopping, enjoying meals and going to hospital. At that time the natural disaster such as a huge earthquake suddenly occurred. They intend to go back to home as soon as possible in order to confirm their family's safety and to help their family. Meanwhile, they want to evacuate from there to guard themselves against severe damages by the earthquake. Many refugees concentrate onto evacuation and emergent traffic roads altogether. There possibly happen many obstacles and disturbances along the evacuation roads. Here, we tried to reconstruct the behavioral simulation model of return home for such people. The simulation was examined in Sapporo City, Japan. Sapporo has 1.9million population and is the fifth largest city in Japan. It has a lot of snow in winter. If an earthquake occurs in winter, the damage will increase more by indirect affects on snow and cold condition.

The study is concluded as 1) The multi-agent simulation model which analyze the behavior of return home includes three kinds of agents are prepared, namely, the return people agents, the node agents and the goal agents. Those agents interact among one another and were evaluated as returning to the objective points in ea... district. 2) The limited time enough to reach the point was estimated by using MAS. It is difficult for evacuator to reach the points by the limited time. This means their performances were incompatible with their ideas. 3) The conditions of aged people returning home were very severe compared with those of young people. It is necessary to ask them to abandon their return. 4) The people who lead the others to return home should be prepared, because they take the other people to the objective points quickly and safely.5) It is effective for returning people to have expanded roads for evacuation. It should be considered that the main evacuation roads are improved as wider routes. Thus, it should be indispensable to arrange the comprehensive and systematic returning system.

In the future study, the accurate estimation is possible to be examined due to a combination between multi-agent simulation model and geographic information system (GIS) in detail.

REFERENCES

- Batty, M (2001) Exploring Isovist Fields: Space and Shape in Architectural and Urban Morphology, **Environment and Planning B**, 28:123-150.
- Horvitz,E.L, Breese,J.S. and Henrion,M.(1988). Decision Theory in Expert systems and artificial Intelligence, **International Journal of Approximate Reasoning**,2. 247-302.
- Kagaya,S., Aitsuki,T., Uchida,K.(2007) Analysis of Human Behavior Representation in the Central Business District of Sapporo Using a Multi-Agent Simulation, **Studies in Regional Science**, Vol.37, No.2 , pp519-534.

Negishi,A., Kagaya,S., Uchida, K. and Hagiwara, T.(2004) A Study on Application of Rule Base by Considering Earthquake Experience to Seismic Evacuation Simulation, **Proceeding in Infrastructure Planning**, JSCE,(in Japanese).

Russell S. and Norvig, P (1995) **Artificial Intelligence, A Modern Approach**. Prentice Hall.

Ulieru, M and Norrie, D. (2000) Fault Recovery in Distributed Manufacturing Systems by Emergent holonic Re-Configuration, A Fuzzy Multi-Agent Modeling Approach, Information Science, 7669, 101-125.

Statistical Characterization and Prediction of Sea Waves Based on Buoy Data

Che-Yu Chang¹ and Bilal M. Ayyub²

¹ Graduate Research Assistant, ² Professor and Director

Center for Technology and Systems Management, Department of Civil and Environmental Engineering, University of Maryland College Park, MD 20742, USA
301-405-1956 (Tel), ba@umd.edu

ABSTRACT

Designing marine and maritime systems require the probabilistic characterization of sea waves in the time-history and spectral domains. These probabilistic models include parameters that can be empirically estimated based on limited data in durations, locations and applicability to particular designs. Characterizing the statistical uncertainties associated with the parameters and the models is an essential step for risk-based design methods. This paper introduces proposed statistical methods to assess confidence intervals for prediction of sea conditions at points of interest in the sea environment. The methodology is briefly introduced and demonstrated using illustrative simulation examples based on notional information.

Key words : statistical characterization, time history, spectral analysis, confidence interval

NOTATIONS

- c_k = autocovariance coefficient
- d = distance between buoy and point of interest
- f = wave spectrum
- H_s = significant wave height
- H_{st} = significant wave height from time history
- H_{sL} = lower confidence limit of significant wave height
- H_{sU} = upper confidence limit of significant wave height
- LCL = lower confidence limit
- UCL = upper confidence limit
- M = truncation point; the number of autocovariance coefficients considered, and also the number of discretized points for the periodogram

N	=	number of data discretized points of time history
n	=	number of independent data points of time history; independent sample size
Pdg	=	periodogram
T_m	=	wave modal period
T_{mt}	=	wave modal period from time history
T_z	=	up-zero-crossing period
T_L	=	lower confidence limit of wave modal period
T_U	=	upper confidence limit of wave modal period
wb	=	weight factor
ω	=	angular frequency
ν	=	degrees of freedom
λ_k	=	lag window
$f_p^{max}; f_p^{Dm}; f_p^{Mq}$	=	maximum spectral frequency estimated by different approaches

INTRODUCTION

Sea-state characterization is required for understanding the sea environment, predicting vessel travel response, designing marine and maritime systems, etc. Hamilton (2009) presented a method for characterizing spectral sea wave conditions by clustering the wave spectra. Cruz and Sarmento (2007) characterized sea state by linear wave theory approach and using boundary element method. This paper proposes a statistical approach for sea-state characterization using simulated sea wave surface elevation data. The approach presents the sea-state characteristics in the time and spectral domains by sea-state parameters, wave modal period and significant wave height obtained from the sea wave surface elevation time-history. In spectral domains, the sea wave characteristics are presented using periodograms constructed from the time histories. Statistical hypothesis testing is performed to define the confidence intervals of these two selected sea-state parameters for sea-condition prediction. Several approaches of modal period estimation are compared with the proposed method and discussed in this paper using illustrative examples.

SPECTRAL ANALYSIS

This section describes the elements needed for characterizing a time history including periodogram analysis, confidence intervals, and independent sample size.

Periodogram Analysis

The characteristics of a time series can be presented in the frequency domain by applying spectral analysis on the time series as described by Chatfield (2004). A periodogram shows how the variance of a time series is distributed over frequency. The periodogram, denoted as Pdg , can be calculated from the time series data, and is the Fourier transform of the autocovariance function. By the fact that the variance of the periodogram is a constant independent of the sample size, the periodogram requires modification to enhance estimation and prediction. One approach to modify the periodogram is to apply lag window on a truncated autocovariance function as follows:

$$Pdg(\omega_p) = \frac{1}{\pi}(\lambda_0 c_0 + 2 \sum_{k=1}^M \lambda_k c_k \cos(\omega_p k)) \tag{1}$$

in which $\{c_k\}$ is the autocovariance coefficient at time lag k , $\{\lambda_k\}$ is a set of weights called the lag window, and $M (<N)$ is the truncation point. The Parzen window is used in this study. The precision of $\{c_k\}$ decreases as k increases since the coefficient is based on fewer terms. The choice of the truncation point M can be subjective or based on common practices. A compromise value is chosen in this study as (Chatfield 2004): $M = 2\sqrt{N}$. Jenkins and Watts (1968) showed that the quantity $vPdg(\omega)/f(\omega)$ is approximately chi-square distributed with v degrees of freedom given by

$$v = \frac{2N}{\sum_{k=-M}^M \lambda_k^2} = \frac{2N}{\lambda_0^2 + 2 \sum_{k=1}^M \lambda_k^2} \tag{2}$$

The $100(1-\alpha)\%$ confidence limits for $f(\omega)$ at different frequencies ω are given by

$$LCL(\text{lower confidence limit}) = \frac{vPdg(\omega)}{\chi_{v, \frac{\alpha}{2}}^2}; \quad UCL(\text{upper confidence limit}) = \frac{vPdg(\omega)}{\chi_{v, 1-\frac{\alpha}{2}}^2}$$

Independent Sample Size

For a time series that has independent observations, the number of discretized points, N , can be treated as sample size. However, when the time series observations are correlated, it is necessary to obtain the sample size which represents the number of independent points of the time series, denoted as n , in order to use well established statistical methods for hypothesis testing as described by Ayyub and McCuen (2004). The sample size n can be estimated using the variance of the time series variance expressed in as follows (Priestly 1981):

$$n = \frac{2S^4}{\frac{2}{N}(c_0^2 + 2 \sum_{m=1}^{N-1} (1 - \frac{|m|}{N}) c_m^2)} \tag{3}$$

in which c is the covariance coefficient, N is the number of discretized points, and S^2 is the variance for the time history. The confidence intervals are evaluated based on the sample size which indicates the independent number of observations, the degrees of freedom ν expressed by Eq. 2 needs to be modified and replaced by n obtained from Eq. 3. Time histories for three buoys of a duration 500 seconds with various discretized points are examined shown in Figure 1. Modal period and significant wave height for the three buoys are summarized in Table 1. The degrees of freedom computed by Eq. 2 is expressed as "Existing Method" while that estimated by Eq. 3 is shown as "Proposed Method" and is different for three different buoys.

STATISTICAL CHARACTERIZATION APPROACH

This section provides the statistical characterization procedure which involves the statistical hypothesis testing. Comparison of several approaches for determining the modal period is discussed.

Table. 1 Modal periods and significant wave heights of buoys 1, 2, and 3.

Buoy	Modal period (BT)	Significant wave height (BHs)
1	7 sec	2.0 m
2	6 sec	1.0 m
3	8 sec	1.5 m

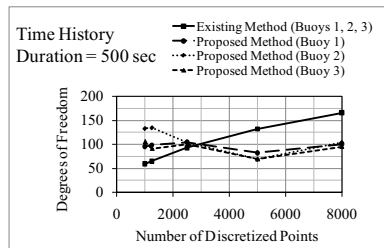


Fig. 1 Buoy independent sample size for various discretized points.

Statistical Hypothesis Testing

In this study, the periodograms constructed from the buoy wave surface elevation time histories are used to illustrate the sea wave characterization in the spectral domains. Statistical hypothesis testing is performed to describe the sea wave characteristics from different buoys, to perform goodness-of-fit of wave spectrum, and to interpolate the buoy data and predict the sea-state characteristics at particular locations of interested. The null hypothesis, denoted by H_0 , represents the equality of two spectra $f_1(\omega)$ and $f_2(\omega)$; while the alternative hypothesis, denoted by H_1 ,

indicates that a significant difference of two spectra exists. This leads to the following hypotheses: $H_0: f_1(\omega) = f_2(\omega)$; $H_1: f_1(\omega) \neq f_2(\omega)$. The quantity $\nu Pdg(\omega)/f(\omega)$ is approximately chi-square distributed with ν degrees of freedom. Consider a statistic X given by the following ratio:

$$X_i = \frac{Pdg_1(\omega_i) f_2(\omega_i)}{Pdg_2(\omega_i) f_1(\omega_i)}, \quad i = 1, 2, \dots, M \tag{4}$$

The random quantity of Eq.4 is distributed according to F -distribution with ν_1 and ν_2 degrees of freedom, denoted as $F(\nu_1, \nu_2)$. In the case when the null hypothesis $H_0: f_1(\omega) = f_2(\omega)$ is true, X_i does not depend on the underlying spectra and can be rewritten in the following form:

$$X_i = \frac{Pdg_1(\omega_i)}{Pdg_2(\omega_i)}, \quad i = 1, 2, \dots, M, \quad \text{if } H_0 \text{ is true} \tag{5}$$

Based on Eq. 5, the following form is suggested to test the null against the alternative hypothesis as:

$$Q = \sum_{i=1}^M X_i \tag{6}$$

Since the quantity X_i in Eq. 5 are independent and identically distributed, according to the central limit theorem, Q for a large sample size is normally distributed with the mean and variance as:

$$E(Q) = M \left(\frac{\nu_2}{\nu_2 - 2} \right), \quad \nu_2 > 2 \tag{7}$$

$$Var(Q) = M \left(\frac{2\nu_2^2(\nu_1 + \nu_2 - 2)}{\nu_1(\nu_2 - 2)^2(\nu_2 - 4)} \right), \quad \nu_2 > 4 \tag{8}$$

Note that M is the number of autocovariance coefficients considered.

Comparison of Several Approaches for Modal Period Estimation

The modal period T_m , or the spectral peak frequency $2\pi/T_m$, is evaluated in this study from the time history by using zero-upcrossing period expressed as follows:

$$T_{mt} = \begin{cases} 1.41T_z & \text{for Bretschneider spectrum} \\ 1.28T_z & \text{for Jonswap spectrum} \end{cases} \tag{9}$$

where T_z is the zero-upcrossing period. Some other approaches to estimate the

spectral peak frequency are available, such as simple maximum, Delft, and weighted mean methods. The Delft method for determining the spectral peak frequency is to find the centroid of the spectral band between the lower and upper spectral density, expressed as (IAHR 1989; Young 1995): $f_p^{Dm} = \int_{f_1}^{f_2} fF(f)df / \int_{f_1}^{f_2} F(f)df$. The weighted mean method estimates the spectral peak frequency by applying a weighting exponent on the spectral densities and evaluating the spectral peak frequency as follows (Sobey and Young 1986; Young 1995): $f_p^{Mq} = \int fF^q(f)df / \int F^q(f)df$.

Table. 2 Several approaches to estimate modal periods of buoys 1, 2, and 3. Relative errors to the original modal periods are shown in parenthesis.

Method	Original	Used in this study	Simple maximum	Delft	Weighted mean
Modal period	T_m	$T_m = 1.4 T_z$	$T_m = 2\pi/f_p^{max}$	$T_m = 2\pi/f_p^{D60}$	$T_m = 2\pi/f_p^{M4}$
Buoy 1	7 sec	7.14 sec (2.04%)	7.21 sec (3.06%)	7.10 sec (1.42%)	6.79 sec (-2.95%)
Buoy 2	6 sec	6.34 sec (5.74%)	6.31 sec (5.21%)	6.23 sec (3.91%)	6.09 sec (1.57%)
Buoy 3	8 sec	7.95 sec (-0.57%)	7.77 sec (-2.88%)	7.66 sec (-4.23%)	7.46 sec (-0.84%)

NUMERICAL EXAMPLE

A sea wave characterization example is presented in this section using simulated buoy vertical displacement data. The buoy vertical displacement is taken as the sea wave surface elevation simulated from Bretschneider spectrum in this study. Two sea-state parameters, sea wave modal period T_m and significant wave height H_s , are selected to describe the wave characteristics in the time domain. A sea spectrum goodness-of-fit is then performed on each buoy by applying statistical hypothesis testing, using Eqs. 6 to 8, on selected sea spectra and on the periodogram which illustrates the wave characteristics in the spectral domains. Bretschneider and Jonswap spectra are selected for the sea spectrum goodness-of-fit and are constructed using the estimated sea-state parameters, wave modal period T_m , and significant wave height H_{st} , calculated from the time history by Eqs. 9 and 10.

$$H_{st} = 4 \sqrt{\text{variance of time history}} \quad (10)$$

The sea spectrum goodness-of-fit is performed by fitting the Bretschneider and Jonswap spectra to the adjusted periodogram. Once the fitted spectrum type is defined, the confidence intervals of the selected sea-state parameters are then analyzed for sea-condition prediction by applying statistical hypothesis testing on the buoy adjusted periodogram and the adjusted periodograms constructed from the fitted spectrum type for a range of sea-state parameters sets. The sea wave surface elevation time histories of three buoys are analyzed in this example. Table 1 summarize modal periods and significant wave heights of these three buoys. Time histories for these buoys are generated from Bretschneider wave spectra using the modal periods and significant wave heights from Table 1. The duration of these buoy time histories is 1500 sec starting from 0.5 sec with a constant interval of 0.5 sec. The number of total data points of each buoy time history is 3000.

Parametric Analysis

The selected two sea-state parameters, sea wave modal period T_m and significant wave height H_s , are analyzed in this section. One parameter is fixed while the other is analyzed within a range of values. The confidence intervals are defined by performing hypothesis testing, using Eqs. 6 to 8, on the adjusted periodograms of buoys and adjusted periodograms constructed from the sea spectra of a range of sea-state parameters sets. Table 4 shows the 95% confidence intervals for the three buoys on the modal period T_m for the significant wave height $H_s = H_{st}$ and on the significant wave height H_s for the modal period $T_m = T_{mt}$.

Table 4 95% confidence intervals of the significant wave height H_s and the modal period T_m of buoys 1, 2, and 3.

95% Confidence Interval Limits	Buoy 1 $T_{mt}=7.14$ sec $H_{st}=1.99$ m	Buoy 2 $T_{mt}=6.34$ sec $H_{st}=0.97$ m	Buoy 3 $T_{mt}=7.95$ sec $H_{st}=1.54$ m
Lower modal period limit T_L	6.87 sec	6.12 sec	7.64 sec
Upper modal period limit T_U	7.79 sec	6.88 sec	8.60 sec
Lower significant wave height limit H_{sL}	1.95 m	0.95 m	1.50 m
Upper significant wave height limit H_{sU}	2.07 m	1.01 m	1.60 m

CONCLUSIONS

This study presents sea environment conditions in the time and spectral domains when given only wave surface elevation time history. Comparisons of several modal period approaches show that these methods produce estimations within 6% relative errors to the original modal periods used to simulate the time histories. The proposed method produces the best estimation for buoy 3 while the Delft and the weighted methods provide the best evaluation for buoys 1 and 2, respectively. Independent sample size is estimated which is needed for performing statistical analysis. The statistical basis of the proposed method enables the characterization of sampling variability and associated uncertainties by estimating the confidence intervals of the sea-state parameters.

REFERENCES

- Ayyub, B. M., and McCuen, R. H. (2004). "Probability, Statistics, and Reliability for Engineers and Scientists," Second Edition, Chapman & Hall/CRC, FL.
- Chatfield, C. (2004). "The Analysis of Time Series: An Introduction," Sixth Edition, Chapman & Hall/CRC.
- Cruz, J.M.B.P., and Sarmiento, A.J.N.A. (2007). "Sea State Characterisation of the Test Site of An Offshore Wave Energy Plant," *Ocean Engineering*, 34(5-6), 763-775.
- Hamilton, L. J. (2010). "Characterising Spectral Sea Wave Conditions with Statistical Clustering of Actual Spectra," *Applied Ocean Research*, 32(3), 332-342.
- IAHR (1989). "List of Sea-State Parameters," *Journal of Waterway, Port, Coastal, and Ocean Engineering*, 115(6), 793-808.
- Jenkins, G. M., and Watts, D. G. (1968). "Spectral Analysis and Its Applications," Holden-Day, San Francisco, CA.
- Priestley, M. B. (1981). "Spectral Analysis and Time Series," Academic Press Inc., NY.
- Sobey, R. J. and Young, I. R. (1986). "Hurricane Wind Waves-A Discrete Spectral Model," *Journal of Waterway, Port, Coastal and Ocean Engineering*, 112(3), 370-389.
- Young, I. R. (1995). "The Determination of Confidence Limits Associated with Estimates of the Spectral Peak Frequency," *Ocean Engineering*, 22(7), 669-686.

Measuring Validity of Reasoning Process for Transportation Planning using Bayesian Inference and Dempster-Shafer Theory

Nopadon Kronprasert, Ph.D. Student¹ and Shinya Kikuchi, Ph.D., PE, Professor²

¹ Department of Civil and Environmental Engineering, Virginia Tech, 7054 Haycock Road, Falls Church, VA 22043, USA (703) 342-8232, email: nopkron@vt.edu

² Department of Civil and Environmental Engineering, Virginia Tech, 7054 Haycock Road, Falls Church, VA 22043, USA (703) 538-8436, email: kikuchi@vt.edu

ABSTRACT

When evaluating the validity of the reasoning process of a transportation plan, a reasoning map facilitates discourse. If the truth values are attached to the premise and each link of the map, the overall truth of the reasoning process can be measured. The map is useful to examine the sensitivity of the truth with respect to the changes in knowledge and opinions. In calculating the truth, Bayesian inference measures it in probability measure. Dempster-Shafer (D-S) theory measures it in Belief and Plausibility. This paper examines the differences between these two methods using an example that deals with selection of the mode of public transportation in a large commercial complex.

INTRODUCTION

The traditional mechanism to measure the validity of a reasoning map is Bayesian inference. In recent decades, Belief and Plausibility measures in the domain of Dempster-Shafer (D-S) theory are introduced to measure the truth when knowledge about causalities is incomplete. Each approach has its own mathematical and axiomatic trait; accordingly interpretations of the results are different (Kikuchi and Pursula, 1998; Kikuchi and Chakroborty, 2006). This paper applies these two approaches to a reasoning map that attempts to justify construction of an automated people mover in a large commercial complex.

Given a set of goals, a developer wants to introduce an automated people mover (APM) that circulates the commercial complex at Tysons Corner, Virginia. Based on a newspaper article written by a proponent of APM (Offutt, 2010), a reasoning map is developed. The validity of this reasoning process is evaluated by Bayesian inference and D-S theory for the APM to achieve the goals.

CALCULATION PROCESS

Strength of Inference by Bayesian Probability Theory

For an inference scheme, given X and $X \rightarrow Y$, the truth of Y is given by,

$$p(Y_j) = \sum_{X_i \in X} p(Y_j | X_i) \cdot p(X_i) \tag{1}$$

where X_i and Y_j are a set of states of parent node X and child node Y , $X_i \in X$ and $Y_j \in Y$ respectively. $p(X_i)$ is the truth value of premise X_i and $p(Y_j|X_i)$ is the conditional probability of Y_j with respect to X_i .

Figure 1 applies this mechanism to a five-node reasoning map, and the probability distribution of the final node E is calculated. The conditional probability distributions of relations $(A,B) \rightarrow C$, $B \rightarrow D$, $(C,D) \rightarrow E$ constitute the knowledge. The premise is the conditions of A and B , all in probabilities. In order to apply Bayesian inference, one must have the complete probability distribution for each premise and each relation.

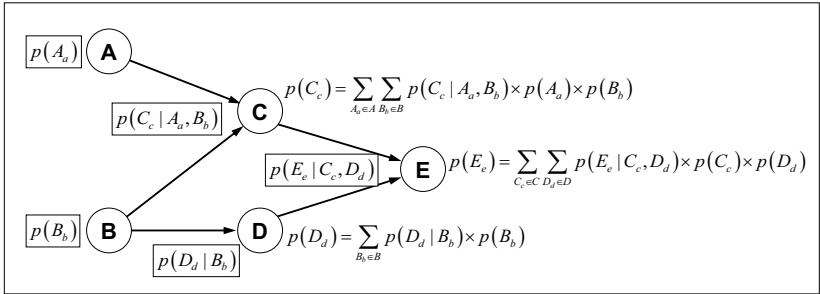


Figure 1. Bayesian inference

Strength of Inference by D-S Theory

For an inference scheme, given X and $X \rightarrow Y$, D-S theory computes the truth of Y as follows.

$$m(Y_j) = \sum_{X_i \in X} m(Y_j | X_i) \cdot m(X_i) \tag{2}$$

where X_i and Y_j are a power set of states of parent node X and child node Y , $X_i \subseteq X$ and $Y_j \subseteq Y$, respectively. For example, if the states of $X = \{X_1, X_2, X_3\}$ in Bayesian inference, then $X_i = \{X_1\}, \{X_2\}, \{X_3\}, \{X_1 \cup X_2\}, \{X_1 \cup X_3\}, \{X_2 \cup X_3\}$, or $\{X_1 \cup X_2 \cup X_3\}$ in D-S inference. $m(X_i)$ is the truth value of premise X_i and $m(Y_j|X_i)$ is the conditional basic probability assignment of Y_j with respect to X_i . Equation (2) is the counterpart of Equation (1) in Bayesian inference.

The counterpart of Figure 1 in D-S theory is Figure 2; where the truth value of E is calculated by following: $(A,B) \rightarrow C$, $B \rightarrow D$, and $(C,D) \rightarrow E$.

$$m(C_c) = \sum_{A_a \subseteq A} \sum_{B_b \subseteq B} m(C_c | A_a, B_b) \cdot m(A_a) \cdot m(B_b) \tag{3}$$

$$m(D_d) = \sum_{B_b \subseteq B} m(D_d | B_b) \cdot m(B_b) \tag{4}$$

$$m(E_e) = \sum_{C_c \subseteq C} \sum_{D_d \subseteq D} m(E_e | C_c, D_d) \cdot m(C_c) \cdot m(D_d) \tag{5}$$

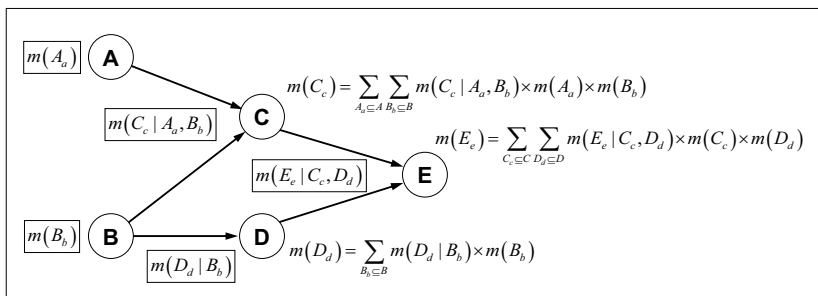


Figure 2. Dempster-Shafer inference

Once $m(E)$ is given, one can compute the Belief and Plausibility measures for E .

$$Bel(E) = \sum_{X|X \subseteq E} m(X), \text{ and } Pl(E) = \sum_{X|X \cap E \neq \emptyset} m(X) \tag{6}$$

The main difference between Bayesian inference and D-S inference is the use of available information (or evidence or knowledge). The former requires complete information about every state of premise and every pair of relation. The latter handles partial information about the combination of subsets. Accordingly, the strength of truth at E harbors greater uncertainty than the case of Bayesian inference in Eq.(1).

Construction of Knowledge about Premises and Relations in D-S Theory

Prior to inferring the consequence using D-S inference, knowledge about every premise and relation can be constructed by aggregating multiple expert opinions. Each expert assigns the basic probabilities to every state in premise and every state in relation. Information about premise X and relation $X \rightarrow Y$ from two sources can be combined through the Dempster’s rule of combination (DRC) as expressed in Equations (7) and (8), respectively.

$$m_X(X_i) = \frac{\sum_{A, B | A \cap B = X_i} m_X^{(1)}(A) \cdot m_X^{(2)}(B)}{1 - \sum_{A, B | A \cap B = \emptyset} m_X^{(1)}(A) \cdot m_X^{(2)}(B)} \tag{7}$$

$$m_{X \rightarrow Y}(Y_j | X_i) = \frac{\sum_{A,B|A \cap B = Y_j} m_{X \rightarrow Y}^{(1)}(A | X_i) \cdot m_{X \rightarrow Y}^{(2)}(B | X_i)}{1 - \sum_{A,B|A \cap B = \emptyset} m_{X \rightarrow Y}^{(1)}(A | X_i) \cdot m_{X \rightarrow Y}^{(2)}(B | X_i)} \quad (8)$$

where $m_X^{(1)}(X_i)$ and $m_X^{(2)}(X_i)$ are the truth values of X_i from Sources 1 and 2, respectively. $m_{X \rightarrow Y}^{(1)}(Y_j | X_i)$ and $m_{X \rightarrow Y}^{(2)}(Y_j | X_i)$ are the truth values of a relation between X_i and Y_j from Sources 1 and 2, respectively. The numerator shows the truth values of the consistent evidence toward the same X or $X \rightarrow Y$, and the denominator normalizes the truth after eliminating the truth values of the conflicting evidence.

D-S theory allows inferring the truth of proposition based on incomplete knowledge; this is not the case of Bayesian inference. For details of mathematics of this formula, among the available references are Shafer (1976), Yager (1987), Dubois and Prade (1988), Klir (1999; 2006), and Ayyub and Klir (2006).

APPLICATION TO TRANSIT PLANNING

The two approaches are applied to test the validity of the reasoning process for introduction of an automated people mover (APM) that serves travel demand from/to four new METRO stations in Tysons Corner, Virginia. Figure 3 shows the reasoning map. The map consists of 8 relations and 13 variables—four for the characteristics of APM (types of guideway, vehicle capacity, non-stop operation, and station spacing), one external factor (demand), six outcomes (service frequency, fleet size, in-vehicle speed, accessibility, wait time, and total travel time), and two goals of the project (cost and ridership).

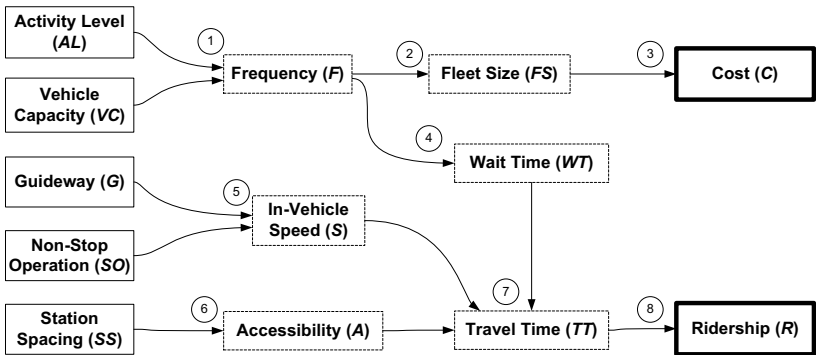


Figure 3. Reasoning map for evaluation of APM

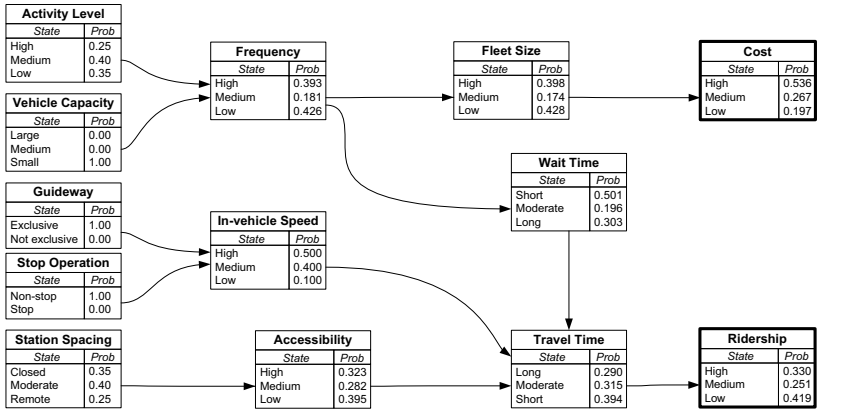
The strength of causal relations among the parameters is obtained from an expert in transit planning, and it is shown in Table 1. The strength of knowledge about each relation is given by $p(Y|X)$ in Bayesian probability theory and $m(Y|X)$ in D-S each. The former represents the strength of one outcome relative to all possible outcomes under the same given premise, and the latter represents the strength of one or more outcomes relative to all possible combinations under the same given premise. The following conditions must be satisfied: $\sum_{X_i \in X} p(Y | X_i) = 1$ and $\sum_{X_i \in X} m(Y | X_i) = 1$.

Table 1. Information used in a reasoning map

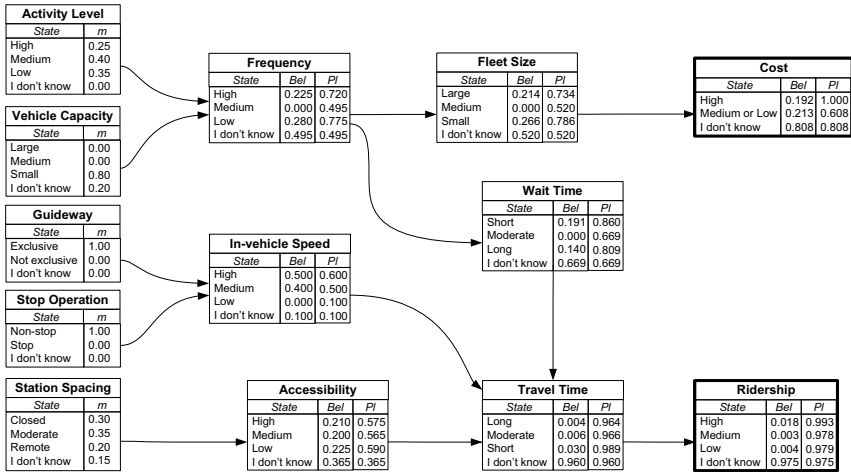
Relation	Degree of Truth	
	$p(Y X)$	$m(Y X)$
R1: Activity Level (<i>AL</i>) and Vehicle Capacity (<i>VC</i>) → Frequency (<i>F</i>)		
R1-1: If <i>AL</i> is large and <i>VC</i> is small, then <i>F</i> is high	0.90	0.90
R1-2: If <i>AL</i> is medium and <i>VC</i> is medium, then <i>F</i> is medium	0.75	0.75
R1-3: If <i>AL</i> is small and <i>VC</i> is small, then <i>F</i> is low	0.80	0.80
R2: Frequency (<i>F</i>) → Fleet size (<i>FS</i>)		
R2-1: If <i>F</i> is high, then <i>FS</i> is large	0.95	0.95
R2-2: If <i>F</i> is medium, then <i>FS</i> is medium	0.85	0.85
R2-3: If <i>F</i> is low, then <i>FS</i> is small	0.95	0.95
R3: Fleet size (<i>FS</i>) → Cost (<i>C</i>)		
R3-1: If <i>FS</i> is large, then <i>C</i> is high	0.90	0.90
R3-2: If <i>FS</i> is medium, then <i>C</i> is medium	0.60	0.60
R3-3: If <i>FS</i> is small, then <i>C</i> is low or medium	—	0.80
R4: Frequency (<i>F</i>) → Wait time (<i>W</i>)		
R4-1: If <i>F</i> is high, then <i>W</i> is short	0.85	0.85
R4-2: If <i>F</i> is low, then <i>W</i> is long	0.50	0.50
R4-3: If <i>F</i> is medium, then <i>W</i> is short or moderate	—	0.80
R5: Guideway (<i>G</i>) and Stopping Operation (<i>SO</i>) → Speed (<i>S</i>)		
R5-1: If <i>G</i> is exclusive and <i>SO</i> is non-stop, then <i>S</i> is high	0.50	0.50
R5-2: If <i>G</i> is exclusive and <i>SO</i> is non-stop, then <i>S</i> is medium	0.40	0.40
R6: Station spacing (<i>SS</i>) → Accessibility (<i>A</i>)		
R6-1: If <i>SS</i> is closely spaced, then <i>A</i> is high	0.60	0.60
R6-2: If <i>SS</i> is reasonably spaced, then <i>A</i> is medium	0.50	0.50
R6-3: If <i>SS</i> is remotely spaced, then <i>A</i> is low	0.90	0.90
R7: Speed (<i>S</i>), Accessibility (<i>A</i>), and Wait time (<i>WT</i>) → Travel Time (<i>TT</i>)		
R7-1: If <i>S</i> is high, <i>A</i> is high, and <i>WT</i> is short, then <i>TT</i> is short	1.00	1.00
R7-2: If <i>S</i> is high, <i>A</i> is high, and <i>WT</i> is long, then <i>TT</i> is long	0.20	0.20
R7-3: If <i>S</i> is high, <i>A</i> is low, and <i>WT</i> is short then <i>TT</i> is moderate	0.35	0.35
R7-4: If <i>S</i> is low, <i>A</i> is high, and <i>WT</i> is short then <i>TT</i> is short	0.65	0.65
R7-5: If <i>S</i> is medium, <i>A</i> is medium, and <i>WT</i> is medium then <i>TT</i> is short	0.90	0.90
R7-6: If <i>S</i> is high, <i>A</i> is low, and <i>WT</i> is long, then <i>TT</i> is long	0.50	0.50
R7-7: If <i>S</i> is low, <i>A</i> is high, and <i>WT</i> is long, then <i>TT</i> is moderate	0.40	0.40
R7-8: If <i>S</i> is low, <i>A</i> is low, and <i>WT</i> is short, then <i>TT</i> is long	0.55	0.55
R7-9: If <i>S</i> is low, <i>A</i> is low, and <i>WT</i> is long then <i>TT</i> is long	1.00	1.00
R8: Travel time (<i>TT</i>) → Ridership (<i>R</i>)		
R8-1: If <i>TT</i> is long, then <i>R</i> is low	0.90	0.90
R8-2: If <i>TT</i> is moderate, then <i>R</i> is medium	0.50	0.50
R8-3: If <i>TT</i> is short, then <i>R</i> is high	0.60	0.60
R8-4: If <i>TT</i> is short, then <i>R</i> is high or medium	—	0.50

Note: — means that it is not applicable in Bayesian inference.

Figures 4(a) and 4(b) show the results from Bayesian and D-S inference. The degree of support associated with each state variables is presented in probability $p(\cdot)$, and belief $Bel(\cdot)$ and plausibility $Pl(\cdot)$ in Bayesian and D-S inference, respectively.



4(a) Bayesian probability theory



4(b) Dempster-Shafer theory

Figure 4. Truth values of parameters in reasoning maps

When the two approaches are compared, Bayesian inference requires the complete knowledge of causality for every pair of the relationship. D-S theory not only allows

to affix “I don’t know” to some of the paired relations. but also to the nested sets, e.g., X_1 is related to “ Y_1 or Y_2 ” (R3-3 and R4-3 in Table 1). This is particularly useful for reasoning process in transportation planning, where uncertainty in causalities and/or where two or more opinions exist. Thus, the impacts of data collection or knowledge enhancement on the integrity of reasoning are evaluated.

The uncertainty in D-S theory are measured by two measures: the measure of non-specificity $N(m)$, and measure of discord $D(m)$. Non-specificity refers to ambiguity due to imprecise knowledge. The measure of non-specificity increases when the truth value of “I don’t know” state increase and the truth values of all specific states decrease. Discord refers to ambiguity due to conflicting information. The measure of discord increases when the truth values of two or more states are even. These two uncertainty measures are calculated as follows.

$$N(m(A)) = \sum_{A \in \Theta} m(A) \cdot \log_2 |A| \quad (9)$$

$$D(m(A)) = - \sum_{A \in X} m(A) \log_2 \left(\sum_{B \in X} m(B) \frac{|A \cap B|}{|B|} \right) \quad (10)$$

The details of these uncertainty measures can be found in Klir and Wierman (1999). Table 2 shows the uncertainty measures associated with each variable in a reasoning map shown in Figure 4(b).

Table 2. Uncertainty measures of a reasoning map in the D-S theory

Variables	Measures of Uncertainty		
	Non-specificity, $N(m)$	Discord, $D(m)$	Total Uncertainty, $TU(m)$
Frequency	0.785	0.926	1.417
In-vehicle speed	0.158	0.936	1.095
Fleet size	0.825	0.608	1.433
Accessibility	0.579	1.006	1.584
Wait time	1.060	0.448	1.508
Travel time	1.521	0.062	1.583
Cost	1.156	0.413	1.569
Ridership	1.546	0.039	1.584

Figure 4(b) and Table 2 show the propagation of uncertainty in decision-making process. In Figure 4(b), the amount of uncertainty propagates from the starting nodes to the end nodes. *Bel* values decreases and *Pl* values increase. The results show that travel time and ridership are the two least specific variables according to the non-specificity measure in Table 2 and the *Bel* of “I don’t know” in Figure 4(b). Frequency, speed, and accessibility are the three most conflicting variables according to the measure of discord in Table 2. Moreover, consider the total amount of uncertainty, which is the sum of non-specificity and discord measures, the uncertainty of each variable is generally very high compared to the maximum total uncertainty of 1.585. This table suggests that more information is needed in order to reduce the uncertainty about the truth of the reasoning map.

CONCLUSIONS

This paper has reviewed the characteristics of Bayesian inference and D-S theory inference in the context of evaluating an APM investment in a commercial complex. The calculation processes of the two approaches are examined, given X and $X \rightarrow Y$, and the abilities to handle "I don't know" in the casual knowledge are tested for the two inference mechanisms using an example.

In transportation planning, investment decisions are made based on loosely defined reasoning processes. In many cases knowledge is haphazard and case specific. Further, experts have different opinions. Bayesian inference does not have an explicit way to treat uncertainty in knowledge; sometimes it is treated assuming equal probability among the alternatives, but this does not distinguish between unknown and truly equal probabilities. Further, information to every pair of sets must be given. D-S inference, on the other hand, accommodates unknown by assigning values to power sets. Thus, not only the effects of additional information can be measured. Hence, use of both Bayesian inference and D-S theory will be useful in understanding of the effects of additional information and also the integrity of reasoning.

REFERENCES

- Ayyub, B. M. and Klir, G. J. (2006). *Uncertainty Modeling and Analysis in Engineering and the Sciences*, Florida: Taylor & Francis Group.
- Dubois, D. and Prade, H. (1988). Representation and combination of uncertainty with belief functions and possibility measures, *Computational Intelligence, Vol.4, No.3*, pp.244-264.
- Kikuchi, S. and Chakroborty, P. (2006). Place of possibility theory in transportation analysis. *Transportation Research Part B, 40(8)*, pp.595-615.
- Kikuchi, S. and Pursula, M. (1998). Treatment of uncertainty in study of transportation: Fuzzy set theory and evidence theory. *Journal of Transportation Engineering, Vol.24, No.1*, pp. 1-8.
- Klir, G. J. and Wierman, M. J. (1999). *Uncertainty-Based Information: Elements of Generalized Information Theory*, Helidelberg: Physica-Verlag.
- Klir, G. J. (2006). *Uncertainty and Information: Foundations of Generalized Information Theory*, New Jersey: John Wiley & Sons.
- Offutt, S. (2010). "The last mile in Tysons Corner, part 3: PRT?", *Greater Greater Washington*, March 12, 2010. <http://greatergreaterwashington.org/post.cgi?id=5181>
- Shafer, G. (1976). *A Mathematical Theory of Evidence*, Princeton, NJ: University Press.
- Yager, R. R. (1987). On the Dempster-Shafer framework and new combination rules, *Information Sciences, Vol.41, No.2*, pp.93-137.

A Simulation Framework for the Path Planning of Unmanned Autonomous Systems

M.-W. Kang¹, S. Wang², M.K. Jha¹, C.-C. Chen², and P. Schonfeld²

¹ Center for Advanced Transportation and Infrastructure Engineering Research (CATIER), Department of Civil Engineering, Morgan State University, 1700 E. Cold Spring Lane, Baltimore, MD 21251; PH (443)-885-1442; FAX 443-885-8218; email: min-wook.kang@morgan.edu, manoj.jha@morgan.edu

² Department of Civil & Environmental Engineering, 1173 Glenn L. Martin Hall, University of Maryland, College Park, MD 20742; PH (301)-405-3160; FAX (301)-405-2585; email: slwang@umd.edu, frank542@umd.edu, pschon@umd.edu

ABSTRACT

This paper presents a simulation framework designed to plan the movements of unmanned autonomous systems (UAS's) in hazardous environments, to coordinate their actions, predict their behavior and evaluate their mission success in various combat situations. Current simulation methods do not predict the complex interrelations among vehicles, operating environments, and paths, thus providing inadequate tests. A family of methods for coordinating, positioning, routing and assessing diverse military units or "agents" (such as unmanned ground vehicles) is described in this paper. The methods are tested and evaluated through computer simulations to ensure suitability for operating unmanned autonomous systems (UAS's). The path evaluation is performed using a dynamic GIS, distance transform, and genetic algorithms. The optimization algorithms for use in testing future unmanned systems are based on multiple objectives and criteria, including: (1) timeliness, (2) detectability & exposure time, (3) probabilities of survival & mission completion; (4) energy use; and (5) obstacle avoidance. A series of tests are presented which mimics real-world combat situation to test the effectiveness of the developed algorithms.

INTRODUCTION

Background

Unmanned Autonomous Systems (UASs), such as Unmanned Ground and Air Vehicles are increasingly used by the armed forces in carrying out tactical missions in combat situations (Frederick et al., 2005). However, these systems pose many technological challenges in ensuring their autonomy and trustworthiness in carrying out critical missions. For example, UASs often face multiple hazards and have to make complex decisions while carrying out their tactical missions through unfamiliar and hostile battlefield environments. The intelligence and capabilities of UASs are increasing over time and so is the complexity of their interactions with each other and with the environments in which they operate. Since the military is increasingly

relying on UAS's, and the UAS's may operate close to humans, it is important to comprehensively predict and test the behavior of such systems in order to anticipate problems and emergent behavior, and avoid surprises when lives are at stake.

Motivation

To date, our team has developed several valuable test and evaluation (T&E) methods for assessing the actions of UAS's as well as optimizing those actions according to various objectives, criteria, and constraints (Jha et al., 2008 and 2010). A common thread of those methods is that various missions, UAS characteristics and environments are pre-specified, and then paths, speeds and other control actions are optimized in real time (and often re-optimized as new information is acquired) in order to best satisfy the mission requirements and other evaluation criteria. The more elaborate versions of the methods developed by our team analyze and coordinate the actions of multiple UAS's, for example in searching and eliminating hazards in a specified area.

Based on our previous works (Jha et al., 2008 and 2010), this paper presents a simulation framework designed to plan the movements of UAS's in hazardous environments, to coordinate their actions, predict their behavior and evaluate their ability in carrying out mission success in various combat situations. Specifically, we develop a family of methods for coordinating, positioning, routing and assessing diverse military units or "agents" (such as unmanned ground vehicles). The methods are tested and evaluated through computer simulations to ensure suitability for operating unmanned autonomous systems (UAS's). The path evaluation is performed using a dynamic GIS, distance transform, and genetic algorithms. The optimization algorithms for use in testing future unmanned systems are based on multiple objectives and criteria, including: (1) timeliness, (2) detectability & exposure time, (3) probabilities of survival & mission completion; (4) energy use; and (5) obstacle avoidance.

The path finding methodology is described in the next Section and is followed by the description of the simulation framework in Section 3.

PATH FINDING METHODOLOGY

Genetic Algorithm (GA)-Based Path Finding

In GA-based path planning, paths between origins and destinations are evaluated based on the expected benefit of reaching the destination (B_f), the benefit of destroying enemies along the path (B_d), the expected travel cost of the agent (C_t), and the expected cost of losing that agent (C_e). Thus, an optimized path is determined based on maximizing the net benefit function $N = B_f + B_d - C_t - C_e$. In order to determine such four components in benefit measurement, other information such as locations of enemies, the sensor ranges and maximum shooting ranges for both friendly agents and enemies, are considered. Thus the net benefit for any given path with m agents and n enemies is defined as

$$N = vP_{m,n} + \sum_{i=1}^m tW_i - \sum_{u=1}^{n+1} c_d L_u P_{u-1,i} - c_e (1 - P_{m,n}) \quad (1)$$

where, v = value of reaching the destination and completing the mission;

$P_{m,n}$ = agent's cumulative survival probability after passing segment m and enemy ' n '

t = value of destroying an enemy (\$);

W_i = the cumulative survival probability of an enemy

c_d = unit travel cost (\$/m)

c_e = cost of losing agent (\$)

L_u = length of the segment ' u ' (m)

The cumulative survival probability (W_i) considers a series of conditional probabilities including: being within or outside the sensor detected range, available line of sight, and shooting ranges. The sensor ranges and maximum shooting ranges are determined by exploiting the spatial information from a GIS. The probability of visual detection is also affected by sensor ranges and line-of-sight (LOS) analysis based on the available terrain information.

$$K_{u,i} = k_{u,i} P(V_{u,i}^a | R_{u,i}^a) P(R_{u,i}^a), \text{ where } k_{u,i} = k_{\max} - (k_{\max} A_{u,i}) / R_{\max}^a \quad (2)$$

$$D_{u,i} = d_{u,i} P(V_{u,i}^e | R_{u,i}^e) P(R_{u,i}^e), \text{ where } d_{u,i} = d_{\max} - (d_{\max} A_{u,i}) / R_{\max}^e \quad (3)$$

The probability values depend on the distance between enemies and selected intermediate points along the candidate paths of the friendly agent. The probability of (line-of-sight) visibility (denoted as $P(V_{u,i}^a | R_{u,i}^a)$ or $P(V_{u,i}^e | R_{u,i}^e)$, from the agent or enemy's viewpoints, respectively) is conditional on the given probability of being within or outside the sensor ranges (denoted as $P(R_{u,i}^a)$ or $P(R_{u,i}^e)$), while the probability of destroying or being destroyed by enemy is conditional on the previously determined probability of visibility. A similar factor in the agent's cumulative survival probability is considered on the enemies' side, in the so-called cumulative destruction probability, which estimates the damage to each enemy. W_i is then derived from the cumulative product of probability of destroying enemies at different location along the path (i.e., 1 minus the cumulative destruction probability of each enemy).

$$W_i = 1 - \prod_{u=1}^m (1 - K_{u,i}) \quad (4)$$

With given origins and destinations (start and end points on the map), a GA is adapted in this path planning model to optimize a path with maximum net benefit. The GA process starts with generating a set of initial paths between given start and end points. Each path is then evaluated with the proposed information/GIS-based path evaluation function. As an evolution process, "parent paths" with higher net benefits are selected for reproducing the offspring paths in order to form the next generation, in which the "strong" offspring tend to replace the "weak" parents. The whole GA search process is stopped when there is no significant improvement in benefit between the paths found in the previous and current generations.

Distance Transformation with Weighted Travel Cost

Due to the complexity of surrounding environments, finding best paths of the friendly agents based only on the minimum distance to the target (i.e., destination) is not sufficient and lacks reality. The best path should guide the agent to reach the target as quickly as possible and to avoid no-go areas and highly risky regions exposed to enemies. As such, a weighted travel cost model which comprehensively evaluates friendly agent's energy consumption (with consideration of the slope of terrain, surface distance, and friction) and degree of exposure to the enemies is also developed here to find the preferred path. A mathematical formulation that minimizes total travel cost of the agent under specified constraints can be expressed as Equation (5). The path finding problem can be reduced to finding a set of successive points, and the Distance Transformation (DT) algorithm is used to find the best set of points. Four types of constraints are used for the formulation, and these are (i) upper and lower limits of the search space, (ii) No-go areas, (iii) slope constraint, and (iv) enemies' sensor search range.

$$\begin{aligned} \text{Minimize } C_{path}^T &= \sum_{i=1}^{n^{IP}+1} C_{i-1,i}^T \\ &= \sum_{i=1}^{n^{IP}+1} \left[(\omega^S D_{i-1,i}^S) (\omega^V F_{i-1,i}^V) \left(\frac{(\omega^F F_{i-1}^F + \omega^E F_{i-1}^E) + (\omega^F F_i^F + \omega^E F_i^E)}{2} \right) \right] \quad (5) \end{aligned}$$

$$\begin{aligned} \text{Subject to: } \lambda_{low} &\leq \lambda_i \leq \lambda_{upper} & \forall \lambda_i \in \mathcal{A} \\ \lambda_i &\notin \mathcal{A}_{NG} & \forall \lambda_i \in \mathcal{A} \\ \theta_{min} &\leq \theta_{i-1,i} \leq \theta_{max} & \forall \lambda_i \in \mathcal{A} \\ R_e^e &< d_i^e & \forall \lambda_i \in \mathcal{A}; \forall e^k \in \mathbf{E}^{\text{known}} \end{aligned}$$

where, C_{path}^T = Total travel cost of the friendly agent from start point to target,
 $C_{i-1,i}^T$ = Weighted travel cost between two successive points of \mathcal{A} ;
 $D_{i-1,i}^S$ = Surface distance between two adjacent points (λ_{i-1} and λ_i);
 $F_{i-1,i}^V$ = Vertical factor between two adjacent points (λ_{i-1} and λ_i);
 F_i^F = Value of friction factor at i^{th} point (λ_i);
 F_i^E = Agent's degree of exposure to all known enemies at i^{th} point (λ_i);
 $\omega^S, \omega^V, \omega^F, \omega^E$ = Weights for D^S, F^V, F^F , and F^E , respectively;
 \mathcal{A} = A set of successive points between the start and target locations;
 $\lambda_i \in \mathcal{A} = [\lambda_0, \dots, \lambda_i, \dots, \lambda_{n^{IP}+1}]$; \mathcal{A} is a subset of the search space (\mathcal{O});
 n^{IP} = The total number of points in \mathcal{A} ;
 λ_S, λ_T = Start and target locations of friendly UGR; $\lambda_S = \lambda_0$; $\lambda_T = \lambda_{n^{IP}+1}$;
 λ_{low} = Lower limit of the search space; $\lambda_{low} = (x_{low}, y_{low}, z_{low})$;
 λ_{upper} = Upper limit of the search space; $\lambda_{upper} = (x_{upper}, y_{upper}, z_{upper})$;
 \mathcal{A}_{NG} = No-go areas in the search space;
 $n(\mathbf{E}^{\text{known}})$ = The total number of enemies whose locations are pre-identified.

Besides the GA-based search method, we have also developed a Distance Transformation (DT)-based path finding method with the weighted travel cost function. DT is a simple algorithm which determines a transformed distance between

a particular point and target point. It is very popular for solution of path planning with both initially known and unknown field topology, and has been widely used for robot path planning in various environments (Kang et al., 2010; Marzouqi et al., 2005; Taylor et al., 2005; Wang et al., 2001). In DT, the path is generated by following the steepest gradient of the distance transform values from start to target. It can provide an efficient path in the presence of obstacles, and the minimum cost obtained by DT is the summation of incremental distances from one cell to another on a grid map. The weighted travel cost function shown in Equation (5) is used to find the least-cost path of the friendly UGV from any point to the target in the search space. DT propagates from the source cell (i.e., target), marking all free cells with an incrementing value.

SIMULATION FRAMEWORK

The simulation mechanism of the proposed model itself is centered by path planning algorithm, display interface and rules/roles characteristics. Visualization then demonstrates the simulation results as well as animation.

Framework of Fixed-Step Simulation Model

The features and assumptions of the fixed step simulation model are as follows:

- New information about locations of the friendly agents and enemies are updated continuously.
- Movements of the agent and enemies occur interactively with their moving “steps”. Only constant speeds are implicitly considered at this model development stage.
- Our agent makes a round trip to its destination, returning to its starting point.
- New enemies are generated during the agent’s mission and return trip.

There are three “activities” designed in this fixed step simulation model, any of which may be considered “new information”, either on new locations or different numbers of enemies:

- Move Agent: the agent moves with specified steps to targeting coordinates. The coordinates are the outputs of optimized path. Those targeting stations are the locations where agent re-optimizes the remaining path.
- Move Enemy: enemies move with specified steps toward the future location of agent.
- Add/Destroy Enemy: enemies are randomly added and/or destroyed when the friendly agent is moving toward the destination or back to origin. Whenever new enemies appear, the re-optimization process is applied to the remaining path. Whenever an encounter occurs, an enemy may be destroyed based on the shooting distance and killing probability.

Figure 1 shows the process of designed simulation model. The model starts with finding initial optimized path with loaded information for the GA or DT-based search. Model then drives the actions of moving for agents or enemies by following the path with segments and coordinates. In this model, the friendly agent and enemies

are responding iteratively to each other’s movements. That is, any agent’s movement is followed by enemies’ movement which is toward the agent’s future location. Since the agent is moving in “steps”, there will be several “stations”, marked for each “step”, along the agent’s optimal path. The movements of both sides are simulated by the given step which is specified as one of the simulation inputs. Re-optimization only occurs when our agent receives new information. The model can also design round trips for agents, from origin to destination, and then return to origin. The major difference between the directional trips is the relevant information from both agent and enemies. That is, when agent reaches the destination and is ready to return, the agent’s start and end points are switched, the path search is repeated and all the future movement will follow the new optimized path.

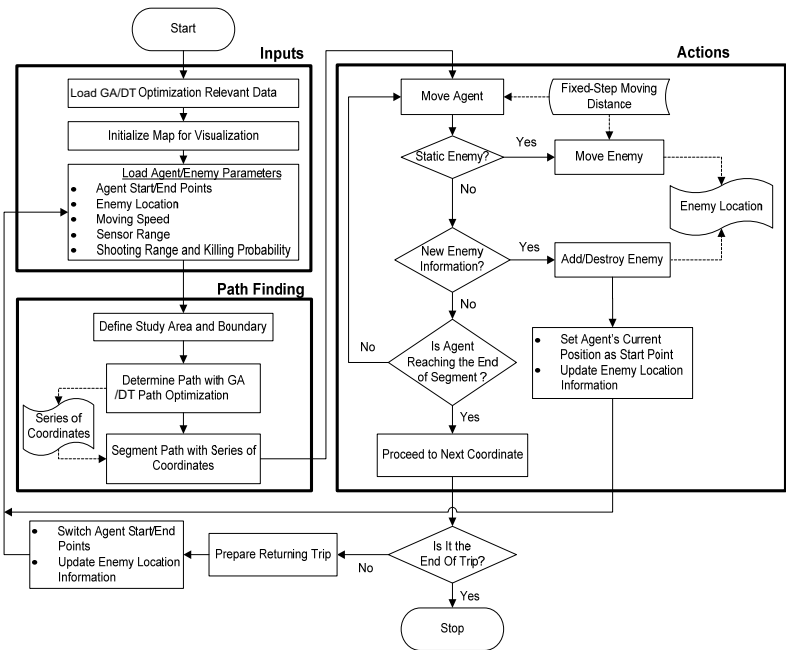


Figure 1. Fixed-Step Simulation Model with GA or DT-Based Optimization

CASE STUDY

Simulation with Moving Agent and Static Enemies

In order to easily present the relative location changes of the friendly agent and enemies, visualization with base map and “moving dots” is first developed. As shown in Figure 2(a), the agent is first indicated as a black dot on the map. With known enemies, a path is then determined for the agent from the start point to the destination (Figure 2(b)). By following the coordinates of the given path, the agent then moves along the path (Figure 2(c) and (d)).



Figure 2. Visualization of a Moving Agent with Static Enemies

Simulation in a Dynamic Environment

In this example the target of the friendly agent is a moving object, and its surrounding environment is time-varying where the elements of the environment change over time. Some large and small hilly mountains are located in the middle of the simulation environment, and three mobile enemies are initially placed in a south-west region of the friendly agent. The mission assigned to the agent is to chase and destroy the enemies distributed in the environment. Thus, calculation of least-cost paths, enemy movement, and agent's exploration to catch the enemy are iteratively processed during the simulation. Figure 3 shows trajectories of the moving objects during the simulation.

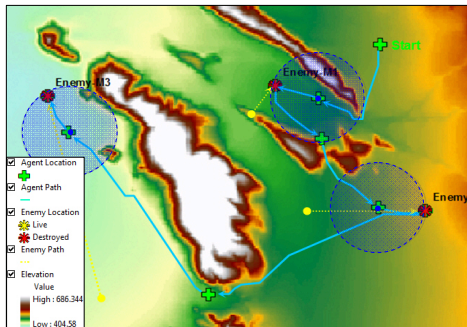


Figure 3. Path Planning for Chasing Multiple Mobile Enemies

When the simulation begins, the friendly agent first chases Enemy-M1 (i.e., target 1) because it is the closest from the agent. After the first target is destroyed, the agent moves for the next closest targets (Enemy-M2 and Enemy-M3 sequentially). The simulation runs until all the enemies are destroyed. In most of simulation runs, it has been observed that the friendly agent catches all the enemies since it is assumed to be faster than the enemies'. However, if its speed is less than or equal to the enemies', it may not be able to catch all the enemies unless it has intelligence to predict enemies' movements in advance. The path planning method proposed in this study will be further improved with consideration of variable speeds and intelligent behaviors of moving objects in a future study.

Hill Climbing Ability

In the proposed model, the friendly agent is designed to travel on mountainous regions based on its hill climbing ability. It can move forward, if its hill climbing ability (i.e., maximum slope that the agent can overcome) is higher than the slope between its current and next points. Figure 4(a) shows least-cost paths of the agent in a hilly terrain with different hill climbing abilities. As shown in the figure, the agent can cut across the hilly terrain with $\pm 40^\circ$ maximum slope to reach the target location; this is the shortest among the alternatives described in the figure. However, with $\pm 3^\circ$ maximum slope it is observed that the UGV travels only through the plain area, producing the longest travel distance.

Least-Cost Paths from Multiple Start Points

Assuming that there is no enemy in the simulation environment and that the mission of the friendly agent is to reach a known target, Figure 4(b) shows least-cost paths to the target from multiple starting points. Note that the maximum slope that the friendly agent can overcome is set to $\pm 14^\circ$ (25%) in this example. As shown in the figure, all six paths completely avoid the high slope regions in mountainous areas and are relatively direct to the target. The result indicates that the surface distance and slope factors are simultaneously evaluated to find the least-cost path.

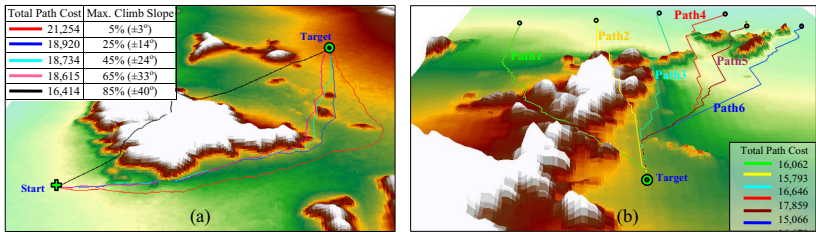


Figure 4. Least-Cost Paths (a) with Different Hill Climbing Abilities and (b) from Various Origins

CONCLUSION

In this study, an evolutionary path finding algorithm (i.e., GA-based search method) and a DT-based weighted travel cost method have been developed to position and route friendly agents (e.g., unmanned autonomous systems (UAS's)) in a hostile environment. A simulation framework has also been developed for testing the path planning methods as well as visualizing activities of moving objects (i.e., the agents and enemies) in the given environment. Through a series of case studies, it has been shown that the proposed path planning methods can find efficient paths and provide useful results.

A variety of GIS input data (such as terrain, land-cover, and ground elevation) and known/unknown information about the obstacle are provided in the simulation model to find the best paths of the friendly agent as well as to help it effectively navigate in the environment. In the proposed simulation model, the military path planning is dealt with two sub-problems: (1) global path finding and (2) local navigation based on the result of the path finding method. These two sub-problems

are iteratively processed one after another during the simulation; in the first stage, suitable locations where the friendly agent starts operating is determined (or given), and next the path from the start and target location is calculated. Navigation of the agent in a hostile environment is then processed in the second stage based the path found in the first stage.

The simulation model presented here can be developed into a versatile tool for testing and evaluating (in a simulated battlefield environment) the characteristics and performance of robotic vehicles, sensors, path planning algorithms and control, cooperation and information dissemination policies. The value and effectiveness of such factors in a wide range of missions and circumstances can be explored especially well by simulating the interactions of multiple agents on opposing teams.

ACKNOWLEDGMENTS

This work is funded by the Test and Evaluation/Science and Technology (T&E/S&T), Test Resource Management Center (TRMC) of the U.S. Department of Defense through the Scientific Research Corporation. The authors thank Mr. Shannon Arnold of Office of the Secretary of Defense (OSD) TRMC T&E/S&T for the support.

REFERENCES

- Frederick, P., Kania, R. Rose, M.D. Ward, D. Benz, U. Baylot, A. Willis, J. and Yamauchi, H. (2005). "Spaceborne Path Planning for Unmanned Ground Vehicles (UGVs)," Presented at MILCOM, Atlantic City, NJ. <http://ieeexplore.ieee.org/stamp/stamp.jsp?arnumber=01606139>>(July 2010).
- Jha, M.K., Schonfeld, P., Kikuchi, S., Kang, M.-W., Wang, S. and Kronprasert, N. (2010). *Software-Simulated Test and Evaluation of Military Missions Using Positioning and Routing Algorithms: Phase II Report*, Test and Evaluation/Science and Technology (T&E/S&T), Test Resource Management Center (TRMC), Department of Defense.
- Jha, M.K., Schonfeld, P. and Kikuchi, S. (2008). "Software-Simulated Test and Evaluation of Military Missions Using Positioning and Routing Algorithms" *Phase I Report*," Test and Evaluation/Science and Technology (T&E/S&T), Test Resource Management Center (TRMC), Department of Defense.
- Kang, M.-W., Jha, M.K. and Karri, G.A. (2010). "Determination of Robot Drop Location for Military Path Planning using GIS Application," *Proc., 4th WSEAS International Conference on Computer Engineering and Applications*, 194-200.
- Marzouqi, M. and Jarvis, R. (2005). "Covert Path Planning in Unknown Environments with Known or Suspected Sentry Location," *Proc., IEEE/RSJ International Conference on Intelligent Robots and Systems*, 1772-1778.
- Taylor, T., Geva, S. and Boles, W. (2005). "Directed Exploration Using a Modified Distance Transform," *Proc., Digital Imaging Computing: Techniques and Applications*, 365 - 370
- Wang, H., Chin, Y.T., Tay, L.P. and Wang, H. (2001). "Vision Guided AGV Using Distance Transform," *Proc. 32nd International Symposium on Robotics*,19-21

Development of Gap Acceptance Fuzzy Models using data from Driving Simulator Experiments

R. Rossi¹, M. Gastaldi¹, G. Gecchele¹

¹Department of Structural and Transportation Engineering, University of Padova, Via Marzolo, 9 – I35131 Padova (Italy); PH +390498275563; FAX +390498275577; email: riccardo.rossi@unipd.it

ABSTRACT

This paper describes the application of fuzzy models of drivers' gap-acceptance behavior at priority intersection; differently from other experiences, in this work gap-acceptance data were collected from experiments of driving behavior performed using a fixed-base driving simulator. The experiments have been conducted at the Transportation Laboratory of the University of Padova, using STSoftware[®] driving simulator.

The proposed fuzzy model allows to overcome problems related to both non-homogeneous explanatory variables and to uncertain and imprecise information on the system. Nevertheless, the findings appear interesting because allow to better understand the effects of explanatory variables not detectable from direct observations (on site) on driver's gap-acceptance behavior with the aim to use this knowledge to perform effective operational analysis (maneuver capacity and LOS assessment).

INTRODUCTION

In studies of vehicular gap acceptance behavior, the choice to accept or reject a gap¹ of a certain size is generally considered the result of a driver decision process which includes, as inputs, subjective estimates of a set of explanatory variables, given specific objective factors. These subjective evaluations are usually affected by a high degree of uncertainty, which can be properly treated both by classical probabilistic models (Tepley et al., 1997a; Tepley et al., 1997b; Maze, 1981) and by fuzzy system theory (Rossi and Meneguzzo, 2002; Rossi et al., 2009; Rossi et al., 2010a); calibration and validation of these models are usually based on gap-acceptance data collected at real intersection using, for instance, observation based on video survey. Starting from the considerations that driving simulators can provide reliable observations of drivers' behaviors (Blana, 1996; Farah et al., 2007), and considering the relevant effects of certain objective and subjective variables on gap-acceptance behavior (Adebisi and Sama, 1989; Wennel and Cooper, 1981) and observing that some of these variables are not detectable from direct observations (driver's education level, employment status, income, driving styles, etc.), in this work a set of experiments using driving simulator have been designed and developed with the aim to measure even the effects of some of these variables. A fuzzy theory-based model

¹ Gap is the time interval from two successive vehicles of the major stream.

of gap-acceptance using driving styles variables and other variables commonly used (time interval type and size, driver's gender) as explanatory ones has been estimated and validated. This work is an extension of previous studies concerning gap-acceptance behavior at priority intersections conducted by Transportation Laboratory of Padova University (Rossi and Meneguzzer, 2002; Rossi et al., 2009; Rossi et al., 2010a;).

The choice to use driving simulator experiments in this specific situation is justified on the basis of the findings carried out in Rossi et al. (2010b) where the driving simulator capability to represent real situation (with reference to the study case) has been demonstrated.

The paper is organized as follows. Section 2 is dedicated to a brief description of the laboratory experimental design. Section 3 describes the identification of the proposed fuzzy model and Section 4 its validation. Section 5 deals with the descriptive capability of the model. Concluding remarks are presented in Section 6.

LABORATORY EXPERIMENTAL DESIGN

The virtual environment has been built considering as reference a real three-leg priority intersection located in a sub-urban area near Venice (Figure 1). An high level of detail in three-dimensional representation of the real context has allowed to create a realistic virtual environment.

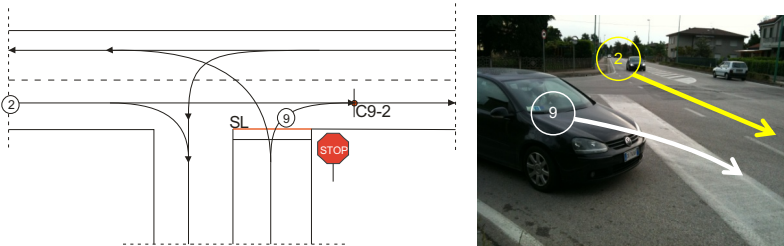


Figure 1 - Layout and pictures of the real three-leg priority intersection.

The driving experiments have been conducted at the Transportation Laboratory of the Department of Structural and Transportation Engineering (University of Padova) using STSoftware[®] driving simulator (Figure 2).



Figure 2 - STSoftware[®] driving simulator.

Our experiment explored how subjects (making right turn maneuver from minor street) select gaps presented in the same order as we had observed in the real situation. Each driver involved in the experiment responded to a questionnaire which collects socioeconomic information, such as age, gender, marital status, education, income and driving experience (years of driving, kilometers driven per year). In addition to personal information, the questionnaire included the multidimensional driving style inventory (MDSI) developed by Taubman Ben-Ari et al. (2004).

The MDSI is able to characterize four domains of driving style:

- reckless and careless driving, which refers to deliberate violations of safe driving norms, and the seeking of sensations and thrill while driving;
- anxious driving, which reflects feelings of alertness and tension as well as ineffective engagement in relaxing activities during driving;
- angry and hostile driving, which refers to expressions of irritation, rage, and hostile attitudes and acts while driving, and reflects a tendency to act aggressively on the road, curse, blow horn, or “flash” to other drivers;
- patient and careful driving, which reflects a well-adjusted driving style, and refers to planning ahead, attention, patience, politeness, keeping calm while driving as well as obeying traffic rules.

Twenty-four drivers relatively balanced as concerns gender were selected. They were chosen from students, staff of the University and people from outside the University according to the following characteristics:

- no experience with the driving simulator,
- at least 3 years of driving experience and
- average annual driven distance on rural roads of at least 5.000 km (3.100 mi).

Driving simulator software provides many parameters related to driver behavior; with regard to the purpose of this study, only major stream vehicles arrival time at the conflict point and test driver’s arrival and departure time at the stop line were considered. The data were organized in a database and then processed using a software procedure that allows to extract gap-acceptance information for each driver. For more detail about the experiment see Rossi et al. (2010b).

MODEL IDENTIFICATION

A total of 1.871 decisions (gap/lag acceptances and rejections) were recorded in the experiment; the average number of decisions per drivers’ approach to the minor street stop line was 2,36 (during a test the same driver approached about 7 times the intersection and each driver made at least four test during the experiment). A summary of the data collected during the experiment is shown in Table 1.

Table 1 - Sample of drivers' observed decisions

Type of interval	Total number of decisions (acceptances and rejections)	Average number of decisions per driver's approach
Gap	1.078	
Lag ²	793	2,36
Total	1.871	

With reference to MDSI in the following table a summary of measures (based on a six level scale of assessment) of test drivers driving style is shown.

Table 2 - Sample of drivers' driving style characteristics (MDSI classification)

Gender	Nr.	Reckless		Anxious		Angry		Patient	
		mean	SD	mean	SD	mean	SD	mean	SD
Male	14	2,15	0,40	2,62	0,46	1,94	0,41	4,52	0,46
Female	10	2,10	0,44	3,05	0,44	1,75	0,60	4,26	0,54
Total	24	2,14	0,39	2,71	0,48	1,90	0,44	4,47	0,47

SD: standard deviation

Starting from the consideration that the time interval size between vehicles on the primary street is the most important factor affecting gap-acceptance behavior (as widely reported in literature) and considering that driver evaluates this variable in subjective terms, in this work we consider time interval as fuzzy variable; others fuzzy variables are driver's "Recklessness" and "Anxiety". Interval type (lag or gap) and drivers' gender are objective factors and then treated as crisp variables in the model. With reference to driving style measures, "Angry" style is not considered because it is not significant (mean value less than 2, see Table 2) and "Patient" style is implicitly considered as opposite to "Recklessness" or "Anxiety".

For the identification of the fuzzy model knowledge base (membership functions of the premise and consequence fuzzy sets, and rules of inferences of the fuzzy inference system) the so-called FPA (Fast Prototype Algorithm, Glouennec 1999) has been used.

The fuzzy system knowledge base obtained was characterized by five triangular fuzzy sets in the domain of the time interval size, by two triangular fuzzy sets in the domain of variables "Recklessness" and "Anxiety" and by two "singletons" in the domain of the crisp variables "type of interval" and "gender". Forty-four rules (42 compensatory and 2 non-compensatory) have been identified (see Table 3). A simple Mamdani-type method of inference has been adopted (see Klir and Yuan, 1995). A satisfactory value of goodness-of-fit has been obtained ($R^2=0,78$).

² Lag is a residual part of a major-stream gap measured from the time when the minor-stream drivers arrives at the stop line (and start the gaps selection) until the next major-stream vehicle arrives to the conflict point.

Table 3 – Fuzzy model knowledge base characteristics.

	variable	Shape	number
Premise	Time Interval	Triangular	5
	Recklessness	Triangular	2
	Anxiety	Triangular	2
	Interval Type	Singleton	2
	Gender	Singleton	2
Consequence	Acceptance	Triangular	2
Number of rules	Compensatory	Non-Compensatory	Tot.
	42	2	44

In Figure 3 a graphical representation of the fuzzy sets of the premises and consequence are shown.

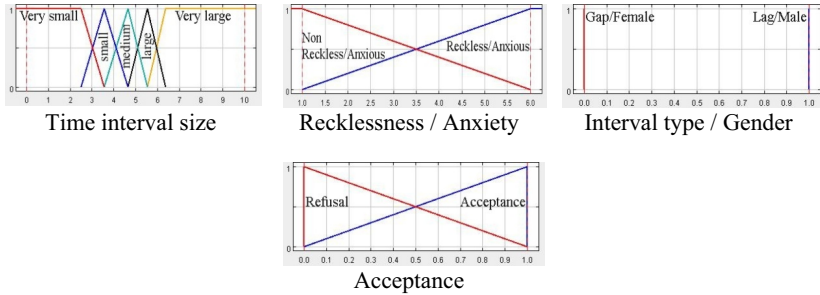


Figure 3 – Fuzzy model premises and consequence fuzzy sets.

As an example the two non-compensatory and two compensatory rules are:

- *If Interval Size is Very Small Then Refusal*
- *If Interval Size is Very Large Then Acceptance*
- ...
- *If driver is Male And Reckless And Non-anxious And Interval Type is Gap And Interval Size is Small Then Acceptance*
- *If driver is Female And Non-reckless And Anxious And Interval Type is Lag And Interval Size is Medium Then Refusal*

MODEL VALIDATION

The model effectiveness has been evaluated by means of the ROC curve analysis (Fawcett, 2006). The basic idea of ROC curve analysis may be explained by considering an experiment with only two possible outcomes, 1 and 0, that are denoted as *positive* and *negative* outcomes.

In the case under analysis the “acceptance” domain was divided in two parts with a threshold equal to 0,5: the left side was defined as a negative outcome (gap/lag rejection) and the right side (gap/lag acceptance) as a positive one. The outcomes

obtained from model rules, and represented by fuzzy sets, have been determined using the centroid defuzzification method. This method allows to identify a synthetic measure (“acceptance index”) representative of the output fuzzy set, giving a compact information about the “acceptance” of a gap/lag for certain values of the premise variables (centroid method, see Klir and Yuan (1995)).

Under these assumptions the basic metrics of ROC analysis become:

- True Positive (TP): the model predicts an acceptance and the driver accepted a gap/lag of a certain size;
- False Positive (FP): the model predicts an acceptance and the driver rejected a gap/lag of a certain size;
- True Negative (TN): the model predicts a rejection acceptance and the driver rejected a gap/lag of a certain size;
- False Negative (FN): the model predicts a rejection and the driver accepted a gap/lag of a certain size;

the probability of correctly identifying positive outcomes may be defined as:

- TPR (True Positive Rate) = number of TP/(number of TP + number of FN)

and the probability of correctly identifying negative outcomes as:

- TNR (True Negative Rate) = number of TN/(number of TN + number of FP)

The ROC curve describes the relationship between TPR, called “sensitivity”, and (1-TNR), called “1-specificity”, for all possible classification thresholds. The ROC curve may be interpreted as describing the relationship between the “percentage of hits” and the “percentage of false alarms” obtained with the model. The Area Under the ROC Curve (AUC) is related to the accuracy of the model predictions, and increases with it; in particular, when this area is equal to 1,0 the model produces perfect forecasts, and when it is equal to 0,5 the model produces random forecasts.

Consequently a set of metrics can be derived, that are:

- F-measure = $2 / \{1 / [\text{number of TP} / (\text{number of TP} + \text{number of FP})] + 1 / \text{TPR}\}$
- Percent right = $[(\text{number of TP} + \text{number of TN}) / (\text{number of outcomes})] * 100$
- Youden Index = $J = \text{TPR} + \text{TNR} - 1$

The maximum value of F-measure, Youden Index and AUC is equal to 1 (perfect model); obviously a good model should have high values of metrics AUC, F-measure, Percent right and Youden Index. The metrics computed (Table 4) show good performance of the estimated model to represent the observed decisions.

Table 4 – Fuzzy model knowledge base characteristics.

Youden Index	F-Measure	Percent Right	AUC
0,85	0,91	92,78%	0,97 ± 0,004

DESCRIPTIVE CAPABILITY OF THE MODEL

Using the “acceptance index”, it is possible to build “acceptance curves” that allow to use the model as predictive tool (and to validate it over the calibration sample). When a gap/lag of a certain size has an acceptance index greater than or equal to the 0.5 threshold, it is considered “acceptable”, otherwise it is considered “unacceptable”. In Figure 4 some acceptance curves for the model are shown; we

observe that the oscillations of the acceptance index that are visible in all the curves may be explained by the specific shape of the membership functions (triangular) and by the structure of the adopted inference rules.

The descriptive capability of the model appear significant and substantially coherent with previous results reported in literature (in the knowledge of the authors, previous findings on driving style effect on gap-acceptance behavior at priority intersection are not reported); some remarks follow:

- females (non-reckless and non-anxious) seem to need wider time interval regardless of interval type;
- reckless males seem to need smaller time interval than non-reckless males;
- reckless males show a more aggressive behavior than reckless females;
- anxious males seem to need wider interval than non-anxious males.

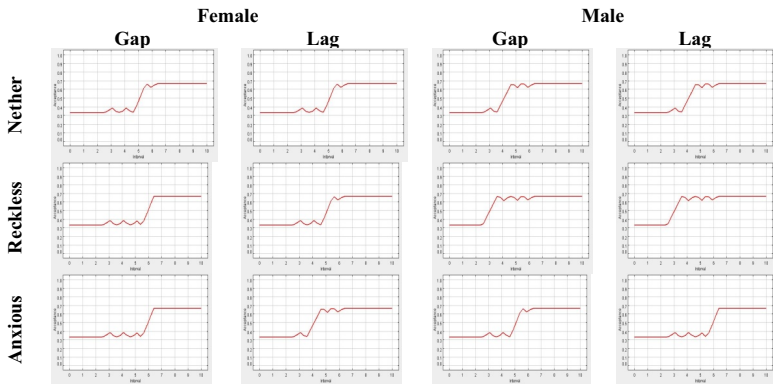


Figure 4 – Fuzzy gap-acceptance model. Acceptance curves as a function of “Gender”, “Time Interval type”, “Driving style” and “Time interval size”.

CONCLUSIONS AND REMARKS

In this work, using data collected from laboratory experiments of driving behavior (questionnaire and driving simulator sessions), a fuzzy model of gap-acceptance behavior at priority intersections has been developed. Laboratory experiments allowed to observe and record information about explanatory variables not detectable from direct observations (on site) allowing to include them in models with the aim to better describe, understand and simulate driver’s choices. On the other hand the use of a fuzzy model allowed to overtake problems concerning non-homogeneous explanatory variables and uncertain and imprecise information on the system.

The proposed fuzzy model has included driving styles variables (“recklessness”, “patient style”, “anxiety”) in addition to some variables commonly used (time interval type and size, driver’s gender).

The results obtained appear interesting:

- the proposed fuzzy model demonstrates good capability in representing real driver’s gap acceptance behavior;

- with reference to commonly used variables, the descriptive capability of the model appear substantially coherent with previous results reported in literature;
- the driving styles variables “recklessness” and “anxiety” have a significant influence on gap-acceptance behavior.

Nevertheless, there are some directions in which this work could be extended:

- analysis of other factors that could affect gap-acceptance behavior (speed and type of approaching vehicles on the main road, driver’s education level, employment status, income, past involvement in car accidents, fatigue, etc.);
- extension of the sample size (number and stratification) in order to better represent the population of drivers and their driving styles.

REFERENCES

- Adebisi, O. and Sama, G. N. (1989). Influence of stopped delay on driver gap acceptance behavior, *Journal of Transportation Engineering*, 115 (3), 305-315.
- Blana, E. (1996), Driving simulator validation studies: a literature review. Institute of Transport Studies, University of Leeds, Working Paper 480. ISSN 0142-8942.
- Farah, H., Polus, A., Bekhor, S., Toledo, T. (2007), Study of passing gap acceptance behavior using driving simulator, *Advances in Transportation Studies an International Journal*, Special Issue, 9-16.
- Fawcett, T. (2006). “An introduction to ROC analysis”. *Pattern Recognition Letters*, 27(8), 861–874.
- Glorennec, P.-Y. (1999). Algorithmes d’apprentissage pour systems d’inférence floue. Editions Hermès, Paris.
- Maze, T.H. (1981). A probabilistic model of gap acceptance behavior. Transportation Research Record 795, *Transportation Research Board*, National Research Council, Washington, DC, 8-13.
- Rossi, R., and Meneguzzer, C. (2002). “The effect of crisp variables on fuzzy models of gap-acceptance behaviour”, Proceedings of the 13-th Mini-EURO Conference “Handling Uncertainty in the Analysis of Traffic and Transportation Systems”, Bari (Italy), 240-252.
- Rossi, R., Gastaldi, M., and Meneguzzer, C. (2009). “Transferability analysis of Logit models of gap acceptance behavior”. In: Proceedings of the "XIII Meeting of the Euro Working Group on Transportation". Padova, 23-25 September: Padova University Press, ISBN/ISSN: 978-88-903541-4-4.
- Rossi, R., Gastaldi, M., and Meneguzzer, C. (2010a). “Comparative evaluation of Logit and Fuzzy Logic models of gap-acceptance behavior”, TRISTAN VII, Seventh Triennial Symposium on Transportation Analysis, Tromsø, Norway, 20-25 June, 2010.
- Rossi, R., Gastaldi, M., and Meneguzzer, C. and Gecchele, G. (2010b). “Gap-acceptance behavior at a priority intersection: field observations versus experiments with a driving simulator”, accepted for presentation at TRB 90th Annual Meeting, Washington D.C., 23-27 January 2011.

- Taubman-Ben-Ari, O., Mikulincer, M., and Gillath O. (2004). The multidimensional driving style inventory - scale construct and validation. *Accident Analysis and Prevention*, 36(3), 323-332.
- Teply, S., Abou-Henaidy, M. I., and Hunt, J. D. (1997a). Gap acceptance behaviour – aggregate and Logit perspectives: Part 1, *Traffic Engineering and Control*, 9, 474-482.
- Teply, S., Abou-Henaidy, M. I., and Hunt, J. D. (1997b). Gap acceptance behaviour – aggregate and Logit perspectives: Part 2, *Traffic Engineering and Control*, 10, 540-544.
- Wennel, J. and Cooper, D. F. (1981). Vehicle and driver effects on junction gap acceptance, *Traffic Engineering and Control*, 22 (12), 628-632.

Entropy Approach to Risk-Analysis of Critical Infrastructures Systems **S.A. Timashev, A.N. Tyrnin**

One of the main yet unsolved problems in the theory of risk is construction of adequate models of complex systems which are comprised of critical infrastructures (CI). These models should allow design of simple and effective quantitative methods of risk analysis and safety control of operating systems. Interaction of elements (subsystems) of complex systems is hard to present explicitly. Another difficulty when modeling CIs is the heterogeneity of the input information which describes functioning of the various elements of CI. Traditional models of representation based on series-parallel connections of CI elements not always give adequate description of CI systems [1]. Usage of the logic-probability models [2, 3], and graph theory models [4] demands greater efforts and presence of significant prior information on the subject of research, which is not always possible.

Modern physics has a useful tool, namely, the entropy concept, for convolution of all significant parameters of a problem into one. Entropy is a universal physical parameter, which allows uniting various displays of the physical world in one single parameter. Thus, it may serve as a common denominator. The modern informational concept of entropy is flexible and permits accurate and precise interpretation in terms of that section of science where it is applied. It is increasingly widely used in modern science for description of structural disorganization; degree of destruction of connections between elements of a system, and generally, for description of the degree of degradation of any closed system, including territorial CIs [5-8]. It is possible to decompose the total entropy of a system into its components – entropies of interaction, configuration, local, structural, etc., which allows making decisions on how to maximize/minimize them. Hence, entropy can be considered as a universal parameter and is ideally fit for being used in risk-management of complex systems, which are represented as a population of interdependent critical infrastructures (ICIs) [4, 9]. In this setting, ICIs are modeled as subsystems of a system. This approach allows optimizing the strategies of renewal of CIs and is a step to integrating models of ICIs into decision support systems. Possibilities can be seen of creating principally new models of early diagnostics and monitoring of systems resilience, revealing correlation between limit states of ICI structures and the corresponding level of their entropy. It is also possible to estimate the maximal permissible levels of the specific entropies (thermodynamic, informational, social, communicative, etc.) for various types of interdependent CI at which their resilience and social longevity is not violated.

In this paper basic problems are considered of developing the entropy-probabilistic approach for solving problems of assessing the safety of interdependent CI. This approach allows overcoming the problem of heterogeneity of source data, as all physical parameters of various engineering problems are brought down to one dimensionless measure – the system entropy.

Proceed to description of the basic concept of the described above approach. Let X be some random variable (RV) with known probability density function (PDF), which describes the functioning of a single CI (for instance, its output). If, further, X is a discrete RV which can take a finite number of values x_1, \dots, x_n , then

$$P_X(x_i) = p_i, \sum_{i=1}^n p_i = 1, p_i \geq 0, i = 1, 2, \dots, n.$$

In this case the CI entropy is defined as

$$H(X) = -\sum_{i=1}^n p_i \log p_i, \quad (1)$$

And is named informational entropy [10]. The unit of measure of information and entropy depends on the type of the logarithm foundation in (1).

As the law of distribution of the RV is known, it is possible to express the entropy in the integral form

$$H(X) = -\int_{-\infty}^{+\infty} p(x) \log p(x) dx, \quad (2)$$

where $p(x)$ is the PDF of the RV X . The entropy calculated using the formula (2), is referred to as entropy of the PDF, or differential entropy.

Comparing (1) and (2) it is easy to see, that informational entropy (1) and differential entropy (2) differ from each other only by a constant. However, the differential entropy, being a numerical characteristic (functional) of the PDF $p(x)$, has a clear interpretation and, consequently, is more preferable to use. For convenience use in (2) the natural foundation of the logarithm, i.e., define entropy as

$$H(X) = -\int_{-\infty}^{+\infty} p(x) \ln p(x) dx.$$

Consider interdependent CI as elements of a certain complex system S . Then system S can be presented in the form of a multi-dimensional random variable $\mathbf{X} = (X_1, X_2, \dots, X_n)^T$. Each element X_i of this vector is one-dimensional random variable, which characterizes the functioning of the corresponding CI of the complex system being studied.

System elements can be interdependent or independent. Keeping this in mind, define the entropy of the multi-dimensional random variable \mathbf{X} by the formula

$$H(\mathbf{X}) = -\int_{-\infty}^{+\infty} \dots \int_{-\infty}^{+\infty} p(x_1, x_2, \dots, x_n) \ln p(x_1, x_2, \dots, x_n) dx_1 dx_2 \dots dx_n, \quad (3)$$

and, at this, $H(\mathbf{X}) \leq \sum_{i=1}^n H(X_i)$, where the equality is reached only under condition of mutual independence of RVs X_1, X_2, \dots, X_n .

Introduce two following pre-conditions.

1°. Consider that all components X_i of the random vector

$$\mathbf{X} = \begin{pmatrix} X_1 \\ X_2 \\ \dots \\ X_n \end{pmatrix}$$

have normal distribution $X_i \sim N(a_i, \sigma_i^2)$, i.e. $p_{X_i}(x) = \frac{1}{\sqrt{2\pi\sigma}} e^{-\frac{(x-a_i)^2}{2\sigma_i^2}}$, $i = 1, 2, \dots, n$.

2°. The covariance matrix

$$\Sigma = \{\sigma_{ij}\}_{n \times n} = \begin{pmatrix} \text{cov}(X_1, X_1) & \text{cov}(X_1, X_2) & \dots & \text{cov}(X_1, X_n) \\ \text{cov}(X_2, X_1) & \text{cov}(X_2, X_2) & \dots & \text{cov}(X_2, X_n) \\ \dots & \dots & \dots & \dots \\ \text{cov}(X_n, X_1) & \text{cov}(X_n, X_2) & \dots & \text{cov}(X_n, X_n) \end{pmatrix} = \begin{pmatrix} \sigma_1^2 & \sigma_{12} & \dots & \sigma_{1n} \\ \sigma_{21} & \sigma_2^2 & \dots & \sigma_{2n} \\ \dots & \dots & \dots & \dots \\ \sigma_{n1} & \sigma_{n2} & \dots & \sigma_n^2 \end{pmatrix}$$

of the random vector \mathbf{X} is known or can be determined via a sample set of X_i .

Define entropy $H(\mathbf{X})$. Introduce vector of mathematical expectations $\mathbf{a} = (a_1, a_2, \dots, a_n)'$. Then, in view of 1° and 2°

$$p(x_1, x_2, \dots, x_n) = \frac{1}{(2\pi)^{\frac{n}{2}} |\Sigma|^{\frac{1}{2}}} \exp\left\{-\frac{1}{2}(\mathbf{X}-\mathbf{a})\Sigma^{-1}(\mathbf{X}-\mathbf{a})^T\right\},$$

where $|\Sigma|$ is the determinant of matrix Σ . Further, transform (3):

$$\begin{aligned} H(\mathbf{X}) &= - \int_{-\infty}^{+\infty} \dots \int_{-\infty}^{+\infty} p(x_1, \dots, x_n) \ln \left\{ \frac{1}{(2\pi)^{\frac{n}{2}} |\Sigma|^{\frac{1}{2}}} \exp\left\{-\frac{1}{2}(\mathbf{X}-\mathbf{a})\Sigma^{-1}(\mathbf{X}-\mathbf{a})^T\right\} \right\} dx_1 \dots dx_n = \\ &= \ln \left[(2\pi)^{\frac{n}{2}} |\Sigma|^{\frac{1}{2}} \right] \int_{-\infty}^{+\infty} \dots \int_{-\infty}^{+\infty} p(x_1, \dots, x_n) dx_1 \dots dx_n + \\ &+ \frac{1}{2} \int_{-\infty}^{+\infty} \dots \int_{-\infty}^{+\infty} p(x_1, \dots, x_n) (\mathbf{X}-\mathbf{a})\Sigma^{-1}(\mathbf{X}-\mathbf{a})^T dx_1 \dots dx_n = \\ &= \ln \left[(2\pi)^{\frac{n}{2}} |\Sigma|^{\frac{1}{2}} \right] + \frac{n}{2} = \frac{1}{2} \ln [(2\pi)^n |\Sigma|] + \frac{1}{2} \ln e^n = \frac{1}{2} \ln [(2\pi e)^n |\Sigma|]. \end{aligned}$$

Thus, the entropy of the random normal vector \mathbf{X} is equal to

$$H(\mathbf{X}) = \frac{1}{2} \ln [(2\pi e)^n |\Sigma|]. \tag{4}$$

From (4) it can be seen, that entropy $H(\mathbf{X})$ is an elementary function of the determinant of covariance matrix Σ . Therefore, relation (4) represents a simple mathematical model, which allows constructing simple optimization algorithms. In order to use this approach, some prerequisites should be described.

In [7] it is shown, that in some cases, the safest state of a structure is when it is maximally indeterminate, i.e. when the structure entropy is maximal (provided the structure design is robust). It stands to reason to use this principle when analyzing complex systems of ICI.

Pre-conditions 1°, 2° are based on the central limit theorem CLT. If conditions of a problem do not allow considering vector \mathbf{X} as normal, perform a "power" linearization of the source data. The essence of this transformation consists in that random components X_i are considered having Gaussian distribution with average values and variances equal to their sample estimations.

Formulate following principle (hypothesis): "The system entropy growth corresponds to the system safety growth." This hypothesis does not contradict the findings of a number of publications [4-8]. This principle is not universal, but is valid for a certain class of structures. Using this principle, the problem of maximizing the safety of complex systems can be simplified and unified. Namely, it can be substituted by a more formalized problem of increasing the entropy of an observable structure or CI. Now, the entropy of the whole system can be increased through the increase of the level of indeterminacy of one or several of its subsystems. At this, the known difficulty arises as to which "point(s)" of the system the limited resources should be applied and what would be the optimal distribution of the aforementioned resources, in order to achieve the necessary level of security for the system in consideration. In order to solve this problem, introduce the concept of "points of growth-POG". The essence of this concept consists in purposeful concentrating operating actions only in specific POGs. As the system is an interconnected single whole, hence, by acting on correctly chosen POGs of the system, it is possible to increase the system safety up to the needed level.

Thus, when modeling safety of complex systems of CI it is necessary to formulate following three important problems, which wait for solution:

1. Is there and what is the universal criterion of effective management of a system of ICI?
2. How and which POGs to choose for activating the processes which ensure the subsequent effective operation of the whole system?
3. What minimal resources are needed to jump-start these processes?

The analysis of the proposed basic entropy-probabilistic model (EPM) of CI system safety in the form of (3), (4) shows, that one of the formalistic paths for increasing (maximizing) entropy of a multi-dimensional RV is by adding some normally distributed RV U to one of its components X_1, X_2, \dots, X_n . Its variance σ_u^2 is an equivalent to acting on a corresponding component of the random vector \mathbf{X} . In practice it could be an input of additional resources (including financial) into one of the CIs – POGs. Coherence of CIs and their interconnectivity will lead to increase of safety of the whole system.

From (4) it follows that the criterion function of the given method of entropy maximization has the form

$$H(X_1, X_2, \dots, X_i + U, \dots, X_n) = \frac{1}{2} \ln \left[(2\pi e)^n (|\Sigma| + \sigma_u^2 M_{ii}) \right],$$

where M_{ii} is the minor of i -th line and i -th column of matrix Σ .

Hence, the problem of maximization of entropy takes the form:

$$\begin{cases} H(X_1, X_2, \dots, X_i + U, \dots, X_n) \rightarrow \max, \\ \Sigma_X = \Sigma, \\ \sigma_u^2 = \sigma^2, \\ \text{cov}(U, X_i) = 0, \quad i = 1, 2, \dots, n. \end{cases} \tag{5}$$

The problem (5) permits realization of efficient control of the system of CI. Its solution will ensure maximal increase of system entropy and safety.

If there is a possibility of simultaneous action on several CIs, the problem (5) can be generalized. In this case act additively on the multi-dimensional RV \mathbf{X} by an additional vector, which elements do not depend on elements of the initial RV. Now the problem comes down to maximal increase of entropy of a multi-dimensional RV by adding normally distributed random variables U_i ($U_i \sim N(a_{u_i}, \sigma_{u_i}^2)$) to the components X_i of RV \mathbf{X} . Now consider that $\text{cov}(X_i, U_i) = 0, i = 1, 2, \dots, n$. Denote:

$$\mathbf{U} = \begin{pmatrix} U_1 \\ U_2 \\ \dots \\ U_n \end{pmatrix}, \quad \mathbf{\Omega}_u = \begin{pmatrix} \sigma_{u_1}^2 \\ \sigma_{u_2}^2 \\ \dots \\ \sigma_{u_n}^2 \end{pmatrix}.$$

Demonstrate that the entropy of vector $\mathbf{X}^* = \mathbf{X} + \mathbf{U}$ will be defined using formula

$$H(\mathbf{X}^*) = \frac{1}{2} \ln \left[(2\pi e)^n \left(|\Sigma| + \sum_{i=1}^n \sigma_{u_i}^2 M_{ii}^* \right) \right], \tag{6}$$

where

$$M_{11}^* = \begin{vmatrix} \sigma_2^2 + \sigma_{u_2}^2 & \sigma_{23} & \dots & \sigma_{2n} \\ \sigma_{32} & \sigma_3^2 + \sigma_{u_3}^2 & \dots & \sigma_{3n} \\ \dots & \dots & \dots & \dots \\ \sigma_{n2} & \sigma_{n3} & \dots & \sigma_n^2 + \sigma_{u_n}^2 \end{vmatrix}, \quad M_{22}^* = \begin{vmatrix} \sigma_1^2 & \sigma_{13} & \dots & \sigma_{1n} \\ \sigma_{31} & \sigma_3^2 + \sigma_{u_3}^2 & \dots & \sigma_{3n} \\ \dots & \dots & \dots & \dots \\ \sigma_{n1} & \sigma_{n3} & \dots & \sigma_n^2 + \sigma_{u_n}^2 \end{vmatrix},$$

...

$$M_{mm}^* = \begin{vmatrix} \sigma_1^2 & \sigma_{12} & \dots & \sigma_{1,n-1} \\ \sigma_{21} & \sigma_2^2 & \dots & \sigma_{2,n-1} \\ \dots & \dots & \dots & \dots \\ \sigma_{n-1,1} & \sigma_{n-1,2} & \dots & \sigma_{n-1}^2 \end{vmatrix} = M_{mm}.$$

As the entropy of a n-dimensional normally distributed RV \mathbf{X} is defined by formula (4), hence, at passage to \mathbf{X}^* in the design formula for the entropy, only the covariance matrix will vary. It will become

$$\Sigma^* = \begin{pmatrix} \sigma_1^2 + \sigma_{u_1}^2 & \sigma_{12} & \dots & \sigma_{1n} \\ \sigma_{21} & \sigma_2^2 + \sigma_{u_2}^2 & \dots & \sigma_{2n} \\ \dots & \dots & \dots & \dots \\ \sigma_{n1} & \sigma_{n2} & \dots & \sigma_n^2 + \sigma_{u_n}^2 \end{pmatrix}.$$

Calculate its determinant:

$$\begin{aligned} |\Sigma^*| &= \begin{vmatrix} \sigma_1^2 + \sigma_{u_1}^2 & \sigma_{12} & \dots & \sigma_{1n} \\ \sigma_{21} & \sigma_2^2 + \sigma_{u_2}^2 & \dots & \sigma_{2n} \\ \dots & \dots & \dots & \dots \\ \sigma_{n1} & \sigma_{n2} & \dots & \sigma_n^2 + \sigma_{u_n}^2 \end{vmatrix} = \begin{vmatrix} \sigma_1^2 & \sigma_{12} & \dots & \sigma_{1n} \\ \sigma_{21} & \sigma_2^2 & \dots & \sigma_{2n} \\ \dots & \dots & \dots & \dots \\ \sigma_{n1} & \sigma_{n2} & \dots & \sigma_n^2 \end{vmatrix} + \\ &+ \sigma_{u_1}^2 \begin{vmatrix} \sigma_2^2 + \sigma_{u_2}^2 & \sigma_{23} & \dots & \sigma_{2n} \\ \sigma_{32} & \sigma_3^2 + \sigma_{u_3}^2 & \dots & \sigma_{3n} \\ \dots & \dots & \dots & \dots \\ \sigma_{n2} & \sigma_{n3} & \dots & \sigma_n^2 + \sigma_{u_n}^2 \end{vmatrix} + \sigma_{u_2}^2 \begin{vmatrix} \sigma_1^2 & \sigma_{13} & \dots & \sigma_{1n} \\ \sigma_{31} & \sigma_3^2 + \sigma_{u_3}^2 & \dots & \sigma_{3n} \\ \dots & \dots & \dots & \dots \\ \sigma_{n1} & \sigma_{n3} & \dots & \sigma_n^2 + \sigma_{u_n}^2 \end{vmatrix} + \dots \\ &\dots + \sigma_{u_n}^2 \begin{vmatrix} \sigma_1^2 & \sigma_{12} & \dots & \sigma_{1,n-1} \\ \sigma_{21} & \sigma_2^2 & \dots & \sigma_{2,n-1} \\ \dots & \dots & \dots & \dots \\ \sigma_{n-1,1} & \sigma_{n-1,2} & \dots & \sigma_{n-1}^2 \end{vmatrix} = |\Sigma| + \sum_{i=1}^n \sigma_{u_i}^2 M_{ii}^*. \end{aligned}$$

From which the validity of the formula (6) follows automatically.

Hence, knowing the formula of modification of the entropy of RV \mathbf{X} , it is possible to establish those of its components, adding to which new random variables U_i will lead to maximal increase of system entropy. Thus, the following problem of nonlinear programming is formulated:

$$\left\{ \begin{array}{l} H(\mathbf{X} + \mathbf{U}) \rightarrow \max_{\Omega_x}, \\ \Sigma_{\mathbf{X}} = \Sigma, \\ \sum_{i=1}^n \sigma_{u_i}^2 = D, \\ \sigma_{u_i}^2 \geq 0, \quad i = 1, 2, \dots, n, \\ \text{cov}(U_i, X_j) = 0, \quad i = 1, 2, \dots, n, \quad j = 1, 2, \dots, n. \end{array} \right. \quad (7)$$

Solution of the problem (7) allows ensuring maximal increase of entropy of a multi-dimensional RV.

Example. As an illustration of implementation of the EP model give the solution of the problem (7). Generate sample of volume $N = 100$ for a certain random vector of dimension $M = 3$. The complete correlation matrix is equal to

$$\Sigma = \begin{pmatrix} 0.818 & 0.751 & 0.120 \\ 0.751 & 0.857 & 0.459 \\ 0.120 & 0.459 & 0.836 \end{pmatrix}.$$

Calculate entropies of all the components and for the random vector as a whole on the sample set: $H(X_1) = 1.772$, $H(X_2) = 1.667$, $H(X_3) = 1.427$, $H(X) = 3.506$. Let $D = 1$. Then following problem can be formulated:

$$\left\{ \begin{array}{l} H(X_1 + U_1, X_2 + U_2, X_3 + U_3) \rightarrow \max_{\Omega_x}, \\ \Sigma_{\mathbf{X}} = \Sigma, \\ \sum_{i=1}^3 \sigma_{u_i}^2 = 1, \\ \sigma_{u_i}^2 \geq 0, \quad i = 1, 2, 3, \\ \text{cov}(U_i, X_j) = 0, \quad i = 1, 2, 3, \quad j = 1, 2, 3. \end{array} \right. \quad (8)$$

where $H(\mathbf{X}^*) = \frac{1}{2} \ln \left[(2\pi e)^3 \left(|\Sigma| + \sum_{i=1}^3 \sigma_{u_i}^2 M_{ii}^* \right) \right]$, $|\Sigma| = \begin{vmatrix} 0.818 & 0.751 & 0.120 \\ 0.751 & 0.857 & 0.459 \\ 0.120 & 0.459 & 0.836 \end{vmatrix} = 0.0128$,

$$M_{11}^* = \begin{vmatrix} 0.857 + \sigma_{u_2}^2 & 0.459 \\ 0.459 & 0.836 + \sigma_{u_3}^2 \end{vmatrix}, \quad M_{22}^* = \begin{vmatrix} 0.818 & 0.120 \\ 0.120 & 0.836 + \sigma_{u_3}^2 \end{vmatrix}, \quad M_{33}^* = \begin{vmatrix} 0.818 & 0.751 \\ 0.751 & 0.857 \end{vmatrix}.$$

The solution of problem (8) gives: $\sigma_{u_1}^2 = 0.364$, $\sigma_{u_2}^2 = 0.635$, $\sigma_{u_3}^2 = 0.001$. Thus maximum value of an entropy is equal $H(\mathbf{X}^*) = 3.596 > 3.506$.

Conclusion

1. The hypothesis is formulated that increase of the entropy of a complex system corresponds to the increase of safety of its operation. The based on it entropy-probabilistic EP approach of modeling robust interdependent CIs is proposed.

2. The basis of entropy-probabilistic EP is the representation of the system in the form of a multi-dimensional normal random vector. As the criterion of effectiveness the maximal increase of entropy is used due to the increase of the indeterminacy of the components of the RV, which characterizes the utility of the system.

3. The virtues of the proposed EP approach are as follows:

- Simplicity of realization;
- It can be used for solving problems of efficient safety control of CIs systems
- Universality and applicability for complex systems of various natures.

References

1. Borge, D. (2001). *The Book of Risk*. John Wiley & Sons, Inc.
2. Crouhy, M., Galai, D., Mark, R. (2006). *The Essentials of Risk Management*. McGraw-Hill.
3. King, J. (2001). *Operational Risk: Measurement and Modeling*. Wiley. Chichester, UK.
4. Wallace, W.A., Mendonca, D., Lee, E, Mitchell, J., Chow, J. (2006). *Managing Disruptions to Critical Interdependent Infrastructures in the Context of the 2001 World Trade Center Attack*. *Critical Infrastructures*, 4, 235–264.
5. Wilson, A.G. (1970). *Entropy in Urban and Regional Modelling*. Pion Limited. London.
6. Timashev, S. A. (2008). Risk- and Entropy-Based Quantitative Definition and Solution of Regional Resilience and Strategic Preparedness. In: *Safety of Critical Infrastructures and Territories: II All Russia Conference / Abstracts of Papers*. Yekaterinburg, Ural Branch Russian Academy of Sciences, ISBN 5-7691-2016-9,261-265
7. Skorobogatov, S.M., Khaykov, A.A. (1993). A design of structures using crack indeterminacy and information entropy. *Proceedings of International Conference Concrete 200*. Scotland, Dundee, Sept. 1993, 12 p.
8. Haken, H. (1988). *Information and Self-Organization. A Macroscopic Approach to Complex Systems*. Springer-Verlag Berlin Heidelberg.
9. Rinaldi, S.M., Peerenboom, J.P., and Kelly, T. K. (2001). Identifying, Understanding, and Analyzing Critical Infrastructure Interdependencies. *IEEE Control Systems Magazine* (December), 11-25.
10. Cover, T.M., Thomas, J.A. (2006). *Elements of Information Theory*. Second Edition. John Wiley & Sons, Inc.

Author contact information

S.A. Timashev,¹ and A.N. Tyrsin²

¹Science and Engineering Center «Reliability and Safety of Large Systems and Machines», Ural Branch, Russian Academy of Sciences, Yekaterinburg, Russia, 54a, Studencheskaya street, 620049; e-mail: timashevs@cox.net

²Science and Engineering Center «Reliability and Safety of Large Systems and Machines», Ural Branch, Russian Academy of Sciences, Yekaterinburg, Russia, 54a, Studencheskaya street, 620049; e-mail: at2001@yandex.ru

A survey of network theoretic approaches for risk analysis of complex infrastructure systems

Sarah LaRocca and Seth Guikema

Johns Hopkins University
Department of Geography and Environmental Engineering
Baltimore, Maryland

Abstract

Many critical infrastructure systems are comprised of complex physical, geographical, and logical networks. Such systems include electric power, drinking water, wastewater, cellular communication, internet, and transportation. These systems are vulnerable to hazards, both natural (e.g. hurricanes and earthquakes) and man-made (e.g. terrorism and accidents), which can induce failures in network elements and reduce system performance. In conducting risk and reliability analyses for complex infrastructure systems, network theory has been used to understand the effect of perturbations of individual network elements on overall system performance. In this paper, we present a survey of research that has employed this network theoretic approach and provide a discussion of future research needs in the field.

1 Introduction

Critical infrastructure systems form the foundation for the economic prosperity, security, and public health of the modern world [17]. As such, vulnerabilities in these complex, interdependent systems pose a significant threat to society. Understanding these vulnerabilities and improving the safety, reliability, and performance of such systems has therefore become an increasingly significant concern to decision-makers in both the public and private realm.

Infrastructure systems can be broadly defined as physical entities that provide the basic services necessary for maintaining the health, security, economy, and environmental quality of the world. Examples of such systems include electric power, drinking water, wastewater, cellular communication, internet, and transportation. These examples can each be more generally classified into one of four categories of infrastructure: information and communication; transportation; energy; and water. These categories primarily represent physical systems, and are the traditional focus of infrastructure risk and reliability analyses. However, infrastructure can encompass other systems as well, such as banking and finance, safety and security, health services, government, manufacturing, and food supply [8].

Infrastructure systems are prone to failures, which can arise from a variety of sources including natural disasters, terrorism, and accidents. Seemingly small or isolated infrastructure failures have the potential for far-reaching consequences. In August 2003, sagging power lines in Ohio caused a fire that triggered cascading failures through the electric power grid in the northeastern U.S and Canada, leaving 50 million customers without

power. Other infrastructure systems dependent on the power system also experienced failures: banks were forced to close; computers could not operate; and cellular communications were interrupted (due to both loss of power in cell towers and system overload from increased call volume) [5]. During Hurricane Katrina in August 2005, approximately 50 breaches occurred in levees throughout New Orleans. In addition, pumping stations failed to function due to loss of electric power, evacuation of pump operators, and flooding of the stations themselves. In total, 1,118 people were confirmed to have died in Louisiana as a direct result of the storm; direct property damage was estimated to be \$21 billion and public infrastructure damage was estimated to be \$6.7 billion [4]. As demonstrated by these examples of failures, vulnerabilities in infrastructure systems can lead to devastating consequences. It is therefore crucial to identify these vulnerabilities and understand the consequences of failures.

Current methods for modeling infrastructure systems include simulation, optimization, decision analysis, input-output analysis, and network theory. In this paper, we will examine existing approaches for modeling infrastructure vulnerabilities using network theory. First, we will introduce the use of networks, or graphs, to represent infrastructure systems. We will describe commonly used measures of network topology, discuss various network models, and present characteristics of real-world networks. Next, we will discuss the concept of network vulnerability and introduce methods for quantifying it. We will discuss modeling infrastructure vulnerability under two different scenarios: natural (random) and intelligent (targeted) threats; we also compare static versus dynamic network vulnerability models. Finally, we will identify research needs in the field.

2 Network topology

Many infrastructure systems can be described as networks, or graphs. Mathematically, a graph can be described by $\mathcal{G} = \{\mathcal{V}, \mathcal{E}\}$, where \mathcal{V} is the set of vertices, or nodes, and \mathcal{E} is the set of edges, or links. For directed graphs, the elements of \mathcal{E} are ordered pairs of distinct vertices, while for undirected graphs, the elements of \mathcal{E} are unordered pairs of distinct vertices. For example, a traffic network of one-way streets can be represented by a directed graph, and a traffic network of two-way streets can be represented by an undirected graph. Electric power transmission systems can also be represented easily as a graph; here, generators, substations, and junction poles are the set of vertices, \mathcal{V} , and the transmission lines are the set of edges, \mathcal{E} .

The total number of nodes in a graph is equal to the number of elements in \mathcal{V} , that is, $N = |\mathcal{V}|$. Correspondingly, the number of edges in a graph is equal to the number of elements in \mathcal{E} , that is, $M = |\mathcal{E}|$ [10].

Any given graph can be uniquely represented by an $N \times N$ adjacency matrix, A . If there exists an edge from some vertex i to some vertex j , then the element a_{ij} is 1; otherwise, it is 0. Undirected graphs always have symmetric adjacency matrices. In some applications, it is useful to not only specify whether an edge exists, but to assign the edge a value, typically a number in the range $(0, 1]$; for instance, Refs. [6, 7] use the value of a_{ij} to represent varying levels of functionality in power transmission lines.

Network topology can be described by a variety of measures. Four measures are particularly useful for characterizing the structure of a network: average path length, clustering coefficient, degree distribution, and betweenness [2].

2.1 Average path length

Average path length describes the mean of the shortest distance between all pairs of nodes. That is,

$$\ell = \frac{1}{N(N-1)} \sum_{i \in \mathcal{V}} \sum_{j \in \mathcal{V}} d_{ij}, \quad (1)$$

where d_{ij} is the shortest path (i.e., number of edges) between node i and node j . Average path length is sometimes also referred to as characteristic path length or average geodesic length. A related topological parameter is the diameter of a network, where diameter is defined as the ‘longest shortest path,’ that is, $\max_{i,j} d_{ij}$.

2.2 Clustering coefficient

The clustering coefficient was introduced by Watts and Strogatz in 1998 [21] as a means of quantifying the degree to which nodes are clustered in a graph. An example of clustering can be seen in social networks; often, ‘cliques’ form, in which every person knows every other person [2]. Suppose a node i is connected to k_i other nodes, or neighbors. Then, the total number of edges that can exist between each of these neighbors is $\frac{1}{2}k_i(k_i - 1)$. Let \mathcal{E}_i be the actual number of edges that exist between each of the neighbors. Then the clustering coefficient for a given node i is defined as follows:

$$C_i = \frac{2\mathcal{E}_i}{k_i(k_i - 1)}. \tag{2}$$

A clustering coefficient equal to 1, implying that $\mathcal{E}_i = \frac{1}{2}k_i(k_i - 1)$, indicates that every neighbor of node i is connected to every other neighbor of node; that is, the neighbors of node i form a complete clique.

2.3 Degree distribution

The nodal degree, k , of a given node is defined as the number of edges that are incident the node; the average degree of a network, $\langle k \rangle$, is defined as:

$$\langle k \rangle = \frac{1}{N} \sum_{i \in V} k_i. \tag{3}$$

Typically, the nodes in a given network do not all have the same degree; rather, the distribution of nodal degrees in the network can be described by some probability density function, $P(k)$, which gives the probability that a randomly selected node has exactly k edges [2]. The nodal degrees of a random graph are Poisson-distributed. However, real-world networks generally do not follow this degree distribution. Many networks follow a power law degree distribution, where $P(k) \sim k^{-\gamma}$ for some constant γ , while others have been shown to have an exponential degree distribution.

2.4 Betweenness centrality

Another important measure of network topology for infrastructure vulnerability analysis is the betweenness coefficient, which is defined as the total number of shortest paths passing through a given node. Relatedly, the betweenness centrality of a node is defined as follows:

$$BC_k = \sum_i \sum_j \frac{\rho_{ikj}}{\rho_{ij}}, i \neq j \neq k, \tag{4}$$

where ρ_{ij} is the number of shortest paths from node i to node j and ρ_{ikj} is the number of these paths that pass through node k [10]. Although one might expect that a high nodal degree leads to a high betweenness coefficient, in fact, the relationship between nodal degree and betweenness is not well-defined. The authors in Ref. [10] present the correlation between nodal degree and betweenness for various types of graphs, and it is clear that the relationship changes depending on other properties of the graph. Betweenness, which is sometimes referred to as load (particularly with respect to electric power networks) [1, 7, 6, 12, 14, 15, 16, 20] and betweenness centrality are useful measures of the importance of a node because they quantify the number of shortest paths that will become longer if the node is removed from the graph. Table 1 presents a summary of measures of topology used in studies of infrastructure network vulnerability.

3 Network vulnerability

Infrastructure vulnerability can be regarded as the sensitivity of a system to threats and hazards (e.g. natural disasters and terrorism). The concept of vulnerability can be divided into two components: robustness (i.e., the ability of a system to retain function when exposed to perturbations) and resilience (i.e. the ability of a system to adapt to regain function after perturbations)[13]. In this section, we will examine approaches for assessing both the robustness and resilience of infrastructure systems; Table 1 summarizes methods used in past and current research in the field. In general, the majority of approaches consist of some key components: 1) simulating or obtaining real data for a network model (e.g. a random graph or an electric power transmission grid); 2) measuring the topological characteristics of the network; 3) inducing random or targeted failures in network elements; and 4) assessing static and/or dynamic performance of the network, typically by means of additional topological characteristics.

3.1 Modeling networks

There are a variety of ways to develop models for infrastructure networks. Ideally, we would always be able to use network models created directly from real-world systems with highly detailed data for analyzing vulnerabilities. However, for multiple reasons, it is often difficult to obtain data: it may be highly sensitive (e.g. electric power grids), may be poor quality (e.g. water distribution systems), or may simply not exist (e.g. the internet). Additionally, even if perfect data existed for every system in the world, it would be computationally prohibitive to perform simulations for every individual network. Therefore, it is sometimes useful to simulate networks whose properties are similar to real networks, in order to understand the effects of network topology on vulnerability.

The majority of research presented in Table 1 focuses on either simulated random networks [3, 7, 8, 9, 10, 11, 14, 15, 16] or electric power grids [1, 7, 6, 11, 12, 14, 18, 19, 22] (or both). Additional infrastructure networks examined include the Internet [7, 14] and the Tokyo gas supply system, water supply system, and sewerage system [19]. However, aside from in Ref. [19], studies of the vulnerability of water-related infrastructure networks are noticeably absent.

3.2 Simulating failures

The assumptions used in simulating network failures vary among studies, but in general the result of a failure is the removal of one or more network elements from the graph. Two types of failures are often examined: random and targeted. Random failures, sometimes referred to as errors [3], represent those resulting from natural phenomena such as hurricanes, earthquakes, and natural deterioration due to aging. Typically, for a given iteration one node is randomly selected for removal, with every node being equally likely to be selected. Network elements are randomly removed in this manner until some stopping criterion (e.g. fraction of nodes removed or network disconnection) is reached. A variant on this approach involves assigning probabilities of failure to each network element using additional information, such as fragility curves [8, 22]. In this approach, more than one network element may fail in a given time step.

Table 1: Selected network theoretic approaches for modeling network vulnerability.

*D = degree-based; L = load-based; F = fragility-curve based; B = betweenness-based; R = range-based.

Reference	Network type	Topology measure	Threat type	Simulation type	Performance measure
Albert <i>et al.</i> 2004 [11]	North American power grid	Degree Load	Random Targeted (D,L)	Static Dynamic	Connectivity loss
Crucitti <i>et al.</i> 2004a [7]	Erdős-Rényi model Barabási-Albert model The Internet Western U.S. electric power grid	Degree Load	Random Targeted (L)	Dynamic	Network efficiency
Dueñas-Osorio and Vemuru 2009 [8]	IEEE test power transmission systems Synthetic electric transmission and distribution systems	Degree Clustering coefficient Redundancy ratio Network efficiency	Random (F) Targeted (L)	Static Dynamic	Connectivity loss Cascading susceptibility
Estrada 2006 [9]	Food web Electronic circuit Protein structure Drug users Gene transcription Random graph	Degree Betweenness Spectral properties	Targeted (D,B)	Static	Largest connected component
Holmgren 2006 [11]	Erdős-Rényi model Modified Barabási-Albert model Western U.S. electric power grid Nordic power grid	Degree Average path length Clustering coefficient	Random Targeted (D)	Static	Largest connected component
Kinney <i>et al.</i> 2005 [12]	North American power grid	Degree Load	Random Targeted (L)	Dynamic	Network efficiency
Motter and Lai 2002 [14]	Scale-free Homogeneous The Internet Western U.S. electric power grid	Degree Load	Random Targeted (D,L)	Dynamic	Largest connected component
Pepyne 2007 [16]	IEEE test power transmission systems Synthetic small-world electric transmission systems	Clustering coefficient Average path length Load	Random	Dynamic	Line loading Number of grid outages
Rosas-Casals <i>et al.</i> 2007 [18]	European electric power grid	Degree Nearest neighbor degree Average path length Clustering coefficient	Random Targeted (D)	Static	Largest connected component
Shoji and Tabata 2007 [19]	Tokyo electric power system Tokyo gas supply system Tokyo water supply system Tokyo sewage system Tokyo interdependent infrastructure systems	Degree Average path length Clustering coefficient Largest connected component Size of isolated components Accessibility ratio	Random	Static	Degree Average path length Clustering coefficient Largest connected component Size of isolated components Accessibility ratio
Simonsen <i>et al.</i> 2008 [20]	UK electric power transmission grid N.W. U.S. power transmission grid	Degree Load	Random	Static Dynamic	Largest connected component
Winkler <i>et al.</i> 2010 [22]	Texas power transmission and distribution grids IEEE test power transmission systems	Degree Clustering coefficient Network meshedness Network centralization Average edge length	Random (F)	Static	Betweenness loss Largest connected component Abnormally loaded nodes

Targeted failures, sometimes referred to as attacks [3], primarily represent intelligent threats (i.e., terrorism). Because the goal of an attack is typically to cause the most damage possible, network elements are selected for removal in decreasing order of apparent importance. The importance of a network element is usually measured by either degree or betweenness. After the most important network element has been removed from the network, subsequent elements are selected for removal in one of two ways: 1) the network element with the next highest importance as initially calculated (i.e., from the initial importance ranking of network elements) is chosen; or 2) importance (e.g. degree of betweenness) is recalculated for the remaining network elements and the network element with the new highest importance is chosen [10]. Again, network elements are removed in one of these manners until some stopping criterion is reached.

Random and targeted failures can be imposed on both nodes and edges; however, in a given simulation, failures are generally restricted to one type of network element. Node failures are most commonly considered, but studies of edge failures exist [10, 15, 16, 20].

Simulating failures using these methods typically represents a static network state. However, it is important to also consider dynamic networks, in which the failure of a network element can cause a redistribution of the flows of physical quantities. Such dynamics are particularly important when modeling real systems such as electric power grids, where the failure of one network element, such as a substation, can lead to cascading failures throughout the network due to flow overloads[14]. A typical approach for dynamic network vulnerability simulations involves assigning a capacity to each node, typically defined to be proportional to initial load, for example,

$$C_i = \alpha L_i, \quad (5)$$

where α is a tolerance parameter of the network [6, 7, 12, 14, 20]. A node failure is induced using one of the methods described above, and the resulting flow redistribution is calculated. If flow through any of the nodes exceeds the node's capacity, that node fails, and flows are again recalculated. The simulation continues in this manner until the network performance has reached an equilibrium.

3.3 Measuring vulnerability

Network performance must be measured during and after failure simulations to quantify the vulnerability of a network. A common measure of performance is the relative size of the largest connected component, $S = N'_S/N_S$, where N_S is the number of nodes in the largest connected component of the network prior to the failure(s) and N'_S is the number of nodes in the largest connected component of the network after the failure(s) [3, 9, 10, 11, 14, 18, 19, 20, 22]. Relatedly, the average size of isolated component clusters, $\langle s \rangle$, can also be calculated.

Network efficiency is frequently used to measure performance when simulating cascading failures, and is defined as follows:

$$E = \frac{1}{N(N-1)} \sum_{i,j} \frac{1}{d_{ij}}, \quad (6)$$

where N is the number of nodes in the network and d_{ij} is the distance of the shortest path between i and j [6, 7, 12, 15].

Another measure of performance that has been used for electric power grids is connectivity loss, defined as follows:

$$CL = 1 - \frac{1}{N_D} \sum_i \frac{N_G^i}{N_G}, \quad (7)$$

where N_G is the total number of generators, N_D is the total number of distribution substations, and N_G^i is the number of generators connected to substation i [1, 8].

4 Conclusions

Although significant progress has been made toward understanding infrastructure network vulnerability, there remains much work to be done. There are several areas of research that will be beneficial to the field. First, the majority of studies that have been completed for specific infrastructure systems focus on electric power transmission. Future studies should be conducted on other systems including water distribution, water treatment, gas supply, and cellular communications. Eventually, once individual systems are better understood, the vulnerability of interdependent infrastructure systems should be examined, as in Ref. [19]; a given system's performance when subjected to hazards may vary significantly when interdependencies between it and other infrastructure systems exist.

Secondly, physical performance models should be incorporated into studies of infrastructure network vulnerability. Of the studies of electric power systems discussed in this paper, only Ref. [16] incorporated a power flow model, and that was a simpler DC power flow model rather than a full AC power flow model. Additionally, the use of physically-based failure probability estimates (such as those obtained from fragility curves in Ref. [22]) should be expanded.

Lastly, although attempts have been made to characterize the relationship between network topology and vulnerability, it is difficult to draw strong conclusions based on a small sample size. Therefore, it would be beneficial to conduct vulnerability analyses on a large number of networks with widely varying topological characteristics. Because real data are difficult to obtain, this is likely to be best achieved through the use of simulated random networks.

The study of vulnerabilities in infrastructure networks provides an understanding of the effects of hazards on systems that are crucial to the functioning of our societies. The information gained from such studies can be used to target reinforcements in infrastructure networks and reduce the probability of failures in critical network elements. Additionally, an improved understanding of the effects of failures on network behavior will result in more optimal post-failure responses, ultimately resulting in fewer costs to society.

5 Acknowledgments

This work was partially supported by a Graduate Research Supplement from the National Science Foundation (CMMI 0826365) and by a National Science Foundation Graduate Research Fellowship to Sarah LaRocca. This support is gratefully acknowledged.

References

- [1] R. Albert, I. Albert, and G. Nakarado. Structural vulnerability of the North American power grid. *Physical Review E*, 69(2):1–4, 2004.
- [2] R. Albert and A.-L. Barabási. Statistical mechanics of complex networks. *Reviews of modern physics*, 74(1):47–97, 2002.
- [3] R. Albert, H. Jeong, and A. Barabási. Error and attack tolerance of complex networks. *Nature*, 406(6794):378–382, 2000.
- [4] American Society of Civil Engineers Hurricane Katrina External Review Panel. The New Orleans hurricane protection system: what went wrong and why: a report. Technical report, 2007.
- [5] K. Belson and M. Wald. '03 blackout is recalled, amid lessons learned, August 13 2008.
- [6] P. Crucitti, V. Latora, and M. Marchiori. A topological analysis of the Italian electric power grid. *Physica A: Statistical Mechanics and its Applications*, 338(1-2):92–97, 2004.

- [7] P. Crucitti, V. Latora, and M. Marchiori. Model for cascading failures in complex networks. *Physical Review E*, 69(4):3–6, 2004.
- [8] L. Dueñas Osorio and S. Vemuru. Cascading failures in complex infrastructure systems. *Structural Safety*, 31(2):157–167, 2009.
- [9] E. Estrada. Network robustness to targeted attacks. The interplay of expansibility and degree distribution. *The European Physical Journal B*, 52(4):563–574, August 2006.
- [10] P. Holme, B. Kim, C. Yoon, and S. Han. Attack vulnerability of complex networks. *Physical Review E*, 65(5):56109, 2002.
- [11] A. J. Holmgren. Using graph models to analyze the vulnerability of electric power networks. *Risk analysis : an official publication of the Society for Risk Analysis*, 26(4):955–69, August 2006.
- [12] R. Kinney, P. Crucitti, R. Albert, and V. Latora. Modeling cascading failures in the North American power grid. *The European Physical Journal B-Condensed Matter and Complex Systems*, 46(1):101–107, 2005.
- [13] V. Latora and M. Marchiori. Vulnerability and protection of infrastructure networks. *Physical Review E*, pages 1–4, 2005.
- [14] A. Motter and Y.-C. Lai. Cascade-based attacks on complex networks. *Physical Review E*, 66(6):2–5, December 2002.
- [15] A. Motter, T. Nishikawa, and Y.-C. Lai. Range-based attack on links in scale-free networks: Are long-range links responsible for the small-world phenomenon? *Physical Review E*, 66(6):1–4, December 2002.
- [16] D. L. Pepyne. Topology and cascading line outages in power grids. *Journal of Systems Science and Systems Engineering*, 16(2):202–221, June 2007.
- [17] S. Rinaldi. Modeling and simulating critical infrastructures and their interdependencies. *Proceedings of the 37th Annual Hawaii International Conference on System Sciences, 2004.*, pages 54–61, 2004.
- [18] M. Rosas-Casals, S. Valverde, and R. V. Solé. Topological Vulnerability of the European Power Grid Under Errors and Attacks. *International Journal of Bifurcation and Chaos*, 17(07):2465, 2007.
- [19] G. Shoji and M. Tabata. Modeling of interdependency associated with a system failure of critical infrastructure networks in views of a seismic disaster risk.
- [20] I. Simonsen, L. Buzna, K. Peters, S. Bornholdt, and D. Helbing. Transient Dynamics Increasing Network Vulnerability to Cascading Failures. *Physical Review Letters*, 100(21):1–4, May 2008.
- [21] D. J. Watts and S. H. Strogatz. Collective dynamics of 'small-world' networks. *Nature*, 393:440–442, 1998.
- [22] J. Winkler, L. Dueñas Osorio, R. Stein, and D. Subramanian. Performance assessment of topologically diverse power systems subjected to hurricane events. *Reliability Engineering & System Safety*, 95(4):323–336, 2010.

Regional Social and Economic Risks as Conditions of Formation of Critical Infrastructures

Alexander V. Shibin¹, Julia L. Shibina², Alexander A. Kuklin³

¹ The Institute of economics of the Ural branch of the Russian Academy of Science, the center of economic security, the Moscovskaya str., 29, Yekaterinburg, Russian Federation, 620014, PH+79045433775, email: a_shibin@list.ru

² The Ural Federal University, The Department of economics and management, Mira str., 19, Yekaterinburg, Russian Federation, 620002, PH+79049821877, email: zaitsevajulial@mail.ru

³ The Institute of economics of the Ural branch of the Russian Academy of Science, the center of economic security, the Moscovskaya str., 29, Yekaterinburg, Russian Federation, 620014, PH+73433710719, email: alexkuklin49@mail.ru

ABSTRACT

It is known, that in case of world economic destabilization prognostic mistakes can not only lead to deterioration of a government but also promote strengthening of crisis tendencies in regions. It makes experts to improving algorithms of social and economic forecasting and gradually to replacing 'static' and 'quasi-static' models of a society by 'dynamic', which includes nonlinear feedback through elements of an economic infrastructure. Quite often this feedback becomes "critical", that is it starts process of transition of territory's economic complex to a new condition with unpredictable in advance properties. In these cases we often speak about occurrence of "critical infrastructures", those are capable to affect essentially on social, economic, environmental, etc. safety of territory. In advance, it is not always known, that infrastructures can appear critical, therefore the risk-analysis should include a stage of their detection on the basis of preliminary formed system of criteria. Designing of criteria of criticality and carrying out risk-analysis becomes complex methodological problem in conditions of continuous change of the importance of parameters of regional social and economic system. Their decision demands participation of the big number of experts which should understand each other and for this purpose to apply the uniform approach to definition of concept of "critical infrastructures". Until now different authors define in their own way terms they use. There is a situation then the significant number of infrastructures drops out of consideration as "critical" because they did not render essential influence on social and economic position of region. The role of the specified infrastructures can suddenly increases in conditions of world crisis. The specified circumstance has caused necessity of revealing of such "latent" potential infrastructures and has become the reason of performance of the presented research.

In the work we started with discussed before assumption, according to which occurrence of critical infrastructures influences essentially on stability and as a

consequence on safety of regional social and economic system (hereinafter – «regional SES») [1].

Thus, for revealing conditions of "criticality" of an economic infrastructure it is necessary to make the list and to estimate a level of regional risks. The analysis of publications of various authors has shown that usually basic risks and concept of safety of the regional SES are connected with conditions of existence and ability to react to external influences. Thus existence of regional system during life cycle is postulated as preservation of its qualitative definiteness even at change of structure of system and functions of its elements [2] (figure 1). Thus as one of a condition of occurrence of a "critical" infrastructure it is necessary to consider occurrence of preconditions for change of qualitative definiteness of the regional SES.

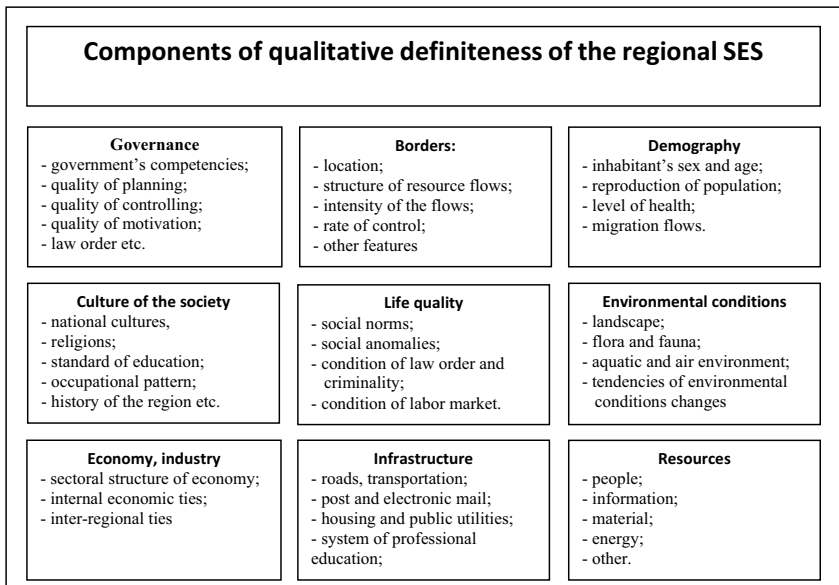


Figure 1. Components of qualitative definiteness of regional SES

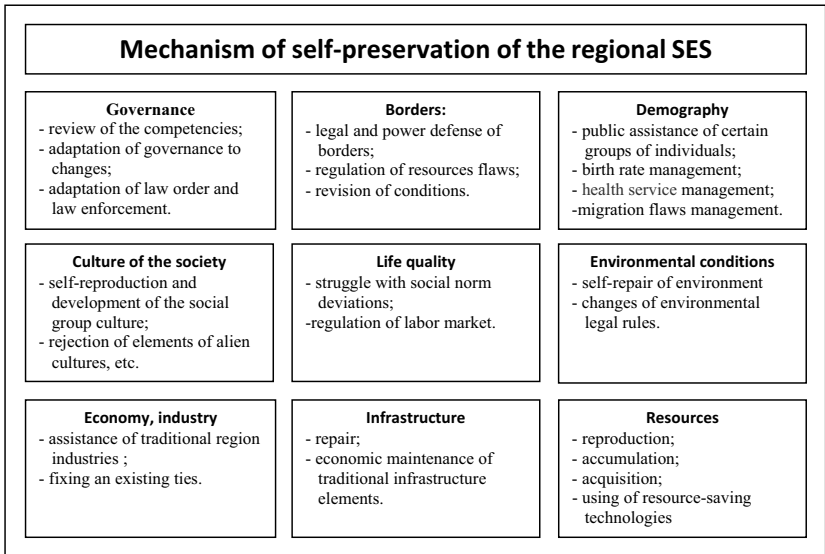


Figure. 2. Mechanism of self-preservation of regional SES

Endeavor of SES to support its security (stability) is one of the reasons of the purposeful self-organization, which shows itself in setting and updating of goals of self-development, changing of structure, and element’s functions. Stability of the regional SES is achieved by using of a complex of mechanisms, which provide maintaining of attribute characteristics in different spheres (figure 2), and closely associate with ability to self-organization. In turn, internal source of system’s self-organization is continuous process of appearance and settling contradictions. So their presence is necessary condition of system safety. Accordingly, some elements of infrastructure might be critical, because they can strongly affect (in comparison with other factors) on ability of the regional SES to be self-organized, that provides required stability.

For example, researches, those are made in the Institute of Economics of the Ural Branch of Russian Academy of Science, show, that one of the most important condition of authoritarian state functioning is existence of powerful shadow economy. Hidden “shadow” mechanisms are results in people self-organization as a response to numerous and not always reasonable prohibitions and restrictions, those are set by strict vertical governance. Being peculiar means of people self-defense from excessive government regulation, they facilitate decreasing of social tension level and increasing indirectly national security.

Analysis has shown that the ability of regional SES to be self-organized is connected with its internal diversity level, which is defined by people freedom level in economic, political, social, cultural, and others spheres.

It is known, there is the definite level of required diversity for every stage of system progress [2]. Critical infrastructures might have a significant influence on diversity level of the regional infrastructure by means of effecting on differentiation (system's tendency to structural and functional diversity of its elements), and on lability (mobility of element's functions with maintenance of stability of system structure in whole).

Indeed, differentiation of the regional SES depends significantly on number of behavior stereotypes that society supports. Behavior stereotypes in modern society undergo strong influence by means of mass media and social networks on the internet. So, the government ability to affecting information flows becomes tool of socio-cultural diversity management.

On the other hand, regional SES lability in many cases is defined as the ability of inhabitants of the region to change their type of activity. In turn, this ability depends on average level and quality of education, and on existence of formal (legal) and economic restrictions. These factors also are strongly affected by government, so relevant infrastructures might be used by government as the mechanisms of changing of ability of the regional SES to be self-organized.

So, government influence on the regional infrastructure with the purpose of maintenance of required internal diversity level becomes one of the most important goals of the regional management system. Thus, indicators that are shown at figure 3 might be used as particular indices of management efficiency. It should be considered, that for maintenance of processes of self-organization, the controlling mechanism should have needed quantity of feedback [1,3-5]. Otherwise critical infrastructures might cause intensification of destructive factors, such as [4]:

- Low efficiency of the management system (as a result, prevalence of destructive factors over factors that compose system);
- Breach of law of proportionality (a sharp decrease of quantity of elements required for the system's functioning, and an increase of quantity of useless components);
- Shortage of external and internal resources;
- Bad conductivity of channels for substances, energy, information;
- Mismatch of goals of system's element with each other, and their mismatch to system goals.

To find out the criticality of the infrastructure, it is needed to define quality of the regional SES management, which provides elimination of the departure of sub-system parameters of the regional system from the norm. Our information search allows us to say, that in this case also might be used different systems of indicators, which are targeted on the estimation of the follows basic characteristics of quality of management system of the regional SES:

- Quality of planning;
- Quality of regulating and motivating legal norms;
- Quality of organization structure;

- Quality of communications in management system;
- Quality of control.

According to the Constitution of Russia Federation, competencies of regional and local authorities are restricted by federal law, i.e. they are derivatives of the competencies of federal state run public authorities, and characteristics of quality of management system of SES, that are listed above, should be defined in accordance with this dependence.

Mechanism, by means of that regional and federal management systems affect on “dynamic security” of the regional SES, is shown on figure 4. The specified mechanism includes components that are managing the scopes of life activities, infrastructure, and also the management system of SES itself that should be able to adapt to the changing external conditions.

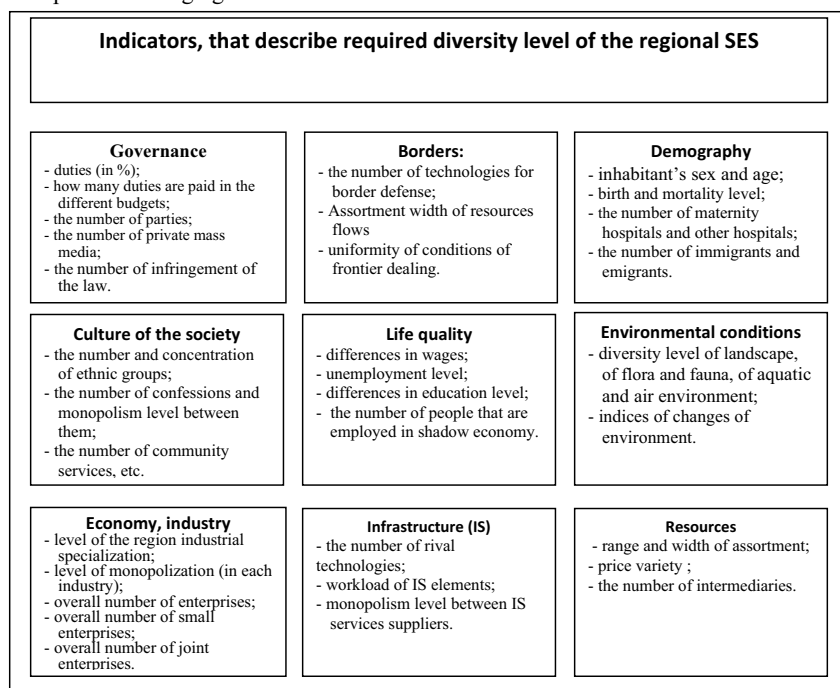


Figure 3. Indicators, that describe required diversity level of the regional SES

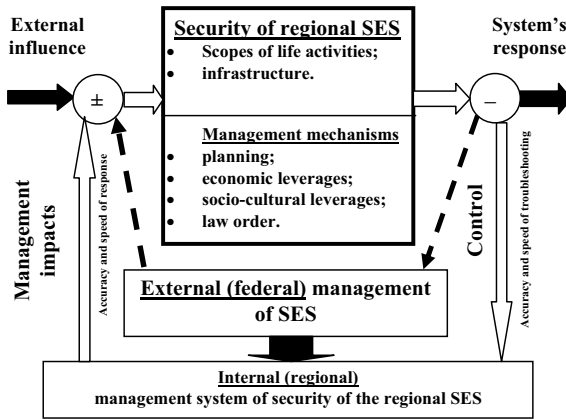


Figure 4. Management mechanism of the “dynamic security” of the regional SES

Improving the complex diagnostic [7], that was devised in the Institute of Economics of the Ural Branch of Russian Academy of Science, we proceeded from the assumption that it is possible to design security indicators of twelve scopes of life activities: investments, production, researches and development, external economic activity, finance, energy sector, inhabitant's standards of living, labor market, demography, law order, supply of provisions, environmental conditions (X_i , where i – indicator number). We suggest adding characteristics of regional economic infrastructure (thirteenth scope of life activity) to the system of indicative rates, and taking into account non-linear ties between certain infrastructure elements and other parts of regional economic system that appear during the crisis (see figure 4).

So, in developing models crisis influence on the regional economic security shows itself in two ways:

- Through the averaged normalized estimation of the thirteenth indicative block $C_{13} = (1/N_{13}) * \sum X_i$, which is added supplementary to the complex diagnostic method of assessment of the regional economic security;
- Through the changing of the indicator rates that compose other blocks of the complex diagnostic method of assessment of the regional economic security.

Composing metrics of the thirteenth indicative block (this block defines infrastructure status and its influence on the regional economic security) it is supposed to keep in mind the follow principles:

1. Performance of an economic system should be assessed only from the point of view of the larger system, where the investigated system is a part, a subsystem.

2. Multifactor assessment describes simplified model that is made of available data, rather than performance of the system. Thus the choice of the indicators might be random, because used criteria have as a rule a multivariate essence.
3. Inherently, criteria might be static and dynamic. Statics defines internal structure and potential of a system, and dynamics reflects tendencies of development and a lag effect measure.

In addition, detection of the set of the indicators of territory infrastructure status is connected with settling of problems that are caused by lack or misrepresentation of the data. There are the follow problems:

- Lack of complete statistic data about all municipalities that are parts of the investigated region of the Russian federation (some part of the data is not published, some part is published with delay for some years), and there is a tendency to information hiding;
- It occurs frequently distortion of the indices reflecting social situation in regions because they are politicized;
- Imperfection of the techniques of defining of some indices that results in significant departure of the assessment from the real situation;
- Considerable rate of the information noise in the formal statistical collection in consequence of including of unimportant indices that do not have economic sense in it.

Taking into account called before principles and restrictions, we propose to use the follow indicators of economic infrastructure status:

1. Output (intensity) of infrastructure;
2. Effectiveness of functioning;
3. Technological and environmental security;
4. Liability (mobility) of some infrastructure elements;
5. Infrastructure manageability on the region level.

Taking into account infrastructure influence on other scopes of life activity (indicator rates that compose corresponding blocks in the method of assessment of the complex regional security) would be executed in follow way.

At first, by the use of nonlinear mathematical programming it would be defined prognostic characteristics (indicator rates of the economic security) of the most probable stable condition of the regional economic system (in concordance with the scopes of life activities) in which it would be possible the next nearest crisis transition.

Then it should define critical elements of economic infrastructure that cause the possibility of the transition of the scopes of life activities in the specified condition, and it should be defined parameters of these elements at which a transition to a new condition has a maximum probability.

Then, by use of mathematical simulation it is supposed to define probability of transition of the whole regional economic system to each probable stable condition.

Finally, on the base of the data about probable prognostic characteristics of new conditions of the scopes of life activities and the probabilities of transition in

each of these conditions, it would be defined adjusted indicative rates of security of the life scope activity.

References

1. Tsygichko V.N. To a manager – about decision-making. Moscow: INFRA-M, 1996.272 p.
2. Krajnyuchenko I.V., Popov V.P. Global evolutionism and synergetics of a noosphere. Monograph. Rostov-on-Don: APSN, SKNC, VS, 2003.330 p.
3. Urmantsev Yu.A. Evolyutsionika, or the general theory of systems of the nature, society, thinking // The Collection “System, Symmetry, Harmony”, Moscow: Mysl, 1988, p.38-124.
4. Krajnyuchenko I.V., Popov V.P. System outlook. The theory and analysis. Textbook for higher school. Pyatigorsk. INEU, 2005. 218 p.
5. Whitehead A. Selected works on philosophy. Translated from English. Compiler Kasavin I.T. Editing and introductory article by Kissel M.A. Moscow. Progress, 1990. (Western philosophical thinking).
6. Ordinance of the President of the Russian Federation from 4/28/2008 № 607 “About an estimation of efficiency of activity of local governments of city districts and municipal areas”
7. Tatarkin A.I., Kuklin A.A., Romanova O.A., Chukanov V.P., Kozitsyn A.A. Regional economic security: unity of theory, research methodology, and practice. Yekaterinburg, the Ural State University, 1997. 240 p.
8. Biyakov O.A. Region economic space: the process approach. Kemerovo. Kuzbassvuzizdat, 2004. 244 p.

Decomposition Methods for Restoring Infrastructure Systems

Burak Cavdaroglu ^{*†§} Sarah G. Nurre^{*} John E. Mitchell[‡]
Thomas C. Sharkey^{*} William A. Wallace^{*†}

December 23, 2010

Abstract

We consider a new class of integrated network design and scheduling problems, with important applications in the restoration of services provided by civil infrastructure systems after an extreme event. Critical services such as power, waste water, and transportation are provided by these infrastructure systems. The restoration of these services is necessary for the society to recover from the extreme event as quickly as possible. The class of integrated network design and scheduling problems considered by this work focuses on a set of selected arcs to install into an existing network (i.e., network design decisions) and then scheduling these arcs on a set of work groups. Unlike previous network design problems, the network must be operating at intermediate points in time so that the scheduling decisions associated with the design decisions have a significant impact on the objective of the problem. The operations of the network at intermediate points in time will be evaluated by determining the amount of satisfied demand in the network. We also discuss exact methods to solve this class of large scale optimization problems by employing decomposition techniques. Our methods are tested on a realistic data set representing the (disrupted) power infrastructure of New Hanover County, NC. These results indicate that our methods are capable of providing better computational performance to decision-makers.

1 Introduction

The restoration of services provided by infrastructure systems is critical for society to recover from extreme events. Society relies on the services provided by these systems in order to operate effectively in both their daily operations and the recovery efforts from these extreme events. Therefore, the managers of these systems are faced with demanding choices in formulating their restoration efforts after the extreme event.

^{*}Department of Industrial and Systems Engineering, Rensselaer Polytechnic Institute, Troy, NY 12180.

[†]The work of this author was supported by the US Department of Homeland Security under Award Number: 2008-ST-061-ND 0001. The views and conclusions contained in this document are those of the authors and should not be interpreted as necessarily representing the official policies, either expressed or implied, of the US Department of Homeland Security.

[§]Primary author, e-mail: cavdab@rpi.edu.

[‡]Department of Mathematical Sciences, Rensselaer Polytechnic Institute, Troy, NY 12180.

These managers can often formulate effective restoration efforts to restore the services provided by their infrastructure without consideration of the other infrastructures or priorities associated with the overall recovery efforts from the extreme event. However, it will be important for the managers to consider the priorities and goals of the overall recovery effort when formulating the restoration plans for their infrastructure after an extreme event. This research examines a novel class of integrated network design and scheduling problems whose solutions can be used as a decision support aid to help managers form restoration plans aligned with the priorities of the overall recovery effort to the extreme event.

The operations of an infrastructure system can be modeled using a network-based representation where flows in the network model the services provided by the system and disruptions within it can be modeled as the removal of nodes and arcs from the network (see, e.g., Lee et al. [2]). The restoration efforts associated with the system will focus on installing or repairing physical components within the system and can be modeled as installing nodes and arcs into the network. Therefore, we can view this selection of nodes and arcs (or, equivalently, physical components) as *network design* decisions. Traditional network design problems are often only concerned with the performance of the end design of the network; however, the driving performance metric, especially in the eyes of the public, in evaluating the restoration efforts is how well the services provided by the system come back online. This means that the network design decisions will be evaluated as they are being implemented, so that the scheduling decisions associated with them will have a significant impact on the objective. In particular, the performance of the network at time t , which is composed of the original network plus the nodes and arcs completed prior to t , will be evaluated by determining the (weighted) amount of flow that can be sent from supply nodes to demand nodes.

The analysis of civil infrastructure systems is complex since they are interdependent (see O'Rourke [6]); disruptions in one can spread to others causing cascading failures (see Wallace et al. [8], Mendonca and Wallace [3], and Chang et al. [1]). Rinaldi et al. [7] note that managers of the infrastructure systems have become inclined to consider these interdependencies; however, the managers of a particular infrastructure will have little knowledge of the structure and operations of the other systems. Therefore, the use of models that contain information about the operations of the other infrastructure systems will not necessarily be available to the managers of a particular infrastructure. However, we can expect that the managers of an individual infrastructure will understand the direct connections of it with other infrastructures and, therefore, can weigh the services provided to connections that feed into other infrastructures more heavily. Our class of problems can be used to model this situation and, further, explore the effects on the restoration plan of an infrastructure when we consider these interdependencies.

This paper proposes an integrated network design and scheduling (INDS) problem that can be applied to a variety of infrastructure systems. This class of problems is most applicable to single-commodity infrastructure systems which include, for exam-

ple, power, waste water, and supply chain systems. The resolution of the problem can assist the managers of these systems in formulating their restoration efforts considering the priorities (e.g., interdependencies) of their infrastructure system within the overall recovery effort from the extreme event. We provide an integer programming formulation of the problem that effectively links the network design decisions with the scheduling decisions in the problem. We also discuss exact methods to solve this class of large scale optimization problems by employing decomposition techniques. These methods are then tested extensively on realistic data sets representing infrastructure systems in New Hanover County in North Carolina. These results demonstrate the power of our proposed methods in formulating their restoration efforts according to the priorities of the emergency managers of the region.

2 Integer Programming Formulation

The mathematical model of our integrated network design and scheduling (INDS) problem involves an underlying network $G = (N, A)$ where N is the set of nodes and A is the set of arcs. There is a set of supply nodes, $S \subseteq N$, and a set of demand nodes, $D \subseteq N$. Each arc $(i, j) \in A$ has an associated capacity u_{ij} while each supply node $i \in S$ has a supply capacity s_i and each demand node $i \in D$ has a demand d_i . We are interested in sending flow (respecting the flow capacities of the arcs and the supply/demand capacities of the nodes) from the supply nodes to the demand nodes where each unit of flow that arrives at demand node $i \in D$ is given a weight of w_i . The performance of the network is evaluated by determining the maximum amount of weighted flow that can be sent from the supply nodes to the demand nodes. There is a set of arcs, A' , that we can install into the network. Without loss of generality, this can model problems where we can install both nodes and arcs into the network since a node can be 'split' into two nodes and an arc (or two arcs). We are interested in scheduling a subset of the arcs in A' onto a series of parallel identical work groups, $k = 1, \dots, K$, in order to install them into the network. Therefore, each arc $(i, j) \in A'$ has an associated processing time, p_{ij} , and capacity, u_{ij} . We assume, without loss of generality, that the processing times are integral. We further assume that we are in a non-preemptive environment so that a task must be processed without interruption. We will let $A'(t) \subseteq A'$ denote the set of completed arcs at time periods $t = 1, \dots, T$. We will evaluate the network at time period t , where we will let f_t denote the maximum weighted flow in the network $G(t) = (N, A \cup A'(t))$. Therefore, f_t provides the performance of the network at time t . The objective function of our integrated network design and scheduling problem will then measure how well the network comes online, i.e., we will maximize

$$\sum_{t=1}^T \omega_t f_t,$$

where ω_t provides the weight we associate with the performance of the network at

time t . These weights represent the ‘importance’ of the operational network at time t relative to the importance in other time periods. By setting $\omega_t = \omega$ for $t = 1, \dots, T$, we can model situations where the performance of the network in each time period is equally important. We can also model situations where the performance of the network early in the horizon is not as important as the performance later on. This would be common, for example, in infrastructures where it is clear that the services will be disrupted in the short term but we wish to ensure that most of the requested services are met quickly after this initial period. The INDS problem was proven to be NP-hard even for problems with a single work group, single supply node, and single demand node in Nurre and Sharkey [5].

We propose an integer programming (IP) formulation for the core INDS problem. The variables in the IP formulation of the INDS problem can be broken down into three types of variables: (i) network flow variables, (ii) network design variables, and (iii) scheduling variables. The network flow variables include continuous variables x_{ijt} for $(i, j) \in A \cup A'$ and $t = 1, \dots, T$ that represent the flow on arc (i, j) in time period t and continuous variables v_{it} for $i \in D$ that represent the amount of demand met at node i in time period t . The network design variables include binary variables z_{kij} for $k = 1 \dots, K$ and $(i, j) \in A'$ that represent the decision that arc (i, j) is assigned to and processed by work group k and β_{ijt} for $(i, j) \in A'$ and $t = 1 \dots, T$ that represent that arc (i, j) is available in time period t . The scheduling variables include binary variables α_{kijt} for $k = 1, \dots, K$, $(i, j) \in A'$, and $t = 1, \dots, T$ that represent the decision that work group k is working on arc (i, j) in time period t . The constraint set of the integer programming formulation will link the network design decisions and the network flow decisions (i.e., we can only send flow on arcs completed prior to time period t in time period t) as well as the scheduling decisions (i.e., if arc (i, j) is available in period t then we must have processed it before t). The formulation of the INDS problem is:

$$\max \sum_{t=1}^T \sum_{i \in D} \omega_t w_i v_{it}$$

subject to (IP)

$$\sum_{(i,j) \in A \cup A'} x_{ijt} - \sum_{(j,i) \in A \cup A'} x_{jit} \leq s_i \quad \text{for } i \in S, t = 1, \dots, T \tag{1}$$

$$\sum_{(i,j) \in A \cup A'} x_{ijt} - \sum_{(j,i) \in A \cup A'} x_{jit} = 0 \quad \text{for } i \in N \setminus \{S \cup D\}, t = 1, \dots, T \tag{2}$$

$$\sum_{(i,j) \in A \cup A'} x_{ijt} - \sum_{(j,i) \in A \cup A'} x_{jit} = -v_{it} \quad \text{for } i \in D, t = 1, \dots, T \tag{3}$$

$$0 \leq v_{it} \leq d_i \quad \text{for } i \in D, t = 1, \dots, T \tag{4}$$

$$0 \leq x_{ijt} \leq u_{ij} \quad \text{for } (i, j) \in A, t = 1, \dots, T \tag{5}$$

$$0 \leq x_{ijt} \leq u_{ij} \beta_{ijt} \quad \text{for } (i, j) \in A', t = 1, \dots, T \tag{6}$$

$$\sum_{(i,j) \in A'} \alpha_{kijt} \leq 1 \quad \text{for } k = 1, \dots, K, t = 1, \dots, T \tag{7}$$

$$\sum_{t=1}^T \alpha_{kijt} \leq p_{ij} z_{kij} \quad \text{for } (i, j) \in A', k = 1, \dots, K \quad (8)$$

$$\beta_{ijt} + \sum_{k=1}^K \alpha_{kijt} \leq \sum_{k=1}^K z_{kij} \quad \text{for } (i, j) \in A', t = 1, \dots, T \quad (9)$$

$$\beta_{ij(t+1)} + \alpha_{kij(t+1)} \geq \beta_{ijt} + \alpha_{kijt} \quad \text{for } (i, j) \in A', k = 1, \dots, K, t = 1, \dots, T \quad (10)$$

$$\beta_{ij(t+1)} \geq \beta_{ijt} \quad \text{for } (i, j) \in A', t = 1, \dots, T - 1 \quad (11)$$

$$\alpha_{kijt}, \beta_{ijt}, z_{kij} \in \{0, 1\} \quad \text{for } (i, j) \in A', k = 1, \dots, K, t = 1, \dots, T \quad (12)$$

The objective is to maximize the cumulative weighted flow arriving at the demand nodes over the horizon of the problem. Constraints (1)-(6) are typical network flow constraints over the arcs available in the network in period t . They ensure that the flow generated at a supply node does not exceed its supply capacity (1), the amount of flow delivered to a demand node is equal to the satisfied demand at the node (3) while not exceeding the requested demand at the node (4), and the flow on an available arc does not exceed its capacity (5)-(6). Constraints (7)-(12) link the network design decisions with the scheduling decisions. Constraint (7) ensures that each work group is processing at most one arc in each time period. Constraints (8)-(10) ensure that an arc $(i, j) \in A'$ is selected by at most one work group and, if selected by a work group, is processed in a non-preemptive manner by the work group.

3 Decomposition Method

The computational times required to solve the INDS problem should be satisfactory with the computational resources available to the managers of the infrastructure systems since the restoration planning and scheduling decisions will need to be made in real time. For this purpose, we develop a customized decomposition method, in which the problem is solved in two steps.

Figure 1 demonstrates how the decomposition method is applied by solving the master problem (MP) and the subproblem (SP) iteratively. First, the master problem decides the flows on each arc (x_{ijt}) in the network, the assignment of tasks to work groups (z_{kij}) , and when the arcs that can be installed into the network will become available (β_{ijt}) . The master problem is defined by deducting the scheduling decisions out of the original IP formulation discussed in Section 2. Therefore, the objective function and constraints (1)-(6) of the the original INDS problem also appears in the formulation of MP problem. The remaining constraints of the MP problem are given by valid inequalities in (13)-(19).

$$\beta_{ij,t+1} \geq \beta_{ij,t+1}, \quad \text{for } ij \in A', t \in \{1, 2, \dots, T - 1\} \quad (13)$$

$$\sum_{t=1}^{p_{ij}} \beta_{ij,t} = 0, \quad \text{for } ij \in A' \quad (14)$$

$$\sum_{k=0}^K z_{kij} \leq 1, \quad \text{for } ij \in \mathbf{A}' \tag{15}$$

$$\sum_{k=0}^K z_{kij} \geq \beta_{ij,t}, \quad \text{for } ij \in \mathbf{A}', t \in \{1, 2, \dots, T\} \tag{16}$$

$$\sum_{ij \in \mathbf{A}'} (\beta_{ij, \min\{T-1, t+p_{ij}\}} - \beta_{ij,t}) \leq K, \quad \text{for } t \in \{2, \dots, T+1\} \tag{17}$$

$$\sum_{ij \in \mathbf{A}'} z_{kij} \cdot p_{ij} \leq T, \quad \text{for } k \in \{1, \dots, K\} \tag{18}$$

$$\beta_{ij,t} = 0, \quad \text{for } ij \in \mathbf{A}', t \in \{1, \dots, p_{ij}\} \tag{19}$$

At the second step, the subproblem checks whether the availability of arcs decided in the master problem can be satisfied with a scheduling plan. In the subproblem, we sort the jobs by their *due time* (i.e. the first time period when they will be available in the network) in ascending order for each work group. If the completion time of any task assigned to a work group does not exceed its *due time*, then the solution found by the master problem will have a feasible schedule. Since the master problem is more relaxed than the original INDS formulation given in Section 2, we can conclude that the optimal solution is attained. If the solution of the master problem can not be feasibly scheduled with the subproblem, we add (20)-(21) into MP and solve the new master problem again until SP finds a feasible schedule.

$$\sum_{ij \in s'_k} \beta_{ij, \text{comptime}_{ij}} + \text{cut}_{k, \text{iteration}} \leq |s'_k|, \tag{20}$$

$$\sum_{ij \in s'_k} z_{ij,k} + (1 - \text{cut}_{k, \text{iteration}}) \leq |s'_k| \tag{21}$$

In constraints (20)-(21), s'_k represents the first $|s'_k|$ tasks that can be feasibly assigned to work group k , where the order of jobs is determined by the subproblem. $\beta_{ij, \text{comptime}_{ij}}$ represents the decision that arc (i, j) is available at the completion time of arc (i, j) decided by SP. A new decision variable $\text{cut}_{k, \text{iteration}}$ is also defined to ensure that only one of (20) and (21) would be a strong valid inequality in the master problem. In other words, this constraint pair forces the solution in the next iteration either not to assign all tasks in s'_k to a work group or not to finish all tasks in s'_k at their completion times (comptime_{ij}) decided by the current iteration of SP.

The focus of this section is on examining a case study representing the power infrastructure of New Hanover County, NC. The network model of power infrastructure has 377 nodes and 386 arcs under normal operations. This may seem that there is not much redundancy in the system but we note that there is a good level of redundancy in the transmission network in the county. There are 37 nodes and 46 arcs in the transmission network. We have added 340 demand nodes and 340 arcs connecting the demand points to appropriate distribution substations in our model of this infrastructure. These demand nodes and arcs then model the distribution network in the county. The components that are damaged in this case study correspond to components that are vulnerable

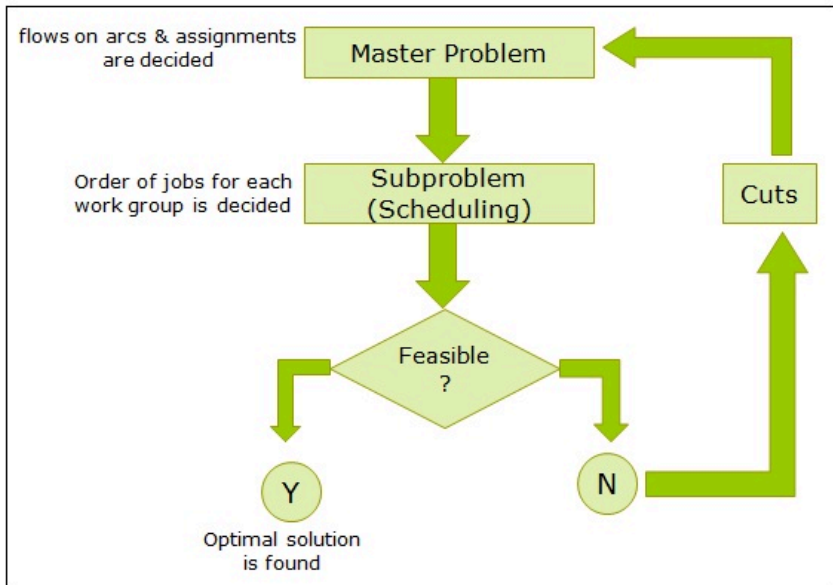


Figure 1: Decomposition Method

to either wind damage or from flooding during a hurricane, especially when the eye of the hurricane passes to the south of the county. The INDS problem has $N = 377$ nodes, and two damage scenarios where there are either 10 disrupted arcs ($A = 376$ arcs and $A' = 10$) or 40 disrupted arcs ($A = 346$ arcs and $A' = 40$). The horizon of the problem is equal to $T = 30$ where, roughly, each time period represents a six hour block of time so that the horizon is roughly a week. The number of work groups in this study is equal to $K = 1$ or $K = 2$.

CPLEX 12.1 is used to solve the integer programming (IP) formulation of INDS problem and the decomposed problem. The comparison of both formulations' computational performances is provided in Figure 2. First table shows the results when w_i and w_t values are constant. Second table compares the computational times when the demand nodes are weighed (w_i) according to the priorities of emergency manager of the county. Third table gives the results when time weights (w_t) are weighed more heavily later in the horizon by setting $w_t = t/T$. The results indicate that almost in all cases decomposition method provides a significant improvement in computational performance. When $K = 2$ and $A' = 40$, the decomposition method solves INDS problem even at least 5 times faster.

Constant node & time weights			
RUN TIME (sec)		IP formulation	DECOMPOSITION
Scenario 1 (10 damaged arcs)	K = 1	5	6
Scenario 2 (40 damaged arcs)		119	31
Scenario 1 (10 damaged arcs)	K = 2	438	9
Scenario 2 (40 damaged arcs)		2155	379

Varying node weights according to county EM priorities time (w_i)			
RUN TIME (sec)		IP formulation	DECOMPOSITION
Scenario 1 (10 damaged arcs)	K = 1	4	6
Scenario 2 (40 damaged arcs)		110	20
Scenario 1 (10 damaged arcs)	K = 2	760	5
Scenario 2 (40 damaged arcs)		5047	180

Increasing time weights over time (w_t)			
RUN TIME (sec)		IP formulation	DECOMPOSITION
Scenario 1 (10 damaged arcs)	K = 1	4	7
Scenario 2 (40 damaged arcs)		64	22
Scenario 1 (10 damaged arcs)	K = 2	292	5
Scenario 2 (40 damaged arcs)		3884	174

Figure 2: Computational Time Results

4 Conclusions

This research has developed a novel integrated network design and scheduling problem that can be used to model the problem of restoring services provided by infrastructure systems after an extreme event disrupts them. The model is general enough to be applicable to a variety of infrastructures, including the power, water, waste water, and emergency supply chain infrastructures (see Nurre et al. [4]). The core INDS problem combines two very difficult classes of optimization problems in network design and scheduling. We have developed an integer programming formulation that is able to provide the exact optimal solutions to the small case studies quickly. However, this integer programming formulation is not able to determine the optimal solution for more complex problems.

In order to overcome the issue of the computational complexity, we introduce the decomposition method, and apply it in a realistic case representing power infrastructure of New Hanover County, NC. The results suggest that decomposition method significantly improves the computational performance.

References

- [1] S.E. Chang, T.L. McDaniels, J. Mikawoz, and K. Peterson. Infrastructure failure interdependencies in extreme events: power outage consequences in the 1998 ice storm. *Natural Hazards*, 41:337–358, 2007.
- [2] E.E. Lee, J.E. Mitchell, and W.A. Wallace. Restoration of services in interdependent infrastructure systems: A network flows approach. *IEEE Transactions on Systems, Man, and Cybernetics, Part C: Applications and Reviews*, 37(6):1303–1317, 2007.
- [3] D. Mendonca and W.A. Wallace. Impacts of the 2001 world trade center attack on new york city critical infrastructures. *Journal of Infrastructure Systems*, 12(4):260–270, 2006.
- [4] S.G. Nurre, B. Cavdaroglu, J.E. Mitchell, T.C. Sharkey, and W.A. Wallace. Restoring infrastructure systems: An integrated network design and scheduling problem. Sept 2010. Submitted to *Operations Research Special Issue: Operations Research for the Public Interest*.
- [5] S.G. Nurre and T.C. Sharkey. Restoring infrastructure systems: An integrated network design and scheduling problem. In *Proceedings of the 2010 Industrial Engineering Research Conference*.
- [6] T.D. O’Rourke. Critical infrastructure, interdependencies, and resilience. *The Bridge: National Academy of Engineering*, 37(1):22–29, 2007.
- [7] S. M. Rinaldi, J. P. Peerenboom, and T. K. Kelly. Identifying, understanding, and analyzing critical infrastructure interdependencies. *IEEE Control Systems Magazine*, 21(6):11–25, 2001.
- [8] W.A. Wallace, D. Mendonca, E. Lee, J.E. Mitchell, and J. Chow. Managing disruptions to critical interdependent infrastructures in the context of the 2001 world trade center attack. *Beyond September 11th: An Account of Post-Disaster Research*, pages 165–198, 2003.

Strategic Planning for Power System Restoration

Carleton Coffrin
Brown University
Providence, RI
02912, USA

Pascal Van Hentenryck
Brown University
Providence, RI
02912, USA

Russell Bent
Los Alamos National Laboratory
Los Alamos, NM
87545, USA

Abstract

This paper considers the power system restoration planning problem (PSRPP) for disaster recovery, a fundamental problem faced by all populated areas. PSRPPs are complex stochastic optimization problems that combine resource allocation, warehouse location, and vehicle routing considerations. Furthermore, electrical power systems are complex systems whose behavior can only be determined by physics simulations. Moreover, these problems must be solved under tight runtime constraints to be practical in real-world disaster situations. This work is threefold; It formalizes the specification of PSRPPs, introduces a simple optimization-simulation hybridization necessary for solving PSRPPs, and presents a complete restoration algorithm that utilizes the strengths of mixed integer programming, constraint programming, and large neighborhood search.

1 Background & Motivation

Every year seasonal hurricanes threaten coastal areas. The severity of hurricane damage varies from year to year, but significant power outages are always caused by seasonal hurricanes. Power outages have significant impacts on both quality of life (e.g. crippled medical services) and economic welfare. Therefore, considerable human and monetary resources are always spent to prepare for and recover from power threatening disasters. At this time, policy makers work together with power system engineers to make the critical decisions relating to how money and resources are allocated for preparation and recovery of the power system. Unfortunately, due to the complex nature of electrical power networks, these preparation and recovery plans are limited by the expertise and intuition of the power engineer. Furthermore, the National Hurricane Center (NHC) of the National Weather Service in the United States (among others) is highly skilled at generating ensembles of possible hurricane tracks but current preparation methods often ignore this information.

This paper aims to solve this disaster recovery problem more rigorously by combining optimization techniques and disaster-specific information given by NHC predictions. The problem is not only hard from a combinatorial optimization standpoint, but it requires modeling of a complex physical system (i.e. the electrical power network) which is a challenging sub-problem. The electrical power industry has developed several tools for modeling the power system's behavior (e.g. T2000, PSLF, Powerworld, PSS), each with its own strengths and weaknesses. Furthermore, the electrical power industry recognizes there is not a single model for understanding the behavior of an electrical power network. For that reason, this work seeks to build solution procedures that are independent of any specific electrical power simulation tool.

The paper considers the following abstract disaster recovery problem: How to store supplies throughout a populated area to minimize the amount of time each customer is without electricity after a disaster has occurred. It makes the following technical contributions:

1. It formalizes the Power System Restoration Planning Problem (PSRPP).
2. It proposes a Constraint Programming and Simulation Hybrid System for optimization of complex network-flow systems

3. It proposes a multi-stage hybrid-optimization decomposition for PSRPPs, combining Constraint Programming, Large Neighborhood Search, and Power Simulation.
4. It validates the approach on power restoration for hurricane recovery in the United States.

Section 2 of this paper reviews similar work on power system recovery and vehicle routing problems. Section 3 presents a mathematical formulation of the power system recovery problem and sets up the notations for the rest of paper. Section 4 discusses the methodology for a hybrid simulation-optimization framework. Section 5 presents the a high level model of the problem. Section 6 reports experimental results of the algorithm on some benchmark instances to validate the approach and Section 7 concludes the paper.

2 Previous Work

Power engineers have been studying power system restoration (PSR) since at least the 1980s (see [1] for a comprehensive collection of work) and the work is still ongoing. The goal of PSR research is to find fast and reliable ways to restore a power system to its normal operational state after a black-out event. This kind of logistics optimization problem is traditionally solved with techniques from the Industrial Engineering and Operations Research sciences. However, PSR has a number of unique features that prevent the application of traditional optimization methods, including:

1. **Steady-State Behavior:** The flow of electricity over a power system is governed by the laws of physics (e.g., Kirchoff's current law and Ohm's law). Hence, evaluating the behavior of the network requires solving a system of non-linear equations. This can be time-consuming and there is no guarantee that a feasible solution can be found.
2. **Dynamic Behavior:** During the process of modifying the power system's state (e.g., energizing components and changing component parameters), the system is briefly subject to transient states. These short but extreme states may cause unexpected failures [2].
3. **Side Constraints:** Power systems are comprised of many different components, such as generators, transformers, and capacitors. These components have some flexibility in their operational parameters but they may be constrained arbitrarily. For example, generators often have a set of discrete generation levels, and transformers have a continuous but narrow range of tap ratios.

The PSR research recognizes global optimization is an unrealistic goal in such complex non-linear systems and adopts two main solutions strategies. The first strategy is to use domain expert knowledge (i.e. power engineer intuition) to guide an incomplete search of the solution space. These incomplete search methods include *Knowledge Based Systems* [16], *Expert Systems* [10, 3, 5], and *Local Search* [12, 13]. The second strategy is to approximate the power system with a linear model and solve the approximate problem optimally [17]. Some work has hybridized both strategies by designing Expert Systems that solves a series of approximate problems optimally [14, 9].

Interestingly, most of the work in planning PSR has focused on the details of scheduling power system restoration [2, 3]. More specifically, what is the best order of restoration and how should system components be reconfigured during restoration? In fact, these methods assume that all network components are operational and simply need to be reactivated. In this study we consider the restoration of damaged components which must be repaired before reactivation can occur. This introduces two additional decision problems: (1) Are replacement parts available for a given repair; (2) How can the restoration teams be routed effectively perform all of the repairs? To the best of our knowledge PSRPPs are the first PSR application that considers strategic storage decisions and vehicle routing decisions.

Given:Power Network: \mathcal{PN} Repositories: $R_{i \in 1..r}$
Capacity: RC_i Vehicles: $V_{i \in 1..m}$
Capacity: VC
Start Depot: D_i^+
End Depot: D_i^- Network Items: $N_{i \in 1..n}$
Item Type: NT_i
Maintenance Time: M_i Items Types: $I_{i \in 1..t}$
Volume: IV_i Scenario Data: $S_{i \in 1..s}$
Scenario Probability: P_i
Item Damage: $ND_i \subset \{1..n\}$
Travel Time Matrix: $T_{i,1..l,1..l}$ **Output:**The items to store at each repository
Delivery schedules for each vehicle in each scenario**Let:** T_i = completion time of the last repair in scenario i
Unserved Power $_i(t)$ = the size of the blackout area
in watts at time t in scenario i **Minimize:**

$$\sum_i P_i * \int_0^{T_i} \text{UnservedPower}_i(t) dt$$

Subject To:Vehicle and repository capacities
Vehicles start and end locations
Travel matrix times
Electrical power system behavior

Figure 1: Power System Restoration Problem Specification

3 The Power System Restoration Problem (PSRPP)

In formalizing PSRPPs, a populated area is represented as a graph $G = \langle L, T \rangle$ where $L_{1..l}$ represents those locations of interest to the restoration problem, i.e., the basic components of the electric power network (e.g., lines, buses, and generators), storage depots and repair vehicle locations. The vehicles can travel to any node of the graph but the edge distances, $T_{1..l,1..l}$, are not generally Euclidean and may be a metric space due to transportation infrastructure and road damage. The primary output of a PSRPP are: (1) which items should be stored at each warehouse; (2) for each scenario and each vehicle, a delivery schedule that minimizes the power restoration objective. Figure 1 summarizes the entire problem, which we now describe in detail.

Electrical Power Network An electrical power network model is necessary to understand the behavior of the power network. Especially how the behavior changes as the restoration procedure occurs. However, there are many competing models for representing electrical power networks. To remain flexible in that regard this specification considers an abstract power network model \mathcal{PN} . The only requirement on the abstract model is that it can implement the interface described in Section 4.

Electrical power networks are comprised of many different components, e.g. lines, generators, loads, capacitors, and transformers. In this work we classify each network item, i , in to a particular item type NT_i . We assume that items of type t are homogeneous in terms of their size IV_i . The power network model \mathcal{PN} captures how different components effect the total power flow in the network.

Objective The objective function aims at minimizing the total watt hours of blackout that occur after the disaster. This is simply the amount of electrical demands that are unserved until some time T . More formally,

$$\text{Minimize } \sum_i P_i * \int_0^{T_i} \text{UnservedPower}_i(t) dt$$

It is not obvious if it is possible to use available optimization and simulation tools to reason over the continuous time domain. However, the restoration process can be seen as a series of discrete events. Those are the times that each job is completed and the state of the power network components (i.e. is it damaged or not). The set of discrete events that effect the PSRPP objective can be calculated from the vehicle delivery schedules. Three pieces of aggregate information must be calculated: (1) the time that each job is completed $T_{i,j}$ (2) the time of the succeeding job $Next_{i,j}$ (3) a function that can calculate the amount of unserved power at some time $UnservedPower_i(t)$. Given these discrete events the integral above can be calculated with the following summation:

$$\text{Minimize } \sum_i P_i * \sum_j \text{UnservedPower}_i(T_{i,j})(Next_{i,j} - T_{i,j})$$

In Section 4 we discuss the details of how the $UnservedPower_i(t)$ function can be implemented in practice.

Side Constraints The first set of side constraints concerns the storage locations which represent the electric company warehouses in the populated area. Each repository $R_{i \in 1..n}$ has a maximum capacity RC_i to store the repair items. The volume of the items stored at warehouse i cannot exceed RC_i .

The second set of side constraints concerns the routing. We are given a fleet of m vehicles $V_{i \in 1..m}$ which are homogeneous in terms of their capacity VC . At any time in the routing process the volume of items carried by vehicle i cannot exceed VC . Each vehicle has a unique starting depot D_i^+ and ending depot D_i^- , and after delivering an item j it must wait for the maintenance time M_j before continuing onto its next delivery task.

Stochasticity PRSPs are specified by a set of s different disaster scenarios $S_{i \in 1..s}$, each with an associated probability P_i . After a disaster, some parts of the power network are damaged and each scenario has a set ND_i of network items that are inoperable due to the disaster damage. Finally, site-to-site travel times $T_{i,1..l,1..l}$ (where $l = |L|$) are given for each scenario and capture transportation infrastructure damage.

Unique Features Different aspects of this problem were studied before in the context of vehicle routing and power system restoration, and both have proven to be difficult problems in their own right. The vehicle routing community has produced many insightful algorithms for solving pickup and delivery routing problems (PDP). Unfortunately these techniques have focused on simple objectives (e.g. minimum travel distance) and are not easily adaptable to the kind of complex objective present in PSRPPs. The power system restoration community has produced many helpful strategies for calculating good restoration schedules. However, they usually ignore the intricacies of transportation and installation in these schedules. The optimization community has studied many problems involving uncertainty, however is uncommon to see second stage problems that involve difficult optimization problems (e.g. vehicle routing, power restoration scheduling). By combining all three aspects of these problems PSRPPs produce restoration preparations that are robust over several disaster contingencies and can be executed with all the details of transportation and installation taken into consideration.

4 A Framework for Optimization with Simulation

As we have discussed before, there are many different models for electrical power networks. This work seeks to develop optimization tools that are independent of any specific model. For this reason we adopt a very simple and abstract power simulation interface in the hope that it can be implemented by any power network model. In the context of restoration there is only one principle attribute for each item on the power network, that is, which items are fully operational

and which items are inoperable due to physical damage. We call this information the damage state of the network. All of our algorithms ask one simple question, “Given a particular damage state, how much real power reaches the network load points?”. More formally, given a power network model \mathcal{PN} , and a damage state \mathcal{DS}_i , we define the function:

$$\text{DemandsMet}(\mathcal{PN}, \mathcal{DS}_i)$$

That returns a real number representing the amount of power severed at each load node in the power network. This interface is very simple and the amount of reasoning we can do with it is limited, but this is the price of generality. If we adopt a more specific power network model we may be able to perform stronger reasoning, but one of the goals of this work is to understand how successful a very generic interface can be. The experimental results demonstrate that this simple interface is sufficient for designing effective local search algorithms. This simple interface also assumes that all the network loads have equal priority. Our future work will consider how to extend this interface to support priorities for emergency services and contractual obligations.

Recall the power restoration objective from Figure 1, this objective can be calculated using the DemandsMet function is the following way: Given some time t let damage state \mathcal{DS}_t be the set of non-operation items at time t . Also let MaxPower be the maximum amount of power served when the power system is fully repaired. Then the power restoration objective can be modeled as follows,

$$\text{Minimize } \sum_i P_i * \int_0^{T_i} \text{MaxPower} - \text{DemandsMet}(\mathcal{PN}, \mathcal{DS}_t) dt$$

The constraint programming (CP) paradigm (from the artificial intelligence community) has proven to be effective for solving a variety of combinatorial optimization problems. Specifically constraint programming is often the state-of-the-art solution technique for complex scheduling and vehicle routing problems. Because we are developing an algorithm for a combined scheduling and vehicle routing problem with many side constraints a constraint programming framework is a natural choice. However, due to the complexity of the problem we use large neighborhood search (LNS) to find high-quality solutions with in the runtime requirements. In the rest of this paper we give the high level intuition for how the DemandsMet function can be used in algorithms for modeling the behavior of an electrical power network.

5 The Basic Approach

This section presents the basic approach for solving the PSRPP. Previous work on location routing (e.g. [7, 4, 15]) has shown that reasoning over a storage problem and a routing problem simultaneously is extremely hard computationally. Furthermore we suffer from additional computation challenges due to the overhead of electric power simulation. To address these difficulties, we propose two primary stages in our algorithm that decomposes the storage, customer allocation, and routing decisions. The two primary stages, and the key decisions of each stage are as follows:

1. **Storage & Customer Allocation:** Which repositories store the repair items and how are the items allocated to each damaged item in each scenario?
2. **Restoration Routing:** For each scenario, what is the best routing plan to minimize the power restoration objective?

The decisions of each stage are independent and can use the optimization technique most appropriate to their nature. The first stage is formulated as a Mixed Integer Program (MIP). This is very natural as MIPs are excellent for two-stage stochastic programming. The second stage is solved using CP but LNS is used for larger instances where a pure CP approach is impractical. This is also a natural choice as CP and LNS are successful at combinatorial optimization of Vehicle Routing Problems (VRP) with unique side constraints. Previous work has shown that problem decomposition can bring significant runtime benefits with minimal degradation in solution quality [6].

Benchmark	r	m	s	n	$\text{Max}(ND_i)$	LNS Timeout (seconds)
BM1	8	13	3	326	22	1200
BM3	8	13	18	266	61	1200
BM4	8	13	18	326	121	1200

Table 1: PSRPP Benchmark Statistics

Stochastic Storage The stochastic storage problem consists in choosing where to store repair items and how those items are allocated to the scenario damage. In practice, the repository storage constraints may prevent full restoration of the electrical grid after a disaster. Therefore, a smart selection of restoration items is necessary to ensure the maximum amount of power is served in each disaster scenario. For this reason we choose to model this as a multi-objective optimization problem consisting of two parts. The first part of the objective consists of minimizing the total unserved demands after all the restoration is complete. The second part consists of minimizing the distance of each repair item to its damage location. The relative importance of the objectives are controlled with parameters W_p and W_t respectively. More precisely, given a decision variable D_{sij} , that indicates that an item from repository i is used to repair network item j in scenario s , then the stochastic storage objective consists in minimizing,

$$W_p * \sum_s P_s * (\text{MaxPower} - \text{DemandsMet}(\mathcal{PN}, \{j : \bigvee_i D_{sij} = 0\})) + W_t * \sum_s P_s * \sum_{i,j} T_{sij} * D_{sij}$$

subject to the repository storage capacity constraints, RC_i .

Restoration Routing Once the storage and repair allocation are computed, the uncertainty is revealed and the second stage reduces to a deterministic multi-depot, multiple-vehicle capacitated routing problem whose objective consists in minimizing the power restoration objective (defined in Section 3). This problem is similar to classic Pickup and Delivery VRPs however evaluation of the power restoration objective requires the use of an electrical power model. More precisely, given a decision variable T_i that represents the repair time of item i and $Next_i$ the time of the job succeeding i , then the restoration routing objective consists in minimizing,

$$\sum_i (\text{MaxPower} - \text{DemandsMet}(\mathcal{PN}, \{j : T_j \leq T_i\})) * (Next_i - T_i)$$

subject to the travel time matrix and vehicle capacity constraints. The addition of power simulation to the objective function adds considerable computational complexity compared the classic routing objectives (e.g. minimum travel distance).

6 Benchmarks & Results

Benchmarks The benchmarks were produced by Los Alamos National Laboratory and are based on the infrastructure of the United States. The disaster scenarios were generated by state-of-the-art hurricane simulation tools similar to those used by the National Hurricane Center. Their sizes are presented in Table 1(The table also depicts the algorithm parameters). The size of the largest ND_i set is included because it is a good metric for difficulty of a benchmark. It is also important to emphasize that, these benchmarks are significantly large in size compared similar work in this field.

The Algorithm Implementation and the Baseline Algorithm The final algorithm was implemented in the COMET system [8] and the experiments were run on Intel Core 2 Duo CPU 2.53GHz machines running OS X 10.5. The power simulator IEISS (a proprietary power simulation tool of LANL) was used to evaluate the behavior of the power system. To validate our results, we compare our PSRPP algorithm to a variant of the same algorithm that models what is done in practice. The baseline algorithm is designed to model the decision making process of an

Benchmark	BM1	BM3	BM4
Baseline	192866	606090	668064
PSRPP	141919	328673	355695
Improvement	26.4%	45.8%	46.8%

Table 2: PSRPP Benchmark Results (Power Restoration Objective)

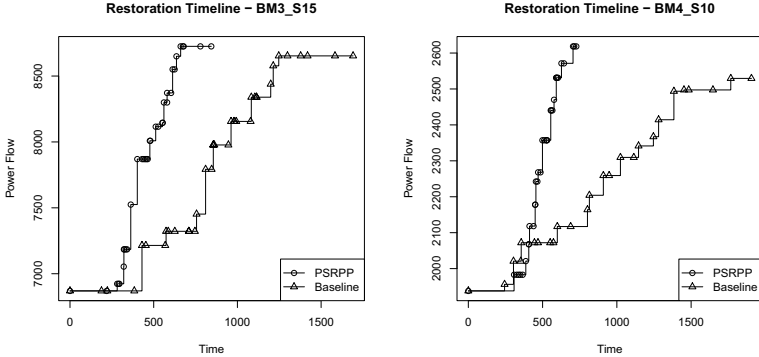


Figure 2: PSRPP Routing Results Comparison

electric power utility before and during the recovery process. There is little documentation on the process utilities use for stockpiling supplies for disaster recovery. Therefore, we design a simple greedy heuristic to model the storage decision process. Having no information about which disasters will occur, the utility may assume each item in the network has an equal probability of being destroyed in a disaster. In that case we should stockpile restoration items relative to their occurrence in the network (subject to the storage capacity constraint). Furthermore, it is not clear where to store the restoration items, so we choose to place them in equal quantity in each warehouse. After a disaster has occurred the utility’s process goes roughly like this: (1) the power system engineers use their intuition for the network to prioritize the restoration actions based upon contractual obligations and restoration of emergency services; (2) restoration teams are dispatched to make the necessary repairs; (3) crews prefer to fix all broken items near the area they are dispatched to. We model this process in the routing stages of the PSRPP algorithm in the following way: (1) the restoration order is fixed by a greedy heuristic that has full understanding of the electrical network’s behavior. It repeatedly chooses to repair the item that will bring the largest increase in network flow. This roughly captures the knowledge that a power systems engineer uses to organize a restoration effort; (2) the routing problem is similar to the one discussed in Section 5 but the routing objective is different because each vehicle crew works independently to do their repairs as fast as possible. The objective seeks to minimize the total travel distance of each vehicle and not power restoration objective. This variant of the PSRPP algorithm roughly approximates current power system restoration procedures and is thus a good baseline for comparison.

Results Table 2 compares the quality of the power restoration objective of the PSRPP algorithm and the baseline algorithm. As you can see the PSRPP algorithm brings a 26% improvement over the baseline on smaller benchmarks and up to 45% on larger benchmarks. Each benchmark has several disaster scenarios, each with a unique vehicle routing problem. Figure 2 illustrates the benefits of the restoration routing aspects of this problem over the baseline on two scenarios the 15th scenario of benchmark 3 (left), and the 10th scenario of benchmark 4 (right). Results on other scenarios are similar but omitted for space reasons.

7 Conclusion

This paper presented a novel problem in the field of humanitarian logistics, the Power System Restoration Problem (PSRPP). The PSRPP models the strategic planning process for post disaster power system recovery. This paper proposed a multi-stage stochastic hybrid optimization algorithm that yields high quality solutions to real-world benchmarks provided by Los Alamos National Laboratory (LANL). The algorithm uses a variety of technologies, including MIP, constraint programming, and large neighborhood search, to exploit the structure of each optimization sub-problem. The experimental results on hurricane disaster benchmarks indicate that the algorithm is practical from a computational standpoint and produce significant improvements over existing relief delivery procedures.

References

- [1] M. Adibi. *Power System Restoration(Methodologies & Implementation Strategies)*. 2000.
- [2] M.M. Adibi and L.H. Fink. Power system restoration planning. *Power Systems, IEEE Transactions on*, 9(1):22–28, feb. 1994.
- [3] M.M. Adibi, L.R.J. Kafka, and D.P. Milanicz. Expert system requirements for power system restoration. *Power Systems, IEEE Transactions on*, 9(3):1592–1600, aug. 1994.
- [4] M. Albareda-Sambola, J. A. Diaz, and E. Fernandez. A compact model and tight bounds for a combined location-routing problem. *Computer & Operations Research*, 32:407-428, 2005.
- [5] J.J. Ancona. A framework for power system restoration following a major power failure. *Power Systems, IEEE Transactions on*, 10(3):1480–1485, aug. 1995.
- [6] Elvin Coban and John N. Hooker. Single-facility scheduling over long time horizons by logic-based benders decomposition. In Andrea Lodi, Michela Milano, and Paolo Toth, editors, *CPAIOR*, volume 6140 of *Lecture Notes in Computer Science*, pages 87–91. Springer, 2010.
- [7] L. I. Burke D. Tuzun. A two-phase tabu search approach to the location routing problem. *European Journal of Operational Research*, 116:87-99, 1999.
- [8] Inc. Dynadec. Comet 2.1 user manual. <http://dynadec.com/>, 2009.
- [9] J.A. Huang, L. Audette, and S. Harrison. A systematic method for power system restoration planning. *Power Systems, IEEE Transactions on*, 10(2):869–875, may. 1995.
- [10] J.A. Huang, F.D. Galiana, and G.T. Vuong. Power system restoration incorporating interactive graphics and optimization. pages 216–222, may. 1991.
- [11] James P. Ignizio. A review of goal programming: A tool for multiobjective analysis. *The Journal of the Operational Research Society*, 29(11):pp. 1109–1119, 1978.
- [12] A.L. Morelato and A.J. Monticelli. Heuristic search approach to distribution system restoration. *Power Delivery, IEEE Transactions on*, 4(4):2235–2241, oct. 1989.
- [13] H. Mori and Y. Ogita. A parallel tabu search based approach to optimal network reconfigurations for service restoration in distribution systems. volume 2, pages 814–819 vol.2, 2002.
- [14] T. Nagata, H. Sasaki, and R. Yokoyama. Power system restoration by joint usage of expert system and mathematical programming approach. *Power Systems, IEEE Transactions on*, 10(3):1473–1479, aug. 1995.
- [15] G. Nagy and S. Salhi. Nested heuristic methods for the location-routing problem. *Journal of Operational Research Society*, 47:1166-1174, 1996.
- [16] T. Sakaguchi and K. Matsumoto. Development of a knowledge based system for power system restoration. *Power Apparatus and Systems, IEEE Transactions on*, PAS-102(2):320–329, feb. 1983.
- [17] M.H. Yolcu, Z. Zabar, L. Birenbaum, and S.A. Granek. Adaptation of the simplex algorithm to modeling of cold load pickup of a large secondary network distribution system. *Power Apparatus and Systems, IEEE Transactions on*, PAS-102(7):2064–2068, jul. 1983.

Preparedness of Finnish electricity users against major disturbances in supply of electric power

J. Sarsama¹, R. Molarius¹, P. Verho², J. Strandén² and H. Krohns²

¹ VTT Technical Research Centre of Finland, P.O. Box 1300, FI-33101 Tampere, Finland, Tel. +358 20 722 111, Fax +358 20 722 3494, email: firstname.lastname@vtt.fi

² Tampere University of Technology, Department of Electrical Energy Engineering, P.O. Box 692, FI-33101 Tampere, Finland, Tel. +358 3 311 511, Fax +358 3 3115 2088, email: firstname.lastname@tut.fi

ABSTRACT

The reliability of electricity supply is in modern societies generally on a very high level. However, there have been power interruptions that have severely impacted on the functioning of a society, and on the safety and well-being of citizens – and the possibility for severe interruptions remains also in future. Responsibility to prepare against power interruptions does not rest in Finland only with network operators, but responsible are also electricity users and public actors like rescue services and municipalities. The topic of this paper is the preparedness of Finnish electricity users against major disturbances in supply of electric power. The paper is based on a questionnaire study directed to 86 Finnish distribution system operators. According to the questionnaire, with a response rate of about 60 per cent, it seems that there would be a need to enhance the preparedness against major disturbances in almost every electricity user type.

INTRODUCTION

The reliability of electricity supply is in modern societies generally on a very high level. However, there have been power interruptions that have severely impacted on the functioning of a society, and on the safety and well-being of citizens. Alone in 2000s severe disturbances have occurred e.g. in Northern America, Italy, UK (London), Europe, Sweden and Finland (U.S.-Canada 2004, UCTE 2004, National 2003, UCTE 2007, Swedish 2008a and 2008b, Forstén 2002). Due to the storm Gudrun (Erwin) in Sweden in 2005 the interruptions were up to about 45 days (Swedish 2008a). The storms Pyry and Janika that hit in a row to Finland in 2001 affected over 800,000 customers (about 30 % of the customers nationwide), and in about 1,600 households interruptions were longer than five days (Forstén 2002). Ex-

amples of societal consequences of the power interruptions caused by the above-mentioned storms e.g. are shortly described in (Strandén et al. 2009).

Along with severe interruptions the understanding about the criticality of the electric power supply infrastructure has grown. This has lead, e.g. in Finland and Sweden to legislative changes, mainly focusing on the responsibilities of distribution system operators (DSO). In Finland the so called standard compensation practice was introduced less than two years after the 2001 storms. (Strandén et al. 2009) The idea of the practice is to direct DSOs to develop their networks and operations so that the reliability of power supply and the management of interruptions are enhanced.

The concrete means by which DSOs have developed their networks are e.g. relocation of the overhead lines from forest to roadside, increasing the amount of underground cabling or network automation as mentioned e.g. in (Strandén et al. 2009). As the economic lifetime of different network parts and components is typically decades (30-50 years), the rate at which the network investments change reliability characteristics of the distribution network, is limited. In addition there are also other types of threats that can cause severe interruptions. According to (Ministry of Defence 2006) electrical networks are an important target for possible terrorism. Also the fact that the operating and control systems of electrical networks are in many respects dependent on data communication systems, is one source of vulnerability problems (Ministry of Defence 2006). So the possibility to severe interruptions remains and thus also a need to a certain level of preparedness in the society against these kinds of incidents.

Responsibility to prepare against power interruptions does not rest in Finland only with network operators, but responsible are also electricity users and public actors like rescue services and municipalities. The roles of electricity users and public actors become important especially in case of severe interruptions.

There has been published some studies that discuss the topic of preparedness of electricity users against power interruptions (Silvast 2007 and 2008, Palm 2009, Helsloot & Beerens 2009, Nieminen Kristofersson 2007, Murphy 2004). However these mainly focus on ordinary households, and do not cover the preparedness of other electricity user types (e.g. water and wastewater utilities; fuel supply & filling stations; municipal health centres etc.) or the focus is in "normal" interruptions, not specifically in major disturbances. At least in Finland there has not been carried out a study, where the whole field of electricity users in respect to their preparedness against major disturbances would have been covered.

The topic of this paper is the preparedness of Finnish electricity users against major disturbances in supply of electric power. The paper is based on a questionnaire study directed to Finnish distribution system operators. The concept of 'major disturbance in supply of electric power' (abbreviations used later "major disturbance" or simply MD) was defined in the study in the following way: *a long lasting or a widespread interruption in the supply of electric power, during which the fire and rescue services and one or more other public actor (municipality, police, etc.) need, in addition to the DSO, to start implementing measures for reducing possible severe consequences to people and property.*

This paper is based on an on-going research project carried out by Tampere University of Technology and VTT Technical Research Centre of Finland. The pro-

ject is funded mainly by the Finnish Funding Agency for Technology and Innovation. The aim of the project is to create a common concept for the exchange of information between distribution system operators and the rescue services and municipal authorities in major disturbances in supply of electric power and by this means to enhance the situational awareness of these bodies.

METHODS AND MATERIALS

The questionnaire – realized by an Internet-based Digium software (Digium 2010) – was addressed in spring 2010 to the greater part of Finnish DSOs. Two out of total 88 DSOs were left out because of their small size and very small number of customers. Contact persons, to whom the questionnaire was sent, were mainly in the positions of operation manager, network manager or CEO. DSOs were recommended to apply teamwork when answering to the questionnaire. It was thought that in this way the answers would better represent “company level”, and that teamwork would make answering easier.

The question related to the topic of this paper, together with the answering options, is presented in the table 1. In the questionnaire there were listed altogether 37 electricity user types, but in this paper the focus is in those 19 that are listed in the table. The electricity user types included into this article are those, which were estimated to have – in case of a MD – immediate or rather immediate effect on the functioning of the society or on the safety or well-being of citizens. Electricity user types left out from this article are such as e.g. “Hotels and spas” and “Downhill skiing centres” for which a MD is mainly a business risk.

Table 1. *Question on the preparedness of electricity users against MDs.*

Task: Estimate the current level of preparedness of the following electricity user types to maintain their own operations/functioning in the major disturbances in the supply of electric power.		
Preparedness level of the given electricity user type is...		
A) Over-dimensioned	D) Insufficient	G) There doesn't exist on the company's geographical area of responsibility the given electricity user type.
B) Sufficient	E) No preparedness at all.	
C) Fairly sufficient	F) Don't know/not possible to estimate.	
1. Hospitals	5. Children's day care centres	12. Shopping centres, hypermarkets
2. Municipal health centres	6. Schools, educational institutions	13. Other shops and stores
3. Critical home care patients dependent on the supply of electric power, e.g. patients with respiratory disorders	7. District heat production and distribution	14. Banking services and money traffic
4. Old people's homes and other service accommodation units	8. Water and wastewater utilities	15. Fuel supply, filling stations
	9. Tele and data communication	16. Households in general
	10. Mass media (radio, TV)	17. Housing companies
	11. Logistics centres, goods terminals	18. One-family houses in urban areas
		19. One-family houses in rural areas

51 DSOs answered to the questionnaire during its answering period of about five weeks. As one of the DSOs answered on behalf of two DSOs belonging to the same corporation, the correct number of attended DSOs was 52 and the corresponding response rate was about 60 %. The response rate was on a quite high level and the coverage of the attended DSOs of the whole branch was even higher: The attended 52 DSOs represented between 81-85 % of the total network length, customers and electric energy distributed in Finland in 2008.

As the answer option A (see table 1) was not chosen a single time in any of the given answers (issue that is a result itself), the measure of *preparedness level*

(symbol P) was used as a first means to get an idea on the preparedness level of different electricity user types. Measure P was constituted by reducing from the percentage value of “positive” answers (“preparedness sufficient” or “preparedness fairly sufficient”) the percentage value of “negative” answers (“preparedness insufficient” or “no preparedness at all”). The calculation of these percentage values was based on the amount of answers given in answer options B-F (see table 1).

RESULTS

A clear majority (17 out of 19) of the electricity user types got negative preparedness level values. In other words, preparedness of the 17 electricity user types (to maintain ones own operations/functioning in MDs), was estimated to be negative. Only in the case of hospitals (P = 67) and mass media (P = 30) the relation was estimated to be opposite i.e. there were given more positive answers than negative ones. In the figure 1 are presented the electricity user types with negative P values and their corresponding percentage values in different answer options.

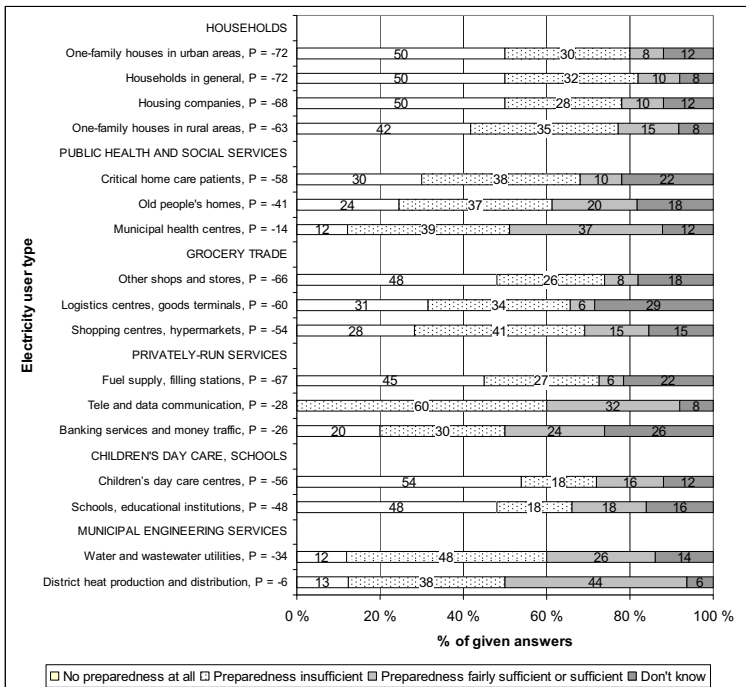


Figure 1. Electricity user types with negative preparedness level (P) values.

The electricity user types are presented in the figure 1 under more general category headings such as *Households, Public health and social services* etc., and under each heading user types are listed in the descending order of calculated P values. In respect to the presented percentage values of given answers in the figure 1, it is worth noting that these are based on a high number of given answers. In case of a clear majority of different electricity user types presented in the figure 1, the number of answered DSOs varied between 48 and 51 (whereas the total number of participated DSOs was 51, see prev. chapter). Only in case of user types “Logistics centres, goods terminals” and “Shopping centres, hypermarkets” and the positively assessed user types – “Hospitals” and “Mass media” (not included in the figure 1) – the number of answered DSOs was a bit lower i.e. 35-44. This was because in case of these user types, the number of answers in the answer option G (*There doesn't exist on the company's geographical area of responsibility the given electricity user type, see table 1*) was somewhat higher than in case of other user types.

Households. The three electricity user types related to households and the corresponding sum category – households in general – were all ranked to be rather poorly prepared (P between -72 and -63). 50 % of answers in electricity user types – one-family houses in urban areas, households in general and housing companies – were in class “no preparedness at all”. About 30 % of answers were in class “preparedness insufficient” and about 10 % in class “preparedness fairly sufficient or sufficient”, in electricity user type – one-family houses in urban areas – even less i.e. 8 %. Electricity user type – one-family houses in rural areas – was assessed to be a somewhat better prepared compared to other electricity user types related to households. In this 42 % of answers were in class “no preparedness at all”, 35 % in class “preparedness insufficient” and 15 % in class “preparedness fairly sufficient or sufficient”. The proportion of answers in class “don't know” in case of the four electricity user types related to households varied between 8-12 %.

Public health and social services. In this category, the calculated preparedness levels varied quite a lot (P between -58 and -14). Electricity user type – critical home care patients – was assessed to be, on the basis of the calculated preparedness levels, the weakest prepared. 30 % of answers related to it were in class “no preparedness at all”, whereas in case of electricity user type – old people's homes – the corresponding figure was 24 % and in case of municipal health centres 12 %. In all electricity user types 37-39 % of answers were in class “preparedness insufficient”. In class “preparedness fairly sufficient or sufficient” the proportion of answers varied between 10 and 37 %, being the worst in case of home care patients and the best in case of municipal health centres. In case of electricity user types – home care patients and old people's homes – proportion of “don't know” answers was also quite high, 18-22 %.

Grocery trade. In this category the calculated preparedness levels varied between -66 and -54. Electricity user type – other shops and stores – was assessed to be, on the basis of the calculated preparedness levels, the weakest prepared. 48 % of answers related to it were in class “no preparedness at all”, whereas in case of the two elec-

tricity user types – logistic centres & goods terminals and shopping centres & hypermarkets – the corresponding figure varied between 28 and 31 %. In the class “preparedness insufficient” the proportions of answers varied between 26-41 %, being the worst in case of shopping centres & hypermarkets and the best in case of other shops and stores. In the class “preparedness fairly sufficient or sufficient” the proportion of answers varied from 6 % (logistics centres & goods terminals) to 15 % (shopping centres & hypermarkets). In case of electricity user type – logistics centres & goods terminals – the proportion of “don’t know” answers was quite high, close to 30 %.

Privately-run services. In this category the calculated preparedness levels – from -67 to -26 – and the distributions of answers between different electricity user types varied quite a lot. Electricity user type – fuel supply & filling stations – was assessed to be, on the basis of the calculated preparedness levels, the weakest prepared. 45 % of answers related to it were in class “no preparedness at all”, whereas in case of electricity user type – banking services and money traffic – the corresponding figure was 20 % and in case of tele and data communication it was a pure zero i.e. there was not a single answer in this class. The proportion of answers in the class “preparedness insufficient” varied from 27 % (in case of fuel supply & filling stations) to 60 % (in tele and data communication). In the class “preparedness fairly sufficient or sufficient” the proportion of answers varied between 6 and 32 %, being the worst in case of fuel supply & filling stations and the best in case of tele and data communication. The proportion of answers in class “don’t know” varied a lot, being between 8-26 %. Highest proportion of “don’t know” answers was in case of banking services and money traffic whereas the lowest figure was in electricity user type tele and data communication.

Children’s day care centres and schools. Electricity user types belonging to this category were very much identical in respect to the given answers. This was the case especially in classes “preparedness insufficient” and “preparedness fairly sufficient or sufficient”, for which the corresponding figures were between 16 and 18 % for both electricity user types. In the class “no preparedness at all” the proportion of answers varied between 48 and 54 %, being worse in case of children’s day care centres and better in case of schools and educational institutions. The proportion of answers in the class “don’t know” was between 12-16 %.

Municipal engineering services. Electricity user types belonging to this category were quite much identical in respect to the given answers. Electricity user type – water and wastewater utilities – was assessed to be, on the basis of the calculated preparedness levels, somewhat weaker prepared against MDs than the electricity user type district heat production and distribution (P values -34 and -6). In both user types 12-13 % of answers were in class “no preparedness at all”. In the class “preparedness insufficient” the proportion of answers varied between 38 and 48 %, being worse in case of water and wastewater utilities. In the class “preparedness fairly sufficient or sufficient” the proportion of answers varied between 26 and 44 %, being worse in case of water and wastewater utilities and better in case of district heat production

and distribution. The proportion of answers in the class “don’t know” varied between 6-14 %.

DISCUSSION

Estimations given by the DSOs on the preparedness of different electricity user types against MDs were in most of the cases negative (earlier described preparedness level measure P got negative values). In other words it was assessed more often that there was no preparation at all, or the preparedness was assessed to be insufficient, compared to that, that the preparedness would have been assessed to be sufficient or fairly sufficient. This was true in case of all 19 electricity user types assessed, except hospitals and mass media (radio, TV).

One of the worst prepared categories of electricity users seemed to be households. In case of “households in general” – as an object of estimation – 50 % of the answered DSOs had an opinion that there was no preparation at all. About one third of the answers was in vote “preparedness insufficient” and only 10 % had an opinion that the preparedness was fairly sufficient or sufficient. The result is surprisingly pessimistic and it can be considered to be even a somewhat too pessimistic, when compared to study results presented by e.g. Silvast (2007). In his study it was asked from 115 household customers of the two DSOs about their preparation for power failures. According to answers e.g. 100 % of the respondents had candles and matches, 98 % flashlight and batteries and 80 % battery-operated radio (Silvast 2007).

One explanation to the discrepancy presented above could be the following: DSOs have focused in their estimations to those preparedness measures, which are valuable in long power interruptions, lasting days or even weeks. So, it is possible that the DSOs have ignored the above mentioned “ordinary” preparedness measures by thinking that if the preparedness is based only on those, it can be rather difficult to cope with long power interruptions without any other preparedness measures. So DSOs have possibly thought such preparedness measures as gas cooking stove and its fuel, extra food supply, fireplace or some other heat source independent from electricity, reserve power unit etc.

According to this study, it seems that there would be a need to enhance the preparedness against MDs in almost every electricity user type. However further studies are needed to get a more detailed picture about the preparedness level of different user types, before it is reasonable to carry out any improvement actions (e.g. advisement or education of certain user types, enforcing possible supplementary requirements to certain user types through legislation). The topic of the study presented in this article, was the preparedness assessment of the different electricity user types carried out by DSOs. This can be found in that sense as a reasonable task, that most probably DSOs have better understanding about the current legislative situation concerning the roles and duties of the different actors in severe interruptions, than e.g. electricity users have. In other words the DSOs most probably understand – at least in a general level – better the need of different user types to prepare against MDs compared to that, how the different user types themselves understand this need. According to some studies about one third of households (in rural areas) for example felt that they don’t have any responsibility to be prepared against power interruptions

(Palm 2009). On the other hand the DSOs' knowledge on the preparedness of individual electricity users can't be at the same level as it is in the case of individual electricity users themselves. Or at least DSOs can't have the same level of detailed knowledge that the individual electricity users have about the concrete preparedness measures they have against MDs. This can however vary quite a lot between DSOs. For example in case of smaller DSOs, the knowledge – also about the concrete preparedness measures – can be on a better level than in the bigger ones.

It is suggested, that in possible further studies the preparedness of different electricity user types would be studied in a more detailed way and then compared to a "sufficient" preparedness level. Finding out the preparedness of electricity users by asking it directly from them is most probably not the best way to do it. Instead one should try to find out the concrete preparedness measures that the different electricity user types have applied, and on the basis of that information then try to find out the preparedness of different electricity user types. One favourable moment to investigate the preparedness of electricity users against MDs is – if possible – to do it shortly after some major disturbance and to use electricity users that have indeed experienced the MD as a source of information. In this way it can be achieved most probably much better understanding about the concrete preparedness measures used and about the problems experienced in the preparation. In respect to research method, probably the most suitable one is an interview study.

A series of summer storms occurred in Finland in summer 2010. These caused severe problems to electricity supply in some areas. In some cases the problems in the supply of electric power lasted about two weeks in permanently lived residences. In respect to this series of incidents the Finnish Accident Investigation Board (located within the Ministry of Justice) started in August 2010 an official investigation in order to improve safety and prevent future accidents. This investigation, for its part, will hopefully give a somewhat deeper understanding on the topic under studying.

It is important first to investigate the problem area – preparedness of electricity users against major disturbances – detailed enough and only after that start to implement possible improvement actions (e.g. changes to legislation or regulations). Otherwise the proposed improvement actions can later reveal to be excessive or otherwise inadequate. On the other hand, it is not however – on the basis of the findings of this study – justified to leave the problem area without further investigations or studies. Major disturbances in the supply of electric power are an important incident type from the functioning of the society point of view, as well as from the point of view of individual citizens, and the possibility of these can't be ruled out in the perceivable future.

REFERENCES

- Digium. (2010). [online]. Collect and report data with Digium software. <http://www.digium.fi/en/digium-software>. (Oct. 15, 2010).
- Forstén, J. (2002). Sähköön toimitusvarmuuden parantaminen [*Improving the Reliability of the Electricity Supply*, in Finnish]. The Ministry of Trade and Industry, Finland. 42 p.

- Helsloot, I., & Beerens, R. (2009). Citizens' Response to a Large Electrical Power Outage in the Netherlands in 2007. *Journal of Contingencies and Crisis Management*. Volume 17 Number 1 March 2009. 64-68.
- Ministry of Defence: The Security and Defence Committee. (2006). [online]. Government Resolution on The Strategy for Securing the Functions Vital to Society. Finland. Available:
http://www.defmin.fi/files/858/06_12_12_YETTS_in_english.pdf. 68 p.
- Murphy, B. L. (2004). Emergency Management and the August 14th, 2003 Blackout. Institute for Catastrophic Loss Reduction. Paper Series – No. 40. 9 p.
- National Grid Company. (2003). Investigation Report into the Loss of Supply Incident affecting parts of South London at 18:20 on Thursday, 28 August 2003.
- Nieminen Kristofersson, T. (2007). Sårbar men inte ensam – en studie av några drabbades erfarenheter av Kemiraolyckan, tsunamin och stormen Gudrun [*Vulnerable but not alone – A study on the experiences of some affected by the Kemira accident, the tsunami and the storm Gudrun*, in Swedish]. Lund University Centre for Risk Analysis and Management. Report 1014. 84 p.
- Palm, J. (2009). Emergency Management in the Swedish Electricity Grid from a Household Perspective. *Journal of Contingencies and Crisis Management*. Volume 17 Number 1 March 2009. 55-63.
- Silvast, A. (2007). Infrastructure, Security and Society – Energy Perspective. *The 19th International Conference on Electricity Distribution (CIRED 2007)*. May 21-24, 2007, Vienna. 4 p.
- Silvast, A. (2008). Being at-risk or taking risks? Day-to-day experiences of electricity blackouts. *International Conference on Infrastructure Systems: Building Networks for a Brighter Future*. November 10.-12, 2008, Rotterdam. 5 p.
- Strandén, J., Nurmi, V.-P., Verho, P. & Marttila, M. (2009). State of Preparedness of Finnish Society for Major Disturbances in Distribution of Electricity. *International Review of Electrical Engineering (I.R.E.E.)*. Vol. 4. 211-219.
- Swedish Energy Agency. (2008a). Storm Gudrun – What can be learnt from the natural disaster of 2005? Eskilstuna, Sweden. 72 p.
- Swedish Energy Agency. (2008b). Storm Per – Lessons for a more secure energy supply after the second severe storm in the 21st century. Eskilstuna, Sweden. 72 p.
- UCTE. (2004). [online]. Final Report of the Investigation Committee on the 28 September 2003 Blackout in Italy. April 2004. Available:
https://www.entsoe.eu/fileadmin/user_upload/_library/publications/ce/otherreports/20040427_UCTE_IC_Final_report.pdf. 128 p.
- UCTE. (2007). [online]. Final Report – System Disturbance on 4 November 2006. January 2007. Available:
https://www.entsoe.eu/fileadmin/user_upload/_library/publications/ce/otherreports/Final-Report-20070130.pdf. 85 p.
- U.S.-Canada Power System Outage Task Force. (2004). [online]. Final Report on the August 14, 2003 Blackout in the United States and Canada: Causes and Recommendations. April 2004. Available:
<https://reports.energy.gov/BlackoutFinal-Web.pdf>

Development of Spatial Risk Profiles of Cargo Rail Systems

Bilal M. Ayyub¹, Kristen Markham², and Che-yu Chang²

¹ Professor and Director, ² Graduate Research Assistant
Center for Technology and Systems Management, Department of Civil and
Environmental Engineering University of Maryland, College Park, MD 20742; PH
(301) 405-1956; email: ba@umd.edu, ksmark87@gmail.com, cchang1@umd.edu

ABSTRACT

Cargo rail systems entail uncertainties and associated risks, particularly with the transport of hazardous materials. The risk associated with their release is assessed through the development of spatial risk profiles which vary based on several analytical and computational steps. The complete assessment of risk involves scenario identification, evaluation of the consequences based on inventories of assets and a hazard assessment to obtain the final risk profile along the rail. Using this framework any given length of railway can be analyzed for risk given the appropriate spatially mapped information on the areas surrounding the rail tracks. The proposed risk quantification and management framework is consistent with current quantitative risk analysis practices in order to enable all-hazard decision making. The methodology is briefly introduced and demonstrated using illustrative examples based on notional information.

1 INTRODUCTION

Each year in the United States alone millions of tons of materials are shipped across the country. Railroads and the freight they carry are a critical part of this mass shipment effort, transporting a variety of goods and resources, a significant portion of which is composed of chemicals and other hazardous materials. These materials, if released, are potentially harmful to human health and the environment.

This paper presents and demonstrates a risk analysis methodology developed using an integrated GIS-based and Critical Asset and Portfolio Risk Analysis (CAPRA) approach to assess risks of railroad incidents, using a case study. A programming framework based on Geographic Information Systems (GIS) data is used to assess the consequences of a railroad incident along the freight railways systems that traverse the city. An inventory of all assets affected for a given location and distance from the railway is determined, approximating the total population, properties, roadways and other important assets within this range.

The proposed CAPRA framework of risk analysis incorporates the potential consequences, vulnerabilities and threats associated with a rail incident. This framework allows for the calculation of the relative risk along a rail beyond the raw consequences data.

2 BACKGROUND

2.1 Hazardous Material and Railways

Of the vast variety of materials shipped across the country via train, a significant portion is composed of materials that are harmful to human health and to the environment. Materials of this nature are called dangerous goods, or hazardous materials (hazmats).

Nearly 155 million tons of chemicals are transported by rail in North America each year, or approximately 500,000 shipments per day (Chemical Week 2001; HMTUSA 1990) which constitutes 1.75 million rail cars of hazardous materials (AAR, 2004). Of the 42% of all intercity freight that is shipped by rail, 20% are chemicals (AAR, 2004). Rails also play the unique roll of providing support to the Department of Defense Strategic Rail Corridor Network for the movement of Department of Defense shipments.

2.2 Consequences of a Rail Incident

Hazardous materials transported by rail can cause a significant threat to the surrounding vicinity if leaked from their storage containers. Beyond the failure of the container itself, a variety of events can cause the occurrence of spillage of a hazardous material into the environment, the most drastic being the overturning or derailling of a railroad car. Based on the particular incident's situation, the affected area surrounding the rail incident can be determined depending on the radial distance from the location that may be affected.

2.3 City Case Study

As an example to better quantify the risk assessment framework proposed, a city is chosen as a case study. This city has an extensive network of cargo-carrying railways – passing within close quarters of residential, commercial and industrial properties. It functions as central transportation hub transit point for the movement of freight within the United States. Rail accidents involving hazardous materials have occurred previously, causing million in damages to the surrounding area.

3 CAPRA METHODOLOGY FOR RAIL RISK

3.1 CAPRA Methodology

The approach recommended for rail security assessment is the Critical Asset and Portfolio Risk Analysis (CARRA) Methodology (Ayyub et al., 2007). In general, CAPRA is a five-phase process including the following steps:

- Scenario Identification
- Threat Probability Assessment
- Vulnerability Assessment
- Consequence and Criticality Assessment
- Benefit-Cost Analysis

3.2 Approach: CAPRA Risk Equation

Of most importance to the CAPRA methodology for this application is the way in which risk is calculated. CAPRA uses the following base equation to build its risk model:

$$R = C \times V \times T$$

For this case study, using this equation Risk (R) is defined as the product of the Consequences (C), Vulnerabilities (V), and Threats (T) associated with a railroad incident. The consequences associated with the railway incidents due to the variability can occur along a railway, however it is also easily quantifiable. Programming using Geographic Information Systems (GIS) software is used research to retrieve all known data about assets affected for a given location and radial distance from the incident location.

4 ADAPTION OF CAPRA TO RAIL RISK ANALYSIS

4.1 Scenario Identification

For the first step of the CAPRA analysis, the scenario identified is the derailment, crash, or other incident in which the behavior of a railroad train, rail car, or set of rail cars causes spillage or release of hazardous materials into the surrounding environment. Based on a database kept by the Federal Railroad Administration Office of Safety Analysis, from 1975-2009 in the example city, there were 218 reported derailments, 35% of which were caused by track defects, 7% from equipment malfunction, 41% from operation or human error and 1.5% from rail & highway collisions. A report on "Railroad Derailment Factors Affecting Hazardous Material Transportation Risk" from 2007 indicated that of all railroad derailments, 11% of all hazardous material cars leaked hazardous material.

4.2 Threat Probability Assessment

The most recent and most relevant data on the shipment rates of hazardous materials comes from the Commodity Flow Survey (CFS) completed in 1997. This survey was referenced in the US General Accounting Office's Report to Congress in April 2003 as being "suitable" and "sufficiently accurate" for their purposes. Thus in this report this survey's data is also accurate enough for the purposes of this risk analysis. The CFS reports the percentage of tons shipped in the US as well as the percentage of ton-miles traveled, separated by type of hazardous material. These are summarized in Table 1.

Table 1. Rail Shipment as a Percentage of Hazardous Materials by all Modes of Transportation

<i>Hazmat Class</i>	<i>% Tons</i>	<i>%Ton-miles</i>
Explosives	< 1%	< 1%
Gases	13 %	52%
Flammable Liquids	2%	12%
Flammable Solids	55%	90%
Oxidizing Subst. / Peroxides	34%	63%
Poisonous and Infectious Subst.	31%	51%
Radioactive	N/A	N/A
Corrosives	27%	41%
Misc.	28%	58%
Total	6%	28%

This data can be useful in the valuation of the consequences found for a particular rail point calculated in the previous section.

4.3 Vulnerabilities

The third step, *Security Vulnerability and Hazard* is less quantifiable and less variable along the railway. Rather than a variable, each is treated more as a coefficient multiplied by the variable consequences to reduce the estimated losses. Train derailment causing potential hazardous chemical spillage can happen due to a wide range of causes. The derailment rate is dependent on a variety of different factors, most of which can be correlated with the track class that is being used (class 1-5). Previous studies have found derailment rates of 1 per million freight train miles (Anderson and Barkan), and 3.5 per 100 million accidents per vehicle km (5.63 per 100 million accidents per vehicle mile) (Bubbico et al. 2004), with an average of 69.2

vehicles per train according to 2008 Freight Rail Fleet Statistics in Progressive Railroading. These numbers and statistics about the Vulnerabilities of the rail cars loaded with hazardous materials can be useful in the valuation of the consequences found for a particular rail point calculated in the Consequences section. As part of the CAPRA framework these and other relevant information found on hazardous material transport by rails can help better quantify the vulnerabilities of hazardous materials being transported.

4.4 Consequences

For the fourth step, *Consequence and Criticality Assessment*, the consequences associated with a particular rail incident are assessed, then tallied to provide the required estimates of loss for a particular scenario. This step is the focus of this paper and is discussed in the following section.

4.5 Benefit and Cost Analysis

The final step – *Benefit-Cost Analysis*- is not addressed in this paper, however it could be applied in future work in deciding where the best locations along the rail would be to focus efforts on constructing risk mitigating strategies.

5 ASSET INVENTORY

5.1 Assets Affected by Rail Incidents

The key assets of concern identified in this research include the follow four main categories:

- *People*
- *Property*
- *Roadways*
- *Other Specific Assets*

Identifying information in the GIS data that falls into one or more of these categories can help quantify the consequences of a particular incident.

5.2 Available Asset Data and Analysis

Based on the information available, the following data sets were used for information on the assets potentially affected by a rail incident.

Population Count

There are multiple methods that can be used to estimate the population affected. The one used in this study uses the 2000 Census Tract data and population count for each tract to count the total number of people in a specified area.

Property

The property loss (in dollars) that could result from a rail incident is needed. Real property or similar datasets provide a variety of information about each property, including the cost of the property in dollars. While this may not perfectly represent the cost of the buildings on the property it has a strong enough correlation to make the assumption that high property values typically indicate that the building(s) located on that property also have higher value and thus high cost of replacement if damaged. In addition values for the approximate square footage are given.

Roadways

The length of roadways within influence areas can be estimated with respective daily traffic volumes and movement of goods. Information on roads (small alleyways to large highways), would provide a strong bases for valuation.

Other Specific Assets

There are many buildings and other structures throughout the city of importance (e.g. government buildings, schools, etc...). The properties of each of these specific assets include the relevant information that would enable consequence estimation including the approximate number of people that could be affected.

5.3 Inventory Collection Along the Railway Using GIS

Several programs were custom created using GIS to tally the asset inventories along the rail. The following steps were used to determine the consequences of potential hazardous material incidents along the railways:

- Identify a point(s) where an incident could occur along the rail and specify a distance(s) from the incident point(s) that could be affected by the theoretical incident.
- Create circular influence circle(s) around the point(s) at specific distances to analyze for affected consequences.

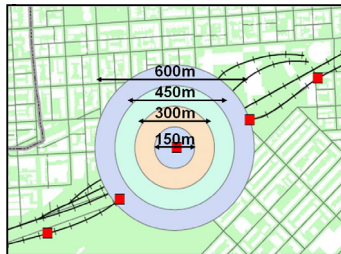


Figure 1. Multiple influence circles around the point of interest

- Identify all data that lies within the influence circle(s) assuming no wind effects.

Interpretation of Data

A summary table of the results is generated that enumerates the population affected, the approximate cost of the properties within the influence area (broken down by Residential, Commercial and Industrial), the linear footage of the roads affected and finally a count of the specific assets affected. In this particular example data is outputted for the four influence circles with diameters of 150, 300, 450 and 600 meters.

Table 2. Population affected by influence area radius

	Census Method	Real Prop
150 m	435 people	696 people
300 m	783 people	696 people
450 m	793 people	696 people
600 m	1004 people	1413 people

Table 3. Property affected by influence area radius

	Total \$	Property Affected					
		Residential	Commercial		Industrial		
150 m	\$5,584,100	\$4,640,000	0 sq ft	\$0	0 sq ft	\$944,100	6475 sq ft
300 m	\$11,272,900	\$5,394,500	3659 sq ft	\$0	0 sq ft	\$5,878,400	275,517 sq ft
450 m	\$12,633,700	\$5,394,500	3659 sq ft	\$0	0 sq ft	\$7,239,200	330,939 sq ft
600 m	\$20,967,810	\$12,701,340	36,058 sq ft	\$237,600	8209 sq ft	\$8,028,870	355,544 sq ft

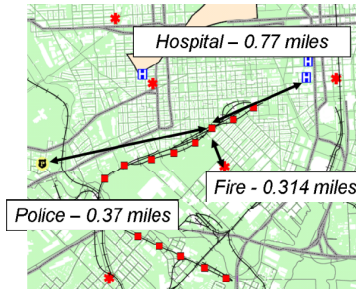
Table 4. Roads and Assets affected by influence area radius

	Roads Affected	Assets Affected
150 m	0 LF	1
300 m	9388 LF	2
450 m	9388 LF	2
600 m	9388 LF	5

6 COUNTERMEASURES AND MITIGATION ACTIONS

In response to the potential incidents that may occur the distance from the closest fire and police stations governs how quickly mitigation resources can arrive at the scene of the incident. Incident points with closer response resource can be interpreted as having less risk since the response time to that incident should be shorter. This calculation is important to the final risk calculations.

For a given incident point, there is one Police Station, Fire Station and Hospital that are closest to the incident that could provide the fastest response. Measured in linear distance rather than by road travel distance, the distances calculated may not be accurate enough to be used for estimated travel times to the incident, however they are still a good indicator of how close the closest set of resources is to the incident and relative to other incident points, how quickly the response efforts could arrive on scene.

**Figure 2.** Closest Response Resources Available for a Given Incident Point

7 RISK PROFILES

Risk profiles can be estimated using Equation 1. Graphs of the consequences along the length of the rail segment are generated, showing areas of higher risk with elevated consequences. Profiles of consequences along an example rail segment have been completed to demonstrate the usefulness of such profiles. Figure 5 is an example of the output generated for the property damage costs. Similar risk profiles can be created for assets, roads, and people affected. 14 points were chosen for analysis spaced approximately 300m apart along the rail.

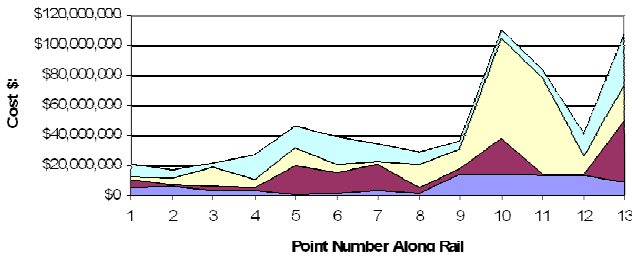


Figure 3. Property affected at 150, 300 450 and 600 meter diameter influence areas

From these graphs it is seen that around points 11 to 13 a high total cost of properties would be affected. Decision analysis is based on the benefit-cost ratio. The benefits of the proposed countermeasures and consequence mitigation strategies are weighed against their respective costs to choose the most effective solution. Strategy tables are generated to compare the alternatives as an aid in this decision.

8 CONCLUSION

This paper presents and demonstrates a risk analysis methodology developed using an integrated GIS-based and the Critical Asset and Portfolio Risk Analysis (CAPRA) approach to assess risks of railroad incidents for a hypothetical city. The risk analysis methodology consists of the following analytical phases: (1) scenario identification, (2) consequence and criticality assessment, (3) security vulnerability assessment, (4) hazard likelihood assessment, and (5) benefit-cost analysis. In this study, the first three phases are demonstrated, and all the phases are described.

The methodology was created to support decisions for those who are either (1) a city planner seeking to find the segments of rail with the highest risk potential in the case of a rail incident, or (2) a first responder to a rail incident who needs to know what potential assets, people and important buildings could possibly be affected. The CAPRA framework of risk analysis can be utilized which incorporates the potential consequences, vulnerabilities and threats associated with a rail incident. This framework allows for the calculation of relative risk along a rail beyond the raw consequences data used to accomplish the first objective. Future efforts may include: (1) adding any additional information or data available to the data set currently in use, (2) assessing the vulnerabilities and threats associated with rail incidents, (3) finalizing a valuation table to quantify the risk based on the consequences, threats and vulnerabilities, and (4) creating a more thorough output table for first responders to use to respond to incidents along the railway system.

ACKNOWLEDGMENTS

The authors would like to acknowledge the support of the Maryland Emergency Management Agency, and information provided by Mr. Pat Nowlan and Mr. Rodney Giacomelli.

REFERENCES

- Ayyub, B.M., McGill, W.L., and Kaminskiy, M., 2007, Critical asset and portfolio risk analysis: An all-hazards framework, *Risk Analysis*, 27(4), 789–801.
- Hazardous Materials Transportation Uniform Safety Act of 1990. P.L. 101-615, 104 Stat. 3244, codified at 49 U.S.C.App. 1801, et seq.
- Association of American Railroads, 2004, AAR Statement of Hazmat Transport Through DC and AAR Statement to Dist. of Columbia City Council, Washington DC.
- Anderson and Barkan, 2007, Railroad Derailment Factors Affecting Hazardous Material Transportation Risk. Transportation Research Board. Washington, DC.
- Bubbico et al., 2004, Risk analysis for road and rail transport of hazardous materials: A simplified approach, *Journal of Loss Prevention in the Process Industries*, Vol 17.
- Chemical Week, 2001, Rail Transport-Is Safety on the Right Track? New York, NY.
- Federal Railroad Administration Office of Safety Analysis, 2010, Washington, DC.
- Glickman, T.S. and P.K. Raj, 1993, A Comparison of Theoretical and Actual Consequences in Two Fatal Ammonia Incidents. Waterloo, Canada
- US General Accounting Office, 2003, Report to Congress on Rail Safety and Security, Washington DC.

Probabilistic study of cascading failures in complex interdependent lifeline systems

Isaac Hernandez-Fajardo & Leonardo Dueñas-Ororio

Department of Civil Engineering. Rice University, Houston, TX, USA.

Abstract

Urban distributed lifelines constitute critical infrastructure elements with their continuous interaction guaranteeing the service and well-being of growing urban populations. However, their interdependence and exposure make them inherently fragile to perturbations. This paper proposes a methodology for the probabilistic study of interdependent urban systems response affected by cascading failures induced by natural hazards. This methodology manages interdependence uncertainty by including a probabilistic parameter, $Istr$, to control intersystemic damage propagation. In parallel, the methodology simulates cascading failures using a load nodal betweenness and a local capacity factor α . The combination of $Istr$ and α allows the exploration of different conditions of interdependence coupling and local robustness. A test application on two interdependent networks under seismic hazard revealed that interdependence escalation induces fragility amplification with increases on α having limited effect on systemic fragilities. This result questions the effectivity of local retrofiting on the global fragility of interdependent systems.

1 Introduction

Urban distributed lifeline systems are key elements of society. Many of the services allowing modern life in cities depend on the continuous functionality of critical infrastructure systems, like the the power and water distribution networks. Today, these systems are threatened by different factors. Aging, deregulation, climate change, terrorism, and natural hazards are threats to consider when attempting to recommend intervention actions for these systems.

An additional factor of interest is interdependence among systems. Systems that depend on each other will eventually share their own weaknesses with each other. This factor must be highlighted in an age of deregulation where the responsibility for preparation and action in systems becomes more diffuse as systems become more interdependent. At the same time, cascading failures, i.e. the event of flow readjustment within a system inducing failures by capacity exceedance, must be taken into account. This type of failure may very well induce catastrophic losses in independent systems, while also contributing to major blackouts in interdependent services.

Previous research have shed some light in the response of interdependent systems and the influence of cascade failures. Motter and Lai (2002) studied cascading failures in individual networks created by flow readjustment. The authors identified and removed critical nodes to trigger cascading failures. Their work introduces a simple model to simulate cascading failures, but does not include provisions on managing uncertainty or interdependence. Dobson and Carreras (2004) proposed a model of cascading failures that assigns additional loads to surviving components according to the initial number of failed nodes. The authors are able to find distributions for the number of failed components and show how the amount of initial load influences the outcome

of cascade failures. Crucitti et al. (2004) describe a new model for cascading failures induced by dynamical flow redistribution. The authors emphasize that elements must not be removed, but rather the flow traversing them must be delayed by the redistribution-induced flow increase. Variations on the original ideas for the simulation of cascading failures are developed further by Wang et al. (2008), Wu et al. (2008), and Bao et al. (2009). These works present diverse application of the simulation of cascading failures to study the behavior of well-known artificial networks (scale-free and small world network). Dueñas-Osorio and Vemuru (2009) apply a methodology to simulate cascading failures to the analysis of individual test networks subjected to the action of natural hazards and deliberate topological-based attacks. These authors discuss the influence of intervention measures on the performance of cascade-prone systems. Finally, Buldyrev et al. (2010) evaluate the probability of existence of a stable mutually connected component given that a percentage of nodes have been removed in a pair of interdependent theoretical networks of the same size. Their study shows that interdependent networks with broad degree distributions perform worse than coupled networks with lower-degree distributions, mostly due to the presence of prone-to-disconnection low-degree nodes.

This short review demonstrates that the interest in the issue of cascading failures in interdependent networks has grown recently. It is also clear that the mentioned works do not include a complete methodology to include the effect of cascading failures in the probabilistic fragility analyses of interdependent networks. This paper introduces an algorithm and methodology to assess the influence of cascading failures in the fragility of heterogeneous interdependent networks. Also, while focusing on natural hazards as triggers of damage, the methodology explicitly includes uncertainty in the description of interdependence. The suitability of the methodology is tested with two power and water interdependent systems subjected to earthquake hazard. The results of this analysis show that interdependent fragility is indeed worsened by the likelihood of cascading failures. Also, it is shown that increases in local flow capacity of the elements of systems have a limited effect on reducing inter-systemic fragility.

2 Fragility of individual systems

This paper studies the influence of cascading failures in the fragility of interdependent distributed lifeline systems. This subject involves several layers of complexity, namely individual systems, interdependence, and cascading failures themselves. This section deals with the first, basic layer, that is the fragility of individual distributed systems.

2.1 *Model of urban spatially distributed systems*

This paper uses simple, directed graphs for the model of urban distributed lifelines. A graph is a mathematical entity formed by nodes and the links among them (Diestel 2005). In this representation, power substations or pumping stations are nodes, while cables or pipes connecting operation or service stations are represented by links. The key element needed for the representation of distributed systems is their connectivity. This work uses adjacency matrices to encapsulate the connectivity relations between different nodes of a system. An adjacency matrix is a square matrix with dimensions equal to the number of nodes in the associated system. The matrix starts as a matrix of zeros with ones added in the positions associated to links. To do so, a position (i, j) in the matrix is associated to the link connecting node i to node j . As a consequence

of this, the number of nonzero entries in the matrix correspond to the number of links within the system.

2.2 Fragility of components

Fragility is herein understood as the probability of a system or a component exceeding a given level of damage under the intensity of an external perturbation. The graph representation locates the source of the fragility of a system in the fragility of its nodes and links. Naturally, the values of fragility usually depend of the interaction of the strength properties of a component, with the intensity and nature of the external perturbation. As a result, in many cases the allocation of fragility is concentrated in the nodes. This assumption is used for the systems in the test example. Component-level fragility can be obtained from expert judgment, experience, and physical or computational models. The information on fragility used in this paper is obtained from HAZUS-MH (Federal Emergency Management Agency 2010), a technical manual and application developed by the federal government of the United States to assess losses from natural hazards. Figure 1a presents a typical set of component-level fragility functions. These curves show how the fragility of a component soars with increasing values of the intensity of the exciting perturbation.

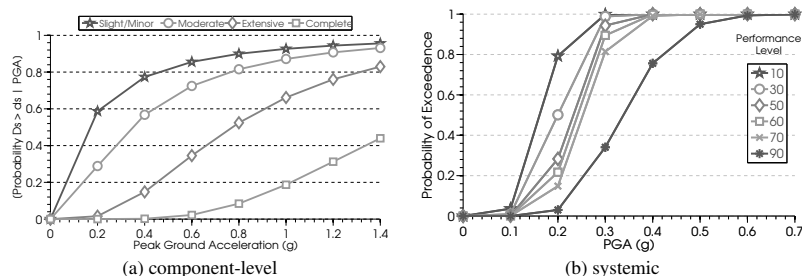


Figure 1: a) Component-level fragility functions for a water reservoir in a water network. Each fragility curve describes how the probability of a component exceeding a particular level of damage changes with hazard intensity; b) Systemic fragility functions for a water system display how systemic probabilities of exceedance change against values of hazard intensity.

2.3 Systemic fragility

An important consequence of the connectivity of networks is the fact that the failure or malfunction of a component can have consequences spreading across the whole system. In this sense, the fragilities of components and their interaction are the elements controlling the fragility of a system. Network algorithms can be used to examine such interaction. The assessment of disconnection failure, for example, is an important step in measuring that interaction. When a system is affected by a perturbation some nodes fail by the direct action of the perturbation on them, while some others survive; however, some of the surviving nodes can be left disconnected from critical components of the system (supply nodes, for example). In this condition the node will not be an

operational element for the system. The node is for all purposes operating in itself, but non-operational for the system. This failure by *disconnection* shows how the relations between components control the fragility of the system, and how systemic fragility is an emergent property of the system itself.

Two general approaches are used to measure systemic fragility, an integrity approach and a serviceability approach. Under an integrity approach what counts as fragility deterioration is the reduction in the number of connecting paths between the key set of elements of the system: the supply (or origin) nodes and the demand (or destination) nodes. The comparison of the final connectivity conditions with the original state of connecting paths over the whole set of consumption nodes provides a measure of the final fragility of the system. In contrast, a serviceability approach focuses on measuring how the service capacity of the system decreases after perturbation. This process requires a study of how flow redistribution within the system affects the flow arriving to the different consumption points. In consequence, in the serviceability approach the delivery capacity in the consumption nodes is examined before and after the action of a perturbation, and an element-by-element comparison is used to measure the change in systemic service capacity. It should be noticed that integrity approaches require less information than serviceability approaches. Also, the analysis of services will involve detailed analysis of flow redistribution. For simplicity, the test example in this paper uses connectivity loss, CL , (Albert et al. 2004) an integrity-based metric, for measuring systemic performance. CL compares the number of connecting paths between supply and demand nodes before and after the action of perturbation. The resulting values from the comparison are averaged to arrive to a final value of systemic loss of connection. CL is defined in mathematical terms as follows,

$$CL = 1 - \frac{1}{|N_D|} \sum_{i=1}^{|N_D|} \left(\frac{P_f}{P_o} \right)_i \quad (1)$$

where N_D is the set of demand nodes, and P_o and P_f are the number of original and surviving connecting paths between surviving demand and supply nodes, respectively. Note that a zero value for CL denotes survival of the connecting paths of the system, while a value of one stands for complete disconnection of supply points.

3 Cascading failures in interdependent systems

Urban distributed lifeline systems work together as part of a common urban service infrastructure. Hence, a realistic model for the systemic fragilities must include the interdependence among them. This requirement is important in the light that damage, and therefore fragility, can travel across systems. This statement establishes that the fragility of system components, their relations within a system and their relations with external systems play a role in systemic fragility. An additional fragility factor is cascading failures. In the description presented in section 2, the fragility of an individual system depended only on the direct and indirect (disconnection) effects of the hazard on the system components. However, an additional source of damage within systems is caused by the redistribution of transmission loads. When elements of a system are perturbed, the reorganization following the perturbation may induce damage by excess of the flow transmission capacity of elements. These type of failures are called cascading failures. The influence of this type of failure in the general fragility of a system is addressed here for the case of interdependent systems.

3.1 Interdependence among distributed systems

This paper's framework for interdependence representation is based on Dueñas-Ororio et al. (2007). In this model, interdependence has two characteristics: localization and intensity. The localization feature is understood as that interdependence is located in the set of links (interdependence links) connecting nodes in different systems. These interdependence links are directed links forming the interdependence interface between systems. The representation of this interface is done in terms of interdependence matrices. An interdependence matrix is a construction conceptually similar to an adjacency matrix; however, a generic interdependence matrix is a rectangular matrix, with the nodes of the *master* system in the rows of the matrix, and the nodes of the *slave* system in the columns. The qualification of master and slave is essential and is expressed in the directionality of the interdependence links. For example, for systems *A* and *B*, the interdependence matrix $Im(a, b)$ contains the interdependence links denoting dependence of nodes of system B on nodes of system A; naturally, the matrix $Im(b, a)$ will represent the reverse dependence relationship.

The intensity property of the interdependence model offers a direct quantification of the probability that the transmission event will take place. The parameter called interdependence strength, $Istr$, measures the likelihood that the slave node will fail given that its master node in an external system has failed. $Istr$ may be associated to the reliability of a back-up system for the slave node. A lack of back-up will be represented by $Istr = 1$, while a total reliance on back-up systems will be represented by $Istr = 0$.

3.2 Cascading damage propagation

Cascading failures occur as a consequence of flow distribution within a system. When some components are affected by external perturbation, the system adapts its inner flow patterns to respond to the absence of the failed components. In this process, it is possible that a highly loaded component is charged with an additional load surpassing its transmission capacity and inducing failure to the otherwise surviving element. In some conditions this process can trigger a chain reaction leading to the collapse of large portions of the system. In the case of interdependence systems this situation can lead not only to failure in the local system, but also to increased fragility in external systems.

This paper uses the strategy presented in Motter and Lai (2002) for modeling cascading failures. The initial load capacity of the components in the system is obtained by measuring the node-betweenness of the elements. In this paper, node-betweenness measures the number of paths between supply and demand nodes in a system. This amount is compared to the maximum number of possible paths between these sets of nodes for a final betweenness value for all the nodes. The initial capacity is increased by a multiplying factor to arrive to the final capacity of each element. The structure of the procedure can be expressed as,

$$C_f(i) = (1 + \alpha)btwn(i) \quad (2)$$

where $C_f(i)$ stands for final capacity, $btwn(i)$ represents node-betweenness, and α is a parameter representing the additional load capacity. The index i identifies nodes in the system.

After a perturbation has struck the system under study, a new betweenness can be calculated. The betweenness for each node is then compared to the capacity C_f

obtained by fixing an α value; if the increment in betweenness exceeds the defined capacity of the element, the element fails as a result of a cascading failure.

3.3 Simulation of cascading damage in interdependent distributed systems

The main concern of this paper is the evaluation of the fragility of interdependent systems under cascading failures triggered by the action of an external perturbation. This perturbation can be a natural hazard or a man-made attack. The scope of this work deals only with natural hazards, specifically earthquake events. The approach to study systemic fragility under these situations consists on using Monte Carlo simulation to probe the effects of hazard action, systemic damage, interdependent action, and cascading effects in separate modules. Simulation is required because there is no explicit function to represent the performance of the system as a function of the performance of its components. Also, the interdependence and cascading failures factors introduce external, dynamic features into the performance analysis. These features reduce the possibility of having a closed-form interpretation of individual systemic response, although some developments on this specific issue are known (See Simonsen (2005), for example). The simulation procedure used for the test example is described in algorithm 1.

Algorithm 1 Steps in the simulation of cascading failures in interdependent systems

1. All systems descriptions are loaded (S_1, S_2, \dots). All systems are undamaged. Node capacities $C_f(i)$ assessed.
 2. Simulation of hazard action. Direct damage to nodes in all systems found.
 3. Network analysis to identify disconnected elements. Indirect damage identified.
 4. **while** There is additional damage in any system **do**
 5. Cascading failures assessment. New betweenness ($btwn(i)$) calculated for all nodes. nodes exceeding their capacities fail.
 6. Interdependence simulation. Failed nodes in one system transmit their damage to slave nodes in other systems. Matrices Im and parameter $Istr$ instrumental in this step.
 7. **end while**
 8. Calculation of systemic performance metric (CL) for all systems involved
-

The process described in algorithm 1 is repeated for a number of simulations required to arrive to stable results in the estimations of systemic probabilities (5000 simulations for the test example). The actual number of simulations is a function of the degree of reliance in the estimation of systemic probabilities as well as of the fragilities of the components. Many more simulations are required to study systems with components highly unlikely to fail. In the case of systems subjected to the action of natural hazards, the number of simulations are relatively small, as the components fail more frequently. Once the simulation process is completed, the resulting vectors of performance metrics for each system are analyzed. Statistics on these values are used to generate estimations of probabilities of the systems exceeding performance levels of interest. The results are put together into systemic fragility functions as the ones shown in Figure 1b. Although apparently similar to the input fragility functions for

components, systemic fragility functions incorporate the effects of the fragility of components, systemic relationships, interdependence interaction, and cascading failures. In this sense, these curves provide a general perspective of the expected behavior of a system working within a super-system of urban infrastructures.

4 A test example: fragility of interdependent power and water networks

The test example involves the study of the probabilistic seismic response of two interdependent power and water networks with topologies representative of real networks. The power network (S1) has 59 nodes and 146 links. The water network (S2) has 49 nodes and 142 links. The fragility description for individual components was based on HAZUS-MH estimates for systems affected extensively by seismic hazard. The seismic action is described by uniform peak ground accelerations (PGA) in the range of 0.1g to 0.7g. In terms of interdependence, the matrix for the dependence of the power system on the water system has 45 links. The matrix for the reverse relationship (water-on-power) has only nine links. The interdependence links in the power-on-water dependence are distributed along the different nodes of the power system. In contrast, the interdependence links in the water-on-power dependence concentrate on the supply nodes on the water system. Interdependence effects are contrasted by using $Istr = 0$ and $Istr = 1$ in the estimations. Also, two capacity factors α of 0.5 and 1.0 are used. 5000 simulations are carried out to generate the systemic fragility estimates. Figure 2 presents the systemic fragility functions for values of $Istr$ of 0 and 1, for a fixed value of $\alpha = 0.5$.

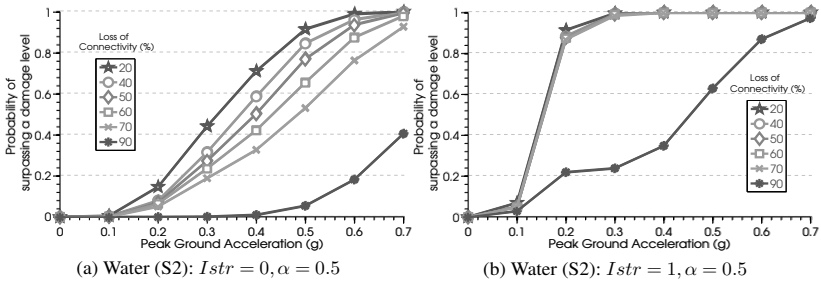


Figure 2: Individual and fully interdependent fragility functions for interdependent S1 and S2. The increase in interdependence strength induces soaring of systemic probabilities of exceedance

The results for S1 show only minor changes. The 90% connectivity loss (stars curve) under a PGA of 0.2g changed from 0.81 for $Istr = 0$ to 0.89 for $Istr = 1$, an increase of 10.2%. For the same conditions of PGA and target level, S2 shows an increase from 0.0 ($Istr = 0$) to 0.22 ($Istr = 1$). These comparisons reveal two facts. First, increasing the probability of interdependence action does increase the fragility of systems. Second, the power system (S1) is not extensively affected by its dependence on the water system (S2). In sharp contrast, the water system is strongly impacted by

its dependence on the power system. In the first place, Figure 2c shows a relatively strong water system, with values as large as 0.6g of PGA being required for assured systemic collapse; however, Figure 2d displays how interdependence effects drive the system to collapse assurance for PGAs as low as 0.3g. Results in Figure 3 evidence the effects of local capacity represented by the factor α . An increase of α from 0.5 to 1.0 reduces the probabilities of exceedance at every level; the more visible case being the high-level 90% *CL*. As an example, the probability of the system exceeding 90% *CL* at 0.3g decreased from 0.24 for local capacity $\alpha = 0.5$ to 0.04 for $\alpha = 1.0$, a reduction of 83% in the probability of exceedance.

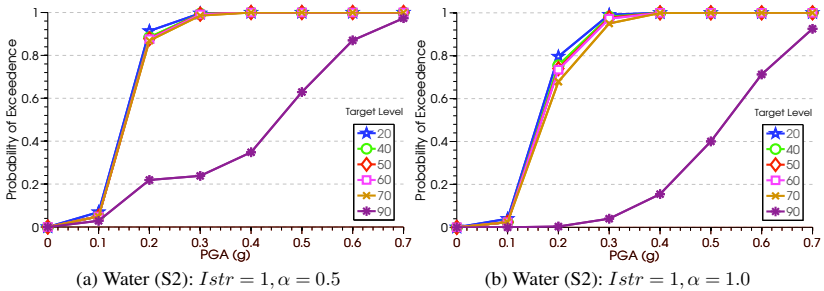


Figure 3: Fully interdependent water system fragility functions for different values of local capacity. Increases in capacity of components decrease the probabilities of exceedance, but may not be a cost-effective intervention alternative alone

5 Conclusions

This paper introduces a methodology to study the influence of cascading failures in the fragility of interdependent urban distributed systems. This methodology integrates strategies presented in the literature to arrive to new developments in the subject of fragility of interdependent networks. The methodology was applied to a test example of two interdependent water and power networks. The results from the test reveal that the influence of interdependence is a major factor defining the final outcome of fragility estimates in interdependent systems. This was clearly evidenced by the fact that the water system's strength to earthquake hazard was altered by its dependence on the functionality of the weak power system. In another important point, the response of the interdependent-weaken water system improved when the local capacity (α factor) was increased. This outcome denotes how, even in the case of interdependent systems, the system's strength benefits (i.e. fragility decreases) from additional transport capacity of the components. Nevertheless, the positive changes in the fragility were not able to counteract the effects of interdependence or even induce large effects at all levels of hazard intensity. In this sense, local capacity appears more like a temporal buffer to unexpected perturbation to the system, than a long-term intervention alternative to enhance the strength or resilience of a distributed system. It seems to be the case that measures of local intervention (capacity enhancements) will be cost-effective only when accompanied by topological modifications or other interventions of global scope.

References

- Albert, R., I. Albert, & G. L. Nakarado (2004, Feb). Structural vulnerability of the north american power grid. *Phys. Rev. E* 69(2), 025103.
- Bao, Z., Y. Cao, L. Ding, & G. Wang (2009). Comparison of cascading failures in small-world and scale-free networks subject to vertex and edge attacks. *Physica A: Statistical Mechanics and its Applications* 388(20), 4491 – 4498.
- Buldyrev, S. V., R. Parshani, G. Paul, H. E. Stanley, & S. Havlin (2010). Catastrophic cascade of failures in interdependent networks. *Nature* 464(7291), 1025–1028.
- Crucitti, P., V. Latora, & M. Marchiori (2004, Apr). Model for cascading failures in complex networks. *Phys. Rev. E* 69(4), 045104.
- Diestel, R. (2005). *Graph Theory* (Third ed.), Volume 173 of *Graduate Texts in Mathematics*. Springer-Verlag, Heidelberg.
- Dobson, I. & B. A. Carreras (2004). A loading-dependent model of probabilistic cascading failure. In *Probability in the Engineering and Informational Sciences*, pp. 15–32.
- Dueñas-Osorio, L., J. I. Craig, & B. J. Goodno (2007). Seismic response of critical interdependent networks. *Earthquake Engineering & Structural Dynamics* 36(2), 285–306.
- Dueñas-Osorio, L. & S. M. Vemuru (2009). Cascading failures in complex infrastructure systems. *Structural Safety* 31(2), 157 – 167. Risk Acceptance and Risk Communication, Risk Acceptance and Risk Communication.
- Federal Emergency Management Agency, F. (2010). *HAZUS-MH MR4 Technical Manual*. Washington D.C.: Federal Emergency Management Agency, (FEMA).
- Motter, A. E. & Y.-C. Lai (2002, Dec). Cascade-based attacks on complex networks. *Phys. Rev. E* 66(6), 065102.
- Simonsen, I. (2005, November). Diffusion and networks: A powerful combination! *Physica A: Statistical Mechanics and its Applications* 357(2), 317–330.
- Wang, J., L. Rong, L. Zhang, & Z. Zhang (2008). Attack vulnerability of scale-free networks due to cascading failures. *Physica A: Statistical Mechanics and its Applications* 387(26), 6671 – 6678.
- Wu, Z.-X., G. Peng, W.-X. Wang, S. Chan, & E. W.-M. Wong (2008). Cascading failure spreading on weighted heterogeneous networks. *Journal of Statistical Mechanics: Theory and Experiment* 2008(05), P05013.

Vulnerability assessment of infrastructure networks by using hierarchical decomposition methods

C. Gómez, J. Buriticá, M. Sánchez-Silva

Department of Civil and Environmental Engineering, University of Los Andes

L. Dueñas-Osorio

Department of Civil Engineering, Rice University

Abstract

Socioeconomic development and sustainability highly depend on the construction and operation of infrastructure networks. Therefore, robustness, reliability, and resiliency of infrastructure networks are vital to the economy, security and wellbeing of any country. When exposed to natural or man-made hazards, the estimation of the vulnerability and the extent of damage, potentially caused to infrastructure networks, is a complex and computationally expensive task. This paper presents a model that combines a *systems approach* with strategies for detecting community structures within networks to make vulnerability estimates. Then, by means of a clustering-based decomposition, a hierarchical representation of the network is derived. This is used to obtain information (i.e., evidence) at different levels of abstraction avoiding the complexity and computational cost of a full evaluation of the network. This simplified model of the network favors the efficient assessment of risk and vulnerability for decision-making regarding, for instance, resource allocation and risk mitigation. In this paper, the conceptual foundations and the practical implementation of the proposed model are presented and discussed. Furthermore, the applicability and the challenges of the model are presented through a practical application.

key words: Clustering, vulnerability, complex networks, systems approach, hierarchical model.

1 Introduction

Infrastructure networks are essential to the socioeconomic development of any country; therefore, studying their performance is important to support decisions about risk mitigation, future developments, investments and maintenance policies that lead to efficient and reliable operation. A primary concern in infrastructure management is the detection of critical elements that might compromise the objective (e.g., performance) of the system. This topic is highly related to vulnerability analysis, which deals with the system's susceptibility to failure when exposed to potentially damaging scenarios. Since infrastructure networks exhibit high complexity, in most practical applications simplified and/or approximate methods are required to achieve practical and efficient descriptions of the possible system's performance.

Systems thinking has gained momentum during the last years as a way to deal with complexity and to obtain a conceptual insight into the problem internal structure (Blockley and Godfrey (2000)). A key feature of this approach is that, by means of a hierarchical representation, it provides descriptions of the systems at different levels of abstraction that can be used to better understand the network performance. For example, this representation provides information about both the network components and their relationships. Hierarchical network descriptions

can be constructed by recursively decomposing it into subsystems (clusters within the network) as it has been proposed by (Gómez et al.).

Network vulnerability analyses are motivated by the importance of global networks (e.g., Internet, communications, power distribution systems) and the dramatic consequences of their failure. Thus, the objective of the paper is to present an approach to evaluate infrastructure network vulnerability based on a systems approach. The proposed methodology uses a recursive clustering strategy to unravel the network's internal structure. Critical network elements are identified based on a combined index that integrates their role within the hierarchical structure and their contribution to the system reliability at every level.

The paper is organized as follows: a review of vulnerability methods is presented in section 2. The use of the systems approach and clustering methods to construct a hierarchical representation of infrastructure networks is shown in section 3. Section 4 describes the hierarchical approach to vulnerability analysis. In section 5, an illustrative example is presented to explain the methodology. Finally, section 6 presents a discussion on the results and future research work.

2 Vulnerability analysis

Berdica and Mattsson (2007) define network vulnerability as a susceptibility to incidents that can result in a serviceability loss. In a wider context, the vulnerability of a system is represented as a loss function defined in terms of varying intensities of a given event and is commonly measured in economic terms. Within the context of network analysis, the vulnerability depends on the way in which the network performance is evaluated. For instance, it may be evaluated in terms of *connectivity* between two selected nodes; or as a *global performance* indicator, e.g., total accessibility of transportation networks. Vulnerability analysis is important for risk management because it provides information about critical scenarios, which contributes to design and implement better risk management strategies (U.S. Department of Energy Office of Energy Assurance (2002)).

A global measure of network vulnerability evaluates the change in performance when the network is exposed to a set of damaging scenarios $d_i \in D$ (D is the set of all possible failure scenarios) (Schuchmann (2010); Latora and Marchiori (2005); Bell et al. (2008)). Then, if $F(S)$ defines a performance measure (i.e. functionality) of the system S , the relative drop in the system's performance for a given scenario d_i can be computed as follows:

$$V(S|d_i) = \frac{F(S) - F(S|d_i)}{F(S)} \quad (1)$$

where $F(S|d_i)$ describes the system's performance measure given the occurrence of damaging scenario d_i . Because a comprehensive vulnerability analysis requires the assessment of all $d_i \in D$, the overall vulnerability can be calculated as $V(S) = \max_i \{V(S|d_i)\}$ (Latora and Marchiori (2005)). The main disadvantage of this approach is that it requires an exhaustive analysis of a vast number of possible scenarios, which is commonly infeasible computationally. Vulnerability can be evaluated also in terms of connectivity loss (Barzel and Biham (2009); Albert and Barabási (2002); Gong et al. (2008); Erath et al. (2009); Nazarova (2009)). In this case, the assessment focuses on evaluating the marginal increment in the minimum connectivity length between two nodes; this is, using the *shortest-path* as a performance measure F in Equation 1.

Because vulnerability is a concept tightly related to a hazardous event (i.e., there is not vulnerability if there is not a threatening event), most vulnerability analysis focuses on simulating *attacks* to the system (potential damaging events) and evaluating the system response. Along this line, a well-known vulnerability assessment technique is the formation of *attack trees* (Ammann (2002); Swiler et al. (1997)), which are structures that represent all possible sequences of attacks (hazards) to the system. The purpose of this attacks is to evaluate the extent of damage caused that may result from a sequence of attacks to the network (Qu et al.).

An alternative approach to evaluate the network's vulnerability is to focus on evaluating the network response as a result of random failure scenarios (Jha et al. (2000); Wang and Guo (2010)). These methods use Bayesian analysis and statistics that provide measures of vulnerability based on the concept of survivability, i.e., keeping the system serviceability above a given threshold. An example of these type of indexes is the *fault-tolerance* index that refers to the statistical probability of an accidental fault(s), not to malicious attack (Ellison et al. (1997)). This index measures the capacity of the network to keep a minimum functionality only under high probably events occurrence, even if there exists low-probably events that caused a general failure.

The last set of indices focus on evaluating directly the relative importance of edges on the network performance. Importance of edges may be evaluated using different metrics. A common approach is to use utility functions in agreement with the problem at hand. In these cases, vulnerability, using connectivity as performance measure, evaluates the relative importance of scenarios \vec{e}_i as (Jenelius et al. (2006)):

$$I(\vec{e}_i) = \frac{\sum_s \sum_{t \neq s} w_{s,t} * c_{s,t}(\vec{e}_i)}{\sum_s \sum_{t \neq s} w_{s,t}} \quad (2)$$

where $w_{s,t}$ is the relative importance of the path between nodes s and t ; and $c_{s,t}(\vec{e}_i)$ is an over-cost in the path between s and t for a given failure scenario \vec{e}_i .

3 Managing network complexity by a systems approach

Graph theory provides a natural way of modeling networks. A graph $G(V, E)$ consists of a set of nodes (vertices) $V = \{v_1, v_2, \dots, v_n\}$ and a set of connecting edges (also called links or arcs) $E = \{e_1, e_2, \dots, e_m\}$. The network structure is usually defined by the *adjacency matrix*, which describes how vertices are connected (i.e., $a_{ij} = 1$ if v_i and v_j are connected, and $a_{ij} = 0$ otherwise). In the case of complex infrastructure networks, the calculation of performance measures and the solution of graph flow/cost problems are computationally expensive tasks, because usually the number of operations grow exponentially with the number of elements (nodes, links).

3.1 Hierarchical Network description

This approach is based on a novel way of handling network representation (Gómez et al.) based on systems thinking (Checkland (1981)), which is built upon the idea that a system can be described as a set of interacting components (subsystems) organized hierarchically (Blockley and Godfrey (2000)). In the hierarchy, every level represents a *fictitious network* of subsystems that compose the whole network; upper levels are constituted of few large subsystems whereas lower levels consist of many simple elements.

This way of rearrangement of information leads to a set of models (*fictitious networks*) of the system at different levels of abstraction. This is useful for supporting decisions within a variety of scopes and to make a more efficient assignment of resources. Each level in the hierarchy provides different evidence to the decision-making process. Therefore, the level of detail in the analysis may change depending upon the nature of the decision problem at hand. Focusing on the decision-maker needs, the problem can be significantly simplified in terms of computational requirements every time a decision is required for which relevance of information is more valuable than its specificity.

The hierarchical representation of a network system leads to a collection of graphs (one for every level or fictitious network) $G^{(l)}(\Lambda^{(l)}, E^{(l)})$ where $\Lambda^{(l)}$ and $E^{(l)}$ are the sets of fictitious nodes and links at level l with $1 \leq l \leq L$, and L represents the number of levels used to describe the system. In a fictitious network, nodes correspond to clusters and edges are parallel arrangements of connecting edges between clusters. Note that at the bottom level both the fictitious and the real networks are the same (Gómez et al.).

Let's define node i of the fictitious network at hierarchical level l as $\mathbf{V}_i^{(l)}$. Then, at the top of the hierarchy (i.e., $l = 1$), the network is interpreted as a single unit (i.e., one fictitious node), which consists of all actual nodes v_i . The set of vertices at level 1 is given by a single fictitious node $\Lambda^{(1)} = \{\mathbf{V}_1^{(1)}\} = \{v_1, v_2, \dots, v_n\}$. In the second level ($l = 2$), the network is described by d_2 fictitious nodes: $\Lambda^{(2)} = \{\mathbf{V}_1^{(2)}, \mathbf{V}_2^{(2)}, \dots, \mathbf{V}_{d_2}^{(2)}\}$, with $\mathbf{V}_1^{(2)}, \mathbf{V}_2^{(2)}, \dots, \mathbf{V}_{d_2}^{(2)} \subset \mathbf{V}_1^{(1)}$.

In synthesis, every level $l \in 1, \dots, L$ of the hierarchy constitutes a fictitious network composed of d_l subsystems. The union of the subsystems at a specific level constitutes the system's representation at that (l -th) level of abstraction. A key decision-making element from this section is the possibility to explore decision-making at different levels according to the problem scope.

3.2 Clustering and network decomposition methods

Identifying patterns within the network around which communities of elements can be grouped is commonly known as clustering and it is useful to simplify large and complex problems. The objective of clustering methods is to generate a partition of the network into k subgroups (Filippone et al. (2008)). Conceptually, most clustering approaches are based on developing a similarity measure m_{ij} between pairs of vertices (v_i, v_j) and an iterative process of vertex grouping up to a point where a minimum or maximum similarity value is achieved. *Recursive clustering* (Gómez et al.) is proposed to detect *communities* and *communities of communities* until the infrastructure network consists of a single unit (i.e., elements are grouped successively) without previous information about the system's structure.

Alternatives for clustering include supervised methods such as the NJW-Method (Ng et al. (2001)) and the k -means algorithm (Macqueen (1967)) require key information (e.g., the number of clusters) to be defined beforehand, whilst unsupervised methods, such as the *Markov Clustering Algorithm*, MCL (van Dongen (2000)), do not. Furthermore, there are sophisticated alternatives such as *kernel-based methods* (Graepel and K. Obermayer (1998); Ryo and Sadaaki (2005); Scholkopf et al. (1998)) and *spectral methods* (Shi (2000); Ng et al. (2001); Verma and Meila (2003)) that allow for more complex partitionings.

4 Vulnerability detection using hierarchical representations of network systems

A network vulnerability analysis includes the following tasks: (1) System identification and characterization; (2) Definition of evaluation criteria (e.g., form, strength); (3) Identification of possible failure scenarios; (4) Assessment of potential losses per scenario; (5) Evaluation of vulnerability indexes. These issues are addressed in this section according to the systems approach.

4.1 Overall strategy for network vulnerability assessments

A proposal for system identification and characterization was discussed in section 3 and is one of the main contributions of this paper. Regarding the criteria to evaluate vulnerability, in this paper we combine both *form* and *resistance*. In other words, the proposed network vulnerability analysis will focus on identifying critical links for connectivity (importance) while at the same time taking into consideration failure probability. Failure scenarios involve the removal of a set of elements as a result of an external damaging event; for example, a set of nodes and links that fail and are removed from the network as a result of an earthquake.

In the proposed approach, the hierarchical network representation is used to make more efficient analyses by reducing the number of scenarios to be evaluated in the upper levels. In this sense, vulnerability assessment is directed towards detecting critical elements (links or nodes) for the network performance. These elements are detected as a result of the network's emergent properties at different levels of abstraction, i.e., how individual elements participate in

the connections between macroscopic components (subsystems) at different levels of abstraction. Under this connectivity-based approach, the higher in the hierarchy an actual link is found to belong to any fictitious link, the greater importance is assigned to it.

The impact of a failure scenario on the network is commonly evaluated in terms of costs, which may be evaluated in different ways. For instance, in transportation networks costs are commonly assumed to be proportional to physical distances. Therefore, the Dijkstra's algorithm for finding *shortest-paths* within networks (before and after link removal) is proposed as a measure of the impact of the damage (lack of an element) in the network.

4.2 Vulnerability Index

Based on a systems approach, a hierarchical description of the network is obtained by successive clustering (section 3). Since the hierarchical representation provides different simplified representations of the system, the vulnerability assessment is level-dependent. Thus, if the vulnerability analysis focuses on identifying critical links (i.e., based on the impact that the removal of the edge may cause on the network), it is possible to define an index that evaluates the contribution of an edge to the system vulnerability as:

$$V^{(l)}(e_j) = I^{(l)}[e_j] \cdot c_l \cdot (F_1(e_j) \cdot F_2(e_j)) \quad (3)$$

where $I^{(l)}[e_j]$ is an indicator function that denotes whether the actual node e_j belongs to a fictitious link at level l . Note that only edges that belong to fictitious links will have an impact on the network vulnerability at a specific level. The weighting factor c_l is a level-dependent coefficient based on global descriptors of the network, and depends on three factors that account for the level in the hierarchy, the reduction of the actual system as a result of clustering and the connectivity of the fictitious network. It is defined as:

$$c_l = \left(\frac{L-l+1}{L} \right) \left(\frac{n - |\Lambda^{(l)}| + 1}{n} \right) \left(\frac{1}{K^{(l)}} \right) \quad (4)$$

where L denotes the total number of hierarchy levels, n is the total number of network nodes; $|\Lambda^{(l)}|$ is the cardinality of the set of fictitious nodes at level l ; and $K^{(l)}$ is the k -connectivity of the fictitious network at level l (Brandes and Erlebach (2005)). The first factor accounts for the fact that more complex subsystems rely on fewer actual links as moving up in the hierarchy; other weighting functions can be used depending upon the problem. The second term defines a degree of clustering at level l ; i.e., the ratio of fictitious nodes with respect to the actual number nodes. Finally, the third factor takes into consideration the connectivity of fictitious networks at every level. The k -connectivity of a network evaluates the number of elements that need to be removed to disconnect the network. Note that all three factors are defined within the interval $[0, 1]$ and decrease as the network description becomes closer to the actual network.

The factors $F_1(e_j)$ and $F_2(e_j)$ evaluate how the *form* (i.e., topological importance according to connectivity within the hierarchy) and the *strength* (failure probability) contribute to the vulnerability of actual links e_j respectively. The factor $F_1(e_j)$ describes the importance of the edge j at level l and is computed as:

$$F_1(e_j) = \sum_{s,t \in V} \frac{D^{(j)}(s,t) - D(s,t)}{D(s,t)} \quad (5)$$

where $D(s,t)$ is the shortest-path between any pairs of nodes s and t , whilst $D^{(j)}(s,t)$ denotes the same index after removing link j . Finally, $F_2(e_j)$ describes the contribution of the actual edge e_j to the probability of failure of the fictitious link it belongs to. Because fictitious links are parallel arrangements of actual links, $F_2(e_j)$ can be computed as:

$$F_2(e_j) = 1 - \frac{\prod_{i \in \Phi \setminus \{e_j\}} P_f(e_i) - \prod_{i \in \Phi} P_f(e_i)}{\prod_{i \in \Phi \setminus \{e_j\}} P_f(e_i)} \quad (6)$$

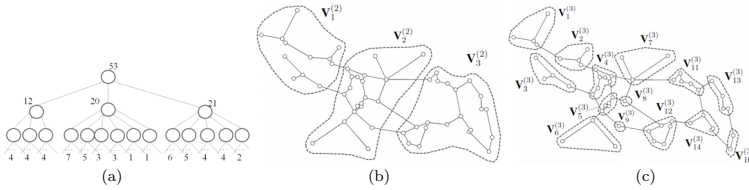


Figure 1: Hierarchical decomposition of the Colombian transportation network (a), and its second (b) and third (c) levels

where Φ is the set of edges that conform the fictitious link, $\Phi \setminus \{e_j\}$ denotes the removal of the link j and $P_j(e_i)$ is the failure probability of the i -th actual link. Note that this is a measure of the relative contribution of the failure probability of the edge e_j to the failure of its associated fictitious link in a given level. Thus, the factor $F_2(e_j)$ will be larger for elements with higher failure probabilities. Note that this factor grows as the analysis moves down in the hierarchy.

The proposed index $V^{(l)}(e_j)$ can be used for ranking the edges according to their relative contribution to the vulnerability at each hierarchical level. The final result is a ranking of links with decreasing contribution to vulnerability (either globally or by level). Thus a global index for a link can be computed as: $\max_l(V^{(l)}(e_j))$. This value provides valuable information for decision-making and risk management, e.g., resource-allocation for maintenance, replacement, etc.

5 Illustrative example

In this section, the strategy to evaluate the vulnerability of the Colombian highway network is presented; it consists of 53 nodes and 59 links representing relevant industrial and touristic points in the country. For the purpose of this example, the failure probability of links is assigned proportionally to their distance; i.e., $p_j = \lambda d_j$ with λ such that $\max_j P_j = 10^{-3}$. A hierarchical description of the network is shown in Figure 1 and obtained by means of successive clustering. The clustering method uses the kernel k -means algorithm (Dhillon et al. (2004)), complemented by the MCL algorithm (van Dongen (2000)), which is used as the initialization mechanism. Four hierarchical levels were obtained, with 1, 3, 14 and 53 nodes at each level.

The level-dependent coefficient c_l is calculated as a function of its three factors (Equation 4). The values of the first factor for every level (top to bottom) are $[1, 0.75, 0.5, 0.25]$, whereas for the second factor (clustering) they are: $[1, 51/53, 40/53, 1/53]$, and for the third (connectivity): $[1, 1/2, 1/13, 1/51]$, thus obtaining $c = [1, 0.36, 0.029, 0.0001]$. The importance $F_1(e_j)$ of every link individually was evaluated using Equation 6. $F_1(e_j)$ captures the impact on the shortest-path after removing an edge e_j . Finally, $F_2(e_j)$ corresponds to the failure probability.

The ranking of edges at each level can be made based on the following measure: $V^{(l)}(e_j) = I^{(l)}[e_j] \cdot F_1(e_j) \cdot F_2(e_j)$. In order to obtain a combined global ranking, the level coefficients c_l need to be included (see section 4). The evaluation of the transportation network, in the 3rd level in the hierarchy, is shown in Figure 2. The values of $F_1(e_j)$ are presented in Figure 2a and the values of $F_2(e_j)$ are shown in Figure 2b. The global indicator is presented in Figure 2c; the thickness of lines denote the value of the index and dotted lines indicate that the link does not belong to fictitious edges at level 3.

The global index indicates that the critical links are those that belong to many shortest-paths and have low redundancy. These results provide valuable information for strategic planning of risk management, i.e., assigning investment priorities in maintenance or adding redundancy where necessary.

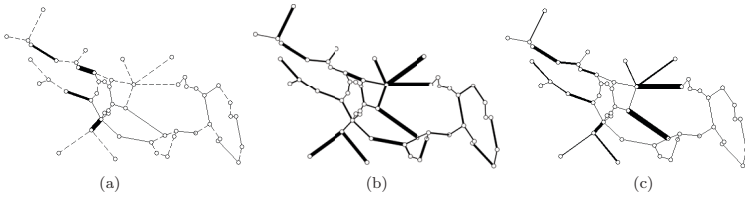


Figure 2: Ordering of links according to importance only at levels 3 (a), failure probability (b) and the global combined indicator

6 Conclusions

In this paper, a novel approach to vulnerability and risk assessment was presented; it is based on a systems approach and the hierarchical decomposition of infrastructure networks to deal with systems complexity. The hierarchical representation allows for the system description at different levels of abstraction, providing insight about the emergent properties of the network and reducing the computational cost of scenario evaluations. These benefits are relevant in vulnerability analysis because they unravel elements of high betweenness beyond intuition, i.e., those connecting different macroscopic subcomponents; and second, because the analysis of failure scenarios is reduced as the analysis moves up in the hierarchy. The paper focuses on the evaluation of critical links within the network. Thus, the contribution of every edge to the network vulnerability is evaluated by an index that takes into consideration two basic criteria: form (importance in connectivity) and strength (failure probability). Furthermore, the index also takes into consideration the hierarchical description of the network. The proposed approach is explained through a practical example. Further research focuses on the formalization of a methodology that includes reliability and damage propagation assessment.

7 Acknowledgments

The authors gratefully acknowledge the financial support by Centro de Estudios Interdisciplinarios Básicos y Aplicados (CEIBA) for this project.

References

- Albert, R. and Barabási, A.-L. (2002). Statistical mechanics of complex networks. *Rev. Mod. Phys.*, 74(1):47–97.
- Ammann, P. (2002). Scalable, graph-based network vulnerability analysis. In *In Proceedings of the 9th ACM Conference on Computer and Communications Security*, pages 217–224. ACM Press.
- Barzel, B. and Biham, O. (2009). Quantifying the connectivity of a network: The network correlation function method. *Phys. Rev. E*, 80(4):046104.
- Bell, M. G. H., Kanturska, U., Schmöcker, J.-D., and Fonzone, A. (2008). Attacker-defender models and road network vulnerability. *Philos. Trans. R. Soc. Lond. Ser. A Math. Phys. Eng. Sci.*, 366(1872):1893–1906.
- Berdica, K. and Mattsson, L.-G. (2007). Vulnerability: A model-based case study of the road network in stockholm. In Murray, A. T. and Grubestic, T. H., editors, *Critical Infrastructure, Advances in Spatial Science*, pages 81–106. Springer Berlin Heidelberg.
- Blockley, D. and Godfrey, P. (2000). *Do it differently: systems for rethinking construction*. Thomas Telford, London.
- Brandes, U. and Erlebach, T. (2005). *Network Analysis: Methodological Foundations (Lecture*

- Notes in Computer Science / Theoretical Computer Science and General Issues*). Springer, 1 edition.
- Checkland, P. (1981). *Systems thinking, systems practice*. John Wiley and Sons, Chichester, UK.
- Dhillon, I., Guan, Y., and Kulis, B. (2004). A unified view of kernel k-means, spectral clustering and graph cuts. Technical report.
- Ellison, R., Ellison, R. J., Fisher, D., Fisher, D. A., Linger, R. C., Linger, R. C., Lipson, H. F., Lipson, H. F., Longstaff, T., Longstaff, T., Mead, N., and Mead, N. R. (1997). Survivable network systems: An emerging discipline. Technical report.
- Erath, A., Birdsall, J., Axhausen, K. W., and Hajdin, R. (2009). Vulnerability Assessment Methodology for Swiss Road Network. *Transportation Research Record*, (2137):118–126.
- Filippone, M., Camastra, F., Masulli, F., and Rovetta, S. (2008). A survey of kernel and spectral methods for clustering. *Pattern recognition*.
- Gómez, C., Sánchez-Silva, M., nas Osorio, L. D., and Rosowsky, D. Hierarchical representation of infrastructure systems for risk-based decision-making. Structure and infrastructure engineering.
- Gong, B., Liu, J., Huang, L., Yang, K., and Yang, L. (2008). Geographical constraints to range-based attacks on links in complex networks. *New Journal of Physics*, 10(1):013030.
- Graepel, J. and K. Obermayer, W. B. (1998). Fuzzy topographic kernel clustering. In *Proc. 5th GI Workshop Fuzzy Neurosystems*, pages 90–97.
- Jenelius, E., Petersen, T., and Mattsson, L. (2006). Importance and exposure in road network vulnerability analysis. *Transportation research Part A – Policy and practice*, 40(7):537–560.
- Jha, S., Wing, J., Linger, R., and Longstaff, T. (2000). Survivability analysis of network specifications. In *Dependable systems and networks (DSN)*, pages 53–58. Press.
- Latora, V. and Marchiori, M. (2005). Vulnerability and protection of infrastructure networks. *Physical Review E*, 71(1, Part 2).
- Macqueen, J. B. (1967). Some methods of classification and analysis of multivariate observations. In *Proceedings of the Fifth Berkeley Symposium on Mathematical Statistics and Probability*, pages 281–297.
- Nazarova, I. A. (2009). Solution methods for the vertex variant of the network system vulnerability analysis problem. *Journal of computer and systems sciences international*, 48(4):581–591.
- Ng, A. Y., Jordan, M. L., and Weiss, Y. (2001). On spectral clustering: Analysis and an algorithm. In *Advances in Neural Information Processing Systems 14*, pages 849–856. MIT Press.
- Qu, G., Hariri, S., and Raghavendra, C. S. A framework for network vulnerability analysis. In *Proceedings of the First IASTED International Conference on Communications, Internet, Information Technology*.
- Ryo, I. and Sadaaki, M. (2005). Lvq clustering and som using a kernel function. *Journal of Japan Society for Fuzzy Theory and Intelligent Informatics*, 17(1):88–94.
- Scholkopf, B., Smola, A., and Muller, K. (1998). Nonlinear component analysis as a kernel eigenvalue problem. *Neural Comput.*, 10:1299–1319.
- Schuchmann, G. (2010). Road network vulnerability-evaluation of measures in ranking damages and developments. *Periodica polytechnica – civil engineering*, 54(1):61–65.
- Shi, J. (2000). Learning segmentation by random walks. In *Advances in Neural Information Processing*, pages 470–477. MIT Press.
- Swiler, L. P., Phillips, C., and Gaylor, T. (1997). A graph-based network-vulnerability analysis system. In *Sandia National Laboratories, Albuquerque, New*, pages 97–3010. ACM Press.
- van Dongen, S. (2000). *Graph Clustering by Flow Simulation*. PhD thesis, University of Utrecht.
- Verma, D. and Meila, M. (2003). A comparison of spectral clustering algorithms. Technical report.
- Wang, J. A. and Guo, M. (2010). Vulnerability categorization using bayesian networks. In *CSIIRW '10: Proceedings of the Sixth Annual Workshop on Cyber Security and Information Intelligence Research*, pages 1–4, New York, NY, USA. ACM.

Sustainability: Complexity, Regulations and Decisions

Tonatiuh Rodriguez-Nikl¹ and Colin B. Brown²

¹ M. ASCE, Ph.D., P.E., Instructor, School of Civil and Construction Engineering, Oregon State University, 220 Owen Hall, Corvallis, OR, 97331, Ph: (541)737-2057, Fax: (541)737-3052, rodrigto@enr.orst.edu.

² Dist. M. ASCE, Ph.D., P.Eng., Professor Emeritus, Department of Civil and Environmental Engineering, University of Washington, Seattle, WA, and Courtesy Faculty, School of Civil and Construction Engineering, Oregon State University, Corvallis, OR.

ABSTRACT

Success in the design and use of civil engineering systems often rests on the synergy with ideas that initially appear to be only peripherally related to the main topic. As more ideas are incorporated into a system greater synergies may become possible, but they may become at the same time more elusive because of the increasing system complexity and the difficulty in considering so many ideas. The complexity of the system results from both technical and social considerations. Under these circumstances it is common to simplify the problem by the introduction of rules and regulations. The setting in which decisions are made will compel civil engineers to participate in decision making processes that are subjective and uncertain. This is different than the rational decision making model in which they are trained and with which they are most comfortable. This paper explores how system complexity, regulations, and decisions are related. This is done in the context of sustainability, a theme in contemporary discourse with higher levels of uncertainty and complexity. It is of particular interest to determine how large the system boundary should be for purposes of decision-making. It is proposed that the boundary be governed by the principle of decision invariance, i.e., as the system boundary changes, the decision does not change. The principle of surprise inevitability is then offered as a reminder that unlikely but potentially dangerous outcomes should be expected, planned for, and to the extent possible avoided.

INTRODUCTION

A central undertaking in civil engineering is the making of decisions that meet the project objectives, in the face of uncertainty, and in a defined period of time. In the best of all worlds such decisions take account of all matters and are the best amongst all alternatives. However, the time constraint may limit how many matters can be considered and thus limit the reduction of uncertainty. During decision making one must specify the system in which matters critical to these decisions are embedded. Two separate concerns limit the extent of the system considered. First, the ability of

human beings to consider ideas is bounded. A figure often quoted is that the number of ideas that can be effectively considered simultaneously is seven, plus or minus two (Miller 1956). Decisions tend to be made with even fewer ideas: rationally with three and intuitively with more (Dijksterhuis et al. 2006). Second, there is a sense that vagueness increases with the enlargement of a system. Civil engineering practice involves an interplay with human agencies that are included in the encompassing system. In this way humanistic, vague ideas have to be introduced into decision making. The preferred focus of most engineers seems to be on technical solutions to specific, well defined problems narrow in scope, yet this may expend unnecessary effort on detailed design of artifacts that do not function well in the encompassing systems. Consideration of the encompassing systems can make the difference between success or failure of the artifact. The concept of including all relevant, but at the same time complicating entities, into a decision scheme is independent of whether it is a massive civil engineering venture or a simple structure.

This paper discusses three related elements: (a) sources of complexity in civil engineering systems, (b) the effect of constraints (primarily regulations) in reducing complexity, and (c) aspects of decision-making strategies. The section on decision making includes suggestions for how the engineer might approach decision-making with regards to complex systems. These elements are then discussed in the context of sustainability.

COMPLEXITY

For realistic decision-making the total system under consideration will include multiple entities and connections, each with their associated complexities. Both entities and connections will be evident in the decision schemes. The expanding system boundaries move the decisions from narrow, though often difficult, technical matters to complex interactions between technical professions and agencies. As the system expands further the interactions will involve society and its aspirations.

Technical Complexity: In general, each entity requires particular technical expertise. The interaction between them ensures complications in language and communication. Even when these entities are all technical in nature, they often have few common technical characteristics. Any combination of such entities in a decision scheme will therefore involve technical complexity. The final system considered will include more than just quantitative, technical considerations. The education and practice of those participating will vary and accommodations to these diverse views will have to occur as decisions are made. However, due to their technical nature, there is a likelihood of a common professional culture in the protagonists and decisions will likely be understood by all parties.

Social Complexity: Another world of complexity exists when the civil engineer steps outside the technical domain. The system boundaries tend to enlarge into regions that incorporate humanistic concerns. Zadeh (1973) conceived a Principle of Incompatibility that applies to these situations:

Stated informally, the essence of this principle is that as the complexity of a system increases, our ability to make precise, and yet significant

statements about its behavior diminishes until a threshold is reached beyond which precision and significance (or relevance) become almost mutually exclusive characteristics.

An increasing number of stakeholders have become participants in civil engineering decisions and this results in greater social complexity.

REGULATIONS

The system in which engineering work is embedded can be highly complex, but constraints can be imposed, which by their prescriptive nature reduce the number of options considered by the engineer. Ideally these constraints limit the complexity of the system to a manageable degree. Regulations can take the form of non-binding but convenient industry standards or legally binding rules generated from within and without the profession. They can be narrow in scope and applied only to the particular problem or to broader social, legal and technical regulations.

Such important technical regulations are readily adopted by the profession. They clear up various complexities and vagueness without affecting the objectives of the decision scheme. However, the impact of the civil rights and environmental movements of the 1970s imposed a broadening of goals in the decision process. The consequent regulations introduced matters that had not been previously significant in civil engineering decision making. The influence of these regulations can result in multiple objectives in the decision scheme that cannot always be reconciled.

Of particular importance to the engineer are codes of practice. There exists a justifiable belief that such enforcement will ensure satisfactory technical results. Over the last half century codes have covered more topics and have become more specific in their requirements. As a consequence professional concern has focused more on meeting the letter of the code and less on seeking what could happen in a particular problem. Despite the comprehensiveness of the code, failures occur much more frequently than would be anticipated from the safety levels provided. The actual frequency of failure is two or three orders of magnitude greater than those levels anticipated in codes (values of 1:100 to 1:1000 failures a year for different types of structures have been estimated as being typical). This difference indicates a major discrepancy between reality and the code models and assumptions. This ontological uncertainty, i.e., uncertainty due to imperfect knowledge about underlying phenomena, receives scant attention. The focus in codes is on statistical and modeling uncertainty and not on ontological uncertainty (Melchers 2007). Thus, despite the fact that regulations facilitate decisions by reducing issues considered by the engineer, there are still levels of uncertainty that are not being plumbed.

DECISIONS

Civil engineers are introduced to the methods of rational decision-making and to some extent utilize them in professional practice. However, the political world is full of subjective uncertainty and involves decision making in a humanistic and vague environment. These realities described by Zadeh have to be confronted in decisions that

involve extensive professional system considerations. The model that engineers usually employ is quantitative and based both on data and values that are a matter of opinion, e.g., values that are distant in time such as the inflation and discount rates, technical improvements and costs, and financial arrangements. Ideally, decisions involve identifying all alternative actions and the consequences that could be induced by each alternative, the chances of the consequences occurring and the benefits and costs for each alternative. These benefits and costs are expressed at present worth values with associated decisions on future inflation and on discount rates. The selection of alternatives, probabilities, future costs and benefit, future inflation rates and a discount rate are highly subjective. On this basis the engineer accepts subjectivity and partial information as fundamental in decision making even when the process appears to be founded on rationality. In practice even this scheme is overly-optimistic and only a few alternatives that satisfy the constrained objectives are considered. The one that displays the best weighted benefits is selected. This process of "satisficing" (Simon 1957) takes into account the impossibility of identifying all of the real alternatives, actual objectives and constraints, truly realistic modeling, completing the work within the time available in the decision process and the ability to balance many ideas at the same time.

There is a dichotomy presented to civil engineers: on the one hand they are urged to expand their thinking when making decisions and to include ever wider system boundaries; on the other hand they have to make responsible decisions that are based on a limited number of ideas and alternatives. The system ultimately considered in decision making should be extensive enough to encompass the first concern and yet small enough to allow the practice of the other. To accomplish these goals, the following criterion is offered:

Decision invariance: the size of the system should be bounded by the invariance of the decision. If the decision is maintained with an extension of the system boundary then a likely limit to the decision system has been attained.

In addition, engineers need to be concerned with surprises. The term "surprise" is used here with a clear meaning. A surprise has a small chance of happening compared to the chances of other possible events. If the consequences of a surprise are great, and if it has been ignored in decision-making, then it can upend previously detailed cost-benefit assessments. It is unlikely that surprise can be avoided. Perrow (1999), for instance, argues extensively that in sufficiently complex and closely-coupled systems, surprises ("accidents" as he calls them) are inevitable. These considerations suggest the second criterion:

Surprise Inevitability: complex systems will inevitably contain surprises. This should be recognized explicitly and solutions should be robust in the face of surprise.

In effect this means that during the decision-making process the question "what can happen here?" should be asked regularly and in good faith.

SUSTAINABILITY

Recent trends in sustainability are encouraging growing numbers of engineers to expand the scope of their work to include environmental and social ramifications in addition to the more traditional technical and economic factors. Engineers now consider soft topics that are often outside their usual experience and education. As an example, concrete designers are contending with a potential EPA ruling to reclassify coal ash waste as hazardous (EPA 2010). The EPA is considering this action in the wake of the fly ash spill in the Tennessee Valley Authority. Although use of fly ash in concrete is common and can have environmentally beneficial uses, this decision risks upsetting public relations, financial, and legal aspects of fly ash use in concrete. Irrespective of whether the EPA action is justified or not, it has brought a large group of engineers closer to toxicologists, public health professionals, ecologists, and others. In this and other situations, the increased number and vagueness of the topics under consideration contribute to a more complex system as previously described.

There are attempts to reduce complexity by codifying sustainability related requirements. In the United States Leadership in Energy and Environmental Design (LEED) is a popular points-based evaluation and certification mechanism for building design. The International Code Council (ICC) is developing the International Green Construction Code (IGCC). This is a model green code structured like other ICC codes, e.g., the International Building Code. The American Society of Civil Engineers is developing a sustainability rating system similar to LEED to be applied to the entire infrastructure (ASCE 2010). This list is not exhaustive. An aspect that these approaches have in common is reducing a problem to the relatively simple task of first satisfying requirements and then choosing from a menu of optional features. Points-based codes award points to the optional requirements and a minimum number of points is required. The problem becomes as simple as choosing the most economical option provided that the minimum number of points has been earned.

As convenient as these approaches are, there are also dangers. There is a temptation to dwell on meeting the letter of the code rather than considering what could occur in a particular setting. This is particularly relevant to sustainability, which is in such an early stage of code development. It is likely that in some important ways these codes are imperfect and incomplete. It is also possible to dwell on the immediate green (environmentally less invasive) aspect of a project to the detriment of other important considerations (see e.g. FEMA 2010). It is important for engineers in this setting to ensure that other matters of significance are not overlooked. Given the relative infancy of green codes it cannot be expected that all such tradeoffs are captured by the codes. Rather, it is up to engineers to exercise judgment.

The two suggestions made in this paper, decision invariance and surprise avoidance, can help engineers focus their thinking, especially during this dynamic period of code development. With codes in their infancy and new green technologies developed seemingly daily, there are myriad ways for surprises to occur. Simply following the codes cannot be sufficient. It is likely that there will be unintended consequences of applying new materials and systems. Engineers need to imaginatively

seek out these consequences. The question “what can happen here?” should be asked regularly.

To illustrate these ideas we consider the hypothetical design of a new house that is within a 100 year flood plain. The designer is striving to be environmentally responsible and for this reason is focusing on reducing material use in the raised foundation. Fig. 1 provides a simplified diagram of issues that would influence the elevation chosen by the designer. This diagram shows the decision being made in white together with the different considerations that inform it either directly or indirectly. An arrow in the diagram indicates that the consideration at the tail of the arrow affects or informs the factor at the head.

The conventional issues affecting the elevation of the house are represented in light grey in Fig. 1. These include issues that are common in any construction project such as first costs, ongoing costs, and construction issues. Particular to flood-prone regions are flood insurance premiums, which are affected by the regulatory flood plain elevation (RFPE) and the Federal Emergency Management Agency (FEMA). FEMA also has a direct influence on the RFPE.

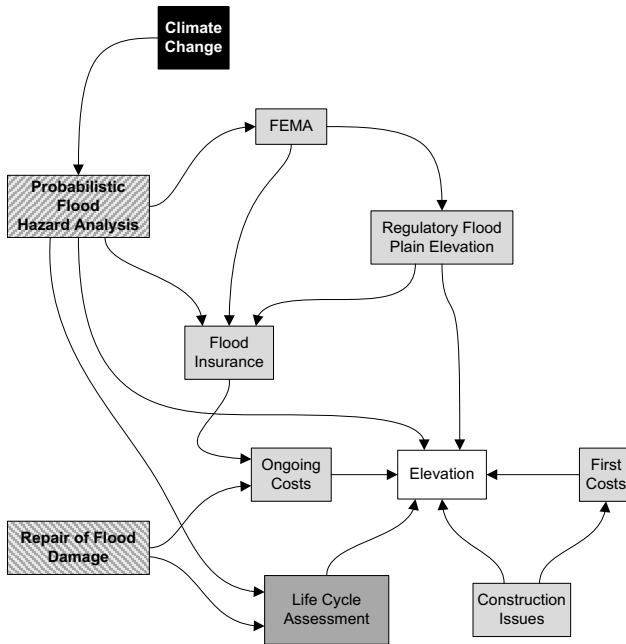


Figure 1. Design considerations for the elevation of a house in a flood plain (including environmental impacts). The object of the decision is in white. Initial considerations are in light grey. As the system is expanded additional considerations are included: first those in dark grey, then grey and white hatches, then black.

Consideration of environmental factors requires a small expansion of the conventional system to include a life cycle assessment (LCA), which is represented in dark grey in Fig 1. An LCA assesses the environmental impacts of a project through its entire life cycle. The LCA may be performed according to established methodologies such as ISO 14040 or it may simply reflect the informal considerations of the designer. In either case, the resulting LCA also influences the elevation selected. If the system were not expanded any further, the LCA would determine that a lower elevation results in lower material usage. This would tend to push the designer to choose a lower elevation.

Including an LCA is the minimal expansion that would be necessary to consider environmental aspects. However, further considerations could result in a changed decision. A further expansion could explicitly include the flooding hazard (represented with a grey cross hatch in Fig. 1). Additional factors now considered are a probabilistic flood hazard analysis and the repair required if a flood were to occur. Repair includes the house itself and its belongings, may involve full demolition and replacement of the house, and includes both financial cost and environmental impact. With these two additional considerations it is possible to determine how much an increased elevation would reduce the probability of damage and thus the expected costs and environmental impacts due to repair. It could then be determined whether this reduction counteracts the increased impacts from the larger amount of material used to achieve that elevation.

It is seen in this example how the further expansion of the system changes the nature of the decision. When considering only narrow environmental considerations the decision involves minimizing the height subject to regulatory constraints. With the system expanded to include the flood hazard the decision involves finding an optimum height that may exceed the minimum but that optimizes the outcome based on life cycle costs and environmental impacts. The two decisions not only result in a different choice of elevation, they are also qualitatively different approaches to the problem.

A final expansion may include consideration of the estimated effects of climate change (represented in black in Fig. 1). Climate change predictions will affect the potential flood hazard. Depending on the region, future rainfall and thus future flood hazard may be expected to rise or fall. In either case the variance will increase. It may be the case that this additional expansion may not substantively change the decision. At this point we would invoke the principle of decision invariance and may decide that, the decision being unchanged, our system is sufficiently large to permit consideration of all necessary issues.

CONCLUSION

This paper explores how system complexity, regulations, and decisions are related. The discussion is grounded in examples in the context of sustainability, a theme in contemporary discourse with levels of uncertainty and complexity with which civil engineers are not accustomed. As a guide for decision makers it is proposed that the size of the system boundary be governed by the principles of decision invariance, i.e., as the system boundary changes, the decision does not change. The principle of sur-

prise inevitability is also proposed as a reminder that surprise can always occur and must be considered to the extent possible.

REFERENCES

- ASCE (2010). "ILC Works to Help Develop Sustainability Rating System". *ASCE News*, 35(5).
- Dijksterhuis, A., Bos, M.W. Nordgren and van Baaren, R.B. (2006). On Making the Right Choice: The Deliberation-Without-Attention Effect, *Science*; 311; 1005-1007.
- EPA (2010). Coal Combustion Residuals - Proposed Rule. <<<http://www.epa.gov/osw/nonhaz/industrial/special/fossil/ccr-rule/index.htm>>> (8 Sep, 2010).
- FEMA (2010). Natural Hazards and Sustainability for Residential Buildings, FEMA P-798, Federal Emergency Management Agency.
- Melchers, R.E., (2007). Structural reliability theory in the context of structural safety, *Civil Engineering and Environmental Systems*, 24(1), 53-69.
- Miller, G.A., (1956). The magical number seven, plus or minus two. Some limits on our capacity for processing information, *Psychological Review*, 24, 1. 343-352.
- Perrow (1999). *Normal Accidents: living with high-risk technologies*, Princeton University Press.
- Simon, H.A., (1957). *Administrative Behavior*, 2nd Edition, Free Press, New York.
- Zadeh, L., (1973). Outline of a new approach to the analysis of complex systems and decision processes, *Transactions of Institute of Electrical and Electronics Engineers*, SMC-3(1), 28-44.

A systems approach to vulnerability assessment

Jitendra Agarwal, Mei Liu, David Blockley
Department of Civil Engineering
University of Bristol
Bristol BS8 1TR (UK)

Abstract

A system is vulnerable if any small damage produces consequences which are disproportionately large. The damage may come from unknown sources. Consequently any inherent weaknesses in the form of the system need to be explored. In this paper, we present a systems approach to analyse the vulnerabilities of a system and hence to manage risks. The form of the system is organized into a hierarchical model that can be systematically examined for weak points. The approach can be applied to many networked systems including lifelines. Here it is briefly illustrated through a simple structural system and a road network.

Introduction

In recent years, with increasing threat of climate change and terrorism, vulnerabilities of infrastructures have gained more importance in public policy (e.g. IPPR 2009). Civil engineering infrastructures are complex systems which can fail in many different ways with far-reaching consequences. To avoid such failures, an analysis of demand and capacity of a system or even exploring some ‘what if’ scenarios is no longer sufficient. Instead an approach is required where interdependent vulnerabilities across systems are identified so that risks can be managed accordingly.

In different disciplines different approaches to define and assess vulnerability are used. For example, seismic vulnerability of structures is usually associated with a seismic event of a given intensity. Vulnerability for social systems is related to their adaptability and stability to damage and change. Vulnerability of transport networks is often related to reductions in their serviceability levels. Topological features are also used to arrive at a measure of network vulnerability. In this paper, a systems approach to identify vulnerabilities in the form and connectivity of a system is presented. The proposed method uses a graph model of the system and leads to a hierarchical representation of the system which can then be systematically examined for vulnerable failure scenarios. The approach can be applied to many different networked systems e.g. structures, road networks, water supply systems, energy distribution systems etc.

The purpose of the paper is to review the concepts of vulnerability, robustness and risk in civil engineering systems; to present a vulnerability and risk analysis procedure within a generic systems approach and finally to illustrate the methodology through two examples - a structure and a road traffic network.

Vulnerability, robustness and risk

A system is vulnerable if any damage produces consequences that are disproportionate to that damage. If a system is vulnerable in any single way it is not robust or resilient. Traditionally, risk is determined as the product of probability of failure and the ensuing consequence. For a complex system, it is not easy to estimate the probabilities and the consequences. For example, it is difficult to know when and where a terrorist strike might occur. The success or failure of a system is judged on whether it continues to function but the extent of the consequences is also very important. The consequences of a failure event depend upon the following three factors: (a) the form of the system, (b) the level of demands on the system (and consequently the severity of any damage) and (c) the level of preparedness for dealing with unforeseen events.

Risk is the product of probability of occurrence of an event and its consequences in a particular context and so the risk of a failure scenario is the product of the likelihood of the whole failure scenario of non-independent events and the resulting consequences in a particular context. Failure scenarios that are vulnerable may be of low probability but if they have high consequences then they must be considered. It is worth noting that many risk analysis studies assume that critical scenarios are available. We propose a generic vulnerability and risk analysis framework as shown in Fig 1. The analysis of the form of the system (Step 1) which leads to the identification of vulnerable scenarios (Step 2) is central to the methodology of this paper. If the consequences of these scenarios are judged to be unacceptable *irrespective of how they might be realized by some unknown action*, the form of the system can be improved before proceeding any further. Modern day systems are interdependent and consequences will invariably extend to the other systems (Step 3). For example, the loss of a bridge (say, due to a joint failure) can have a severe impact on the transport network of which it is a part. A separate vulnerability analysis could be carried out for the transport network and the results could be appropriately incorporated in the risk calculations for the bridge. An analysis of the likelihood of various scenarios (Step 4) is a systematic process of identifying all possible known actions which could trigger the vulnerabilities in a system. Risks associated with different scenarios due to all possible known actions can now be assessed (Step 5). These risks could be managed (Step 6), for example, by improving the form of the system, putting measures in place to control the severity of actions. However it is important to note that the risk of a vulnerable scenario due to an unknown action cannot be calculated. This is a potentially important source of incompleteness in any estimate of risk (Blockley, Godfrey 2000)

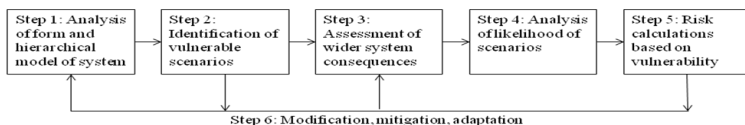


Figure 1. A framework for vulnerability and risk analysis

A systems approach to vulnerability analysis

The vulnerability and risk analysis framework proposed here is based on a systems approach which recognises the importance of incompleteness. The properties of the components of the system and their interactions are used to create a hierarchical model of the system. This is then used to identify vulnerable scenarios on which risk calculations are based.

Systems concepts and measure of form

A system is considered as a set of interacting process objects (Blockley and Godfrey 2000) which are arranged and connected together in an appropriate form. They interact with each other in order to deliver a process or to fulfil a role in a higher level process. The nature of objects may differ substantially from one system to the other. For example, beams and columns are objects in a structure and pipes are objects in a water supply network. Such a system can also be represented as a graph model in terms of nodes and links. The links are the channels of communication between nodes. In most systems there is one channel per link (e.g. electrical current or fluid flow), however, there can be more channels along a link (e.g. up to six degrees of freedom in a structure). Associated with each link is a parameter describing a quality of the form of the link. This parameter depends upon various components in a system and their relationships (for example in mechanical and electrical systems, see Shearer *et al* 1967). Relationships are expressed in terms of across and through variables. The across variables balance around the circuit and the through variables balance across any section through the circuit. Table 1 summarises some of the variables for different systems including structures, water supply and traffic networks. The parameter used here to describe a quality of the form of a link is either transmittance or impedance. In a road network a wide road with high transmittance will attract traffic flow whereas in a structure a large stiff structural component will attract the flow of force.

Vulnerability is susceptibility to some kind of damage or adverse event because the form of the system has certain characteristics. Form and function are closely related in that an appropriate form is required to achieve a particular function. If the form is damaged then the function will also be affected. Disproportionate consequences derive from a form that is inappropriate because it 'unzips' when subjected to one or more specific demands (which may not have been anticipated) in an unacceptable way. Hence vulnerability is examined by concentrating on the way in which the form of a system is affected by any arbitrary damage. Then the results can be combined with the analysis of response to different specific demands.

Hierarchical model of a system

As stated earlier, the proposed approach uses a graph model of a system. A path in a graph is a sequence of nodes and links. A path through an appropriate combination of nodes and links provides the means by which a system resists the demands upon it and obey Kirchoff's Laws (Shearer *et al* 1967). A path may result in closed loops. For example in a structure (Agarwal *et al* 2003), a ring is capable of maintaining equilibrium through a balanced flow of forces. In an electrical network, the essential form required to conduct a balanced flow of electricity is a closed loop. Clusters of

these paths of rings and loops are then formed according to their degree of connectivity and well-formedness (defined below). The objects in a cluster are more tightly connected to each other than to those outside the cluster. These clusters are grown by including neighbouring clusters to provide a second level of definition of the system. This process of clustering is repeated to form even higher levels of definition in a hierarchy until there is one single cluster, the whole system.

Well-formedness is a measure of a quality of the form of a system and is a central concept of the theory. In one sense it represents the tightness of a cluster which is not based on the topology of the network alone. Rather the well-formedness measure uses the number and the form of connections as well as the quality of flow through a path. To keep the discussion general, we assume that it is a function of the weightings (w) of the links within the system and the way they are connected. The weightings will be arrived at in different ways for different systems, as shown in Table 1. How these weights are combined to obtain well-formedness again depends upon the nature of the system. In an abstract case, well-formedness may be assumed to be proportional to the sum of the weightings, w , of the links into a node and the well-formedness of a cluster is obtained by summing the well-formedness of the constituent parts.

Unzipping and identification of vulnerable scenarios

A system can fail in different ways but the failure scenarios with disproportionately large consequences are of direct interest here particularly when the nature or the likelihood of the actions is not known. The hierarchical representation of a system, as described above, is searched for various failure scenarios by systematically 'unzipping' the clusters. Four particular scenarios are of interest. The first is the *minimum demand failure scenario* which is the easiest way in which a system can be damaged with some loss of function no matter how small. The second is the *total failure scenario* where all the objects are disconnected irrespective of the effort. Next is the *maximum failure scenario* with the highest consequences with least effort. Finally the *minimum failure scenario* is a failure scenario with the minimum consequences irrespective of damage demand.

A failure scenario is a sequence of deteriorating events leading to some degree of separation from a reference cluster within the system. A deteriorating event is the removal of a link and is the basic unit of damage. For example, a part of a structure can become a mechanism or a part of a road network can be blocked to traffic. A deterioration event may be caused by a specific or random action considered as part of a risk calculation as discussed in the next section.

Associated with each failure scenario is a measure of damage demand and a measure of consequences to the form of the system. Damage demand is related to the weighting parameter, w , describing the form of a link. Consequences are considered at two levels – firstly, to the form of the system itself and secondly, to the wider system including other interconnected systems. The former will be referred to as separation and it is measured by the ratio of the change in well-formedness due to damage to the well-formedness of the whole intact system. Total separation occurs when the system becomes completely disconnected from a reference cluster. The reference is that part of the meta-system which acts as a source or a sink. For

example in structures the reference is usually the ground (but may be a particularly important or sensitive part of a structure) and the points of contact are the supports. A transport network will potentially have many reference clusters where the traffic originates or arrives.

The susceptibility of a system to disproportionate consequences in the event of damage or failure is measured using a vulnerability index. This is the ratio of the consequences to the relative damage demand. Thus the higher the vulnerability index the more vulnerable a system. Because both consequences and relative damage demand are non-dimensional numbers, the vulnerability index can be used to compare the form of different systems.

Table 1. Parameters contributing to the form of different systems

<i>Attribute</i>	<i>Electrical circuits</i>	<i>Structures</i>	<i>Traffic</i>	<i>Water pipes</i>	<i>Organisations</i>
<i>Across variable (Potential)</i>	Voltage (V)	Velocity (\dot{x})	Need (v)	Pressure difference (h)	Driver of need & purpose
<i>Through variable (Flow)</i>	Current (I)	Force (F)	Flow (f)	Flow (Q)	Flow of change
<i>Dissipative component R</i>	Resistance $V = RI$	Damping $F = c\dot{x}$	Resistance to movement	Resistance to flow	Dissipation of energy / conflict
<i>Across storage component C (Accumulation)</i>	Capacitance $I = C \frac{dV}{dt}$	Mass (Inertia) $F = m\ddot{x}$	Parking	Internal reservoir	Message passing time / inertia
<i>Through storage component L (Delay)</i>	Inductance $V = L \frac{dI}{dt}$	Flexibility (Inverse of Stiffness) $F = kx$	Length of link	Length of link	Response time / delay
<i>Weighting parameter describing form of a link (w)</i>	Impedance	Stiffness	Transmittance (ease of flow)	Transmittance (ease of flow)	Impedance

Likelihood of failure scenarios and risk calculation

The likelihood of a failure scenario with the potential to cause large consequences can be estimated by considering all conceivable combinations of actions on the system that may contribute to that scenario. The assessment of the likelihood of a failure scenario is made by choosing (a) a measure of the evidence that an action is likely to cause damage, (b) a measure of the confidence in that assessment and (c) a measure of the likelihood (importance) of that action irrespective of the degree of damage it may cause.

The above measures can be either numeric or linguistic. Where the actions are quite precisely known (e.g. dead load) single point values may be appropriate. For actions with large uncertainties (e.g. wind load) stochastic parameters or interval numbers can be used to assess extremes. For actions such as accidental damage or sabotage linguistic grades for damage may be the best that can be done. But these linguistic descriptions can be mapped to an interval number using various schemes which recognise and help decision makers to manage incompleteness (Dester and Blockley, 1997, Blockley, Godfrey 2000).

In summary risk is the combination of the chance and consequences of an event in a stated context. Vulnerability analysis gives the relative size of the consequences of damage to the effort of producing that damage no matter the chance of it happening. The assessment of likelihood of a failure scenario combined with the vulnerability index gives a measure of risk to the form of the system. Clearly, this risk may be part of a wider risk assessment and managed within that wider system.

Example applications

Structures

The function of a structure is to transmit forces between points in space in an acceptable manner. A consideration of form is as essential to structural integrity as it is to other attributes such as aesthetics. Indeed in some modern structures there may be an uneasy tension between the architectural aesthetic and the engineering functional requirements of form. This highlights the need for better methods for analysing structural form to avoid unintended vulnerabilities. A load path is defined by a structural ring which, by its configuration, is capable of resisting an arbitrary set of applied forces. For a pin-jointed structure, a ring has three members and this ring in itself is just one load path. A structural ring fails if it cannot carry any forces i.e. when it becomes a mechanism. The quality of its form is a function of the member properties, their orientation and connectivity. This quality, called well-formedness Q , is obtained using the stiffness sub-matrices k_{ij} associated with the joints in a structural ring i.e. $Q = \frac{1}{N} \sum \det(k_{ij})$ where $i=1, 2, \dots$, number of joints N . Any reduction in the well-formedness of a ring indicates damage to the structure.

Structural vulnerability analysis has been extensively reported (Lu et al 1999; Agarwal et al, 2001, 2003). Primitive structural rings made up of joints and members at the first and familiar level of definition of a structure are first identified. Structural clusters are then grown by including the neighbouring members according to a well-defined algorithm. The final top level cluster is the entire structure. The hierarchy of clusters are then progressively damaged or 'unzipped' by a series of deteriorating events (e.g. introducing a pin into a member) to form various failure scenarios. The analysis concludes by finding failure scenarios that are vulnerable. The algorithms for clustering and unzipping are given in Lu et al (1999), Agarwal et al (2001, 2003) and illustrated through many examples. Fig 2 illustrates the clustering hierarchy for a pin-jointed tower structure. One vulnerable scenario is the failure of member 2 which would obviously cause the whole structure to collapse. Intuitively one might choose member 1 to cause total failure but this requires more effort to cause damage.

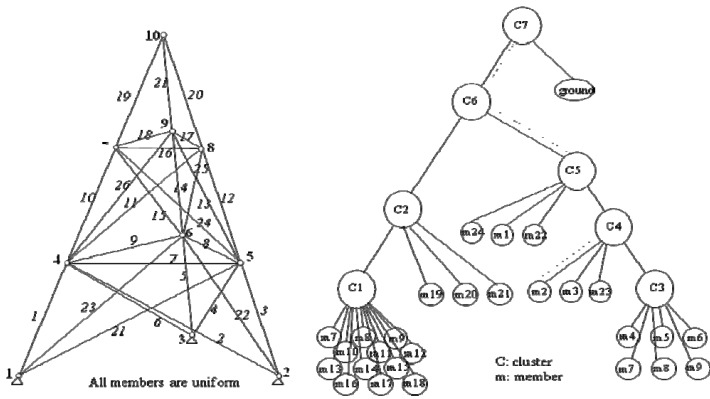


Figure 2. An illustration of clustering and unzipping for a structure

Transport networks

A road network can be represented as a connected, directed, weighted graph. There is traffic potential (i.e. a need to travel) between any two nodes that drives the flow of traffic along links in some way. Usually it is the shortest path between the nodes or the path with the shortest travel time. However, real networks are far more complex and the consequences of the failure of one of more links need to be analysed with respect to the whole system. It is not uncommon to see 'knock-on' effects of the failure of a major road on many minor roads.

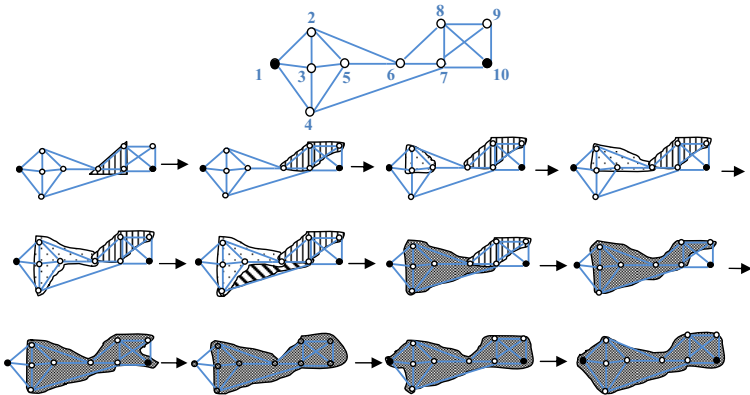


Figure 3. Clustering sequence for a simple transport network

Algorithms for the vulnerability analysis of road networks using the systems approach described above are currently being developed. A measure of transmittance which depends on capacity speed and length and orientation is used to calculate well-formedness. The clustering process starts with the identification of loops with the best well-formedness and higher level clusters are formed by including the neighbouring loops so as to increase the well-formedness of the cluster. If there is no increase in the well-formedness, a new loop is started and the process continued. Figure 3 shows the clustering sequence for a simple network. Here nodes 1 and 10 are reference nodes as population centres and the rest of the nodes are traffic junctions. The cut set (9-10,8-10,7-10) is the total and maximal failure scenario.

Conclusion

A system is vulnerable if any damage produces disproportionately large consequences. Vulnerability together with threat can produce high risks. If there is no identified action that might trigger the vulnerability then it is a hazard rather than a risk. However in any real situation an unintended, unforeseen or unanticipated action may occur and the vulnerability triggered. In other words the combination of an active threat and the vulnerability creates a real risk to the system and its users but an unforeseen vulnerability to an unanticipated action creates a potential incompleteness in a risk analysis that cannot be disregarded. To manage such risks, a vulnerability and risk analysis framework has been outlined where vulnerabilities present in a system are identified through an analysis of form and connectivity. The management of incomplete risks requires systems of monitoring and control which is beyond the scope of this paper.

Vulnerability analysis as described proceeds by clustering constituent parts of a system according to their well-formedness until the whole system is one cluster. A search through the clustering hierarchy leads to an identification of vulnerable scenarios. For structural systems, the approach is well-developed and current work is leading to the development of the approach for road networks. The approach is generic to any system that can be modeled using a graph.

References

- Agarwal, J., Blockley, D.I. and Woodman, N. J. (2001) Vulnerability of Systems, *Civil Engrg & Env Systems*, 18, 141-165.
- Agarwal, J., Blockley, D.I. and Woodman, N.J. (2003) Vulnerability of Structural Systems, *Jnl of Structural Safety*, 25, 263-286.
- Blockley, D. I. and Godfrey, P. (2000) *Doing it Differently*, Thomas Telford.
- Dester, W. S. and Blockley, D. I. (1997) Hazard Assessment: The Representation and Analysis of Evidence of Hazard, *Proc. of ICOSAR'97*, Kyoto, Japan.
- IPPR (2009) *Shared responsibilities: A national security strategy for the UK*, London, IPPR.
- Lu, Z., Yu, Y., Woodman, N. J. and Blockley, D. I. (1999) A Theory of Structural Vulnerability, *The Structural Engineer*, 77, 17-24.
- Shearer, J. L., Murphy, A. T., Richardson, H. H. (1967) *Introduction to System Dynamics*, Addison-Wesley.

System Reliability Analysis of Fatigue-induced Sequential Failure

Young-Joo Lee¹ and Junho Song²

¹University of Illinois at Urbana-Champaign, Newmark Civil Engineering Laboratory, Room 3148, 205 N. Mathews Ave., Urbana, IL 61801; PH (217) 418-9011; email: ylee74@illinois.edu

²University of Illinois at Urbana-Champaign, Newmark Civil Engineering Laboratory, Room 2207, 205 N. Mathews Ave., Urbana, IL 61801; PH (217) 244-9307; FAX (217) 265-8040; email: junho@illinois.edu

ABSTRACT

Various structural systems are subjected to the risk of fatigue-induced failures. If such structural systems do not have an adequate level of redundancy, local failures may initiate sequential failures toward system-level failures. In order to analyze the reliability of fatigue-induced sequential failures of such structures, the **Branch-and-Bound** method employing system reliability **Bounds** method (termed as B^3 method) was recently developed. Using a disjoint cut-set formulation, the B^3 method identifies critical sequences of fatigue-induced failures in the decreasing order of their likelihood as it systematically updates both lower and upper bounds on the system failure probability without additional system reliability analyses. The updated bounds provide reasonable criteria for terminating the B^3 analysis without missing critical sequences or estimating the system-level risk inaccurately. However, the original B^3 method is not readily applicable to continuum structures because of its limitations in describing general stress distributions in limit-state formulations, evaluating stress intensity range based on the crack length, and dealing with slow convergence of the bounds for structures with high redundancy. In this paper, the B^3 method is generalized to overcome these limitations, and demonstrated by a numerical example of aircraft longeron structure.

1 INTRODUCTION

Various structural systems such as aircraft, bridges and offshore structures are often subjected to the risk of fatigue-induced failures caused by repeated loading during their life cycle. Such structural systems should be designed and maintained such that they keep an adequate level of structural redundancy to prevent local fatigue-induced failures from progressing toward system collapse. For risk-informed structural design and maintenance of such structural systems, it is thus essential to quantify the risk of fatigue-induced sequential failures toward system level failures such as collapse.

Monte Carlo simulation is the most straightforward method to deal with such problems; however, when structural analysis demands time-consuming computational simulations or when the probability of system-level failure is low, the computational time costs required for converged results can be exceedingly high. A variety of non-sampling-based methods were thus developed, many of which employ the branch-

and-bound (B&B) method (Murotsu 1984) to identify critical failure sequences efficiently through an event-tree type search. Despite many research efforts, existing B&B based approaches are still either time-consuming or prone to miss critical failure sequences.

In order to overcome these challenges, a new **Branch-and-Bound** method employing system reliability **Bounds** method (termed as B^3 method) was proposed (Lee & Song 2010a, b). Unlike other existing B&B based approaches, the B^3 method identifies disjoint failure sequences in order to (1) obtain *both* the lower and upper bounds of the system risk; (2) achieve monotonic decrease in the updates of the lower bounds as the search process proceeds; and (3) update the bounds of the system risk without performing additional system reliability analyses. The updated bounds provide reasonable criteria for terminating the B&B search without missing critical sequences or estimating the system-level risk inaccurately. The B^3 method has been successfully demonstrated by examples of a multi-layer Daniels system (Lee & Song 2010a) and a three-dimensional truss structure (Lee & Song 2010b).

However, most of the existing studies on the risk quantification of fatigue-induced sequential failure focus on relatively simple *discrete* structures such as truss, and there have been few studies on risk quantification of more complex continuum structures. Despite the abovementioned merits, the original B^3 method still has the following limitations in the risk quantification of fatigue-induced sequential failures of continuum: (1) far-field stress, a basic parameter in the fatigue crack growth formulation of the B^3 method, is not conspicuous for a continuum in general; (2) it is not always feasible to derive an analytical relationship between the stress intensity range and the crack length using so-called geometry function for a continuum having complex stress distribution; and (3) structural complexity of a continuum often results in many dominant failure sequences with a similar level of likelihood, which prevents fast convergence of the lower and upper bounds during the B^3 analysis.

In order to overcome these challenges, this paper generalizes the B^3 method in three phases: (1) the limit-state function is modified to deal with a general stress distribution instead of a far-field stress; (2) an external computer program is integrated with the B^3 computational framework to estimate the stress intensity range with the general stress distribution without relying on analytical geometry function; and (3) an additional search termination criterion is introduced for efficient system reliability analysis of a continuum. In this paper, the B^3 method introduced in Lee & Song (2010a, b) is termed as the “original” B^3 method while the approach presented in this paper is referred to as the “generalized” B^3 method.

2 GENERALIZED BRANCH-AND-BOUND METHOD EMPLOYING SYSTEM RELIABILITY BOUNDS (B^3 METHOD)

2.1 Generalization I: limit-state function formulations for general stress distribution.

First, consider the following crack-growth model (Paris & Erdogan 1963):

$$\frac{da}{dN} = C(\Delta K)^m \quad (1)$$

where a denotes the crack length, N is the number of load cycles, C and m are the material parameters, and ΔK denotes the range of the stress intensity factor. In the

original B³ method, the stress intensity range is evaluated by an analytical function of far-field stress and crack length, i.e. by Newman’s approximation (Newman & Raju 1981). In order to deal with structures under general stress distribution, however, the generalized B³ method does not rely on Newman’s approximation in formulating the limit-state function for crack failures. Integrating Equation 1 from the initial condition to the current time point, the relation between the time duration T and the corresponding crack length a is derived as

$$\int_{a_0}^a \frac{1}{[\Delta K]^m} da = C \cdot N = C \cdot v_0 \cdot T \tag{2}$$

where a_0 is the initial crack length, and v_0 is the loading frequency. At the i -th component, a crack failure is assumed to occur when the crack exceeds a critical length a_{ci} . Then, the limit-state function for the component’s failure within an inspection cycle $[0, T_s]$ is described as

$$g_i(\mathbf{X}) = T_i^0 - T_s \leq 0, \text{ where } T_i^0 = \frac{1}{C v_0} \int_{a_i^0}^{a_{ci}} \frac{1}{[\Delta K]^m} da \tag{3}$$

where a_i^0 is the initial crack length of the i -th component, T_i^0 is the time required for the crack growth from a_i^0 to a_{ci} , and \mathbf{X} denotes the vector of random variables. In order to describe the failure sequences as *disjoint* events in the B&B search, we first formulate the case in which the i -th component fails before failures at any other components. The probability of this system event is described as

$$P_i = P \left\{ \left[\bigcap_{\forall j \neq i} (T_i^0 < T_j^0) \right] \cap (T_i^0 < T_s) \right\} \tag{4}$$

The event in Equation 4 is a parallel system event consisting of n component events. The probability can be computed by component reliability analyses of the n events and a subsequent system reliability analysis. Similarly, the probability of a general failure sequence $\{1 \rightarrow 2 \rightarrow \dots \rightarrow (i-1) \rightarrow i\}$ is described as

$$P_i^{1, \dots, (i-1)} = P \left\{ \left[\bigcap_{\forall j \neq 1} (T_1^0 < T_j^0) \right] \cap \left[\bigcap_{\forall k \neq 1, 2} (T_2^1 < T_k^1) \right] \cap \dots \cap \left[\bigcap_{\forall l \neq 1, \dots, i} (T_i^{1, \dots, (i-1)} < T_l^{1, \dots, (i-1)}) \right] \right. \\ \left. \cap (T_1^0 + T_2^1 + \dots + T_i^{1, \dots, (i-1)} < T_s) \right\} \tag{5}$$

where $T_i^{1, \dots, (i-1)}$ denotes the time required for the failure at the i -th component since the sequential failure $\{1 \rightarrow 2 \rightarrow \dots \rightarrow (i-1)\}$. Unlike T_i^0 in Equation 3, i.e. the time until the first failure for an undamaged structure, the time terms introduced for damaged structures (such as $T_i^{1, \dots, (i-1)}$ in Equation 5) should be computed with the effects of load redistributions considered. For efficient evaluation of the limit-state functions during component reliability analyses, a recursive formulation is derived for a general failure sequence $\{1 \rightarrow 2 \rightarrow \dots \rightarrow (i-1) \rightarrow i\}$ as

$$T_i^{1,\dots,j-1} \approx \frac{1}{Cv_o} \int_{a_i'}^{a_i} \frac{1}{[\Delta K_i^{1,\dots,j-1}]^m} da - \sum_{k=1}^{j-1} \int_{a_i'}^{a_i} \frac{1}{[\Delta K_i^{1,\dots,k-1}]^m} T_k^{1,\dots,k-1} \quad (6)$$

where $\Delta K_i^{1,\dots,j-1}$ denotes the range of the stress intensity factor at the i -th component after the occurrence of the failure sequence $\{1 \rightarrow 2 \rightarrow \dots \rightarrow (i-1) \rightarrow i\}$. The details of the derivation are available in Lee & Song (2011). Although an approximation was made for efficiency, a numerical example showed that the impact of the approximation is negligible.

2.2 Generalization II: evaluating stress intensity range using external software

The generalized limit-state function formulation in Equation 6 makes it necessary to compute the range of stress intensity factor ΔK along crack length a for complex stress distributions, which cannot be described by a far-field stress in general. Among a variety of existing computer programs and methods, AFGROW® (Harter 2006) is used to find the a - ΔK relation in this research. AFGROW® provides Component Object Model (COM) Automation interfaces that allow users to control AFGROW® in other Windows applications such as MS Excel®. Figure 1 (left) illustrates the computational framework of the generalized B³ analysis in this paper. The main B³ analysis code in MATLAB® repeatedly calls ABAQUS® to obtain the stress distribution from the Finite Element (FE) analysis for given Random Variables (RVs) and damage conditions, and the stress distribution is transferred to AFGROW® for estimating the corresponding stress intensity range along crack length, which is the basic information for the estimation of the limit-state function in Equation 6.

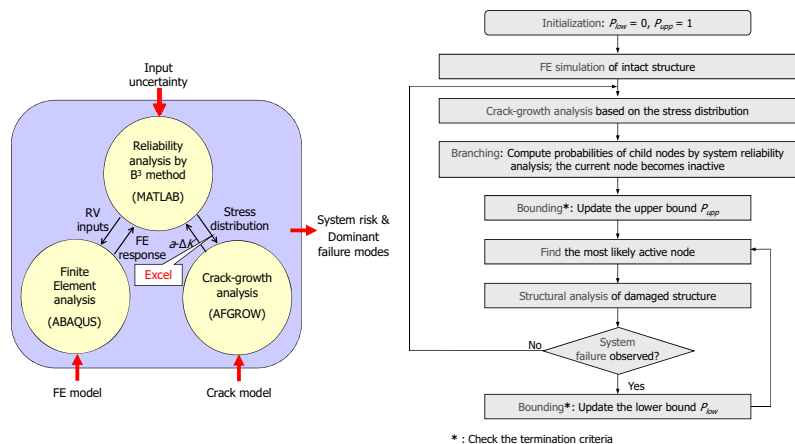


Figure 1. Computational framework of the generalized B³ method (left) and flow chart of the generalized B³ method (right).

2.3 Generalization III: additional termination criterion for systematic search scheme.

The systematic search scheme of the generalized B^3 method is identical to that of the original B^3 method except for an additional analysis termination criterion and the crack-growth analysis process described in Section 2.2. Figure 1 (right) illustrates the search procedure by a flow chart. The search starts by setting the lower and upper bounds of the system failure probability (denoted by P_{low} and P_{upp}) as zero and one, respectively. These bounds are continuously updated as the search process identifies cases of system failures and non-failures and computes their probabilities.

After performing the first FE analysis and crack-growth analysis, the first child nodes are branched out from the initial node and their probabilities in Equation 5 are calculated. As suggested in the original B^3 method (Lee & Song 2010a, b), we use the First-Order Reliability Method (FORM) and the Second-order Reliability Method (SORM) for component reliability analyses (Der Kiureghian 2005). For the parallel system reliability analysis, we use a multivariate normal integral method by Genz (1992), which enables us to calculate the probabilities of large-size parallel systems accurately and efficiently. Based on the probability calculations, the first bounding is made and P_{upp} is decreased by the probability of the newly-identified non-failure case.

The next step is to compare all the nodes except for system-failure, non-failure, and “parent” nodes for selecting the one with the highest probability. Then, a new FE analysis is performed using an FE model reflecting the damage scenario of the selected node. If the FE analysis reveals that the selected node represents a system failure case, P_{low} is increased by the probability of the node. On the other hand, if the FE analysis reveals that a system-level failure does not occur, another crack-growth analysis and branching process are performed to find the probabilities of child nodes originating from the selected node.

This repeated process of “branching” and “bounding” is continued until the following termination criteria are satisfied. If finding the most critical paths is the main interest, one can terminate the search process when the most recently identified system failure sequence has a probability lower than a given threshold or the required number of identified failure sequences is satisfied. This is because the systematic search scheme guarantees finding the failure modes in the decreasing order of their likelihood. On the other hand, if risk quantification (RQ) of system failure is of interest, one can terminate the process when the gap of the bounds or the contribution of the newly-identified failure sequence is negligible compared to the overall risk level identified by the bounds. In the generalized B^3 method, it is proposed to terminate the search process for RQ if any of the following conditions is satisfied:

- gap of two bounds / upper bound $< \varepsilon_1$
- lower-bound increment / upper bound $< \varepsilon_2$

where ε_1 and ε_2 are predetermined values that are fairly small compared to 1.0, which define the convergence level of a particular analysis. For the numerical example in this paper, $\varepsilon_1=0.05$ and $\varepsilon_2=0.001$ are used. In the original B^3 method, only the first convergence condition was considered as termination criterion for RQ, which worked well in verification examples of discrete structures such as a three dimensional truss structure. However, more complex structures with higher level of structural

redundancy tend to have many competing failure sequences with similar likelihood. For the risk analysis of such structures, it may require a huge number of searches and structural analyses to satisfy the first criterion. The second criterion is thus introduced to identify whether the speed of the convergence becomes too slow so that one can avoid continuing search process that does not update the bounds significantly. The performance of the newly-suggested termination criteria are tested and compared to that of the old criteria in the following numerical example.

3 NUMERICAL EXAMPLE: AIRCRAFT LONGERON

In order to test the applicability of the proposed method to continuum structures, let us consider an aircraft longeron system, which is a non-discrete structural system with higher level of complexity compared to truss-type structures. A longeron is a thin strip of metal, wood, or carbon fiber, to which the skin of the aircraft is fastened, and it has been widely used in many studies of the risk analysis of fatigue-induced sequential failures for the following advantages: First, despite their structural complexity, it is easy to identify “hot spots” that have relatively high stresses, which are generally located around fasteners. Second, local failure of a fastener can be described as the event that its crack length exceeds a critical level. Lastly, it is relatively simple to reflect the failure of the identified component in the FE model.

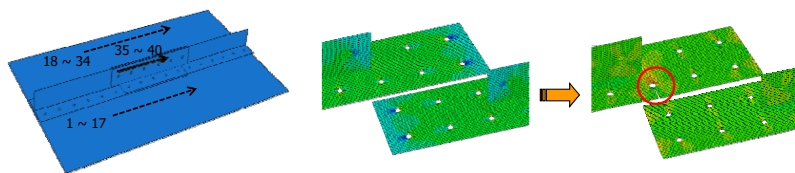


Figure 2. Longeron FE model (left); and the load-redistribution after a local failure (right).

3.1 Structural configuration and loadings

Figure 2 shows an FE model of longeron system developed in ABAQUS® and one example of the load redistribution caused by local failure(s) (red circle). A big plate on the bottom is a part of the aircraft skin, and the assembled structure along the center line represents the longeron. It is assumed that the main material of the skin and longeron is aluminum. All the parts are attached together by 0.25-inch diameter fasteners, which are made of steel and simulated by spring elements. The total number of fastener holes is 40, and their numbering choice is displayed in Figure 2 (left). Assuming the longeron system is located in an upper fuselage under bending caused by vertical acceleration, the system is subjected to pure tension/compression loads, which cause an initial crack of around each fastener hole to grow from hole to the nearest edge. The loading frequency (ν_0), the inspection cycle (T_i), and the critical crack lengths are given as 60/hour, 2,000 hours, and 12.7mm, respectively. These parameters are assumed to be deterministic.

3.2 Statistical parameters and component/system failure definitions

This example deals with the following random variables to represent the uncertainties: (1) C (mean: 1.202×10^{-13} , c.o.v.: 0.533, Lognormal distribution); (2) m (mean: 3.0, c.o.v.: 0.02, Lognormal distribution); (3) initial crack length a_i (mean: 0.11 mm, c.o.v.: 1.0, Exponential distribution); and (4) external load intensity I (mean: 103 MPa, c.o.v.: 0.1, Lognormal distribution). These statistical parameters were determined based on a comprehensive literature survey performed by Lee & Song (2010b). In this example, one random variable I is used to describe the uncertainty in the loading, and each of 40 fastener holes has one random variable of a_0 . In addition, based on findings from preliminary FE analyses, the hot spots around all fastener holes are located on the two center parts shown in Figure 2 (right). For that reason, two random variables are assumed to represent C and m for each part. Therefore, a total of 45 random variables are used. All random variables are assumed to be statistically independent of each other except the following cases for which non-zero correlation coefficients are assigned: (1) between parameters (C) of two different parts (correlation 0.6); (2) between parameters (m) of two different parts (correlation 0.6); (3) between initial crack lengths (a_0) of two different fastener holes (correlation 0.6); and (4) between C and m of two different or the same parts (correlation -0.2).

In addition, it is assumed that the section around a fastener hole fails when its crack length reaches its critical crack length. Upon the occurrence of such section failure, the corresponding crack is embodied in the FE model, which causes stress redistribution. As an attempt to accurately identify system failure cases via FE analyses instead of heuristic criteria, in this example, it is assumed that the structural system fails if any local yielding occurs in the system. The yield strengths of aluminum or steel are given as 289.4 and 496 MPa, respectively. It should be noted that this is an example of system failure criteria that can be used during a B^3 search. One can introduce a set of his/her own system failure criteria based on the objectives and safety concerns of a target structure.

3.3 Analysis results

With the new termination criteria described in Section 2.3, the lower and upper bounds are respectively 1.400×10^{-3} and 1.563×10^{-3} after only 151 FE simulations. With the old criteria, however, both bounds are respectively 1.469×10^{-3} and 1.546×10^{-3} for 458 FE simulations. It was already proved that the actual system risk is closer to the upper bound rather than the lower bound (Lee and Song 2010a, b). Without no significant update in the upper bound, the old criteria requires 5 more days to perform more than 300 FE simulations. This additional computational time is consumed mostly for identifying many negligible failure sequences and updating the lower bound slightly. This is because the longeron system has many competitively similar failure sequences.

In addition, the critical failure sequences are identified in the decreasing order of their likelihood. Some of the major patterns (1st, 3rd, and 4th) are listed in Table 1. In the table, we can observe various system failure modes on different locations and materials. It is also noteworthy that each of the identified failure sequences has another failure scenario with the exactly same probability due to the symmetry of the longeron around its center line.

Table 1. Critical failure sequences of longeron system

Failure sequences	Probability ($\times 10^{-4}$)	Yielding material & location (S: steel, A: aluminum)
5 (or 22)	2.607	S yielding at #35 fastener
23 \rightarrow 5 (or 6 \rightarrow 22)	0.743	S yielding at #35 fastener
23 \rightarrow 4 (or 6 \rightarrow 21)	0.336	A yielding at around #23 (or #6) hole

4 SUMMARY AND CONCLUSIONS

In this paper, the Branch-and-Bound method employing system reliability Bounds (the B^3 method) is generalized in order to overcome limitations in risk analysis of continuum structures. To achieve this goal, (1) the limit-state function was modified to deal with general stress distribution instead of far-field stress; (2) an external computer program such as AFGROW® was incorporated into the B^3 computational framework to estimate the stress intensity range with the general stress distribution; and (3) the termination criteria of B^3 analysis was modified to avoid unnecessary simulations. The proposed method was applied to an example of aircraft longeron system. The merits of the proposed approach were successfully demonstrated.

REFERENCES

- Der Kiureghian, A. (2005). "First- and Second-order Reliability Methods." *Engineering Design Reliability Handbook*, edited by E. Nikolaidis, D.M. Ghiocel, and S. Singhal, Chap. 14. Boca Raton, FL: CRC Press.
- Genz, A. (1992). "Numerical computation of multivariate normal probabilities." *Journal of Computational and Graphical Stat.*, 141-149.
- Harter, J.A. (2006). "AFGROW user guide and technical manual." *AFRL-VA-WP-TR-2006-XXXX*. WPAFB, OH: Air Force Research Laboratory.
- Lee, Y.-J. and Song, J. (2010a). "Risk analysis of fatigue-induced sequential failures by branch-and-bound method employing system reliability bounds." *IFIP WG7.5 Working Conference on Reliability and Optimization of Structural Systems*, April 7-10, Munich, Germany.
- Lee, Y.-J. and Song, J. (2010b). "Identification of critical sequences of fatigue-induced failures by branch-and-bound method employing system reliability bounds." *Proc. 12th AIAA NDA Conference*, April 12-15, Orlando, FL.
- Lee, Y.-J. and Song, J. (2011). "Risk quantification of fatigue-induced sequential failures by branch-and-bound method employing system reliability bounds." *Proc. 11th International Conference on Applications of Statistics and Probability in Civil Engineerin.* August 1-4, ETH Zurich, Switzerland.
- Murotsu, Y. (1984). "Automatic generation of stochastically dominant modes of structural failure in frame." *Structural Safety*, 2(1), 17-25.
- Newman, J.C. and Raju, I.S. (1981). "An empirical stress intensity factor equation for the surface crack." *Engng. Fract. Mech.*, 15, 185-192.
- Paris, P.C. and Erdogan, F. (1963). "A critical analysis of crack propagation laws." *J. Basic Eng.*, Trans. ASME., 85, 528-534.

Sample Treatment of Uncertainties in Earthquake Portfolio Risk Analysis

By

Craig Taylor¹, William Graf², Yajie (Jerry) Lee³,
Charles Huyck⁴, and Zhenghui Hu⁵

¹ AffM. ASCE, Research Director, Baseline Mgmt. Co. Inc. and Research Professor, USC, 5402 Via Del Valle, Torrance, CA 90505, cetaylor@earthlink.net

² M. ASCE, Associate, URS Corporation; 915 Wilshire Blvd., Ste 700; Los Angeles, CA 9017, william_graf@urscorp.com

³ Senior Risk specialist, URS Corporation, 915 Wilshire Blvd, Ste 700, Los Angeles, CA 90017; jerry_lee@urscorp.com

⁴ Executive Vice President, Imagecat, Inc., Union Bank of California Bldg., 400 Oceangate Ste 1050, Long Beach, CA 90802, USA, ckh@imagecatinc.com

⁵ Systems Analyst, Imagecat, Inc., Union Bank of California Bldg., 400 Oceangate Ste 1050, Long Beach, CA 90802, zh@imagecatinc.com

ABSTRACT

Previous papers and presentations by the authors have proposed that robust simulation should be used to define uncertainties in catastrophe risk analyses for portfolios and/or systems. Robust simulation begins with a “preferred” comprehensive model that turns out to be comprised of non-unique solutions for many technical issues. Uncertainties in this “preferred” model can be estimated either endogenously, that is, through alternative distributions used in the simulation process, or exogenously, through alternative comprehensive model simulations. This paper elucidates how these uncertainties are estimated through the examination on the one hand of available earthquake hazard models and (e.g., GMPE, kinematic) and selected uncertainties (e.g., directivity, focal depth), and on the other hand of available building vulnerability models (statistical, opinion-based, engineering) and selected uncertainties (e.g., structural period, strength, ductility). The goal of this paper is thus to define more clearly what count as “alternative credible models” and how they may be used to estimate uncertainties in the resulting portfolio loss distributions.

BACKGROUND

In recent years, the overarching question “How does one account for uncertainties in catastrophe risk analysis?” has become more prominent. Within traditions of statistical and probability theory, the narrow tradition of using the distinction between “epistemic” and “aleatory” uncertainty has been demonstrated to yield considerable incoherence. Endogenous or nominal uncertainties account for uncertainties given the models used, but not those uncertainties resulting from the use of alternative models (parameters, data, or assumptions).

The practice in several major disciplines—long-term policy analysis, global climate change, climate conditioning for hurricane prediction, missile risk analysis, and earthquake portfolio analysis, provides a key to how to address this overarching question. Robust simulation methods permit several alternative accounts to be evaluated as precisely and coherently as they permit. The diverse answers that these alternative accounts produce can be used to serve as the uncertainty as currently understood. This approach to the overarching question, and the question itself, both assume that there must be alternative credible solutions, that is, acceptable alternative models, assumptions, parameters, or data. (See Taylor et al., 2010 and cited documents.)

For earthquake portfolio risk analysis, the minimum suite of models includes those for exposure data, those of hazards, and those for buildings, contents, and downtime. This paper briefly covers these types of models in the context of a validation study of commercial and multi-family dwelling and to illustrate how—as is common—many alternative credible models can be found even as one seeks a “preferred” model.

This paper first illustrates how non-unique approaches and solutions are ubiquitous in defining earthquake hazard models, and numerous credible ones are available. Next, validations of existing loss models clarifies not only uncertainties in hazards, but also in exposures and buildings as well.

Alternative Credible Models for Earthquake Hazards

Earthquake hazard models cover sources and rates of occurrence, the transmission and distribution of seismic waves, and ground deformations resulting from rupture and response of local ground conditions to incoming seismic waves.

Earthquake source models may be point-source (epicenter, hypocenter, center-of-energy release) or planar. The latter may be restricted to accounting for dip angle, focal depth, fault width, fault length, magnitude, and strike angle, or may include additional elements as in the case of kinematic modeling. In the broadband simulation approach used by Graves and Pitarka [2010, in press], many more variables must be included (e.g., fault rupture speed and pattern, stress drop, asperities). Additionally, rates of occurrence may consider some combination of (a) time-independence, ignoring only foreshocks and aftershocks (b) cyclical “strain build up” models for characteristic earthquakes, and/or (c) clustering of major earthquakes resulting from near-term transfer of strains to fairly local fault zones as a consequence of a major earthquake. (see Jackson and Kagan, 1996; Rundle et al., 2006; Petersen et al., 2008)

Models of transmission and distribution of earthquake strong ground motion waves as embodied in ground motion prediction equations (GMPE) have been discussed in the “Next Generation Attenuation” (NGA) project as discussed for instance by Stewart and Archuleta (2008). Different teams of investigators were provided with

the same enlarged database. Yet, for a large number of reasons, these diverse teams with diverse model requirements did not first of all necessarily use the same dataset for their modeling and did not arrive at the same results. As a general rule, the numerous different theories that exist in modeling earthquakes and their strong ground motions yield from somewhat to very divergent results. Controversies over site amplification effects exist as for instance questions have arisen concerning the validity of using average shear wave velocity for the first 30 meters of depth.

Thus, one can find in models of earthquake sources, rates of occurrence, the transmission and distribution of waves, and even permanent deformations alternative models that arise out of credible efforts. No models appear to be absolutely decisive; some may have specific advantages over others, but have some disadvantages as well. For instance, the use of a “directivity” parameter in strong ground motion attenuation functions may have advantages after earthquakes, but may require more speculations before them.

Alternative Credible Models for the Seismic Vulnerability of Buildings

Alternative credible models for the seismic vulnerability of buildings can be drawn from a number of sources:

1. Opinion-based models. These are heuristic models based on expert opinion. An example is ATC-13, which predicts damage to general classes of building as a function of ground shaking intensity (MMI).
2. Historical performance. Anecdotal accounts of damage to various classes of buildings in earthquakes may be available, and sometimes limited conditional statistics are also found. (Unconditional statistics require the same level of information about the undamaged structures as the damaged ones). Even where sound statistics may have been compiled (e.g., Wesson et al, 2005), these may not be directly relevant, if the buildings we wish to model were built to recent (and presumably better) seismic building codes, while the statistics relate to older structures, built in a specific time and place, representing local design, construction and inspection practice.
3. Analytical design models (e.g.: SAP2000, RISA, ETABS, PERFORM-3D). These analytical models usually represent the major structural elements in an explicit way. They range from linear elastic models to nonlinear inelastic, with the earthquake demands represented as equivalent static forces, spectral demands or acceleration time histories. Engineering design models are usually more expensive and time-consuming to construct, requiring complete design documents. The outputs include stresses and strains, accelerations and displacements, but usually not repair costs, casualty counts or downtime. These models are often deployed in forensic studies of damage, or in detailed study of index buildings for the calibration of engineering risk models (see below). These models serve to improve our understanding of the structural

characteristics associated with damage (weakness, excessive flexibility, irregularity in plan and height, lack of ductility, etc.).

4. Engineering risk models. These models may use physics-based principles, but they often make radical simplifications and abstractions. Current models (e.g., HAZUS-MH, or Assembly-Based Vulnerability [Porter et al, 2002]) are only partially calibrated. Engineering risk models may include some set of rational parameters, while excluding others, and the parameters are adjusted to suit the particular structure(s) in question. Another concern is the range of cases within the competency of such models. For instance, HAZUS uses a single-degree-of-freedom representation of the building's structure and so is not fully competent for high-rise construction, which necessarily involves multiple modes of vibration.

As an example of the difference between these classes of models, we can compare damage models for wood-frame residential construction in California. The figure below plots mean damage factor (repair cost as a fraction of building replacement value) as drawn from ATC-13 (opinion-based), Wesson et al (historical), and HAZUS-MH (Engineering risk).

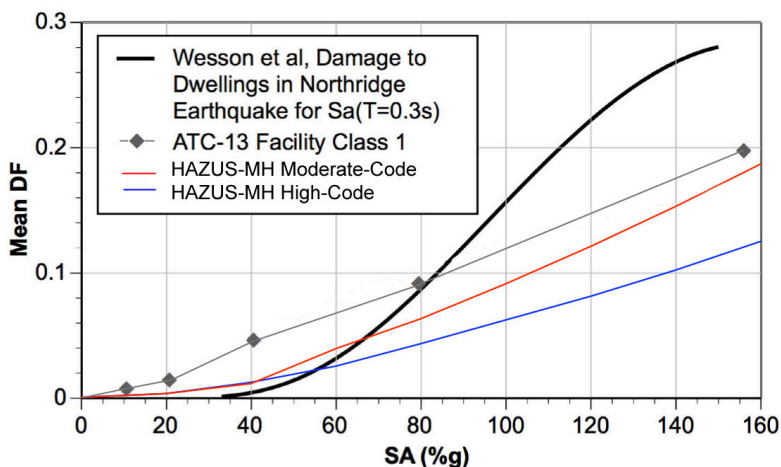


Figure 1 – Comparison of Models Based on Opinion and Statistics with an Engineering Risk Model

Modeling Uncertainties in Seismic Vulnerability

Ideally, all credible models should be considered to span the range of uncertainties, with a “preferred” model being selected as the baseline risk. Often the selection of a preferred model is a practical choice. The selection of the type of model depends largely upon the size of the building inventory, the time and budget available for

modeling, as well as the availability of engineering and exposure data for the buildings under study. Such practical considerations may restrict the set of credible models to simple variants of a single model.

Once the type of structural vulnerability model is selected, the uncertainties need to be managed. Endogenous parameters will have some uncertainty, perhaps modeled by a statistical distribution. Some relevant characteristics may remain completely unknown (e.g., load path discontinuities), and the model will have some scatter even if every endogenous parameter were perfectly known, contributing to some irreducible uncertainty.

At present, we do not dispose of adequate statistical loss data from seismically instrumented buildings to establish “budgets” for the uncertainty in building damage and loss for known (recorded) ground shaking. Limited unconditional data exists for noninstrumented buildings (e.g., Wesson et al, 2005), but these present the added difficulty of estimating the ground shaking and its uncertainty at exposure locations known only by ZIP and extracting valid damage relationships with almost no data on engineering characteristics. For non-instrumented sites, we are confronted with the challenge of segregating the uncertainties associated with ground motion from the uncertainties of building damage given ground motion.

Conclusions

This paper focuses on the sorts of considerations yielding alternative credible models for earthquake hazards and earthquake building vulnerability models. Potential and actual applications of robust simulation for earthquake hazards and risk are widespread. Incoherence in an aleatory/epistemic distinction to yield “total” uncertainty has given rise to the need for a method—as needed—to account for “exogenous” uncertainties. (See Taylor et al., 2009) Other models—macroeconomic, systems, diverse perils—and alternative methods—non-parametric, parametric—produce additional considerations for defining preferred and alternative credible models. The bounds of “exogenous” uncertainties can be identified through the search for an simulation of the credible models most divergent from the “preferred” model.

References

Graves, Robert W. and Arben Pitarka, “Broadband Ground-Motion Simulation Using A Hybrid Approach,” *the Bulletin of the Seismological Society of America*, October, 2010 (in press).

Jackson, D. D. and Y. Y. Kagan, (2006), “The 2004 Parkfield Earthquake, the 1985 Prediction and Characteristic *Earthquakes*: Lessons for the Future,” *the Bulletin of the Seismological Society of America*, Vol. 96, No. 4B, pp. S397-S409, September.

National Institute of Building Sciences and Federal Emergency Management Agency (NIBS and FEMA), 2003. Multihazard Loss Estimation Methodology, Earthquake Model, HAZUS®MH Technical Manual and Users *Manual*, Washington, D.C.

Petersen, Mark D., Arthur D. Frankel, Stephen C. Harmsen, Charles S. Mueller, Kathleen M. Huller, Russell L. Wheeler, Robert L. Wesson, Yuehuan Zeng, Oliver S. Boyd, David M. Perkins, Nicolas Luco, Edward H. Field, Chris J. Wills, and Kenneth S. Rukstales, (2008), *Documentation for the 2008 Update of the United States National Seismic Hazard Maps*, U. S. Department of the Interior, U. S. Geological Survey, Open-File Report 2008-1128.

Porter, K. A., Beck, J. L. and Seligson, H. A., Scawthorn, C. R., Tobin, L. T., Young, R., Boyd, T., 2002. Improving Loss Estimation for Woodframe Buildings. Volume 1 Technical Report and Volume 2 Appendices, Consortium of Universities for Research in Earthquake Engineering, Richmond, CA.

Rojahn, C., 1985. ATC-13: Earthquake Damage Evaluation Data for California, Applied Technology Council, Redwood City, CA.

Rundle, John B., Paul B. Rundle, Andrea Donnellan, P. Li, W. Klein, Gleb Morein, D. L. Turcotte, and Lisa Grant, (2006), *Tectonophysics* 413, 109-125.

Stewart, Jonathan P., Ralph J. Archuleta, Maurice S. Power, (2008), "Special Issue on the Next Generation Attenuation Project," *Earthquake Spectra*, Vol. 24, No. 1, February.

Taylor, C., D. Perkins, R. Murnane, W. Graf, and Y. Lee, (2009), "Epistemic Uncertainty, Rival Models, and Closure," submitted to *Natural Hazards Review*, 3/2009.

Taylor, Craig, Yajie Lee, William Graf, Zhenghui Hu, and Charles Huyck, (2010), "Robust Simulation and Cat Diagnostics for Treating Uncertainties in Catastrophe Risk Analysis," Shanghai, China, International Symposium on Reliability Engineering and Risk Management (ISPERM2010), organized by Tongji University and Kanagawa University.

Wesson, Robert L., Perkins, D. M., Leyendecker, E. V., Roth, R. J., Petersen, M. D., 2004. Losses to single-family housing from ground motions in the 1994 Northridge, California, earthquake, *Earthquake Spectra* 20, No. 3, 1021-1045.

Probabilistic Application in Seismic Vulnerability Assessment of Structures

Mohsen.Javanpour¹, Panam.Zarfam²

¹ M.Sc Structural Engineering,Iran,email:mohsen.javan1982@gmail.com

² Ph.D Structural Engineering, Department of Civil Engineering Islamic Azad University Science and Research Branch Tehran, Iran, email:pzarfam@gmail.com

Abstract

A formal probabilistic framework for seismic assessment of a structural system can be built around the expression for the probability of exceeding a limit state capacity, a measure of the reliability of system under seismic excitations. Common probabilistic tools are implemented in order to derive a simplified closed-form expression for the probability of exceeding a limit state capacity. This closed-from expression is particularly useful for seismic assessment and design of structures, taking into account the uncertainty in the generic variables, structural “demand” and “capacity” as well as the uncertainty in seismic excitations. This framework implements non linear dynamic analysis procedures in order to estimate variability in the response of the structure (“demand”) to seismic excitations. Alternative methods for designing a program of nonlinear analyses and for applying the results of dynamic analysis, particularly as it relates to displacement-based “demand” and “capacity” estimation, are discussed.

Keywords— Dynamic, Nonlinear, Probabilistic, Seismic

Introduction

This paper presents an analytical foundation for probability-based formats for seismic design and assessment of structures. These formats are designed to be suitable for code and guideline implementation. The framework rests on non-linear, dynamic seismic analysis. The formats can be used to ensure that the structural seismic design can be expected to satisfy specified probabilistic performance objectives, and perhaps (more novel) that it does so with a desired, guaranteed degree of confidence. Performance objectives are presumed to be expressed as the annual probability of exceeding a structural performance level. Structural performance levels are in turn defined as specified structural parameters (e.g., ductility, strength, maximum drift ratio, etc.) reaching a structural limit state (e.g. onset of yield, collapse, etc.). The degree of confidence in meeting the specified performance objective may be quantified through the upper confidence bound on the (uncertain) probability. In order to make such statements, aleatory (random) uncertainty and epistemic (knowledge limited) uncertainty must be distinguished. The main goal of this paper provide fundamental and novel method for calculating probability of the vulnerability of structures using statistical distribution is in addition to simply being more efficient, more accurate performance of structures likely to be able to offer us. (Being symmetric is one of the important characteristics of this distribution which should be noted).Logistic distribution was additionally investigated and it was illustrated that this distribution is very much like the Log-Normal distribution from the aspect of statistic specifications. The presented mathematics papers¹ are suggestive of this claim, too.

¹ - Raminta Stockute, Andrea Veaux, Paul Johnson (2006). “Logistic distribution”

Limit State Probability P_{LS}

The final product of the proposed probabilistic procedure is called the probability of exceeding a structural limit state, where the limit state is the condition that, $D > C$. In order to be brief, we will refer to it as the limit state probability P_{LS} . For the case that we are mainly interested in, i.e. the collapse limit state, it is also reasonable to call this quantity the failure probability. Therefore, we seek:

$$P_{LS} = P[D > C] \tag{1}$$

General Solution Strategy

In order to determine $P_{LS} = P[D > C]$, we are going to decompose the problem into more tractable pieces and then reassemble it. First, we introduce a ground motion intensity measure IM (such as the spectral acceleration, S_a , at say 1 second period), because the level of ground motion is the major determinant of the demand D and because this permits us to separate the problem into a seismological part and a structural engineering part. To do this, we make use of a standard tool in applied probability, The Total Probability Theorem (see Appendix B), TPT which permits the following decomposition of P_{LS} with respect to an interface variable (here, the spectral acceleration):

$$P_{LS} = P[D > C] = \sum_{all\ x} P[D > C / S_a = x].P[S_a = x] \tag{2}$$

In Equation (2) we have introduced S_a as the intensity measure. In simple words, the problem of calculating the limit state probability has been decomposed into two problems that we already know how to solve. The first problem to calculate the term $P[S_a = x]$ or the likelihood that the spectral acceleration will equal a specified level, x . This Likelihood is a number we can get from a Probabilistic Seismic Hazard Analysis (PSHA) of the site. The second problem is to estimate the term $P[D > C / S_a = x]$ or the conditional limit state probability for a given level of ground motion intensity, here represented by, $S_a = x$.

Randomness and uncertainty as the sources of variability

The probability-based seismic assessment and design procedure presented here aims to evaluate the probability P_{LS} that the limit state variable exceeds a limit state threshold LS . Our first objective here is to derive the limit state probability assuming that randomness is the only source of uncertainty in the design variables. We will follow the displacement-based solution strategy discussed in previous section. in order to derive the limit state probability. Our objective here is to derive the limit state frequency when there is both randomness and uncertainty in the design variables such as spectral acceleration hazard, drift demand given spectral acceleration and drift capacity. Our derivations are going to be based on the assumption that to a first approximation we can represent all the epistemic uncertainty in variable X by the uncertainty in its median. The model becomes:

$$X = \hat{\eta}_x \varepsilon_\eta \varepsilon_x \tag{3}$$

Where $\hat{\eta}_x$ is the current point estimate of the median of X , the unit-median random variable ε_η represents the epistemic uncertainty as to the true value the median of X , and the unit-

median random variable ε_x represents the aleatory randomness of X. We are also going to assume that the deviation from median ε_n , can be properly modeled by a Lognormal distribution. In general, of course, the epistemic uncertainty in β_x should also be taken into account. Also, the shape of the distribution of may not be Logistic.

Spectral Acceleration Hazard

The hazard curve estimation involves many scientific assumptions (see Kramer 1996). In other words there is uncertainty in the evaluation of a hazard curve. That’s why spectral acceleration hazard curves are normally provided as mean and 84th percentile hazard curves (As shown in Figure 1). Here we are going to take into account the uncertainty in the evaluation of the spectral acceleration hazard. In the previous sections, we found it advantageous to approximate the hazard curve by a power-law relationship as proposed by Kennedy and Short (1994) and Luco and Cornell (1998):

$$\begin{aligned}
 H_{S_a}(S_a) &= k_0 x^{-k} \Rightarrow \boxed{k_0 \text{ and } k \text{ are parameters defining the shape of the hazard curve}} \\
 \hat{H}_{S_a}(x) &= k_0 x^{-k} \Rightarrow \boxed{\text{median estimate of the uncertain hazard curve}}
 \end{aligned}
 \tag{4}$$

Further we introduce the random variable ε_{UH} that represents the uncertainty in the spectral acceleration hazard, so that we have:

$$H_{S_a}(x) = \hat{H}_{S_a}(x) \varepsilon_{UH}
 \tag{5}$$

Here we have assumed that ε_{UH} is a Logistic random variable whose statistical parameters have the following characteristics:

$$\begin{aligned}
 \text{median}(\varepsilon_{UH}) &= \eta_{\varepsilon_{UH}} = e^{\text{mean}(\ln \varepsilon)} = 1 \\
 \sigma_{\ln(\varepsilon_{UH})} &= \beta_{UH} \Rightarrow \boxed{\text{Where } \beta_{UH} \text{ reflects the degree of uncertainty in the PSHA estimation}}
 \end{aligned}
 \tag{6}$$

We recognize the spectral acceleration hazard itself as an uncertain (random) variable, $\tilde{H}_{S_a}(x)$, which can be represented as the median (“best”) estimate times this uncertain deviation, $\tilde{\varepsilon}_{UH}$:

$$\tilde{H}_{S_a}(x) = \hat{H}_{S_a}(x) \tilde{\varepsilon}_{UH}
 \tag{7}$$

Note the use of a “tilda” to denote a random variable, when clarity is needed. Considering our assumption about $\tilde{\varepsilon}_{UH}$ being Logistic, we can observe from the above equation that the hazard for any value of S_a itself is a Logistic random variable (i.e., instead of having a single deterministic value assigned to it, it has a probability distribution). We can write the spectral acceleration hazard as:

$$\tilde{H}_{S_a}(x) = \hat{H}_{S_a}(x) \varepsilon_{UH} = k_0 x^{-k} \varepsilon_{UH}
 \tag{8}$$

The mean hazard curve can be written as:

$$\bar{H}_{Sa}(x) = \hat{H}_{Sa}(x) \text{mean}(\varepsilon_{UH}) = \hat{H}_{Sa}(x) e^{\frac{1}{6}\beta_{UH}^2} \tag{9}$$

This equation is based on a property of the Logistic variables.

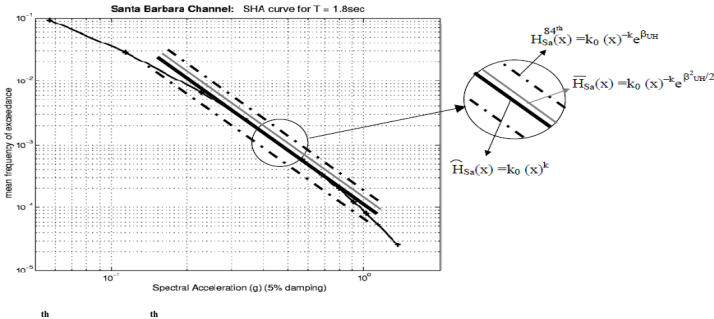


Figure 1.16 , median and 84 percentile spectral acceleration hazard corresponding to a damping ratio equal to 5 and a structural fundamental period of 1.8 seconds.

Probability of Exceeding a Drift Demand value – Drift Hazard

The drift demand variable (given a specified Sa level) was introduced as the median demand value times a random variable ε representing the random variation (e.g., record-to-record) around the median value. We assumed that ε has a Logistic distribution:

$$D = \eta_D(x)\varepsilon \tag{10}$$

Randomness is assumed to be the only source of variability in the above expression. In general, the median drift demand is also an uncertain quantity. The uncertainty in the median drift demand is caused by the limited knowledge and data about modeling and analysis of the structural system especially in the highly non-linear range and/or exact numerical values of the parameters of structural model.

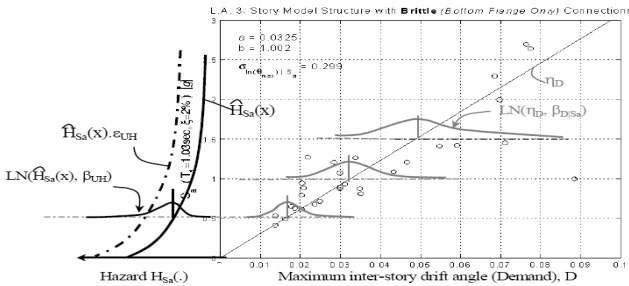


Figure 2. Basic components for the evaluation of drift hazard with uncertainty in the estimation of spectral acceleration hazard, $\hat{H}_{S_a}(x)$

The uncertainty is also caused by using a finite number of non-linear analyses to estimate the median value. The scatter of the displacement-based response indicating record-to-record variability implies that the estimate of the median $\hat{\eta}_D(x)$ can depend on the particular sample of records used and its size. In order to distinguish this type of uncertainty from the one that we considered in the previous section, we refer to it as epistemic uncertainty. The median inter-story drift can be expressed as the product of its median estimate, $\hat{\eta}_D(x)$ and a random variable ε_{UD} (UD stands for the uncertainty in evaluation of D) representing the uncertainty involved in the evaluation of $\eta_D(x)$:

$$\eta_D(x) = \hat{\eta}_D(x) \cdot \varepsilon_{UD} \Rightarrow \boxed{\text{With replacing } \eta_D(x) \text{ in equation 11}} \Rightarrow D = \hat{\eta}_D(x) \cdot \varepsilon_{UD} \cdot \varepsilon \tag{11}$$

In order to be consistent with, ε_{UD} , we now subscript ε with RD, standing for the randomness (aleatory uncertainty) in drift demand evaluation. Finally the drift demand is represented as:

$$D = \eta_D(x) \varepsilon_{UD} = \hat{\eta}_D(x) \cdot \varepsilon_{UD} \cdot \varepsilon_{RD}$$

Where $\varepsilon_{UD}, \varepsilon_{RD}$ are assumed to be independent and to have Logistic distributions with following characteristics:

$$\eta_{\varepsilon_{RD}} = \eta_{\varepsilon_{UD}} = e^{mean(\ln(\varepsilon))} = 1, \sigma_{\ln(\varepsilon_{UD})} = \beta_{UD}, \sigma_{\ln(\varepsilon_{RD})} = \beta_{RD} \tag{12}$$

Our objective in this section is to derive the probability that the drift demand D exceeds a specific value d. In order to minimize the calculation efforts, we'll make use of the drift demand hazard that was derived by Javan Pour and Zarfam (2010) assuming that there was no variability due to uncertainty. The drift hazard or the annual frequency that the drift demand exceeds a specific value was derived from Equation 13 as:

$$H_D(d) = \nu \cdot P[D > d] = k_0 (S_a^d)^{-k} \cdot e^{\frac{9}{4} \frac{k^2}{\pi^2 b^2} \beta^2_{RD}} = H_{Sa} (S_a^d) e^{\frac{9}{4} \frac{k^2}{\pi^2 b^2} \beta^2_{RD}} \tag{13}$$

The spectral acceleration hazard for a given value of deviation in its evaluation, ε_{UH} , can be found from Equation 8 as:

$$\begin{aligned} H_{Sa/\varepsilon_{UH}}(x) &= \hat{H}_{Sa}(x) \cdot \varepsilon_{UH} = k_0 \cdot x^{-k} \cdot \varepsilon_{UH} \boxed{\text{Replacing the opposite value for spectral acceleration hazard in Equation 13}} \\ &\Rightarrow \\ \Rightarrow H_{D/\varepsilon_{UH}}(d) &= \nu \cdot P[D > d] = \tilde{H}_{Sa/\varepsilon_{UH}}(S_a^d) e^{\frac{9}{4} \frac{k^2}{\pi^2 b^2} \beta^2_{RD}} = \hat{H}_{Sa}(S_a^d) \cdot \varepsilon_{UH} e^{\frac{9}{4} \frac{k^2}{\pi^2 b^2} \beta^2_{RD}} \tag{14} \\ &\boxed{\text{drift demand hazard for a given value of deviation in spectral acceleration hazard } \varepsilon_{UH}} \end{aligned}$$

In the next step, we derive the drift hazard function for a given value of deviation in spectral acceleration hazard, ε_{UH} , and the given value of deviation of the median drift demand, ε_{UD} :

$$H_{D/\varepsilon_{UH}, \varepsilon_{UD}}(d) = v.P[D > \varepsilon_{UH}, \varepsilon_{UD}] = \hat{H}_{S_a/\varepsilon_{UD}}(S_a^d) \cdot \varepsilon_{UH} e^{\frac{9}{4} \frac{k^2}{\pi^2 b^2} \beta^2_{RD}}$$

$$\hat{H}_{S_a/\varepsilon_{UD}}(S_a^d) = \hat{H}_{S_a}(S_a^{d/\varepsilon_{UD}}) \Rightarrow \boxed{\text{The term } \hat{H}_{S_a/\varepsilon_{UD}}(S_a^d) \text{ median spectral acceleration hazard for the spectral acceleration that corresponds to drift } d \text{ for a given value of deviation}} \quad (15)$$

In order to be able to calculate the above value, we need to find $S_a^{d/\varepsilon_{UD}}$ or the spectral acceleration corresponding to drift d for a given value of deviation ε_{UD} in drift evaluation.

$$\eta_D(x) = a \cdot x^b \cdot \varepsilon_{UD} \quad (16)$$

$S_a^{d/\varepsilon_{UD}}$ or the spectral acceleration corresponding to drift d for a given value of deviation ε_{UD} in drift evaluation can be evaluated by setting $\eta_D(x)$ in Equation 18 equal to d and solving for $S_a^{d/\varepsilon_{UD}}$. Hence, we can define $S_a^{d/\varepsilon_{UD}}$:

$$S_a^{d/\varepsilon_{UD}} = \left(\frac{d}{a\varepsilon_{UD}}\right)^{\frac{1}{b}} = \left(\frac{d/\varepsilon_{UD}}{a}\right)^{\frac{1}{b}} = S_a^{d/\varepsilon_{UD}} \quad \boxed{\text{Replacing the value for } S_a^{d/\varepsilon_{UD}} \text{ from Equation 17 in Equation 15}} \Rightarrow$$

$$H_{D/\varepsilon_{UH}, \varepsilon_{UD}}(d) = v.P[D > \varepsilon_{UH}, \varepsilon_{UD}] = \hat{H}_{S_a/\varepsilon_{UD}}(S_a^d) \cdot \varepsilon_{UH} e^{\frac{9}{4} \frac{k^2}{\pi^2 b^2} \beta^2_{RD}} = \hat{H}_{S_a}(S_a^{d/\varepsilon_{UD}}) \cdot \varepsilon_{UH} e^{\frac{9}{4} \frac{k^2}{\pi^2 b^2} \beta^2_{RD}} \quad (17)$$

The graphic interpretation of $S_a^{d/\varepsilon_{UD}}$ can be seen from Figure 3. In simple words, this means that we find the corresponding S_a value from the median curve $a \cdot x^b \cdot \varepsilon_{UD}$:

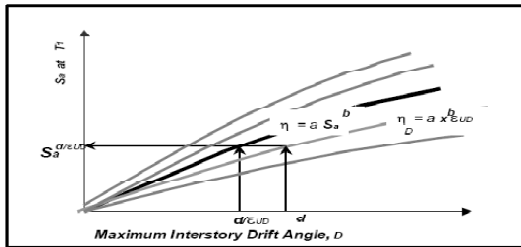


Figure 3. Spectral acceleration corresponding to the inter-story drift ratio value d for a given value of deviation of median drift,

$\hat{H}(S_a^{d/\varepsilon_{UD}})$ Can be calculated from Equations 17 and 4 as follows:

$$\hat{H}_{S_a}(S_a^{d/\epsilon_{UD}}) = k_0 \left(\frac{d}{a\epsilon_{UD}}\right)^{\frac{-k}{b}} \quad (18) \Rightarrow \boxed{\text{Substituting the value of } \hat{H}(S_a^{d/\epsilon_{UD}}) \text{ from Equation 18 in Equation 17 results in}}$$

$$\Rightarrow H_{D|\epsilon_{UH}, \epsilon_{UD}}^{(d)} = \hat{H}_{S_a}(S_a^{d/\epsilon_{UD}}) \epsilon_{UH} e^{\frac{9}{4} \frac{k^2}{\pi^2 b^2} \beta^2_{RD}} = k_0 \left(\frac{d}{a\epsilon_{UD}}\right)^{\frac{-k}{b}} \epsilon_{UH} e^{\frac{9}{4} \frac{k^2}{\pi^2 b^2} \beta^2_{RD}} = k_0 \left(\frac{d}{a}\right)^{\frac{-k}{b}} e^{\frac{9}{4} \frac{k^2}{\pi^2 b^2} \beta^2_{RD}} \epsilon_{UH} \epsilon_{UD}^{\frac{k}{b}} \quad (19)$$

In short, we have an expression for the drift hazard conditioned on the spectral acceleration hazard and variables representing the uncertainty in drift, which is a simple analytical function of ϵ_{UH} and ϵ_{UD} , the random variable representation of those two uncertainties. Where the spectral acceleration hazard could be interpreted as an uncertain variable,

$$\tilde{H}_{S_a}(S_a^d) = k_0 \left(\frac{d}{a}\right)^{\frac{-k}{b}} \epsilon_{UH} \quad (20)$$

We can interpret the drift hazard itself as an uncertain (random) variable $\tilde{H}_D(d)$ which is a function of the uncertain spectral acceleration hazard $\tilde{H}_{S_a}(S_a)$ and uncertainty in drift prediction ϵ_{UD} :

$$\tilde{H}_D(d) = v.P[D > d] = k_0 \left(\frac{d}{a}\right)^{\frac{-k}{b}} e^{\frac{9}{4} \frac{k^2}{\pi^2 b^2} \beta^2_{RD}} \tilde{\epsilon}_{UH} \tilde{\epsilon}_{UD}^{\frac{k}{b}} = \tilde{H}_{S_a}(S_a^d) e^{\frac{9}{4} \frac{k^2}{\pi^2 b^2} \beta^2_{RD}} \tilde{\epsilon}_{UD}^{\frac{k}{b}} \quad (21)$$

The product of independent Logistic random variables raised to powers, such as k/b , is again a Logistic random variable (Javan Pour and Zarfam, 2010). Therefore, we can conclude that the drift hazard is also a log-normal random variable whose distribution parameters can be calculated based on the information about the distribution characteristics of ϵ_{UH} and ϵ_{UD} from Equations 6 and 12:

$$\text{median}(\tilde{H}_D(d)) = \tilde{H}_D(d) = \text{median}(\hat{H}_{S_a}(S_a^d) e^{\frac{9}{4} \frac{k^2}{\pi^2 b^2} \beta^2_{RD}} \epsilon_{UH} \epsilon_{UD}^{\frac{k}{b}}) =$$

$$\hat{H}_D(d) = \hat{H}_{S_a}(S_a^d) e^{\frac{9}{4} \frac{k^2}{\pi^2 b^2} \beta^2_{RD}} \Rightarrow \boxed{\text{The drift hazard } \tilde{H}_D(d) \text{ is an uncertain quantity with median}}$$

$$\beta_{UH_D} = \sqrt{\beta_{UH}^2 + \frac{k^2}{b^2} \beta_{UD}^2} \Rightarrow \boxed{\text{Fractional standard deviation}} \quad (22)$$

And, also mean value $\bar{H}_D(d)$ is equal to:

$$\bar{H}_D(d) = \hat{H}_D(d) e^{\frac{1}{6} \beta_{UH_D}^2} = \hat{H}_{S_a}(S_a^d) e^{\frac{9}{4} \frac{k^2}{\pi^2 b^2} \beta^2_{RD}} e^{\frac{1}{6} \beta_{UH_D}^2} \boxed{\text{with substituting } \beta_{UH_D}} \Rightarrow$$

$$\bar{H}_D(d) = \hat{H}_{S_a}(S_a^d) e^{\frac{9}{4} \frac{k^2}{\pi^2 b^2} \beta^2_{RD}} e^{\frac{1}{6} \beta_{UH}^2} e^{\frac{1}{2} \frac{k^2}{b^2} \beta_{UD}^2} = \bar{H}_{S_a}(S_a^d) e^{\frac{9}{4} \frac{k^2}{\pi^2 b^2} \beta^2_{RD}} e^{\frac{1}{6} \frac{k^2}{b^2} \beta_{UD}^2}$$

$$= \boxed{\bar{H}_{S_a}(S_a^d) e^{\frac{9}{4} \frac{k^2}{\pi^2 b^2} \beta^2_{RD}} e^{\frac{1}{6} \frac{k^2}{b^2} \beta_{UD}^2}} \Rightarrow \boxed{\text{Probability of Exceeding a Drift Demand value - Drift Hazard}} \quad (23)$$

CONCLUSION

According to investigations conducted by the author determined that the log normal probability distribution, the probability of the vulnerability of structures to be very conservative calculation. According to the research was clear that the likely vulnerability of structures using the Log normal distribution approximately 20% of the structures more vulnerable than the Logistic distribution shows (Figures 4 and 5), the fact considers less risk, but designing structures in discussion of economic problems and desirable structural safety with regard to reasonable risk of the most essential things. Therefore it is suggested to calculate the probability of structural vulnerability of the Logistic distribution probability distribution simple, symmetrical, and the likelihood and ability to accurately calculate the probability of occurrence and the response it has caused (Bader taking some reasonable risks) instead of Log normal probability distribution use.

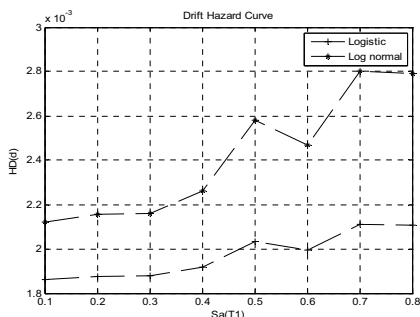


Figure 4. Drift Hazard Curve by Power-Law Method

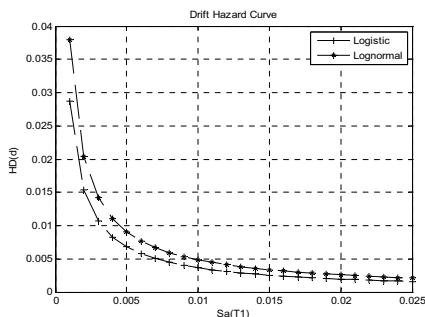


Figure 5. Drift Hazard Curve in a Highly Specific Level of Earthquake

REFERENCE

Javan pour, M., and Zarfam, P. (2010). " Probabilistic Application in Seismic Vulnerability Assessment of Existing Reinforced Concrete Structures by Nonlinear Dynamic Analysis", International Conference on Building Science and Engineering, France, Paris, ISSN: 2070-3724, Paper FR67000

Kennedy, R. P., and Short, S. A. (1994). "Basis for seismic provisions of DOE-STD-1020", UCRL-CR-111478 and BNL-52418, Lawrence Livermore National Laboratory and Brookhaven National Laboratory.

Kramer, S. L., (1996), "Geotechnical earthquake engineering", Prentice Hall.

Luco, N., Cornell, C. A. (1998). "Seismic drift demands for two SMRF structures with brittle connections", Structural Engineering World Wide 1998, Elsevier Science Ltd., Oxford, England, 1998, Paper T158-3.

Options for the Treatment of Uncertainty in Seismic Probabilistic Safety Assessment of Nuclear Power Plants

Tamas J. Katona

Nuclear Power Plant Paks, 7031 Paks, Hungary, e-mail: katonat@npp.hu

ABSTRACT

In the paper two possible ways are presented for the improvement of the probabilistic seismic safety analysis of nuclear power plants. The fragilities of structures and equipment used in safety analysis are presented as function of peak ground acceleration, although it is not an adequate damage indicator. In the paper an interpretation is given for cumulative absolute velocity as damage indicator. The possibility for derivation of conditional probability of failure for cumulative absolute velocity is also shown. In the paper an attempt is also made for outlining some new options for nuclear power plant seismic fragility development based on the interval and p-box-concept. These theoretical tools might be used in case of large number and variety of types of components, failure modes. The proposed methods can be adopted for simplification of the screening, which requires enormous experience.

INTRODUCTION

One of the most complex cases for assessing the nuclear power plant (NPP) safety is the evaluation of the response of the plant to an earthquake load and the risk related with this. Well-defined set of plant systems and structures and components (SSCs) are required to be functional during and after the earthquake for ensuring the plant safety. The frequencies of core damage caused by an earthquake are calculated by plant logic convoluting with component fragilities; see ANSI/ANS-58.10 (2003).

For evaluation of core damage frequency the seismically induced plant damage state frequency f_{ij} has to be calculated via:

$$f_{ij} = - \int_0^{\infty} f(a)_i \frac{dH_j}{da} da', \quad (1)$$

where the fragility curve, $f(a)_i$ is the i -th representation of the conditional probability of core damage. The fragility is defined as the conditional probability of core damage as a function of a – PGA at free surface. The dH_j/da is the probability density function of the applied seismic load expressed in terms of peak ground acceleration, taken from the j -th hazard curve.

The seismic probabilistic safety assessment (PSA) results are very much affected by uncertainties of the methodologies for quantification the seismic hazard and plant fragility. In the standard methodology definition of the fragility is mainly based on extrapolation of the design and testing information. Once the potential

failure modes of a particular SSC are identified, for each failure mode, the median capacities are to be evaluated by conducting limit state analyses using the specific failure criteria with the applied loading and operating conditions, ageing, etc. The seismic fragility development needs enormous experience and specific knowledge in seismic and structural engineering, also involvement very high-qualified system engineers.

Experience shows that plants survive much larger earthquakes than it has been considered in the design base. Positive examples are the nuclear power plants surviving earthquakes larger than those considered in design base (see the case of Kashiwazaki-Kariwa NPP, 2007).

The new designs of plants the seismic contribution to the total core damage frequency became a more critical issue since the internal events core damage frequency is very low.

Therefore new developments and R&D effort have to be made for improving the methodology of seismic PSA and fragility analysis. Recently research activities are going on in the frame of International Atomic Energy Agency, in the area of hazard characterization and fragility development triggered mainly by Kashiwazaki-Kariwa nuclear power plant cases, focusing also on finding of damage indicators, including CAV, relevant for nuclear power plant SSCs.

In the paper the authors view is presented regarding possibilities for improvements of seismic fragility developments for nuclear power plants. Two aspects of treatment of the uncertainty for plant fragility are considered:

- possibility for derivation of conditional probability of failure for cumulative absolute velocity as load parameter, instead of PGA;
- utilization of some new achievements in probability theory like interval and p-box theory for the better description of SSCs behavior.

The paper highlights some options for further discussion and consideration rather than a closed up methodology.

PROPOSALS FOR IMPROVEMENTS IN FRAGILITY DEVELOPMENT

Fragility versus CAV

The median and design base capacities used in seismic fragility development are scaled in PGA. The experience shows that the PGA is not the most appropriate damage indicator. One can say, that the structure will not fail for sure if the design base earthquake (Safe Shutdown Earthquake – SSE) will happen. However, it is not obvious whether the structure will resist or fail if an earthquake will happen with PGA higher than those for SSE. Besides of the randomness of the resistance of the structure, damage of the structure may depend on the PGA, length of strong motion, frequency content of the vibratory motion, etc. Therefore it is rather difficult to validate the fragility as conditional probability of failure versus PGA.

According to the experience the cumulated absolute velocity seems to be an adequate damage indicator; see EPRI (1988).

CAV is calculated as simple integral over the time history of absolute value of acceleration component:

$$CAV = \int_0^T |a(t)| dt. \quad (2)$$

The standardized CAV is calculated applying a noise-filter for the amplitudes less than $\pm 0.025g$. The variability of standardized CAV at fixed PGA could be essential, Katona, 2010.

First of all it has to be understood why the CAV could be an appropriate damage indicator.

Let consider the equation (2) and apply the mean value theorem for the integral. The $|a(t)|$ is an integrable function and its mean value on T is equal to $E \{ |a(t)| \}$. Equation (2) can be rewritten as

$$CAV = \int_0^T |a(t)| dt \cong T * E \{ |a(t)| \}. \quad (3)$$

According to the equation (3) the CAV can be considered as product of two random variables, the duration of strong motion T and the mean of absolute value of ground acceleration time history. Generally the variables T and $E \{ |a(t)| \}$ are not independent.

For the sake of simplicity let's assume that $a(t)$ is a stationary normal random process with zero mean and probability density function $f_a(a)$ and autocorrelation function $R(\tau)$. In this case the random process $z(t) = |a(t)|$ has the density function $f_z(z) = 2f_a(z)U(z)$, and its mean value is as follows:

$$E \{ |a(t)| \} = \int_{-\infty}^{\infty} |a| f_a(a) da = \sqrt{\frac{2}{\pi}} R(0) \quad (4)$$

where $R(0) = R(\tau=0)$ is the autocorrelation function of $a(t)$ at $\tau=0$. We can write further for $R(0)$ that

$$R(0) = \frac{1}{2\pi} \int_{-\infty}^{\infty} S_{aa}(\omega) d\omega, \quad (5)$$

where $S_{aa}(\omega)$ is the power spectral density (PSD) function of $a(t)$. Since we intend to explain the qualitative features of the CAV we may assume that $a(t)$ is an ideal band-limited process with PSD:

$$S_{aa}(\omega) = \begin{cases} S_0 & \text{if } \omega_1 \leq \omega \leq \omega_2 \\ 0 & \text{elsewhere} \end{cases}.$$

It seems that the excitation energy is concentrated within a narrow frequency range. Thus the equation (5) for $R(0)$ can be written as follows:

$$R(0) = \frac{1}{2\pi} \int_{-\infty}^{\infty} S_{aa}(\omega) d\omega = \frac{S_0}{\pi} (\omega_2 - \omega_1) = \frac{S_0}{\pi} \omega_c \frac{\Delta\omega}{\omega_c} \quad (6)$$

where $\Delta\omega$ is the bandwidth, and the ω_c is the median frequency.

Further we can introduce the number of load cycles N during the strong motion, via

$$T\omega_c = T \frac{2\pi}{T_c} = 2\pi N ,$$

and we can rewrite equation (3) as follows:

$$CAV = T \sqrt{\frac{1}{\pi^2} \omega_c \frac{2S_0\Delta\omega}{\omega_c}} = \sqrt{\frac{2}{\pi}} \sqrt{T} \sqrt{N} \sqrt{\frac{2S_0\Delta\omega}{\omega_c}}$$

If $a(t)$ is band-limited we can represent it by a sum of sine functions as $a(t) = \sum_{i=1}^n A_i \sin(\omega_i t + \phi_i)$ or for the sake of simplicity by a single sine with median frequency ω_c and $2S_0\Delta\omega = A_c^2$. Thus the CAV can be expressed as:

$$CAV = T \sqrt{\frac{1}{\pi^2} \omega_c \frac{2S_0\Delta\omega}{\omega_c}} = \sqrt{\frac{2}{\pi}} \sqrt{T} \sqrt{N} \sqrt{\frac{2S_0\Delta\omega}{\omega_c}} = \sqrt{\frac{2}{\pi}} \sqrt{T} \sqrt{N} \frac{A_c}{\sqrt{\omega_c}}$$

On the basis of above considerations we may conclude that the CAV is proportional to the product of strong motion duration and energy (RMS) of the strong motion acceleration time history $a(t)$. The CAV is reflecting the main parameters of damage phenomena; it is proportional to load cycles causing e.g. fatigue-ratcheting type damage. Qualitatively it is obvious. However the dependence of the CAV on the strong motion duration, T , number of load cycles, N , and median frequency, ω_c and amplitude of the alternating load, A_c (the ground motion) is rather interesting. The CAV is proportional to the $\omega^{-1/2}$. It means the higher the mean frequency of excitation the possibility of a damage will be less, which corresponds to the observations and to the fact that majority of structures have characteristic frequencies between 2 and 20 Hz. The results obtained above establish the link between ground motion characteristics and features of the structure.

Dependence of CAV as damage indicator on the features of the vibratory motion (length of strong motion, frequency content, PGA) mentioned above indicates that probability of damage/failure P_{fail} is depending on a load vector $\bar{X} = (x_1, x_2, \dots)$ rather than on a single parameter; see Katona (2010). This approach might seem theoretically precise, however definition of the dependence of fragility on the components of the load vector requires enormous effort. Also the characterization hazard should correspond to the description of fragility. The real need is to establishing a method based on use of CAV as a nonnegative single load parameter $x \geq 0$. (For the sake of simplicity of writing CAV will be denoted below simple by x). Equation (8) should be rewritten as follows:

$$P_{fail} = \int_0^{\infty} h(x) P(x) dx .$$

Assuming that, if a failure occurs for a value of CAV equal to x , then it is occurs for all values larger than x . In this case the conditional probability distribution function $P(x)$ coincides with the cumulative probability distribution function of the failure load parameter λ , i.e. of the smallest value of the load parameter that the structure is unable to withstand,

$$P(x) = \mathbf{Prob}(\lambda \leq x).$$

From the equation above we can calculate the average value of the failure load parameter, i.e. the average CAV-value of failure:

$$\bar{\lambda} = \int_0^{\infty} x' \frac{dP(x)}{dx} dx'.$$

With other words, for the effective use of CAV in fragility analysis, the value $\bar{\lambda}$ has to be evaluated from the empirical data (damages of earthquakes, fragility tests) for all type of SSCs and failure modes. Obviously, the experience and knowledge embodied in the fragility development in terms of PGA should be utilized in the frame of a CAV based methodology, too. Moreover, the use of fragilities expressed in terms of PGA might be reasonable in case of some component types and failure modes.

Options for fragility representation and uncertainty accounting

Not practical to quantify the seismic PSA models using continuous families of seismic hazard curves and associated equipment fragility distributions. Instead of using families of seismic hazard curves, $\{p_j, H_j\}$ as well as the set of equipment fragility distribution, $\{q_i, f_i\}$ point estimates of hazard and fragility are used with subsequent uncertainty analyze. Moreover, in the practice the point estimate of the hazard curve is approximated by stepwise function with low number of intervals (<10) and the same might be done for the approximate representation of fragility curve. Equation (1) might be rewritten as follows:

$$f = - \int_0^{\infty} f(a) \frac{dH}{da'} da \approx \sum_{k=1}^n \left\{ \tilde{f}_k \left(\frac{dH}{da} \right)_k \right\} \Delta a_k, \quad (9)$$

where $f(a)$ and dH/da' denote the selected point estimates of hazard and fragility sets. Each failure fraction \tilde{f} represents the mean conditional likelihood for the given seismic induced failure at the designated seismic acceleration interval $[a_k, a_{k+1}]$. In the recent practice the analysis of uncertainties is based on the probability theory: point estimates are used in combination with Monte-Carlo sensitivity analysis.

Another method for quantifying uncertainty in the model represented by Eq. (14) can be based on interval probability or p-box theory. Instead of point estimates, the upper and lower bounds of the distribution functions might be used for replacing the sets $\{p_j, H_j\}$ and $\{q_i, f_i\}$ by probability boxes specified by a left side and a

right side distribution functions. For the fragility the following representation can be applied (see e.g. Tucker, Ferson (2003) and Ferson et al. (2003))

$$\{\{q_i, f_i\}\} \rightarrow [\bar{F}(x), \underline{F}(x)],$$

where $[\bar{F}(x), \underline{F}(x)]$ is the probability-box specified by a left side $\bar{F}(x)$, and a right side $\underline{F}(x)$ distribution functions, where $\underline{F}(x) \leq \bar{F}(x)$ for all $x \in \mathfrak{R}$, consisting of all non-decreasing functions $F(x)$ from the reals into $[0,1]$ so, that $\underline{F}(x) \leq F(x) \leq \bar{F}(x)$. $[\bar{F}(x), \underline{F}(x)]$ is a p-box for a random variable x whose distribution $F(x)$ is unknown except that it is within the p-box. From a lower probability measure \underline{P} for a random variable X , one can compute upper and lower bounds on distribution functions.

It is often convenient to express a p-box in terms of its inverse functions d and u defined on the interval of probability levels $[0, 1]$. The function u is the inverse function of the upper bound on the distribution function and d is the inverse function of the lower bound. These monotonic functions are bounds on the inverse of the unknown distribution function F ,

$$d(p) \geq F^{-1}(p) \geq u(p),$$

where p is probability level.

The most trivial case for the use of p-box is the screening according to ruggedness of the component. The screened out SSCs with certain capacity are assumed to resist a given level of vibratory motion. The failure fractions for each group of components are determined by their respective screening fragility distributions.

The rugged components might be described by p -box with a lower bound \underline{x} (PGA or any other damage indicator) below of that no failure may occur and an upper bound of \bar{x} above that the failure will occur for sure. In this case the only information needed (or available) is that

$$\underline{P}_{fail} = \begin{cases} 0, & \text{if } x \leq \bar{x}, \\ 1, & \text{otherwise,} \end{cases}$$

$$\bar{P}_{fail} = \begin{cases} 0, & \text{if } x \leq \bar{x}, \\ 1, & \text{otherwise,} \end{cases}$$

where p -box might be defined in case when the minimum, maximum or median and/or other percentiles of failure distribution are known.

The probability bounds might be calculated for cases in which the distribution family is specified by interval estimates of the distribution parameters. If the bounds on mean, μ and standard deviation σ are known, bounds on the distribution can be obtained by computing the envelope of all lognormal distributions L that have parameters within the specified intervals:

$$d(p) = \max_{\alpha} L_{\alpha}^{-1}(p),$$

$$u(p) = \min_{\alpha} L_{\alpha}^{-1}(p),$$

where $\alpha \in \{(\mu, \sigma) | \mu \in [\mu_1, \mu_2], \sigma \in [\sigma_1, \sigma_2]\}$.

Real benefit from this type of representation of probability distribution might be obtained if the fragility of a particular failure mode of a component is known approximately only, small sample size of damage histories, inconsistency of data, or the modeling of failure component is uncertain (e.g. if the set of possible failure modes might be incomplete).

The same procedure might be applied generally, i.e. to the fragility and hazard functions. Interval representation might be also applied to the equation (9) as it is shown below

$$\sum_{k=1}^n \left\{ \tilde{f}_k \left(\frac{dH(a)}{da} \right)_k \right\} \rightarrow \sum_{k=1}^n \left\{ [f_k, \underline{f}_k], [\bar{h}_k, \underline{h}_k] \right\}$$

where $[\tilde{f}_k, \underline{f}_k]$ and $[\bar{h}_k, \underline{h}_k]$ are stepwise interval representations of the point estimates of hazard $h(a) = \frac{dH(a)}{da}$, and fragility functions $f(a)$ in equation (14).

Considering the trivial case of known lognormal distribution for upper and lower bounds of the box the 5% and 95% of confidence might be selected and for the acceleration intervals $[a_k, a_{k+1}]$ and $[\tilde{f}_k, \underline{f}_k]$ pairs might be calculated.

The methods mentioned above allow convolution of several failure modes in the fault tree of a component. Calculation of failure fractions for load intervals $[a_k, a_{k+1}]$ provides certain flexibility in the plant modeling especially when the plant model represented by event trees depends on the excitation level for example due to onset of new global failure modes, e.g. soil liquefaction.

More details on the possible application of the theoretical tools mentioned above one can find in Katona (2010).

Explicit numerical methods exist for computing bounds on the result of addition, subtraction; multiplication and division of random variables when only bounds on the input distributions are given, see Tucker, Ferson (2003) and Ferson et al. (2003). These algorithms have been implemented in software and have been extended to transformations such as logarithms and square roots, other convolutions such as minimum, maximum and powers, and other dependence assumptions.

CONCLUSION

The basic issue of seismic PSA is the definition of component and plant fragilities. Sparse statistical information exists on behavior of complex structures/machines under earthquake loads. In the seismic PSA practice the component fragility development is based on the design information anchored into

PGA. Other representation of load, for example using cumulative absolute velocity as load parameter may improve the calculation of probability failure. As outlined in the paper an adequate interpretation can be given for using the CAV as damage indicator.

The other possible way for the seismic PSA improvements might be the utilization of bounding approach which complements traditional probabilistic analyses when analysts cannot specify precise parameter values for input distributions or point estimates in the model, precise probability distributions for some or all of the variables in the risk model, etc. Upper and lower bounds on parametric values can be provided, typically from expert elicitation. There are several advantages of utilization of interval and p-box description of uncertainties. The proposals for improvement of fragility description outlined in the paper represent combination interval analysis and probability theory. These methods are successfully used in other areas of risk analysis.

REFERENCES

- ANSI/ANS-58.21-2003 (2003), External Events PRA Methodology, March 2003.
- EPRI (1988), Criterion for determining Exceedance of the Operating Basis Earthquake, EPRI NP-5930, July 1988.
- Katona T.J. (2010), Options for the treatment of uncertainty in seismic probabilistic safety assessment of nuclear power plants, *Pollack Periodica* 5:(1) pp. 121-136. (2010)
- Tucker W. T., Ferson S. (2003) Probability bounds analysis in environmental risk assessments, *Applied Biomathematics*, 100 North Country Road, Setauket, New York, 2003
- Ferson S, Kreinovich V., Ginzburg L., Myers D. S., Sentz K. (2003), Constructing probability boxes and Dempster-Shafer structures, Unabridged version, SAND2002-4015, Unlimited Release, Printed January 2003.

Seismic Investigation for the Temple of Antioch Reconstruction

Ece Erdogmus, Ph.D., A.M.ASCE¹, Terri Norton, Ph.D., A.M. ASCE², Cody M. Buckley³, Kyle Kauzlarich⁴, Brad Petersen⁴

¹ Associate Professor of Architectural Engineering, Durham School of Architectural Engineering and Construction, University of Nebraska-Lincoln, 205A PKI, 1110 S. 67th St. Omaha, NE 68182-0816, eedogmus2@unl.edu

² Assistant Professor of Construction Engineering and Architectural Engineering, Durham School of Architectural Engineering and Construction, University of Nebraska-Lincoln

³ Graduate Research Assistant, Architectural Engineering, Durham School of Architectural Engineering and Construction, University of Nebraska-Lincoln

⁴ Undergraduate Research Assistant, Architectural Engineering, Durham School of Architectural Engineering and Construction, University of Nebraska-Lincoln

ABSTRACT

Founded in the middle of the 1st century A.D., Antiocheia ad Cragum was one of the larger Roman cities of the Mediterranean coast region of modern Turkey. This coastal region of Anatolia was known as Rough Cilicia in antiquity. The ancient city, now in a state of ruin, includes an imperial Temple, which was first identified by archaeologists in the 1960s. In 2004, a new project started, with the goal of studying, excavating, and perhaps partially restoring the Temple to a state of “site museum”.

Several theories have been postulated regarding the collapse of the original temple. Since the temple is located near the East Anatolian Fault, it is highly probable that a seismic event aided in the collapse. In order to better understand the performance of the temple under seismic loading, virtual and physical models of the temple are being created. This paper provides an overview of the project and details the progress being made in seismic analysis. The first author is the architectural engineering director of this project that is conducted in collaboration with art historians and archaeologists, and under the observations and rules of the Turkish Ministry of Culture.

INTRODUCTION

Antiocheia ad Cragum was one of the larger Roman cities of the Mediterranean coast region of modern Turkey, which was known as Rough Cilicia in antiquity. This city was founded in the middle of the 1st century A.D. and was an important provincial coastal city of the Roman Empire at the time. The ancient city, now in a state of ruin, includes an imperial Temple, which was first identified by archaeologists in the 1960s. It remained in this ruinous state until it was re-discovered (under heavy vegetation) by the archeologists of this project during a 10-year long surface survey project in the late 1990's (Figure 1).

This temple offers the unique opportunity to research what is likely to be a completely preserved, albeit collapsed, building. Such a study, however, is a challenge for both the engineering and art history/archaeology disciplines, as it includes more unknowns than available information.

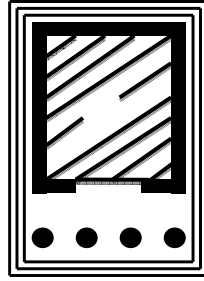


Figure 1. Temple Site Images. (Left) Initial status of the temple after the clearing of vegetation, (Right) example of *prostyle* layout.

The structure is situated on a terrace overlooking the ancient city, visible from the ancient colonnaded road when approached from the still preserved city gates. Based on stylistic evidence and sculptural decoration observed on site, the temple appears to date to the early 3rd century A.D. The researchers also hypothesize that the temple faced the main entry of the city and featured four columns in its front *façade*, indicative of a *prostyle* layout (Figure 1). While the building served as a temple to the Roman imperial cult, the identity of the first emperor worshipped in the temple is still unknown. In addition, fieldwork has shown that the temple contained what appears to be a vaulted substructure, which suggests the possibility of preserved remains that may be religious in nature.

In 2004, a new and comprehensive project on the Temple started with the first author as the architectural engineering director. The project is conducted in collaboration with art historians and archaeologists, and under the observations and rules of the Turkish Ministry of Culture. The goal of this project is to study, excavate, and partially restore this Temple to the state of a well-conserved site museum.

This paper summarizes the project and details the progress being made in the seismic analysis of the temple.

PROJECT ORGANIZATION

In an attempt to develop an organized structure to the project and to offer advice for other complex projects of similar nature, the researchers have classified the project tasks into preconstruction and reconstruction phases (Figure 2). Currently the preconstruction phase is in progress, and it includes several tasks, as illustrated in Figure 2.

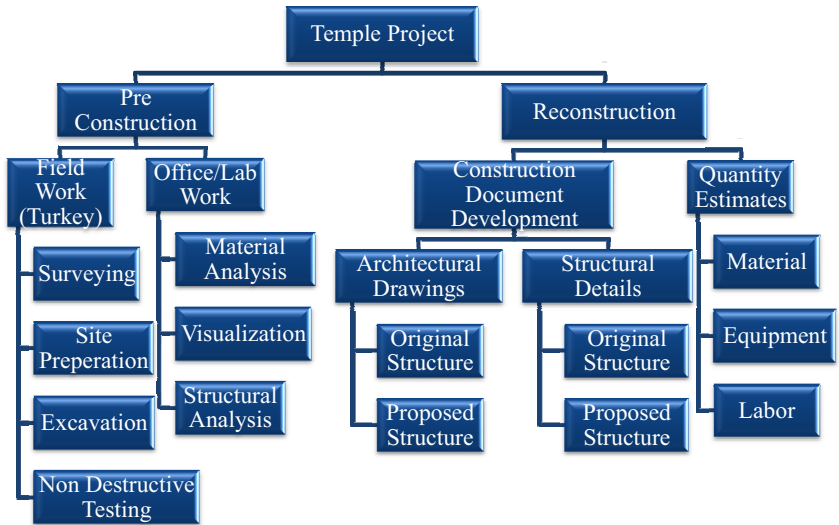


Figure 2. Project Breakdown. The above illustration demonstrates the tasks associated with each phase of the project.

Every summer since 2005, excluding 2006 and 2010, Erdogmus and two collaborators (UNL Art History professor Michael Hoff and Clark University Art History professor Rhys Townsend) along with a team of students carried out the fieldwork tasks shown in Figure 2. Previous project progress summaries can be found in the following publications: Erdogmus *et. al.*, 2007; Erdogmus and Skourup, 2007.

Data and material samples collected in the field are brought back to the University of Nebraska (UNL), where they are used for material analysis, visualization, and analysis efforts. At this time, it is anticipated that the preconstruction phase will require at least 2 more years.

LABORATORY WORK

The fieldwork has provided the team with various types of data that need to be processed in the laboratory or on computers using visualization software. Although the analysis work is still in its earlier stages, progress is being made in each task illustrated in Figure 2. The following sections detail the progress being made in the seismic analysis of the temple. Although most of this progress can be placed under the structural analysis task, the other two tasks have played important roles that will be mentioned.

LITERATURE REVIEW

The ultimate goal of this project is the partial reconstruction of the Temple of Antioch to a state of “site museum”. Given the temple’s current collapsed state a great deal of analysis must be conducted to gain an understanding of the temple. Furthermore this analysis will be vital to the final reconstruction.

Several theories have been postulated regarding the collapse of the original temple. One prominent theory is that a seismic event aided in, if not completely caused, the collapse. Since the temple is located near the East Anatolian Fault in a region susceptible to the extensional tectonics of the Aegean Sea, this theory is certainly plausible. Coupled with the fact that this area experienced high seismic activity in the 5th century, this theory is highly likely and warrants further attention (Stiros, 2001).

Unfortunately, information about dry stone masonry under seismic loading is scarce. In order to understand the seismic behavior of dry stone masonry Vasconcelos *et al.* (2006) suggests considering static cyclic and dynamic tests. In the past, three distinct testing approaches have been used to conduct seismic research on unreinforced masonry structures. These approaches include cyclic tests, dynamic shake table tests, and pseudo-dynamic tests. According to Calvi *et al.* (2006), cyclic testing provides more accurate measurements of forces and displacements while dynamic testing accurately simulates seismic action.

For the purposes of this project, dynamic shake table testing and finite element analysis are the primary methods of investigation being employed. Progress in these two areas is detailed below.

PHYSICAL MODEL

In order to perform dynamic shake table testing a 1:25 scale model of the temple was created using a 3D plotter. The 3D plotter created the model pieces with compressed powder having a density of 1500 kg/m³. This partial model was comprised of (4) columns, (4) column bases, and a two piece pediment.

The partial model was tested on a QUANSAR shake table with the goal of obtaining the natural frequency and mode shapes of the model. The testing setup involved gluing the column bases to a piece of timber that was clamped to the shake table. Once the board was secured, the columns and each pediment piece were stacked on top of the bases. The setup process is detailed in Figure 3. In addition to the model, a displacement sensor was mounted to gather displacement and acceleration data during the testing.

The model was exposed to a forcing function that produced lateral movement parallel to the length of the model. The forcing function used was a simple harmonic sine function, whose frequency and amplitude were altered during testing. Data was collected for several test runs and is currently being processed.

This initial test was not without issues and left much room for improvement. The primary issue was the size of the model. At a 1:25 scale, the entire model shown in Figure 3 stood at a height of 6.25” while the columns were only 3.5” tall. However, due

to the relatively small size (18" x 18") and weight limit (7 kg) of the shake table, a larger model simply was not feasible.

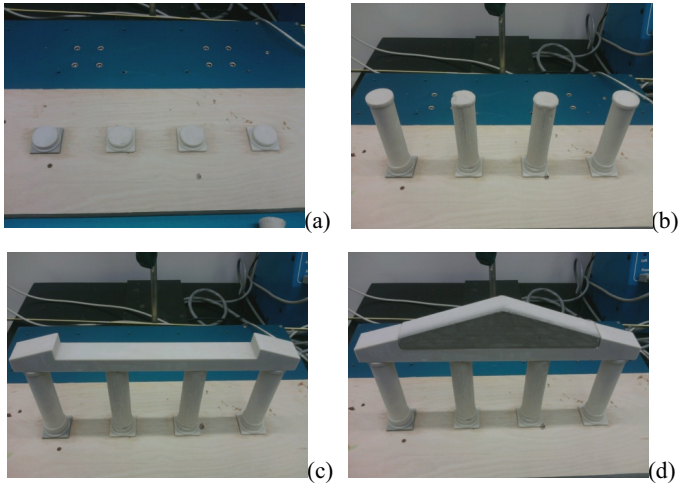


Figure 3. Shake Table Setup. (a) Column bases are glued to timber, (b) Columns are stacked on bases, (c) First pediment piece is placed on columns, (d) Final pediment piece is placed

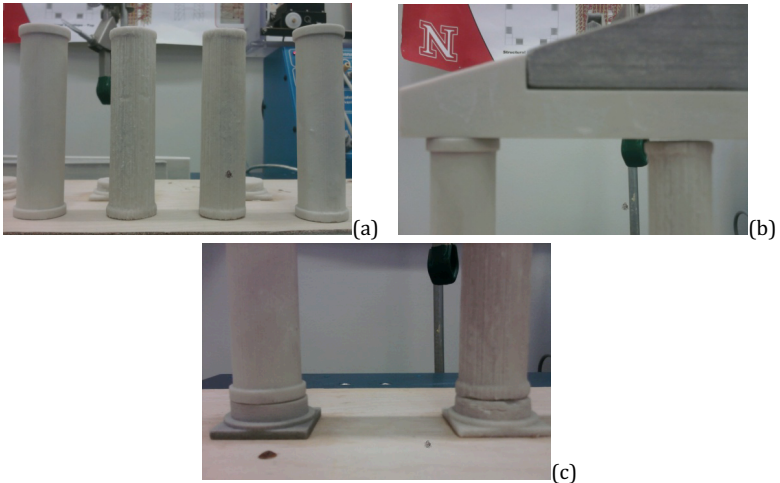


Figure 4. Non-uniformity in Model. (a) The two outer columns are of better quality than the inner two, (b) The pediment did not evenly rest on all columns due to non-uniform height as seen in the right column, (c) Quality differed even in the bases.

Another issue was the use of the 3D plotter which could not produce pieces any larger than those used. In fact, due to the cost of the compressed powder only the *façade* could be produced economically. With only the *façade*, the model was only tested with lateral movement parallel to its length. Without the support of the rest of the structure, lateral movement perpendicular to the *façade* would not produce any useful data. The powder used to create the pieces was not the best material choice as it could be damaged rather easily and resulted in non-uniformity among the columns. The result was columns with differing heights and finishes (Figure 4).

In order to improve the data received from the shake table a larger model must be constructed. However, in order to test a larger model, a larger shake table is also needed. Currently the team is exploring different possibilities for the next model that include: using concrete or mortar for the temple pieces, finding a larger shake table, or even creating a shake table.

FINITE ELEMENT MODELING

Currently, finite element models of the hypothetical architecture of the Temple are being created by the team in ANSYS, a finite element modeling software (Figure 5). These models rely on information from visualization models for geometry and material analysis results for material properties. Thus far, the density and coefficient of friction for marble have been determined as $2,800 \text{ kg/m}^3$ and 0.966 respectively.

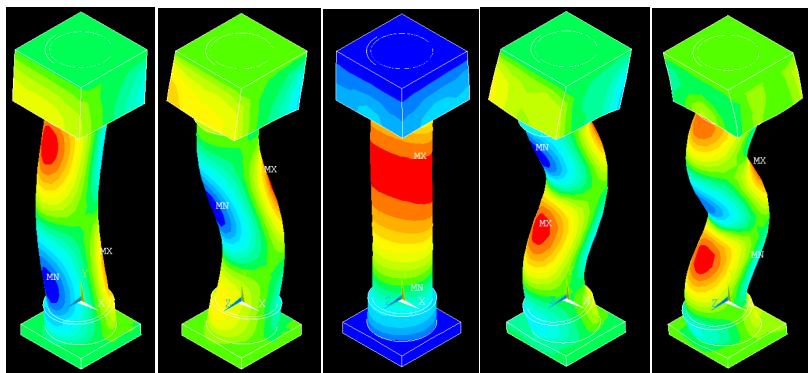


Figure 5. ANSYS Testing. The above photos illustrate mode shapes obtained while testing one column in ANSYS.

The purpose of these models is to predict the natural frequencies and modes of the temple before they are physically tested. By creating ANSYS models, the team can verify if a certain scale model will yield significant results. The photos in Figure 5 illustrate mode shapes obtained from a preliminary column model. This model assumes that the column is a single continuous mass. Currently the model is being modified to reflect the segmented pieces and dry masonry joints of the column. Hand calculations are being used to verify model results under free vibration. Once

verified, these models will be subjected to seismic loads and used to predict the behavior of physical models

CONCLUDING REMARKS AND FUTURE WORK

Currently the project is still in the pre-construction phase. Work has begun on the structural analysis, material analysis, and visualization of the temple. Fieldwork is performed every year and the data is brought back to the universities for analysis. There is potential for the introduction of new technologies to the temple site with the goal of integrating the data collection and visualization efforts. One such possibility is the use of a laser scanner that can be used for surveying the site and transferring 3D point clouds to aid in the temple rendering process.

After the pre-construction phase, work will commence on the reconstruction phase. During this phase, the “philosophy” of the reconstruction will first be established and architectural and structural detail plans will be drawn. Once these are approved, estimates will be taken in order to prepare for the work in the field and raise the necessary funds. Once all necessary office work has been completed, the project will be completed in the field. This project breakdown can be viewed in Figure 2.

The reconstruction of the Temple of Antioch is a very complex project that requires well-organized and compromising interdisciplinary cooperation. Due to the project experts’ occupations as university professors and the students’ class requirements, fieldwork is performed for 1-2 months each year. While analysis work is conducted by the team all year, it is difficult to keep a uniform level of progress and continuity with the rotation of students. Additionally there are various requirements that the Turkish government asks of researchers working on national heritage sites. Together, these factors lengthen the project considerably. Project Directors (Erdogmus, Hoff, and Townsend) have tentatively placed the completion date in the year 2020.

ACKNOWLEDGEMENTS

The funding for this project is provided by National Science Foundation, Harvard Loeb Library Foundation, and numerous UNL internal grants, including Layman Grant, interdisciplinary grant, and UCARE (Undergraduate Creative Activities and Research Experiences). The authors extend their deepest gratitude to Drs. Michael Hoff and Rhys Townsend for their art history and archeology expertise, and for the fruitful collaboration they provide. A special thanks is also extended to the Turkish Ministry of Culture, Mayor and governor of Gazipaşa, Alanya Museum, and the people of Guney Village.

REFERENCES

- Calvi, G.M., et al (1996). “Testing Masonry Structures for Seismic Assessment.” *Journal of Earthquake Engineering Research Institute*.
- Erdogmus, E., Hoff, M., Townsend, R., Turkmen, S. (2007). “Interdisciplinary Assessment of A Roman Temple: Antiocheia Ad Kragos (Gazipasa, Turkey)”, *Proceedings of the International Symposium on Studies on Architectural*

Heritage, Yildiz Technical University Research Center for Preservation for Historical Heritage, 163-170.

- Erdogmus, E., Skourup, B.N. (2007). "Review of Available On-site Assessment and Strengthening Techniques for the Reconstruction of an Ancient Roman Temple," *Proceedings of the 10th North American Masonry Conference*, The Masonry Society, TMS.
- Stiros, Stathis C. . "The AD 365 earthquake and possible seismic clustering during the fourth to sixth centuries AD in the Eastern Mediterranean: a review of historical and archaeological data." *Journal of Structural Geology*. 23. (2001): 545-562. Print.
- Vasconcelos, G. et al (2006). "Experimental Investigations on Dry Stone Masonry Walls." *First International Conference on Restoration of Heritage Masonry Structures*.

Multicriteria Optimization under Uncertainty: Average Criteria Method

L.E.K. Achenie¹, I.V. Datskov² and G. M. Ostrovsky³

¹ Department of Chemical Engineering, Virginia Polytechnic and State University, Blacksburg, VA 24060. Author to whom all correspondence should be addressed (Achenie@vt.edu).

² OSISOFT, 777 Davis Street, Suite 250, San Leandro, CA 94577

³ Karpov Institute of Physical Chemistry, Vorontsovo Pole 10, Moscow 103064, Russia.

Abstract. This paper discusses chemical process models for which the only uncertainties of interest are model parameters. In an earlier paper the authors addressed multicriteria optimization in the presence of model and process uncertainty at the design stage. Specifically the authors discussed extensions of the average criterion method, the worst-case strategy and the ε -constraint method under the following conditions: (a) at the design stage the only information available about the uncertain parameters is that they are enclosed in a known uncertainty region T , and (b) at the operation stage, process data is rich enough to allow the determination of exact values of all the uncertain parameters. The suggested formulation assumed that at the operation stage, certain process variables (called control variables) could be tuned or manipulated in order to offset the effects of uncertainty. This formulation made the conventional assumption that there was only one type of uncertain parameters. In this paper, the authors consider the more realistic case, where the uncertain parameters fall under at least two classes at the operation stage, namely (a) those that can be determined with enough accuracy and (b) those that cannot be determined with such accuracy given the available process data. The case study is an application to a direct methanol fuel cell.

1. INTRODUCTION

Often the performance of chemical processes cannot be estimated only by one objective criterion and it is necessary to take into account several conflicting criteria, for example (a) process economics and environmental requirements, and (b) integration of process design and control. The importance of multicriteria optimization (MCO) has been discussed by a number of researchers (see for example Luyben and Floudas, 1994, Caballero et al., 1997).

Process simulations are further complicated by the presence of uncertainty in the process models and some process variables. Therefore, we cannot reliably carry out MCO without simultaneously considering process and model uncertainty. Furthermore, under an industrially-relevant scenario we cannot rely on commonly used assumption that any uncertain parameter can be determined accurately enough given the available process data at any time instant during the operation stage. For convenience let us refer to the last assumption as *Assumption 1*.

In an earlier paper by us (Ostrovsky et al., 2006) we employed *Assumption 1*. In this paper we remove this assumption and identify two types of uncertainty at the operation stage. The first type represents the parameters which can be determined accurately enough, meaning that accurate and fast responsive sensors are present. The second type represents the parameters which cannot be determined accurately enough.

This is the case when sensors have significant measurement error, delay in response or there are no sensors present to make measurements from which specific parameters can be inferred. In this paper we have to consider mathematical formulations with both types of uncertain parameters simultaneously.

2. PROBLEM FORMULATION

The MCO problem under parametric uncertainty at the design stage can be formulated as

$$\begin{aligned} \min_{d,z} (f_1(d,z,\theta), \dots, f_p(d,z,\theta)) \\ g_j(d,z,\theta) \leq 0, \quad j = 1, \dots, m \end{aligned} \quad (1)$$

where d is an n_d -vector of design variables, z is a n_z -vector of control variables and θ is a vector of uncertain parameters over the domain T . The minimization is over a set of p (possibly conflicting) performance criteria $f_i(d,z,\theta)$. Constraints $g_j(d,z,\theta)$ in the problem are design specifications. The design variables (associated with the design stage of the chemical process) are fixed during the operation stage. Examples of design variables are reactor volume, heat exchanger area, length and diameter of the flow pipes. The control variables primarily represent tunable parameters that can be adjusted during the operation of the chemical process; examples are temperatures, flow rates and pressures.

When the set of uncertain parameters is divided into two sets reflecting their level of accuracy at the operation stage (as discussed earlier), the MCO under uncertainty becomes

$$\begin{aligned} \min_{d,z} (f_1(d,z,\theta^1,\theta^2), \dots, f_p(d,z,\theta^1,\theta^2)) \\ g_j(d,z,\theta^1,\theta^2) \leq 0, \quad j = 1, \dots, m \end{aligned} \quad (2)$$

Here θ^1 is a set of vectors of the first type of uncertain parameters over the domain T^1 and θ^2 is a set of vectors of the second type of uncertain parameters over the domain T^2 .

When **Assumption 1** holds, the vector of uncertain parameters θ in (1) is considered known at the operation stage and becomes the conventional MCO problem, referred to in this paper as the *nominal MCO problem*. For simplicity we omit θ from the formulation in (1) and introduce the notation $x = (d, z)$. The main concept in the MCO problem is the *Pareto Set* (PS) (*non-inferior set of points*) defined as follows: any point \bar{x} (such that $g(\bar{x}) \leq 0$) belongs to PS if in the small vicinity of \bar{x} we cannot find a point $\bar{\bar{x}}$ (such that $g(\bar{\bar{x}}) \leq 0$) at which there is at least one criterion j such that

$$\begin{aligned} f_j(\bar{\bar{x}}) < f_j(\bar{x}) \\ f_i(\bar{\bar{x}}) \leq f_i(\bar{x}), \quad i \neq j \end{aligned}$$

This means that at any point in a PS, it is not possible to improve a criterion $f_i(x)$ without making another criterion $f_j(x)$ ($j \neq i$) worse.

There are several methods for solving the nominal MCO problem (i.e. absence of parametric uncertainty) and building the PS curve under the following condition: *there is*

complete information about uncertain parameters at the design stage. We consider the following methods: the average criterion (AC) (Sophos et al., 1980) and the worst case strategy (WCS) (Clark and Westerberg, 1983). All these methods reduce the MCO problem to a one-criterion optimization problem. There are two general approaches for this reduction. In the approach employed by AC and WCS, a convolution of the original criteria $f_1(x), \dots, f_p(x)$ ($i = 1, \dots, p$) serves as the objective function. A review of these and other methods can be found in our paper Ostrovksy et al. (2006).

3. PROPOSED SOLUTION APPROACH FOR MCO UNDER UNCERTAINTY

We distinguish between two types of variables, namely the design and control variables. The design variables correspond to the design stage and can vary only at this stage. While the control variables can be tuned during both stages of the CP. This work is focused on the case when at the operation stage we have incomplete information about uncertain parameters. This means that at the operation stage we do not have enough process data for determination of accurate values for all uncertain parameters. In this case we define two groups of uncertain parameters. The first group represents parameters which can be determined exactly at any time instant at the operation stage; at the design stage the only available information about this group is given by the associated domain T^1 . The second group represents uncertain parameters which cannot be determined accurately enough at any time instant at the operation stage. Thus the only information at both stages is given by the associated domain T^2 . The presence of the second group of uncertain parameters complicates derivations of MCO under uncertainty. To solve the resulting MCO problem under uncertainty, we will employ extensions of the average criterion (AC) method and the worst-case strategy (WCS). Both methods are discussed in our paper Ostrovksy et al. (2006). However, in the current paper, we will focus only on the AC method.

We will use the following general approach for the extension of the AC method. First, we will transform each criterion $f_i(d, z, \theta^1, \theta^2)$ to a new criterion $\tilde{f}_i(d)$, which depends only on the design variables. With $\tilde{f}_i(d)$ ($i = 1, \dots, p$) we will be able to use the AC method for solving the MCO problem under uncertainty. From now on we will use the phrase “convolution method” to denote the phrase “AC method”.

Consider the following optimization problem

$$\begin{aligned} \min_z \int_{T^2} F(f_1, \dots, f_p, \alpha) \mu(\theta^2) d\theta^2 \\ \max_{\theta^2 \in T^2} g_j(d, z, \theta^1, \theta^2) \leq 0 \quad j = 1, \dots, m \end{aligned} \tag{3}$$

Here $F(f_1, \dots, f_p, \alpha)$ is a convolution of p criteria f_1, \dots, f_p , which is constructed using the convolution method and α is a vector of parameters. We will suppose that at the operation stage, Eqn. (3) is solved for each θ^1 . Let us construct a new set of criteria as

$$\tilde{f}_i(d, \alpha) = \int_{T^1} f_i(d, z^*(d, \theta^1, \alpha), \theta^1) \mu(\theta^1) d\theta^1 \tag{4}$$

These criteria employ the optimal solution $z^*(d, \theta^1, \alpha)$ obtained from (3).

The function $\bar{f}_i(d, \alpha)$ is a mean value of the original criterion $f_i(d, z, \theta^1, \theta^2)$ at the operation stage since for each θ^1 Eqn. (3) is solved. Again we can use the same convolution method for solving the MCO problem while employing the functions $\bar{f}_i(d, \alpha)$ (here we will use the same parameters α , used in the construction of the convolution $f(f_1, \dots, f_p, \alpha)$). Designate the solution as $[d^*, \bar{f}_i^*]$ ($\bar{f}_i^* = \bar{f}_i(d^*, \alpha)$). Using the convolution method with $\bar{f}_i(d, \alpha)$ ($i=1, \dots, p$) for all values of α , satisfying (4) traces a curve (surface) in the space of the \bar{f}_i ($i=1, \dots, p$). This curve (termed Decision Maker, DM curve) is an analog of the conventional PS in the sense that the DM must make a final decision using the curve. From engineering consideration he must select a point $[\bar{d}, \bar{\alpha}]$ from this curve as the solution of the MCO problem.

Let us analyze the results. During the operation stage for each θ^{1j} , $\alpha = \bar{\alpha}$, and $d = \bar{d}$, the control variables z are obtained from (3) using the convolution method (i.e. we solve a conventional MCO problem). Thus, the resulting value of z corresponds to one of the points on the Pareto set for the functions $f_i(\bar{d}, z, \theta^{1j}, \theta^2)$. Now consider the values $\bar{f}_i(\bar{d}, \bar{\alpha})$ ($i=1, \dots, p$). These are obtained by solving Eqn. 3 or Eqn. 5 from our paper Ostrovskiy et al., 2006. Again we obtain a solution, which corresponds to one of the points of the conventional PS for $\bar{f}_i(d, \bar{\alpha})$. Therefore, for each $\bar{f}_i(d, \bar{\alpha})$ we cannot obtain a better MCO solution than $\bar{f}_i(\bar{d}, \bar{\alpha})$. It is clear that the solution can be realized, since at each time instance, Eqn. (3) is solved and the resulting $z^*(d, \theta^1, \bar{\alpha})$ is used for construction of all $\bar{f}_i(d, \bar{\alpha})$. We will apply this general approach for solving the MCO problem using the convolution method.

If Eqn. (3) is a convex program, then a local optimization algorithm is adequate for obtaining a global solution, otherwise a global optimizer is needed. Global optimization algorithms can be classified as either stochastic or deterministic. For example Luh et al. (2003) considered stochastic methods (specifically the genetic algorithm family) in order to converge to globally optimal solutions for an MCO formulation. Several deterministic global optimizers rely on branch and bound and convex/concave estimators (see for example Ostrovskiy et al., 2003b).

EXTENDED AVERAGE CRITERIA METHOD

In the extended average criteria (AC) method, we formulate the MCO problem as

$$\begin{aligned}
 f^*(d, \theta^1, \alpha) &= \min_z \int_{\bar{r}^2} f(d, z, \theta^1, \theta^2, \alpha) \mu(\theta^2) d\theta^2 \\
 \max_{\theta^2 \in \bar{r}^2} g(d, z, \theta^1, \theta^2) &\leq 0 \quad j = 1, \dots, m
 \end{aligned}
 \tag{5}$$

where

$$f(d, z, \theta^1, \theta^2, \alpha) = \sum_{k=1}^p \alpha_k f_k(d, z, \theta^1, \theta^2) \tag{6}$$

$$\sum_{k=1}^p \alpha_k = 1 \quad \alpha_k \geq 0$$

Let $z^*(d, \theta^1, \alpha)$ be the solution to the problem. Then $\bar{f}_i(d, \alpha)$ is given by Eqn. (4). The new criteria $\bar{f}_i(d, \alpha)$ ($i=1, \dots, p$) do not depend on the control variables z and uncertain parameters $[\theta^1, \theta^2]$. Now we can directly use the method of minimization of the weighted average criterion

$$\min_d \bar{f}(d, \alpha) \tag{7}$$

where

$$\bar{f}(d, \alpha) = \sum_{k=1}^p \alpha_k \bar{f}_k(d, \alpha) \tag{8}$$

This is a bi-level optimization problem, since for calculation of $\bar{f}_k(d, \alpha)$ we must use $z^*(d, \theta^1, \alpha)$, which is the solution of Eqn. (5). It has been proven that the bi-level optimization problem is multi extremal and nondifferentiable. To make matters worse, during the calculation of the objective function of Eqn. (7), we must recalculate p multidimensional integrals at each value of d . Therefore we need to reduce Eqn. (7) to a simpler problem. By substituting in Eqn. (8) the expression for $\bar{f}_k(d, \alpha)$ from Eqn. (4) and rearranging, we obtain

$$\bar{f}(d, \alpha) = \int_{T^1} \left[\sum_{k=1}^p \alpha_k f_k(d, z^*(d, \theta^1, \alpha), \theta^1, \theta^2) \right] \mu(\theta^1) d\theta^1 \tag{9}$$

The term inside the square brackets is the optimal value of the objective function of the internal optimization Eqn. (5), and since for a given θ^1 the optimal value of z does not depend on the values of z for other θ^1 , we can rewrite Eqn. (9) as

$$\bar{f}(d, \alpha) = \min_{z(\theta^1)} \int_{T^1} \int_{T^2} \left(\sum_{k=1}^p \alpha_k f_k(d, z, \theta^1, \theta^2) \right) \mu(\theta^2) \mu(\theta^1) d\theta^1 d\theta^2 \tag{10}$$

$$\max_{\theta^2 \in T^2} g_j(d, z, \theta^1, \theta^2) \leq 0$$

Here $z(\theta^1)$ is a multivariable function with respect to the uncertain parameters θ^1 and $j = 1, \dots, m$. By substituting the expression for $\bar{f}(d, \alpha)$ from (10) in Eqn. (7) we obtain

$$\min_{d, z(\theta^1)} \int_{T^1} \int_{T^2} \sum_{k=1}^p \alpha_k f_k(d, z, \theta^1, \theta^2) \mu(\theta^2) \mu(\theta^1) d\theta^1 d\theta^2 . \tag{11}$$

$$\max_{\theta^2 \in T^2} g_j(d, z(\theta^1), \theta^1, \theta^2) \leq 0, \forall \theta^1 \in T^1 \tag{12}$$

In order to guarantee existence of the solution of the problem we must supplement this problem with the following constraint Ostrovsky et al (2003a)

$$\chi_2(d) \equiv \max_{\theta^1 \in T^1} \min_z \max_{\theta^2 \in T^2} \max_{j \in J} g_j(d, z, \theta^1, \theta^2) \leq 0 \tag{13}$$

The system of equations in Eqns. (11) and (13) constitute a two-stage optimization problem (TSOP2). Therefore, we can use the split and bound method (SB) described in Ostrovsky et al (2003a) to solve this problem.

Suppose the decision maker selects the point $[\bar{d}, \bar{\alpha}]$ from the DM curve. This means that if we solve (5) at each time instance during the operation stage, the mean of $f_i(\bar{d}, z, \theta^1, \theta^2)$ will be equal to $\bar{f}_i(\bar{d}, \bar{\alpha})$. We note that if we apply the direct approach for formulation of an MCO optimization problem on the basis of the AC method we will obtain TSOP as Eqn. (9). Thus in this case the direct approach gives the same result as the extended AC method approach.

4. COMPUTATIONAL EXPERIMENTS

In this case study we will illustrate the effect of uncertainty on multicriteria optimization of the Direct Methanol Fuel Cell (DMFC). The DMFC uses methanol in the form of liquid or vapor, to generate electrical energy. The main disadvantage is the voltage drop associated with crossover of methanol through the membrane. The direct methanol fuel cell model is from Scott et al. (1997) and is summarized in the appendix of our paper Ostrovsky et al. (2006).

In the DMFC the most important problem is to decrease the cell voltage drop associated with crossover of methanol through the membrane. A proposed solution is to increase the pressure of oxygen (air) on the cathode side. Thus, in the first study case we constructed two conflicting criteria, which characterize the performance of the DMFC. One criterion ($f_1[V]$) represents the crossover overpotential and the other ($f_2[V]$) represents the cost of pressurizing; we employed a correlation similar to one in Douglas (1988).

$$f_1 = \eta_{crossover} \qquad f_2 = \left(\frac{P_{cathode}}{P_{ref}} \right)^{0.29} - 1 \tag{14}$$

The results (Fig. 1) were as expected; with an increase in the cost of pressurizing (f_2), the performance (curve 1) of the DMFC drops as a result of increasing crossover overpotential (f_1). Note that for TSOP1 (only one type of parametric uncertainty), a significant increase in crossover overpotential occurred, resulting in poor DMFC performance (curve 2). In TSOP2 (two types of parametric uncertainty), no significant differences were detected (curve 3), except that the feasibility region is reduced significantly. This leads to conservative design, since the design and control variables are very close to their bounds. Other case studies can be found in our paper, Ostrovsky et al. (2006).

5. CONCLUSIONS

We have discussed an extension of the average criterion method (AC) method for solving the multicriteria optimization problem under uncertainty for a chemical process when there are two distinct types of uncertainty present. Specifically we have considered the

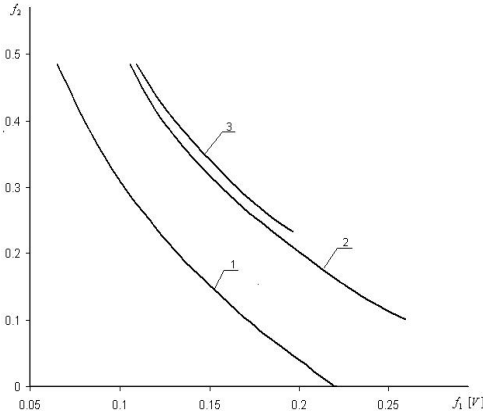


Figure 1. Pareto curve and DM curve for the Case Study.

Nominal case (Pareto) = curve # 1, TSOP 1 (DM) = curve # 2, TSOP 2 (DM) = curve # 3

more realistic case where the uncertain parameters fall under at least two classes at the operation stage, namely (a) those that can be determined with enough accuracy and (b) those that cannot be determined with such accuracy given the available process data. In all three approaches we exploit the degrees of freedom afforded by the presence of the control variables at the operation stage.

6. NOTATION

a_i	Scalar constant
a, a^*	Vector constant
d	Vector of design variables (with dimension n_d)
$f_i^i(*), f^i(*)$	Performance criterion
$\bar{f}^2(*), \bar{f}_i^i(*), \bar{f}^2(*)$	Performance criterion
$f^{i*}, f_k^{(p)}, \bar{f}^{2*}(*), \bar{f}^{2*}(*)$	Optimal value of performance criterion
$g_j(*)$	Scalar constraint
$g(*)$	Vector constraint
$E\{*\}$	Expected value
J, \bar{J}	Index set
w_i	Weight (scalar)
$x, \bar{x}, \bar{\bar{x}}, x^*, x^{(k)}$	A point
z	Vector of control variables (with dimension n_z)
$z^*(*)$	Optimal vector of control variables (with dimension n_z)

z^i	$z(\theta^i)$
<u>Greek</u>	
$\varepsilon_i, \bar{\varepsilon}_i, \alpha_k, \beta, \gamma$	Scalar constant
θ	Vector of uncertain parameters over the domain T
θ^i	A given value of θ
θ_i^N	Nominal value of θ
$\delta\theta_i$	Deviation fraction
$\rho(*)$	Probability density function
$\chi_1(*), \bar{\chi}_1(*)$	Feasibility function

7. REFERENCES

- Clark, P.A. and Westerberg, A.W. (1983). "Optimization for design problems having more than one objective." *Comput. Chem. Eng.*, 7: 259.
- Caballero, R., Ruiz, F. and Steuer, R.E. (1997). *Advances in multiple objective and goal programming*. Berlin: Springer-Verlag.
- Douglas, J. (1988). *Conceptual Design of Chemical Processes*. McGraw-Hill.
- Luh, G.C., Chueh, C.H. and Liu, W.W. (2003). MOIA: "Multi-Objective Immune Algorithm". *Eng. Opt.*, 35(2):143–164.
- Luyben, M.L. and Floudas, C.A. (1994). "Analysing the interaction of design and control-1, a multiobjective framework and application to binary distillation synthesis". *Comp. Chem. Eng.* 18: 933.
- Ostrovsky, G.M., Achenie, L. E. K., Datskov, I. and Volin, Y. (2006). "An Approach to Multicriteria Optimization under Uncertainty," *Chemical Engineering Science*, **61**, 2379-2393.
- Ostrovsky, G.M., Datskov, I.V., Achenie, L.E.K, and Volin, Yu.M. (2003a) "Process uncertainty: the case of insufficient process data at the operation stage". *AIChE Journal*, 49: 1216-1240.
- Ostrovsky, G.M., Achenie, L. E. K., and Sinha, M. (2003b) "A Reduced Dimension Branch-and-Bound Algorithm for Molecular Design," *Comp. Chem. Eng.*, **27**(4), 551-567.
- Scott, K., Taama, W. and Cruickshank, J. (1997). "Performance and modeling of a direct methanol solid polymer electrolyte fuel cell". *Journal of Power Sources*, 65: 159-171.
- Sophos, A., Rodstein, F. and Stephanopoulos, G. (1980). "Multi-objective analysis in modeling the petrochemical Industry". *Chem. Eng. Sci.*, 35: 2415.

National-Level Infrastructure Risk Evaluation Framework and Best Practices

Yujie Lu¹, Qingbin Cui², Longquan Mao³, Liang Chen³

¹Ph.D. Candidate, School of Economics and Management, Tongji University, 1239 Siping Road, Shanghai 200092, China; Research Assistant, Department of Civil & Environmental Engineering, University of Maryland, College Park, MD 20742, USA; PH(240)460-9966; Email: lyj0415@gmail.com

²Ph.D., Assistant Professor, Department of Civil & Environmental Engineering, University of Maryland, 1157 Glenn L. Martin Hall, College Park, MD 20742; PH (301) 405-8104; Email: cui@umd.edu

³Nanjing Construction Quality Supervision Bureau, 30-33 Yudao Street, Nanjing, Jiangsu Province, 210016 China

Abstract

The national infrastructure is the most essential society component serving for civil activities, economic prosperity, and public safety every day. Its absence or failure will result in tremendous devastation to nation's growth and competitiveness. Nevertheless we can't manage and drive the infrastructure to a right direction unless the infrastructure conditions and risks are properly evaluated. And current researches mainly focus on single or multiple projects, seldom study the risk evaluation from the overall national level. This paper first constructs a national-level risk evaluation framework from four levels: ultimate outcome, immediate determinants, underlying determinants, basic determinants; then assesses the infrastructure condition based on ASCE quadrennial infrastructure report card case. Various methodologies, assessment objectives, evaluation breakdown structure, gauging criteria and data sources are discussed though the case. The result of this research can be used for investigating national infrastructure risks systematically, supporting the national infrastructure funding allocation, and assisting to policy decisions making.

Introduction

National-level infrastructure evaluation is necessary and essential both for public awareness and policy decision makers, not only providing infrastructure deterioration facts and enacting the practices, but also sustaining well-maintained, efficient, safe and secure infrastructure system to meet the needs of a growing quality of life.

To evaluate the national infrastructure is necessary for two primary reasons. First, it identifies the current infrastructure condition and projects the future satisfying level.

So far, lots of countries have tried their efforts to gauging the infrastructure conditions. From 1998 on, the American Society Civil Engineers (ASCE) publishes the quadrennial national-level infrastructure condition evaluation in report card fashion and most years only earned D score. Delayed maintenance and chronic underfunding are main contributors to the infrastructure nearly every year. An increasing more countries, such as United Kingdom, Australia, New Zealand, the South African, start to evaluate their infrastructure condition((ICE 2010), (Engineers Australia 2005), (PricewaterhouseCoopers 2004), (SAICE 2006)). Second, the infrastructure evaluation is a critical document supporting for policy decision because infrastructure usually needs large numbers of investment and various financing approaches. American Recovery and Reinvestment Act, an economic stimulus package passed in February 2009, sets aside more than \$132 billion for a wide range of infrastructure projects including roads, transit, energy grid and passenger rail and etc partially in light of engineers' testimony. In the long term, 2009 ASCE report card indicates that the America will still need 2.2 trillion to pull all infrastructures back to good conditions in next five years (ASCE 2009). This paper presents an extensive discussion including the related research review, risk evaluation framework, and ASCE best practices.

Literature Review

Over the last several decades, there are abundant efforts have been done to evaluate and improve infrastructures. According to Mishalani and McCord (2006), the academic community focused their researches on condition assessment, deterioration forecasting, better inspection, and maintenance decision-making by adopting a spectrum of methodologies including material science(Al-Ostaz et al. 2009) statistics(Chu and Durango-Cohen 2008), econometrics (Kobayashi et al. 2008), and operations research(Madanat et al. 2006). Those research tackle different infrastructure problems including pavement (Prozzi and Hong 2008) (Chu and Durango-Cohen 2008), water distribution system/pipeline (Grigg 2006) (Hong et al. 2006), sewer pipeline (Wright et al. 2006), traditional steel structure (Melchers 2006) , Brick facilities (Cascante et al. 2008) and etc. In addition, there are various literatures about topics including Infrastructure Asset Management(USACE 2005, Infrastructure Canada 2007, GAO 2004, FHWA 2007) , infrastructure evaluation sources and technology((Madanat et al. 2006), (Cascante et al. 2008), (Maser 2005), (Buchheit et al. 2005)), and future evaluation development((Mishalani and McCord 2006), (Al-Ostaz et al. 2009)) etc.

Risk Evaluation Framework

Based on infrastructure evaluation cases around the world, we develop the conceptual framework for the national-level infrastructure condition risk evaluation (Figure 1).

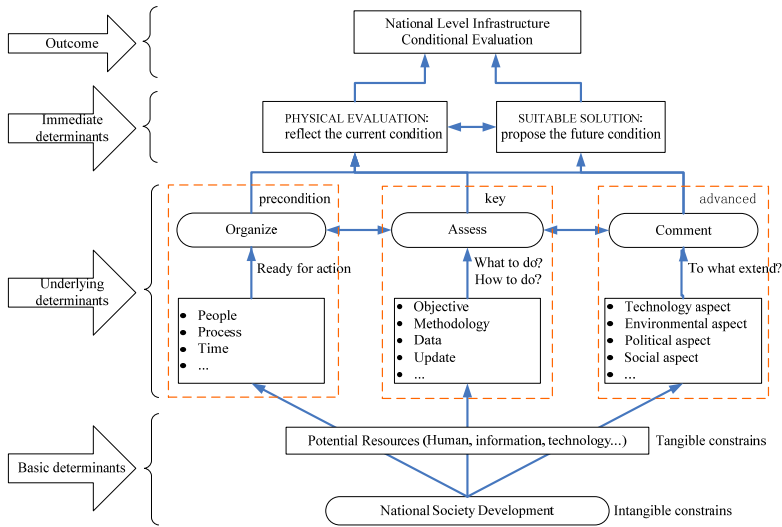


Figure 1. National-level infrastructure condition risk evaluation framework

The first level is the overall outcome for the whole infrastructure condition evaluation expressed by the report, public presentation or online video.

The second level is the immediate determinants, which includes physical evaluation and suitable solution as two main components. The evaluation is based on the real infrastructure situations and most of used knowledge mainly comes from the civil engineering industry; meanwhile the solution may propose the future infrastructure development and involve with interdisciplinary and miscellaneous issues besides infrastructure, such as economics, finance, political policy, etc.

The third level, named underlying determinants, covers detail variables for all risk evaluation. Before implementing a evaluation, highlighted with preconditions, every related recourse should be well organized including finding knowledge professionals, designing process flow, and planning time schedule, etc. Then, highlighted in the middle box, assessment becomes the key part of the whole evaluation process since it regulates rules for gauging the infrastructure performances and delivers the background information for the following comment. Condition assessment mainly focus on “what to do” and “how to do” from both quality and quantity aspects, including objective, methodology, data, update, problems, etc. The last part determines the infrastructure future status and possible efforts though answering the question of “to what extend”. Related concerns may include

technology aspect, economic aspect, environmental aspect, political aspect, social aspect and etc. Those determinants appear more subjective and advanced comparing to the condition assessment, since it regulates the higher strategy level may changes in light of society development.

The lowest level named as basic determinants, which includes potential resources and national society development status. In detail, potential resources means all the possible resources which is required to perform this evaluation, such as human resource, information resources, technology resources, etc. Whereas those resources become the tangible constrains when they are unavailable; national society development is the background of the whole evaluation, and could be either opportunities or constrains.

The following paragraphs will mainly discuss on the assessment section of this framework through the US ASCE report card case study from 1988 to 2009.

ASCE report card case study

The American Society of Civil Engineers, founded in 1852, is the United State's oldest national civil engineering organization. The ASCE and its members are committed to protecting the health, safety, and welfare of the public, and as such, are equally committed to improving the nation's public infrastructure by depicting the condition and performance of nation's infrastructure in the familiar form of a school report card(ASCE 2009). This original concept of report card came from the National Council on Public Works Improvement, which created by the public works improvement act of 1984 (P.L.98-501) and published the first edition of America's infrastructure report card in 1988(NCPWI 1988). Since adopting this idea from 1998, the American Society Civil Engineers (ASCE) published the quadrennial national-level infrastructure condition evaluation report card and the latest edition released on January 2009. To keep information updated, the ASCE also publishes the brief biennial follow-up report to tracks latest progress including relevant legislation, investment and improvement. The following contents will explore report card assessment methodology, breakdown structure, and evaluation criteria and data sources in sequence.

Methodology. Generally, the report card evaluates the infrastructure from both quality and quantity aspects through multiple methods in different scenarios and phases as described the following Figure 2. The assessment starts based on available public data and professionals' opinions in the input process. comprehensive literature review and interviewing with professionals are mainly adopted. And due to limited resources, ASCE can only collect second-hand data instead of investigate those

abundant data by itself. Then based on the GPA Grading, Scenario analysis, Subjective Probability Method, Connoisseur method (also called expert evaluation) and Delphi method, each category’s original score and potential solutions are drafted; Subsequently, all ASCE experts gather to standardize their criteria by connoisseur method again, and feedback the results to the previous steps in order to adjust each category’s score. Finally in the output process, with final scores and recommended solutions, the official report card is completed. (*Note: it’s worth mention that ASCE may only take partly or similar of those methods in practice in lieu of strictly performing them in the whole process.*)

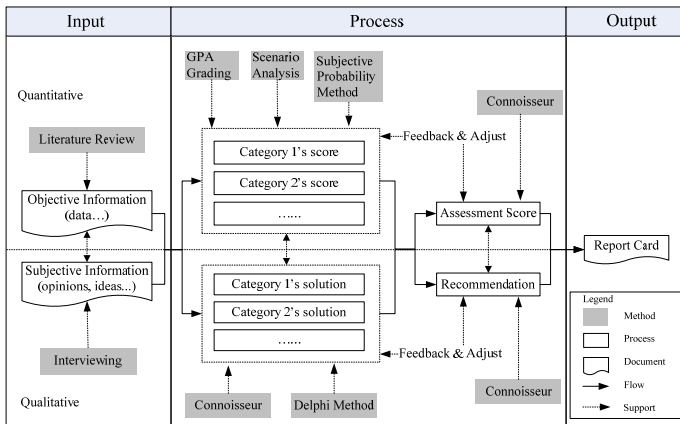


Figure 2. ASCE report card evaluation methodologies

Objectives. The definition of infrastructure represents the basic physical structures and services facilities needed and necessary for a nation. Under the public concerns for long-lasting and reliable infrastructure, increasing numbers of infrastructure objectives have been studied from 9 to 15 during 1988-2009 including dams, drinking water, hazardous waste, levees, solid waste, wastewater, aviation, bridges, inland waterways, rail, road, transit, public parks and recreation, school, energy. Those objectives can be grouped into four categories including water and environment, transportation, public facilities, energy. Nevertheless, some categories still miss from the latest report partially because of haven’t been paid enough attention yet. Some of missing items belong to existing categories, such as bicycle paths, public shelters; while some are new, such as telecommunication, national positioning system and etc.

Evaluation Breakdown structure. After defining all the objectives, the assessment structure framework can be developed to gauge both overall categories and single subjects. The structure is composed by both horizontal and vertical categories shown

as Figure 3. Each category’s criteria are decided by infrastructure professionals, who are all experts in their fields of practice or academy. Based on their review and analysis of available data, each category’s score is calculated and followed by the final overall score. For example, national dam assessment can be conducted firstly by acquiring information from national information sources like Association of State Dam Safety Officials, Federal Emergency Management Agency, etc., then by assessing with corresponding criteria, like safety, quality, etc. Once every category is assessed with a score, the national grade can be assigned by averaging all categories scores without weight. The similar procedure for regional classification by first assigning regional score and then national overall grade. The overall score can be assigned by either category or regional classification, and both two evaluation systems can be found in past report card.

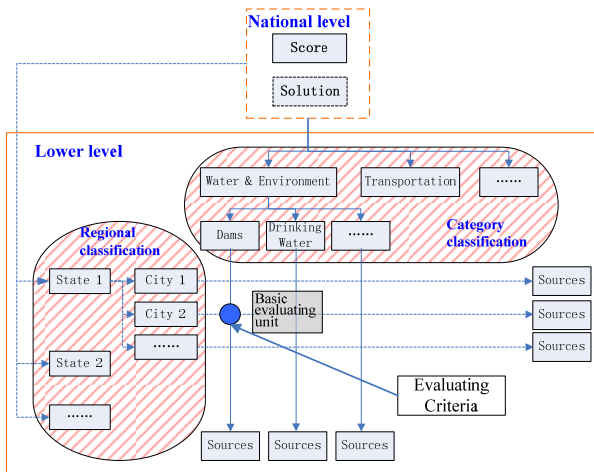


Figure 3. report card assessment breakdown structure

Assessing criteria. Assessing criteria are key components impacting the evaluation result, and may vary according to different categories. There are general criteria for the whole evaluation(see Table 1); and specific sub-criteria developed for different categories or subjects flexibly by their characters. Those criteria keep changing for upcoming challenges. In 2009 edition, there is a new criterion called resilience, the scope of which includes security, disaster preparedness and mitigation, and response and recovery activities. This concept of evaluating resilience embodies a shift from a strategy based on pure protection to one that ensures the system capability withstanding both natural and human-caused multihazard threats, as well as recovering critical service promptly following such events.

Table 1 ASCE report card assessing criteria (1988-2009)

year	General criteria
1988	Performance, condition, capacity, investment, spending (concluded by author)
1998	(no record)
2001	Condition, Performance, capacity vs. need, funding vs. need
2005	Condition, capacity, funding vs. need
2009	Capacity, physical condition, operations and maintenance ability, current and future needed cost Funding, public safety, system's resilience

Data sources. The data availability and accuracy is important during the infrastructure evaluation process, and could impact the quality of evaluation result to some extent. In order to ensure the information coverage, the report card refers all national infrastructure information sources, including but not limited to reports, publish papers, data, hearing materials, testimony, government documents, laws, statutes and etc. In addition, there are various professional organizations and institutes participating as the assistances during the whole process.

Conclusion

During the last two decades, comprehensive analysis and methods to address infrastructure risk evaluation issues are key steps to improve long term national infrastructure. This research mainly focuses on the proposing an integrated risk evaluation framework for national-level infrastructure, and illustrates the evaluation's assessment though ASCE report card cases. Nevertheless, more efforts need to be developed to sustain the national infrastructure to meet the current and future social needs, such as national-level infrastructure public policy research, infrastructure funding allocation algorithm, different levels government roles analysis and etc.

References

- Al-Ostaz, A., Cheng, A., Mullen, C., and Song, C. (2009). "Aging Infrastructure: Evaluation, Repair, Improvement and Protection." *Ole Miss Project 63888 Pub 48 - Aging infrastructure for DHS infrastructure workshop*.
- ASCE. (2009). "2009 Report Card for America's Infrastructure." *American Society of Civil Engineers*.
- Bernhardt, K. L. S., Loehr, J. E., and Huaco, D. (2003). "Asset Management Framework for Geotechnical Infrastructure." *Journal of Infrastructure Systems*, 9, 107.
- Buchheit, R. B., Garrett Jr, J. H., McNeil, S., and Chen, P. (2005). "Automated Procedure to Assess Civil Infrastructure Data Quality: Method and Validation." *Journal of Infrastructure Systems*, 11, 180.

- Cascante, G., Najjaran, H., and Crespi, P. (2008). "Novel Methodology for Nondestructive Evaluation of Brick Walls: Fuzzy Logic Analysis of MASW Tests." *Journal of Infrastructure Systems*, 14, 117.
- Chu, C. Y., and Durango-Cohen, P. L. (2008). "Empirical Comparison of Statistical Pavement Performance Models." *Journal of Infrastructure Systems*, 14, 138.
- Engineers Australia. (2005). "2005 Australian Infrastructure Report Cards." <http://www.engineersaustralia.org.au/irc/>, accessed by 2010 August.
- Grigg, N. S. (2006). "Condition assessment of water distribution pipes." *Journal of Infrastructure Systems*, 12, 147.
- Hong, H. P., Allouche, E. N., and Trivedi, M. (2006). "Optimal scheduling of replacement and rehabilitation of water distribution systems." *Journal of Infrastructure Systems*, 12, 184.
- ICE. (2010). "State of the Nation." <http://www.ice.org.uk/News-Public-Affairs/State-of-the-Nation>, *Institution of Civil Engineers*, accessed by 2010 August.
- Kobayashi, K., Ejiri, R., and Do, M. (2008). "Pavement Management Accounting System." *Journal of Infrastructure Systems*, 14, 159.
- Madanat, S., Park, S., and Kuhn, K. (2006). "Adaptive optimization and systematic probing of infrastructure system maintenance policies under model uncertainty." *Journal of Infrastructure Systems*, 12, 192.
- Maser, K. (2005). "Automated Systems for Infrastructure Condition Assessment." *Journal of Infrastructure Systems*, 11, 153.
- Melchers, R. E. (2006). "Recent progress in the modeling of corrosion of structural steel immersed in seawaters." *Journal of Infrastructure Systems*, 12, 154.
- Mishalani, R. G., and McCord, M. R. (2006). "Infrastructure condition assessment, deterioration modeling, and maintenance decision making: Methodological advances and practical considerations." *Journal of Infrastructure Systems*, 12, 145.
- NCPWI. (1988). "Fragile Foundations: A Report on America's Public Works." *National Council on Public Works Improvement, Washington, DC*.
- PricewaterhouseCoopers. (2004). "Infrastructure Stocktake: Infrastructure Audit." *Ministry of Economic development, New Zealand*, http://www.med.govt.nz/templates/MultipageDocumentPage_9024.aspx.
- Prozzi, J. A., and Hong, F. (2008). "Transportation Infrastructure Performance Modeling through Seemingly Unrelated Regression Systems." *Journal of Infrastructure Systems*, 14, 129.
- SAICE. (2006). "The SAICE Infrastructure Report Card for South Africa." *The South African Institution of Civil engineering*, <http://www.civils.org.za/>.
- Sunkpho, J., Garrett Jr, J. H., and McNeil, S. (2005). "XML-based inspection modeling for developing field inspection support systems." *Journal of Infrastructure Systems*, 11, 190.
- Wright, L. T., Heaney, J. P., and Dent, S. (2006). "Prioritizing Sanitary Sewers for Rehabilitation Using Least-Cost Classifiers." *Journal of Infrastructure Systems*, 12, 174.

Probabilistic Performance Risk Evaluation of Infrastructure Projects

Byung-Cheol Kim

Assistant Professor, Dept. of Civil Engineering, Ohio University, 114 Stocker Center,
Athens, OH 45701-2927, USA; PH (740) 593-1478; FAX (740) 593-0625; email:
kimb@ohio.edu

ABSTRACT

Forecasting is a critical function of project control and management. Reliable forecasting enables the project manager to make better informed decisions for timely control actions to prevent or mitigate adverse project outcomes, especially schedule delays and/or cost overruns. Recently, a new probabilistic method for project schedule forecasting was developed based on the Kalman filter method and the earned value method. In this paper, the Kalman filter forecasting method for schedule is extended to formulate a consistent and practical method for project schedule and cost performance forecasting. A numerical example is presented to demonstrate how the new method can be efficiently employed in real projects. Monte Carlo simulation is also conducted to evaluate the accuracy of the proposed method.

INTRODUCTION

Forecasting is a critical function of project control because it provides the project manager with early warnings of potential problems so that timely actions can be taken before it becomes too late. Common forecasting methods in the construction industry, for example the critical path method (CPM) and the earned value method (EVM), are mostly deterministic and fail to provide the project manager with necessary information about the range of possible outcomes and the probability of completing the project on time and within budget. Furthermore, common practices for schedule and cost forecasting in the project management community and the construction industry are dealing with schedule and cost separately. For example, the critical path method is only for schedule performance monitoring and controlling, while the earned value method is recommended only for cost performance forecasting (Fleming and Koppelman 2006). Methodologically, CPM and EVM provide predictions based on different assumptions about the relationship between the past performance and the future performance. Furthermore, the CPM requires detailed activity-level progress information while the EVM uses project-level summary performance metrics such as the planned value (PV), the earned value (EV), and the actual cost (AC).

This paper introduces a new probabilistic forecasting method, the Schedule and Cost Kalman filter method (S-CKFM) for consistent prediction of project

schedule cost performance based on the earned value metrics. The S-CKFM was formulated by extending the Kalman filter forecasting method for schedule performance (Kim and Reinschmidt 2010) and integrates forecasting of project duration and cost at completion within a consistent probabilistic framework. The Kalman filter provides a mathematically sound framework for updating previous forecasts with new progress data on actual performance. The objective of this paper is to introduce the S-CKFM and demonstrate how the S-CKFM provides probabilistic predictions on both schedule and cost predictions simultaneously. With a simple bridge project, the benefits of a probabilistic approach and the ease of implementing the S-CKFM in real projects are demonstrated. In the application, predictions by Monte Carlo simulation are also provided and compared with the outcomes by the S-CKFM.

FORMULATION OF THE S-CKFM

The schedule-cost Kalman filter method is formulated by extending the Kalman filter method for project duration at completion (Kim and Reinschmidt 2010) to incorporate forecasting of project cost at completion. The schedule Kalman filter model (SKFM) aims at probabilistic forecasting of project duration at completion using the baseline progress curve and actual progress from periodic progress reports. In the SKFM, the Kalman filter provides a probabilistic framework for integrating prior knowledge based on pre-construction planning and posterior observations from actual progress reports. Furthermore, inherent uncertainty in actual progress measurements is systematically taken into account within the Kalman filter method (Kim and Reinschmidt 2010).

Figure 1 (a) shows the input requirements of the SKFM along with conceptual probability curves for the estimated duration at completion (EDAC). The SKFM starts with the planned project duration, the budget at completion (BAC), and the baseline progress curve (PV curve) that depicts the cumulative project-level progress at a specific time until the project complete. In addition, a probability distribution of the project duration is required as shown with prior $p(\text{EDAC})$ in Figure 1 (a). The prior EDAC probability curve represents the degree of accuracy in the original estimate of the project duration. Once a project starts and the earned value at each reporting period is being monitored and reported, the SKFM updates the prior EDAC probability curve to a posterior EDAC curve. In the SKFM, the Kalman filter combines the prior information with the new information observed by a progress monitoring and reporting system with some errors in such a manner that the error is minimized statistically (Maybeck 1979). Obviously, this updating process is repeated after each reporting period throughout the project execution period.

Given the inputs displayed in Figure 1, the procedures developed for the SFKM can also be used for the S-CKFM except that the state of the system is now defined with four state variables instead of two in the SKFM. That is, in addition to the two state variables (the time variation and the rate of time variation) in the SKFM, two new system variables (the cost variance and the rate of cost variance) are added in the S-CKFM. These four variables are collectively used to monitor, track and forecast schedule and cost performance simultaneously.

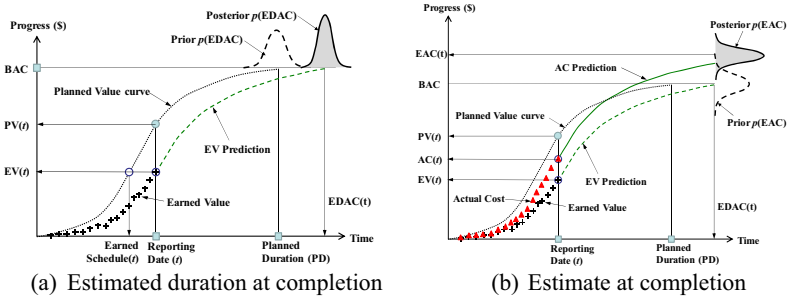


Figure 1. Schedule-Cost Kalman filter forecasting

APPLICATIONS AND DISCUSSION

In this section, practical application of the S-CKFM for probabilistic estimation of project duration and cost at completion is demonstrated with a prestressed concrete girder bridge project from the literature (Antill and Woodhead 1990). The bridge has three spans and is planned with 32 schedule activities. Table 1 summarizes the precedence relationships among all activities along with single-point estimates of the duration and cost of each activity. In addition, variability of activity durations and costs is considered by assuming normal distributions with means of single-point estimates shown in Table 1 and coefficient of variation of 0.2. In this example, a simulation approach is also applied and compared with the S-CKFM. Monte Carlo simulation, or simply simulation, is a technique for formal risk analysis in project scheduling and cost estimating. Based on the information in Table 1 and the variability assumption of activity durations and costs, a simulation approach is applied to generate stochastic S-curves for the earned value and for the actual cost of the bridge project. All the simulation outcomes in this paper were obtained from 10,000 S-curves. Figure 2, however, displays first 200 progress curves for earned value and actual cost of the 10,000 randomly generated progress curves. From this simulation results, probability distributions for the project duration and cost can be generated (Hulett 1996).

The primary issue of this paper is to update the probabilistic estimates of project duration and cost at completion in a *progressive* way. That is, the prior estimates of the project duration and cost need to be updated as the project proceeds and more information accrues revealing actual performance of the project periodically. Periodic progress reports, usually biweekly or monthly, are considered here a reliable source for forecasting future performance. In order to demonstrate how the S-CKFM updates its predictions in real project environments, a pair of earned value and actual cost curve is chosen to simulate a likely actual progress of the project. Figure 3 shows the earned value curve and actual cost curve used in the analysis following. It should be noted that, in theory, each progress curve in Figure 2 has the same probability of becoming the actual progress of the project. Therefore, the randomly generated S-curves in Figure 3 must be considered one of the probable outcomes of the project due to the network structure and the variability of activity durations and

costs. Figure 3 also shows the baseline progress curve against which the earned value and actual cost are compared.

Network Simulation Results

First, the network schedule simulation is applied using the data available at week 10. At this point, actual finish dates of the finished activities are used to determine the status of the project in terms of EV and AC. Then, with the remaining activities, including ongoing activities, the simulation approach is again applied to generate two groups of 10,000 likely progress curves of EV and AC, respectively. Figure 4 displays the likely progress curves of EV and AC generated for the remaining tasks. From the outcomes, the expected value and standard deviation of the estimated duration at completion (EDAC) and the estimate at completion (EAC) at week 10 can be calculated. Of course, this progressive simulation approach can be applied after each reporting period, with new EV, and AC values. Figure 5 shows the outcomes at week 30.

Table 1. Project data of the prestressed concrete girder project.

Activity ID	Description	Predecessor	Duration (weeks)	Cost (\$1,000)
1	Mobilization	none	6	9
2	Girder casting yard	none	6	18.6
3	Drive piles in Abutment A	1	4.8	7.8
4	Cofferdam - install at Abutment A	3	3	16
5	Erect falsework in Span 1	1	5	12
6	Erect falsework in Span 2	5	5	12
7	Erect falsework in Span 3	6	5	12
8	Drive piles in Pier no. 1	4, 5	4.6	6
9	Drive piles in Abutment B	7, 8	4.8	7.8
10	Reinforced concrete, Abutment A	4, 5	4	15
11	Cofferdam remove & install at Pier 1	8, 10	4	21
12	Drive piles in Pier no. 2	6, 11	4.6	6
13	Reinforced concrete, Pier 1 (1/2)	6, 11	4	16.5
14	Cofferdam remove & install at Pier 2	12, 13	4	21
15	Reinforced concrete, Pier 1 (2/2)	13,	4	16.5
16	Reinforced concrete, Pier 2 (1/2)	7, 14	4	16.5
17	Manufacture PC Girders, Span 1	1, 2	14	96
18	Cofferdam remove & install Abut. B	9, 15, 16, 17	4	21
19	Reinforced concrete, Abutment B	10, 18	4	15
20	Cofferdam remove from Abut. B	19	3	3
21	Reinforced concrete, Pier 2 (2/2)	15, 16, 17	4	16.5
22	Manufacture PC Girders, Span 2	17	13	96
23	Manufacture PC Girders, Span 3	22	13	96
24	Erection of PC Girders, Span 1	15, 17	3	5.4
25	Erection of PC Girders, Span 2	21, 22, 24	3	6
26	In-situ concrete deck, Span 1	21, 22, 24	3	9
27	Erection of PC Girders, Span 3	20, 23, 25, 26	3	6.6
28	In-situ concrete deck, Span 2	20, 23, 25, 26	3	9
29	In-situ concrete deck, Span 3	27, 28	3	9
30	Approaches, handrails, etc.	27, 28	6	21
31	Remove falsework, all spans	29	4	6
32	Clean up and move out	31	2	6

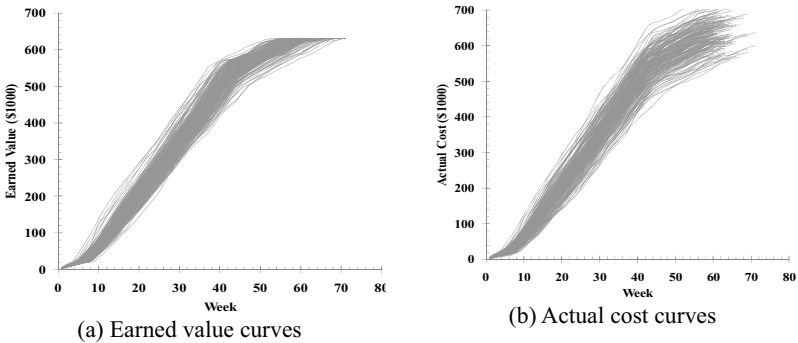


Figure 2. Simulated progress curves of the bridge project.

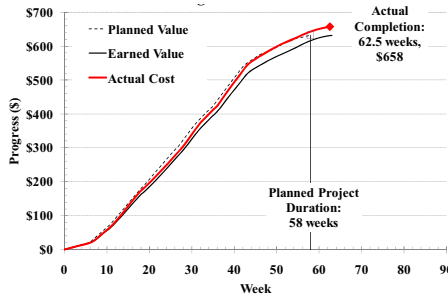


Figure 3. Progress curves of the three-span bridge project.

In this paper, probabilistic distributions of the EDAC and the EAC are estimated at weeks 0, 10, 20, 30, 40, and 50 and shown in Figure 6. The thick solid lines in Figure 6 represent the mean of the posterior distribution of the EDAC and the EAC. The upper and lower bounds (UB and LB, respectively) are determined at 90% prediction intervals. That is, the upper bound indicates the value of EDAC (or EAC), which has 5% probability of schedule (or cost) overruns. Collectively, the three curves (the expected value, the lower bound, and the upper bound) show the range of possible outcomes at the time of forecasting. The results in Figure 6 indicate that as the project progresses the EDAC deviates from the prior estimates 61 week to the actual outcome 62.5 week. And more importantly, the actual duration at completion lies inside the prediction intervals throughout the analysis period. Note also that the standard deviation narrows down as more tasks finish and the variability of the remaining tasks decreases. The results of EAC also show similar patterns regarding the profile of the mean and standard deviation of EAC.

Kalman Filter Forecasting Method

The same project was analyzed with the S-CKFM. In contrast to the simulation approach, S-CKFM does not require detailed activity-level data. Major input is the three basic performance indicators in the earned value method (PV, EV, and AC) and prior estimates of the project duration and cost at completion. The prior probabilistic

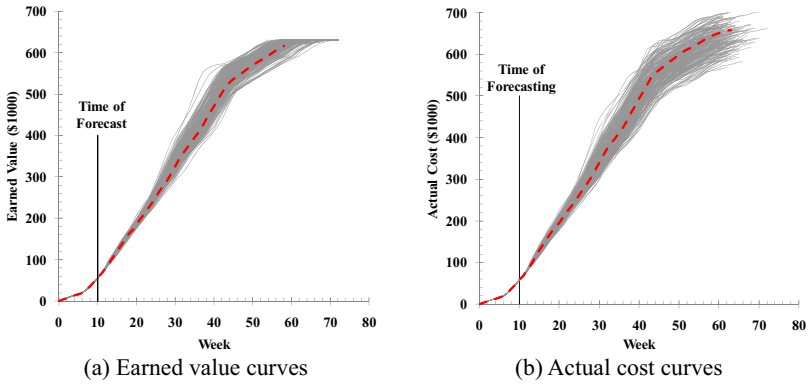


Figure 4. Simulated progress curves of the remaining works at week 10.

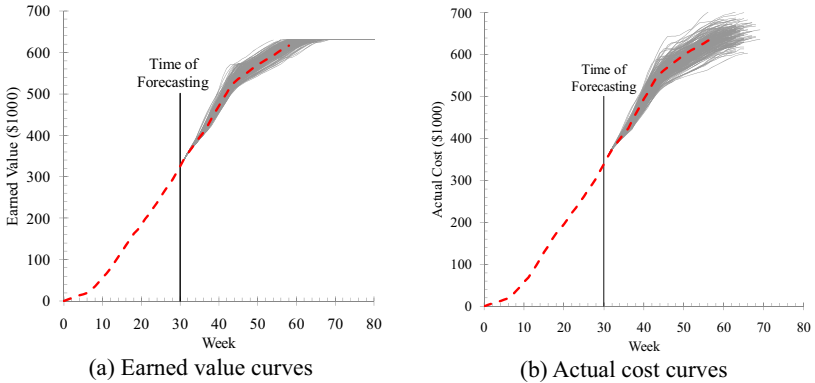


Figure 5. Simulated progress curves of the remaining works at week 30.

estimates can be made in various ways (Kim and Reinschmidt 2009; 2010). A practical way of estimating the initial uncertainty in project duration and budget is the three-point method (or the PERT estimate), which uses the optimistic value, the most likely value, and the pessimistic value. In this paper, the three-point method is adopted and the value of each parameter is determined from a preliminary simulation analysis.

The S-CKFM is then repeatedly applied to update the probability distributions of EDAC and EAC from the beginning of the project up to week 60. Because of the computational efficiency of the S-CKFM compared to the simulation approach, predictions are in fact updated each week (Figure 7) instead of a few selected points as for the simulation approach. The results in Figure 7 can be summarized as follows.

- The EDAC starts to deviate from the prior estimate of 58 weeks (Figure 3) toward the final project duration of 62.5 weeks after 8 weeks. Similar pattern is also observed in the EAC profile. This is attributed to a nature of the Kalman filter.

That is, the Kalman filter updates prior estimates in the light of new information. However, the degree of impact of the new information on the prior estimates is determined by relative accuracy and significance of the new information compared to the accuracy of the prior estimates. In this case, the EV and AC of the project do not show noticeable deviation from the PV until approximately week 10.

- As more actual data accrue, both the EDAC and the EAC curves approach their final outcomes. For schedule forecasting purpose, the S-CKFM provides an accurate EDAC as early as week 26. In the case of EAC, the project team gets earlier indicator of the final outcome as early as week 18. These results indicate that, for the given situation, the S-CKFM can be effectively used to provide timely warnings about potential schedule and cost problems at the end of the project.
- Last conclusion is about the reliability of the S-CKFM. Both EDAC and EAC curves indicate temporary fluctuations throughout the analysis period. However, the risk that the project team is misinformed about the true status of the project due to these noises can be significantly reduced by referring to the prediction bounds. For both EDAC and EAC, prediction bounds (UB and LB) narrow down as more tasks in the project are finished, which indicate the project team can get more reliable estimates of the range of possible outcomes. More importantly, both the actual project duration and the actual project cost stay inside the prediction bounds throughout the analysis period.

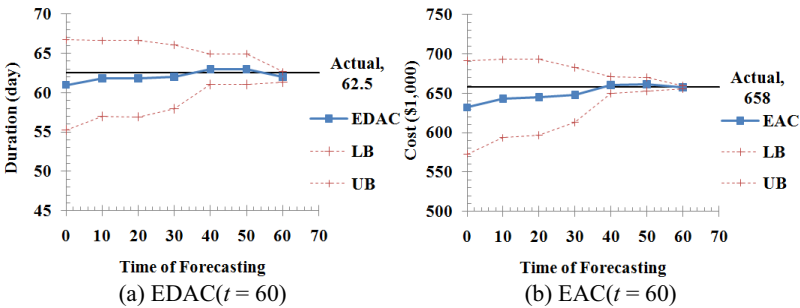


Figure 6 Simulation predictions at every 10 weeks.

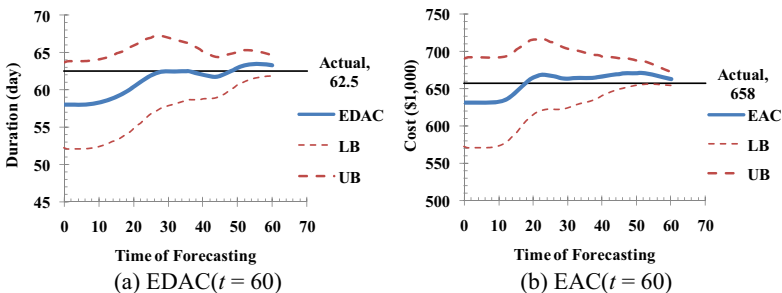


Figure 7 S-CKFM predictions from the beginning to week 60.

It should be noted that additional information about the range of possible outcomes, which deterministic approaches cannot convey, can mitigate the risk of misguided decisions by the project team. It will also help the project manager and the owner develop a better insight into the real status of their projects and make better informed decisions as to whether interruptive control actions for detailed project review or corrective actions are necessary or not.

CONCLUSIONS

In this paper, a new probabilistic method for forecasting of project duration and cost at completion during the execution period is introduced. The schedule and cost Kalman filter forecasting method (S-CKFM) is formulated by extending a previous research by the author about for probabilistic forecasting of project duration at completion. From a practical point of view, the S-CKFM is an easy-to-use and intuitive method which can be efficiently incorporated to any EVM-based performance reporting systems without additional burden of data collection or data analysis.

With a hypothetical project of a three-span prestressed concrete bridge, the S-CKFM is successfully applied to provide reliable predictions about the project duration and cost at completion. A comparison with the simulation results revealed that the S-CKFM provides reliable forecast without any requirements for extensive data acquisition for activity-level progress as the simulation approach does.

REFERENCES

- Antill, J. A., and Woodhead, R. W. (1990). *Critical path methods in construction practice*, 4th Ed., Wiley-Interscience.
- Fleming, Q. W., and Koppelman, J. M. (2006). *Earned value project management*, 3rd Ed., Project Management Institute, Newtown Square, PA.
- Hulett, D. T. (1996). "Schedule risk analysis simplified." In: *PM Network*, 23-30.
- Kim, B.-C., and Reinschmidt, K. F. (2009). "Probabilistic forecasting of project duration using Bayesian inference and the Beta distribution." *Journal of Construction Engineering and Management*, 135(3), 178-186.
- Kim, B.-C., and Reinschmidt, K. F. (2010). "Probabilistic forecasting of project duration using Kalman filter and the earned value method." *Journal of Construction Engineering and Management*, 136(8), 834-843.
- Maybeck, P. S. (1979). *Stochastic models, estimation, and control Volume 1*, Academic Press, Inc.

Optimal Planning of Public Works Using Improved Genetic Algorithm

Koichiro Nakatsu¹, Hitoshi Furuta² and Ken Ishibashi³

¹Postdoctoral fellow, Doctor of Informatics, Faculty of Informatics, Kansai University, 2-1-1 Ryozenji-cho, Takatsuki, Osaka, 569-1095, Japan; Tel & Fax: +81-72-690-2348; e-mail: inside2@sc.kutc.kansai-u.ac.jp

²Professor, Doctor of Engineering, Faculty of Informatics, Kansai University, 2-1-1 Ryozenji-cho, Takatsuki, Osaka, 569-1095, Japan; Tel & Fax: +81-72-690-2348; e-mail: furuta@res.kutc.kansai-u.ac.jp

³Student, Master of Informatics, Graduate School of Informatics, Kansai University, 2-1-1 Ryozenji-cho, Takatsuki, Osaka, 569-1095, Japan; Tel & Fax: +81-72-690-2348; e-mail: ken_ishibashi@furuta-lab.jp

ABSTRACT

The purpose of this research is to establish an appropriate program for the long/middle term planning of public works. This planning needs to satisfy various constraints such as the order relations among construction projects and annual budget. Therefore, in order to solve this planning problem as a combinatorial optimization, it is necessary to search for solutions in very complicated solution space. In this optimization, Genetic Algorithm (GA) is more likely to be trapped by a local optimum due to the lack of diversity among individuals. In this study, an attempt is made to develop a decision support system for the optimal planning by using Improved GA. The proposed method adopts a local search which aims at satisfying constraint of the order relations. This local search can prevent that the search of GA tends to converge to a local optimum. Numerical examples are presented to demonstrate the applicability of the proposed method through the comparison with Simple GA computation.

INTRODUCTION

In general, construction projects consist of many works that have order relations to each other. Therefore, in order to establish a plan of construction project, it is first necessary to satisfy the order relations. Moreover, it is often necessary for the plan to simultaneously satisfy the requirements of multiple construction projects with a limited budget. It is obviously desirable to establish a program that can give the maximum benefit such by an appropriate budget allocation.

The purpose of this research is to establish an appropriate decision making system for the long/middle term planning of public works. In order to solve this planning problem as a combinatorial optimization, it is necessary to optimize it under various constraints such as financial, technical and erection constraints. Genetic Algorithm (GA) has been proven to be very powerful in solving combinatorial problems. However, it is difficult for GA to search for practical solutions in a problem which has complicated constraints. The search of Genetic Algorithm (GA) is more likely to be trapped by a local optimum due to the lack of diversity among individuals.

In this study, an attempt is made to develop a decision support system for the optimal planning by using Improved GA. The proposed GA adopts the local search which uses the repair process of gene based on Baldwin effect. This local search can obtain solutions which satisfy constraints by repairing genes which violate constraints of order relations. Furthermore, this repairing of genes can prevent that GA tends to converge to a local optimum, because genetic array of individual does not change in the repair process of genes based on Baldwin effect; but only the fitness is changed as individual's information. Therefore, the proposed method can search for solutions with keeping the diversity among individuals. Numerical examples are presented to demonstrate the applicability of the proposed method through the comparison with Simple GA computation.

LONG/MIDDLE TERM PLANNING OF PUBLIC WORKS

In this study, the planning problem is formulated according to the work by Furuta et al. in 1998. Here, it is assumed that there are N projects $P_1 \sim P_N$ proceeding simultaneously. Each project has n_j ($j = 1 \sim N$) works which are represented by y_{ij} ($i = 1 \sim n_j, j = 1 \sim N$). In order to establish an appropriate plan for these projects, the objective function, constraints and decision variable are defined as follows:

Objective function: $O \rightarrow \max$ (1)

Constraints:

- Order relations among works in each project
- If a constraint of annual budget exists, this is represented as follows:

$$\sum_{j=1}^N \sum_{i \in Y_{jk}} c_{ij} \leq B_k \quad (k = 1 \sim K) \tag{2}$$

Moreover, if no work continuing over years exists, the following constraint is given:

$$\sum_{Y_{jk}} t_{ij} \leq 12 \quad (j = 1 \sim N, k = 1 \sim K) \tag{3}$$

Design Variable: Y_{jk} ($j = 1 \sim N, k = 1 \sim K$) (4)

where, O represents the objective function evaluated in the process of works. For example, O represents the early completion of all projects or the summation of benefit to the inhabitants with the completion of each project. If prerequisite works shown in Table 1 exist as constraints, the order relations are represented as an arrow diagram shown in Figure 1. Each project has the order relations presented in Figure 1. At work i in project j , c_{ij} is the construction cost and t_{ij} is the construction period (month) for completing. B_k is the annual budget on k year. Y_{jk} is the set of works which are done on k year in project j . K is the year when all projects have been completed. In Equation (3), 12 means that the works on the year are completed within 12 months.

Table 1. Example of prerequisite works

Work number	5	6	7	8	9
Prerequisite works	1	3	4 6	2 5 6	7 8

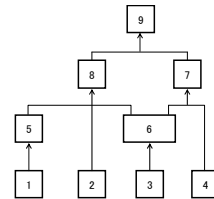


Figure 1. Arrow diagram

PLANNING OF MULTIPLE CONSTRUCTION PROJECTS SIMULTANEOUSLY BY USING GENETIC ALGORITHM

In this study, the coding of gene follows the method proposed by Furuta et al. In the problem, the order for works of projects is determined. The total number of works is represented by Equation (5).

$$NDV = \sum_{j=1}^N n_j \tag{5}$$

All works are numbered in order of the project and the number of work. The order of the number from 1 to NDV represents the genetic array in the problem. For example, in the case with $N = 2$ and $n_1 = n_2 = 4$, the genetic array is represented as follows:

$$[7 \ 4 \ 3 \ 6 \ 8 \ 5 \ 2 \ 1]$$

Then, this array is interpreted by decoding to works of projects; as follows:

$$[y_{32} \ y_{41} \ y_{31} \ y_{22} \ y_{42} \ y_{12} \ y_{21} \ y_{11}]$$

This means that the works are finished in this order. If the problem has constraints such as Equation (2) and/or (3), the annual plan needs to satisfy the constraints. In the above example, the plan is shown in Table 2, if the schedule was decided as follows:

$$[y_{32} \ y_{41} | y_{31} \ y_{22} \ y_{42} \ y_{12} | y_{21} \ y_{11}]$$

This problem should satisfy the order relations of projects simultaneously. In the study of Furuta et al., an attempt was made to satisfy the order relations by introducing the special genetic operators into Simple GA. First, this method creates

the genetic arrays for initial individuals satisfying the order relations. Next, new individuals are generated without violating the order relations because order crossover is used in the crossover operation. Finally, this GA does not use the mutation because the mutation operator is likely to violate the order relations. Then, this method can satisfy the constraints. However, the constraint satisfaction method has some limitations about the design space. Therefore, the search of Simple GA is more likely to be trapped by a local optimum due to the lack of diversity among individuals.

In this study, an attempt is made to satisfy the order relations by applying the local search with the repair of gene based on Baldwin effects to Simple GA. The algorithm of the Improved GA is as follows:

- STEP 1: Generation of initial population
 - STEP 2: Evaluation
 - STEP 3: Local Search
 - STEP 4: Natural Selection
 - STEP 5: Crossover and mutation
- STEPs 2 to 5 are repeated until the convergence is achieved.

The local search satisfies the order relations through two processes. First, in the case of the order relations shown in Figure 1, the repair of gene is performed as shown in Figure 2. In Figure 2, the array labeled “before” represents the genetic array violating the order relations and the array labeled “after” represents the genetic array repaired to satisfy the order relations. The colored portions in the arrays are changed by the repair. Table 3 presents an example of repair. In the repair, a work violating the order relations is stored in the waiting work list shown in Table 4 at the year. Then, the order of the genetic array is repaired in order to implement a waiting work at the year when it can start.

Next, in the local search, the repaired genetic array is used for the calculation of fitness only; the genetic array of individual is not changed. This is because the local search is based on Baldwin effect. Then, it is expected that the constraint satisfaction used in the proposed method has no limitation about the design space.

Table 2. Example of plan

Year	1	2	3
Project 1 (Y_{1k})	y_{41}	y_{31}	y_{21}, y_{11}
Project 2 (Y_{2k})	y_{32}	y_{22}, y_{42}, y_{12}	

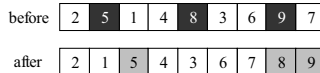


Figure 2. Example of the repair of gene

Table 3. Example of repaired plan

Year	Done works
1	2, 1
2	5, 4, 3
3	6, 7
4	8, 9

Table 4. Waiting work list

Year	Waiting works
1	5
2	8
3	8, 9

NUMERICAL EXAMPLES

The applicability of the proposed method will be verified by several numerical examples. The data of each work in each project used in the numerical examples are shown in Table 5.

In Table 5, "Cost" represents the cost (unit) for each work and "Period" represents the months necessary for each work. "Prerequisite" represents works needed to complete previously in order to start the work. In this study, an attempt is made to apply the proposed method to two planning problems; Example 1 and Example 2. Projects shown in Table 5 are dealt with simultaneously in the problems. 4 projects (project 2, 4, 6 and 7) are considered in Example 1 and all projects are considered in Example 2. The objective function of these problems is shown in Figure 3.

In the problem, w_j is provided to beneficiaries as a quantified service measure by completing project j . The service degree of each project is accumulated every year with the progress of works. In this study, the summation of service measure of each project is normalized to 1. Therefore, non service measure is calculated by subtracting this summation from 1. The objective of this problem is the minimization of accumulated non service degree which is the colored portion in Figure 3. The service measure of each project shown in Table 5 is 22, 23, 25, 11.5, 22, 6 and 26 for project 1 through 7 respectively.

In the numerical examples, constraints are considered as follows; (1) order relations, (2) annual budget and (3) period for works. The constraint (1) is shown as prerequisite works in Table 5. The constraint (2) is that the total of cost for works in a year is less than the annual budget; solutions must satisfy Equation (2). The annual budgets used in each example are shown in Table 6. The constraint (3) means that no work is continuing over years as shown in Equation (3).

The parameters of Simple GA and the proposed method applied in the numerical examples are shown in Table 7. The mutation applied in the proposed method is the exchange of portions selected from a genetic array randomly. The results obtained by 20 times executions of the two methods are shown in Table 8.

It is seen from Table 8 that solutions obtained by the proposed method were better than Simple GA in the two examples. First, the results of the methods were almost the same in Example 1. This means that search performance of Simple GA is equal to that of the proposed method in a small problem. However, there were differences in the results between Simple GA and the proposed method in Example 2. The search of Simple GA is considered to result in the convergence to a local optimum due to the lack of diversity among individuals. In Example 2, the search processes in the case that a solution with the best evaluation was obtained by the methods are shown in Figure 4.

In Figure 4, the search of Simple GA converged prematurely. On the other hand, it is seen that the proposed method was able to search a better solution than

Simple GA. In the problem with many constraints, the number of solutions which satisfy all constraints is very fewer than solutions violating constraints. Therefore, in the search of Simple GA, the larger the problem is, the more difficult it is to keep the diversity among individuals because individuals violating constraints are not generated.

Table 5. Data of each work in each project used in numerical examples

Project No.	Work No.	Cost	Period	Prerequisite	Project No.	Work No.	Cost	Period	Prerequisite	
1	1	40	3		4	9	375	6	1, 2	
	2	160	9	1		10	375	6	2, 4	
	3	100	6			11	375	6	2, 4	
	4	50	9	3		12	375	6	2, 4	
	5	100	6			13	330	6	3, 9	
	6	50	9	5		14	340	6	3, 5, 10	
	7	230	9			15	330	6	5, 6, 12	
	8	180	9	2, 7		16	90	6	8, 13, 14, 15	
	9	270	9	1, 2, 3		17	200	3	6	
	10	200	6	4, 9		5	1	55	6	
	11	200	6	4, 6, 9			2	50	6	1
	12	150	6	10, 11			3	50	6	
	13	40	3	12			4	50	6	3
	14	150	3	8			5	415	9	1, 3
2	1	230	6				6	200	6	2, 4, 5
	2	230	6				7	40	6	2
	3	160	6				8	15	1	7
	4	110	6	1, 2, 3	9		20	3	4	
	5	230	3	7	10		10	1	9	
	6	230	3	7	6	1	250	9		
	7	130	6	4		2	70	6	1	
	8	200	9	1, 2		3	250	9		
	9	140	3	5, 6, 8		4	70	6	3	
	10	100	3	5		5	20	3		
	11	20	1	6		6	20	6	5	
3	1	2250	12			7	200	9	1, 3	
	2	750	12			8	100	6	5	
	3	1000	12			9	35	3	4, 6	
	4	650	9			10	20	3	2	
	5	650	9			11	10	1	10	
	6	700	9			12	15	3	6	
	7	500	6	1, 2, 4		13	5	1	12	
	8	500	9	2, 3, 5, 6	1	600	6			
	9	150	3	7, 8	2	600	6			
	10	350	6	1, 3	3	200	6			
4	1	500	12		4	150	6	1, 2, 3		
	2	400	9		5	500	6	7		
	3	150	6	2	6	500	6	7		
	4	400	9		7	580	6	4		
	5	150	6	11	8	600	9	1, 2		
	6	1100	9		9	370	6	5, 6, 8		
	7	340	9		10	250	3	5		
	8	230	6	6, 7	11	30	3	6		

In the search of the proposed method, individuals violating constraints are generated. However, the proposed method can search solutions with keeping the diversity of individuals with the use of the local search based on Baldwin effect. Furthermore, the local search can use gene information of individual violating constraints by use of genetic array repaired to satisfy order relations in the decision for fitness. For example, it can be expected that the local search obtains global optimum easily even if there are few solutions which satisfy constraints around global optimum in the problem space of GA. Therefore, it is considered that the proposed method was able to obtain better solutions than Simple GA without being trapped by local optimum as shown in Figure 4.

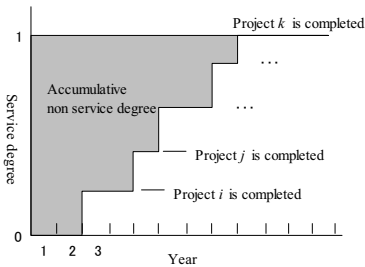


Figure 3. Objective function

Table 6. Annual budget of each example

Year	Annual budget (unit)	
	Example 1	Example 2
1	300	500
2	900	1500
3	1500	2500
4	2000	3500
5	2700	4500
6	2700	4500
7	3500	6000
After	3500	6000

Table 7. Parameters used in numerical examples

Method	Simple GA	Proposed method
Population size	2000	2000
Crossover rate	0.8	0.6
Mutation rate	0.00	0.01
Generation	500	500

Table 8. Result of numerical examples

Problem	Example 1		Example 2	
	Simple GA	Proposed method	Simple GA	Proposed method
Best Evaluation	4.308	4.218	5.472	4.376
Worst Evaluation	4.744	4.519	6.129	4.956
Average	4.471	4.320	5.895	4.680

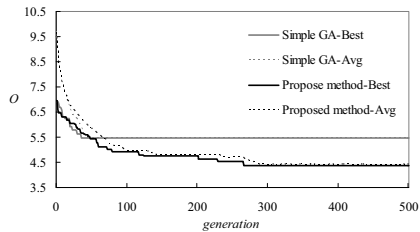


Figure 4. Search process

CONCLUSIONS

In this study, an attempt was made to develop a decision support system for the optimal planning of public works by using Improved GA. In order to search an optimal solution under multiple constraints, the proposed GA adopted the local search which used the repair process of gene based on Baldwin effect. Through numerical examples, it was demonstrated that the proposed method can obtain more appropriate solutions than Simple GA regardless of the size of problem. The proposed method can search for solutions with keeping the diversity of individuals with the use of the local search based on Baldwin effect. Furthermore, the local search can use gene information of individual violating constraints by use of genetic array repaired to satisfy order relations in the decision for fitness.

In this planning problem, Simple GA satisfied constraints by embedding order relations in the coding of gene. On the other hand, the proposed method dealt with order relations as constraints and satisfied constraints by using the local search. Then, the proposed method can be expected to improve the search performance in various problems under multiple constraints, because the constraints satisfaction method used in the proposed method has no limitation about the design space.

REFERENCES

- H. Furuta, H. Sugimoto, Y. Inoue, T. Yokota, A. Hirose and T. Nakatani (1998). "Application of GA to long/middle term planning of road network project", *Journal of Structural Engineering*, JSCE, Vol. 44A, pp.497-502 (in Japanese).
- E. Aiyoshi and K. Yasuda (2007). "Metaheuristics", *The Institute of Electrical Engineering of Japan*, pp.15-27 (in Japanese).
- Kim, W. C. Ku (2006). "Enhance the Baldwin Effect by Strengthening the Correlation between Genetic Operators and Learning Methods", *IEEE Congress on Evolutionary Computation*, pp.3302-3308.

Quantitative Risk Assessment, Public Policy, and Decision-making

Vilas Mujumdar¹, P.E., S. E.

¹VSM Associates, 9905 Trosby Court, Vienna, VA 22181, PH (703) 938-2117;
email: v_mujumdar41@yahoo.com

ABSTRACT

Effective hazard reduction depends to a large degree on informed public related to risks, risk consequences, and risk management practices. *Quantitative risk analysis* can estimate probabilities of damages considering different variables as well as the costs associated with the damages.

In a community, several engineered systems act together interdependently to provide operating functionality. Interdependence among systems is not well understood and thus meaningful measures of system vulnerability are difficult to derive. To minimize the impact of a damaging natural hazard on a community, actions by several levels of decision-makers are necessary. Effective public policies have to consider not only the quantitative analysis of physical systems but also economic consequences for the society, and socio-political rationality. The focus of this paper is on long –term actions taken by the public officials in minimizing the loss of functionality in a community, by combining quantitative analysis with the qualitative aspects of the decision-making reality in the context of public policy.

1. GENERAL BACKGROUND

1.1 *Quantitative Risk Assessment*

Quantitative risk assessment approach states risk in numerical terms. On the other hand, Qualitative approach does not express a numeric value but classifies the risk in words like “low”, “medium” and “high”. It is based on expert opinions.

Quantitative risk assessment is primarily focused on physical facilities, and engineers are concerned with risk analysis and assessment of these. *Quantitative risk analysis* can identify the variables, define their relationships and consider the interaction based on these relationships. Risk assessment involves assessing the probability of a hazard, the vulnerability of physical facilities to the hazard, and the resulting consequences. Such assessment is possible for physical facilities as the vulnerabilities in physical systems can be estimated based on experimental data. The severity of damage to the structural systems can be translated into estimating non-

structural systems damage, and damage to equipment supported on structural systems. Thus, it is possible to assess the risk numerically for a single facility. Probabilities of damage for different variables can be determined as well as the costs associated with the damage and the overall risk. In a community, overall damage to physical facilities can be aggregated if data is available for the quantity of different types of facilities, material used for construction, and their age. However, even in the engineering systems, the interdependent nature of the infrastructure systems and consequent vulnerabilities and damages as a result of these combined behaviors must be considered.

1.2 *Public Policy*

Public officials, on the other hand, have to consider the entire community as a system. The physical civil infrastructure systems are *sub-systems* in the overall community system. . Other subsystems that compliment the engineering systems are economic sub-system, and societal sub-system. When a hazard strikes, all systems in a community are impacted and the overall safety and the amount of damage depend on the type and degree of interdependency that exists among engineering systems, economic systems, and societal systems. Overall risk assessment needs to give due consideration to these interdependencies. Public policies have to be made without complete information and recognizing the lack of capacity to process all the information. The resulting enacted public policy related to hazards may not be *optimal*, but attempts to benefit all segments of a society in some way. It is an outcome of a process that considers qualitative analysis in conjunction with quantitative analysis to assess cost-benefit aspects of a public policy.

1.3 *Decision-making*

All decisions that are made by private owners or public officials to address a specific scenario involve risk. Whether a risk is implicitly covered or explicitly assessed depends on the environment in which such decisions are taken. In a democratic environment, arriving at a decision and implementing it is an art; this author argues that the underlying basis for a decision ought to be based on scientifically robust data, analyses, and expert opinions.

Decision-making in the public sector is not always based on considerations of overall risk. There are many reasons for this: lack of time, lack of credible information, inability to process all information, lack of consensus and finally political considerations. Decisions also tend to be modified by different stakeholder interests. To minimize the impact of a damaging natural hazard on a community system, actions at several levels of decision-makers are necessary. Some actions are immediate in nature and others are meant for long-term. On a long-term basis decision-makers are interested in minimizing the loss of functionality in a community by creating resiliency. Such an effort requires creating redundancy and robustness in physical systems; resourcefulness in the socio-economic fabric of the community, institutional structures and by educating the populace at large on the risk posed by a natural hazard.

2. PHYSICAL CIVIL INFRASTRUCTURE SYSTEM

In the context of civil engineering systems, the example of physical civil infrastructure will be perhaps better understood. The case is further illustrated by using a seismic hazard affecting the physical civil infrastructure in a community. Physical civil infrastructure can be considered as a complex coupled engineering system that provides resources and services necessary for *functioning and sustainability* of the society. Physical civil infrastructure that is considered critical for functioning of a community comprises of *transportation networks, water and wastewater utility systems, electric power network, gas pipelines and distributions systems, and communication systems*. These systems are integrally connected and interact with socio-economic systems to form a complete community system.

2.1 System-based approach

It is necessary to define and understand a “system”. This author defines a system as “*a group of independent but connected elements or subsystems forming a unified whole, that interact coherently and synergistically to achieve a beneficial purpose*”.

A systems approach provides:

- A holistic perspective
- Melds individual discipline contributions into an unified effort considering interdependencies
- Forms a structured development process from *conception to operations*

A system can be ‘static’ or ‘dynamic’. A static system is non-adaptive due to absence of feedback loops. A dynamic system can be adaptive or non-adaptive depending on the ability to respond to input from the feedback loops.

A dynamic system considers input from subsystems and *adapts/modifies* system behavior to achieve desired outcome; and considers stakeholder input to deliver cost-effective solutions, which leads to dynamic decision – making framework. However, it often requires contribution from diverse disciplines, and determination of degree and nature of interaction among sub-system or components.

2.2 Behavior of systems

The character of a system is dependent on how the components or subsystems are connected and the types of connections themselves. When the components are connected to each other in a linear chain-link fashion, the resulting system is called a *series* type. When the components are connected in such a way that at least two routes are available from one point to another, the system is called a *parallel* type. A system may have combination of both series type and parallel type connections resulting into a *hybrid* system. When the components are not connected in any defined way or the connections are not discernible, the system is characterized as a *random* type. Another defining characteristic of a system is the type and behavior of links connecting the components. The linkages can be *linear or non-linear* (see Figure1).

Built environment, which comprises civil physical infrastructure, are static systems and the linkage is rigid and linear. That is, under a particular hazard such as earthquake, the behavior is predictable with the use of fragility curves. However, the

linkages with economic and societal systems are non-linear and flexible. This is due to the fact that under a hazard, the economic and societal systems adjust and the response is modified. The predicted behavior is difficult as the exact nature of this relationship is not known as there is non-linearity and randomness associated with it.

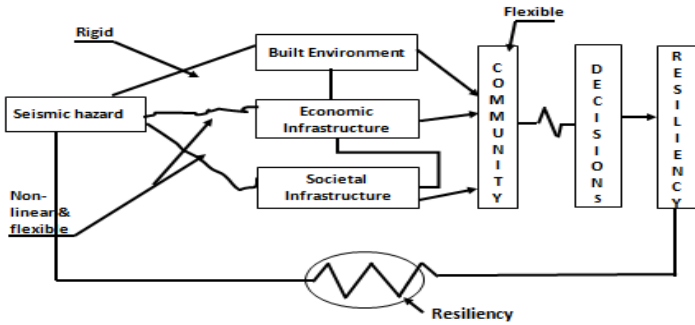


Figure 1. - Types of Linkages among Sub-systems

2.3 Individual infrastructure system

When considerations go beyond a single facility to an infrastructure system such as water utility where civil engineers are responsible for the design of the entire system, the design and risk considerations are different than in a single facility. A *water supply system* consists of various sizes of pipes, branches, and pump stations. Fragility curve for each of the components needs to be generated. These fragilities would indicate the most vulnerable components in the system. However, to determine the vulnerability of the entire system, one has to determine the joint fragilities considering the fragilities of all components together working in the system. The joint fragility curves must be generated for various levels of damage to assess the probable damage to the system under a wide range of intensities of hazards. This is a difficult task that must be undertaken to understand the system behavior. Quantitative analyses methods in conjunction with the data on the component fragilities and network analysis would enable determining the system fragility. Thus, it is possible to determine fragility for a single infrastructure system.

2.4 Interdependency among infrastructure systems

As difficult as it is to derive joint fragility of a system considering the contributions of different components, in a community various systems are also interdependent. Modeling interdependency among various infrastructure systems is critical to understanding the behavior of the total infrastructure system. Although

interdependencies can be categorized as geographical, physical, and hierarchical, for infrastructure systems, this author proposes a different categorization: *system engineering design basis*; *operational basis*. Following examples of interdependency are given for illustration purposes:

1. System engineering design basis
 - a. Water system with electrical network
 - b. Transportation network with electrical network
 - c. Electrical network with communication systems
 - d. Wastewater system with electrical network
2. Operational basis
 - a. Hierarchical – within organizations
 - b. Organizational – between organizations
 - c. Socio-economic systems

When the electrical network is damaged, it impacts the water networks because the pumping stations are affected. This may be in addition to the direct damage to the water system due to the hazard. Therefore, the water system is considered dependent on the electrical system. To determine the impact of damaged water system on customers, the impact of electrical system on the water system needs to be modeled. This requires joint fragilities to be derived. Similarly electrical system impacts transportation system since traffic signals are affected.

3 PUBLIC POLICY – GENERAL

3.1 *Public policy authority and Influence*

In the US, public policy is made at several levels. At the federal level, congress is responsible and at the state level, state elected legislators are responsible. At the local level, cities and counties can also make public policies specific to their jurisdictions through elected public officials. Regulations by administrators of various governmental organizations can be promulgated for specific situations that are *in effect enforceable* documents just like codes. Many entities try to influence the public policy as their own interests are at stake. Lobbyists engaged by large businesses, charitable organizations, political action committees, state and local governments, special interest groups, and general public through direct contact with the elected officials. Because it is such a complex process imbued with so many interests, the eventual policy outcome is at best, a compromise

3.2 *Public policy- natural hazards*

In natural hazards area, three considerations dominate. The demand at each stage is different and the public policy considerations for each stage are necessarily different. (see Figure 2).

Public Policy Considerations

A. Prior to major hazard event

Mitigation	<ul style="list-style-type: none"> a. Has upfront costs b. Need economic incentives c. <i>Don't fix till it is broke</i>
-------------------	---

B. During major hazard event

Response	<ul style="list-style-type: none"> a. Societal Preparedness b. Timeliness – efficiency c. Resource availability d. Resource Mobilization
-----------------	--

C. After major hazard event

Recovery	<ul style="list-style-type: none"> a. Strong economy – private industry b. Govt. Programs for Reconstruction
-----------------	--

2

Figure 2.- Stages in a Hazard Event

As can be seen in figure 2, *during a major hazard event*, the policy is required for emergency management requiring immediate assistance and resource mobilization for that effort. The main concern is safety of population and providing basic survival needs as well as the medical care. A policy must be in place for such emergencies. For example, all counties in California are required to have an emergency management plan and a separate entity to provide the emergency response. There is usually no disagreement within legislators for this situation.

Before the event, however, the policy considerations require studying mitigation efforts. These measures have upfront cost. The policy discussions revolve around priorities among competing claims on the resources and enacting laws to enforce retrofit measures. Many stakeholders are involved and unless economic incentives are given, owners have very little motivation to retrofit their facilities voluntarily.

After a major event, the considerations are significantly different. Governments and the private industry are interested in a strong economic recovery and a robust environment for further investments in the community. Reconstruction of damaged facilities takes a priority for a community. This is also the period where discussions take place on the long-term retrofit, land-use, and insurance- regulation policies.

Since stakeholders are involved in protecting their own interests, making decisions in a society that is acceptable to all becomes extremely difficult and time-consuming. A societal decision-making model is shown in figure 3. The common area of interaction and agreement between various actors is very small. (see Figure 3)

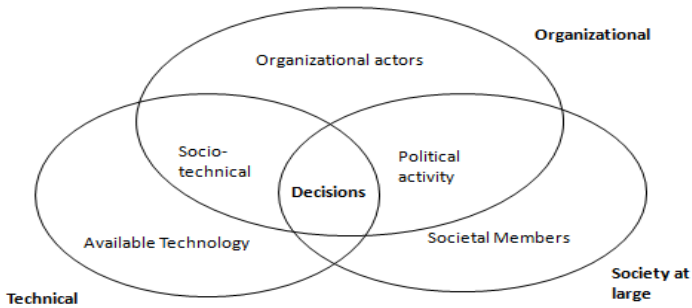


Figure 3.- Societal Decision-making Model

4 DECISION-MAKING –NATURAL HAZARDS

4.1 Decision-making in public sector

In public sector decision-making is fraught with many issues. Some of these are: *separate regulations for Federal facilities or federally assisted facilities; multiple agencies promulgate regulations– lack of clarity in areas of responsibility; federal versus state authority; and federal government as a “resource of last resort”.*

Satisficing is a decision-making strategy which is often employed, which attempts to meet criteria for adequacy rather than identify an optimal solution. For near optimal solutions the cost of obtaining complete information can be considered in the decision outcome. Satisficing occurs in consensus building when the group looks towards a solution everyone can agree on.

It is suggested that to minimize the impact of a natural hazard on a community, public policy component must be incorporated in integrated analysis. As pointed out by the Subcommittee on disaster reduction, in 2004, *Protecting American communities from disasters ---- depends on policy makers adopting an integrated approach to disaster risk reduction, drawing on existing knowledge ----- combined with new information on risks –”.*

Multi-Criteria Decision Analysis (MCDA) methods can be used which allows quantitative and qualitative attributes to be evaluated that are necessary to take into account different interests of multiple stakeholders.

5 SUMMARY

In summary, this paper identifies various aspects that need to be considered by public officials before they make a decision:

- Public officials have to address the larger issue of health and life safety of a community
- The assessment of risk to physical systems need to evaluated considering interdependencies of various systems
- Joint fragilities need to be generated based on these interdependencies
- The overall community system comprises of physical civil infrastructure systems along with socio-economic systems
- Given the technical risk assessments and other socio-economic considerations, public officials have to make decisions even though complete information may not be available
- The decisions are made considering qualitative information along with the quantitative analysis
- Final decisions are not always optimal but satisfy most of the stakeholders

It is the responsibility of engineering profession to provide robust and credible information on behavior of physical systems. Based on this engineering data base, public officials can make risk-informed decisions that are rational.

6 REFERENCES

1. American Lifelines Alliance Power Systems, Water, Transportation and Communications Lifeline Interdependencies March 2006 (DRAFT)
2. Rinaldi, S, Peerenboom, J, and Kelly, T. Identifying, Understanding and Analyzing Critical Infrastructure Interdependencies. *IEEE Control System Magazine*; 21:11-25.
3. Department of Homeland Security, National Infrastructure Protection Plan 2006. Department of Homeland Security
4. L. Nozick, M. Turnquist, D. Jones, J. Davis, C. Lawton, 'Assessing the Performance of Interdependent Infrastructures and Optimizing Investments', *Proceedings of the 37th Annual Hawaii International Conference on System Sciences*, Island of Hawaii, January 2004.
5. Jamie E. Padgett, Reginald Des Roches, 'Methodology for the development of analytical fragility curves for retrofitted bridges' *Earthquake Engineering and Structural Dynamics*, 2008;37:1157-1174, Wiley Inter Science
6. Mujumdar, V, "Multi-hazards, Vulnerability, Mitigation, and Decision-making in Public policy Context", *University of Illinois*, Urbana-Champaign, IL Feb.2009
7. Mujumdar, V., "A Need for Risk-Consistent Approach to Multi-Hazard Engineering"., *Symposium on Emerging Developments in Multi-Hazard Engineering*, New York, New York, Sept. 18, 2007

Research on the establishment of mega public building safety risk assessment system in China

Chen Liang¹, Mao Longquan², Feng Ye³, Cheng Hu³

¹Nanjing Construction Quality Supervision Station, No.33 Yudao Street, Nanjing, Jiangsu Province, 210000; email: 13386555@163.com

²Nanjing Municipal Commission of Housing and Urban-rural Development, No.185 Guangzhou Road, Nanjing, Jiangsu Province, 210000; email: mlq_2006@sina.com

³Project Management Research Institute, Civil Engineering College, Southeast University, Nanjing, Jiangsu Province, 210096; email: youliang_h@163.com

ABSTRACT

Based on the mega public building safety management status in China, the related legal system and government supervision mechanism still need to be improved. However, as many a mega public building with high technology is being built or has been operated in China, safety risk may exist to some extent. Therefore, this article puts forward the establishment of mega public building safety inspection system. The researches will contain legislation, inspection contents, confirmation of inspection methods or procedures, qualification of inspection organization and inspectors.

INTRODUCTION

With rapid economic growth and improvement of people's living standard in China, a lot of mega public buildings with unique structure have been built, such as Beijing Olympics Stadium, newly constructed tower for China Central Television, Canton Tower in Guangzhou and so on. Their technical requirements have exceeded the existing construction standards, which may cause technical difficulties and increase risks. As the characteristics of public and service of mega public building, their safety management methods are different from other kinds of buildings. The reason is not only about its unique shape but also about the fact that there are much higher quality requirements for the building structure and construction processes. In addition, during service life of building, wear and tear of structures, changes of architectural composition, owners' incorrect use and climatic deterioration may bring about building safety hazards. Based on that, Construction Project Management Institute of Southeast University and Nanjing Construction and Installation Engineering Quality Supervision Station carried out a research named "mega public building safety risk assessment system" in 2009 commissioned by the Ministry of Housing and Urban-Rural Development of the Peoples' Republic of China.

LEGAL RESEARCH FOR MEGA PUBLIC BUILDING RISK ASSESSMENT SYSTEM

The establishment of each kind of systems requires rules and regulations for guarantee. Based on the status quo of building safety management in China, the existing management system just focuses on the verification and safety management of dangerous houses. Meanwhile relevant laws and regulations are limited. Taking the Construction Law of the Peoples' Republic of China as an example, as the most essential law in the field of construction, Construction Law is mainly about quality and safety management in the stage of design and construction, but seldom about the safety management of existing buildings (the Eighth National People's Congress Standing Committee, 1997).

Therefore, in order to reinforce the safety management of existing buildings the Law should be revised. For example, from the perspective of the management scope, the content of building maintenance, reinforcement, and demolition should be incorporated into it, especially the government regulatory supervision measures, qualification management of inspection organizations and inspectors as well as implementation process of structure periodic inspection system and dangerous building safety appraisal system. In addition, the law should also include sustainable development management, construction waste disposal, building energy conservation and reduction measures.

Besides the revision of Construction Law, a series of regulations are drawn up, which are also necessary for the establishment of a mega public building safety risk assessment system. Consequently, this paper will propose the establishment of existing building safety management regulation as another legal support for the proposed system. Concretely, the regulation should be included the contents, such as safety precautions, procedures and supervision of existing building demolition, operation safety management measures like structure periodical inspection of the existing building system; building maintenance management and dangerous housing management.

THE DEFINITION OF MEGA PUBLIC BUILDING RISK ASSESSMENT TARGET AND INSPECTION RANGE

So far, there have not been any unified definition standards for mega public building in the world. In terms of relevant Chinese standards, qualitative and quantitative definitions of mega public buildings are mainly based on floor area. In the Design Standard for Energy Efficiency of Public Building Detail Regulation of China, mega public building is defined as a single building or annexed building whose floor area is more than 20,000 m² (Ministry of Housing and Urban-Rural Development of the People's Republic of China, 2005). However, the classification standard based on floor area is not the same among different kinds of buildings. And it is not all-inclusive that the floor area is the only quantitative indicator. As the

author focuses on safety risks that will cause personal injuries and property damages at the stage of operation period, those which are not large enough but may hold the crowd gathered in a short time or of which internal facilities may influence social activities will also be incorporated into the discussion in this paper. Therefore, besides the floor area, crowd intensity and particularity of buildings will also be the quantitative analysis indicators for defining the mega public building and the reasons are shown as follows.

Based on the floor area for definition

In this paper, floor area is applicable as a quantitative indicator for defining the volume of public building and the number of 20,000 m² still can be the boundary line. The reason is, on the one hand, floor area is the most familiar and visual technique data. On the other hand, the building whose floor area is larger than 20,000 m² may face more safety risks. Meanwhile, it is to be noted that floor area is not the only indicator and will be combined with the following factors for definition.

Based on the particular type of building for definition

Even though the floor area of some of the buildings is less than 20,000 m², they may have important role of public service. Once an accident happens, there will be a negative impact on the society and even a great loss of property and lives. Therefore, these kinds of public buildings with particular purposes can be classified into mega public buildings. Concretely, the following kinds of building can be incorporated into mega public building in this paper (See Table 1).

Table 1 Types of public buildings with particular purposes

Types of public buildings with particular purposes
• national and provincial television building
• national and provincial power dispatching center
• provincial post office building
• regional city fire control center
• regional city telecommunication control center
• regional financial service center like the People's Bank of China and four major commercial banks
• city executive office building
• library with more than one million books
• the county-level or above archives
• the research center where the value of scientific equipment is more than 100,000,000 Yuan (RMB)

Based on the crowd intensity for definition

Although some of public buildings, like multi-storey schools, do not have any special purposes and their floor areas are not more than 20,000 m², they are urban

public spaces with thick crowds. Once an incident happens, a great loss will take place. Therefore, this kind of buildings should be incorporated into the safety management category of public buildings. The author argues that the standard of crowd intensive degree is more than 500 people. Based on that, mega public building with a dense crowd is referred to as the public space that enables more than 500 people frequently or regularly to gather such as the school, library, dormitory, commercial center, office building, catering center, tourist building, medical center, stadium, exhibition hall, memorial, mercantile exchange center and places of public entertainment.

Based on risk threatened area for definition

Some of the high-rise buildings such as television tower or cistern which may threaten the public safety around them if an incident happens should also be incorporated into the safety management category. Thereby, in this paper, the high-rise building whose threatened area is more than 100m to the public will also be taken into consideration.

Overall, mega public buildings in this paper are shown in the following Table 2.

Table 2 Types of mega public buildings

Types of mega public buildings
<ul style="list-style-type: none"> ● All kinds of single public buildings whose floor area is more than 20,000 m²
<ul style="list-style-type: none"> ● power and telecommunication, financial and other special end-use public buildings of city-level or above;
<ul style="list-style-type: none"> ● all kinds of public buildings that enable more than 500 people to gather;
<ul style="list-style-type: none"> ● High-rise building whose threatened area is more than a radius of 100m.

THE ACCREDITATION OF MEGA PUBLIC BUILDING RISK ASSESSMENT ORGANIZAITONS AND CHECKERS

A great many mega public buildings with unique structures, new materials and construction processes have been built and operated. The main method to control risks and solve technique problems of construction is the expert seminar in China. However, experts do not have to bear legal responsibilities of final results after seminars. But the safety assessment of mega public buildings is more complicated compared with other kinds of buildings. And the assessment of these complicated construction processes and particular design is the high requirement for the assessment organizations. As an independent third-party advisory agency, mega public building risk assessment organization not only needs to meet the technical requirements of industry, but also should shoulder legal responsibility of the result report. Consequently, the government should implement strict qualification access restrictions for the inspection organization. The so-called access mechanism of

assessment agency is referred to as setting up certain requirements on the registered capital, technicians, organization, equipment and internal management system for the assessment agency to ensure the quality of assessment. During the establishment of mega public building risk assessment organization access mechanism, the following points should be mainly concerned with:

- In view of technical requirements and limited resources, assessment agency can be divided into two levels, Class A and Class B according to its qualification. Class A institute can take business in the whole country and its qualification management is taken on responsibility by the national Ministry of Housing and Urban-rural Development. Meanwhile, Class B institute can only make contract to do a job within the province and its qualification management also assumes responsibility by provincial government department. In addition, registered capital, equipment and the technical personnel should be considered into the accreditation standard of assessment organization.
- As the assessment is a relatively complicated job which contains of fire safety control, public sanitation prevention and control, disaster reduction and construction safety, general risk assessment cannot meet all the requirements of the assessment job. Therefore, the business scope can be sub-divided into special assessment and comprehensive assessment. Disaster safety assessment and fire safety control assessment before the construction belong to the scope of special assessment. While, design quality assessment, construction safety assessment, existing building safety assessment are all about comprehensive assessment.
- Building management relates to different kinds of fields such as structure, water supply and drainage, electricity, air condition and so on. As a consequence, it is necessary for the assessment agency to meet these technical requirements, otherwise it cannot take up business of relevant fields.

According to the mentioned-above requirements of the accreditation of risk assessment agencies and drawing on the experience of other relevant fields, this article puts forward assess standards for agencies and inspectors as shown in the following Table 3.

Table 3 Qualification Requirement Table of Inspection Organizations and Inspectors

	Class A	Class B
Registered capital	More than 5,000,000 Yuan	More than 3,000,000 Yuan
Professionals	Not less than 32 full time technicians including not less than 8 registered architects; 8 certified structure engineers; 6 registered construction engineers; 10 accredited professionals in other relevant fields or a certain number of senior engineers. Moreover, the number of each Grade A registered architects and Grade A certified structure engineers is no less than 3.	Not less than 24 full time technicians including not less than 6 registered architects; 6 certified structure engineers; 4 registered construction engineers; 8 accredited professionals in other relevant fields or a certain number of senior engineers. Moreover, the number of each Grade A registered architects and Grade A certified structure engineers is no less than 1.
Management mechanism	There is a sufficient sound organization management system.	
Equipment	Owning necessary technical support such as facilities, equipment and regular workplace.	
Others	Having the qualification of Class B of more than 3 years, without illegal record and having the ability to take business of tow mega public buildings.	None

Moreover, knowledge, experience and skill of inspectors may have an impact on the assessment work to some extent. Professional qualification is a main method for the government to control the admission of those professional and technical works that have direct advantageous and disadvantageous relations with public benefits. And it is also a necessary standard prerequisite of entry to the profession for the accreditation inspectors. Their jobs are on the one hand to provide adequate assessment report and on the other hand to bring forward relevant countermeasures and suggestions. The professional qualification has another ideal of potential quality assurance and commitments for clients. The existing relevant qualification in the construction field includes certified structure engineers, certified civil engineers, registered architects, registered construction engineers, certified geotechnical engineers and so on. Based on the characteristics of the risk job, although the establishment of a new kind of professional qualification certification system will no doubt help to achieve the expectation of clients or government, it also wastes a lot of resources.

MEGA PUBLIC BUILDINGS RISK ASSESSMENT PROCEDURE

Mega public building risk assessment procedure is mainly based on the popular method in the world, i.e. the four-step process shown in the following fig.1 which contains hazard identification, exposure assessment, dose-response assessment and risk characterization which was put forward in the National Research Council in 1983.

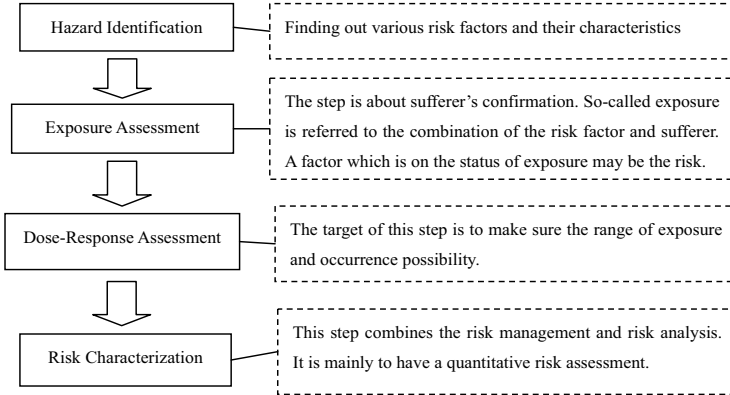


Fig.1 Risk Assessment Procedure Flowchart

Obviously, the job of assessment is a kind of process that is risk identification, risk characterization and taking measures. According to the features of risk assessment, mega public building risk assessment procedures which are shown in the following fig.2 including application step, preparation step, inspection steps and evaluation conclusion (National Research Council, 1983).

Agency Commission

The person in charge of mega public building safety management should submit a application report to the government department before inspection, and then employ an accreted agency for the assessment. If not, the government will urge them to do so and punish them. Moreover, the person in charge will reach a preliminary agreement of fees with the agency. Then both of the two sides will sign a contract which will be kept on the record later.

Inspection Preparation

Inspection agencies should establish an evaluation group in which there are two accredited inspectors and other necessary professionals. The person in charge should provide relevant construction materials and technical documents to the evaluation group. According to the materials, inspectors may map out a project which will include the purpose, object, content, standard, method, budget, timing, procedure, equipment and so on. These conditions will also include the contract signed by the

two sides.

Risk identification

Inspectors will analyze all of the materials to determine the damage position, choose the proper method such as data analysis method, eye-measurement method, nondestructive analysis method and so on. During the assessment, inspectors should pay much attention to the potential safety hazards and make a record.

Conclusion

Inspectors should draw the conclusion from the site condition. If necessary, a countercheck is needed. And then a conclusion report should be made and submitted to the government department for record.

If disaster happens, the mentioned-above procedures must be simplified. For example, there is no commission step but direct assignment of agency as well as the submission procedure of conclusion report to the government department.

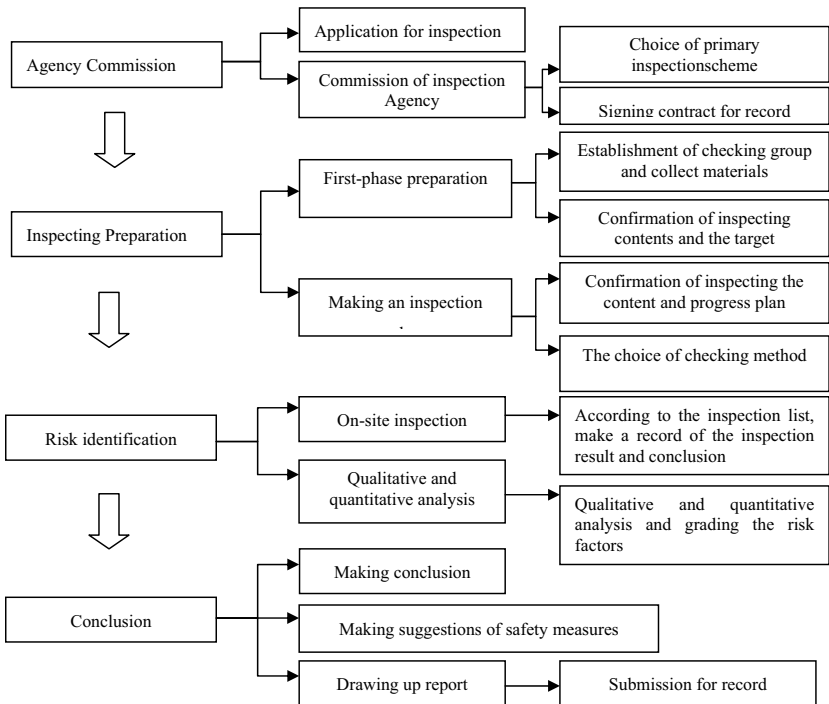


Fig.2 Mega public building safety checking flowchart

MEGA PUBLIC BUILDING SAFETY ASSESSMENT PROCEDURE REGULATIONS

Mega public building safety inspection system consists of time point setting, establishment of the inspection organization, inspector's constitution, selection of checking methods, implementation of inspecting procedures, confirmation of inspecting content and result conclusion. Each of these will play a key role of the inspecting job. Failure of each procedure may go against the governmental supervision and even make the whole system losing the principle of transparency, publicity and equity. Therefore, in order to make the realization of standardization of the whole procedure, the author will put forward procedure regulations of mega public building safety inspection system which will be a text format specification of the whole inspecting procedure. But it has been noticed that practice procedure is not unchangeable. During the practice, the inspection organizations and inspectors can make a corresponding change of inspecting methods or procedures according to the characteristics of buildings. Generally, the procedure regulations of mega public building safety inspection consist of five parts.

Concretely, the general rule is the original version of the procedure regulations of each stage which is mainly about omnibus description of the inspection job on the perspective of the life cycle. Its specific contents should include first of all, defining the jobs of assessment and making clear the emphasis of the inspection job; secondly, the confirmation of the target and inspection agency as well as the inspector's constitution; thirdly, expatiation of inspection procedures, contents and conclusion report. As the inspection procedures are being phrased, according to the characteristics of the inspection job during each stage and based on the regular rule, inspection procedures regulations of each stage are necessary, such as mega public building safety inspection procedure regulation of the design stage, mega public building safety inspection procedure regulation of the construction stage, mega public building safety inspection procedure regulation of the operation stage and mega public building main risk resource inspection procedure regulation of construction stage. Concretely, these four parts should be focused on the description of inspection procedures, selection of inspection methods and the requirements of the conclusion report. Meanwhile, the regulations should be enclosed with the table of inspection procedures, the report template, format requirements, material lists provided by the person in charge of mega public building safety management.

CONCLUSION

This paper mainly introduces the establishment of mega public building safety risk assessment system in China which includes legal researches, inspection contents, inspection methods, inspection procedures, inspection organizations and inspectors. This system will make a profound impact on the building safety management in China. It can not only make the whole building supervision system more regularly,

but also serve to realize the building life-cycle management system. Furthermore, the establishment of mega public building safety inspection system will be an example of a new management model change in the future.

REFERENCES:

- The Eighth National People's Congress Standing Committee (1997), *Construction Law of the Peoples' Republic of China*, Retrieved on September 25, 2009, from http://www.gov.cn/ziliao/flfg/2005-08/05/content_20920.html
- The Ministry of Housing and Urban-Rural Development of the People's Republic of China (2005), *Design Standards for Energy Efficiency of Public Buildings Detail Regulation of China*. Beijing: China Architecture and Building Press
- National Research Council (1983), *Risk Assessment in the Federal Government: Managing the Process*, Washington, D.C.: National Academy of Press.

A new model of supervision of Chinese government over building

safety: based on the third-party assessment mechanism

Cheng Hu¹, Mao Longquan², Huang Youliang¹, Zhao Xin¹,

1 Project Management Research Institute, Civil Engineering College, Southeast University, No.2 Sipailou, Nanjing, Jiangsu Province, 210000;

Email: pmri@seu.edu.cn

2 Nanjing Municipal Commission of Housing and Urban -rural Development, No.185 Guangzhou Road, Nanjing, Jiangsu Province, 210000;

Email: mlq_2006@sina.com

【Abstract】 With rapid development of Chinese urbanization, the number of city buildings is growing rapidly. The original building safety supervision system: supervision functions are divided into many departments, supervision focused on the spot, could no longer be effective. There exist problems with the deficiency of executive resources, blind management zone and unclear responsibility. By employing third-party assessment agencies as a "chain" of building safety management, the original divided and intermittent administration functions can be integrated into an organic network, so the supervision system could evolve into a long-lasting and adaptive management system. This paper mainly researches the construction approach and the operating mechanism of this new regulatory model, clarifies the responsibilities of the parties involved in this model. It is hoped that this model can provide a feasible solution to the public management reform on building safety supervision in China.

【Key words】 building safety, government supervision, third-party mechanism

Building safety management is one of the responsibilities of the government .In China, these duties are distributed to different departments. However, the state of building safety management is not optimistic. "5.12" earthquake and other disasters also highlight the deficiency of the current building safety supervision system. It is urgent to study and solve this problem.

1. Analysis of present state of building safety supervision in China

Governments of all levels pay close attention to the building safety. The government has promulgated a series of laws and regulations related to the building safety. These laws have covered the domain from "Building ordinance" the fundamental law of construction to State Council code, urban government rules and regulations. The government also adopts a series of management tools, including the administrative examination and approval, periodic inspection, on-site inspection and other means. These laws and tools have formed a set of supervision systems at all

levels and covered the whole life cycle of the building safety. However as the urban building scale grows fast, the system can no longer meet the needs of the state. Chart 1 outlines the present state of Chinese building safety supervision in China and its deficiency.

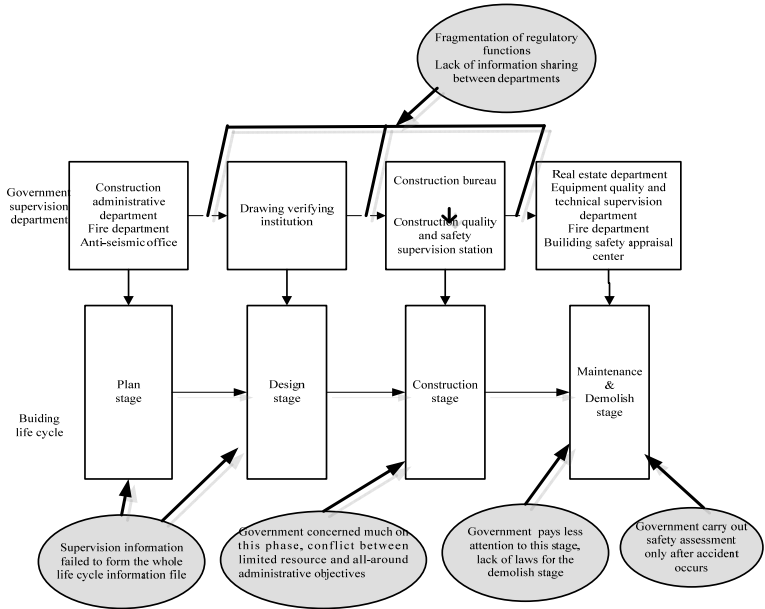


Fig1-present Chinese building safety supervision system

From chart 1 we can conclude the characteristic of the present building safety administration supervision system as follows:

(1) Fragmentation of administration functions

In the present administration system, the building safety public administration function belongs to different departments according to the phase and the type of work it takes. The supervision of building plan phase belongs to the urban planning department. The construction executive department is in charge of the design and the construction phase. The safety of the operational phase is the responsibility of urban real estate department. The building fire protection safety is the function of public fire department. The safety of elevators and other special equipment is the duty of the quality and technical supervision department. We may find that the supervision system is dissevered factitiously .On one hand, this arrangement makes the building owner face different government departments, and this may increase the social cost.

On the other hand, repeated inspection or absent supervision may occur in some areas. This may leave the hidden danger of supervision behind, and also it is a waste of precious government supervision resources.

(2) Absence of the government supervision for the building operational phase

Since the implementation of reform and open-up policies, the urban construction has seen fast development which progresses by leaps and bounds. The statistical data have demonstrated that the annual average completed residential areas amounts to 630,000,000 square meters in the past three years. With more and more buildings facing the aging problem, the safety of the building structure and the building equipment is becoming prominent day by day.

However, since government supervision has formed a tradition that it pays more attention to the construction phase and less attention to the building maintenance phase, through establishing administrative permission, controlling administrative examination and approval, the state and municipal government intend to prevent the possible management risk in the construction phase. By inviting construction quality and safety supervision stations to carry out on-site inspection, the government means to control the entity quality and safety of the building. But the government actually pays little attention to the safety of building operational phase. An obvious example is that there are few laws or regulations related to the building maintenance and demolition phase at present.

(3) Conflict between limited supervision resources and all-around administrative objectives

Unlike the fact that government pays little attention to the building maintenance phase, it concerns lots about the construction quality and safety. Governments at all levels spend much time and resources in inspecting the building quality and safety in case that a construction accident occurs in their district. However as China has entered a fast growing urbanization era, limited administrative supervision resources are unable to meet the all-around administrative goals.

Take the building quality supervision as an example, according to one report from the Ministry of Construction, there were 2659 quality surveillance organizations and approximately 42,000 professionals engaged in this field all over the country by the end of 2008. And at the same time the house construction area around the country was 4,740,000,000 m². In most big or medium-sized cities, The average surveillance area per person was about 30,000 m² in the early 90s , and now this figure has increased from about 500,000 to 1,000,000 m² . Supervision resources are insufficient for a long time.

(4) Emergency management mechanism

The government concerns less about the building maintenance phase, and this attention is mainly laid on the urban dangerous house. But even in this small field, government supervision is still insufficient. Regular house safety check is organized by house owners, after having discovered possible danger, they apply for a building

safe assessment. But in everyday life, there are only a few house owners carrying out a regular house check, and this risk-preventive measure plays a less important role in the building safety management. In many situations, related government departments organize safety inspections after accidents occur. This kind of emergency management can do little to prevent potential building hazards, and it is also impossible to form a persistent building protection mechanism.

2. Supervision model for building safety based on the third-party assessment mechanism

These are many factors influencing building safety management, involving the building's life cycle in each phase. The use phase of a building is a stage in which the risks from entity quality conformation of construction phase appear gradually and the risks from use process accumulate gradually. As shown by survey data, most accidents occur in the use phase, such as building collapse, suspender shedding, could find reasons in the design and construction phase

This characteristic of building safety management causes the concern and research of building life cycle risk management. In fact, the thought of life cycle risk management is also adequate for the safety regulation that government exerts on building. Under the current regulatory regime, different authorities carry out building regulations in different phases. Due to the lack of effective collaboration among these authorities, a lot of regulatory information runs off in the phase transition. The result is that the building risks hidden in the early phase couldn't cause enough concern in late phase, and it may lead to a waste of limited regulatory resources because of repeated inspection.

The building safety supervision system is suitable for organization arrangement of the current administration system. The change which aims to the supervision system will both face the resistance layer upon layer and that huge price must be paid. The reform of the present building safety supervision system must meet both two requirements, i.e. one is to satisfy the methodology of building total life cycle, and the other is that it cannot create big change to the immediately supervision system. The third party assessment mechanism, which profits from both the building supervision patterns of developed countries and regions and the existing administrative reform successful experience in China, was proposed under this mentality.

By employing third-party assessment agencies as a "chain" of building safety management, the original division and intermittent administration functions can be integrated into an organic network, so the supervision system could evolve into a long-lasting and adaptive management system

It's the mandatory stipulation of the law that the building safety owner has the

obligation to control the safety risk under the new supervision pattern, and the building safety owner must regularly require the third party to implement the routine building safety assessment according to the stipulation. The report of assessment can be used to collect the building safety control information in relevant jurisdiction, and also works out the safety control measures for government. As the specialty technical service provider, the third party assessment organization writes up the fitness report, and it must undertake the corresponding technical responsibility. The government carries on the assessment information to set up a file, and then puts it into the unified supervision information platform of government. As a result, the building' life cycle time information supervision system can be established, making the building life cycle time safety control possible. The restructuring government supervision pattern is shown in the chart as follows:

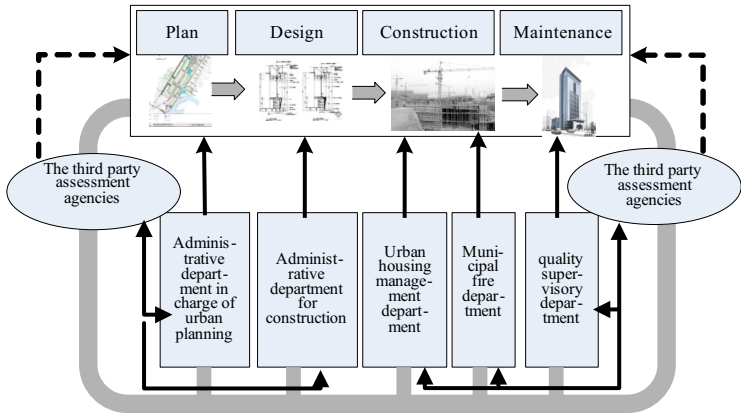


Figure 2. The building safety supervision system with the third party assessment mechanism

3. Establishment of the new building safety supervision system

When introducing the third-party assessment mechanism into the government supervision system, consideration should be taken to every phase and every department affected by this change. From the perspective of system theory, this paper considers that the new supervision system can be made up of four sub-systems, and the new supervision system can be expressed by the following diagram:

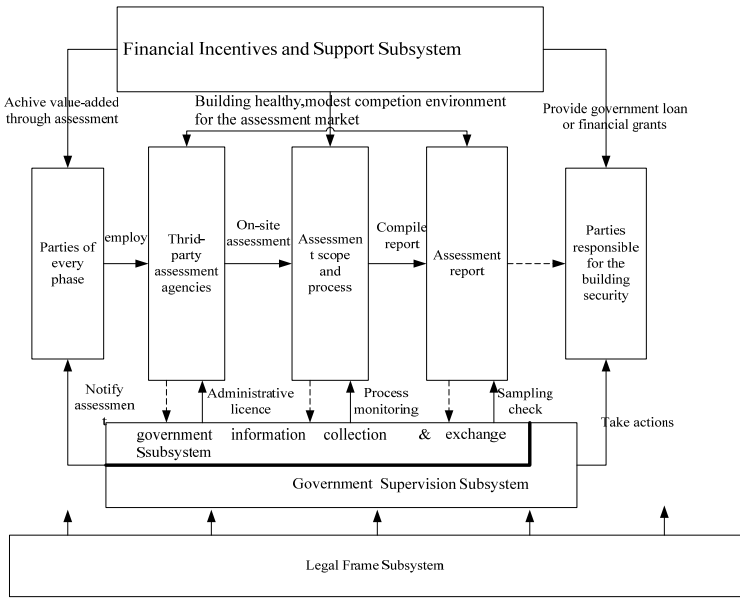


Fig 3. Government supervision system based on third-party mechanism

-----> Information flow

(1) Legal frame subsystem

The original idea of the government’s overall supervision has been changed by the introduction of third party assessment in the government regulatory system, which has extended the scope of government’s supervision to the stage of use and removal, adjusted and re-defined building safety regulatory functions of government. The third party is responsible for preparing the assessment report, which should be the basis of safety management measures by the government, giving a certain power to assessment agencies. In the re-organized system, the safety management of building is not any way of automatically application, voluntary identification and self-management by the householder, but a mandatory safety management obligation. Clearly, definition by the laws, regulations and all normative documents is needed for the redefinition of the functions of government regulations, the restraint over the power of third-party assessment agencies and the constraint regulations for safety assessment obligation of the person responsible for building safety. Some enabling and compulsory regulation and safeguards rules to the operation of other system must be determined by the sub-system of the legal frame in the implementation of the whole supervision process of safety supervision system. Sub-system of Legal

Frame provides protection to the orderly operation of other sub-systems.

(2) Third-party assessment sub-system

The third-party assessment operation system is the main part of the re-organized supervision system. This sub-system mainly serves to deal with the process reengineering after the introduction of third-party assessment mechanism in government regulation. In this sub-system, the person responsible for building safety commissions the safety assessment of building to the qualified third-party rating agencies voluntarily, according to compulsory safety assessment obligation under the laws and regulations. Assessment agencies should comply with the appropriate specifications in each stage of safety assessment of building and prepare the assessment report in the specified assessment scope. The assessment report should be submitted to the appropriate government regulatory authorities, which should give instructions to the person responsible for building safety on the basis of contents and conclusions of the assessment report and take some corresponding management initiatives

(3) Government information collection, exchange and supervision sub-system

In the process of safety supervision over life-cycle of building by the government, a lot of supervision information is produced. If there are no proper preservation and delivery of them, it would not only bring potential safety risk, but also bring about duplicate regulation with different departments. Therefore, reengineering system makes arrangement with government information collection and exchange. As the provider for a third party service technical support, the assessment institution acquires the power and duties to issue assessment report. For the sake of preventing appraisers from abusing their appraise power, it is necessary for the government to execute strict management over a third party assessment institution. The government supervision over a third party assessment institution consists of checking up the qualification of a third party assessment institution, granting permit to appraisers, supervising assessment process of assessment institution and appraisers, double-checking the assessment report, etc.

(4) Financial incentives and support subsystem

According to government regulation theory and the research results on the effect of government supervision, the government supervision over the regulation object is rather like a game of "a cat-mouse game". In the case of lacking effective market incentive, the regulation object often sacrifices the interests of the third party to cope with the government. The market economy has its own stabilizer of economy. The government supervision over the main body of building safety management is required to comply with the basic law. The financial incentives and supportive sub-system is the "balance stabilizer" which adjusts the interests between enforceable governmental supervision object and various participants. In the process of building safety supervision, the government could guide building safety sponsors to integrate safety appraise in building safety management. The preservation and

increase of the value of buildings resulting from building safety management would play an active role in initiative appraisal. In addition, the government should not only execute strict management, but also create a healthy, orderly, appropriate competition market environment for a third party assessment institution which would prevent over competition just as general service industry. Enforceable safety appraisal stipulates the obligation of all participants and at the same time should provide financial support for building safety sponsors who are in financial difficulties, the financial support in the form of government subsidy and government loan, etc.

4. Conclusion and prospect

Based on analysis of the current status and the disadvantages of the building safety system in our country, a scheme which inducts a third party assessment institution to reconstruct government building safety supervision mode was produced. The government supervision system is presented in this paper on the viewpoint of system theory and integration theory, which would provide a brand-new idea for solution to the reform of governmental institutions.

References:

- Guo Handing (2005) "Discussion on government supervision and management mechanism for construction quality" Journal of East China Jiaotong University. Vol.22 No.5,44-47
- Guo Yunchong.(2009) "Housing and urban-rural development ministry :Vice minister's speech on the construction quality supervision national conference."MUD history, http://www.mohurd.gov.cn/ldjh/jsbfd/200911/t20091111_196753.htm>(Sep.1, 2010)
- Liu Jing ,Mao Longquan .(2009)."Study on the whole life cycle risk assessment system about the large-scale public building in China".Journal of Construction Economy.,Vol 316,5-9
- 2007/2008/2009 Yearly statistical data National Bureau of Statistics.MUD history, <http://www.stats.gov.cn/>(Oct.10,2010)
- Yuan Chunyan.(2008)Researches on the system of the existing building safety and crisis management in city, doctoral dissertation of Xi'an University of Architecture and Technology

Development of Spatial Risk Profiles Resulting from Sea Level Rise

Bilal M. Ayyub¹, Michael Kearney², Josue Ramirez³,
Kristen Markham³, Che-Yu Chang³

¹Professor and Director; ²Professor of Geography; ³Graduate Research Assistant

¹Center for Technology and Systems Management, Department of Civil and Environmental Engineering, University of Maryland College Park, MD 20742, USA
301-405-1956 (Tel), ba@umd.edu

ABSTRACT

Risks from future sea level rise entail significant uncertainties concerning overall potential impacts, the specific threats faced by particular areas, and what benefit or costs are associated with strategies for addressing such risks. Quantitatively assessing these risks requires the development of spatial risk profiles based on several analytical and computational steps of hazard likelihood assessment, scenario identification, consequence and criticality assessment based on inventories of assets along coastal areas particularly of population centers, vulnerability and inundation assessment, and benefit-cost analysis to manage risks. The proposed risk quantification and management framework is consistent with quantitative risk analysis practices in order to enable decision making. The methodology is briefly introduced and demonstrated using illustrative examples based on notional information.

Key words : Times Infrastructure, Inundation, Natural hazard, Protection, Risk, Sea level rise

BACKGROUND

By the end of this century, some estimates suggest at least 100 million people worldwide will be affected by rising sea levels. This number, large as it may be, hinges on the relatively conservative upper end of scenarios for future sea level rise of the Fourth Assessment of the Intergovernmental Panel on Climate Changes (IPCC 2007). Among many climate scientists there exists considerable disquiet that this top end estimate could prove too low, as the contribution from polar ice melting still remains highly uncertain. The resulting impacts on global sea levels could be a rise on the order of 19.6 feet. An increase in the global trend is likely, and this increase will be on the order of two to two-and-a-half times what occurred in the 20th century, historically

a period of the highest rate of sea level rise in the last thousand years (Kearney 2008). The challenge of such a sea level rise is indeed formidable, and requires immediate attention in order to examine associated risks and to assess the socioeconomic impacts for the purpose of developing appropriate long-term measures and mitigation strategies (Ayyub 2003). The impacts on other parts of the globe such as southern Asia can be total devastation for particular countries.

One of the important economic consequences of sea level rise that merits immediate attention is the impact on ports and the transportation arteries that support them. As an example, in the Chesapeake Bay the Port of Baltimore has experienced in recent years a 28% growth in foreign cargo, amounting to 32 million tons in 2004. The Port is directly responsible for 19,000 direct jobs (\$2.4 billion in personal wages and salary), \$2 billion in business revenue, and generates \$278 million in state, county and municipal taxes (State of Maryland Governor's Office 2006). The total economic impact is well beyond these estimates. Comparable figures are available for the Port of Norfolk and Portsmouth in Virginia, plus with the nation's largest naval installation, the added impact on national security and the ability to project national power to areas across the world.

SEA-LEVEL RISE AND ASSOCIATED RISKS

Fairbridge (1960, 1961) documented that the ocean levels rose and fell over long time scales producing what has become known as the Fairbridge Curve of the Holocene Eustatic Fluctuations based on detailed observations off Western Australia and afterwards from elsewhere in the world. He formulated the hypothesis that sea levels had been rising for the last 16,000 years and that the rise showed regular periodic oscillations of rise and fall over this period with oscillations continued throughout the last 6,000 years to the present time, but with diminishing amplitude. The oscillations include a relatively short periodicity component of relatively rapid rises and falls of up to four meters, although up to three meters is more common, taking place over periods of no more than 10 or 20 years. This short-periodicity component would now have catastrophic consequences for the world. Over the next 100 years and possibly within our lifetime such an occurrence is likely. The periodicities are revealed in a rich variety of sources, including: geology; geomorphology; glaciations; sediments; sand dunes; beach rock; the circulation of the ocean; geomagnetic records; and the records of the isotopes of carbon, oxygen, beryllium, chlorine and hydrogen in tree rings, ice

cores, biota, rocks, air and water (Mackey 2007; Finkl 1995 and 2005).

Changes in the average sea level involve several primary categories of variables that are interdependent with nonlinear associations: (1) temperature and salinity levels of oceans; (2) worldwide carbon inventory; (3) the shape of the basins that contain the oceans; (4) the volume of water in these basins; and (5) local variations in land adjacent to the ocean basins. Global warming causes the oceans to warm up; this in turn causes thermal expansion of the oceans leading to rising sea level. Global warming also causes the poles to warm up leading to the melting of land-based ice sheets, glaciers, and ice caps. These variables can form a basis for defining scenarios as recommended by the IPCC (2007) with associated probabilities. Defining risk as the potential of losses for a system resulting from an uncertain exposure to a hazard or as a result of an uncertain event (Ayyub 2003) offers a basis for risk quantification for identified risk events or event scenarios and associated rates, system vulnerabilities and potential consequences. Risk can be viewed to be a multi-dimensional quantity that includes event-occurrence rate (or probability), event-occurrence consequences, consequence significance, and the population at risk; however, it is commonly measured as a pair of the rate (or probability) of occurrence of an event, and the outcomes or consequences associated with the event's occurrence that account for system weakness, i.e., vulnerabilities. Another common representation of risk is in the form of an exceedance rate (or exceedance probability) function of consequences. In a simplified notional (or Cartesian) product, it is commonly expressed as:

$$\text{Risk} = \text{Event rate} \times \text{Vulnerability} \times \text{Consequence} \quad (1)$$

This equation not only defines risk but also offers strategies to control or manage risk: by making the system more reliable through vulnerability reduction or by reducing the potential losses resulting from a failure or impacting event rates.

RISK MODEL

Probabilistic risk analysis as described by Ayyub (2003) can be used to develop the overall risk analysis methodology suitable for quantifying and managing risks associated with sea-level rise. Risk assessment is a systematic process for quantifying and describing the nature, likelihood and magnitude of risk associated with some substance, situation, action or event, including consideration of relevant uncertainties (Ayyub 2003). Ayyub et al. (2007) developed an approach called the Critical Asset and Portfolio Risk Analysis (CAPRA) Methodology. In general, CAPRA is a five-phase

process. CAPRA consists of several steps as shown in Figure 1 and discussed below:

- Scenario Identification: This step characterizes the missions applicable to an asset, portfolio, and region and identifies hazard and threat scenarios that could cause significant regional losses should they occur.
- Hazard Likelihood Assessment: This step produces estimates of the annual rate of occurrence for each threat or hazard scenario including the time-variant hazard profile associated with sea-level rise for a region.
- Vulnerability Assessment: This step estimates the effectiveness of measures to protect, reduce hazard intensity, detect, delay, respond to, and eliminate a hazard that might cause harm to a region.
- Consequence and Criticality Assessment: This step estimates the loss potential for each scenario identified for the region by considering the maximum credible loss, fragility of the target elements, effectiveness of mitigation strategies, and effectiveness of consequence-mitigation measures to respond to and recover.
- Benefit-Cost Analysis: This step assesses the cost-effectiveness of proposed countermeasures and consequence mitigation strategies produced from the developing of strategy tables.

Risk associated with sea-level rise is quantified using a regional seal-level rise (S) probability distribution f_S at time t , scenarios of underlying variables (i) defining S and respective probabilities P_i , regional storm rate (λ) that is dependent on S and i , scenarios of underlying variables (j) defining λ_j and respective probabilities Q_j , and the conditional probability $P(C > c)$ with which a consequence valuation (C) exceed



Fig. 1 The critical asset and portfolio risk analysis (CAPRA) methodology.

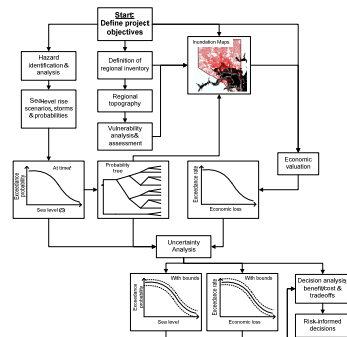


Fig. 2 A risk methodology for seal-level rise at a particular region.

different levels (c) for i, j and coastal state at time t . A loss-exceedance probability at time t can be expressed as follows:

$$P(C > c; t) = \sum_i P_i \left(\int f_S \left(\sum_j \lambda_i Q_j P(C > c | i, j) \right) ds \right) \quad (2)$$

where f_S is probability density function of sea level (S) at time t ; P_i is the probability of a scenario of underlying variables (i) defining S ; λ is regional storm rate that is dependent on S and i ; Q_j is the probability of a scenario of underlying variables (j) defining λ ; and $P(C > c | i, j)$ is the probability that the consequence C exceeds c under a state defined by the pair (i, j) and the corresponding state of the coast at time t . Summations are over all scenario types i and j using a suitable discretization. The increased storm activities would include wave run-up. This model is consistent with recently developed and used risk model for natural hazards, such as the risk model for developing protection strategies of hurricane-prone regions (Ayyub, et al. 2009a and 2009b). Figure 2 defines a logic and computational flow diagram for the proposed risk methodology for sea-level rise at a particular region starting with hazard identification and definition, followed by inventory definition to estimate losses based on inundation mapping, and finally constructing risk profiles and estimating associated uncertainty.

RISK MANAGEMENT

The risk management phase assesses the cost-effectiveness of proposed countermeasures and consequence mitigation strategies for reducing the risk associated with an asset or portfolio of assets or a region. In the context of sea-level rise, countermeasures aim to reduce vulnerabilities of coastal lines, property and asset exposure, impact on resources and populations, and land use changes. Consequence mitigation strategies aim to reduce the potential consequences given the occurrence of a successful scenario. Risk management entails decision analysis for a cost-effective reduction of risk given finite available resources. The benefit of a risk mitigation action can be assessed as the difference between the risk before and after implementation (Ayyub 2003). The probability that a favorable benefit-to-cost ratio will be realized can be represented as:

$$P\left(\frac{\text{Benefit}}{\text{Cost}} \geq 1\right) = 1 - P(\text{Benefit} - \text{Cost} \leq 0) \quad (3)$$

THE CITY OF BALTIMORE AS A CASE STUDY

This section provides a preliminary demonstration of the proposed methodology

using publically available information on the City of Baltimore.

Hazard Analysis

The first step is to estimate the sea level rise as a function of time. Data obtained from the National Oceanic and Atmospheric Administration (NOAA) website was used as lower bound on the estimates. The data includes current sea level-rise trends for the city of Baltimore recorded for over 100 years at a Baltimore (NOAA station # 8574680) and its record goes back to the year 1902. Figure 3 shows current sea level trends for Baltimore along with a trend line. This trend line is used to estimate future sea level elevations using a linear trend for the purpose of demonstration, and it is specific for the station location. The resulting linear trend is: $\text{Sea level} = 0.0031y - 5.8699$, where y is the year, such as 1992.

Land, Asset and Resource Inventory

Much information is available in geographical information system (GIS) format about the City of Baltimore, thus in an effort to most efficiently and effectively analyze this information and how it can be potentially affected by sea-level rise, it is important to first identify what type of information is needed to sufficiently capture the key assets to define the consequences of greatest concern. The key assets of concern identified in this case study include the following main categories: (1) People; (2) Land and Environment; (3) Property; (4) Roadways and Railways; (5) Other Specific Assets. The properties of each of these specific assets include the relevant information that would enable consequence estimation including the approximate number of people that could be affected.

Inundation Mapping and Risk Profile

Assuming that the city of Baltimore does not have a coastal protection system in place, and therefore is vulnerable to sea-level rise, the development of inundation maps requires topographical maps for the City of Baltimore. These maps were obtained from the United States Geological Service (USGS) website. The GIS data are represented by pixels containing the average elevation of a portion of land in Baltimore with an approximate area of 10 meter by 10 meter. A time line for the risk profile for the City of Baltimore is shown in Figure 4 by focusing and zooming in on the coastal areas. Figure 5 shows the trends of the inventory components affected by inundation.

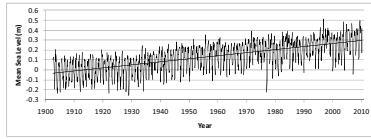


Fig. 3 Mean sea level trend for Baltimore, MD.

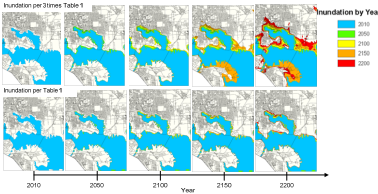


Fig.4 A demonstration of the format of the timeline of the risk profile of the City of Baltimore due to sea-level rise.

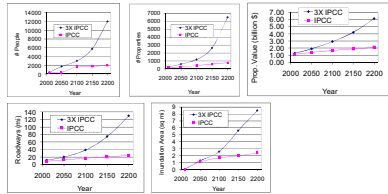


Fig. 5 Inundation inventory components to quantify the risk profile.

CONCLUDING REMARKS AND NEXT STEPS

Quantifying risk using a probabilistic framework produces hazard (elevation) and loss-exceedance probability curves based on a spectrum of sea-level rise scenarios according to the mean sea level as a function of time and increased storm rates with associated surges, waves and precipitation with uncertainty quantification. The methodology provides a process for evaluating the loss potential for a region covering land-use changes, population affected, and property at risk by considering the topography and asset inventory for the region. The quantification of risk will enable decision makers to consider various alternatives to manage risk through setting appropriate policy relating to land use, land-use changes, infrastructure planning, building requirements and permits, water resource planning, and the enhancement of consequence mitigation measures.

This preliminary, conceptual framework for quantifying risks associated sea-level rise requires refinement and development of computational details. Moreover the state of the inventory requires further developing by focusing on the coastal areas of the City of Baltimore and other areas within the United States. The inventory used in this paper is developed for rail safety studies and is incomplete and/or inaccurate along the coastal lines. The increase in storm activity with wave run-up intensity escalation due to the rising sea level requires further investigation. The impacts of such

increased activities at coastal lines would lead to interdependence with land-use and human-activity change.

REFERENCES

- Ayyub, B. M. (2003). *Risk Analysis in Engineering and Economics*, Chapman & Hall/CRC Press, FL.
- Ayyub, B. M., Foster, J., McGill, W. L. (2009a). "Risk Analysis of a Protected Hurricane-Prone Region I: Model Development." *ASCE Natural Hazards Review*, 10:2(38), 38-53.
- Ayyub, B. M., McGill, W. L., Foster, J., Jones, H. W. (2009b). "Risk Analysis of a Protected Hurricane-Prone Region II: Computations and Illustrations," *ASCE Natural Hazards Review*, 10:2(38), 54-67.
- Ayyub, B. M., McGill, W. L., Kaminskiy, M. (2007). "Critical Asset and Portfolio Risk Analysis for Homeland Security: An All-Hazards Framework." *Risk Analysis International Journal*, Society for Risk Analysis, 27(3), 789-801.
- Fairbridge, R. W. (1960). "The Changing Level of the Sea." *Scientific American*, 202 (5), 70-79.
- Fairbridge, R. W. (1961). "Eustatic Changes in Sea-Level", *Physics and Chemistry of the Earth*. L. H. Ahrens, K. Rankama, F. Press and S. K. Runcorn, eds., Pergamon Press, London, UK, 4, 99-185.
- Finkl, C. W., Jr., ed. (1995). "Holocene Cycles: Climate, Sea Levels, and Sedimentation. A Jubilee Volume in Celebration of the 80th Birthday of Rhodes W. Fairbridge.." *J. of Coastal Research*, Special Issue 17.
- Finkl, C W., Jr., ed. (2005). "The Sun, Earth and Moon In Honor of Rhodes W. Fairbridge." *J. of Coastal Research*, Special Issue 42.
- IPCC. (2007). *Climate Change 2007: Synthesis Report. Contribution of Working Groups I, II and III to the Fourth Assessment Report of the Intergovernmental Panel on Climate Change*, Geneva, Switzerland.
- Kearney, M. S. (2008). "The potential for significant impacts on Chesapeake Bay: Sea Level Impacts and Ecology." *The Likelihood and Character of Large and Disruptive Climate Change*. M. McCracken, ed., EarthScan London, U.K., 85-100.
- Mackey, R. (2007). Rhodes Fairbridge and the Idea that the solar System Regulates the Earth's Climate, *J. of Coastal Research*, Special Issue No. 50.
- Vermeera, M., and Rahmstorf, S. (2009). "Global sea level linked to global temperature" <www.pnas.org/cgi/doi/10.1073/pnas>.

Evaluating the Source of the Risks Associated with Natural Events

P. Gardoni¹ and C. Murphy²

¹ Zachry Department of Civil Engineering, Texas A&M University, 3136 TAMU, College Station, TX 77843-3136; PH (979) 845-4340; FAX (979) 845-6156; email: pgardoni@civil.tamu.edu

² Department of Philosophy, Texas A&M University, 4237 TAMU, College Station, TX 77843-4237; PH (979) 862-4856; FAX (979) 845-0458; email: cmmurphy@philosophy.tamu.edu

ABSTRACT

Tornadoes, hurricanes, droughts, and earthquakes are example of natural events that pose risks to society. The first objective of this paper is to demonstrate why we cannot simply apply to risks associated with natural events insights and frameworks for moral evaluation developed in the literature by considering ordinary risks, technological risks and the risks posed by anthropogenic climate change. The second objective is to develop a framework for the moral evaluation of the source of the risks associated with natural events. Our discussion concentrates on the way the construction and modification of the built and natural environments can alter the probability of occurrence of natural events and the character and magnitude of the impact that such events have. We propose a standard of reasonable care for decisions about the built and modified natural environment, which accounts for technical and resource constraints and the place of natural hazard mitigation in public policy.

INTRODUCTION

Between 1991 and 2005 almost 1 million people were killed and 3.5 billion people were directly affected by natural disasters such as earthquakes, wind storms, droughts, and floods (UNISDR 2005). Given the devastating consequences natural disasters can have for communities, devising and implementing effective mitigation measures against future natural disasters is, in the words of the Hyogo Declaration of the report of the United Nations World Conference on Disaster Reduction in 2005, “one of the most critical challenges facing the international community” (United Nations 2005). Risk is often defined as a set of scenarios, their associated probability of occurrence and consequences (Kaplan and Gerrick 1981; Hansson 2007). Risks associated with natural events are potentially damaging or destructive natural events that might occur in the future. Risk analysis is the process of determining the probabilities and potential consequences, and evaluating the assessed risks (Vose 2000; Bedford and Cooke 2001). Risk analysis forms the foundation for natural hazard mitigation policies.

The first objective of this paper is to demonstrate that we cannot simply apply to risks associated with natural events insights and frameworks for moral evaluation developed by considering ordinary risks, technological risks and the risks posed by anthropogenic climate change. We illustrate the distinctive questions the risks

associated with natural events by considering a recent critique of traditional risk analysis offered in the context of technological risks by Jonathan Wolff (2006). Wolff has argued that the *cause* or *source* of a risk, that is, how “a hazard comes into being, or is sustained, or perhaps, permitted,” should also be considered as an independent variable considered in risk evaluation. While Wolff’s insight seems importantly relevant when considering technological risks, ordinary risks, and even risks due to anthropogenic climate change, it is not immediately clear how his insight would apply to risks posed by natural events. Natural events are not created by our actions in the same way as technology, nor do we permit or allow natural hazards in the way we may permit other kinds of risks. Furthermore, insofar as we play some role in sustaining natural hazards, it is not obvious how we play this role and so what would be the subject of moral evaluation for the source of the risks in such cases. As we discuss later, actions that affect natural events are not co-extensive with actions that contribute to anthropogenic climate change.

The second objective of this paper is to identify the source of the risk in the context of hazards associated with natural events and to develop a framework for the moral evaluation of this source. To identify the source, we discuss the way the construction and modification of the built and natural environments can alter the probability of occurrence of natural events and the character and magnitude of the impact that such events have. We then argue for the need to develop a standard of reasonable care for decisions about the built and modified natural environment, which accounts for technical and resource constraints, as well as the place of natural hazard mitigation in public policy. One interesting outcome of our discussion is that it demonstrates that the scope of moral concern and evaluation when thinking about risk, development, and global justice needs to be significantly broadened. In particular, the engineered built environment and implications of engineering for the natural environment should be a central concern.

The next section of this paper identifies the source of the risks due to natural events. The second section distinguishes this source from the source of three other kinds of risks and argues that differences in the mechanism of each source lead to differences in the moral questions that are relevant to ask about the source in each case. The third section develops a framework for evaluating the source of the risks due to natural events.

THE SOURCE OF A RISK

In the context of technological risks, Wolff (2006) has recently argued that any evaluation of risks must take into consideration the source of a risk, or how risks are created and maintained. Using Wolff’s example, consider three different scenarios in which an individual dies in a house fire; the three scenarios are identical except for the cause of the fire. In the first case, an electrical fault that led to the fire is caused by a “freak accident” or a random mishap. In the second, the fault is caused by negligent workmanship. In the third, it is caused by deliberate arson. In these three cases, the cause of the house fire is different. When considering mitigation action for house fires, Wolff notes, all three risks would be judged equally urgent to mitigate if we only consider the consequences and probability of occurrence. However, Wolff argues that the public typically differentiates among how these kinds of risks are caused. Those risks stemming from malice, for example, are more threatening and more urgent to

address than risks caused by accident. To capture these differences, we must include the source of a risk in our moral evaluation of risks. In this section, we define the source of risks associated with natural events. We then highlight key differences between the mechanism of this source and the mechanisms of the source of three risks typically discussed in the literature: ordinary risks, technological risks, risks due to anthropogenic climate change.

Our interest in this paper is the source of risks associated with natural events. Tornadoes, hurricanes, droughts, and earthquakes are examples of natural events that pose risks to society. Such natural events pose risks because they may occur, but there is uncertainty surrounding their time, location and magnitude of occurrence, the nature and severity of their impact on society, and a given society's resilience (or ability to recover from such events).

Risks from natural events are not a product of our creation; we cannot bring about a tornado in the way that we can cause a house fire through deliberate arson. Natural events are produced by, for example, unusual changes in atmospheric conditions or movements in tectonic plates. Thus, we are not, strictly speaking, the direct source of such risks. However, our actions do influence the character and extent of such risks and it is important to appreciate the complex mechanism through which risks associated with natural events are realized. By spelling out the ways in which we influence such risks we can understand how we can constitute an indirect source of such risks.

Both dimensions of risk, the probability of occurrence of natural events and the character and magnitude of the impact that such events have, are affected by the built environment and modifications to the natural environment. The built environment refers to the man-made structures and infrastructure systems that, linked to the natural environment, provide the physical and technological setting of human life and activities. Examples of such infrastructure systems include the transportation infrastructure (e.g., roads, bridges, airports, subways, railways, seaports), energy infrastructure (e.g., electric grids, natural gas pipelines), water and waste management infrastructures (e.g., sewage collection and disposal, drinking water systems, dams, irrigation systems, landfills), and communication infrastructure (e.g., telephone and mobile phone networks, internet servers) (Oxford English Dictionary 2010). The natural environment refers to organic living and non-living things. The natural environment includes natural resources, such as water, air, and climate; naturally existing energy; systems, such as vegetation, animals, soil. Modifications to the natural environment include those activities that alter or use natural resources and systems. Examples of modifications we make to the natural environment include land development by deforestation or the reclamation of wasteland or flooded land so that it can be cultivated, for example by diverting river streams, building dams, levees, or canals. Dams can also serve other purposes, such as providing electricity. Anthropogenic climate change can lead to indirect modifications to the natural environment (or be a product of such changes).

Though we do not create or produce natural events, we can influence the probability of occurrence of some natural events directly and indirectly, and to varying degrees, in virtue of how we construct and modify the built environment and in virtue of how we modify the natural environment. Similarly, choices in the construction and

modification of the built environment and modification of the natural environment influence the likely severity of the consequences of natural hazards.

Consider earthquakes, a potentially economically devastating hazard which 75 million Americans in 39 states face (United States Geological Survey 2010). Though it is virtually impossible to affect their probability of occurrence, given current technological knowledge and capability, we can reduce the impact of earthquakes by not building in seismically active areas or improving the seismic design of structures (e.g., buildings and bridges) and construction practice in such areas. Similarly, the seismic performance of older structures may be improved by retrofitting them, a process through which they are brought up to current design standards. For example, cross-bracing, where diagonal steel beams are added to a structure, might improve its lateral resistance and ability to dissipate energy and in turn its ability to withstand earthquakes. Finally, we can reduce the impact of a hazard by improving a society's resilience and ability to respond to a disaster in a timely and well informed way. We can improve the resilience of a society by increasing the redundancy of structures and infrastructures. For example, having alternate routes for transportation by building a second bridge in an area of high commerce reduces the consequences of one bridge failing from a seismic event.

Landslides are natural events whose probability of occurrence and severity are affected by our actions. One kind of modification of the natural environment, namely, aggressive deforestation, directly increases the likelihood of landslides. The probability of occurrence is also affected by factors beyond our actions, including severe storms, earthquakes, and volcanic activity, all of which can increase slope instability. When deforestation is done for the sake of creating livable areas, which are then constructed, landslides become more potentially devastating in their impact.

CONSIDERATIONS INFLUENCING THE MORAL EVALUATION OF THE SOURCE OF RISKS

There are important differences among the source of risks associated with natural events and the source of the risks considered in the literature, ordinary risks, technological risks and the risks posed by anthropogenic climate change. Ordinary risks are those stemming from routine daily or recreational activities, for example, mountain climbing (Hansson 2004; Sunstein 2002). Technological risks are produced by the creation and use of artifacts and their associated services (Franssen et al. 2009). Examples of technological risks include the risks posed by nuclear power, toxic wastes, smoking, driving, and concerns with occupational safety (Shrader-Frechette 1985; Wolff 2006). A third category of risks are those associated with complex systems, like the climate (Hansson 2007). Risks due to climate change in part stem from anthropogenic increases in greenhouse gas levels, including carbon dioxide (CO₂) and methane (CH₄). Burning fossil fuels in part through, for example, industrial and transportation activities, accounts for the majority of anthropogenic CO₂ sources, though changes in land use patterns are another important cause (Gardiner 2004). Causes of CH₄ emissions include "fossil fuels, cattle, rice agriculture and landfills." Once we understand the mechanism by which different kinds of risks are created, sustained, influenced, and mitigated, we can begin to morally evaluate the actions that brought this mechanism about. In this section, we distinguish these questions to ask

about the source of risks associated with natural events, from those to ask about technological risks, ordinary risks, and risks from climate change.

In the case of ordinary risks and some technological risks, we are in a position to choose whether or not to assume certain risks. We can choose to engage in certain activities, like mountain climbing, and assume ordinary risks. Human actions lead to the creation of technology, and to the risks that stem from the objects and artifacts of our creation; such risks would not exist without our actions. For example, we design and construct nuclear reactors or, as in Wolff's example, houses. Second, users of artifacts can create or cause risks through their actions. In the case of houses, for example, a poor electrical connection creates the risk of house fires.

Given that such risks are a function of our choices, one general question to consider is which sources of risk we should allow. In other words, we can identify what individuals should be able to do or create, given that they themselves, as well as possibly others, may be harmed through their actions. This is in part a question of which risks we will allow in the basic structure of a community. We can specify which artifacts we will allow people to create, as well as which actions or activities we will permit individuals to engage in. We can also specify constraints on the ways that people will be permitted to use certain artifacts. In fact, philosophical discussions of ordinary and technological risks attempt to make such distinctions. Theorists distinguish, for example, between those actions or technologies that are too dangerous to be permissible and those which, though potentially harmful, are permissible, sometimes in light of their associated real or potential benefits. Discussions furthermore specify criteria for attributions of responsibility for any harms realized in risky activities or by technological creation and use, and how responsibility tracks being a source of a risk (McKerlie 1986).

By contrast, though we exert influence on the character of risks associated with natural events, we do not create or, in most cases, choose to assume such risks. As noted earlier, hurricanes are a kind of natural event that exists independent of our actions; unlike artifacts, they are not a function of our making. Furthermore, we are not one of the sole avenues through which a particular natural event is brought about, in the way that, through deliberate arson, we can cause a house fire. Finally, though we have some control over our exposure to natural events, in most cases it is not appropriate to talk about individuals choosing to assume risks associated with natural events. While it may be a theoretical possibility to move the communities that are vulnerable to natural hazards, that is not a practical possibility, both because there are few areas of the world not vulnerable to a natural hazard of some kind and because it is not a reasonable option for many people to move to a different region or even country to avoid certain risks.

Because risks associated with natural events are not risks that we create, the question of which risks communities should permit does not arise in the same way. Instead, the choices communities face with regard to risks associated with natural events concerns questions about the design, construction, and modification of the built and the modification of the natural environment, including mitigation actions that should be taken to reduce the impact of future natural events. This is a question about the management, not strictly speaking about the acceptance, of risks. Given the threat posed by natural events, risk management involves communities asking what level of

potential disruption they will allow, not whether they will allow their community to face risks associated with natural events.

Risks from anthropogenic climate change are similar to the risks from natural hazards in that risks from climate change are influenced by our actions. Thus, the source of risks in both cases is indirect, linked to our actions which in turn have implications for the climate system or for natural events. Like ordinary risks and technological risks, risks due to anthropogenic climate change raise questions of responsibility. However the central question in this context is who bears responsibility for mitigation action; in this respect risks associated by natural events and risks due to anthropogenic climate change are similar.

Despite these similarities, the character of the link between responsibility and mitigation is importantly different for risks due to anthropogenic climate change and risks associated with natural hazards. Philosophical discussions of responsibility for risk mitigation in the context of climate change concentrate on justifying and defining the demands of intergenerational justice, that is, the requirements of people now alive to prevent harm to future generations (Moellendorf 2009). A second question considered is what constitutes fairness of the distribution of greenhouse gas emissions, and whether and how much our answer to this question should take into consideration historical contributions to greenhouse gas levels and who is most at risk by climate change (Harris 2003). This second question arises in part because of the gap between those who influence the character of risks posed by climate change and those who are most vulnerable to such risks.

For risks associated with natural events, the question of responsibility for mitigation is not primarily or fundamentally a question of intergenerational justice. Mitigation action, or the failure to take mitigation action, characteristically affects current as well as future generations. Furthermore, the issue of distribution of responsibility for mitigation action has a different character in the context of risks associated with natural hazards. There is less distance between those who influence the character of risks posed by natural events and those who are vulnerable to such risks. Construction in the United States does not change or negatively impact the risks associated with natural events in Haiti (setting aside indirect implications of such construction for greenhouse gas emissions) the way that construction in Haiti does.

Finally, it is important to recognize that the scope of the actions which affect the risks due to anthropogenic climate change and the risks associated with natural events are different. The actions which influence the risks associated with natural events are broader than the actions that influence greenhouse gas emissions. For example, reinforcing existing structures can directly reduce the likely severity of the consequences of a future earthquake, but have little influence on greenhouse gas emissions. In addition, not all of the consequences of anthropogenic climate change will be of interest when considering risks associated with natural events. In the case of risks associated with natural events, our interest is not fundamentally with the impact of our actions on greenhouse gas emissions and subsequent climate change. Rather, our interest is in the impact of our actions on the probability and severity of natural events. Thus, changes in greenhouse gas emissions will be of interest insofar as their impact on climate changes affects the probability of occurrence or severity of impact of natural events. That is only insofar as greenhouse gas emissions contribute to climate change in

ways that lead to increases in the probability of occurrence or severity of the impact of natural events will anthropogenic sources of greenhouse gas emissions will be relevant for evaluating the risks due to natural events.

THE MORAL EVALUATION OF THE SOURCE OF THE RISKS ASSOCIATED WITH NATURAL EVENTS

Our actions influence the character of the risks stemming from natural events. It is the interaction, between the natural and the built environments and a natural event, which is the source of a risk in the context of natural hazards. In this section we develop a framework for the moral evaluation of the source of the risks associated with events. Our evaluation concentrates on the decisions made with respect to how to construct and modify the built environment, as well as how to modify the natural environment, insofar as these decisions influence the risks associated with natural events. Our discussion takes as its starting point concepts and standards from tort law. We argue that tort law has theoretical resources that can inform the evaluation of the decisions in which we are interested.

The central issue in tort law is determining who should bear the costs of misfortune or disaster, the direct victim(s), the community, or those responsible for the misfortune or disaster itself (Coleman 2003). A necessary condition for an individual to be held liable for misfortune or disaster, and so be responsible for the costs, is that he or she commits a wrong. Wrongdoing in this context is understood to mean breaching a standard of conduct to which he or she should and could instead adhere, including the kinds of risks individuals have a right to impose on others or have the obligation to mitigate. Such standard in tort law is called a standard of reasonable care. This standard articulates how a reasonable person would act, when appropriately constraining his/her actions in light of the legitimate interests of others.

The content of the standard of reasonable care categorizes actions in different ways. Some actions are absolutely prohibited and others are permissible so long as done with reasonable precaution. Absolutely prohibited actions are sufficiently harmful that individuals have a duty not to engage in them (Coleman 2003). An individual is liable for harm caused by him or her engaging in a prohibited activity. For permissible actions, an individual can be liable for harm insofar as she acted recklessly or negligently, failing to exercise due precaution or care. Precaution is defined in part by foreseeability; that is, to claim that someone must refrain from certain actions depends on what consequences we can anticipate following from our action.

Tort law provides useful theoretical resources for thinking about how to morally evaluate decisions regarding the built and modified natural environments that have implications for the risks associated with natural events. The standard of care focuses our attention on what it is reasonable to expect from those involved in constructing and modifying the built and natural environments, including engineers, architects, policy makers, and construction companies. The standard of care for each group will be different because the kinds of decisions they make with respect to the built and natural environments are different. For example, policy makers define the boundaries of the built environment and boundaries of permissible modifications to the natural environment. They specify whether construction can occur in a particular region as well as what kinds of buildings and facilities can be located in that region. Engineering professional organizations specify minimum guidelines for design and construction

through their professional codes.¹ Engineers and architects make choices about the specific design of structures and infrastructure. Construction companies make choices about materials for construction within the boundaries set by law and the code. In what follows, we outline the general kinds of considerations that should inform an evaluation of each kind of decisions.

The first thing to recognize is that the standard of reasonable care for decisions about the built and modified natural environment will be constrained by current knowledge about possibilities for the design, construction, and modification of the built and natural environments. This knowledge sets boundaries for the range of possibilities in our action. In the case of the built environment, reasonable options regarding construction may include building or not building in a particular area, or constructing a building using specific materials (e.g., steel, concrete, or wood). In the case of the modification of the built environment, choices may be whether to retrofit an existing building or not, and if so how. Choices with the natural environment involve, for example, land development by deforestation or the reclamation of wasteland or flooded land so that it can be cultivated, for example by diverting river streams, building dams, levees, or canals.

Whether a given choice should be viewed as satisfying the standard of care will depend on three factors. First, the influence of such decisions on the probability of occurrence and the associated consequences of natural hazards must be considered. For some natural hazards, choices may not impact the probability of occurrence. For other hazards, choices may influence the probability of occurrence. More frequently, choices will influence the likely consequences of a natural hazard. For example, revising building codes, retrofitting existing structures, changing zoning laws, or restricting land use may diminish the likely consequences of an earthquake. Specification of any standard for reasonable care requires determining how foreseeable is the increase in the probability of occurrence or severity of the impact of natural hazards in any given case. Technical knowledge can inform the criteria of foreseeability. Importantly, given that the state of engineering knowledge is expanding with new research findings, the boundaries of possibility may increase and uncertainty may be reduced over time as knowledge increases.

The second factor that should inform the reasonable standard of care is available resources; economic constraints delimit practical boundaries for possibilities. Engineers design and construct buildings and systems under resource constraints. Resource constraints set some boundaries around which technical options are financially feasible in any particular context. Thus, choices that have a greater increase in the probability of occurrence or consequences than alternatives may satisfy a standard of care if such choices are the only financially feasible alternative.

Furthermore, the standard of care must take into account competing priorities of individuals and communities. Not all financially feasible alternatives that most reduce vulnerability to hazards should automatically be pursued. Reduced vulnerability to hazards is not the only thing that matters to either individuals or communities. Individuals often have a number of valuable goals they want to pursue, all of which may depend on financial resources to be feasible. It can be reasonable for individuals to

¹ For an overview of standards for engineering see Strand and Golden (1997).

trade off certain gains in safety, by for example buying more affordable homes in order to increase the resources available to pursue other goals and objectives that matter. At the policy level, hazard mitigation is not the only priority that matters. Hazard mitigation is one of a number of important objectives of governments and communities to pursue. Other important objectives include, for example, education and health.

Given these competing alternatives, the standard of care may be sufficiently broad to accommodate and indeed reflect reasonable disagreement about how to weigh and compare competing values. Some individuals may be more risk-averse than others. Likewise, some communities may place a higher priority on natural hazard mitigation than on, for example, national defense. The specification of what should reasonably be expected should be general enough to allow for some choice in the means used to achieve a particular goal. The standard for reasonableness can be updated in light of increases or decreases in general resources, which would suggest fewer or additional resources to be put towards natural hazard mitigation.

However, there will be constraints on the kind of variation that is reasonable. For example, implicit in any formulation and justification of standards will be the assumption of background conditions of distributive justice. Any analysis of the standard of reasonable care for the construction of the built environment and modification of the natural environment must account for the more serious resource constraints that many developing countries, for instance, face. At the same time, extreme and unreasonable resource scarcity among groups within a community or among poorer communities nationally, if not taken into account, may result in standards for reasonable care reflecting the constraints of poverty, rather than reasoned judgments about the relative value of natural hazard mitigation as opposed to other competing goods. Thus, it is necessary to identify a threshold kind and level of resources that is needed within communities and at the global level for any justifiable standard of reasonable care.

When the construction of the built and modified natural environment cannot be justified on the basis of the standard of reasonable care, we can examine where the source(s) of the fault lies. In some contexts, fault may lie with the global community, insofar as the global distribution of resources is such that it is impossible for a community to fulfill any minimal reasonable standard of care. In other cases, it may be government officials and policy makers who are responsible for the failure to meet a reasonable standard of care, insofar as governments fail to allocate the minimally justifiable resources to natural hazard mitigation or fail to support and supplement the efforts of professional organizations to come up with professional standards. Alternatively, individual contractors may be responsible for the failure to fulfill reasonable standards of construction that were both possible to fulfill and required by law. Multiple levels of failure may be present in certain cases. As these examples illustrate, the evaluation of the character of the built and modified natural environments will be complex. Diverse actors, including policy makers and members of the business community, as well as the general public, influence the character of the built and natural environments. The multiple actors involved in creating the built and modifying the natural environments compound the challenge of both assigning responsibility for its construction and ascribing intentions to actors judged responsible. However, the complexity of the evaluative process offers no principled reason to refrain from

attempting to come up with appropriate categories and engaging in particular moral assessments.

ACKNOWLEDGEMENTS

This research was supported primarily by the Science, Technology, and Society Program of the National Science Foundation Grant (STS 0926025). Opinions and findings presented are those of the authors and do not necessarily reflect the views of the sponsor.

REFERENCES

- Bedford, T., and R. Cooke, R. 2001. Probabilistic risk analysis: foundations and methods. Cambridge, UK: Cambridge University Press.
- Coleman, Jules. 2003. Theories of Tort Law. The Stanford Encyclopedia of Philosophy. <http://plato.stanford.edu/entries/tort-theories/>. Accessed 23 March 2010
- Franssen, Maarten, Gert-Jan Lokhorst, and Ibo van de Poel. 2009. Philosophy of Technology. Stanford Encyclopedia of Philosophy. <http://plato.stanford.edu/entries/technology/#AnaTec>. Accessed 23 March 2010
- Gardiner, Stephen M. 2004. Ethics and Global Climate Change. *Ethics* 114: 555-600
- Hansson, Sven Ove. 2004. Philosophical Perspectives on Risk. *Techné* 8(1): 10-35
- Hansson, Sven Ove. 2007. Risk. Stanford Encyclopedia of Philosophy. <http://plato.stanford.edu/entries/risk/>. Accessed 23 March 2010
- Harris, Paul G. 2003. Fairness, Responsibility, and Climate Change. *Ethics and International Affairs* 17(1): 149-156
- Kaplan, S., and B.J. Gerrick. 1981. On the quantitative definition of risk. *Risk Analysis* 1: 11-27
- McKerlie, Dennis. 1986. Rights and Risk. *Canadian Journal of Philosophy* 16: 239-252
- Moellendorf, Darrel. 2009. Justice and the Assignment of the Intergenerational Costs of Climate Change. *Journal of Social Philosophy* 40(2): 204-224
- Shrader-Frechette, Kristin. 1985. Technological Risks and Small Probabilities. *Journal of Business Ethics* 4:431-445
- Strand, M.N., and K.C. Golden. 1997. Consulting Scientist and Engineer Liability: A Survey of Relevant Law. *Science and Engineering Ethics* 3 (4): 357-394
- Sunstein, Cass R. 2002. Risk and Reason. Cambridge: Cambridge University Press.
- UN International Strategy for Disaster Reduction (UNISDR). 2005. Disaster Statistics 1991-2005. <http://www.unisdr.org/disaster-statistics/impact-killed.htm>. Accessed 23 March 2010
- United States Geological Survey. 2010. <http://www.usgs.gov/hazards/earthquakes/>. Accessed 23 March 2010
- Vose, D. 2000. Risk analysis: a quantitative guide. New York: Wiley
- Wolff, Jonathan. 2006. Risk, Fear, Blame, Shame and the Regulation of Public Safety. *Economics and Philosophy* 22:409-427

Florida International University's Wall of Wind: a tool for improving construction materials and methods for hurricane-prone regions

Aly Mousaad Aly¹, Girma Bitsuamlak², Arindam Gan Chowdhury³

Laboratory for Wind Engineering Research, International Hurricane Research Center, Department of Civil and Environmental Engineering, Florida International University, Miami, Florida 33174, USA.

¹PH (786) 200 2145; email: aalysaye@fiu.edu; aly.mousaad@polimi.it

²PH (305) 348 6755; email: girma.bitsuamlak@fiu.edu

³PH (305) 348 0518; email: chowdhur@fiu.edu

ABSTRACT

Hurricane winds are one of the governing design environmental loads for structures. In coastal regions such as Florida, hurricanes cause enormous loss to life and property. Research focusing on the complex interaction between hurricanes and the built environment is therefore needed for developing a cohesive approach to build hurricane resilient coastal communities. At the International Hurricane Research Center (IHRC), Florida International University (FIU), research is going in stages on the construction of a large state-of-the-art Wall of Wind (WoW) facility for potential full- and large-scale wind engineering testing. In this paper, a technique for simulating hurricane winds at the WoW is presented and investigated. Wind profiles were simulated using turning vanes, and/or adjustable planks mechanism with and without grids. Assessments of flow characteristics were performed in order to enhance the WoW's flow simulation capabilities. The full-scale testing facility will be capable of generating hurricane wind and wind-driven rain field with proper characteristics to allow better understanding of category 1 to 4 hurricane (using Saffir-Simpson scale) effects on structures. The facility will be large enough to engulf full- and large-scale models of single-story buildings built using actual construction materials. This will help improve code provisions, innovative hurricane mitigation development, and producing solutions which bridge the disciplines of wind engineering and structural engineering.

INTRODUCTION

In recent years, full-scale testing and measurements of wind effects on the built environment have been playing an important role in the construction and retrofitting of more resilient structures. On the other hand, lack of awareness of the complex interaction between hurricane winds and the built environment during the construction of such structures, may lead to rickety designs with a result of enormous loss to life and property (Emanuel 2005; National Science Board 2008; Pielke et al. 2008). Wind-structure interaction complexity as well as lack of reliable full-scale data during destructive wind events, made full-scale industrial wind engineering testing essential for developing a cohesive approach for building more economical and

hurricane resilient coastal communities. To overcome scaling issues and enhance capabilities to conduct destructive testing under hurricane winds and rain, researchers at Florida International University (FIU) have introduced a testing facility, the Wall of Wind (WoW) (see Figure 1). However, modeling proper hurricane wind characteristics for the facility is a big challenge. For example, unlike for flow in wind tunnels, the mean wind speed decreases along the flow direction. This requires setting the test models as close as possible to the fans exit. In addition, it is necessary to generate wind flow with as large wind speed as possible to simulate destructive hurricane forces. For these reasons, wind field management for the facility requires techniques that are not necessarily similar to those in wind tunnels.



Figure 1. New 12-fan WoW (under construction) beside the 6-fan WoW (on the right) at FIU.

In 2003, research team at the International Hurricane Research Center (IHRC), FIU, started planning for the construction of large-scale testing facility to produce an experimental data-base for better understanding of the effects of extreme winds on structures (Leatherman et al. 2007). With this vision, IHRC has first developed a 6-fan WoW testing facility suitable for experimentation and destructive testing of large-scale, low-rise structures (Bitsuamlak et al. 2009; Gan Chowdhury et al. 2009). However, the maximum wind speed produced by the facility is still lower than what is required for some destructive tests. To allow for better understanding of hurricane-induced effects on residential buildings and other structures through large-scale and destructive testing, a more powerful 12-fan WoW with electric fans (see Figure 1) is under construction.

The aim of this research is to generate wind fields with proper characteristics that mimic hurricane winds within the atmospheric boundary layer for the new facility for potential WoW testing. The paper focuses on a preliminary evaluation of the performance of the 12-fan WoW by examining numerically and experimentally its potential flow characteristics.

METHODOLOGY

A small-scale replica (1:15) of the 12-fan WoW facility with adjustable planks mechanism was fabricated to reduce the effort required for developing a mechanism to generate proper wind profiles (see Figure 2). The replica consists basically of 12 fans placed on an arc to produce concentrated flow and thus enhance the wind speed. The air blown from the fans goes inside a contraction used for further speed

enhancement. The exit section has a width of about 15.5 in (around 395 mm) and a height of about 11 in (around 280 mm). The WoW is housed in a structural building which replicates a full-scale building constructed for providing protection from environmental conditions (e.g., sun and rain). The building model was constructed using wood beams covered by polystyrene transparent sheets.

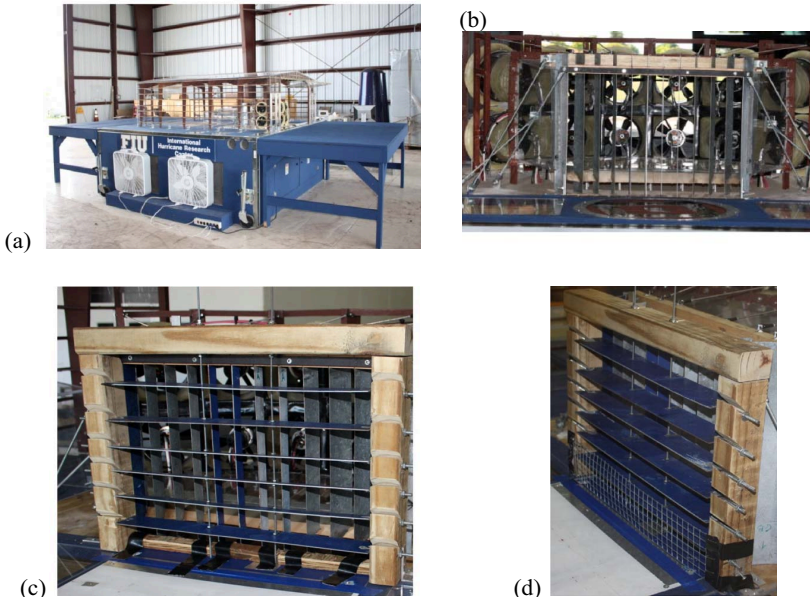


Figure 2. 12-fan WoW: (a) Scaled 1:15 replica; (b) Configuration I; (c) Configuration II; (d) Configuration III.

An easily adjustable planks mechanism was constructed for the purpose of managing the mean wind speed profile. The mechanism consists basically of a wooden frame where horizontal steel planks are supported by hinges for ease of adjustment [Figure 2(c-d)]. Two vertical threaded steel guides are used to help keep in place the planks at a certain pitch angle, and to help prevent wind-induced oscillations in the vertical direction. The pitch angle of each plank can be adjusted through the hinged supports and the vertical steel guides to offer a wide range of atmospheric boundary layer (ABL) profiles. A total number of six steel planks were used. This arrangement was found to best achieve two purposes: reduce the deviations of the mean wind speed data points about the target profiles, and keep the blockage produced by the planks as low as possible.

Cobra probes (Turbulent Flow Instrumentation) were used for wind speed measurements. The multi-hole pressure probe can capture the 3D velocity variation within a high range of frequencies. The probe has a frequency response of up to 5000 Hz. In comparison to hot-wires, Cobra probe is robust and can withstand moderate knocks and contaminated flow. Furthermore, the probe can provide flow mapping in

test sections and around model or full-scale objects, offering a replacement of hot-wires and other types of anemometers. Four Cobra probes arranged vertically as shown in Figure 3(a) were used for wind velocity assessment. The assessment provided insight into the wind field generated with and without the flow management devices and explored mean wind speed as well as turbulence intensity profiles. The probes were mounted on a steel bar which was fixed by means of two vertical steel rods secured to a movable carriage (traverse system). The carriage can be moved in a horizontal plane allowing measurements at grid-like locations. Wind speeds were measured at a sampling rate of 1750 Hz. Such high frequency of acquisition was very important for capturing the most significant content of the signal and hence accurate estimate of turbulence intensities. Each test was performed for duration of one minute which was sufficient to have a wind speed record with a stationary mean value for each individual test.

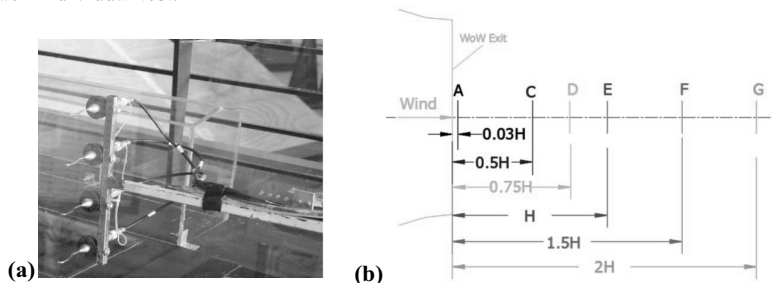


Figure 3. Wind velocity components were measured using turbulent flow Cobra probes: (a) Cobra probes, (b) Measuring locations.

WIND FIELD MANAGEMENT

Three wind profiles were simulated under three different configurations as follows:

Configuration I. In this configuration, the WoW flow was simulated with vertical turning vanes of thin plate cross-sections and without any planks or mesh (see Figure 2-b). Three locations were considered for wind speed measurements. The measuring locations considered are A, C, and E, as designated in Figure 3(b). Measurements were conducted at two different wind speeds and referred to as 15% and 35%. These ratios are actually related to the percentages of the power (throttle ratio) given to fan motors that can generate mean wind speeds (U_{ref}) of about 20m/s and 40m/s respectively at a reference height of 6.4 inches (162.6 mm). The measured profiles are compared to those predicted by a computational fluid dynamics (CFD) study accomplished by RWDI Inc. Figure 4 shows mean wind speed and turbulence intensity profiles at the three measuring locations. Results show that there is a good agreement between mean wind speed profiles measured and those predicted by the CFD study for the two throttle ratios, especially at locations C and E. Such agreement will attest the importance of CFD simulations in the area of wind engineering. Turbulence is generally low and the use of this configuration for testing bridges as well as some aeronautical applications could be promising.

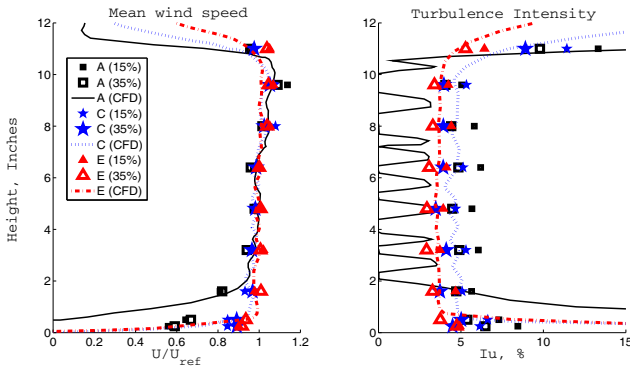


Figure 4. Mean wind speed and turbulence intensity profiles under Configuration I at locations A, C, and E.

Configuration II (suburban terrain). The objective of this configuration is to generate a wind field with a power law profile that mimic suburban terrain (power law exponent $\bar{\alpha} = 1/4$). This configuration was achieved by adjusting planks pitch angles as follows: 8.5° , 13° , 15° , 8.5° , 3.5° , and 1.5° (starting from the lower plank). In addition, a wooden prism with a length of 15.5 in (393.7 mm), a width of 1 in (25.4 mm), and a height of 0.625 in (15.9 mm) was placed on the floor under the lower plank to create some blockage in the lower part of the boundary layer [Figure 2(c)]. Figure 5(a) shows mean wind speed and turbulence intensity profiles measured at locations C, E, and G of Figure 3(b) under Configuration II. Results show that mean wind speed profiles at E and G are in agreement with the target profile (suburban terrain). However, mean wind speed profile at C shows some irregularities at the lower part of the boundary layer (the scatter of the measured data at C is the highest among all of the locations considered). This is due to the fact that location C is closer to the flow exit from the planks mechanism where the wind flow was subjected to sudden changes in the wind speed with less homogeneity and had not enough time to be properly mixed as was the case at locations E and G.

Configuration III (open terrain). The intention of this configuration is to produce a wind field with a power law typical to flow over open terrain ($\bar{\alpha} = 1/6.5$). This configuration was attained by adjusting planks pitch angles as follows: 0° , 6° , 6° , 5.5° , 0° , and 0° (starting from the lower plank). Furthermore, a steel mesh was secured at the lower part of the planks mechanism to generate some blockage in the lower part of the boundary layer [see Figure 2(d)]. Figure 5(b) shows mean wind speed and turbulence intensity profiles achieved at locations C, D, E, F, and G of Figure 3(b) under Configuration III. The figure shows that mean wind speed profiles at all of the five measuring locations are in agreement with the target open terrain profile. One can also see that mean wind speed profiles have lower irregularity when compared to the profiles obtained under Configuration II. This is mainly attributed to the fact that the planks pitch angles are generally lower than those of Configuration II. Figure 6 shows mean wind speed surface plot at locations C.

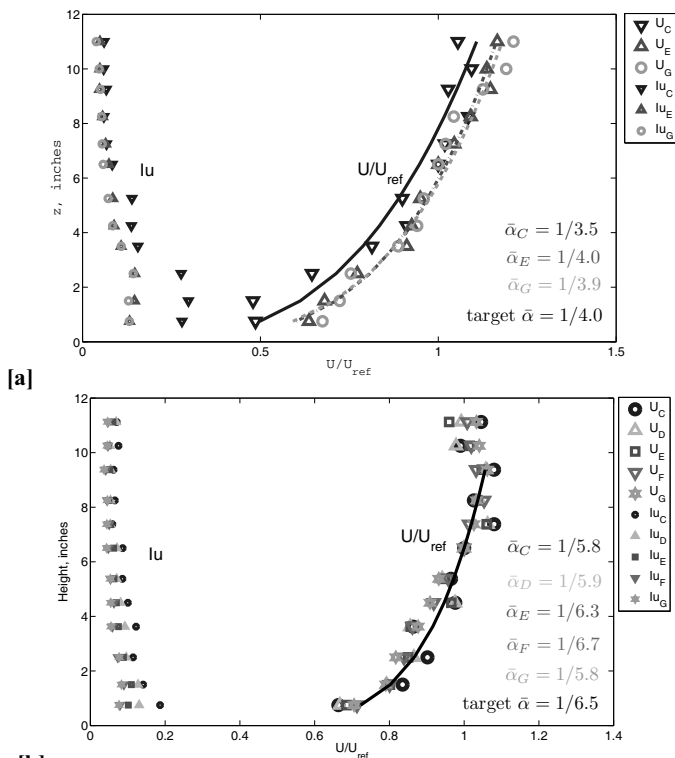


Figure 5. Mean wind speed and turbulence intensity profiles: [a] Configuration II (suburban terrain); [b] Configuration III (open terrain).

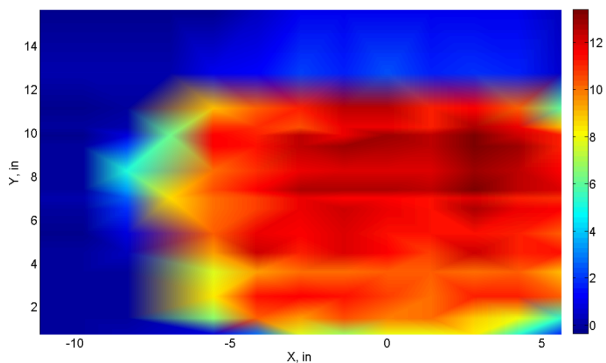


Figure 6. Mean wind speed (m/s) surface plot at section C.

DISCUSSION

Wind profiles obtained under Configuration I, where only vertical turning vanes were used, are useful for performing tests on aeroelastic models of long-span cable-stayed or suspended-span bridges. Deck section model tests also can be performed using dedicated tools. In addition, this configuration could be promising for high wind speed, low-turbulence aeronautical applications.

WoW simulations are sufficiently flexible to generate commonly used mean wind velocity and turbulence intensity profiles (i.e., mean wind power law or logarithmic profiles). Furthermore, the WoW is capable of generating hurricane profiles measured through the Florida Coastal Monitoring Program (FCMP) as described by Yu (2007). The wind profiles simulated in this study provide a tool for future tests at the full-scale facility (low-rise, tall buildings, and long-span bridges). In addition to the possibility of providing low-turbulence test section as well as typical ABL profiles, the 12-fan WoW will allow, through large-scale and destructive testing, better understanding of category 1 to 4 hurricane effects on residential buildings and other structures. This will help improve code provisions and innovative hurricane mitigation development. The electric 12-fan system is expected to have lower noise compared to the noise emitted from the existing 6-fan WoW and will require less maintenance. Furthermore, the electric fans have high static head (when compared to the current fans of the 6-fan WoW, driven by diesel engines). Since this system is indoors (Figure 1) it will also be controllable and the weather conditions will not affect test schedules, hence allowing more tests to be conducted within a given time frame.

The full-scale FIU WoW facility has the following vision: holistic full-scale simulation of hurricane wind forces with realistic mean and turbulence characteristics; coupling/hybridizing dynamic wind loading with nonlinear structural/material response; monitoring performance levels and progressive damages for different wind force levels; providing a controllable, programmable, and repeatable hurricane test environment; eliminating scaling issues, and yielding realistic Reynolds and Strouhal numbers; simultaneous testing for high wind forces and impinging rain; simultaneous testing of high wind forces and wind-borne debris impact (using debris propelling devices) on components and the entire structure, including the effects of breach of envelope on internal pressure. Four different types of tests are anticipated at the new full-scale facility: (a) Aeroelastic (long-span bridges, sensitive structural elements, and super-tall buildings), (b) Aerodynamic (pressure tests on low-rise buildings, large roofs, high-rise buildings, and aerodynamic mitigation), (c) Hydro-aerodynamic (wind-driven rain intrusion through roof secondary water barriers, soffits, and window/door/wall interfaces), and (d) Destructive (roof tile and shingle tests, roof fascia tests, and wind-borne debris).

CONCLUSIONS

Wind fields assessed experimentally at the small-scale 12-fan WoW facility are in agreement with CFD results. Such agreement will attest the significance of CFD simulations in the area of wind engineering. The adjustable planks mechanism proposed in this research allows for generating different mean wind speed profiles. Suburban terrain ($\bar{\alpha} = 1/4$) and open terrain ($\bar{\alpha} = 1/6.5$) are achieved with

Configuration II and Configuration III, respectively. Wall of Wind testing technology combined with potential wind profiles offers great benefits for future-oriented wind engineering applications involving bridges, buildings, wind-induced rain, and destructive testing at large scales. This is imperative for the improvement of code provisions, innovative hurricane mitigation development, and for producing solutions which bridge the disciplines of wind engineering and structural engineering.

REFERENCES

- Bitsuamlak, G.T., Gan Chowdhury, A. and Sambare, D. (2009), "Application of a full-scale testing facility for assessing wind-driven-rain intrusion", *Build. Environ.*, **44**(12), 2430-2441.
- Bitsuamlak, G., Dagnew, A. and Gan Chowdhury, A. (2010), "Computational assessment of blockage and wind simulator proximity effects for a new full-scale testing facility", *Wind Struct.*, **13**(1), 21-36.
- Emanuel, K. (2005), "Increasing destructiveness of tropical cyclones over the past 30 years", *Nature* 436(7051), 686-688.
- Gan Chowdhury, A., Simiu, E. and Leatherman, S.P. (2009), "Destructive Testing under Simulated Hurricane Effects to Promote Hazard Mitigation", *Nat. Hazards Review J. ASCE*, **10**(1), 1-10.
- Huang, P., Gan Chowdhury, A., Bitsuamlak, G. and Liu, R. (2009), "Development of devices and methods for simulation of hurricane winds in a full-scale testing facility", *Wind Struct.*, **12**(2), 151-177.
- Leatherman, S.P., Gan Chowdhury, A. and Robertson C.J. (2007), "Wall of Wind Full-Scale Destructive Testing of Coastal Houses and Hurricane Damage Mitigation", *Journal of Coastal Research*, **23**(5), 1211-1217.
- National Science Board (2007), "Hurricane warning: the critical need for a national hurricane research initiative", NSB-06-115, 1-36.
- Pielke, R. A., Jr.; et al. (2008), "Normalized Hurricane Damage in the United States: 1900-2005", *Nat. Hazards Review J. ASCE*, **9**(1), 29-42.
- Yu B. (2007), *Surface mean flow and turbulence structure in tropical cyclone winds*, Ph.D. dissertation, Florida International University: Miami (FL); 2007.

Risk management of Long Term Infrastructure Projects “PPP-BOT projects” by using Uncertainty, Probabilistic and Stochastic Methods and Models

Meghdad Attarzadeh, David Kim Huat Chua, Michael Beer

Department of Civil Engineering, National University of Singapore, Block E1A #07-03, 1Engineering Drive 2, Singapore, 117576, Tel (DID): 65-65164643

Email: Meghdad@nus.edu.sg

Abstract :

Risk Management is one of the vital factors for success in long term projects. According to some researchers which consider the risks in long term and large structures projects, risk management is the order of the day and one of the critical success factors (CSFs) of PPP-BOT projects. The concept of risk in these projects, where the risks are generally high, involves contingency and uncertainty. So it is essential to employ uncertainty, probabilistic and stochastic methods and to use related models to manage risks in these projects. In this paper some Probabilistic and Stochastic methods, tools and software are used in real cases to show their role and benefits in the life cycle risk management of Long Term Infrastructure Projects; namely PPP-BOT projects and these have been compared with current methods. Finally a framework for these methods has been proposed to examine dependability modeling under uncertainty by using proposed global dynamic environment model.

Key words:

Risk management, Probabilistic methods, Fuzzy set, Dependability modeling under uncertainty, Construction project simulation, Monte Carlo Simulation, PPP

1. Introduction:

Public private partnership (PPP) is collaboration between the public and private sectors for the purpose of delivering a project or a service traditionally provided by the public sector and offers one means of achieving this by attaining a win-win-win situation among the public sector (government), private sector (concessionaire) and end user. Although increasing market for PPPs for the development and operation of infrastructure projects has been reported [1], only a few of them have been successfully completed [2,3]. One significant reason is that the commonly used financial evaluation methods only consider the benefits and cost of the private sector. With the fast pace of market-oriented transformations in infrastructure, a delicate balance has to exist among the private sector capacity and benefits, government regulatory function, and public and end user satisfaction simultaneously. In other words it is related to the level of risk management in each phase. To support this process through all stages of a project it is necessary to identify, assess and manage the risks, so that the amount of risk can be rightly apportioned during the negotiation stages. This basic work and the process of updating the risk assessment and the process of risk mitigation and control – often summarized under the term risk management – are supported and organized by the especial and proper process [2]. The advantage of a probabilistic approach lies in the fact that by using values lying within a bandwidth and modeled by a defined distribution density the reality can be modeled better than by using deterministic figures.

In this research uncertainty environment has been used to cover both probabilistic models and fuzzy set theory. Fuzzy sets are used for decision making based on incomplete or insufficient data, and probabilistic models is used as a decision making based on complete information about the probability. The research methodology that is discussed later, suggests improved investment decisions will follow from more knowledgeable assessments of project risks that will lead to improved project selection which in turn results in improved project performance. It sustains future investment enthusiasm in the new procurement method. Due to the difficulties in estimating the long-term uncertainties and wider-risk profiles at the tendering stage, this research suggests using uncertainty, probabilistic and stochastic risk analysis techniques (such as fuzzy sets, probability models and Monte Carlo simulation) to enhance traditional decision making methods. Also this study considers risk analysis incorporating financial evaluation method for the delivery of PPP projects, taking into account all the viewpoints of the relevant stakeholders including the government, sponsors, and lenders. At the last step of current research, dependability modeling under uncertainty is considered by utilizing proposed global dynamic environment model in a framework.

2. Simulation process model:

In the modeling process of risks and uncertainty through the life cycle negotiation simulation, the idea is that: deterministic and uncertain parameters that are constructed the model, each uncertain parameter follow specific distribution.

For model procedure it is necessary to follow three steps:

1. Identify the major risk factors that could have serious effects on the uncertain parameters.
2. Establish an empirical or assumed distribution for each of the identified risk factor (discrete or continuous form).
3. Examine the effects of the risk factors on the uncertain parameters as negotiable concession items.

2.1. *Model assumptions and details:*

The two main parameters in this model are:

- *Deterministic parameters:* such as construction period as estimated by public party, return rate as estimated by private party (MARR) and tariff/toll regime as estimated by the end-user willing to pay.
- *Uncertain parameters:* in order to achieve proper model of risk management some steps must be done:

Step1: Firstly identify essential and significant risks and uncertainty as well as concession items involve in life cycle negotiation PPP-BOT project from each party's point of view (as CSFs if manage properly) as follows:

- *Concession period:* According to Zhang and Kumaraswamy [4] establishing an appropriate *concession period* is important to the success of a PPP project. Being protected by an assured minimum "revenue stream", the concessionaire is entitled to raise the tariff/toll in case their actual profit falls short of the anticipated return. Projects with a shorter concession period could hence result in a higher tariff/toll regime, and this is obviously not desirable from the user's standpoint. The studies show that the risks and uncertainties, such as a

change in inflation rate, traffic flow and operation cost could influence the decision on the concession period.

- Cost in year t (C_t) comprises all the expenses could be influenced by many risk factors such as
 - Inflation rate fluctuation represent by normal probability distribution.
 - Operation and maintenance cost follow a uniform distribution (interval between a pessimistic and optimistic estimation).
- Operation revenue in year t (R_t) is determine by number of user (follow normal distribution) and tariff/toll regime (deterministic parameter)

Step2: Having established the deterministic and uncertain parameters, the simulation can proceed by inputting these parameters. By repeating the simulation cycle a number of times, the cumulative frequency distribution of the negotiable concession items can be generated. So the cumulative probability for each possible negotiable concession item can also be identified.

Step3: With the simulation results, the public partner can determine negotiable concession item that would guarantee the concessionaire to gain the anticipated IRR under the proposed tariff/toll regime with a particular confidence level (probability). Note that the simulation output would include the cumulative probability of all different IRR (IRR_{min} , $IRR_{expected}$ and IRR_{max}) and the criteria for determining an appropriate negotiable concession items. Besides, different scenarios could be considered during the simulation process. These could be set to facilitate the decision-makers to trade off between deterministic and uncertain parameters like series of IRR and tariff/toll regime at the one side and negotiable concession items such as concession period and tariff/toll rate in the other side. Figure 1 demonstrates Simulation process model.

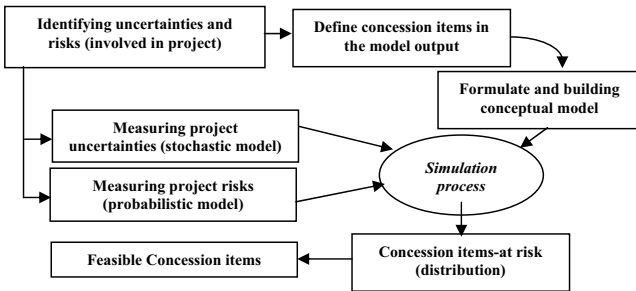


Figure 1: Simulation Process modeling for feasible concession items determination

2.2. Selection of input concession items (random variable) for PPP-BOT risk management model:

- Input model variable (uncertain variable- Private & Public sectors and Lenders perspectives)
- Negotiation items : Concession and construction period, Base price (tariff), Demand quantity, Return rate (IRR)
- Negotiation & project risks:
 - Completion time, construction cost: follow lognormal dist., O&M cost: follow uniform dist.

- Market demand, sale price (income), inflation, foreign exchange rate, and interest rate: follow normal dist.

2.3. Selection of output indicators for PPP Risk management Model:

We need methods which take return and risk into account simultaneously. Indicator-at-risk systems provide a decision criterion with a confidence level (probability). Table 1 show all Indicator-at-risk based on related perspectives. Ye and Tiong defined the NPV-at-risk [5], a measure of minimum expected return from the project at a given confidence level. Indicator-at-risk measures of maximum potential change in value of portfolio of financial instrument with a given probability over a present horizon. $IND\text{-at-risk} = IND_{\alpha} = \mu_{(IND)} - Z_{(\alpha)} \cdot \sigma$
 Decision rule: The project is acceptable with a confidence level of $1-\alpha$ if the $IND\text{-at-risk}$ at given confidence interval is greater than zero.

Table 1: indicators of all parties' perspective:

Indicator	Deterministic environment	Uncertainty environment
Public sector 's perspective	VFM (Value for Money) SLR ('Total Revenue/Total Cost' ratio @ end of Concession period)	VFM-at-risk SLR-at-risk
Lenders 's perspective	DSCR (Debt Service Cover Ratio) LLCR (Loan Life Cover Ratio) TIE (Time Interest earned)	DSCR-at-risk LLCR-at-risk TIE-at-risk
Private sector 's perspective	NPV IRR	NPV-at-risk IRR-at-risk

2.4. Simulation process model example:

Yongjian et al. applied the Simulation model to a real case (bridge project in Romania) which has been extended here[6]. The project was procured under a PPP contract with a concession period of 30 years (O&M costs is about US\$0.8 million) and requires US\$300 million over 6 years. Debt-equity ratio is 7:3, with an annual debt interest rate of 2.5% and income tax rate is 16%. Monte Carlo simulation (5000 iteration) was carried out on a simulation model to obtain the generated financial results for various confidence levels on different parties' Perspective involve in project. (See table 2 & 3)

Table 2: generated financial results

Perspective	variable	Mean value	SD	Maximum	minimum
Government	SLR	1.53	0.08	1.77	1.30
lenders	DSCR	1.06	0.03	1.14	0.98
lenders	TIE	2.68	0.02	2.71	2.63
sponsors	NPV(US\$, million)	72.61	8.86	102.04	43.55
sponsors	IRR (%)	15.00	0.007	13.10	16.90

Table 3: financial results for various confidence level

Perspective	variable	99% CL	90% CL	50% CL
Government	SLR-at-Risk	1.36	1.43	1.53
lenders	DSCR-at-Risk	1.00	1.02	1.06
lenders	TIE-at-Risk	2.64	2.66	2.68
sponsors	NPV-at-Risk(US\$, million)	51.99	61.08	72.67
sponsors	IRR-at-Risk (%)	13.50	14.10	15.00

As can be seen the financial evaluation method is based on NPV-at-risk method, which incorporates a risk analysis using confidence levels and discount rate concepts

to give more equitable results for all parties involved in the PPP project. Therefore by these simulation results, negotiations objectives will be promptly obtained.

2.5. Illustration of negotiation simulation model - manage risks and uncertainty through life cycle of PPP-BOT Projects:

To demonstrate the application of negotiation simulation model in order to manage variables as uncertainties such as completion time, construction cost, market demand, sale price, operation and maintenance (O&M) cost, inflation, foreign exchange rate and interest rate and bring them in to account, an real example that Ye and Tiong discussed [5], has been considered. The question is that when all uncertainties treat as random variables which follow specified probability distribution (Must be determine from experiences according to entity of that uncertainty) and take them in to account to evaluate and compare projects A and B (say based on NPV method) which one must be select to invest? To answer this question Trade-off between risk and uncertainty in one side and their return in other side should be considered.

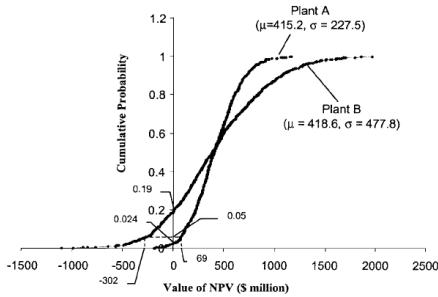


Figure 2: Comparison of NPV Distributions at Plants A and B [5]

Monte Carlo simulation was done on the described simulation model. NPV distributions of both projects are shown in Figure 2. As can be seen NPV-at-Risk of project A at 95% confidence level is M\$ 69 >0 so it is feasible. Also the probability of NPV=0 of project A is 0.024, in other word there is 97.6% (=1-0.024) confidence that NPV of project A is greater than zero. Although the expected NPV (μ) of project B is greater than project A (is in 50% confidence level), due to uncertainty management as discussed before project A should be selected to invest and Project B with confidence level greater than 81% would be rejected.

3. Utilizing Simulation model to establish appropriate negotiable Concession items

In the case where a concessionaire's actual profit falls short of the expected return then this will result in a raise of the toll/tariff. So, optimal concession period will help to balance the interests of both the government and investor in order to avoid renegotiations. S.Thomas et al. introduced a simulation model which it be developed here [7]. With the simulation results, the public partner can determine a concession period that would guarantee the concessionaire to gain the anticipated IRR under the proposed toll/tariff regime with a particular confidence level.

To determine it, three different scenarios on IRR: (IRR_{min}, IRR_{expected}, IRR_{max}) have been considered. Decision-makers trend is tradeoff amongst the concession period,

toll/tariff regime and IRR. To illustrate this simulation model a real case (BOT road project in Hong Kong) with the following details has been considered: construction period: 5 years with M\$100 cost, annum O&M cost =15% of annum operation revenue, discount rate: 13%, concession period: 15 years. In the deterministic environment, output calculates: NPV = M\$8.04, PBP =13.42 years

3.1. Incorporating risk factor in the simulation process- base scenario:

Uncertain parameters:

- Inflation rate: follows N-dist.: $\mu = 2.5\%$ and $SD=2\%$, Traffic flow: follows N-dist with $SD=20\%$, O&M cost (% of revenue): follow U. dist. [0.13, 0.17].
- IRR min = 0.13 , IRR expected =0.14, IRR max = 0.15

IRR	Table 4: Cumulative probability of concession period (deterministic environment)								
Year	13	14	15	16	17	18	19	20	21
IRR _{min}	0.004	0.129	0.551	0.878	0.982	0.998	1	1	1
IRR _{expected}	0	0.013	0.149	0.480	0.798	0.941	0.986	0.996	1
IRR _{max}	0	0	0.012	0.094	0.338	0.605	0.804	0.914	0.964

3.2. Renegotiation 1- changes in IRR:

Assume after negotiation of IRR: IRR_{min} =0.125, IRR_{expected} =0.135, IRR_{max} remains unchanged at 0.15. Table 5 shows results.

IRR	Table 5: Cumulative probability of concession period (Renegotiation 1)								
Year	13	14	15.5	16	17	18	19	20	21
IRR _{min}	0.052	0.3	0.901	0.95	1	1	1	1	1
IRR _{expected}	0	0.052	0.533	0.75	0.95	0.97	1	1	1
IRR _{max}	0	0	0.052	0.12	0.37	0.62	0.78	0.914	0.96

3.3. Renegotiation 2- Impact of different toll regimes: assume 20% higher:

Note that by comparing this result with the base scenario, it can be seen that the concession period is very sensitive to the toll regime as the concession period can be shortened by 3 years if the toll regime is increased by 20%.

IRR	Table 6: Cumulative probability of concession period (Renegotiation 2)								
Year	11	12	13	14	15	16	17	18	19
IRR _{min}	0.01	0.25	0.85	0.3	0.901	1	1	1	1
IRR _{expected}	0	0.05	0.505	0.052	0.533	1	1	1	1
IRR _{max}	0	0.01	0.163	0	0.052	1	1	1	1

4. Applying Fuzzy set simulation model to evaluate negotiable Concession items:

The combined features of the simulation and fuzzy multi-objective decision model (Max IRR, Min Tariff regime, Min concession period for private - end user-public sector perspectives respectively) enable the scenario most likely to result in a win-win concession scheme to be identified for government- concessionaire -end user. In this model concession items such as investment return (IRR_{min}) and tariff regime as a deterministic variable in model input; and concession period r.v. in model output are utilized. A practicable strategy would be to institute feasible options based on the concession periods and different combinations of IRR and tariff regimes; and finally select one which would balance the interests of all major stakeholders simultaneously.

At first current objective function must be transfer to fuzzy objective function. As f_i is a fuzzy set, f_{iinf} and f_{isup} are the inferior and superior boundaries of $f_i(x)$ and $\mu_{f_i}(x)$ or

$\mu_i(x)$ is the degree of membership that x belongs to f_i , so for the Max and Min objectives, membership functions that are used respectively shows by equations 1&2:

Eq. (1): $\mu_i(x) = \left[\frac{f_{i(x)} - f_{i\text{inf}}}{f_{i\text{sup}} - f_{i\text{inf}}} \right]$ Eq. (2): $\mu_i(x) = \left[\frac{f_{i\text{sup}} - f_{i(x)}}{f_{i\text{sup}} - f_{i\text{inf}}} \right]$ Eq. (3): $\mu_y = \max_j \min_i \{ \mu_{ij} \}$

Non-inferior solution is deduced by the max–min composition as expressed by equation 3, where ω_i is the weight of objective i .

4.1. Fuzzy set simulation model example:

Consider BOT road project which described in part 3. Incorporating risks and uncertainties factors in the fuzzy set simulation model has studied in three scenarios:

- Scenario 1:
 - Major risks and uncertainties:
 - Inflation rate—the rate of change follows N.dist. : $\mu = 2.5\%$, $SD = 2\%$.
 - Traffic flow —follows N dist.: $SD = 20\%$ of the first year’s traffic volume, and
 - O&M cost —follow a uniform dist. in the interval [0.13, 0.17].
- Scenario 2:
 - Minimum expected IRR=0.12
 - Tariff regime: the tariff is 10% less than the most likely tariff.
- Scenario 3:
 - Minimum expected IRR=0.14
 - Tariff regime: the tariff is 20% more than the basic tariff.

Result of simulation by calculating Cumulative probability of concession period for three scenarios, is summarized in table 7.

Table 7: Concession items for three scenarios- deterministic environment			
Concession items	Scenario 1	Scenario 2	Scenario 3
IRR (%)	13	12	14
Tariff coefficient	1	0.9	1.2
Concession period (years)	16.37	17.40	14.17

4.2. Evaluating of three scenarios:

Assuming the possible interval for IRR is [8%, 20%] and the concession period is [10, 25], degree of membership of scenario 1 to the objective of maximal IRR and degree of membership of scenario 1 to the objective of minimal concession period are showed by equations 4&5:

Eq. (4): $\mu_{13} = \frac{13\% - 8\%}{20\% - 8\%} = 0.42$ Eq. (5): $\mu_{13} = \frac{25 - 16.37}{25 - 10} = 0.58$

Evaluation results for three tariff regimes: moderate, satisfied and unsatisfied, 0.5, 0.7 and 0.3 are the degree of membership for those tariff regimes. Degree of membership matrix has been summarized in table 8. Non-inferior solution can be deduced based on the degree of membership matrix through the max– min composition as follow. It can be concluded that Scenario 1 is the most preferable with the preference order being Scenarios 1, 2 and 3.

$$\mu_y = \max_j \min_i \{ \mu_{ij} \} = \max_{1 \leq j \leq 3} \min_{1 \leq i \leq 3} \begin{pmatrix} 0.42 & 0.33 & 0.50 \\ 0.50 & 0.70 & 0.30 \\ 0.58 & 0.51 & 0.72 \end{pmatrix} = \max_{1 \leq j \leq 3} (0.42 \quad 0.33 \quad 0.30) = 0.42 = \mu_{11}$$

In order to consider the objective priority, weighting coefficient has been set to $w = \{0.3, 0.5, 0.2\}$. So calculation is change as follow. As can be seen in this result,

Scenario 2 is the most preferable; the preference order now becomes Scenarios 2, 1 and 3.

$$\mu_{ij} = \max_j \min_i \{(\mu_{ij})^m\} = \max_{1 \leq j \leq 3} \min_{1 \leq i \leq 3} \begin{pmatrix} 0.77 & 0.72 & 0.81 \\ 0.71 & 0.84 & 0.55 \\ 0.90 & 0.87 & 0.94 \end{pmatrix} = \max_{1 \leq j \leq 3} (0.71 \quad 0.72 \quad 0.55) = 0.72 = \mu_{21}$$

Concession items	Scenario 1	Scenario 2	Scenario 3
IRR (%)	0.42	0.33	0.50
Tariff coefficient	0.5	0.70	0.30
Concession period (years)	0.58	0.51	0.72

5. **Conclusion:**

As it has been discussed in this paper, these studies infer that in order to manage well all risks and uncertainties, a model which considers them in dynamic environment manner is the best way. The results of studies in a global dynamic environment model are shown in figure 3. Other interesting issues in this context are the utilization of game theory and the consideration of the UK’s VFM toolkit, which are, however, beyond the scope of this paper.

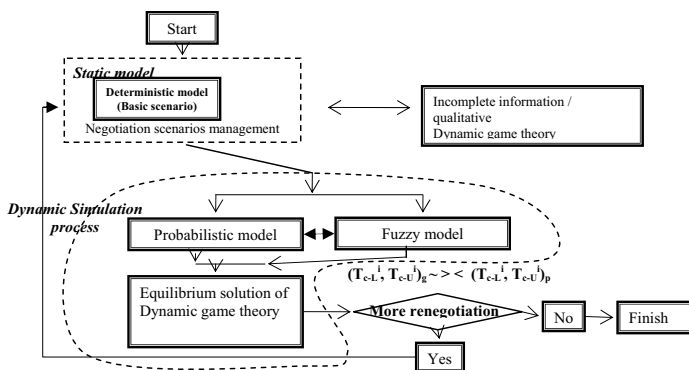


Figure 3: Global dynamic environment model- negotiation concession items

6. **References:**

1. Wang YD. *BOT trap. Global Entrepreneur*, 2002,2.
2. Meghdad Attarzadeh “Economic appraisal of BOT projects - financial risks management model” MSc. Thesis, Amirkabir University of Technology, 2007.
3. Ramin Dehdashtian “Critical success factors of BOT contracts in Iran” MSc. Thesis, Amirkabir University of Technology, 2007.
4. Zhang XQ, Kumaraswamy MM. “Hong Kong experience in managing BOT projects” J Constr Eng Manage ASCE 2001; 127(2):154-62.
5. Ye S D, Tiong R L K. “NPV-AT-RISK method in infrastructure project investment evaluation” J Constr Eng Manage ASCE 2000, 126(3): 227-233.
6. Yongjian et all. “Equitable financial evaluation method for Public-Private Partnership projects” Tsinghua Science and Technology 2008.
7. S.Thomas et al. “A simulation model for optimizing the concession period of public private partnerships schemes” Intern.J Proj. Manag.2007,25:791-798

Mixing good data with bad: how to do it and when you should not

J. Siegrist

Applied Biomathematics, 100 North Country Road, Setauket, NY 11733; PH (631) 751-4350; FAX (631) 751-3425; email: jacksie@eden.rutgers.edu

ABSTRACT

Is it a good idea to mix data that have been collected with painstaking attention to proper protocols and careful measurement using highly precise instruments with data that have been hastily collected by poorly paid, sloppy, and unmotivated people with bad instruments and shoddy protocols under uncontrolled conditions? Interval statistics is one convenient method that accounts for the different qualities of data in an analysis. High quality data have tighter intervals and poor quality data have wider intervals, and the two can be legitimately pooled using interval statistics. Thus, it is possible for an analyst to combine good data and bad, but is it advisable to do so? We provide illustrations that show that under some circumstances, including more data without regard for its quality decreases the amount of uncertainty in the output of an analysis. Ordinarily, statistical judgment would frown on throwing away any data, but as demonstrated by these examples, it seems clearly advantageous to ignore this judgment under certain situations. More data does not always lead to more power, and increasing the precision of measurements sometimes provides a more efficient return on research effort.

INTRODUCTION

Investigators are often concerned with whether it is wise to combine data of differing quality. Some data may have been collected with painstaking attention to proper protocols and careful measurement using high-resolution instrumentation, while other data may have been hastily collected by poorly paid, sloppy, and unmotivated people with bad instruments and shoddy protocols under uncontrolled conditions. Several questions arise with such a mixture of data in hand. Is it possible to pool good data and bad in a single analysis? Is it advisable to do so?

Conventional statistical practice recommends always including all data available for an analysis. Increasing sample size results in a better characterization of variability, which in turn decreases the amount of sampling error. A smaller amount of sampling error is beneficial because it allows one to make statistical inferences with a higher degree of certainty. In practice this reduced uncertainty takes the form of higher power for a statistical test.

There are, however, multiple kinds of uncertainty. Most fields recognize two primary kinds of uncertainty, one dealing with unavoidable variability due to stochasticity or randomness, which can be modeled using probability distributions, and one dealing with doubt due to imperfect or incomplete information, which can be modeled using intervals. For example, when weighing a single object many times,

each particular measurement may vary slightly from the last, due to random measurement errors, and the variation across measurements can be modeled as a probability distribution. Each single measurement, however, is subject to uncertainty because the scale has some minimum resolution. There is no way to assign a probability distribution to a single datum, so an interval must be used to model the uncertainty about the value of each measurement.

Various fields have independently recognized and named these two kinds of uncertainty, so that there is a confusing ambiguity in terminology among different disciplines, but one of the earliest and most familiar classifications is that of Knight (1921), who recognized *risk* as concerning variability and *true uncertainty* as concerning ignorance. Engineers commonly refer to these as *aleatory uncertainty* and *epistemic uncertainty* (Apostolakis 1999). Both of these cause *uncertainty* about particular outcomes, resulting in *ambiguous* decisions. In statistical inference, the amount of ambiguity in a decision is the same as the amount of power in a statistical test.

If there is more than one kind of uncertainty, then there is more than one way to reduce uncertainty in statistical inferences. Reducing sampling error by increasing sample size is only one means of increasing the power of a statistical test. Ultimately, any action, even preferentially withholding data from analysis, should be desirable and allowable if it decreases the uncertainty about the inference.

So should increasing sample size be an unqualified recommendation in statistical analysis? When the data available are a mixture of data sets of varying quality, this is not necessarily the case. Statistical analysis using measurements modeled as intervals provides one method to account for these two kinds of data. The good data have narrow intervals and the bad data have wide intervals. The data can be pooled using intervalized statistics (Ferson et al. 2007). Thus one *can* combine good data and bad using these methods.

But it is a different and deeper question to ask whether it is *advisable* to combine fairly precise data with rather imprecise data. Might not the imprecision in the latter dilute the informativeness of the former? Numerical experiments were performed in order to address this question.

METHODS

Simulations were performed that consisted of generating two small data sets, each with a different amount of imprecision around the individual measurement. The uncertainty about a statistic for the more precise data alone was then compared to the uncertainty about a statistic for the precise data pooled together with the imprecise data. This procedure was repeated for different amounts of imprecision in the bad data.

For each data set, 10 points, representing measurements, were randomly chosen from a normal distribution with a mean of 15 and a standard deviation of 2. For the good data, a negligible amount of uncertainty was added as an interval placed symmetrically around each point such that the precision of the measurements was ± 0.1 . This means that the true value of the measurand might be smaller than the reported value by as much as 0.1 or it might be larger than the reported value by as much as 0.1. For the bad data, the width of the interval placed symmetrically around

each point was multiplied by a constant imprecision factor for each set of simulations, with the imprecision factor varying from 1 time to up to 40 times wider among the sets of simulations.

For each collection of measurements the 95% confidence interval of the median was calculated by finding the critical values for the Kolmogorov-Smirnov test for goodness-of-fit for the observed median (Sokal and Rohlf 1969, p. 574). These critical values, D_α , can be computed as

$$D_\alpha = \sqrt{\frac{-\ln\left(\frac{1}{2}\alpha\right)}{2n}}$$

in which α is the specified significance level and n is the number of measurements made. The 95% confidence interval around the cumulative distribution can be determined by computing $F_i \pm D_{0.05}$ for the frequency, F_i , associated with each value or class, Y_i . These Kolmogorov-Smirnov bounds are illustrated for a single replicate at several different levels of imprecision in Figure 1.

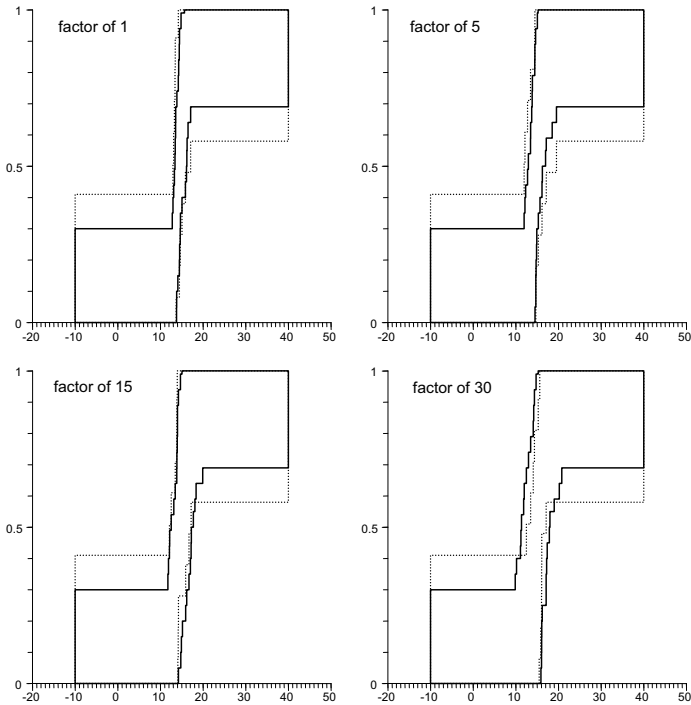


Figure 1. Kolmogorov-Smirnov 95% confidence intervals around the cumulative frequency distributions of measurements for one random simulation for different precision factors. The good and bad data combined is represented by the solid line and the partial data set, with only high-precision data, is represented by the dashed line. The precision factors are shown in the upper left corner of each plot and represent how many times more imprecise the imprecise data are than the precise data. The amount of imprecision is measured by the width of the intervals around the measurements.

For each imprecision factor the simulation was replicated 100 times. The number of simulation in which the interval around the median for the pooled data was smaller than the interval median for the good data alone was used as a measure of the desirability of increasing sample size by including the imprecise measurements.

RESULTS

When the imprecision in the bad data is *small*, for example only 5 times worse than it is for the good data, then pooling together the good and bad data is beneficial, tending to *decrease* the uncertainty about the median. In this case the median for the smaller but more precise data set contains the median for the pooled data set 96% of time. When the imprecision in the bad data is *large*, for example 30 times worse than it is for the good data, then pooling together the good and bad data is detrimental, tending to *increase* the uncertainty about the median. In this case the median for the smaller but more precise data set contains the median for the pooled data set only 13% of the time. The relationship between the percent of trials in which pooling is beneficial and how much more imprecise the bad data is than the good data (the precision factor) is illustrated in Figure 2. For this particular parameterization, a precision factor of about 20 results in approximately equal performance for both the pooling all data strategy and the ignoring the imprecise data strategy.

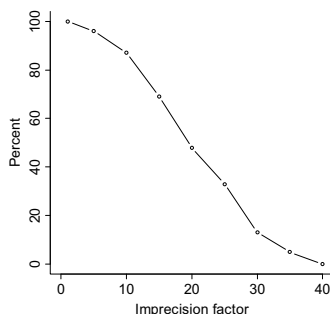


Figure 2. The percent of trials in which the full data set has less uncertainty about the median than the partial data decreases as the imprecision about some of the measurements increases. The less precise data have interval widths that are larger than the more precise data according to the imprecision factor. In the partial data set

the less precise measurements are excluded. For each imprecision factor 100 simulations were run.

CONCLUSIONS

Pooling imprecise data with precise data can be beneficial in that the overall uncertainty of the pooled data can be lower than that of either data set alone. As long as the more imprecise data are not too imprecise, having the large sample size helps more than it hurts. The more imprecise the bad data are, however, the more likely that the imprecision in the bad data will ruin the good data by making the uncertainty in the outcome larger than it would be for the good data alone. In this case it is beneficial and acceptable to ignore the imprecise data entirely.

Ordinarily, statistical judgment would frown on throwing away any data, but in the case of this example, it seems clearly advantageous under some circumstances to ignore this judgment. Moreover, it seems reasonable that there should be *no penalty* for doing so, because throwing away the more imprecise data does not constitute 'peeking' at the data in the Pearsonian sense. Different perspectives and different models of measurement imprecision could result in different decisions in particular situations about whether pooling or throwing away the bad data is better, but there are broad tradeoffs consistent across different perspectives.

This work assumes that both the good data and the bad data are sampled randomly from the same distribution. Alternatively, if the different data sets were measuring different parts of a distribution, and the amount of imprecision were related to the magnitude, then throwing away the bad data would not be appropriate because this action would decrease the representativeness of the data. Ignoring the bad data is only valid if the imprecision of the data has no relationship to the values of the data.

Neglecting measurement uncertainty is common in statistical practice. Most statistical analyses focus on sampling uncertainty, and power analyses used to inform guidance may consequently be unduly swayed by the increase in sample size. Conventional wisdom among statisticians holds that all data values are measured with error, so empiricists are counseled to hand over all of the data and let the statistical analysis sort things out. This results in project managers investing in more samples rather than more precise measurements, at least when those samples meet basic (but often rather loose) data quality standards. Quality assurance protocols generally contain particular criteria that are intended to exclude data that are likely to be biased, or to place data into classes of quality. For example, in a quality assurance project plan for the US Environmental Protection Agency, criteria were devised to place data into one of four categories: acceptable; unrestricted use; acceptable, use with caution; conditionally acceptable for limited uses; not acceptable. Data that meet these minimal criteria for acceptance are all admitted to the analysis as equal in quality. Data quality, however, varies continuously, and ideally the output of an analysis should depend on the varying quality of the data.

Intervals are, perhaps, the most natural form of representation for most measurements. Any measurement instrument has some resolution that limits the precision of the measurements made. The resolution of a ruler is determined by the density of tick marks, the resolution of a microscope by the properties of the light

used, the resolution of a monitoring program by how often observations are made, the resolution of a digital scale by the number of digits displayed. These limits to resolution make all measurements ultimately discrete. A plus or minus interval around a scalar measurement indicates that the true value could be anywhere within the given interval.

This work suggests that sometimes the better investment in terms of the benefiting the statistical inference to be made may be in increasing the precision of measurements.

ACKNOWLEDGEMENTS

This work was supported by a subaward to Applied Biomathematics from the National Science Foundation Division of Social and Economic Sciences award number 0756539 to PI Adam Finkel. The content is solely the responsibility of the authors and does not necessarily represent the official views of the National Science Foundation.

REFERENCES

- Apostolakis, G. (1999). The distinction between aleatory and epistemic uncertainties is important: An example from the inclusion of aging effects into probabilistic safety assessment. *Proceedings of the PSA '99*, August 22–25, 1999, American Nuclear Society, Washington D.C.
- Ferson, S., Kreinovich, V., Hajagos, J., Oberkampf, W., and Ginzburg, L. (2007). “Experimental uncertainty estimation and statistics for data having interval uncertainty.” Sandia National Laboratories Technical Report SAND2007-0939, Albuquerque, New Mexico.
(<http://prod.sandia.gov/techlib/access-control.cgi/2007/070939.pdf>)
- Knight, F. H. (1921). *Risk, Uncertainty, and Profit*. Hart, Schaffner, and Marx Prize Essays, no. 31, Houghton Mifflin, Boston and New York.
- Sokal, R. R. and Rohlf, F. J. (1969). *Biometry*, W. H. Freeman and Company, San Francisco.

Study on the Method Selection for Building Safety Risk Assessment in China

Mao Longquan¹, Huang Youliang², Chen Liang³, Yang Wu²

¹ Nanjing Municipal Commission of Housing and Urban-rural Development, No.185 Guangzhou Road, Nanjing, Jiangsu Province, 210000; email: mlq_2006@sina.com

² Project Management Research Institute, Civil Engineering College, Southeast University, Nanjing, Jiangsu Province, 210096; email: youliang_h@163.com

³ Nanjing Construction Quality Supervision Station, No.33 Yudao Street, Nanjing, Jiangsu Province, 210000; email: 13386555@163.com

ABSTRACT

A lot of uncertainties can be encountered in the process of building design, construction and use, and they tend to affect the safety of building in the building occupancy phase. The study was launched to select an appropriate risk assessment method which can be used to make a proper evaluation of uncertainties, and it would be better that the assessment of a building's safety risk is convenient and fast while the staff only use some simple inspection methods. The characteristics of risk factors were analyzed, and several risk assessment methods were compared. Finally, a suitable building safety risk assessment framework was put forward. However, the specific risk assessment approach requires further study, and more in-depth analysis should be made in selection principle of selecting the risk assessment methods.

Keywords: *Building; Safety risk; Selection principle; Assessment methods*

Building safety risk, which will affect the safety of building during the building occupancy phase, goes through the life cycle of building. These risks are formed in various stages of the project, and then accumulated to the building occupancy phase. Once they reach a certain level, accidents will happen. The safety of the building is related to people's lives and property. so the safety risk assessment throughout the whole lifetime of the building is necessary. Although, as a unique product, the building safety risk assessment is different from other areas, the risk assessment of building safety has its own characteristics. The risk assessment methods, which can be used in other common areas, are not applied to it. As a special product, buildings should have a comprehensive risk assessment process and methods.

1. Features of building safety risk Assessment

Building safety risk includes all risk factors covering the whole process of building from the design phase to the occupancy phase. To identify and assess these

risk factors systematically, it's necessary to study the characters of safety risk assessment of building. Generally speaking, the building safety risk has the following characteristics[1].

1) **Systematization**

There exist a number of risk factors in the building use phase. As for the time dimension, it covers risk factors from the building design phase to the building occupancy phase. As for the spatial dimension, it includes risk factors of all parts and various aspects. Thus, the risk evaluation of building safety should assure the systematization and integrity of risk factor identification.

2) **Complexity**

The complexity of building safety risk assessment is reflected into two aspects. On one hand, the building safety risks are composed of many factors, which cover people, materials, machinery management and environment, etc. Therefore, the risk evaluation of building safety process will take all risk factors of building safety risk factors into account. On the other hand, building safety risk assessment process is complex and requires that the status of the entity with the specification, the drawings and other technical data are compared and analyzed to evaluate risk factors. The process is professional and technical, and only specialized evaluators can be competent.

3) **Continuity**

The building formation process proceeds by stages, and building safety risk assessment should focus on different contents at different stages. Therefore, the building safety risk assessment also needs to be distributed in each appropriate point to continue. Assessment at each time point constitutes the building safety risk assessment information of the entire life, and assessment results at some point act as safety risk assessment factors which will be considered into the risk assessment of the next assessment time point.

4) **Fuzziness**

The safety risk assessment of buildings has been formed mainly for the evaluation of the established things. However, the causes leading to these risk factors are difficult to trace. And the evaluations of most risk factors are not quantifiable and can only use the fuzzy words to describe the status and level of risk factors. Therefore, the process of the evaluation of risk factors is inevitably full of ambiguity and subjectivity. Such ambiguity and subjectivity are bound to affect the selection of evaluation methods.

5) Low Probability

The event of low probability generally refers to the event whose occurrence possibility is less than 5%. While the fatal risk event of low probability refers to the event that the relative probability is small, but it can lead to heavy casualties and serious consequences. The risk accidents of building safety are the events of low probability. The low probability and uncertainty of those events result in attracting insufficient attention of its public. The research on risk assessment of low probability events is still in its infancy. Therefore, quantitative research is not easy. So, most of the risk assessment approaches are qualitative at this stage.

2. Comparison between several risk assessment methods

There are many methods which can be used to assess the risk, though the most widely used methods are fuzzy comprehensive evaluations, fault tree analysis, risk matrix analysis, analytic hierarchy process, and risk factor check list. The risk assessment methods are both qualitative assessment methods and quantitative risk assessment methods. There are not only simple risk assessment methods such as risk factors checklist, but also complex methods such as fault tree analysis. Different methods have different practical fields. The research staff analyzed the above methods from several aspects of the definition, application fields, advantages and shortcomings. A comparative analysis result is shown in Table 1.

Table 1. Comparative Analysis Result of Several Risk Assessment Method[2]

Assessment Method	Advantages	Shortcomings	Application Field
Fuzzy Comprehensive Evaluation	(1)Facilitating quantitative analysis on risk factors; (2)Evaluation results are more continuous; (3)The evaluation method is systemic, and the results are objective and comprehensive.	(1)A complex system of risk indicators is necessary; (2)Other methods should be used to establish the weight of risk factors; (3)The operability is weak because of doing multi-level fuzzy operations.	Economic, Machinery, Electronics, Chemicals, Metallurgy, Medicine.
Fault Tree Analysis	(1)Risk identification is comprehensive and systemic; (2)The method is intuitive, clear and logical	(1)It should be experienced and familiar with the system. (2)Large data of model lead to hard quantitative calculation (3)Actual operation also is not convenience.	Aerospace, Nuclear Engineering, Military, Chemical, Mechanical, Economic..
Risk Matrix Analysis	(1)Determination of risk level is intuitive. (2)Research and application are mature.	(1)It is hard to obtain the level of risk loss and the level of risk probability; (2)To determine the allowable upper and lower risks result in hard operation.	Economic, Chemical, Civil engineering

<p>Analytic Hierarchy Process</p>	<p>(1)It is convenience to consider the various criteria that make the assessment process more realistic, comprehensive and reasonable; (2)Clearly, quantitative identification of risk factors by decision-makers is the foundation of multi-criteria decision.</p>	<p>(1)A complex system of risk indicators is necessary; (2)To calculate the weight of risk factors requires extensive survey and the calculation process of complex. (3)It is more suitable for comparative analysis on risk possibility of single factors but not for assessing the level of system-oriented risk,</p>	<p>Economics, Management, Chemicals, Machinery and Environmental engineering.</p>
<p>Risk Factors Checklist</p>	<p>(1)It has sufficient time to organize experienced personnel to prepare and make it more systemic and complete. (2)According to the required standards, norms and regulations, implementation will be checked and accurate evaluation can be proposed. (3)A wide range of applications, different checking objects with different checklists. (4)It is easy to grasp, so the lack of knowledge and experience of staff is made up for to some extent.</p>	<p>(1)It only can do qualitative evaluation but not quantitative evaluation. (2)Evaluation objects should already exist. (3)A lot of checklists should be pre-prepared for different needs. It is heavy workload and the quality of checklist is limited by the staff's level of knowledge and experience.</p>	<p>Chemical, Mechanical, Nuclear power</p>

3. Determination of Building Security risk Assessment Methods

Building safety risk assessment method should include two aspects, namely, identification methods of risk factors and assessment methods of the risk level. Taking the characteristics of building safety risks into account, it could be found that there are many obstacles and difficulties in risk assessment if common methods are directly used. So, we propose to identify risk factors with the method of Fault Tree Analysis, and then use these factors to develop a risk-factor checklist. When the risk checklist is fixed, two scoring methods are considered, and a new systematic method is proposed for building safety risk assessment, which is called "weighted scoring method with negative item".

1) Risk level assessment standard

Learning from China's current standards, such as "Civil Standard of Reliability Evaluation" (GB50292 – 1999) [3] and "Dangerous Building Appraisal Standards" (CJ13-86) [4], the research staff classified the building safety status into four categories by A, B, C, D, which are corresponding to safe, generally safe, local unsafe, serious unsafe (see Table 2). Also, risk factors are described to four levels by a, b, c, d (see Table 3).

Table 2. Description of Building Safety Level

Grade	Safety	Conclusion Corresponding to the Status
A	safe	Normal use, there was no evidence of potential risks in building safety
B	generally safe	Normal use, while there exist some minor potential risks, and the repair or reinforcement should be taken on deadline
C	local unsafe	Suspended, there exist important potential risks, and only the repair or reinforcement is approved by the relevant administrative authority, it could be continue to use.
D	seriously unsafe	Stop using, there are significant potential risks, the mandatory building appraisal procedures must be started up.

Table 3. Level Description of Risk Factors

Grade	Feature Description
a	Does not affect the safety of the house
b	Does not affect the building safety on the whole, there may be a few unsafe factors that require control.
c	Significant impact on building safety, some appropriate measures should be taken to deal with the unsafe factors
d	Serious impact on building safety, and measures must be taken immediately

It's obvious to know that not all the various risk factors are equal in practical engineering. Some risk factors, once it occur, will affect the safety of the whole building; while some risk factors only affect the local building safety, instead of threatening the entire building. Therefore, researchers identified the general factors into four levels of grade a, b, c, and d. for those key risk factors, they are divided into four grades of a, b, c, d. The classification of risk factors will directly affect the assessment conclusion, and the specific impact mechanism will be further introduced in the follow article.

2) The establishment of risk-factor checklist

In order to find out various systematic risk factors which affect building safety, I think the Fault Tree Analysis method should be selected to identify risk factors. And the risk factors should be identified separately in different assessment entities and different building types. In view of the risk factors which have been indentified, the Delphi method was used in the screening important factors, in reference to relevant laws, regulations and standards, the risk-factor checklist has been drawn up. The content of checklist is as follows[5]:

(1) Check section means the classification of risk factors. Generally, multi-factors may exist in one part of the building, in order to prevent misdiagnosis of risk factors in the process of detection. The risk factors of the same classification is grouped together for the integrity of the risk assessment.

(2) The score column reflect the final findings of the evaluation personnel. If an entity assessment lacks a risk factor which is not suitable for the item, then these risk factors should be eliminated from the entire risk assessment.

(3) The division of assessment grade is the standard which should be followed in the risk assessment for assessing manpower. The division rests on various standards and regulations currently in effect.

(4) Negative items refer to some very important factors existing in the risk factors which have been identified. When these risk factors happen, the evaluator can judge the risk level of the building directly. Some key risk factors are chosen by researchers, and their risk level is divided as “c” negative level and “d” negative level.

3) The implementation of risk assessment

Entering the spot, evaluating the management institution should first confirm the building types and the stage situated currently, and draw up the appropriate risk-factor checklist. The evaluation personnel identify the potential safety risks of the building in accordance with the risk -factor testing form, through eye survey, instruments, measurement and other techniques, then judge the level of risk factors. In the process of risk assessment, evaluation personnel should make right judgment rest on own experience and refer to following documentation. Different risk factors should refer to different documentations. Taken together, these documentations contain:

- ① Drawings;
- ② Engineering geological investigation documentations;
- ③ Eelevant national laws, administrative regulations, and rules;
- ④ Engineering design organization for the construction;
- ⑤ worksite data, which include materials, approach inspection documents, materials reinsert report, the test report, quality inspection documents;
- ⑥ Previous risk assessment report of the building, and relevant risk prevention.

4) Determination of the level of risk assessment

In the light of the assessment results of risk-factor checklist, researchers gave a corresponding value to the level of a, b, c, d, and then we would reach assessment conclusion of the building safety risk level.

Researchers assigned the corresponding value W_a, W_b, W_c, W_d to the level of a, b, c, d, and $W_a = 4, W_b = 3, W_c = 2, W_d = 1$. The number of occurrences of each level is counted as K_a, K_b, K_c, K_d . So, a total scoring of one routine assessment time point could be obtained, it was:

$$S = W_a \cdot K_a + W_b \cdot K_b + W_c \cdot K_c + W_d \cdot K_d \quad (1)$$

And the effective scoring was:

$$F = S/N = \frac{W_a \cdot K_a + W_b \cdot K_b + W_c \cdot K_c + W_d \cdot K_d}{K_a + K_b + K_c + K_d} \quad (2)$$

Corresponding to the value of four levels of a, b, c, d, four subsection intervals are defined for the four assessment grades of A, B, C, D.

Grade A: $F \in [3.5, 4.5]$; Grade B: $F \in [2.5, 3.5]$

Grade C: $F \in [1.5, 2.5]$; Grade D: $F \in [1, 1.5]$

Then the grade of risk assessment can be determined by the interval where the F belongs to. However, there are some flaws in the above calculation of the risk assessment grade.

(1) It's too rigid that the dividing value of the subsection intervals between grade A, B, C, D, such as $F = 2.49$, it should be judged to grade C as described above, while if $F = 2.5$, the assessment conclusion will be grade B. Obviously, the above two results of safety rating appear very disparate, while the actual risk condition is not so disparate as the result appears.

(2) The risk assessment result is a weighted average score, the score may not truly reflect the level of safety. For instance, one result contains a lot of "a" and "c", while there is a small quantity of "b" and not "d", in an assessment. For example:

$$F = S/N = \frac{W_a \cdot K_a + W_b \cdot K_b + W_c \cdot K_c + W_d \cdot K_d}{K_a + K_b + K_c + K_d} = \frac{4 \times 6 + 3 \times 1 + 2 \times 3 + 0}{6 + 1 + 3} = 3.3 \in [2.5, 3.5]$$

According to the above method, the results can be judged as grade B. It's clear that the result is not consistent in the actual level of the building safety. The high scores are simply attributed to the fact that the result contains more "a".

In response to these shortcomings, the research staff made appropriate improvements. The summary is as follows.

(1) Set crucial risk factors as negative items. Negative items are divided into level "c" and level "d". If the risk element is commented level "d", the conclusion of the risk evaluation is D. As the same, on the premise of the absence of risk element of

level “d”, if the risk element is commended level “c”, the conclusion of the risk evaluation is C.

(2) If negative items are not effective, the risk level is defined with the score of risk evaluation, which is calculated by steps mentioned above. Meanwhile, the percentage of level c should be checked, if the Kc is more than 20%, the level should be degraded one level.

(3) If the score of risk assessment is at the interval of ± 0.05 of the critical value of risk classification, the final risk classification will be judged with the actual risk status of the construction by the risk evaluator. If the risk evaluator considers it affirmative, the higher level above the critical value of the classification interval is chosen; otherwise, the lower level is chosen. For example, the critical value $F=2.5$, which is the cutoff level between grade B and C. If the risk assessor considers the building safety status affirmative, B is chosen finally; on the contrary, C is chosen.

The above points are the improvements that aim to the method of weighted scoring risk- factor checklist method, and we call it "weighted scoring method with negative item".

4. Framework of risk assessment procedures for large public building safety in China

Large-scale public buildings are often the symbol of local economy and culture, and so their safety risks attract the attention of people particularly. The pace of construction of large-scale public buildings is at an alarming rate in China. Moreover, the holding of 2008 Beijing Olympic Games and 2010 Shanghai World Expo carried the construction of large public buildings in chain forward into a booming stage. In this context, commissioned by the Ministry of Construction, the study group composed of Project Management Institute of Southeast University and Institute of Quality Supervision Station of Construction and Installation of Nanjing studied "large-scale public building risk assessment system". With the above idea, we built the procedures of large public building safety evaluation. The main framework includes the followings.

1) Identification of safety risk factors for China's large-scale public buildings

The identification of safety risk factors of large-scale public buildings should departure from each of the possible loss of risk, find out the entire risk event, and then try out all possible risk factors and make a list of them. Researchers need to analyze a large number of accident cases to extract reasonable risk factors. Figure 1 shows the identification process of large public building safety risk factor.

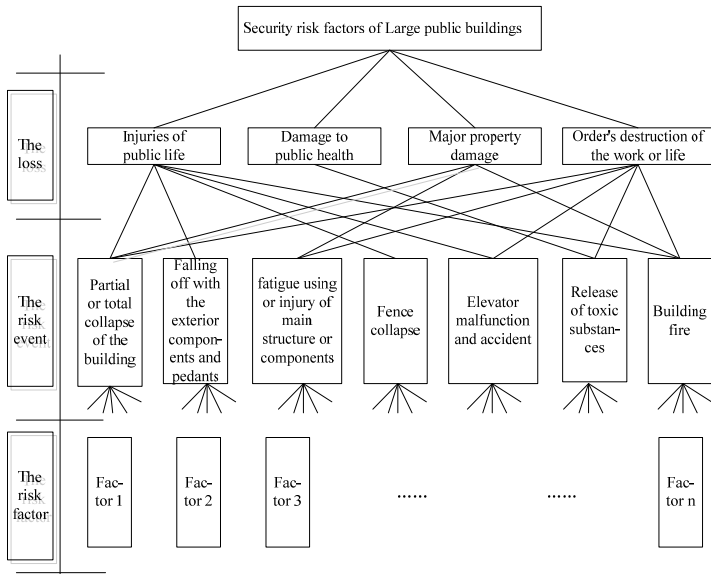


Figure 1. The structure of risk identification of large public buildings

2) The establishment of risk-factor checklist of large-scale public buildings

Take the assessment point of the completion of foundation as an example, in accordance with the above process of identification, the risk-factor checklist can be established as it is shown in Table 4.

Table4. The example of the risk-factor checklist

Check section	Risk factors	scoring				Unsuitable	Division standard of assessment level	Negative level
		a	b	c	d			
Foundation [6]	Uneven settlement of foundation						<ul style="list-style-type: none"> ● a: No obvious settlement; ● b: The settlement is within a reasonable area; ● c: The settlement exceeds the reasonable area to a small extent; ● d: The settlement seriously exceeds the reasonable area. 	d
.....						<ul style="list-style-type: none"> ● 	

3) The implementation of risk assessment of large public buildings

The on-site risk assessment can be carried out after the establishment of risk-factor checklist. In accordance with various basis data on the time point of risk assessment, the risk assessment personnel can get the risk level through some simple

tools' measurement. Take an implementation process of a risk assessment as an example, and the part of the assessment results was shown in Table 5.

Table 5. The example of a risk assessment result

Check Section	Risk Factors	Scoring					Division Standard of Assessment Level	Negative Level
		a	b	c	d	Unsuitable		
Foundation	Uneven settlement of foundation			✓			<ul style="list-style-type: none"> ● a: No obvious settlement; ● b: The settlement is within a reasonable area; ● c: The settlement exceeds the reasonable area to a small extent; ● d: The settlement seriously exceeds the reasonable area. 	d
Foundation beam	Normative of reinforcement layout in foundation beam		✓				<ul style="list-style-type: none"> ● a: Foundation beam reinforcement meets relevant standards and in line with design specifications; ● b: The layout of foundation beam reinforcement meets the requirements, but there is little error; ● c: The layout of foundation beam reinforcement does not comply with relevant standards, specifications and design diagrams 	c
.....						<ul style="list-style-type: none"> ● 	

4) The determination of risk assessment level of large public buildings

The appropriate level of risk assessment result could be obtained after the management of the on-site inspection data. The level's determination of risk assessment should go through the following steps:

(1) Check negative items and see whether it takes effect. If it goes into effect, the grade of risk can be determined directly, otherwise, go to the next step;

(2) According to the results of risk-factor level, scoring the grade of risk assessment;

(3) If the score of risk assessment is in the field of ± 0.05 of the critical value of risk classification, the grade of the risk assessment can be given in accordance with the method introduced above;

(4) The percentage of level c should be checked, if the K_c is more than 20%, the level should be degraded one level. Otherwise, the calculating result will go into effect.

5) The risk assessment conclusion of large public buildings

The corresponding potential risks can be found based on the risk assessment result, and then the management measures should be developed and carried out.

5. Conclusion

The development status of China's large-scale public buildings was considered, and the framework for risk assessment procedures was proposed through the study of building safety risk. The methodology system is composed of methods of identification and assessment. So, fault tree analysis was used to identify risks, and the checklist method is proposed to assess the safety risk of large public buildings. However, due to the lack of empirical data, the assessment approach of China's large-scale public buildings is qualitative in most of the time. The authors consider that a number of quantitative risk assessment methods, which can make the risk assessment results more convincing, will be incorporated into the existing building assessment method framework in the future study.

REFERENCES

- Kou Liping. (2008). "Study on risk assessment theory and standardization method of assembly occupancies". *A dissertation submitted to China University of Geosciences for doctor degree*, section 4.2, Beijing.
- Zhang Nailu. (2007). "*Security Assessment Technology*", Xi'an University of Electronic Technology Press, Xi'an, 124-130.
- China Bureau of Quality and Technical Supervision & Ministry of Construction of People's Republic of China. (1999). "*Civil Standard of Reliability Evaluation*" (GB50292 - 1999) , Beijing.
- Wang Hongde. (2008). "*Management Practices of Security Evaluation*", China Water Conservancy Press, Beijing, 105-108.
- China Bureau of Quality and Technical Supervision & Ministry of Construction of the P.R of China. (1999). "*Code for acceptance of construction quality of building foundation*"(GB5002-2002), section 5.0.Beijing.
- China Bureau of Quality and Technical Supervision & Ministry of Construction of the P.R of China. (1999). "*Code for acceptance of constructional quality of concretes structures*"(GB5004-2002), section 5.0.Beijing.

Decision-Making Model for Offshore Offloading Operations Based on Probabilistic Risk Assessment

C. E. Patiño Rodríguez^{1,2} and G. F. M. Souza²

¹Department of Industrial Engineering, Engineering College, University of Antioquia, Calle 67 # 53 – 108, Medellín, Colombia; email: cpatino@udea.edu.co

²Department of Mechatronics and Mechanical System, Polytechnic School, University of São Paulo, Av. Prof. Mello Moraes, 2231, Cidade Universitária, São Paulo, Brasil; email: gfmsoza@usp.br

ABSTRACT

This paper presents a risk-based analysis method aiming at defining the risk profile associated with an offloading operation. For offloading operations the risk profile is usually evaluated considering that the environmental condition will not suffer considerable changes during offloading that has an approximate duration of 24 hours, varying based on the tanker size. The method follows four basic steps: Accident Modeling, Failure probability assessment with Bayesian techniques, Evaluation of consequences, and Markovian process to aid decision making. The method is applied to evaluate the risk profile of an offloading operation in Campos Basin, Brazil. The method is used to model the risk scenario associated with shuttle tanker main engine failure as initiating event. The changes in environmental conditions have great influence in risk profile and increase the probability of disconnection.

INTRODUCTION

The occurrence of accidents in complex systems, such as offshore and onshore oil and gas processing plants, are financially expensive because the accidents can cease plant operations and even can cause harm to people, property and environment. The identification of vulnerable factors that cause unacceptable operating scenarios is a challenge in the risk assessment of complex systems. The risk assessment seeks to minimize undesirable events probability and their impact both on the environment and on the people involved in the operations measured as economic consequences.

The current method for crude oil export in deepwater is through the use of FPSO (Floating Production Storage and Offloading). This trend is being repeated globally, not only in the waters of Brazil, but also in West Africa and in various locations in Asia (Huijer 2005). The offshore operations in Brazil represent more than 75% of oil exploration operations and the shuttle tankers have become the main way to distribute the crude oil produced offshore (Reis, 2004).

The tandem offloading operation is a complex and difficult marine operation. FPSO may weathervane (rotate according to the weather) around its turret and may also have significant low frequency motions in the horizontal plane (surge, sway and yaw) due to waves and wind actions. In order to stay connected for loading and at the same time maintain a safe separation distance, shuttle tanker has to position itself aligned with the FPSO position (Roed, et al 2009).

The incidents in maritime operations often involve the analysis of low-probability events for which few data are available and the quantification of risk requires the quantification of the likelihood of rare accidental events, which normally cannot be done without employing expert judgment. Bayesian techniques are useful because of their ability to deal with sparse data and to incorporate a wide variety of information gained based on expert judgment, (Aven and Kvaloy 2002).

This paper, aiming at providing safety for offloading operations in deepwater oil fields, considering both FPSO and shuttle as one integrated system, presents the application of risk-based analysis techniques to evaluate offloading operations between a FPSO and a shuttle tanker that could be used to develop actions and procedures to minimize the consequences of an accident for the operation. Applying a quantitative risk analysis based on Bayesian techniques, the relation between the probability of occurrence of each hazardous event and its consequence could be found.

DYNAMIC RISK ASSESSMENT METHODOLOGY

Risk can be represented by the Eq. (1) which relates the undesired event’s occurrence probability and the consequences.

$$Risk = (p_i, c_i) \tag{1}$$

where p_i is the i^{th} event occurrence probability, and c_i is the effect of the i^{th} event occurrence.

For complex systems, the possibility that an unexpected scenario shows up is related to an initial event or failure which happens in a specific component. For each one of the system or subsystems’ components it is necessary to know the probabilities that the unexpected condition (failure) shows up and its consequences and states must be evaluated. In this context, another important decision making aspect in complex systems is the need for creating a model which can consider dynamic characteristics of system. In the case under analysis these characteristics are given by the transition between states corresponding to safety operating zones. The method is based on probability risk assessment and Markovian process to aid decision making (see Figure 1). To calculate the probability of accident scenario, the Bayesian approach is used, and to estimate the probabilities that the system is in a given state stochastic models are applied. The methodology can be summarized in three steps: Accident Modeling, Failure probability assessment with Bayesian techniques, Evaluation of consequences with Markovian process to aid decision making.

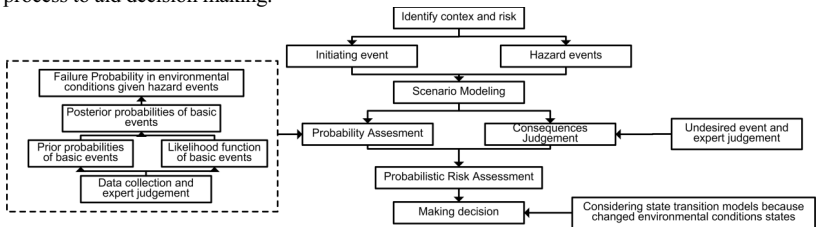


Figure 1. Probabilistic risk assessment methodology

Accident Modeling

The first step identifies the objective of the risk assessment and selects the undesirable consequences of interest. These consequences may include items like degrees of harm to environment or degrees of loss of operation performance.

To determine the hazard events “brainstorming” technique is used involving experienced personnel on the procedures used for the practice of routine operations. A question-answer technique based on PHA (Preliminary Hazard Analysis) concepts is used. The accident modeling is finished with scenario modeling based on the use of the event tree.

An event tree is used to identify the various paths that the system could take, starting with the initiating event and studying the failure progress as a series of successes or failures of intermediate events called hazard events, until an end state is reached. The sequence of events is named failure scenario for which the consequences are estimated.

Failure probability assessment

In this step the probability of occurrence of a failure scenario is calculated combining two conventional reliability analysis methods: Fault Tree Analysis (FTA) and Event Tree. The probability of each failure scenario is determined by summing the probability of each set of events which lead to this particular outcome. Each sequence probability is obtained by simply multiplying the probabilities of the events represented in a given branch of the event tree in case of independence case if there is dependence between events the Bayesian methods are used. The probabilities of the hazard event are obtained by solution of fault trees associated with each hazard event.

Bayesian Ideas and Data Analysis

The Bayesian techniques are appropriate for use in offshore offloading operations analysis because the Bayesian statistical analysis involves the explicit use of subjective information provided by the expert judgment, since initial uncertainty about unknown parameters of failure distribution of basic events must be modeled from a priori expert opinion or based on insufficient data and evidence collected.

The Bayesian method starts identifying the parameter to be estimated. This involves the consideration of the form of the likelihood function appropriate to the evidence that will be collected. The second step is development of prior probabilities to describe the system current state of knowledge. Next step incorporates information through the collection of evidence and construction of the likelihood function selected in the stage one. The final step results in new probabilities using Bayes’ theorem, called posterior distribution, to describe your state of knowledge after combining the prior probabilities with the evidence (Singpurwalla 2006). Using Bayes’ Theorem in its continuous form, the prior probability distribution of a continuous unknown quantity, $P_0(x)$ can be update to incorporate new evidence E, as shown in Eq. 2.

$$P(x|E) = \frac{L(E|x) \cdot P_0(x)}{\int L(E|x) \cdot P_0(x) \cdot dx} \quad (2)$$

where $P(x|E)$ is the posterior probability distribution of the unknown quantity x given evidence E, and $L(E|x)$ is the likelihood function (Lindley 1965).

Evaluation of consequences and making decision

In reliability and risk analysis, the transition rates correspond to hazard rate between two operational states. In this case the probability of changes during offloading operation that could cause changes in the risk profile is modeled as Semi-Markov Process to allow for non-exponential distributions for sojourns times. The Semi-Markov process shows the probability that the position of shuttle tanker will change from operational zone to alert zone in a given environmental condition. That change affects the decision of continuing the offloading operation. The decision-making theory can further be used to evaluate the need for disconnection in case of occurrence of an environmental change coupled to a critical component failure in the shuttle tanker. Consequences of hazardous events or abnormal incidents on the shuttle tanker and offloading operation are described and explained. The classifications for major and catastrophic events are presented in Table 1.

Table 1. Relative severity criteria for hazardous events classification (Patino Rodriguez, et al. 2009)

Description	Set		
	Personal	Facilities	Environment
Major III	Serious harm to people in installation and/or outside	Major damage of the installation, with possible repair	Contamination of environment below maximum concentration
Catastro- phic IV	Single fatality or multiple severe harm to people inside and outside of installation	Damage or degradation without possible repair or repair take a long time to do	Contamination of environment above maximum concentration

Hence, let *ST* be a variable that represents a state of system, and let *K* to be a scenario. The probability that *K* be true given the system is in the state *ST* can be represented by Eq. (3).

$$P(K|ST) = \frac{P(ST|K) \cdot P(K)}{P(ST)} \tag{3}$$

where *P(ST|K)* is the probability that the system was in the *ST* state given a scenario *K*, *P(K)* is the probability that a scenario *K* be true, and *P(ST)* is the probability that the system is in the state *ST*.

APPLICATION OF THE METHODOLOGY

The method is applied on the analysis of the offloading operation considering a shuttle tanker with dynamic positioning systems (DP).

From the point of view of the shuttle tanker, tandem offloading operation can in principle be summarized into the following five operational stages (Patino-Rodriguez, et al. 2009): 1. Approach: tanker approaches FPSO and stops at a pre-defined distance; 2. Connection: messenger line, hawser and loading hose are connected and the tug boat is connected to the tanker stern; 3. Loading: oil is transferred from FPSO to tanker; 4. Disconnection: manifold is flushed, and loading hose and hawser are disconnected; and 5. Departure: tanker reverses away from FPSO while sending back hawser messenger line, and finally sails away from oil field, (MCGA 2005).

Patino Rodriguez et al. (2009) found 56 hazardous events for shuttle tanker. The connection stage is the phase with the highest number of hazardous event. In fact this stage involves more activities associated with mooring hawser and hose connection, beside the smallest distance between shuttle tanker and FPSO. Most of the events

characterized as catastrophic are related to Dynamic Positioning System (DPS) failures. The initiating event selected as for risk assessment is “(DPS) Failure”. The considered accident sequence is shown in Figure 2 modeled as an accident progression of four hazard events: 1) Auxiliary Engine Failure, 2) Main Engine Failure, 3) Tug Failure and 4) Towing Cable Failure.

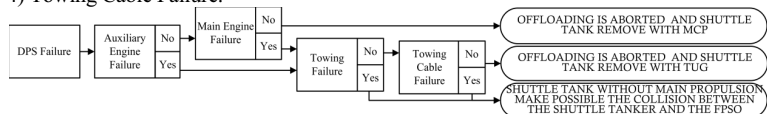


Figure 2. Event Sequence Diagram of the accident progression for offloading operation

The fault tree for the four hazard event that appears in the event tree was developed. For all basic events of the fault trees the parameter to be estimated is failure rate, and the Poisson distribution is selected as likelihood function. Analyzing the type and source of information (expert judgment and literature data) as well as the nature of the time to failure that is the random variable of interest, Gamma distribution is selected as appropriate “Prior Distribution” (Siu and Kelly 1998). The Bayesian model for estimating failure rates is applicable under the assumption of homogeneous empirical data and also that the expert judgments are used to construct the prior distribution. Using Bayes’s theorem (Eq. 2) the posteriori distribution is obtained:

$$P(\lambda|E) = \frac{\left[\frac{(\lambda-t)^r}{r!} \cdot e^{-\lambda t} \right] \cdot \left[\frac{\beta^\alpha \cdot \lambda^{\alpha-1}}{\Gamma(\alpha)} \cdot e^{-\beta \cdot \lambda} \right]}{\int_0^\infty \left[\frac{(\lambda-t)^r}{r!} \cdot e^{-\lambda t} \right] \cdot \left[\frac{\beta^\alpha \cdot \lambda^{\alpha-1}}{\Gamma(\alpha)} \cdot e^{-\beta \cdot \lambda} \right] \cdot d\lambda} \cong \left[\frac{(\beta+t)^{\alpha+r} \cdot \lambda^{\alpha+r-1}}{\Gamma(\alpha+r)} \right] \cdot e^{-(\beta+t) \cdot \lambda} \quad (4)$$

As an example the posterior distribution is calculate for fuel system failure (see Fault Tree in Figure 3) one of the components of main engine. The posterior mean value of failure rate is calculated by substituting in Eq. (4) the mean failure rates measured in failure/hours for fuel system failure $E[P_0(\lambda)]$ and standard deviation $S[P_0(\lambda)]$ measured in failure/hours (see Table 2). To do this, we use data obtained form database (Lee 1996) and (OREDA 2002) because of the difficulty to obtain operation history reports from FPSO and shuttle tanker. In the future these data may be enriched with the opinion of experts.

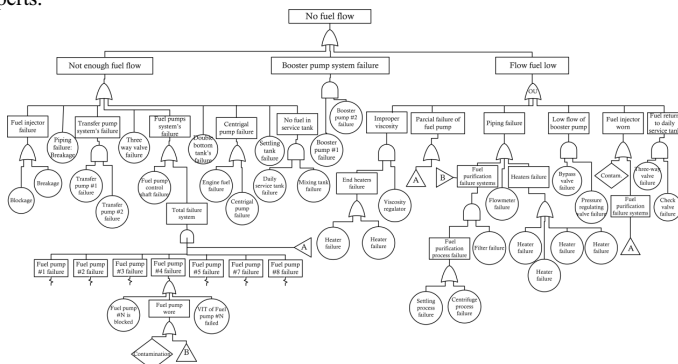


Figure 3. Fault Tree for fuel system failure

Using probability theory and assuming that the fuel system is operated for $t=43800$ h (time between maintenance), the probability of “No fuel flow” is $8.390E-04$.

Table 2. Failure rates and standard deviations of some basic events.

Equipment	$E[P_0(\lambda)]$	$S[P_0(\lambda)]$	$P(\lambda E)$	Equipment	$E[P_0(\lambda)]$	$S[P_0(\lambda)]$	$P(\lambda E)$
Cent. pump	7.36E-04	1.20E-04	3.95E-04	Motor cent. pump	1.13E-04	2.81E-05	8.62E-05
Main tank	2.13E-04	2.13E-04	2.06E-05	Daily tank	9.50E-06	9.11E-06	6.87E-06
Fuel Pumps	1.43E-03	1.13E-03	3.55E-05	Control shaft	3.00E-05	3.00E-05	1.30E-05

The prior and posterior densities of basic event that have more influence on system failure are shown in Figure 4, associated with the failure of the centrifugal pump.

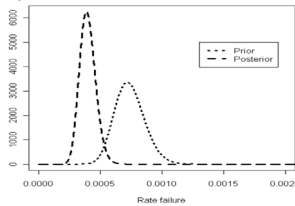


Figure 4. The prior density and posterior density for centrifugal pump failure

The same procedure is used for other subsystems and the probability of hazard event “main engine failure” is found by solving the fault tree associated with that failure. In the same way that procedure is applied to find the failure rates of all hazard events as shown in Table 3.

Table 3. Posterior probabilities for hazard events involve of the offloading operation and a 90% interval estimate for rate failure

Hazard Event	$P(\lambda E)$ [failure/h]	90% interval estimate for rate failure	
		5%	95%
DPSFailure	1.58E-05	3.18E-07	5.29E-05
Auxiliary Engine Failure	1.97E-04	1.01E-04	3.18E-04
Main Engine	4.95E-05	9.70E-06	1.14E-04
Tug Failure	2.28E-05	1.17E-06	6.82E-05
Towing Cable Failure	2.18E-03	0.001837	0.002555

Figure 5 gives a further description of the risks and the probability of each consequence category (scenario K) is calculated by adding the probabilities of the branches that ends with the same consequence category.

The failure scenarios presented in Figure 5 can occur at any time during offloading operation. It is essential to consider the probability of the change of the shuttle tanker position from operational zone to alert zone, as shown Figure 6, during offloading.

The Semi-Markov process shows the probability that the position of shuttle tanker will change from operational zone to alert zone in a given environmental condition. Thus, the random variable which is modeled as Weibull distribution corresponds to the angle ϕ angle between FPSO and shuttle tanker at time t . In this case, the two states are: operational zone and alert zone.

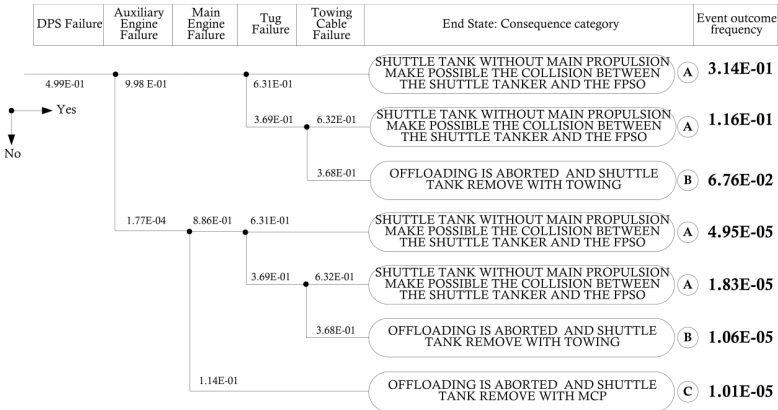


Figure 5. Event tree for the offloading operation

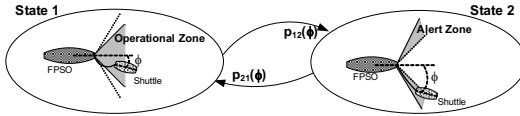


Figure 6. Markov state transition diagram

The transitions between states (λ_{ij}) are characterized by transition probability matrix M , shown in Eq. (5).

$$\lambda_{ij}(\phi)d\phi = pr \left\{ \begin{array}{l} S_n - S_{n-1} \in (\phi, \phi + d\phi) \cap Z(S_n) = j \\ Z(\phi_{n-1}) = i \cap S_n - S_{n-1} > \phi \end{array} \right\} \Rightarrow$$

$$M = \begin{bmatrix} (1 - \lambda_{12}(\phi))d\phi & \lambda_{21}(\phi)d\phi \\ \lambda_{12}(\phi)d\phi & (1 - \lambda_{21}(\phi))d\phi \end{bmatrix} \quad (5)$$

Where S_n is the time of next transition and S_{n-1} is the time of last transition with respect to ϕ . Z is the state at angle ϕ . Therefore, it is the probability, that the process will transfer to state j in an infinitesimal time interval $(\phi, \phi+d\phi)$, given that it is in state i at time t .

The angle ϕ is estimated via de Numerical Offshore Tank (NOT) simulator which is an advanced offshore system simulator. The simulator reproduces ship motion in the presence of waves, wind and currents. For the present study the current speed is 0.71 m/s (South), the wave height is 2.9 m and period 5.91 s and the wind speed is 11.16 m/s (Southeast). According to the standards of the offloading operation in Brazil this angle within the operational zone should not be greater than 45 degrees. The parameters and transition rate equation are shown in Table 4.

Using a recurrent algorithm, the probability ($P(ST)$) that the shuttle tanker is inside the operational zone, without any failure, is 0.7918. In the same way, inducing the hazard events in ship dynamics simulator it is possible to determine the probability that the system is in the ST state given a scenario K as shown in Table 5.

Table 4. Parameters and transition rate for offloading operation

State	Parameters weibull distribution				Transition rate equation
	Consequences category				
	0	C	B	A	
Inside the operational zone	$\beta=1.6; \eta=12.9$	$\beta=1.6; \eta=13.1$	$\beta=1.5; \eta=12.0$	$\beta=1.7; \eta=14.3$	$\frac{\beta}{\eta} \left(\frac{\phi_k}{\eta} \right)^{\beta-1}$
Outside the operational zone	$\beta=10.9; \eta=30.1$	$\beta=8.6; \eta=60.5$	$\beta=8.5; \eta=60.4$	$\beta=7.3; \eta=63.2$	

Table 5. Probabilities in that the tanker is inside a given location each

State	Consequences category			
	P(ST)	P(K=C)	P(K=B)	P(K=A)
Inside the operational zone	0.7918	0.19546	0.039312	0.03528
Outside the operational zone	0.2082	0.80454	0.96069	0.96472

Applying Eq. (2) the probability that a scenario K is true given the system is in the state ST is obtained. For instance, the probability that shuttle tanker is without main propulsion, making possible the collision between the shuttle tanker and the FPSO, given that shuttle tanker is in the inside the operational zone is:

$$P(K = C | ST = 1) = \frac{(0.1954) \cdot (0.43)}{0.7918} = 0.1059$$

CONCLUSION

The tandem offloading operation is a complex and difficult marine operation. The duration of the operation takes about 24 hours based on FPSO storage capacity and oil transfer rate. Shuttle tanker loss of position in powered condition and subsequently collision with FPSO is the most significant risk.

The proposed method for risk assessment seems to be suitable for complex systems analysis since it allows not only the identification of critical consequences but also is a tool to make decision because it allows a quantitative evaluation of accident progression in systems that change their operational condition during the time. The development of the fault tree and even tree is important for the understanding of the functional relation between system components and the relationship with accident progression. Based on the modeling of each accident scenario, the Bayesian analysis is performed considering the evidence of database and knowledge of offloading operation.

For the case under analysis, which considered that the position between FPSO and shuttle tanker during offloading operation can be defined by two operational states, the probability that a failure scenario is true given the system is in a specific operational state is obtained. Both states have the distribution of positions represented by a Weibull probability function.

The method is a proactive methodology to prevent accidents through risk assessment aiming at identifying and depicting a system, in order to reduce failures and to minimize consequences of the hazardous events. The results of the analysis support the development of mitigating scenarios for the causes of hazardous events and contingency scenarios for the consequences of hazardous events.

REFERENCES

- Aven, T., and Kvaloy, J. T. (2002). Implementing the Bayesian paradigm in risk analysis. *Reliability Engineering and System Safety*, 78, 195-201.
- Huijer, K. (2005). *Trends in Oil Spills from Tanker Ships 1995-2004*. London: International Tanker Owners Pollution Federation.
- Lee, F. P. (1996). *Loss prevention in the process industries* (Vol. 3). Oxford: Butterworth Heinemann.
- Lindley, D. V. (1965). *Introduction to probability and statistics : from a bayesian viewpoint*. Cambridge: Cambridge University Press.
- MCGA. (2005). *Ship and Cargoes*. Acesso em 2008, disponível em Maritime and Coastguard Agency: [http://www.mcga.gov.uk/c4mca/stscontingencyplan291105 .pdf](http://www.mcga.gov.uk/c4mca/stscontingencyplan291105.pdf)
- OREDA. (2002). *Offshore Reliability Data Handbook*. Norway: OREDA Participants.
- Patino Rodriguez, C. E., Souza, G. F., and Martins, M. R. (2009). Risk-based analysis of offloading operations with FPSO production units. *Proceedings of COBEM*. Gramado: ABCM.
- Reis, S. P. (2004). *Transporte marítimo de petróleo e derivados na costa brasileira: Estrutura e implicações ambientais*. Rio de Janeiro: Universidade Federal do Rio de Janeiro.
- Roed, W., Mosleh, A., Vinnem, J. E., and Aven, T. (2009). On the use of the hybrid causal logic method in offshore risk analysis. *Reliability Engineering and System Safety*, 94, 445-455.
- Singpurwalla, N. D. (2006). *Reliability and Risk: A Bayesian Perspective*. London: John Wiley and Son Ltda.
- Siu, N. O., and Kelly, D. L. (1998). Bayesian parameter estimation in probabilistic risk assessment. *Reliability Engineering and System Safety*, 62, 89-115.

Preliminary Risk Analysis of a Liquefied Natural Gas Regasification System in an Offshore Unit

Schleder, Adriana Miralles¹; Martins, Marcelo Ramos²; Souza, Gilberto Francisco Martha³.

¹Graduate student, Naval Architecture and Ocean Engineering Department University of São Paulo, Brazil; Mail Stop Av. Prof. Mello Moraes, 2231 – São Paulo, Brazil 05508 030 PH (11) 3091-5348; email: adrianamiralles@usp.br

²Prof. Dr., Naval Architecture and Ocean Engineering Department University of São Paulo, Brazil; Mail Stop Av. Prof. Mello Moraes, 2231 – São Paulo, Brazil 05508 030 PH (11) 3091-5348; email: mrmartin@usp.br

³Prof. Dr., Mechanical Engineering Department University of São Paulo, Brazil; Mail Stop Av. Prof. Mello Moraes, 2231 – São Paulo, Brazil 05508 030 PH (11) 3091-9656; email: gfmnsouza@usp.br

ABSTRACT

Nowadays, LNG Import Terminals (where the storage and regasification process is conducted) are mostly onshore; the construction of these terminals is costly and many adaptations are necessary to abide by environmental and safety laws. Moreover, an accident in one of these plants might produce considerable impact in neighboring areas and population; this risk may be even worse due to the possibility of terrorist attack.

Under this perspective, a discussion is conducted about a vessel known as FSRU (Floating Storage and Regasification Unit), which is a storage and regasification offshore unit, that can work miles away from the coast and, because of this, can be viewed as an option for LNG storage and regasification.

The goal is to develop a Preliminary Risk Analysis, which will map potential hazardous events, equipment and operation of critical points at the FSRUs Regasification System, based on the Reliability Theory and the Risk Analysis Theory. This analysis is essential to define a maintenance plan based on the Reliability Centered Maintenance.

The results intend to clarify the operational risks of the system and might improve the development of an effective maintenance plan, which can provide good operability with appropriate safety levels.

INTRODUCTION

Natural gas is becoming an important energy source option, as it is clean energy as compared with traditional fuels and a significant alternative to diversify the

national matrix energy. However, in general, the production centers is much far of the consumers; therefore, in order to guaranty the economical viability of this source, the development of liquefied natural gas (LNG) transport, which reduces the original volume amount in 600 times, and the regasification technologies are essential.

In this view, a new option to supply LNG arises, the Floating Storage and Regasification Unit (FSRU). As the regasification process usually occurs on onshore plants, the processing in vessels (offshore) is pioneering. These vessels were used just for transporting liquefied gas, but it were transformed to be enabled to gasify LNG. Due to the offshore regasification process being a recent process, with no failures history for analysis and maintenance plan development, our goal is to perform a preliminary risk analysis and build a base for developing an efficient methodology for building an appropriate maintenance plan for the regasification system.

Preventive maintenance is crucial in this case, because an accident with liquefied natural gas may be catastrophic, causing personal, environmental and materials damages.

THE REGASIFICATION SYSTEM

As mentioned previously, the system studied is the regasification system of a FSRU. Since the 1940s, vessels have been used for LNG transportation; however, these vessels began to process the gas regasification and directly supply the net pipes just a few years ago. The regasification process adds new hazards to operations, because besides LNG, there is now compressed gas in process. Accidents along this process may reach the storage tankers causing huge fires or explosions.

In the vessel studied, a Cascade System was used, shown in Figure 1. In this system, the LNG is heated in two stages. At first, by propane compact heat exchanger, its temperature increases from 13.15° K to 263.15°K. In the next stage, the gas is heated by sea water in a shell&tube heat exchanger, and the temperature reaches 288° K. The propane used in the first phase works in a closed loop. Outside the LNG heat exchanger, its temperature is about 268,15°K and it is liquefied; hence, it is pumped into a titanium heat exchanger and heat, by sea water, until 273°K and vaporizes. It then returns to the LNG exchanger.

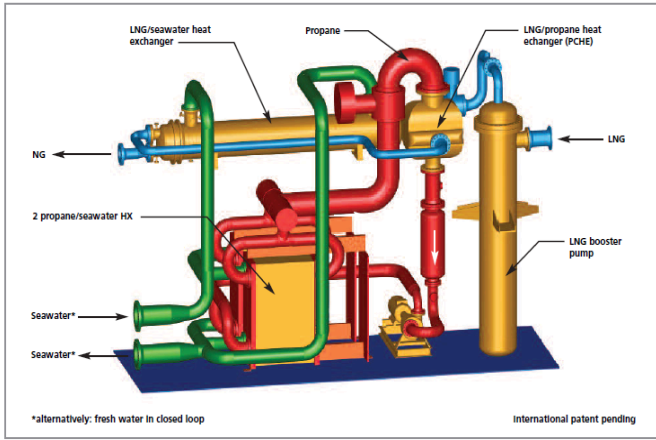


Figure 1. Regasification System (Source: Hamworthy site)

In this cycle, there are hazardous elements: LNG, compressed natural gas and propane.

NATURAL GAS

Natural gas is a hydrocarbon mix composed mostly of methane (about 98%), followed by propane, ethane, butane, hexane and others substances in minor proportions.

Physico-chemical analyses of natural gas allow drawing some conclusions:

- Natural gas density is lower than air, so it spreads easily and does not pose asphyxia risk in ventilated areas. Yet it may cause asphyxia by lack of oxygen in confined spaces;
- Natural gas poses fire risk if exposed to flame; however, its flammability range is narrow, thus hazards decrease;
- It has a high ignition point; in other words, it does not flare up even at high temperatures;
- Being natural gas composed mostly of methane, natural gas toxicity can be said to be equal to methane toxicity, that is, it will be dangerous just for people exposed to large amounts.

LNG

LNG is natural gas condensed to -160°C . It is a cryogenic liquid, which presents hazards due to the very low temperature and the high freezing power.

PROPANE

Propane is used in this system due to its thermodynamic properties and low freezing point. Analyzing propane properties, it is possible to draw some conclusions:

- The very low freezing point is appropriate for heat exchange with LNG, since other substances could freeze and cut off the system flow;

- Propane has a high self-ignition point and a narrow flammability range, which decreases the risk of explosion.

METHODOLOGIES

PRELIMINARY HAZARD ANALYSIS (PHA)

As ABS (2000) defines the PHA technique is a broad, initial study that focuses on identifying apparent hazards, assessing the severity of potential mishaps that could occur involving the hazards, and identifying means (safeguard) for reducing the risks associated with the hazards.

After knowing the system and elements, it is necessary to identify hazards (IMO 2007) ; for this, the Preliminary Hazard Analysis (PHA) technique was chosen. This analysis allows a better system view, making it easier to understand its operation. Next, hazards are classified and the probable causes are studied.

PHA identified the main hazards and they were classified by severity and frequency, according to tables 1 and 2 parameters.

Table 1. Frequency Classes

Class	Frequency	Description
A	Very remote	Scenarios that happen only if multiple failures occur. It is not expected through the system life cycle
B	Remote	Scenarios related to large equipment failure.
C	Unlikely	Scenarios related to any equipment failure or human fault.
D	Likely	Expected at least once through the system life cycle.
E	Frequent	Likely to occur at least once a year.

Table 2. Severity Classes

Class	Severity	Description
I	Negligible	Events related to no damages or not measureable damages.
II	Marginal	Events related to negligible damages.
III	Critical	Events which cause external environment impact with small recovery time. May cause moderate personnel injury.
IV	Catastrophic	Events which cause huge external environment impact with long recovery time. May cause severe injury or death.

Using these standards, a PHA was developed and the obtained results are shown in Table 3:

Table 3. Preliminary Hazardous Analysis Table.

System or function	Hazardous element	Triggering event 1	Hazardous condition	Potential accident	Effect	F	S	Corrective Measures
1 LNG Tubing	LNG	LNG Large Leak	Enough LNG to cause asphyxia for lack of oxygen	People without oxygen	Personnel injury	A	IV	- periodic inspections in tubing, heat exchangers and pumps; - installation of gas detector and alarms; - workers training;
			Enough LNG to initiate a reaction.	Explosion or fire	Personnel injury and materials damages	B	IV	
		LNG Small Leak	Enough LNG to cause freezing	Freezing when touching skin	Personnel injury	C	III	
			Enough LNG to cause freezing	Tubing and surrounding equipment freezing	Material damages	D	III	
2 Propane Tubing	Propane	Propane Small Leak	Enough Propane to cause freezing	Tubing and surrounding equipment freezing	Material damages	D	III	inspections in tubing, heat exchangers and pumps; - installation of gas detector and alarms; - workers training;
				Freezing when touching skin	Personnel injury	C	III	
		Propane Large Leak	Enough Propane to cause asphyxia for lack of oxygen	People without oxygen	Personnel injury	A	IV	
			Enough Propane to initiate a reaction.	Explosion or fire	Personnel injury and materials damages	B	IV	
3 Natural gas tubing	Compressed natural gas	Compressed gas Large Leak	Enough gas to cause asphyxia for lack of oxygen	People without oxygen	Personnel injury	A	IV	inspections in tubing, heat exchangers and pumps; - installation of gas detector training;
			Enough gas present to initiate a reaction.	Explosion or fire	Personnel injury and material damages	B	IV	

Using the frequencies and severity classes, the risk matrix (Figure 2) is developed (ABS 2003). It shows the risks classes.

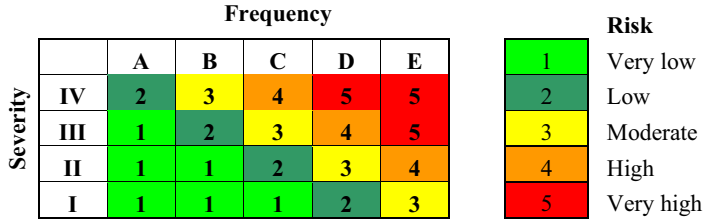


Figure 2. Risk Matrix

Setting the hazards from the HPA table in this matrix, the number of hazards for each risk class is obtained (Figure 3):

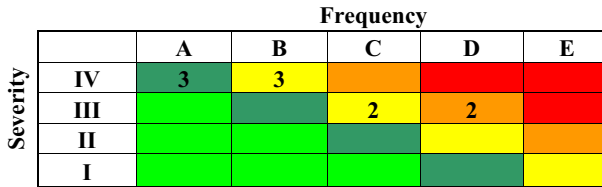


Figure 3. Risk Matrix of Regasification System

FAULT TREE ANALYSIS (FTA)

As ABS (2000) defines Fault Tree Analysis (FTA) is a deductive analysis that graphically models (using Boolean logic) how logical relationships among equipment failures, human errors and external events can combine to cause specific mishaps of interest. These FTs allow verifying what causes the event and using the diagram, knowing the failures rates, it is possible to calculate the top event probability; the top event is the undesired event that was chosen for qualitative and quantitative analysis.

To continue risk analysis, risks classified as “High” and “Moderate with severity IV”, in Figure 3, were chosen to be the top events of Fault Trees (FTs). Figure 4 shows the fault tree of the LNG Explosion event, in which the necessary base elements to trigger the undesired event are exposed. FTs were built for each risk classified as “High” or “Moderate with severity IV”, however just the FT of the LNG Explosion will be presented here due to restricted space.

DISCUSSION AND CONCLUSIONS

Adopting the techniques presented in this research, it is possible to check the most significant hazards and their causes. The study illustrated that the PHA technique is effective to conduct the risk assessment for the chosen system. In turn, the Fault Trees are very useful to understand the interactivity between subsystems and equipment.

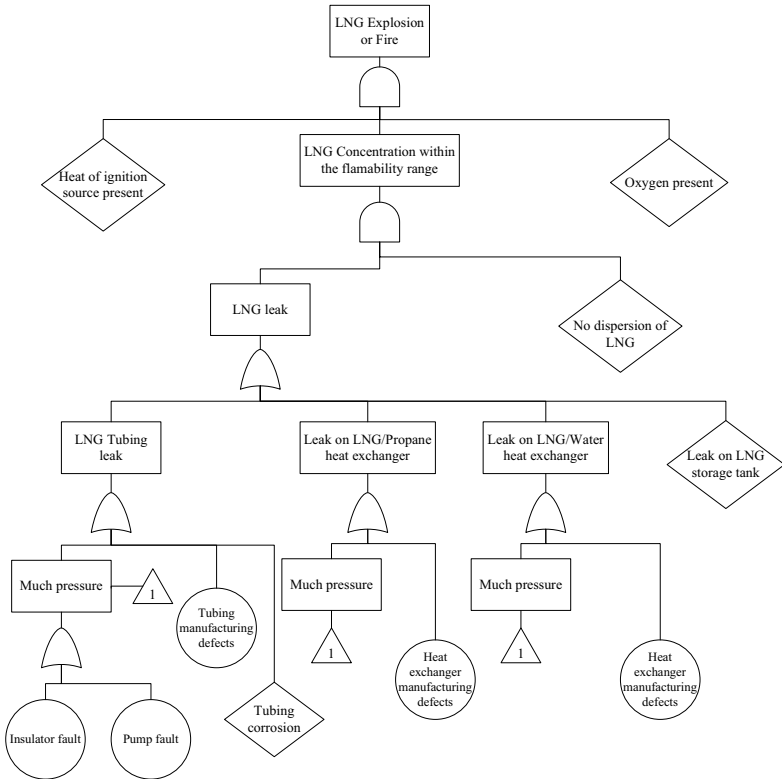


Figure 4. Fault Tree “LNG Big Leak with Explosion or Fire”

To make the analysis more efficient it is essential to get more information about the system and equipment. The detection and alarm systems were not included in this analysis, but they influence the risk analysis, for example these equipments may contribute in LNG or CG dispersion, what will change FTs likelihoods. In future works, including these systems in the analysis is recommended. This preliminary risk analysis allowed knowing the main hazards of a FSRUs Regasification System (explosions, fires and freezing) and the more likely causes.

Large leaks deserve attention since they are associated with high levels of severity, mitigating and preventive measures should thus be proposed. Propane and LNG small leaks are classified as High risk, hence deserving attention, too. In both cases the FT analysis shows that the reliability of heat exchangers, pumps and tubes must be high for the use condition; they are the FT base elements.

In the case of pipes, it is worth noting that two elements contribute for occurrence of leaks: increase of pressure and tubing defects.

The increase pressure may be caused by an unexpected heat loss of the LNG or Propane. If the insulator fails and LNG or Propane heat inside tubing, the gas expands and possibly causes a tubing rupture. As a preventive measure it is proposed a control system to supervise heat exchange along the pipe and a meticulous maintenance plan of the refrigeration system.

Tubing defects may be caused by manufacturing defects or pipe corrosion and the LNG constitution is a significant corrosion cause. Thus, this study suggests a tight control of the LNG constitution before the storage tanks being loaded.

The other developed FTs provided more data about the system, however they present many similar base elements, which demonstrates that the measures proposed above may avoid more than one risk. The FTs also show that the labor training is crucial since it prevents accidents where the worker touches the cryogenic liquid and also prepares the worker to deal with the control and alarm systems.

Other measures suggested are: the implementation of physical protection to avoid pipe rupture on critical locations; periodic inspections; installation of gas detectors and alarms; and labor training. These measures intend to reduce likelihood of the potential events classified as High and Moderate.

This study is a preliminary analysis; it was possible to check the main potential hazardous events and what causes these events. More information about the system is necessary to improve the results. Continuing the risk analysis through the quantitative analysis is recommended, including beyond the history failure equipment expert opinion to improve the analysis.

In this investigation was not found a study about the system operation and the consequences of a regasification system failure in the vessel; a failure in this system may reach other areas of the vessel, such as the LNG tanks, and cause dangerous fires and explosions. Therefore, a future work may study the effects of an undesired event in the regasification system on other FSRU systems.

REFERENCES

- American Bureau of Shipping (ABS). (2000). "Risk Assessment Applications for the Marine And Offshore Oil and Gas Industries", Guidance Notes.
- American Bureau of Shipping (ABS). (2003). "Risk Evaluations for the Classification of Marine-Related Facilities", Guidance Notes.
- Ayyub, B.A. (2001) "RISK Analysis for Engineers and Economics", Chapman & Hall / CRC, EUA.
- International Maritime Organization (IMO). (2007) – "Liquefied Natural Gas (LNG) Carriers Details of the Formal Safety Assessment", Maritimar Safety Committee-83rd session-Agenda item 21.
- Foss, M. M. (2003). "LNG Safety and Security". Bureau of Economic Geology. University of Texas. <http://www.beg.utexas.edu/energyecon/lng> (Mar. 3, 2010).
- Blackwell, B. (2009). "Golar LNG: Delivering the World's First FSRU". <http://www.golarlng.com> (Mar. 29, 2010).
- Hamworthy Gas Systems. (2010), "LNG Systems for Marine Application". <http://www.hamworthy.com/en> (Mar. 3, 2010).

Seismic risk assessment and sensitivity analysis in terms of life-cycle repair cost

Alexandros A. Taflanidis¹

¹University of Notre Dame, Department of Civil Engineering and Geological Sciences, Notre Dame, IN, 46556, USA, email: a.taflanidis@nd.edu

ABSTRACT

A probabilistic framework is discussed in this paper for assessment and sensitivity analysis of seismic risk, characterized as the life-cycle repair cost. A comprehensive methodology is initially discussed for earthquake loss estimation that uses the nonlinear time-history response of the structure to estimate the damage in a detailed, component level. A realistic, stochastic ground motion model is then adopted for describing the acceleration time history for future seismic excitations. In this setting, the life-cycle repair cost can be quantified by its expected value over the space of the uncertain parameters for the structural and excitation models. Estimation of this cost through stochastic simulation is suggested and a probabilistic sensitivity analysis approach is also presented, aiming to identify the structural and excitation properties that probabilistically contribute more to this cost.

INTRODUCTION

Risk assessment in earthquake engineering requires proper integration of (i) approaches for treating the uncertainties related to the seismic hazard and to the structural behavior, (ii) methodologies for quantifying structural performance and ultimately characterizing risk, as well as (iii) algorithms appropriate for stochastic analysis. Undoubtedly the most relevant description of this risk is in terms of the anticipated economic losses and various novel approaches have been developed to establish such a risk description (Ang and Lee 2001; Porter et al. 2001; Fragiadakis et al. 2006; Kircher et al. 2006; Goulet et al. 2007). In this paper a probabilistic framework is presented for characterization of seismic risk in terms of the life-cycle repair cost. Basis of this framework is a comprehensive methodology for estimating seismic losses that uses the nonlinear time-history response of a structure under a given seismic excitation to calculate damages in a detailed component level (Porter et al. 2001; Goulet et al. 2007). An efficient stochastic simulation approach is then discussed for risk assessment and for a novel probabilistic sensitivity analysis, aiming to identify the critical risk factors that contribute more to this cost.

LIFE-CYCLE SEISMIC COST ASSESMENT

For evaluation of seismic cost adoption of appropriate models is needed for the structural system itself, the earthquake excitation and for loss evaluation. The characteristics of these models are not known with absolute certainty, though. Uncertainties may pertain to the properties of the structural system, to the variability

of future seismic events, or to parameters related to the fragility of the system components. For explicitly incorporating these uncertainties in the modeling process, let $\theta \in \Theta$, denote the augmented vector of model parameters where Θ represents the space of possible model parameter values. Vector θ is composed of *all* the model parameters for the individual structural system, excitation, and loss evaluation models. The uncertainty in these model parameters is then quantified by assigning a probability model $p(\theta)$ to them, which incorporates our available knowledge about the system and its environment into the model and it addresses future variability for both the seismic hazard, as well as for the structural system and its performance.

In this setting, the overall cost, for a specific structural configuration and seismic excitation, described by θ , is denoted by $h(\theta)$. *Seismic risk* is then characterized as expected life-cycle cost and is ultimately simply given by the expected value of $h(\theta)$ over the chosen probability models

$$C = \int_{\Theta} h(\theta)p(\theta)d\theta \quad (1)$$

Since the models adopted for characterization of the earthquake losses can be complex the expected value (1) cannot be calculated, or even accurately approximated, analytically. An efficient alternative approach is to estimate this integral by *stochastic simulation*. In this case, using a finite number, N , of samples of θ simulated from some importance sampling density $q(\theta)$, an estimate for (1) is given by the *stochastic analysis*:

$$\hat{C} = 1/N \sum_{j=1}^N h(\theta^j)p(\theta^j)/q(\theta^j) \quad (2)$$

where vector θ^j denotes the sample of the uncertain parameters used in the j^{th} simulation and $\{\theta^j\}$ corresponds to the entire sample set. The importance sampling density $q(\theta)$ is used to improve the efficiency of this estimation, by focusing the computational effort on regions of the Θ space that contribute more to the integrand of the stochastic integral. The simplest selection is to use $q(\theta)=p(\theta)$, then the evaluation in (2) corresponds to direct Monte Carlo analysis.

Finally, though appropriate selection of the individual system, excitation and performance evaluation models, along with the estimation (2), this approach provides an end-to-end simulation based framework for detailed characterization of life-cycle seismic cost. This framework puts no restrictions on the complexity of the structural and excitation models used or in the probability models chosen for their uncertain characteristics. Thus, it allows for an efficient and accurate estimation of the economic losses, and can take into account all uncertainties about the properties, excitation and performance of the structural system through its entire lifetime. Next the loss estimation methodology and stochastic ground motion model used in this study are reviewed. Then an extension of this framework is discussed to additionally quantify the importance of each of the model parameters in affecting the overall cost.

LOSS ESTIMATION METHODOLOGY

For estimating earthquake losses the comprehensive methodology described in (Porter et al. 2001) and (Goulet et al. 2007) is adopted. In this methodology the

nonlinear time-history response of the structure under a given excitation is used for a detailed evaluation of economic losses. For the direct losses, the components of the structure are grouped into n_{as} damageable assemblies. Each assembly consists of components of the structural system that have common characteristics with respect to their vulnerability and repair cost. Such assemblies may include, for example, beams, columns, wall partitions, contents of the building, and so forth. For each assembly $j=1, \dots, n_{as}$, $n_{d,j}$ different damage states are designated and a fragility function is established for each damage state $d_{k,j}$, $k = 1, \dots, n_{d,j}$. These functions quantify the probability $P_e[d_{k,j} | EDP_j, \theta]$ that the component has reached or exceeded its k^{th} damage state, conditional on some engineering demand parameter (EDP_j) which is related to the time-history response of the structure (for example, peak transient drift, peak acceleration, maximum plastic hinge rotation, etc.). Damage state 0 is used to denote an undamaged condition. A repair cost $C_{k,j}$ is then assigned to each damage state, which corresponds to the cost needed to repair the component back to the undamaged condition. The expected losses in the event of the earthquake are given by:

$$L(\theta) = \sum_{j=1}^{n_{as}} \sum_{k=1}^{n_{d,j}} P[d_{k,j} | \theta] C_{k,j}$$

where $P[d_{k,j} | \theta]$ is the probability that the assembly j will be in its k^{th} damage state and the explicit dependence on EDP_j has been dropped. The probability $P[d_{k,j} | \theta]$ may be readily obtained from the information from the fragility curves:

$$P[d_{k,j} | \theta] = P_e[d_{k,j} | \theta] - P[d_{k+1,j} | \theta] \quad P[d_{n_{d,j},j} | \theta] = P_e[d_{n_{d,j},j} | \theta]$$

GROUND MOTION MODEL

The life-cycle assessment framework discussed here requires development of a probabilistic model of the entire ground motion time history that will adequately describe the uncertainty in future earthquake events. The approach used in this study for this purpose is adoption of a stochastic ground motion model. The parameters of such models are correlated to earthquake (type of fault, moment magnitude and epicentral distance) and site characteristics (shear wave velocity, local site conditions) by appropriate predictive relationships. Description of the uncertainty for the earthquake characteristics and the predictive relationships leads then to a complete probabilistic model for future ground-motion time-histories. In particular, a point-source stochastic ground motion model (Boore 2003) is adopted here with the specific source spectrum developed by Atkinson and Silva (2000) for California seismicity. According to this model, the time-history for a specific event magnitude, M , and source-to-site distance, r , is obtained by filtering a white-noise sequence \mathbf{Z} through a time-domain envelope function $e(t; M, r)$; and a frequency-domain amplitude spectrum $A(f; M, r)$. This process is illustrated in Figure 2. The characteristics for $A(f; M, r)$ and $e(t; M, r)$ used in this study are same as the ones considered in (Taflanidis and Beck 2009). The model parameters in this case consist of the seismological parameters $[M, r]$, and the high-dimensional white-noise sequence, \mathbf{Z} .

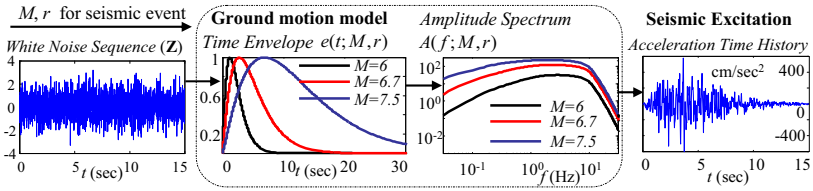


Figure 2: Stochastic ground motion model and generation of a sample ground motion

PROBABILISTIC SENSITIVITY ANALYSIS

The life-cycle repair cost assessment framework may be seemingly extended to additionally investigate the sensitivity of this cost with respect to each of the uncertain model parameters. Foundation of this methodology (Taflanidis 2009) is the definition of an auxiliary probability density function that is proportional to the integrand of the life-cycle cost integral

$$\pi(\theta) = h(\theta)p(\theta) / \int_{\Theta} h(\theta)p(\theta)d\theta \propto h(\theta)p(\theta) \quad (3)$$

where \propto denotes proportionality. The sensitivity analysis is established by comparing this auxiliary distribution $\pi(\theta)$ and the prior probability model $p(\theta)$; based on the definition of $\pi(\theta)$ in (3) such a comparison does provide information for $h(\theta)$. Bigger discrepancies between distributions $\pi(\theta)$ and $p(\theta)$ indicate greater importance of θ in affecting the system performance, since they ultimately correspond to higher values for $h(\theta)$. More importantly, though, this idea can be implemented to each specific model parameter θ_i (or even to groups of them), by looking at the marginal distribution $\pi(\theta_i)$. Comparison between this marginal distribution $\pi(\theta_i)$ and the prior distribution $p(\theta_i)$ expresses the *probabilistic* sensitivity of the seismic risk with respect to θ_i . Uncertainty in all other model parameters and stochastic excitation is explicitly considered by appropriate integration of the joint probability distribution $\pi(\theta)$ to calculate the marginal probability distribution $\pi(\theta_i)$.

A quantitative metric to characterize this sensitivity is the relative information entropy, which is a measure of the difference between distributions $\pi(\theta_i)$ and $p(\theta_i)$

$$D(\pi(\theta_i) || p(\theta_i)) = \int \pi(\theta_i) \log(\pi(\theta_i) / p(\theta_i)) d\theta_i \quad (4)$$

with larger values for $D(\pi(\theta_i)||p(\theta_i))$ indicating bigger importance. An analytical expression, though, is not readily available for the marginal distribution $\pi(\theta_i)$. An alternative stochastic-sampling approach is discussed next, based on generation of a set samples $\{\theta^k\}$ from the joint distribution $\pi(\theta)$. Such samples may be obtained by any appropriate stochastic sampling algorithm, for example by the accept-reject method. Furthermore this task may be seemingly integrated within the stochastic analysis (2): each of the samples θ^j from (2) can be used as a candidate sample in the context of the Accept-Reject algorithm. Projection, now, of the samples from $\pi(\theta)$ to the space of *each* of the model parameters provides samples for the marginal

distributions $\pi(\theta_i)$ for each of them separately. Thus using the same sample set $\{\theta^k\}$ this approach provides simultaneously information for all model parameters. For scalar quantities, as in this case, the relative entropy (4) may be efficiently calculated by establishing an analytically approximation for $\pi(\theta_i)$ based on the available samples, through Kernel density estimation and then numerically calculating the scalar integral (4) (Taflanidis 2009).

This approach ultimately leads to an efficient sampling-based approach for calculating the relative information entropy for different parameters, which can be performed concurrently with the risk assessment, exploiting the readily available system model evaluations to minimize computational burden. Comparing the value for this entropy between the various model parameters leads then to a direct identification of the importance of each of them in affecting risk. Parameters with higher value for the relative entropy will have greater importance.

ILLUSTRATIVE EXAMPLE

Structural, excitation models. For the illustrative example, a three-story, office building is considered. The building is a non-ductile reinforced concrete, perimeter moment-frame structure with height for each story is 3.9 m. A planar shear frame model (illustrated in Figure 2) with hysteretic behavior and deteriorating stiffness and strength is assumed (using a distributed element model assumption for the deteriorating part). The lumped mass of the top story is 935 ton while it is 1215 ton for the bottom two. The initial inter-story stiffnesses k_i of all the stories are parameterized by $k_i=k_{in}\theta_{ki}$, $i = 1,2,3$, where $[k_{in}]=[700.0, 616.1, 463.6, 281.8]$ MN/m are the most probable values and θ_{ki} are nondimensional uncertain parameters, assumed to be correlated Gaussian variables with mean value $\theta_{ki}=1$ and covariance matrix with elements $\mathbf{K}_{ij}=(0.1)^2\exp[-(i-j)^2/2^2]$. For each story, the post-yield stiffness coefficient α_i , stiffness deterioration coefficient β_i , over-strength factor γ_i , yield displacement $\delta_{y,i}$ and displacement coefficient η_i have mean values 0.1, 0.2 0.3, 0.22% of story height and 2, respectively (see Figure 3 for proper definition of some of these parameters). All these parameters are treated as independent Gaussian variables with coefficient of variation 10%. The structure is assumed to be modally damped. The damping ratios for all modes are treated similarly as Gaussian variables with mean values 5% and coefficients of variation 10%.

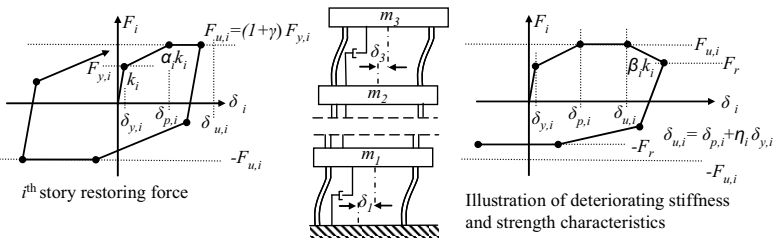


Figure 2: Structural model

Seismic events are assumed to occur following a Poisson distribution and so are independent of previous occurrences. The uncertainty in moment magnitude M is modeled by the Gutenberg-Richter relationship truncated on the interval $[M_{min}, M_{max}] = [5.5, 8]$, leading to the PDF $f(M) = b \exp(-bM) / [\exp(-bM_{min}) - \exp(-bM_{max})]$ and expected number of events per year $v = \exp(a - bM_{min}) - \exp(a - bM_{max})$. Only events with magnitude greater than $M > 5.5$ are considered since earthquakes with smaller magnitude are not expected to lead to significant damage to the structure and thus will not contribute significantly to the expected life-cycle cost. The regional seismicity factors are selected as $b = 0.9 \log_e(10)$ and $a = 4.35 \log_e(10)$, leading to $v = 0.25$. For the uncertainty in the event location, the logarithm of the epicentral distance, r , for the earthquake events is assumed to follow a log-normal distribution with median $\log(20)$ km and coefficient of variation 0.4.

Expected repair-cost. The total value of the losses from all future earthquake excitations, is taken as the quantity representing lifetime repair cost:

$$h(\theta) = L(\theta) v t_{lif}$$

where t_{lif} is the lifetime of the structure (taken here 60 years) and $L(\theta)$ is the cost given the occurrence of an earthquake event.

For $L(\theta)$ losses only repair cost due to damage is considered here. Each fragility function is a conditional cumulative log-normal distribution with median x_m and logarithm standard deviation b_m , as presented in Table 1. This table also includes the expected cost per element $\$/n_{el}$, where n_{el} corresponds to the number of elements that belong to each damageable assembly in each direction of each floor. For the structural contents and the acoustical ceiling, the maximum story absolute acceleration is used as the EDP and for all other assemblies the maximum inter-story drift ratio is used as the EDP. For estimating the total wall area requiring a fresh coat of paint, the simplified formula developed in (Goulet et al. 2007) is adopted. According to this formula, a percentage of the undamaged wall area is also repainted, considering the desire of the owner to achieve a uniform appearance. This percentage depends on the extent of the damaged area and is chosen here based on a lognormal distribution with median 0.25 and logarithmic standard deviation 0.5.

Table 1. Characteristics of fragility functions and expected repair costs per storey

	x_m	b_m	n_{el}	$\$/n_{el}$		x_m	b_m	n_{el}	$\$/n_{el}$
$d_{k,j}$	Structural components				$d_{k,j}$	Partitions			
1 (light)	$1.4\delta_{y,i}$	0.2	30	2000	1 (patch)	0.33%	0.2	500	180
2 (mod.)	$(\delta_{y,i} + \delta_{p,i})/2$	0.35	30	9625	2 (replace)	0.7%	0.25	500	800
3 (signif.)	$\delta_{p,i}$	0.4	30	18200	$d_{k,j}$	Acoustical Ceiling			
4 (severe)	$\delta_{u,i}$	0.4	30	21600	1 (damage)	1g	0.7	10^3m^2	25
5 (collap.)	3%	0.5	30	34300	$d_{k,j}$	Paint			
$d_{k,j}$	Contents				1 (damage)	0.33%	0.2	3500m^2	25
1 (damage)	0.7g	0.3	40	1000					

Results and discussion. Results from the lifetime repair cost assessment are illustrated in Figures 3. The total lifetime repair cost for the structure is estimated at \$328,430. The biggest contribution to this cost comes from the non-structural components; repairing the partitions and repainting any damaged surfaces. The structural components also do have a fairly significant importance, whereas the acceleration sensitive assemblies, i.e., the building contents or the acoustical ceiling only a small one. Also most damages and associated repair costs are anticipated in the first two floors.

The sensitivity analysis results for the uncertain model parameters are reported in Table 2. The relative entropy $D(\pi(\theta)|p(\theta))$, calculated as described in Section 5, is presented with respect to the total cost, as well as with respect to the repair cost for the different damageable assemblies. Due to space limitations, results are reported here only for the model parameters that have non-negligible values for $D(\pi(\theta)|p(\theta))$. It is evident that M has the highest importance in influencing seismic risk (highest value for the entropy), with r also having a significant, but smaller, impact. The structural model parameters have a relatively only small contribution. The comparison between the different damageable assemblies shows that the repair cost for structural components demonstrates a relatively larger sensitivity to structural characteristics. Another interesting trend is that for the ceiling, and especially for the contents of the buildings the sensitivity with respect to the seismic hazard is significantly smaller.

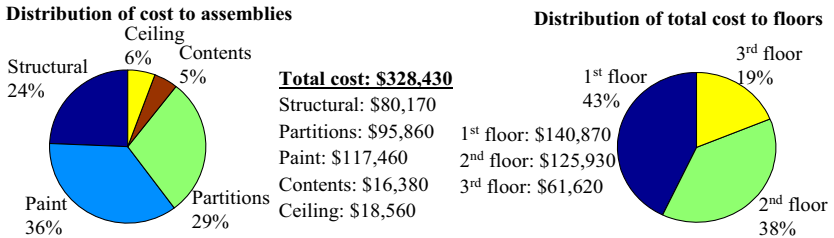


Figure 3: Total lifetime repair cost and its distribution to different damageable assemblies and floors.

Table 2. Relative entropy $D(\pi(\theta)|p(\theta))$ with respect either the total repair cost or the repair cost for different assemblies

	Total cost	Repair cost per assembly				
		Structural	Partitions	Paint	Contents	Ceiling
M	2.281	2.600	2.149	2.492	1.043	2.021
r	0.754	0.819	0.690	0.788	0.580	0.812
ζ_i	0.006	0.016	0.011	0.005	0.021	0.019
$\delta_{y,1}$	0.017	0.041	0.020	0.013	0.010	0.017
$\delta_{y,2}$	0.008	0.029	0.004	0.004	0.004	0.007
$\delta_{y,3}$	0.004	0.009	0.010	0.008	0.004	0.003

CONCLUSIONS

A probabilistic framework was discussed in this paper for assessment and sensitivity analysis of the life-cycle seismic repair cost of structural systems. Though appropriate selection of system and probability models, this approach efficiently takes into account all uncertainties about the properties, excitation and performance of the structural system through the specified lifetime. A computationally efficient approach for a probabilistic sensitivity analysis was also presented, based on advanced stochastic sampling concepts. This sensitivity analysis aims at identifying the structural and excitation properties that contribute more to the total lifetime repair cost. The framework was illustrated in an illustrative example for a three-storey non-ductile reinforced- concrete office building.

ACKNOWLEDGMENTS

This research effort is supported by NSF grant CMMI-1030726. This support is greatly appreciated.

REFERENCES

- Ang, H.-S. A., and Lee, J.-C. (2001). "Cost optimal design of R/C buildings." *Reliability Engineering and System Safety*, 73, 233-238.
- Atkinson, G. M., and Silva, W. (2000). "Stochastic modeling of California ground motions." *Bulletin of the Seismological Society of America*, 90(2), 255-274.
- Boore, D. M. (2003). "Simulation of ground motion using the stochastic method." *Pure and Applied Geophysics*, 160, 635-676.
- Fragiadakis, M., Lagaros, N. D., and Papadrakakis, M. (2006). "Performance-based multiobjective optimum design of steel structures considering life-cycle cost." *Structural and Multidisciplinary Optimization*, 32, 1-11.
- Goulet, C. A., Haselton, C. B., Mitrani-Reiser, J., Beck, J. L., Deierlein, G., Porter, K. A., and Stewart, J. P. (2007). "Evaluation of the seismic performance of code-conforming reinforced-concrete frame building-From seismic hazard to collapse safety and economic losses." *Earthquake Engineering and Structural Dynamics*, 36(13), 1973-1997.
- Kircher, C. A., Whitman, R. V., and Holmes, W. T. (2006). "Hazus earthquake loss estimation methods." *Natural Hazards*, 7(2), 45-59.
- Porter, K. A., Kiremidjian, A. S., and LeGrue, J. S. (2001). "Assembly-based vulnerability of buildings and its use in performance evaluation." *Earthquake Spectra*, 18(2), 291-312.
- Taflanidis, A. A. (2009). "Stochastic subset optimization with response surface methodologies for stochastic design." *1st International Conference on Soft Computing Technology in Civil, Structural and Environmental Engineering*, 1-4 September, Madeira, Portugal.
- Taflanidis, A. A., and Beck, J. L. (2009). "Life-cycle cost optimal design of passive dissipative devices." *Structural Safety*, 31(6), 508-522.

Influence of socio-economic consequences of world economic crisis on a shadow economy

A.S. Naydenov¹

¹Center for Economic Security, Institute of Economics of Ural Branch of Russian Academy of Sciences, 29 Moskovskaya street, Yekaterinburg, Russia, 620014; www.eng.uralcses.ru; PH +7 (343) 3715701, +7 (912) 6648664; email: naidenov@list.ru

ABSTRACT

Results of previous research of shadow economy show powerful impact of crisis tendencies in economy on shadow economic activity. Moreover, during crises a scale of shadow economy grows considerably, therefore an importance of learning this part of economy is increasing. So far as economic crisis cause activation of all forms of shadow activities an estimating quantitative influence of socio-economic consequences of the world economic crisis on a shadow economy is of interest.

In order to achieve goal the economy-mathematical model was designed. The economy-mathematical model of a shadow economy in the conditions of the world economic crisis was used to forecast a development of the regional shadow economy under the influence of the world economic crisis. Short-term forecasts of the development of a regional shadow economy were obtained for the Russian regions.

INTRODUCTION

An importance of state administration rise significantly during the world economic crisis. Meanwhile, efficiency of administration depends on the presence of impartial and credible information on the state of object of governance. Compliance with this requirement is complicated by a shadow economy which is unregistered and unobserved. Thus an estimating scale of shadow economy and shadow activity is a first-priority aim, and achieving of this aim is a necessary condition of an efficient state policy.

During economic crises an importance of studying and evaluating of shadow economy grows significantly because of the influence of socio-economic consequences of crisis tendencies on shadow economy – as a rule shadow activity increase due to its ability to stabilize economic and social situation.

B.T. Ryabushkin insist that the reason of shadow economy growth is a misbalance between economic sector, between demand and supply, and that cause disturbance of reproduction process (Ryabushkin, 2003). And shadow economy can make up for gaps in economy with shadow operations. A.A. Kuklin and A.N. Dyagtereva say about “compensation function” of shadow economy (Kuklin, Dyagtereva, 2005).

So, the importance of studying shadow economy in crisis conditions of economic activity is of obvious importance. But this task demands for precise and objective methodology and mathematical technique which were created in the research.

METHODOLOGY OF RESEARCH

The basis of methodology is the econometric model of shadow economy under the influence of socio-economic consequences of the world economic crisis. The description of the procedure of shadow economy modeling is given in the figure 1.

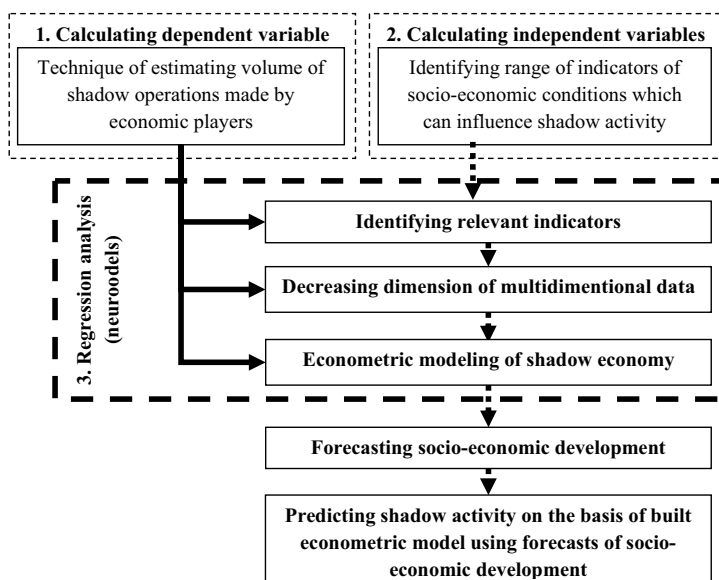


Figure 1. Description of shadow activity modeling procedure

The model of shadow economy is a polynomial function of shadow economy and arguments of the function are economic indicators of socio-economic conditions determined by economic crisis.

Dependent variable of the function is a volume of shadow operations conditioned by unregistered economic activity. This variable is calculated with help of special technique designed by authors earlier. This technique is using statistics of tax inspections of different groups of taxpayers.

As it has been already mentioned the arguments of the econometric function are economic indicators of socio-economic conditions determined by economic crisis. These indicators are selected through the several steps (see figure 1):

1. Identifying range of indicators of socio-economic conditions which can influence shadow activity. These indicators are indices provided by Federal Statistics Service and revealing all aspect of socio-economic development in Russian regions. All these indicators were grouped in 10 sets (figure 2).

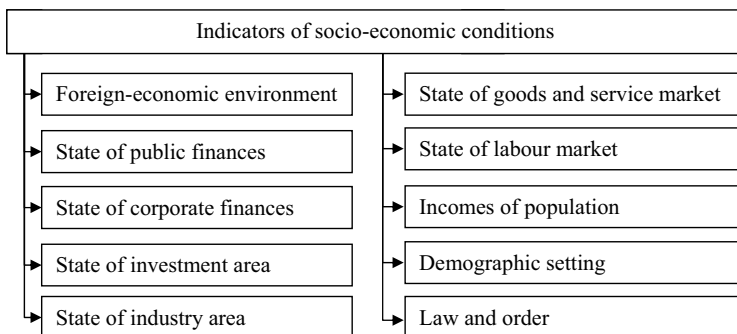


Figure 2. Groups of indicators of socio-economic conditions which can influence shadow activity

2. Identifying relevant indicators. Actually this step is devoted to detecting those indicators which has no any effect of shadow economy. The reason of such narrow approach is that we used here correlation analysis. And this method has disadvantage: only linear link can be identified while influence of socio-economic conditions on shadow economy is usually nonlinear. That is why in order to escape mistake of rejecting relevant indicators we used faint bounds.
3. Reduction of data dimension. Inclusion of big number of indicators permit to take into account all aspect of socio-economic life but it makes difficult to build econometric model. In order to avoid this problem we used modified method of principal components to decrease the volume of statistical data. As a modification of method of principal components we used criteria of external informativity:

$$Ip = I - ||R_X - R_{X'}||,$$

where R_X – correlation matrix of initial indicators;

$$R_{X'} - \text{correlation matrix of indices } \delta'_j = \sum_{v=1}^p q_{jv} * y_v ;$$

p – number of principal components;

v – index of principal component in range 0 and p ;
 j – index of initial indicator;
 y_v – principal component v .

Statistical finding were used further in the econometric modeling of shadow economy. The model was built with help of neuro-analysis, Group Method of Data Handling. This method is the realization of inductive approach for mathematical modeling of complex systems. The main advantage of this method is its ability to build mathematical model of socio-economic process on the basis of observations with lack of information. Modeling was automated through the instrumentality of special mathematical software designed for emulation of neuronet.

The Kolmogorov-Gabor polynomial was used as a supporting function of the econometric model:

$$Y(x_1, \dots, x_n) = a_0 + \sum_{i=1}^n a_i x_i + \sum_{i=1}^n \sum_{j=i}^n a_{ij} x_i x_j + \sum_{i=1}^n \sum_{j=ik=j}^n \sum_{k=j}^n a_{ijk} x_i x_j x_k + \dots,$$

where x – observation;

a – polynomial coefficients.

Next the forecast of shadow economic activity was made using the econometric model of shadow economy. Forecasting was made on the basis of the prediction of socio-economic development which determined the shadow activity. Socio-economic development was predicted with help of expert judgements made by state authorities, Federal Statistics Service and academic experts.

PRINCIPAL FINDINGS

Research was devoted to studying and forecasting of shadow economy under the influence of the world economic crisis in the regions of the Ural Federal District of Russia.

Identifying range of indicators of socio-economic conditions which can influence shadow activity showed 59 most important of them among all parameters of socio-economic development tracked by Federal Statistics Service.

Further analysis of socio-economic indicators was based on statics of period 2006 – 2009 (quarterly). Finding of relevant indicators and reduction of data dimension brought to the statistics limited to 8-15 most important indicators (dependently on particular territory). Using Kettel-criteria for every region 4 most informative indicator were detected (which explain all together more then 82% of the total dispersion of the obtained data).

Factor weights show that the commonly gotten principal components have the following meaning content, dependently on the region:

1. General state of socio-economic environment (effectiveness of companies, tax proceeds, gross volume of retail sales, population incomes, etc.).
2. Spirit of enterprise (index of industrial production, index of employment, proceeds of corporate taxes, etc.).
3. Level of prices.

4. Investment activity (total volume of investments, volume of foreign investment, etc.).
5. Financial state of banking area (gross margin, number of banks, total value of past-due loans, etc.).
6. State of public finances (value of public expenditures, value of budgetary payments, etc.).

Relying on the obtained data the econometric models of shadow economy was made for the region of the Ural Federal District of Russia. As it has been already mentioned dependent variable of the function is a volume of shadow operations conditioned by unregistered economic activity. The figure 3 shows an estimated volume of shadow operations in several Russian regions comparing with the gross tax base.

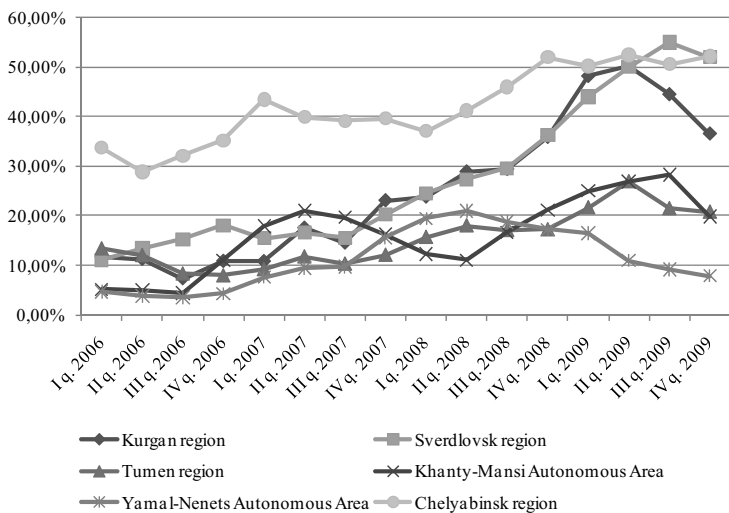


Figure 3. Dynamic of shadow activity in Russian regions (members of Ural Federal District), rate of shadow operations and gross tax base, %

The results of modeling shadow economic activity in the regions of the Ural Federal District of Russia under the influence of economic crisis are presented in the figures 4-6.

The findings show the differences in economic situation concerning shadow economy. Such territories as Kurgan region, Sverdlovsk region, Yamal-Nenets Autonomous Area are characterized as territories with big shadow sector of economy, which rapidly grew during the world crisis and is dropping down in the

period of economic stabilization. Still it is hardly probable that the volume of shadow operations will fall below the precrisis level.

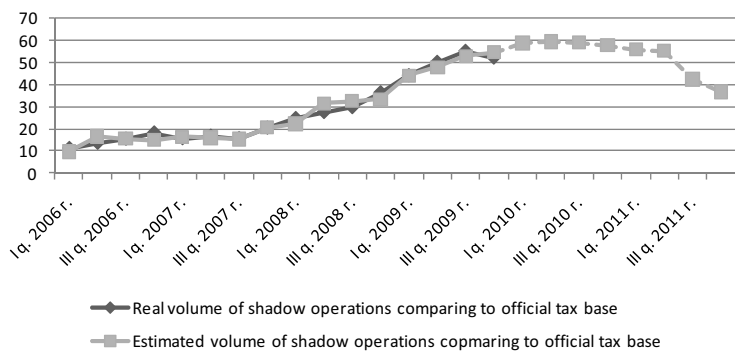


Figure 4. Comparison of real and estimated by the model volume of shadow operations comparing to the official tax base (Sverdlovsk region), %

Other regions of the Ural Federal District have another scenario. Tumen region, Chelyabinsk region and Khanty-Mansi Autonomous Area are likely to save the current position. The most severe situation is in Khanty-Mansi Autonomous Area. This region will probably suffer from the further growth of shadow economy.

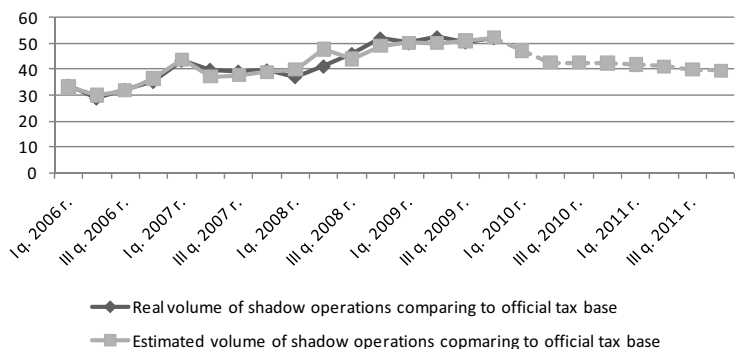


Figure 5. Comparison of real and estimated by the model volume of shadow operations comparing to the official tax base (Chelyabinsk region), %

Chelyabinsk region has the most stable situation among all regions of the Ural Federal District. After beginning of the world economic crisis Chelyabinsk

region experienced small increase of shadow activity: from 40% to 50% of the official tax base. However, this region had the biggest volume of shadow operations comparing with other regions before the world economic crisis.

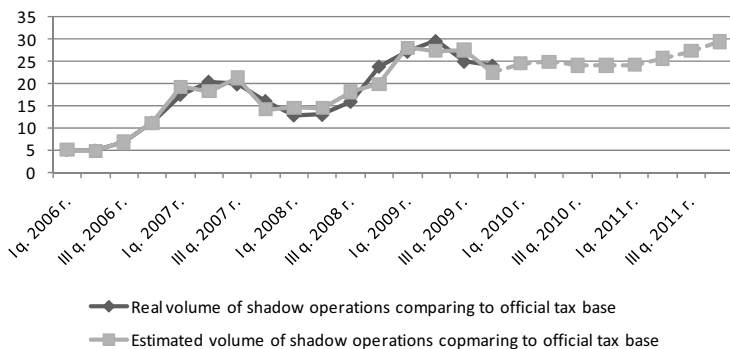


Figure 6. Comparison of real and estimated by the model volume of shadow operations comparing to the official tax base (Khanty-Mansi Autonomous Area), %

CONCLUSION

Thus the result of the research is the econometric model which was used for the predicting shadow economic activity under the influence of the world economic crisis. The forecast was made for the regions of the Ural Federal District till 2011.

Findings show significant differences in the dynamic of the shadow economy with regard to considered territories. Such regions as Kurgan region, Sverdlovsk region and Yamal-Nenets Autonomous Area are predicted to have decrease in shadow activity down to precrisis level, while Chelyabinsk region, Tumen region and Khanty-Mansi Autonomous Area are likely to save present position till the end of 2011.

The econometric model of shadow economy is of practical interest for short-time and medium-time forecasting, for improvement of social and economic state policy and for developing of the measure directed to counteracting to a negative influence of the shadow economy on the economic complex of region.

REFERENCES

- Ryabushkin, B.T. (2003). Methods of estimating shadow and informal sectors of economy, Finances and statistics, Moscow.
- Kuklin A.A., Dyagtereva, A.N. (2005). Economic paradoxes or paradoxical economy?, Economics, Moscow.

Classification and Moral Evaluation of Uncertainties in Engineering Modeling

C. Murphy¹, P. Gardoni² and C.E. Harris, Jr.³

¹Department of Philosophy, Texas A&M University, 4237 TAMU, College Station, TX 77843-4237; PH (979) 862-4856; FAX (979) 845-0458; email: cmmurphy@philosophy.tamu.edu

²Zachry Department of Civil Engineering, Texas A&M University, 3136 TAMU, College Station, TX 77843-3136; PH (979) 845-4340; FAX (979) 845-6156; email: pgardoni@civil.tamu.edu

³Department of Philosophy, Texas A&M University, 4237 TAMU, College Station, TX 77843-4237; PH (979) 845-5697; FAX (979) 845-0458; email: e-harris@philosophy.tamu.edu

ABSTRACT

Engineers must deal with risks and uncertainties as a part of their professional work and, in particular, uncertainties are inherent to engineering models. Models play a central role in engineering. Models often represent an abstract and idealized version of the mathematical properties of a target. Using models, engineers can investigate and acquire understanding of how an object or phenomenon will perform under specified conditions. This paper defines the different stages of the modeling process in engineering, classifies the various sources of uncertainty that arise in the each stage, and discusses the categories into which these uncertainties fall. The paper then considers the way uncertainty and modeling are approached in science, in order to highlight the very different criteria appropriate for the development of models and the treatment of the inherent uncertainties in engineering. Finally, the paper puts forward nine guidelines for the treatment of uncertainty in engineering modeling.

INTRODUCTION

Dealing with risk and uncertainty is an important part of the professional work of engineers. Uncertainties are involved in understanding the natural world and in knowing the performance of engineering works. Such uncertainties produce risk. In the standard account risk is the product of a set of possible consequences and their associated probabilities of occurrence (Kaplan and Garrick, 1981), where the probabilities quantify the likelihood of occurrence of the potential consequences in light of the underlying uncertainties.

One important use of models in engineering risk analysis is to quantify the likelihood or probability of the occurrence of specific events or a set of consequences. This paper focuses on the classification and moral evaluation of the various sources of the uncertainties that underlie the modeling process in engineering. While an extensive literature exists on the evaluation, including the moral evaluation, of risk, little attention has been paid to the evaluation of the various kinds of uncertainties and, consequent to that evaluation, the determination of the proper response by engineers to them.

There are five sections in this paper. The first provides a brief description of the role of modeling in engineering. The second identifies three stages in engineering modeling and the types of uncertainty associated with each stage. The third and

fourth sections discuss the different goals of science and engineering, a contrast which is especially important for this discussion. We proceed to a consideration of the ways this general contrast plays out with regard to risk, uncertainty, and the use of models. The fifth section articulates criteria for evaluating the uncertainties faced by engineers, drawing on our account of the distinctive function of engineering.

MODELING IN ENGINEERING

Models play a central role in engineering. Engineers Armen Der Kiureghian and Ove Ditlevsen (2009) write: “Engineering problems, including reliability, risk and decision problems, without exception, are solved within the confines of a model.” Using models, engineers can investigate and acquire understanding of how an object or phenomena will perform under specified conditions. Models are often used by engineers to predict the performance of products. Computer simulations are often used to derive results from mathematical equations or solve equations, especially in cases where models are dynamic, or evolving over time, or to solve optimization problems. For example, Monte Carlo simulations might be used to estimate the probability of occurrence of a specified event by repeating the same simulation a number of times using randomly generated values for the input random variables.

UNCERTAINTY IN ENGINEERING MODELING

It is generally recognized that there are uncertainties inherent in the modeling process. However, there exists no systematic account of the specific kinds of uncertainty that arise in the various stages of modeling. We argue in this section that there are three main stages in which uncertainty must be treated in modeling: (1) development of a model, (2) application or implementation of a model, and (3) analysis of the results of a model. Below we identify and discuss the specific kinds of uncertainty associated with each stage of modeling, drawing on the categories of uncertainty found in Gardoni et al. (2002) and Hansson (2006).

Uncertainty in Developing a Model. The uncertainties in developing a model are:

- ***Model Inexactness:*** This type of uncertainty arises when approximations are introduced in the formulation of a model. There are two essential problems that may arise: error in the form of the model, and missing variables.
- ***Mistaken Assumptions:*** Models are based on a set of assumptions. Uncertainties might be associated with the validity of such assumptions.
- ***Measurement Error:*** The parameters in a model are typically calibrated using a sample of the measured quantities of interest and the basic variables considered in the model. These observed values, however, could be inexact due to errors in the measurement devices or procedures, which then leads to errors in the calibration process.
- ***Statistical Uncertainty:*** Statistical uncertainty arises from the sparseness of data used to calibrate a model. In particular, the accuracy of one’s inferences depends on the observation sample size. The smaller the sample size, the larger is the uncertainty in the estimated values of the parameters.

Uncertainty in Applying or Implementing a Model. Once a model has been developed, uncertainties surround the application or implementation of the model. Such uncertainties include:

- **Randomness in the Basic Variables:** This type of uncertainty reflects the variability or randomness in the basic variables used as inputs in the developed model.
- **Volitional Uncertainty:** This type of uncertainty is associated with the choices or decisions made in light of the developed probabilistic models and their outcomes.
- **Human Error:** This type of uncertainty is associated with errors in the application of a model by human beings, e.g., using a model in a non-applicable area or range, incorrectly applying a model in an applicable area or range, illegitimate manipulating a model or data, or forcing a model to have a required outcome.

Uncertainty in the Results of a Model. There are two different kinds of uncertainties that surround the results of a model:

- **Endoxastic uncertainty:** This type of uncertainty is inherent in the results of a model and affects our confidence in them. It is generated by all the uncertainties described earlier when discussing the uncertainties in the development and application of a model.
- **Metadoxastic uncertainty:** This uncertainty concerns the degree of confidence we should have in a model itself or the choice between alternative models. As Hansson (2006) notes, in practice, attention is paid only to the most credible risk assessment and “other possible assessments with lower but non-negligible credibility will have no influence on the calculations.”

Aleatory Uncertainties vs. Epistemic Uncertainties. In the context of modeling, the different uncertainties described above can each be characterized as either aleatory uncertainties (from the Latin word *alea*, the rolling of a dice), or epistemic uncertainties (from the Greek word *πιστήμη* (*episteme*), knowledge) (Gardoni et al. 2002, Der Kiureghian and Ditlevsen 2009). The difference between the two types of uncertainties is that aleatory uncertainties are irreducible, whereas epistemic uncertainties are reducible, e.g., by the use of improved models, the acquisition of more accurate measurements and the collection of larger samples. Aleatory uncertainties arise from the inherently uncertain or random character of nature. They are thus not influenced by the observer or manner of observation, and as such they cannot be reduced by improving the observation method or protocol. By contrast, epistemic uncertainties often arise from a lack of knowledge, a deliberate choice to simplify matters, errors that arise in measuring observations, and the finite size of observation samples.

The division between aleatory and epistemic uncertainties plays an important role in engineering modeling and is often drawn in a context-dependent manner. Depending on the knowledge engineers take into consideration in a particular case and other pragmatic considerations, a given uncertainty may be described as either aleatory or epistemic. To illustrate, if the design of a safe structure does not depend on state-of-the-art scientific knowledge, and classical mechanics is sufficient to capture the underlying physics of a problem, without using the more recent theory of relativity, the factors not captured by classical mechanics might be considered as aleatory uncertainties in this engineering application.

One important question concerns the basis on which engineers should draw the line between aleatory and epistemic uncertainties in any given case. Furthermore, there is a question of the basis on which we should decide whether efforts should be

undertaken to reduce epistemic uncertainties. The answers to these questions, we argue later in the paper, depend on understanding the goal of engineering in a society and how a given uncertainty impacts the ability of engineers to achieve this goal. Our discussion of the goal of engineering begins first with an analysis of science and the goal of science, which will provide a helpful contrast for understanding the goal of engineering.

THE DISCIPLINE OF SCIENCE

In order to get a better grasp on the unique features of engineering, it will be useful to look first at the sciences. A good scientific theory enhances understanding of the world. Abandoning scientific realism and assuming a more pragmatic attitude, we can say that scientific understanding is the ability to explain natural phenomena, in the sense of predict and control them. Explanation is the ability to predict, and prediction is made in terms of laws and initial conditions. An ideal scientific explanation must be fruitful in suggesting other explanations, as the theory of natural selection has proven to be. The broader the scope of a theory, i.e. the more natural phenomena it can cover, the more desirable the theory or type of explanation is. If an explanation is consistent with other theories and types of explanation, it is more acceptable. Finally, the criterion of “simplicity” has often been cited, although the term is difficult to define (Baker 2010).

Modeling in Science. Models play a central role in scientific practice (Morgan and Morrison 1999), providing instruments for “experimentation, measurement, and theory development” (Gould 2003). Learning through models involves constructing a representation relation between the model and target, investigating dimensions of the model to demonstrate certain theoretical claims about it, and converting these claims into claims about the target system.

Uncertainty in Scientific Modeling. Models contribute to our understanding of a new fact or enhancing the accuracy of scientific predictions. In science, aleatory uncertainties refer to those uncertainties inherent in nature. Epistemic uncertainties are not inherent in nature, but rather stem from our lack of knowledge or certainty about, for example, the accurateness of our model. Given that the goal of the scientific enterprise is understanding, any epistemic uncertainty should be reduced. The presence of epistemic uncertainties calls into question the claim to have acquired a new fact, or to have increased the accuracy of scientific predictions.

THE DISCIPLINE OF ENGINEERING

In contrast to science, the aim of engineering is not understanding nature for its own sake, but the creation of artifacts and technology. Inventions such as the pulley, level, and wheel are examples of engineering artifacts. The pyramids of Egypt and the roads and aqueducts built by the Romans are examples of technology. Engineers draw on a variety of sources to devise possible solutions, including science, and they are often inspired by nature. Indeed, a central feature of modern engineering is the application of mathematics and modern (post-Galilean) science (especially physics) to make useful objects.

One could say that engineering is applied science, and this definition has considerable merit, but it obscures the fact that engineering has unique features that differentiate it from science. First, engineering is goal-specific and aims at the

fulfillment of a purpose that often has a local or specific character: constructing a particular bridge, developing a particular chemical process, developing a new headlamp for an automobile, developing a new composite, and so forth.

Second, unlike scientific theories and explanations, past technologies are not “refuted” and may exist alongside newer ones if they continue to satisfy some human need. A technologically unsophisticated plow may be more useful in developing countries because it may be easier to use, more easily repaired by the local population, and produced more cheaply. Even though sailing ships have been replaced in commerce, they are still useful for teaching the skills of navigation and for recreation. Some technologies have, however, been abandoned or fallen into disuse in favor of others. The history of the progression from sailing ships to steamships, to diesel-powered ships, to atomic-powered ships is an interesting example.

Third, engineering resolves the underdetermination problem with quite different criteria than the ones appropriate in science. If scientific theories are underdetermined by the facts, engineering problems are underdetermined in that there can usually be more than one solution to an engineering problem. This is because there is no unique criterion by which to decide what counts as the best solution to a given problem, which makes it difficult to rank alternative solutions, and the solution space is often not well-defined, which makes it difficult to account for all possible solutions when selecting the solution to pursue. To use terminology from mathematics, engineering problems are ill-conditioned; that is, there is more than one solution in part because not all inputs are known. Criteria for good engineering design, or external constraints, help limit the possible number of engineering solutions. These include availability of resources; the cost-effectiveness of the design; ease of manufacture, construction and repair; safety; environmental impact and sustainability; elegance and aesthetic appeal; and others.

Values and norms are implicit or even explicit in many of the design criteria used by engineers. To illustrate, the determination of the appropriate ratio between cost and function must take into account the value of the engineering work to society and the ease of manufacture. Safety is often given an overriding importance, setting the parameters within which choices about cost and function can be made (Moller et al. 2006; Macpherson 2008). The goals to be achieved by the structure or product are suffused with moral and social considerations. Marketability is in part a function of the desire of consumers for a product. Elegance and aesthetic appeal are clearly value considerations. Considerations of environmental impact and sustainability reflect societal values that are becoming more important. Engineers must identify, understand and interpret these value-laden constraints. In normal design, there may be a general understanding of how to apply these criteria; in radical design, the application of the criteria may not be clear or at least controversial. (van de Poel and Gorp 2006).

Treatment of Uncertainty in Engineering. We noted earlier that given that the central goal of the scientific enterprise, there is always reason to reduce epistemic uncertainty in scientific models. The very presence of epistemic uncertainties calls into question the claim to have succeeded in furthering the goal of science. However, the same treatment of uncertainty, including epistemic uncertainty, is not required in engineering. In contrast with science, the central goal of engineering is not

understanding for its own sake, but rather the creation, modification, and invention of useful artifacts and technology that both satisfy the societal needs to which they are designed to respond and respect central societal constraints. Given this goal, the question then becomes: how should uncertainty be treated in engineering modeling? Below we develop a set of guidelines for the treatment of uncertainty in engineering modeling, which are designed to promote the central goal of engineering.

In our view, the starting point for any set of guidelines must be recognition of the fact that uncertainty is inherent in the engineering enterprise. Innovation and invention are central to the drive in engineering to create useful objects for communities. By their nature, innovation and invention are uncertain, carrying unforeseen consequences and risks. In our view, if engineers were required to avoid uncertainties at all cost, we would undermine the capacity of engineers to be innovative and inventive, and, ultimately, we would severely limit the ability of engineers to fulfill their role in society. Accepting some degree of uncertainty is necessary to realize the aspiration for innovation and invention. However, recognizing the need to accept at least some uncertainties does not give engineers complete freedom in creating new technologies regardless of the associated uncertainties and risk. That is, the inventive and innovative character of engineering does not entail that all uncertainty must be accepted. We believe engineers must innovate in a responsible manner. Below we spell out what constitutes the appropriate way for engineers to deal with uncertainties.

The first guideline is that engineers acknowledge the uncertainty inherent in their work. While this guideline might seem obvious, this is not a trivial point in practice. Engineers far too often only consider point estimates of the model inputs or outcomes that either ignore or do not explicitly account for the uncertainties in the inputs or outcomes. However, by not explicitly accounting for the uncertainties, it might be difficult to assess the actual risk, which requires knowing the actual capacity and the likely departure from it. So, engineers should explicitly account for the underlying uncertainties in their work. Acknowledging uncertainty is a precondition for making principled and well-educated decisions about how to treat uncertainties and about the acceptability of risks.

The second guideline is that engineers evaluate the necessity or importance of innovation and invention in any particular case. If there is no societal need for or value in, for example, a new technology or a newly designed artifact (e.g., in terms of reduced costs, longer reliability, or higher safety), then putting forward a new technology or design might not be justified. A new technology or design will carry new uncertainties. In this case, using more familiar technologies and normal designs might be preferable.

For those cases where innovation is judged important or necessary, engineers must then evaluate the associated new uncertainties as acceptable or not. The third guideline is that engineers must determine whether such uncertainties are aleatory or epistemic. The division between aleatory and epistemic uncertainty reflects the distinction between reducible and non-reducible uncertainties. As we noted earlier, judgment is involved in drawing the line between epistemic and aleatory uncertainties. The external constraints informing engineering problems should influence where the boundary between aleatory and epistemic uncertainties is drawn.

Aleatory uncertainties, such as randomness in the basic variables, are those that cannot be reduced by a modeler or the manner of modeling. Thus the choice an engineer faces is either to accept or reject such uncertainties, along with the technologies that create such uncertainties. The fourth guideline is that engineers evaluate the acceptability of aleatory uncertainties on the basis of the acceptability of the risks associated with them.

The fifth guideline is similar to the fourth but it applies to the epistemic uncertainties. In this case, the decision to accept (in full or in a reduced form) or reject such uncertainties should be based on the comparison of the potential costs and benefits associated with accepting optimally reduced uncertainties against the potential costs and benefits of not accepting them. The optimal reduction of epistemic uncertainties should be based on the maximization of the associated benefits computed as the benefits brought by the new technology and as a result of the reduced uncertainties discounted by the resources invested to reduce such uncertainties. In such discounting exercise, the engineer should also properly weight the potential benefits by their associated probabilities. Furthermore, there is uncertainty surrounding any estimation of costs and benefits; it is necessary to decide how to factor in the surrounding uncertainty when conducting or acting on the basis of a cost-benefit analysis.

It should be noted that when deciding whether to reduce a given epistemic uncertainty, engineers should consider the influence that such uncertainty has on the success of a solution to a given engineering problem and the successful protection of the public welfare. The more influence an epistemic uncertainty has on such successes, the greater the obligation to take steps to reduce it.

It may be necessary in some cases to prioritize the reduction of those epistemic uncertainties that are judged to have an important impact on the successful solution of an engineering problem and the protection of the public welfare. The sixth guideline is that engineers make such prioritization based on two factors: the size of the different kinds of uncertainties and the relationship between a given uncertainty and external constraints. Holding importance constant, a greater uncertainty should be prioritized over a smaller uncertainty.

The seventh guideline concerns metadoxastic uncertainties. Engineers must strive to keep up with scientific discoveries, as an additional potential resource for reducing the metadoxastic uncertainties surrounding the results of a model. Furthermore, a method for accounting for metadoxastic uncertainties should be developed. One method for accounting for metadoxastic uncertainty could be to specify the degree of confidence in a particular analysis linguistically. That is, we could have categories of assessments of which we are, for example, "highly confident," "confident," or "less confident." The basis for specifying confidence levels could be our general understanding of the problem, based on the comprehensiveness of both the models and the endodoxastic uncertainties accounted for in the analysis. The more comprehensive our knowledge, the more confidence we should have in the accuracy of the assessment.

The eighth guideline is that engineers should communicate to the public, in particular the portion of the public that will be exposed to the risks associated to the uncertainties, and to policy makers that there is uncertainty surrounding their work.

Communication helps ensure public scrutiny, transparency, completeness and fairness in the analysis and modeling.

The ninth and final guideline is that engineers continue to monitor their projects, in full recognition that the project's success remains uncertain. Engineers should be attentive to the possibility of unforeseen problems and consequences arising and modify their design in ways that account for increased knowledge (Wetmore 2008).

It is valuable and important for engineers to incorporate these guidelines in their research and practice. First, there are predictable negative consequences that arise from the failure to consider and respond effectively to uncertainty. Engineers may fail to actually satisfy the societal needs that drive the modeling process, because their analysis is inaccurate, or engineers may waste or misallocate resources or undermine safety by not taking uncertainty into account in a responsible and appropriate manner. Second, appreciating the uncertainty surrounding engineering modeling is important to ensure that the public forms reasonable expectations regarding the risks associated with new technology and engineering products and reasonable expectations regarding what we can demand of engineers in their work.

CONCLUSION

Risk and uncertainty, especially uncertainty inherent to engineering modeling, are a central part of engineering work. We have offered a classification of the types of uncertainty in developing, applying and interpreting models generally and discussed some of the differences between science and engineering. Finally, we have considered some of the special problems associated with uncertainty in engineering modeling and suggested nine guidelines for dealing with uncertainty in engineering, especially with regard to modeling. These guidelines are developed based on the central goal of engineering and the nature of different types of uncertainties in modeling.

REFERENCES

- Baker, A. (2010). Simplicity. Stanford Encyclopedia of Philosophy. <http://plato.stanford.edu/entries/simplicity/>. Accessed 11 June 2010.
- Der Kiureghian, A., and Ditlevsen, O., (2009). "Aleatory or epistemic? Does it matter?" *Structural Safety*, 31(2), 105-112.
- Gardoni, P., Der Kiureghian, A., Mosalam, K.M., (2002). "Probabilistic capacity models and fragility estimates for RC columns based on experimental observations," *ASCE Journal of Engineering Mechanics*, 128(10), 1024-1038
- Hansson, S.V. (2006). Economic (Ir)rationality in Risk Analysis. *Economics and Philosophy*, 22, 231-241.
- Kaplan, S., and Gerrick, B.J. (1981). On the quantitative definition of risk. *Risk Analysis*, 1, 11-27.
- Macpherson, J.A.E. (2008). Safety, Risk Acceptability, and Morality. *Science and Engineering Ethics* 14(3), 377-390.
- Moller, N., Hansson, S.O., and Peterson, M. (2006). Safety is more than the antonym of risk. *Journal of Applied Philosophy*, 23(4), 419-432.
- Morgan, M., and Morrison, M. (1999). *Models as Mediators: Perspectives on Natural and Social Science*. New York: Cambridge University Press.
- van de Poel, I., and Gorp, A.C. (2006). The Need for Ethical Reflection in Engineering Design: The Relevance of Type of Design and Design Hierarchy. *Science, Technology, & Human Values*, 31(3), 333-360.
- Wetmore, J.M. (2008). Engineering with Uncertainty: Monitoring Air Bag Performance. *Science and Engineering Ethics*, 14, 201-218.

Making urban territories more resilient to flooding by improving the resilience of their waste management network. A methodology for analysing dysfunctions in waste management networks during and after flooding.

Hélène BERAUD¹, Bruno BARROCA¹, Damien SERRE², Gilles HUBERT¹

¹ *Université Paris Est – Marne la Vallée, LEESU UMR MA 102*

² *EIVP (École des Ingénieurs de la Ville de Paris)*

In view of all the damage caused by flooding that has affected large numbers of regions throughout the world over the last ten years, urban areas appear to be little prepared for facing up to this type of catastrophe. Today, improving their resilience, i.e. their capacity to recover rapidly after flooding, appears to be a real issue at stake in societies' sustainable development.

Due to their organization in the form of subsystems¹, the multiple aspects of their functions and the dynamics that drive them, these urban territories must be considered as complex systems². Within these urban systems, technical networks³ are physical links between inhabitants and the actors involved, the symbolic links of belonging to the same community, to the same organized territory (Lacoste quoted by Dupuy, 1991). As supports and even objects of interactions between the different sub-systems in the urban system and with the outside environment, they supply, unify and irrigate all the constituent elements of urban territories. In this way, networks participate in organizing and regulating the system by being the vector of relations between its different constituent elements. "Physically connecting the elements in the system unifies them and creates the network's operating conditions at the same time. In the same way, it makes a certain mode of operation and evolutions in the system possible" (Dupuy, 1984). This strategic position makes networks extremely influent in the dynamics of maintaining the global urban system. In turn, they can be generators of incidents by interrupting flows or vectors in the propagation of unforeseen turns of events. Therefore, characterizing their resilience to flooding may prove to be interesting in for providing a better understanding of urban resilience.

In this context, we have decided to work on the resilience of waste management networks. Because they raise essential questions on sanitation and public health and because they often have a strong visual and psychological impact, these networks appear to be real issues at stake in crisis management. After flooding, the volume of waste generated is often significant and of a different sort (mixed, even polluted wet waste). Faced with this situation, waste management poses a real problem. What should be done with this waste? How should it be collected? Where can it be stored? How should it be processed? Who is in charge? Providing answers to these questions is all

¹ Sub-systems are internal components in a system.

² A complex system can be defined as "an object, which, in a given environment, endowed with given aims, exercises an activity and sees its structure develop as time goes by without it losing its one and only identity" (Le Moigne 1977). In this article, the term "system" is always to be understood in the sense of a complex system.

³ In this article, the term network is understood in the sense of an urban technical network as defined by Gabriel Dupuy in "Urban planning for networks: Theories and methods", i.e. meshing that supports a service.

the more strategic inasmuch as post-flood waste is the visual sign of the catastrophe. As a result, cleaning up is populations' and local actors' first reflex in order to forget what has happened, but also in order to start up again as quickly as possible. Therefore, it would appear primordial to improve waste management networks' resilience to flooding (Beraud *et al.*, 2010).

First and foremost, improving the resilience of an organization requires understanding the way it operates in order to identify what dysfunctions it may contain. A methodology needs to be developed for this purpose, capable of analyzing a waste management network's way of operation under normal and crisis conditions. In this way, risks and potential dangers resulting from the urban system being flooded can be identified and the means of prevention for improving the waste management network's resilience to flooding can be brought out.

Choosing the right methodology is not an easy task. Numerous methods of risk analysis exist. For the most part they are of industrial origin. As a result, it is not always easy to use them for studying social systems such as urban technical networks, as these systems possess characteristics that differ considerably from industrial systems. "Multiple responsibilities with regard to the design, build, operation and maintenance of networks, separated amongst numerous actors who do not regularly communicate together and share information" are, for example, one of the particularities of risk control in an urban environment (Prost, in Blancher, 1998). As a result, the way in which networks operate may appear to be extremely complex: the diversity and involvement of actors, different scales and territories to be taken into account, the issues at stake concerning the public service mission, catastrophic consequences, that are immediate and those with important repercussions when they are interrupted, etc. This complexity makes it extremely difficult to model urban networks (Maiolini, 1992), whereas applying methods used in the world of industry requires that models are created beforehand. Therefore, there are real methodology stakes in play when transferring these methods from industrial engineering to urban engineering.

This article will present the methodology set up followed by initial results.

I. DEFINITION OF A METHODOLOGY FOR ANALYZING A WASTE MANAGEMENT NETWORK

Our aim is to determine the impact of flooding on waste management networks⁴. Therefore, first and foremost we must understand the way in which these networks operate in order to highlight their dysfunctions. As a result, in this article we will limit our analysis to waste management processes: from collecting, to processing and upgrading. Therefore waste production is not included: this is considered as being a system adjustment or modification variable that may disrupt the system's way of operation.

⁴ This analysis takes account of all types of waste (company, household and agricultural waste, etc.).

A. From systematic modelling to functional analysis: a study of the way in which waste management networks operate

Studying the way a waste management network operates requires for it be considered as a complex system. It is, in fact, an object formed by elements or sub-systems organized for one purpose, an ultimate goal (“managing waste”), and which are in constant interrelation between each other and with the outside environment (the urban system, the wider environment). With this systemic conception of a waste management network not only a global analysis of the object can be made, highlighting the interdependencies and interrelations that structure it, but evolutions, and dynamics that model the network, can also be thought out.

Understanding how a system operates requires for its structure, its environment and its functions⁵ to be analysed, as well as its operating conditions (Villemeur, 1988). This is all made possible by the use of a functional analysis. This method “enables us to understand the way in which the system under study operates and to make a synthetic description of it: it (the method) defines its limits, its environment and its structure and it discovers the functions that are provided” (Peyras, 2002). As such, using this method enables the principles of operation of the waste management system to be established and its mechanisms to be determined.

Several methods of functional analysis exist. We have decided to use the APTE method (Application aux Techniques d’Entreprise) frequently used for analyzing organizations. It has the advantage of making a functional analysis - a description of the functions fulfilled by the system - together with a morphological analysis - a description of the system (components, environment and relations).

The APTE method is carried out in two phases:

- An external functional analysis shows why the system exists, it shows what purpose it serves and it clearly reveals its main functions, i.e. the functions for which the system was created;
- An internal functional analysis enables the internal operation of the system to be understood (the morphological analysis) and it reveals the functions that enable the system to attain its objectives.

This method is based on the use of two tools: the functional block diagram and the functional analysis chart (Peyras, 2002). The first tool is a representation of the system, its outside environments and the interactions that irrigate it. The second tool results from the block diagram. It presents the system’s different functions.

The analysis of the way in which the waste management network operates will be carried out for each crisis phase: in the pre-crisis period⁶, in the crisis period⁷, and in the post-crisis period⁸. This will show how functions evolve due to flooding.

Once this operation has been carried out, any potential dysfunctions in the network will become apparent.

⁵ In this case the term function is defined in the sense of standard NF X50-150, i.e. the action of a product or one of its constituents expressed in terms of its final purpose.

⁶ Pre-crisis: flooding is announced, but water-levels have not risen yet.

⁷ Crisis: flooding has arrived.

⁸ Post-crisis: flood levels have dropped, but the region’s operating system has not returned to normal as yet.

B. Revealing dysfunctions in a waste management network

The study of potential dysfunctions in the waste management system will be carried out with the help of the FMECA method (Failure Modes, Effects and Criticality analysis), which is one of the operational safety methods most used in industry and, over the past few years, in civil engineering. An inductive method for analyzing potential failures in a system, it is generally carried out in three main phases: (1) Breaking down the system by means of a functional analysis, (2) Identifying failure modes⁹, (3) Describing the effects of the failure modes that have appeared in the system. Then, a preventive action strategy can be defined to enable the waste management system to maintain active during crisis and post-crisis periods.

In an 'operational safety' approach, this method generally covers three stages carried out one after the other: the product FMECA, whose objective is to check that the system carries out its functions correctly in the operating phase; the process FMECA that examines whether the product obtained is compliant with what is produced; and the resource FMECA which investigates the resources needing to be implemented (Peyras, 2002). These phases will not all be required for our case study. As we only wish to identify potential dysfunctions in the waste management network during flooding, our analysis will only cover its operating cycle. For this reason, we will only be applying the product FMECA.

Our initial results are described below. They concern the functional analysis of the waste management network.

II. INITIAL RESULTS: FUNCTIONAL ANALYSIS OF THE WASTE MANAGEMENT NETWORK

A. Structural analysis of the waste management network

As we have defined above, we are limiting our study to cover solely the management processes that correspond to the domains belonging to the different system processes. The waste management network is, in fact, composed of a "Waste management process" system which is broken down into five sub-systems that correspond to the five stages in waste management: Collecting, storing, transporting, treating and upgrading. This process system is related to elements from the outside environment through which and for which it exists: waste, producers of waste, the society, rule-making authorities (*State, European Community, State decentralized services, etc.*), organizing authorities (*Territorial communities, producer associations, etc.*), sensitive environments (*water, soil, air, biodiversity, etc.*), aggressive environments (*natural catastrophes, bad weather, climate change, etc.*), networks, companies that use secondary raw materials and the world market.

B. External functional analysis

On the basis of this description of the system, we must then define why the system exists. To do this, its main functions and its constraint functions need to be defined.

⁹ Failure mode: The way in which the failure appears

Main functions (MF) correspond to the relations created by the organization between certain of its constituent elements and the outside environment. They express the system's purpose. As for constraint functions (CF) they express the requirements of an element from outside the system made on the system itself.

These functions will be defined by studying the relations that exist between the system and outside constituents. The diagram below presents these relations.

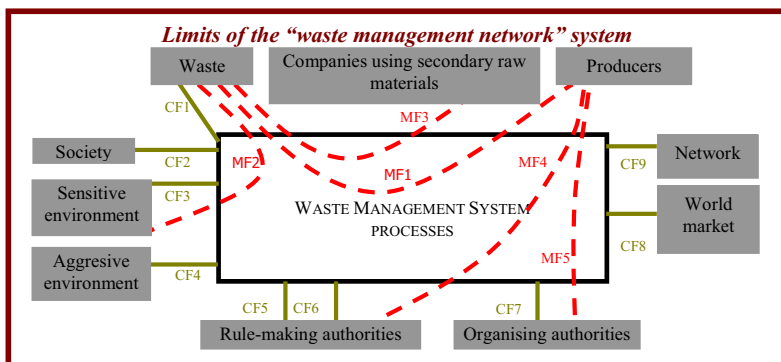


Figure 1: External functional block diagram of the "waste management network" system

Five main functions and nine constraint functions have been defined. However, these functions may be brought together under three denominations that correspond to the major missions of a waste management process.

1. Managing waste in a way adapted to the type of flow (*MF1: Managing waste generated by producers, MF3: Upgrading waste in the form of new products or new raw materials, MF5: Enabling the organizing authority to make waste producers pay for treating their waste, CF2: Meeting society's expectations in terms of sanitation, health and safety, CF6: Meeting control organization requirements, CF7: Being remunerated by the organizing authority, CF8: Taking account of world market evolutions for choosing the system process, CF9: Operating by means of infrastructures and networks*),
2. Limiting impacts on the environment (*MF2: Limiting effects of waste on the environment, MF4: Inciting producers to reduce the waste they generate by means of different standardization and rule-making tools, MF5: Enabling the organizing authority to make producers of waste pay for waste-treatment, CF3: Respecting sensitive environment and reducing pollution of water, earth and air in view of regulations in force, CF5: Complying with regulations, CF6: Meeting control organization requirements*),
3. Maintaining waste management in operation (continuity of service, obligations in terms of sanitation and public safety) (*CF2: Meeting society's expectations in terms of sanitation, health and safety, CF4: Inciting producers to reduce the waste they generate by means of different standardization and rule-making tools*).

These three missions are the reasons why waste management system processes, and therefore whole networks, exist. For this reason, the way the latter operates internally must enable these main missions to be carried out successfully.

C. Internal functional analysis

Characterisation of the internal operation of a waste management network necessitates defining the role of every component inside the system i.e. determining the different

relations that connect the components in the system to each other and to the outside environment. These different relations define the so-called design functions that enable the system to execute the missions for which it was created. The diagram below represents these relations.

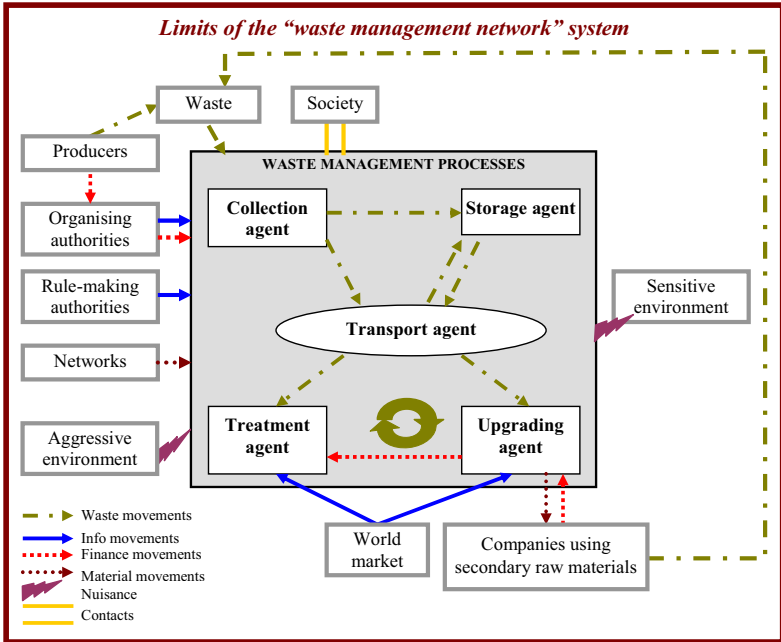


Figure 2: Internal functional block diagram of the “waste management network” system.

This work on defining relations and then defining functions, was carried out in normal operating periods and in flood periods. The following table is an extract of the results that we obtained. It presents the functions carried out by the collecting agent to meet the three main missions of the global system (managing waste, limiting impacts on the environment and maintaining activity) in normal operating and flood conditions.

Table 1: Extract of the internal functional analysis table: Collection agent analysis

MAIN MISSIONS	DESIGN FUNCTIONS NORMAL CONDITIONS	DESIGN FUNCTIONS FLOOD CONDITIONS		
		PRE-CRISIS	CRISIS	POST-CRISIS
WASTE MANAGEMENT	Collecting waste	Collecting waste	Collecting waste in the flooded zone	Collecting normal waste and post-flood waste
	Centralising waste before transport to the point of treatment	Centralising waste before transport to its point of treatment	Centralising waste before transport to its point of treatment	Centralising waste before transport to its point of treatment
	Receiving remuneration for services provided			

	Defining collection rounds depending on waste flows	Anticipating evolutions in waste movement with the arrival of flooding	Reorganising collection rounds	Reorganising collection rounds depending on new missions to be carried out.
			Facing up to possible breaks in networks	Managing evolutions in waste flows
			Managing evolutions in waste movements	Informing on post-flood waste collection conditions
LIMITING IMPACTS ON THE ENVIRONMENT	Complying with regulations	Complying with regulations	Complying with regulations	Complying with regulations
	Quantifying waste collected and invoicing it to producers	Quantifying waste collected and invoicing it to producers	Quantifying waste collected and invoicing it to producers	Quantifying waste collected and invoicing it to producers
				Cleaning zones impacted by flooding as rapidly as possible.
				Remaining in contact with services in charge of health control
CONTINUING TO MANAGE WASTE	Honouring commitments to maintain activities	Reorganising rounds	Remaining in contact with the different partners in waste management during evolutions in the crisis situation.	Remaining in contact with treatment and transport organisations that will have to take action afterwards.
	Remaining in regular contact with partners, organising / regulating authorities so as to maintain activities.	Informing producers in flood areas on the actions to take for reducing post-flood waste	Keeping the organising authority informed of evolutions in activity.	Keeping the organising authority informed of evolutions in activity.
		Keeping the organising authority informed of changes in activity.		

The work on analysing the way in which the waste management network operates, presented here via the waste collection agent, highlights the large number of functions that elements in the system need to carry out so that the system can fulfil its three main missions (managing waste, limiting impacts on the environment and maintaining services), at the three different periods in the crisis. It must be remembered that, when there is a flood, the actors involved must deal with new missions. As a result, as soon as a rise in water levels is announced, the collection agent must slightly modify the way it operates in order to take account of the forthcoming flood. It must be remembered that the agent's duties to maintain public services oblige it to pursue its missions during crisis and post-crisis periods. Therefore, it has to anticipate and prevent dysfunctions. During flood periods, if waste collection is stopped for flood areas, it is maintained outside flood areas. It is for this reason that the collection agent's missions are

modified. In the post-crisis period, the collection agent must also handle new missions that have appeared with the production of post-flood waste. Therefore, solutions must be found urgently for collecting very considerable quantities of new waste, whilst continuing to collect normal waste at the same time.

CONCLUSION

As we have demonstrated above, improving the resilience of waste management networks to flooding passes by preventing any dysfunctions in the network. To do this, an analysis must be carried out of the way in which the waste management network operates, followed by an inventory of any possible dysfunctions and their characterisation. Our research has shown that, despite the numerous adaptations required, risk analysis methods coming from industry prove to be the most suitable for studying a system as complex as a waste management network. As a result, the functional analysis method was chosen for showing how this complex system operates. Then, applying the FMECA method reveals any potential dysfunctions.

The first results presented here on the scale of sub-systems in the process system reveal the appearance of new functions during flood periods. These new functions, which are essential for enabling the system to fulfil its three main missions (managing waste, limiting impacts on the environment and maintaining services), require considerable human, technical and financial resources. This initial analysis is not sufficient for measuring these resources. It must be more detailed, on a smaller scale, i.e. within each sub-system (collection, storage, treatment, etc.) so as to be able to assess the way the system operates on a scale that can be used for applying preventive measures. The dysfunction analysis phase, which will enable us to list potential failures in the way the system operates, can then be applied on these two levels (sub-systems of the process system and components in the sub-system of the process system).

BIBLIOGRAPHY

- BERAUD H., BARROCA B., and HUBERT G. (2010), *Flood resilience urban territories Geophysical Research Abstracts*, Vol. 12, EGU2010-7875, 2010 EGU General Assembly 2010
- BLANCHER P. (Dir.) (1998), *Risques et réseaux techniques urbains*, Lyon, CERTU, 169 p.
- DUPUY G. (1984), Villes, systèmes et réseaux : le rôle historique des techniques urbaines, *Réseaux*, vol. 2, n° 4, 1984, p. 3 – 23
- DUPUY G. (1991), *L'urbanisme des réseaux : théories et méthodes*, Paris, A. Colin, 198 p.
- LE MOIGNE J.-L. (1977), *La théorie du système général. Théorie de la modélisation.*, Paris, PUF, 258 p.
- MAIOLINI J.-L. (1992), *Sûreté de fonctionnement des réseaux urbains. Deux études de cas : les réseaux d'alimentation en eau potable et les galeries techniques visitables*, Projet de fin d'études, sous la direction de OLIVIER D., ENPC, 41 p + annexes.
- PEYRAS L. (2002), *Diagnostic et analyse de risques liés au vieillissement des barrages. Développement de méthodes d'aide à l'expertise*, Thèse, sous la direction de VERGNE A., Aix-Marseille II, 199 p.
- VILLEMEUR A. (1988), *Sûreté de fonctionnement des systèmes industriels. Fiabilité - Facteurs humains – Informatisation*, Paris, Eyrolles, 795 p.

A Polynomial Chaos Approach for Uncertainty Analysis of Chloride-Induced Corrosion in Concrete Structures

B. Saassouh and Z. Lounis

National Research Council, Institute for Research in Construction, Ottawa, ON,
Canada

Bassem.Saassouh@nrc.gc.ca, Zoubir.Lounis@nrc.gc.ca,

ABSTRACT

Chloride-induced corrosion has been identified as one of the main causes of deterioration of concrete structures, such as highway bridges, etc. The development of a performance-based approach is critical to ensure adequate safety, serviceability and durability of concrete structures, built in chloride-laden environments, as well as to help identify appropriate maintenance strategies to extend their service life. This paper presents a polynomial chaos response surface approach for the probabilistic modeling of chloride-induced corrosion of carbon steel reinforcement in concrete structures that takes into account the uncertainties in the parameters that govern the physical models of chloride ingress into concrete and corrosion of carbon steel, including concrete diffusivity, concrete cover depth, surface chloride concentration and threshold chloride level for onset of corrosion. A case study of highway bridge deck was used to illustrate the applicability, accuracy and computational efficiency when compared to crude Monte Carlo simulation.

INTRODUCTION

In porous solids, such as concrete structures, chlorides can penetrate into concrete via different physical mechanisms, such as diffusion, capillary absorption, etc. which lead to the corrosion of the steel reinforcement. The corrosion of the steel reinforcement leads to concrete fracture through cracking, delamination and spalling of the concrete cover, reduction of concrete and reinforcement cross sections, loss of bond between the reinforcement and concrete, and reduction in strength and ductility. As a result, the safety, serviceability and service life of concrete structures are reduced. In the last decades, the Fickian diffusion process was used to model the chloride diffusion and the initiation time to corrosion using the concept of chloride threshold as an indicator of corrosion resistance of reinforcing steel to chloride attack. In practice, the design of durable concrete structures is mainly based on specifying a minimum concrete cover depth (depending on the environmental exposure), a maximum water-to-cement ratio (to achieve low chloride diffusivity), and as well the use of more corrosion resistant reinforcing steels. However, a considerable level of uncertainty may be associated with one or more of the above identified parameters. This is due to: (i) heterogeneity and aging of concrete with temporal and spatial

variability of its chloride diffusivity; (ii) variability of concrete cover depth, which depends on quality control, workmanship and size of structure; (iii) variability of surface chloride concentration, which depends on the severity of the environmental exposure; and (iv) uncertainty in chloride threshold level that depends on the type of reinforcing steel, type of cementing materials, test methods, etc. It is clear that the combination of these uncertainties leads to a considerable uncertainty in the model output (e.g. the time to corrosion initiation). This uncertainty in the model output could have serious consequences in terms of reduced service life, inadequate planning of maintenance and increased life cycle costs. The objective of this paper is twofold: (i) present physical models of chloride transport and corrosion of carbon steel reinforcement in concrete structures; and (ii) present a polynomial chaos approach for the probabilistic modeling of chloride-induced corrosion that takes into account the uncertainties in the parameters that govern the physical models. The proposed approach enables a modeling that represents the whole response of the system in a meta-model format, instead of the estimation of the mean, variance or the tail of the response.

CHLORIDE TRANSPORT PROBLEM

Chloride diffusion process

The main transport mechanisms of chlorides into concrete are diffusion and adsorption. However, adsorption occurs in concrete surface layers that are subjected to wetting and drying cycles, and it only affects the exposed concrete surface down to 10-20 mm (Weyers et al. 1993; Tuutti 1982). Chloride diffusion is a transfer of mass by random motion of free chloride ions in the pore solution, resulting in a net flow from regions of higher to regions of lower concentration (Crank 1975). The rate of chloride ingress is proportional to the concentration gradient and the diffusion coefficient of the concrete (Fick's first law of diffusion). Since in the field, chloride ingress occurs under transient conditions, Fick's second law of diffusion can be used to predict the time variation of chloride concentration for one-dimensional flow. It can be expressed as follows: (Crank 1975):

$$\frac{\partial C_{x,t}}{\partial t} = \frac{\partial}{\partial x} \left(D \frac{\partial C_{x,t}}{\partial x} \right)$$

where $C_{x,t}$ is the concentration of chlorides at depth x and time t ; D is the diffusion coefficient. Under the assumptions of a constant diffusion coefficient, constant surface chloride content C_s as the boundary condition, and the initial condition specified as $C=0$ for $x>0$, $t=0$, Crank's solution yields (Crank 1975):

$$C_{x,t} = C_s \left(1 - \operatorname{erf} \frac{x}{2\sqrt{Dt}} \right)$$

where $\operatorname{erf}(\cdot)$ is the error function. In the modeling of chloride ingress as Fickian process, several simplifying assumptions are made (Zhang and Lounis 2006).

Corrosion initiation

The corrosion initiation stage corresponds to the process of chloride ions (chlorides) ingress into concrete, while the steel remains passivated. The corrosion initiates when the concentration of chloride ions in contact with the steel reaches a threshold level C_{th} (Tuutti 1982) that destroys the passivation of the steel. Therefore, the duration of the initial stage, which is often used as a quantitative indicator of service life or durability of concrete structures, depends on the rate of chloride penetration in concrete. Ideally, the corrosion initiates at time \tilde{T}_t at which the concentration of chlorides at the steel level becomes equal or greater than the chloride threshold (C_{th}):

$$C_{d,\tilde{T}_t} \geq C_{th}$$

Where d represents the concrete cover depth of the steel. From this equation, the approximated initiation time to corrosion can be deduced as follows:

$$\tilde{T}_t = \frac{d^2}{4D \left[\text{erf}^{-1} \left(1 - \frac{C_{th}}{C_s} \right) \right]^2}$$

In this deterministic model, the four governing parameters are assumed as independent that are critical for corrosion protection: (i) structural parameter: concrete cover depth d ; (ii) material parameters: chloride diffusion coefficient D , which is an indicator of the rate of chloride penetration into concrete, and chloride threshold value C_{th} , which is an indicator of the corrosion resistance of reinforcing steel; and (iii) environmental parameter: surface chloride concentration C_s , which is a measure of the corrosivity or load or exposure risk of concrete structures. Given the inherent complexity and heterogeneity of concrete as a corrosion medium, there exists a large uncertainty in the above mentioned parameters and in the proposed model. In the following section, a probabilistic approach based on the polynomial chaos expansion will be used to model the uncertainties in the above four parameters.

PROBABILISTIC MODELING OF CORROSION USING POLYNOMIAL CHAOS EXPANSION

Uncertainty modeling

As mentioned above, the model and its associated parameters can exhibit a considerable level of variability (e.g. concrete cover depth, diffusion coefficient, etc.), which may have coefficients of variation of 20% or higher while the concrete cover for high quality control can present a narrow scatter with lower coefficients of variation (Stewart and Rosowsky 1998; Lounis and Mirza 2001). The values of these parameters used in deterministic models are mainly based on the mean values or

some conservative characteristic values of the variables. The deterministic models can predict only two states, i.e. corrosion or non- corrosion. It is clear that the use of deterministic models, which assume concrete as a homogeneous medium, cannot predict the extent of corrosion for a reference period of time (it is either 0% or 100% corrosion). Although such models present a powerful tool for selection of proper parameters at the design stage for new structures, they have serious shortcomings regarding the selection of appropriate maintenance strategies for structures in service. A probabilistic modeling of the performance of concrete structures has much to offer with regard to simplicity as compared to attempts to formulate purely deterministic models (Frangopol *et al.* 1997; Mori and Ellingwood 1993).

Prediction of Corrosion Probability

In order to calculate the probability of corrosion of reinforcing steel embedded in concrete structures several methods can be used, depending on the complexity of the model (e.g. linear or non-linear ...) and the accuracy desired. The probability of corrosion corresponds to the integral of the probability density function $f_X(x)$ on the corrosion domain (See equation below).

$$P_f = \int_{g(C_s, d, D, C_{th}) < 0} f_Y(C_s, d, D, C_{th}) dx$$

$$\text{With } g(C_s, C_{th}, D, d) = C_{th} - C_s \left(1 - \operatorname{erf} \frac{d}{2\sqrt{Dt}} \right)$$

Where g is the limit state or performance function, which is a highly nonlinear function.

To calculate this integral (i.e. probability of corrosion P_f), several methods can be proposed. The most obvious and simple to implement is the Monte Carlo Simulation (MCS). This method attempts to characterize the whole domain of failure so it needs an important number of simulations (i.e. slow convergence rate). Advanced methods use a more efficient way to select simulations, which are based on two main concepts: (i) the approximation of the nonlinear state function; and (ii) efficient method of simulations (e.g. experimental designs).

Other methods attempt to represent the whole response of the system, such as a polynomial chaos expansion that allows constructing a probabilistic response surface. The response of a concrete structure subjected to chloride attack is a random output that can be explicitly represented in a suitable space using the polynomial chaos (PC) basis (Soize & Ghanem 2004). The response is thus cast as a series of multivariate polynomials. In this setup, characterizing the random response is equivalent to computing the coefficients in the representation, i.e. the coordinates of the response in the PC basis. This can be efficiently achieved by using non intrusive approaches, namely the projection strategy and the regression strategy. These

schemes allow one to compute the coefficients of the PC expansion by means of a set of deterministic model evaluations, i.e. without modifying the underlying computer code. Inexpensive moment, sensitivity and reliability analyses (Sudret 2008) are then easily carried out using a suitable post-processing of the PC expansion coefficients.

Polynomial chaos representation

Consider a structural system described by a numerical model that can be analytical or more generally algorithmic (e.g. a finite element model). Suppose that this model has M uncertain input parameters that are represented by *independent* random variables $\{X_1, \dots, X_M\}$ gathered into a random vector \mathbf{X} of prescribed joint probability density function $f_{\mathbf{X}}(\mathbf{x})$. Hence the model response denoted by $Y = \mathcal{M}(\mathbf{X})$ is also random. For the sake of simplicity, Y is assumed to be scalar throughout the paper (in case of a vector response \mathbf{Y} , the following derivations hold true for each component). Provided that the random variable Y has a finite variance, it can be expressed as follows (Soize & Ghanem 2004):

$$Y = \mathcal{M}(\mathbf{X}) = \sum_{\alpha \in \mathbb{N}^M} a_{\alpha} \psi_{\alpha}(\mathbf{X}) \tag{1}$$

This expansion is referred to as the *generalized polynomial chaos (PC) representation* of Y . The a_{α} 's are unknown deterministic coefficients and the ψ_{α} 's are multivariate polynomials, which are orthonormal with respect to the joint PDF $f_{\mathbf{X}}$ of the input random vector \mathbf{X} , i.e. $E[\psi_{\alpha}(\mathbf{X}) \psi_{\beta}(\mathbf{X})] = 1$ if $\alpha = \beta$ and 0 otherwise.

Basis of polynomial chaos expansion

As emphasized above, it is supposed that the input random vector \mathbf{X} has independent components $X_i, i=1..M$. Thus, its joint probability density function (PDF) may be written as:

$$f_{\mathbf{X}}(\mathbf{x}) = \prod_{i=1}^M f_{X_i}(x_i)$$

where $f_{X_i}(x_i)$ = the marginal PDF of X_i .

Let $\{\pi_j^{(i)}, j \in \mathbb{N}\}$ be a family of orthonormal polynomials with respect to f_{X_i} . Most common distributions can be associated to a specific type of polynomials, e.g. normalized Hermite (resp. Legendre) polynomials for standard normal variables (resp. uniform variables over [-1,1]). The multivariate basis $\{\psi_{\alpha}, \alpha \in \mathbb{N}^M\}$ of the representation in Eq. 1 is built by from the M resulting families of univariate polynomials as follows:

$$\psi_{\alpha}(\mathbf{X}) = \prod_{i=1}^M \pi_{\alpha_j}^{(i)}(X_i)$$

For computational purposes, the series in Eq. 1 are truncated in order to retain only a finite number of terms. One commonly retains those polynomials whose total degree $|\alpha| = \sum_i \alpha_i$ does not exceed a given p :

$$Y = \mathcal{M}(\mathbf{X}) \approx \sum_{|\alpha| \leq p} a_\alpha \psi_\alpha(\mathbf{X}) \quad (2)$$

Characterizing the random response Y is thus equivalent to computing the finite set of unknown coefficients $\{a_\alpha, |\alpha| \leq p\}$. This may be achieved using non intrusive techniques respectively known as *projection* and *regression* methods, as shown in the sequel.

Estimation of coefficients of polynomial chaos expansion

The estimation of the coefficients can be done by many strategies, including:

- classic simulation strategy like Monte Carlo Simulation, Latin Hyper Cube
- projection strategies.

Here below, an overview of the main projection strategies is given:

(i) Integration strategy

Due to the orthonormality of the PC basis, the PC coefficients can be computed by pre-multiplying Eq. 2 by ψ_α and by taking their expectations. Therefore, the exact expression of each coefficient a_α can be written as follows:

$$a_\alpha = E[\psi_\alpha(\mathbf{X}) \mathcal{M}(\mathbf{X})] \equiv \int_{D_X} \psi_\alpha(x) \mathcal{M}(x) f_X(x) dx$$

where D_X denotes the support of the random vector \mathbf{X} . The multidimensional integral in the above equation may be computed either by simulation techniques, such as Monte Carlo simulation, Latin Hypercube (McKay et al. 1979) or quadrature (Sudret 2008).

(ii) Regression strategy

Another alternative is the *regression* strategy, which consists in adjusting the truncated PC expansion to the model under consideration. It is possible to recast Equation 2 using a vector notation as follows:

$$Y = \mathcal{M}(\mathbf{X}) \approx \mathcal{M}_p(\mathbf{X}) = \mathbf{a}^T \boldsymbol{\psi}(\mathbf{X})$$

where \mathbf{a} (resp. $\boldsymbol{\psi}$) gathers the coefficients $\{a_\alpha, |\alpha| \leq p\}$ (resp. the basis polynomials $\{\psi_\alpha, |\alpha| \leq p\}$). Sudret (2008) shows that the PC coefficients in Equation 2 are the solution of the optimisation problem below:

$$\mathbf{a}^* = \underset{\mathbf{a} \in \mathbb{R}^p}{\operatorname{argmin}} \int_{D_X} (M(x) - \mathbf{a}^T \boldsymbol{\psi}(x))^2 f_X(x) dx$$

where P denotes the number of multi-indices in the set $\{a_\alpha, |\alpha| \leq p\}$, which is given by:

$$P = \binom{M+p}{p}$$

This problem can be solved by an integral discretization and by choosing a suitable *experimental design* (using the PDF of \mathbf{X}). Hence, let us consider an experimental design $\mathbf{X} = \{\mathbf{x}^{(1)}, \dots, \mathbf{x}^{(N)}\}^T$ such that \mathbf{X} represents a set of N realizations of the input random vector, and $\mathbf{Y} = \{y^{(1)}, \dots, y^{(N)}\}^T$ be the corresponding model evaluations $\{y^{(i)} = \mathcal{M}(\mathbf{x}^{(i)}), i = 1, \dots, N\}$. In this case the estimated coefficients are those that minimize the following squared residual:

$$\hat{\mathbf{a}} = \underset{\mathbf{a} \in \mathbb{R}^P}{\operatorname{argmin}} \left[\sum_{i=1}^N (\mathcal{M}(\mathbf{x}^{(i)}) - \mathbf{a}^T \boldsymbol{\psi}(\mathbf{x}^{(i)}))^2 \right]$$

The solution reads as:

$$\hat{\mathbf{a}} = (\boldsymbol{\Psi}^T \boldsymbol{\Psi})^{-1} \boldsymbol{\Psi}^T \mathbf{Y}$$

where the *data matrix* $\boldsymbol{\Psi}$ is defined by:

$$\boldsymbol{\Psi} = \begin{pmatrix} \psi_{\alpha_1}(\mathbf{x}^{(1)}) & \dots & \psi_{\alpha_p}(\mathbf{x}^{(1)}) \\ \vdots & \ddots & \vdots \\ \psi_{\alpha_1}(\mathbf{x}^{(N)}) & \dots & \psi_{\alpha_p}(\mathbf{x}^{(N)}) \end{pmatrix}$$

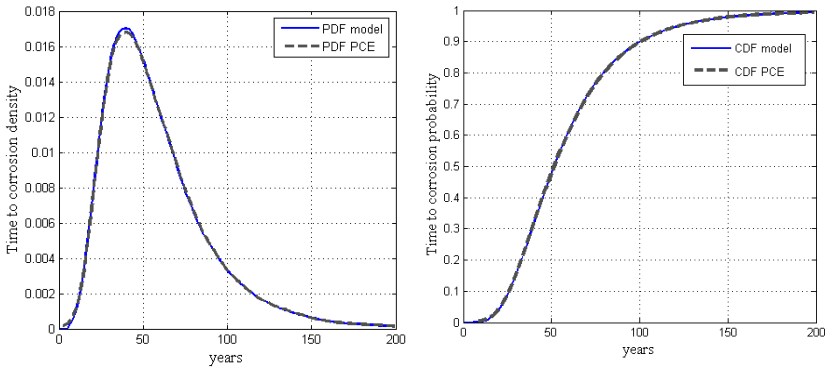
upon introducing the ordering $\{|\alpha| \leq p\} \equiv \{\alpha_1, \dots, \alpha_p\}$ of the multi-indices. Note that in order to make this problem well-posed, the experimental design \mathbf{X} must be selected in such a way that the *information matrix* $\boldsymbol{\Psi}^T \boldsymbol{\Psi}$ is well-conditioned. This implies that the size N of the design (*i.e.* the number of model evaluations) has to be large enough, and necessarily greater than P .

ILLUSTRATIVE EXAMPLE

The probabilistic model proposed herein is illustrated on a high performance concrete (HPC) highway bridge deck reinforced with conventional carbon steel with two different types of HPC mixes that yield similar diffusion coefficients of 0.2 cm²/yr. HPC1 is made with a low w/c ratio (no supplementary mineral admixtures) and HPC 2 contains 10% of silica fume. The parameters values are based on examples taken from Lounis and Daigle (2008) and are listed in Table 1:

Table 1. Data for Bridge Deck Case Study

	C_s Kg/m ³	Depth mm	Diffusion cm ² /year	C_{th} Kg/m ³
Mean value	6	70	0.2	0.7
Coefficient of variation	30%	20%	25%	20%

**Figure 1. PDF and CDF of corrosion initiation time using PCE and MCS models**

In this example, the parameters are assumed to be independent and follow lognormal distributions. The time-varying probability of corrosion is evaluated over 200 years. Fig.1 shows the probability density function (PDF) and cumulative density function (CDF) of the corrosion initiation time obtained using the polynomial chaos expansion (PCE) with 200 simulations. Fig.1 shows also the PDF and CDF of the corrosion initiation time using Monte Carlo simulations (MCS) with 100,000 simulations. It can be seen from Fig.1, that PCE with only 200 simulations provides similar predictions to MCS with much higher number of simulations. This example illustrates the following: (i) the applicability of the polynomial chaos expansion for non-linear chloride transport and corrosion problems; (ii) Accuracy of the PCE when compared to MCS; and (iii) PCE can provide reliable results at a lower computational cost.

CONCLUSIONS

In this paper, a probabilistic modeling of chloride transport and chloride-induced corrosion of concrete structures using the polynomial chaos expansion (PCE) is

presented. It is found that the PCE approach provides accurate results and is more efficient than Monte Carlo simulation, even for the highly nonlinear performance function. The case study showed that similar results are obtained using PCE with much lower computational cost.

REFERENCES

- Crank J. (1975). *The Mathematics of Diffusion*. Oxford: Clarendon press
- Frangopol, D.M., Lin, K.Y., and Estes, A.C. (1997). Reliability of reinforced concrete girders under corrosion attack. *ASCE J. of Struct. Eng.*, 123(3), 286-297.
- Lounis, Z., and Mirza, M. S. (2001). Reliability-based service life prediction of deteriorating concrete structures. *Proceedings of 3rd International Conference on Concrete Under Severe Conditions*, Vancouver, 965-972.
- Lounis, Z. and Daigle, L. (2008). Reliability-based decision support tool for life cycle design and management of highway bridge decks. *Conf. of Transp.Ass. Canada*, Toronto, pp. 1-19.
- McKay, M.D., et al. (1979). A comparison of three methods for selecting values of input variables in the analysis of output from a computer code. *Technometrics* 2, 239-245.
- Mori, Y., and Ellingwood, B. 1993. Reliability-based service life assessment of aging concrete structures. *ASCE J. of Struct. Engrg.*, 119(5),1600-1621.
- Soize, C, and Ghanem, R. 2004. Physical systems with random uncertainties: Chaos representations with arbitrary probability measure. *SIAM J. Sci. Comput*, 26(2), 395-410.
- Stewart, M., and Rosowsky, D.V. 1998. Structural safety and serviceability of concrete bridges subject to corrosion. *ASCE J. of Infrast. Systems*, 4(4), 146-155.
- Sudret, B. (2008). Global sensitivity analysis using polynomial chaos expansions. *Reliab. Eng. Syst. Safety*, 93, 964-979.
- Tuutti, K. 1982. *Corrosion of Steel in Concrete*. Swedish Cement and Concrete Research Institute. Stockholm.
- Weyers, R.E. et al. (1993). *Concrete Bridge Protection, Repair, and Rehabilitation Relative to Reinforcement Corrosion: A Methods Application Manual*. SHRP-S-360, NRC.
- Zhang, J., and Lounis Z. 2006. Sensitivity study of control parameters for onset of corrosion Induced by chloride diffusion. *Cement & Concrete Research*; 36 (7):1312-1323.

Method Of Assessment of Human-induced Area Risks and Creation of Risk Map Using Geoinformation Systems

Yu.I. Shokin¹, V.V. Moskvichev², V.V. Nicheporchuk³

¹Institute Of Computational Technologies SB RAS 6 Acad. Lavrentjev avenue, 630090 Novosibirsk, Russia PH +7 (383) 330-6150; FAX +7 (383) 330-6342; email: ict@ict.nsc.ru

²Special Designer-Technology office SB RAS, 53, Mira avenue, Krasnoyarsk, Russia, 660000; PH +7(391) 227-4916; FAX +7 (391) 227-5536; email: fortuna@icm.krasn.ru

³Institute Of Computational Modelling SB RAS, Akademgorodok, 50, build. 44, Krasnoyarsk, Russia, 660036; PH +7(391) 290-7453; FAX +7 (391) 290-7476; email: valera@icm.krasn.ru

ABSTRACT

The general scheme for processing the results of the area risk monitoring, requirements for the data bank structure and functioning are presented. The algorithms of processing statistical and expert information for obtaining quantitative estimates of the area risks and creating thematic maps of different detailization of the considered territories are given.

INTRODUCTION

The notion «human-induced risk» includes both the risks of occurring technogenic and environmental emergency situations connected with the human activity and risks of occurring natural disasters endangering the human life.

The relevance of the given work is related to the fact that at present there aren't any regulatory and procedural documents, regulating the principles of quantitative estimates of the human-induced area risks. However, scientific research results are being widely used by different government authorities when planning and implementing mitigation of emergencies and other negative consequences of human activity, risk reduction and mitigation of the consequences of the accidents and disasters.

The assessment of human-induced risks requires a complex approach which takes into account the total list of hazards, their sources and development on the considered area. Besides mathematically strict methods of probabilistic modeling, methods of expert assessment are widely used. Most methods of the area risk assessment are based on statistical information on the quantity of events, including the type, time, scale and other characteristics.

The qualitative estimates of the area risks with further creation of the thematic maps are obtained in the following sequence:

- design and arrangement of the data storage of statistical and expert information;
- development of methods of the data analysis using different informational technologies;

- creation of analytical documents (maps, reports), necessary for making decisions.

Given below are the algorithms, tested in practice, for obtaining the values of human-induced risks and creating thematic maps of the areas of the Krasnoyarsk Region.

MATHEMATICAL APPARATUS FOR THE RISK ASSESSMENT

When analyzing natural and human-induced emergency risks, the probability of hazards occurrence can be written as:

$$P_S = F_{PS} \{P_N, P_T, P_O\}, \quad (1)$$

where P_N is the probability of undesired event due to the human factor; P_T is the probability established by the state of the technosphere objects; P_O is the probability conditioned by the state of the environment. Functional (1) is also the same for the probabilities of integrated, graded and object risk implementation.

Damages U_S from accidents in a general case can be presented as:

$$U_S = F_{US} \{U_N, U_T, U_O\}, \quad (2)$$

where U_N is the damages to the population at the interaction of primary and secondary damage effects when the accidents occur; U_T is the damages to technosphere objects; U_O is the damages to the environment. The values U_N , U_T and U_O are measured both in physical units (for example, death toll, quantity of objects destroyed and area of the areas damaged), and their equivalents (for example, economic and money indicators) (Makhutov N.A., 2007).

Based on these data the area risk indicator is calculated by the formula:

$$R(S) = P(S) \cdot U(S), \quad (3)$$

where S is the event, $P(S)$ is the probability of the event, $U(S)$ is the damages.

Individual risk R_i is determined using the data of the emergency statistics as the probability of the human death from a certain reason at a certain point (x, y) of the considered area, using the formula

$$R_i(x, y) = \frac{1}{N} H \lambda_j \iint_S E_j P_j(x, y) \varphi(x, y) dx dy, \quad (4)$$

where H is the accident frequency in the considered area; λ_i is the probability of j -th accident scenario occurrence; E_j is the probability of adverse effect appearance in the j -th accident scenario in the i -th area; P_j is the probability of human death from the adverse effect; N is the population of the considered area, $\varphi(x, y)$ is the population density of the considered area.

Collective risk R_k of death in the considered area due to the accident at a hazardous object was calculated as follows

$$R_k = \sum_j H \lambda_j \sum_i E_j P_{ij} N_i, \quad (5)$$

Complex risk R_c was determined as the average death toll during a year from different reasons or their combination in the considered area

$$R_c = \frac{1}{L} \sum_{j=1}^m \sum_{i=1}^n N_i(Q_j) \cdot P_i(Q_j), \quad (6)$$

where $N_i(Q_j)$ is the death toll from the hazard source Q_j ; $P_i(Q_j)$ is the probability of the hazard Q_j appearance in the considered area in a time unit; L is the total population number in the considered area; m is the number of hazard types; n is the number of damage zones with different human death probabilities.

To estimate social risk it is necessary to have statistical database with observation series long enough (30-40 years). As a rule, there isn't such a database in most areas of Russia. Therefore, it is allowable to determine the social risk by the calculation method using the data on the operation time of the equipment on hazardous industrial objects of the area and number of people in a possible damage zone. The frequency F of the death of 10 and more people is calculated by the formula

$$F = k \frac{T}{N} 10^{-4}, \quad (7)$$

where T is the actual average operation time of the dangerous equipment; k is the coefficient of the hazard severity ($k = 0.05$ when endangering society, $k = 0.5$ when endangering the staff); N is the population number in the damage zone.

The possible population number in the damaged zones was taken according to the list of hazardous objects in the considered area. The operation time of the equipment was set based on the information of the expert centers, dealing with the diagnostics of the technical condition of hazardous industrial objects. Risk functions were constructed as the diagrams "frequency of events – death and injured toll" based on the calculation results.

ORGANIZATION OF DATA COLLECTION AND PROCESSING

For the human-induced risk assessment it is necessary to estimate risk indicators, range of allowed values, frequency of monitoring data collection and processing. This determines the structure of the system of monitoring environmental risk parameters and frequency of data collection and processing.

The aim of creating data storage and database is to generalize and analyze the indicators of the human-induced risks for further forecasting situation in the areas, decision-making on the measures to be taken and the estimation of their efficiency. Here, the following tasks are to be solved:

- systematization of data on the area risk sources;
- automatic data conversion into the format necessary for the risk analysis;
- construction of the risk maps using GIS;
- forecast of the possible situation, including forecast using expert methods;
- preparation of summarized reports according to the forms approved.

The general scheme of the data collection and processing is presented in Fig. 1.

The given scheme consists of three blocks: obtaining, storing and processing the data. The means of collection and primary analysis of the data are necessary for the formal description of physico-geographical, economical, administrative and other area characteristics, objects and infrastructure. These data are collected once a year

and used for quantitative estimates of the area vulnerability, assessment of emergency consequences (scale, losses and damages).

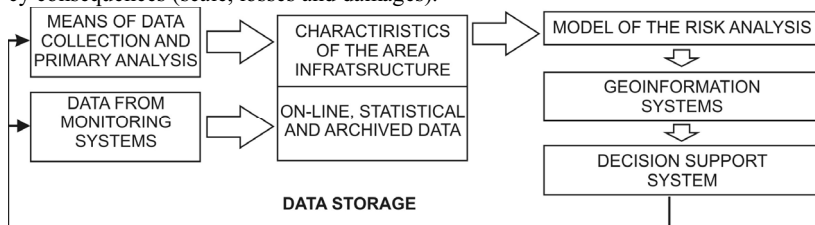


Figure 1. Scheme of obtaining the data and human-induced risk assessment.

On-line data on the situation are daily collected by the territory groups. However, mainly statistical data representing the dynamics of events in a certain period, which were primary analyzed and tested for validity, are used for the risk analysis.

To show the whole variety of emergencies the following approach can be used. For the total emergency list, based the statistical data of the studied area, one creates the Table with the indicators:

- area of occurrence;
- observation period;
- quantity of events;
- total amount of the injured;
- summarized damage.

Therefore, the data storage shall include data necessary for making calculations using formulas (4-7).

This scheme represents the highest level of abstraction. When designing the scheme of the data for the risk assessment, each element of this scheme should be divided into several tables depending on the detailization level of the results anticipated.

CARTOGRAPHIC RESOURCES

Cartographic database is the basis for visualization of risk values by using cartograms and creating thematic risk maps, preparing reports and analytical materials. According to these objectives it is necessary to employ cartographic data of three succeeding scales:

- small-scale digital maps (M1:1000 000) – for the analysis and visualization of the aggregated information on the subject as a whole;
- medium-scale digital maps (M1:200 000) – for modeling and mapping risks in municipal areas, specially protected natural areas and industrial ones;
- large-scale digital plans (M1:10 000) – for modeling and mapping risks in industrial cities and towns, where the state of the environment is regularly monitored.

The data are to be stored in standard formats (for example, Shape, MapInfo) and to have meta description (projection, data and development sources, content, degree of secrecy etc).

Vector maps with the scale of M1:200 000 and less have the following characteristics: projection GK Pulkovo, 1942 г., zones from 12 to 20 (depending on the subject of the Siberian region). Software assets for the visualization of the risk maps are organized as a multi-level model. Cartographic resources are used on three user's levels given as Researcher level, Expert level and Manager level.

ALGORITHMS OF CONSTRUCTING RISK MAPS

Level of the subject (municipal area). The scheme of mapping risk indicators for large areas is given in (Shakhramanyan, M.A., 2002). It reflects three stages of work: preliminary, mapping itself and the stage of the map delineation.

The algorithm of mapping includes the following steps:

1. The choice of the map scale. The results of calculating the area risk zones which are less than 10 km (the zones of floods, oil spills etc.), can more conveniently be illustrated on large- scale maps: M1:25 000 and larger. On small-scale maps one can demonstrate the results of complex risk calculation, the area seismicity, the distribution of the natural hazards (NH) and other kinds of hazards which do not require any specification.

2. The process of the initial data preparation includes the creation of thematic tables of the phenomena for the process of mapping, the development of the thematic layers of the risk sources (river bottoms, pipelines, transport routes of dangerous substances, hazardous industrial objects, waterworks etc.).

3. The easiest way of risk mapping is classifying the area units (municipal formations, district forestries, geological provinces) according to one or several indicators (given in the left part of the scheme). The areas with different indicators can be shown by the colour, shading or by a set of diagrams for each object.

Shown in the right part of the scheme in Figure 3 is the way of the construction of the regular grid or contour lines characterizing the risk values for each space point. These values will be the highest near the risk sources arranged according to their significance on the basis of the normalized indicators. Such a map will be sensitive to the removal/appearance of the risk source as well as to the change of its significance. For example, by changing the equipment or introduction of new technologies with the reduced amount of dangerous substances one can reduce the indicators of the area risk in the local area, adjacent to the hazardous industrial object.

4. Another way of classifying the areas according to a definite indicator is the choice of the captions style (colour, slope etc).

5. Since the sources of the technogenic risk in Siberia are, as a rule, concentrated in a small size area, then, for illustration, large industrial agglomerations are arranged into separate fragments of the scale larger than the main map. A cumulative table or a plot of indicators distributed according to the territories also helps to improve the perception of the map.

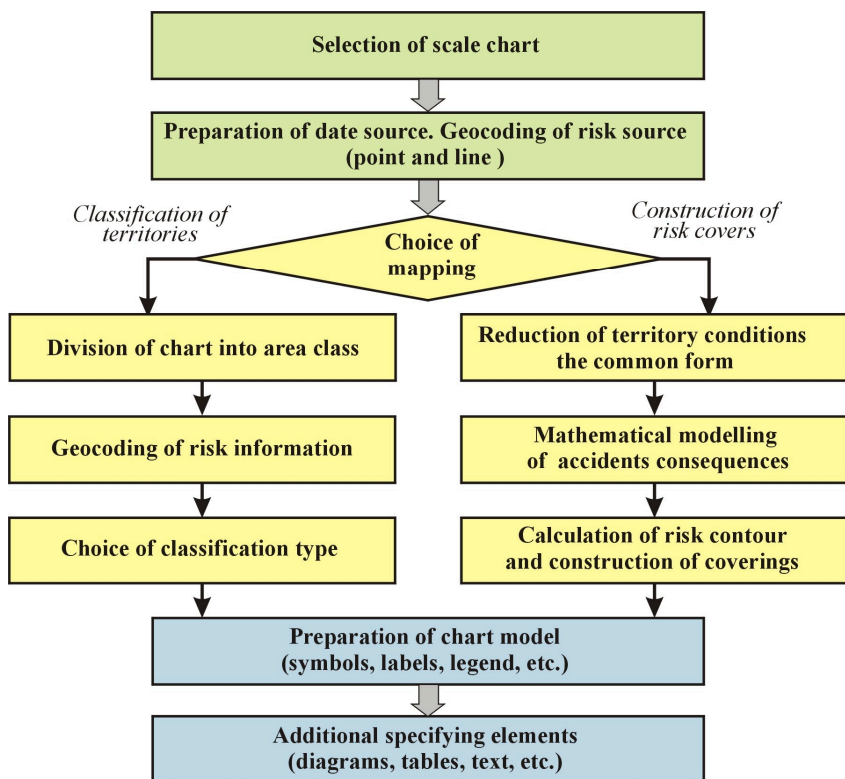


Figure 2. Scheme of constructing the risk maps.

The constructed maps intended for publication in press or on a site is accompanied by a corresponding explanatory note containing the description of the initial data for the calculation, comparison of the obtained risk values with the all-Russia or international indicators, the characteristic of the measures for the risk mitigation (if necessary).

An approximate list of the maps included into the Area risk atlas is determined according to (Moskvicev V. V., 2007). It includes the following more 20 different maps.

The maps intended for publishing should be specified to the levels of municipal areas since the mapping of large areas at the level of a constituent of a federal district in the size of a printed sheet is only possible at a small scale of mapping. To obtain the full actual picture of human-induced risk distribution, especially for the areas with high population density it is necessary to use medium-scale maps, e. g. M1:200 000 and larger.

The total number of risk maps for the constituent, with regard to detalization can amount to 30-50, and the number of thematic levels – to several tens.

Presentation of the ready map montages in digital form has a number of advantages in comparison with the printed variant. It is the change of topographic substrates (raster patterns, satellite images, hill shading), a possibility to use several succeeding scales in one project, managing the mapping of thematic layers, work with a great number of attributive data for each spatial object.

An easier way of risk mapping is shown in the left part of the scheme, it is the classification of the area units (municipal formations, district forestries, geological provinces etc.) according to one or several indicators. Areas with different indicators can be shown by the colour, shading or a set of diagrams for each object. Such a way of mapping is computerized by the specialists of the laboratory of applied computer science of the Institute of Computational Modeling of the SB RAS. The system of on-line analytical data processing (OLAP) «Analytic» is supplemented by the GIS-module which allows automatic creation of cartograms of risk indicator distribution on the basis of the statistical data analysis.

The subject level (municipal area). The algorithm of modeling natural and human-induced hazards at the level of a city (the map M1:10 000 and larger) is presented in [4]. The fundamental difference from the given above way of mapping large area risks is the necessity of estimating the consequences of possible emergencies: natural hazards, accidents at industrial objects, transport, environmental emergencies. Besides, for the level of a city cartograms are more seldom used (for example, classification of the city districts according to the risk type).

The process of the map construction includes five stages.

1. The creation of point-like thematic layer of hazardous
2. The estimation of the consequences for each type of emergencies.
3. The subdivision of the area according to the risks of natural hazards.
4. Rating of the obtained risk zones from various emergencies and summation

of the risk values in the zones of intersection.

5. The creation of the regular grid with the values of the individual risks in each point of the described space with the help of the module 3-D Analyst. Thus, the Grid-surface illustrates the risk values in each arbitrary point in the area of the municipal formations.

Then, the values of individual risks from the selected hazardous industrial objects are plotted on the city digital map by means of using GIS and the probabilistic Grid-surface showing the interpolated value of the individual risk for the whole area of the municipal centre (city) is constructed with the help of the module ArcGIS Geostatistical Analyst.

THE MAIN DIRECTIONS ON EMERGENCY PREVENTION AT THE REGIONAL LEVEL

On the basis of the Russian and foreign experience and with regard to the region peculiarity three main directions of activity on the prevention of emergencies at the regional level can be distinguished.

1) The creation of the scientific basis of the safety measures for the population and areas in the conditions of the risk of natural hazards and technogenic emergencies.

2) Identification of hazards for industrial regions, objects and natural areas.

3) Improvement of the methods and means of hazards monitoring, accident and disaster prevention.

Taking the program measures should be the main goal of the administrative structures of the entities of the Russian Federation responsible for the protection of population and areas from emergencies. This approach is implemented at the federal level and should be accepted at the regional level. The ideology of the regional approach in implementing the program measures, conceptual and strategic developments on increasing the safety level including working out the main directions of activity on the example of the Krasnoyarsk Region are more systematically presented in the collective monograph (Safety of Russia, 2001).

The implementation of the mentioned directions will allow one to control and manage natural and technogenic safety, to develop economic mechanisms of safety management including the insurance of hazardous objects and population living in the possible impact zone in emergencies; these measures will lead to decreasing the amounts of compensational payments from the budgets of the local authorities and provide more stable functioning of the economic potential and will increase competitive (investment) advantages of the region.

REFERENCES

- Lepikhin, A. M. (2010). "Estimation methods of ecological risk by the example of Krasnoyarsk region". *Problems of safety and extreme situations*. Moscow, 1, 31-42.
- Makhutov, N.A. (2007). "Legal and normative regulation of the safety of technosphere objects". *Safety and persistence of technical systems: Proceedings of the II All-Russian conference*. – Krasnoyarsk, Institute of Computational Modeling of SB RAS, 2007. – p. 5-12.
- Moskvichev, V. V. (2007). "Estimation and division into districts of extreme situations risk for Krasnoyarsk region territory". *Problems of safety and extreme situations*. Moscow, 5, 124-133.
- "Safety of Russia (2001). Legal, socio-economic, scientific and technical aspects. Regional safety problems. Krasnoyarsk Region". Moscow: «Znaniye», 500.
- Shakhramanyan, M.A.(2002). "Methods of complex risk assessment for the population from natural hazards and technogenic emergencies". *Moscow : All-Russian Research Institute of Civil Defense and Emergencies*, Moscow, 2002. 21-35.

Closed-form Approximation to Annual Failure Probabilities

Ramesh Kumar¹ and Paolo Gardoni², M.ASCE

¹Zachry Dept. of Civil Engineering, Texas A&M University, College Station, TX, 77843, PH (979) 224-4473; FAX (979) 845-6156; ramesh-kumar@neo.tamu.edu

²Zachry Dept. of Civil Engineering, Texas A&M University, College Station, TX, 77843, PH (979) 845-4340; FAX (979) 845-6156; pgardoni@civil.tamu.edu

ABSTRACT

Accurate and time-efficient methods for computing annual failure probabilities are important for effective implementation of performance-based and reliability-based optimal design. This work provides a general approximate closed-form solution to compute the annual failure probability of components or systems. We show an application of the proposed approach to an example elasto-plastic SDOF system and compare the solution with those obtained numerically and using an alternative approximate closed-form solution currently available in the literature. We find that the proposed approximate closed-form performs better than the one in particular at low ductility levels. The proposed solution also gives insights into the physical phenomena by expressing failure probability in the terms of key parameters.

INTRODUCTION

Fragility functions have been increasingly used to express the vulnerability of components or systems. They are defined as the conditional probability that the component or system does not meet a specified performance level for given measure(s) of demand. The annual probability that the component of system does not meet a specified performance level can be computed by integrating the fragility function multiplied by the annual probability density function of the quantity(ies) the fragility is conditioned on. Such integration can often be computed only numerically. Alternatively, in the context of seismic hazard, Cornell et al. (2002) proposed an approximate closed-form to estimate the annual probability of failure of a component or system. However, such approximate form relies on the assumption that the component or system demand follows a Pareto distribution. However, in general such assumption is not satisfied.

In this work, we propose a novel approximate closed-form solution that does not rely on the assumption of a Pareto distribution for the demand and as result has a higher accuracy than the one proposed by Cornell et al. (2002). The proposed formulation is also more general and can also be applied to hazards other than the seismic one. The closed-form solution gives insights into the physical phenomena by expressing the failure probability in the terms of key structural and hazard parameters. The proposed formulation is particularly valuable for an efficient implementation of performance-based and reliability-based optimal design. As an example, we apply the proposed method to a single-degree-of-freedom systems (SDOF) that mimics the behavior of reinforced concrete (RC) bridges designed based on Caltrans specifications. We show how various structural properties like the natural period, shear force and displacement at

yield govern the failure probability. We also compare the results obtained using the proposed approach with those obtained following Cornell et al. (2002) and a numerical integration.

ANNUAL FAILURE PROBABILITY

In general, the failure of a structural component of system can be written by introducing the limit state function $g(\mathbf{x}, S) = C(\mathbf{x}) - D(\mathbf{x}, S)$ as $F = [g(\mathbf{x}, S) \leq 0]$, where $C(\mathbf{x}) =$ probabilistic capacity model for a specific performance level, $D(\mathbf{x}, S) =$ corresponding probabilistic demand model, $\mathbf{x} =$ a vector of material and geometrical properties of the structure, and $S =$ a load intensity measure. The outcomes of $C(\mathbf{x})$ and $D(\mathbf{x}, S)$ are random due to the randomness inherent in \mathbf{x} and S , and the uncertainty in the modeling of the structural behavior.

The annual failure probability is commonly used as a basis for making recommendations for design of new systems and, maintenance and repair of existing deteriorating systems (e.g., Cornell et al. 2002; Stewart and Val 2003; Kong and Frangopol 2003). The annual failure probability, $P_A(F)$, of a component or system due to a load with intensity S , can be computed as follows:

$$P_A(F) = P(F|E)P_A(E) \tag{1}$$

where, $P(A|B) =$ conditional probability of A given B , $E =$ occurrence of the load, $P_A(E) =$ annual probability of E , and

$$P(F|E) = \int P(F|S = s, E) f_{S|E}(s|E) ds \tag{2}$$

where, $P(F|S = s, E)$ is commonly referred as a fragility function, and $f_{S|E}(s|E) =$ probability density function of S given E . Using Eqs. (1) and (2), we can write

$$P_A(F) = \int P(F|S = s, E) h_s(s) ds \tag{3}$$

where, $h_s(s) = f_{S|E}(s|E)P_A(E)$, which is related to the annual probability of exceeding a corresponding value of S also known as the hazard function, $H_S(s) = P(S > s)$, as

$$h_s(s) = \frac{d}{ds} [1 - H_S(s)] \tag{4}$$

The hazard function, $H_S(s)$, is commonly modeled as a Pareto distribution (Cornell et al. 2002)

$$H_S(s) = P(S > s) = \begin{cases} 1 & s \leq S_{\min} \\ k_0 s^{-k_1} & s > S_{\min} \end{cases} \tag{5}$$

where k_0 and k_1 are regional constants and $S_{\min} = (1/k_0)^{1/k_1}$.

In this paper we discuss approximate closed-form methods to compute $P_A(F)$. In the following sections we propose a closed-form solution to compute $P_A(F)$ and compare the proposed solution with an existing solution by Cornell et al. (2002).

PROPOSED SOLUTION

This section develops an approximate closed-form expression for $P_A(F)$ using Eq. (3). First approximate forms for $C(\mathbf{x})$ and $D(\mathbf{x}, S)$ are developed. Then the failure probability is written conditioning on the value of S using the probability density functions (PDF) of $C(\mathbf{x})$ and $D(\mathbf{x}, S)$. Thereafter, the conditional failure probability is integrated with the annual PDF of S to compute $P_A(F)$.

Probability distribution of capacity and demand. Often the models $C(\mathbf{x})$ and $D(\mathbf{x}, S)$ are constructed using a variance stabilizing transformation (e.g., taking the natural logarithm of the quantities of interest) so that the standard deviation of the modeling error is approximately constant (homoskedasticity assumption) and the error follows a normal distribution (normality assumption) (e.g., Gardoni et al. 2002 and 2003, Ramamoorthy et al. 2006, Choe et al. 2007.) As a result, Choe et al. (2007) proposed the following expression for failure probability:

$$P(F|S=s, E) = P[C(\mathbf{x}) - D(\mathbf{x}, S) < 0 | S=s, E] = \Phi \left[\frac{\hat{D}(\mathbf{x}, s) - \hat{C}(\mathbf{x})}{\sqrt{\sigma_D^2 + \sigma_C^2}} \right] \quad (6)$$

where, $\hat{C}(\mathbf{x})$ and σ_C = point estimates of the mean and standard deviation of $C(\mathbf{x})$, $\hat{D}(\mathbf{x}, S)$ and σ_D = point estimates of the mean and standard deviation of $D(\mathbf{x}, S)$, and $\Phi(\cdot)$ = standard normal cumulative distribution function (CDF). Point estimates are obtained by considering the mean values of \mathbf{x} and any model parameter in the expressions of $C(\mathbf{x})$ and $D(\mathbf{x}, S)$. In order to achieve a closed-form solution of the integral in Eq.(3), we use the following form for $\hat{D}(\mathbf{x}, S)$ proposed by Cornell et al. (2002) and Ramamoorthy et al. (2006):

$$\hat{D}(\mathbf{x}, S) = b(\mathbf{x}) \ln[S] + a(\mathbf{x}) \quad (7)$$

where, $a(\mathbf{x})$ and $b(\mathbf{x})$ = structural parameters.

Next, using Eqs. (5) and (7), the hazard function, $H_{\hat{D}}(r)$, for $\hat{D}(\mathbf{x}, S)$ can be written as

$$H_{\hat{D}}(r) = P[\hat{D}(\mathbf{x}, S) > r] = P\left[S > \exp\left(\frac{r-a}{b}\right)\right] \quad (8)$$

$$\Rightarrow H_{\hat{D}}(r) = \begin{cases} 1 & r \leq \alpha \\ \exp[-\lambda(r-\alpha)] & r > \alpha \end{cases} \quad (9)$$

where, $\lambda = k_1 / b(\mathbf{x})$, $\alpha = a(\mathbf{x}) + [b(\mathbf{x}) / k_1] \ln(k_0)$. Furthermore, using Eqs. (4) and (9), $h_{\hat{D}}(r)$ for $\hat{D}(\mathbf{x}, S)$ can be shown to be a shifted exponential distribution.

Performing change of variables, we can write

$$P_A(F) = \int P(F|S=s, E) h_S(s) ds = \int P(F|\hat{D}=r, E) h_{\hat{D}}(r) dr \quad (10)$$

Finally, using the derived expression for $h_{\hat{D}}(r)$, the integral in Eq. (10) is carried out as follows:

$$\int P(F|\hat{D} = r, E)h_{\hat{D}}(r)dr = \int_{\alpha}^{\infty} \Phi\left[\frac{r - \hat{C}}{\sigma}\right] \lambda e^{-\lambda(r-\alpha)} dr \tag{11}$$

$$\int_{\alpha}^{\infty} \Phi\left[\frac{r - \hat{C}}{\sigma}\right] \lambda e^{-\lambda(r-\alpha)} dr = -e^{-\lambda(r-\alpha)} \Phi\left[\frac{r - \hat{C}}{\sigma}\right] \Big|_{\alpha}^{\infty} + \int_{\alpha}^{\infty} e^{-\lambda(r-\alpha)} \left\{ \frac{1}{\sigma} \phi\left[\frac{r - \hat{C}}{\sigma}\right] \right\} dr \tag{12}$$

$$= e^{-\lambda(r-\alpha)} \Phi\left[\frac{r - \hat{C}}{\sigma}\right] \Big|_{\alpha}^{\infty} = \Phi\left[\frac{\alpha - \hat{C}(\mathbf{x})}{\sigma}\right] \tag{13}$$

Using $z = (r - \hat{C}) / \sigma$, we get

$$\int_{\alpha}^{\infty} e^{-\lambda(r-\alpha)} \left\{ \frac{1}{\sigma} \phi\left[\frac{r - \hat{C}}{\sigma}\right] \right\} dr = \int_{(\alpha - \hat{C})/\sigma}^{\infty} e^{-\lambda(\sigma z + \hat{C} - \alpha)} \phi[z] dz \tag{14}$$

$$= e^{-\lambda(\hat{C} - \alpha)} \int_{(\alpha - \hat{C})/\sigma}^{\infty} \frac{1}{\sqrt{2\pi}} \exp\left(-\sigma\lambda z - \frac{1}{2}z^2\right) dz \tag{15}$$

$$= e^{(\lambda^2\sigma^2/2)} e^{-\lambda(\hat{C} - \alpha)} \int_{(\alpha - \hat{C})/\sigma}^{\infty} \phi[z + \lambda\sigma] dz = e^{(\lambda^2\sigma^2/2)} e^{-\lambda(\hat{C} - \alpha)} \Phi\left[\frac{\hat{C}(\mathbf{x}) - \alpha - \lambda\sigma^2}{\sigma}\right] \tag{16}$$

$$\Rightarrow P_A(F) = \Phi\left[\frac{\alpha - \hat{C}(\mathbf{x})}{\sigma}\right] + e^{-\lambda[\hat{C}(\mathbf{x}) - \alpha]} e^{(\lambda^2\sigma^2/2)} \Phi\left[\frac{\hat{C}(\mathbf{x}) - \alpha - \lambda\sigma^2}{\sigma}\right] \tag{17}$$

where, $\sigma = \sqrt{\sigma_D^2 + \sigma_C^2}$.

Cornell et al. (2002) first developed the marginal probability distribution for $\delta(\mathbf{x}) = \exp[D(\mathbf{x})]$. This was done by integrating out S from $D(\mathbf{x}, S)$ using a Pareto distribution for S to obtain distribution for $D(\mathbf{x})$ and then computing the distribution of $\delta(\mathbf{x})$. However, for simplification, the integration was performed using approximate limits that lead to a Pareto marginal distribution for $\delta(\mathbf{x})$. The resulting expression for $P_A(F)$ is as follows:

$$P_A(F) = H_S \left\{ \exp\left[\frac{C(\mathbf{x}) - a(\mathbf{x})}{b(\mathbf{x})}\right] \right\} \exp\left[\frac{1}{2} \frac{k_1^2}{b^2(\mathbf{x})} \sigma_C^2\right] \exp\left[\frac{1}{2} \frac{k_1^2}{b^2(\mathbf{x})} \sigma_D^2\right] \tag{18}$$

However, a Pareto distribution for $\delta(\mathbf{x})$ is not a good approximation because the distribution has a minimum value greater than zero, which is inconsistent with a lognormal distribution for the demand. In particular, the minimum value of $\delta(\mathbf{x})$ can be computed as

$$\delta_{\min}(\mathbf{x}) = k_0^{b(\mathbf{x})/k_1} \exp\left[a(\mathbf{x}) + \frac{1}{2} \frac{k_1}{b(\mathbf{x})} \sigma_D^2\right] \tag{19}$$

APPLICATION OF THE PROPOSED FORMULATION TO A SDOF SYSTEM SUBJECT TO SEISMIC HAZARD

In this section, we use the proposed method to compute $P_A(F)$ of an elasto-plastic SDOF system subject to seismic hazard. We compare the result of the proposed approach with those obtained following Cornell et al. (2002) and numerically integrating Eq. (3). The SDOF represents the behavior of RC bridges in San Francisco, CA designed as per Caltrans specifications (Caltrans 2006). The deformation mode of failure of the SDOF system is considered in writing $g(\mathbf{x}, S)$. This mode of failure is selected because Caltrans specifications require bridges to be designed to fail in lateral deformation of the columns under seismic loading. It is also noted that the capacity and demand models used in this example are for illustration purposes only. The formulation in Eq. (17) is general and does not rely on the specific models used.

Deformation Capacity. Following Gardoni et al. (2002), the random deformation capacity of an elasto-plastic SDOF system is written as

$$C(\mathbf{x}) = \ln \left[\frac{\hat{\Delta}_y(\mathbf{x}) + \hat{\Delta}_p(\mathbf{x})}{H} \right] + \sigma_c \varepsilon \quad (20)$$

where, $\hat{\Delta}_y$ = displacement at yield, $\hat{\Delta}_p$ = displacement capacity, H = height of the SDOF system and ε is a standard normal random variable. For simplicity the bias correction terms in Gardoni et al. (2002) have been ignored in Eq.(20). However, they can be incorporated in this formulation as a terms added to the mean value.

Seismic Deformation Demand. Following Gardoni et al. (2003), the seismic deformation demand $D(\mathbf{x}, S)$ on an elasto-plastic SDOF is written as

$$D(\mathbf{x}, S) = \hat{D}(\mathbf{x}, S) + \sigma_D \varepsilon \quad (21)$$

Ignoring the bias correction terms

$$\begin{aligned} \hat{D}(\mathbf{x}, S) &= \ln \left[S \hat{\Delta}_y / H \right] & S \leq 1 \\ &= \ln \left\{ \left[1 + \frac{1}{c} (S^c - 1) \right] \hat{\Delta}_y / H \right\} & S > 1 \end{aligned} \quad (22)$$

where, $S = S_a(T_n) / A_y$, $S_a(T_n)$ = spectral acceleration computed from elastic response spectrum for given natural period, T_n , $A_y = F_y / w$, F_y = shear force at yield, w = the weight of the structure, and $c = T_n / (1 + T_n) + 0.42 / T_n$. The spectral acceleration $S_a(T_n)$ is commonly modeled as a Pareto random variable as shown in Eq. (5).

Computation of annual failure probability. Implementation of the proposed solution to this example relies on the accuracy of Eq. (7) in capturing the behavior of an elasto-plastic SDOF system given in Eq. (22). The first part of Eq. (22) (i.e., $S \leq 1$) can be ignored because the contribution of $P_A(F | S \leq 1)$ to $P_A(F)$ is negligible since the structure is likely to stay elastic when $S \leq 1$ and hence is unlikely to fail. Hence, we can write

$$P_A(F) = P_A(F | S > 1) P_A(S > 1) \quad (23)$$

$$P_A(F|S > 1) = \left[\int_1^\infty P(F|S = s, E) h_{S|S>1}(s|S > 1) ds \right] \tag{24}$$

Comparing Eq. (7) with Eq.(22) for $S > 1$, it is found that $a(\mathbf{x}) = \ln[\Delta_y / H]$. Also we choose a value for $b(\mathbf{x})$ that provides the best fit in the range $1 \leq S \leq (\mu_{S|S>1} + 2\sigma_{S|S>1})$, which turns out to be $b(\mathbf{x}) = c^{0.55}$. It is seen that Eq. (24) is analogous to Eq. (3) with a difference that in Eq. (24) the annual failure probability and the annual PDF for S are conditioned on $S > 1$. Therefore, the proposed solution is applicable to this problem with suitable corrections required for conditioning on $S > 1$, which are discussed next.

The conditional hazard function $H_{S|S>1}(s)$ can be derived as follows:

$$P(S_a > s_a) = 1 \quad s_a \leq S_{a,min} \tag{25}$$

$$= k_0 s_a^{-k_1} \quad s_a > S_{a,min}$$

$$P(S > s | S_a > A_y) = P(S_a > s A_y | S_a > A_y) \tag{26}$$

$$P(S_a > s A_y | S_a > A_y) = \frac{P(S_a > s A_y \cap S_a > A_y)}{P(S_a > A_y)} \tag{21}$$

$$\Rightarrow P(S > s | S_a > A_y) = \frac{P(S_a > A_y)}{P(S_a > A_y)} = 1 \quad s \leq 1 \tag{27}$$

$$= \frac{P(S_a > s A_y)}{P(S_a > A_y)} = s^{-k_1} \quad s > 1$$

Therefore,

$$H_{S|S>1}(s|S > 1) = P(S > s | S > 1) = \begin{cases} 1 & s \leq 1 \\ s^{-k_1} & s > 1 \end{cases} \tag{28}$$

The mean and the standard deviation are given as $\mu_{S|S>1} = k_1 / (k_1 - 1)$ and $\sigma_{S|S>1} = \sqrt{k_1 / [(k_1 - 1)(k_1 - 2)]}$, respectively. Now, $H_{\hat{D}|S>1}(r)$ is given by Eq.(9) by substituting $k_0 = 1$ because in Eq. (28) the coefficient of $s^{-k_1} = 1$. Next, $h_{\hat{D}|S>1}(r)$ can be obtained using Eq.(4). The value of $P_A(F|S > 1)$ is given by Eq. (17). Finally, we compute the value of $P_A(F)$ using Eq. (23), where $P(S > 1)$ is computed by substituting A_y for s_a in Eq (25):

$$P(S > 1) = P(S_a > A_y) = k_0 A_y^{-k_1} \tag{29}$$

Numerical Examples, Results and Discussions. Table 1 gives the structural properties of an example SDOF with $T_n = 0.20$ sec. For San Francisco, CA the corresponding values of k_0 and k_1 are 0.009 and 4.512, respectively. Using k_0 and k_1 the mean values for $S_a(T_n = 0.2) = 0.45g$. Figure 1 shows that the plots of the generalized annual reliability index, $\beta_A = -\Phi^{-1}[P_A(F)]$, versus the ductility capacity $\hat{\mu}_c = [(\hat{\Delta}_y + \hat{\Delta}_p) / \hat{\Delta}_y]$.

The plots compare the results obtained using the proposed solution with the results obtained following Cornell et al. (2002) and a numerical integration of Eq. (3) using Eqs. (4) - (6) and (22).

It can be seen that, for this example, the proposed approach is more accurate than the solution obtained following Cornell et al (2002), in particular at lower values of $\hat{\mu}_c$. Using Eq. (13), the corresponding minimum ductility demand in the approach by Cornell et al. (2002) is found to be $\mu_{d,min} = H\delta_{min}(\mathbf{x})/\Delta_y = 1.17$. Consistently, $P_A(F)$ found using Cornell et al. (2002) gives inaccurate results for $\hat{\mu}_c$ values close to $\mu_{d,min}$. The proposed solution does not rely on the assumption of a Pareto distribution for $\delta(\mathbf{x})$ and hence is consistently accurate while maintaining the simplicity and convenience of a closed-form.

Table 1. Example SDOF system

Property	Symbol	SDOF 1	Units
Natural period	T_n	0.20	sec
Mass	m	3.0E05	kg
Shear force at yield	F_y	981.25	kN
Height	H	5.0	m

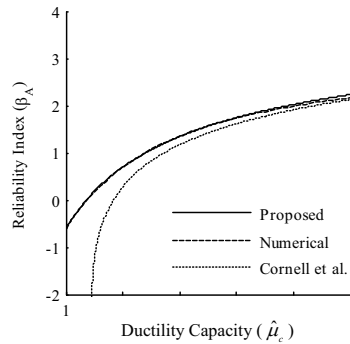


Figure 1. Reliability Index for example SDOF

CONCLUSIONS

An efficient implementation of a performance-based design and reliability-based optimal design require accurate and time-efficient methods for computing failure probabilities. While numerical methods are the most versatile, they are time consuming. If possible, approximate closed-form solutions should be used for time-efficiency.

This work develops an approximate closed-form solution to the annual failure probability of components and systems. The structural capacity and demand conditioned on intensity measure are assumed to be lognormally distributed, and the intensity measure is assumed to follow a Pareto distribution. These assumptions are well supported in particular by the existing literature on seismic hazards. As an application, we used the proposed approach on an example single-degree-of-freedom (SDOF) system. We found that, for the example SDOF considered, the proposed solution performs better than the existing approximate closed-form solution in particular at low ductility levels. The closed-form solution also gives insights into the physical phenomena by expressing the failure probability in the terms of key structural and hazard parameters.

REFERENCES

- Choe, D., Gardoni, P., and Rosowsky, D. (2007). "Closed-form fragility estimates parameter sensitivity and Bayesian updating for RC Columns." *J. Eng. Mech.*, 133(7), 833–843.
- Cornell, C. A., Jalayer, F., Hamburger, R. O., and Foutch, D. A. (2002). "Probabilistic Basis for 2000 SAC Federal Emergency Management Agency Steel Moment Frame Guidelines." *J. Struct. Eng.*, 128(4), 526–533.
- Federal Emergency Management Agency (FEMA), "NEHRP guidelines for the seismic rehabilitation of buildings." *FEMA-273*, 1997.
- Gardoni, P., Der Kiureghian, A., and Mosalam, K. M. (2002). "Probabilistic Capacity Models and Fragility Estimates for RC Columns Based on Experimental Observations." *J. Eng. Mech.*, ASCE, 128(10), 1024–1038.
- Gardoni, P., Mosalam, K. M., and Der Kiureghian, A. (2003). "Probabilistic seismic demand models and fragility estimates for RC bridges." *J. Earthquake Eng.*, 7(1), 79–106.
- Kong J. S., and Frangopol D. M. (2003). "Life-Cycle Reliability-Based Maintenance Cost Optimization of Deteriorating Structures with Emphasis on Bridges." *J. Struct. Eng.*, 129(6), 818–828.
- Ramamoorthy, S. K., Gardoni, P., and Bracci, J. M. (2006). "Probabilistic demand models and fragility curves for reinforced concrete frames." *J. Struct. Eng.*, 132(10), 1563–1572.
- Stewart M. G., and Dimitri V. V. (2003). "Multiple Limit States and Expected Failure Costs for Deteriorating Reinforced Concrete Bridges." *J. Bridge Eng.*, 8(6), 405–415.
- Structural Engineers Association of California (SEAOC). "Performance based seismic engineering of buildings", *vol. I. Vision 2000 Report*, California, 1995.
- Caltrans, (2006), *Seismic Design Criteria, Version 1.4*, California Department of Transportation, Sacramento, California.

Use of Quantitative Risk Assessment in Structural Design

Nasim Uddin¹, Mohammed A. Mousa²

¹ Professor, Department of Civil, Construction and Environmental Engineering,
University of Alabama at Birmingham, 1075 13th Street South, Birmingham, AL
35294-4440

PH: 205-934-8432, email: nuddin@uab.edu

² Graduate Student, Department of Civil, Construction and Environmental
Engineering, University of Alabama at Birmingham, 1075 13th Street South,
Birmingham, AL 35294-4440

PH: 205-243-3215, email: mmousa@uab.edu

ABSTRACT

Civil engineers, in particular, have the primary responsibility for the design and planning of civil structures, including protective systems to minimize losses of lives and economies during extreme hazard events. Structural failures in recent earthquakes and hurricanes have exposed the weakness of current design procedures and shown the need for new concepts and methodologies for building performance evaluation and design. Although the uncertainty of seismic load has been well recognized by the profession, the incorporation of uncertainty in most building code procedures have been limited to the selection of design loads based on return period. To strike a balance between the possible high initial cost and potential large losses over the structure's lifetime, the life-cycle cost and the uncertainty in the hazards and system capacity need to be carefully considered. Moreover, to strictly enforce performance goals, the target probabilities need to be set directly for the limit states rather than for the design earthquake or hurricane etc. Therefore, the total cost over the life time of the structure should be considered when optimizing the design for natural hazard. The future or damage cost of the structure due to natural hazard is calculated based on quantitative risk assessment (QRA). This paper presents a methodology for the design optimization based on the QRA. A case study for a three story residential wood building is presented in order to demonstrate the concept.

Keywords: Design Optimization, QRA, Life Cycle Cost, Natural Hazard

INTRODUCTION

Despite most of recent structures have been designed according to the desired code requirements, wide spread structural failures during recent natural hazards such as hurricanes and earthquakes have shown the weakness of the current design methods. It has demonstrated an urgent need for a new approach for structural design that accounts for the risk due to natural hazards. Among these is the total life cycle cost (LCC) over the life time of the structure. LCC is the sum of all costs that are incurred over the life span of the structure. It includes direct costs that are required to construct, maintain, and eventually dispose the structure and also expands to include indirect costs that are incurred from the use of the structure as well as the damage cost due to hazard loads. Although the concept of LCC itself is not new, its applications in infrastructure management has recently begun to gain widespread acceptance in the United States [Makow 1995]. Ehlen [1999] has examined the LCC of three FRP bridge decks and compared them with a convention reinforced concrete deck. The study indicated that one of the FRP decks was a life-cycle- cost effective than the others. Leeming [1993] applied the LCC concept to examine structural type of a new bridge while Smith and Obaide [1993] evaluated the cost implications of different bridge-maintenance choices including repair, refurbishment, and replacement.

Risk assessment is a step in a risk management procedure and it is the determination of quantitative value of risk related to a concrete situation and a recognized hazard. In general economic terms, Quantitative Risk Assessment (QRA) requires calculations of the two main components of risk (R); the magnitude of the potential loss L , and the probability P_L of the occurrence of that loss.

$$R = P_L \times L \quad (1)$$

In engineering economic terms, risk is a function of the probability of occurrence of a hazard, P_h (e.g., earthquake or hurricane), the probability of the damage (P_d) and the potential adverse consequence that result from that hazard, C_q [Ang 2006]. Risk in engineering may be expressed in quantitative terms as:

$$R = P_h \times P_d \times C_q \quad (2)$$

OBJECTIVES

The main objective for this paper is to provide a methodology based on the research work conducted by Kang and Wen (2000) for design optimization for structures against the effect of multihazards loading such as earthquake, hurricane, or windstorm. The concept is based on QRA, and considers also the uncertainty in hazard loading. In addition to design optimization concept, the paper also demonstrates the method through a case study of three story residential wood building for seismic loading.

METHODOLOGY

The design methodology for the case study involves six main steps. These steps are summarized in the flow chart illustrated in Figure 1. LFRS that is referred in Figure 1 stands for Lateral Force Resisting System for seismic loading.

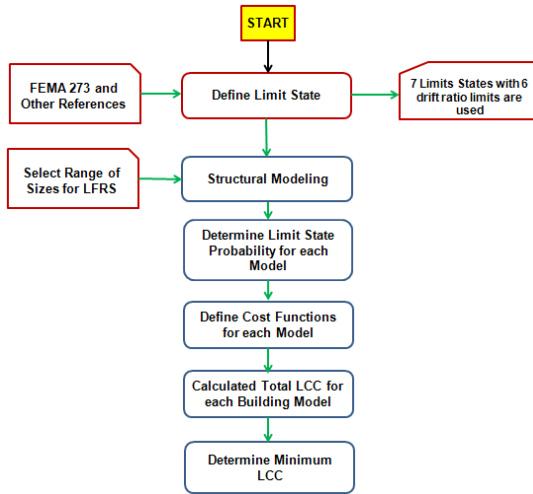


Figure 1. Flowchart for the optimum design based on QRA

Defining limit states is the first step for a design based on QRA. It is a criterion to define the failure of the structures. Currently, most of building codes and design guidelines define the structural limits states in terms of the performance level and drift limits. The definition has been expanded into seven limit states based on the damage level according to Earthquake Damage Evaluation Data for California [ATC-13 (1985)] and a Benefit-Cost Model for the Seismic Rehabilitation of Buildings [FEMA 227 (1992)]. They range from none to destroyed damage.

Structural Modeling: The structure under consideration is first modeled to obtain the structural member sizes. The modeling step starts with designing the structure according to the building code requirements and specifications to obtain the standard member sizes for the Lateral Force Resisting System (LFRS). Then, a range of LFRS sizes are selected below and above the standard sizes. Further, another range of hazard loading (i.e., seismic in this case) is assumed and each structure is modeled and analyzed for each loading scenario and the corresponding drift is calculated.

Determining Limit State Probability: Probability is a way of expressing knowledge or belief that an event will occur or has occurred. In general, the probability is used for predicting what might happen in the future under the condition of uncertainty. The probability for each limit state is calculated for each hazard loading. The procedure for determining the limit state probability is illustrated in Figure 2. This procedure comprises of many steps and it depends on the nature of the hazard loading (i.e., seismic or wind or both). To obtain the equations used for determining the limit state probability, the procedure used was similar to that used previously by Kang and Wen [2000]. Using the annual probability of exceedance versus drift ratio curve, the following formulas are used to obtain the limit state probability for different limits states:

$$P_f = 1 - \left\{ -\frac{1}{\nu} \left[\ln(1 - P_a(\Delta > \Delta_1)) \right] \right\} \tag{3}$$

$$P_i = \frac{1}{\nu} \{ \ln[1 - P_a(\Delta > \Delta_i)] - \ln[1 - P_a(\Delta > \Delta_{i-1})] \} \tag{4}$$

$$P_n = \frac{1}{\nu} \{ -\ln[1 - P_a(\Delta > \Delta_{n-1})] \} \tag{5}$$

where f , i , and n represents the first, any middle and last limit states probabilities, respectively. In the case study section, these formulas will be applied to demonstrate their applications.

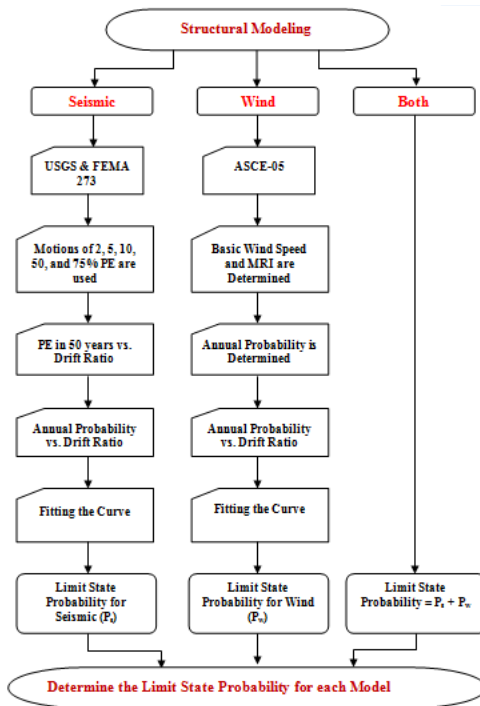


Figure 2. Procedure for determining the limit states probability

Defining Cost Functions: The LLC composed of direct and indirect costs. The total direct cost is then can be expressed as:

$$C_D = C_c + C_m + C_d \tag{6}$$

Where C_D is the direct cost, C_c is the construction cost, C_m is the maintenance cost, and C_d is the disposal cost. After each structure is designed, the initial cost can be

calculated based on the member sizes. The source of the direct cost data can be found through material manufacturers, fabricators, government agencies, previous studies, universities, and contractors. The indirect costs are those resulting from the damage of the building due to the hazard. It called also damage cost. According to FEMA 227 [1992], the damage cost includes the cost of repair or building damage (C_d), loss of contents (C_c), Relocation cost (C_r), Economic loss (C_e), Injury cost (C_i) and loss of life or fatality cost (C_f). Thus, the total indirect can be expressed as:

$$C_{ID} = C_d + C_c + C_r + C_e + C_i + C_f \quad (7)$$

FEMA 227 [1992], FEMA 228 [1992], FEMA 174 [1989], and ATC-13 [1985] provide detail values for all the damage costs. The summation of direct and indirect costs yields the total LCC. However, since some of the direct costs (maintenance and disposal costs) and all indirect costs are expected to be occurred in future, thus they should be discounted to reflect their present worth. The indirect costs are obtained by multiplying the failure cost by the limit state probabilities.

LLC formulations: To account for the failure cost due to single hazard, Wen and Ang [2000] has the proposed the following formula:

$$LCC = C_0 + C_f P_f \frac{v}{\lambda} (1 - e^{-\lambda t}) + \frac{C_m}{\lambda} (1 - e^{-\lambda t}) \quad (9)$$

where C_0 is the initial cost, C_f is the failure cost, C_m , P_f is the failure probability due to single hazard, λ is the discount rate, v is the occurrence rate per year, and t is the structure life time. However, to include the disposal cost and to account for multiple hazards, equation (10) can be extended as following:

$$LCC = \left[C_c + \frac{C_m}{\lambda} (1 - e^{-\lambda t}) + \frac{C_d}{\lambda} (1 - e^{-\lambda t}) \right] + \left[\sum_{i=1}^n C_{fi} P_{fi} \frac{v}{\lambda} (1 - e^{-\lambda t}) \right] \quad (10)$$

The first part of equation (10) represents the direct cost whereas the second part represents the indirect cost. It should be noted that if the annual limit state probability is used, the occurrence rate per year factor (v) is taken as unity. *Minimum LCC:* After determining the costs for each structure, the direct and indirect costs are plotted for all structures. For structures designed for lower loads will have lower initial costs, but large expected failure costs. On the other hand, those designed for higher load will increase their initial costs and reduce the expected failure costs. The optimal design level can be determined at the point of the minimum total life-cycle cost.

CASE STUDY

In order to demonstrate the presented design methodology, a three story residential wood building is considered as a design example. Only seismic hazard was considered. It is similar the design example provided in FEMA 451 [2006] which was located at Seattle, Washington with site coordinates of 47.69° N, 122.32° W. However, since the design needs to be in high seismic region, the design was revised to be appropriate for Los Angeles; California at site coordinates of 34° N, 118° W. These coordinates are important in order to determine the seismic design parameters. The building's dimension is 148 ft long by 56 ft wide with 27 ft height. The Lateral Force Resisting System (LFRS) is composed of plywood diaphragms and shear walls. Figure 3 shows the main LFRS for this building. The shear walls in the longitudinal

direction are located on the exterior faces of the building and along the corridor. In the transverse direction, the end walls and one line of interior shear walls provide lateral resistance.

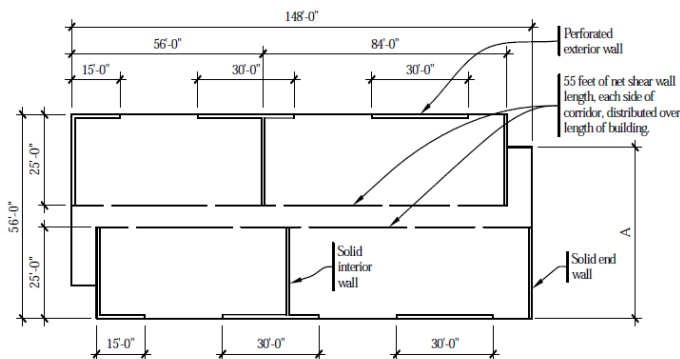


Figure 3. Layout of the main LRFS [FEMA 451 (2006)]

Defining Limit States: ATC-13 [1985] and FEMA 227 [1992] defines the limit states whereas FEMA 273 [1997] defines the performance level along with only three drift ratio limits. To extend the drift limits and make them compatible with the limit states, Table 1 was developed based on the mentioned specifications for the wood structures.

Table 1: Drift ratio limits for each limit state level for wood buildings

Limit State Level	Structural Performance Level	Damage State	Allowable Drift Ratio Limit (%)
I	Immediate Occupancy	None	$\Delta < 0.5$
II	Immediate Occupancy	Slight	$0.5 < \Delta < 0.7$
III	Life Safety	Light	$0.7 < \Delta < 1.0$
IV	Life Safety	Moderate	$1.0 < \Delta < 1.5$
V	Life Safety	Heavy	$1.5 < \Delta < 2.0$
VI	Collapse Prevention	Major	$2 < \Delta < 3$
VII	Collapse Prevention	Destroyed	$\Delta > 3$

Structural Analysis: The building is designed first for seismic loading according to NEHRP provisions [FEMA 450 (2003)] to obtain the standard member sizes. It should be mentioned the total building deflection is composed of shear wall and diaphragm deflections which are determined according to equation FEMA 451 [2006]. After conducting the code design, eight building models was assumed in order to determine the optimum design. The models were obtained by changing the dimension of the design output by 10% below and above the code design. The nail spacing was kept the same for all models while the plywood thickness and the area of end posts were changed. The models along with the dimensions are listed in Table 2. The code design is corresponding to S4.

Determining Limit States Probability: Five motions were used in order to obtain the limit states probability. The motions are 2%, 5%, 10%, 50%, and 75%

Table 2: Member sizes for the 3-story wood building models

Structure	Shear Walls		Diaphragms	
	Plywood Thickness (in.)	End Posts Area (in ²)	Plywood Thickness (in.)	End Posts Area (in ²)
S1 (70% St D)	0.35	40.25	0.35	24.15
S2 (80% St D)	0.4	46	0.4	27.6
S3 (90% St D)	0.45	51.75	0.45	31.05
S4 (St D)	0.5	57.5	0.5	34.5
S5 (110% St D)	0.55	63.25	0.55	37.95
S6 (120% St D)	0.6	69	0.6	41.4
S7 (130% St D)	0.65	74.75	0.65	44.85
S8 (140% St D)	0.7	80.5	0.7	48.3

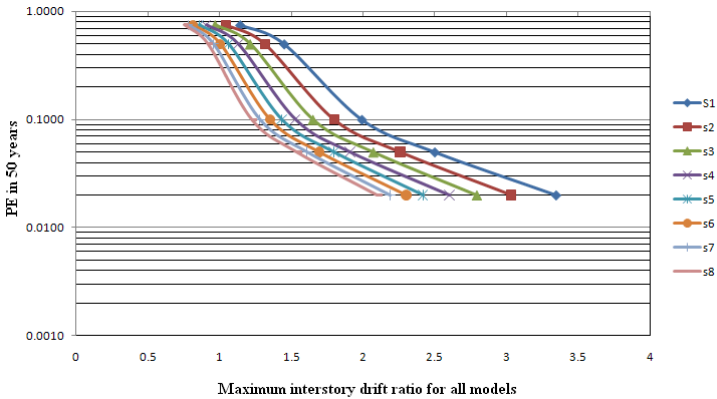


Figure 4. Maximum interstory drift ratio and probability of exceedance in 50 years for the 3-story wood building at Los Angeles

probability of exceedance (PE) in 50 years. The spectral acceleration parameters (S_s and S_1) for 2%, 5%, and 10 % PE were obtained from The National Seismic Hazard Mapping Project of USGS [2008] for the Los Angeles site. The parameters for 50% and 75% PE were obtained according to FEMA 273 [1997]. Each model listed in Table 2 is analyzed for each motion and the critical drift is determined. Figure 4 shows the critical drift for each model along with the PE. The annual probability is then determined according to the formula provided by USGS [2008]. Accordingly, new set of curves are then developed to illustrate the relation between the annual PE and the Corresponding maximum interstory drift for each building model. These curves are further fitted using power function using EXCEL software in order to obtain the limit states probability thereafter. Figure 5 shows the annual PE versus drift ratio along with the curve fitting and the power equation of the curve for S1 only. It should be mentioned that the y-axis which as a logical function. The fitting

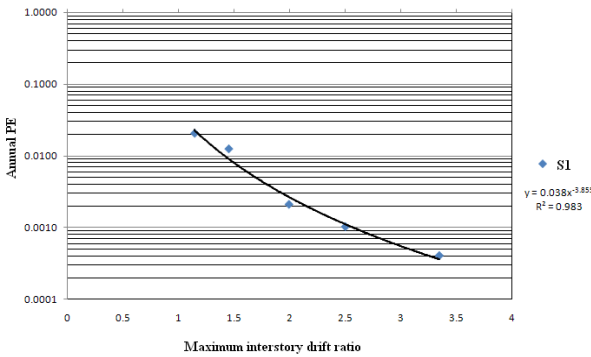


Figure 5. Maximum interstory drift ratio versus the annual PE with curve fitting using a power function for S1

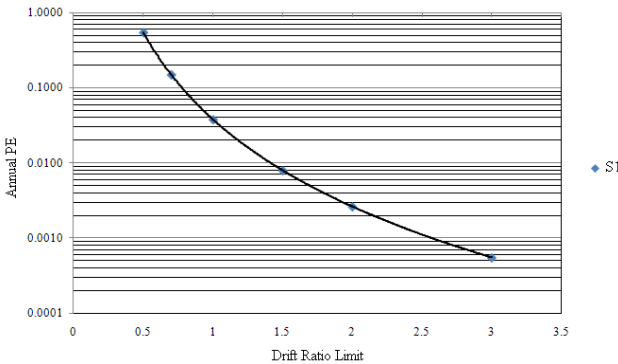


Figure 6. Drift ratio limit versus the annual PE for S1

equation provided for each curve is then used in order to generate a new curve describing the relation between the annual probability of exceedance and the drift limits for each building model (Figure 6). From the curves of drift ratio limit versus the annual PE for each model, and using equations 3-5, the limit state probabilities can be determined.

Determining Cost Function: All direct cost items were obtained through contactors, fabricators and previous studies. Based on the last mentioned sources, direct costs for all building models are listed in Table 3. The disposal and maintenance costs were assumed zero for all models. Regarding to the indirect cost, s mentioned before the damage cost is composed of six damages costs according to equation (7). FEMA 227 [1992], FEMA 228 [1992], FEMA 174 [1989], and ATC-13 [1985] specifications were used to calculate all these costs. All these standards

provide the basic costs according to 1985 year. Accordingly, these costs were transferred into its 2010 worth using the discount rate of 2.7% according to the latest value provided by OMB [2010]. These costs depend mainly on the social function classification of the structure. The structure under consideration is classified as residential low rise building. The main items included in the indirect cost calculations are: basic cost value, total area of the structure, central damage factor (CDF), number of months required relocation and rental, number of persons occupied by the structure, injure rate, and death rate.

Table 3: Direct cost for all models

Model	Direct Cost (\$)	Indirect Cost (\$)	Total LCC (\$)
S1	350000	2,978,696	3,328,696
S2	400,000	2,021,889.44	2,421,889
S3	450000	1,459,976	1,909,976
S4	500000	1,106,682	1,606,682
S5	550000	877,506	1,427,506
S6	600000	702,091	1,302,091
S7	650000	575,536	1,225,536
S8	780000	486,222	1,266,222

The total LCC is calculated according to equation (10). As shown in equation (10), the failure LCC cost is calculated by the multiplying the total indirect cost listed by the limit state probability, and then the results are transformed into future costs by using equation (10). Life time of 50 years was used in the calculations of the indirect costs. Table 3 and Figure 7 show the direct, and indirect and total LCC for each model. As shown in Table 3 and Figure 7, the code design model is not the optimum design whereas S7 building model is the QRA criteria.

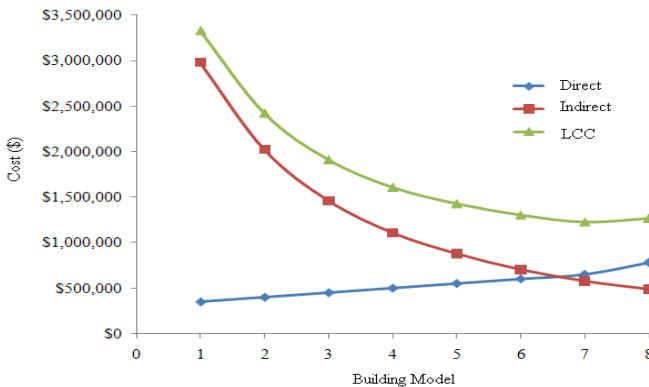


Figure 7. Direct, Indirect, and LCC for building models

SUMMARY

A methodology for optimum design based on the QRA was presented in this paper. The indirect or damage cost involved in the LCC is calculated based on the

concept of QRA. The QRA depends on three main parameters; resulting damage, probability of resulting damage, and probability of hazard occurrence. Further, a case study of residential wood building was also presented as a design example. Based on the results of this case study, the code design was not the optimum one over the structures' life time. Accordingly, this raised the weakness of the current code methods and therefore the need for a new advanced design method should be highly considered in order to minimize the damage and/or the failure of the new structures.

REFERENCES

- Ang, A. H-S., "Practical Assessments of Risk and Its Uncertainty", IFIP WG 7.3 Working Group Conf. Proc., Taylor & Francis Publishers, Netherlands, 2006a.
- Applied Technology Council (ATC) (1985) "Earthquake Damage Evaluation Data for California", ATC-13, California.
- Ehlen, M. A. (1999). "Life-Cycle Costs of Fiber-Reinforced-Polymer Bridge Decks." *Journal of Materials in Civil Engineering*, 224-230.
- Federal Emergency Management Agency (FEMA) (2006). "NEHRP Recommended Provisions: Design Examples, FEMA 451, 2003 Edition, Washington, D.C.
- Federal Emergency Management Agency (FEMA) (2003). "NEHRP Recommended Provisions for Seismic Regulations for New Buildings and Other Structures." FEMA 450, 2003 Edition, Washington, D.C.
- Federal Emergency Management Agency (FEMA) (1997) "NEHRP Guidelines for the Seismic Rehabilitation of Buildings, FEMA 273, 1st Edition, Washington, D.C.
- Federal Emergency Management Agency (FEMA) (1992) "Benefit-Cost Model for the Seismic Rehabilitation of Buildings, FEMA 227: Volume 1 & 2, Washington, D.C.
- Federal Emergency Management Agency (FEMA) (1989) "Establishing Programs and Priorities for the Seismic Rehabilitation of Buildings" Handbook, FEMA 174, Washington, D.C.
- Kang, Y.-J., Wen, Y. K. (2000) "Minimum Life-Cycle Cost Structural Design Against Natural Hazards" Structural Research Series No. 629, University of Illinois at Urbana-Champaign.
- Leeming, M. B. (1993). "The application of life cycle costing to bridge." *Journal of Bridge Management*, London, U.K., 574-583.
- Makow, M.J. (1995), "Highway management systems: state of the art." *Journal of Infrastructure System*, ASCE, 1(3), 186-191.
- Smith, N. J., and Obaide T. (1993). "Whole-life costing of steel bridges." *Journal of Bridge Management*, London, U.K., 519-639.
- Office of Management and Budget "Guidelines and discount rates for benefits-cost analysis of federal programs, Appendix C." (2010), OMB Circular No. A-94, Washington, D.C.
- U.S Geological Survey (2008), <http://earthquake.usgs.gov/earthquakes/>
- Wen, Y. K. ., and Ang, A. H-S., "Reliability and Cost-Effective of Structures with Active Control," *Intelligent Structures-2: Monitoring and Control*, Proc. Of the International Workshop on Intelligent Systems, Perugia, Italy, 27-29, Elsevier Applied Science.

Statistical Tools for Populating/Predicting Input Data of Risk Analysis Models

G. L. Pita^{1*}, R. Francis^{2*}, Z. Liu³, J. Mitrani-Reiser⁴, S. Guikema⁵, J.-P. Pinelli⁶

¹PhD Candidate, Civil Engineering Department, Florida Institute of Technology. Visiting student at Johns Hopkins University. gpita@my.fit.edu

²Assistant Professor, Department of Engineering Management and Systems Engineering, The George Washington University. seed@gwu.edu

³Graduate Student, Civil Engineering Department, Johns Hopkins University. zliu36@jhu.edu

⁴Assistant Professor, Civil Engineering Department, Johns Hopkins University. jmitrani@jhu.edu

⁵Assistant Professor, Department of Geography and Environmental Engineering, Johns Hopkins University. sguikema@jhu.edu

⁶Professor, Civil Engineering Department, Florida Institute of Technology. pinelli@fit.edu

ABSTRACT

By quantifying economic risk due to damage to building stock, regional loss models for natural hazards are critical in the creation of regional policies, including evacuation strategies and zoning. The increasingly complex interaction between natural hazards and human activities requires more and more accurate data to describe the regional exposure to potential loss from physical damage to buildings and infrastructure. While databases contain information on the distribution and features of the building stock, infrastructure, transportation, etc., it is not unusual that portions of the information are missing from the available databases. Missing or low quality data compromise the validity of regional loss projections. Consequently, this paper uses Bayesian Belief Networks and Classification and Regression Trees to populate the missing information inside a database based on the structure of the available data. A case study is presented to evaluate results.

INTRODUCTION

Catastrophe (or cat) models are essential for predicting future losses in a specific region and/or of a portfolio of properties due to a disaster, such as a hurricane, earthquake, or large-scale oil spill. These tools could also be used to: identify vulnerable sub-areas in geographic regions and insurance portfolios, to help decide how best to allocate post-event resources and inform other emergency response plans, to help inform hazard mitigation policies, and to inform stakeholders of their expected risk given the physical location and the quality of their assets. However, in order to perform an accurate hazard risk assessment for a region/portfolio, it is

* First Authors

necessary to have reasonably complete and accurate data on the inventory of buildings, lifelines, and other engineered systems.

Traditional catastrophe models, such as HAZUS (OES 2006) use census tract data to populate their building and lifeline inventory databases. Although inventory data at the census tract level is useful, it only allows for gross damage analysis of the built environment. Other risk assessment models, such as MAEviz have attempted to refine risk assessment inventories using advanced technological and statistical tools to populate these inventories. MAEviz contributors (e.g., French and Muthukumar 2006) use LIDAR and aerial photography to determine building footprint classifications (e.g., rectangular, H-shaped, etc.), and use multinomial logistic regression models and artificial neural networks to estimate building structural types (e.g., wood, concrete, etc.). Although this work is limited to a small geographic region, the results are promising and indicate that statistical tools can be successfully used for populating building and lifeline inventory databases.

We extend statistical modeling of building and lifeline inventory databases to imputation of missing building and lifeline inventory data. This is an important problem because building inventory data is often incomplete. The original building stock data is collected from tax assessor records, which often have missing values for specific data fields and which sometimes have erroneous information for a given property. Moreover, because building datasets are recorded not for the purpose of describing a building's strength characteristics but for tax collection and insurance ratemaking purposes, information needed for strength estimation may be missing.

In this paper we explore the use of a variety of graphical models to populate structural features such as the roof shape of buildings for use in a hurricane risk assessment model. This paper presents the results for roof shape classification using Bayesian Belief Networks (BBN) and Classification and Regression Trees (CART). Classification accuracies are also provided, and recommendations are given for the use of these models for other risk assessment applications. Although we have evaluated the performance of other data mining techniques for populating missing values, the scope of this paper is restricted to the application of graphical models for multiple imputation of missing values. These alternative methods include support vector machines (SVM), Bayesian additive regression trees (BART), and multivariate adaptive regression splines (MARS). For more information on these other methods see Hastie et al. (2001).

BACKGROUND

Missing data. Missing data is a problem in statistical analysis for diverse types of problems and applications as missing values can bias predictions or inferences unpredictably (Helsel, 1990, 2005; Helsel and Cohn 1988). As discussed above, building stock data is particularly prone to missing data. Several methods have been developed for dealing with missing data. The most widely accepted method is multiple imputation using the EM algorithm (Dempster et al., 1977). The intuition behind this approach is to perform a random walk over all the possible values of the

missing data given parameter values that could be expected to produce to the observed data set.

Graphical models. In this paper, we take a different approach to missing data prediction by using BBNs and CART to classify the observed values based on other covariates in the data set. Assuming that the missing values are missing at random, we then predict the classification of the missing values based on the other covariates. We use this approach to predict roof shape (RS) in several Florida counties, applying Bayesian Belief Networks (BBNs) and classification and regression trees (CART) as our data mining techniques (Hastie et al., 2001).

A Bayesian Belief Network (BBN) is a graphical representation of a probability model. Nodes represent marginal and conditional probability density functions, and arcs represent probabilistic relevance. A BBN is a directed graph Q , with edges e and k nodes θ . The values of the nodes of the BBN are ζ_θ . For $i, j \in k$ the probability that a node θ_i takes the value ξ_{θ_i} can be written:

$$\Pr(\xi_{\theta_i} | \xi_{\theta_j}, j \in 1, 2, K, k, i \neq j, \Theta)$$

Consider, as an example, a simple case with three random variables: A, B, and C. Suppose B and C are conditional on the outcome of A, and conditionally independent from each other given the outcome of A. This causal relationship can be represented by the simple BBN in Figure 1.

The conditional distribution represented by this graph is shown in the following equation:

$$\Pr(A, B, C) = \Pr(B|A)\Pr(C|A)\Pr(A)$$

BBNs are easily extended to prediction and filtering applications. Suppose we want to predict the value of θ_i given the values of θ_j for $i, j \in k$. The prediction for the value of θ_i , $\hat{\zeta}_{\theta_i}$, is given by the rule:

$$\hat{\zeta}_{\theta_i} = f(\theta_j, \Theta) = \max \left[\Pr(\xi_{\theta_i} | \xi_{\theta_j}, j \in 1, 2, K, k, i \neq j, \Theta) \right]$$

This is the Bayes' classifier (Hastie et al., 2001). The Bayes' classifier simply says that the prediction for a node value is its most probable value given the BBN structure and observed node states, θ . Both BBNs and CART makes predictions according to the Bayes' classifier.

The other statistical model we focus on in this paper is that of Classification and Regression Trees [CART] (Breiman, et al., 1984; Hastie et al., 2001). CART is a tree-based data mining model. The tree is characterized by recursive, binary splitting over a set of covariates such that the variance over the dependent variable within the binary groups is minimized. CART is fully nonparametric and no causal assumption is necessary to construct CART models. The most important consideration in

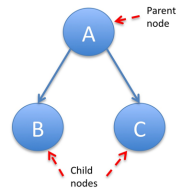


Figure 1 Example BBN with one parent and two children.

developing CART models is the use of cross-validation to avoid overfitting. Overfitting is a particular danger in flexible, non-parametric methods such as CART, because the dataset may be recursively split until each data point contains its own terminal node. Thus, the tree is typically pruned through cross-validation, penalizing the tree for complexity while accounting for prediction accuracy.

Cross validation. In this paper, the constructed BBNs and CART models were evaluated through k-fold cross validation. k-fold cross validation consists of recursively randomly splitting the database into a training set used to fit a model, and a testing set to test the prediction accuracy of the trained model.

CASE STUDY: ROOF SHAPE PREDICTION IN FLORIDA LOW-RISE BUILDINGS

In a survey of building stock data performed by the authors (Pita et al., 2008), it was observed that roof shape—the most important building feature needed to characterize the overall ability of a house to resist hurricane-induced pressures—is the most frequently missing variable from property assessors’ data and other public records in the state of Florida. In addition, counties often record this information by combining gable and hip roof shapes into a single category, making it difficult to identify the actual roof shape. It is particularly important to distinguish hip and gable roof shapes because the distribution of pressures that the wind exerts on the roof differs considerably in both cases, significantly impacting the overall vulnerability of a structure.

A case study is presented where statistical models are used to predict roof shape categories (RS = [gable, hip, other]) based on other building characteristics. The case study is performed on multi-family buildings (2368 buildings for Marion and 2238 for St. Lucie) of St. Lucie and Marion counties for which the datasets have all the variables of interest. These variables and categories are described in Table 1.

Table 1: Building feature variables (from Pita et al., 2008).

Variables	Categories
Exterior Wall	Concrete Block / Masonry (CB), Timber
Year Built	before 1960; 1961-1970; 1971-1980; 1981-1993; 1994-2001; 2002-2010
Roof Cover	Shingles, Tiles, Metal, Other
Roof Shape	Gable, Hip, Other
Building Value (\$)	<50,000; 50,000 – 73,000; 73,001 – 100,000; 100,001 – 300,000; > 300,000
Number of Stories	1, 2, 3

BBN Imputation Model for Roof shape. A Bayesian Belief Network (BBN) was used to better understand the underlying relationships amongst the building characteristic and to predict the roof shape in our case study counties. Netica® and Matlab® were used to develop the BBN models. The probabilistic relationships were

defined by expert knowledge together with statistical analysis of the relationships between them through a cluster analysis of the variables. An example of the network structure and the resulting conditional probabilities that relate the nodes for St. Lucie County is depicted in Figure 2.

The construction of the BBN model involved the use of expert knowledge to identify the variables that are most relevant for predicting roof shape. These variables were chosen from the property appraiser data and, based on expert knowledge, were reduced to a set that are most likely to infer roof shape. The selection of the covariates and their respective links in the BBN model was validated by lengthy calculations of the conditional probabilities for a given roof shape given each of the alternative states (e.g., 1, 2, or 3) of the other variables (e.g., number of stories); the covariates are all listed in Table 1. The BBN model ranked the variables most influential for predicting roof shape (for both counties) in descending order: year built, building value, roof cover, exterior wall and finally number of stories. Therefore, it is critical that for future regional studies, we collect data that includes the year built and the building value.

The relationships amongst the variables, or links shown in Figure 2, were identified using expert knowledge and based on the results of the conditional probabilities calculation described above. The expert knowledge is particularly important for determining the direction of the links (or arrows in Figure 2) in the network. The number of links between nodes should be kept to a minimum; otherwise, the complexity of BBN increases quickly. Therefore, even though further links could be created between the nodes of our networks, these relationships are not significant enough to increase the predicting accuracy between variables and are discarded.

The last issue in the construction of the BBN is deciding the number of unique states to include for each variable. The selection of states for discrete variables (i.e., *roof shape* and *number of stories*) is straightforward. However the BBN accuracy is sensitive to the discretization of continuous variables, such as *year built* and *building value*, that are additionally ranked as most influential variables. Therefore, a careful study of building practices, population migration, and the evolution of building codes in the state of Florida was carried out to discretize the variable *year built*. The results of this study are given in Table 1. Note that since building code enforcement and regulations are not homogeneous for all counties in Florida, the discretization of *building value* for the entire State may not be feasible to use. Similarly, the influence of the number of unique states *building value* on the BBN accuracy was also thoroughly investigated; results are also given in Table 1.

Table 2: Predicting accuracy of roof shape using the BBN models

Model	10-fold Cross Validation	Predicting the other county
St. Lucie	0.76	0.68
Marion	0.73	0.68
Combined	0.71	St. Lucie: 0.72 Marion: 0.72

The predictive accuracy of two BBN models was analyzed. One through 20% cross-validation, to predict roof shape of portions of the same dataset used to fit the network. The other model predicted roof shape of one county through a BBN fitted with the other available county and vice versa. The results are displayed in Table 2.

CART Imputation Models for Roof shape. In order to improve the predictive accuracy, we also applied a CART model to classify roof shapes for St. Lucie County and Marion County. Because gable roofs are the dominant class for these two counties, we developed two kinds of CART models: one model only predicts the gable roof class; the other model predicts all the roof shapes at once in the building stock. An example of the classification tree for predicting gable roof is given in Figure 2.

In this tree, *RC_gravel* is a binary variable: if it is equal to 1 then the roof cover material is gravel, and if it is equal to zero the roof cover material is not gravel. *Year Built* is the year the building was built and *BuildingVal* is the value of a building. When each branch breaks off to the left, it means that the logical statement is true for that node, and the right branch is the false case. For the CART model that only predicts the gable roof class, like in Figure 2, the predicted result is gable roof if the probability is larger than or equal to 0.5, otherwise we say it is not gable roof. However, the models that predict all roof shapes at once result in a group of probabilities for each roof shape. For this type of CART model, we use the maximum probability of the entire group to determine roof shape.

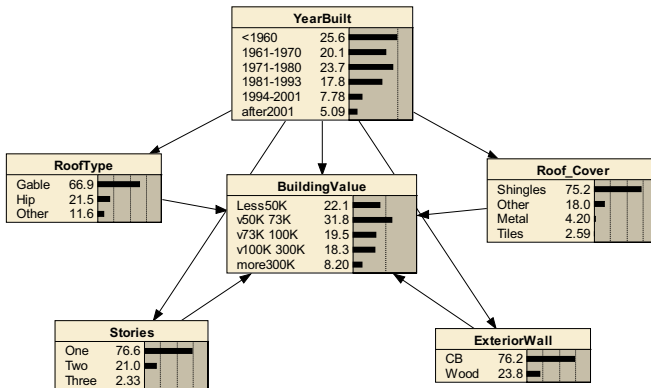


Figure 1: BBN for St. Lucie County database (Netica®)

Table 3. Predicting accuracy of roof shape using the CART model fitted with the St. Lucie County building database

Model		Gable	All
Predicting accuracy	St. Lucie	0.82	0.81
	Marion	0.67	0.72

Table 4. Predicting accuracy of roof shape using the CART model fitted with the Marion County building database.

Model		Gable	All
Predicting accuracy	Marion	0.82	0.82
	St. Lucie	0.66	0.66

In order to estimate the predicting accuracy of our models, we do hold out tests for each model. Typically we set the number of hold out tests to be 60 and hold out 20% of the data set each time. The criteria we used to compare models' accuracy is the fraction correct that is the percentage of the number of correct predictions over the total number of predictions. The hold out tests results are for St. Lucie and Marion Counties are given in Table 3, Table 4 and Table 5. The first row of each table is the mean fraction correct of the hold out tests for each county. The other rows are the fraction correct that we used one data set's CART model to predict other data sets.

Table 5: Predicting accuracy of roof shape using the CART model fitted with the combined building databases of St. Lucie County and Marion County.

Model		Gable	All
Predicting accuracy	St. Lucie & Marion	0.80	0.79
	St. Lucie	0.81	0.80
	Marion	0.79	0.78

DISCUSSION

For the present case study results show that BBN models work well for predicting the data set that they are built on (73% to 76%). The accuracy drops to about 68% when predicting roof shapes of the other available dataset (e.g., using St. Lucie data to predict for Marion County). CART models do better with around 82% predicting accuracy for cross-validation and about the same at 67% for predicting one county roof shape with a model fitted with the other county. For this case study it seems not optimal to use a single county's classification tree to predict other counties' roof shape. The low accuracy in both models to predict a county's roof shape using a model fitted on another's data might be rooted in the differing buildings stock characteristics of both available counties. Marion is an inland northern-central county with no significant hurricane history while St. Lucie is a coastal south-east county with hurricane history and higher population density (although less inhabitants).

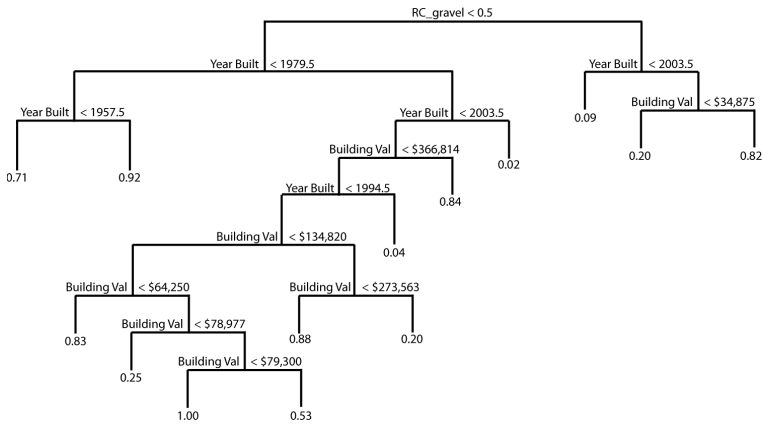


Figure 2 Classification tree for predicting gable roof in St. Lucie County.

CART models showed better results for this case study; however, it seems premature to indicate the superiority of CART over BBN for this problem without analyzing more counties. For both datasets combined into a single dataset, the BBN has 72% prediction accuracy when predicting individual county data using a model fit to the combined dataset. On the other hand, the classification tree fitted to the combined dataset has prediction accuracies of 80% and 78% for St. Lucie and Marion counties' roof shapes. Thus, using a CART model fit to the combined dataset to find a common pattern of the distribution of the roof shapes, then using this pattern to predict the attributes of individual county datasets seems promising. The use of a single model still needs to be applied to many more counties. We intend to collect more data to explore patterns for predicting roof shapes for the entire state by: (1) fitting a CART model for a single dataset that combines all collected data, or (2) fitting a CART model for datasets disaggregated by several regions that share similar common building construction patterns. Construction and evaluation of these models on such comprehensive datasets will enable us to more strongly evaluate the validity of graphical models for supporting catastrophe modeling in risk assessment.

ACKNOWLEDGEMENTS

This research is supported by the State of Florida through a Department of Financial Services (FDFS) grant to the Florida International University International Hurricane Research Center, and the National Science Foundation through CMMI 0826365. The opinions, findings, and conclusions expressed in this paper are not necessarily those of the FDFS. The help of St. Lucie and Marion property appraisers is gratefully appreciated. Thanks to Fausto Fleites and Hsin-Yu Ha for helping to process the databases.

REFERENCES

- Dempster, A., Laird, N., & Rubin, D. (1977). «Maximum likelihood from incomplete data via the EM algorithm». *Journal of the Royal Statistical Society, Series B*, 39(1), 1-38.
- French, S.P., and Muthukumar, S., 2006. "Advanced Technologies for Earthquake Risk Inventories". *Journal of Earthquake Engineering*, 10(2): 207-236.
- Hastie, T., Tibshirani, R., & Friedman, J. (2001). *The elements of statistical learning theory*. New York: Springer.
- Helsel, D. (1990). "Less than obvious: statistical treatment of data below the detection limit". *Environmental Science and Technology*, 24(12), 1766-1774.
- Helsel, D. (2005). "More than obvious: better methods for interpreting nondetect data". *Environmental Science and Technology*, 39(20), 419A-423A.
- Helsel, D., & Cohn, T. (1988). "Estimation of descriptive statistics for multiply censored water quality data". *Water Resources Research*, 24, 1997-2004.
- Jensen, F.V., (1996) *An Introduction to Bayesian Networks*. UCL Press. London.
- Kjaerulff, U.B. and Madsen, A.L. (2008), *Bayesian Networks and Influence Diagrams*. Springer Verlag. New York.
- (OES) Office of Emergency Services, 2006. "Data Standardization Guidelines for Loss Estimation – Populating Inventory Databases for HAZUS®MH MR-1." A report prepared by ImageCat, Inc. and ABS Consulting, Inc. for the California Governor's Office of Emergency Services, March 2006.
- Pearl, J. (1988). *Probabilistic Reasoning in Intelligent Systems: Networks of Plausible Inference*. San Francisco, CA: Morgan Kaufmann.
- Pearl, J. (1998). *Bayesian networks*. Los Angeles, CA: UCLA Computer Science Dept.
- Pita, G. L. , Pinelli, J.-P. , Subramanian, C.S. , Gurley, K., Hamid, S. (2008), "Hurricane Vulnerability of Multi-Story Residential Buildings in Florida". *Proceedings ESREL 2008*. Valencia, Spain.

Integrating Risk Management within the Project Delivery Process at Caltrans: A transportation project case study

PEDRO MARIA-SANCHEZ¹, ROSS CATHER², LOU MELENDEZ³, ROBERT LOWRIE⁴

¹California Department of Transportation, 4050 Taylor Street, San Diego, CA, 92110; PH (619)718-7821; FAX (619) 688-2508; email: pedro_maria-sanchez@dot.ca.gov

²California Department of Transportation, 4050 Taylor Street, San Diego, CA, 92110; PH (619)688-3633; FAX (619) 688-3122; email: ross_cather@dot.ca.gov

³California Department of Transportation, 4050 Taylor Street, San Diego, CA, 92110; PH (619)688-3328; FAX (619) 688-3122; email: lou_melendez@dot.ca.gov

⁴California Department of Transportation, 4050 Taylor Street, San Diego, CA, 92110; PH (619)688-6784; FAX (619) 688-3122; email: bob_lowrie@dot.ca.gov

ABSTRACT

The purpose of this exercise was to apply the risk management concepts for assessing the project's risk profile, quantify the risks in terms of cost, validate the cost estimate and to propose mitigation strategies for managing the risks. The California Department of Transportation (CALTRANS) has developed a Project Risk Management Handbook; the guidelines of this document were followed on this study. The Cabrillo Bridge is located in Balboa Park and was built for the 1915 Panama-California Exposition. Currently the project is in the environmental phase and is set for completion in spring 2010. The project team was faced with a decision to move forward with a replacement or with rehabilitation. It was believed that significant public controversy and opposition would arise with a replacement alternative because the Cabrillo Bridge is an integral part of the City's Balboa Park, a public facility which is listed as a National Historic Landmark.

A Risk Management Team was formed and its members represent the project different functional units. The results show the possibility to obtain a cost contingency based on specific risks within the risk register and uncertainty with the items of the project cost estimate, instead of assigning a contingency value without any reference to identified risks or uncertainty conditions. In addition, the results validated the alternative recommended by the value analysis study. This paper demonstrates the viability for performing concurrently risk management and value analysis, having done this; it will provide very valuable feedback to the value analysis study plus will contribute with quantifiable data for sustaining a decision over a selected alternative. In addition, it will formalize the use of risk management with CALTRANS current process for delivering projects.

PURPOSE

The purpose of this exercise was to implement Caltrans' risk management methodology for the Cabrillo Bridge project, which is at the environmental phase. A cost risk analysis was conducted in order to address the project's uncertainties while creating a risk register and performing uncertainty analysis for the project cost estimate for each of the three alternatives. Contingency percentages were able to be obtained for each alternative. The risk management team (RMT) was involved in the whole risk management process (planning, identification, analysis and response).

Additionally, Caltrans does not have a formal process of implementing risk management within its project delivery process. The results obtained on this study will provide a relevant support for the implementation and for developing a permanent program in risk management.

SCOPE OF WORK

The scope is to identify, analyze, quantify and respond to the project's risks as mandated by CALTRANS within its Office of Statewide Project Management Improvement (OSPNI) and the Project Risk Management Handbook (Second Edition, May, 2007). The work presents the cost risk analysis results for the alternatives selected for this study. In addition, it will include recommendations and risk mitigation strategies.

In addition, this study will show the feasibility of implementing risk management within Caltrans project delivery process.

A cost risk analysis was carried out for the risks identified as critical within the risk registers and for the project cost estimate (uncertainty in unit prices and item quantities). The results obtained from both analyses were put together in order to show the total project cost with risk.

PROJECT ALTERNATIVES

The Project Study Report (PSR) proposes five alternatives to address deficiencies of the bridge and one "No Build" alternative. Three of the alternatives propose to address the deficiencies through seismic retrofit and structural rehabilitation and two separate alternatives address those deficiencies through complete bridge replacement.

Two of the three seismic and rehabilitation alternatives propose a two-staged approach. The third one "Alternative VA" proposes a seismic retrofit project that combines Stage 1 (providing safe access for bridge inspection and scoping for final design of the structure rehabilitation to be done in Stage 2) and Stage 2. The stages are therefore to be done concurrently, with design measures to reduce the risk of cost overruns as recommended

by the multidisciplinary Value Analysis (VA) Team. Alternatives 3 and 4 propose complete bridge replacement and are therefore projects that do not require Stage 1 work.

The "Alternative VA" is the PSR recommended alternative and therefore it was chosen for risk analysis from amongst the three proposing retrofit and rehabilitation. It along with the two alternatives that propose complete bridge replacement for a total of three alternatives comprised the risk analysis agenda. The "No Build" alternative was not considered for risk analysis for obvious reasons.

CALTRANS RISK MANAGEMENT PROCESS

The risk management methodology follows CALTRANS' guidelines and methodology described with the Project Risk Management Handbook developed by the OSPNI. The quantitative cost risk analysis used the Monte Carlo simulation method included in the @ Risk software.

Risk identification

The risk identification meeting held with the RMT provided the first input data for creating the risk registers. It is important to mention that three different alternatives were analyzed at the same time. Figure 1 shows the risks identified per alternative and risk category.

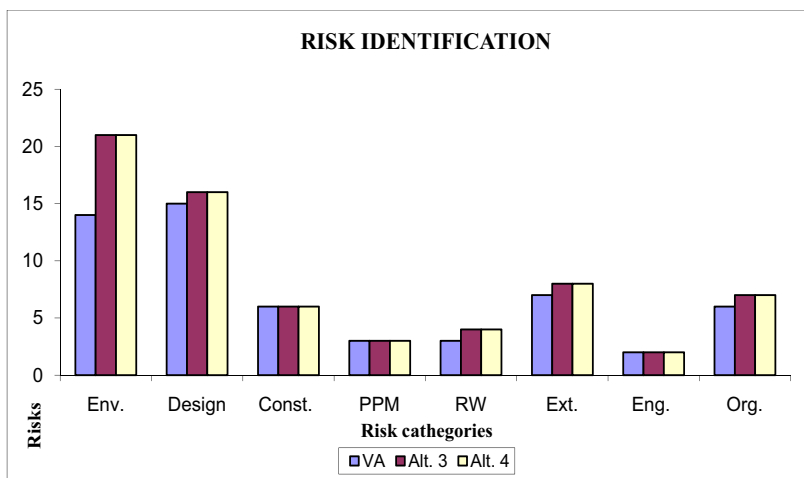


Figure 1. Identified risks per the alternative

It is important to mention that for alternatives 3 and 4, the same number of risks (67 risks) were identified, this make sense because the scope of these alternatives is similar. Whereas in the case of the VA alternative; 56 risks were identified. The higher concentration of risks was with the environmental and design categories. Additionally, 21 environmental risks were identified for alternatives 3 and 4. A checklist was used to facilitate the risk identification and very valuable input from the entire RMT was obtained using brainstorming. In addition, project data from the Project Study and the Value Analysis reports was considered. The risk registers were created and used as the basis for the qualitative analysis.

Qualitative Cost Risk Analysis

The RMT evaluated the probability and impact for each risk. A risk matrix (see Figure 2) was used in order to combine the risk probability and impact values and for obtaining a risk score. Whenever the risk score falls into the red zone of the risk matrix, it was considered critical. For example, if a risk has a high probability and a high impact, then this is risk considered critical. In that way, the risks contained in each risk register were classified in terms of their criticality. Figure 3 shows the critical risks per alternative obtained in the qualitative assessment. Alternative 4 has the highest number of critical risks with a total of seven, followed by the VA alternative and alternative 3 with six critical risks each.

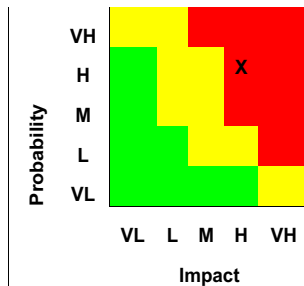


Figure 2. Risk matrix

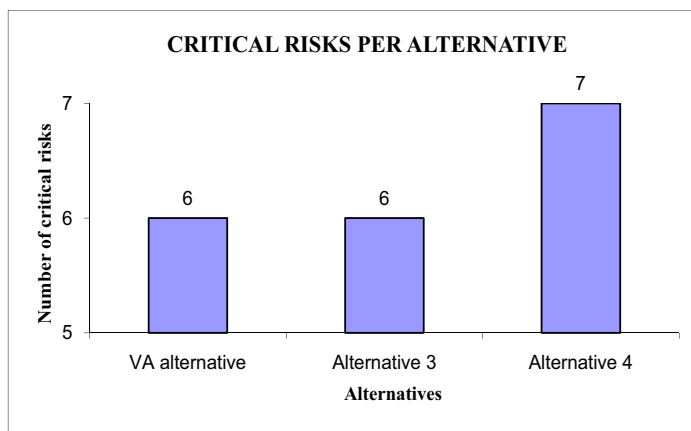


Figure 3. Critical risks per alternative

The results obtained with the qualitative analysis conform the basis for implementing the quantitative analysis for the risk registers and the project cost estimate; which uses only the most critical risks.

Quantitative Cost Risk Analysis

The quantitative risk assessment input data was obtained automatically while performing the qualitative risk analysis. This was possible because within the Risk Register, a range of probable risk cost impacts was created and linked to the risk score. In other words, once a risk score was obtained through the qualitative assessment; it was possible to select a cost range representative for its impact. Representing this cost range, the input data (minimum and maximum values) for the probability distribution to be used with the simulation model. The risk matrix, the cost range and the risk scores were validated with the RMT.

The quantitative risk impacts and probabilities were analyzed using a combination of professional judgment and project data. It was an iterative, consensus-building approach to estimate the elements of each risk. Risk scores were quantified using probability distributions (density functions), the risk cost impacts were entered into the @ Risk software in the form of probability density functions. A Monte Carlo simulation model was developed for the risk register and for the project cost estimate. The results are shown in the following sections.

Figure 4 shows the results obtained with the cost risk analysis for the Risk Register for the three alternatives. The values of the first column represent the contingency proposed

with the project cost estimate. The simulated risk cost values (50 % confidence level) for the risk register items are the ones shown in the second column. These values included only the most critical risks identified per each alternative. It is possible to notice that alternative 4 is the one requiring a higher contingency (\$19.22 million) and the VA alternative is the one requiring the least contingency (\$11.41 million).

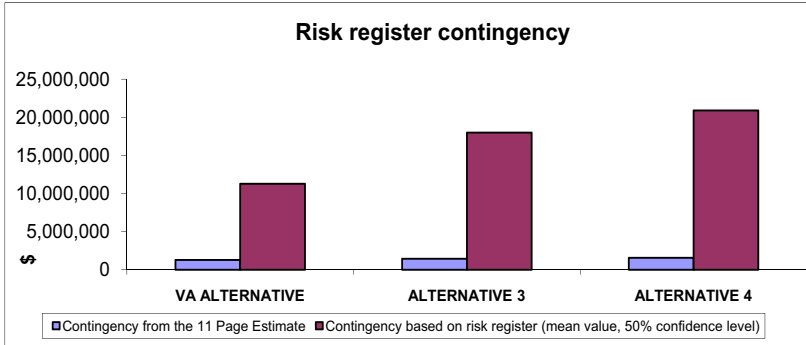


Figure 4. Risk register contingency per alternative

The following results (Figure 5) enclosed the cost risk analysis performed into the project cost estimate for each alternative, while assuming uncertainty for the quantity items and for the unit prices. The values of the first column are basically the project cost estimate calculated by the project engineer without the contingency amount. The values of the second column represent the results obtained with the risk model for a 50% confidence level.

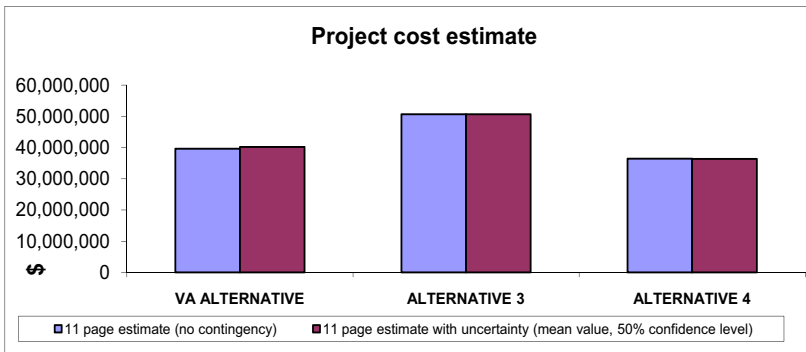


Figure 5. Project cost estimate

As can be observed from Figure 5, the results obtained with the risk analysis model are very similar to the project cost estimates values for the three alternatives. This exercise validates the process used by the project engineer for determining the project cost with no risk assessment. Nevertheless, is the objective was to get a higher confidence level, then, a contingency will be needed.

The total project costs per alternative with and without risks are shown in Figure 6. Alternative 3 has the highest cost with and without risk (total cost without risk is \$52.1 million and with risk, is approximately \$68.37 million) at 50% confidence level.

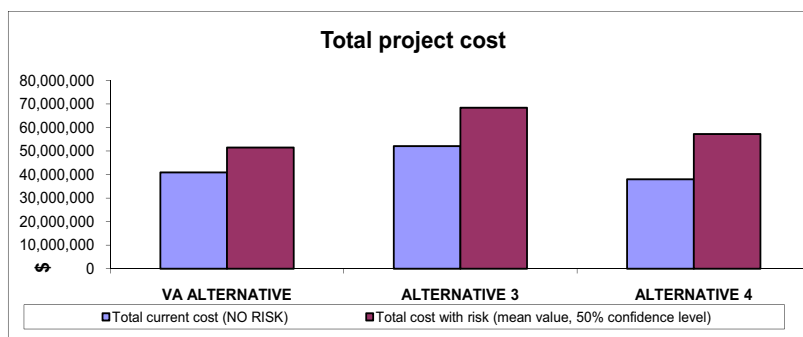


Figure 6. Total project cost

In second place came alternative 4 with a total cost without risk of \$38.0 million and \$57.22 million with risk. The lower total cost with risk came for the VA alternative with a value of \$52.31 million and \$40.9 million without risk. By calculating the difference between both estimates (with and without risk), it is possible to obtain the contingency in money terms.

4.4 Risk Response and Monitoring

Several risk response strategies were recommended by the RMT and the risk owners. As part of the agreement for monitoring the risk management plan, the risk manager will be addressing the status of the risk management plan in regular meetings, usually in a monthly basis. The following table shows some examples of the proposed risks responses.

Table 1. Risk responses

RISKS	RESPONSE
Unidentified Materials/Geotechnical/Foundation issues	Request updated Geotechnical/Foundation report
Unknown condition of interior/exterior concrete on existing structure	Design with contingency factors and Contract Change Order in construction
High political visibility or unreasonable expectations for delivery	Discuss with City of San Diego

RECOMMENDATIONS

The complete risk management process was implemented for this project for quantifying the risks impacts in money terms. Nevertheless, it is recommended to perform a similar study but with emphasis in analyzing the impacts of risks in time terms (delays). Additionally, a formal request its being prepare for submission to CALTRANS executive staff for implementing formally risk management as part of its project delivery process.

REFERENCES

- CALTRANS (2007). "Project Risk Management Handbook: Threats and opportunities." Office of Statewide Project Management Improvement (OSPMI), Sacramento, Calif.
- CALTRANS (2008). "Project Study Report: Threats." California Department of Transportation District 11 San Diego, Calif.
- CALTRANS (2009). "Value Analysis Study Report." California Department of Transportation District 11 San Diego, Calif.
- Wayne, L.W. (2001). "Simulation Modeling using @Risk." Thomson Learning, Duxbury, Canada.

The Relationship between Hazards Vulnerability and Stage of Economic Development in Haiti and Chile

Lan Nguyen¹ and Ross B. Corotis¹

¹Department of Civil, Environmental and Architectural Engineering, University of Colorado, Boulder, Colorado 80309, USA; PH (303) 735-0539; FAX (303) 492-7317; email: corotis@coloado.edu

ABSTRACT

Both Haiti and Chile were subjected to major earthquakes less than two months apart. The loss of life and devastation in Haiti, however, was much worse, despite the magnitude of the earthquake being smaller. This paper investigates the underlying relationship between the implicit level of risk accepted for natural hazard vulnerability, and the level of economic, social and political development of the country. In particular, it reports on a study of seismic hazard and code development/enforcement for two countries at very different levels of development, illustrated through a case study.

1. INTRODUCTION

On January 12th, 2010, a magnitude Mw 7.0 earthquake hit Haiti. The seismic moment Mw relates to the work done from rupture and energy released from the earthquake. This earthquake received worldwide attention due to its widespread destruction.

Six weeks later, on February 27, 2010, a more powerful earthquake (Mw 8.8) hit Chile. Unlike Haiti, however, relatively few people died and few buildings were destroyed. Several international teams are investigating the sources of structural damage in the Haiti earthquake, trying to determine the cause of such extensive loss. This paper examines the status of building codes in the two countries, and the role they may have played on the resilience of the societies after an earthquake. To understand the circumstances surrounding the two countries, one must be aware of the demographics, the geology, and the seismic history of the two countries.

2. BACKGROUND OF THE TWO EARTHQUAKES

2.1 Haiti. The earthquake that struck Haiti happened at 04:53 PM local time (21:53 Coordinated Universal Time (UTC)). The main shock epicenter was located about 25 km west-southwest of the city of Port-au Prince shown in Figure 1. Within two weeks after the primary shock, there were 59 aftershocks with magnitudes 4.5 or greater (USGS, 2010).

Although Haiti had not experienced large earthquakes in the last 150 years, large earthquakes occurred there in 1701, 1751, 1770, and 1860. The 1770

earthquake resulted in the widespread destruction of buildings in Port-au-Prince and Léogâne. The earthquakes in Haiti are a result of east-west sliding movement between the Caribbean plate and the North American plate. The Mw 7.0 earthquake involved three faults including the newly discovered Léogâne fault which contributed 85 percent of the energy released during the earthquake (Israel)

2.2 Chile. On February 27, 2010, an earthquake with magnitude Mw 8.8 hit the central region of Chile. The main tremor occurred off the coast of the country at 3:34 am local time (6:34 UTC). Following the primary shock, over 300 aftershocks occurred with magnitudes of 5.0 or greater over the period of two months. In fact, twenty-one of these were at magnitudes 6.0 or greater (USGS, 2010). The epicenter of the 2010 earthquake was 105 km (65 miles) north-northwest of Concepción off the coast of the country shown in Figure 2. As the main earthquake occurred, the ocean floor warped and caused a destructive tsunami (Universidad de Chile, 2010). The earthquake moved the city of Concepción three meters (ten feet) to the west of its previous location, and moved the capital, Santiago, about 28 centimeters (11 inches) to the west-southwest (AON Benfield, 2010).

On March 3, 1985, an earthquake with a moment magnitude of 8.0 struck the same region, causing millions of dollars of damage to buildings and infrastructure in Santiago, although only 177 people died in that earthquake (USGS, 1985). The largest earthquake ever recorded in the world happened in Chile on May 22, 1960 with moment magnitude of 9.5 and killed approximately 2000 people in Southern Chile, Hawaii, Japan, and Philippines (H. Carrol Talley, 1960). In the 20th century, over 75 earthquakes of magnitude 7.0 and higher struck Chile (Universidad de Chile, 2010)

The type of 2010 Chile earthquake typically occurs at the subduction zones. In the case of Chile, the earthquake occurs at the boundary of two plates, with the Nazca plate moving eastward and sliding beneath the South American plate. The subduction zones are known to produce the most powerful earthquakes on earth since the geological make-up of the subduction zone allows more stress to build up before the energy is released in the form of an earthquake (Hayes, 2009).

2.3 Earthquake Differences Between Haiti and Chile. The 2010 Chile earthquake was much stronger than the 2010 Haiti earthquake. The energy released from the earthquake in Chile was about 500 times more than in the earthquake in Haiti. In the past, Chile reacted to the strength and frequency of the earthquakes it experienced with a strict seismic building code, which Haiti lacks. The building codes enacted in Chile can be credited with significantly reducing the loss of life after earthquakes including the 2010 earthquake. It is obvious that the physics of earthquakes striking a region have a significant impact on seismic design. In addition, there are other factors that have a large influence on the design of structures: population density, and the wealth of the region where earthquakes occur.

3. POPULATION AT RISK AND AFFECTED

3.1 Haiti. Over nine million people live in Haiti. Most of these people live in rural areas, and 80% of the population is living under the poverty line (CIA, 2010).

More than 1.5 million people were directly affected by the earthquake, which is more than 15% of the population of the entire country. The number of recorded casualties exceeded 222,570 deaths, and there were 300,000 injuries. At least four people were killed by a local tsunami in the Petit Paradis area near Léogâne. There are 1.3 million people now living in temporary shelters (United Nations, 2010). The estimated damage after the earthquake is 7.8 billion US dollars.

3.2 Chile. The population density in Chile is much greater than in Haiti, and more than eight million people live in the area affected by the earthquake in Chile. According to the Chile National Institute of Statistics, more than two million people live in the six regions directly affected by the earthquake: Concepcion, Talca, San Fernando, Valparaiso, and Santiago (AON BenField, 2010). The damage estimation is much higher in Chile than in Haiti: 30 billion US dollars. In contrast to Haiti, only 521 people in Chile died and 12,000 were injured from the earthquake and the resulting tsunami (USGS, 2010).

4. DAMAGE EXPERIENCED

4.1 Haiti. In addition to the loss of life, the earthquake destroyed over 105,000 homes and damaged more than 208,000 in the Port-au-Prince area and in much of southern Haiti. Critical infrastructure such as hospitals, government buildings, roads, and bridges were all rendered useless due to significant damage (USGS, 2010).

4.2 Chile. There was also significant damage to buildings and infrastructure due to the Chile earthquake. The earthquake in Chile damaged 370,000 houses, 4013 schools, and 79 hospitals (EERI, 2010b). Among the damaged buildings, there were 54 constructed of reinforced concrete, of which four suffered total or partial collapse (EERI, 2010b). Overall, there was a lot less disruption after the Chile earthquake, even though it was much more powerful than the Haiti earthquake.

4.3 Significance of the Effects of the Two Earthquakes. Despite the large magnitude of the Chile earthquake, the number of deaths, injuries, and buildings damaged were considerably less than in Haiti, a country that experienced a smaller earthquake but has no seismic code (Bhatty, 2010). The estimated dollar amount of the damage in Haiti approximates to 65% of its 2009 GDP. Chile's damage amount in dollars was estimated to be higher, due to the existence of more modern buildings and infrastructure, but approximates to only 11% of its 2009 GDP. Chile is a wealthier country than Haiti, and is considered a First World country. The government of Chile recognizes the seismic threat and enforces a strict building code throughout the country (Harris, 2010). In fact, Chile building code NCH 433 (1996) is an earthquake resistant design code. The standard was based on the perceived need to ensure the survival of most buildings, following the occurrence of the Mw 8.0 earthquake that happened on March 3, 1985 (Moehle, 2010)

In major earthquakes such as the one that occurred in Chile in 2010, the primary goal is to protect human life by preventing the collapse of structures. The Chile earthquake moment magnitude of 8.8 was larger than the design earthquake considered in the code. Therefore, it is not surprising that there was some damage

after the earthquake. Because of the economic position of the country, Chile has the ability to reduce future earthquake losses in terms of both lives and economics, and it is expected that they will further update and improve their seismic building code.

A later section of this paper will investigate the seismic building code in Chile, and to consider whether a similar standard could be adopted by a developing country like Haiti, even though the building types in both countries and their economic standings are completely different.

5. SOCIAL, ECONOMIC AND POLITICAL CONSIDERATIONS

5.1 Haiti. Haiti is the poorest country in the western hemisphere. GDP of the country as a whole was 11.99 billion US dollars and 1,300 US dollars per capita in 2009 (CIA, 2010). Over the past five years, the economy of Haiti grew slowly with the small annual percentage of 2.3% from 2004 to 2009 after a decline of 0.7% from 2000 to 2004 (US Department of State, 2010). This economic situation combined with natural hazards in the form of earthquakes and hurricanes places Haiti in a unique position. A concern is the degree to which this level of poverty and lack of social and economical resources increases the amount of risk the government is willing to have its citizens take. For the future, will the devastation that the citizens of the country experienced change the acceptability of this risk to human life?

Earthquakes are not the only natural hazards to strike Haiti. In the past, Haiti has suffered hurricanes and tropical storms, such as in 2008, when 800 people were killed within two months due to four such storms (CIA, 2010). This history is important because if the country regularly experiences severe weather and natural hazards, but no building codes are established and enforced to protect the people, it reflects on the priorities of the Haitian government. Perhaps these decisions could be the result of the government's limited knowledge of seismic structural design, or its willingness to assume a high level of risk due to competing economic factors for limited resources. An important question is whether some of the financial aid promised Haiti should be required to be used for seismic code development and enforcement for the reconstruction of Port-au-Prince and its environs.

Another concern is the political situation in the country. Ever since the country won its independence from France in 1804, Haiti has been plagued with economic instability and political corruption. There have been 55 leaders of Haiti since the country won its independence, but only nine of them were able to complete their presidential terms. The remaining leaders died during their terms, were killed, or were forced out of office (Buss, 2008). Many of these leaders were reported to have taken advantage of their citizens and the island's natural resources for personal and political gain. Citizens were often aware of this, and as a result, there were few times in the country's history where there was peace (Buss, 2008).

5.2 Chile. In contrast with Haiti, Chile has a reputation of being the strongest and most stable economy in South America. During the early 1990s, Chile's reputation made it an international role model for economic. It was also during this time period that Chile's seismic design code was adopted, indicating that Chile's strong economic status helped give it the opportunity to develop and improve other aspects of its society. In 1996, NCh433 was adopted and included a similar analysis procedure

those that appear in the 1997 UBC. As a result, strong earthquakes struck the country, but because the buildings were overall well-designed and up to code, there was a minimal loss of life.

Chile had experienced political instability in the past (Schneider, 2007), but in contrast with Haiti, Chile was able to move forward economically and socially, making sure that their citizens were treated fairly. In the early 1970's, the Chilean economy was struck by depression, inflation, and workers' strikes. In 1973, the Chilean government was overthrown by a military coup that later would be known for committing human rights violations, torture, and even murders. In the 1980's, Chile had recovered economically, and the government gradually began to grant its people more freedom (Schneider, 2007). Chile's GDP in 2009 was 242.2 billion US dollars and 14,600 per capita. The GDP of Chile increased with an annual average near 4 percent since 1999 (CIA, 2010).

6. BUILDINGS AND CODE ENFORCEMENT

6.1 Haiti. Haiti has a wide array of buildings, but, unfortunately, many of them are not designed for seismic loads (Harris, 2010). Buildings in the country can be divided into two categories: those built between 1800 and 1920, and those built from 1920 to the present. The buildings constructed prior to 1920 are categorized as historic buildings. They are: timber frame, unreinforced masonry and reinforced concrete buildings (EERI, 2010a).

In general, timber frame buildings perform well during an earthquake (EERI, 2010a). In Bois Verna, a neighborhood of Port-au-Prince, 200 wooden houses known as 'gingerbread' houses withstood the earthquake (Klarreich, 2010). These timber frame structures are light and flexible, with diagonal members and interior wooden planks spanning horizontally across the wall framing, providing lateral structural strength. The houses that stood were in relatively good condition prior to the earthquake. In many cases, however, there was serious damage to these structures due to the deterioration of wood members from termites and wood rot, thus weakening the structural members.

Unlike timber structures, unreinforced masonry buildings typically fail under earthquakes, with damage ranging from diagonal cracking in wall sections to collapse. Failures can be attributed to the lack of brick ties or brick headers between brick wythes, lack of reinforcement, weak stone at critical points, poor quality due to aggregate quality, inadequate cement or lime and poor maintenance (EERI, 2010a).

Concrete buildings can also fail during an earthquake. In Haiti, the concrete structures adopted a European style with heavy domes and Roman arches. Rigid first floors and massive concrete dome roofs caused the second floor to act as a soft story. This is the case of failure in the National Presidential Palace. (EERI, 2010a)

In the early 20th century, Haitian engineers and architects were educated in France. They were familiar with the French building design code-AFNOR, and these engineers were teaching at the University of Haiti. There were no earthquake provisions, however, in these codes. Structures designed by the Haitian engineers-both in the past and today-were primarily reinforced concrete with moment resisting frame and unreinforced hollow concrete masonry infill (EERI, 2010a). Infill

masonry structures suffered damage both in infill and the surrounding columns. In both reinforced concrete and reinforced masonry, smooth bars were used as reinforcement, and they were widely spaced in the structure. This appeared to be the causes of failures, especially in structural columns (EERI, 2010a).

Another important issue is the lack of supervision in building construction in Haiti. Engineering is only taught at the university level, and limited knowledge is transferred. There is an absence of building code and record keeping, and there is no inspection or regulation in the construction process (Bhatty, 2010). Seismic design is up to the individual and not subject to oversight by the government (EERI, 2010a).

The general practice in Haiti is that the builder is also the designer (except buildings designed and built by outside companies such as the Digicel building, which survived the earthquake (EERI, 2010a). The establishment of a seismic building code would almost certainly require that structures be designed by an engineer and inspected by a government official to ensure the code is being followed. The international community has pledged a large amount of financial support to assist in the rebuilding of Haiti. The challenge for the world is to show Haiti what to do with structural design, without having Haiti permanently rely on the international community. The long tradeoffs between more robust structures and other demands of society will eventually need to be addressed by Haiti's own people and government.

6.2 Chile. Unlike Haiti, Chile has a nationalized building code and it is enforced rigorously by the government. The seismic structural code of Chile, NCh433 (1996), has many provisions based on ACI 318-95. It does not, however, limit vertical irregularities in calculating the seismic response coefficient C (Moehle, 2010), as compared to the Uniform Building Code, 1997 that referenced ACI 318-95 and was used in the United States shortly after NCh433 was established in Chile. Nor does NCh433 require the provisions of ACI that address boundary elements in walls. Because of this, what was found in many walls that failed were concentrations of vertical bars at both ends, and widely spaced bars in the middle (Leon, 2010). With tensile strength of the wall concentrated at the ends, the steel could not reach yield, and brittle crushing of concrete occurred. In contrast, ACI requires hooks or U-stirrups to resist buckling of vertical edge reinforcement (ACI 318, 1995).

NCh433 1996 Section 8 for secondary elements enforces the anchorage and tying of non structural components. According to an EERI news letter report (EERI, 2010b), the enforcement of this provision in Chile actually depended on the building owner. About 60% of the 130 hospitals were harmed by nonstructural failures, which caused a substantial dollar loss to the economy. (EERI, 2010b)

There is certainly no building that can be designed to be completely earthquake-proof. The cost of constructing such a structure would be too expensive. The earthquake that happened in Chile in February 2010 showed that Chile's design code and enforcement were able to protect many lives and minimize structural damage. Although many buildings were damaged beyond repair, lives were saved by preventing total collapse. The results of this earthquake served as a lesson to Chile in its approach to seismic codes. The importance of an effective seismic building code as well as proper detailing and enforcement were well demonstrated. The consequences of damage to nonstructural elements were also demonstrated, which in some buildings was the only form of damage (Miranda, 2010).

7. COMPARISONS AND CONCLUSIONS

This paper discusses the differences between the earthquake effects in Haiti and Chile. Powerful earthquakes occur more frequently in Chile than in Haiti, and Chile as a developed, stable country was able to enforce a modern, strict building code. Although the dollar amount of damage in Chile was large, the code minimized the loss of lives, and the economic loss was a much smaller fraction of the GDP.

The difference in the construction methods and the building types in Haiti and Chile have a tremendous impact in the aftermath of an earthquake. Because there is a standardized building code in Chile, fewer people died than in Haiti. The irony of the building code, however, is that the repair costs of a modern building are much higher than in a building typically found throughout the developing world. Because of what happened to Haiti in January, it is critical to have a building code in place because human lives cannot be replaced. One challenge facing Haiti if it were to enact a seismic building code, however, is the affordability in relation to the tradeoffs of other needs of society. This ongoing research will next incorporate the longstanding modern country of New Zealand and how its codes affected their recent earthquake.

Observations from Haiti have shown that those buildings that were designed to resist seismic loads performed well during the earthquake. Low quality materials and lack of inspection and quality control compounded the severe damage the earthquake caused to the country. Historic patterns of prior earthquakes in the area predict that earthquake with an even larger magnitude could happen any time. This knowledge should be used along with help from the international community when rebuilding Port-au-Prince to develop and enforce proper design and construction practices for Haiti's structures. An active role in rebuilding Haiti is the best way to mitigate the suffering and ensure that this devastation would not be seen again.



Figure 1. Location of the Haiti Earthquake Epicenter



Figure 2. Location of the Chile Earthquake Epicenter

REFERENCES

- ACI Committee 318; Building Code Requirements for Structural Concrete (ACI 318-95) and Commentary (ACI 318R-95)
 AON Benfield(2010). "Even Recap Report: 02/27/2010 Chile Earthquake (2010)"

- http://www.aon.com/attachments/reinsurance/201003_ab_if_event_recap_chile_earthquake_impact_forecasting.pdf>03/30/2010.
- Bhatty, Ayesha(2010). "Haiti devastation exposes shoddy construction". *BBC News, London*. Jan. 15, 2010 <http://news.bbc.co.uk/2/hi/8460042.stm>>(8/3/2010)
- Buss, Terry F. and Adam Gardner (2008). "Haiti in the balance: why foreign aid has failed and what we can do about it". Washington: Brookings Institution. 21-27.
- Central Intelligence Agency(2010). The World Factbook <http://www.cia.gov/library/publications/the-world-factbook/geos/ha.html> >(9/10/2010)
<https://www.cia.gov/library/publications/the-world-factbook/geos/ci.html> >(9/30/2010)
- EERI (2010a). "The Mw 7.0 Haiti Earthquake of January 12, 2010: Report #2, 2010". *EERI Special Earthquake report*. May, 2010
- EERI (2010b). "Learning from Earthquake: The MW 8.8 Chile Earthquake February 27th, 2010". *EERI Special Earthquake report*. Jun. 2010
- Harris, James (2010). Direct Contact July 7, 2010. Denver, CO.
- Haynes, Gavin (2009). "The Subduction Zone Analysis". http://gogeometry.com/project_brainstorming/earthquake_geometry_of_fault >(9/10/2010)
- Instituto Nacional De Normalizacion Official Chilean Standard NCh433 (1996).
- Israel, Brett (2010). "Surprises Reveal in Wake of Massive Haiti Quake"<http://www.ouramazingplanet.com/haiti-earthquake-fault-lines-tsunami> >(10/13/2010)
- Klarreich, Kathie (2010). "Port-au-Prince, Six months after a devastating earthquake, many are looking to the past as possible was forward. Rediscovering Haiti's gingerbread houses". *Times*, July 26, 2010
- Leon, Roberto (2010). "The February 27, 2010 Chile Earthquake". Atlanta. *EERI Preliminary Reports*, 2010
- Midanda, Eduardo, M. Gilberto, P. Gokhan and R. Rodrigo (2010). "Brief Report on Earthquake Reconnaissance after the M 8.8 February 2010, Maule, Chile Earthquake". *EERI Preliminary Reports*, 2010. 13-14
- Moehle, Jack(2010). "27 February Offshore Maule, Chile Earthquake 2010". *EERI Preliminary Reports*, 2010.
- Schneider, Ronald M. (2007). "Latin American political history: Patterns and Personalities", West-view Press, Boulder, CO, 351-353, 4 and 471-47
- Servicio Sismologico (2010). Universidad de Chile, <http://ssn.dgf.uchile.cl/> >10/3/2010.
- H. Carroll Talley, Jr. and William K. Cloud (1960). "United States Earthquakes 1960". U.S. Department of Commerce, Coast and Geodectic Survey.
- The U.S. Department of State, Bureau of Western Hemisphere Affairs. <http://www.state.gov/r/pa/ei/bgn/1982.htm#econ> > 8/14/2010
- United Nations (2010). "Security Council SC/10026".<http://www.un.org/News/Press/docs/2010/sc10026.doc.html>> (9/17/2010)
- USGS (2010). "Offshore Valparaiso, Chile 1985 March 03, Magnitude 7.8, 1985"
<http://earthquake.usgs.gov/earthquakes/world/events/19850303.php>> (8/8/2010)
- USGS (2010). "Magnitude 7.0 - HAITI REGION, 2010 January 12"<http://earthquake.usgs.gov/earthquakes/centeqsww/Quakes/us2010rja6.php>> (7/10/2010)
- USGS (2010). "Magnitude 8.8- OFFSHORE MAULE, CHILE"<http://earthquake.usgs.gov/earthquakes/eqinthenews/2010/us2010tfan/>> (07/10/2010)

Applying Heuristics to Civil Engineering

X. J. Irias¹

¹ East Bay Municipal Utility District, Department of Engineering and Construction, 375 11th Street, Oakland, CA 94607; PH (510) 287-1002; email: xirias@ebmud.com

ABSTRACT

Uncertainty analysis is an area of vital interest to all engineers, including those engaged in policy formation as well as those charged with design or construction of novel solutions. While an array of tools has arisen to help assess and manage uncertainty, many fundamental challenges remain, among them the role of human judgment in risk analysis.

Heuristics theory is a theory of human judgment and perception, made famous by 2002 Nobel Prize winner Daniel Kahneman, and his associate Amos Tversky. An understanding of heuristics theory can help us leverage quantitative uncertainty analysis by making the role of human judgments manifest, and by giving us techniques to reduce bias in those judgments.

This paper reviews recent research in the area of heuristics and bias and proposes applications to civil engineering domains. Case studies of actual projects and situations are reviewed to highlight the interaction of heuristics with uncertainty modeling and analysis. The paper also highlights the challenges of communicating uncertainties, in particular how to close the gap between perceived risk and quantified risk and how perceived benefits keenly influence perceived risk.

INTRODUCTION

Uncertainty looms large today in the mind of engineers, and appropriately so given that every aspect of engineering work confronts uncertainty or, more precisely, risk at multiple levels. A major portion of project management is concerned with managing risk posed by uncertain costs and schedules. At the technical level, every day in the life of a project from the first day of conceptual planning to the final day of operations is an exercise in risk management. Consider the many questions engineers seek to answer: Will it work? How might it fail? What is an appropriate design load? What is an appropriate factor of safety? All of these questions are fundamentally about risk.

Many authors including notably Petrosky have reviewed the historic role of failure in risk management. Indeed, trial and error has guided risk management since the days of the pyramids, as multiple angles were tried before settling on 51.85 degrees as the steepest practical angle (Greenberg 2000). Gothic cathedrals pushed the limits and occasionally exceeded them, as exemplified by the failure of Beauvais Cathedral in 1573.

In more recent times, there is an unmistakable attempt to supplement trial-and-error methods with quantified risk analysis. For example, in 1975, the Nuclear Regulatory Commission began requiring a formal risk assessment known as WASH-1400/

NUREG/75-014 (NRC 2007). That trend toward quantifying or at least enumerating risk has increased with time, not only within the nuclear industry but in other high consequence endeavors such as dam building and operation; the Federal Energy Regulatory Commission (FERC) now requires dam owners to prepare a Potential Failure Modes Analysis (PFMA). A PFMA is not highly quantitative, but attempts to rank failure modes to highlight areas of concern and screen out non-credible risks. FERC is currently exploring ways to more formally quantify risks identified in PFMA's (Hydroworld 2010).

The trend toward quantified risk is not limited to high-consequence facilities like dams and nuclear reactors. The increasing use of "factored loads" rather than allowable stress design is an attempt to explicitly quantify uncertainty in loading and performance alike. Utility owners increasingly use risk assessment as a tool to manage their aging infrastructure and to balance the risk of asset failure with the cost of asset maintenance or replacement.

In short, as our society increasingly relies upon ever more sophisticated and complex engineered systems, we engineers in turn rely upon ever more sophisticated and complex risk management tools. A central question is therefore whether those tools are sufficient for the task and whether they are being used optimally.

LIMITS OF QUANTITATIVE METHODS

The original WASH-1400 report of 1975 quantified the risk of a person dying from a nuclear accident at a mere one in 20,000,000,000 annually (Rasmussen 1975). That optimistic view of nuclear safety has, over the years, come under serious attack, though the particulars vary (some probabilities are probably understated, but some consequences are likely overstated, for example). Perhaps more important than the technical underpinnings of WASH-1400 is that the analysis simply did not *seem* credible to many, particularly when viewed in the harsh light of reality. To a lay person, if nuclear accidents were essentially impossible, then how could Three Mile Island (TMI), Chernobyl, and other accidents have happened? An accident like TMI should only happen on average once every 400 years according to WASH-1400.

Dissecting WASH-1400 might miss the larger picture and obscure the benefits of risk quantification. In fact, WASH-1400 brought to light an important failure mode, observed at TMI four years after the publication of WASH-1400, that of small-scale coolant losses. At the time of plant licensure, the impacts of this possible failure mode had been considered negligibly small. So, while imperfect in some particulars, WASH-1400 should be considered a milestone in risk quantification and a step forward in our goal to identify, disclose and discuss risks.

We might hope that more recent risk quantifications would show a highly advanced state of the art relative to those of 1975. Unfortunately, some shortcomings with risk quantification are fundamental and thus plague even the most recent attempts. As an example, consider the Three Gorges Dam on the Yangtze River, with a design flood said in 2003 to be based on a 10,000-year recurrence (The Australian 2000). By 2007, that assessment was downgraded to only 1,000 years; then in 2008, it was downgraded to only

100 years. As of 2010, the dam's safety is being called into question for floods with recurrence intervals estimated in decades rather than thousands of years. In short, the original design basis has been missed by at least a factor of 100.

The example risk assessments discussed, WASH-1400 and the Three Gorges project, span a 35-year interval of quantitative risk assessments, and fairly capture the essential shortcomings of virtually all quantitative risk assessments of low-probability events:

1. They model only known risks and hence suffer a systematic error of optimism.
2. They are reliant on expert judgment and hence prone to expert bias.
3. They tend to be stated with a confidence far exceeding their actual precision.

These limitations cannot be vanquished with technology or other means, as they are grounded in the very essence of uncertainty, without which there'd be no need to model risk in the first place. The shortcomings can, however, be mitigated. For that mitigation, we turn not to computer models but to the field of heuristics.

HEURISTICS

Heuristics theory is a theory of human judgment and perception, made famous by 2002 Nobel Prize winner Daniel Kahneman, and his associate Amos Tversky.

A heuristic is a "rule of thumb" that one uses to make judgments in the face of uncertainty, including judgments of relative worth of alternatives, and likelihood of alternative futures. Kahneman and others identified a series of named heuristics such as "availability" that explain and predict human judgments in a wide range of areas.

One way to understand heuristics is by contrast with other models of human cognition. In fact, the current thinking is that heuristic thoughts within our brains run "in parallel" with a more analytic pathway. The heuristic pathway is often called "System 1," with the analytic pathway called "System 2." System 1 is characterized by lightning-fast judgments with minimal data, while System 2 is characterized by relatively slow judgments that rely on complete data. To borrow an analogy from a well-known television show, Captain Kirk is the epitome of System 1, while Mr. Spock epitomizes System 2.

Outside of *Star Trek*, in the mind of each of us, both systems are in effect, operating in parallel. However, System 1, being faster and more frugal of data, invariably "finishes first" and hence governs most of our judgments and actions. System 2 operates by exception, providing a check on System 1 and occasionally overriding it.

Much research has been done to prove not only that System 1 exists but also that it governs most human judgments. The most straightforward way to prove these facts is to conduct experiments in which System 1 reaches different conclusions than System 2. Those experiments also then prove unequivocally the presence of bias in System 1.

If our knowledge of heuristics stopped there, it would still be useful since the very fact that our judgments inescapably rely on heuristics over reason, and are prone to bias, would give us insights into the judgment process.

Kahneman won the 2002 Nobel Prize for going much farther. As a start, he defined “prospect theory” to build upon classical utility theory as espoused by Daniel Bernoulli. Classical utility theory is a starting point and is briefly reviewed next.

CLASSICAL UTILITY THEORY

The cornerstone of much risk management is minimizing the “expected value” of an array of losses, or conversely of maximizing the “expected value” of gains. Sometimes the losses are expressed in financial terms, so the goal of risk management is to minimize the expected value of financial losses.

Such a crude approach misses something very fundamental, something so fundamental it has been called a “law” in reference to work done in 1738 by the mathematician Daniel Bernoulli, who opined the “Law of Diminishing Marginal Utility.” Marginal utility theory explains a host of outcomes, including the very human perception that we value a high probability of a moderately good financial outcome over a smaller probability of a fantastically good financial outcome. This is not an irrational quirk, but is rather perfectly rational. The “utility” of a billion dollars to most of us is far, far less than one thousand times the utility of a million. This truth was explored by Daniel Bernoulli’s cousin in a riddle known as the St. Petersburg paradox. The paradox describes a game in which a coin is tossed repeatedly until a heads results; the payout, or “pot,” is seeded with one dollar prior to the first toss, and then doubled prior to each subsequent toss. The question is how much one should pay to play the game.

A moment’s reflection reveals that the “expected value” of the payout is infinite. Why then is a rational player not willing to wager her life savings, or more, to play it? In fact, the typical person is only willing to pay \$25 or so, a far cry from “infinity” indicated by a present-value analysis. Among the potential explanations for the paradox, diminishing marginal utility offers a compelling explanation. Other explanations have been postulated, including a human tendency to simply disregard very improbable outcomes when mentally aggregating risk. But common to all explanations is the notion that the “expected value” of the various possible dollar outcomes does not provide useful guidance.

Further, none of these explanations offer any guidance to the practitioner seeking to manage risks that involve low-probability, high-consequence events, such as dam failures, core meltdowns, and collapse of important buildings. It is precisely for this type of event that formal risk management might be desired in the first place, since it is in this arena that our “common sense” judgment of risk may be worth little to none, and available data to validate the risk assessment will be relatively sparse. In cases like this, naïve risk assessments based on calculating an expected value of alternative

cash flows would be disastrously out of step with human values. Utility theory tells us enough to identify the problem with such an approach, but not enough to resolve the problem. For that we turn to prospect theory, discussed next.

PROSPECT THEORY

Prospect theory was developed by Kahneman and Tversky because it better modeled actual human choices than did utility theory. According to prospect theory, people evaluating a series of possible future outcomes will accord each a mental “weight,” in a similar manner as Daniel Bernoulli might have imagined a mental assignment of “utility” for possible dollar payouts. But there is an important difference: the assignment of utility under prospect theory is non-symmetric. Simply put, *people abhor losses more than they value gains*. This fundamental truth is the building block for a compelling explanation of a range of human behaviors, including risk aversion; preference reversals; biases, including those in favor of the status quo; and intransitivity of preference. Those behaviors comprise a large part of what we otherwise refer to as expert judgment, and thus a keen understanding of this topic is crucial to proper use of expert judgments for risk assessments.

Our experts, being presumably human, will exhibit preferences consistent with prospect theory, even if they believe themselves immune to the perceived irrationality of non-symmetric preferences predicted by prospect theory. This means that generally they will give more weight to a situation framed as a loss than to an equivalent gain. And perhaps surprisingly, they will tend to make optimistic forecasts of the future, because of a tendency to treat the situation at hand as more unique than it really is (and hence to ignore, for example, histories of prior problems or assume a rosier future). This pairing of “timid choices and bold forecasts” is memorably described in a paper by Kahneman (Kahneman 2000).

If the fundamental idea of prospect theory is that people feel losses more sharply than gains, this begs the question of what exactly a loss is, in the context of risk management. If one is modeling a dam failure, for example, are not all of the various failure scenarios “losses” anyway?

The answer is that the way we frame a question is supremely important. The framing of a question can establish the reference point from which excursions are perceived as either losses or gains. For example, an experiment developed by Kahneman, known as the Disease Problem, poses the following question:

Imagine that the United States is preparing for the outbreak of an unusual disease that is expected to kill 600 people. Two alternative programs to combat the disease have been proposed. Assume that the exact scientific estimates of the consequence of the programs are as follows: If Program A is adopted, 200 people will be saved. If Program B is adopted, there is a one-third probability that 600 people will be saved and a two-thirds probability that no people will be saved. Which of the two programs would you favor, Program A or Program B?

The problem is also offered with this alternative formulation:

Imagine that the United States is preparing for the outbreak of an unusual disease that is expected to kill 600 people. Two alternative programs to combat the disease have been proposed. Assume that the exact scientific estimates of the consequence of the programs are as follows: If Program C is adopted, 400 people will die. If Program D is adopted, there is a one-third probability that nobody will die and a two-thirds probability that 600 people will die. Which of the two programs would you favor, Program C or Program D?

The majority preference for A over B should come as no surprise given prospect theory's finding that people are risk-averse. But the preference for D over C is somewhat surprising since C and D are just Programs A and B restated. The explanation is that when A is framed as a loss of 400 lives rather than a gain of 200 lives, it is avoided.

Obviously, framing dependencies should strike fear into the heart of anyone seeking to rely upon expert judgments for risk assessments. If our experts reverse their opinions depending on the phrasing of a question, how can we rely upon their judgments?

It turns out that framing dependencies are but one of many vulnerabilities of expert judgments. They are also prone to a number of biases, such as anchoring, status quo bias, base rate neglect, and scope neglect, to name a few. All of these biases would clearly undermine the accuracy of expert predictions. On top of poor accuracy, we must also add that expert opinions tend to be stated with unwarranted confidence and a false sense of their precision. These problems, and ways to combat them for purposes of improving our risk assessments, are discussed next.

BIAS REDUCTION

Some major biases are briefly described as follows:

Anchor bias results when a judgment is "anchored" to a reference point, and then adjusted either insufficiently or not at all. Anchoring per se is not at all bad. For example, one might estimate the expected price of a project by starting with the price of a prior similar project, and then scale the price up or down to account for differences. The anchor bias refers to the fact that we tend to anchor on even random data, and having anchored we often do not adjust sufficiently.

Status quo bias is an excessive fondness for status quo, a bias which is readily understood by loss aversion. It is worth noting that a status quo bias was probably adaptive in our evolution as humans, as it discourages impetuous changes. It is a real problem, however, when applied to low-probability events; for example, an executive may downgrade a facility's vulnerability to a Probable Maximum Flood by noting that the dam in question has withstood "Mother Nature's worst" since 1920, not considering that the event under consideration occurs only every 10,000 years so a 90-year period of non-failure does not constitute strong evidence in favor of the status quo.

Base rate neglect is a tendency to focus too much on the particulars of a situation and forget the more general tendency. For example, one may study a detailed schedule analysis for a project that shows completion of a facility in one year, and be inclined to ignore the base rate, which is that other facilities of that type tend to take two years.

Scope neglect is the tendency to ignore magnitude. This bias goes beyond the well-known “a single murder is a tragedy, but a million deaths is only a statistic.” It also comes into play when comparing small numbers or large numbers. For example, an expert may provide an off-the-cuff risk estimate of “one in a million” at one moment and “one in a thousand” at another moment, because in her mind these numbers are essentially the same thing, as are one million versus one billion. Obviously, when included in a quantitative model, factors of one thousand impact final results.

The most effective countermeasure to bias is to actively counter it with reality checks. Sometimes, for example, with recurring problems like weather prediction or simpler engineering problems, all that is needed is habitually checking one’s judgments against actual outcomes. For predictions of less common events, when data are not available, the next best thing is to seek what Kahneman calls an “outside view.” This can be done literally by asking somebody less involved in the project; an outsider knows fewer details and is automatically less prone to status quo bias or scope neglect.

That still leaves anchoring effects and scope neglect as major problems. Anchoring effects can be explored by framing the relevant questions in different ways and seeing if the experts’ answers change. It is crucial to recognize that there is no such thing as a truly “neutral” framing; indeed, it is difficult or impossible to consider opinion to even exist distinct from its elicitation. Scope neglect can be reduced by breaking the problem into pieces such that an expert’s subjective probability is neither close to zero nor close to 1.0. Vick, in *Degrees of Belief*, provides a good discussion of ways to convert subjective judgments to numeric values.

Finally, the precision of experts tends to be overstated (Christian 2004). Even when experts are told to provide a range rather than a single number, and even when given guidance that the range ought to be as large as necessary to achieve a given confidence level (e.g., a 90% confidence level), experts very consistently overrate the precision of their own estimates. In the cited paper, Christian recounts a study (Hynes and Vanmarke 1976) in which experts are asked to predict the height of fill required to cause failure of an embankment. In the study, a lay audience on average outperformed the experts in both accuracy and precision. Certainly this would argue for keeping a close watch on the number of significant digits ascribed to expert judgments.

SUMMARY

Expert judgment is an essential and indeed inescapable part of risk management, as expert judgments define what risks are modeled in the first place, and often assign numeric values to important parameters in a risk assessment.

Expert judgments rely on heuristics, which have been studied extensively by psychologists in the field of behavioral economics. Knowledge of heuristics and associated biases can improve our risk assessments, and also improve our interpretation of risk assessments done by others.

REFERENCES

- Christian, John T. (October 2004). *Journal of Geotechnical and Geoenvironmental Engineering*, "Geotechnical Engineering Reliability: How Well Do We Know What We Are Doing?"
- Greenberg, Ralph (2000). *The Slopes of the Pyramids*, at <http://www.math.washington.edu/~greenber/pyressay.html>
- Hydroworld, volume 29, issue 6 (September 2010). "Dam Safety: Room for Improvement," at <http://www.hydroworld.com/index/display/article-display/5231889973/articles/hydro-review/volume-29/issue-6/cover-story/dam-safety-room-for-improvement.html>
- Hynes, M., and Vanmarke, E. (1976). *Proc., Engineering Mechanics Division Specialty Conference*, University of Waterloo Press, Waterloo, Ont., Canada "Reliability of Embankment Performance Predictions" (referenced by Christian, October 2004)
- Kahneman, Daniel (2000). "Timid Choices and Bold Forecasts," *Choices, Values and Frames*
- Nuclear Regulatory Commission (2007), at <http://www.nrc.gov/about-nrc/regulatory/risk-informed/history.html#HistoricalSummary>
- Rasmussen, *Reactor safety study: An assessment of accident risks in U. S. commercial nuclear power plants*, October 1975, Table 6-3, available at http://www.osti.gov/energycitations/product.biblio.jsp?query_id=6&page=0&osti_id=7134131
- The Australian (July 24, 2010). *China dam faces flood stress test*, available at <http://www.theaustralian.com.au/news/world/china-dam-faces-flood-stress-test/story-e6frg6so-1225896277213>

Probabilistic and Optimization Considerations in Multihazard Engineering

Dat Duthinh and Florian Potra

National Institute of Standards and Technology, Gaithersburg, MD. 20899, USA

ABSTRACT

In accordance with the ASCE Standard 7-05, in regions subjected to wind and earthquakes, structures are designed for loads induced by wind and, separately, by earthquakes, and the final design is based on the more demanding of these two loading conditions. Implicit in this approach is the belief that the Standard assures risks of exceedance of the specified limit states that are essentially identical to the risks inherent in the provisions for regions where only wind or earthquakes occur. We show that this belief is, in general, unwarranted, and that ASCE 7 provisions are not risk-consistent, i.e., in regions with significant wind and seismic hazards, risks of exceedance of limit states can be up to twice as high as those for regions where one hazard dominates. This conclusion is valid even if the limit states due to wind and earthquake are defined differently, as is the case in ASCE 7. We also describe an optimization approach to multi-hazard design that achieves the greatest possible economy while satisfying specified safety-related and other constraints. We present two applications to illustrate our approaches.

KEYWORDS: Building technology; earthquakes; interior point; limit states; multihazard; optimization; safety; solar energy; wind loads.

INTRODUCTION

The design of structures in the United States is governed by load combinations specified in the ASCE Standard 7 (2005). In regions prone to both earthquakes and strong winds, structures are designed for loads induced by wind and, separately, by earthquakes. The final design is based on the more demanding of these two loading conditions and is in general suboptimal. Implicit in this approach is the belief, which has so far prevailed in the code-writing community, that the Standard assures risks of exceedance of the limit states being considered that are essentially identical to the risks inherent in standard provisions for regions where only wind or earthquakes occur.

The first part of this paper draws the attention of the design, code-writing, and insurance communities to the fact that this belief is, in general, unwarranted. We show that ASCE 7 Standard provisions are not risk-consistent, in the sense that structures in regions with significant wind *and* seismic hazards can have risks of exceedance of limit states that can be up to twice as high as corresponding risks implicit in the provisions for regions where only one of these hazards dominates. This is true in spite of the fact that such risks are notional; that the failure modes for wind and earthquake can differ from each other; and that the ASCE 7 Standard uses different design approaches for wind and earthquakes.

The paper is organized as follows. First we explain, by using probabilistic tools, the nature of the misconception that has led to the development of the current – inadequate – ASCE design criteria for multi-hazard regions. In the second part, we suggest an optimization approach, namely the interior point method, in multihazard design. For simplicity we address the case in which the loads corresponding to a nominal probability of exceedance of the failure limit state are specified. We explore the potential of optimization under multiple hazards as a means of integrating the design so that the greatest possible economy is achieved while satisfying specified safety-related and other constraints. We consider two case studies – a water tower and a solar tower – to illustrate the main points presented in this paper.

RISK OF EXCEEDANCE OF LIMIT STATES INDUCED BY TWO HAZARDS

We now show that implicit in ASCE 7 provisions are risks of exceedance of limit states due to two distinct hazards that can be greater by a factor of up to two than risks for structures exposed to only one hazard. An intuitive illustration of this statement follows. Assume that a motorcycle racer applies for insurance against personal injuries. The insurance company will calculate an insurance premium commensurate with the risk that the racer will be hurt in a motorcycle accident. Assume now that the motorcycle racer is also a high-wire artist. In this case the insurance rate would increase as the risk of injury, within a specified period of time, in either a motorcycle or a high-wire accident will be larger than the risk due to only one of those two types of accident. This is true even though the nature of the injuries sustained in a motorcycle accident and in a high-wire accident may differ. The argument is expressed formally as:

$$P(s_1 \cup s_2) = P(s_1) + P(s_2) \quad (1)$$

Equation 1 also holds for a structure for which $P(s_1)$ is the probability of the event s_1 that the wind loads are larger than those required to attain the limit state associated with design for wind, and $P(s_2)$ is the probability of the event s_2 that the earthquake loads are larger than those required to attain the limit state associated with design for earthquakes. (Note that, as in the earlier example, it is assumed that s_1 and s_2 cannot occur at the same time.) $P(s_1 \cup s_2)$ is the probability of the event that, in any one year, s_1 or s_2 occurs. It follows from Eq. 1 that $P(s_1 \cup s_2) > P(s_1)$, and $P(s_1 \cup s_2) > P(s_2)$, i.e., the risk that a limit state will be exceeded is increased in a multi-hazard situation with respect to the case of only one significant hazard. If $P(s_1) = P(s_2)$ the increase is twofold. Note that s_1 and s_2 can differ, as they typically do under ASCE 7 design provisions. In spite of such differences, it is the case that, both for earthquakes and wind, inelastic behavior is allowed to occur during the structure's lifetime. For seismic loading, only the mean recurrence interval (MRI) (i.e., the inverse of the risk of exceedance) of the maximum considered earthquake is specified; the MRI of the onset of post-elastic behavior is unknown. For wind loading, the MRI of the onset of nonlinear behavior is specified; however, nonlinear behavior is also possible and allowed to occur during the structure's life.

We now consider a model developed by Pearce and Wen (1984) that has been invoked in support of the current ASCE 7 provisions for design in regions with both strong earthquakes and hurricanes. For illustration purposes we consider, in this model, the case in which two time-dependent loads $X_1(t)$ and $X_2(t)$ occur. If

$$Z = \max [X_1(t) + X_2(t)] \text{ in } (0, t) \quad (2)$$

the probability that Z exceeds a level s during the interval $(0, t)$ is

$$G_Z(s) \approx 1 - \exp \{-[v_1 (1 - P_{X_1}(s)) + v_2 (1 - P_{X_2}(s)) + v_{12} (1 - P_{X_1+X_2}(s))]t\} \quad (3)$$

in which the terms v_1 , v_2 and v_{12} are the annual mean s -upcrossing rates of X_1 , X_2 , and X_1+X_2 , and P_{X_1} , P_{X_2} , and $P_{X_1+X_2}$ are the marginal cumulative distribution functions of X_1 , X_2 , and X_1+X_2 respectively. The rate v_{12} can be approximated by $v_1 v_2 (\tau_1 + \tau_2)$, in which τ_1 and τ_2 are the durations of X_1 and X_2 ; it represents (approximately) the annual probability of a coincidence in time of the loads X_1 and X_2 (Ellingwood, personal communication, 2008); v_{12} for coincident wind and earthquake is negligibly small, so wind and earthquake may be treated as mutually exclusive. However, inspection of Eq. 3 shows that, in spite of the fact that wind and earthquake are mutually exclusive, $P_Z(s)$ is increased if both wind and earthquakes can occur at a site, contrary to the assumption implicit in the ASCE 7 provisions.

That assumption is that, because wind and earthquake hazards have negligible probability of occurring at the same time, structures may be analyzed first as if they were subjected to only one of the hazards, and second as if they were subjected only to the other hazard; the design selected for each member then corresponds to the higher of the respective demands. In this approach the increase in the probability of exceeding a limit state in the presence of two hazards is not taken into account. This would imply that the insurance rates for structures subjected to two significant hazards should be the same as for their counterparts subjected to one hazard. This implication would be correct only if the current ASCE 7 Standard design criteria applied to regions with both wind and earthquake hazards were modified so that risks in such regions be brought in line with risks in single-hazard regions.

CASE STUDY 1

Table 1 Structural member dimensions

Structural member	Shape	D_o or a (mm)	t (mm)
Tank Roof	Ellipsoidal shell		6.3
Tank middle	Cylindrical shell		9.5
Tank bottom	Ellipsoidal shell		9.5
Balcony girder	Square box	609.6	12.7
Legs	Circular tube	711.2	12.7
Horizontal braces	Circular tube	304.8	6.35
Diagonal braces	Circular tube	50.8	6.35

To illustrate the concepts discussed above, we present a case study for locations in South Carolina where the effects of wind and earthquake are important. Figure 1 shows a 1500 m³ water tank consisting of a cylindrical middle part of diameter 13.68 m and height 4.50 m, and semi-ellipsoidal roof and bottom of major axis 13.68 m and minor axis 8.90 m. The tank is supported at 1.12 m above the juncture between the bottom and the middle parts by a balcony ring girder of square box cross section, supported in turn by six vertical 53.64 m legs. The legs are braced by three sets of hexagonal horizontal braces placed at equal vertical distances between the ground and the balcony girder. In addition, the water tower is stiffened with diagonal braces consisting of steel tubes prestressed to a tensile stress of 125 MPa. The material is steel with 200 GPa modulus of elasticity, 2.0 GPa tangent modulus, and 400 MPa yield strength. Table 1 lists the outside dimensions (diameter D_o or side a) and thickness t of the structural members. The tank model also has a hollow 1.09 m diameter, 6.3 mm wall thickness vertical core used for pumping water (not visible in Fig. 1).

Since P- Δ (load-deflection) effects are important, a nonlinear, large deflection finite-element model (FEM) of the water tower is created to accurately capture the deformations of the balcony girder and the top end conditions of the legs. The FEM uses 4200 thin shell elements (with four nodes each) to model the tank and core, and 1800 beam elements (with two nodes each) to model the balcony ring girder, legs and braces. Static, push-over analysis is used, whereby load is applied gradually, first gravity, followed by wind or earthquake. The most unfavorable direction of lateral loading is parallel to a pair of diametrically opposite legs denoted as +x and -x.

Wind load: The basic wind speed is 45 m/s (100 mi/h) (ASCE 7-05, Fig. 6.1) and the required importance factor is 1.15. The strength design load combination is 0.9 D + 1.6 W, where D is dead load and W wind load. The weight of water, with the tank filled to maximum operating capacity (94 % of tank volume), is included in D. For this load combination, the total foundation reaction is 13.9 MN vertical and 572 kN horizontal. The +x and -x legs vertical reactions are 3.54 MN and 1.10 MN respectively, so the wind effects account for a relative difference of 105 % from the reactions without wind. The maximum deflection is 0.140 m (0.23 % of total height). For this loading, the structure is close to the limit of small deflection, linear elastic behavior.

Seismic load: According to ASCE 7-05 Eqs. 11.4.6 and Fig. 22.2 (map for 1-s spectral response acceleration $S_1 = 0.20$ g at location selected, where g is the acceleration of gravity), the design spectral response horizontal acceleration S_a for this structure is:

$$S_a = \frac{S_{D1}}{T} = \frac{(2/3)F_v S_1}{T} = \frac{(2/3) \cdot 1 \cdot 0.20 \text{ g}}{4.08} = 0.033 \text{ g} \quad (4)$$

where S_{D1} is the design spectral response acceleration parameter at 1-s period, F_v is the long-period site coefficient, and $T = 4.08$ s is the first natural period of the structure. ASCE 7-05 provides maps for parameters S_s and S_1 that correspond to the

ground motion of 0.2 s and 1.0 s spectral response acceleration with 5 % of critical damping of the maximum considered earthquake (with 2% probability of exceedance within a 50-year period) for site class B. Load effects include vertical seismic design acceleration A_v :

$$A_v = 0.14 S_{DS} = 0.14 \cdot (2/3) F_a S_s = 0.14 (2/3) \cdot 1.0 \cdot 0.75 g = 0.07 g \quad (5)$$

where S_{DS} is the design spectral response acceleration parameter at 0.2-s period, and F_a is the short-period site coefficient.

For the strength design load combination 0.9 D + 1.0 E, the total foundation reaction is 15.0 MN vertical and 500 kN horizontal. The +x and -x legs' vertical reactions are 3.80 MN and 1.20 MN, so the seismic effects account for a relative difference of 104 % from what the reactions would be without earthquake loads. The maximum deflection of the structure is 0.155 m (0.25 % of total height). The structural behavior is seen to be very similar under seismic load and wind load. This strongly suggests that the risk of exceedance of an undesirable state is greater for the structure subjected to wind or earthquakes than for the structure subjected just to wind or just to earthquakes.

It is not possible in the present state of the art to calculate the risk of exceedance of the seismic limit state. Nevertheless, it is clear that in the case of two hazards the risk of exceedance of an undesirable state – a limit state associated with the one or both hazards – can be significantly greater than the risk associated with only one of the hazards.

In the second part, we investigate ways of optimizing a structural design subjected to multiple hazards.

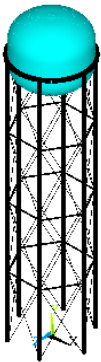


Fig.1 Water tower

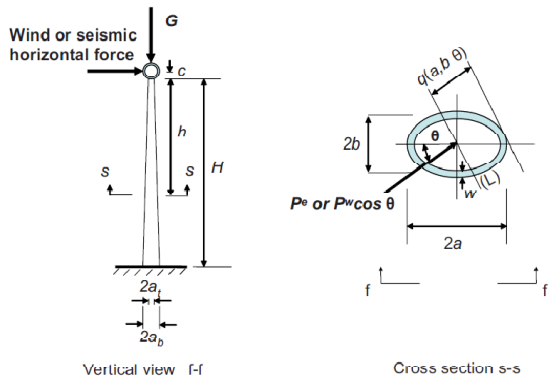


Fig. 2 Vertical view and cross section of solar column

MULTIHAZARD DESIGN AS A NONLINEAR PROGRAMMING PROBLEM

We consider a set of n variables (i.e., a vector) (d_1, d_2, \dots, d_n) characterizing the structure. In a structural engineering context we refer to that vector as a *design*. Given a single hazard, we subject those variables to a set of m constraints

$$g_1(d_1, d_2, \dots, d_n) \leq 0, g_2(d_1, d_2, \dots, d_n) \leq 0, \dots, g_m(d_1, d_2, \dots, d_n) \leq 0. \quad (6)$$

Examples of constraints are minimum or maximum member dimensions, allowable stresses or design strengths, allowable drift, allowable accelerations, and so forth. A design (d_1, d_2, \dots, d_n) that satisfies the set of m constraints is called *feasible*. Optimization of the structure consists of selecting, from the set of all feasible designs, the design denoted by $(\bar{d}_1, \bar{d}_2, \dots, \bar{d}_n)$ that minimizes a specified *objective function* $f(d_1, d_2, \dots, d_n)$. The objective function may represent, for example, the weight or cost of the structure. The selection of the optimal design is a nonlinear programming problem (NLP) for the solution of which a variety of techniques are available. Here we do not consider topological optimization, but rather, limit ourselves to structures whose configuration is specified, and whose design variables consist of member sizes.

As noted earlier, in multi-hazard design each hazard i ($i=1,2,\dots,N$) imposes a set of m_i constraints. Typically the optimal design under hazard i is not feasible under (i.e., does not satisfy the constraints imposed by) hazard $j \neq i$. For example, the optimal design that satisfies the drift constraints under one hazard may not satisfy drift constraints (i.e., may not be feasible) under another hazard. Common engineering practice is to obtain separately feasible designs d^i corresponding to each hazard i ($i=1, 2, \dots, N$). Those designs are used to construct an envelope d such that the constraints imposed under all hazards are satisfied. However, such a design will in general be suboptimal.

The NLP is clearly more difficult to solve in the multi-hazard than in the single hazard case. However, progress made during the last two decades in the field of nonlinear programming (see, e.g., Wright, 2005) now renders the solution of complex multi-hazard problems a practical possibility.

CASE STUDY 2

Description of structure: We consider the structure of Fig. 2, representing one in a long row of columns free at the top and fixed at the base that support a pipe filled with water. The water is heated by ground-level, computer-controlled rotating mirrors that focus reflected solar rays onto the pipe. The resulting heat is used for power generation. For the sake of simplicity and clarity in the illustration of our approach we assume that, in response to functionality requirements, the supporting structure consists solely of the columns (i.e., no bracing or other members are present). The column is subjected to a gravity load G due to the weight of the pipe and the water it contains, and to the wind load P^w and seismic load P^e acting non-simultaneously. The seismic load can act from any direction. The wind load, however, is a function of the wind velocity direction. Its magnitude is $P^w = P_0^w \cos\theta$, where θ is the angle between the direction of the wind velocity vector and the normal to the longitudinal axis of the

pipe. The horizontal cross section of the column is tubular and elliptical in shape, with constant thickness w . The major axis of the outer ellipse, $2a(h)$, at a cross section with coordinate h (see Fig. 2) varies linearly between $2a_t$ at the top of the column and $2a_b$ at the base; its direction coincides with the normal to the longitudinal axis of the pipe. The minor axis of the outer ellipse, $2b(h)$, at a cross section with coordinate h varies linearly between $2b_t$ at the top of the column and $2b_b$ at the base. Had the column been exposed to seismic hazard alone, a circular cross sectional shape would have been warranted. However, because the wind force is largest when its direction is normal to the longitudinal axis of the pipe, the section modulus of the cross section needs to be larger in that direction. One interesting output of the procedure is the ratio a/b corresponding to the optimal multi-hazard design. In the absence of earthquakes, that ratio should be as large as possible. In the absence of wind, the ratio should be unity. For the multi-hazard design, an intermediate ratio will be appropriate. That ratio will be neatly yielded by the optimization procedure.

Stresses: The compression stresses due to *gravity* loads are the sum of the force G and of the column weight from the top to the cross-section with coordinate h , divided by the area of the column at that cross section. The combined stress also includes the maximum compression stresses due to *bending* induced by a horizontal force P acting at elevation $H+c$ above the column base in the direction θ with respect to the major axis of the column cross section.

Multi-hazard optimization: We wish to find the design variables a_t, b_t, b_b, w so that the largest compression stress in the column not exceed the allowable stress σ_{all} . The design variables are subjected to the constraints

$$w_{min} \leq w \leq b_{t,min} = 38.1 \text{ mm} \leq b_t \leq a_t \leq a_b \leq a_{b,max} = 228.6 \text{ mm} \quad (7)$$

where w_{min} and $b_{t,min}$ are the lower bounds of w and b_t , respectively, and $a_{b,max}$ is the upper bound of a_b . The largest compression stresses in the column under earthquake and wind loading are, respectively,

$$\sigma_{mh}^e(\mathbf{d}, h) = \sigma_g(\mathbf{d}, h) + [\sigma_b(\mathbf{d}, h, P^e, \theta = \pi/2, h)] \leq \sigma_{all}, \quad 0 \leq h \leq H \quad (8)$$

$$\sigma_{mh}^w(\mathbf{d}, h) = \sigma_g(\mathbf{d}, h) + \max_{\theta \in [0, \pi]} [\sigma_b(\mathbf{d}, h, P^w, \theta, h)] \leq \sigma_{all}, \quad 0 \leq h \leq H \quad (9)$$

Denoting

$$\bar{g}_{mh}^w(\mathbf{d}, h) = \sigma_{mh}^w(\mathbf{d}, h) - \sigma_{all} \quad (10)$$

$$\bar{g}_{mh}^e(\mathbf{d}, h) = \sigma_{mh}^e(\mathbf{d}, h) - \sigma_{all} \quad (11)$$

the multi-hazard optimization problem becomes

$$\min_{a_t, b_t, b_b, w} f(\mathbf{d}, h) \quad (12) \quad \text{such that} \quad \bar{g}_{mh}^w(\mathbf{d}, h) \leq 0, \quad \bar{g}_{mh}^e(\mathbf{d}, h) \leq 0, \\ w_{min} \leq w \leq b_{t,min} = 38.1 \text{ mm} \leq b_t \leq a_t \leq a_b \leq a_{b,max} = 228.6 \text{ mm},$$

where the objective function f is the weight of the column. The optimization problem (12) is in general considerably more difficult to solve than its counterparts where each hazard is considered separately. However, its solution can be obtained efficiently by using modern optimization techniques.

Optimization algorithm: The inequalities $\bar{g}_{mh}^w(a_t, b_t, b_b, w, h) \leq 0$ and $\bar{g}_{mh}^e(a_t, b_t, b_b, w, h) \leq 0$ in (12) impose infinitely many constraints on the design variables a_b , b_t , b_b , and w (i.e., they impose a constraint for each value of h). For this reason, we replace these constraints by a finite number of constraints of the type

$$\bar{g}_{mh}^w(\mathbf{d}, h_i) \leq 0, \quad i = 1, 2, \dots, k, \quad (13)$$

where $0 \leq h_1 \leq h_2 \leq \dots \leq h_k \leq H$ is a finite partition of the interval $[0, H]$. The set of coordinates h_i , denoted by \mathbf{H} , is obtained as follows. Initially the set consists of four points: 0, $H/2$, H , and $rand_1$, where $rand_1$ is a random number in the interval $[0, H]$.

We replace in (10) and (11) the allowable stress σ_{all} by $\sigma_{all} - \varepsilon/(2\pi w)$. (In our calculations we chose $\varepsilon = 0.1$.) We then compute the maximum stresses under the wind hazard and the earthquake hazard, msW and msQ , respectively, and, to within a tolerance of 0.01ε , the coordinates $h = hW$ and $h = hQ$ at which those stresses occur. We return the set (a_b, b_t, b_b, w) as the solution of the optimal design problem if the stresses msW and msQ are both smaller than $\sigma_{all} - 0.01\varepsilon$. If this is not the case, we update the set \mathbf{H} by adding to it the point hW if $msW > \sigma_{all} - 0.01\varepsilon$, the point hQ if $msQ > \sigma_{all} - 0.01\varepsilon$, and the point with coordinate $rand_2$, and repeat the procedure until the requisite tolerance in the stresses msW and msQ is achieved.

Numerical results. We assume the following values for the constants defining our case study: $H = 3.66$ m, $c = 0.305$ m, vertical applied load $G = 31\,150$ N, $P^e = 8\,010$ N, $P^w = 8\,010$ N, $\gamma = 76\,846$ N/m³. We have considered for a_b the upper bound $a_{b,max} = 230$ mm; for w the lower bounds $w_{min} = 5.1$ mm or $w_{min} = 3.8$ mm, and for b_t the lower bound $b_{t,min} = 38.1$ mm. We assume that the column is constructed of A36 steel with allowable stress $\sigma_{all} = 110.3$ MPa.

Table 2 lists the quantities a_b , b_t , b_b , w , msW , hW , msQ , and hQ , as well as the number of iterations $iter$ required to achieve the specified tolerance. Note that in all cases w is equal to w_{min} . This is due to the greater efficiency of increasing the larger axis of the ellipse, thereby achieving a larger section modulus than had the material been placed in a thicker member closer to the center of the ellipse. If a constraint had imposed a sufficiently small upper limit on that axis, the result $w > w_{min}$ could have been obtained in some cases. For an actual design the dimensions shown in Table 2 would have to be slightly modified for constructability. The resulting weights and stresses would be modified accordingly.

Table 2 Multihazard Optimization

w_{\min}	b_t	a_t	b_b	w	Weight	msW	hW	msQ	hQ	iter
5.08	40.64	63.98	144.8	5.08	167.24	110.3	1 834	110.3	1 793	7
3.81	46.16	73.66	167.3	3.81	145.54	110.3	1 834	110.3	1 806	9
2.54	56.46	91.23	206.1	2.54	124.20	110.3	1 839	110.3	1 821	8

Dimensions: mm; weight: N; and stresses: MPa.

CONCLUSIONS

The notional risk of exceedance of limit states implicit in the ASCE 7 Standard can be greater by a factor of up to two for regions where both wind and earthquake loads are significant than for regions with only one significant hazard. This is true even if, as in the ASCE 7 Standard, the limit states differ for wind and earthquakes. In addition to design implications, our argument has implications for insurance assessments, which depend on the type of structure. The paper also shows the advantage of an optimization approach in a multi-hazard context as it provides an integrative framework allowing the structure to be optimized under constraints associated with all the hazards to which the structure is exposed, thereby achieving the most economical design consistent with the constraints of different types (e.g., constructability constraints) imposed on the structure. In general, multi-hazard optimization poses substantially greater challenges than optimization under a single hazard. However, recent progress in optimization theory and practice, and in particular the revolutionary development of interior point theory and algorithms, should allow the routine solution in the future of optimization problems under multiple hazards for structures of increasingly greater complexity.

REFERENCES

- ASCE 7-05 Standard (2005) *Minimum Design Loads for Buildings and Other Structures*, American Society of Civil Engineers, Reston, Virginia.
- Pearce, T.H. and Y.K. Wen (1984) "Stochastic Combinations of Load Effects," *ASCE J. Struct. Eng.* **110**:1613-1629.
- Wright, M. H. (2005) "The Interior-Point Revolution in Optimization: History, Recent Developments, and Lasting Consequences," *Bull., New Ser., Am. Math. Soc.*, **42**:1, 39–56.

ACKNOWLEDGMENT

We are grateful to Dr. Emil Simiu who inspired us to perform this work.

Asset Management of Structures Using Hybrid Structural Health Monitoring and Structural Uncertainty Analysis Procedure

M. Modares¹ and J. Mohammadi²

¹Department of Civil, Architectural and Environmental Engineering, Illinois Institute of Technology, AM 213, 3201 South Dearborn St., Chicago, IL 60616; PH (312) 567-5714; FAX (312) 567-3519; email: mmodares@iit.edu

²Department of Civil, Architectural and Environmental Engineering, Illinois Institute of Technology, AM 228, 3201 South Dearborn St., Chicago, IL 60616; PH (312) 567-3629; FAX (312) 567-3519; email: mohammadi@iit.edu

ABSTRACT

The safety and mobility of the population is dependent on the structural integrity of existing infrastructures. This requires a continuous monitoring program for condition assessment of infrastructures to guarantee their safe and reliable operation. A comprehensive structural health monitoring system involves a combination of advanced structural analyses integrated with field investigation using sensors and performance data acquisition. In this work a new engineering decision-making method for condition assessment of infrastructures is developed that is based on a hybrid experimental structural health monitoring (performance of non-destructive tests for structure's response) and theoretical structural uncertainty analyses (interval finite element analysis of structures) procedure.

In many cases, the application of results obtained from the health monitoring program of a structure is limited. Furthermore, the conventional deterministic structural analyses are incapable of considering uncertainties in experiments, system properties and loads, thereby resulting in error when estimating the state of health of a structure. This work proposes a new methodology that utilizes the results from structural health monitoring applications, combined with uncertainty analyses, in an effort to offer a more robust process for estimating the condition, energy conservation, and sustainable design of a given structure. On a broad sense, the results of this study will be applicable to the decision making process in determining a structure's demand for retrofit or reconstruction. The developed methodology along with an illustrative example is presented.

INTRODUCTION

A major cost and management issue related to existing infrastructures is condition assessment which typically produces very subjective and highly variable results. The subjectivity and variability of existing condition assessment protocols can be attributed to two major issues: 1) The application of results obtained by health monitoring of a structure is limited due to presence of errors and uncertainties, and 2) the conventional structural analysis schemes are incapable of considering uncertainties in experiments, system properties, data compilation, and loads, thereby resulting in error when estimating the health condition of a structure.

The model herein is essentially a condition assessment framework developed for incorporating engineering uncertainty analyses with structural health monitoring outcomes to achieve a more robust procedure for result interpretation and any follow-up engineering decision-making process. Moreover, this work demonstrates the capability of an analytical model whose input is the result of an experimental or field data collection with incorporation of possible uncertainties and errors. This leads to an establishment of a framework for a better engineering decision-making process geared for management of existing infrastructure systems.

The model uses the induced stresses in existing structure's components, which are obtained from engineering uncertainty analysis (interval finite element method), and determines whether critical components meet the initial design criteria or they have sustained failure/damage. Then, an asset management framework for decision-making is developed to determine whether to replace or repair based on the quantity and intensity of failed/damaged components. This creates a protocol for asset management of structures based on their performance and functionality.

Having the ability to use structural health monitoring data, integrated with an enhanced finite element method (capable of considering errors), produces the necessary information to make knowledgeable decisions regarding inspections, rehabilitation and repairs

STRUCTURAL HEALTH MONITORING

The structural health and condition of in-service structures is usually assessed through visual inspections and nondestructive testing & evaluation (NDT/NDE) methods conducted on a pre-set schedule. The goal of structural health monitoring system is to employ sensing instruments to provide information pertaining to the condition of the structure (Chang 2003).

The today's practice of structural health monitoring involves a host of structural parameters for which the data is compiled either continuously or intermittently. The availability of compact data acquisition systems along with the wireless technology has made the process of data compilation more affordable and convenient. It is envisioned that in the near future, more engineers and owners would take the advantage of the wireless instrumentation and data acquisition process in developing a system that can continuously be used to monitor the state of the health of their structures.

However, the challenge to this process would be the efficient use of the compiled data and development of a process via which the actual condition of a structure can be assessed accurately and the results be used reliably to determine what decision will need to be made in regard to the structure's need for repair, retrofit or reconstruction.

ENGINEERING UNCERTAINTY ANALYSIS

In the present era of modern technology, engineering analysis plays a fundamental role in design of structural systems. Engineering analysis has two main parts, simulation/analysis and optimization/design. The reliability of these two parts depends on how effectively the system behavior is predicted and how successfully the optimal solutions are achieved. Engineering uncertainty analysis requires that the procedures for analysis accommodate different sources of uncertainties and errors. One way to quantify the presence of uncertainty in a system is to use unknown-but-bounded or interval variables. The concept of interval numbers has been originally applied in the error analysis associated with digital computing. Quantification of the uncertainties introduced by truncation of real numbers in numerical methods was the primary application of interval methods (Moore 1966). The interval methods have been used for structural uncertainty analyses (Muhanna and Mullen 2001, Modares et al 2006).

Interval Variable

A real interval is a closed set defined by extreme values as:

$$\tilde{Z} = [z', z''] = \{z \in \mathfrak{R} \mid z' \leq z \leq z''\}$$

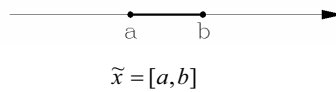


Figure 1. An interval variable

In this work, the symbol (\sim) represents an interval quantity. One interpretation of an interval number is a random variable whose probability density function is unknown but non-zero only in the range of the interval.

Interval Finite Element Method

In this work, a methodology is developed to perform interval finite element analysis on an existing structure with displacements/rotations and strains defined as interval variables obtained by measurements.

$$[K]\{\tilde{U}\} = \{\tilde{F}\}$$

where, $[K]$ is the stiffness matrix, $\{\tilde{U}\}$ is the interval displacement vector resulting from experimental data collection with incorporation of uncertainties and $\{\tilde{F}\}$ is the interval external force vector. The results of these analyses include the upper and lower bounds on the internal forces and stresses. The bounds on the internal stresses will then be used in the engineering decision making part of this work. This information relating to the structures health (records) will be used for effective decision making regarding repair or reconstruction.

Hybrid Procedure

Upon the application of data in the methods developed in this work, the outcome will be the structure's performance records with elements of uncertainties incorporated in them. These records essentially represent the structure's response in terms of several key parameters, which determine the condition of the structure. The records are then used in the evaluation of the condition assessment of the structure and development of strategies that can be used in the asset management and scheduling of the structure for repair and or reconstruction.

The interval finite element method reported in this work utilizes displacement history. However, in most cases, the existing data is in the form of acceleration history. This is because accelerometers are less expensive, and can easily be implemented on a structure to compile data, than are displacement transducers. Since the acceleration data will need to be converted into displacement histories before use in the techniques proposed in this research, an extra error may then appear in the response of the structure. This error can also easily be estimated and incorporated in the uncertainty level inherent in the developed method.

METHODOLOGY FRAMEWORK

The framework for the developed method is developed through five phases. These five phases are divided into three major nodes (Figure 2) defined below.

Node 1: Data Acquisition

Phase 1: Structural Health Monitoring

In this phase, displacement and/or other response data in several identified key performance parameters for existing structures are obtained. For example, stress ranges will be an important parameter in investigation of cracks in critical components of a steel girder in a bridge.

The information for these parameters needs to be translated from data that may only be available for strain and acceleration of the structure. This phase involves extracting information for key performance parameters of the structures from what is available through structural monitoring and data acquisition processes.

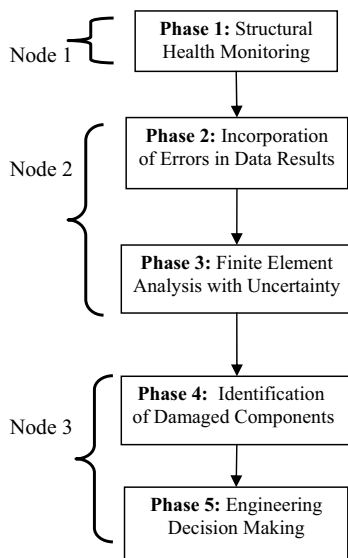


Figure 2. Methodology Framework

Node 2: Structural Uncertainty Analysis***Phase 2: Incorporation of Errors in Data Results***

In this phase, the presence of any uncertainty or impreciseness in data (due to measurement or sensor errors, for example) is incorporated through quantification of the experimental data as intervals of uncertainty. This phase involves a critical review of compiled data and use of statistical analyses to determine the various levels of uncertainties that may be inherent in the data. The quantification of uncertainties is performed through the analysis of variation in the data, comparison with expected norms, reported sensor errors, sampling errors, and uncertainties related to sensor locations.

Phase 3: Finite Element Analysis with Uncertainty

Interval finite element analysis is performed using the updated experimental data for the structure in order to obtain the bounds on the induced components' forces and stresses. In this phase, the interval finite element analysis utilizes the data with uncertainty, quantified by interval representation, to establish bounds for the results. Specifically, the results on this phase contain the bounds on induced stresses in each component of the structure. These results are used in engineering decision making as explained in Phase 5 of the developed method.

Node 3: Results Evaluation and Decision-Making Protocol***Phase 4: Identification of Damaged Components***

Based on the induced stresses in existing structure's components obtained from interval finite element analysis, it is determined whether, those components meet the initial design criteria or, they must be labeled as failed and/or damaged. This evaluation determines the safety of each component of the structure based on induced stresses in the elements. The results from this phase are used to detect the damaged components in the structure and whether the structure has suffered significant damage in its elements that for practical purposes has reached a failure state.

Phase 5: Engineering Decision Making

In this phase, the asset management framework is developed for decision-making on whether to replace or repair the structure based on the quantity and intensity of failed/damaged components. The quantity and intensity of the damage or failure of the structure's components is used to establish a framework for decision making on whether to repair or replace the structure based on both safety and economical considerations.

NUMERICAL EXAMPLE

Problem Definition

As a numerical example, the developed method is utilized for a sign support structure mounted on an interstate highway bridge. The structure experienced a failure at a member (Figures 3 and 4). The sign support structure consisted of two 25.4ft (64.52 cm) towers and a 73ft (185.42 cm) girder. The towers' horizontal and vertical members were made up of steel pipes with outer diameter of 6.18 in (15.7 cm) and a thickness of 0.239 in (0.61cm).

The horizontal and vertical girder members were made up of aluminum pipes with outer diameter of 4.75 in (12.06 cm) and a thickness of 0.1875 in (0.476 cm). The girder and towers diagonal members were aluminum pipes with outer diameter of 2 in (5.08 cm) and a thickness of 0.1875 in (0.476 cm). The modulus of elasticity for steel and aluminum were 29000 ksi and 10900 ksi, respectively. The Poisson's ratio for both the metals was 0.3.



Figure 3: The failure location of the sign support structure

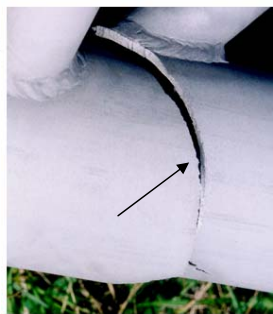


Figure 2: The detailed view of the failed member

Structural health monitoring was conducted on this structure by measurements on base acceleration on the towers induced by the passage of an eighteen-wheel truck. The experiments were performed fourteen times and the induced accelerations were recorded (Zalewski and Huckelbridge 2005).

Problem Solution

The model was implemented on the structure is using three-dimensional beam elements. The structure model has 92 nodes and 197 elements (Figure 5).

The interval finite element analysis was performed using MATLAB software source-code programming.

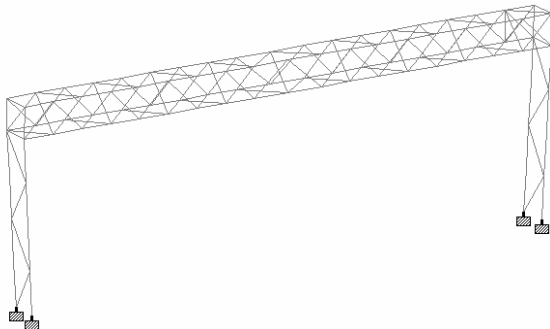


Figure 5: The finite element model of the structure

In order to obtain the deflections at the base of the towers, the induced accelerations due to truck passage were used to estimate the displacements. The results for fourteen measurements were combined as intervals of base displacements for the purpose of determining the errors and uncertainties in the data acquisition processes. The intervals for towers' displacements are summarized in Table 1.

Table1: Interval Deflections

<i>Tower</i>	<i>Interval Displacements (in.)</i>
East	[0.0307, 0.2653]
West	[0.0306, 0.3392]

The structure was analyzed using the interval of tower base displacements obtained from the health monitoring procedure. The bounds on forces and stresses in the structure's members were then determined. The upper bound of maximum normal stress in the girder is:

$$\sigma = 5.9423 \text{ ksi}$$

This stress occurs in the diagonal member of the girder adjacent to the tower, which is the actual failed member (Figures 3 and 4). Therefore, the results from the developed method correlate with the actual structure.

CONCLUSION

This work develops a new methodology for asset management and engineering decision-making for infrastructures using a combination of experimental health monitoring (performance of non-destructive tests for structure's response) and theoretical structural uncertainty analyses (interval finite element analysis of structures). Establishing a relationship between structural health monitoring and engineering uncertainty analysis will provide an increased confidence in the results of condition assessment program for infrastructure management. The results of this project have significant impact not only in academic pursuits but also in practical applications.

REFERENCES

- Chang, F.K. (2003). "Structural Health Monitoring 2003: From Diagnostics & Prognostics to Structural Health Management". *Proc. 4th International Workshop on Structural Health Monitoring*, DEStech, Stanford, CA.
- Modares M., Mullen, R. L. and Muhanna R. L., (2006). "Frequency Analysis of Structures with Bounded Uncertainty," *Journal of Engineering Mechanics*, ASCE, 132 (12), 1363-1371.
- Moore, Ramon E., (1966). "Interval Analysis", *Prentice Hall*, Englewood, NJ.
- Muhanna, Rafi L. & Mullen, Robert L., (2001). "Uncertainty in Mechanics Problems, Interval-Based Approach." *Journal of Engineering Mechanics* June 2001, 557-566.
- Zalewski, B. F. and Huckelbridge, A. A., "Dynamic Load Environment of Bridge-Mounted Sign Support Structures: A Special Student Study Final Report, Ohio Department of Transportation, Report no. ST/SS/05-002, June 2005.

Structural Health Assessment using only Noise-Contaminated Responses

Ajoy Kumar Das¹ and Achintya Haldar²

¹Doctoral Student, Dept. of Civil Engineering & Engineering Mechanics, University of Arizona, P.O. Box 210072, Tucson, AZ 85721; PH (520) 621-2266; FAX: (520) 621-2550; email: akdas@email.arizona.edu

²Professor, Dept. of Civil Engineering & Engineering Mechanics, University of Arizona, P.O. Box 210072, Tucson, AZ 85721; PH (520) 621-2142; FAX: (520) 621-2550; email: haldar@u.arizona.edu

ABSTRACT

A novel nondestructive Structural Health Assessment (SHA) technique, known as the Generalized Iterative Least-Squares Extended Kalman Filter with Unknown Input (GILS-EKF-UI) method, is being developed at the University of Arizona. The procedure can detect defects in new, deteriorated or rehabilitated existing structures or just after large natural or manmade events. Most SI-based SHA approaches use excitation and response information to identify a structure. Excitation information is not available in most cases. It could be noise-contaminated and the SI concept may not be applicable. For large complicated real structures, it may not be possible to measure responses at all dynamic degrees of freedom and they always contain noise. Addressing all the issues, the GILS-EKF-UI method is being developed and is presented here.

INTRODUCTION

Recent study reveals that many aging infrastructures worldwide are structurally deficient and do not meet the current safety and design guidelines. According to USDOT FHWA, out of about 600,000 bridges in the USA, 12% of them are structurally deficient. An efficient inspection procedure, replacing the traditional visual inspection technique, is urgently needed. Structural health assessment (SHA) has generated multi-disciplinary research interest from many different directions. SHA using an inverse identification technique, called System identification (SI), has become a very popular research item. The basic idea is that the dynamic responses of structures are expected to be different in the presence of defects and if the system can be identified using altered responses, it will identify the defective members. Some of them are summarized in (Doebling et al. 1996; Housner et al. 1997; Humar et al. 2006).

A basic SI-based procedure contains three essential components: (1) excitation information that generated the responses, (2) the system to be identified, generally represented in algorithmic form like finite elements, and (3) measured response information. In most cases, the information on the input excitation is not available or it contains so much noises that SI-based algorithm cannot be used. The finite element – based representation of the system may not be unique. The measured dynamic responses, even by smart sensors, will contain noise and may not represent the true

response. Furthermore, it may not be economically feasible to measure dynamic responses at all dynamic degrees of freedoms (DDOFs). Considering implementation potential, it will be highly desirable if a system can be identified using only limited amount of noise-contaminated response information measured at parts of a structure and completely ignoring the information on excitation. Such a novel SI technique is being developed at the University of Arizona and is presented here.

CONCEPT OF GILS-EKF-UI METHOD

The GILS-EKF-UI procedure is a two-stage time-domain SI technique that combines two methods, namely, Generalized Iterative Least-Squares with Unknown Input (GILS-UI) (Katkhuda et al. 2005) and Extended Kalman Filter Weighted Global Iteration (EKF-WGI) (Hoshiya and Saito 1984) method. In Stage 1, based on the location of measured responses, a substructure is identified and using the GILS-UI procedure, the stiffness and damping parameters of all the elements in the substructure are indentified. The concept is shown in Figs. 1 and 2. As a byproduct, it also generates the time history of the excitation(s) that caused the responses. The information obtained in Stage 1 is judiciously used to implement Stage 2 to identify the whole structure using EKF-WGI. Both stages are briefly discussed below.

Stage 1 - Mathematical concept of GILS-UI method - The governing differential equation of motion using Rayleigh damping for the substructure can be expressed as:

$$\mathbf{M}_{sub} \ddot{\mathbf{x}}_{sub}(t) + (\alpha \mathbf{M}_{sub} + \beta \mathbf{K}_{sub}) \dot{\mathbf{x}}_{sub}(t) + \mathbf{K}_{sub} \mathbf{x}_{sub}(t) = \mathbf{f}_{sub}(t) \tag{1}$$

where \mathbf{M}_{sub} is the global mass matrix; \mathbf{K}_{sub} is the global stiffness matrix; $\ddot{\mathbf{x}}_{sub}(t)$, $\dot{\mathbf{x}}_{sub}(t)$, and $\mathbf{x}_{sub}(t)$ are the vectors containing the acceleration, velocity, and displacement, respectively, at time t ; $\mathbf{f}_{sub}(t)$ is the input excitation vector at time t ; α , β are the mass and stiffness proportional Rayleigh damping coefficients. For a two dimensional frame and a substructure containing $nesub$ number of elements (in Figure 1 and 2, $nesub = 2$), the mass and stiffness matrices can be expressed as:

$$\mathbf{M}_{N_{sub} \times N_{sub}} = \sum_{i=1}^{nesub} \mathbf{M}_{6 \times 6}^i \tag{2}$$

$$\mathbf{K}_{N_{sub} \times N_{sub}} = \sum_{i=1}^{nesub} \mathbf{K}_{6 \times 6}^i = \sum_{i=1}^{nesub} k_i \mathbf{S}^i = k_1 \mathbf{S}^1 + k_2 \mathbf{S}^2 + \dots + k_{nesub} \mathbf{S}^{nesub} \tag{3}$$

where \mathbf{M}^i and \mathbf{K}^i are global mass and stiffness matrix for the i^{th} element, respectively; k_i is the i^{th} element stiffness parameter which is a function of length L_i , moment of inertia I_i , and material elastic modulus E_i , and N_{sub} is the number of DDOFs.

For simplicity, Eq. 1 can be reorganized as:

$$\mathbf{A}_{N_{sub} \cdot m \times L_{sub}} \mathbf{P}_{L_{sub} \times 1} = \mathbf{F}_{N_{sub} \cdot m \times 1} \tag{4}$$

where

$$\mathbf{P}_{L_{sub} \times 1} = [k_1, k_2, \dots, k_{nesub}, \beta k_1, \beta k_2, \dots, \beta k_{nesub}, \alpha] \tag{5}$$

where \mathbf{A} is an $N_{sub} \cdot m \times L_{sub}$ matrix composed of system response vectors of velocity and displacement at each DDOF for all m time points; \mathbf{P} is the $L_{sub} \times 1$ vector containing unknown system parameters i.e. stiffness and damping at the element level; L_{sub} is the total number of unknown parameters; and \mathbf{F} is a $N_{sub} \cdot m \times 1$ vector

composed of unknown input excitations and inertia forces at each DDOF. Minimizing the least squares procedure, Wang and Haldar (1994) suggested an iterative procedure to estimate all the unknown system parameters, L_{sub} .

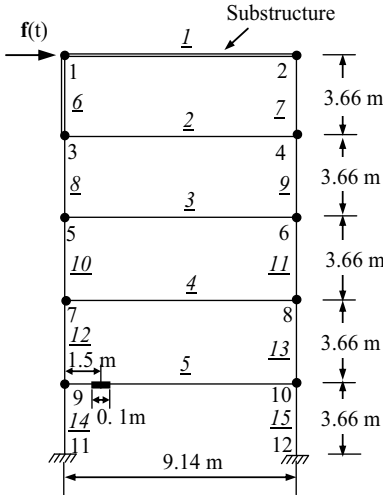


Figure 1. Five-story frame under sinusoidal excitation.

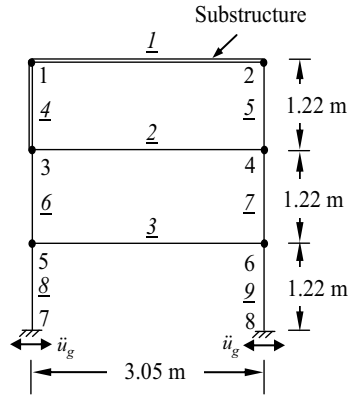


Figure 2. Three-story frame under seismic excitation.

Stage 2 - Mathematical concept of EKF-WGI method - The Extended Kalman Filter Weighted Global Iteration (EKF-WGI) (Hoshiya and Saito 1984) procedure is generally used when input excitation information is available, but the output responses are not available at all the DDOFs and they are noise contaminated. To circumvent the situation of SI without excitation information, the information from Stage 1 is used to implement EKF in Stage 2.

For the implementation of EKF, the differential equation in state-space form and the discrete time measurements can be expressed as:

$$\dot{\mathbf{Z}}_t = f(\mathbf{Z}_t, t) \tag{6}$$

$$\mathbf{Y}_{t_k} = h(\mathbf{Z}_{t_k}, t_k) + \mathbf{V}_{t_k} \tag{7}$$

where \mathbf{Z}_t is the state vector at time t ; $\dot{\mathbf{Z}}_t$ is the time derivative of the state vector; f is a nonlinear function of the state; \mathbf{Y}_{t_k} is the measurement vector; h is the function that relates the state to the measurement; \mathbf{V}_{t_k} is a zero-mean white noise process represented by $E[\mathbf{V}_{t_k} \mathbf{V}_{t_j}^T] = R_k \delta_{k-j}$, where δ_{k-j} is the Kronecker delta function; that is $\delta_{k-j} = 1$ if $k = j$, and $\delta_{k-j} = 0$ if $k \neq j$.

The filtering process in EKF can be started after initialization of state vector $\mathbf{Z}(t_0|t_0)$, which can be assumed to be Gaussian random variable with state mean $\hat{\mathbf{Z}}(t_0|t_0)$ and error covariance of $\mathbf{P}(t_0|t_0)$ i.e. $\mathbf{Z}(t_0|t_0) \sim N(\hat{\mathbf{Z}}(t_0, \mathbf{P}_{t_0}))$. The basic

filtering process in EKF is the same Kalman filter (KF), i.e. propagation of the state mean and covariance from time t_k to one step forward in time t_{k+1} , and then updating them when the measurement at time t_{k+1} becomes available. Mathematically the steps are expressed as:

(i) Prediction of state mean $\hat{\mathbf{Z}}(t_{k+1}|t_k)$ and its error covariance matrix $\hat{\mathbf{P}}(t_{k+1}|t_k)$ for the next time increment t_{k+1} as:

$$\hat{\mathbf{Z}}(t_{k+1}|t_k) = \hat{\mathbf{Z}}(t_k|t_k) + \int_{t_k}^{t_{k+1}} \hat{\mathbf{Z}}(t|t_k) dt \tag{8}$$

$$\mathbf{P}(t_{k+1}|t_k) = \Phi [t_{k+1}, t_k; \hat{\mathbf{Z}}(t_k|t_k)] \bullet \mathbf{P}(t_k|t_k) \bullet \Phi^T [t_{k+1}, t_k; \hat{\mathbf{Z}}(t_k|t_k)] \tag{9}$$

(ii) Using measurement $\mathbf{Y}(t_{k+1}|t_k)$ and Kalman gain $\mathbf{K}[t_{k+1}; \hat{\mathbf{Z}}(t_{k+1}|t_k)]$ available at time t_{k+1} , updated state mean $\hat{\mathbf{Z}}(t_{k+1}|t_{k+1})$ and error covariance matrix $\hat{\mathbf{P}}(t_{k+1}|t_{k+1})$ can be obtained as:

$$\hat{\mathbf{Z}}(t_{k+1}|t_{k+1}) = \hat{\mathbf{Z}}(t_{k+1}|t_k) + \mathbf{K}[t_{k+1}; \hat{\mathbf{Z}}(t_{k+1}|t_k)] \bullet \{\mathbf{Y}(t_{k+1}) - h[\hat{\mathbf{Z}}(t_{k+1}|t_k), t_{k+1}]\} \tag{10}$$

$$\begin{aligned} \mathbf{P}(t_{k+1}|t_k) = & \{\mathbf{I} - \mathbf{K}[t_{k+1}; \hat{\mathbf{Z}}(t_{k+1}|t_k)] \bullet \mathbf{M}[t_{k+1}; \hat{\mathbf{Z}}(t_{k+1}|t_k)]\} \bullet \mathbf{P}(t_{k+1}|t_k) \\ & \bullet \{\mathbf{I} - \mathbf{K}[t_{k+1}; \hat{\mathbf{Z}}(t_{k+1}|t_k)] \bullet \mathbf{M}[t_{k+1}; \hat{\mathbf{Z}}(t_{k+1}|t_k)]\}^T \\ & + \mathbf{K}[t_{k+1}; \hat{\mathbf{Z}}(t_{k+1}|t_k)] \bullet \mathbf{R}(t_{k+1}) \bullet \mathbf{K}^T [t_{k+1}; \hat{\mathbf{Z}}(t_{k+1}|t_k)] \end{aligned} \tag{11}$$

where, $\Phi [t_{k+1}, t_k; \hat{\mathbf{Z}}(t_k|t_k)]$ is the state transfer matrix from t_k to t_{k+1} ; $\mathbf{K}[t_{k+1}; \hat{\mathbf{Z}}(t_{k+1}|t_k)]$ and $\mathbf{R}(t_{k+1})$ is the Kalman gain matrix and diagonal noise covariance matrix, respectively, at time t_{k+1} . Detail procedure for their calculation can be found in Katkhuda and Haldar (2008). In the present study diagonal entries in the noise covariance matrix \mathbf{R} are considered to be 10^{-4} .

Prediction and updating processes are carried out for all m time points completing a *local iteration*. After completing the local iteration, Hoshiya and Saito (1984) suggested a weighted global iteration procedure to ensure stability and convergence in the identified stiffness parameters. To start the global iteration process $\hat{\mathbf{Z}}^{(1)}(t_m|t_m)$ and $\mathbf{P}^{(1)}(t_m|t_m)$ obtained at the end local iteration process are used. In the second global iteration a weight factor w , a large positive number, is introduced into error covariance matrix to amplify the covariance values of the stiffness parameters. In this study w is considered to be 100 and 1000 depending on the applications. The same prediction and updating phases of local iterations are carried out for all the time points and a new set of state vector and error covariance matrix are obtained at the end of second global iteration. The global iteration process is continued until the estimated relative error in stiffness parameters at the end of two consecutive global iterations becomes smaller than a predetermined convergence criterion (ε). ε is considered to be between 0.1 and 100 in this study. If they diverge, the best estimated values are considered based on minimum objective function $\bar{\theta}$ (Hoshiya and Saito 1984).

The GILS-EKF-UI procedure is clarified further with the help of examples.

EXAMPLE 1 - FIVE-STORY FRAME UNDER SINUSOIDAL EXCITATION

A five-story one-bay two-dimensional steel frame, as shown in Figure 1, is considered. The frame consists of fifteen members; five beams and ten columns made of A36 steel. Assuming the bases are fixed; the frame can be represented by 30 DDOFs. All beams are made of W21×68 and all columns are made of W14×61 section. The actual theoretical stiffness values k_i evaluated in terms of $(E_i I_i / L_i)$ shown in column 2 in Table 1b. The first two natural frequencies of the frame are estimated to be 3.70 Hz and 11.72 Hz. Following the procedure suggested in Clough and Penzien (1993), the Rayleigh damping coefficients α and β are estimated to be 1.0599 and 0.000619, respectively, corresponding to 3% modal critical damping.

To obtain the analytical responses in terms of acceleration, velocity, and displacement time histories, the frame was excited horizontally by applying a sinusoidal load $f(t) = 0.045 \sin(20t)$ kN at Node 1. ANSYS (ver. 11) was used to calculate responses measured at 0.00025 s interval. Since excitation information is not required in the GILS-EKF-UI method, after obtaining the response information, the excitation information is completely ignored. In all cases, responses between 0.02-0.32 s, for a total duration of 0.3 s were used for the identification purpose.

Health assessment - At first defect-free state of the frame is considered. In Stage 1, the substructure, shown in Figure 1, is identified accurately using responses at all 9 DDOFs. Results are presented in columns 3 and 4 in Table 1a. Maximum error in stiffness identification is 0.00154%. In Stage 2, the whole frame is identified. The identified stiffness values using responses at 9 and 18 DDOFs are shown in columns 3 and 5, respectively, in Table 1b. The error in identification for 9 DDOFs is 4.72% whereas it is 1.72% for 18 DDOFs indicating the benefit of extra responses.

To clarify health assessment capabilities in presence of defects, two types of defective states are considered. For defect 1, beam 5 at the first story level is considered to be broken. In the analytical model the broken state is represented by 0.1% of the cross sectional area and moment of inertia of the defect-free state. In defect 2, the thicknesses of the flange and web is considered to be reduced by 50% over a length of 10 cm in member 5 at a distance of 1.5 m from node 9 (see Figure 1). This results in reduction of cross-sectional area by 50.47% and moment of inertia by 52.14% at that location. The location of substructure in Stage 1 is kept the same for all the defective cases. In stage 1, the substructure is identified accurately and the results are presented in columns 5 and 7 in Table 1a. Then using responses at 18 DDOFs, the whole frame is identified in Stage 2. The identification results for defective case 1 are shown in column 7 in Table 1b. The stiffness value for beam 5 sharply decreases to 1251 instead of 13476 indicating its broken state. Results for defective case 2 are presented in columns 8 and 9. In this case, the stiffness value for beam 5 decreases by the maximum amount of 2.15%. This indicates that the member contains defects but not as severe as in defective case 1.

EXAMPLE 2 - THREE-STORY FRAME UNDER SEISMIC EXCITATION

A three-story single bay two dimensional steel frame shown in Figure 2 is considered. The same frame was tested in the laboratory by exciting it by sinusoidal

and impulsive forces. The frame consists of nine members; three beams and six columns. Steel section of size S4x7.7 was used for all the beams and columns. Assuming the bases are fixed; the frame can be represented by 18 dynamic degrees of freedom (DDOFs). Before testing the frame in the laboratory, the actual values of cross sectional area, mass, and moment of inertia were estimated to be 14.14 cm², 11.5 kg/m, and 238.7 cm⁴, respectively, using exhaustive experimental studies (Martinez-Flores 2005). The same values are used in developing the present analytical model. The actual theoretical stiffness values k_i evaluated in terms of ($E_i I_i / L_i$) are summarized in column 2 in Table 2b. To simulate gravity load, a uniformly distributed load of 3675 N/m is applied on all the floor beams. The first two natural frequencies of the frame are estimated to be 2.0915 Hz and 7.3063 Hz. α and β are estimated to be 0.2454 and 0.0004068, respectively.

Table 1. Stiffness parameter (EI/L) identification for five story frame.
(a) Stage 1 – Identification of substructure.

Member	Nominal	Identified (EI/L) values in (kN-m)					
		Defect-free		Defect 1		Defect 2	
		Identified	Error (%)	Identified	Error (%)	Identified	Error (%)
(1)	(2)	(3)	(4)	(5)	(6)	(7)	(8)
k_1	13476	13478	0.0153	13478	0.0127	13478	0.0153
k_6	14553	14555	0.0154	14555	0.0128	14555	0.0154

(b) Stage 2 – Identification of whole frame.

Member	Nominal	Identified (EI/L) values in (kN-m) for the whole frame						
		Defect-free				Defect 1	Defect 2	
		9 DDOF		18 DDOF		18 DDOF	18 DDOF	
		Identified	Error (%)	Identified	Error (%)	Identified	Identified	Error (%)
(1)	(2)	(3)	(4)	(5)	(6)	(7)	(8)	(9)
k_1	13476	13594	0.88	13490	0.10	13305	13490	0.10
k_2	13476	13369	-0.80	13512	0.26	13290	13511	0.26
k_3	13476	13794	2.36	13492	0.12	16197	13493	0.12
k_4	13476	13904	3.18	13626	1.11	6793	13618	1.05
k_5	13476	13746	2.00	13397	-0.58	1251	13187	-2.15
k_6	14553	14529	-0.16	14535	-0.12	14476	14536	-0.12
k_7	14553	14444	-0.75	14537	-0.11	14603	14538	-0.10
k_8	14553	14115	-3.01	14534	-0.13	14328	14534	-0.13
k_9	14553	14987	2.98	14534	-0.13	14318	14534	-0.13
k_{10}	14553	13866	-4.72	14342	-1.45	17427	14354	-1.37
k_{11}	14553	14026	-3.62	14331	-1.53	17325	14343	-1.44
k_{12}	14553	14025	-3.62	14382	-1.18	13242	14271	-1.94
k_{13}	14553	13986	-3.89	14331	-1.52	12657	14317	-1.62
k_{14}	14553	14321	-1.59	14758	1.41	15037	14847	2.02
k_{15}	14553	14352	-1.38	14803	1.72	16202	14815	1.80

The frame was excited by El. Centro earthquake ground motion at the bases i.e. at nodes 7 and 8. Again using ANSYS, analytical responses are calculated in

terms of displacements, velocity and acceleration at 0.00025 s interval. For all cases, responses between 1.52-2.37 s, for duration of 0.85 s were used for the identification purpose. After obtaining the responses, the seismic excitation information is completely ignored in the subsequent identification process.

Health assessment - Defect-free state of the frame is considered first. In Stage 1, the substructure (see Figure 2), is identified accurately using responses at all 9 DDOFs. Results are presented in columns 3 and 4 in Table 2a. Maximum error in stiffness identification is 0.002%. In Stage 2, the whole frame is identified. Columns 3 and 5 in Table 2b are showing the results using responses at 9 and 12 DDOFs (i.e. three responses at nodes 1, 2, 3 and only horizontal responses at 4, 5, 6), respectively. It can be noticed that identified stiffness values for 12 DDOFs case shows significant improvement from 9 DDOFs case and are very close to the actual theoretical values indicating that the frame is defect-free.

Table 2. Stiffness parameter (EI/L) identification for three story frame.

(a) Stage 1 – Identification of substructure.

Member	Nominal	Identified (EI/L) values in (N-m)					
		Defect-free		Defect 1		Defect 2	
		Identified	Error (%)	Identified	Error (%)	Identified	Error (%)
(1)	(2)	(3)	(4)	(5)	(6)	(7)	(8)
k_1	96500	96498	-0.002	100	-99.90	96498	-0.002
k_4	241250	241244	-0.002	241410	0.066	241245	-0.002

(b) Stage 2 – Identification of whole frame.

Member	Nominal	Identified (EI/L) values in (N-m) for the whole frame			
		Defect-free		Defect 1	Defect 2
		9 DDOF	12 DDOF	12 DDOF	12 DDOF
		Identified	Identified	Identified	Identified
(1)	(2)	(3)	(4)	(5)	(6)
k_1	96500	96946	96225	442	95194
k_2	96500	94334	96893	95985	98702
k_3	96500	79379	94840	96235	-2104
k_4	241250	229117	237739	236935	236311
k_5	241250	238014	239033	237021	233666
k_6	241250	182932	242091	240039	245882
k_7	241250	208766	248598	245101	240446
k_8	241250	496563	247199	250292	250677
k_9	241250	165941	240178	234827	248391

To verify health assessment capabilities in presence of defects, two types of defective states are considered for this frame also. For defect 1, beam 1 at the third story level is considered to be broken whereas for defect 2, beam 3 at the first story level is considered to be broken. In the analytical models the broken states are represented by 0.1% of the moment of inertia at defect-free state. The substructure is not altered for the defective cases. In Stage 1, the substructure is identified accurately and the results are summarized in columns 5, 6, 7, and 8 of Table 2a. Then using responses at 12 DDOFs the whole frame is identified as shown in columns 5 and 6 in

Table 2b. For defective case 1, the identified stiffness value for beam 1 is 442 instead of 96500. On the other hand, for defective case 2, the stiffness value for beam 3 is -2104. Obviously, the numbers indicate that the members are broken.

CONCLUSION

Concept of a novel SI-based SHA procedure, denoted as GILS-EKF-UI, is briefly discussed. The procedure is finite element based and can identify defects by tracking changes in stiffness parameters at the element level of a structure. The essential feature of the procedure is that it does not require information on input excitation and uses limited number of noise contaminated responses during the identification process. The procedure is clarified with the help of two examples: a five story frame excited by sinusoidal loading and a three story frame excited by seismic ground motion. The procedure accurately identified the defect-free and defective states of the frames and the severity of defects. The procedure can be used for rapid diagnostic purpose as a part of a broader SHA and maintenance strategy.

REFERENCES

- ANSYS version 11.0 (2007). The Engineering Solutions Company.
- Bridge Programs Structure Type by Year Built as of Dec. 31 (2009). U.S.D.O.T. FHWA, available at <http://www.fhwa.dot.gov/bridge/structyr.htm>.
- Clough, R.W. and Penzien, J. (1993) *Dynamics of Structures*. Second Edition, McGraw-Hill Inc.
- Doebbling, S., Farrar, C., Prime, M. and Shevitz, D. (1996). "Damage Identification and Health Monitoring of Structural and Mechanical Systems from Changes in their Vibration Characteristics: A Literature Review." Los Alamos National Laboratory, Report No. LA-13070-MS.
- Hoshiya, M. and Saito, E. (1984). "Structural Identification by Extended Kalman Filter", *J. Engrg. Mech.*, ASCE, 110(12), 1757-1770.
- Housner, G., Bergman, L., Caughey, T., Chassiakos, A., Claus, R., Masri, S., Skelton, R., Soong, T., Spencer, B. and Yao, J. (1997). "Structural Control: Past, Present and Future." *J. Engrg. Mech.*, ASCE, 123(9), 897-971.
- Humar, J., Bagchi, A. and Xu, H. (2006). "Performance of Vibration-based Techniques for the Identification of Structural Damage." *Struct. Health Monitoring*, 5(3), 215-241.
- Katkhuda, H., Martinez-Flores, R. and Haldar, A. (2005). "Health Assessment at Local Level with Unknown Input Excitation." *J. Struct Engrg*, 131(6), 956-965.
- Katkhuda, H. and Haldar, A. (2008). "A Novel Health Assessment Technique with Minimum Information." *Struct. Cont. & Health Monitoring*, 15(6), 821-838.
- Martinez-Flores, R. (2005). "Damage Assessment Potential of a Novel System Identification Technique – Experimental Verification." Ph. D. Thesis. Department of Civil Engineering and Engineering Mechanics, University of Arizona, Tucson, Arizona.
- Wang, D. and Haldar, A. (1994). "An Element Level SI with Unknown Input Information", *J. Engrg. Mech.*, ASCE, 120(1), 159-176.

Statistically detecting clustering for rare events

J. Siegrist¹, S. Ferson¹, J. Goode¹, and R. Grimson²

¹Applied Biomathematics, 100 North Country Road, Setauket, NY 11733; PH (631) 751-4350; FAX (631) 751-3425; email: jacksie@eden.rutgers.edu

²Clinical Statistics, 3 Birdseye Circle, Stony Brook, NY 11790; PH (631) 751-8986; FAX (631) 751-4250; email: ClinicalStat@aol.com

ABSTRACT

Cluster detection is essential for recognizing design flaws and cryptic common-mode or common-cause dependencies among events such as component failures, but when such events are rare, the uncertainty inherent in sparse datasets makes statistical analysis challenging. Traditional statistical tests for detecting clustering assume asymptotically large sample sizes and are therefore not applicable when data are sparse—as they generally are for rare events. We describe several new statistical tests that can be used to detect clustering of rare events in ordered cells. The new tests employ exact methods based on combinatorial formulations so that they yield exact *p*-values and cannot violate their nominal Type I error rates like the traditional tests do. As a result, the new tests are reliable whatever the size of the data set, and are especially useful when data sets are extremely small. We characterize the relative statistical power of the new tests under different kinds of clustering mechanisms and data set configurations.

INTRODUCTION

Risk analysis is normally concerned with events with low probability and high consequence, which makes conventional statistical analyses that depend on asymptotic approximations to known distributions difficult to apply. Using those approximate methods for the analysis of small populations results in incorrect *p*-values, so that it cannot be determined if the observed pattern is significantly different from random or not. Simulation studies show that the Type I error rates for traditional tests such as chi-square or the log-likelihood ratio (G-test) are routinely much larger than their nominal levels when applied to small data sets. As a result these tests can seriously overestimate the evidence for clustering and thus cause more alarm than is warranted. In other cases, traditional cluster tests can fail to detect clusters that can be shown by other methods to be statistically significant, and it is difficult to anticipate whether the traditional test will overestimate or underestimate the probability of clustering for a particular data set. Moreover, these tests are sensitive to a specific kind of deviation from randomness and may not provide the most appropriate measure of clustering from a specific mechanism. Thus, traditional asymptotic approaches provide an inefficient and misleading analysis of the available data. As an alternative, the combinatorial approach provides *exact* statistical tests for very small

population sizes, but is computationally expensive, so it is typically impractical for populations that are much larger than around 20.

The set of tests examined are all applicable to ordered data sets, such as sequences of events over time or over increasing distance in space. The statistical detection of clusters can be applied to a wide range of engineering problems, but the tests for ordered data examined here are especially useful for problems such as monitoring the degradation of structures and processes in order to determine if there might be increases in failure rates during certain periods of time or in particular locations. In these situations, statistical evidence for clustering can be used to justify more detailed studies of suspected causes and to justify emergency interventions.

One example of how cluster detection could be used in engineering is a study of the degradation of wires in the cables of a suspension bridge. In this case, the cells are the separate panels that allow access to the cable through the protective housing, which are arranged in a single sequence along each cable. Sampling of wires is necessarily destructive so that sample size is limited in order to prevent severe damage from the study itself. In this case, clustering of significantly degraded wires along the length of the cable might suggest that certain locations are subjected to more extreme weathering or that certain parts of the cable are under more extreme stress than the rest. Evidence for such a cause would then justify more intense monitoring or planning for more frequent repairs.

METHODS

Exact Tests

We studied the following tests, some of which are novel and unpublished: (1) binomial maximum test, (2) empty cells test, (3) hypergeometric maximum test, (4) longest run of empty cells test, and (5) range-scan test. The null hypothesis for each test is that events are randomly distributed among cells. The alternative hypotheses are different for each test and are reflected in each individual test's sensitivities. Using different tests for each special situation provides the most sensitive possible detection of a clustering or other non-random occurrence in incidence relative to the usual background patterns.

(1) *Binomial Maximum Test*: This test has two versions, one for surveillance, detecting a cluster in the most recent window of time, and the other for retrospectively detecting a cluster in any of the windows of time (Grimson and Mendelsohn 2000). The first tests whether the r events observed in the most recent k days is significantly larger than the $N - r$ number of events observed in all of the remaining $C - k$ days if there N total events and C total days. If events are equally likely to occur on any day, then the p-value can be derived from the binomial distribution by making the probability of success equal to k / C :

$$P_1(R \geq r | C, N, k) = \sum_{i \geq r} \binom{N}{i} \left(\frac{k}{C} \right)^i \left(\frac{C-k}{C} \right)^{N-i}$$

The second version tests whether any of the windows, not just the most recent one, represent a significant amount of clustering. The expression for the exact p-value is complicated but an approximation that is accurate to within three decimal places for $p \leq 0.4$ is:

$$P_2(M \geq \max | C, N) \approx \left(1, C \sum_{i \geq \max} \binom{N}{i} \left(\frac{1}{C} \right)^i \left(\frac{C-1}{C} \right)^{N-i} \right)$$

The two expressions are related as follows (Grimson and Mendelsohn 2000):

$$P_2(M \geq \max | C, N) \approx \min(1, CP_1(R \geq \max | C, N, 1))$$

(2) *Empty Cells Test*: For sparse data (when $N \leq 2C$) the number of empty cells observed, E , can be used to measure the degree of clustering (Grimson and Oden 1996), with the exact p-value given by:

$$P(E \geq e) = \frac{\sum_{k \geq e} (C)_{C-k} S(N, C-k)}{C^N}$$

in which $(C)_{C-k} = C(C-1)...(k+1)$ and $S(N, C-k)$ is a Stirling number of the second kind (Roberts 1984). Significant clustering based on empty cells suggests that there may be concentration of events in particular space-time units at the expense of the remaining space-time units, or that a threshold that permits events to occur has only been exceeded in particular space-time units.

(3) *Hypergeometric Maximum Test*: The probability of randomly selecting r or more of the N events during the k most recent of C time units is given by:

$$P(\geq r) = \binom{C+N-1}{N}^{-1} \sum_{i \geq r} \binom{C-k+N-1-i}{C-k-1} \binom{k-1+i}{k-1}$$

(4) *Longest Run of Empty Cells Test*: The number of Bose-Einstein arrangements of N objects in C cells with a maximum capacity of K objects per cell is given by (Grimson 1979, Mancuso 1998, notation follows Mancuso 1998, p. 35):

$$M(N, C, K) = \sum_{j=0}^C (-1)^j \binom{C}{j} \binom{C+N-j(K+1)-1}{C-1}$$

The probability that a run of empty cells of length R is greater than or equal to the observed length r for N objects in C cells is given by (Grimson, Aldrich, and Drane 1992, Mancuso 1998, notation follows Mancuso 1998, p. 35):

$$P(R \geq r) = 1 - \left(\frac{\sum_{j=1}^{\min(N,C)} M(C-j, j+1, r-1) j! S(N, j)}{C^N} \right)$$

where $S(N, j)$ is a Stirling number of the second kind (Roberts 1984).

(5) *Range-scan Test*: The range-scan test is suited to surveillance and is most useful for detecting an outbreak given that there are events on the current day and that previous events occurred recently. For a window size w that contains all N events in C time units the p-value is:

$$P(W \leq w) = \frac{1}{C^{N-1}} + \frac{1}{C^N} \sum_{i=2}^w (C-i+1) (i^N - 2(i-1)^N + (i-2)^N), \text{ for } w \geq 2$$

$$\text{and } \frac{1}{C^{N-1}} \text{ for } w = 1$$

Power Tests

Each exact test was evaluated by describing its power with reference to the procedures outlined in Hutwagner et al. (2005). Each test was evaluated using a collection of synthetic data. The synthetic data simulated several clustering mechanisms (alternative hypotheses) to be tested against the null hypothesis of a randomly generated distribution. These simulations varied the number of cells C from 10 to 100 with intervals of 10, the number of cases N from $0.2 * C$ to $2 * C$ with intervals of $0.2 * C$, the strength of clustering s from 0 (no clustering) to 1 (perfect clustering) with intervals of 0.1, the lookback window L from $0.2 * C$ to $0.8 * C$ with intervals of $0.2 * C$, and the kind of clustering among four models outlined below. The results of 500 simulations for each possible configuration of parameters were used to estimate the power of each test.

Clustering Mechanisms

Descriptions of the clustering models employed follow. An example of a simulated data set for each mechanism is illustrated in Figure 1. The example data sets were created with 10 cells, 10 cases, a cluster strength of 0.8, and, where applicable, a look back window 3 cells wide.

- (1) *Affected region*. Sequences of cells of random lengths are chosen at random, then events are randomly sprinkled only within those susceptible sequences.
- (2) *Cure singles*. Events are randomly sprinkled across cells. With a probability equal to the cluster strength, single events within cells are then moved at random to cells that already have more than one event.
- (3) *Drop in*. Events are randomly sprinkled across cells, but there is a positive feedback because the probability of falling into any given cell is weighted by the proportion of events that are currently in each cell.
- (4) *Lookback infect*. With a probability equal to the cluster strength, events fall randomly within any cell within a specified window. Otherwise, events fall randomly into any cell.
- (5) *Random sprinkle*. Events have equal probability of falling in any cell.
- (6) *Sprinkle grow*. The probability of an event falling in a cell is weighted in proportion to the number of events in that and in neighboring cells.
- (7) *Susceptible cells*. A set of susceptible cells is chosen at random, the number of cells determined by the clustering intensity. Events are randomly sprinkled across only the susceptible cells.
- (8) *Threshold effect*. This mechanism is similar to cure singles, except that the threshold for curing is set to two events per cell.

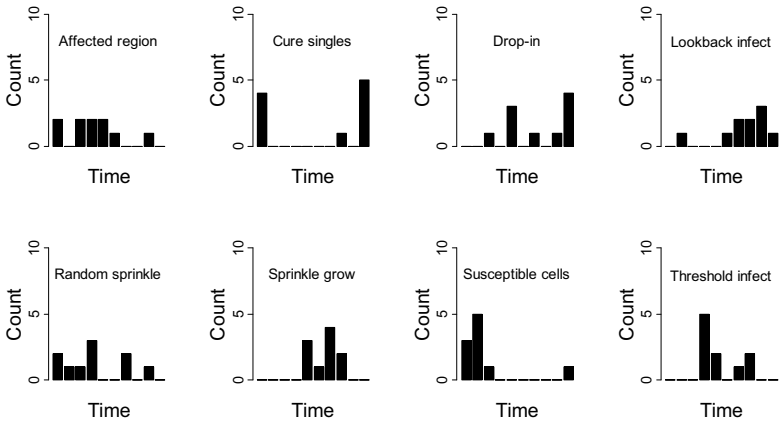


Figure 1. Examples of simulated data sets created using different clustering methods. Each example has the same total number of events and clustering intensity.

RESULTS

A threshold power of 0.8 was used as a criterion for the minimal acceptable power for a test. The strength of clustering associated with this threshold power is the minimal degree of clustering that the test can be used with. We call this minimal degree of clustering the *detectability* for the test. Many power curves failed to reach a power of 0.8 at any clustering strength. For these tests the detectability was defined as 1.

The average detectability for each test across all of the simulation parameterizations was: 0.88 for the binomial max, 0.41 for the empty cells, 0.90 for the hypergeometric max, 0.90 for the longest run of empties, and 1.00 for the range-scan. These average detectabilities along with quantiles and outliers are illustrated in Figure 2.

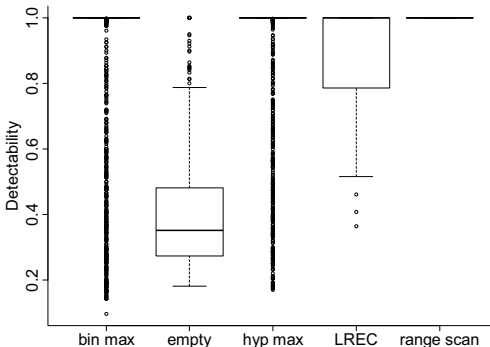


Figure 2. The empty cells test is the only test powerful enough for general use. Detectability is the minimal cluster strength that is required in order for the test to have power greater than our threshold of acceptance of 0.8. Tests are binomial maximum (bin max), empty cells (empty), hypergeometric maximum (hyp max), longest run of empty cells (LREC), and range scan.

The binomial max and the hypergeometric max tests have acceptable power for only the lookback window mechanism. The average detectability for these two tests for this mechanism is 0.52 for the binomial max and 0.60 for the hypergeometric max (Figure 3). For comparison, the average detectability for the empty cells test is 0.42 for this same mechanism.

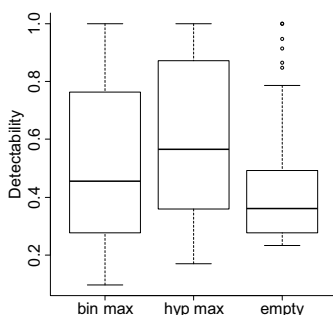


Figure 3. The detectability for the lookback clustering mechanism for the binomial max (bin max), hypergeometric max (hyp max) and empty cells (empty) tests. The empty cells test has the best performance even for this particular mechanism, while the other two tests have acceptable performance only for this particular mechanism.

CONCLUSIONS

These combinatorial tests allow for the determination of exact p-values. This ensures that for these exact tests, false alarms for clustering are no higher than the specified error rate. This guarantee is not present when using conventional cluster tests that require distributional assumptions that are only met with asymptotically large data sets. While the rate of Type I error is dependable for these exact tests, the power to find clusters that do exist, representing the Type II error rate, differs wildly among these tests. For applications that require conservative detection of clusters, such that false alarms are never created above the specified rate, any of these tests are useful. For applications that require detecting all possible clusters, the test used must be chosen carefully.

The empty cells test is the only test that has sufficient power over the wide range of parameterizations explored, but even this test should not be used when the clustering strength is very weak (around 0.2 in these simulations). The longest run of empties test and the range scan test have consistently weak power and should not be used for any of the mechanisms tested. The binomial max and the hypergeometric max tests are acceptable when clustering is known to be caused by a mechanism similar to the lookback window mechanism used here, but the empty cells test

outperforms these tests even for this particular mechanism, so that there does not appear to be any advantage to using any test except for the empty cells test. These results are, however, dependent on how representative are the clustering mechanisms used.

ACKNOWLEDGEMENTS

This work was supported by the National Institute of Allergy and Infectious Diseases award number 2R44AI077146-02. The content is solely the responsibility of the authors and does not necessarily represent the official views of the National Institute of Allergy and Infectious Diseases or the National Institutes of Health.

REFERENCES

- Grimson, R.C. (1979). "The clustering of disease." *Mathematical Biosciences*, 46, 257–278.
- Grimson, R.C., Aldrich, T.E. and Drane, J.W. (1992). "Clustering in sparse data and an analysis of rhabdomyosarcoma incidence." *Statistics in Medicine*, 11, 761–768.
- Grimson, R.C. and Mendelsohn, S. (2000). "A method for detecting current temporal clusters of toxic events through data monitoring by poison control centers." *Clinical Toxicology*, 38, 761–765.
- Grimson, R. C., and Oden, N. (1996). "Disease clusters in structured environments." *Statistics in Medicine*, 15, 851–871.
- Hutwagner, L. C., Thompson, W. W., Seeman, G. M., and Treadwell, T. (2005). "A simulation model for assessing aberration detection methods used in public health surveillance for systems with limited baselines." *Statistics in Medicine*, 24, 543–550.
- Mancuso, J.P. (1998). *Exact Null Distributions of Runs Statistics for Occupancy Models with Applications to Disease Cluster Analysis*, Ph.D. Dissertation, Department of Applied Mathematics and Statistics, Stony Brook University, Stony Brook, NY.
- Roberts, F. S. (1984). *Applied Combinatorics*, New Jersey, Prentice-Hall.

A Bayesian Framework to Predict Deformations during Supported Excavations Based on a Semi-Empirical Method

J. K. Park¹, S.M.ASCE, P. Gardoni², M.ASCE, and G. Biscontin³, M.ASCE

¹Graduate Student, Zachry Department of Civil Engineering, Texas A&M University, College Station, TX, 77843-3136; PH (979) 422-9888; email: jkpark0215@tamu.edu

²Associate Professor, Zachry Department of Civil Engineering, Texas A&M University, College Station, TX, 77843-3136; PH (979) 845-4340; email: pgardoni@civil.tamu.edu

³Associate Professor, Zachry Department of Civil Engineering, Texas A&M University, College Station, TX, 77843-3136; PH (979) 845-6303; email: gbiscontin@civil.tamu.edu

ABSTRACT

The ground movements induced by the construction of supported excavation systems are generally predicted in the design stage by empirical/semi-empirical methods. However, these methods cannot account for the site-specific conditions and for information that become available as an excavation proceeds. A Bayesian updating methodology is proposed to update the predictions of ground movements in the later stages of excavation based on recorded deformation measurements. As an application, the proposed framework is used to predict the three-dimensional deformation shapes at four incremental excavation stages of an actual supported excavation project.

INTRODUCTION

Evaluating the magnitude and distribution of ground movements adjacent to a supported excavation is an important part of the design process in particular when excavating in an urban environment. Although numerical modeling is a powerful tool in many design situations, it can be costly and requires considerable training to implement and interpret results. Therefore, empirical/semi-empirical methods are most commonly used to predict induced ground movements due to a supported excavation. Empirical/semi-empirical methods have five major limitations. First, designs based on empirical/semi-empirical methods can be overly conservative, especially when dealing with layered soil conditions and complex geometries (Long 2001; Finno et al. 2007). Second, much of the current empirical/semi-empirical methods have evolved from important empirical observations carried out since the 1940's. The construction materials and methods of support systems have been improved to both enhance the safety and reduce ground movements. Third, empirical/semi-empirical methods do not account for the site-specific characteristics of the soil and loading conditions, and for the information in the measurement data as they become available during the excavation process. Fourth, the empirical/semi-empirical methods have incomplete linkage between horizontal displacements and surface settlements. Fifth, they do not account for the uncertainty in the estimates of the deformations and therefore they cannot be used to assess the degree of safety of a design and for a reliability-based optimal design. This paper presents a

Bayesian framework that addresses these five limitations and updates the predictions of ground movements in the later stages of excavation based on the recorded deformation measurements.

EXCAVATION-INDUCED GROUND MOVEMENTS BY EMPIRICAL AND SEMI-EMPIRICAL METHODS

Several empirical and semi-empirical methods are available to predict the excavation-induced maximum horizontal displacement (Clough and O'Rourke 1990; Kung et al. 2007) and the surface settlement profile (Clough and O'Rourke 1990; Ou et al. 1993; Kung et al. 2007). Analysis of excavation-induced ground movements generally consists of the following four steps: (1) estimate the maximum horizontal displacement, $\delta_{h,max}$; (2) estimate the deformation ratio, $\theta_R = \delta_{v,max} / \delta_{h,max}$, where $\delta_{v,max}$ is the maximum surface settlement; (3) calculate $\delta_{v,max}$; and (4) estimate the surface settlement profile. Clough and O'Rourke (1990) proposed the normalized semi-empirical chart shown in Figure 1(a) to estimate $\delta_{h,max}$ for excavations in soft to medium soft clay. The chart provides curves of the normalized horizontal displacement, $\delta_{h,max} / \theta_{He}$, versus the system stiffness, $EI / \gamma_w \theta_{h,avg}^4$, where θ_{He} = the excavation depth, EI = the wall stiffness, γ_w = the unit weight of water, and $\theta_{h,avg}$ = the average support spacing. The curves are parameterized with respect to the load-resistance ratio, L_R , given by Terzaghi (1943) as

$$L_R = \frac{5.7\theta_{Sub}B}{(\gamma\theta_{He} + q)B - \theta_{Sub}\theta_{He}} \tag{1}$$

where, θ_{Sub} and θ_{Sub} = the undrained shear strength above and below the excavation, respectively, B = the width of the excavation, γ = the unit weight of the soil, and q = the surcharge. Clough and O'Rourke (1990) proposed dimensionless settlement profiles for estimating surface settlements for the different soil types as shown in Figure 1(b).

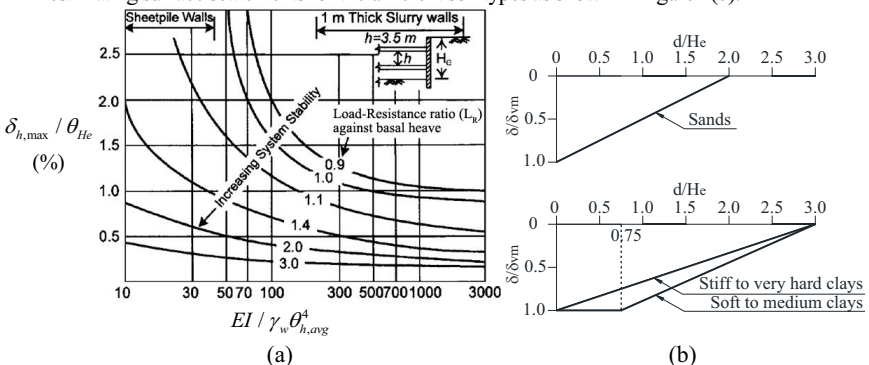


Figure 1. Design charts for (a) maximum horizontal displacements (b) surface settlement profile for excavations (after Clough and O'Rourke 1990)

More recently, Kung et al. (2007) developed regression equations to estimate δ_{hm} , R , δ_{vm} . For the surface settlement profile, they proposed following expressions

$$\begin{aligned}
 \delta_v / \delta_{v,\max} &= (1.6 \times d / \theta_{He} + 0.2) && \text{for } 0 \leq d / \theta_{He} \leq 0.5 \\
 \delta_v / \delta_{v,\max} &= (-0.6 \times d / \theta_{He} + 1.3) && \text{for } 0.5 \leq d / \theta_{He} \leq 2.0 \\
 \delta_v / \delta_{v,\max} &= (-0.05 \times d / \theta_{He} + 0.2) && \text{for } 2.0 \leq d / \theta_{He} \leq 4.0
 \end{aligned}
 \tag{2}$$

where, δ_v = the vertical settlement at the distance d . In this paper, we have used the Clough and O'Rourke (1990) chart to estimate $\delta_{h,\max}$ and $\delta_{v,\max}$, and Kung et al. (2007) equations have used to estimate a surface settlement profile.

ANALYTICAL FORMULATION OF SEMI-EMPIRICAL CHART

The first step in the proposed approach is to define analytical expressions for the curves in the Clough and O'Rourke chart. A mathematical description of these curves is needed to update the predictions of the ground movements in the later stages of excavation based on recorded deformation measurements. The Box and Cox transformation (1964) is used to formulate the following analytical expression:

$$\left[\frac{(\delta_{h,\max} / \theta_{He})^{(\theta_1 + \theta_2 L_R)} - 1}{(\theta_1 + \theta_2 L_R)} \right] = (\theta_3 + \theta_4 L_R) + (\theta_5 + \theta_6 L_R) \left[\frac{(EI / \gamma_w \theta_{h,\text{avg}}^4)^{(\theta_7 + \theta_8 L_R)} - 1}{(\theta_7 + \theta_8 L_R)} \right]
 \tag{3}$$

where, $\theta_{BC} = (\theta_1, \dots, \theta_8)$ = a set of unknown model parameters first estimated by fitting the model in Eq. (3) to the existing curves in the Clough and O'Rourke chart, and later updated as deformation measurements become available.

PROBABILISTIC BAYESIAN SEMI-EMPIRICAL METHOD

Mathematical formulation

A probabilistic model that describes the deformation at the k th excavation stage can be written as

$$D_k = \hat{d}_k(\theta_{CO}) + \sigma \varepsilon_k, \quad k = 1, \dots, m
 \tag{4}$$

where, $D_k = \delta_{h,\max}$ or $\delta_{v,\max}$ \hat{d}_k = the deformation estimate of $\delta_{h,\max}$ or $\delta_{v,\max}$ by the Clough and O'Rourke (1990) chart, $\theta_{CO} = (\theta_{Sub}, \theta_{Sub}, \theta_R)$ = a set of unknown parameters, $\sigma \varepsilon_k$ = the model error, σ = the unknown standard deviation of the model error, ε_k = a random variable with zero mean and unit variance. In assessing the probabilistic model, the following three assumptions are made: (a) the homoskedasticity assumption for the model variance, (b) the normality assumption for ε_k , and (c) ε_k at two different excavation stages are uncorrelated. The total deformation and deformation estimates at the j th excavation stage can be described as

$$\begin{aligned}
 D_j &= \Delta D_1 + \dots + \Delta D_j = \sum_{i=1}^j \Delta D_i \\
 \hat{d}_j(\theta_{CO}) &= \Delta \hat{d}_1(\theta_{CO}) + \dots + \Delta \hat{d}_j(\theta_{CO}) = \sum_{i=1}^j \Delta \hat{d}_i(\theta_{CO})
 \end{aligned}
 \tag{5}$$

where $\Delta D_j = D_j - D_{j-1}$ = the incremental deformation measurements at the j th excavation stage, $\Delta \hat{d}_j(\theta_{CO}) = \hat{d}_j(\theta_{CO}) - \hat{d}_{j-1}(\theta_{CO})$ = the incremental deformation estimates at the j th excavation stage, $D_0 = \hat{d}_0(\theta_{CO}) = 0$. Using Eq. (4) we can define the deformation residual as $r_k(\theta_{CO}) = [D_k - \hat{d}_k(\theta_{CO})]$. If the deformation has been recorded at the j th stage, the

deformation at the k th stage can be obtained by adding the predicted incremental deformation $\Delta D_{j+1}, \dots, \Delta D_k$ to the measured deformation at the j th stage. It follows that

$$r_k(\theta_{CO}) = D_k - \hat{d}_k(\theta_{CO}) = (\Delta D_{j+1} + \dots + \Delta D_k) - [\Delta \hat{d}_{j+1}(\theta_{CO}) + \dots + \Delta \hat{d}_k(\theta_{CO})] \quad (6)$$

The Clough and O'Rourke (1990) chart only provides estimates of $\delta_{h,max}$. However, the location of $\delta_{h,max}$ and the deformation profile cannot be estimated from the chart. Therefore, a functional form for the shape of the deformation profile is needed to compare with the field inclinometer data.

The three-dimensional profile of ground movements

This study adopts the shape of the three-dimensional deformation profiles perpendicular and parallel to an excavation as shown in Figure 2.

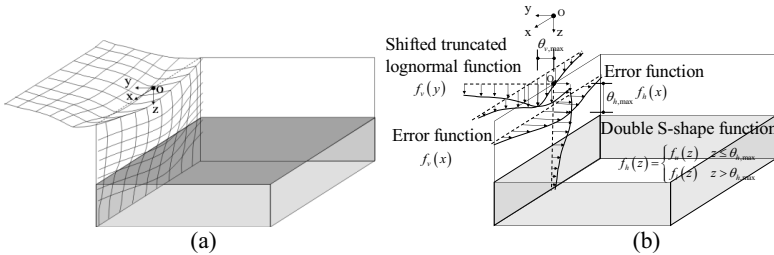


Figure 2. The three-dimensional ground movements (a) conceptual view (b) different functions to describe the deformation profiles

These shape functions are established after consideration of numerous alternatives with the objective of capturing the correct shape while maintaining a relatively simple form. After $\delta_{h,max}$ and $\delta_{v,max}$ have been computed, the following procedure is proposed to predict the three-dimensional ground movements.

- 1) The horizontal displacement profile is determined using an appropriate distribution type. The double S-shape distribution function (Gardoni et al. 2007) is introduced in this study for this purpose.

$$f_h(z) = \begin{cases} f_u(z) & z \leq \theta_{h,max} \\ f_l(z) & z > \theta_{h,max} \end{cases} \quad (7)$$

where, $f_u(z)$ and $f_l(z)$ = two S-shape functions defined one above and one below $\theta_{h,max}$ which is the unknown location of $\delta_{h,max}$,

$$f_u(z) = \delta_{h,max} \left[\frac{\theta_{u1} - (z - \theta_{u3})}{\theta_{u1}} \right]^{\theta_{u2}+1} \times \left[\left(\frac{\theta_{u1} - z}{\theta_{u1}} \right) (\theta_{u2} + 1) - (\theta_{u2} + 2) \right] + \delta_{h,max}, \quad (8)$$

$$f_l(z) = \delta_{h,max} \left[\frac{\theta_{l1} - (z - \theta_{l3})}{\theta_{l1}} \right]^{\theta_{l2}+1} \times \left[\left(\frac{\theta_{l1} - z}{\theta_{l1}} \right) (\theta_{l2} + 1) - (\theta_{l2} + 2) \right] + \delta_{h,max}$$

and $\theta_{u1}, \theta_{u2}, \theta_{u3}, \theta_{l1}, \theta_{l2}, \theta_{l3}$ = unknown parameters. The location of $\delta_{h,max}$ is assumed that it will locate at the center of the excavation in the x direction.

- 2) The horizontal displacement parallel to an excavation is defined by the complementary error function (Finno and Roboski 2005),

$$f_h(x) = \delta_{h,\max} \left\{ 1 - 0.5 \times \operatorname{erfc} \left[\frac{(0.5B - |x| - \theta_{h1}) / \theta_{h2}}{\theta_{h2}} \right] \right\} \quad (9)$$

where, θ_{h1} and θ_{h2} = unknown parameters.

- 3) The ground surface settlement profile perpendicular to the excavation is estimated using a shifted truncated lognormal distribution,

$$f_v(y) = \frac{1}{\sqrt{2\pi}\theta_{v1}(y - \theta_{v2})} \times \exp \left\{ -\frac{1}{2} \left[\frac{\ln(y - \theta_{v2}) - \theta_{v3}}{\theta_{v1}} \right]^2 \right\} \times \frac{1}{1 - F_Y(0)} \quad (10)$$

where, θ_{v1} , θ_{v2} , and θ_{v3} = unknown parameters, and

$$F_Y(0) = 0.5 \times \left\{ 1 - \operatorname{erf} \left[\frac{\ln(-\theta_{v2}) - \theta_{v3}}{\sqrt{2}\theta_{v1}} \right] \right\} \quad (11)$$

The location of $\delta_{v,\max}$ is assumed be at the center of the excavation, and the distance from the excavation, $\theta_{v,\max}$ needs to be estimated and updated from the field measurement data.

- 4) The surface settlement parallel to an excavation can also be described by the complementary error function,

$$f_v(x) = \delta_{v,\max} \left\{ 1 - 0.5 \times \operatorname{erfc} \left[\frac{(0.5B - |x| - \theta_{v4}) / \theta_{v5}}{\theta_{v5}} \right] \right\} \quad (12)$$

where, θ_{v4} and θ_{v5} = unknown parameters.

The different functions describing the deformation profiles are summarized in Figure 2(b). The four shape functions $f_h(z)$, $f_h(x)$, $f_v(y)$, and $f_v(x)$ define the three-dimensional ground movements around the excavated area. Note that all the shape functions are mirrored about the centerline of the excavation to give a distribution along the full wall and at the same location, we should have the same deformation value, $f_h(x=0) = f_h(z = \theta_{h,\max}) = \delta_{h,\max}$ and $f_v(x=0) = f_v(y = \theta_{v,\max}) = \delta_{v,\max}$. At the location of $\theta_{v,\max}$, the derivative should be zero, $f_v'(x=0) = f_v'(y = \theta_{v,\max}) = 0$. This limits the number of unknown parameters by eliminating 4 unknown parameters.

ASSESSMENT OF THE PROBABILISTIC BAYESIAN SEMI-EMPIRICAL METHOD

The proposed probabilistic approach uses a Bayesian updating rule to incorporate all types of available information, such as field measurements, and engineering experience and judgment. The Bayesian updating is used to assess the unknown model parameters and also provides a convenient way to update the model as the new set of measurement data become available. The prior distribution, $p(\Theta)$, should be constructed using the knowledge available before the observations used to construct the likelihood function are made. In reality, we typically have information about the unknown parameters, prior to the excavation. The Bayesian approach requires such prior information in the form of a prior distribution of the unknown parameter. In this study, θ_{BC} , θ_{CO} , and θ_{SF} are assumed to be independent, respectively. The objective information is entered through the likelihood function, $L(\Theta | \mathbf{D}_k)$. The likelihood function can then be written as

$$\begin{aligned}
 L(\Theta | \mathbf{D}_k) &\propto \prod_{\text{equality data}} P[\sigma \varepsilon_k = r_k(\theta_{CO})] \times \prod_{\text{lower bound data}} P[\sigma \varepsilon_k > r_k(\theta_{CO})] \times \prod_{\text{upper bound data}} P[\sigma \varepsilon_k < r_k(\theta_{CO})] \\
 &\propto \prod_{\text{equality data}} \left\{ \frac{1}{\sigma} \varphi[r_k(\theta_{CO})] \right\} \times \prod_{\text{lower bound data}} \left\{ \Phi[-r_k(\theta_{CO})] \right\} \times \prod_{\text{upper bound data}} \left\{ \Phi[r_k(\theta_{CO})] \right\}
 \end{aligned}
 \tag{13}$$

where, $\varphi(\cdot)$, $\Phi(\cdot)$ = the standard normal probability density and cumulative distribution functions. In the Clough and O'Rourke chart, one of three possible outcomes can be realized: (1) the D_k is observed in the range of $0.9 \leq L_R \leq 3.0$; (2) the measured D_k is a lower bound to the possible displacement if $L_R < 0.9$; (3) the measured D_k is an upper bound to the possible displacement if $L_R > 3.0$. Numerical solutions are the only option to compute the posterior statistics and the normalizing constant because the proposed model is nonlinear in the unknown parameters. In this paper, a Markov Chain Monte Carlo (MCMC) algorithm is used to compute the posterior statistics. Markov chains are generated with the likelihood formulation of the probabilistic models based on the initial points and a prior distribution until a convergence criterion is met. We adopt the Geweke's convergence diagnostic to decide when to terminate the MCMC simulations (Geweke 1992). We terminate the simulation when the Geweke's convergence diagnostic is sufficiently large, i.e., larger than 0.95.

APPLICATION OF THE PROBABILISTIC BAYESIAN SEMI-EMPIRICAL METHOD

The proposed probabilistic approach is applied to an actual supported excavation project for the Robert H. Lurie Medical Research Building in Evanston, Illinois. The prior distribution models are selected depending on the range of the parameters summarized in Table 1. The means for θ_{CO} are based on previous research results (Finno and Roboski 2005). The standard deviations are based on an assumed value for the coefficient of variation (COV). The means for θ_{BC} are based on the initial fitting result of original Clough and O'Rourke chart. Figure 3 compares the predicted horizontal displacements after each excavation stage for the west side of the Lurie excavation site with the corresponding field measurements. The proposed approach can accurately capture the horizontal displacement profile based on site specific measurements as they become available.

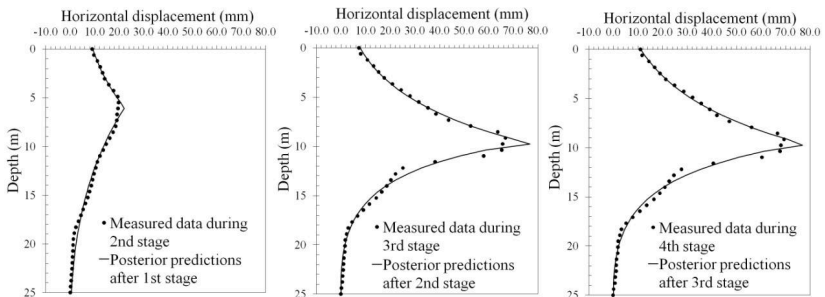


Figure 3. Comparison of measured and predicted horizontal displacements

Similarly, Figure 4 compares the surface settlements profiles after each excavation

stage. The proposed approach gives good predictions of the maximum settlement and its location. Figure 5 shows the complete three-dimensional horizontal deformation profiles and surface settlement profiles after the 3rd excavation stage. It is also possible to predict the deformations for different sides of the excavation.

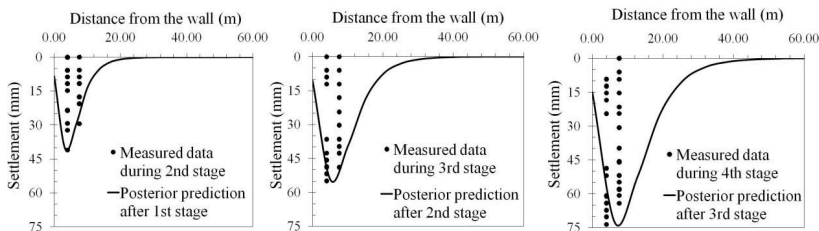


Figure 4. Comparison of measured and predicted surface settlements

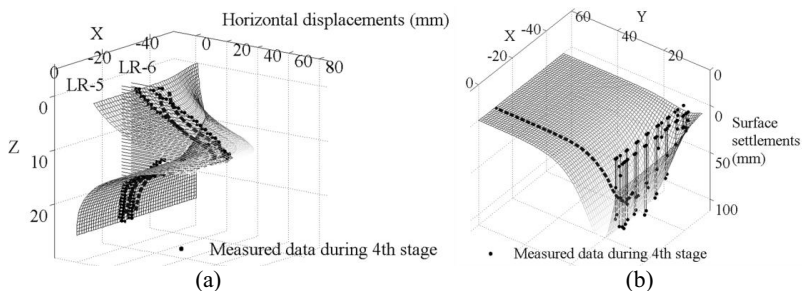


Figure 5. Comparison of measured and predicted (a) horizontal displacements (b) surface settlements based on posterior estimates for Lurie case (after stage 3)

Table 1. Prior distributions, means, and standard deviations

Physical meaning	Parameter ranges	Distribution models	Mean	COV
The soil properties (θ_{CO})	$0 < \theta_{Sub} < \infty$	Lognormal	50.0	0.2
	$0 < \theta_{Sub} < \infty$	Lognormal	30.0	0.2
	$0 < \theta_R < \infty$	Lognormal	0.5	0.2
The shape function parameters (θ_{SF})	$-\infty < \theta_{u1} < \infty$	Normal	10.0	0.2
	:	:	:	:
	$-\infty < \theta_{v5} < \infty$	Normal	10.0	0.2
The Box and Cox transformation parameters (θ_{BC})	$-\infty < \theta_1 < \infty$	Normal	-0.5	0.2
	:	:	:	:
	$-\infty < \theta_8 < \infty$	Normal	0.2	0.2

CONCLUSIONS

A probabilistic framework is proposed to predict deformations during supported excavations based on a semi-empirical method. A Bayesian approach is used to assess the unknown soil parameters by updating prior information based on site specific field measurements. The updated model parameters are then used to develop new and more accurate predictions of the deformations in the subsequent stages until the end of the excavation project. The key advantage of this proposed approach for practicing engineers is that they can use a semi-empirical chart together with simple calculations to evaluate three-dimensional displacement profiles without the need for constitutive laws or complex calculations. The developed approach provides a sound basis for decision about the design of excavation projects and can be used for optimizing the design of supported excavation systems. The proposed approach can also be used for an adaptive reliability-based optimal design of the excavation system in which the design is modified after each excavation stage to minimize costs and maintain a minimum reliability requirement.

REFERENCES

- Box, G. E. P., and Cox, D. R. (1964). "An Analysis of Transformations." *Journal of the Royal Statistical Society. Series B (Methodological)*, 26(2), 211-252.
- Clough, G. W., and O'Rourke, T. D. (1990). "Construction Induced Movements of Insitu Walls." *Design and Performance of Earth Retaining Structures*, L. A. H. Philip Lambe, ed., ASCE, Ithaca, New York, 439-470.
- Finno, R. J., Blackburn, J. T., and Roboski, J. F. (2007). "Three-Dimensional Effects for Supported Excavations in Clay." *Journal of Geotechnical and Geoenvironmental Engineering*, 133(1), 30-36.
- Finno, R. J., and Roboski, J. F. (2005). "Three-dimensional responses of a tied-back excavation through clay." *Journal of Geotechnical and Geoenvironmental Engineering*, 131(3), 273-282.
- Gardoni, P., Reinschmidt, K. F., and Kumar, R. (2007). "A probabilistic framework for Bayesian adaptive forecasting of project progress." *Computer-Aided Civil and Infrastructure Engineering*, 22(3), 182-196.
- Geweke, J. (1992). "Evaluating the accuracy of sampling-based approaches to the calculation of posterior moments." *Bayesian Statistics 4* J. M. Bernardo, J. Berger, A. P. Dawid, and A. F. M. Smith, eds., Oxford University Press, Oxford, UK, 169-193.
- Kung, G. C., Juang, C. H., Hsiao, E. L., and Hashash, Y. A. (2007). "Simplified model for wall deflection and ground-surface settlement caused by braced excavation in clays." *Journal of Geotechnical and Geoenvironmental Engineering*, 133(6), 731-747.
- Long, M. (2001). "Database for Retaining Wall and Ground Movements due to Deep Excavations." *Journal of Geotechnical and Geoenvironmental Engineering*, 127(3), 203-224.
- Ou, C. Y., Hsieh, P. G., and Chiou, D. C. (1993). "Characteristics of Ground Surface Settlement during Excavation." *Canadian Geotechnical Journal*, 30(5), 758-767.
- Terzaghi, K. (1943). *Theoretical soil mechanics*, John Wiley & Sons, New York.

A Bayesian Network Approach for Identification of Critical Components of a System

M. Bensi and A. Der Kiureghian¹

¹ University of California, Berkeley, Department of Civil and Environmental Engineering, CA 94720-1710, emails: mtbensi@gmail.com, adk@ce.berkeley.edu

ABSTRACT

Bayesian networks (BNs) have characteristics and capabilities that make them useful for assessing and responding to risk due to natural and man-made hazards posed to infrastructure systems. In this paper, we emphasize the use of the max-propagation algorithm of the BN for identifying critical components in a system subject to an arbitrary hazard. The paper begins with a brief introduction to BNs. This is followed by brief descriptions of inference and max-propagation in a BN, and use of the latter for identifying critical components. Limitations of the methodology are discussed. Two simple examples demonstrate the use of the proposed algorithm.

INTRODUCTION

A Bayesian network (BN) is a probabilistic graphical model that represents a set of random variables and their probabilistic dependencies. The variables may represent demand or capacity values, or the states of components and systems. BNs are graphical and intuitive, facilitate information updating, can be used for identification of critical components within a system, and can be extended by decision and utility nodes to solve decision problems. Thus, BNs have characteristics and capabilities that make them extremely useful for assessing and responding to risks due to natural or man-made hazards posed on civil infrastructure systems.

The goal of this paper is to demonstrate the use of one capability of BNs, known as the max-propagation algorithm, for identifying critical components and minimum cut sets (minimum set of components whose joint failure constitutes failure of the system) in an infrastructure system. This work is a subset of a broader effort to develop a BN methodology for seismic infrastructure risk assessment and decision support (Bensi 2010). The paper begins with a brief introduction to BNs. Then short descriptions of inference in a BN and the max-propagation algorithm are presented. The value of using the algorithm for identifying critical components and minimum cut sets is presented through use of two simple examples. The paper ends with a brief discussion of the capabilities and limitations of the approach.

BRIEF INTRODUCTION TO BAYESIAN NETWORKS

A BN is a directed acyclic graphical model consisting of a set of nodes representing random variables and a set of links representing probabilistic dependencies, typically causal relationships. Consider the simple BN shown in Figure 1 modeling five random variables $X = \{X_1, \dots, X_5\}$ and their probabilistic relationships. For example, random variable X_3 is probabilistically dependent on random variables X_1 and X_2 , as represented by arrows going from nodes X_1 and X_2 to node X_3 . In the BN terminology, X_3 is a *child* of X_1 and X_2 , while X_1 and X_2 are the *parents* of X_3 . Additionally,

X_4 is defined conditionally on its parent node X_1 and X_5 is defined conditionally on X_4 . Each node is associated with a set of mutually exclusive collectively exhaustive states. To be able to utilize exact inference algorithms, it is generally necessary to discretize all continuous random variables in the BN (with the exception of BNs with continuous Gaussian nodes without discrete children). We will not address BNs with continuous nodes in this paper, but additional details can be found in Lauritzen (1992), Lauritzen & Jensen (2001), and Langseth et al. (2009). For discrete nodes, probabilistic dependencies are encoded by attaching to each node a *conditional probability table* (CPT), providing the conditional probability mass function (PMF) of the random variable given each of the mutually exclusive states of its parents. For random variables without parents (e.g. X_1, X_2), a marginal probability table is assigned.

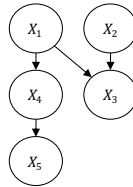


Figure 1. A simple BN

The joint distribution of the random variables in the BN is constructed as a product of the conditional distributions as

$$p(\mathbf{x}) = \prod_{i=1}^n p(x_i | pa(x_i)) \quad (1)$$

where $pa(x_i)$ is the set of parents of node X_i , $p(x_i | pa(x_i))$ is the CPT of X_i and n is the number of random variables (nodes) in the BN. Thus, for the BN in Figure 1, the joint PMF is

$$p(x_1, x_2, x_3, x_4, x_5) = p(x_5 | x_4) p(x_4 | x_1) p(x_3 | x_1, x_2) p(x_1) p(x_2) \quad (2)$$

BNs are useful for answering probabilistic queries when one or more variables are observed. That is, BNs efficiently compute the conditional distribution of any subset \mathbf{X}' of the variables in the BN given observations (or evidence) on any other subset \mathbf{X}^e of the variables. This process is known as inference. Suppose observations have been made on nodes X_3 and X_5 in Figure 1 and that the conditional distribution $p(x_2 | X_3 = x_3, X_5 = x_5)$ is of interest. This posterior distribution can be computed by first marginalizing the joint distribution in Figure 1 to obtain the joint distributions over subsets of the variables:

$$p(x_2, x_3, x_5) = \sum_{x_1, x_4} p(x_1, \dots, x_5) \quad (3)$$

$$p(x_3, x_5) = \sum_{x_1, x_2, x_4} p(x_1, \dots, x_5) \quad (4)$$

The desired conditional distribution is then obtained as

$$p(x_2|X_3 = x_3, X_5 = x_5) = \frac{p(x_2, x_3, x_5)}{p(x_3, x_5)} \quad (5)$$

While it is possible to obtain updated distributions as shown above, this is not a computationally efficient approach to performing probabilistic inference in non-trivial BNs. Instead, *inference engines/algorithms* are available that efficiently perform calculations in BNs. A variety of algorithms are available, including exact and approximate methods (e.g. Dechter 1996; Langseth et al. 2009; Madsen 2008; Yuan and Druzdzel 2003, 2006). One of the most basic exact inference algorithms is the *elimination algorithm*. While not used heavily in practice, it forms a basis for more efficient algorithms and is thus briefly described here. Furthermore, understanding the elimination algorithm facilitates an intuitive understanding of max-propagation.

The elimination algorithm is used to determine the distribution of a subset of random variables in the BN by incrementally eliminating nodes from the BN that do not belong to the subset of interest. Mathematically, elimination of a node corresponds to summing the joint distribution of the random variables over all states of the node to be eliminated. Again, consider the BN in Figure 1 and suppose that the joint distribution of X_3 and X_4 is of interest. Nodes X_1 , X_2 and X_5 must be eliminated from the BN to obtain this quantity. Thus, the joint distribution must be summed over all states of X_1 , X_2 and X_5 . For example, the elimination of X_1 results in the joint distribution of the remaining variables X_2, \dots, X_5 :

$$\begin{aligned} p(x_2, x_3, x_4, x_5) &= \sum_{x_1} p(x_5|x_4)p(x_4|x_1)p(x_3|x_1, x_2)p(x_1)p(x_2) \\ &= p(x_5|x_4)p(x_2) \sum_{x_1} p(x_4|x_1)p(x_3|x_1, x_2)p(x_1) \\ &= p(x_5|x_4)p(x_2)\phi(x_4, x_3, x_2) \end{aligned} \quad (6)$$

Note that in the second line the summation operator has been moved as far to the right as possible. This means that the sum need only be performed over the product of CPTs which include the variable X_1 . The result of the sum is a table or *potential* over the remaining variables: $\phi(x_4, x_3, x_2) = p(x_3, x_4|x_2)$. The above process is repeated for the elimination of X_2 and X_5 . The order in which the variables are eliminated (i.e. the summation operations are performed) has a significant impact on the size of the CPTs/potentials that must be multiplied at each stage, and consequently the memory demands of the elimination algorithm. In the above example, the largest memory demand comes from the product of three CPTs (involving four nodes) when eliminating X_1 : $p(x_4|x_1)p(x_3|x_1, x_2)p(x_1)$. Alternate elimination orders can be found that result in decreases in computational demands because they require smaller products. The elimination algorithm is “query sensitive,” i.e. the entire algorithm must be re-run for each quantity of interest. Thus, the elimination algorithm is efficient from the viewpoint of computer memory, but it is inefficient from a computational time perspective because it does not reuse computations when considering different combinations of evidence and/or desired posterior distributions. Alternative options for performing exact inference that facilitate such reuse exist, e.g. the junction tree algorithm (Jensen

and Nielson 2007). Available software applications (e.g. DSL 2007; Hugin Expert A/S 2008), facilitate inference in complex BNs.

THE MAX-PROPAGATION ALGORITHM

The outcome of the *max-propagation algorithm* provides the most-probable configuration of node states for a given evidence scenario. The algorithm can be applied to find the most likely configuration for any subset of nodes in the BN given evidence on a different subset. The exact version of the algorithm (in contrast to an approximate algorithm, see Yuan et al. 2004) is carried out using the inference procedures described in the previous section, but with summations over random variables replaced by maximization operators (Jensen and Nielson 2007). To differentiate the inference methods described above from the max-propagation algorithm, the methods above are generally referred to as *sum-propagation* algorithms. Thus, the use of the max-propagation is not conceptually more difficult than conventional use of sum-propagation. Max propagation is likewise implemented in many available software applications (e.g. DSL 2007; Hugin Expert A/S 2008). A brief introduction to max propagation is presented below.

Recall that the joint distribution of all random variables in the BN is constructed as a product of the conditional distributions, $p(\mathbf{x}) = \prod_{i=1}^n p(x_i | pa(x_i))$. In the case of no evidence, the most probable configuration of node states in the BN corresponds to the largest entry in the joint probability table $p(\mathbf{x})$. Let p^* be the probability associated with the most probably configuration. It follows that

$$p^* = \max_{\mathbf{x} \in \mathbf{X}} p(\mathbf{x}) = \max_{\mathbf{x} \in \mathbf{X}} \left[\prod_{i=1}^n p(x_i | pa(x_i)) \right] \quad (7)$$

Thus, the objective of the algorithm is to find the configuration of nodes which corresponds to p^* . As was the case for sum-propagation, the maximization operator can be moved as far to the right as possible to reduce the size of products that must be considered when computing the maximum of a particular joint distribution. This likewise implies that local operations can be used to determine this quantity.

When it is of interest to know the maximal probability of a subset of nodes in the BN, the above procedure is modified by first eliminating (i.e. “summing-out”) all variables that do not belong to the subset of interest and for which evidence has not been observed. Then the maximization is performed over the remaining potentials conditioned on the evidence. It is important to note that because summations must be performed before the maximization, there are constraints on the order in which operations (e.g. elimination of variables) can be performed. This constraint results in computational demands that are larger than the demands associated with performing sum-propagation or max propagation over all nodes in the BN (Jensen and Nielson 2007).

EXAMPLE APPLICATIONS

We utilize two simple example systems to demonstrate the use of the max-propagation algorithm for identification of critical components, particularly components in critical minimum cut sets (MCSs). We choose systems with predictable topologies and correlation structures to facilitate intuitive interpretation of results ob-

tained from the analyses. Given sufficient computational resources, we believe the methodologies are applicable to more general and realistic infrastructure systems. Limitations to this extrapolation are described in the Discussion section of the paper. The goal of the example assessments contained herein is to determine the most probable set of components to cause failure of the infrastructure system, i.e. to determine the “weak link” in the system. Such information can be useful for assisting infrastructure owners/managers with allocation of resources, selection of retrofit strategies, emergency planning, and other operational objectives.

The example system shown in Figure 2a consists of eight numbered square components connecting source and sink nodes. For simplicity, we consider only the failure of the square components. The system has five MCSs: {1,2,3,4}, {1,2,3,5}, {1,2,3,6}, {7}, {8}. Assuming binary component and system states, one possible BN topology modeling the performance of this system is shown in Figure 2b. The state of the system is represented by node S_{sys} , which is in the failure state if any node MCS_i is in the failure state. Nodes MCS_i represent system MCSs and are in the failure state only if all nodes in the MCS are in the failure state, otherwise node MCS_i is in the survival state. The states of the components are modeled by nodes C_i . The assumed (arbitrary) component failure probabilities are shown in Table 1. As should be evident from the BN, the component states are assumed to be statistically independent.

Table 1. Assumed component failure probabilities

Component	1	2	3	4	5	6	7	8
Pr(failure)	0.25	0.2	0.15	0.2	0.1	0.15	0.1	0.05

Note that the BN topology in Figure 2b is not constructed with the goal of maximizing computational efficiency, but is chosen for its simplicity and transparency. Optimization of BN topologies for modeling system performance is the subject of other work (Bensi et al. 2010).

In order to determine the most critical components for survival of the system, evidence is entered that the system has failed. The max propagation algorithm is used to identify the configuration of node states most likely the result in this evidence scenario. For this entered evidence, it is most likely that system failure results from the failure of component 7. This is an intuitive result because component 7 is part of the system bottleneck.

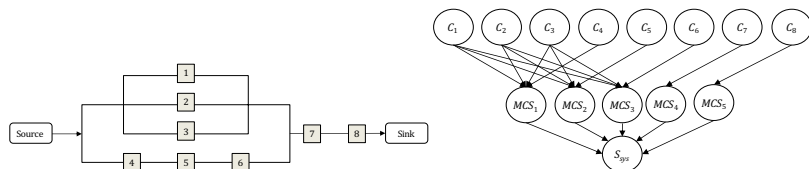


Figure 2. (a) Example system 1; (b) BN modeling performance of system

Next consider that additional evidence is entered into the BN indicating that it is known that components 7 and 8 are in the survival state (e.g. due to the inspection of the components). Application of the max-propagation algorithm under the new evidence scenario reveals that the set of components most likely to result in system fail-

ure is now {1,2,3,4}. Once again, this result is expected. If the bottleneck is known to be operational, in order for the system to fail, the complete set of parallel components (components 1-3), must fail. Furthermore, at least one of the components in series (components 4-6) must fail. Because component 4 is the least reliable, it is a member of the most likely set of components to cause system failure for the evidence scenario.

The above methodology is not limited to binary components. Extending the methodology to multistate components is easily done by augmenting the construction of the conditional probability tables through use of the Max-Flow Min-Cut theorem (Elias et al. 1956; Ford and Fulkerson 1956) as described in Bensi (2010). Conceptually, the topology of the network need not change when modeling multi-state instead of binary components. However, consideration of more states will increase memory demands and may require use of more efficient formulations, see Bensi et al (2010).

Next, the slightly larger system in Figure 3a is considered. Ten components connect a source and sink. Once again, we only consider failure of the square components. The system has twelve MCSs and system performance is modeled in a manner similar to the procedure described above. The resulting BN is shown in Figure 3b. For the purpose of illustration, components in the system are arbitrarily grouped into four classes, A-D. The component states are correlated through common parent nodes, corresponding to each class, as shown by nodes and links with dotted edges in Figure 3b. Nodes A-D are binary with the assumed failure probabilities shown in Table 2.

Table 2. Assumed failure probabilities for nodes A-D

Class	A	B	C	D
Pr(failure)	0.04	0.02	0.03	0.01

Each binary node C_i is defined such that there is 0.9 probability that the node will be in the same state as its parent node, and a probability of 0.10 that it will be in the opposite state. This correlation structure is chosen for its simplicity and predictability. More sophisticated correlation structures are necessary for modeling realistic demands on infrastructure, such as those resulting from earthquakes, see Bensi (2010).

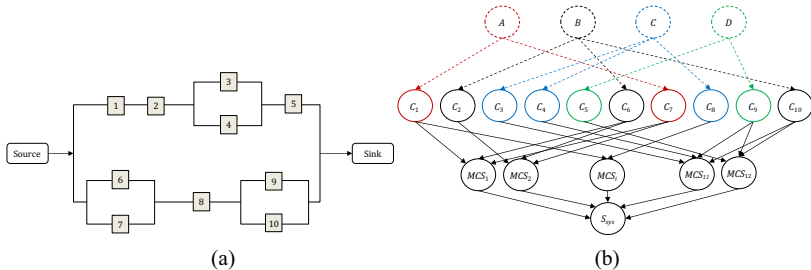


Figure 3. (a) Example system 2; (b) BN modeling performance of system

The procedure described for the previous example is repeated: evidence is entered at node S_{sys} and the max propagation algorithm is utilized to determine the configuration of node states most likely to result in the observed system failure state. Given the assumed failure probabilities and correlation structure, the failure of components 3, 4,

and 8 is most likely to cause system failure. When correlation between component states is neglected (i.e. nodes *A-D* are removed and the component failure probabilities are defined according to their class), the failure of the system is most likely to result from failure of components 1 and 8. If evidence is entered indicating component 8 is in the survival state and the procedure repeated, the most likely set of components to result in system failure is instead components 1, 6 and 7. This result is unchanged if correlation is neglected. Similar analyses can be performed for any combination of observations that have been made about the state of any node in the BN. Note that, as opposed to the first example, the results in this example are not as easily predictable.

DISCUSSION

The max-propagation algorithm is useful for indentifying weak points within a system. Inclusion of sophisticated demand structures allow this task to be performed for any arbitrary hazard and potential evidence scenario. However, care must be exercised when using the algorithm. The procedure described previously is only applicable to generally reliable components, i.e. components that are more likely to be in the survival state than in the failure state. For components for which this is not true, the max propagation algorithm will not produce meaningful results, i.e. it will find that all such components are most likely to be in the failure state when evidence is entered indicating the system has failed. Instead, for such “unreliable” components, an inverse procedure can prove meaningful. That is, the informative observation for such components corresponds to system survival and the algorithm can be used to identify the “strongest link” in the system (i.e. the set of components most likely to result in system survival). Finally, recall that, in the above examples, all nodes were binary. However, when modeling more complex demands and systems, it may be necessary to utilize discretized versions of continuous random variables. For example, seismic demands placed on the components of an infrastructure system are typically measured using continuous metrics, e.g. peak ground acceleration, spectral acceleration. Furthermore, these metrics are typically defined as a function of continuous random variables representing earthquake magnitude, source-to-site distance, and other quantities. The max-propagation algorithm is sensitive to discretization. For discretized versions of continuous random variables the algorithm will identify the discretization interval with the largest probability mass. If continuous random variables are discretized with unequal intervals, certain states may be associated with more probability mass simply because they are associated with a larger interval. This can significantly bias results obtained from the procedure described above.

CONCLUSION

The max-propagation algorithm is used to identify the most probable configuration of node states in a Bayesian network for a given evidence scenario. The paper demonstrates how the max-propagation algorithm can be used to identify critical components or weak links in an infrastructure system with generally reliable components. The paper begins with a brief introduction to BNs and the max-propagation algorithm. The paper demonstrates the usefulness of the algorithm through two simple

examples. Finally, several cautionary words are offered regarding the limitations of the methodology.

REFERENCES

- Bensi, M. (2010). "A Bayesian Network Methodology for Infrastructure Seismic Risk Assessment and Decision Support." Ph.D Thesis., University of California, Berkeley.
- Bensi, M., Der Kiureghian, A., and Straub, D. (2010). "Bayesian network modeling of system performance." *Proceedings of IFIP WG 7.5 Working Conference on Reliability and Optimization of Structural Systems*, Munich, Germany.
- Dechter, R. (1996). "Bucket Elimination: A unifying framework for probabilistic inference." *Uncertainty in Artificial Intelligence*, UA1996, 211-219.
- DSL. (2007). *GeNIe 2.0 by Decision Systems Laboratory* (<http://genie.sis.pitt.edu/>).
- Elias, P., Feinstein, A., and Shannon, C. (1956). "A note on the maximum flow through a network." *Information Theory, IRE Transactions on*, 2(4), 117-119.
- Ford, L. R., and Fulkerson, D. R. (1956). "Maximal flow through a network." *Canadian Journal of Mathematics*, 8(3), 399-404.
- Hugin Expert A/S. (2008). *Hugin Researcher API 7.0* (www.hugin.com). Hugin Expert A/S, Denmark.
- Jensen, F. V., and Nielson, T. D. (2007). *Bayesian Networks and Decision Graphs*. Springer-Verlag, New York.
- Langseth, H., Nielsen, T. D., Rumi, R., and Salmerón, A. (2009). "Inference in hybrid Bayesian networks." *Reliability Engineering & System Safety*, 94(10), 1499-1509.
- Lauritzen, S. L. (1992). "Propagation of probabilities, means and variances in mixed graphical association models." *Journal of the American Statistical Association*, 87, 1098-1108.
- Lauritzen, S. L., and Jensen, F. V. (2001). "Stable local computation with conditional Gaussian distributions." *Statistics and Computing*, 11(2), 191-203.
- Lauritzen, S. L., Jensen, F. V., and Olesen, K. G. (1990). "Bayesian updating in causal probabilistic networks by local computations." *Computational Statistics Quarterly*, 4, 269-282.
- Lauritzen, S. L., and Spiegelhalter, D. J. (1988). "Local Computations with Probabilities on Graphical Structures and Their Application to Expert Systems." *Journal of the Royal Statistical Society. Series B (Methodological)*, 50(2), 157-224.
- Madsen, A. L. (2008). "Belief update in CLG Bayesian networks with lazy propagation." *International Journal of Approximate Reasoning*, 49(2), 503-521.
- Yuan, C., and Druzdzel, M. (2003). "An importance sampling algorithm based on evidence pre-propagation." *In Proceedings of the 19th Annual Conference on Uncertainty in Artificial Intelligence (UAI03)*.
- Yuan, C., and Druzdzel, M. (2006). "Importance sampling algorithms for Bayesian networks: Principles and performance." *Mathematical and Computer Modelling*, 43(9-10), 1189-1207.
- Yuan, C., Lu, T., and Druzdzel, M. (2004). "Annealed MAP." *Proceedings of the 20th conference on Uncertainty in artificial intelligence*, AUAI Press, Banff, Canada, 628-635.

Damage Detection in Water Distribution Pipe Network Using Bayesian Framework and System Reliability Analysis

Won-Hee Kang¹ and Junho Song²

¹University of Illinois at Urbana-Champaign, Newmark Civil Engineering Laboratory, Room 3148, 205 N. Mathews Ave., Urbana, IL 61801; PH (217) 781-0545; email: wkang3@illinois.edu

²University of Illinois at Urbana-Champaign, Newmark Civil Engineering Laboratory, Room 2207, 205 N. Mathews Ave., Urbana, IL 61801; PH (217) 244-9307; FAX (217) 265-8040; email: junho@illinois.edu

ABSTRACT

When a natural or man-made hazard occurs, it is essential to detect damaged components in lifeline networks to enable rapid recovery of the utility service in the impacted areas. However, inspections of individual network components such as buried pipes are often impractical due to exceedingly large costs and time. This paper presents a new system reliability method using a Bayesian method developed for identifying network components with higher conditional probabilities of damage given post-disaster network flow monitoring data. This method achieves an optimal matrix-based representation of the problem for efficient damage detection. The developed method is demonstrated by a water pipeline network consisting of 15 pipelines. The conditional probabilities of damage in 15 pipelines given post-disaster network flow observations are obtained by a Bayesian method for damage detection purpose. The results of the post-disaster damage detection by the proposed system reliability method are compared to those by Monte Carlo simulations and by the matrix-based system reliability method without selective expansion scheme in order to demonstrate the accuracy and efficiency.

1 INTRODUCTION

Urban lifeline networks are large and complex systems consisting of a variety of structural components that are spatially distributed. When a natural or man-made hazard occurs, these networks are often susceptible to structural failures of multiple components such as pipe leakages and breakages. For timely recovery of the utility services in the impacted areas, rapid post-disaster inspections and repairs are desirable. However, physical inspections of all individual pipes in terms of leakages and breakages are often impractical since they are mostly buried underground and excavations would require exceedingly large costs and time. Therefore, it is desirable to have a stochastic framework that can estimate the likelihood of structural damage of network components based on network flow monitoring data such that components with higher likelihood of damage can be inspected with a priority. The framework

needs to account for the uncertainties in component damage and their impacts on the system-level performance through efficient and accurate system reliability analyses.

In order to facilitate such stochastic damage detection of pipeline networks, this study proposes an efficient system reliability method for estimating the conditional probabilities of water pipeline damage given flow monitoring data, based on the Bayesian framework introduced in Poulakis et al. (2003) and the Matrix-based System Reliability (MSR) method (Kang et al. 2008, Song & Kang 2009). Finding such conditional probabilities is fairly time-consuming since the size of the matrices used by the MSR method increases exponentially as the number of components increases. To overcome this computational challenge, the proposed method finds the optimal problem size of the matrices for efficient and accurate stochastic damage detection. As a numerical example, the method is applied to a water distribution network consisting of 15 pipelines subjected to an earthquake event. The conditional probabilities of pipeline damage given network outflow observations are estimated for damage detection purpose. The results are compared to those by existing methods.

2 PROPOSED SYSTEM RELIABILITY METHODS

2.1 Uncertainty quantification of system quantity

Consider a system consisting of n components, each of which has d_i component damage states, $i = 1, \dots, n$. Thus, the system has a total of $d_1 \times d_2 \times \dots \times d_n$ system states determined by component damage states. Let $P_{i,(j)}$, $i = 1, \dots, n$, $j = 1, \dots, d_i$, denote the probability that the i -th component is in the j -th state. If all the component events are statistically independent of each other, the probability of each system state is obtained as the product of the corresponding component probabilities, i.e.

$$\mathbf{p} = \begin{bmatrix} P_{(1,1,\dots,1)} \\ P_{(2,1,\dots,1)} \\ \vdots \\ P_{(d_1,d_2,\dots,d_n)} \end{bmatrix} = \begin{bmatrix} P_{1,(1)} \times P_{2,(1)} \times \dots \times P_{n,(1)} \\ P_{1,(2)} \times P_{2,(1)} \times \dots \times P_{n,(1)} \\ \vdots \\ P_{1,(d_1)} \times P_{2,(d_2)} \times \dots \times P_{n,(d_n)} \end{bmatrix} \quad (1)$$

where \mathbf{p} is the “probability vector” (Lee *et al.* 2010), and $P_{(\dots)}$ denotes the probability of the system state determined by the damage states of the components shown in the subscript. For example, $(2, \dots, 1)$ in the subscript of $P_{(2,1,\dots,1)}$ indicates that all the components are in the first damage state except that the first component is in the second damage state.

Next, we introduce the “component quantity” to represent the performance of the component in a particular damage state. For example, the flow capacity of a pipeline can be considered as a component quantity during a system reliability analysis. Let $q_{i,(j)}$, $i = 1, \dots, n$, $j = 1, \dots, d_i$ denote the component quantity of the i -th component in the j -th damage state, which corresponds to $P_{i,(j)}$. For a given set of component quantities, one can find the corresponding performance of the system, which is represented by a “system quantity.” For example, the flow capacity of a network can be considered as a system quantity. This system quantity can be obtained

by a problem-specific algorithm for a given set of component quantities. For each system state shown in Equation 1, the system quantities can be evaluated as follows.

$$\mathbf{q} = \begin{bmatrix} Q_{(1,1,\dots,1)} \\ Q_{(2,1,\dots,1)} \\ \vdots \\ Q_{(d_1,d_2,\dots,d_n)} \end{bmatrix} = \begin{bmatrix} f(q_{1,(1)}, q_{2,(1)}, \dots, q_{n,(1)}) \\ f(q_{1,(2)}, q_{2,(1)}, \dots, q_{n,(1)}) \\ \vdots \\ f(q_{1,(d_1)}, q_{2,(d_2)}, \dots, q_{n,(d_n)}) \end{bmatrix} \tag{2}$$

where \mathbf{q} is termed as the “quantity vector” (Lee *et al.* 2010), $Q_{(\dots)}$ denotes the system quantity of the system state determined by the component states in the subscript, and $f(\)$ denotes the problem-specific algorithm or function that evaluates the system quantity for the given set of component quantities. For example, the maximum flow capacity algorithm was used in Lee *et al.* (2010) to evaluate the network flow capacity as a system quantity of a bridge transportation network.

Using the probability vector (Equation 1) and the quantity vector (Equation 2), one can obtain probability functions and statistical parameters of the system quantity of interest, Q by matrix calculations (Lee *et al.* 2010). For example, the mean, variance and the cumulative distribution function (CDF) of the system quantity are calculated respectively as follows.

$$\begin{aligned} \mu_Q &= \mathbf{q}^T \mathbf{p} \\ \sigma_Q^2 &= \mathbf{p}^T (\mathbf{q} * \mathbf{q}) - \mu_Q^2 \\ F_Q(q) &= P(Q \leq q) = \sum_{\forall i: q_i \leq q} p_i \end{aligned} \tag{3}$$

where “*” denotes the element-wise multiplication of the two vectors, and p_i and q_i are the i -th elements of the vectors \mathbf{p} and \mathbf{q} , respectively.

It is noteworthy that this matrix-based approach decouples two tasks “system (or network) analysis” and “probability calculations” such that introduction of additional system quantities to the analysis does not require re-computing the probabilities. On the other hand, changes in probabilities due to time-varying performance of components, often caused by structural deterioration in civil infrastructures, do not require re-performing network flow analyses (Lee *et al.* 2010).

2.2 Bayesian method for stochastic system damage detection

When post-disaster observations on system quantities, $\mathbf{Q} = \{Q^1, Q^2, \dots, Q^m\}$ (e.g. outflow quantities at different locations in a network) are available, we can update the probabilities of system states described in Section 2.1 based on the system state observations for damage detection purpose. This stochastic damage detection process should account for various uncertainties such as those in flow measurement, statistical parameters in fragility models, and mathematical models introduced for components and system quantity. However, modeling each of these uncertainties individually is often challenging due to the lack of knowledge and data. Therefore, this study deals with these uncertainties by introducing random variables describing

the uncertain errors in predicting the system quantity by the mathematical model of the system. In the numerical example of this study, the error of each system state prediction is described by a zero-mean normal random variable.

Using a Bayesian framework (Poulakis *et al.* 2003), the conditional probabilities of system states given post-disaster observations on system quantities, $\mathbf{Q} = \{Q^1, Q^2, \dots, Q^m\}$ are evaluated as follows.

$$\begin{aligned}
 \mathbf{p}_{\mathbf{Q}} &= \begin{bmatrix} P_{(1,1,\dots,1)\mathbf{Q}} \\ P_{(2,1,\dots,1)\mathbf{Q}} \\ \vdots \\ P_{(d_1, d_2, \dots, d_n)\mathbf{Q}} \end{bmatrix} \\
 &= \frac{1}{C} \begin{bmatrix} \prod_{k=1}^m \varphi[(Q^k - Q_{(1,1,\dots,1)}^k) / \sigma] \cdot P_{(1,1,\dots,1)} \\ \prod_{k=1}^m \varphi[(Q^k - Q_{(2,1,\dots,1)}^k) / \sigma] \cdot P_{(2,1,\dots,1)} \\ \vdots \\ \prod_{k=1}^m \varphi[(Q^k - Q_{(d_1, d_2, \dots, d_n)}^k) / \sigma] \cdot P_{(d_1, d_2, \dots, d_n)} \end{bmatrix} \tag{4}
 \end{aligned}$$

where $\mathbf{p}_{\mathbf{Q}}$ denotes the probability vector updated by the observation \mathbf{Q} , $P_{(\dots)\mathbf{Q}}$ is the conditional probability of the system state given the observation \mathbf{Q} , $Q_{(\dots)}^k$ is the k -th system quantity predicted by a problem-specific algorithm, $\varphi(\cdot)$ denotes the probability density function of the standard normal distribution, σ is the standard deviation of the normal random variable introduced to describe the aforementioned uncertainty in the system quantity prediction, and C is the normalization factor that makes the sum of the elements in the vector unity.

Since the size of this vector increases exponentially with the number of component events, we propose a method to obtain the updated system state probabilities efficiently. The main idea is to reduce the number of system states by combining damage states of components that do not contribute to the system performance significantly. Suppose we aim to obtain the conditional probability of damage for the l -th component in the system. First, we combine the damage states of all components except the l -th component such that each component has only one damage state, and thus becomes deterministic. This reduces the number of the system states to d_l . The mean of the component quantities is chosen as the deterministic component quantity after the damage states are combined. The mean of the i -th component quantity ($i \neq l$), \bar{q}_i is obtained as

$$\bar{q}_i = \sum_{j=1}^{d_i} P_{i,(j)} \cdot q_{i,(j)} \tag{5}$$

Next, we try to restore the damage states of one of the components to reduce the error. In order to gain maximum improvement in the accuracy, we aim to find the

component whose recovery of the damage states would make the biggest change in the probability of the l -th component's damage. This component damage probability can be obtained by summing up the elements in Equation 4 that belongs to the damage case of the l -th component. For each component except the l -th, we compute the probability and find the component whose recovery makes the biggest change. The number of the system states is then multiplied by the number of the damage states of the selected component. We repeat this process until the damage probability of the l -th component converges. This study uses the following convergence criterion:

$$|P_l^D - P_{l,prev}^D| \leq \epsilon \tag{6}$$

where P_l^D denotes the probability of the l -th component's damage by the current updated probability vector, $P_{l,prev}^D$ is the probability at the previous step, and ϵ is a small threshold value.

3 APPLICATION TO A WATER PIPELINE NETWORK

3.1 Description of water pipeline network

The method proposed in Section 2.2 is demonstrated by the water pipeline network example shown in Figure 1. The network consists of 15 pipes (links) indexed by the numbers in circles. The pipeline intersections (nodes) are indexed by the numbers in squares. The network receives water inflow from a tank and distributes the water through three outflow locations. It is assumed that for the inflow rate $0.1 \text{ m}^3/\text{sec}$, the rate of each outflow for undamaged condition is $0.0333 \text{ m}^3/\text{s}$.

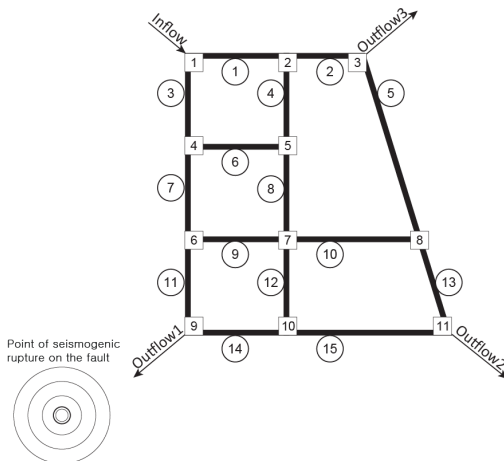


Figure 1. A water pipe network with 15 components.

The flow rates of the undamaged pipes, $q_i, i = 1, \dots, 15$, are computed using the following equation (Lewis *et al.* 2004):

$$q_i = \frac{\pi D_i^4}{128\mu} \left(\frac{p_i^{(1)} - p_i^{(2)}}{L_i} \right) \quad (7)$$

where D_i and L_i are the diameter and the length of the i -th pipe ($i=1, \dots, 15$), $\mu (=9.6 \times 10^{-4} \text{ N}\cdot\text{s}/\text{m}^2)$ is the dynamic viscosity of water, and $p_i^{(1)}$ and $p_i^{(2)}$ are the pressures at the node with the lower index number and that with the higher index number of the i -th pipe, respectively. The diameter of each pipe is assumed to be 0.25 meter while the lengths of the pipes are given as 1.0, 1.0, 1.0, 1.0, 2.1, 1.0, 1.0, 1.0, 1.0, 1.7, 1.0, 1.0, 1.0, 1.1, and 2.0 km (from Pipe 1 to 15). The pipe flow rates for a given set of inflow and outflow values are obtained as follows. At each node, the sum of the flow rates should be zero. For example, at Node 1, the sum of q_1 , q_3 and the inflow rate is zero; and at Node 2, the sum of q_1 , q_2 and q_4 is zero. These 11 equations representing nodal equilibrium conditions are described in terms of 15 pipe flow rates q_i , $i=1, \dots, 15$. By replacing these by the right-hand side of Equation 7, we obtain 11 equations given in terms of $p_i^{(1)}$ and $p_i^{(2)}$, $i=1, \dots, 15$. These pressure terms can be replaced by the pressures at the corresponding nodes. Therefore, one can solve these 11 equations for the 11 nodal pressures. Then, we substitute these into Equation 7 to obtain the pipe flow rates q_i , $i=1, \dots, 15$.

When the water pipe network is subjected to an earthquake event, pipes can be damaged, which reduces the flow rates. The failure probabilities of the pipes are estimated by use of the following “repair rate” given as a function of the peak ground velocity (PGV) in the HAZUS technical manual (FEMA 2008), which is defined as the average number of failures per unit length (km) of a pipe:

$$\text{repair rate} \cong 0.0001 \times (\text{PGV})^{2.25} \quad (8)$$

The failure probability of each pipe is approximately computed by the product of the pipe’s length and the repair rate. Note that this paper deals with failures by ground shaking only by use of the repair rate model in Equation 8, while the ground failure is ignored.

The PGV is computed from the following attenuation relationships (Campbell 1997):

$$\begin{aligned} \ln(\text{PGV}) = & \ln(\text{PGA}) + 0.26 + 0.29M - \\ & 1.44 \ln[r + 0.0203 \exp(0.958M)] + \\ & 1.89 \ln[r + 0.361 \exp(0.576M)] + \\ & (0.0001 - 0.000565M)r - 0.12F - \\ & 0.15S_{SR} - 0.30S_{SR} - \\ & 0.75 \tanh(0.51D)(1 - S_{HR}) - f_V(D) \end{aligned} \quad (9a)$$

where

$$\begin{aligned}
\ln(\text{PGA}) = & -3.512 + 0.904M - \\
& 1.328 \ln\{\sqrt{r^2 + [0.149 \exp(0.647M)]^2}\} + \\
& [1.125 - 0.112 \ln r - 0.0957M]F + \\
& [0.440 - 0.171 \ln r]S_{SR} + \\
& [0.405 - 0.222 \ln r]S_{HR} +
\end{aligned} \tag{9b}$$

where PGA is the peak ground acceleration, M denotes the earthquake magnitude, assumed to be 7.0 for the earthquake scenario in this example, F represents the fault type, assumed to be 0 for strike-slip type faulting, S_{SR} and S_{HR} define the local site conditions, assumed to be alluvium or firm soil ($S_{SR} = S_{HR} = 0$), D denotes the depth to bedrock, assumed to be 0.45 km, r is the distance between the center of each pipe and the epicenter. The distances of the pipes are 5.7, 6.3, 5.0, 5.6, 6.1, 4.8, 4.1, 4.8, 4.1, 5.0, 3.4, 4.1, 5.6, 4.1, and 4.7 km (From Pipe 1 to 15). For $D < 1$ km, $f_i(D)$ is given as

$$f_V(D) = -0.30(1 - S_{HR})(1 - D) - 0.15(1 - D)S_{SR} \tag{9c}$$

The failure event of a pipe is further divided into three damage states in terms of the water flow rate losses: 25%, 50%, and 100% losses. Their probabilities are assumed to be 0.75, 0.07, and 0.18, respectively, which are modified from a proposed water loss distribution in Zolfaghari and Niari (2009). Thus, the probabilities of these three damage states of each pipe given an earthquake magnitude are computed by the product of the failure probability obtained by use of the repair rate in Equation 8 and the probabilities of water losses. There is one more case, 0% water loss, and the corresponding probability is one minus the failure probability of the pipe. In sum, each pipe has four damage states represented by 0%, 25%, 50%, and 100% water loss. Therefore, there exist four component quantities, i.e. $q_{i,(1)}=q_i$, $q_{i,(2)}=0.75q_i$, $q_{i,(3)}=0.5q_i$ and $q_{i,(4)}=0$. The corresponding component probabilities $P_{i,(1)}$, $P_{i,(2)}$, $P_{i,(3)}$ and $P_{i,(4)}$ are computed as explained above.

3.2 Stochastic damage detection of water pipeline network

Suppose, after an earthquake event with $M=7.0$ occurs, the three outflow rates are observed as 1.20×10^{-2} , 2.05×10^{-2} and 1.21×10^{-3} m³/s (from Outflow 1 to 3). Using the Bayesian method introduced in Section 2.2, we calculate the updated probabilities that the pipes are damaged and thus experience any loss of water flow rate, i.e., 25%, 50% or 100% water loss. In order to account for the aforementioned uncertainties in the problem, the errors in the system quantity predictions are assumed to be zero-mean Gaussian random variables with the standard deviations σ assumed to be 1% of the inflow rate 0.1 m³/s. Due to the exceedingly large size of the vector, the updated probability vector in Equation 4 cannot be evaluated directly or by MCS.

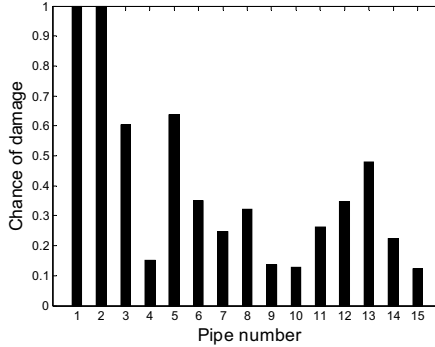


Figure 2. Component damage probabilities based on the complete vector of the updated probabilities obtained by a supercomputer ($\sigma=1\%$ of inflow).

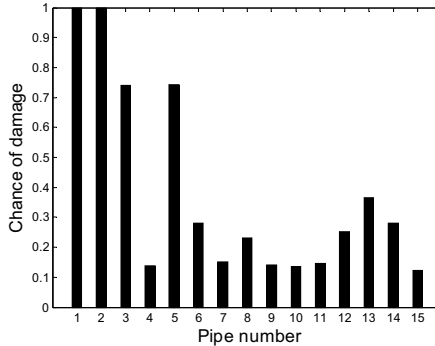


Figure 3. Component damage probabilities based on the incomplete vector of the updated probabilities obtained by the method proposed in Section 2.2 ($\sigma=1\%$ of inflow).

To test the accuracy of the method proposed in Section 2.2, we evaluate the updated probability vector in Equation 4 completely using a supercomputer (Abe Dell Intel 64 Linux Cluster), i.e. without using the approximation by the method. A total of $4^{15} (\approx 10^9)$ flow analyses are required. By summing up the updated probabilities corresponding to the damage of each component, the component damage probability is calculated (see Figure 2). Next, the same analysis is conducted by Matlab® on a personal computer with AMD dual core 2.0 GHz, using the efficient method proposed in Section 2.2. The convergence criterion in Equation 6 is slightly modified as follows to perform stochastic damage detection of multiple pipes in parallel:

$$\frac{1}{n} \sum_{i=1}^n |P_i^D - P_{i,prev}^D| \leq \varepsilon \quad (10)$$

where $n=15$ is the number of the components, and $\epsilon=0.15$ is the threshold value used in this example. This convergence criteria indicates that the analysis is continued until the average error of the component damage probabilities is smaller than the prescribed threshold value ϵ . Although the analysis stopped after only 6 of 15 components recovered a full set of damage states, the results in Figure 3 show a good agreement with those by the complete vector evaluated by the supercomputer (Figure 2).

From these results, we observe that Pipes 1 and 2 have almost 100% chance to be damaged given post-disaster outflows, which means they should be inspected with a top priority. Pipes 3 and 5 also have relatively high chances of damage and need to be inspected.

Figure 4 shows the component damage probabilities estimated by Monte Carlo Simulation (10^5 samples). Even after a three-day analysis (by the same personal computer), the component damage probabilities are significantly different from the true solutions in Figure 2 and fail to identify most critical components.

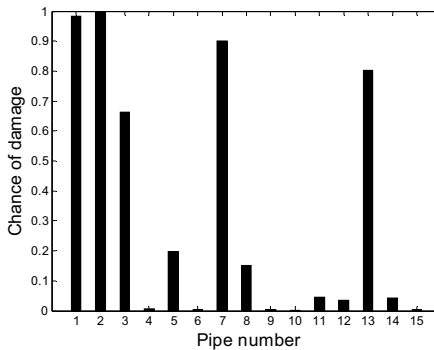


Figure 4. Component damage probabilities by Monte Carlo simulations (10^5 samples, $\sigma=1\%$ of inflow).

In order to test the impact of the assumed value of σ in Equation 4, two higher levels of errors $\sigma = 5\%$ and 10% of the inflow are used. Figure 5 and Figure 6 show the component damage probabilities obtained by the method proposed in Section 2.2 with 5% and 10% errors, respectively. It is seen that the damage probabilities of Pipes 1 and 2 remains the highest but decrease while other pipes' probabilities increase, which makes damage detection a challenging task. As the errors increase even more, the post-disaster damage probabilities approach the original probabilities before observations because the likelihood functions in the Bayesian framework do not provide much information about damage due to large uncertainties in the prediction by the mathematical model. Further study is needed to find actual level of the uncertainties in stochastic damage detection.

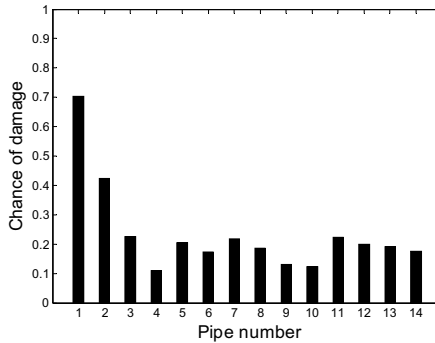


Figure 5. Component damage probabilities based on the incomplete vector of the updated probabilities obtained by the method proposed in Section 2.2 ($\sigma=5\%$ of inflow).

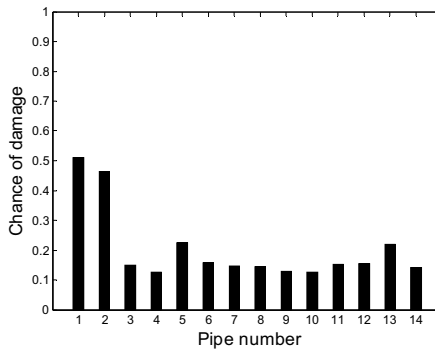


Figure 6. Component damage probabilities based on the incomplete vector of the updated probabilities obtained by the method proposed in Section 2.2 ($\sigma=10\%$ of inflow).

4 CONCLUSION

In this study, an efficient system reliability method is developed based on the matrix-based system reliability method in order to facilitate post-disaster damage detection for water pipeline networks. A Bayesian framework is developed to compute the conditional probabilities of component damage given post-disaster network flow observations. The developed method was successfully applied to a water pipe network consisting of 15 pipelines. The efficient stochastic system damage detection method identifies the same critical components as full vector calculations, which were done by use of a supercomputer due to its exceedingly large computational cost.

The results demonstrate the high efficiency and reasonable accuracy of the proposed method while Monte Carlo simulations were not able to detect components with high probabilities of damage despite large computational cost. The proposed method is applicable for other general complex systems as well. A further study is needed for investigating the impact of model errors on stochastic damage detection and for rapid post-disaster decision makings on a variety of lifeline networks.

ACKNOWLEDGEMENTS

The authors would like to thank the U.S. National Science Foundation for funding under grant number CMMI 1031318. Any opinions, findings and conclusions or recommendations expressed in this material are those of the authors and do not necessarily reflect the views of the National Science Foundation. We also greatly acknowledge an allocation of advanced computing resources supported by the National Science Foundation (System: NCSA Abe - Dell Intel 64 Linux Cluster).

REFERENCES

- Campbell, K. (1997). "Empirical near-source attenuation relationship for horizontal and vertical components of peak ground acceleration, peak ground velocity, and pseudo-absolute acceleration response spectra." *Seismological Research Letters*, 68(1), 154-179.
- Federal Emergency Management Agency (FEMA) (2008). "HAZUSMH-MR4 Technical Manual", FEMA, Washington D.C., USA.
- Guenard, Y.F. (1984). "Application of system reliability analysis to offshore structures. Report 1", *Reliability of Marine Structures Program*, Stanford Univ., Stanford, CA, USA.
- Huang, S.M., Fu, S.C. and Jiang, J.B. (2008). "Flow analysis of water supply networks post-earthquake." *Proceedings of the 14th world conference on earthquake engineering*, Beijing, China.
- Kang, W.-H., Lee, Y.-J., Song, J. and Gencturk, B. (2010). "Further development of matrix-based system reliability method and applications to structural systems." *Structural and Infrastructure Engineering: Maintenance, Management, Life-cycle Design and Performance*, in press (DOI: 10.1080/15732479.2010.539060).
- Kang, W.-H., Song, J. and Gardoni, P. (2008). "Matrix-based system reliability method and applications to bridge networks." *Reliability Engineering and System Safety*, 93, 1584-1593.
- Lee, Y.-J. and Song, J. (2010). "Risk analysis of fatigue-induced sequential failures by branch-and-bound method employing system reliability bounds." *IFIP WG7.5 Working Conference on Reliability and Optimization of Structural Systems*, April 7-10, Munich, Germany.
- Lee, Y.-J., Song, J., Gardoni, P. and Lim, H-W. "Post-hazard flow capacity of bridge transportation network considering structural deterioration of bridges." *Structural and Infrastructure Engineering: Maintenance, Management, Life-*

- cycle Design and Performance*, in press (DOI: 10.1080/15732479.2010.493338).
- Lewis, R.W., Nithiarasu, P. and Seetharamu, K.N. (2004). "Fundamentals of the Finite Element Method for Heat and Fluid Flow." *Wiley & Sons*.
- Murotsu, Y. 1984. "Automatic generation of stochastically dominant modes of structural failure in frame." *Structural Safety* 2(1): 17-25.
- Poulakis, Z., Valougeorgis, D. and Papadimitriou, C. (2003). "Leakage detection in water pipe networks using a Bayesian probabilistic framework." *Probabilistic Engineering Mechanics*, 18, 315-327.
- Song, J. and Kang, W.-H. (2009). "System reliability and sensitivity under statistical dependence by matrix-based system reliability Method." *Structural Safety*, 31(2), 148-156.
- Song, J. and Der Kiureghian, A. (2003). "Bounds on system reliability by linear programming." *Journal of Engineering Mechanics*, 129(6), 627-636.
- Zolfaghari, M. R. and Niari, M.A. (2009). "Probabilistic Seismic Damage Assessment for Water Supply Networks following Earthquake." *Proceedings of the 2009 ASCE Technical Council on Lifeline Earthquake Engineering Conference*, Oakland, CA, USA.

Bayesian Network for Post-Earthquake Decision on Monitored Structures

S.Broglio¹ and A.Der Kiureghian²

¹Department of Structural Engineering, ROSE School, IUSS, Università di Pavia, via Ferrata 1, 27100 Pavia (Italy); email: sbroglio@roseschool.it.

²Department of Civil and Environmental Engineering, University of California, 723 Davis Hall, Berkeley, CA 94720-1710,; email: adk@ce.berkeley.edu.

ABSTRACT

In this paper the problem of assessing the condition and making decisions for strategic structures, e.g. hospitals, police and fire stations, and highway/railway bridges, immediately after an earthquake is investigated. Nowadays it is possible to monitor such structures with placement of sensors, such as accelerometers, strain gages and seismographs. Due to their low cost and easy operation, it is possible to place a large number of such sensors in various parts of a structure or its surrounding ground. The question then arises as to how to post-process the large amount of data obtained from such sensors and from seismological sources that become available shortly after the earthquake. A Bayesian network (BN) framework for processing such evolving information is proposed herein. This probabilistic information, together with information on the costs associated with inspection and closure of the structure, is then used to formulate a decision problem regarding the optimal action to take in the aftermath of an earthquake. An example demonstrates the methodology for a typical building structure.

INTRODUCTION

In this study we address the problem of assessing the condition and making decisions for critical or strategic structures that need to be operative in the immediate aftermath of an earthquake. Nowadays it is possible to monitor such structures in a very detailed way with placement of sensors, such as accelerometers and strain gages. The large amount of data becoming available from sensors or from other seismological sources can be processed to assess the condition of the structure and make decisions about its operation in the immediate aftermath of the earthquake.

In this study we propose a Bayesian network (BN) framework for processing the evolving information that becomes available, not only from the sensors placed in the structure, but also from seismological sources or recordings of the ground motion that become available shortly after an earthquake. The BN allows rapid probabilistic updating of the state of the structure in light of any observed evidence. The probabilistic inference in BNs can be *predictive* or *diagnostic*. In the first case, the probability distribution of a node representing, e.g., the state of the structure, is computed based on prior marginal and conditional distributions of the other nodes, which may represent demand and capacity values. The diagnostic analysis involves the computation of the posterior probability of each node considering observations on one or more nodes in the BN.

Many analyses technique can perform predictive analyses, but diagnostic analyses are peculiar to BNs. For this reason, the BN methodology is highly

useful for applications involving monitoring of structures. The updated probabilistic information about the state of the structure, together with information on the costs associated with various states of the structure, is used to formulate a decision problem regarding the optimal action to take. This may include continued operation or closure of the structure, or conduct of various levels of inspection before a final decision is made. An example demonstrates this process. A simple structural model and highly simplified structural analysis methods are purposely used to avoid masking the main idea of using the BN for information updating and decision support.

BRIEF BACKGROUND ON BAYESIAN NETWORKS

A Bayesian Network (BN) is a graphical model representing the joint probability distribution of a number of random variables using a Directed Acyclic Graph (DAG) and Probability Mass Functions (PMFs). The random variables in the network may represent capacity or demand quantities, or the states of components or systems. Figure 1 shows a simple BN with four nodes, each representing a random variable. In BN terminology, variables X_2 and X_3 are said to be the *children* of X_1 , while variable X_1 is defined as a *parent* of X_2 and X_3 . Likewise, variable X_2 is a *parent* of X_4 , while X_4 is a *child* of X_2 .

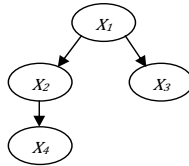


Figure 1. A Simple BN as a Direct Acyclic Diagram (DAG).

Each node X_i in the BN represents a discrete or discretized random variable with a finite set of mutually exclusive and collectively exhausted states. Continuous random variables can also be considered, but exact inference algorithms only work for discrete variables (with the exception of linearly dependent Gaussian random variables). The distribution of each variable X_i is represented by a Probability Mass Function conditioned on its parents, $p(x_i|pa(X_i))$, where $pa(X_i)$ is the set of parents of X_i . If a variable has no parents, it is described by its marginal PMF, $p(x_i)$. One can show that the joint PMF of all the random variables in the network can be written as

$$\begin{aligned}
 p(x_1, x_2, \dots, x_n) &= p(x_1|pa(X_1))p(x_2|pa(X_2)) \dots p(x_n|pa(X_n)) \\
 &= \prod_{i=1}^n p(x_i|pa(X_i))
 \end{aligned}
 \quad (1)$$

Equation 1 states that a random variable X_i , conditional on its parents $pa(X_i)$, is statistically independent of all its parents' ancestors.

BNs are suitable for answering probabilistic queries when one or more variables are observed. Upon receiving information on one or more variables (nodes), the distributions of all other variables in the network are updated. Let $e = \{X_1 = x_1\}$ denote the observed information or *evidence*, i.e. we have observed that random variable X_1 is in state x_1 . The conditional distribution of any other set of the variables given this evidence is obtained by use of the Bayes'

rule. For example, the updated joint distribution of random variables X_2 and X_3 given e is

$$p(x_2, x_3 | x_1) = \frac{p(x_1, x_2, x_3)}{p(x_1)} \quad (2)$$

It is seen that this calculation requires the lower-level joint PMF $p(x_1, x_2, x_3)$ and the marginal PMF $p(x_1)$. These are obtained from the joint distribution in (1) through a process of *marginalization*. Efficient algorithms are available for this purpose (see Jensen and Nielson, 2007). So-called *d-separation* rules, which determine how information propagates in a BN, facilitate rapid updating of distributions even when the BN involves large number of random variables.

MODEL FOR STRUCTURAL RESPONSE

The example structure considered here is a 5-storey reinforced concrete building with a moment-resisting frame, regular in elevation. The height of each story is 3.0 m (i.e. total height 15m). The total mass of the building is assumed to be known and equal to 1500 tons.

Simplified procedures are used herein in order to obtain the general BN framework used for the definition of the structural response. If the response of the structure is defined using response spectra, the period of the structure needs to be computed. Several approximate methods are available in the literature for estimating the period of a building. A predictive equation proposed by Crowley *et.al* (2006) has the form

$$T = (0.043)H + E_T \quad (3)$$

where T is the period in seconds, H denotes the height of the building in meters (here assumed known to be 15m), and E_T is the model error term, which is assumed to be a zero-mean normal random variable with standard deviation equal to 0.10. The distribution of T is truncated in the range [0.50 1.10], which is a reasonable range of values for cracked reinforced concrete buildings with infill panels with openings.

The input motion is defined in terms of its response spectrum. Predictive equations defining the response spectrum in terms of earthquake and site characteristics are given by Campbell & Bozorgnia (2006). These equations involve the earthquake magnitude, distance to nearest point of the fault rupture, the shear-wave velocity of the site, etc. Bensi *et al.* (2010) used these relations to develop a BN model of the seismic demand. Here, we use the model by Bensi *et al.* to define the median spectral acceleration (S_{AM}). Figure 2 shows the position of the building relative to the fault and Table 1 lists some of the assumed distributions or relations in the model by Bensi *et al.* (2010). Figure 3 shows a simplified version of Bensi's BN seismic demand model inside the dotted rectangle.

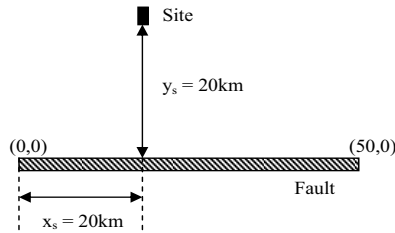


Figure 2. Position of the building relative to the fault.

Table 1. Parameters used in the predictive equations for spectral acceleration

Building coordinates	Deterministic $x_s = 20\text{km}$; $y_s = 20\text{km}$;
Epicenter position, \mathbf{x}_e	Uniform probability distribution along the fault
Magnitude, m	Truncated exponential distribution (Gutenberg and Richter, 1944)
Rupture Length, R_L	$\log(R_L) = a + bm + \varepsilon\sigma$ (Wells et al., 1994)
Left-end coordinate of the rupture, \mathbf{x}_r	$U(x_e - \min(R_L, x_e), x_e - \max(0, R_L - (F_L - x_e)))$ (Bensi et al., 2010)
Site-to-fault distance in X direction, x_d	$\max((x_r - x_s), x_e - \min(x_r + R_L, 0))$ (Bensi et al., 2010)
Joyner-Boor distance, R_{jb}	$R_{jb} = \sqrt{x_d^2 + y_s^2}$

Passing from the median to the real value of spectral acceleration, S_{ar} , the error term in the regression formula must be taken into account. In the Campbell-Bozorgnia attenuation relationship, the variance representing the total variability is a function of magnitude, distance and the considered period. An investigation of these relations revealed that, for the range of periods considered, the influence of magnitude, distance and period on the total standard deviation is insignificant. Hence, in this study the standard deviation of the logarithmic spectral acceleration is assumed to be constant and equal to 0.60.

Two sensors are placed at the 1st and 5th floor levels of the building. A simplified predictive model of the median value floor accelerations, \hat{a}_i , in terms of the real spectral acceleration is considered as shown in equation (4) below, where M_b is the mass of the building, S_{ar} is the real spectral acceleration, T is the period as computed in (3), z_i is the height of the story considered measured from the ground level and m_i is the mass of the single story. It is based on the assumption of linear distribution of the lateral forces (and then accelerations) along the height of the building (Petrini *et al.*, 2004). The logarithm of the floor acceleration is associated with a model error term (E_a), which is assumed to be a zero-mean normal random variable with assumed standard deviation equal to 0.20 and it is introduced to get the real value of the floor acceleration (a_i) as in (5).

$$\hat{a}_i = M_b \cdot S_{ar}(T) \cdot \frac{z_i}{\sum_{i=1}^{n\text{-story}} m_i z_i} \quad (4)$$

$$\log(a_i) = \log(\hat{a}_i) + E_a \tag{5}$$

Equation (4) gives a crude approximation of the floor acceleration. Other, more refined methods will be used for further development of the proposed framework.

Figure 3 shows the complete BN model, where nodes are included for accelerations of floors 1 and 5. Terms representing errors in the predictions of the period, the response spectrum ordinate, and the floor accelerations, denoted E_i , are included. These are zero-mean normal random variables with standard deviations listed in Table 2. Note that the errors for the two floor accelerations are assumed to be correlated, hence the directed link between them. The correlation coefficient between these two error terms is assumed to be 0.5.

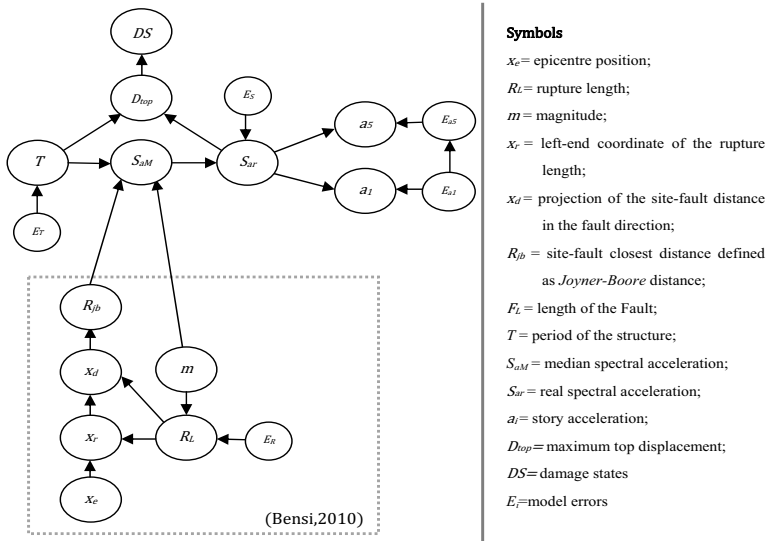


Figure 3. Bayesian Network for definition of structural response.

Table 2. Standard deviations of model errors.

Parameter	Standard deviation
Spectral Acceleration (S_{ar})	0.60
Rupture Length (R_L)	0.23
Period (T)	0.10
Floor acceleration (a_1 and a_5)	0.20

DECISION UNDER UNCERTAINTY

The BN can be used to support decision-making under uncertainty. The tool used to solve the decision problem is called Influence Diagram (ID), which is a BN that is extended with addition of decision and utility nodes. Each decision node has

states indicating the available alternatives. Decision alternatives considered in this study include continued operation or closure of the building, or conduct of an inspection before a final decision regarding closure/operation is made. Each of these alternatives is related to direct and indirect losses. Direct losses are those related to the damage of the building itself, while indirect losses are due to business interruption if the building is closed, and the cost of liability if the building is left open, depending on the damage state of the building. These are represented by utility nodes. For this example, the total cost of direct and indirect losses is considered in an approximate way as a percentage of the total cost of replacement of the building, as shown in Table 3. The cost of inspection is assumed to be 1% of the replacement cost.

Table 3. Total direct and indirect costs expressed as percentage of the cost of replacement.

	no damage		slight		moderate		extensive		complete	
	close	open	close	open	close	open	close	open	close	open
cost	1	0	1.02	0.02	1.1	0.6	1.5	6.0	2.0	12

The Influence diagram used in this study is given in Figure 4. Rectangular nodes in this graph represent decision nodes. They are: conduct or not conduct an inspection (*INSPECTION*), and continue operation or close the building (*FINAL DECISION*). These nodes are related to utility nodes, shown as hexagons, which state the costs associated with each decision alternative (C_i is the cost of inspection and C_{tot} is the total cost related to closure or non-closure of the building). The *DS* chance node represents the probability distribution of the damage state of the building and the *INFO* node is the test-likelihood matrix used to indicate the quality of the inspection, as shown in Figure 4.

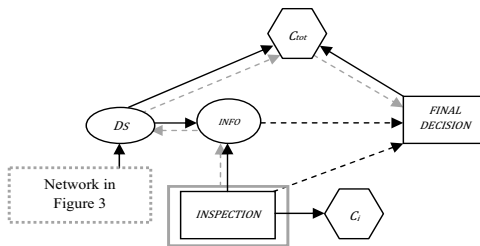


Figure 4. Influence diagram (ID).

If the decision maker decides to perform an inspection of the structure before the final decision, the network will be updated following the grey-path. The additional information obtained performing the inspection updates the probability distribution of the state of the building and, thus, influences the final decision.

Table 4. Test-likelihood matrix as considered in this study

Inspection outcome	Real Damage States				
	no damage	Slight	moderate	extensive	complete
no damage	0.8	0.1	0	0	0
slight	0.2	0.7	0.1	0	0
moderate	0	0.2	0.7	0	0
extensive	0	0	0.2	0.8	0.2
complete	0	0	0	0.2	0.8

EXAMPLE APPLICATION

In order to demonstrate the methodology, a scenario example is given in this section considering the networks represented in Figure 3 and Figure 4. It is assumed that a sequence of evidence becomes available after an earthquake. The information comes from different sources and is summarized in Figure 5.

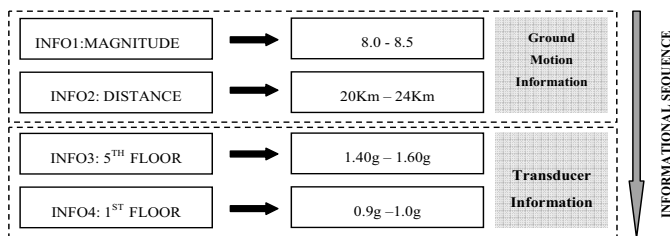
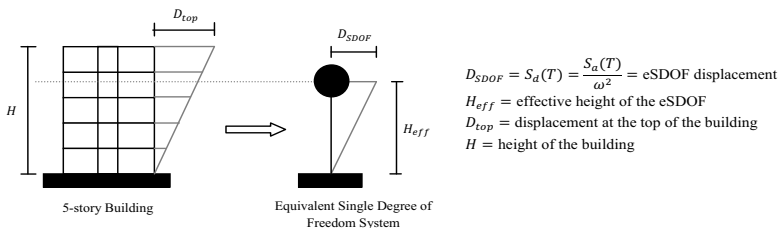


Figure 5. Informational sequence.

The evolution of the damage state probability distribution (i.e. the PMF of node *DS* in the network) is given in the form of bar charts in Figure 7. Table 5 shows the damage states considered in this study. They are defined in terms of the maximum drift ratio, which for the simplified model considered here is equal to the ratio of the maximum top displacement to the total height of the building, assuming a linear displacement profile (see Figure 6). It can be seen in Figure 7 that the PMF of the damage states moves towards higher damage values as the evidence sequence increasingly suggests a high intensity ground motion.



$$D_{SDOF} = S_a(T) = \frac{S_a(T)}{\omega^2} = \text{eSDOF displacement}$$

$$H_{eff} = \text{effective height of the eSDOF}$$

$$D_{top} = \text{displacement at the top of the building}$$

$$H = \text{height of the building}$$

Figure 6. Simplified scheme for determining the top displacement for the 5-story building.

Table 5. Definition of damage states as function of drift ratio.

Damage State	Drift Ratio
No-Damage	0-0.0033
Slight Damage	0.0033-0.0053
Moderate Damage	0.0053-0.0133
Extensive Damage	0.0133-0.0333
Complete Damage	> 0.0333

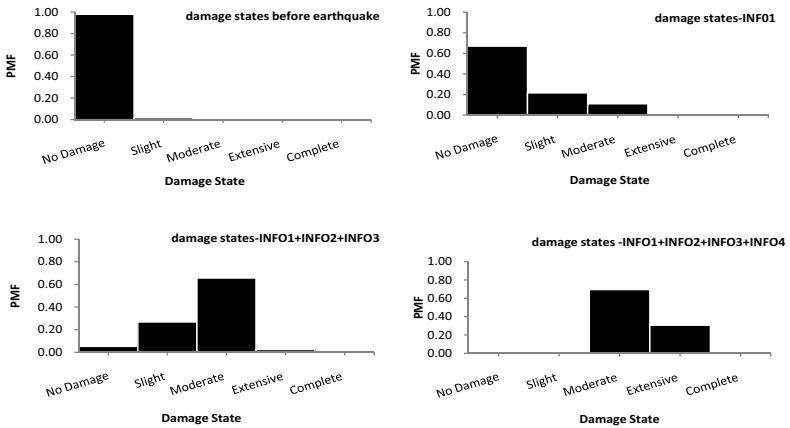


Figure 7. Evolution of damage state probability distribution.

Given the sequence of evidence in Figure 5 and the test-likelihood in Table 4, the PMF of the indicated damage states before inspection is performed is shown in Figure 8. With this distribution and the cost values in Table 3, the ID given in Figure 4 indicates that an inspection should be performed before making the final decision regarding the closure or non-closure of the building.

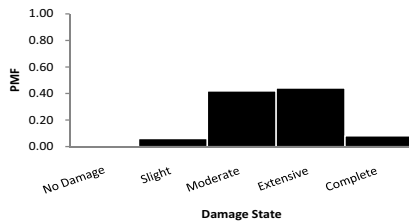


Figure 8. Probability distribution of damage state indication before performing inspection.

The optimal decision alternatives for closure or non-closure of the building for each damage state indication by the inspection are presented in Table 6. An optimal decision for no-damage state indication is not given since, considering the

evidence sequence in Figure 5, this damage state indication has zero probability of occurring, as can be seen in Figure 8.

Table 6. Optimal decision alternatives for different damage states.

Result of inspection	No-damage indicated	Slight damage indicated	Moderate damage indicated	Extensive damage indicated	Complete damage indicated
Optimal Decision	-	OPEN	OPEN	CLOSE	CLOSE

CONCLUSIONS

Thanks to the reduction in price of sensors, it is increasingly feasible to monitor structures during earthquake events. The Bayesian network and associated influence diagram are powerful and efficient tools for processing the information gained from such sensors in order to support decision-making in the aftermath of an earthquake. In this paper a simple building example is used to demonstrate the effectiveness of the BN-ID framework. The example uses simplified methods of modeling the building and evaluating its response so this analysis does not mask the underlying concepts of the BN and ID methodology. These modeling and analysis will be refined in future developments in order to obtain more realistic results for practical applications.

REFERENCES

- Bensi, M., A. Der Kiureghian and D. Straub (2010). Bayesian network for infrastructure seismic risk assessment: challenges and opportunities. *Proc., 7th Intern. Conf. on Urban Earthquake Engineering & 5th Intern. Conf. on Earthquake Engineering*, Tokyo, Japan, March 3-5, 2010.
- Campbell, K.W., Bozorgnia, Y. (2007) *Campbell-Bozorgnia NGA Ground Motion Relations for the Geometric Mean Horizontal Component of Peak and Spectral Ground Motion Parameters*. 2007. Report 2007/02, Pacific Earthquake Engineering Research Center (PEER), University of California, Berkeley.
- Gutenberg, B., and Richter, C. F. (1944). "Frequency of earthquakes in California" *Bulletin of the Seismological Society of America*, 34(4), 185-188.
- Jensen, F. V., and Nielson, T. D. (2007). *Bayesian Networks and Decision Graphs*. Springer-Verlag, New York.
- Petrini, L., Pinho, R., Calvi, G.M. (2004). *Criteri di Progettazione Antisismica degli Edifici*. IUSS Press, Pavia, Italy.
- Straub, D., Der Kiureghian, A. (2009) "Bayesian Network Enhanced with Structural Reliability Methods: Methodology," *ASCE Journal of Mechanics* 186 (10), 1248-1258..
- Wells, D.L., Coppersmith, K.J., (1994) "New Empirical Relationship among Magnitude, Rupture Length, Rupture Width, Rupture Area, and Surface Displacement," *Bulletin of the Seismological Society of America* 84(4), 974-1002.

RISK-BASED FRAMEWORK FOR STREAM REPAIR PROJECTS

Peggy A. Johnson¹

¹Professor and Head, Dept. of Civil and Environmental Eng., Penn State University, University Park, PA 16802; PH (814) 863-3084; email: paj6@psu.edu

ABSTRACT

The phrase “stream restoration” has become commonplace to describe a wide variety of stream intervention practices. Rather than using the term “restoration” to cover the broad range of stream interventions, many of which are not restoration at all, the Center for Watershed Protection has moved to using the phrase “stream repair”. In this paper, a risk-based framework is presented for planning and designing stream repair projects, particularly in the vicinity of infrastructure. The method incorporates a wide variety of uncertainties, including non-quantifiable types, such as aesthetics, failure consequences, etc., providing a systematic approach to reducing risk prior to implementation. Individual components of a stream repair project, as well as the overall design, are considered. The results provide a basis for decision-making in determining the best option for stream repair and provides a powerful tool for communication between practitioners engaged in design, environmental funding and permitting agencies, infrastructure owners, and other stream stake-holders.

INTRODUCTION

The phrase “stream restoration” has become commonplace to describe a wide variety of stream intervention practices. The Federal Interagency Stream Restoration Working Group (FISRWG) (1998) based their definition of stream restoration on the definition provided by the National Research Council (1992), which stated that restoration is reestablishment of the structure and function of ecosystems. According to FISRWG, it is not possible to recreate a system exactly, due to the dynamic nature of that system. Rather, the restoration process recreates the self-sustaining behavior of the ecosystem by reestablishing the general structure, function, and dynamic processes of the stream. The Center for Watershed Protection (Center for Watershed Protection, 2009) has moved to using the phrase “stream repair” rather than “restoration” to cover the broad range of stream interventions, many of which are not restoration at all. This terminology has been adapted in this paper.

Expenditures related to stream restoration and repair have exceeded an average of \$1 billion dollars per year since 1990 (Bernhardt et al. 2005). Nationally, costs range from \$100 - \$875 per meter of restored stream length (Moerke and Lamberti 2004). Despite federal and state mandates to improve aquatic ecosystem conditions, ten-figure annual stream restoration expenditures, and the emergence of a

consulting industry specializing in this area, the success of restoration projects has been mixed (Kondolf et al. 2001; Downs and Kondolf 2002; Johnson et al. 2002). Given the high costs associated with natural channel design and the uncertainty and risk associated with these projects, the development of a simple tool that can be used to assess the uncertainty and risk associated with a particular stream repair project would constitute a substantial contribution to the science.

In this paper, a risk-based framework for planning and designing stream repair projects is presented that is capable of incorporating a wide variety of uncertainties, including non-quantifiable types, and provides a systematic approach to reducing risk prior to implementation. The risk-based framework has the capacity to provide systematic evaluation of individual components of a restoration project as well as the overall design, incorporate a wide range of uncertainties and concerns (aesthetics, failure consequences, etc.), incorporate uncertainty inherent in the system, include impacts on infrastructure, and provide adaptability of projects to changes in climate and land use.

BACKGROUND

In the design and implementation of stream repair, there are numerous factors that contribute to uncertainty, thereby increasing the risk of the design (Johnson, 1996; Johnson and Rinaldi, 1998). Johnson and Brown (2001) provided numerous sources of uncertainty involved with stream restoration design. Of these sources, only the uncertainty in specific design parameters (e.g., Manning's n and critical shear stress) and the equations that incorporate these design parameters have been quantified (Johnson 1996; Wilcock 2004). Johnson and Brown (2001) developed an approach, based on a Failure Modes and Effects Analysis (FMEA), to incorporate uncertainty in the design of a channel rehabilitation project in northern Pennsylvania. They suggested that this approach was useful for justifying decisions and determining which design components required particular attention. The FMEA is described in more detail below. Niezgodna and Johnson (2007) later developed a two-step method of incorporating uncertainty and risk in stream restoration design, combining design failure modes and effects analysis (DFMEA) and risk quantification. The analysis involved a detailed sediment transport modeling effort to lower the risk of failure. The sediment transport and alluvial channel modeling design methods were shown to reduce uncertainty and risk by detecting design deficiencies that the initial design, which was based on simplistic incipient motion analyses, overlooked.

Failure modes and effects analysis (FMEA) is a tool widely used in the electrical and manufacturing industries to qualitatively and systematically identify potential component failure modes and assess the effects of associated failures on the operational status of the system (Dushnisky and Vick, 1996). The FMEA is implemented to determine failure modes and remove their causes before the design is implemented (McCollin, 1999). Thus, the preventative action in the FMEA implies modification of the system design for risk reduction before the design is in place. Formulation of the FMEA begins with identification of the system and all of its

components (Dushnisky and Vick, 1996). Next, the range of possible failure modes is defined as mutually exclusive, collectively exhaustive events. The effects of each of the failure modes on the system are then listed, along with the consequences, likelihoods of occurrence (as a qualitative description), and methods of detection. The user chooses numeric ratings, typically on the scale of 1–10, for consequence and likelihood of occurrence criteria, with the largest values associated with the most severe consequence level and the highest likelihood of occurrence. By using ratings for consequences and occurrence, in addition to a rating for detectability (likelihood that a design control will detect or prevent a failure), failure modes can be prioritized to place a greater level of effort on higher priority failures (Niegoda and Johnson, 2007). The most common method of establishing prioritization among failure modes is through the use of risk priority numbers (RPN). The RPN is the product of the numeric ratings (e.g., 1 through 10) for occurrence (O), consequence (C), and detectability (D) of a given failure mode, with the largest values associated with the most severe consequence level and the highest likelihood of occurrence. There are several limitations or drawbacks to FMEA. These limitations, along with more advanced and expanded methods of FMEA proposed for this research, are discussed below.

DEVELOPMENT AND ANALYSIS OF THE FMEA

The FMEA involves steps to assess the failure modes and their associated consequences, severity, and detectability. A set of generalized tables were developed to provide the rankings from 1-10 for each of the three elements of a classic FMEA: consequences, likelihood, and detection. Risk Priority Numbers (RPN) are commonly used to analyze the results of the FMEA:

$$RPN = S * O * D \quad (1)$$

where S = severity, O = occurrence, and D = detection (steps 4-6 above). There is no physical meaning to the RPN; however, the larger the number, the higher the risk. Attention may be needed for those failure modes with high RPNs. Since multiple failure modes might have similar RPNs for different reasons, another measure, Criticality (C), is also often computed.

$$C = S * O \quad (2)$$

A high value of criticality (both high severity and high occurrence) will usually merit special attention. Both of these measures, RPNs and Criticality, will be computed and ranked for all failure modes to determine which failure modes may be problematic in a given design.

RPN and C provide relative measures to determine which failure modes require attention. In the planning and design phases, those components having failure modes with high RPN and/or C should be redesigned to reduce the project risk. However, there are no criteria for what defines an acceptable level of risk for the overall project

or individual failure modes based on RPN and C. Attempting to correct multiple components because of high RPNs could result in an over-designed and costly project. Thus, in this project, advanced FMEA measures will be applied to assist in determining acceptable levels as follows.

The total risk estimate (TRE) (Bluvband and Grabov, 2009) will be calculated as a measure of the “riskiness” of the overall project:

$$TRE = \frac{\sum_{i=1}^n RPN_i}{n * 1000} * 100\% \quad (3)$$

where n = number of failure modes. Bluvband and Grabov (2009) suggest using TRE = 17%, (corresponding to the multiplied midpoint (5.5) values for three RPN components ranked on a scale of 1 to 10), as a significant point or threshold above which the project is “risky”. In addition, the use of simple scree-type plots, as suggested by Bluvband et al. (2004) and Bluvband and Grabov (2009) were explored as a tool to supply additional insight into the relative meaning of the RPNs. The plot is formed by ordering the RPNs and plotting them versus the n^{th} cause. The result is typically a plot that has a gentler slope at the lower RPNs and a steeper slope for higher RPNs. Where the RPNs are seen to increase rapidly in the steeper part of the curve may be considered to be the RPNs and associated failure modes that are in need of more attention.

To decide on a final design, and in order to develop a true picture of risk, economic factors must be considered. Niezgodna and Johnson (2007) developed a two-step method for this purpose in which the first step was a simple FMEA process and the second step used initial and expected failure costs to quantify risk and provide a basis for deciding on a design. Although this method showed promise for an individual case for which cost information was available, the expertise and substantial data requirements for the associated sediment transport model would be limiting factors in most applications.

RPNs, Criticality, TRE’s, and scree-type plots were used to analyze the results of the FMEA and provide meaning and recommendations for which components require redesign or other special attention. Based on these results, the stream repair design can be adjusted in order to lower the level of risk for specific components as well as the overall project. The resulting FMEA for the redesign will then be compared to the original to assure that the risk level has been lowered sufficiently to an acceptable level.

The potential for this system is demonstrated based on an FMEA conducted by Niezgodna and Johnson (2007). The FMEA was conducted for three design scenarios, based on the level of sediment transport calculations for the same stream reach to be restored. The 14 failure modes identified for this case resulted in RPNs ranging from 32 to 512 and total RPN of 4224, 2392, and 1584, respectively, for the simple,

moderate, and detailed design methods (see Table 1). While it is clear that the simple method resulted in a much higher RPN, it is not clear that 4224 is worthy of concern or that there is a significant difference between 2393 and 1584, which might result in concerns regarding the design. The individual RPNs for the 14 failure modes had a wide range, but there is no basis for determining which of those failure modes requires corrective actions other than to select the relatively high values for treatment. Criticality was not computed.

The final design selection in this case was based on the FMEA and an analysis of the total expected costs (initial plus cost of failure). The detailed design method (#3 in Table 1) was selected. Based on the proposed research in this current project, an analysis of a scree-type curve and the TRE values could be used to come to more detailed conclusions regarding the overall project and the concern level for individual failure modes. The TRE values for the three methods are 30.2, 17.1, and 11.3, as listed in Table 1. Using the threshold level of 17% suggested by Bluvband and Grabov (2009), the conclusion would have been similar to the complex cost analysis results in the original study. However, the former method required substantial data, expert knowledge of sediment transport modeling, and a significant time commitment. In this simpler method, these three factors are substantially reduced. As stated earlier, the basis for using 17% will be explored as part of this project.

Table 1. RPNs for 14 failure modes and 3 design methods based on Niezgodna and Johnson (2007).

Failure Mode	Simple (1)	Moderate (2)	Detailed (3)
1	96	64	32
2	128	72	48
3	144	96	64
4	160	96	64
5	256	96	64
6	256	144	96
7	256	144	96
8	320	192	96
9	360	192	128
10	360	192	128
11	384	240	144
12	480	288	192
13	512	288	192
14	512	288	240
RPN Sum	4224	2392	1584
TRE =	30.2	17.1	11.3

The individual RPN values could also be examined using a scree-type plot of the ranked RPNs, as shown in Figure 1. From this Figure, it can be concluded that for RPNs greater than 100, the slope of the scree plot increases sharply. Thus, these RPNs should be given careful attention and corrective actions should be taken to improve the design. The use of this type of plot in both the planning and design stages of stream restoration or modification projects is also a subject of this proposal.

CONCLUSIONS

The results of this study provides a simple method for use in determining the best management practices for stream repair that incorporates uncertainty and is capable of considering important factors in adapting to current and future hydrologic and land use conditions. Uncertainty is inherent in all engineering design. Numerous methods exist for assessing uncertainty; however, the enormous complexity of stream hydraulics and erosional processes of the river channel in designing stream repair projects render quantitative methods of computing uncertainty unfeasible. The method presented here seeks to reduce uncertainty in the planning and design phase through a systematic FMEA approach.

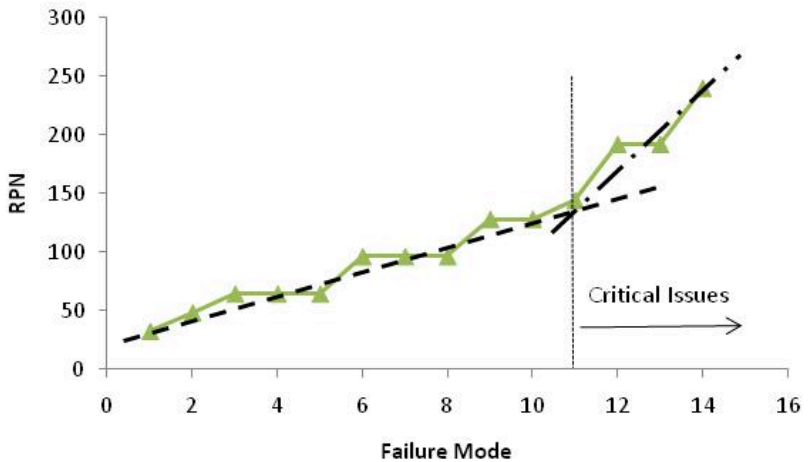


Figure 1. RPN values for 14 failure modes based on data from Niezgoda and Johnson (2007). RPN values are given in Table 1.

These results can also provide a powerful tool for communication between practitioners engaged in design, environmental funding and permitting agencies, infrastructure owners, and other stream stake-holders, such as state and local environmental agencies, watershed organizations, and scientists. The proposed method could be used for deciding whether a stream repair design is feasible and for

choosing the best alternative design based on several simple tests. This may result in an overall more cost-effective approach to creating sustainable designs that move us further toward the goal of managing the impacts of stormwater, infrastructure, climate changes, and land use changes, to protect this valuable asset.

REFERENCES CITED

- Bernhardt, E.S., M.A. Palmer, J.D. Allan, G. Alexander, K. Barnas, S. Brooks, J. Carr, S. Clayton, C. Dahm, J. Follstad-Shah, D. Galat, S. Gloss, P. Goodwin, D. Hart, B. Hassett, R. Jenkinson, S. Katz, G.M. Kondolf, P.S. Lake, R. Lave, J.L. Meyer, T.K. O'Donnell, L. Pagano, B. Powell, and E. Sudduth. 2005. Synthesizing U.S. river restoration efforts. *Science* 308:636-637.
- Bluvband, Z., and Grabov, P., 2009. Failure Analysis of FMEA. Annual Reliability and Maintainability Symposium - 2009 Proceedings: International Symposium on Product Quality and Integrity, Fort Worth, TX.
- Blivband, Z., Grabov, P., Nakar, O., 2004. Expanded FMEA (EFMEA). Annual Reliability and Maintainability Symposium - 2004 Proceedings: International Symposium on Product Quality and Integrity, Los Angeles, CA, 31-36.
- Center for Watershed Protection, 2009. Stream Repair. http://www.cwp.org/Resource_Library/Restoration_and_Watershed_Stewardship/stream.htm. Last accessed on August 10, 2009.
- Downs, P.W. and G.M. Kondolf. 2002. Post-project appraisals in adaptive management of river channel restoration. *Environmental Management* 29(4):477-496.
- Dushnisky, K. and Vick, S.G., 1996. Evaluating risk to the environment from mining using failure modes and effects analysis. In *Uncertainty in the Geologic Environment: From Theory to Practice*, Proceedings of Uncertainty '96, July 31-August 3, 848-865.
- FISRWG (1998). *Stream Corridor Restoration: Principles, Processes, and Practices*. By the Federal Interagency Stream Restoration Working Group (FISRWG) (15 Federal agencies of the US gov't). /GPO Item No. 0120-A; SuDocs No. A 57.6/2:EN 3/PT.653. ISBN-0-934213-59-3.
- Johnson, P. A., 1996. Uncertainty of hydraulic parameters. *Journal of Hydraulic Eng.*, 122(2), 112-114.
- Johnson, P.A., and Brown, E.R., 2001. Incorporating uncertainty in the design of stream channel modifications. *Journal of the American Water Resources Association*, 37(5), 1225-1236.
- Johnson, P.A., and Rinaldi, M., 1998. Uncertainty in Stream Channel Restoration. *in Uncertainty Modeling and Analysis in Civil Engineering*, B.M. Ayyub (ed.), CRC Press, New York, Chapter 22.
- Johnson, P.A., Tereska, R.L., and Brown, E.R., 2002. Using technical adaptive management to improve design guidelines for urban in-stream structures. *Journal of the American Water Resources Association*, 38(4), 1143-1152.
- Kondolf, G.M., M.W. Smeltzer, and S. Railsback. 2001. Design and performance of a channel reconstruction project in a coastal California gravel-bed stream. *Journal of Environmental Management* 28:761-776.

- McCollin, C., 1999. Working around failure. *Manufacturing Engineering*, 78(1), 37-40.
- Moerke, A.H. and G.A. Lamberti. 2004. Restoring stream ecosystems: lessons from a midwestern state. *Restoration Ecology*, 12(3), 327-334.
- National Research Council. 1992. *Restoration of Aquatic Ecosystems*. Committee on Restoration of Aquatic Ecosystems-Science, Technology and Public Policy. National Academy Press, Washington, DC.
- Niezgoda, S.L., and Johnson, P.A. 2007. Case Study in Cost-Based Risk Assessment for Selecting a Stream Restoration Design Method for a Channel Relocation Project. *Journal of Hydraulic Engineering*, Vol. 133 (5), 468-481.
- Wilcock, P. R., 2004. Sediment transport in the restoration of gravel-bed rivers. Proc., 2004 ASCE-EWRI World Water and Environmental Resources Congress, Critical Transactions in Water and Environmental Resource Management, Salt Lake City, Utah, 1-11.

Managing Climate Change Uncertainty in Water Supply Planning

X. J. Irias¹ and A. R. Coate²

¹ East Bay Municipal Utility District, Department of Engineering and Construction, 375 11th Street, Oakland, CA 94607; PH (510) 287-1002; email: xirias@ebmud.com

² East Bay Municipal Utility District, Department of Watershed and Natural Resources, 375 11th Street, Oakland, CA 94607; PH (510) 287-1663; email: acoate@ebmud.com

ABSTRACT

Climate change is without a doubt one of the greatest sources of uncertainty today. Even among the majority of scientists who agree that it is happening and will continue to happen, there is a tremendous range of projections as to the specific impacts, their timing and their geographic extent. There's not even agreement over the magnitude of uncertainty surrounding the various projections.

All of this uncertainty poses a huge challenge for many organizations, but for none more so than water supply agencies, since climate change may directly impact both water supply and water demand.

East Bay Municipal Utility District (EBMUD) is a major water utility in California that recently considered climate change along with other future unknowns when it updated its water supply program through 2040. This paper discusses the process by which EBMUD considered the massive uncertainty posed by climate change in the context of other unknowns to formulate a flexible, defensible water supply strategy that would be robust in the face of the continually evolving scientific data over the next two decades. During this process, EBMUD considered not only the range of scientific projections, but also their possible reliability; and considered not only what we might do if various projections are correct, but what we might do if they are low or high. The discussion of the process and final outcomes should be of interest to all practitioners charged with helping society manage the tremendous uncertainties associated with climate change.

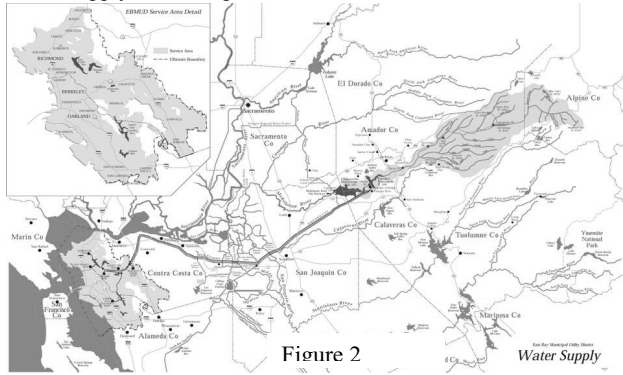
INTRODUCTION

EBMUD provides water to 1.4 million people in the San Francisco Bay Area, as shown in Figure 1. The utility's primary water source is snowmelt from the Mokelumne River system, as shown in Figure 2. A supplemental supply from an adjacent river, the Sacramento River, is also available during dry years.



Figure 1.

As a water-wastewater utility on the coast, climate change poses many challenges to EBMUD even beyond water supply; for example, the need to consider sea level rise impact on low lying wastewater collection and treatment and water transmission facilities and the need to consider mitigating climate change by minimizing our carbon footprint. However, the focus of this paper is on water supply planning specifically. Even this somewhat narrowed focus involves a tremendous number of “known unknowns,” as well as some likely unknowns not even fully understood.



Exponential population growth in California since the gold rush of 1848 has placed increasing stress on water supplies statewide. EBMUD has, since its formation in 1928, met its water supply primarily through storage and transmission of Mokelumne River water. In the 1970s EBMUD initiated programs to promote water conservation by customers and began to recycle treated wastewater to reduce potable water demand. In recent years, EBMUD has improved dry-year reliability with supplies from the Sacramento River and local aquifer storage and recovery. Despite these efforts, fundamental challenges remain, given that California’s climate is semi-arid and subject to periods of drought. It is those periods of drought that shape EBMUD’s water supply strategies since in non-drought years, there is more than sufficient water to meet demands. The long-term level of drought risk is not well known, given that we have only 100 years of data on river flows and precipitation.

EBMUD periodically updates its water supply outlook. The most recent update is known as Water Supply Management Program (WSMP) 2040, which forecasts supply and demand through the year 2040 and proposes methods to meet demands. WSMP 2040 was completed in 2009 to update the previous WSMP that was completed in 1993, and hence it was the first major water supply planning effort for EBMUD that had the benefit of current thinking on global climate change and its impacts on water supplies.

IMPACTS OF CLIMATE CHANGE ON WATER SUPPLY

For purposes of the quantity side of water supply planning, climate change impacts may be categorized as follows (Bates, IPCC, 2008):

1. Increased water demand due to air temperature rise. For example, irrigation use will tend to increase with temperature.

2. Decreased average annual precipitation; there's also a chance of increased precipitation, which is a flood control issue, but for a water supply planner, it's the downside risk that matters.
3. Increased year-to-year variability in runoff, leading to longer and/or deeper droughts.
4. Change in timing of runoff due to earlier snowmelt; if the snow-pack melts too soon, it will be released as part of flood control operations and hence not available for water supply.
5. Change in type of precipitation, e.g., more rain and less snow. Snow acts as a "reservoir" of sorts, so this can decrease our working storage.
6. Decrease in runoff per unit of precipitation, owing to increased sublimation/evaporation due to higher temperatures, and higher ground absorption due to reduction in average precipitation.

Modeling of the impacts described above is relatively uncharted territory for water utilities. Clearly, the cumulative amount of uncertainty is staggering since each of the six factors listed is subject to huge uncertainty not only as estimated by competing global circulation models, but also by regional variation. While the extent and impact of any one of the six factors is quite uncertain, their cumulative impacts are even more uncertain since the six factors may coincide in ways not well understood, and their impacts may add in highly non-linear ways.

The list given here focused on water quantity alone. Changes in water quality, in particular higher temperatures and related fisheries management challenges, are also anticipated, but are beyond the scope of this paper.

STATE OF PRACTICE

Recognizing that drought years represent the limiting condition for water supply, it is crucial to understand not only how climate change might affect the "average year," but more importantly how it will impact the frequency and severity of droughts.

Various water utilities were contacted to gain an understanding of the current state of practice with regard to modeling of drought conditions and modeling of climate change impacts on water supply.

Generally, water utilities surveyed build drought planning around one or more "scenario droughts," which typically are replays of specific historic droughts, optionally with an adjustment such as a time extension or scaling. In a 2002 survey of eight agencies, four agencies planned for a replay of a specific historic drought and two (one of them EBMUD) planned for a specific historic drought with a modification such as a repeat or an extra dry year. Additionally, single severe dry years were analyzed by some agencies, with 1977 being the dry year of record for most of the utilities.

It should be noted that it's very difficult to make meaningful comparisons among a group of utilities, even the eight utilities that are all California-based and all serving similar customer classes (municipal and industrial). Most of the utilities other than EBMUD have relatively diverse supplies, contrasted with EBMUD which relies on a single river for 95% of its water in a normal year. Assumptions also vary regarding the operational strategies that might recognize a drought is underway and reduce demands. Finally, the

utilities vary in terms of their service level objectives (i.e., degree of rationing) during a scenario drought, ranging from an objective to meet the scenario drought with negligible customer impact to accepting significant cutbacks. This range in performance objectives is likely tied to a number of factors, including varying perceptions about the likelihood of one's scenario drought occurring and the degree of water supply reliability acceptable to a given agency.

In short, even before climate change is considered, drought planning in California is an inexact science, stemming from limited data with which to approximate natural phenomena that are poorly understood. A gross generalization, but one that is perhaps helpful to capture the relative immaturity of current practice, is that utilities generally analyze the one or at most two drought scenarios rather than dozens, hundreds or millions of possible scenarios. Utilities also typically rely on historic and watershed specific records of less than 100 years while greater or longer droughts are believed to have occurred in previous centuries based on tree ring growth studies. This one-or-two scenario approach contrasts with the risk management approach practiced in other disciplines. For example, a beam's structural analysis would not be considered complete if live loads were only analyzed at a single location. A dam's safety would not be considered adequate unless all credible seismic hazards had been considered. In disciplines for which a single "scenario" is common, for example, wind load on a small building, that expedient approach is taken not due to lack of knowledge about the likely range of wind loads, but for the opposite reason, i.e., that the wind load scenarios are well understood and a single envelope case may safely be used.

In the field of drought planning, the reasons for the one-or-two scenario practice are rather the opposite; far from modeling limited scenarios because we're confident we understand the phenomena being modeled, we model limit scenarios because we don't have the data or tools to do better. Other hydrologic planning endeavors, such as determination of Probable Maximum Flood (PMF), are similarly prone to the problem of sparse data relative to the planning horizon and, accordingly, it is not uncommon for PMFs to be revised upward, sometimes dramatically, following a larger-than-average flood. But drought planning is even more confounding because of the extreme difficulty in extrapolating from one watershed to another; diverse sources; and, in many cases, the climatic differences between source watersheds and the area where the water is used.

To the nascent science that is drought planning, we introduce the additional uncertainties posed by climate change. A 2007 survey of eleven utilities revealed that five of the eleven were not attempting to analyze agency-specific impacts, relying instead on statewide climate simulations and the assumption that their basic planning scenarios were sufficiently conservative and/or that their systems were inherently "adaptive" enough. Of the remaining five, four were in the process of performing some type of "sensitivity analysis," at least one of which was focused on making adjustments to their drought scenarios. Two of the eleven utilities generated and analyzed multiple scenarios presumably with the same end goal in mind as those performing sensitivity analyses, for example, to adjust their drought scenarios.

Accounting for climate change is an emerging science and there are not yet standardized approaches and widely understood, accepted terminology to allow classifications of approach and methodology. It should thus be recognized that there were no bright lines

in the classification of these eleven utilities; one agency's comprehensive scenario analysis may be judged by another to be a sensitivity analysis. A reasonable distinction might be that a sensitivity analysis would evaluate variables individually or in limited groupings (for example, vary temperature rise), while a scenario analysis would evaluate all variables simultaneously, with each unique vector of variables defining a "scenario" for consideration. It is not known whether such a distinction was discussed with survey respondents.

EBMUD's own state of practice for hydrologic planning going into the WSMP 2040 process was, like the other utilities surveyed, shaped by a major issue: that of limited data stemming from a relatively short historical record. Figure 3 shows the annual runoff for all known years, color-coded as to classification.

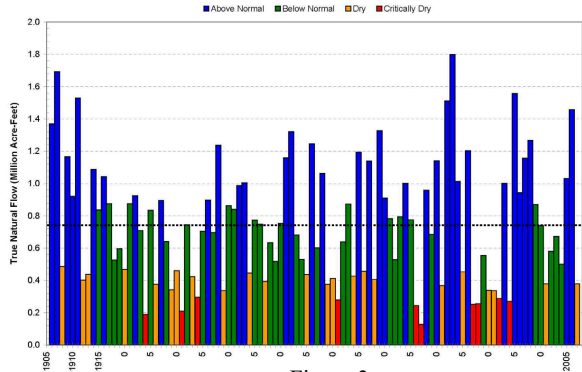


Figure 3.
Mokolunne River Runoff 1906-2007
Source: WSMP 2040

ALTERNATIVE APPROACHES

Having taken a quick look at some common practices for addressing the uncertainties associated with drought planning in the face of climate change, it is appropriate to consider alternative approaches to manage this uncertainty or, more precisely, the alternatives to manage the uncertain *impacts* of climate change.

Alternatives include:

1. Ignore climate change. Assume that its impacts, to the extent they arrive, will be relatively minor and/or gradual, allowing time for adaptation.
2. Be extremely conservative. Do not seek to quantify the various impacts and their uncertainties, but jump directly to solutions such as greater storage and/or diversification of supply.
3. Perform sensitivity analyses of some important parameters such as temperature and precipitation in order to make some educated judgments about overall water supply impacts.
4. Develop multiple scenarios and assess impacts. Optionally attempt to estimate, if not their absolute probabilities, their relative likelihoods compared to one another.

Even if a primary strategy is chosen from the above list to manage the overall system-wide uncertainties posed by climate change, at the tactical level, the various alternatives may be combined. For example, one might temporarily "ignore" climate change for a specific facility sizing analysis if the facility won't be built right away, while favoring

diversity of supply per alternative #2, and performing sensitivity analysis or scenario analysis (#3 or #4) to help choose between two specific supply alternatives.

Alternative 1—Ignore

Ignoring climate change is certainly the cheapest option when considering only the cost of the planning process. Despite the seeming lack of diligence associated with ignoring a known risk, this alternative might be optimal for a utility that has ample fallbacks. For example, a utility that has multiple supply sources, and no looming long-term capital investment decisions, could reasonably take a wait-and-see approach.

On the other hand, a utility with relatively little diversity of supply and contemplating various options to meet future demands would not be well advised to simply ignore climate change. Doing so would expose the utility's facilities to risk of early obsolescence, since many water facilities have lifetimes in the 100-year range.

Alternative 2—Extreme Conservatism

Extreme conservatism as a general panacea for uncertainty increases costs. Even if one is willing to pay, and even if one is willing to bear other potential non-monetary costs of overbuilding, e.g., environmental impacts from dam-building, climate change poses such significant uncertainty that the obvious problem is: how conservative is conservative enough?

Alternative 3—Sensitivity Analysis

Sensitivity analysis, in this particular context, has been termed the “bottom-up approach,” since rather than seek to precisely model future hydrology, it instead models the impacts of some possible climate change outcomes on facilities based on larger scale modeling results. For example, if we consider a 20% reduction in average precipitation to be a likely outcome, we could model our system's performance in that circumstance. After exploring that variable, we might move on to another, such as early runoff, and again model our system's performance.

The analyst who seeks to perform a sensitivity analysis faces some choices. What is a reasonable range of a “likely outcome” such as temperature rise? How should the various outcomes be combined, or bundled, if at all: for example, should a rise in temperature be bundled with a drop in precipitation? Should it also be bundled with an “early spring” and would the answer change if such a bundling is at times unconservative? Should the various “outcomes”, i.e., major variables, vary “in phase” with one another during a modeling run, or be temporally offset?

These concerns hint at a major problem when performing most stochastic modeling: unknown correlations among pseudo-independent variables. A modeler may be oblivious to these concerns, or consciously choose to ignore them, but that will not diminish their effect. Depending on the quality of the modeling choices, the final results may be very useful, utterly meaningless, or somewhere in between. To the extent that correlations among variables are misdiagnosed, the cumulative modeling error may understate the effects of climate change. This error of understatement is in addition to that inherent in

any modeling effort, i.e., only known major variables get modeled at all. For example, if we ignore the reduction in the runoff/precipitation ratio that would almost certainly accompany reduced precipitation, we introduce a non-conservative error in the hopes that the magnitude of the error is small enough to not invalidate our overall conclusions.

Despite the limitations of sensitivity analysis, it may yield some insights to guide decision-making. An advantage of sensitivity analysis over “scenario analysis,” discussed next, is relatively low cost and low complexity.

Alternative 4—Scenario Analysis

Scenario analysis in this context is a major step up from sensitivity analysis in terms of cost and complexity. Instead of varying a single variable or “bundle” of variables at one time, all model variables are varied simultaneously to form a “scenario.” For example, a scenario might consist of a value for air temperature increase, a value for change in average precipitation, a selected shift in that precipitation over the year, and an assumed runoff/precipitation ratio for marginal changes to precipitation. This package of variables, which is a vector representing a single point in an n-dimensional sample space, is then analyzed in the usual way, for example, analyzing system performance under various drought planning sequences.

A clear issue here is the explosion of analytical effort – in effect, we have scenarios within scenarios, since a drought planning sequence is itself a scenario, as is a given contemplated set of capital options, water demand, etc. The analytical effort for a single scenario may be huge, and clearly thousands or millions of scenarios would be needed to get reasonable coverage in a “brute force” manner.

At first glance, one might hope to brush aside concerns of analytical effort by counting on the power of computers. In theory, if one could generate the appropriate pool of scenario vectors and model system performance with each vector, one would gain an understanding of system performance over a very wide range of possible scenarios. Such an approach is endorsed by the Intergovernmental Panel on Climate Change (Bates 2008), even if at present such an effort may be beyond the resources available to most water agencies.

A moment’s reflection on the huge uncertainties in the model and its inputs prompts further thought; rather than searching for the optimal management approach to handle a single future, we ought to consider searching for a management approach that performs reasonably well against a wide range of possible futures. This notion is part of Robust Decision Making (RDM) as promoted by RAND Corporation (Groves, 2005). The general idea is that we want a system that is “robust” With RDM, we develop and study a very large number of scenarios with the goal of ensuring that our system performs “good enough” against a very wide range of scenarios, i.e., that our needs are “satisfied” in the face of a wide range of possible futures, even if not optimally for even one of those possible futures.

However, there appear to be some barriers to widespread adoption of RDM for climate modeling.

1. We don't know what robust really means, despite serious work on the subject (Jen, 2003). Is robustness simply "good enough" performance against a wide range of inputs, or is it more, such as "ductile" behavior as the inputs approach extreme values? If we accept that ductility is desirable, how do we quantify it?
2. We don't really know how to numerically judge "system performance" for a single scenario, let alone millions of scenarios, so it's difficult to have the computer pick the "limiting" scenarios. This problem is not entirely unique to RDM, since virtually any kind of computer optimization, such as genetic algorithm optimization, requires some way to quantify performance. Optimizing toward a robust solution rather than a single-scenario optimal solution makes the quantification process more difficult, given our inability to precisely define and measure robustness as mentioned above, and hence our inability to quantify appropriate tradeoffs associated with competing solutions.
3. We don't have a straightforward way of gauging the probability of a given scenario or even quantifying the *relative* probabilities of two different scenarios with any confidence. Put another way, constructing a valid sample space, i.e., a sample space within which all selections are equally likely, is a formidable challenge; without such a hypercube, any sort of "Monte Carlo" analysis may be extremely misleading. This problem impacts Monte Carlo analysis in a variety of disciplines, even if not always addressed. In the field of climate change, we lack knowledge about the probability distributions of the various unknowns and their correlations. Given the non-linear nature of climate modeling, it's not clear that various simplifying assumptions are appropriate.

These problems are not unknown among practitioners, but their general solution remains a challenge. Nonetheless, the concept of seeking a robust solution, one that will perform reasonably well even in the face of huge uncertainty, has huge allure. Further developments in practical applications of RDM for climate modeling of water supplies will be awaited eagerly.

SUMMARY

Scenario analysis is the future for climate change planning, particularly for larger regions. However, at the present time, its full value is difficult to capture. Obvious barriers include epistemic uncertainties (i.e., scarce or sparse data), poor and non-existent regional climate change models, and practical constraints on resources available for modeling. Even setting all of those barriers aside, other prerequisites remain unfulfilled, including a straightforward metric for system performance, a way to generate a valid sample space, and agreement on what robustness means in a quantitative sense.

In light of the current problems with scenario modeling, EBMUD has opted to use sensitivity analysis. Recognizing the limits of that method, EBMUD has further built flexibility into its overall water supply management by adopting a portfolio approach for water supply, to not only diversify water supply, but be able to adjust in future years if climate change or other factors require it.

Climate change adaptation remains an exciting area literally full of unknowns.

REFERENCES

- Bates, B.C., Z.W. Kundzewicz, S. Wu and J.P. Palutikof, Eds., 2008: Climate Change and Water. Technical Paper of the Intergovernmental Panel on Climate Change, IPCC Secretariat, Geneva, 210 pp. at <http://www.ipcc.ch/pdf/technical-papers/climate-change-water-en.pdf>
- Groves, David, *New Methods for Identifying Robust Long-Term Water Resources Management Strategies for California*, 2005, available at http://www.rand.org/pubs/rgs_dissertations/RGSD196/
- Jen, Erica, *Stable or Robust? What's the Difference?*, 2003 available at <http://www.santafe.edu/media/workingpapers/02-12-069.pdf>

Improvements in Hurricane Surge Response Functions: Incorporating the Effects of Forward Speed, Approach Angle and Sea Level Rise

I. E. Udoh¹ and J. L. Irish²

¹*Coastal and Ocean Engineering Division,
Zachry Department of Civil Engineering, Texas A&M University, 3136 TAMU
College Station, TX 77843
E-mail: uniport2texas@tamu.edu
Phone: 979-402-2836*

²*Coastal and Ocean Engineering Division
Zachry Department of Civil Engineering, Texas A&M University, 3136 TAMU
College Station, TX 77843
E-mail: jirish@civil.tamu.edu
Phone: 979-845-4586*

ABSTRACT

Applying surge response functions (SRFs) in the estimation of peak hurricane surge is valuable to coastal management and safe-evacuation planning. These SRFs make use of the meteorological characteristics for expected storms as input, and were developed by Irish et al. (2009) using generalized dimensionless scaling laws and optimally selected sets of hydrodynamic hurricane simulations for the open coast and within more complex regions like coastal bays. With improvements to the existing form of the SRFs, reliable extreme-value hurricane flooding estimates can be obtained. Hurricane forward speed and approach angle are important meteorological parameters that can induce variations in surge estimates. Recent studies suggest that in the future sea level rise (SLR) may accelerate and major hurricanes may intensify. Here we present a methodology applied to modify the scaling laws to incorporate the effects of forward speed; we also introduce considerations being made towards developing scaling laws for approach angle and sea level rise effects.

Keywords: Surge Response Functions (SRFs), Forward Speed, Approach Angle, Sea Level Rise (SLR)

1 INTRODUCTION

Damage causable by hurricanes could be tremendous. Many efforts have been made by coastal engineering researchers to improve the tools used in hurricane surge estimations, flood prevention/control and coastal planning. Being able to accurately estimate surge for expected storms is not only important in the event of an expected hurricane, but provides an increased level of confidence that the methodologies used

in obtaining such estimates may be applied in design of flood prevention/control structures toward achieving the same ultimate goal of limiting the damage to lives, property and the environment as much as possible. Surge Response Functions (SRFs) are one approach which may be applied in the determination of hurricane surge, with an acceptable level of accuracy.

Considering that the scaling laws used in developing SRFs comprise of meteorological characteristics which control the behavior of hurricanes, it is pertinent that as many of these parameters as possible be accounted for in developing representative functions for surge estimation. The most important storm meteorological parameters include the central pressure (c_p), storm size (R_p), propagation or forward speed (V_f), approach angle (θ) and the steepness of the radial wind velocity distribution, typically represented by the Holland B (Holland, 1980) parameter. For an estimation tool to be considered fully robust (in addition to acceptable accuracy), the effects of these important parameters, in addition to spatial parameters (like the continental shelf width) which directly influence hurricane surge generation, should be explicitly accounted for in its skill. Our objective therefore is to incorporate the influences V_f and θ into the existing form of the SRFs, and to account for the effects of climate change through the inclusion of Sea Level Rise (SLR) in the SRFs.

2 LITERATURE REVIEW

2.1 Effects of Forward Speed, Approach Angle and Sea Level Rise

The influence of varying forward speeds and approach angles on peak surge estimates have been described in a number of works such as Resio et al (2009) to be small relative to those of c_p and R_p , but if ignored these effects though small may affect the accuracy of SRF estimates depending on the shoreline location and related contributing factors. Irish et al (2008) found that varying forward speeds between 2.6m/s and 10.2m/s could increase peak surges up to about 15% to 20% depending on the bottom slope. They also found significant variations among peak surges produced by storms with more oblique angles than storms with angles perpendicular to the shoreline, while holding forward speed constant. Rego and Li (2009) found significant variations in peak surge magnitudes and flood volumes while varying forward speeds in their numerical simulations. U.S. Army Corps (2007) observed variations in peak surge while simulating shore-normal, clockwise-rotated and counter-clockwise rotated storms propagating across a straight coast.

Estimates of SLR reported in the IPCC report (2009) suggest an increasing trend due to melting ice resulting from observed increasing average global temperatures. For some areas, these SLR increases may be a lot more significant than at others due to variations in continental shelf slopes and local sea surface temperatures. Ignoring these increasing trends may lead to under-estimation of total water levels for an

expected storm; thus we consider it more appropriate to include SLR effects into the SRFs in a way that accurately represents its contribution to peak surge.

2.2 Previous Works on Surge Response Functions in the Open Coast

Prior to the current research discussed in this work, the SRFs developed by Irish et al (2009) for the Texas coast were modified by Song (2009, in preparation) to include the effects of storm size and continental shelf width. The dimensionless SRF parameters developed by Irish et al. (2009) are expressed as:

$$x'_1 = \frac{x - x_o}{R_p} - \lambda - F(1 - R')H(1 - R') \tag{1a}$$

$$\zeta'_1 = \frac{\gamma \zeta}{\Delta p} + m_x \Delta p \tag{1b}$$

where x and x_o are distance to the coastal location of interest and the hurricane landfall position along the shoreline. The parameter λ is a constant which describes a linear correlation between R_p and the alongshore distance between the storm eye at landfall (x_{eye}) and the location of peak surge ($x_{\zeta_{peak}}$) as in equation 2, and Δp is the central pressure deficit.

$$x_{\zeta_{peak}} - x_{eye} \cong \lambda R_p \tag{2}$$

In equation (1a), the third term was developed to modify the effects of the first two terms while correcting secondary influences due to relatively small storms that make landfall close to the location of interest. Irish et al classify these small storms, for the Texas coast, as storms with R_p less than a threshold value, $R_{thresh}=25$ km. They define the kernel in the third term in equation 1a, $F(1-R')$ as:

$$F(1 - R') = \begin{cases} a_1(1 - R') + b_1 & (\lambda \leq x' \leq 0) \\ a_2(1 - R') + b_2 & (0 \leq x' \leq \lambda) \\ 0 \rightarrow (\lambda \leq |x'|) \end{cases} \tag{3}$$

and $H(1-R')$ is a Heaviside function defined as:

$$H(1 - R') = \begin{cases} 0 \rightarrow (R' \geq 0) \\ 1 \rightarrow (otherwise) \end{cases} \tag{4}$$

where R' is the dimensionless hurricane size defined as $R' = \left(\frac{R_p}{R_{thresh}} \right)$

The dimensionless surge parameter (ζ'_1) expressed in equation 1b is obtained by normalizing peak surge results from simulated storms using hurricane central pressure deficit. Its first term accounts for the momentum transfer due to surface wind stress, while

the second term accounts for additional wind-drag effects. The coefficient m_x is defined as a site-dependent coefficient, determined by linear regression. Song's (2009, in preparation) work modified equation (1b) to the form:

$$\zeta'_2 = \frac{\zeta_x \gamma_w}{\Delta p} - m_R(x) \chi(L_{30}) \psi_x \left\{ \frac{R_p}{L_{30}} \right\} + m_x \frac{\Delta p}{\gamma_w} \quad (5)$$

The coefficient $m_R(x)$ is a location-dependent constant that varies along the Texas coast.

3 NUMERICAL SIMULATIONS – Model and Scenarios

3.1 Numerical Model - ADCIRC

Our numerical simulations are performed using the 2-dimensional depth-integrated (DDI) version of the high resolution finite element model, ADCIRC (Luettich and Westerink, 2006). The domain of the finite element grid used in ADCIRC in this research spans the Gulf of Mexico, Atlantic Ocean and Caribbean Sea. The model solves the generalized continuity and momentum equations for water elevations and currents, using meteorological parameters as input. The resolution of the numerical grid along the Texas coast is very high (on the order of 50m), allowing the model to resolve output with high accuracy. The ADCIRC grid is shown on figure 1.

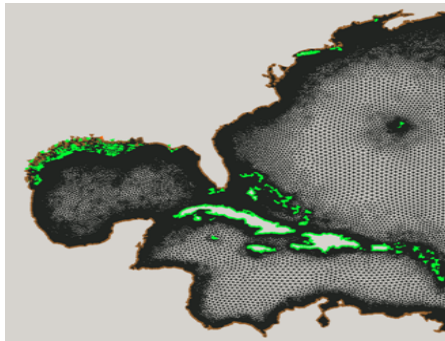


Figure 1: ADCIRC grid

3.2 Hurricane Scenarios Simulated

In selecting the set of storms for numerical simulations towards assessing the effects of forward speed and approach angle, we strived to effectively cover a realistic range of values for meteorological parameters while keeping the number of simulations required as low as possible. Simulations for the forward speed effect covered slow, medium and fast-moving storms combined with two values of central pressures, while holding the hurricane size and the Holland B parameter constant at 32.780km and

1.27 respectively. Tables 1 and 2 show examples of the scenarios simulated on one hurricane track for the V_f effect, and at each landfall location for the θ effect. For the V_f effect, least 6 simulations per track are performed over 16 tracks covering the Texas coast while at least 3 simulations per landfall location are performed for the θ effect, as shown in figure 2.

Table 1: Typical storm scenarios for the V_f effect

Storm ID	Yeye (deg)	Xeye (deg)	V_f (m/s)	C_p (mb)
1	24.760	-95.897	2.058	900
2	24.760	-95.897	5.659	900
3	24.760	-95.897	8.746	900
4	24.760	-95.897	3.087	960
5	24.760	-95.897	6.688	960
6	24.760	-95.897	10.289	960

Table 2: Typical storm scenarios for the θ effect

Storm ID	Yeye	Xeye	Angle	V_f	C_p
1	25.941	-95.460	15 > SN	11	930
2	25.941	-95.460	30 > SH	11	930
3	25.941	-95.460	15 < SH	11	930
4	25.941	-95.460	SN	11	930

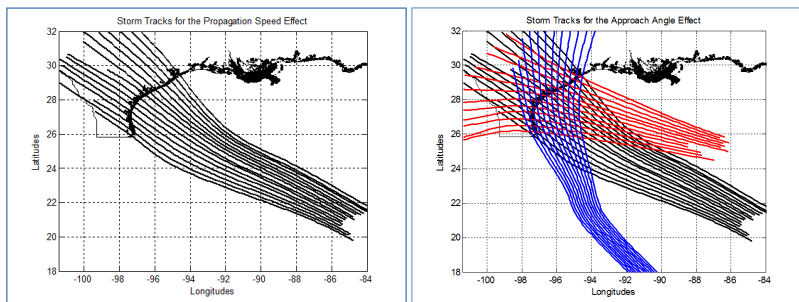


Figure 2: Simulation Tracks for the V_f (left) and θ (right) effects

4 Developing Scaling Laws for V_f and θ

4.1 Forward Speed in SRFs – Scaling Laws (in development)

After preliminary analyses of results from V_f simulations we found that a major influence on peak surge, in relation to the variations of forward speeds, is the amount of time during which the storm propagates over the continental shelf, considering some reference depth such as L_{30} defined in Song (2009, in preparation). We

therefore hypothesize that the non-dimensional peak surge is a function of a non-dimensional time-dependent parameter ψ_t , defined in equation 6.

$$\psi_t = f\left(\frac{L_{30}}{V_f}, \frac{L_{30}^*}{V_f^*}\right) \quad (6)$$

where L_{30} is the continental shelf width at the 30m depth contour, while L^* and V_f^* are characteristic shelf width and representative *medium* forward speed respectively, for a given storm track. The form of the SRFs which includes ψ_t is denoted, ζ'_3 .

4.2 Considerations for Approach angle and SRL

Based on preliminary simulations for approach angle simulations, we expect that the shoreline orientation relative to approach angle will influence peak surge significantly, hence will contribute to the form of the SRFs. As a first approach to incorporating a non-dimensional approach angle parameter into the non-dimensional SRF form, we are considering a formulation of the form shown in equation 7.

$$\psi_\phi = f(\theta, \phi, \mu) \quad (7)$$

where:

ϕ is the shoreline orientation and μ is a location-dependent coefficient incorporating any other contributing influences. We also propose to incorporate estimates of SLR normalized by water depth, h_0 or a more appropriate characteristic length scale, so that the non-dimensional SLR parameter is:

$$\psi_{SLR} = f(SLR, h_0) \quad (8)$$

5 Preliminary Results and Conclusions

For an arbitrary station on the wide shelf area of the Texas coast, we show the performance of the ψ_t formulation. In figure 3, all circular red dots correspond to V_f surge data points, while all other marker shapes and colors correspond to previous simulations by Irish et al (2008) and Song (2009, in preparation). The distribution of the red dots tends to collapse fairly well on pre-existing data, suggesting significant potential for this formulation to contribute to accurate SRF predictions. Work is ongoing to improve on parts of this distribution with high scatter, and to incorporate and analyze θ and SLR data with the proposed formulations.

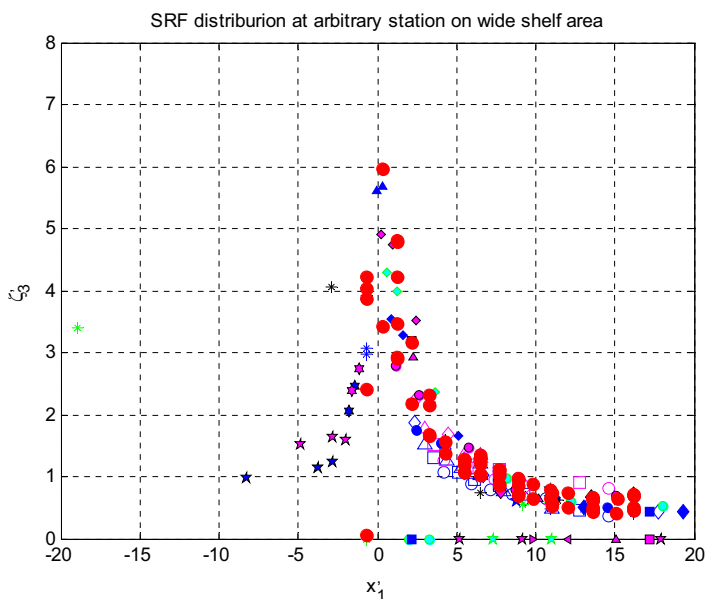


Figure 3: SRF plot for an arbitrary station on wide continental shelf area

List of References

1. Irish, J. L., Resio, D. T. (2008): A hydrodynamics-based Surge Scale for Hurricanes, *Ocean Engineering* 37.
2. IPCC Report, AR4 (2007): Summary for Policy Makers, Page 7.
3. Luetlich, R., Westerink, J. (2006): Formulation and Numerical Implementation of the 2D/3D ADCIRC Finite Element Model Version 44.XX.
4. Rego, J. L., Li, C. (2009): On the Importance of the Forward Speed of Hurricanes in Storm Surge Forecasting – A numerical study, *Geophysical Research Letters*, 36, L07609.
5. Resio, D. T., Irish, J. L., Cialone, M. (2009): A Surge Response Function Approach to Coastal Hazard Assessment, Part 1: Basic Concepts.
6. U.S. Army Corps of Engineers IPET Report (2007): Estimating Hurricane Inundation Probabilities.
7. Song, Y. K., Irish, J. L., Chang, K. (2009, in preparation): A Surge Response Function Approach to Coastal Hazard Assessment, Part 3: Improvements for wide extent of the Texas coast.

A Comparison of Top-Down Statistical Models With Bottom-Up Methods for Power System Reliability Estimation in High Wind Events

Roshanak Nateghi, Seth D. Guikema

Department of Geography and Environmental Engineering,
Johns Hopkins University, Baltimore, MD, 21218.

December 15, 2010

Abstract

The North American electric power grid is considered to be the largest and most complex technical system in the world. Reliability of this heterogeneous and highly interconnected systems is paramount since our national security, digital economy, and transportation and water systems require robust operation of the electric power system. The focus of this paper is on comparing top-down statistical approaches with bottom-up engineering models that are used in estimating the reliability of power systems during hurricanes and high wind events. It then gives a synthesized overview of the advantages and disadvantages of each approach and highlights areas in which additional research is needed.

1 Introduction

Major power outages can affect millions of customers and businesses and lead to catastrophic social and economic impacts. For example the cost incurred by a large utility affected by storms is estimated to range from \$100,000 to \$1,00000 per hour (Zhou et al. 2006). Power outages can occur due to a variety of reasons such as erroneous planning and operation, equipment failure, non-optimal load conditions and severe weather (Cheng et al. 2009). The restoration of interrupted power due to transmission equipment failure can typically be done within a day, even during the events where a large geographic area is impacted. However, restoration efforts in the cases of outages caused by severe weather conditions and earthquakes take much longer since there are significant, wide-spread damages throughout the power system infrastructure of an area. For example, it was estimated that about 1.3 million customers of one of the largest utilities in the central Gulf Coast Region in the U.S. lost power after the landfall of hurricane Katrina in 2005 and the outage lasted for up to about 12 days in some areas. Because of the high costs associated with failures and the dependence of other critical infrastructure systems on electric power systems, the availability of accurate, practical methods for assessing and managing the risk of failure of these systems during hurricanes and other high wind events is critical. This paper reviews the two basic classes of

approaches: top-down methods and bottom-up methods. Top-down methods use characteristics of the overall system, the hazard, and the area to estimate failure risk. Bottom-up methods break the system down into its constituent parts, estimate the failure of these components, and then roll this back up to overall system failure risk. Each has strengths and weaknesses.

Power systems are comprised of three major subsystems, namely, generation, transmission and distribution. The susceptibility of these subsystems to natural hazards vary significantly. For instance, generation plants in the U.S. are generally designed to withstand high wind loads and flood hazards. The transmission subsystems are designed with large tree setbacks and can withstand many high-wind events. They typically have sufficient redundancy in the system to ensure reduced frequency of power interruptions except in the most extreme high wind events. The subsystem that is most vulnerable to wind hazards is the distribution section of the system. The elements of the distribution system are not designed with as high of standard as the elements of the generation and transmission systems, and the tree set back distances are lower. Consequently, this paper focuses on the reliability models of power distribution systems affected by hurricanes and other high wind events.

A wide range of methods have been proposed in the literature for modeling power system reliability during hurricanes and other high-wind events. Before outlining the major modeling approaches, it is worth introducing the more widely used reliability indices in power systems. The two common types of reliability indices that are frequently used are customer load point indices and system indices. The customer load point indices are a measure of the expected number of outages for individual customers. The most common systems indices are the System Average Interruption Duration Index (SAIDI) (Eq.1) and the System Average Interruption Frequency Index (SAIFI) (Eq.2). These indices can be estimated using historical data or predicted through stochastic methods (Balijepalli et al. 2004).

$$SAIDI = \frac{\sum(\text{number of hours of customers out for each power interruption})}{\text{total number of customers in the service area}} \quad (1)$$

$$SAIFI = \frac{\sum(\text{number of customers out for each power interruption})}{\text{total number of customers in the service area}} \quad (2)$$

Sometimes a third index, CAIDI, is used which is the quotient of SAIDI or SAIFI. These indices, however, should be interpreted with caution as the definition of outage varies across utilities. Also the number of customers used in the formula could be misleading since a business that serves several customers could be counted as one customer. Moreover, the indices do not incorporate temporal or spatial variance of the outage (Reed et al. 2007).

2 Bottom-up Engineering Approaches

The first of the two major types of methods that have been proposed for modeling power distribution system reliability during hurricanes and other high-wind events are bottom-up engineering methods. As outlined above, these methods decompose the system into its constituent components, estimate the reliability of each of these components, and then combine these component-level reliability estimates into an overall estimate of the system function or reliability.

2.1 Fragility-based Models

The fragility curves represent the probability of a single component failure as a function of the adverse event parameter such as wind speed. For example, Reed et al. (2007) used the following relationship to estimate fragility of an urban power system during four storms.

$$\text{Fragility} = p(\text{damage} | (\text{gust wind speed})^2) = \frac{\text{damaged feeder length}}{\text{total length of feeders}} \quad (3)$$

The reason for using the feeders' length rather than the number of feeders in Eqn.3 is due to the fact that the feeders are not equivalent in their length, or the number of customers that they serve. So their exposed length is a better measure of the structural damage. Simulations are used to estimate the probability density function of component failures as a function of the relevant storm parameter by incorporating estimates of the demand parameter and component failure rates. Storms typically cause simultaneous failure of the system components. In order to implement simultaneous fragility analysis for several components, it is necessary to assume conditional independence given the demand parameter value. However, the assumption of conditional independence is not necessarily valid during a hurricane, hence the results should be interpreted with caution. The number of customers can then be predicted through coupling fragility models with network topological data based on connectivity of the customers to the grid. Fragility curves usually do not incorporate a wide range of covariates that could help explain the spatial variance of outages or temporal variance of restoration efforts (such as the number of crews available that has an impact on restoration times). Their accuracy for making future predictions has also not been widely tested. The analysis is commonly used to estimate the number of outages, and have been further extended to also model the number of customers without power (restoration curves).

Han et al. (2008) developed an improved fragility curve using a Bayesian approach to combine reliability models and failure data. Deunas-Osorio et al. (2009) advanced this combined modeling method even further by including a wider range of failure types that are not usually incorporated in fragility models.

2.2 Non-Fragility Modeling Approaches

Discrete transition Markov process is another method that could be used for reliability assessments. This method models the functionality of each individual lifeline and their combination as a system post-disaster. In this approach, each subsystem's state at each step of the restoration process is assumed to be random. It is also assumed that the probability of the next step is only affected by that of the previous step, and independent from all the other stages of the process. The transition probability matrix is dependant on the level of restoration resources available to each of the subsystems of the lifeline. Interactions can be incorporated into the model by defining the transition probability matrix such that the probabilities are a function of both the available resources and the states of the other subsystems (Zhang et al. 1992). While this approach can explicitly account for uncertainties, it requires accurate estimates of model parameters and probabilities. The modeling is thus complicated by the great level of detailed information needed to define the transition probability matrices.

Another structurally similar procedure is discrete event simulation approach since it is also simulation-based representation of the restoration process. However, discrete event simulation

models each repair crew and each significant element of the system, (e.g. transformers) explicitly. The model is data-intensive and requires detailed information about the restoration process of a specific utility (Cagnan et al. 2006). Another approach is deterministic resource constraint method. In this method the actual progress of the restoration procedure is modeled in a simplified manner, through a set of equations that are functions of both time and space. The constraints are incorporated into the model by specifying the number of repairs that can be implemented by the available crew in any given time period. The repair rates are typically estimated using historic data or expert opinion. Optimization methods are implemented to minimize the average outage restoration time, using decision variables such as the number of crews available, and constraints such as budget and system topology. Sensitivity analysis is then carried out to measure the impact of different decision variables that are input to the model on restoration times. This approach assumes that the restoration effort is only limited to the repair phase and ignores the inspection phase and damage assessment stage. Moreover, as implied by its name, deterministic resource constraint method ignores the uncertainties associated with expected restoration times.

In the network approach, the power system is modeled as a series of supply and demand nodes interconnected through either functional or non-functional links. Here, recovery is defined to be customers being connected to the supply node. Graph theory and optimization methods are combined to achieve plans that yield minimized mean restoration times. The advantage of this approach is integrating spatial and temporal variations of restoration (Nojima and Kameda 1992). Contrary to deterministic resource constraint methods and Markov processes that primarily depict the restoration process, network models are typically developed to obtain optimal restoration strategies.

3 Top-down Statistical Methods

The second group of models proposed in the literature for power system reliability estimation during severe weather is top-down models. These models utilize characteristics of the whole system, the geographic area, and the hazard for model development.

3.1 Empirical curve fitting approaches

A restoration curve shows the percentage of customers out in the service area whose power has been restored over time, or the percentage of demand met as a function of time since the occurrence of the event. The data used for plotting the restoration curves is either derived from historical data, or elicited from experts through iterative questionnaire approach. In this method, the restoration curves are either fitted to the plotted data or a distribution is assumed for them and the observed data is subsequently used to estimate the parameters of the distribution. This approach does not model the restoration process explicitly. Moreover, the uncertainties involved, and decision variables (such as the number of crews available) are not directly incorporated into the models. Only one restoration curve is typically obtained at a system-wide level (Cagnan and Davidson 2004).

3.2 Statistical Models

Multivariate regression based statistical methods are top-down models that use a wide range of input covariates such as characteristics of the power system and the service area, together with the historical outage data and storm characteristics to make future predictions about the number of customers without power, number and duration of outages and numbers of damaged poles and transformers.

From what we are aware of, Liu et al. (2005) was the first paper that used a statistical model to provide predictions for location and number of outages during a hurricane at a detailed geographic scale; with outages being defined as non-transitory activation of a protective device. They used Negative Binomial Generalized Linear Model (NB GLM) which is a type of count data regression model. NB GLM is employed to estimate the number of outages in the service area at the grid cell level. The data that went into their model consist of the number of transformers, types of land cover, types of trees, hurricane wind speed, and soil characteristics in each grid cell. They mainly focused on model fit and did not examine predictive accuracy. The major limitation of their model is that it includes hurricane and company indicator variables that makes the use of the model for future scenarios problematic. Liu et al. (2008) further improved their previous models by using a Generalized Linear Mixed Model (GLMM) to incorporate spatial variations. However, the model results indicated that adding spatial correlation did not significantly improve their model's fit.

Han et al. (2009) built from Liu et al.'s work to remove the indicator variables by using a more extensive set of input covariates that could be measured prior to a hurricane making landfall. The additional data incorporated into their (NB GLM) framework included the time between hurricanes, the central pressure difference of the storm and a wider range of geographic and climatic variables. The goodness of fit they achieved was comparable to that of Liu et al.'s. Moreover their predictive accuracy evaluation was found to be promising for the system as a whole, but showed that the model generally tended to overestimate the number of outages in the rural areas and underestimate their number in urban areas. They further improved the model by using a Poisson Generalized Additive Model (GAM) framework and found that the GAM approach greatly improves the predictive accuracy.

Guikema et al. (2010) used statistical methods to model power system damage caused by hurricanes. In their model they defined damage to be the number of poles to be replaced. Their predictive models included a combination of statistical and data mining techniques. They compared the predictive accuracy of seven approaches, including Bayesian Additive Regression Trees (BART), Classification and Regression Trees (CART), Negative Binomial Generalized Linear Models (GLM), and Poisson Generalized Additive Models (GAM). The hold-out validation tests indicated that it is more challenging to predict damage than the number of outages due to the input data being less complete.

Liu et al. (2007) implemented survival analysis techniques to model power outage restoration times during hurricanes and ice-storms. They used the two methods of Accelerated Failure Time models (AFT) and Cox Proportional Hazard models (Cox PH), and recommended the implementation of the AFT model, since its output was substantially easier to interpret. They did not implement hold-out validation testing or report the out-of-sample predictive accuracy of their models. Nateghi et al. (2010) compared a range of survival analysis and data mining techniques to model power outage duration induced by hurricane landfalls, using hold-out validation testing to

compare the actual predictive accuracy of the methods. The survival methods included AFT and COX PH and the data mining techniques included BART, CART and MARS. They found that Bayesian Additive Regression Trees can predict power outage durations most accurately.

4 Discussion

Electric power disruption are costly to the society. Sustained power outages have large impacts on other lifelines, and they have severe societal and economical consequences. Ensuring the reliability of power systems and reduced restoration times after failures are therefore critical. This paper summarizes the key approaches proposed in the literature to model the reliability of power systems in areas prone to hurricanes and other high-wind events. The main approaches are broadly categorized into bottom-up engineering models (both deterministic and probabilistic), and top-down statistical models. There are advantages and disadvantages associated with both approaches.

Statistical analyses include both regression-based parametric models and semi-parametric and non-parametric data mining techniques. These methods allow for incorporating a wide set of covariates that could be measured before the hazard impacts the system. The input variables could help explain the variance in outage locations and durations with reasonable predictive accuracy. Statistical models are particularly useful when there is extensive hard data available about the performance of the system during past adverse events. However, it should be noted that the quality of the models' outputs are critically dependent on the size, quality and suitability of the input data (Guikema et al. 2009). If the right kind of data is not used, and the past data incorporated in the model is not representative of the future performance of the system under study, the accuracy of the results will be questionable. In that case the model results should be treated with caution. Moreover, there are usually a number of simplifying assumptions made prior to using most statistical models (such as normality and independence) that need to be justified before interpreting the model results.

Model validation is also critical for top-down models because, in the presence of extensive data, and especially in the case of using more flexible non-parametric approaches, there is always the risk of over-fitting the data. Over-fitted models can explain the past patterns of the system well, but have little predictive value for future events. Random hold-out cross validation tests should be performed to examine the out-of-sample predictive accuracy of the models prior to using them for future forecasts.

If top-down models are developed with input variables that are not specific to a utility company or a particular hazard, they can be reused for various systems and future events to yield results with reasonable predictive accuracy. The computational burden of the statistical analysis depends on the nature of the techniques implemented (model efficiency), the computational resources available and volume of the input data used. The computational times are usually reasonable which is a great advantage for utility companies. Reasonable model run times facilitate implementing damage estimates rapidly prior to the adverse event taking place.

Bottom-up models (such as fragility analysis and deterministic and probabilistic simulations) can include more information about the topology and structure of the network than the statistical methods. However, since the components of the system are modelled individually, the computational burdens of the engineering models are generally far greater than that of the statistical

techniques. If the models are further extended to include the network information and dynamic power flow simulations, the computational times will increase to the point of being prohibitive for rapid, pre-event reliability estimation.

Bottom-up models are particularly useful when there is not a lot of hard data available at the system level, and expert knowledge is the best available source of information. This data is typically more appropriately used at the detailed component level and then rolled up to system-level estimates through an appropriate model. The models can incorporate the engineering behaviour of the system through the use of detailed engineering performance models, but this results in the models becoming specific to that particular system and of little use for making pre-storm predictions for a different system. Moreover, while the fragility models yield great insights into the behaviour of the impacted system, their predictive accuracy has not been widely validated for hurricanes and other high-wind events.

In summary, top-down approaches allow for incorporating a wide range of relevant variables that could be measured prior to the occurrence of the undesirable event. Their computational burden is reasonable and their accuracy is highly dependent on the quality and representativeness of their input data and the suitability of the models used. The bottom-up approaches can include more detailed information about the topology and structure of the system, but they are computationally intensive and their predictive accuracy has not been widely examined. A combination of both approaches can yield great insights into power system behaviour after disasters and also reasonable predictions of power system reliability measures (e.g. Winkler et al. 2009). There is room for future research to include more topological information of the system in statistical models as they do not typically include such information. Also additional research is needed to couple the engineering approaches with power flow models so that the fragility models can be used to estimate outages based on connectivity of customers to the network.

References

- [1] Balijepalli, N., Venkata, S.S., Christie, R.D., " Modeling and Analysis of Distribution and Reliability Indices." October 2004;19(4):1950-1955.
- [2] Cagnan,Z., Davidson, R., and Guikema, S.D., "Post-earthquake restoration planning for Los Angeles electric power," *Earthquake Spectra*,vol.22,no.3,pp.1-20,Aug. 2006.
- [3] Cheng, D., "Integrated System Model Reliability Evaluation and Prediction for Electrical Power Systems :Graph Trace Analysis Based Solutions Integrated System Model Reliability Evaluation and Prediction for Electrical Power Systems : Graph Trace Analysis Based Solut. Simulation." Doctor of Philosophy Thesis, Virginia, 2009.
- [4] Davidson, R.A., Liu, H., Sarpong, I.K., Sparks, P., and Rosowsky, D.V, "Electric Power Distribution System Performance in Carolina Hurricanes", *Natural Hazards, Review*, Feb 2003.
- [5] Guikema, S.D., S.R. Han, S.M. Quiring. "Pre-Storm Estimation of Hurricane Damage to Electric Power Distribution Systems", submitted to *IEEE Transactions on Reliability*. [under review].

- [6] Guikema, S.D., "Natural Disaster Risk Analysis for Critical Infrastructure Systems: An Approach Based on Statistical Learning Theory." *Reliability Engineering and System Safety*, Vol.94, No.4, pp.855-860,2009.
- [7] Han, S.R., Guikema, S., Quiring, S., Lee, K.H., Davidson, R., and Rosowsky, D., "Estimating the Spatial Distribution of Power Outages during Hurricanes in the Gulf Coast Region." *Reliability Engineering and System Safety*. 2009;94(2):199-210.
- [8] Han, S.R., Guikema, S.D., and Quiring, S.M., "Improving the Predictive Accuracy of Hurricane Power Outage Forecasts using Generalized Additive Models," *Risk Analysis*, Vol.29, No. 10, pp. 1443-1453,2009.
- [9] Han, S.R., "Estimating Hurricane Outage and Damage Risk in Power Distribution Systems." Doctor of Philosophy Thesis, Department of Civil Engineering, Texas A& M University, College Station, TX, 2008..
- [10] Liu, H., Davidson, R.A., Rosowsky, D.V., and J.R. Stedinger. "Negative binomial regression of electric power outages in hurricanes." *Journal of Infrastructure Systems*. 2005;11(4):258-267.
- [11] Liu, H., R.A. Davidson, and T. Apanasovich, "Statistical forecasting of electric power restoration times in hurricanes and ice storms," *IEEE Transactions on Power Systems*, Vol. 22, N o. 4, pp. 2270-2279,2007.
- [12] Liu, H., Davidson, R.A., and Apanasovich, T.V. "Spatial generalized linear mixed models of electric power outages due to hurricanes and ice storms." *Reliability Engineering and System Safety*. 2008;93(6):897-912.
- [13] Nateghi, R., Guikema, S.D. , and Quiring, S.M. "A comparison of methods for predicting hurricane power outage duration," submitted to *IEEE Transactions on Power Systems*, 2009.
- [14] Nojima N., Kameda H., "Optimal strategy by use of tree structure for post-earthquake restoration of lifeline network systems." *Proceedings of the 10th World Conference on Earthquake Engineering*,1992, 5541-5546, Balkema, Rotterdam.
- [15] Nojima, N., Sugito, M., "Empirical estimation of outage and duration of lifeline disruption due to earthquake disaster". In: *Proceedings of the USChinaJapan Workshop on Lifeline Systems*, October 2002.
- [16] Winkler, J., L. Duenas-Orsorio, Stein, R., and Subramanian, D., "Performance assessment of topologically diverse power systems subjected to hurricane events," *Reliability Engineering and System Safety*,2009.
- [17] Reed, D.A., *Electric utility distribution analysis for extreme winds*. Communication. 2008;96:123-140.
- [18] Zhang, R.H."Lifeline Interaction and Post Earthquake Urban System Reconstruction." *Proceedings of 10th World Conference on Earthquake Engineering*,(1992),5475-5480, Balkema, Rotterdam.

Classification of Current Building Stock for Hurricane Risk Analysis

Boback Bob Torkian ¹, Jean-Paul Pinelli ^{*2}, Kurt Gurley ³

¹Graduate Student, Florida Institute of Technology, Melbourne, Florida, USA,
btorkian@fit.edu

^{2*}Professor of Civil Engineering, Florida Institute of Technology, Melbourne, Florida,
USA, *pinelli@fit.edu*

³Associate Professor of Civil Engineering, University of Florida, Gainesville, Florida,
USA, *kgurl@ce.ufl.edu*

ABSTRACT

This article presents a survey which was carried out to identify the most prevalent residential building types, their characteristics and their distribution in the state of Florida. The databases provided by county property tax appraisers were used for the survey. Detailed statistics on different building components are presented along with an analysis of their correlation to the year built of the structures. The results of the survey provided a basis for the generation of different vulnerability matrices in different regions of Florida. The survey, the resulting statistical analysis, and the weighting process of the vulnerability matrices are discussed.

INTRODUCTION

Natural hazards may not be avoidable, but natural disasters are (Prevatt-2010). Societal vulnerability and the characteristics of hazard both combine to produce a natural disaster (Kelman-1998). While in Florida the natural hazard is defined by the hurricanes which regularly hit the state because of its vulnerable geographical location, an important component of the societal vulnerability is the building stock subjected to the hurricane winds. Consequently, it is critical to quantify the economic magnitude of the hurricane risk, and to identify what are the most cost effective mitigation solutions to increase the safety of the existing and new building stock and to avoid repeating past errors when rebuilding in disaster areas. Catastrophe models like the Florida Public Hurricane Loss Model (FPHLM) can play a crucial role in this identification process (Pinelli et al., 2008, 2011; Hamid et al. 2010). This paper describes a survey and analysis of the current Florida personal residential building stock with the aim of improving the building models which are at the core of the FPHLM.

PRELIMINARY DATA COLLECTION

The wind vulnerability of the housing stock in Florida cannot be fully understood without a review of its construction characteristics. A series of databases were collected from county property tax appraisers (CPTA) offices from 32 counties, out of 67 counties in Florida. According to the census these 32 counties account for more than 88% of the

Florida population. These databases contain information on thousands of residential buildings in each county. The available building characteristics vary from county to county, and include some combination of the following: exterior wall material, interior wall material, roof shape, roof cover, floor covering, foundation, opening protection, year built, number of stories, area per floor, area per unit and geometry of the building (Zhang-2003). For the purpose of analyzing the data, the state was divided into four main regions including: North, Central, South and Keys. Monroe County is kept as a separate region because of its unique geographical location (island keys prone to hurricanes). Geography and the statistics from the Florida Hurricane Catastrophe Fund (FHCF) provided guidance for defining regions that would have a similar building mix. For example, North Florida has primarily wood frame houses while South Florida has primarily masonry houses. Figure 1 shows the regional classification, with the counties which provided data in each region indicated with a star.

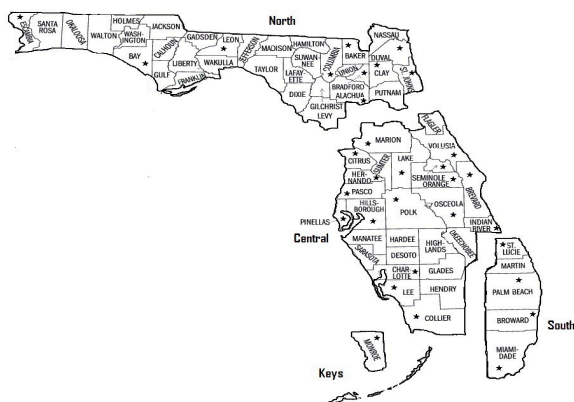


Figure 1: Regional classification-showing counties with data

Because CPTA databases are developed for tax purposes, only a few of them contain all the structural data necessary for modeling. For instance, most databases do not differentiate between gable and hip roof shapes, which makes it difficult to develop statistics on actual roof shape; likewise, data on roof cover or wall type might be missing or incomplete. Consequently, in the counties with missing data, it was extrapolated from average regional statistics. In the case of the Keys region, missing data was extrapolated from the South region.

STATISTICS OF BUILDING COMPONENTS

The key parameters that define the wind vulnerability of residential buildings are exterior wall, roof shape, roof cover, number of stories, foundation, building area and shape, and opening protection, as well as the year built. The attributes for these parameters are listed in Table 1 and Table 2. Statistics on these parameters are presented below.

Table 1: Attributes of the different building components

Exterior Walls	Roof Shape	Roof Cover	Shape of Building
Concrete Blocks	Gable	Shingles	Square
Wood	Hip	Tiles	Rectangle
Metal	Flat	Gravel	L-shape
Glass	Other	Membrane	Irregular
Concrete		Metal	
Other		Wood	
		Concrete	
		Other	

Table 2: Attributes of the different building components (Continued)

Story	Foundation	Building Area(ft ²)	Year Built
One	Pier	Average in County	Pre - 1960
Two	Concrete block	Less than 1000	1960-1970
		1000-1500	1971-1980
	1500-2400	1981-1993	
	Greater than 2400	1994-2001	
	After-2001		

Exterior walls: counties in the south have a higher ratio of concrete block to wood frame walls than central and northern counties. The proportions of concrete block homes in the south, central and north were 86%, 68% and 18% respectively. Figure 2 shows the percentage of concrete block homes in three regions for different eras.

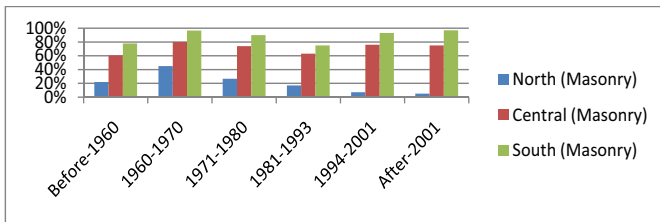


Figure2: Distribution of masonry homes according to year built in the different regions

Roof shape: 93% of buildings have gable or hip roof. Although the aggregated data for roof shape was available in 22 counties, only 5 of these 22 counties differentiated between gable and hip. The data shows that the use of hip roofs increased after 1980, and since 1994 (after hurricane Andrew) the majority of new buildings have hip roofs (Figure 3).

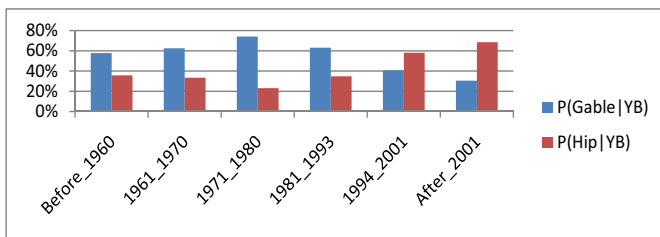


Figure3: Comparison between Gable and Hip roof according to year built in the 5 available counties

Roof cover: Shingle roof cover is by far the dominant roof cover in Florida. Next are tile roofs, which represent 34% of the roof covers in the South. Metal roofs represent a far smaller percentage of roof cover, with the exception of Monroe County where 38% of roofs are metal.

Layout Shape: Only two counties recorded the shape of the buildings. 78% of buildings had a rectangular shape.

Opening protection: Only two counties had records for shutters. In these, 92% of homes did not have any shutters. The South Florida and Florida Building Codes, enacted in 1994 and 2001 require shutters on every building in a high velocity hurricane zone (HVHZ), and windborne debris impact zone (WBDR). This, together with expert opinions, led to the distribution shown in Table 3 for the different wind zones.

Table 3: Modified shutter data for different sub regions

Wind Sub Region	Buildings after 2001		Buildings between 1994-2001		Buildings before 1994	
	With Shutter	Without Shutter	With Shutter	Without Shutter	With Shutter	Without Shutter
High Velocity Hurricane Zone	90%	10%	90%	10%	40%	60%
Wind Borne Debris Region	90%	10%	25%	75%	25%	75%
Inland Region	10%	90%	5%	95%	5%	95%

Number of stories: Single story was by far the dominant height in the 14 counties with information available regarding number of stories (86%).

Building areas: The average of building area and living area were calculated in 15 counties with available values for the building area. Figure 4 shows the evolution in the building area in the South region.

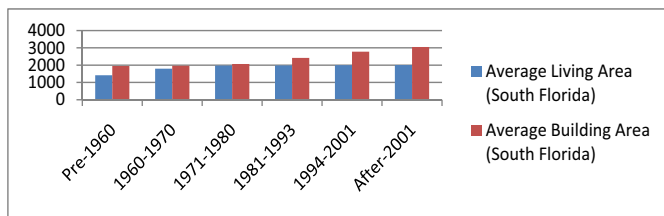


Figure4: Distribution of buildings area in the south region

CONDITIONAL PROBABILITIES

The modelers defined generic structures based on a combination of 5 of the previously mentioned characteristics: number of stories (NS) (either 1 or 2), roof cover (RC) (shingle/tile), roof shape (RS) (either gable or hip), opening protection (OP) (with shutter or without shutter) and exterior wall (EX) (either concrete blocks or timber). The dependencies between these critical building characteristics including year built (YB), and building area (BA) were tested. The analyses showed that all the building characteristics are dependent on the year built, and that, in addition, roof cover is also dependent on the type of exterior wall. No other significant dependencies were identified. The probability of occurrence of each type of home was calculated in each county, within predefined eras, based on the statistics from the survey.

DEFINITION OF VULNERABILITY MATRICES

The vulnerability model uses a component-based Monte Carlo simulation to determine the external damage at various wind speeds for the different building models. The internal damage is then extrapolated from the external damage for each simulation, and the total damage is converted into a damage ratio of damage cost over replacement cost. Once the simulation results have been translated into damage ratios, they are then transformed into vulnerability matrices.

The cells of a vulnerability matrix for a particular structural type represent the probability of a given damage ratio occurring at a given wind speed. The columns of the matrix represent three-second gust wind 10-m wind speeds from 50 mph to 250 mph in 5 mph bands. The rows of the matrix correspond to damage ratios (DR) in 2% increments up to 20%, and then in 4% increments up to 100%. If a damage ratio is $DR = 15.3\%$, it is assigned to the interval $14\% < DR < 16\%$ with a midpoint $DR = 15\%$. After all the simulations have been counted, the total number of instances in each damage interval is divided by the total number of simulations per wind speed to determine the percentage of simulations at any damage state occurring at each speed. These percentages are the conditional probabilities of occurrence of a level of damage, given a certain wind speed. A partial example of a vulnerability matrix is shown in Table 2.

Table 2. Partial example of vulnerability matrix

Damage \ Wind Speed (mph)	47.5 to 52.5	52.5 to 57.5	57.5 to 62.5	62.5 to 67.5	67.5 to 72.5
0% to 2%	1	0.99238	0.91788	0.77312	0.61025
2% to 4%	0	0.00725	0.0806	0.21937	0.36138
4% to 6%	0	0.00037	0.001395	0.007135	0.0235
6% to 8%	0	0	0.000125	0.000375	0.0025
8% to 10%	0	0	0	0	0.000375
10% to 12%	0	0	0	0	0.000375
12% to 14%	0	0	0	0	0.000625
14% to 16%	0	0	0	0	0.0005
16% to 18%	0	0	0	0	0.000125
18% to 20%	0	0	0	0	0.00012
20% to 24%	0	0	0	0	0.00025
24% to 28%	0	0	0	0	0

These matrices, which are at the core of the FPHLM, were calculated for the most common types of single family homes in Florida. These typical buildings are masonry homes or timber box like structures, both with timber truss roofs. Each type of structure is itself modeled with differing strengths as a weak, a medium, and a strong model (Pinelli et al.-2011). Table 5 shows the definition of weak, medium and strong. There were no statistics in the CPTA databases on garage door strength and roof to wall connections type. Instead, these two parameters were assigned depending on the year built to reflect the evolution of the building code and construction practices in each era and sub region. Sub regions which are exposed to higher wind speeds typically develop better, more wind-resistant construction traditions than those struck to lower wind speeds; the concentration of poorly constructed homes in old eras caused older buildings to be more susceptible into hurricane damage.

It is not feasible for the modelers to generate a unique vulnerability matrix for every single home in the state. Instead, 1032 vulnerability matrices were developed for site built homes. The definition of these typical building was a direct result of the survey analyses, as described above. They correspond to different combinations of wall type (frame or masonry), region (North, Central, South), sub-region (high wind velocity zone, wind borne debris region, inland), roof shape (gable vs. hip), roof cover (tile vs. shingle), window protection (shuttered or not shuttered), number of stories (1 or 2), and strength (weak, medium, strong).

Table 5: Basic models – Weak, medium, and strong for one and two story buildings

Model	Garage Door	Sheathing	Roof-Wall connection	Roof shape	Roof Cover	Shutters
Weak	30 psf	6d@12" nails	Toe nails	gable/hip	Unrated Shingle/Tile	shutter/without shutter
modified Weak01	30 psf	8d@6" nails	Toe nails	gable/hip	Rated Shingle/Tile	shutter/without shutter
modified Weak10	30 psf	8d@6" nails	Toe nails	gable/hip	Unrated Shingle/Tile	shutter/without shutter
Medium00	30 psf	8d@12" nails	clips	gable/hip	Unrated Shingle/Tile	shutter/without shutter
modified Medium01	30 psf	8d@6" nails	clips	gable/hip	Rated Shingle/Tile	shutter/without shutter
modified Medium10	30 psf	6d@12" nails	clips	gable/hip	Unrated Shingle/Tile	shutter/without shutter
Strong	52 psf	8d@6" nails	straps	gable/hip	Rated Shingle/Tile	shutter/without shutter

WEIGHTED VULNERABILITY MATRICES

In general, there is little information available in an insurance portfolio file regarding the structural characteristics and the wind resistance of the insured property. Instead, insurance companies rely on the ISO fire resistance classification. Portfolio files have information on ZIP Code and year built. The ISO classification is used to determine if the home is constructed of masonry, timber, or other. The ZIP Code is used to define the region and sub-region. The year the home was built is utilized to assist in defining whether a home should be considered weak, medium or strong. To summarize, region, sub-region, construction type, year built, and by extension strength, are determined, from the insurance files. This leaves the roof shape, roof cover, number of stories, and opening protection options undefined. From the exposure study of the 32 Florida counties, the regional distributions of number of stories, roof shapes, and roof cover by age per region were calculated. For each age group, we define a weighted matrix for each construction type in each region and sub-region. The weighted matrices are the sum of the corresponding vulnerability model matrices weighted on the basis of these statistical distributions.

The year-built or year of last upgrade of a structure in a portfolio might not be available when performing a portfolio analysis to estimate hurricane losses in a certain region. In that case, it becomes necessary to assume a certain distribution of ages in the region, in order to develop an average vulnerability by combining weak, medium, and strong. The tax appraisers' databases include effective year of construction, and thus provide guidance as to how to weigh the combined weak, medium and strong model results, when year-built information is not available in other portfolio files. The results are shown in Figure 5, for the windborne debris zone in Central Florida. The different weighted vulnerability curves are shown for the weak, medium, and strong models, superimposed with the age weighted vulnerability curve.

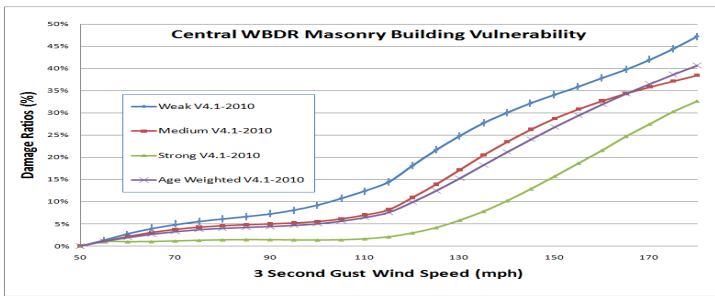


Figure 5. Weighted masonry structure vulnerabilities in the Central wind borne debris region

CONCLUSION

A survey was carried out to evaluate the statistics of current residential buildings in the state of Florida. Key findings of the survey include the following:

- The statistical distributions of key wind vulnerability parameters among the building stock in Florida were quantified both in time and in space. For example: the survey showed the prevalence of masonry homes in South Florida and timber homes in North Florida; it also highlighted the prevalence of gable roofs in older homes and hip roofs in newer homes.
- The dependency between different building parameters was identified and quantified. For example, it was shown that roof shape is heavily dependent on year built, and roof cover on type of exterior wall.
- Typical generic residential models that represent the vast majority of the building stock in Florida were identified. These models were implemented in the Florida Public Hurricane Loss Model.

These results are fundamental to enhance the prediction of hurricane risk in Florida. In particular, based on the results of the survey, it is possible to combine the different models when necessary, to be able to estimate the hurricane risk of insured properties in the absence of any information other than location, age, and type of exterior wall.

A similar study was carried out for commercial residential buildings and is reported elsewhere (Pinelli et al., 2008).

REFERENCES

- Hamid, S., Kibria, B. M. G, Gulati, S., Powell, M., Annane B., Cocke, S., Pinelli, J.-P., Gurley, K., and Chen, S.-C. (2010). "Predicting Losses of Residential Structures in the State of Florida by the Public Hurricane Loss Evaluation Models." *Journal of Statistical Methodology*, pp 552-573.
- Kelman, I., and Karney, B. (1998). "Technology, Volcanoes, and Us". A presentation and abstract at the 23rd Annual Hazards Research and Applications Workshop held in Boulder, Colorado, Natural Hazards Research and Applications Center in Colorado
- Pinelli, J.P., Pita, G. L., Gurley, K., Torkian, B. B., Hamid, S., and Subramanian, C. (2011). "Damage Characterization: Application to Florida Public Hurricane Loss Model," *ASCE Natural Hazard Review*, accepted for publication.
- Pinelli, J.P., Pita, G. L., Subramanian, C., Gurley, K., and Hamid, S. (2008). "Hurricane Vulnerability of Multi-Story Residential Buildings in Florida
- Pinelli, J.-P., Gurley, K., Subramanian, C., Hamid, S., and Pita, G. (2008) "Validation of a probabilistic model for hurricane insurance loss projections in Florida," *Reliability Engineering and System Safety International Journal*, Vol. 93, No 12, pp. 1896-1905
- Prevatt, D. O., Dupigny-Giroux, L. A., and Masters, F. J. (2010). "Engineering Perspective on Reducing Hurricane Damage to Housing in CARICOM Caribbean Islands". *ASCE Natural Hazard Review*.
- Zhang, L. (2003) *Public Hurricane Loss Prediction Model: Exposure and Vulnerability Components*. M.S. Thesis. Civil Engineering Department. Florida Institute of Technology

Probabilistic hurricane surge risk estimation through high-fidelity numerical simulation and response surface approximations

Alexandros A. Taflanidis¹, Andrew B. Kennedy¹, Joannes J. Westerink¹, Jane Smith², Kwok F. Cheung³, Mark Hope¹, Seizo Tanaka¹

¹University of Notre Dame, Department of Civil Engineering and Geological Sciences, Notre Dame, IN, 46556, USA

²Coastal and Hydraulics Laboratory, U.S Army Engineer Research and Development Center, Vicksburg, MS, 39186, USA

³Department of Ocean and Resources Engineering, University of Hawaii at Manoa, Honolulu, Hawaii, 96822, USA

ABSTRACT

An efficient, computational framework is discussed for hurricane risk estimation with emphasis on online applications. Basis of this framework is the characterization of each hurricane scenario through five model parameters: the location and angle of landfall, the central pressure, the forward speed, and the radius of maximum winds. Description of the uncertainty in these parameters, through appropriate probability models, leads then to quantification of hurricane risk as a stochastic integral. For efficiently evaluating this integral, application of response surface methodologies as a surrogate modeling approach is discussed. An illustrative example is presented that considers applications of these tools for hurricane risk estimation for the Oahu Island in Hawaii.

INTRODUCTION

Hurricane surge risk assessment has received a lot of attention the past five years, in response to 2005 and 2008 hurricane seasons. A probabilistic approach, frequently reference as the Joint Probability Method (JPM), has recently emerged as a standard tool for this task (Niedoroda et al. 2008; Irish et al. 2009). This approach relies on a simplified description of hurricane scenarios through a small number of model parameters. Description of the uncertainty in these parameters, through appropriate probability models, leads then to characterization of hurricane risk as a stochastic integral. One of the recent advances in this field has been the development of high-fidelity numerical simulation models for reliable and accurate prediction of surge responses for a specific hurricane event (Resio and Westerink 2008). These models permit a detailed representation of the hydrodynamic processes, albeit at the cost of greatly increased computational effort. This increases significantly the computational cost for estimating hurricane risk, which requires evaluation of the response for a large number of hurricane scenarios. For alleviating this problem an efficient dimensional analysis approach was proposed in (Irish et al. 2009), but the evaluation was restricted to risk calculation for specific locations, rather to an entire

region of interest and the uncertainty only is some of the hurricane model parameters was addressed.

In this work an efficient computational framework is presented for online evaluation of hurricane risk. Based on information from a small number of high-fidelity numerical simulations, a surrogate model is developed for efficient estimation of the surge response for any potential hurricane scenario. During an approaching hurricane event, the uncertainty in the hurricane characteristics is described through probability models provided by the National Weather Service (NWS). The resultant hurricane risk is then estimated at a small computational cost using the already developed surrogate model.

PROBABILISTIC FRAMEWORK

In the proposed framework, each hurricane event is approximately described by only five variables: (i) the location of landfall x_o ; (ii) the angle of impact at landfall θ ; (iii) the central pressure c_p ; (iv) the forward speed during final approach to shore v_f ; and (v) the radius of maximum winds R_m . These variables ultimately constitute the model parameters vector, \mathbf{x} , describing each hurricane scenario. The variability of the hurricane track and characteristics prior to landfall is also important. Directly incorporating, though, this variability in the hurricane description would increase significantly the number of model parameters and so it is avoided here. Instead this variability is approximately addressed by appropriate selection of the hurricane track history prior to landfall, so that important anticipated variations, based on historical data, are efficiently described (Resio et al. 2009).

In this setting, let \mathbf{z} denote the vector of response quantities of interest throughout the entire region of significance. Such response quantities for hurricane risk estimation could include, for example, the (i) the still water level (SWL), defined as the sea level in absence of wind waves, the (ii) wave breakup level (WBL), defined as the sea level including breakup of wind waves on shore, or (iii) the significant wave height H_s along with the corresponding period of wave oscillation T_s . The response vector \mathbf{z} for a specific hurricane scenario, described by the model parameter vector \mathbf{x} , may be accurately estimated by numerical simulation, once an appropriate high fidelity model is established (see discussion later). Since the high-fidelity model requires extensive computational effort for each analysis, a surrogate model is also developed for simplification of the risk evaluation (see discussion later). This surrogate model is based on information provided by a number of pre-computed evaluations of the computationally intensive high-fidelity model, and ultimately establishes an efficient approximation to the entire response vector for each hurricane scenario. The relationship between each component of the actual response z_i and corresponding component of the response that is provided through the surrogate model \hat{z}_i is ultimately expressed as $z_i = \hat{z}_i + \varepsilon_i$ where ε_i is the *total* model prediction error that is established through the various introduced approximations.

Hurricane risk is finally expressed in terms for the response $\hat{\mathbf{z}}$ and the prediction error vector $\boldsymbol{\varepsilon}$. If $p(\mathbf{x})$ is the probability model describing the uncertainty in the hurricane model parameters, then each risk component R_j is expressed by the stochastic integral

$$R_j = \int_X h_j(\mathbf{x})p(\mathbf{x})d\mathbf{x} \quad (1)$$

where X corresponds to the region of possible values for \mathbf{x} and $h_j(\cdot)$ is the risk occurrence measure that ultimately depends on the definition for R_j . Through appropriate selection of $h_j(\cdot)$ all potential hurricane risk quantifications can be addressed through this approach. For example, if R_j corresponds to the expected value for some z_j then $h_j(\mathbf{x}) = \hat{z}_j(\mathbf{x})$. If on the other hand R_j corresponds to the probability that some z_j will exceed some threshold β_j then (Taflanidis and Beck 2008) $h_j(\mathbf{x}) = P_j(\hat{z}_j - \beta_j)$ where $P_j(\cdot)$ corresponds to the cumulative distribution function for the model prediction error e_j . Note that for online risk estimation during an approaching event, the probability model $p(\mathbf{x})$ is ultimately selected through information provided by NWS. Finally the risk integral (1) is estimated by *stochastic simulation*; using N samples of \mathbf{x} simulated from $p(\mathbf{x})$, an estimate for R_j is given by

$$\hat{R}_j = 1/N \sum_{k=1}^N h(\mathbf{x}^k) \quad (2)$$

where vector \mathbf{x}^k denotes the sample of the uncertain parameters used in the k^{th} simulation. Based on the surrogate model this estimation can be efficiently performed and whenever the prediction for $p(\mathbf{x})$ is updated (as the hurricane approaches landfall) the estimate (2) may be also updated.

HIGH FIDELITY MODEL

For a hurricane scenario the surge and wave response is accurately calculated by a combination of the ADCIRC and SWAN numerical models. ADCIRC solves the shallow-water equations for water levels and the momentum equations for currents. The variables are defined on unstructured triangular finite element grids at the vertices (Westerink et al. 2008). Waves are computed using the unstructured version of the SWAN non-phase resolving wind wave model. SWAN solves for wave action density which evolves in time, geographic space and spectral space. Source terms in the governing wave action density equation account for wave growth by wind; action lost due to whitecapping, surf breaking and bottom friction; and action exchanged between spectral components due to nonlinear effects in deep and shallow water. The unstructured grid version of SWAN is based on triangular elements with the action density function being defined at the vertices. Of course, waves and circulation interact despite being well separated in frequency space. SWAN+ADCIRC have been fully integrated into a comprehensive modeling system allowing full interaction between model components. Since the variables for both models are defined at identical locations (i.e. triangle based vertices), there is no interpolation that has to be performed between the two models. Furthermore in the highly efficient parallel implementation of SWAN+ADCIRC, all inter-model communication is intra-core, and while intra-model communications in inter-core, it is predominantly local along the sub-domain edges and only between adjacent sub-domains. This makes the combined code highly scalable and efficient.

Additionally, wave action can increase inundation considerably in the swash zone at the ocean's edge, which is intermittently wet and dry, from wave runup and

drawdown. An approximate approach is adopted here for efficient evaluation of these effects; a large number of one dimensional transects are defined along the perimeter of the region of interest, with each transect extending 1000m inland and up to 2000m offshore. A two dimensional array of initial water levels and wave heights is then defined at the offshore end of each transect, with values based on information about the anticipated wave environment characteristics provided through the initial SWAN+ADCIRC runs. One dimensional Boussinesq model analysis is then performed for all these parameter combinations, yielding a prediction for the wave runup along each transect (Demirbilek et al. 2009). These results are then used through a simple interpolation scheme, to provide an estimate of maximum inundation distance along that transect for any input for wave or water level.

RESPONSE SURFACE METHODOLOGIES

Response surface approaches aim to approximate a complex process, requiring large computational cost for its evaluation, by a simpler mathematical model. This is established by expressing the function corresponding to the initial process $f_j(\mathbf{x}):\mathfrak{R}^{n_s}\rightarrow\mathfrak{R}$, where $\mathbf{x}=[x_1\dots x_{n_s}]\in\mathfrak{R}^{n_s}$ denotes the vector of free variables, through a number of NB prescribed basis functions $b_i(\mathbf{x}):\mathfrak{R}^{n_s}\rightarrow\mathfrak{R}$. The approximation is expressed as a linear combination of the $b_i(\mathbf{x})$ by introduction of coefficients $a_i\{\mathbf{x}\}\in\mathfrak{R}; i=1,\dots,NB$

$$\hat{f}_j(\mathbf{x}) = \sum_{i=1}^{NB} b_i(\mathbf{x})a_i\{\mathbf{x}\} = \mathbf{b}(\mathbf{x})^T \mathbf{a}\{\mathbf{x}\} \quad (3)$$

where $\mathbf{b}(\mathbf{x})$ is the vector of basis functions and $\mathbf{a}\{\mathbf{x}\}$ is the vector containing the coefficients for the basis functions. Different classes of basis functions have been suggested and used in the literature. A common choice is a full second order approximation. The coefficients $\mathbf{a}\{\mathbf{x}\}$ are calculated by initially evaluating $f(\mathbf{x})$ in a set of $NS>NB$ support points $\{\mathbf{x}_I; I=1,\dots,NS\}$, and then by minimizing the mean squared error over these points between $f_j(\mathbf{x})$ and the approximation established through (3). In the Moving Least Squares (MLS) approach the coefficients are dependent on \mathbf{x} , and are selected by minimizing a weighted sum of squared error, with weights that are a function of \mathbf{x} as well

$$J_R\{\mathbf{x}\} = \sum_{I=1}^{NS} w\{\mathbf{x}\} [\hat{f}_j(\mathbf{x}_I) - f_j(\mathbf{x}_I)]^2 = [\mathbf{B}\mathbf{a}\{\mathbf{x}\} - \mathbf{F}_j]^T \mathbf{W}\{\mathbf{x}\} [\mathbf{B}\mathbf{a}\{\mathbf{x}\} - \mathbf{F}_j] \quad (4)$$

where the following quantities are introduced

$$\mathbf{B} = [\mathbf{b}(\mathbf{x}_1) \dots \mathbf{b}(\mathbf{x}_{NS})]^T; \quad \mathbf{F}_j = [f_j(\mathbf{x}_1) \dots f_j(\mathbf{x}_{NS})]^T$$

$$\mathbf{W}\{\mathbf{x}\} = \text{diag} [w(d(\mathbf{x}; \mathbf{x}_1)) \dots w(d(\mathbf{x}; \mathbf{x}_{NS}))]$$

and $w\{d(\mathbf{x}; \mathbf{x}_I)\}$ is a variable weight function with a compact support that depends on some measure of the distance between the interpolation point \mathbf{x} and each of the support points. A typical selection for this distance is

$$d(\mathbf{x}; \mathbf{x}_I) = \sqrt{\sum_{i=1}^{n_s} (\mathbf{x}_i - \mathbf{x}_{i,I})^2} v_i^2 = \sqrt{[\mathbf{v}(\mathbf{x} - \mathbf{x}_I)]^T \mathbf{v}(\mathbf{x} - \mathbf{x}_I)}; \quad \mathbf{v} = \text{diag}(v_1 \dots v_{n_s})$$

with v_i representing the relative weight for each component of x_i . The introduction of the dependence on the distance weights $w\{d\}$ aims at reducing the approximation error at each point by performing a weighted local averaging of the information obtained by the support points that are closer to it. Without these weights, the coefficient vector, \mathbf{a} , would be constant over the whole domain for \mathbf{x} which means that a global approximation would be established (global least squares). The efficiency –i.e. fit to $f(\mathbf{x})$ – of global approximations depends significantly on the selection of the basis functions, which should be chosen to resemble $f(\mathbf{x})$ as closely as possible. Such a selection is not always straightforward. The MLS circumvents such problems by establishing a local approximation for $\mathbf{a}\{\mathbf{x}\}$ around each point in the interpolation domain. This leads to a smaller dependence of the fit on the type of basis functions used. An appropriate support size D should be selected at any point \mathbf{x} so that a sufficient number of neighboring supporting points are included to avoid singularity in the solution for $\mathbf{a}\{\mathbf{x}\}$. This means that D should include at least NB points. Many types of weighting functions have been suggested in the literature. One of the most common is the exponential type of function

$$w\{d\} = [e^{-\left(\frac{d}{cD}\right)^{2k}} - e^{-\left(\frac{1}{c}\right)^{2k}}] / [1 - e^{-\left(\frac{1}{c}\right)^{2k}}] \text{ if } d < D, \quad 0 \text{ else} \quad (5)$$

where c and k are free parameters to be selected for better efficiency. Common values suggested in the literature for these parameters are $c=0.4$, $k=1$.

The minimization of (4) is a standard quadratic optimization problem and yields solution

$$\mathbf{a}\{\mathbf{x}\} = \mathbf{M}^{-1}\{\mathbf{x}\}\mathbf{L}\{\mathbf{x}\}\mathbf{F}_j \text{ where } \mathbf{M} = \mathbf{B}^T\mathbf{W}\{\mathbf{x}\}\mathbf{B} \text{ and } \mathbf{L}\{\mathbf{x}\} = \mathbf{B}^T\mathbf{W}\{\mathbf{x}\}$$

Ultimately D in (5) should be selected so that \mathbf{M} is invertible. Finally from (3)

$$\hat{f}_j(\mathbf{x}) = \mathbf{b}^T(\mathbf{x})\mathbf{M}^{-1}\{\mathbf{x}\}\mathbf{L}\{\mathbf{x}\}\mathbf{F}_j \quad (6)$$

For the hurricane risk estimation this surrogate modeling is implemented for approximation of the response vector $\hat{\mathbf{z}}$, with interpolation points corresponding to the grid of parameter values for which the high fidelity simulations have been performed. The approximation for the entire vector \mathbf{z} is established by approximating each z_j through (6) and is ultimately expressed in a simple mathematical form

$$\hat{\mathbf{z}} = \mathbf{b}^T(\mathbf{x})\mathbf{M}^{-1}\{\mathbf{x}\}\mathbf{L}\{\mathbf{x}\}\mathbf{F} \text{ where } \mathbf{F} = [\mathbf{F}_1 \quad \mathbf{F}_2 \quad \dots \quad \mathbf{F}_{n_z}]$$

This MLS approximation simultaneously provides the *entire* response vector of interest, which is one of its significant advantages over other surrogate models.

APPLICATION TO ONLINE RISK ESTIMATION FOR OAHU

High fidelity model and simulations. The computational domain developed for the high-fidelity simulation of the hurricane response in this study, encompasses a large portion of the northern Pacific Ocean and extends from 0 (equator) to 35 degrees north and from 139 to 169 degrees west. The grid incorporates 1,590,637 nodes and 3,155,738 triangular elements. Minimum grid resolution at the domain edge is 10km, and maximum resolution of 30m is found in complex coastal areas such as bays and

harbors. Bathymetric (Figure 1) and topographic data applied to the grid came from a variety of sources. For the numerical simulation, SWAN applies 10 minute time steps while ADCIRC applies 1 second time steps. A SWAN+ADCIRC simulation runs in 16 wall clock minutes per day of simulation on 1024 cores on Diamond, a 2.8 GHz dual quad core based machine with a 20 Gbit/sec InfiniBand interconnect (<http://www.ercd.hpc.mil/>). This model was validated by simulating tides as well as by hindcasting Hurricane Iniki (1992), comparing to water levels as well as wind wave data.

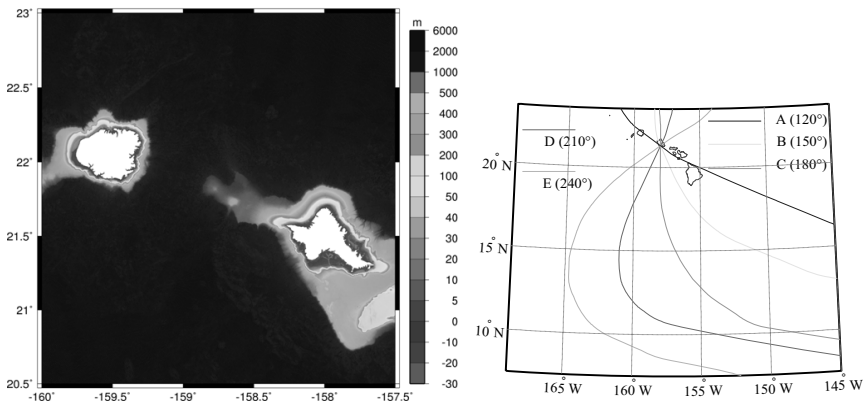


Figure 1: Bathymetry of the grid around Oahu and Kauai (left) and Basic storm tracks considered for the study (right)

Based on information from the NWS on historical storms, a suite of hurricane scenarios was created. These scenarios will ultimately correspond to the support points for the surrogate model, and were chosen so that they cover most future hurricane events that are anticipated to have significant impact on Oahu. Five basic storm tracks were considered, representing different angles of final approach θ . These tracks are shown in Figure 1. Landfall was defined to correspond to the point where each hurricane crosses 21.3 degrees north. A suite of 300 storms was then selected to efficiently describe the entire grid of possible future hurricane scenarios. The response for these storms was then computed by the ADCIRC+SWAN model, a process which required ultimately more than 500,000 computational hours, and all results of interest were stored.

For the wave breakup 750 transects were considered around the island and for each transect a matrix of 169 combinations of wave height and water level was created. The maximum and minimum values of these parameters for each transect were selected based on the information from the 300 runs. For each case the inundation was then predicted by a 1-D Boussinesq analysis. If z_{wj} is the wave break up response at transect j and H_{sj} and z_{sj} are the corresponding wave height and still water level, respectively, then this approach leads to a mapping of the form $z_{wj} = g(H_{sj}, z_{sj} | D)$, where D represents the data obtained through the 169 1-D Boussinesq analyses for each transect.

Surrogate model. Using the pre-computed 300 storms as support points a moving least squares response surface model is built. Full quadratic basis functions are chosen for x_o , θ and v_f and linear for R_m and c_p , whereas for weight the common Gaussian selection (5) is adopted with D adaptively selected so that it includes for each \mathbf{x} 100 support points. Overall, the average error of the response surface approximation was found, through numerous comparisons, to be 5% for wave height and 2% for the still water level. This surrogate model is then used to predict the response, in particular the still water level and significant wave height, for any desired hurricane scenario and *simultaneously* for all locations of interest around the island. The proposed interpolation scheme can then be used to additionally calculate the wave breakup for each transect using as input these two predictions.

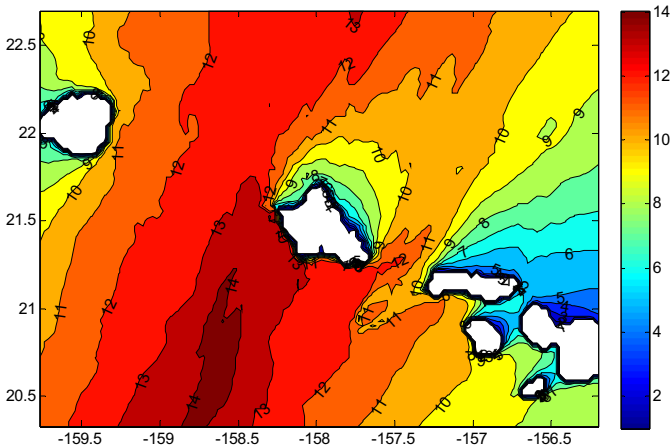


Figure 2: Wave heights (meters) with exceedance probability 10% for a sample hurricane scenario with landfall in Oahu

Online risk assessment tool. During an incoming hurricane event, and prior to landfall the probability distribution for the model parameters $p(\mathbf{x})$ is provided by the NWS and updated during regular time intervals. This probability model can be then used to quantify risk as in (1) and estimate it through stochastic simulation by (2), using the already established surrogate model to evaluate the response for each configuration \mathbf{x} . For implementation of such risk estimation, a risk assessment tool is finally developed. The tool accepts as input the parametric configuration for the most probable hurricane track as well as the estimate for time till landfall, used in the current version to select $p(\mathbf{x})$. Based on this input the output for the most probable hurricane track or the hurricane risk are estimated. The latter is quantified as the threshold with a pre-specified probability of exceedance and is evaluated using $N=2000$ samples for the stochastic simulation (2). The outputs from the risk estimation are finally graphically presented. Figure 2 shows an example. The total time needed for the tool to provide the required output is less than 5 min on a 3.2

GHz single core processor with 2 GB of RAM, which illustrates that it can be efficiently used for online risk evaluation.

CONCLUSIONS

An efficient framework was presented here for hurricane risk estimation with particular emphasis on online risk evaluation. Each hurricane scenario is approximately described through only five model parameters and characterization of the uncertainty in these parameter leads to direct quantification of hurricane risk as a stochastic integral. For efficiently evaluating this integral an approach based on surrogate modeling was examined. For this purpose, a suite of hurricane scenarios is initially created, extending to the entire range of possible values for the model parameters for anticipated future events. The response characteristics for these scenarios, such as wave heights or still water levels, are then accurately predicted through high fidelity numerical simulation models. Based on the information provided by these runs a surrogate model is then built for computational efficiently predicting surge responses. This surrogate model is then used for all evaluations required for the hurricane risk estimation.

ACKNOWLEDGMENTS

This research effort is supported by US Army Corps of Engineering grant W912HZ-09-C-0086. This support is greatly appreciated.

REFERENCES

- Demirbilek, Z., Nwogu, O. G., Ward, D. L., and Sanchez, A. (2009). "Wave transformation over reefs: evaluation of one dimensional numerical models." Report ERDC/CHL TR-09-1, US Army Corps of Engineers.
- Irish, J., Resio, D., and Cialone, M. (2009). "A surge response function approach to coastal hazard assessment. Part 2: Quantification of spatial attributes of response functions." *Natural Hazards*, 51(1), 183-205.
- Niedoroda, A. W., Resio, D. T., Toro, G., Divoky, D., and Reed, C. (2008). "Efficient strategies for the joint probability evaluation of storm surge hazards." Solutions to Coastal Disasters Congress ASCE, Oahu, Hawaii, 242-255.
- Resio, D., Irish, J., and Cialone, M. (2009). "A surge response function approach to coastal hazard assessment – part 1: basic concepts." *Natural Hazards*, 51(1), 163-182.
- Resio, D. T., and Westerink, J. J. (2008). "Modeling of the physics of storm surges." *Physics Today*, 61(9), 33-38.
- Taflanidis, A. A., and Beck, J. L. (2008). "An efficient framework for optimal robust stochastic system design using stochastic simulation." *Computer Methods in Applied Mechanics and Engineering*, 198(1), 88-101.
- Westerink, J. J., Luetlich, R. A., Feyen, J. C., Atkinson, J. H., Dawson, C., Roberts, H. J., Powell, M. D., Dunion, J. P., Kubatko, E. J., and Pourtaheri, H. (2008). "A basin- to channel-scale unstructured grid hurricane storm surge model applied to southern Louisiana." *Monthly Weather Review*, 136(3), 833-864.

Wind Vulnerability Curves for Low-Rise Commercial-Residential Buildings in the Florida Public Hurricane Loss Model

G. L. Pita¹, J.-P. Pinelli², K. Gurley³, J. Weekes⁴, J. Mitrani-Reiser⁵,

¹PhD Candidate, Florida Institute of Technology, Melbourne, FL, *gpita@fit.edu*

²Professor of Civil Engineering, Florida Institute of Technology, Melbourne, FL, *pinelli@fit.edu*

³Associate Professor of Civil Engineering, University of Florida, Gainesville, FL, *kgurl@ce.ufl.edu*

⁴PhD Candidate, University of Florida, Gainesville, FL, *yoyojw17@ufl.edu*

⁵Assistant Professor of Civil Engineering, Johns Hopkins University, Baltimore, MD, *jmitrani@jhu.edu*

ABSTRACT

Regional wind loss predictions depend on vulnerability curves. A state of the art approach for developing the vulnerability curves is presented in the paper. It is based on engineering models that estimate the building damage caused by wind pressures, debris impact, and water penetration. This approach is a substantial improvement over traditional approaches, which derive vulnerability curves for different kind of buildings through curve fitting of historical insurance loss data. This paper describes the engineering model used to develop vulnerability curves for commercial-residential buildings in the Florida Public Hurricane Loss Model.

INTRODUCTION

There is a rising interest in the use of catastrophe (CAT) models in the public and private sector to project losses, mitigate buildings damage, and regulate insurance premiums (Grossi and Kunreuther, 2005). The Florida Public Hurricane Loss Model (FPHLM) commissioned by the State of Florida was initially developed to predict the insured losses to single-family residential buildings (Pinelli et al., 2004, 2006, 2007; Powell et al., 2005). The model has recently been expanded to include commercial-residential buildings as well, which include both low-rise (LR) (1-3 stories) and mid/high rise (MR) (4+ stories) buildings.

The FPHLM, evaluates the damage that wind produces to the envelope of buildings through Monte Carlo simulations subjecting building models to 3-second peak gust wind speeds and debris missile impacts. Interior damage on the other hand is assessed through separate Monte Carlo simulations that compute the intrusion and propagation of wind-driven water through the breaches in the building envelope. Exterior and interior damages are combined to quantify the vulnerabilities of the different building types as a function of wind speed. The description of the whole process is the focus of this paper.

BUILDING TYPES DEFINITION

The commercial-residential LR module of the FPHLM was developed to represent typical condominium and apartment buildings of up to three stories (Figure 1). The characteristics of the buildings were surveyed by the authors in a building exposure

study (Pita et al., 2008). Given the variability of sizes and geometries of these buildings, the program was developed to provide flexibility in choosing a building layout and dimensioning details (footprint, overhang length, roof slope, roof shape, etc.). Most of the existing commercial-residential building inventory in the state of Florida has been built over 1900 to date. The construction practice in Florida changed drastically over this time frame, affecting the capacity (hurricane wind resistance) of buildings from different construction eras. The model presented in this paper can handle three types of construction qualities (weak, medium, and strong) for each damageable building component (roof type, roof sheathing type, roof cover type).



Figure 1: Typical low-rise buildings

Any given strong, medium or weak model may be altered by additional individual or combined mitigation or retrofit measures. For example re-roofing an old apartment is represented by increasing the probabilistic descriptor of capacity for the roof cover. Building models have been produced for each combination of the following: building height (1, 2 or 3 stories), wall type (timber or masonry), roof shape (hip or gable), roof cover (shingles or tiles), strength (weak, medium or strong), and window protection (no protection or with shutters). Table 1 summarizes the building types modeled.

Table 1: LR most prevalent buildings types

Category	Wall type	Roof Cover	Roof shape
Main Building types	Concrete block	Shingles/Tiles	Gable
	Concrete block	Shingles/Tiles	Hip
	Wood	Shingles/Tiles	Gable
	Wood	Shingles/Tiles	Hip
Windows	Shuttered / Not impact-resisting		
Stories	1 / 2 / 3		
Strength	Strong, Medium, Weak		

DAMAGE MATRICES

Exterior damage: The model framework for exterior damage simulation is based on the single-family residential model (Pinelli et al., 2004, 2006, 2007; Cope et al., 2005), which uses a probabilistic description of wind loads and exterior and structural component capacities to estimate physical damage as a function of wind speed. The model uses a Monte Carlo simulation component approach to assess the external

vulnerability at various wind speeds of buildings, accounting for the capacity for each structural component separately (Weekes et al, 2009). This process is summarized in Figure 2.

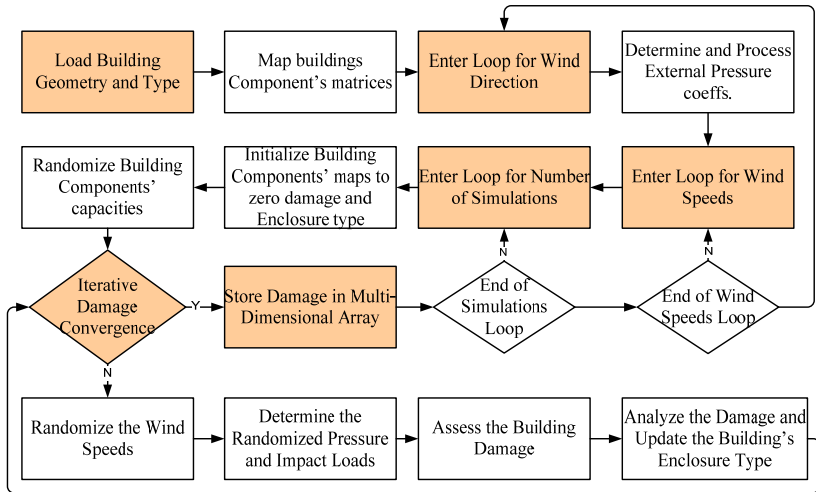


Figure 2: Monte Carlo Simulation procedure to predict external damage

The damage assessment is conducted over a range of wind speeds and wind directions, and results are stored in a damage matrix. Probabilistic damage assessment is conducted by first creating an individual building realization by mapping each component accordingly to typical construction practice. Random capacity values are assigned to the various components based on a probability distribution for each component type. This realization is subjected to a peak 3-second gust wind speed from a particular direction. Directional loads are calculated using randomized pressure coefficients based on wind tunnel data (NIST Aerodynamic Database - <http://fris2.nist.gov/winddata>) and directional modifications to ASCE 7. Damage occurs when the assigned capacity of a component is exceeded by its loading. Once the openings have been checked for failure due to pressure, the damage due to the impact of airborne debris are also evaluated. Damaged components are removed, and a series of checks are performed to determine if lost components will redistribute loading to adjacent components or change the overall loading. For example, loss of a roof-to-wall connection places additional load on adjacent connections, while an envelope breach will potentially alter internal loading and change the overall loading on most components. Iterative convergence is used to produce the final damage state for that building realization. The results of this single simulation are documented based on the final iteration. Then another realization of that building is constructed by assigning new random capacities to each component, and the process repeats for the same 3-second gust, same wind direction, and newly randomized pressure coefficients based on the number of desired simulations the user would like to run.

The process is repeated for eight wind directions and a series of 3 second wind speeds between 50 and 250 mph in 5 mph increments.

The output of the Monte Carlo simulation model is an estimate of physical damage to structural and exterior components. The results are in the form of a four dimensional damage matrix. Each row of the matrix lists results of one simulation. The amount of damage to each of the modeled components for a simulation is listed in the 32 columns of the row. The third dimension represents the peak 3-s gust wind speed between 50 and 250 mph in 5 mph increments, while the fourth dimension represents the 8 angles between 0 and 315 degrees in 45-degree increments.

INTERIOR AND UTILITIES DAMAGE

The FPHLM team developed a novel approach to assess the interior damage. The approach starts from the damage to the buildings' envelope described in the previous section. The model then estimates the amount of wind-driven rain that enters through the breaches and defects in the building envelope and converts it to interior damage. The approach is based on a Monte Carlo simulation that samples exterior damage, probability distributions of rain rate (the depth of rain accumulated per unit of time), and its duration. The model also considers the vertical propagation of water between stories. The interior damage outcome is expressed as total building interior damage or related to each of the envelope components. In both cases the damage is expressed either as a function of wind speed or exterior damage ratio. The method is described in Figure 3.

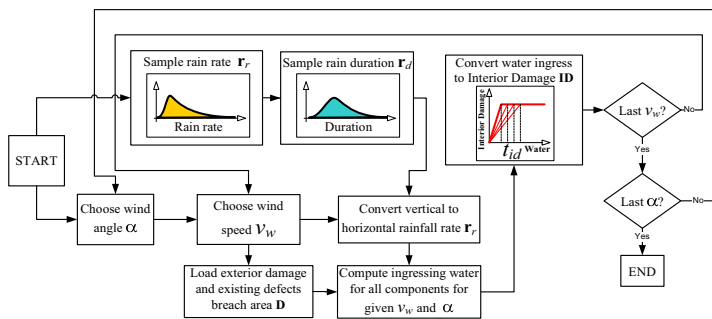


Figure 3: Flowchart of the interior damage model

In order to estimate total (exterior + interior) building damage, the model considers existing defects as well as the wind-induced damage of several exterior building components: roof cover, roof sheathing, wall cover, wall sheathing, gable cover, gable sheathing, windows, doors and sliding doors. For a given wind speed, the model first estimates breach areas of each component from the exterior damage array. An estimated area of existing defects in envelope components is also accounted for from surveys (Mullens et al, 2006) and engineering experience.

Next, the model samples the ground level rain rate in mm/hour, from an empirical probability distribution (Jiang et al., 2008). The rain ground level rain rate is not the same rain that hits the walls of the building (impinging rain). The impinging rain is a

function of ground level rain rate as well as the wind speed hitting the building. The model uses a semi-empirical method proposed by Straube and Burnett (2000) that estimates the impinging rain based on these two variables and the raindrop size spectra. The duration of the rain is also needed to quantify the amount of water entering the building. The duration is sampled from an empirical probability distribution derived from the NOAA Hourly Precipitation Data (NCDC, 1953-2005) counting the rain hours for 23 hurricanes in the period from 1953 – 2005. The product of the breach area by the impinging rain by the duration of the rain conveys the amount of water that enters the building for each simulation (row) of the exterior damage array. This approach estimates the amount of water that enters through each component of the envelope. The total amount of water is calculated by adding the contribution of all components for a given wind speed. The final step maps water inside the building to interior damage with a nonlinear probabilistic relationship.

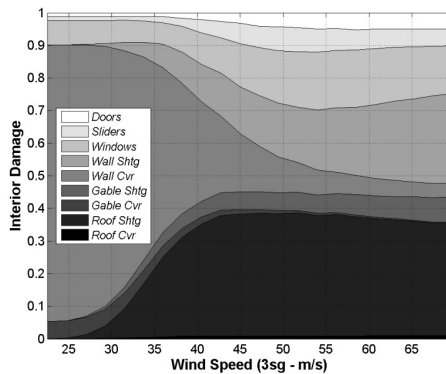


Figure 4: Interior damage as a function of wind speed

Figure 4 depicts the behavior of interior damage as a function of wind speed, for a typical gable roof, timber frame, 1-story multi-family building. The x-axis depicts wind velocity and ranges from 25mph until 65 mph, where complete interior damage occurs. At low speeds the interior damage is governed by the existing defects. Gradually, roof, gable and wall sheathing damage modes become the main sources of damage. Note that the only damage modes that play a constant role in the interior damage generation throughout the wind speed range are the openings, particularly windows. The interior damage due to water penetrating through openings goes through three stages: 1) damage due to existing defects, 2) increasing damage due to breach; and 3) relative decrease as the wall sheathing predominates. This behavior emphasizes the need for protecting the openings of Florida buildings with shutters or impact resisting glass.

LOW-RISE BUILDINGS VULNERABILITY

Building vulnerability relates wind speed to building damage, expressed as fraction of replacement cost. The vulnerability is defined by a matrix whose columns sorted for increasing wind speeds intervals, represent the conditional probability distribution

$P(D_i|V_j)$ of building damage ratio D_i , for a given wind speed V_j . The rows of the matrix correspond to increasing damage intervals. Building damage ratios damage D_i , increase in 2% increments up to 20%, and then in 4% increments up to 100%. The wind speeds range from 50 to 250 mph in 5 mph increments. The vulnerability matrix, shown in Figure 5 can be transformed into a vulnerability curve by computing the mean building damage ratio at each wind speed interval.

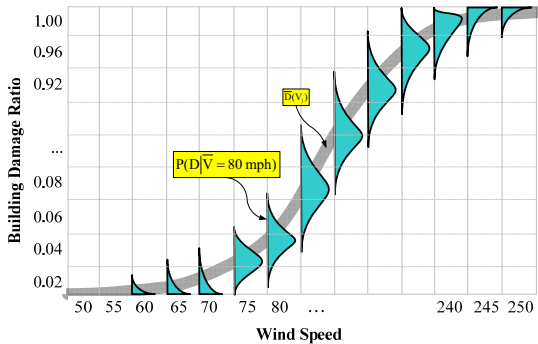


Figure 5: Vulnerability matrix layout

The process to estimate the vulnerability of a particular building type is illustrated in Figure 6. The derivation of building vulnerabilities involves the exterior, interior and utilities damage assessment, and the aggregation of all of the damages weighted by their cost allocation. Total building damage is defined as the ratio of the aggregated damage repair cost, including handling and removal costs, over the cost of the entire building. Given a particular building type, its previously calculated exterior damage array is loaded. Then the costs to replace or fix the damaged components are calculated for all wind speeds and wind directions.

The interior damage is computed according to the methodology presented in the previous section. Finally the damage ratio (DR) is estimated by adding the corresponding costs of damaged envelope components plus damaged interior plus damaged utilities divided over the overall building cost that is contingent upon the type and size of the building. All the costs include material, labor, and disposal of damaged elements, as needed.

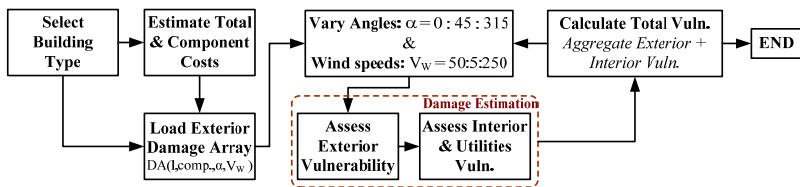


Figure 6: Vulnerability estimation process. (In the damage array, “I”= simulation run number; comp.= component type, e.g. window; α = angles, i.e. wind direction; V_w = wind speeds)

The model also considers the Florida Building Code (FBC) provisions for damage thresholds. When the damage to certain components exceeds given thresholds then the entire component needs to be replaced and brought up to code. For instance, if the roof has more than 25% damage in the High Velocity Hurricane Zone, the whole roof must be brought up to code. Other thresholds apply outside the aforementioned regions. The model incorporates these provisions so that if any of the thresholds is exceeded, then the cost to replace the whole component is computed.

CONCLUSIONS

This paper describes the development of vulnerabilities for commercial-residential low rise building. The methodology is based on a component approach that estimate the damage caused by wind pressures, debris impact, and water penetration of multiple building components. This approach is a substantial improvement over traditional approaches, which derive vulnerability curves for different buildings types through curve fitting of historical insurance loss data.

In particular, a novel approach has been implemented to estimate the interior damage based on the interaction between damage to the envelope of the building and wind-driven rain. Sensitive points of the method include the estimate of vertical rain fall, rain duration, conversion of vertical rainfall into horizontal rainfall and correlation of water intrusion with interior and contents damage. Access to meteorological data, and damage and claim data are important for the validation and calibration of the overall vulnerability model. Next step includes validation of the model for those structures that there is available claim data information.

ACKNOWLEDGMENTS

This research is supported by the state of Florida through a Department of Financial Services (FDFS) grant to the Florida International University – International Hurricane Research Center. Dr. Mitrani-Reiser is supported by NSF grant 0826365. The opinions, findings and conclusions expressed in this paper are not necessarily those of FDFS or NSF.

REFERENCES

- ASCE 7-08, (2008) *Minimum Design Loads for Buildings and Other Structures*, American Society of Civil Engineers.
- Cope, A. , Gurley, K., Gioffre, M. , Reinhold, T., “Low-rise gable roof wind loads: Characterization and stochastic simulation” (2005). *Journal of Wind Engineering and Industrial Aerodynamics*, Volume 93, Issue 9, p. 719-738.
- Grossi, P. and Kunreuther, H., “*Catastrophe Modeling: A New Approach to Managing Risk*.” Springer, New York, 2005
- Gurley, K., Davis, R., Ferrera, S-P., Burton, J., Masters, F., Reinhold, T. and Abdullah, M. (2006), “Post 2004 Hurricane Field Survey – an Evaluation of the Relative Performance of the Standard Building Code and the Florida Building Code”, ASCE Structures Congress, St. Louis, 2006.
- Mullens, M., Hoekstra, R., Nahmens, I., and Martinez, F. (2006). *Water Intrusion in Central Florida Homes During Hurricane Jeanne in September 2004*. University of Central Florida Constructability Lab.

- National Climatic Data Center (NCDC) (1953-2005), *Hourly Precipitation Data – Florida*, National Oceanic and Atmospheric Administration (NOAA). Department of Commerce. ISSN 0364-6114.
- Pinelli, J. -P., C. Subramanian, A. Artiles, K. Gurley, S. Hamid, Validation of a probabilistic model for hurricane insurance loss projections in Florida, Proceedings, ESREL 2006, Estoril, Portugal, September 18-21, 2006.
- Pinelli, J. -P., Simiu, E., Gurley, K., Subramanian, C., Zhang, L., Cope, A., Filliben, J. (2004) “Hurricane Damage Prediction Model for Residential Structures”, *Journal of Structural Engineering*, ASCE, Vol. 130, No 11 , pp. 1685-1691.
- Pinelli, J. -P., Subramanian, C., Garcia, F., Gurley, K., (2007) “A study of hurricane mitigation cost effectiveness in Florida”. *Proceedings ESREL 2007*, Stavanger, Norway.
- Pita, G. Pinelli, J.-P. , Subramanian, C. , Gurley, K. , Hamid, S. (2008), “Hurricane Vulnerability of Multi-Story Residential Buildings in Florida”. *Proceedings ESREL08*, Valencia, Spain.
- Pita, G.L., Pinelli, J.-P., Mitrani-Reiser, J., Gurley, K., Weekes, J., (2011) “Assessment of hurricane induced internal damage to low-rise buildings in the Florida Public Hurricane Loss Model”. Abstract accepted to 13 Int’l Conf. on Wind Engineering, Amsterdam.
- Powell, M., Soukup, G., Cocke, S., Gulati, S., Morisseau-Leroy. N., Hamid, S., Dorst, N., Axe, J., (2005) “State of Florida hurricane loss projection model: Atmospheric science component”. *Journal of Wind Engineering and Industrial Aerodynamics*, 93, (8), 651-674
- Straube, J. and Burnett, E., “Simplified Prediction of Driving Rain Deposition” (2000). *Proc of International Building Physics Conference*, Eindhoven, September 18-21, pp. 375-382.
- Weekes, J. , Balderrama, A. , Gurley, K. , Pinelli, J.-P. , Pita, G.L. , Hamid, S. , “Physical Damage Modeling of Commercial-Residential Structures in Hurricane Winds”. *11th American Conference of Wind Engineering*. Puerto Rico, 2009.
- Zhang, Z., Public Hurricane Loss Prediction Model: Exposure and Vulnerability Components. M.S. Thesis. Civil Engineering Department. Florida Institute of Technology. Melbourne, FL. 2003

Database-Assisted Design: Why and How?

E. Simiu¹

¹Engineering Laboratory, National Institute of Standards and Technology, 100 Bureau Dr., Gaithersburg, MD 20899; PH (301) 975-6076; FAX (301) 869- 6275; email: emil.simiu@nist.gov

ABSTRACT

This paper presents an overview of the Database-Assisted Design (DAD) methodology, and describes its motivation, the technological developments that enabled its development, and its main features. DAD is an integrated methodology that does not just calculate wind loadings, but rather performs the automatic calculation of internal forces and demand-to-capacity indexes, and the detailed verification of the adequacy of the structural design. The paper discusses interpolation issues, wind directionality effects, and the estimation of wind effects with specified mean recurrence intervals. It concludes by noting the potential of using DAD in conjunction with Computational Fluid Dynamics methods.

INTRODUCTION

Inherent in the ASCE 7 Standard provisions for wind loads on rigid buildings are large errors -- in some cases larger than 50% on the unconservative side (Ho et al., 2005; StPierre et al., 2005; Coffman et al., 2010). The errors are due in part to the reduction of vast amounts of aerodynamic data to the far smaller numbers of data contained in tables and plots. For buildings that warrant the use of more accurate procedures than those based on standard tables and plots such errors can be significantly reduced by using the Database-Assisted Design (DAD) methodology. The subsequent sections describe the methodology, and discuss interpolation issues as well as the estimation of mean recurrence intervals of wind effects as functions of wind directionality. The paper ends with a set of conclusions which note the potential of using DAD in conjunction with Computational Fluid Dynamics methods.

DATABASE-ASSISTED DESIGN METHODOLOGY

Essentially, DAD determines wind effects by using large sets of electronically recorded aerodynamic pressure data measured simultaneously in the wind tunnel at large numbers of points on the building surfaces (Figure 1).

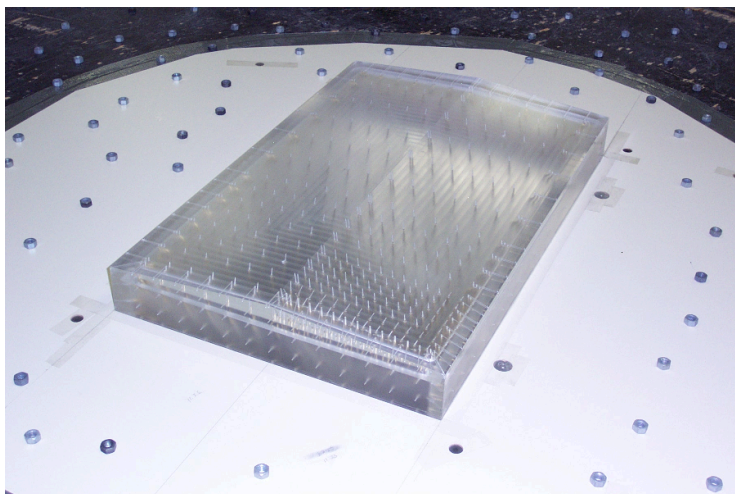


Figure 1. University of Western Ontario Boundary Layer Wind Tunnel building model, with locations of pressure taps. (For detailed credits see section “Acknowledgment.”)

DAD allows the estimation of wind effects with specified mean recurrence intervals by accounting for the directional properties of (a) the extreme wind speeds and (b) the building aerodynamics. The use of DAD procedures is permitted by the ASCE 7-10 Standard (ASCE Commentary Sect. C31.4.2). DAD is evolving into an effective, user-friendly tool. For standard development purposes or for special projects DAD can also be used for nonlinear push-over analyses, which provide information on ultimate capacities under wind and gravity loads (Jang et al., 2003; Duthinh and Fritz, 2002; Duthinh et al., 2007).

DAD takes advantage of the following advances:

1. The number of pressure taps that can be accommodated on a building model envelope is sufficiently large (of the order of hundreds) to provide a realistic representation of the pressure distributions.
2. Pressure time histories can be measured simultaneously at all the pressure taps affecting the loading of components and main wind-force resisting systems.
3. The simultaneous pressure time histories can be stored electronically for use in calculations.
4. The influence coefficients required to calculate the internal forces can be obtained by standard structural analysis programs for the structure of interest, rather than from

generic structures purported to be typical, as was the case for the development of loads on low-rise buildings specified in the ASCE 7 Standard .

5. Time histories of internal forces can be obtained in a routine, user-friendly manner by using software whose input consists of pressure tap locations, stored pressure data, frame locations, and influence coefficients obtained for the structure being designed (Main and Fritz, 2006).

6. DAD software includes a subroutine for calculating statistics of peak values by using the information contained in the entire time history of the internal force of interest. Statistics of peak values are preferable to observed values, which vary from record to record and, therefore, do not allow conclusive comparisons between observations obtained in different experiments. The subroutine allows the estimation of any desired percentile of the peak.

7. DAD software also includes software that effects interpolations based on data for buildings with geometric characteristics close to those of the building being designed.

8. Database-Assisted Design databases, software and examples of its application are publicly available (see www.nist.gov/wind).

The software is aimed at implementing the following sequence of operations. A preliminary structural design is developed and used to obtain influence coefficients. Spatial coordinates of the pressure taps, and measured pressure time series, are provided by the wind tunnel laboratory or are available on file. They are used in conjunction with information on the positions of the structural frames and with the requisite structural influence coefficients to obtain statistics of the peak values of the response of interest for each wind direction.

DAD allows the calculation of the time series of internal forces and/or demand-to-capacity indexes (DCIs) and their peaks, which are used for the design of the Main Wind Force Resisting System and of components such as girts and purlins. The DCIs consist of the left-hand sides of the design interaction equations.

For rigid structures it is convenient to evaluate peak responses (e.g., peak DCIs) corresponding to a unit wind speed. The resulting direction-dependent response quantities are referred to as directional influence factors (DIFs) (Rigato, Chang and Simiu, 2001). Since the linear structural responses being sought are unaffected by dynamic effects, the peak response to the load induced by any arbitrary wind speed can be obtained via multiplication of the corresponding DIF by the square of that wind speed. In this manner, the DIFs can be combined with databases of directional extreme wind speeds from a sufficiently large number of storm events to estimate, by using non-parametric statistical methods, values of the DCIs, or of internal forces, with specified mean recurrence intervals. These values can then be used to redesign the structure. Influence coefficients are computed for the revised structural design, and the analysis procedure is repeated as necessary, until satisfactory convergence is achieved.

The ASCE Standard provisions for low-rise buildings were developed on the basis of tests on a modest number of basic configurations – about ten – that do not represent all the building configurations covered by the provisions. To date a larger number of building configurations have been covered for DAD development purposes by tests conducted at the University of Western Ontario. For DAD to be a

routine tool resulting in safer and more economical designs it is necessary that the acquisition, certification, and archiving of aerodynamic data be expanded in the future. Whenever warranted by economic considerations, ad-hoc wind tunnel tests can be performed for the building being designed.

INTERPOLATION

In practice it is not possible to provide aerodynamic databases for all possible sets of building dimensions corresponding to a given building configuration. Therefore, if pressure records are available for two buildings having the same configuration but somewhat different dimensions, internal forces on a similar building with intermediate dimensions can be obtained by interpolation. We briefly describe the simple and effective interpolation procedure developed in (Main and Fritz, 2006; Main, 2005).

Assume that pressure data are available for two buildings, denoted by A and C, whose dimensions (and/or roof slopes) are relatively close to and, respectively, larger and smaller than those of the building of interest, denoted by B. The coordinates of the pressure taps of buildings A and C are scaled to match the dimensions of building B. Using these scaled coordinates, DIFs are computed by treating the measured pressures on buildings A and C as if they had been recorded on a model having the same dimensions as building B. This procedure can be applied using measurements from only one wind tunnel model (i.e., A or C), but improved accuracy can generally be achieved by making use of measurements from several models, having dimensions that bound those of the structure of interest. The DIFs for the building of interest are then estimated by taking a weighted average of the DIFs corresponding to each of the wind tunnel models, with greater weight being given to results from models that more closely match the dimensions of the building of interest. For details see (Main, 200?). The structure is designed on the basis of those DIF's. An example of this interpolation procedure is given in (Main and Fritz, 2006), in which the results of the interpolation match remarkably well the results based on data obtained directly for the building of interest. For interpolations between buildings with different roof slopes the extent to which this procedure yields satisfactory results remains to be tested. The interpolation software is provided on www.nist.gov/wind.

WIND DIRECTIONALITY AND MEAN RECURRENCE INTERVALS OF WIND EFFECTS

For rigid structures with linearly elastic behavior and orientation defined by an angle φ between a principal axis and the north direction, the wind effect $Q_i(\theta_j, \varphi)$ (e.g., a bending moment, or an axial load) induced by a wind speed $V_i(\theta_j)$ blowing from direction θ_j may be written as

$$Q_i(\theta_j, \varphi) = \kappa(\theta_j, \varphi) V_i^2(\theta_j) \quad (1)$$

the directional effect coefficient $\kappa(\theta_j, \varphi)$ is the wind effect induced in the building with orientation φ by a unit mean wind speed at the top of the building from direction θ_j , and is called the directional influence factor (DIF, see Sect. 2). The mean wind speed at the top of the building blowing from direction j in storm event i is denoted by $V_i(\theta_j)$. This section discusses several approaches used in standards or by wind engineering consultants to account for the directionality of both the aerodynamic effects and the extreme wind speeds.

The approach specified in the analytical procedure of the ASCE 7 Standard consists of using a building *wind directionality factor* $K_d = 0.85$ applied to the wind effect calculated by disregarding wind directionality. The wind effect induced by wind event i is thus defined as

$$Q_i = 0.85 \max_j[\kappa(\theta_j, \varphi)] \max_j[V_i^2(\theta_j)] \quad (2)$$

This approach is the simplest, but can either overestimate or underestimate the response, and is therefore not used by wind engineering laboratories for estimating wind effects on special structures. The angle φ is omitted from the left-hand side of Eq. 2 because the building orientation does not affect the maxima of the directional effect coefficients $\kappa(\theta_j, \varphi)$. ASCE 7 Standard estimates of wind effects are therefore independent of building orientation.

The approach based on *non-parametric statistics* introduced in Sect. 12.7 incorporates the directional aerodynamic and wind climate effects in a simple, transparent, and rigorous manner. This approach requires the development by Monte Carlo simulation of a matrix of wind speeds $V_i(\theta_j)$ in which $j=16$ or 36 , say, $i = 1, 2, \dots, m$, and m is sufficiently large for the number of storm events or the years of record to cover a time interval longer than the mean recurrence interval of the design wind effect (for details see Yeo, 2011). A vector with m components is then created, the i th component of which is the largest of the directional wind effects in the i th storm, $\max_j[Q_i(\theta_j, \varphi)]$. The components of the vector are rank-ordered, and the wind effect with an \bar{N} -yr mean recurrence interval is obtained by standard non-parametric statistical methods.

In principle, *parametric statistics* may also be employed by fitting an extreme value probability distribution to the quantities $\{\max_j[Q_i(\theta_j, \varphi)]\}^{1/2}$, which are proportional to wind speeds. This approach has the advantage of being applicable to the case where m represents the number of storm events for which wind speed measurements are available, rather than the larger number of synthetic storm events obtained by Monte Carlo simulation from the measured wind speeds. The application of extreme value statistics to the quantities $\{\max_j[Q_i(\theta_j, \varphi)]\}^{1/2}$ may be expected to yield results as realistic as their counterparts based on extreme wind speeds. However, no studies have so far been performed to test this proposition.

The *outcrossing* approach is, to our knowledge, currently used by only one or two laboratories. The models include in the data samples non-extreme wind speed data, such as speeds recorded at one-hour intervals (*Wind Tunnel Studies*, 1999, p. 167) or low speeds occurring in peripheral hurricane zones. This typically causes the underestimation of wind effects, a concern noted in (Isyumov et al., 2005). A second

drawback is the perception by structural engineers that the approach is opaque. For details, see (Simiu (2011)).

Some wind engineering consultants have used the *sector-by-sector* approach (Simiu and Filliben, 2006). This approach typically yields unconservative results.

CONCLUSIONS

Aerodynamic data included in the ASCE 7 Standard can be affected by large errors that, in conjunction with simplified methods for estimating wind directionality effects, can result in the significant overestimation or underestimation of wind-induced effects on structures. The Database-Assisted Design (DAD) methodology, made possible by recent developments in pressure measurement technology and by modern computational capabilities, has been developed with a view to achieving improved designs from the standpoints of safety and material consumption. To implement DAD on a broad scale, additional aerodynamic databases need to be developed, either in the wind tunnel or, as may be possible in the near future, by using standard or simplified Computational Fluid Dynamics methods.

ACKNOWLEDGMENT

Figure 1 is taken from C.E. Ho, D. Surry & D. Morrish, *NIST/TTU Cooperative Agreement – Windstorm Mitigation Initiative: Wind Tunnel Experiments on Generic Low Buildings*, Alan G. Davenport Wind Engineering Group, The University of Western Ontario, 2003, a publication funded by the National Institute of Standards and Technology.

REFERENCES

Coffman, B.F., J. A. Main, D. Duthinh, and E. Simiu, "Wind effects on low-rise metal buildings: Database-assisted design versus ASCE 7-05 Standard Estimates," *J. Struct. Eng.* **136**, 744, 2010.

Duthinh, D. and W. P. Fritz, "Safety evaluation of low-rise steel structures under wind loads by nonlinear database-assisted technique," *J. Struct. Eng.* **133** 587-594, 2007.

Duthinh, D., J.A. Main, A.P.Wright, and E. Simiu, "Low-rise steel structures under directional winds: mean recurrence interval of failure." *J. Struct. Eng.* **134** 1383-1388, 2008.

Ho, T.C.E., D. Surry, D. Morrish, and G.A. Kopp, "The UWO contribution to the NIST aerodynamic database for wind loads on low buildings Part I. Archiving format and basic aerodynamic data," *J. Wind Eng. Ind. Aerodyn.* **93** 1-30 (2005).

Isyumov, N. et al., Predictions of Wind Loads and Responses from Simulated Tropical Storm Passages," *Proc.*, 11th Intern. Conf. on Wind Eng., D.A. Smith and C.W. Letchford (eds.), June 2-5, 2003, Lubbock, Texas, 2005.

Jang, S, L.-W. Lu, F. Sadek, E. Simiu, "Database-assisted wind load capacity estimates for low-rise steel frames," *J. Struct. Eng.* **128** 2002 1594-1603, 2002.

Main, J.A. (2007). "Interpolation procedures for database-assisted design." *Proc., 12th Int. Conf. on Wind Engineering*, July 1-6, 2007, Cairns, Australia, 1087-1094.

Main, J.A. and W.P. Fritz, *Database-assisted design for wind: Concepts, software, and examples for rigid and flexible buildings*. NIST Building Science Series 180, National Institute of Standards and Technology, Gaithersburg, MD, 2006.

Rigato, A.,P. Chang, and E. Simiu, "Database-assisted design, standardization, and wind direction effects," *J. Struct. Eng.* **127** (2001) 855-860.

Simiu, E. and J.J. Filliben "Wind tunnel testing and the sector-by-sector approach," *J. Struct. Eng.* **131** 1143-1145, 2005.

Simiu, E., *Design of Buildings for Wind*. Hoboken: Wiley, 2005.

St. Pierre, L.M., G.A. Kopp, D. Surry, and T.C.E. Ho, "The UWO contribution to the NIST aerodynamic database for wind loads on low buildings: Part II. Comparison of data with wind load provisions," *J. Wind Eng. Ind. Aerodyn.* **93** 31-59 (2005).

Wind Tunnel Studies of Buildings and Structures, ASCE Manuals and Reports on Engineering Practice No. 67, American Society of Civil Engineers, Reston, Virginia, 1999.

Yeo, D., "Development of Large Directional Wind Speed Databases," this conference.

Probabilistic Demand Models and Fragility Estimates for Offshore Wind Turbine Support Structures

M. Mardfekri¹, P. Gardoni², and J. M. Roesset³

¹Doctoral Student, Zachry Dept. of Civil Engineering, Texas A&M Univ., College Station, TX, 77843-3136. Email: maryam_mardfekri@tamu.edu

²Associate Professor, Zachry Dept. of Civil Engineering, Texas A&M Univ., College Station, TX, 77843-3136. Email: pgardoni@civil.tamu.edu

³Cain Chair Professor, Zachry Dept. of Civil Engineering, Texas A&M Univ., College Station, TX, 77843-3136. Email: jroesset@civil.tamu.edu

ABSTRACT

A probabilistic model is developed to predict the deformation demand on wind turbine support structures due to the operation of the turbine, and wind and wave loading. An existing deterministic model is corrected by adding a correction term to capture the inherent bias and model error arising from an inaccurate model form or missing variables. The correction term and the model error are assessed using data obtained from detailed three dimensional nonlinear finite element analyses of a set of wind turbine systems considering different design parameters. Fragility of the support structure is then defined as a conditional probability of not meeting a specified deformation performance level. Existing simplified methods for the analysis of the support structure and foundation of wind turbines have limitations in the modeling of the nonlinear behavior of the foundations. Three dimensional nonlinear finite element analyses provide a more rigorous and accurate modeling of the soil mass, pile and their interaction, but they are computationally expensive and time consuming. The proposed probabilistic demand model provides an accurate framework for predicting the deformation of support structure properly accounting for the underlying uncertainties, and for estimating the vulnerability of the wind turbine support structure without the need of conducting complicated nonlinear finite element analyses.

INTRODUCTION

Extensive installation of offshore wind farms for electricity production in the United States and abroad has raised a new concern about the analysis and design of offshore wind turbine support structures. Mono-piles are widely used to resist lateral loads and bending moments resulting from the operation of the turbine as well as wind and wave loading on the tower.

Reliable power production operation of a wind turbine is one of the key factors to reduce the cost of energy. Providing adequate reliability can help reduce the need for costly repairs and downtime. Walford (2006) shows how improving system reliability is critical to reduce the operation and maintenance cost of wind turbines. Furthermore, an accurate assessment of the reliability of wind turbines can be used for a reliability-based optimal design that minimized construction and maintenance costs while maintaining minimum reliability requirements. An important criterion for the design of a wind turbine support structure is to meet the

serviceability criteria of the turbine. The proper operation of wind energy converters relies on the limited movement of the turbine installed at the top of the wind turbine tower. Therefore, this paper assesses the probability that the deformation at the top of the support structure exceeds specified threshold levels.

Computational modeling is being widely used to determine the demand on the support structure of the wind turbines. Computational analyses of the support structure require the accurate modeling of the structural dynamic response of the structure, and the evaluation and modeling of the environmental loading including wind loading, and, for offshore wind turbines, wave and current loading.

Common methods for the analysis of laterally loaded single piles can be generally classified into two categories: Winkler (elastic) foundation models, and continuous models accounting for the coupling of forces and displacements in the soil along the pile. Winkler foundation models are popular because of their simplicity and reasonable accuracy. For nonlinear analyses the p-y method - developed first by Matlock (1970) - is the most commonly used one. To simplify the computational models in most of the analyses of wind turbines, the foundation is modeled by equivalent springs (Reese and Wang, 2008). Reese and Wang (2008) used a design method based on p-y curves (Reese et al., 1975) to take soil-structure interaction into account. Mardfekri et al. (2010) used a three-dimensional (3D) nonlinear finite element model and showed that, depending on the pile diameter and soil type, using common simple models, such as p-y method and particularly modeling the pile using one dimensional beam-column elements may result in inaccurate responses. This is true in particular for the pile sizes typical of foundations of offshore wind turbines.

However, continuous modeling of the pile and the surrounding soil are mostly done using finite element or boundary element models. A 3D nonlinear finite element analysis of a pile foundation in which both the soil and the pile are modeled with 3D finite elements can be quite expensive and time consuming, particularly when incorporating nonlinear behavior of the soil and soil-pile interaction. On the other side, several aeroelastic simulation codes are used in the industry to simulate fatigue, aerodynamics, structural dynamic response, and turbulence. They are mostly used to predict the extreme and fatigue loads of wind turbines. For example, FAST (Jonkman and Buhl Jr., 2005) and ADAMS, developed by MSC corporation, are two commonly used simulators. The main limitation of these simulators is that they are not capable of modeling the foundation behavior and the dynamic soil-structure interaction because they consider the tower to be fixed at the ground level. However, given the side of the superstructure, it is important to account for the effects of the dynamic soil-structure interaction in predicting the deformation at the support structure.

To address the limitations of prevailing approaches in assessing the demand on the support structure of offshore wind turbines, we develop new demand model that accounts for the dynamic nonlinear soil-structure interaction in evaluating the dynamic response of the support structure.

VIRTUAL EXPERIMENTAL DATA

A set of representative configurations are selected to generate virtual experiments later used to calibrate the proposed probabilistic demand models. The representative configurations are selected by conducting an experimental design to maximize the

information content of the cases run and minimize the computational costs associated with running 3D nonlinear finite element analyses. According to Simpson et al. (2001), the design space is defined as the region bounded by the upper and lower limits of each design (input) variable being studied and the sample points should be chosen to fill the design space for computer experiments such that they spread as far from each other as possible. There are several "space filling" designs in the literature; here the Latin hypercube sampling technique introduced by McKay et al. (1979) is used to select the support structure representative configurations. Latin hypercube sampling technique maximize the minimum distance between sample points, while the range of each parameter, x_i , is divided to N strata of equal marginal probability $1/N$, so this method ensures that the sampling has a good coverage of the design space. A total of 1000 configurations will be generated. For now, we have chosen eight configurations to run the simulations and used the obtained results to assess the parameters of the proposed probabilistic demand model.

Finite element models are developed in ABAQUS to simulate the dynamic response of the support structure of typical offshore wind turbines, subjected to wind, wave and turbine operational loading. The finite element model of the support structure is constructed such that it is able to account for the nonlinearity of the soil behavior and soil-structure interaction.

Wind turbulence is simulated using the computer program TurbSim. TurbSim is a stochastic, full-field, turbulent-wind simulator. It uses a statistical or empirical model (as opposed to a physics-based model) to numerically simulate time series of three-component wind-speed vectors (Jonkman, 2009).

The wave loading is modeled using a linear irregular wave model which is commonly used to model stochastic ocean waves. The model can be written as

$$\Phi = \sum_{m=1}^N -A_m \frac{g}{\omega_m} \frac{\cosh k_m (h+z)}{\cosh k_m h} \sin(\omega_m t - k_m x - \phi_m) \quad (1)$$

where Φ = velocity potential, A_m = amplitude of the wave, ω_m = frequency of the wave, determined by solving the dispersion equation of $\omega_m^2 = g k_m \tanh(k_m h)$, g = acceleration of gravity, h = water depth, and $k_m = 2\pi/L_m$ is the wave number, where L_m = wave length. Horizontal water particle velocity, u , and acceleration, \dot{u} , are determined as $u = -\partial\Phi/\partial x$ and $\dot{u} = \partial u/\partial t$, respectively.

Following Det Norske Veritas guideline for design of wind turbines (DNV/Risø, 2002), Morison's equation is used to determine the hydrodynamic forces. The horizontal force on a vertical element dz of the structure at level z is expressed as (Dean and Dalrymple, 1991)

$$dF = dF_D + dF_I = \frac{1}{2} C_D \rho d_p u |u| + C_M \rho \frac{\pi d_p^2}{4} \dot{u} \quad (2)$$

where dF_D and dF_I indicate the drag and inertia forces, respectively, C_D = drag coefficient, C_M = inertia coefficient, d_p = pile diameter, and ρ = density of water. We neglect the velocity and acceleration of the structure and parameters u and \dot{u} indicate the horizontal velocity and acceleration of the water particles.

The aerodynamics of the turbine is simulated by the aid of the computer program FAST (Fatigue, Aerodynamics, Structures, and Turbulence). FAST is a comprehensive aeroelastic simulator capable of predicting both the extreme and

fatigue loads of two- and three-bladed horizontal-axis wind turbines (Jonkman and Buhl Jr., 2005). We use FAST to simulate the wind turbine and produce the time history of the forces at the top of the tower due to the wind and operation of the turbine. The time history of wind loading used as an input for FAST is generated using TurbSim. The result of this simulation is the operational loading on the tower, which is used in the finite element model of the support structure as an external loading in addition to wave loading. Figure 1 show a schematic representation of how ABAQUS, FAST and TurbSim are combined to model the dynamic behavior of a wind turbine system.

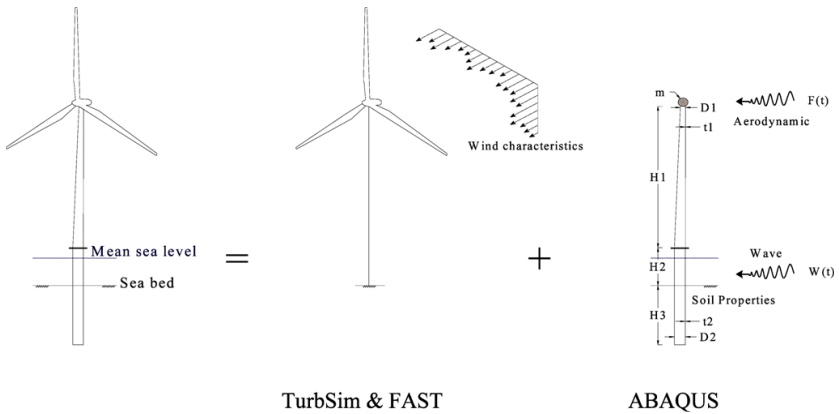


Figure 1. Typical offshore wind turbine support structure configuration

PROBABILISTIC DEMAND MODEL

A probabilistic demand model is a mathematical expression that relates the demand on a structural component to a set of measurable variables such as material properties, structural dimensions and boundary conditions. Ideally a model should incorporate all the available sources of information including the rules of physics and mechanics, and experimental and field data when they are available. Following Gardoni et al. (2002, 2003), we develop a probabilistic demand model by adding a correction term to a selected existing deterministic demand model. The proposed demand model for given material properties, structural dimensions, and boundary conditions, x , and for a given wind and wave loading, w , can be formulated as

$$D(x, w, \theta) = \hat{d}(x, w) + \gamma(x, w, \theta) + \sigma \varepsilon \tag{3}$$

where $D(x, w, \theta)$ = probabilistic demand model, $w = (w_1, w_2)$, w_1 = mean wind speed, w_2 = significant wave height, $\theta = (\theta, \sigma)$, θ = vector of unknown model parameters, $\hat{d}(x, w)$ = selected deterministic demand model, $\gamma(x, w, \theta)$ = correction term for the bias inherent in the deterministic model, $\sigma \varepsilon$ = model error, ε = random variable with zero mean and unit variance, and σ = standard deviation of the model error. In formulating a model, we employ a logarithmic transformation of the data to satisfy the homoskedasticity assumption (the model variance is constant), the normality

assumption (ε has the normal distribution), and the additive form used in Eq. (3).

The correction term, $\gamma(x, w, \theta)$, is added to incorporate the missing terms in the deterministic model into the developed demand models and to correct for the potential bias in $\hat{d}(x, w)$, and it is written as

$$\gamma(x, \theta) = \sum_{i=1}^q \theta_i h_i(x, w) \tag{4}$$

where $\theta = [\theta_i]$, and $h_i(x, w)$ = normalized explanatory functions that are significant in correcting $\hat{d}(x, w)$. The model parameters, $\theta = (\theta, \sigma)$, are estimated by the Bayesian updating method using the virtual data generated in the previous section.

Deterministic demand model. An ideal deterministic model for predicting the demand on the support structure is simple and yet accurate in estimating the displacement at the top of the tower. In the present study, we use computer program FAST as the simulation tool for modeling wind turbine and estimating the deformation demand on the support structure. FAST is selected because it is most commonly used in practice for the design of wind turbines.

Model correction. Correction term, $\gamma(x, w, \theta)$, is intended to correct for the bias inherent in the deterministic model. The main limitation of selected deterministic model is that it models the tower as a cantilever beam fixed at the ground level, so it does not account for the stiffness of foundation. This limitation guides us to define $\gamma(x, w, \theta)$. We select $h_1(x, w) = 1$, to capture potential constant bias in the model that is independent of the variables. The term $h_2(x, w) = \hat{d}(x, w)$ captures any possible under- or over-estimation of the deterministic model. As mentioned in the previous section, the deterministic model ignores the stiffness of the foundation. So we select $h_3(x, w) = \log[(\delta_p + \alpha_p H_h) / H_h]$ where H_h is the hub height and δ_p and α_p are the displacement and rotation at the pile head from p-y method, respectively.

With the definition of the correction terms, Eq. (3) can be rewritten as

$$D(x, w, \theta) = \theta_1 + (1 + \theta_2) \hat{d}(x, w) + \theta_3 \log[(\delta_p + \alpha_p H_h) / H_h] + \sigma \varepsilon \tag{5}$$

Considering $(1 + \theta_2)$ as a parameter, Eq. (5) can be written in a matrix format

$$D(x, w, \theta) = H\theta + \sigma \varepsilon \tag{6}$$

where $H = n \times k$ matrix of known regressors or explanatory functions, n = number of observations, k = number of parameters, and $\theta = k \times 1$ vector of unknown model parameters. A Bayesian updating method is used to estimate the model parameters. Having no prior information about the model parameters, we select a noninformative prior. Following Box and Tiao (1992), the marginal posterior distribution of σ^2 is in the inverse chi-square distribution, with mean and variance of $vs^2 / (v - 2)$ and $2v^2 s^4 / [(v - 2)^2 (v - 4)]$, respectively. The marginal distribution of θ is the multivariate t distribution, where $\hat{\theta} = (H'H)^{-1} H'E$ is the mode and median of θ and its covariance matrix is $vs^2 (H'H)^{-1} / (v - 2)$, where $s^2 = (1/v)(E - \hat{E})'(E - \hat{E})$, $v = n - k$, $\hat{E} = H\hat{\theta}$. Table 1 shows the posterior statistics of developed model parameters. Also Fig. 2 shows a

comparison between measured and predicted drift demand based on deterministic and probabilistic models.

Table 1. Posterior statistics of parameters in demand model

Parameter	Mean	Standard deviation	Correlation Coefficient		
			θ_1	θ_2	θ_3
θ_1	1.341	0.525	1	-0.43	0.82
θ_2	-0.359	0.101	-0.43	1	-0.86
θ_3	0.367	0.121	0.82	-0.86	1
σ^2	0.139	0.046			

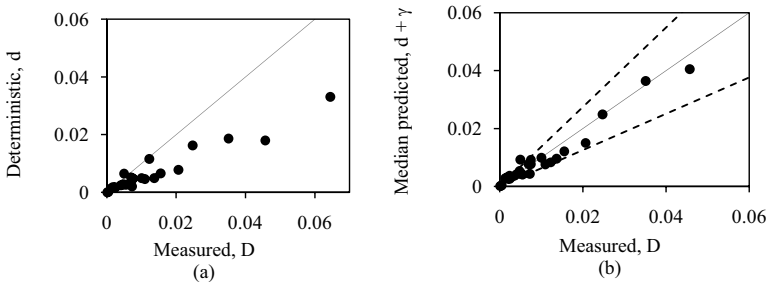


Figure 2. Comparison between measured and predicted drift demand based on a) deterministic and b) probabilistic models

FRAGILITY ESTIMATE

In this paper, fragility is defined as the probability that the deformation demand exceeds a deformation threshold c for given wind and wave conditions. We estimate the fragility of an example support structure using the developed probabilistic demand model. Following the conventional notation in structural reliability theory (Ditlevsen and Madsen, 1996), the fragility of the support structure, $F(w, \theta)$, will be defined as

$$F(w, \theta) = P[g(x, w, \theta) \leq 0 | w] \tag{7}$$

where $g(x, w, \theta)$ = a mathematical model describing the limit state for the corresponding "failure" mode of the support structure. The limit state function is defined as

$$g(x, w, \theta) = C - D(x, w, \theta) \tag{8}$$

where $D(x, w, \theta)$ is obtained from Eq. (3).

We consider different performance level criteria for displacement at the top of the tower as deterministic capacity model. Displacement threshold for the tower top is the maximum displacement, exceeding which may cause a temporary shutdown of the turbine, different damage levels or even collapse of the support structure. Since, these criteria are different for each wind turbine and usually determined by the manufacturer bases on the characteristics of the rotor mounted at the top of the

support structure, the fragility estimates are parameterized with respect to c . Fig. 3 shows how the fragility changes with respect to the wind or wave load and c .

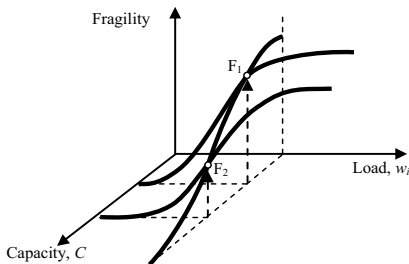


Figure 3. Schematic diagram for the fragility of wind turbine

Approximate Point Estimate of the Fragility. Assume that ε is the most important random variable in Eq. (3), we can estimate the fragility by considering a point estimate of the other variables. This assumption enables us to write the following approximate-form of the fragility:

$$\begin{aligned} \hat{F}(\mathbf{w}) &= F(\mathbf{w}, \hat{\theta}) = P[g(\mathbf{x}, \mathbf{w}, \hat{\theta}) \leq 0 | \mathbf{w}, \hat{\theta}] \\ &= P\left[\{C - D(\mathbf{x}, \mathbf{w})\} \leq 0 | \mathbf{w}, \hat{\theta}\right] \\ &= \Phi\left(-\frac{C - D(\mathbf{x}, \mathbf{w})}{\hat{\sigma}}\right) \end{aligned} \tag{9}$$

where $\hat{\theta}$ = point estimate of parameters. Fig. 4 shows the estimation of fragility for an example wind turbine based on Eq. (9). Properties of the example support structure are presented in Table 2.

Table 2. Properties of the example support structure

Rotor diameter (m)	100.0	Pile Diameter (m)	5.3	E_s (Pa)	1.94E+08
Hub Height (m)	99.0	Pile Penetration (m)	23.0	C_s (Pa)	127400
				ϕ_s (deg)	14.9

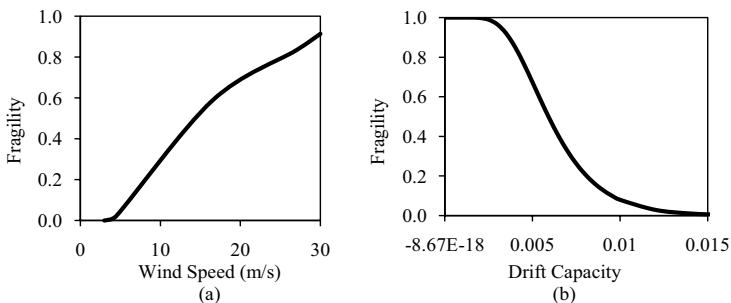


Figure 4. Fragility estimate of an offshore wind turbine for a) a drift capacity of 0.5% and b) a wind speed equal to 21 m/s.

CONCLUSIONS

This paper developed a probabilistic model for the deformation demand in the support structure of wind turbines. In order to facilitate its use in practice, the probabilistic model was constructed by adding a correction term to an existing deterministic model commonly used for the design of wind turbines. The correction term and the model errors were assessed using data obtained from detailed three dimensional nonlinear finite element analyses of wind turbine systems that considered the dynamics soil-structure interaction. The proposed probabilistic demand model is then used to assess the fragility of an example off-shore wind turbine subject to wind and wave loading. The proposed model can be used for the reliability-based optimal design of wind turbines.

REFERENCES

- Box, G.E.P., Tiao, G.C. (1992). *Bayesian Inference in Statistical Analysis*, Wiley, New York.
- Dean, R.G., Dalrymple, R.A. (1991). *Water Wave Mechanics for Engineers and Scientists*, World Scientific.
- Ditlevsen, O., and Madsen, H. O. (1996). *Structural reliability methods*, Wiley, New York.
- DNV/Riso (2002). *Guidelines for Design of Wind Turbines*, 2nd Edition, Det Norske Veritas and Wind Energy Department, Risø National Laboratory.
- Jonkman, J.M., and Buhl Jr., M.L. (2005) "FAST User's Guide." *Technical Report NREL/EL-500-38230*, National Renewable Energy Laboratory, Golden, CO.
- Jonkman, B.J. (2009). "TurbSim User's Guide." Revised August 26, 2009 for Version 1.50. *Technical Report NREL/TP-500-46198*, National Renewable Energy Laboratory, Golden, CO.
- Gardoni, P., Der Kiureghian, A., Mosalam, K.M. (2002). "Probabilistic Capacity Models and Fragility Estimates for RC Columns Based on Experimental Observations." *J. Engrg. Mech.*, ASCE, 128(10), 1024-1038.
- Gardoni, P., Mosalam, K.M., Der Kiureghian, A. (2003). "Probabilistic Seismic Demand Models and Fragility Estimates for RC Columns." *Journal of Earthquake Engineering*, 7(1), 79-106.
- Mardfekri, M., Gardoni, P., Roesset, J.M. (2010) "Modeling Laterally Loaded Single Piles Accounting for Soil-Pile Interactions." *J. Engrg. Mech.*, ASCE (Submitted).
- Matlock, H. (1970). "Correlations for design of laterally loaded piles in soft clay." *Proc., 2nd Annu. Offshore Technol. Conf.*, Paper 1204, 1, 577-588.
- McKay, M.D., Conover, W.J., and Beckman, R.J. (1979). "A comparison of three methods for selecting values of input variables in the analysis of output from a computer code", *Technometrics*, 22(2), 239-245.
- Reese L.C., Wang S.T. (2008). "Design of Foundations for a Wind Turbine Employing Modern Principles." *From research to practice in geotechnical engineering*, 351-365.
- Reese, L.C., Cox, W.R., Koop, F.D. (1975). "Field Testing and Analysis of Laterally Loaded Piles in Stiff Clay." *Proc., 7th Annu. Offshore Technol. Conf.*, Paper 2312, 2, 671-690.
- Simpson, T.W., Lin, D.K.J., and Chen, W. (2001), "Sampling strategies for computer experiments: design and analysis", *International Journal of Reliability and Application*, 2(3), 209-240
- Walford C.A. (2006). "Wind Turbine Reliability: Understanding and Minimizing Wind Turbine Operation and Maintenance Costs." Report Number SAND2006-1100, *Sandia National Laboratories*, Albuquerque, NM 87185 and Livermore, CA 94550.
- http://www.mscsoftware.com/press/press.cfm?pid=1093&Div_id=1

The Use of Aerodynamic and Wind Climatological Databases for High-Rise Reinforced Concrete Structure Design

DongHun Yeo

Engineering Laboratory, National Institute of Standards and Technology, 100 Bureau Dr., Gaithersburg, MD 20899-8611; PH (301) 975-8103; FAX (301) 869-6275; email: donghun.yeo@nist.gov

ABSTRACT

Structural response due to directional wind must be taken into account rigorously and transparently in wind resistant design, particularly for tall buildings. A database-assisted design (DAD) technique makes it possible to account for directional effects on the structural design of tall buildings. To this end, DAD employs a climatological database consisting of the directional wind speeds at a meteorological station relevant to the building site, an aerodynamic database of the pressure coefficient time histories at large numbers of taps on the exterior building surface, and a micrometeorological data set consisting of the ratio of wind speeds at the standard elevation at that site to the mean hourly wind speeds at the top of the building. This study describes the application of the DAD methodology to the design of a 60-story reinforced concrete high-rise structure using the aerodynamic and wind climatological databases. The DAD procedure provides wind-induced responses with any mean recurrence interval, including demand-to-capacity indexes, inter-story drifts, and top-floor accelerations, and compares their compliance with design criteria.

Keywords: Database-Assisted Design (DAD); climatological database; mean recurrence interval; reinforced concrete; wind effects.

INTRODUCTION

Extreme wind speeds, aerodynamic pressures, and the dynamic response of tall buildings are functions of wind direction. The directional dependence must be taken into account clearly and rigorously in the wind resistant design of tall buildings. The database-assisted design (DAD) technique makes it possible to account for the directional effects on the structural design of tall buildings by employing (1) a directional database of the wind speeds at a meteorological station relevant to the building site (i.e., a wind climatological data set, containing, for a large number of storm events, the respective directional wind speeds; the dataset can be developed by Monte Carlo simulation, from smaller datasets of measured wind speeds), (2) a directional database of the pressure coefficient time histories at a sufficiently large number of ports on the exterior building surface, and (3) a micrometeorological data set obtained in the wind tunnel and consisting of the ratio between the directional

mean hourly wind speeds at the elevation of the top of the building and the corresponding directional 3-s or 10-min wind speeds at the standard elevation (typically 10 m) of the meteorological site.

Once the databases (1) and (2) and the data set (3) are made available by the wind engineering consultant, the structural engineer can independently perform the requisite structural calculations and design. The clear division of tasks between the wind engineer and the structural engineer has the advantage of transparency and accountability, in the sense that the wind loading information inherent in the data of (1), (2), and (3) is clearly defined and recorded. If the quality of the wind speed record at the location of concern is relatively unsatisfactory, as can be the case in areas where wind speed data have not been collected over sufficiently long time periods, the assumptions used to develop the requisite wind climatological database (1) must be clearly stated. This provides a basis for developing, via accepted structural reliability techniques, more realistic uncertainty estimates for the response calculations than would be the case if standard safety margins (load factors) or mean recurrence intervals of the wind effects were simply taken from standard provisions developed for ordinary structures under reasonably well known wind climatological conditions. The DAD procedure is illustrated in the paper with reference to a building with reinforced concrete frames.

OVERVIEW OF DAD PROCEDURE

The DAD approach to high-rise buildings is represented in Figure 1. The processes within the box constitute the main algorithm of the High-Rise Database-Assisted Design for Reinforced Concrete structures (HR_DAD_RC) software (Yeo 2010). The DAD procedure is described as follows.

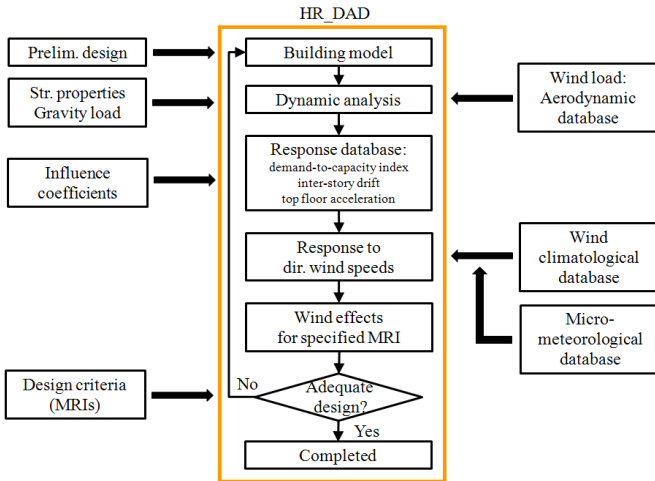


Figure 1. Basic algorithm for HR_DAD

Preliminary design

A preliminary design, performed by the structural engineer, provides *an initial set of structural properties* including building member dimensions. The fundamental natural frequencies of vibration for the preliminary design can be obtained by modal analysis using a finite elements analysis program. The damping ratios are specified by the structural engineer.

Dynamic analysis

Dynamic analyses of the building with the member dimensions determined in the preliminary design employ combinations of wind and gravity loads specified in the ASCE 7-10 Standard (hereinafter ASCE 7-10), Section 2.3 (ASCE 2010). The wind loads in DAD are calculated from the aerodynamic database for each given wind direction. The pressure time histories can be obtained from wind tunnel tests or, in principle, from CFD simulations.

The dynamic analyses are performed by considering the resultant of the wind forces at each floor's mass center, for each wind direction and for reference mean hourly wind speeds at the top of the building of, for example, 20 m/s, 30 m/s, ..., 80 m/s, depending upon the wind speed range of interest at the building location. The directional wind forces acting on each floor are calculated from directional aerodynamic pressures database provided by the wind engineering consultant. The outputs of this phase are the *floor displacements, floor accelerations, and effective (aerodynamic plus inertial) lateral forces at each floor corresponding to the specified set of directional reference wind speeds.*

Influence coefficients for determining internal forces

For each direction and specified wind speed, a time series of internal forces in members were calculated using the effective lateral forces at floor mass centers multiplied by the *influence coefficients* that yield the internal forces due to a unit load with specified direction acting at the mass center of any floor.

Response database

Peak wind effects of demand-to-capacity indexes, inter-story drifts, and top-floor accelerations can be obtained from: time series of internal forces due to wind and gravity loads; floor displacements; and floor accelerations. Using interpolation techniques the structural response can be obtained for any specific wind direction and speed within the specified ranges. The response database is a property of the structure that incorporates its aerodynamic and mechanical characteristics and is independent of the wind climate.

Wind climatological database

A *wind climatological database*, developed by wind engineers, is a matrix of directional wind speeds at 10 m above ground in open exposure, and is developed for a location close to the building of interest. Each row of the matrix corresponds to one

storm event (if a peaks-over-threshold estimation procedure is used) or to the largest yearly speed (if an epochal estimation procedure is used). The columns of the matrix correspond to the specified wind directions. For hurricane winds, a similar matrix of wind speeds is used. Using micro-meteorological relations, reference wind speeds in the wind climatological database are converted to mean hourly wind speeds at the elevation of the top of the building.

Peak directional response

For each direction of each storm event (or year), the peak response of interest is calculated by interpolation from the response database. From a design viewpoint, however, only the largest peak response is retained for each storm event (or year). A vector of the maximum response induced by each storm event is thus created, and its dimension is equal to the number of storm events in the wind climatological database.

Peak wind effects with specified MRIs

The time series of peak wind effects induced by each storm event in the wind climatological database is used to obtain the requisite peak wind effect with the specified MRI. The time series is rank-ordered, the largest wind effect having rank one, and the non-parametric estimation method described in Sect. 2.4.3.2.2 of Simiu and Miyata (2006) can be employed. Note that the estimated peak responses with specified mean recurrence intervals are obtained for wind load effects, not for wind loads.

Based on the assumption that the occurrence of storm events is a Poisson process with constant occurrence rate, the estimated MRI \overline{N}_k associated with k^{th} ranked peak wind effects is

$$\overline{N}_k = \frac{n+1}{vk} \quad (1)$$

where n is total number of storm events in the database. Interpolation is used where necessary.

Adjustment of demand-to-capacity indexes

According to ASCE 7-10, Section 31.4.3, it is prudent for estimates based on the wind tunnel method to be not less than 80 % of the corresponding estimates based on the ASCE 7 analytical method using directional or envelope procedure. For practical reasons this requirement applies to estimates of peak overturning moments in the principal axes with MRIs specified in the Standard. If DAD-based overturning moments do not satisfy this requirement the demand-to-capacity index is adjusted as:

$$B_{ij}^* = \gamma B_{ij} \quad (2)$$

$$\gamma = \frac{0.8}{M_o^{DAD} / M_o^{ASCE7}}$$

where M_o^{DAD} and M_o^{ASCE7} are the overturning moments at base obtained from DAD and ASCE 7-10, respectively, and γ is the index adjustment factor.

Compliance with design criteria

Once peak responses (i.e., demand-to-capacity index, inter-story drift, and acceleration) for specified MRIs are obtained, DAD verifies if the peak responses satisfy design criteria for safety and serviceability. The procedure outlined in Figure 1 is repeated as needed with a modified structural design (e.g., by re-sizing members or by installing dampers) until the results satisfy the design criteria.

Structural responses considered in design

The DAD methodology for safety and serviceability of a RC structure satisfies design specifications in the Building Code Requirements for Structural Concrete and Commentary 318-08 (hereinafter ACI 318-08) and ASCE 7-10 Standards. The responses considered are the demand-to-capacity index, the inter-story drift, and accelerations at the top floor.

Demand-to-capacity indexes

A demand-to-capacity index (DCI) is a quantity used to measure the adequacy of a structural member's strength. In general, this index is defined as a ratio or sum of ratios of the internal force induced by design loads to associated strength provided by the section. An index higher than unity indicates inadequate design of a structural member. For reinforced concrete two demand-to-capacity indexes are of interest: B_{ij}^{PM} for axial and/or flexural loads, and B_{ij}^{VT} for shear and torsion. The index B_{ij}^{PM} pertains to the interaction of axial and/or flexural loads for columns and beams:

$$\begin{aligned} B_{ij}^{PM} &= \frac{M_u}{\phi_m M_n} && \text{(for a tension-controlled section)} \\ &= \frac{P_u}{\phi_p P_n} && \text{(for a compression-controlled section)} \end{aligned} \quad (3)$$

where M_u and P_u are the factored bending moment and axial force at the section, M_n and P_n are the nominal moment and axial strengths at the section, and ϕ_m and ϕ_p are the reduction factors for flexural and axial strengths, respectively. In particular, for columns subject to bi-axial flexure loads, the Bresler reciprocal load method of R10.3.6 in ACI 318-08 (2008) is used for compression-controlled sections, and the PCA (Portland Cement Association) load contour method (PCA 2008) is used for tension-controlled sections.

The index " B_{ij}^{VT} " is associated with interaction equations for shear forces and torsional moment for columns and beams:

$$B_{ij}^{VT} = \frac{\sqrt{V_{ux}^2 + V_{uy}^2 + \left(\frac{T_u p_h b_w d}{1.7 A_{oh}^2}\right)^2}}{\phi_v (V_c + V_s)} \quad (4)$$

where V_c and V_s are the nominal shear strengths provided by concrete and by reinforcement, respectively, V_{ux} and V_{uy} are the shear forces in the x and y axes, respectively. T_u is the torsional moment, ϕ_v is the reduction factors for shear strengths, p_h is the perimeter enclosed by the centerline of the outermost closed stirrups, A_{oh} is the area enclosed by the centerline of the outermost closed stirrups, b_w is the width of the member, and d is the distance from extreme compression fiber to the centroid of longitudinal tension reinforcement.

Inter-story drift

A time series of the x -axis inter-story drift ratios at the i^{th} story, $d_{i,x}$ is

$$d_{i,x}(t) = \frac{[x_i(t) - D_{i,y} \theta_i(t)] - [x_{i-1}(t) - D_{i-1,y} \theta_{i-1}(t)]}{h_i} \quad (5)$$

where $x_i(t)$ and $\theta_i(t)$ are the displacement and rotation at the mass center at the i^{th} floor, $D_{i,x}$ is the distance along the x axis from the mass center on the i^{th} floor to the point of interest on that floor, and h_i is the i^{th} story height between mass centers of the i^{th} and the $(i-1)^{\text{th}}$ floor. A similar expression holds for the y -direction.

The ASCE 7-10 Commentary suggests limits on the order of 1/600 to 1/400 (see Appendix CC.1.2 in ASCE 7-10).

Top floor acceleration

A time series of resultant acceleration at the top floor, $a_r(t)$ is

$$a_r(t) = \sqrt{[\ddot{x}_{top}(t) - D_{top,y} \ddot{\theta}_{top}(t)]^2 + [\ddot{y}_{top}(t) + D_{top,x} \ddot{\theta}_{top}(t)]^2} \quad (6)$$

where accelerations $\ddot{x}_{top}(t)$, $\ddot{y}_{top}(t)$, and $\ddot{\theta}_{top}(t)$ of the mass center at the top floor pertain to the x , y , and θ (i.e., rotational) axes, and $D_{top,x}$ and $D_{top,y}$ are the distances along the x and y axes from the mass center to the point of interest on the top floor.

The resultant value of Eq. (6) is used, rather than accelerations along the principal axes, because peak acceleration is of concern for human discomfort regardless of its direction. While ASCE 7-10 does not provide wind-related peak acceleration limits, for office buildings a limit of 25 mg with a 10-year MRI was suggested by Isyumov et al. (1992) and Kareem et al. (1999).

APPLICATION AND RESULTS

A 60-story reinforced concrete building with rigid diaphragm floors in this study has dimensions 45.72 m in width, 30.48 m in depth, and 182.88 m in height and known as the Commonwealth Advisory Aeronautical Research Council (CAARC) building.. It

has a moment-resistant frame structural system consisting of 2880 columns and 4920 beams, and is similar to the structural

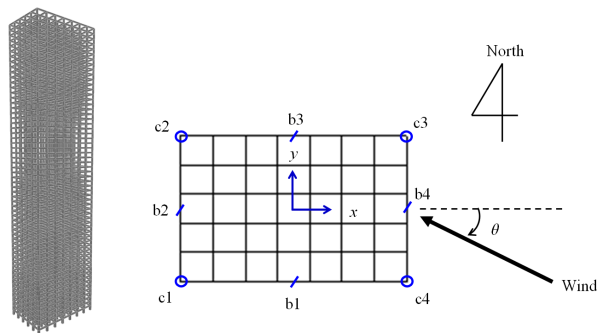


Figure 2. Schematic and plan views of a building

system studied by Teshigawara (2001). The building was assumed to be located near Miami, Florida and to have suburban exposure. The long side of the building was assumed to be normal to the South-North direction. The damping ratio was assumed to be 2 % in all three modes. The building is categorized as Occupancy Category III, whose design MRI is 1700 years.

To illustrate the estimation of structural wind effects on the CAARC building we used synchronous pressure time histories at a total of 120 pressure taps obtained at the Prato (Italy) Inter-University Research Centre on Building Aerodynamics and Wind Engineering (CRIACIV-DIC) Boundary Layer Wind Tunnel. The model scale was 1:500, and the sampling frequency was 250 Hz. The reference model mean wind speed was 23.2 m/s at the top of the building.

For strength design, demand-to-capacity indexes (DCIs) corresponding to mean recurrence intervals (MRI) were obtained for structural members of the building. Figure 2(a) shows the DCIs for the corner column c1 with respect to MRIs. Because ratios of peak overturning moments based on DAD and on ASCE 7 are less than 0.8 for MRI = 1700 years, and the corresponding DCIs are adjusted by multiplying the original indexes by adjustment coefficients γ of 1.19. For the corner columns, DCIs for axial force and bending moments interaction (B_{ij}^{PM}) were 0.95 to 1.00. The DCIs for the shear force and torsional moment interaction (B_{ij}^{TT}) were 0.44 to 0.73. For the spandrel beams, B_{ij}^{PM} ranged from 0.44 to 0.74 and B_{ij}^{TT} were from 0.32 to 0.53.

For serviceability design, DAD provided inter-story drifts along column lines and top-floor accelerations. Figures 2(b and c) show inter-story drift ratios of a corner at the 44th floor and accelerations of a corner at the top floor with respect to MRIs. The largest inter-story drift (i.e., y -direction drift in this study) was $d_{i,y} = 0.0029$ for MRI = 20 years on the four corners at the 44th floor, which is larger than $1/400 = 0.0025$. The top-floor peak resultant accelerations were the largest values being 27.9

mg (i.e., milli-gravitational acceleration) for MRI = 10 years, rather than 25 mg. The design is seen to be governed by serviceability constraints.

DAD's efficiency in determining building response corresponding to various set of simulated pressure time histories makes it possible to assess the significance of the various parameters that determine the response and of uncertainties in those parameters.

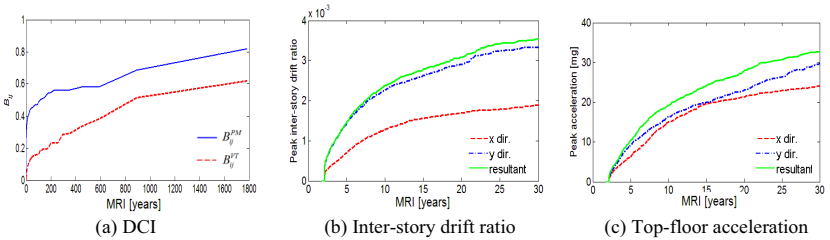


Figure 3. MRI-based peak wind effects

CONCLUSIONS

This paper presented the development of a Database-Assisted Design (DAD) procedure for reinforced concrete buildings, and its application to a 60-story building. The DAD procedure performs dynamic analyses using simultaneous time-series of aerodynamic pressure data and establishes response databases of wind effects for a sufficiently wide range of wind speeds and for a sufficiently large number of wind directions. Response The databases depend on the building's aerodynamic, geometric, structural, and dynamical features, and are independent of the wind climate. DAD appropriately accounts for wind directionality using: wind climatological data that may need to be augmented by simulation (for the description of a procedure for developing augmented wind speed data sets see Yeo 2011); aerodynamic data; and micro-meteorological data. Estimated peak responses obtained from DAD are estimated for the requisite mean recurrence intervals. This requires that the estimates be performed in the wind effects space.

The procedure was illustrated through its application to a specific design of the CAARC building. The design approach presented in this paper provides more accurate and clearer predictions of wind effects than conventional approaches, and is expected to be more economical and efficient when used in conjunction with optimization. Software for implementing the DAD procedure used in this study is available on www.nist.gov/wind.

ACKNOWLEDGEMENTS

The author would like to thank Dr. Emil Simiu for valuable advice and comments, and acknowledges with thanks the previous development of HR_DAD software by

Mihai Iancovici, William P. Fritz, René D. Gabbai, and Seymour M.J. Spence at the NIST. The wind tunnel data developed were kindly provided by Dr. Ilaria Venanzi of the University of Perugia.

REFERENCES

- ACI. (2008). *Building code requirements for structural concrete (ACI 318-08) and commentary*, American Concrete Institute, Farmington Hills, MI.
- ASCE. (2010). *Minimum design loads for buildings and other structures*, American Society of Civil Engineers, Reston, VA.
- Isumov, N., Fediw, A. A., Colaco, J., and Banavalkar, P. V. (1992). "Performance of a tall building under wind action." *Journal of Wind Engineering and Industrial Aerodynamics*, 42(1-3), 1053-1064.
- Kareem, A., Kijewski, T., and Tamura, Y. (1999). "Mitigation of motions of tall buildings with specific examples of recent applications." *Wind and Structures*, 2(3), 201-251.
- PCA. (2008). *PCA notes on 318-08 building code requirements for structural concrete with design applications*, Portland Cement Association, Skokie, IL.
- Simiu, E., and Miyata, T. (2006). *Design of buildings and bridges for wind: a practical guide for ASCE-7 Standard users and designers of special structures*, John Wiley & Sons, Hoboken, NJ.
- Teshigawara, M. (2001). "Structural design principles (chapter 6)." *Design of modern highrise reinforced concrete structures*, H. Aoyama, ed., Imperial College Press, London.
- Yeo, D. (2010). "Database-Assisted Design of high-rise reinforced concrete structures for wind: Concepts, software, and application." *NIST Technical Note 1665*, National Institute of Standards and Technology, Gaithersburg, MD.
- Yeo, D. (2011). "Development of large directional wind speed databases." This conference.

Development of Large Directional Wind Speed Databases

DongHun Yeo

Engineering Laboratory, National Institute of Standards and Technology, 100 Bureau Dr., Gaithersburg, MD 20899-8611; PH (301) 975-8103; FAX (301) 869-6275; email: donghun.yeo@nist.gov

ABSTRACT

For structures sensitive to wind directionality, methods for the estimation of wind effects require the use of time series of directional wind speeds with length exceeding the length of the MRIs of interest. This study proposes a procedure for generating such time series from relatively short synoptic wind data sets. The focus in this paper is on the estimation of the parameters of a probabilistic model of the wind speeds and on errors in the estimation. The wind speed data being generated can be used in the Database-Assisted Design approach to account for directional wind effects.

INTRODUCTION

Inherent in the ASCE 7 Standard (ASCE 2010) wind loading provisions are approximations that may be acceptable for the design of ordinary structures but are deemed unacceptable for the design of special structures, including in particular tall buildings. Among these approximations are those inherent in the use by ASCE 7 Standard of a blanket wind directionality factor. For special structures wind engineering laboratories use more elaborate methods for accounting for directionality effects. In particular, methods that determine wind effects corresponding to specified MRIs by using non-parametric statistical approaches require the use of time series of directional wind speeds that are longer than those MRIs. Hence it is necessary to use simulation techniques to develop long time series of synthetic directional wind speeds from smaller data sets.

The design MRIs of wind effects for wind loads specified in ASCE 7 Standard are 300 years, 700 years, and 1700 years, depending upon the structure's risk category. If design wind speeds are specified regardless of their direction, as is the case for the ASCE 7 Standard, the MRI of the design wind speeds and the MRI of the design wind effects are the same. This is typically not the case if directional wind speeds are used in design.

The procedure used in this study involves three steps. First, probabilistic models are fitted to the directional wind speeds. Second, the fitted models are used to generate by Monte Carlo simulation synthetic directional wind speed records that have any desired length. Third, the uncertainty in the generated wind speeds is assessed. The procedure proposed in the paper yields simple and transparent probabilistic estimates of directional wind speeds for use in structural design.

MODEL OF DIRECTIONAL WIND SPEEDS

This study proposes a probabilistic model for synoptic winds based on (1) a Poisson process representing the arrival of extreme wind events and (2) a translation vector defining directional wind speeds, consisting of a nonlinear transformation of a direction-dimensional Gaussian vector. In this study we make use of the methodology developed by Grigoriu (2009), which is summarized herein.

Let \mathbf{T} be a sequential time series of the extreme wind events. The element T_k describes the time of the k^{th} extreme wind event in the time sequence ($k = 1, 2, \dots, n$, where n is the number of extreme wind events being considered). If it is assumed that the random times T_k are the jump times of a homogeneous Poisson process $N(t)$ ($t > 0$) of intensity $\lambda > 0$, the average number of the extreme wind events during a time $t > 0$ is equal to the expectation $E[N(t)] = \lambda t$ of $N(t)$, where the intensity λ is the rate of arrival of the extreme wind events. The arrival rate of extreme wind events is simply modeled by a homogeneous Poisson processes with mean rate inferred from observations. For example, if the observed number of wind events at a site during a 30-year period is 66, then the estimated rate of arrival is $\lambda = 2.2 \text{ year}^{-1}$.

Suppose that a matrix of synoptic wind speeds \mathbf{V} has n rows and d columns, where n is the number of extreme wind events and d is the direction of the synoptic winds. The element $V_i^{(k)}$ describes the wind speed recorded in the i^{th} direction during the k^{th} wind event ($i = 1, 2, \dots, d$ and $k = 1, 2, \dots, n$) at time T_k . If it is assumed that the wind speed vectors $\mathbf{V}^{(k)}$ representing the extreme wind events are independent vectors of a d -dimensional random vector \mathbf{V} with joint distribution F , the proposed model can be characterized by (1) the intensity λ of the Poisson model N and (2) the distribution of \mathbf{V} . While the estimation of λ of the Poisson process N is simple, the selection of the joint distribution of F of \mathbf{V} is much more complicated because there are no general models for arbitrary non-Gaussian joint distributions. In this study, we assume that \mathbf{V} is a translation vector that accounts in an approximate manner for the correlation between directional wind speeds.

Suppose the components V_i of the directional wind speeds in extreme wind events are defined as follows:

$$V_i = F_i^{-1}[\Phi(G_i)] \quad \text{for } i = 1, 2, \dots, d \quad (1)$$

where F_i denotes the distribution of the i^{th} direction wind speed vector V_i , Φ denotes the i^{th} direction distribution of the standard Gaussian variable with mean 0 and variance 1, G_i is the i^{th} direction correlated standard Gaussian variable with covariance matrix $\rho_{ij} = E[G_i, G_j]$ where $i, j = 1, \dots, d$, and E denotes expectation. Equation 1 establishes a one-to-one correspondence between the wind speed matrix \mathbf{V} and the Gaussian matrix \mathbf{G} . For synoptic winds, however, the available data is typically not sufficient for the estimation of the correlation between directional wind speeds. For this reason it is assumed in this study that directional wind speeds are independent of each other. This assumption is conservative from a structural design viewpoint, as is shown in the paper.

MODEL CALIBRATION

To calibrate the probabilistic model for \mathbf{V} , we estimate the marginal distributions F_i of the directional wind speeds V_i . Since numerous directional wind speed data are

considered as zero when they are not above a threshold u , the distribution F_i of a random variable \mathbf{V} is defined as:

$$F_i(v) = q_i + (1 - q_i)1(v > u)\tilde{F}_i(v) \quad \text{for } i = 1, 2, \dots, d \tag{2}$$

where $1(A)$ denotes the indicator of set A and is equal to 1 and 0 when A is true and false, respectively, q_i is the probability $P(V_i \leq u)$ that V_i is less than or equal to the threshold wind speed u in the i^{th} directional wind speed vector, and $\tilde{F}_i(v)$ is a proper distribution expressing the wind speeds of V_i above the threshold.

We assume that the distribution $\tilde{F}_i(v)$ of a random variable \mathbf{V} is the generalized Pareto distribution (GPD) with parameters (c_i, a_i, u_i) , where c_i is the shape (i.e., tail length) parameter, a_i is the scale parameter, and u_i is the location (i.e., threshold) parameter, in the i^{th} direction (the GPD is an appropriate model for the exceedances over a suitable threshold of extreme value variates; see Galambos et al. 1994). The cumulative distribution function of the generalized Pareto distribution is

$$\tilde{F}_i(v) = \begin{cases} 1 - \left[1 + c_i \left(\frac{v - u_i}{a_i} \right) \right]^{-1/c_i} & \text{for } c_i \neq 0 \\ 1 - \exp\left(-\frac{v - u_i}{a_i} \right) & \text{for } c_i = 0 \end{cases} \tag{3}$$

where the domain is $v \geq u_i$ for $c_i \geq 0$ and $u_i \leq v \leq u_i - a_i/c_i$ for $c_i < 0$. The density function is

$$\tilde{f}_i(v_i) = \begin{cases} \frac{1}{a_i} \left[1 + c_i \left(\frac{v - u_i}{a_i} \right) \right]^{-\left(1 + \frac{1}{c_i}\right)} & \text{for } c_i \neq 0 \\ \frac{1}{a_i} \exp\left[-\left(\frac{v - u_i}{a_i} \right) \right] & \text{for } c_i = 0. \end{cases} \tag{4}$$

In order to estimate the parameters (c_i, a_i, u_i) in the generalized Pareto distribution $\tilde{F}_i(v)$ of above-threshold wind speed data, the study employs the maximum likelihood estimation (MLE, Kotz and Nadarajah 2000) and the de Haan method (de Haan 1994).

To avoid unrealistic or unconservative modeling of non-hurricane wind speeds, we propose that if the estimated value of the GPD tail length parameter is $c_i > -0.01$, the value used in the calculations can be taken as $c_i = -0.01$ (corresponding to within a close approximation to a Gumbel distribution tail), and if the estimated value is $c_i < -0.1$, the value used in the calculations can be taken as $c_i = -0.1$, thereby avoiding distribution tails that may be unconservatively short.

GENERATION OF SYNTHETIC WIND SPEEDS

Once the probability law of the proposed directional synoptic wind speed model has been calibrated to observed wind records at a site, we can apply Monte Carlo simulations to generate directional wind speed data of any length that are consistent with the observed records.

For the generation of directional synoptic wind speeds with annual arrival rate λ over a period of τ years, the following steps are required:

(1) Generate d independent random numbers (r_1, r_2, \dots, r_d) uniformly distributed in the range of (0, 1). If the random number r_i is less than the probability q_i that wind speeds are not higher than the threshold, the generated wind speed in the i^{th} direction is zero. Otherwise, an above-threshold wind speed v is generated from Eq. (5) by another random number r'_i in (0, 1):

$$v = u_i + \frac{a_i}{c_i} \left[(r'_i)^{-c_i} - 1 \right]. \tag{5}$$

(2) Repeat step (1) $n_\tau = \lambda\tau$ times to generate a time series of directional extreme wind speeds over τ years.

ESTIMATION OF MEAN RECURRENCE INTERVALS

Consider a set of n wind speed data at a site where the mean storm arrival rate is λ year⁻¹. If the rate were $\lambda = 1$ storm/year, the estimated probability that the highest speed in the set would be exceeded is $1/(n+1)$, and the corresponding estimated MRI would be $\bar{N} = n+1$ years (Simiu and Miyata 2006). The estimated probability that the q^{th} highest speed in the set is exceeded is $q/(n+1)$, the corresponding estimated MRI in years is $\bar{N} = (n+1)/q$, and the rank of the wind speed with MRI is $q = (n+1)/\bar{N}$.

For a general case of $\lambda \neq 1$, the estimated MRI is $\bar{N} = (n+1)/(\lambda q)$ years. For example, if $n = 999$ synoptic wind speed data, and $\lambda = 0.5$ year⁻¹, the estimated MRI of the event that the highest wind speed in the sample will occur is $\bar{N} = 1000/0.5 = 2000$ years, the estimated MRI of the second highest speed is 1000 years, and so forth. The rank of the speed with a specified MRI \bar{N} is $q = (n+1)/(\lambda \bar{N})$.

The wind speed with an \bar{N} -year mean recurrence interval obtained from wind speeds above a threshold u can be estimated by the generalized Pareto distribution as follows:

$$v(\bar{N}) = u_i - \frac{a_i}{c_i} \left[1 - (\lambda_i \bar{N})^{c_i} \right]. \tag{6}$$

where λ_i is the annual occurrence rate of wind events in the i^{th} direction and can be estimated as $\lambda_i = \lambda \cdot P(V_i > u) = \lambda(1 - q_i)$, where λ is the annual occurrence rate of the wind events in all wind directions and q_i is the probability that wind speeds in the i^{th} direction are less than or equal to the threshold u , as previously explained.

ESTIMATION OF WIND EFFECTS WITH SPECIFIED MRIs

For structural design for wind, the estimation of wind effects -- rather than wind speeds -- corresponding to design MRIs, is of concern to structural engineers. This is the case because, as was mentioned earlier, owing to wind directionality effects, the MRIs of the wind effects induced by directional wind speeds typically differ from the MRIs of the corresponding wind speeds regardless of their direction.

The analytical procedure specified in the ASCE 7 Standard uses a building wind directionality factor $K_d = 0.85$ applied to the wind effect calculated by disregarding wind directionality. This approach is simple, but can either overestimate

or underestimate the response. For structures for which directional wind effects are significant alternative approaches have been developed and are currently being used in practice. Database-Assisted Design (DAD), developed by National Institute of Standards and Technology (NIST), is an integrated design tool for structural design of strength and serviceability (Spence 2009; Yeo 2010) which enables the probabilistic estimation of wind effects while accounting for wind directionality as reflected by measured or simulated wind speed data. The estimation procedure entails the following steps:

(1) Develop an $n \times d$ matrix of directional wind speeds from measured data. The number n of rows is equal to the number of storm events or of years of record, and must be sufficiently large to allow the use of non-parametric estimates of wind effects with MRIs of the order of thousands of years. The number d of columns in the matrix is equal to the number of wind directions being considered (e.g., 8, 16, or 36). The matrix of directional wind speeds at a site, called *climatological wind database*, is developed for long periods exceeding the design MRIs by probabilistic estimates. The procedure of generating synoptic winds from measured data was previously described in the paper.

(2) Transform the $n \times d$ matrix of directional wind speeds into an $n \times d$ matrix of wind effects induced by each directional storms. The wind effects in DAD include demand-to-capacity indexes for structural members, inter-story drifts, and top-floor accelerations. The detailed procedure of DAD is provided in Yeo (2010).

(3) Create a vector of dimension n consisting of the largest wind effect of interest corresponding to each row (i.e., each storm) of the wind effects matrix developed in Step 2. For each storm event only the largest of the directional responses is of interest from a structural design viewpoint and all the other responses are discarded.

(4) Use non-parametric estimates to obtain statistics of the wind effect for which the vector was created in Step 3. This vector is rank-ordered, and the peak responses corresponding to the required mean recurrence intervals are obtained using the non-parametric estimation method (Simiu and Miyata, 2006, p. 33). The peak wind effects of interest can be estimated for the respective specified MRIs.

APPLICATION

We employ the proposed probabilistic model of directional wind speeds to generate synthetic synoptic wind speed series data for large MRIs at Newark, New Jersey. For the calibration of the proposed model for directional synoptic wind speeds, we use observed data from the Automated Surface Observing System (ASOS), a network of about 20000 standardized US weather stations (NCDC 2008). The ASOS data of synoptic winds in Newark have 228 wind events in 36 directions in 10° increments, threshold wind speed of 35 knots (1 knot \approx 0.51 m/s), and measuring duration of 19.94 years. Thus, the annual rate of occurrence for the wind events is $228/19.94 \text{ year} = 11.43 \text{ year}^{-1}$.

Figure 1 shows the distribution of directional speeds of synoptic winds at Newark, NJ.

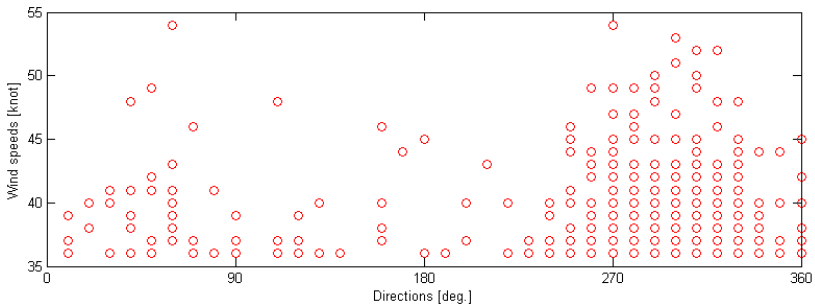


Figure 1. Directional wind speeds of synoptic winds (Newark, NJ)

Because the directional data are not sufficient to calibrate parameters of the generalized Pareto distribution in each direction, this study divides the data by 4 sectors (i.e., 10° to 90° , 100° to 180° , 190° to 270° , and 280° to 360°), and estimates the probability of wind speeds less than or equal to a threshold u , $q_i = P(V_i \leq u)$ and the parameters (c_i, a_i, u_i) for each sector by the MLE and the de Haan method. As shown in Table 1, the probability q_i (Eq. 2) significantly depends on sectors: it is 0.93 for sector 2, and 0.22 for sector 4. For the parameters of GPD, 3 sectors have estimated shape parameters c_i lower than -0.10 ; as indicated earlier, these are assumed to be -0.10 . In contrast, since for section 2 $c_i = -0.08$, this value of the parameter is used without adjustment. The scale parameters a_i are approximately 4 to 7, and the threshold u_i is 35 knots, regardless of sector.

Synthetic wind speeds for 60000 synoptic wind events in Newark, NJ have been generated in 4 sectors by Monte Carlo simulation using parameters estimated from the MLE and the de Haan method. The adjusted parameters of the sectors are used in the simulation. Estimates of parameters (c_i, a_i) and q_i are shown in Table 1. Where two numbers separated by a slash are shown in Table 1, the first and second number is estimated by the MLE and the de Haan method, respectively. The simulation has reliably generated the probabilities q_i that wind speeds are less than or equal to a threshold $u = 35$ knots. The MLE method has estimated parameters of the synthetic data that are relatively closer to those of the ASOS data than the de Haan method. Figure 2 shows empirical and fitted cumulative distribution functions (CDFs) $\hat{F}_i(x)$ of generated above-threshold wind speeds and of adjusted parameters of GPD, respectively, in sector 4 using both estimation methods.

The Monte Carlo simulation has enabled the generation of the time-series of directional synoptic wind speeds of synoptic wind speeds allowing the estimation of wind effects with MRIs of up to 5000 years. Figure 3 shows results based on the MLE and the de Haan method. For any given MRI the wind speeds are generally higher for the MLE method than for the de Haan Method.

Bootstrapping is used to assess the statistical uncertainty in the estimates of the wind speeds v_{MRI} corresponding to MRIs. Classical bootstrapping using empirical distributions to generate replicates of wind speed series is not adequate because v_{MRI} can be out of the range of the wind records and all replicates are constructed from the parameters in the range defined by the record. To overcome this limitation, we use parametric bootstrapping in which replicates are

Table 1. Parameters of the generalized Pareto distributions

	Sector 1 (10° to 90°)	Sector 2 (100° to 180°)	Sector 3 (190° to 270°)	Sector 4 (280° to 360°)
q_i	0.90	0.93	0.71	0.22
a_i	5.72 / 5.58	4.84 / 4.06	6.14 / 5.87	6.53 / 6.58
c_i	-0.15 / -0.24	-0.17 / -0.08	-0.24 / -0.31	-0.30 / -0.43
Adjusted c_i	-0.10 / -0.10	-0.10 / -0.08	-0.10 / -0.10	-0.10 / -0.10
q_i (synthetic data)	0.90	0.93	0.71	0.23
a_i (synthetic data)	5.88 / 5.04	4.76 / 3.61	6.14 / 5.11	6.58 / 5.70
c_i (synthetic data)	-0.11 / -0.10	-0.09 / -0.06	-0.10 / -0.08	-0.11 / -0.09

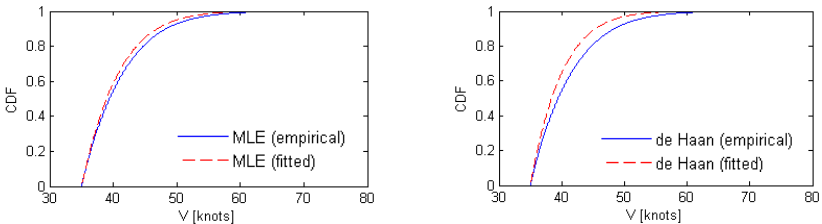


Figure 2. CDF of generated wind speeds (sector 4)

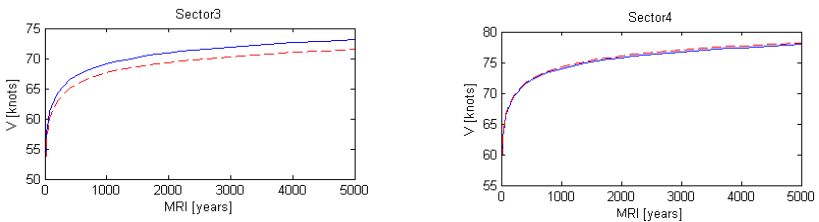


Figure 3. Generated wind speeds with MRIs (— MLE; - - - de Haan)

generated from probabilistic models for directional wind speed data calibrated to the record rather than empirical distribution given by the record. The Monte Carlo simulations are repeated 1000 times to generate 1000 replicates of the directional synoptic wind speeds at a site. Figure 4 shows the resulting scatter plot of parameter estimates in sector 4.

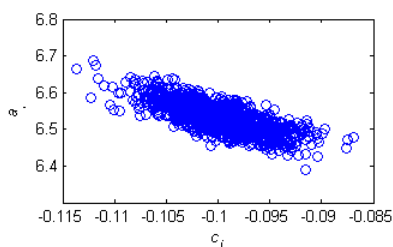


Figure 4. Realizations of estimated parameters (c_i, a_i)

Substituting the generated bootstrap sample values of (c_i, a_i) into Eq. (6) generates the corresponding bootstrap samples of directional wind speeds with any specific MRIs. Sample distributions of the wind speeds v_{MRI} are considered for 20-yr, 100-yr, 2000-yr, and 5000-yr MRIs. For sector 4 their histograms, and statistics of sample wind speeds, are plotted in Figure 5 and summarized in Table 2. The results, reported in detail in the paper, indicate that wind speeds with specified MRIs follow Gaussian distributions (Figure 5), and that the uncertainties in their estimation increase as the MRI increases (Table 2).

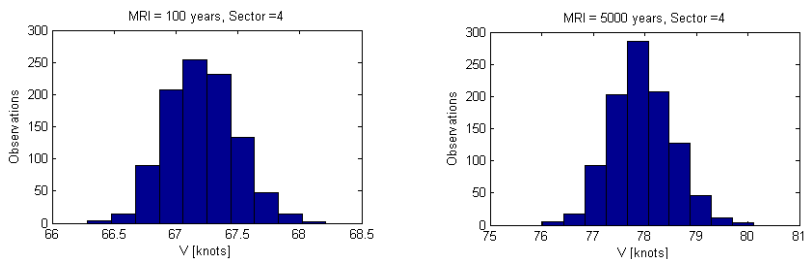


Figure 5. Bootstrap sample distributions of MRIs

Table 2. Estimates of wind speeds with MRIs [knots]

MRI [years]	Mean	Standard error	95% lower limit	95% upper limit
20	61.4	0.005	61.1	61.7
100	67.2	0.009	66.6	67.7
2000	75.8	0.016	74.7	76.7
5000	77.9	0.019	76.7	79.0

Note: Standard error is defined as σ/\sqrt{n} , where σ is the standard deviation of samples, and n is the number of samples

CONCLUSIONS

We proposed an algorithm to generate directional wind speeds of synoptic winds with large design MRIs by Monte Carlo simulations. The probability model in the study

was based on a generalized Pareto distribution with the assumption of directionally independent wind speeds. The parameters of the distribution were estimated from the ASOS data by the maximum likelihood estimation and the de Haan method. Using the Monte Carlo simulation we generated, from the probabilistic model calibrated to the data, synthetic directional wind speeds with large MRIs. Uncertainties in the estimated wind speeds were also estimated. The methodology illustrated in this study is equally applicable to hurricanes and thunderstorm wind speeds.

ACKNOWLEDGEMENTS

This work is based on a methodology developed by Professor Mircea Grigoriu of the Department of Civil and Environmental Engineering, Cornell University. The author would like to thank Dr. Emil Simiu of NIST for useful discussions.

REFERENCES

- ASCE (2010). *Minimum design loads for buildings and other structures*, American Society of Civil Engineers, Reston, VA.
- de Haan, L. (1994). "Extreme Value Statistics." in *Extreme value theory and applications*, J. Galambos, J. Lechner, and E. Simiu, eds., Kluwer Academic Publishers, 93-122.
- Galambos, J., Lechner, J., and Simiu, E. (1994). "Extreme Value Theory and Applications." Kluwer Academic Publishers.
- Grigoriu, M. (2009). *Algorithms for generating large sets of synthetic directional wind speed data for hurricane, thunderstorm, and synoptic winds*. NIST Technical Note 1626, National Institute of Standards and Technology, Gaithersburg, MD.
- Kotz, S., and Nadarajah, S. (2000). *Extreme value distributions: theory and applications*, Imperial college press, London.
- NCDC (2008). *Data documentation for data set 3505 (DSI-3505)*:
<<http://www1.ncdc.noaa.gov/pub/data/documentlibrary/tddoc/td3505.pdf>>
(accessed 11/30/10).
- Simiu, E., and Miyata, T. (2006). *Design of buildings and bridges for wind: a practical guide for ASCE-7 Standard users and designers of special structures*, John Wiley & Sons, Hoboken, NJ.
- Spence, S. M. J. (2009). *High-rise database-assisted design 1.1 (HR_DAD_1.1): Concepts, software, and examples*. NIST Building Science Series 181, National Institute of Standards and Technology, Gaithersburg, MD.
- Yeo, D. (2010). *Database-Assisted Design of high-rise reinforced concrete structures for wind: Concepts, software, and application*. NIST Technical Note 1665, National Institute of Standards and Technology, Gaithersburg, MD.+

Dynamic Displacement Analysis of a Shallow Landslide in Norwood Tuff

Keith E. Beisner¹, Aurelian C. Trandafir², Ronald L. Bruhn³

¹Department of Geology and Geophysics, University of Utah, 115 S. 1460 E., Salt Lake City, Utah, 84112-0111; PH (785) 550-1864; e-mail: keith.beisner@utah.edu

²Department of Geology and Geophysics, University of Utah, 115 S. 1460 E. Rm 449, Salt Lake City, Utah, 84112-0111; PH (801) 585-0491; e-mail: a.trandafir@utah.edu; atrandafir@yahoo.com

³Department of Geology and Geophysics, University of Utah, 115 S. 1460 E. Rm 325, Salt Lake City, Utah, 84112-0111; PH (801) 581-6619; e-mail: ron.bruhn@utah.edu

ABSTRACT

Northern Utah has a long history of landslides occurring on natural and man-made slopes. Earthquake activity in this region may exacerbate the incidence of landslides, thus increasing the potential of landslide related damage to residential structures and transportation corridors. In this context, the present study addresses the earthquake response in drained conditions of a typical, shallow landslide in northern Utah occurring in completely decomposed Norwood Tuff. The slide mass geometry was obtained using a 2-D seismic refraction profile and previously collected geotechnical borehole data. The Newmark sliding block analysis was employed with a translational failure mechanism to determine the permanent dynamic slope displacements under various input accelerograms. The yield coefficient was obtained from pseudo-static limit-equilibrium slope stability analyses using the Slope/W module of the GeoStudio engineering software package. Based on the computational results, a methodology to evaluate the peak ground acceleration threshold that would distinguish between insignificant ground movements and large, potentially damaging slope displacements during an earthquake was developed.

INTRODUCTION

Earthquake and landslide hazards in Utah are associated with risks that include damage to homes and businesses, transportation corridors, and potential loss of human life. While much research has been done on landslides and earthquakes in Utah separately, there is little data relating earthquake energy and landslide displacement thresholds. Northern Utah provides an excellent study area for the potential of earthquake-induced landslides given the large number of active landslides in Norwood Tuff in this region combined with an historically active normal-fault system capable of producing large earthquakes (Figure 1). Urban development in this region is also accelerating and more construction occurs on hill slopes, thus increasing the need for understanding the risks posed by geologic activity in the area.

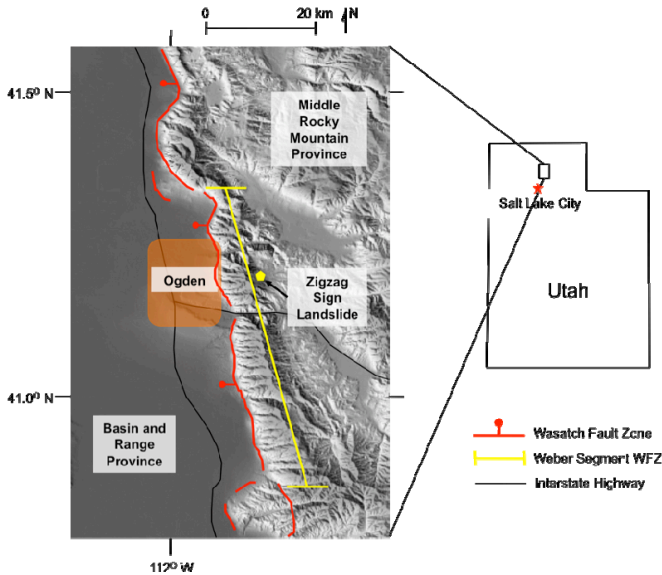


Figure 1. Regional study area.

GEOLOGIC SETTING

Northern Utah is considered part of the Middle Rocky Mountains physiographic province (Stokes, 1977). Coogan and King (2006) mapped the Norwood Tuff, a Tertiary age volcanic unit, as part of the Salt Lake Formation. The volcanic tuff underlies middle and upper Pleistocene glacial deposits. The Norwood Tuff was originally deposited in a near-shore lacustrine environment and subsequent weathering and metamorphism of this material resulted in the formation of claystone, siltstone, and sometimes sandstone layers. The tuff also includes lenses of conglomerate containing chert and carbonate clasts.

Based on available geotechnical information from boreholes, Trandafir and Amini (2009) developed a generalized subsurface profile for the study region. This includes a 0.3-m thick topsoil at the surface underlain by glacial till with thicknesses ranging within 1-5 m (also reaching up to 10 m in some areas). Decomposed Norwood Tuff with thicknesses of 1.0 - 4.5 m underlies the glacial till and grades into fresh bedrock tuff at 7 - 12 m below the ground surface.

Landslide hazards in Northern Utah exist both on natural and man-made slopes. Landslides in this region are responsible for damage to residential homes, transportation corridors, and buried utility and sewer lines (Ashland, 2007). Most landslides experience movement annually during spring and early summer snowmelt due to elevated groundwater levels and saturated soils. While this annual movement is generally not catastrophic, potentially damaging displacements can occur during

unusually high precipitation or after several years of high snowpack, precipitation, and increased groundwater levels.

Landslide activity on cut slopes along the Snowbasin Access Road (State Highway 226) provides a case study for determining the failure threshold in shallow landslides comprised of Norwood Tuff. Previous mapping and reconnaissance surveys show that landslides affect approximately 35% of the cut slopes along the road (Trandafir and Amini, 2009). The landslide study area along the Snowbasin Access Road is located on the footwall side of the Weber Segment of the Wasatch Fault Zone (WFZ). The WFZ is a north-south trending normal fault system that extends 343 km along the western base of the Wasatch Mountain Range. The WFZ is comprised of ten segments, each capable of rupturing independently and generating magnitude 7+ earthquakes. The Weber Segment is one of five central segments that show evidence of multiple surface-faulting earthquakes in the last 6000 years (Duross, 2009). The end-to-end length of the fault is 56 km and the surface trace length is 61 km. The expected moment magnitude of an earthquake on the Weber Segment is 7.17.

The objective of this study is to determine peak ground acceleration thresholds that would trigger large, potentially damaging dynamic displacements of shallow landslides in drained, completely decomposed Norwood Tuff during an earthquake. The proposed approach employs field and laboratory geotechnical data with a Newmark sliding block formulation for assessing drained seismic slope displacements. The results of this study will be helpful in developing effective mitigation strategies against earthquake-induced shallow landslide hazards in completely decomposed Norwood Tuff.

GEOLOGIC ENGINEERING FEATURES OF ZIGZAG SIGN LANDSLIDE

Zigzag sign landslide may be regarded as a typical shallow landslide characterizing the failure mode of cut slopes in Norwood Tuff along the Snowbasin Access Road (Figure 2). The slide can be qualified as a slump-earthflow complex exhibiting translational movement along a planar sliding surface. Deformation features include a slump near the head scarp, formation of a secondary scarp near the center of the landslide, and a thrust system at the toe of the slide. The landslide surface is characterized by a hummocky topography with fractures and sag ponds encountered at various locations. Examination of borehole data combined with dynamic cone penetration tests conducted at the landslide location revealed that the slide mass consisting of completely decomposed Norwood Tuff is underlain by a thinly bedded carbonate rock which is very stiff and dips parallel to the slope face (Trandafir and Amini, 2009).



Figure 2. Image of Zigzag Sign landslide.

The Utah Geological Survey has monitored groundwater conditions for the area (Ashland, 2008). Results from monitoring the Green Pond Landslide and Bear Wallow Landslide, both located along Snowbasin Access Road, indicate an annual increase in groundwater levels following spring snow melt (Ashland, 2008). Zigzag sign landslide experiences slow, down-slope movement and deformation during and immediately following spring snowmelt. The carbonate layer underlying the zone of deformation in the Zigzag Sign landslide may potentially develop perched water tables within the decomposed Norwood Tuff material. As the water levels increase, the pore-water pressure increases and may induce slide mass deformations as driving forces overcome resisting forces within the landslide.

The slide mass geometry was determined using a 45-m long seismic refraction profile with forty-five 4.5 Hz geophones spaced one meter apart and connected to a 16-bit seismograph. A sledgehammer impacting a metal plate at the ground surface was used as a source and 15 stacks of the sledgehammer were used for each shot. The profile was located along the landslide surface perpendicular to the head scarp and parallel to the direction of movement.

Results from the seismic refraction profile indicate a raypath interface at approximately 3-5 m depth throughout the profile. Below this interface the P-wave velocities increase to greater than 1000 m/s, possibly indicating fresh Norwood Tuff below the sliding surface. This interpretation correlates with unpublished geotechnical borehole data showing a stiff, sandy clay at approximately 5 m depth. Slickensides present within this material indicate a potential sliding surface at the interface between decomposed Norwood Tuff and fresh Norwood Tuff bedrock.

Disturbed samples of completely decomposed Norwood Tuff were used for laboratory index property testing. Grain size analysis results show that the completely decomposed Norwood Tuff contains 12% sand, 26% silt, and 62% clay. Additionally, Atterberg's limits tests provided a liquid limit (LL) of 37% and a plasticity index (PI)

of 13%. The plastic limit for completely decomposed Norwood Tuff is 25%. In the Unified Soil Classification System these test results qualify the completely decomposed Norwood Tuff as lean clay.

Static conditions of the deformed Zigzag Sign landslide were modeled for dry conditions with Geostudio engineering software developed by Geo-Slope International, Ltd. The limit-equilibrium method built into Slope/W module was utilized to study the static slope stability. The model geometry was developed using a combination of seismic refraction, borehole, and dynamic cone penetration test data for the Zigzag sign landslide. Groundwater was not considered in the analysis, as the study was performed for dry slope conditions. Bedrock and slide mass material were the two regions modeled (Figure 3). The bedrock was considered impenetrable while the slide mass material was governed by the Mohr-Coulomb failure criterion. Material properties involved in modeling the slide mass included the unit weight of completely decomposed Norwood Tuff – 19.1 kN/m^3 , the effective cohesion – 4.2 kPa , and the effective friction angle – 27° (Trandafir and Amini, 2009). Janbu's method was used to calculate the static safety factor along the sliding surface for the slope without a groundwater table within the slide mass (Janbu, 1954). The safety factor (FS) for the drained, deformed slope is 1.36, thus indicating a stable slope under dry, static conditions.

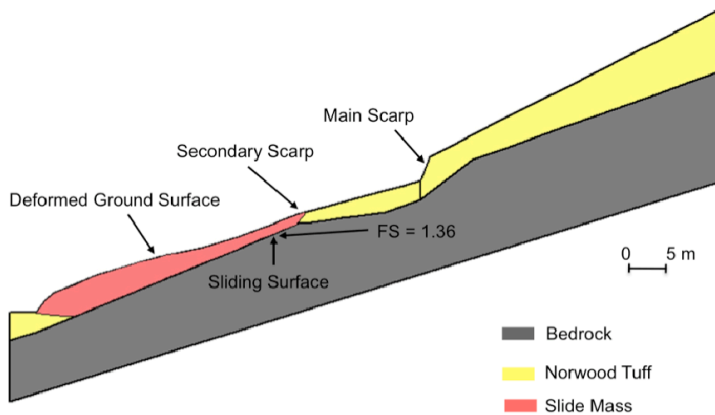


Figure 3. Static analysis of the Zigzag Sign landslide.

DYNAMIC DISPLACEMENT ANALYSIS OF ZIGZAG SIGN LANDSLIDE

A pseudo-static limit-equilibrium analysis with the Slope/W module was employed to determine the drained seismic yield coefficient using the same parameters as the static slope analysis. A trial-and-error approach was employed to adjust the magnitude of the horizontal seismic load acting on the landslide mass until a safety factor equal to one was achieved. The seismic coefficient associated with a

safety factor of one represents the yield coefficient. Because the shear surface of the landslide was already known, the critical slip surface for each trial did not need to be determined. The analysis revealed a yield acceleration (i.e., yield coefficient multiplied by the gravitational acceleration) of 0.25g necessary to achieve a safety factor equal to one for the analyzed landslide in drained conditions.

Since no earthquakes have been yet recorded with modern instrumentation on the Weber Segment of the Wasatch Fault, example earthquakes from around the world were employed to simulate the seismic response of the Zigzag sign landslide. The parameters used to locate records with similar characteristics to the Weber Segment and the study area included normal faulting earthquakes with magnitudes M_0 ranging from 6.7 to 7.7, rupture distance ranging from 0 to 15 km, and rock site conditions with shear wave velocities ranging from 760 m/s to 1500 m/s. Six earthquake events were chosen and scaled to match as closely as possible the target spectrum acceleration. In addition, six seismic waveforms characterized by various Arias intensities were selected to correlate Arias intensity values with displacement and earthquake acceleration thresholds associated with large, potentially destructive landslide movements.

A Newmark sliding block analysis was employed to calculate permanent seismic displacements of the Zigzag Sign landslide (Newmark, 1965) under various horizontal input accelerograms. The finite-difference based numerical integration scheme characterizing the Newmark sliding block procedure was built into a computer code utilized in dynamic displacement calculations. Each acceleration-time history was scaled to various values of the peak earthquake acceleration within 0.1-1.0g using 0.1g increments. For each earthquake event the scaled peak acceleration coefficient (k_m) was plotted against the corresponding calculated permanent displacement (s_p) on a logarithmic scale (Figure 4). Such plot allows us to distinguish between peak earthquake accelerations associated with relatively small permanent displacements and peak earthquake acceleration values that may trigger large, potentially damaging slope movements. The intersection between the tangent to the asymptotic portion of the s_p - k_m curve and the horizontal axis provides the peak ground acceleration threshold (k_m^c, g) for earthquake-induced large, potentially damaging displacements. Peak acceleration values greater than this threshold may be considered unsafe due to an asymptotic increase in permanent seismic displacements with increasing k_m .

The relationship between the critical peak ground acceleration threshold and the amount of energy released by the earthquake was subsequently analyzed using normalized Arias intensities calculated for the positive and negative orientation of each seismic record. The normalized Arias intensity (\bar{I}_A) was calculated as follows:

$$\bar{I}_A = \frac{I_A}{(a_{\max})^2}$$

where I_A represents the Arias intensity calculated for a specific earthquake accelerogram, $a(t)$, characterized by a peak earthquake acceleration $a_{\max} = k_m g$ and a

duration t_s (i.e., $I_A = \frac{\pi}{2g} \int_0^{t_s} a^2(t) dt$).

For the analyzed input earthquakes, \bar{I}_A varied from 1.83 to 63.15 s^3/m . The threshold peak earthquake acceleration coefficient to trigger large, potentially damaging dynamic landslide displacements ranged from 0.55 to 0.70g with an average value of 0.63g and a standard deviation equal to 0.04g (Figure 5).

CONCLUDING REMARKS

Results from the dynamic displacement analysis indicate that peak acceleration values greater than 0.55g should be considered unsafe for shallow landslides in completely decomposed Norwood Tuff due to an asymptotic increase in computed permanent displacement with increasing peak earthquake acceleration beyond this threshold. The analysis also revealed that the coefficient of peak ground acceleration threshold is not dependent on the normalized Arias Intensity of the seismic event.

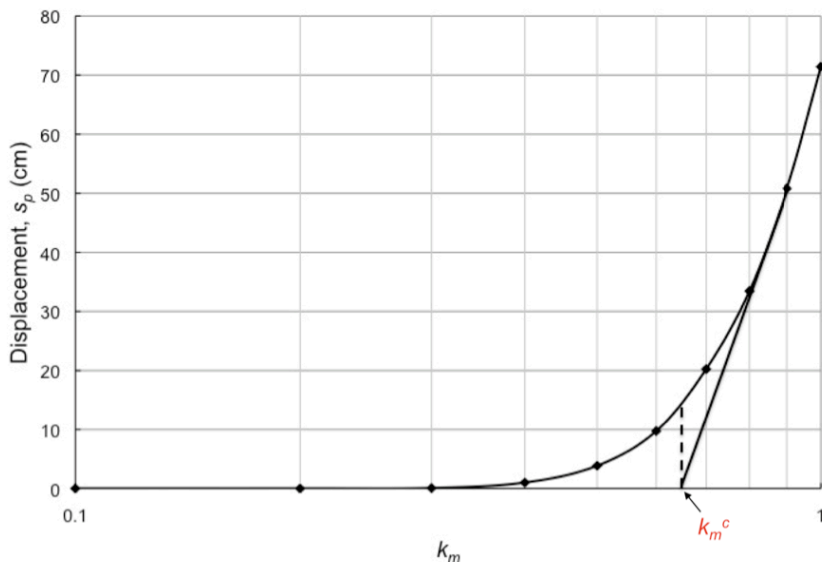


Figure 4. Typical relationship between peak earthquake acceleration coefficient (k_m^c) of a scaled seismic record and corresponding computed permanent landslide displacement (s_p).

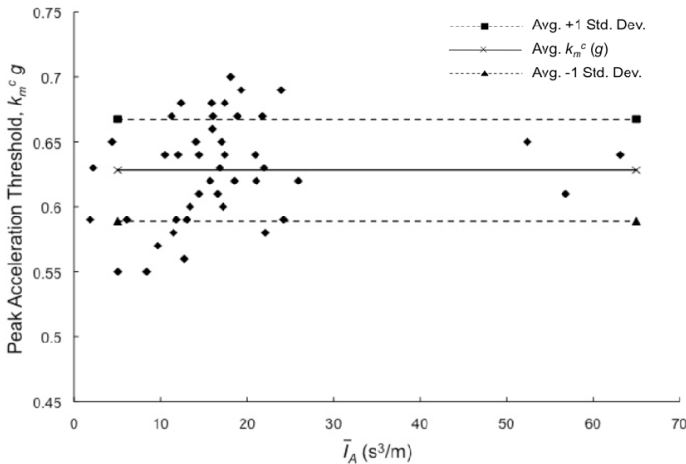


Figure 5. Relationship between the peak earthquake acceleration threshold and normalized Arias intensity.

REFERENCES

- Ashland, F.X. (2007). Active landslides in the Creekside Drive area, Mountain Green, Morgan County, Utah, between June 2005 and December 2006. Utah Geological Survey Report of Investigation 260.
- Ashland, F.X., Giraud, R.E., McDonald, G.N., and Elliott, A.H. (2008). Ground-water conditions in the Green Pond Landslide, Weber County, Utah. Utah Geological Survey Open-File Report 528.
- Coogan, J.C. and King, J.K. (2006). Interim geologic map of the Durst Mountain quadrangle, Morgan and Weber Counties, Utah, Utah Geological Survey.
- Duross, C.B., Personius, S.F., Crone, A.J., McDonald, G.N., and Lidke, D.J. (2009). Paleoseismic investigation of the northern Weber segment of the Wasatch Fault Zone at the Rice Creek trench site, North Ogden, Utah. Utah Geological Survey Special Study 130.
- GEO-SLOPE International, Ltd. (2007). GeoStudio tutorials, Geo-Slope International Ltd, p 485.
- Janbu, N. (1954). Applications of composite slip surfaces for stability analysis. In: Proceedings of the European conference on the stability of earth slopes, Vol. 3. Stockholm, pp. 39-43.
- Newmark, N.M. (1965). Effects of earthquakes on dams and embankments. Geotechnique, Vol. 15 No. 2, pp. 139-149.
- Stokes, W.L. (1977). Subdivisions of the major physiographic provinces in Utah. Utah Geol 4(1), pp. 1-17.
- Trandafir, A.C. and Amini, Z.A. (2009) Yielding mechanism of shallow mass movements in completely decomposed Norwood Tuff: the Zigzag Sign landslide, Utah. Environmental Geology, Vol. 57, No. 6, pp. 1443-1451.

Intra- and Inter-Event Uncertainties of Ground Motion Attenuation Relations

Swagata Banerjee

Assistant Professor, Pennsylvania State University, University Park, PA 16802

Ground motion attenuation relationships have traditionally been used to describe the spatial distribution of earthquake ground motions. Attenuation models provide the ground motion intensities at different locations of the distribution region by combining two key estimates: (i) median values of ground motion intensities and (ii) aleatory uncertainty parameters namely inter- and intra-event uncertainty. The present study simulates inter- and intra-event uncertainties as Gaussian random variable and two-dimensional stationary Gaussian random field, respectively, assuming they are independent events. Earthquake records from Next Generation Attenuation or, NGA database are used for this purpose. Intensity of ground motions are measured in terms of peak ground acceleration (PGA). To use in the simulation process, nonlinear site response model is represented with a suitable probability distribution. Result shows that intra-event uncertainty is more significant than inter-event uncertainty.

INTRODUCTION

The empirical ground motion models (i.e., attenuation relationships) are in use over decades to describe the spatial distribution of earthquake ground motions. The functional form of attenuation relationships can generally be written as

$$\ln(Y_{ij}) = \ln(\hat{Y}_{ij}) + \eta_i + \varepsilon_{ij} \quad (1)$$

where Y_{ij} is the ground motion intensity (such as peak ground acceleration, or PGA) of i^{th} event at j^{th} station and \hat{Y}_{ij} is the median ground motion intensity of the same event at that station. Y_{ij} is a recorded quantity while \hat{Y}_{ij} represents the prediction from empirical attenuation equations. The most recent attenuation models known as Next Generation Attenuation or, NGA models provide the empirical equations for \hat{Y}_{ij} (Abrahamson and Silva 2008, Campbell and Bozorgnia 2007, Boore and Atkinson 2008, Idriss 2007, and Chiou and Youngs 2008). η_i and ε_{ij} are two aleatory uncertainties respectively known as inter-event and intra-event uncertainty, and are introduced in the attenuation model to represent (collectively) the uncertainty associated with the predictive model. Inter-event uncertainty indicates the randomness of seismic events generated from a particular seismic source, while the intra-event uncertainty describes the random nature of a particular seismic event at different sites. Thus the random effect of ground motion distribution is incorporated in the empirical attenuation model. Median ground motion intensities in combination with these two aleatory uncertainties provide the expected intensities of ground motions at various sites in the neighboring region of earthquake epicenter.

Abrahamson and Silva (1992) performed regression analysis to calculate the effect of η_i and ε_{ij} on the ground motion attenuation. They modeled these two uncertainty terms as statistically independent normal random variates with zero mean

values. The standard deviations of these two normal variates (say, τ and σ respectively, for η_i and ε_{ij}) are found to have dependence on the magnitude of generating earthquakes (Abrahamson and Silva 1997). Recent research identified that in addition to earthquake magnitude, τ and σ also depend on soil nonlinearity (Abrahamson and Silva 2008). Closed-form empirical equations are proposed in this literature to represent the standard deviations τ and σ in terms of earthquake magnitude, mean PGA at rock, shear wave velocity at site, and spectral time period. However, no definite correlation between uncertainty terms and the abovementioned source and site parameters is found through which η_i and ε_{ij} can be quantified explicitly. Therefore, the proposed NGA models (including closed-form equations for uncertainty terms) may not provide accurate estimates of ground motion intensities at different locations in the distribution region.

Due to the inherent randomness of the ground motion distribution process, the present study proposes the use of simulation-based approach to model and analyze the aleatory uncertainties. Assuming these are independent variables, inter- and intra-event uncertainties are represented here with a Gaussian random variable and a two-dimensional stationary Gaussian random field, respectively. NGA relationships (only for calculating \hat{Y}_{ij}) and ground motion records from NGA database are used here. Ground motion intensity is measured in terms of PGA, although any other intensity parameter such as spectral accelerations at various periods can also be used for this purpose. To demonstrate the uncertainty simulation, an initial discussion on one of the NGA models and some relevant statistical analyses are necessary.

NGA MODEL BY ABRAHAMSON AND SILVA (2008) FOR MEDIAN GROUND MOTION INTENSITY

Abrahamson and Silva (2008) proposed the next generation attenuation (NGA) model to evaluate the median estimate of ground motion intensities (Eq. 2). This relationship is developed using 2754 recordings from 135 earthquakes.

$$\ln(\hat{Y}) = f_1(M, R_{rup}) + a_{12}F_{RV} + a_{13}F_{NM} + a_{15}F_{AS} + F_{HW}f_4(M, R_{rup}, R_{jb}, R_x, W, \delta, Z_{TOR}) + f_5(PGA_{1100}, V_{S30}) + f_6(Z_{TOR}) + f_8(R_{rup}, M) + f_{10}(Z_{1.0}, V_{S30}) \quad (2)$$

Here \hat{Y} represents the median value of ground motion intensity. f_1 represents the base model which is a function of earthquake magnitude (M) and rupture distance (R_{rup}). R_{rup} is a measure of distance between source and site. F_{RV} , F_{NM} , F_{AS} , and F_{HW} are factors respectively representing the effects of reverse faulting earthquake, normal faulting earthquake, after shock and hanging wall on the ground motion attenuation. f_4 is associated with the hanging wall model which is a function of M , R_{rup} , Joyner-Boore distance (R_{jb}), horizontal distance from top edge to rupture (R_x), width of down-dip rupture (W), fault dip (δ), and depth-to-top of rupture (Z_{TOR}). The site response model is expressed with f_5 that represents the nonlinearity in site soil condition as a function of site shear wave velocity over the top 30 m (V_{S30}) and pick ground acceleration for rock sites (PGA_{1100} ; in this case $V_{S30} = 1100$ m/s). f_6 , f_8 and f_{10} respectively represent depth-to-top of rupture model, large distance model and soil depth model where $Z_{1.0}$ corresponds to the depth to shear wave velocity = 1.0 km/s. a_{12} , a_{13} , and a_{15} are various model coefficients.

In the present study, 487 records of ground motion intensities from 10 different California earthquakes are taken from NGA database (Table 1). These data are selected based on the following criteria:

- (i) All records are from main shocks.
- (ii) Recording sites exclude hanging walls; this criterion is made to avoid statistical uncertainty due to limited available data on hanging walls.
- (iii) Any record beyond 100 km from the source is ignored; this is considered based on the fact that beyond 100 km ground motion intensities attenuate to a great extent which can be ignored for the risk assessment of regional infrastructures.
- (iv) V_{S30} is always considered to be less than V_{LIN} (V_{LIN} is defined as a shear-wave velocity below which site response is nonlinear; Abrahamson and Silva 2008); this is to study the effect of soil nonlinearity on the attenuation relation.

These four criteria yield F_{AS} , F_{HW} and f_8 equal to zero. In addition, the influence of f_{10} on the ground motion attenuation is not studied here primarily for two reasons; (i) very limited data on $Z_{1.0}$ is found in NGA database for some of the earthquakes that are considered in this study (e.g., Coalinga, Landers, Hector Mine and North Palm Spring) and (ii) soil depth (i.e., shallow or deep) is found to have no effect on median PGA (Abrahamson and Silva 2008).

Table 1: Selected earthquakes from NGA database (in alphabetic order)

Earthquake	Year of Occurrence	NGA ID	Magnitude	Fault Mechanism	Z_{TOR} (km)	# of recordings
Coalinga	1983	76	6.36	Reverse	3.4	31
Hector Mine	1999	158	7.13	Strike-slip	0	29
Imperial Valley	1979	50	6.53	Strike-slip	0	33
Landers	1992	125	7.28	Strike-slip	0	21
Loma Prieta	1989	118	6.93	Reverse-oblique	3.8	69
Morgan Hill	1984	90	6.19	Strike-slip	0.5	27
N Palm Springs	1986	101	6.06	Reverse-oblique	4	28
Northridge	1994	127	6.69	Reverse	5	132
San Fernando	1971	30	6.61	Reverse	0	22
Whittier Narrows	1987	113	5.99	Reverse-oblique	14.5	95

Incorporating these selection criteria, Eq. (2) takes the form of Eq. (3). Different components of this equation are described in following paragraphs.

$$\ln(\hat{Y}) = f_1(M, R_{rup}) + a_{12}F_{RV} + a_{13}F_{NM} + f_5(PGA_{100}, V_{S30}) + f_6(Z_{TOR}) \tag{3}$$

Component 1 - Base model (f_1): The base model exhibits a gradual attenuation of ground motion intensity with distance from earthquake source. This is given as

$$f_1(M, R_{rup}) = \begin{cases} a_1 + a_4(M - c_1) + a_8(8.5 - M)^2 + [a_2 + a_3(M - c_1)]\ln(R) & \text{for } M \leq c_1 \\ a_1 + a_5(M - c_1) + a_8(8.5 - M)^2 + [a_2 + a_3(M - c_1)]\ln(R) & \text{for } M > c_1 \end{cases} \tag{4}$$

where $R = \sqrt{R_{rup}^2 + c_4^2}$. Values of a_1 , a_4 , a_5 , a_8 , c_1 and c_4 can be obtained from Abrahamson and Silva (2008).

Component 2 - Effect of faulting (F_{RV} and F_{NM}): Depending on the source mechanism, F_{RV} and F_{NM} can be determined as 1 or 0.

Component 3 - Site response model: This model represents site characteristics. In NGA database, five different soil types namely A, B, C, D, and E are identified based on preferred V_{S30} . Two extreme soil types, class A and E respectively represent hard rock ($V_{S30} > 1500$ m/s) and soft clay ($V_{S30} < 180$ m/s), and other three types fall in between. 487 earthquake records used in this study have V_{S30} ranging from 116.4 m/s to 813.5 m/s and V_{LIN} for PGA is considered to be 865.1 m/s as reported in Abrahamson and Silva (2008). This indicates that for all 10 earthquakes used here, selected recordings are associated with nonlinear site response (as $V_{S30} < V_{LIN}$).

Site response model can be written as (proposed by Abrahamson and Silva 2008)

$$f_5(PGA_{1100}, V_{S30}) = \begin{cases} a_{10} \ln\left(\frac{V_{S30}}{V_{LIN}}\right) - b \ln(PGA_{1100} + c) \\ \quad + b \ln\left(PGA_{1100} + c \left(\frac{V_{S30}}{V_{LIN}}\right)^n\right) & \text{for } V_{S30} < V_{LIN} \\ (a_{10} + bn) \ln\left(\frac{V_{S30}}{V_{LIN}}\right) & \text{for } V_{LIN} \leq V_{S30} < V_1 \end{cases} \quad (5)$$

Values of a_{10} , b , c , and n are obtainable for the literature and $V_1 = 1500$ m/s for PGA.

Component 4 - Depth-to-top of rupture model (f_6): This model is expressed in the form of Eq. (6) where the value of a_{16} is given in Abrahamson and Silva (2008).

$$f_6(Z_{TOR}) = \begin{cases} \frac{a_{16} Z_{TOR}}{10} & \text{for } Z_{TOR} < 10 \text{ km} \\ a_{16} & \text{for } Z_{TOR} \geq 10 \text{ km} \end{cases} \quad (6)$$

Among these four components of Eq. (3), 1, 2 and 4 are introduced to account for the effects of source characteristics and source-to-site distance (i.e., rupture distance R_{rup}). Therefore, summation of these three components will provide a gradual attenuation of PGA from seismic source with increasing R_{rup} . Component 3 introduces nonlinearity in the attenuation model when $V_{S30} < V_{LIN}$. This is the case of the present study.

In order to evaluate median PGA (PGA_{median}) over the entire distribution region, PGA_{1100} needs to be calculated first. This is done by applying $V_{S30} = 1100$ m/s in Eq. (3) which resulted in the following expression of PGA_{1100} .

$$\ln(PGA_{1100}) = f_1(M, R_{rup}) + a_{12} F_{RV} + a_{13} F_{NM} + f_5(V_{S30} = 1100) + f_6(Z_{TOR}) \quad (7)$$

Figure 1 shows the variation of PGA_{median} and PGA_{1100} for two of the earthquakes, Northridge and Loma Prieta, considered herein. This also shows the recorded PGA values (with red open circles) at different recording stations for these two earthquakes. Note that PGA_{1100} has gradual attenuation while PGA_{median} is random. This is due to the fact that f_5 becomes linear for PGA_{1100} (i.e., for $V_{S30} = 1100$ m/s). Similar trends are observed for other earthquake ground motions as well.

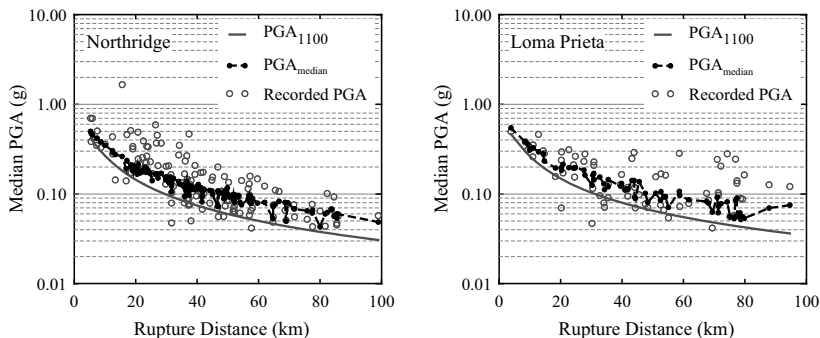


Figure 1. Attenuation of median ground motion intensity

SIMULATION OF NONLINEAR SITE RESPONSE

Uncertainties associated with the current attenuation model can be easily visualized from Figure 1. Besides, the distribution of median PGA (PGA_{median}) is random in nature when the site response is nonlinear (i.e., f_5 is nonlinear). Therefore, utilizing the attenuation relationship described in the preceding section, one cannot estimate the attenuation of PGA_{median} of any scenario earthquake using only information related to source characteristics and source-to-site distance. Distribution of V_{S30} over the entire region is also necessary for this purpose.

In NGA database, information on V_{S30} is available only at the recording stations. For any other sites, V_{S30} must be predicted from that recorded at nearby recording stations. Figure 1 shows random trends of the variation of V_{S30} between any two consecutive recordings. Therefore, the method of interpolation may not provide accurate information of V_{S30} at any arbitrary site other than recording stations. This complexity makes it difficult to estimate median PGA at sites where V_{S30} is not readily available. To overcome this difficulty, the current study assigns a suitable probabilistic distribution for the nonlinear site response. First, 487 values of f_5 from 487 records of 10 earthquakes are calculated. These f_5 values correspond to nonlinear site response according to forth ground motion selection criteria. Figure 2 represents the histogram of 487 values of f_5 . A goodness-of-fit test is performed that resulted in a normal distribution at levels of significance of 0.01 and 0.05. The mean and standard deviation of the normal distribution are estimated to be 0.3002 and 0.1296, respectively. This distribution of f_5 is used to simulate the values of median PGA. Figure 3 represents the calculated PGA_{median} and its simulated values (in blue circles) for Northridge earthquake. Comparison shows good agreement between them.

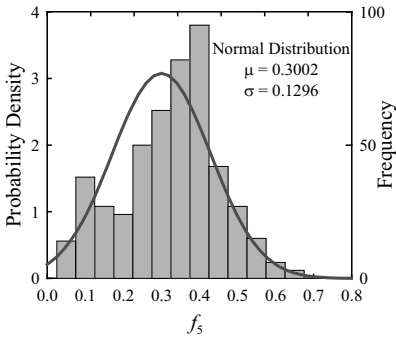


Figure 2. Histogram of 487 values of f_5 and the best-fitted probability distribution

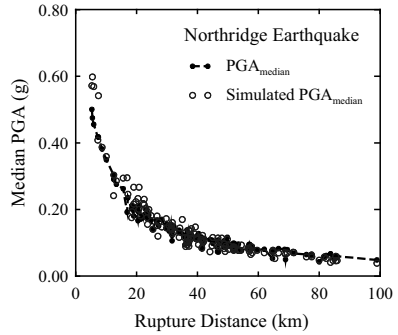


Figure 3. Calculated and simulated PGA_{median} at recording stations

MODELING OF INTER- AND INTRA-EVENT UNCERTAINTY

Modeling of Inter-event Uncertainty: Inter-event uncertainty (η_i) represents the random effect of i^{th} event. This is modeled as a Gaussian random variable with zero mean and standard deviation τ . Therefore the expression becomes, $\eta_i = N(0, \tau)$.

Modeling of Intra-event Uncertainty: The random effect of j^{th} recording of the i^{th} event is represented by intra-event uncertainty (ε_{ij}). A two-dimensional (2D) stationary Gaussian random field with standard deviation σ is considered to model the uncertainty. A region of $40 \text{ km} \times 40 \text{ km}$ is chosen to be the distributed region of the ground motion. The upper cut-off wave number is set to 5 rad/km . Simulation results are discussed in the following section.

SIMULATION RESULTS AND DISCUSSIONS

Two sets of simulations are performed for all 10 earthquakes; (i) Case I with $\tau = \sigma = 0.2$ and (ii) Case II with $\tau = 1.0$ and $\sigma = 0.2$. Figure 4 and 5 show the simulation results obtained in Case I and Case II, respectively for Northridge earthquake. Each figure consists of four plots showing the simulation of median PGA (a) without uncertainty, (b) with inter-event uncertainty, (c) with intra-event uncertainty, and (d) with both uncertainties. All of these plots show randomness of ground motion distribution. The randomness in plot (a) is purely due to the random nature of nonlinear site response, while the same is due to the combined effect of nonlinear site response and aleatory uncertainty (either inter-event or intra-event or both) in other three plots.

In Case I (Figure 4), difference between (a) and (b) is trivial, whereas the same in Case II is significant (Figure 5). This is due to assigned values of standard deviations of inter-event uncertainty (τ). Lower τ does not insert much variation in the ground motion attenuation relationship. In all cases, the effect of inter-event uncertainty remains constant for one simulation and does not changes spatially.

The difference between (a) and (c) in both cases (Figures 4 and 5) are results of intra-event uncertainty. Comparison of (b) and (c) of Figure 4 indicates that intra-event uncertainty is more significant than inter-event uncertainty even if they have same values of standard deviation. The distribution of median intensity of ground motions may become extremely random due to high intra-event uncertainty.

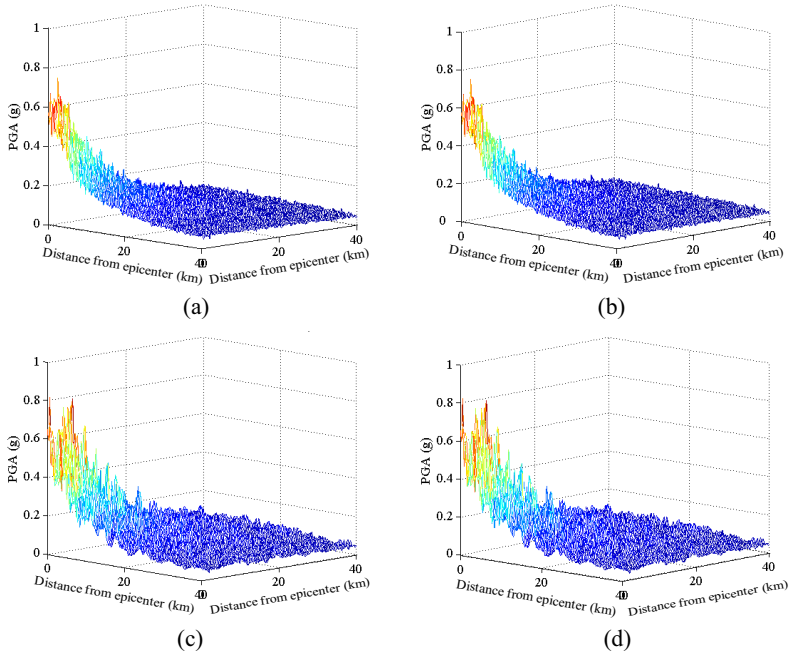
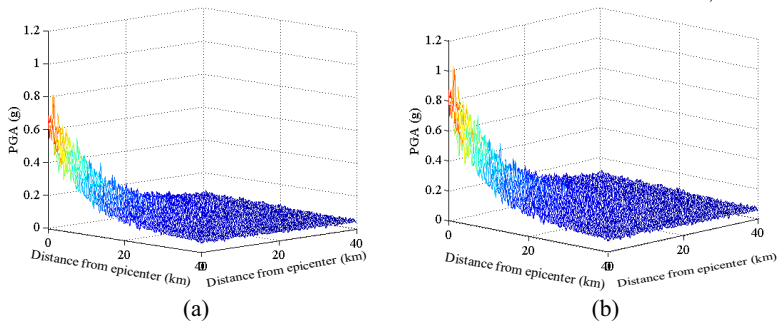


Figure 4. Mean ground motion intensity (PGA) obtained in Case I ($\tau = \sigma = 0.2$); (a) without uncertainty, (b) with inter-event uncertainty, (c) with intra-event uncertainty, and (d) with both inter- and intra-event uncertainties



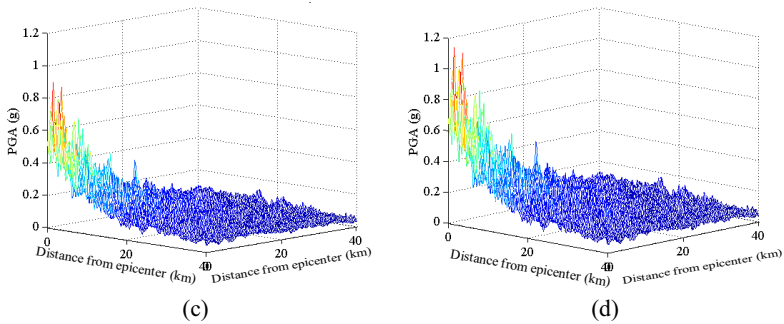


Figure 5. Mean ground motion intensity (PGA) obtained in Case II ($\tau = 1.0$ and $\sigma = 0.2$); (a) without uncertainty, (b) with inter-event uncertainty, (c) with intra-event uncertainty, and (d) with both inter- and intra-event uncertainties

CONCLUSIONS

The study proposed a simulation-based approach to model ground motion distribution associated with uncertainties. Two key findings are (i) nonlinear site response can effectively be presented with a suitable probability distribution and (ii) intra-event uncertainty is more significant than inter-event uncertainty. Future study is underway that will provide more insight in this topic.

REFERENCES

- Abrahamson, N. A., and Youngs, R. R., (1992). "A stable algorithm for regression analyses using the random effects model." *Bulletin of Seismological Society of America*, 82, 505–510.
- Abrahamson, N. A., and Silva, W., (1997). "Empirical response spectral attenuation relations for shallow crustal earthquakes." *Seismological Research Letters*, 68, 94–127.
- Abrahamson, N. A., and Silva, W., (2008). "Summary of the Abrahamson & Silva NGA ground-motion relations." *Earthquake Spectra*, 24 (1), 67–97.
- Boore, D. M., and Atkinson, G. M., (2008). "Ground-motion prediction equations for the average horizontal component of PGA, PGV, and 5%-damped PSA at spectral periods between 0.01 s and 10.0 s." *Earthquake Spectra*, 24, 99–138.
- Campbell, K. W., and Bozorgnia, Y., (2007). "Campbell-Bozorgnia NGA ground motion relations for the geometric mean horizontal component of peak and spectral ground motion parameters." Report PEER 2007/02, Pacific Earthquake Engineering Research.
- Chiou, B. S.-J., and R. R. Youngs (2008). "An NGA model for the average horizontal component of peak ground motion and response spectra." *Earthquake Spectra*, 24, 173–215.
- Idriss, I. M. (2007). "Empirical model for estimating the average horizontal values of pseudo-absolute spectral accelerations generated by crustal earthquakes – Volume 1, Sites with $V_{S30} = 450$ to 900 m/s." Interim report issued for USGS Review.

Effective Shear Strengths of Isotropic Spatially Variable Soil Masses

Jianye Ching¹, M. ASCE and Kok-Kwang Phoon², F. ASCE

¹ Associate Professor, Dept of Civil Engineering, National Taiwan University, Taipei, Taiwan. Email: jyching@gmail.com. Phone: 886-2-33664328. Fax: 886-2-23631558.

² Professor, Dept of Civil and Environmental Engineering, National University of Singapore, Singapore.

ABSTRACT: The purpose of this study is to understand the mechanism of the effective shear strength for a soil mass in the presence of spatial variability. Random field finite element analyses are used to simulate spatial average shear strengths and effective (or overall) shear strengths that govern the failure of a soil mass. Based on the simulation results, it is found that the statistics of spatial average strengths can be estimated by Vanmarcke's theory as to be expected. However, the effective shear strength is found to be close to the average shear strength along the actual slip curve, rather than the spatial average shear strength over the entire soil mass.

INTRODUCTION

Soil properties in the field generally exhibit spatial variability. This is true even if the soil mass is nominally homogeneous, because small scale heterogeneities are always present due to natural geologic processes that create and continuously modify the soil in-situ. One important property is the shear strength of the soil. For most foundation engineering problems, resistances provided by soil mass are the "overall" shear strengths, which are typically related to spatial averaging over a certain region. Spatial variability is usually modeled by a homogeneous (or stationary) random field that can be characterized succinctly in a second-moment sense by a mean value at a point, a variance at a point, and a scale of fluctuation. Vanmarcke (1977) showed that the averaged property of a random field over a region has a mean value identical to the point mean, while the variance is less than the point variance.

Vanmarcke's definition of a spatial average is purely based on an integral of the

random field over a given prescribed volume. The rationale is that the effective shear strength of a soil mass for a particular problem is governed by the spatial average along a slip curve and this spatial average is more relevant than the value at a point. There appears to be an implicit assumption that the spatial average defined along a prescribed slip curve is comparable to the spatial average defined along a *critical* slip curve that depends on mechanics (equilibrium, compatibility, and constitutive relations) and boundary conditions. By definition, the critical slip curve is the curve producing the lowest factor of safety among all possible curves. In principle, it is clear that this critical curve is fundamentally different from an arbitrary trial slip curve that is prescribed rather than emerging as an outcome of a finite element or similar analysis. However, it is unclear at this stage if this fundamental difference would produce effective strengths that are significantly different from simple Vanmarcke-type spatial average strengths.

The objective of this study is to elucidate this query. There are limited studies in the literature that explore this query systematically. The outcome of this study is of practical significance, because it is computationally intensive to identify the critical slip curve and its associated effective strength. In contrast, the second-moment statistics of a Vanmarcke-type spatial average are available in closed-form.

The above comparison is conducted through random field finite element analyses. A rectangular domain is divided into finite elements with shear strengths specified by realizations of a random field. The effective shear strength of the domain is determined by conducting plane-strain compression until failure. Discrepancies between the effective shear strength and the spatial average will be discussed. As to be expected, these discrepancies are mostly related to mechanical principles.

RANDOM FIELD AND SPATIAL AVERAGING

Stationary random fields are widely used primarily because the amount of measured data available in most site investigations would only permit characterization under this second-moment (weak) stationarity assumption. A two dimensional stationary random field for shear strength $\tau_f(x,z)$ can be characterized by its point mean value $E(\tau_f)$, point variance $\text{Var}(\tau_f)$, and auto-correlation function. The auto-correlation function of a stationary random field $\tau_f(x,z)$ is defined as the correlation between two locations with lag distance of Δx and Δz :

$$\rho(\Delta x, \Delta z) \equiv \rho(\tau_f(x, z), \tau_f(x + \Delta x, z + \Delta z)) = \frac{COV(\tau_f(x, z), \tau_f(x + \Delta x, z + \Delta z))}{\sqrt{Var(\tau_f(x, z))} \cdot \sqrt{Var(\tau_f(x + \Delta x, z + \Delta z))}} \quad (1)$$

where Var denotes the variance; COV denotes the covariance. An auto-correlation model widely used in geotechnical engineering literature is the single exponential model:

$$\rho(\Delta x, \Delta z) = \exp(-k_x |\Delta x| - k_z |\Delta z|) \quad (2)$$

where the parameter k_x and k_z are respectively equal to 2 divided by the scales of fluctuation (SOF) in the x (horizontal) and z (depth) directions [denoted respectively by SOF_x and SOF_z]. It is clear that the correlation decreases as Δx and Δz increase. This is consistent with measurements taken from natural soils: soil properties are strongly correlated within a small interval but are weakly correlated over a large interval. The SOF is the correlation length, i.e. the length scale within which two locations are significantly correlated.

Vanmarcke (1977) pointed out that the spatial average of soil properties over a region D has a mean value identical to the point mean but has a variance smaller than the point variance. Let the region D be a rectangular domain defined by $[x_0 \ x_0 + \Delta x]$ and $[z_0 \ z_0 + \Delta z]$. Mathematically, the spatial average over D can be defined as

$$\tau_f^D = \frac{1}{\Delta x \Delta z} \int_{x_0}^{x_0 + \Delta x} \int_{z_0}^{z_0 + \Delta z} \tau_f(x, z) dz dx \quad (3)$$

The variance of τ_f^D is smaller than the point variance $Var(\tau_f)$ due to the cancellation of variability through spatial averaging. Vanmarcke (1977) further defined a variance reduction factor which is equal to the variance of τ_f^D divided by the point variance:

$$\Gamma^2(D) = Var(\tau_f^D) / Var(\tau_f) \quad (4)$$

Using the single exponential model in Eq. (2), Vanmarcke (1977) showed that

$$\Gamma^2(D) = \left[\frac{2\Delta x}{SOF_x} - 1 + \exp\left(-\frac{2\Delta x}{SOF_x}\right) \right] \left/ \frac{2\Delta x^2}{SOF_x^2} \times \left[\frac{2\Delta z}{SOF_z} - 1 + \exp\left(-\frac{2\Delta z}{SOF_z}\right) \right] \right/ \frac{2\Delta z^2}{SOF_z^2} \quad (5)$$

$\Gamma^2(D)$ is a decreasing function of $\Delta x/SOF_x$ and $\Delta z/SOF_z$. These latter two terms may be interpreted as the number of independent segments in the x and z directions.

COMPARISON BETWEEN EFFECTIVE τ_f AND SPATIAL AVERAGE OVER WHOLE DOMAIN

Although Vanmarcke's theory provides useful closed-form solutions for the spatial average, it is not clear if: (1) the effective shear strength is the same as τ_f^D and (2) the statistics of the effective shear strength can be approximated using the statistics of τ_f^D even if (1) is not true. To verify this, random field finite element analyses (FEA) are conducted. The region D is taken to be a plane-strain 36m×10m rectangular area ($\Delta x = 10m$, $\Delta z = 36m$) with 0.1m×0.1m FEA mesh grids. The total number of plane-strain elements is 36,000. The two lateral boundaries are free, the bottom boundary is roller, and the lower-left-most node is a hinge. The upper boundary is subjected to a compression stress. The unit weights of all elements are zeros, the Young's modulus is 40 MN/m², and the Poisson ratio is 0.3. The elastic properties hardly affect the failure load and a high Young's modulus is selected for computational efficiency.

The spatially varying shear strength τ_f is simulated by stationary Gaussian random fields with a point mean $E(\tau_f) = 50 \text{ kN/m}^2$, a point standard deviation $\text{Var}(\tau_f)^{0.5} = 10 \text{ kN/m}^2$, and $SOF_x = SOF_z = SOF$. When assigning the simulated τ_f to each element, the local averaging subdivision algorithm developed and recommended by Fenton and Vanmarcke (1990) is adopted for local averaging within each 0.1m×0.1m element. In this initial study, the shear strength τ_f is assumed to be independent of the confining pressure for simplicity, i.e., $\phi = 0^\circ$.

The spatial average of τ_f over region D, namely τ_f^D , is therefore the average of the 36,000 assigned τ_f values. A single realization of the random field will give a sample of τ_f^D . In this study, 120 realizations are taken for the following 13 chosen SOFs: SOF = 0.01m, 0.1m, 0.3m, 1m, 3m, 10m, 20m, 40m, 100m, 300m, 1000m, 3000m, and 10000m. The case with SOF = 10⁴ m produces a nearly homogeneous mass given the dimension of the domain. The left plot in Figure 1 shows the τ_f^D samples, 120 samples for each SOF. In this plot, τ_f^D samples and SOF are normalized with respect to the point mean 50kN/m² and the mesh width 10m, respectively.

Because τ_f^D is the spatial average of region D, it is expected that its statistical properties can be effectively estimated by Vanmarcke’s theory, i.e., the mean value of τ_f^D is the same as the point mean 50kN/m², and the variance of τ_f^D is equal to the point variance 100 multiplied by the variance reduction factor in Eq. (5). The right plots in Figure 1 show the sample average and sample variance for the τ_f^D samples, 120 samples for each SOF. They are normalized by the mean and variance estimated by Vanmarcke’s theory. It is clear that Vanmarcke’s theory is indeed reasonable for the spatial average τ_f^D , regardless the chosen SOF. This is to be expected and merely validates the correctness of the simulations undertaken in this study.

In this study, the “effective” shear strength means the overall shear strength provided by the entire soil mass. The effective shear strength can be obtained by actually shearing the soil mass to failure, which can be readily achieved in FEA. A normal compression stress is exerted at the upper (top) boundary until non-convergence of the FEA, i.e., failure. The compression stress at failure divided by 2 is taken to be the “effective” shear strength of region D, denoted by τ_f^{FEA} . This FEA simulation is similar to the unconfined compression (UC) test in laboratory, except that it is in plane strain condition. The UC test is taken here because the initial confining pressure has no effect on τ_f^{FEA} due to the $\phi = 0^\circ$ assumption.

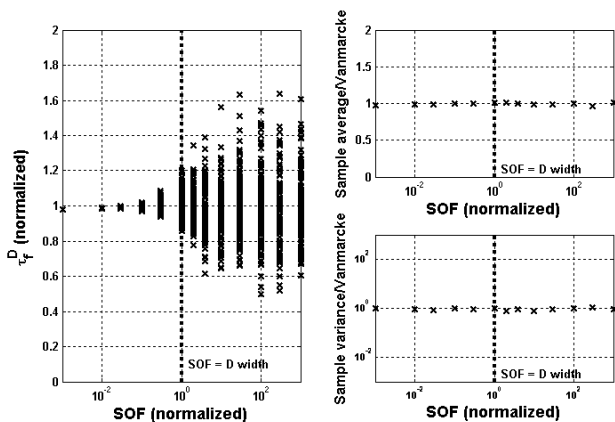


Figure 1 Samples of τ_f^D , their average values and variances under different SOFs, normalized with respect to the estimation from Vanmarcke’s theory.

A single realization of random field gives a sample of τ_f^{FEA} . Similarly, 120 realizations are taken for the 13 chosen SOFs. The left plot in Figure 2 shows the resulting τ_f^{FEA} samples, 120 samples for each SOF. In this plot, the same normalization used previously is taken for both τ_f^{FEA} and SOF. It is clear that τ_f^{FEA} samples behave differently from τ_f^D samples shown in Figure 2, especially when SOF is close to the width of D. The right two plots show the sample average and sample variance of the τ_f^{FEA} samples. Vanmarcke's theory performs satisfactorily when SOF is large but slightly overestimates the sample mean when SOF is close to the width of D, and significantly underestimates the sample variance when SOF is small.

COMPARISON BETWEEN EFFECTIVE τ_f AND SPATIAL AVERAGE ALONG SLIP CURVE

At the point of non-convergence of FEA, the stress states for all elements are recorded. A sophisticated algorithm is applied to identify the actual slip curve where shear failure occurs. This algorithm employs the safety factor (SF) defined by Pham and Fredlund (2003). A search algorithm based on the particle swarm optimization (PSO) (Kennedy and Eberhart 1995) is then applied to find the curve with SF = 1, i.e., the actual slip curve.

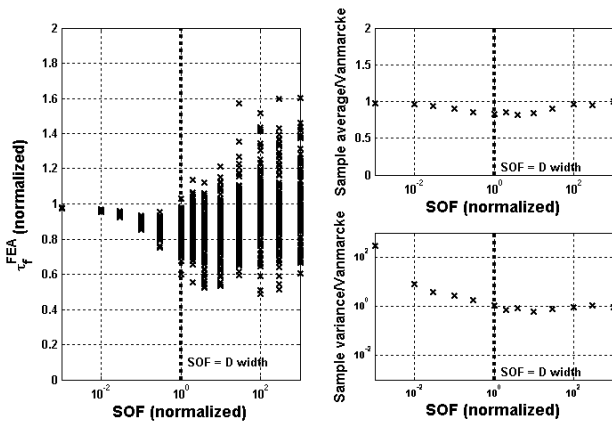


Figure 2 Samples of τ_f^D , their average values and variances under different SOFs, normalized with respect to the estimation from Vanmarcke's theory.

The same algorithm is executed after each FEA simulation of the UC test. The elements that the slip curve passes through are identified, and the assigned τ_f values of these elements are then averaged with weights proportional to the traversing lengths. This average value is therefore the spatial average along the slip curve, denoted by τ_f^{slip} . The left plot in Figure 3 shows the resulting τ_f^{slip} samples, and the right two plots show the sample average and sample variance of the τ_f^{slip} samples, normalized by the sample mean and sample variance of τ_f^{FEA} samples. It is clear that the overall shear strength τ_f^{FEA} has mean and variance that are similar to those of τ_f^{slip} , except for minor deviations in the variance when SOF is 1% to 3% of the width of D.

The consistency shown in Figure 3 leads to the following conclusion: *the effective/overall shear strength of a region D is close to the spatial average shear strength along the actual slip curve, not the spatial averaging over the entire region D.* Note that the latter is close to what is estimated by Vanmarcke's theory, as seen in Figure 1. Therefore, it can be concluded that *Vanmarcke's theory may not be suitable for estimating the mean and variance of the effective/overall shear strength of a region D in this simple plane strain example.*

The minor difference between τ_f^{slip} and τ_f^{FEA} is further explored. It is found that τ_f^{FEA} is typically larger than τ_f^{slip} , and the magnitude of difference seems to correlate well with the irregularity of the actual slip curve. This is reasonable because the overall shear strength τ_f^{FEA} should be the composition of the average shear strength along the slip curve τ_f^{slip} and the dilation effect produced by the irregularity.

CONCLUSION

Although the statistics of the spatial average shear strength over D can be estimated by Vanmarcke's theory, the statistics of the effective/overall shear strength are NOT consistent with those estimated by Vanmarcke's theory. However, the statistics of the effective shear strength are close to those of the spatial average shear strength along the actual slip curve. The effective shear strength is found to be typically slightly larger than the spatial average shear strength along the actual slip curve. The difference is believed to be due to the irregularity of the actual slip curve, i.e., the overall shear strength is the composition of the average shear strength along the slip curve and the dilation effect induced by the irregularity.

In the case where Vanmarcke's theory is taken to estimate the statistics of the effective shear strength, the theory generally overestimates the mean value of the overall shear strength and underestimates the variance. Both errors are unconservative.

The overestimation of the mean value is maximum when the scale of fluctuation is comparable to a characteristic size of the soil mass. The underestimation of the variance increases with decreasing scale of fluctuation.

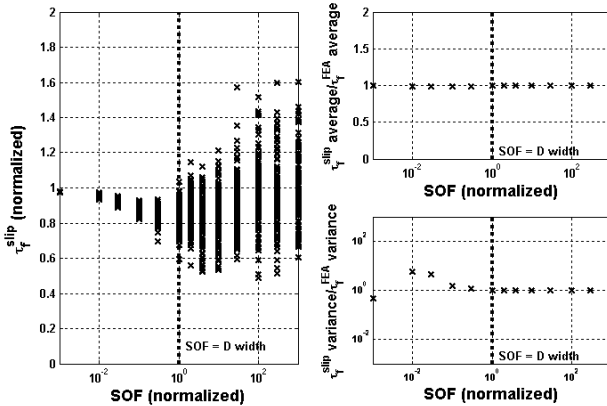


Figure 3 Samples of τ_f^{slip} , their average values and variances under different SOFs, normalized with respect to the sample average and variance of τ_f^{FEA} .

REFERENCES

- Kennedy, J. and Eberhart, R. (1995). Particle swarm optimization. *Proceedings of IEEE International Conference on Neural Networks, Vol IV*, 1942–1948.
- Pham, H.T.V. and Fredlund, D.G. (2003). The application of dynamic programming to slope stability analysis. *Canadian Geotechnical Journal*, 40, 830-847.
- Fenton, G.A. and Vanmarcke, E.H. (1990). Simulation of random fields via local average subdivision, *ASCE Journal of Engineering Mechanics*, 116(8), 1733-1749.
- Vanmarcke, E.H. (1977). "Probabilistic modeling of soil profiles." *ASCE Journal of Geotechnical Engineering Division*, 103(11), 1227-1246.

Transportation Risk Analysis (TRA) of Bosphorus Suspended Bridge, using Probabilistic Approach

H. Aslan¹, H. S. Kuyuk² and M. Aktas³

¹Division of Transportation, Department of Civil Engineering, Sakarya University, Esentepe Campus, A1 Serdivan/Sakarya, PH +90 (264) 2955752 Turkey; email: haslan@sakarya.edu.tr

²Earthquake Research Institute, The University of Tokyo, 113-0032, Yayoi 1-1-1 , Bunkyo-ku, Tokyo, PH +81 (3) 5841 1766, Japan, email: serdarkuyuk@gmail.com

³Department of Civil Engineering, Sakarya University, Esentepe Campus, A1 305 Serdivan/Sakarya, PH +90 (264) 2955727 Turkey; email: muharrema@sakarya.edu.tr

ABSTRACT

The expected destructive earthquake of Istanbul in the near future urges the researchers to determine the proper and effective measures in order to make sure that the Bosphorus related traffic is affected at the possible lowest level. By considering the fact that the traffic on this bridge corresponds to the busiest in Turkey, especially in the peak hours, the amount of lives to be lost when the earthquake hits the bridge must be kept at the minimum levels according to the different scenarios. In this research a probabilistic approach is employed to develop a risk analysis model by manipulating the speeds of the vehicles and the length of the danger.

INTRODUCTION

Istanbul, the biggest metropolitan city of Turkey, is expecting one of the most devastating earthquakes of its history with a huge number of buildings to be collapsed and damaged. The expected earthquake will affect this city from a wide spectrum of daily life, causing many people to die and get wounded. The Bosphorus suspended bridge, without any doubt, is one of the most critical structures of the city. This bridge is not just important as being one of the most important connecting elements of the European and Asian sides of the city, it also represents the highest volumes of traffic of the city as a whole. Determination of proper traffic management strategies will have utmost importance in order to minimize the total number of dead and/or injured people using the bridge for their daily travel purposes (Aktas et. al. 2010). This paper focuses on the issues of the strategies to manage the traffic on the Bosphorus suspended bridge by investigating the occurrence probability of the danger zone lengths and manipulating the average speeds of the vehicles on the bridge.

GENERAL STRUCTURAL AND TRAFFIC PROPERTIES OF THE BOSPHORUS BRIDGE

The Bosphorus Bridge has a length and height of 1071m and 165 mt, respectively and 6 lanes (3+3) being in service since 1973. The average daily traffic on both directions is at about 190.000veh/day (www.kgm.gov.tr). Many researchers have been conducted on the dynamic properties of the bridge. Maximum transverse and vertical displacements of the bridge are calculated 1.36 and 1.154 meter respectively at mid-span (Apaydin N. M., 2010).

The following figure illustrates the fluctuating nature of the traffic volumes available on the bridge for different days of the selected month.

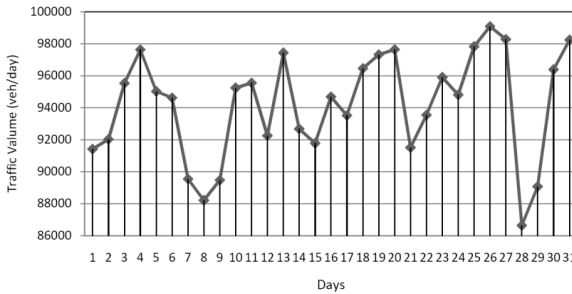


Figure 1. Average number of vehicles per day for one direction (March, 2010)

The same unstable nature of the traffic can be observed as far as the hourly volumes are concerned as shown in the figure below.

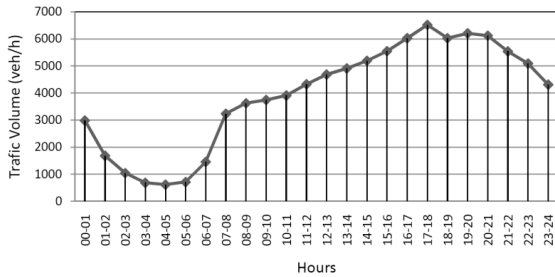


Figure 2. Typical hourly traffic available on the Bosphorus Bridge

Although the average daily traffic (around 3900 veh/h) is already quite high, the peak hour traffic volume of 6000-6500 veh/h (17⁰⁰ - 18⁰⁰) causes unbearable queues with extremely high travel times.

SETTING UP THE MATHEMATICAL STRUCTURE AND COST MATRIX OF THE MODEL

As to determine the best strategies in terms of the speeds on the bridge, a cost matrix was set up to illustrate the number of people to be affected if they are the ones on the danger zone when the earthquake hits the bridge. This matrix has the possible speeds of the vehicles as its rows and lengths of the danger zone as its column. Danger zone describes the critical sections of the bridge in terms of failure and collapse.

Determination of the values of the matrix is based on the model suggested by Greenshields (1935). This model, being one of the macroscopic approaches to relate the speed and density of the traffic, hypothesized that a linear relationship existed between the two parameters of speed and density. The speed that is used in the algorithm is the space-mean speed which is the harmonic mean of the speeds of the vehicles passing a point on a highway during an interval of time. This speed is obtained through the division of the total distance on a section of highway by the total time required by two or more vehicles to travel this distance. The density, on the other hand is the number of vehicles travelling over a unit length of highway at an instant in time.

With these explanations, the mathematical relation is expressed by Greenshields as follows.

$$\bar{u}_s = u_f - \frac{u_f}{k_j} k \quad (1)$$

where;

\bar{u}_s is the space-mean speed of the vehicles corresponding the density of k

u_f is the maximum speed when the density is at its minimum, i.e., 0

k_j is the jam density

The values of this matrix are determined through a design vehicle of 4.5m with four (4) occupants travelling. The value given by the first cell of Table 1 below, for example, represents the total number of people who are calculated to be in the danger zone facing with loosing their lives through determining the number of vehicles using Greenshields' speed and density relationship. Thus the original matrix represents the numbers when related speed and corresponding length of danger zone are the case to represent the real cases as if the earthquake hit and those speed and length values occurred in real life. In other words, each cell value is determined by assuming that the probability of speed and danger zone for that specific value being 1.

The following Table 1 indicates the calculated cost values for these real case scenarios.

Table 1. System cost matrix values

Velocity (km/h)	Danger Zone Length (m)																
	125	150	175	200	225	250	275	300	325	350	375	400	425	450	475	500	
20	218	273	327	382	436	491	545	600	654	709	764	818	873	927	982	1036	1091
30	194	242	291	339	388	436	485	533	582	629	678	727	775	824	872	921	969
40	170	212	255	297	339	382	424	467	509	551	594	636	678	721	763	805	848
50	145	181	218	254	291	327	364	400	437	473	509	546	582	619	655	692	728
60	121	151	182	212	242	273	303	333	364	394	425	455	485	516	546	576	607
70	97	121	145	170	194	218	242	267	291	315	339	364	388	412	436	461	485
80	73	90	109	127	145	164	182	200	218	236	255	273	291	309	328	341	364
90	48	61	73	85	97	109	121	133	146	158	170	182	194	206	218	231	243
100	24	30	36	42	48	55	61	67	73	79	85	91	98	104	110	116	122
110	8	10	12	14	16	18	20	22	24	26	28	30	32	34	36	38	40

As one of the main objectives of this research is to investigate and establish the best set of possible strategies to manage the traffic to minimize the possible dead and injured numbers, the probabilistic distribution of both speed and length values was employed to include all different possibilities and scenarios. Hence, a new cost matrix was suggested to model these situations. Each cost elements of this matrix is calculated through

$$P_{v_j} P_{l_j} C_{ij} \tag{2}$$

where;

i is the total number of the speeds

j is the total number of the danger zone

P_{v_j} is the probability of i.th speed when the length of j is the case

P_{l_j} is the probability of length of the danger zone when the speed of the vehicle is i is the case

C_{ij} is the cost matrix values from Table 1 given above.

The cost matrix elements of the model of this research, thus, are related to the probabilistic distribution of the speeds and length of the danger zones. Four different types of cases were used to represent the probabilistic occurrence of the length of the danger zones as shown in Figure 3 below.

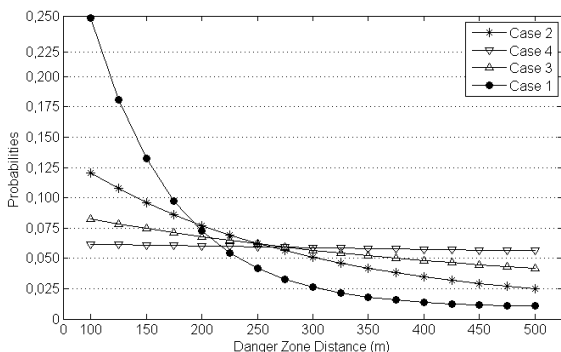


Figure 3. The probabilistic distribution of the Cases

Probability distribution of danger zone distance is assumed as an exponential function. This is due to the historical data related to the occurrence and magnitude of earthquakes and realistic evaluation of the fact that stronger earthquakes cause higher damages. The occurrence probability of 200 m danger zone, for instance, is higher than 500 m danger zone because the probability of the occurrence of earthquake with Magnitude 5 is higher than the occurrence of earthquake with magnitude 7.5. While Case 1 covers this approach, other cases with different standard deviation and mean values, shown in Figure 3, are also assessed for comparison purposes and to investigate the boundaries of this approach. The following Figure 4 depicts the lognormal structure of the averaged space-mean speed of the vehicles within the scope of this research.

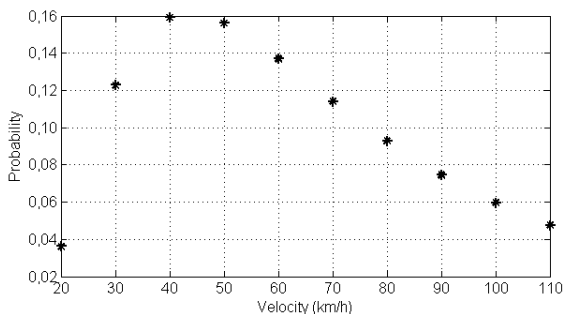


Figure 4 Lognormal distributions of the speeds

The following Table 2 illustrates the probabilistic cost values of the matrix for the distribution type of Case1. A lognormal - probability distribution of the velocities of the vehicles crossing the bridge is assumed to demonstrate the probability and decided with respect to the data available for the bridge. The highest

congestion level of the bridge is generally seen in the entrance of the bridge. As the vehicles enter the bridge, the density is not that much causing the dominant velocity to be at about 50km/h obtained from the many test drives at different times and days of the months.

Table 2 System cost matrix values in terms of probabilistic approach

Velocity (km/h)	Danger Zone Length (m)																
	100	125	150	175	200	225	250	275	300	325	350	375	400	425	450	475	500
20	0.95	1.06	1.14	1.19	1.22	1.23	1.23	1.22	1.20	1.18	1.16	1.13	1.10	1.07	1.04	1.02	0.99
30	2.87	3.19	3.43	3.58	3.67	3.71	3.71	3.68	3.63	3.55	3.48	3.40	3.31	3.23	3.14	3.06	2.99
40	3.26	3.63	3.90	4.07	4.16	4.21	4.20	4.18	4.11	4.04	3.95	3.86	3.76	3.66	3.57	3.47	3.39
50	2.73	3.04	3.27	3.41	3.50	3.54	3.54	3.51	3.47	3.40	3.32	3.25	3.16	3.09	3.00	2.93	2.86
60	2.00	2.22	2.40	2.50	2.56	2.59	2.59	2.56	2.53	2.48	2.43	2.37	2.31	2.26	2.20	2.14	2.09
70	1.33	1.49	1.59	1.67	1.71	1.72	1.72	1.71	1.69	1.65	1.62	1.58	1.54	1.50	1.46	1.43	1.39
80	0.82	0.90	0.97	1.01	1.04	1.05	1.05	1.04	1.03	1.01	0.99	0.96	0.94	0.91	0.89	0.86	0.85
90	0.43	0.49	0.52	0.54	0.56	0.56	0.56	0.56	0.55	0.54	0.53	0.52	0.50	0.49	0.48	0.47	0.46
100	0.17	0.19	0.21	0.22	0.22	0.23	0.23	0.22	0.22	0.22	0.21	0.21	0.20	0.20	0.19	0.19	0.18
110	0.05	0.05	0.05	0.06	0.06	0.06	0.06	0.06	0.06	0.06	0.06	0.06	0.05	0.05	0.05	0.05	0.05

This approach finally produced the concept of “Total Expected System Cost”. which is formulated in the following equation.

$$EC = \sum_{i=1}^n \sum_{j=1}^m P_{v_i} P_{l_j} C_{ij} \tag{3}$$

EC here is the total expected cost of the whole system.

RESULTS AND DISCUSSIONS

The total expected cost of the system can be shown as in Figure 5 for different probabilistic distribution of danger zone distances. As this figure implies, Case 4 represents the worst scenario with the total cost of 360 deaths. This was expected as Case 4 shows boundary condition assuming the probabilistic variation in danger zone length is almost the same regardless of the magnitude of the earthquake. The other cases along with the most realistic approach of Case 1. resulted in lower expected cost values (total number of people in danger). Case 1., having the minimum value of expected cost, is in fact what is expected in real life due the fact that the probability distributions are determined using real data. As we had the actual measured speed values for Bosphorus Bridge, it was decided to model these speeds as a log-normal distribution being the best fitting approach as far as the actual speed distribution is concerned. Although the real-life data are already available, there is still an unknown side of these speeds simply because it is not known which one would be the real-life case when the earthquake hits. This also explains why probabilistic approach is used to determine the best strategies as far as bridge traffic

management is concerned. From this point of view, $P_{v_i,j}$ and $P_{l_i,j}$ represent the probabilistic values of the speeds and danger zone length in case of occurrences of the earthquakes described by 4 different cases above.

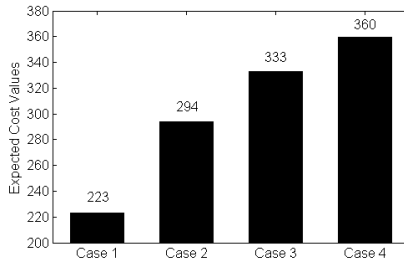


Figure 5. Total expected cost of the system for different cases of the danger zone distance probabilistic distribution

Other interesting findings of this research are shown in Figure 6. These four different graphics sum the general pictures of the expected cost values of the problem in detail regarding these four different cases, respectively.

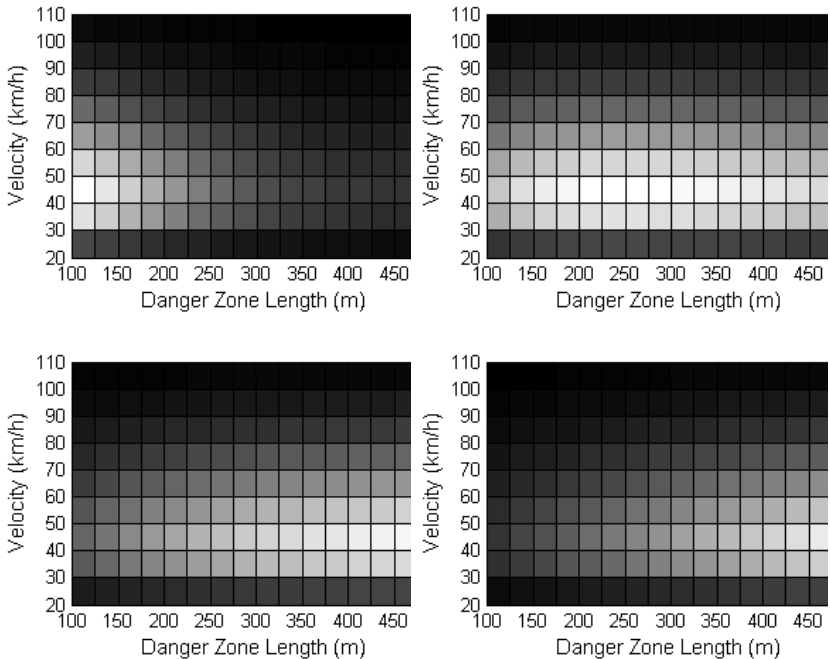


Figure 6 Illustration of the expected cost matrix values for each cell and scenario

The brighter the cells get, the higher the expected cost of the system is obtained as far as the combinations of the velocity and danger zone distance probabilities are concerned. While the brighter cells are located in the left–bottom corner of the first item of the graph indicating the most dangerous combination of the probabilities in terms of Case 1., the brighter section moves to the down part of the right corner of the last item representing Case 4. The darker parts of the graphs are those sections with the safest combinations of speed and length probabilities. Hence, the safest strategies to be implemented and operated by the engineer lie among the darker sections of the graphs. If the Case 1, for example, is the real-life case, then the model suggests that the best strategy to be implemented to operate the traffic is that a density of vehicles on the bridge can allow the vehicles travelling on the danger zone to have at least a speed of 70km/h. This is done through limiting the amount of the vehicles to use the bridge for crossing.

REFERENCES

AKTAS M., KUYUK H. S., ASLAN H., “Traffic Management for Bosphorus Suspended Bridge, Istanbul information based on earthquake real-time information” 14th European Conference on Earthquake Engineering, Ohrid, Republic of Macedonia, 30th August – 3rd September, 2010

Apaydin N. M., (2010) Earthquake performance assessment and retrofit investigations of two suspension bridges in Istanbul Soil Dynamics and Earthquake Engineering 30 702–710

General Directorate of Turkish Highways, www.kgm.gov.tr

Greenshields . B.D. (1935) “ A study of traffic capacity. Highway Research and Board proceedings 14. 448-477

Effects of Spatial Variability of Soil Property on Slope Stability

K. Kasama¹ and K. Zen¹

¹Geo-disaster Prevention Laboratory, Division of Civil and Structural Engineering, Faculty of Engineering, Kyushu University, 744 Motoooka, Nishi-ku, Fukuoka 819-0395, Japan; TEL&FAX +81-92-802-3383; email: kasama@civil.kyushu-u.ac.jp and zen@civil.kyushu-u.ac.jp

ABSTRACT

This paper presents a probabilistic approach to evaluating the geotechnical stability problem by incorporating the stochastic spatial variability of soil property within the numerical limit analyses. The undrained shear strength and unit weight of soil are treated as a random field which is characterized by a log-normal distribution and a spatial correlation length. The current calculations use a Cholesky Decomposition technique to incorporate these random properties in numerical limit analyses. The Random Field Numerical Limit Analyses are applied to evaluate effects of spatial variability of soil property on the slope stability and the failure mechanism. Monte Carlo simulations are then used to interpret the failure probability of slope for selected ranges of the coefficient of variation in soil property and the ratio of correlation length to slope height. Finally, the conventional safety factor of slope stability is evaluated to obtain an objective probability of slope failure.

RANDOM FIELD NUMERICAL LIMIT ANALYSES

Numerical limit analyses

The Numerical Limit Analyses (NLA) used in this study were based on 2-D, plane strain linear programming formulations of the Upper Bound (UB) and Lower Bound (LB) theorems for rigid, perfectly plastic materials presented by Sloan and Kleeman (1995) and Lyamin and Sloan (2002). One of the principal advantages of NLA is that cohesion and friction angle were only input parameters. Figure 1 illustrates a typical finite element mesh used for two dimensional slope stability program with the slope angle of 45°.

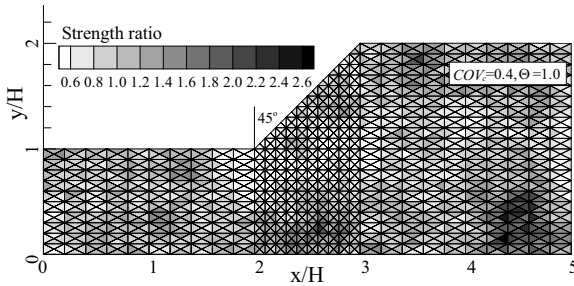


Figure 1. Typical mesh for slope stability considering the spatial variability

Random field realization

The effects of inherent spatial variability are represented in the analyses by modeling the undrained shear strength, c_u , and unit weight, γ , as a homogeneous random field. The undrained shear strength and unit weight are assumed to have an underlying log-normal distribution with mean, μ_c and μ_γ , and standard deviation, σ_c and σ_γ , and an isotropic scale of fluctuation (also referred to as the correlation length), θ_c and θ_γ . Current simulation assumes that correlation length of unit weight θ_γ is similar to that of cohesive strength θ_c . Following Griffiths and Fenton (2004) the current analyses present results based on assumed values of the ratio of the correlation length to slope height, $\Theta = \theta_c/H = \theta_\gamma/H$ as an input parameter.

The mean and standard deviation of $\log c_u$ and $\log \gamma$ are readily derived from μ_c and σ_c and μ_γ and σ_γ as follows (e.g., Baecher & Christian, 2003):

$$\sigma_{\ln c} = \sqrt{\ln(1 + \sigma_c^2)} \quad ; \quad \sigma_{\ln \gamma} = \sqrt{\ln(1 + \sigma_\gamma^2)} \quad (1)$$

$$\mu_{\ln c} = \ln \mu_c - \frac{1}{2} \sigma_{\ln c}^2 \quad ; \quad \mu_{\ln \gamma} = \ln \mu_\gamma - \frac{1}{2} \sigma_{\ln \gamma}^2 \quad (2)$$

The spatial variability is incorporated within the NLA meshes by assigning the undrained shear strength, c_i , and unit weight, γ_i , corresponding to the i th element:

$$c_i = \exp(\mu_{\ln c} + \sigma_{\ln c} \cdot G_i) \quad ; \quad \gamma_i = \exp(\mu_{\ln \gamma} + \sigma_{\ln \gamma} \cdot G_i) \quad (3)$$

where G_i is a random variable that is linked to the spatial correlation length, θ_c and similar G_i is used to calculate c_i and γ_i in this study. Namely, it is assumed that unit weight of i th element, γ_i was assumed to be perfectly correlated with the undrained shear strength of i th element, c_i , which agrees with experimental findings that there is

strong correlation between undrained shear strength and unit weight of soil. Values of G_i are obtained using a Cholesky Decomposition technique using an isotropic Markov function which assumes that the correlation decreases exponentially with distance between two points i, j :

$$\rho(x_{ij}) = \exp(-2x_{ij}/\theta) \quad (4)$$

where ρ is the correlation coefficient between two random values of c_u and γ at any points separated by a distance $x_{ij} = |x_i - x_j|$ where x_i is the position vector of i (located at the center of element i in the finite element mesh). Figure 1 illustrates the spatial distribution of undrained shear strength obtained for a typical mesh for one example simulation with input parameters $\mu_c = 100\text{kPa}$, $COV_c = (\sigma_c/\mu_c) = 0.4$ and $\Theta = 1.0$. The lighter shaded regions indicate areas of higher shear strength. A parametric study has been performed using the ranges listed in Table 1. It is noted that input coefficient of variability of undrained shear strength, COV_c , ranges from 0.2 to 1.0 while input coefficient of variability of unit weight, COV_γ , is fixed at 0.1 because the spatial variability of unit weight is generally less than that of shear strength. Normalized correlation length Θ ranges from 0.25 to 4.0 in addition to very small correlation length which is corresponding that the strength of elements was randomly determined. Although horizontal correlation length is generally larger than vertical one for naturally deposited soils, horizontal correlation length assumed to be identical to vertical correlation length in this study. For each set of parameters, a series of 1000 Monte-Carlo simulations have been performed.

Table 1. Input parameters

Parameter	Value
Angle of slope	45°
Mean undrained shear strength μ_c	100kPa
Coefficient of variability of undrained shear strength, COV_c	0.2, 0.4, 0.6, 0.8, 1.0
Mean undrained shear strength μ_γ	10kN/m ³
Coefficient of variability of unit weight, COV_γ	0.1
Ratio of vertical and horizontal correlation length	1.0 (Isotropic)
Normalized correlation length $\Theta = \theta_c/H = \theta_\gamma/H$	Random, 0.25, 0.5, 1.0, 2.0, 4.0
Monte Carlo iterations	1000

NUMERICAL RESULT

Stochastic stability factor

In order to evaluate the stochastic property of slope stability with the spatial variability of soil property, the computed stability factor for slope can then be reported for each realization, i , of the random field, N_{si} , as follows:

$$N_{si} = \frac{F_s \cdot \mu_\gamma \cdot H}{\mu_c} \tag{5}$$

where F_s is a conventional safety factor of slope. Hence, the mean, μ_{N_s} , and standard deviation, σ_{N_s} , of the stability factor are recorded through each set of Monte Carlo simulations, as follows:

$$\mu_{N_s} = \frac{1}{n} \sum_{i=1}^n N_{s_i} ; \sigma_{N_s} = \sqrt{\frac{1}{n-1} \sum_{i=1}^n (N_{s_i} - \mu_{N_s})^2} \tag{6}$$

Figure 2 shows a 20-bin histogram of the stability factor from one complete series of Monte Carlo simulations with $COV_c = 1.0$ and $\Theta = 0.25$ and 1.0 . Based on goodness-of-fit tests, it is concluded that normal or log-normal distribution functions can be used to characterize the stability factor at a 5% significance level.

Figures 3 summarize the reduction ratio of mean stability factor obtained by equation (6) to deterministic solution for homogeneous slope with μ_c and μ_γ , $R_{N_s} = \mu_{N_s}/N_{sDet}$ (where $N_{sDet} = 5.57$) for combinations of the input parameters (COV_c , Θ). In general, $R_{N_s} < 1$ and hence spatial variability causes a reduction in the expected slope stability. The trends show that the largest reductions in μ_{N_s} occur when the coefficient of variation is high and/or the correlation length is small.

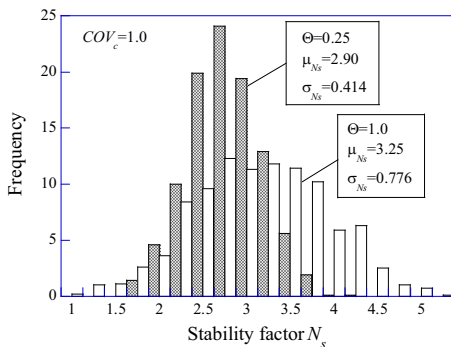


Figure 2. Histogram of stability factor for slope

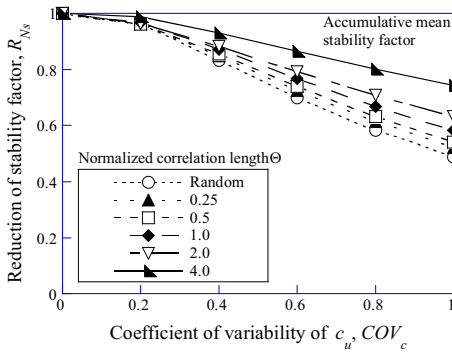
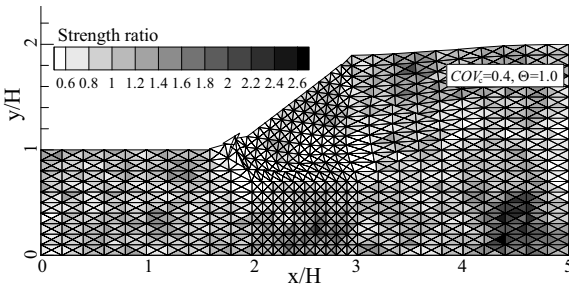
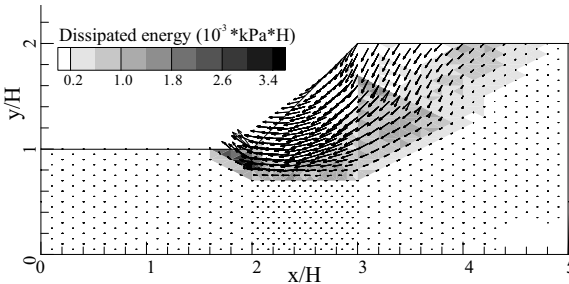


Figure 3. Reduction of stability factor for a given Θ



a) Deformed mesh



b) Dissipated energy and displacement vector

Figure 4. Typical failure mechanism

Failure Mechanism

Figures 4 illustrate typical failure mechanisms from a series of UB calculations for slope with the inclined angle of 45° , $COV_c = 0.4$ and $\Theta = 1.0$. Figure 4a) shows deformed FE mesh and the distribution of input shear strength. Figure b) shows dissipated energy together with the vectors of the computed velocity field. Close inspection shows that the computed failure mechanisms find paths of least resistance, passing through weaker soil elements in the slope. It can be seen that there is a well defined toe failure passing through the weak soil zone near the slope toe and there is a concentration of dissipated energy at the toe of slope. It is suggested that the location of weak soil elements in the slope affects failure mechanism of slope.

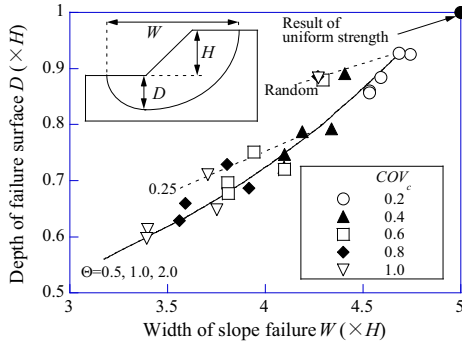


Figure 5. Relationships between width and depth of failure slope

In order to examine effects of spatial variability on the failure mechanism for slope, Figure 5 shows the relationships between mean width of failure zone and mean depth of failure surface obtained from a series of Monte Carlo simulation. It Although the width and depth of failure zone for homogeneous slope are $5.0H$ and $1.0H$ respectively, the mean width and depth of failure zone for slope with spatial variability decreases with increasing COV_c and Θ . It can be suggested that the spatial variability of soil property greatly affects to failure mechanism of slope. Moreover, the location of weak soil elements in slope is important to local failure of slope and the scale of slope failure decreases with increasing the magnitude of spatial variability of soil property.

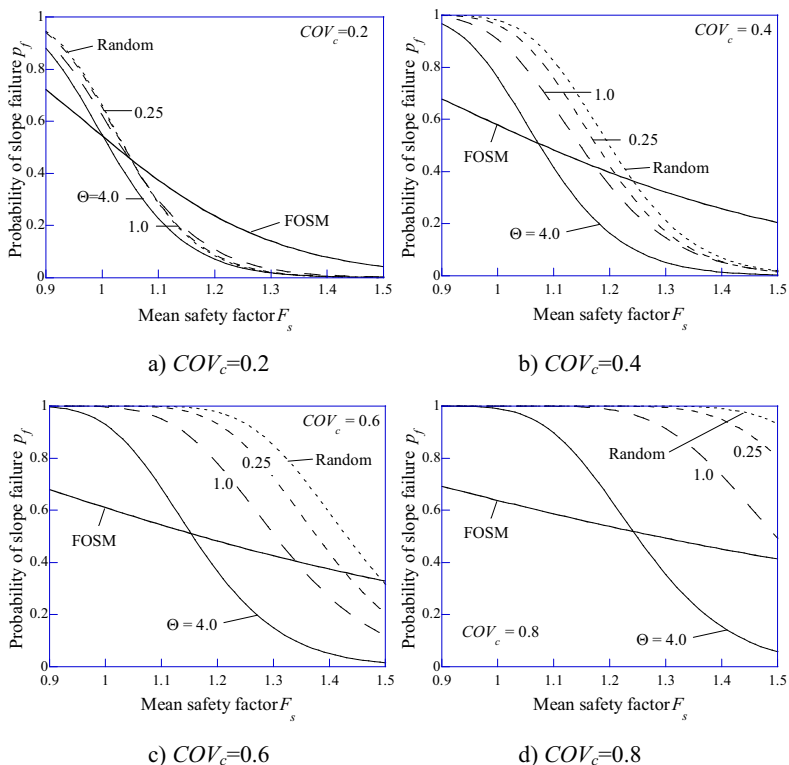


Figure 6. Probability of slope failure compared with FOSM

FAILURE PROBABILITY AND SAFETY FACTOR

In order to link obtained probabilistic results to conventional evaluation for slope stability using safety factor, the relationship between the probability of slope failure and mean safety factor of slope for a given COV_c are shown in Figure 6 together with results of conventional FOSM. The probability of slope failure became over 0.5 even for the mean safety factor of 1.0 because the mean stability factor for slope with spatial variability is less than that for homogeneous slope as shown in figure 3. The probability of slope failure for given COV_c and Θ decreases drastically as F_s increases compared to results of conventional FOSM. Moreover, the probability of slope failure for a given F_s increases with decreasing Θ , which is suggesting that the potential of local failure of slope increases with decreasing Θ . It can be

characterized that the numerical limit analyses incorporated with the random field theory is useful for representing local failure of slope induced by the spatial variability of soil property.

CONCLUSIONS

This paper has presented initial results from a probabilistic study on the slope stability problem using random field numerical limit analyses and Monte Carlo simulation. The spatial variability of soil property reduces the slope stability factor relative to a conventional calculation based on mean soil parameters. The failure zone of slope can be localized by generating failure surface through weak soil elements. Based on the results, the relationship between the conventional safety factor of slope stability and the probability of slope failure is discussed together with results of conventional FOSM.

REFERENCES

- Baecher, G.B. and Christian, J.T. (2003). "*Reliability and statistics in geotechnical engineering*", John Wiley & Sons, Ltd.
- Griffiths, D.V. and Fenton, G.A. (2004). "Probabilistic Slope Stability Analysis by Finite Elements", *J. Geotech and Geoenvi. Eng., ASCE*, Vol.130, No.5, pp.507-518.
- Lyamin, A.V. and Sloan, S.W. (2002). "Lower bound limit analysis using non-linear programming", *Intl. Journal for Numerical Methods in Engineering*, Vol.55, No.5, pp.573-611.
- Sloan, S.W. and Kleeman, P.W. (1995). "Upper bound limit analysis using discontinuous velocity fields", *Comput. Methods Appl. Mech. Eng.*, Vol.127, pp.293-314.

Interval Reliability Analysis for Gravity Retaining System of Deep Excavation

Wang Jingchun¹, Xu Pengfei² and Hou Weihong³

¹College of Civil Engineering, Shijiazhuang Tiedao University, P.O. Code 050043, Shijiazhuang, China; PH (86) 311-87939457; FAX (86) 311-87935085; email: wjc36295@163.com

²Structure Monitoring and Control Institute, Shijiazhuang Tiedao University, P.O. Code 050043, Shijiazhuang, China; PH (86) 311-87939285; FAX (86) 311-87939285; email: xupengfei-1986@163.com

³College of Civil Engineering, Shijiazhuang Tiedao University, P.O. Code 050043, Shijiazhuang, China; PH (86) 311-87936452; FAX (86) 311-87935085; email: wangyu950506@163.com

ABSTRACT

Deep excavation is a complex engineering system. It is necessary to research the system reliability of deep excavation in order to reduce the number of accidents. Considering the interval features of mechanic parameters of retaining system and soils of deep excavation, the interval analysis method was applied to establish two performance functions against overturning and sliding for the gravity retaining system of deep excavation. In terms of the limitation and shortage of the interval calculating rules, the affine arithmetic approach was adopted to compute corresponding reliability index. Then, the interval reliability of some typical systems, such as series system, parallel system, series-to-parallel system, etc, was studied based on the extension principle and the system analysis. The analysis process was given by an engineering example.

INTRODUCTION

In recent years, more deep excavation engineering have been constructed in the city, and more engineering accidents related to deep excavation emerged. It is necessary to research the system reliability of deep excavation in order to reduce the accident influence on urban life. Deep excavation engineering may have many potential failure modes, and every failure mode has many potential reasons, even countless reasons. There is a certain correlation between the potential failure mode and the reason. So, it is better to analyze the safety of deep excavation by using the systematic reliability theory. Reliability calculations of gravity retaining system can be performed by using improved FOSM methods(Xu Chao et al, 1998). Another

popular method employed in the analysis of gravity retaining walls is the reliability index approach (Du Yongfeng et al, 2008). In these methods, the real distributing of the geotechnical mechanics parameters is not represented by probability density function or membership function and the reliability of the retaining system is not accurately calculated. Come from the previous researches, the interval features of parameter value of retaining structure and soils of deep excavation are confirmed. In this paper the interval theory was used to calculate the reliability of gravity retaining of deep excavation, and the system reliability considering the two failure modes of overturning and sliding of retaining structure was analyzed, which could consummate the reliability theory and reduce the accident rate of deep excavation.

NON-PROBABILISTIC RELIABILITY MODEL FOR STABILITY OF GRAVITY RETAINING STRUCTURE

The major unstable modes of gravity retaining structure are overturning, sliding, compressive or shear failure of retaining wall, deficiency of bearing capacity of foundation, piping or quicksand etc. In the check computations of reliability design, various failure mode corresponds to the specific performance functions and the limit state equation. In order to simplify the calculation, the performance function of overturning and sliding instability of retaining wall will be discussed in the following.

Stability against sliding. The failure mechanism is a sliding produced by the wall body along the base. And the mathematical expression is $F_R \geq F_S$. F_R and F_S are the anti-sliding force and sliding force separately.

Stability against overturning. That is the overturning destruction which the wall body turns about the wall toe will not be produced. The mathematical expression is $M_R \geq M_S$. In where M_R and M_S represent the stability moment and the overturning moment.

In conclusion, the limit state equation for the stability of retaining wall's is given by

$$M_1 = g(F_R, F_S) = F_R - F_S = 0, M_2 = g(M_R, M_S) = M_R - M_S = 0 \quad (1)$$

The researches illustrate that the density of soil behind the retaining wall, γ , the internal friction angle, φ , cohesion, c , etc, are the main factors affecting the stability of gravity retaining system in deep excavation. All of those geotechnical mechanics parameters can be obtained from the laboratory or field experiment. For the uncertain factors such as the conditions of engineering geology, the division of petrofabric, the sampling methods, the test conditions, etc, these parameters have the interval features. Therefore, the interval analysis theory will be applied. And the each parameter of the retaining wall will be displayed by using an interval and then the non-probabilistic reliability index of the retaining wall will be gained. Therefore, the performance function of the traditional reliability analysis can be expressed as follows

$$M = g(x) = F - (1 + \delta) = F_R / F_S - (1 + \delta) = M_R / M_S - (1 + \delta) \quad (2)$$

Where the x is the variable of geochemical mechanics parameters in the retaining wall for deep excavation and the 1 is the safety factor when the retaining wall is in the limit state. The δ is the interval increment. All which can be got according to the request of the specification and engineering.

SOLUTION OF NON-PROBABILISTIC RELIABILITY INDEX

Solution for variety interval of response variable. The real variety interval of the response variable is asked to obtain in order to calculate the uncertain non-probabilistic reliability index of the geotechnical mechanics parameters in the retaining structure of deep excavation. For the most problems of retaining structure, the finite element method can be adopted to analyze(Lu Zhenzhou et al, 2002). And the governing equation of the structural system can be represented as

$$K \bullet Y = P, R = R(Y) \tag{3}$$

Where the matrix K is the rigidity matrix of the system and is the function of X . And X is the variable matrix in the inputting interval system. Y is the matrix of nodal displacement. P is the external load matrix. R is the function of the response variable Y . Generally, R equals stress or stain. When all the inputting variable are interval, the equation of the variable matrix as

$$X = [\underline{X}, \overline{X}] = \{ \underline{x}_n, \overline{x}_n \}, P = [\underline{P}, \overline{P}] = \{ \underline{p}_m, \overline{p}_m \} \tag{4}$$

In which n is the number of the geometric dimension and the variable of the geotechnical parameters, m is the number of the nodal, “-” adding on the upper and lower position of the variable indicates separately the values of upper limit and lower limit. Therefore, the response variables Y and R belong to the interval.

Normally, the intervals algorithm is adopted to calculate the changing intervals of the response variable. When the inputting number and its changing interval are minor, the varying interval can be exactly estimated using the intervals algorithm. However, if the number of imputing variable is bigger or the changing interval’s range of the imputing variable is wider, the interval of response variable will be excessively reckoned. Therefore, the affine arithmetic is brought in(Comba et al, 1993).

Considering the correlation of the values involving the interval arithmetic, a refined solution can be drew by the affine arithmetic(Shou Huahao et al, 2006). In the affine arithmetic, an uncertain parameter x (an interval parameter) is represented by the

affine form \hat{x} , which is a linear combination regarding the $\varepsilon_i (i=1,2,L, n)$:

$\hat{x} = x_0 + x_1\varepsilon_1 + x_2\varepsilon_2 + L + x_n\varepsilon_n$, in which, although the value of $\varepsilon_i (i=1,2,L, n)$ is

unidentified, its range is supposed as $[-1,1]$. The corresponding coefficient x_i is real number, which determines the magnitude and the sign of ε_i . Therefore, the interval form and affine form can mutual transmit; the parameter x is given in the interval

$[\underline{a}, \bar{b}]$, the corresponding affine form is $\hat{x} = x_0 + x_1 \varepsilon_1$, $x_0 = (\underline{a} + \bar{b})/2$, $x_1 = (\bar{b} - \underline{a})/2$.

Likewise, given a particular affine form $\hat{x} = x_0 + x_1 \varepsilon_1 + x_2 \varepsilon_2 + L + x_n \varepsilon_n$, the corresponding interval $[\underline{x}, \bar{x}] = [x_0 - \xi, x_0 + \xi]$, $\xi = \sum_{i=1}^n |x_i|$ will be received.

Solution of non-probabilistic reliability index. When the form of structural function $g(\bullet)$ is more complicated, the number of the variable is bigger or the feature of the incensement and reduction about the basic variable x_i is unidentified, following method could be adopted to determine the non-probabilistic reliability index (Guo Shuxiang et al, 2005). $x_i (i=1, 2, L, n)$ is the interval variable. $g(\bullet)$ is the function of x_i . M is the interval variable as well. The basic interval variable is standardized, meanwhile the limit state equation is transmitted into the standard form. The upper and lower bound of the equation satisfy the following condition:

$$M^l = \min_{\delta_i \in \Delta^l} G(\delta_1, \delta_2, \dots, \delta_n), M^u = \max_{\delta_i \in \Delta^l} G(\delta_1, \delta_2, \dots, \delta_n) \quad (5)$$

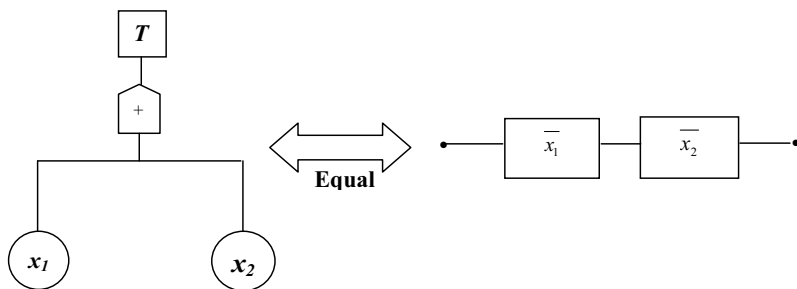
Therefore, the corresponding non-probabilistic reliability index is

$$\eta = M^c / M^r = (M^u + M^l) / (M^u - M^l) \quad (6)$$

CALCULATION FOR SYSTEMS INTERVAL RELIABILITY OF BRACING EXCAVATION

The research on system reliability is a structure reliability problem of multi-functional. A structure can be regarded as the constitution of the several failure models. Therefore, structure system can be considered as a series system, a parallel system or a series-to-parallel system, all of which are made up of the failure models. Then the structural reliability is turned to the reliability calculation of the system. Either overturning or sliding of the gravity retaining system in deep excavation will lead to the structural destruction. Therefore, the structural system is a parallel system.

Failure modes for gravity retaining system of deep excavation. According to the fundamental theory of the system fault tree and the equivalent relationship between fault tree and reliability block diagram, the gravity retaining system for deep excavation has been analyzed and the diagram showing the failure of foundation pit system and the equivalent parallel system can be drawn as Fig.1 (Jiang Xingwei et al, 2005). And x_i means the failure of the i unit; \bar{x}_i means the normal function of the i unit; T is failure and \bar{T} is the system in the normal operation. However, in this Fig 1, the T stands for the function failure of the deep excavation system. x_1 represents the failure of overturning. x_2 represents the failure of sliding.



(a) Fault tree of retaining system

(b) Reliability diagram

Fig.1. Diagram showing the failure of retaining system of deep excavation

Interval reliability analysis of system. For the system and its composed units, the assumption is as follows: there are only two states of performance and failure for the system and the units, and the reliability of the each unit in system is independent. For simplicity, here the traditional probabilistic reliability is named as point reliability to distinguish the interval reliability in the non-probabilistic reliability system. based on the relationship among basic design variables, unit reliability and failure probability, the point reliability R_s and failure probability F_s can be represented as

$$R_s = g(R_1, R_2, L, R_n), F_s = h(F_1, F_2, L, F_n) = 1 - g(R_1, R_2, L, R_n) \tag{7}$$

In which $g(\bullet)$ and $h(\bullet)$ separately stand for the continuous linear function or nonlinear function, $R_i, F_i \in [0, 1], i = 1, 2, L, n$.

In some cases, the reliability of unit in the system is not easily available. However, based on the experiences or the scientific experiments, under the request of the particular accuracy, the upper and lower limit $[R_i, \bar{R}_i], [F_i, \bar{F}_i], (i = 1, 2, L, n), (\bar{R}_i, \bar{F}_i \in [0, 1])$ of the interval reliability or the failure probability of unit can be obtained

The interval reliability and failure probability for the system can be derived from the interval extension of function (Moore, 1979) and the Eq (7) as follows:

$$[R_s] = g([R_1], [R_2], L [R_n]), [F_s] = h([F_1], [F_2], L [F_n]) = 1 - g([R_1], [R_2], L [R_n]) \tag{8}$$

Parallel System. From the analysis of the parallel system illustrated in Fig.2, based on the point reliability of system and interval extension theory the interval reliability of system can be deduced, which is

$$[R_s] = \prod_{i=1}^n [R_i] = \prod_{i=1}^n [\underline{R}_i, \bar{R}_i] = \left[\prod_{i=1}^n \underline{R}_i, \prod_{i=1}^n \bar{R}_i \right] \tag{9}$$



Fig.2 Parallel system

On the basis of the features of parallel system and interval analysis by Sun Hailong (2007), the interval characteristics of the parallel system are: the upper limit for the interval reliability of parallel system equals the arithmetic product of the upper limit of reliability of units in system; the lower limit of system equals the arithmetic product of the lower limit of its units; there is more possibility that the interval reliability of parallel system is less than the reliability of its units, that is $0 \leq P([R_s] \geq [R_i]) \leq 0.5$; as the number of the units become more and more, the reducing chance of the interval reliability of parallel system may become much feasible.

Series System. From the analysis of the series system in Fig.3, the system interval reliability can be obtained as follows:

$$[R_s] = 1 - [F_s] = 1 - \left[\prod_{i=1}^n (1 - \bar{R}_i), \prod_{i=1}^n (1 - \underline{R}_i) \right] = \left[1 - \prod_{i=1}^n (1 - \underline{R}_i), 1 - \prod_{i=1}^n (1 - \bar{R}_i) \right] \quad (10)$$

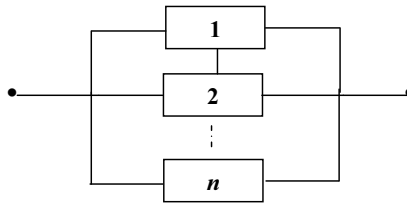


Fig.3 Parallel system

According to the features of series system and interval theory, the interval reliability of series system have the characteristics as follows: the upper limit and lower limit separately cater to $1 - \prod_{i=1}^n (1 - \underline{R}_i) \geq \underline{R}_i$ and $1 - \prod_{i=1}^n (1 - \bar{R}_i) \geq \bar{R}_i$; there is more possibility that the interval reliability of the system may exceed that of the units, that is $0.5 \leq P([R_s] \geq [R_i]) \leq 1$; With the increasing of the unit number, the chance of the enlargement for system interval reliability will become more possible.

Series-to-parallel system. For the parallel-to-series system, the interval reliability of system is

$$[R_s] = \left[1 - (1 - \underline{R}_1 \underline{R}_2)(1 - \underline{R}_3 \underline{R}_4), 1 - (1 - \bar{R}_1 \bar{R}_2)(1 - \bar{R}_3 \bar{R}_4) \right] \quad (11)$$

For the series-to-parallel system, the interval reliability of system is

$$[R_s] = \left[1 - \prod_{i=1}^2 (1 - \underline{R}_i), 1 - \prod_{i=1}^2 (1 - \overline{R}_i) \right] \bullet \left[1 - \prod_{i=3}^4 (1 - \underline{R}_i), 1 - \prod_{i=3}^4 (1 - \overline{R}_i) \right] \quad (12)$$

From the analyses of interval reliabilities between the parallel-to-series system and the series-to-parallel system, it is founded that interval reliability of the former system is more reliable than that of the latter.

ANALYSIS OF ENGINEERING EXAMPLE

Engineering outline. The deep excavation with the gravity retaining structure was put into use in Shanghai, whose typical section was displayed in the Fig.4. Through the experiments of laboratory and site, the density, the internal friction angle, cohesion of soil behind the retaining wall, and the average density of the wall body, $\gamma, \varphi, c, \gamma_0$ were obtained. The number of the each parameter are, $\gamma = [17.8, 18.7]$, $\varphi = [10.8, 11.5]$, $c = [8.2, 9.1]$ and $\gamma_0 = [18, 19]$. The depth of deep excavation is $H=9.8\text{m}$. The retaining wall of deep-mixing pile was adopted. The distance buried into the soil was $D=8.2\text{m}$. The width of the braced wall body was $b=6.5\text{m}$. The load on the ground was uniform load $q=10\text{kPa}$. The soil of the foundation was supposed one layer, and its parameters were gained by the weighting according to the thickness of soil layer.

Analysis process. On the given conditions, the earth pressure on the retaining structure was calculated as follows:

$$E_a = \frac{1}{2} \gamma (H + D)^2 K_a - 2c(H + D) \sqrt{K_a} + \frac{2c^2}{\gamma} + qK_a (H + D), \quad E_p = \frac{1}{2} \gamma D^2 K_p + 2cD \sqrt{K_p} \quad (13)$$

in which, $K_a = \tan^2(45 - \frac{\varphi}{2}), K_p = \tan^2(45 + \frac{\varphi}{2})$.

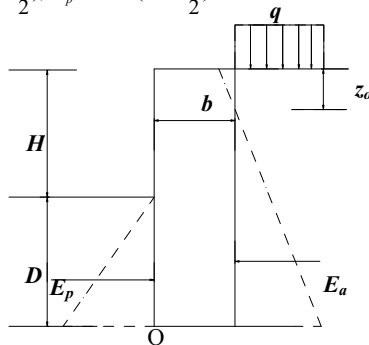


Fig.4 Cross-section of gravity retaining wall and force diagram

Non-probabilistic reliability calculation of stability against sliding. Connecting the Eq.(2) and the calculation method of stability against sliding for retaining wall, the performance function against sliding was set up as below

$$M_1 = \frac{W \tan \varphi + cb + E_p}{E_a} - (1 + \delta_1) \quad (14)$$

Based on the engineering practice and the calculation requirements $\delta_1 = 1$, from the given conditions and Eq.(13) and (14), the operating of affine arithmetic was deduced, then, $M_1 = [0.66, 0.92]$. According to the Eq.(6) and the optimization the non-probabilistic reliability index of stability against sliding was calculated, $\eta_1 = 4.08$.

Non-probabilistic reliability calculation of stability against overturning. Likewise, the performance function of stability against overturning is

$$M_2 = \frac{W \frac{b}{2} + E_p \frac{D}{3}}{(E_a - K_a qH) \bullet \frac{H - z_0}{3} + \frac{K_a qH^2}{2}} - (1 + \delta_2), \quad \left(z_0 = \frac{2c}{\gamma \sqrt{K_a}} \right) \quad (15)$$

For calculation convenience, choose $\delta_2 = 1$. According to the given conditions, Eq.(13) and (15) and the operating of affine arithmetic, the $M_2 = [0.63, 0.82]$ was deduced. According to the Eq.(6) and the optimization the non-probabilistic reliability index of stability against sliding was obtained, $\eta_2 = 5.63$.

Non-probabilistic reliability calculation of system. According to the Fig.1, either overturning or sliding of the gravity retaining wall would lead to structural destruction. So, the retaining structure of deep excavation should be a parallel system. The interval non-probabilistic reliability of retaining system could be deduced from the M_1 , M_2 and Eq.(9), $R_s = [0.416, 0.754]$. According to the Eq.(6) and the optimization the non-probabilistic reliability index of retaining system was gained, $\eta = 3.46$.

From the Fig.4 and the engineering example, it was known that the calculation method of non-probabilistic reliability for gravity retaining system of deep excavation was simple and the result was reasonable, which illustrated that the method in calculating reliability was feasible.

CONCLUSION

Based on the interval features laying the mechanic parameters for the gravity retaining system, the interval analysis was introduced. And affine arithmetic was adopted to solve the problem of interval calculation, which effectively solved the problem of interval extension. Meanwhile, the overturning failure and sliding instability in gravity retaining system were recognized as the parallel system. Then using the typical features of interval system, the non-probabilistic reliability index was calculated. The engineering case made the further verification of the reasonable and feasible for analysis method of non-probabilistic reliability in retaining system of deep excavation. However, a further research and verification need to be enforced in the various failure modes and the complicated system of deep excavation in the future.

REFERENCES

- Xu Chao, Yang Linde (1998). "Analysis of reliability for braced system of gravity foundation pit". *Hydrogeology and Engineering Geology*, 24(6): 34-37
- Du Yongfeng , Yu Yu, Li Hui(2008). "Analysis of reliability of structural systems for stability gravity retaining walls". *Chinese J. of Geotechnical Engineering*, 30(3): 349-353
- Lv Zhenzhou, Feng Yunwen, Yue Zhufeng (2002). "An advanced interval-truncation approach and non-probabilistic reliability analysis based on interval analysis". *Chinese Journal of Computation Mechanics*, 19(3): 260-264
- Comba J. L. D., Stolfi J.(1993). "Affine arithmetic and its applications to computer graphics". In: *Proceedings of Anais do VII SIBGRAPI*, Recife, Brazi: 9-18
- Shou Huahao, Shen Jie (2006). "A survey on research and applications of interval arithmetic and affine arithmetic". *J. of Image and Graphics*, 11(10):1351-1358
- Guo Shuxiang, Zhang Ling, Li Ying (2005). "Procedures for computing the non-probabilistic reliability index of uncertain structures". *Chinese Journal of Computation Mechanics*, 22(2): 227-231
- Jiang Xingwei, Song Zhengji, Wang Xiaochen (2005). "*Reliability and technology of engineering*". Haerhin: Harbin Institute of Technology Press
- Moorse R. E. (1979). *Methods and applications of interval analysis*. Philadelphia: SIAM Publications
- Sun Hailong.(2007). "Interval reliability analysis of some typical systems". *Journal of Nanjing University of Aeronautics & Astronautics*, 39(5): 637-641

Methodology for Risk Analysis of Ground Surface Subsidence

H. A. Kamal¹ and B. M. Ayyub²

¹Building and Energy Technologies Department, Kuwait Institute for Scientific Research, P.O. Box 24885 Safat, 13109 Kuwait, PH (965) 2498-9261; FAX (965) 2498-9099; hkamal@kisir.edu.kw

²Center for Technology and Systems Management, Department of Civil and Environmental Engineering, University of Maryland, College Park, MD 20740; PH (301) 405-1956; FAX (301) 405-2585; ayyub@umail.umd.edu

ABSTRACT

A number of ground surface subsidence occurred within few months in a residential suburb in Kuwait due to sinkholes. Comprehensive studies were carried out to identify the reasons of the subsidence and underground deep cavities were detected. The cause of the sinkholes was attributed to the dissolution of the limestone bedrock and the subsequent raveling of the overburden soil cover. A pilot area was selected and treated by filling the underground deep cavities with cementitious grout materials. This paper develops a basis of a methodology for quantifying the risk of ground surface subsidence due to underground cavities for the above case. The hazard and risk profile development is limited to computing the probability of sinkhole formation over the selected pilot area based on field data and examining spatial characteristics of the cavities. The failure probability is based on a single limit state and failure mode. The spatial analysis of cavities demonstrated an analytical process and confirmed the random layout of cavities without any spatial characteristics at about the same depth. A regression model for predicting grout volume as a function of cavity height was developed.

Keywords: *Sinkhole, Cavities, Subsidence, Risk, Failure probability, Spatial analysis*

INTRODUCTION

Several ground surface subsidences were occurred in Kuwait in the last two decades. In general, principal causes of land subsidence include aquifer-system compaction, drainage of organic soils, underground mining, oil extraction, hydrocompaction, natural compaction, sinkholes, and thawing permafrost (National Research Council, 1991). The consequences of land subsidence can be significant in monetary and land use terms. The costs of identification, stabilization and repair can be enormous with uncertain effectiveness. Developing the means to cost-effectively, yet comprehensively characterize conditions that could lead to subsidence is critical to reducing risk and containing costs to acceptable levels. Pressurized grout remote backfilling has been identified as an effective stabilization method. According to this

method, a cementitious grout is pumped through cased drill holes directly into cavities. This method is effective for stabilizing the surface from underground subsidence. A primary drawback of pressurized grout remote backfilling is its high cost, mainly due to the high cost of Portland cement. A case study is introduced in this paper in order to concurrently demonstrate the methodology.

RISK ANALYSIS

Risk is generally defined as the potential of losses for a system resulting from an uncertain exposure to a hazard or as a result of an uncertain event (Ayyub 2003). It is quantified as the rate that losses will occur due to the non-performance of an engineered system or component. The non-performance be quantified as the probability that specific loads (or demands) exceed respective strengths (or capacities) causing the system or component to fail, and losses are defined as the adverse impacts of that failure if it occurs. Risk can be viewed to be a multi-dimensional quantity that includes event-occurrence rate (or probability), event-occurrence consequences, consequence significance, and the population at risk; however, it is commonly measured as a pair of the rate (or probability) of occurrence of an event, and the outcomes or consequences associated with the event's occurrence that account for system weakness, i.e., vulnerabilities. In a simplified notional (or Cartesian) product, risk is commonly expressed as:

$$\text{Risk} = \text{Event rate (or probability)} \times \text{Vulnerability} \times \text{Consequences of failure} \quad (1)$$

The probability of failure can be influenced by engineers by strengthening of existing structures or by adding additional protection; however the consequence part is highly dependent upon the actions and decisions made by residents, government and local officials. Risk analysis offers a framework to examine tradeoffs related to land subsidence and effectiveness of stabilization methods. Implementation of risk analysis to the land subsidence is challenging because it is a complex system of cavities, water table, groundwater flow, geological and soil characteristics, and land use. In addition, existing capability to accurately predict land subsidence is limited.

METHODOLOGY FOR RISK ANALYSIS

The quantification of a risk profile relating to land subsidence requires the performance of the following steps:

- Define the boundaries of a site of particular interest and characterize the site as follows:
 - Geological strata, types, distribution, and conditions
 - Hydrologic conditions including underground water content, distribution and flows, and precipitation and surface-to-underground flow due to land use
 - Spatial distribution of cavities (x,y,z), their volumes, and associated openings
 - Types of potential land subsidence
 - Built up assets at the site
 - Associated uncertainties

- Define primary cases of potential site conditions and their combinations, and failure modes and associated probabilities by estimating the following:
 - Occurrence probability of each type of land subsidence
 - Extent of land subsidence quantified in terms of surface area and volume, and associated probabilities
- Identify repair options. For each repair option, estimate the following:
 - Updated occurrence probability of each type of land subsidence
 - Updated extent of land subsidence quantified in terms of surface area and volume, and associated probabilities
 - Other impacts on the environment and repair equipment, and crew safety
 - Cost of repair
- Aggregate all scenarios prior to repairs to obtain loss exceedence probability curve representing the risk profiles, and aggregate all repair-impacted scenarios to obtain loss exceedence probability curve representing the risk profiles.
- Quantify the benefits as the difference between the risk profile after repairs and prior to repairs.

CASE STUDY: SINKHOLE OCCURRENCE

Investigation programs were conducted in a residential suburb after the occurrences of a number of sinkholes of various sizes. From the investigation programs, it is revealed that the causes of the sinkholes are the existence of Karst cavities within the Limestone bedrock underlying the overburden soil. The investigations outlined a treatment to minimize the recurrence of the sinkholes. The high cost and uncertainties associated with the treatment have necessitated the performance of a technical review and a need assessment of a risk study that would account for cavity spatial and size distributions, associated detection probabilities, costs, effectiveness, and potential consequences.

Since the development of this residential suburb, eight sudden incidents of ground subsidence have been recorded. The first four sinkhole incidents occurred between 1988 and 1989. The affected area, consisted of around 130 housing units, were evacuated and fenced for further study (Al-Rifaiy, 1990). Four other sinkholes were recorded in 2004. Table 1 lists detail on the eight occurred sinkholes and Figure 1 shows their locations (Abdullah and Kamal, 2005). The suburb site is characterized with an overburden layers consisting of sandy, slightly cemented and dense soil, which overlies the bedrock of the limestone Dammam Formation (Burdon and Al Sharhan 1968, Salman 1979).

Table 1. Recorded ground surface subsidence.

Sinkhole #	Location (Sector)	Date of occurrence	Diameter/length (m)	Width (m)	Depth (m)	
SH1	A1	April 1988	15.0	-	31.0	OTO
SH2	A1	April 1988	4.0	-	7.0	
SH3	A1	October 1988	7.0	-	9.0	
SH4	A1	June 1989	8.0	2.0	1.4	
SH5	A1	June 2004	4.8	2.6	0.83	MEN
SH6	A1	June 2004	1.5	-	0.54	
SH7	A1	June 2004	5.6	5.0	0.4	
SH8	A6	July 2004	7.0	-	6.0	



Figure 1. Location of the recorded sinkholes.

In 2005 to 2007, grouting programs were developed for a pilot area for filling up the upper levels of the Karst cavities identified with the objective of the designed treatment to eliminate the risk of sinkhole re-occurrence by eliminating the possibilities of collapse of the upper level Karst cavities within the limestone bedrock (Kamal, et al. 2007).

PROBABILITY OF SINKHOLE OCCURRENCE

Assessing the probability of sinkhole occurrence requires defining a performance function (*Z*) (Ayyub 2003, and Ayyub and McCuen, 2003) corresponding to a failure mode as

$$Z = R - L \tag{2}$$

where *R* = limiting resistance or strength, and *L* = load in same units. The nonperformance probability, i.e., failure probability, can be computed as the probability of *Z*<0. The nonperformance probability assessment can be expressed in general terms as (Ang and Tang, 1990; Ayyub and McCuen, 2003; Ayyub, 2003):

$$P_n = \int \dots \int f_{X_1, X_2, \dots, X_n}(x_1, x_2, \dots, x_n) dx_1 dx_2 \dots dx_n \tag{3}$$

where *X*₁, *X*₂, ..., *X*_{*n*}, are the basic random variables that define *R* and *L*. The integral of Eq. 3 can be evaluated using Monte Carlo (MC) simulation with conditional expectation (CE). Taking into account the case of a performance function for sinkhole failure on a Karst opening based on a combined shear failure of dry uncemented and cemented sand through a Karst opening, Figure 2. Consider the case of a Karst opening of diameter *D* supporting cemented and uncemented sand that have some shear strength. The performance function (*Z*) for a potential shear failure mode can be expressed as

$$Z = R_{cemented} + R_{uncemented} - (L_{cemented} + L_{uncemented}) \tag{4}$$

or as a simplified equation

$$Z = \sqrt{c^2 - 2c \left[\frac{1}{4} \gamma_c D_{ac} \cos \beta + \frac{K_u \gamma_u H_c}{2\pi} \sin \beta \right] + \frac{\gamma_u D'}{4} - \left[\left(\frac{1}{4} \gamma_c D_{ac} \sin \beta - \frac{K_u \gamma_u H_c}{2\pi} \cos \beta \right) + \frac{\gamma_u D'}{4K_u \tan \phi} \right]} \quad (5)$$

where c = cemented sand cohesive strength, H_c = cemented-sand layer, β = cemented-sand surface angle that can be taken to be 60° , γ_c = cemented-sand unit weight, D = cemented-sand plug bottom diameter, D_{ac} = average diameter for cemented sand plug = $(D + D')/2$, $D' = D - 2 \frac{H_c}{\tan \beta}$, K_c = empirical factor, γ_u = uncemented sand unit weight, ϕ = uncemented sand friction angle, K_u = coefficient of earth pressure = σ_h/σ_v , σ_v = overburden pressure at failure. Table 2 shows the characteristics of the random variables of Eq. 4.

This failure mode is possible as a result of water leading to erosion and weakening of the materials of an arch spanning a Karst opening with sustained sand loading. It results from water table fluctuation or water seeping from the surface to the lower sand layers as a result of household use of land including watering of plants and cleaning driveways and patios. The water action in this case leads to an erosion of the strength of the arch and removal of sand particles from the supporting layers leading to its weakening and eventual failure.

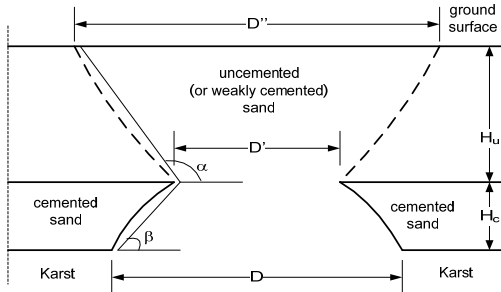


Figure 2. Schematic geological profile for defining failure modes.

Table 2. Characteristics of random variables.

Random Variable	Mean	Coefficient of Variation	Distribution Type
C	40 kN/m ²	0.2	Lognormal
γ	16 kN/m ³	0.1	Lognormal
D	0.5	0.35	Lognormal
H_c	0.05	0.1	Lognormal
β	60 degrees	0.1	Lognormal
K	1.4	0.4	Lognormal
ϕ	30 degrees	0.3	Lognormal

RISK PROFILE FOR THE PILOT AREA

The case of a Karst opening of diameter D supporting cemented and uncemented sand that have some shear strength is used to illustrate the computation of the probability of failure according to the performance function of Eq. 5. Simulation using conditional expectation (Ayyub 2003) is used to this purpose. The variable of the uncemented sand friction angle (ϕ) was used as the control variable that is not randomly generated and its cumulative distribution function was used to compute the failure probability. Equation 5 was rearranged for this purpose as follows:

$$P_f = P \left[X - \frac{\gamma_u D'}{4 K_u \tan \phi} < 0 \right] = P \left[\phi < \tan^{-1} \left[X \frac{4 K_u}{\gamma_u D'} \right] \right] \tag{6}$$

where $X = \sqrt{c^2 - 2c \left(\frac{1}{4} \gamma_u D_u \cos \beta + \frac{K_u \gamma_u H}{2\pi} \sin \beta \right) + \frac{\gamma_u D}{4} \left(\frac{1}{4} \gamma_u D_u \sin \beta - \frac{K_u \gamma_u H}{2\pi} \cos \beta \right)}$. Performing N simulation cycles, the failure probability in the i^{th} cycle according to MC-CE (Ayyub 2003) is computed as follows:

$$P_{fi} = F_{\phi} \left[\tan^{-1} \left[X_i \frac{4 K_{ui}}{\gamma_{ui} D'_i} \right] \right] \tag{7}$$

where the i^{th} subscript to each random variable means an independently generated respective value of the random variable. The failure probability and associated statistical coefficient of variation (COV) for a sample size N can be estimated as

$$\bar{P}_f = \frac{1}{N} \sum_{i=1}^N P_{fi} \quad \text{and} \quad COV(\bar{P}_f) \approx \frac{\sqrt{\frac{1}{N(N-1)} \sum_{i=1}^N (P_{fi} - \bar{P}_f)^2}}{\bar{P}_f}$$

Using the statistical characteristics of the random variables as provided in Table 2 and Table 3 that shows the parameters, the failure probability was estimated based on $N = 100$ simulation cycles to be 0.00022 with $COV = 0.60$.

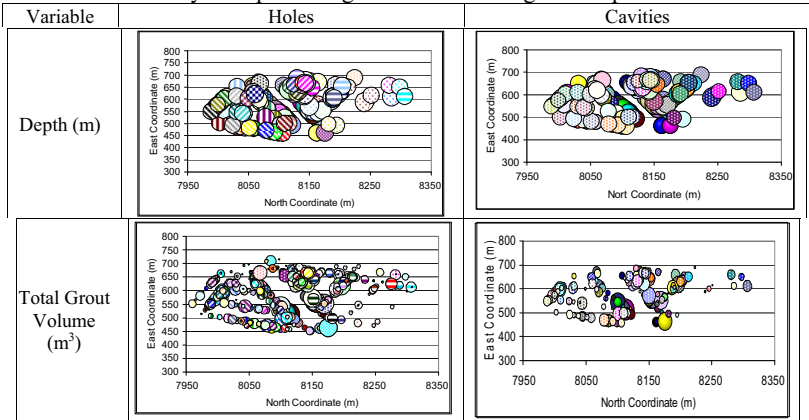
SPATIAL CHARACTERIZATION OF EXPLORATORY HOLES AND CAVITIES

The results of the exploratory holes and cavities were graphically and statistically examined. Table 4 summarizes for the holes and cavities the depths, volume of cavity filling grout, volume of permeation grout, and total volume. The circle area in the figures is proportional to the respective variable magnitude. Figure 3 shows cavity heights which shows that spatial trends are nonexistent in terms of cavity heights. The cavities are at about the same random depth with random spatial locations, volumes, and heights. The cavity height and corresponding grout volume were separately examined to identify any correlation to enable prediction of grout volumes from cavity heights. The regression analysis results, the model has limited prediction capabilities.

Table 3. Statistical characteristics of the random variables.

Variable	Mean	COV	Standard Deviation	Distribution Type	Parameter 1	Parameter 2
Cohesive strength c	40	0.2	8	Lognormal	3.6692691	0.1980422
Unit weight g	16	0.1	1.6	Lognormal	2.7676136	0.09975135
Karst opening D	0.5	0.35	0.175	Lognormal	-0.7509264	0.33993873
Layer thickness H_c	0.05	0.1	0.005	Lognormal	-3.0007074	0.09975135
Beta	1.04667	0.1	0.1046667	Lognormal	0.0406353	0.09975135
K_c	1.4	0.4	0.56	Lognormal	0.2622622	0.38525317
phi	0.52333	0.3	0.157	Lognormal	-0.6906255	0.29356038

Table 4. A Summary of depths and grout volumes using bubble plots.



Note: The area of a circle (i.e., bubble) is proportional to the respective variable provided in the plot

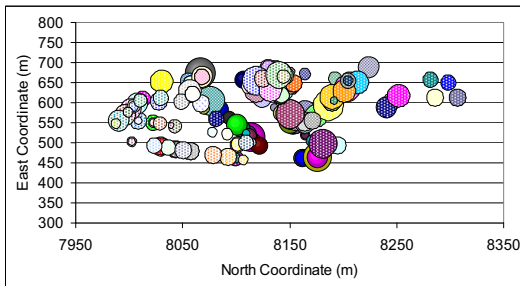


Figure 3. Cavity Heights (The area of a circle is proportional to the respective variable provided in the plot).

SUMMARY AND CONCLUSIONS

A basis of a methodology for quantifying the risk of land subsidence due to underground cavities in Kuwait at a selected area is developed and the methodology is demonstrated. The hazard and risk profile development is limited to computing the probability of sinkhole formation over a selected geographic area based on field data and examining spatial characteristics of the cavities. The development required examining the spatial characteristics of cavities, the development of a prediction model of grout volume, and the development of an example to demonstrate the methodology. The failure probability based on a single failure mode without considering the important effects of the water table was estimated to have a small value of 0.00022 with a coefficient of variation of 0.60. The spatial analysis of cavities demonstrated an analytical process and confirmed the random layout of cavities without any spatial characteristics at about the same depth. A low-reliability prediction model of grout size as a function of cavity height was developed with significant regression coefficients.

ACKNOWLEDGMENT

The authors appreciate the financial support of the Public Authority of Housing Welfare (PAHW) in Kuwait and extend its appreciation to the project team and the management of Kuwait Institute for Scientific Research (KISR) for their dedication, facilitating and continuous support.

REFERENCES

- Abdullah, W. and Kamal, H., "Characterization of Desert Karst Terrain in Kuwait and the Eastern Coastline of the Arabian Peninsula," *Proceedings, Sinkholes and the Engineering and Environmental Impacts of Karst*, San Antonio, Texas, 2005.
- Al-Rifaiy, A., "Land subsidence in the Al-Dhahar residential area in Kuwait: a case history study," *Q. J. of Eng. Geol. London*, (1990), 23, 337-346.
- Ang, A., and Tang, W., *Probability Concepts in Engineering Planning and Design, Volume II: Decision, Risk, and Reliability*, (1990), by the authors.
- Ayyub, B. M., *Risk Analysis in Engineering and Economics*, (2003), Chapman and Hall/CRC Press.
- Ayyub, B.M., and McCuen, R., *Probability, Statistics and Reliability for Engineers and Scientists, Second Edition*, (2003), Chapman and Hall/CRC Press.
- Burdon, D. G., and Al Sharhan, A., "The Problem of Paleokarstic Dammam Limestone Aquifer in Kuwait," *J. Hydrol.*, (1968), 6, 385-404.
- Kamal, H., El-Hawary, Abdullah, W., Abduljaleel, A., Taha, M., Karam, H., Abdul-Salam, S., Al-Sanad, S., Abbas, M., Al-Shatti, F., Al-Elaj, M., Al-Arbied, A., and Al-Furaih, R., *Preparation of Tender Documents, Supervision of Implementation and Evaluation of Treatment Measures of the Pilot Area of Al-Dhahar-Phase II*, (2007), Kuwait Institute for Scientific Research, Kuwait.
- National Research Council, *Mitigating Losses from Land Subsidence in the United States*, *National Academy Press*, (1991), Washington, D. C.,
- Salman, A., *Geology of the Jal Az-Zor-Al-Liyah Area, Kuwait*, (1979), M.Sc. Thesis, Kuwait University, Kuwait.

A Methodology of Constructing Dynamic Risk Maps for Large Metropolitan Areas

E. Guryev¹, L. Poluyan¹ and S. Timashev¹

¹ Science & Engineering Centre «Reliability and Safety of Large Systems and Machines», Ural Branch, Russian Academy of Sciences, Yekaterinburg, Russia, 620049. Ph./Fax: +7-343-374-1682. E-mail: timashevs@gmail.com

ABSTRACT

The paper describes the methodology that was used to construct the dynamic risk map for a virtual large «Russian Gotham» city, which here and thereafter will be named as RG-City. The risk map is the main part of the safety passport (SP) for the RG-City. The SP is a document required by the Russian EMERCOM and the Russian State Agency for Industrial Safety. The SP contains extensive risk analysis of all potential dangerous objects that are located within the boundaries of the city. It analyzes the natural and technological threats/disasters that may occur in the city. While the city is virtual, the components of the methodology and examples are real.

Keywords: Dynamic risk map, Large Metropolitan Areas, natural and manmade disasters.

INTRODUCTION

The methodology of constructing dynamic risk maps (DRMs) for large metropolitan areas (LMAs) consists of following steps [Timashev S.A. 2008, a], [Timashev S.A. 2008, b]:

- Assessment of the potential territorial risk (PTR);
- Assessment of social risk (SR);
- Assessment of risk due to catastrophes and incidents when transporting HAZMATs by railways, on highways or by water;
- Assessments of risk of high and low pressure gas pipelines;
- Assessments of risk associated with hot/cold water supply systems and residential buildings fires;
- Assessment of risk due to natural hazards;
- Construction of social and property loss risk diagrams;
- Constructing risk fields on the digital map of the LMA (in our case – the RG-City);
- Update the risk fields every time some new data on risk comes to life or a new disaster scenario is considered.

Proceed to brief description of each of the above bullets. A full group of disaster scenarios is defined and the distribution of the probability of each scenario assessed, as well as their consequences. The conducted risk analysis shows that main

sources of risk for the metropolitan area of the RG-City are railroads, highways, airport, gas stations, meat processing plant and some facilities that could release chlorine and/or ammonia. As the result, a digital map of the LMA showing the levels of risk (from 10^{-4} to 10^{-11}) is constructed.

The dynamic risk map is a map which is updated every time some new data on risk comes to life. The main goal of such maps is to serve as an early diagnostics tool for decision making persons (DMPs) which are responsible for the well being of the population of the territory studied. The means that are needed for risk mitigation/reduction are then assessed in a timely manner.

POTENTIAL TERRITORIAL RISK (PTR)

PTR is a complex *conditional* measure of risk, which characterizes a potential dangerous object (PDO) or a territory. PTR is a 3D distribution of the conditional probability (frequency) of the possible realization of a negative influence of a specific level. When modeling dangerous technogenic processes associated with discharging harmful substances according to following scheme: "incident-impact process-realization of the impact", the assessment of the PTR for an arbitrary point (x, y) can be made using the following formula:

$$R_{pr}(x, y) = \sum_{i,j} P(A_i) \cdot P_{i,j}(x, y) \cdot P(L_j) \quad (1)$$

where $R_{pr}(x, y)$ is the potential risk, $P(A_i)$ is the probability of an incident according to the i -th scenario, $i=1, \dots, I$, $\{I\}$ is a full group of events (FGE); $P_{i,j}(x, y)$ is the probability of manifestation of the j -th type impact in point for the i -th scenario of discharge, $j=1, 2, \dots, S$, $\{S\}$ is the FGE; $P(L_j)$ is the probability of a lethal (or any other) outcome during manifestation of the j -th type of impact (influence).

The conditional PTR (CPTR), by definition, is describing the potential of the maximal possible risk for concrete influenced objects, which are located in a given point (x, y) of the territory in consideration. This measure of risk is conditional because it does not depend on:

- the very fact that the recipient is at the given point (it is assumed that the recipient is at the given point with probability of 1);
- the probability of the initiating event (it is assumed that $P(A_i) = 1.0$).

Hence, the CPTR does not depend on whether the PDO is in a remote or urban environment, and becomes territorial conditional individual risk (TCIR). TCIR is equal to the probability (frequency) of affecting a human being (according to this or that type of hazard) due to development of a realization of a given type of impact in a point of the territory with given coordinates. In practice it is important to know the distribution of the potential risk for different sources of risk and specific scenarios of catastrophes. TCIR is therefore an *intermediate* measure of risk, which is used to assess the individual and the social risks.

DEFINITION OF SOCIAL RISK

SR characterizes the scale of possible incidents and is defined by the so called F/N diagram (function). Depending on the purpose of the analysis N can be considered as the total number of injured people, number of fatalities or some other parameter that describes the seriousness of the catastrophe. Knowledge of the CPTR and of the distribution of the population across the studied territory allows getting quantitative assessment of the SR for the residents of a LMA.

The SR parameters are defined through the frequency of occurrence (λ , 1/yr) and the probabilistic zone of destruction [$P(x, y)$] for each catastrophe scenario, when accounting for the distribution of the recipients $N(x, y)$ over the considered territory. The number of injured people ($N_{sc, j}$) during a specific i -th scenario of an incident is defined by formula:

$$N_{sc, j} = \int_S n(x, y) \cdot R_i(x, y) ds \quad (2)$$

where λ_j is the frequency of this event.

After calculating the number of injured people for the whole spectrum of possible scenarios ($j = 1, 2, \dots, J$) it is possible to draw the F/N diagram, by summing up all the frequencies of incidents for which the number of injured is more than some preassigned value. Hence, the criteria of acceptable level of risk will be not a number, but a curve, constructed for different incident scenarios. Currently the generally accepted approach to defining the acceptability of risk is using two F/N curves in logarithmic coordinates - one for acceptable risk and the other for unacceptable risk. The area between them is the grey zone where the level of risk is intermediate. The problem of decreasing this kind of risk is solved by accounting for the specificity of the industry, local aspects, and by coordinating with local bodies of self government and supervision. As a variable T in this case it is possible to take the economic (G) and/or ecological (E) damage.

CONSTRUCTING THE RISK FIELDS ON THE DIGITAL MAP OF A LMA

The above results permit constructing integral and local risk fields. These fields are the most valuable forms of visualization first and foremost because they permit synthesizing a large number of nonhomogeneous data in a unique format which allows the decision making persons (DMPs) to easily understand the situation at hand. For constructing risk fields following data are used:

- A listing of the PDOs, described as a full group of N sources of hazard for the LMA in consideration;
- M types of possible incidents for each PDO from the listing, specifics of their occurrence and development;
- Results of drawing the CTPR fields;
- Probabilities of manifestation of the negative potential of these incidents

$$\lambda_j, j = \overline{1, M}.$$

First local risk maps for each PDO are developed. Risk maps are constructed for each type of incident and each scenario that can physically occur in the considered PDO, with a concrete attachment to the source of danger. In this case the formula for calculating the total risk for a given PDO in each geo-cell $R_{\Sigma}(i, j)$ takes the form

$$R_{\Sigma}(i, j) = \sum_{j=1}^M \lambda_j R_I(i, j) = \sum_{j=1}^M \lambda_j \cdot R_I(i, j). \quad (3)$$

In this formula summation of risks is justified by the fact that all the incident scenarios and hence, the destruction zones, are independent.

As a result of these efforts a map $R_{I\Sigma}(i, j)$ of individual risk is formed, which characterizes the integral probability of this or that destructive factor, on the condition that the recipient with probability of 1 is in the given point of space during occurrence of the catastrophe. Having all the local maps they could be synthesized. Conduct summation of all the fields of potential danger for each PDO, taking into account their actual position on the LMA's map:

$$R_{\Sigma}^t(i, j) = \sum_{k=1}^N R_{I\Sigma, k}(i, j). \quad (4)$$

Here again it is justified to summate risks due to the mutual independence of the incidents in the PDO.

After constructing the integral risk field it is possible to assess the influence of the incidents/catastrophes on one object on the possibility of an incident in an adjacent PDO. This is especially important to take into account for scenarios which involve fires and explosions, because in these cases it is highly probable that cascade "domino" type accidents will develop, which, as a rule, lead to maximal economic and social damages.

ASSESSMENT OF RISK DUE TO CATASTROPHES AND INCIDENTS WHEN TRANSPORTING HAZMATS BY RAILWAYS

When analyzing possible scenarios two scenarios are picked for consideration: the most dangerous and the most probable. As the most dangerous scenario an incident on the railway was considered which involves destruction of several railroad tanks containing oil products. According to Russian State rule it is necessary to consider the case when half of all the oil carrying tanks are losing their contents. As a most probable scenario an oil spill from a single railway tank (120 cub.m) was considered. These scenarios can be comprised of following sub-scenarios (SS):

a. Oil products spill

SS 1.1 – oil spill from 25 tanks 80 cub. meters each (2000 m^3); SS 1.2 - oil spill from a single tank (120 m^3). Consequences of such incidents are: atmosphere pollution by oil products evaporation, intoxication of people. Possible secondary types of accidents could be oil spill fire, toxic injury of people, and creation of a fuel-air mixture cloud (FAMC) followed with its explosion.

b. Forming of a burning oil spill

SS 2.1 – oil spill from 25 tanks 80 cub. meters each (2000 m^3) followed by its ignition; SS 2.2 - oil spill from a single tank (120 m^3) followed by ignition of the spill. Dangerous factors which influence people and assets are flame and sparks, elevated temperature of the environment, toxic products from the fire and thermal discomposure of the materiel, smoke, decreased concentration of oxygen in the air. Possible secondary type incidents in this case are: fire ball and explosion, ignition of the technological equipment and transportation means, buildings and structures.

c. Forming of a FAMC followed by a fire ball

SS 3.1- oil spill from 25 tanks 80 cub. meters each (2000 m^3) followed by forming a fire ball; SS 3.2 - oil spill from a single tank (120 m^3) followed by ignition of a FAMC. Consequences of such development of the incident are atmosphere pollution by products of burning oil, intoxication and thermal injury of people. Possible secondary incidents include: explosion, ignition of the technological equipment and transportation means, buildings and structures.

d. Forming of a FAMC followed by its explosion (creation of an air blast wave)

SS 4.1 - oil spill from 25 tanks 80 cub. meters each (2000 m^3) followed by the FAMC explosion; C 4.2 - oil spill from a single tank (120 m^3) followed by the FAMC explosion. In order to assess the most dangerous case the oil product considered in scenarios SS 4.1 – SS 4.2 was benzene. In risk calculations the surrounding air temperature was taken as 20°C . The consequences of this kind of catastrophe development could be: destruction of equipment, air pollution, destruction of flora, and intoxication of people, injuries of people by the blast wave and by equipment projectiles. Due to the blast a fire ball could be created. Possible secondary type incidents in this case are: fire ball, ignition and destruction of the technological equipment and transportation means, buildings and structures. Collective risk for the most probable incident is $2.16 \cdot 10^{-3}$. Collective risk for the most dangerous incident is $6.2 \cdot 10^{-4}$.

In this study chlorine spill on railways was also considered and its consequences evaluated. The typical scenario involves three tanks on a railway station, each containing 60 tons of chlorine. The frequency of this type of incident is $3.2 \cdot 10^{-6}$. The intoxication radii is 2.5 km, the radii of lethal intoxication is 0.87 km.

The average number of fatalities, at average population density for the RG-City being $0.0022 \text{ residents/m}^2$ is 412 people. Collective risk is equal to $1.28 \cdot 10^{-3}$.

ASSESSMENTS OF RISK WHEN TRANSPORTING HAZMATS ALONG HIGHWAYS

The incident frequency during highway transportation for the case when 4 containers with chlorine are transported is equal to $3.8 \cdot 10^{-4}$. It is assumed that each container contains 850 kg of chlorine. Assume that the average time of transportation of chlorine inside the LMA is not more than 2 hours. In this case the radii of intoxication will be 2.5 km, the radii of lethal intoxication is 0.86 km. The average number of fatalities, at average population density for the RG-City being $0.0022 \text{ citizens/m}^2$ is equal to 412 people. Collective risk is equal to $1.42 \cdot 10^{-2}$.

ASSESSMENT OF RISK FOR HIGH (900KPA) AND LOW (50KPA) PRESSURE GAS PIPELINES

The average frequency of loss of containment for small diameter trunk gas pipeline per km yr is $2.8 \cdot 10^{-4}$. The probability of gas cloud explosion is 0.0118. Calculations were conducted taking into account possible deaths of people during destruction of buildings and on the streets of LMA. For high pressure gas pipelines individual risk is $3.91 \cdot 10^{-9}$. For low pressure gas pipelines individual risk is equal to $1.5 \cdot 10^{-9}$. The total individual risk when trunk gas pipelines operate is $5.4 \cdot 10^{-9}$.

ASSESSMENTS OF RISK ASSOCIATED WITH HOT/COLD WATER SUPPLY SYSTEMS AND RESIDENTIAL BUILDINGS FIRES

All calculations are based on the statistics provided by the local ENERCOM based on statistics gathered during the time interval 2002 – 2005. Results of this analysis are not shown in this paper.

ASSESSMENT OF RISKS DUE TO NATURAL HAZARDS

In the RG-City the average duration of a thunderstorm is 90 minutes, the average number of storms per year is 25.6. The average number of thunderbolts per sq.km year as given by the Russian Code GOST 12.1.004-91 is equal to 3 (thunderbolts km^2/yr). According to this code the probability $Q_i(t)$ that a thunderbolt will directly strike a building is found as

$$Q_1(t) = 1 - e^{-N_{ts}\tau_d}, \quad (5)$$

where N_{ts} is the number of direct strikes of a thunderbolt of an infrastructure object, per year; τ_d is the duration of local observations of this phenomenon, years.

For rectangular objects

$$N_{is} = (S + 6H) \cdot (L + 6H) \cdot N_{is} \cdot 10^{-6} . \tag{6}$$

Assume the average height of the RG-City citizen is equal to 1.5 m, the probability of a person being outdoors during a storm is not more than $1.1 \cdot 10^{-3}$. Then the individual risk of being killed by a thunderbolt is not more than $2.6 \cdot 10^{-7}$.

The average number of days when the outside temperature in the RG-City is below $- 25^{\circ}\text{C}$ (according to meteorological data) is ≥ 8 . According to expert assessments the probability that a person would die due to hypothermia is $1.1 \cdot 10^{-7}$ (days⁻¹). Then the individual risk of death due to hypothermia is not more than $8.2 \cdot 10^{-7}$. Loss of people due to earthquakes and hurricanes in the vicinity of the RG-City was never registered. The total individual risk of life loss due to natural hazards in the RG-City is $1.04 \cdot 10^{-6}$.

CONSTRUCTION OF SOCIAL AND PROPERTY LOSS DIAGRAMS

All the above allowed constructing F/N social diagrams for employees of companies that are located in the LMA, its residents and the total diagram (see Figs. 1 through 3) and a generalized F/G diagram for the city (see Fig.4).

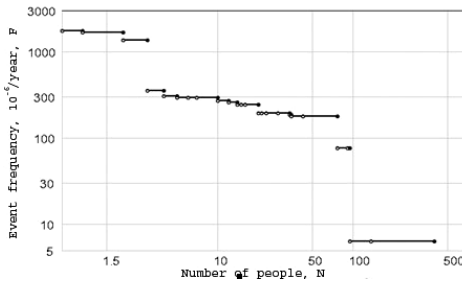


Figure 1. F/N social risk diagram for companies' employees

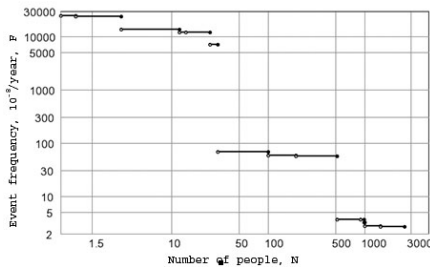


Figure 2. F/N social risk diagram for the population

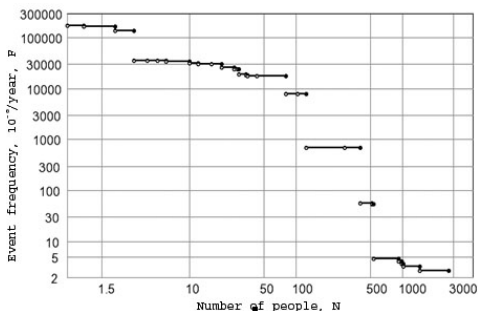


Figure 3. Total social risk F/N diagram

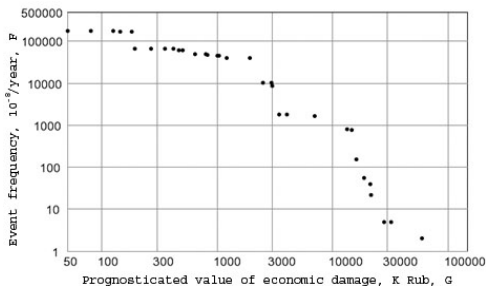


Figure 4. F/G diagram

CONCLUSION

The outlined methodology for constructing individual risk maps is an important and useful tool for providing insight into every decision made by the decision making persons that govern the LMA.

REFERENCES

Timashev S. A. (2008). “Management of risk of interdependent systems of critical infrastructures and territories“ *II All Russia Science and Technology Conference, Safety of Critical Infrastructures and Territories, Yekaterinburg, 7-9.*

Timashev S. A. (2008). “Risk and Entropy Based Quantitative Definition and Solution of Regional Resilience and Strategic Preparedness“ *Ibid.*, 261-265.

A methodology to produce interdependent networks disturbance scenarios

Serge Lhomme¹, Damien Serre¹, Youssef Diab¹, Richard Laganier²

¹Université Paris-Est, Ecole des Ingénieurs de la Ville de Paris, 15 rue Fénelon, 75010, Paris, Tél: +33 1 56 02 11 05; damien.serre@eivp-paris.fr; serge.lhomme@eivp-paris.fr; youssef.diab@eivp-paris.fr

² Université Paris Diderot – Paris 7, Laboratoire PRODIG, 7 rue Thomas Mann, F-75205 Paris Cedex 13

ABSTRACT

Quick urban development coupled with technical failures and climate change have increased flood risk and corresponding challenges to urban flood risk management. In this context, there is a need to understand how networked systems are resilient because societal functions are highly dependent on networked systems and the operability of these systems can be vulnerable to disasters. That is why we develop a methodology for producing interdependent networks disturbance scenarios. In order to take advantage of this methodology software is needed.

INTRODUCTION

In France, as in Europe, river floods have been increasing in frequency and severity [Szöllösi-Nagy & Zevenbergen, 2005] and there are more instances of rivers bursting their banks, aggravating the impact of the flooding of areas supposedly protected by flood defenses. Climate change is expected to exacerbate the frequency and intensity of hydro meteorological disaster [IPCC, 2007]. Moreover, the total urban population is expected to double from two to four billion over the next 30 to 35 years [United Nations, 2006]. This growing rate is equivalent to the creation of a new city of one million inhabitants every week, and this during the next four decades [Flood resilience Group]. So, this quick urban development coupled with technical failures and climate change have increased flood risk and corresponding challenges to urban flood risk management [Ashley et al., 2007], [Nie et al., 2009]. These circumstances oblige to manage flood risk by integrating new concepts like urban resilience. In this context, a first analysis of city needs about decision making tools shows they don't have tools available to help them to prioritize recover actions and of course they are interested in having it. For this, there is an important need to understand failure mechanism that lead to disturb city.

Here, there is a big issue because city is a complex object. Nowadays, the principle is to study the city like a system, especially like a complex one (such systems are not fully predictable, due to the inherent uncertainty in how these systems evolve). Indeed, a system is an *“autonomous entity with regard to its environment, organised in a stable structure (identifiable in the course of time), constituted by interdependent elements, whose interactions contribute in maintaining the system structure and making it evolve”* [Pumain, 1982]. As illustrated in the literature [Pumain et al., 1995], [Sanders, 1992], [Beaujeu-Garnier, 1997] a city appears as a set of components interconnected by networks with some critical infrastructures.

That's why in this paper we will focus on the study of critical infrastructures interdependency. First, we will introduce resilience concept. Secondly, we will introduce the

use of safety methods to study impact of natural hazards on infrastructures. Then we will present the methodology and a tool to produce networks failure scenarios due to flood hazard.

RESILIENCE CONCEPT

Derived from ecology, the concept of resilience is firstly defined as “*the measure of the persistence of systems and of their ability to absorb change and disturbance and still maintain the same relationships between populations or state variables*” [Holling, 1973]. Nowadays this concept is used in many other disciplines (like psychology, economy, environment...). But for risk management this concept is relatively new, especially concerning natural hazard. We study number of other disciplines in order to well understand resilience concept and to define this concept concerning urban flood management. It appears that resilience is usually used in the continuity of existing terms in these various disciplines. The abundance of definitions of disaster resilience and the fact that this concept is shared by many disciplines makes it difficult to have a common definition.

Disaster management has typically focused on analyzing the hazard. Yet, river floods have been increasing in frequency, so researchers and few decision makers recognize the need to analyse not only the hazard but also the vulnerability to each specific hazard. That is why disaster management has been moving away from solely emergency response, initiated during and after a flood event, toward mitigation and preparedness, initiated before an event, in order to reduce impacts more effectively [Wilhite, 1987], [Hooke, 2000]. For Pasche and Geisler, this comprises individual preventive and emergency measures at building and municipal infrastructure and a land use policy to adapt building activities to the risk. Thus for them, flood preparedness is mainly a matter of flood resilient building and hazard awareness. So, in the current discussion on flood resilient cities a strong emphasis is placed on improving the flood performance of buildings. Yet, the city has to be considered as an entity with different systems and vital functions and not merely as a set of concrete buildings [Anema, 2009], [Lhomme et al., 2009].

Networks affect the well-being of the people and the smooth functioning of services and, more generally, of economical activities. For instance, over 19 billion tons of freight valued at \$13 trillion dollars was moved through the U.S. multimodal transportation system during 2002 [U.S. Department of Transportation, 2006]. In fact, the economy of a nation or regions depends heavily upon an efficient and reliable transportation system to provide accessibility and promote the safe and efficient movement of people and good [Chen, 2000]. So, the economy of a nation or regions depends heavily upon an efficient and reliable transportation system, but it's true for other networked systems like electricity, water and telecommunication supply. For instance, the August 2003 electrical blackout in North America, with the loss of a single electricity generation plant in Cleveland, Ohio, a cascading failure of interconnected electrical systems commenced, eventually generating a blackout encompassing eight U.S. states, two Canadian provinces, and nearly 50 million people (ELCON 2004). In fact, the most important in a networked system disturbance, it is the potential domino effects on the others systems.

Evaluating network infrastructures for potential vulnerabilities is an important component of strategic planning, particularly in the context of managing and mitigating service disruptions [Murray et al. 2008]. Yet, multiple networks that innervate the city are particularly sensitive to flooding, through their structures and geographic constraints. There is a need to understand how networked systems are resilient because societal functions are highly dependent on networked systems and the operability of these systems can be vulnerable to disasters. The first step for that is to study their failure modes.

THE USE OF SAFETY METHODS TO STUDY NETWORKS FAILURE MODES AND PRODUCE FAILURE SCENARIOS

It appears that risk analysis is not a discipline but rather an engineer activity who tries to assess the risk. In fact, there are several approaches to fulfill this activity, which are clearly identified and formalized in the industry (nuclear plant, aeronautic...) and also used in civil engineering [Serre et al., 2008]. They can be gathered into two families [Zwingelstein, 1995]: internal methods and external methods (Fig. 1). Internal methods are based on detail knowledge of the system functioning. From modeling, it is possible to predict its future behavior and then to analyze the risks. There are two main approaches: physical modeling and functional modeling thanks to safety methods. External methods are used when modeling of the mechanisms (physical or functional) is technically impossible or inappropriate to the level of knowledge, due to system complexity. There are methods based on statistical analysis and those based on expertise.

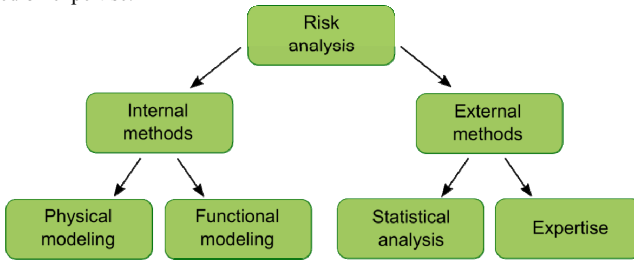


Figure 1. Risk analysis methods

The principle of functional modeling is to study the interactions between components of a system and its environment in order to establish a link between the functions failure, their causes and effects. There are various techniques for functional modeling systems: Analysis of Failure Modes and Effects Analysis (FMEA), FMEA completed by a criticality analysis (FMECA), the methods of the Tree or Consequences Events... Functional modeling allows better understanding how the system operates and that's why it allows better understanding failure mechanisms.

FMEA is a procedure to identify component failures which have significant consequences affecting the system operations in the application considered. FMEA only provides qualitative analysis. First, FMEA requires breaking down the system into components (structural analysis). Then it's necessary to identify the functional structure of the system and how the components contribute to functions. Then FMEA requires defining failure modes of each component and finishing perform analysis for each failure mode of each component and recording results in table (Tab 1).

Network	Components	Fonctions	Failures	Origins	Effects

Table 1. FMEA Structure

After compiling the FMEA data, we can determine the most important failure modes of the systems, their causes and their effects. So, using the FMEA, the failure mechanism model had been defined, and failure scenarios had been designed thanks to events trees. The events trees analysis was developed in early 1970 for risk assessment of nuclear power plants.

Here we are just using the method without quantitative aspects, but this model involves and underlying domino effect induced by networks failure. Indeed, infrastructures and systems do not exist in isolation of one another – telecommunication networks require electricity, as do the sewerage systems. Transportation networks often use sophisticated computerized control and information systems, the generation of electricity requires fuels, etc [Syncera, 2007].

We design networks systems failure scenarios by linking failure causes to failure modes, and then to failure effects (Fig. 2). In this way, the failure mechanisms are modeled as series of functional failures representing the relevant physical processes taking place within the system and leading to loss or deterioration of functions. For these scenarios we adapted the events trees method (Fig. 3) and for the moment we don't work on matrix interdependency. So it's possible to produce failure scenarios using a specific methodology (Fig. 2).

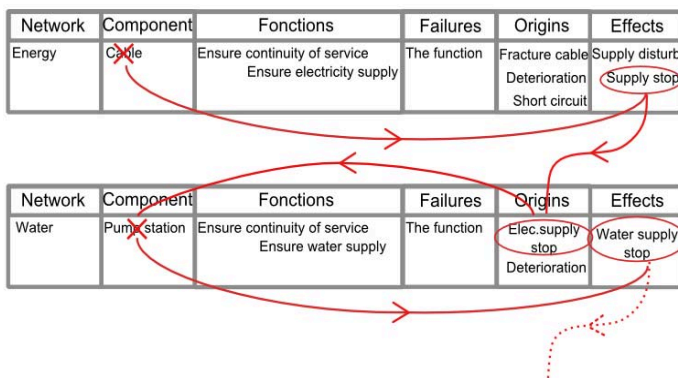


Figure 2. Methodology to produce failure scenarios

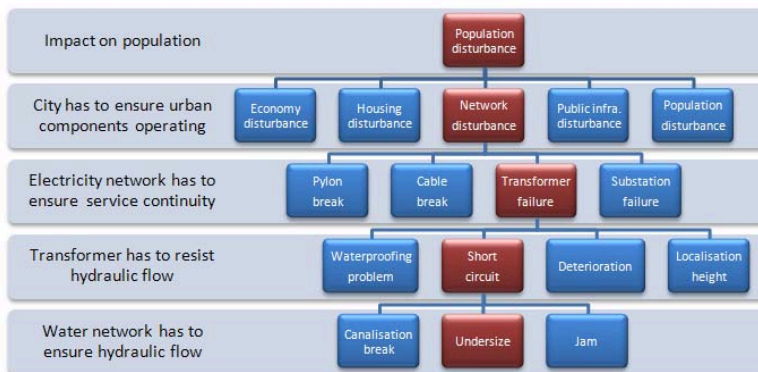


Figure 3. Failure scenario example

A TOOL FOR PRODUCING FAILURE SCENARIOS

The methodology, presented above in the second part, allows producing networks

failure scenarios. Nevertheless, it is only possible producing few scenarios. Maybe these scenarios are the most important and plausible, thanks to a good knowledge and expertise of the networks, but we can't take advantage of the overall FMEA analysis. Indeed structural analysis breakdowns the system into 37 components and at the end of the functional analysis 127 functions were found. Moreover we have to take into account of two interdependency levels: components interdependency and networks interdependency. So, components and/or functions failures combination causes too much scenarios. For these reasons, a tool is needed to automate these scenarios and take advantage of the FMEA analysis.

We design networks systems failure scenarios by linking failure causes to failure modes, and then to failure effects. Actually, this method can be automated because it corresponds to automatics queries (Fig. 4). For this automation we need specific vocabulary in order to automatics queries operate.

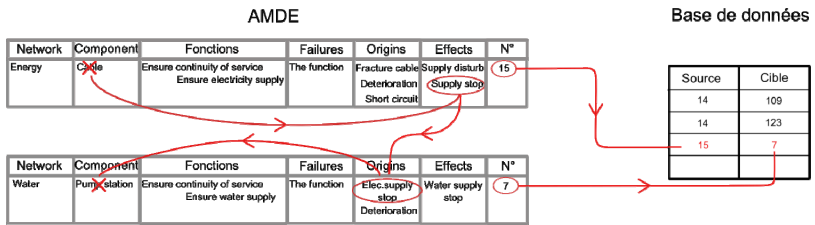


Figure 4. Automation process

The tool responds to three main objectives. The first objective is to allow visualization and update of the FMEA. The second objective is to design failure scenarios. The third objective is to analyze the results and to allow an overall understanding of interdependent networks failure modes thanks to diagram representation of the results. In order to produce failure scenarios we implement FMEA in database and use user interface to display results of users query.

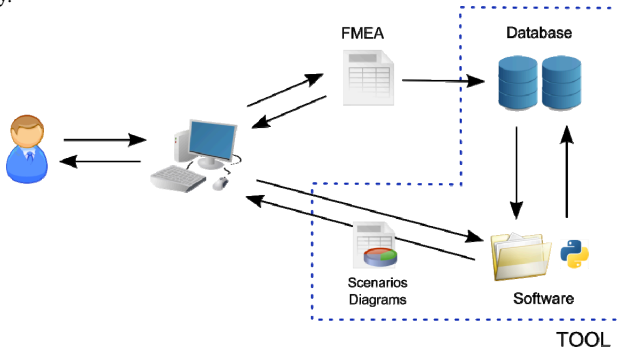


Figure 5. A tool for producing failure scenarios

FMEA visualization allows users to consult at any moment the FMEA table and all the information needed for understanding results. Update FMEA is a very important tool because as we explain above, we need a specific vocabulary for the automation process. Thus in case of error, it is possible to modify it. For instance, when users consult the effects of the

disruption of a component surprising result can be identified. Using an algorithm to establish direct relationship between components, it is possible to use shortest path algorithm for producing failure scenarios. Thus we obtain all the shortest (more direct) relations between components or functions but not all the possible scenarios. It's possible to use others algorithms for producing others scenarios (more complex scenarios).

RESULTS

In France, two main studies on networks vulnerability conclude that electricity networks is the most aggressive networks because all the networks depend on electricity supply. So networks vulnerability studies often recommend focusing actions on electric network. With our tool conclusions are quite different. Indeed three main conclusions have been highlighted.

The study concludes that electrical network is the most aggressive networks (Fig. 6), as others studies, but others network components can be as aggressive as electric components. For instance, electrical and telecommunication pylons are the most aggressive components. This is due to their configurations. Indeed these components are the interface between their own network and transportation network. That is why it is possible to include these components as part of the transportation systems. So, it is difficult to define accurately boundaries of a network due to important interrelation between each network. In other word, it is difficult to determine the most aggressive network because all the networks are highly interdependent.

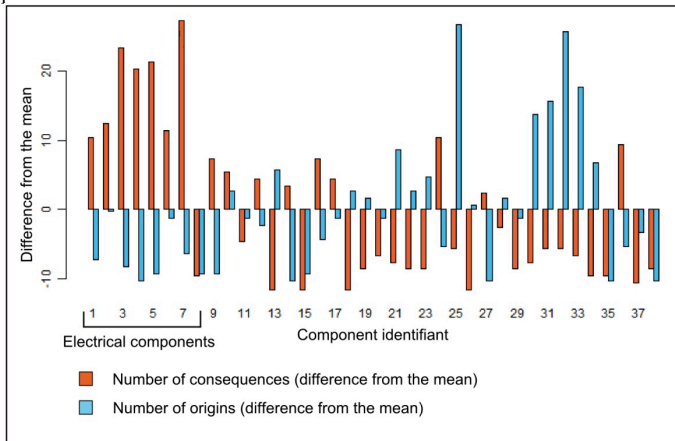


Figure 6. Component failure effects (orange) or causes (blue) diagram

Diagram allows studying not only the most aggressive component but also the most sensitive to the disturbance of others components. The most sensitive components can be impacted by a lot of components. When we study the results, these very sensitive components are involved in more scenarios than the most aggressive components. That is why it doesn't seem pertinent focusing only on aggressive components (electrical networks).

Some components are very problematic. Indeed numerous scenarios involve these specific components. These components are not the origin or the final effect of these scenarios, but components which spread disturbance effect of a component. Thus these

components disturb components which can not directly impact by an origin component. As we can see in the figure below (Fig. 7) the impact of these specific components are most important than the two others indicators (number of causes and effects). So it seems more important focusing on these components to limit impacts of flooding (pump stations, road...).

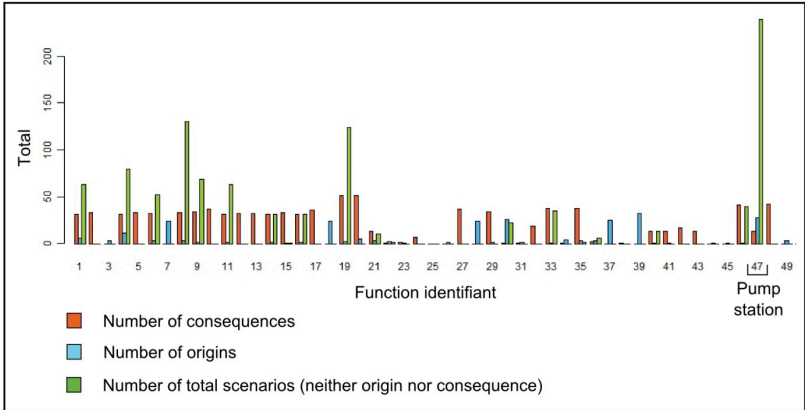


Figure 7. This diagram shows a component which is not the origin or the final effect of scenarios, but a component which spread disturbance effect of others components disturbance

CONCLUSION

Critical infrastructures, especially networks, can be considered as a complex system of multi component systems responding in a non-linear way to stimuli and perturbations. That is why causes of system failures are often incomprehensible. We know relatively little about the causes of these infrastructural breakdowns. So there is a need to produce failure scenarios of interdependent critical infrastructures in order to understand their failure modes. Our methodology, based on functional analysis, allows producing these scenarios and help to understand failure modes. Yet, it is impossible to take advantage of the overall knowledge of the networked systems without our informatics tool.

First application of this tool for networked systems allows highlighting the importance of specific components or functions. Thus if electric appears as the most aggressive network we conclude that we have to prioritize action not especially on electrical network but on these specific components of different networks. This tool will have to be implemented in a GIS in order to produce a tool for assessing resiliency of cities.

REFERENCES

- Anema, K.A. MSc, 2009, *A scoring system for the resilience of critical infrastructure and their interdependent networks in cities*, cost22, 7 p.
- Ashley, R., Blanksby, J., Chapman, J., Zhou J. J., 2007, "Towards Integrated Approaches to Reduced Flood Risk in Urban Areas". In: Ashley, R., Garvin, S., Pasche, E., Vassilopoulos, A., Zevenbergen, C. *Advances in Urban Flood Management*, pp. 415-432.
- Beaujeu-Garnier J., 1997, *Géographie urbaine*, cinquième édition, édition Armand Collin.

- Chen A., Yang H., Lo H. K., Tang W. H., 2000, "Capacity reliability of a road network : an assessment methodology and numerical results", *Transportation Research*, pp. 225-252.
- Holling C. S., 1973, *Resilience and stability of ecological systems*, Annu. Rev. Ecol. Systemat. 4 (1973) 1-23
- Hooke W.H. , 2000, *U.S. participation in international decade for natural disaster reduction*, Natural Hazards Review, ASCE, pp 106-133.
- IPCC (Intergovernmental Panel on Climate Change), *Climate change 2007: The IPCC fourth assessment Report, Summary for Policymakers*, www.grida.no/climate
- Lhomme S., Serre D., Diab Y., 2009, *A GIS prototype to optimize recovery after a flood event*, Cost 22, Conference on Road Map Towards a Flood Resilient Urban Environment.
- Murray A. T., Matisziw T. C., Grubestic T., 2008, "A methodological overview of network vulnerability analysis", *Growth and Change*, Vol. 39 No.4, pp.573-592.
- Nie, L.M., Lindholm, O. and Braskerud B.C., 2009, *Urban flood management in a changing climate*. J. of Water by Norwegian Water Association, Vol. 2, pp. 203-213.
- Pumain D., 1982, *La dynamique des villes*, Editions Economica.
- Pumain D., Sanders L., Saint-Julien T., 1995, *Villes et auto-organisation*, Economica, 191 p.
- Sanders L., 1992 , « Système de Villes et synergie », col. Villes Ed. Anthropos-Economica, 274 p.
- Serre, D., Peyras, L., Tourment, R., Diab, Y., 2008. « Levee performance assessment: development of a GIS tool to support planning maintenance actions », *Journal of Infrastructure System*, ASCE, Vol. 14, Issue 3, pp. 201-213.
- Syncera, 2007, *Quick Scan Halve Meter Ram*, In opdracht van het Ministerie van Verkeer en Waterstaat, DG-Water.
- Szöllösi-Nagy A., Zevenbergen C., 2005, *Urban flood management*, Introduction, pp 1-10.
- WILHITE D.A. , 1987, "The role of the government in planning for drought: Where do we go from here?" *Planning for drought: Toward in societal vulnerability*, D.A. Wilhite and W.E. Easterling (eds.), pp 425-444.
- Zwingelstein G., 1995, « Diagnostic des défaillances: théorie et pratique pour les systèmes industriels », *Traité des nouvelles technologies, série Diagnostic et maintenance*, Hermès, Paris, 1995

Automated Security Risk Analysis Tool for USAF Installation Security

Kenneth J. Knox, Ph.D., P.E.¹

¹Integration Innovation, Inc. (i3), 2518 Highway 77, Suite A, Lynn Haven, FL 32444; PH (850) 303-0583; FAX (850) 271-8720; email: ken.knox@i3-corps.com

ABSTRACT

The demands of deployments and home station security have severely over-tasked Air Force Security Forces. Previous standards-based security doctrine was not flexible enough to allow commanders to manage limited resources to achieve acceptable, balanced risk tailored to the mission and priorities. Security Forces needed to change the paradigm of how they do business, to truly transform. USAF Security Forces are now moving to a risk-based approach to installation security, and are using a standardized model called ForcePRO to identify risks and develop risk management strategies. Developed by Air Force Research Laboratory (AFRL) contractors at Tyndall AFB, Florida, the ForcePRO model and software application were field tested at over 50 Air Force installations in the US, Europe and Southwest Asia. ForcePRO facilitates a thorough, repeatable, and understandable physical security analysis that documents the assets, threats, vulnerabilities and risks facing an installation. It aids in developing risk mitigation strategies to reduce risks exceeding the installation commander's risk tolerance.

A LITTLE HISTORY

“Principles of War” are those “truths” of warfare that usually define success or failure on the battlefield. United States military doctrine identifies nine principles of war, including *Security* (Joint Chiefs of Staff, 2006). The “purpose of security is to never permit the enemy to acquire unexpected advantage,” and encompasses understanding your threats and prudent risk management. Without effective security operations, the US Air Force (USAF) risks losing the initiative in Air, Space, and Cyberspace operations. In the Air Force, the enterprise lead for security—for protecting the force and the airbase both at home and abroad—resides with Security Forces (SF).

The post-Cold War period has hardly been quiet for the US military, with actions in the Persian Gulf, Africa, the Balkans, and Somalia among others. Since 9/11 this high operations tempo has accelerated, marked most recently by Operation Iraqi Freedom in Iraq and Operation Enduring Freedom in Afghanistan. With the simultaneous demands of both overseas deployments and home station security, the Air Force Security Forces were severely over-tasked. It was common for over 50% of an SF unit to be deployed from their home station. With fewer resources, SF leaders had to decide what responsibilities would not be accomplished. Previous standards-based security doctrine was not flexible enough to allow commanders to

manage limited resources to achieve acceptable, balanced risk tailored to the base mission and priorities. In need of a new, transformational business model to provide installation security in a resource-constrained environment, the Air Force Security Forces moved to a risk-based approach using an automated risk analysis tool called **ForcePRO**.

Integrated Defense is the name applied to this new model, and is implemented in a new Air Force Instruction 31-101, *Integrated Defense*. USAF security planners are using Integrated Defense and ForcePRO to identify risks and to develop risk management strategies that are tailored to their installation and threat environment. Simple in concept, ForcePRO was field tested at over 50 Air Force installations in the US, Europe and Southwest Asia (Figure 1). Along with the requirements for airbase security, the ForcePRO assessment also meets the requirements of the Department of Defense’s antiterrorism program, as implemented in DoDI 2000.16 *DoD Antiterrorism (AT) Standards* and DoD O-2000.12-H *DoD Antiterrorism Handbook*.

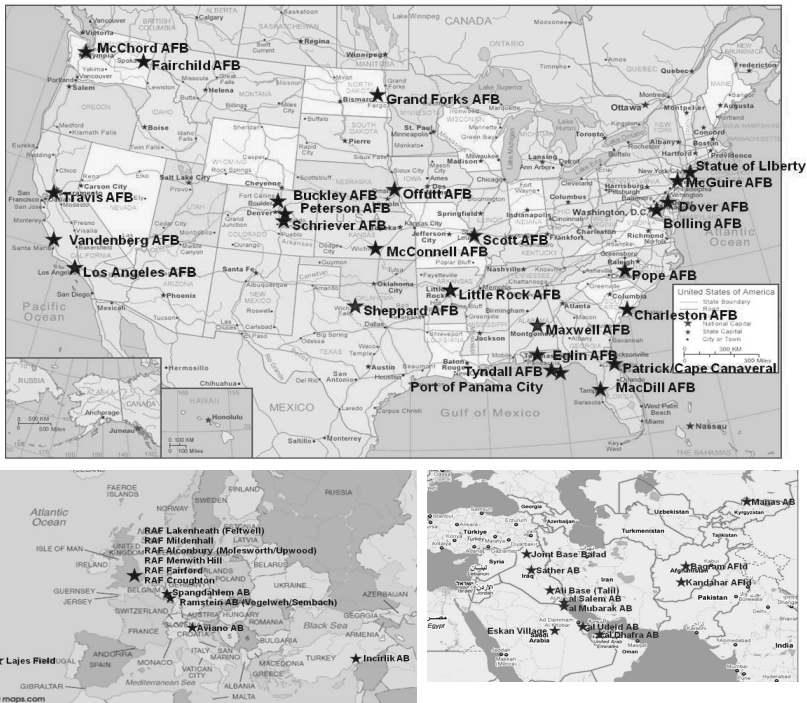


Figure 1. ForcePRO security risk assessments.

Developed by the Air Force Research Laboratory and its contractor Integration Innovation, Inc. (i3), the ForcePRO development program is managed by the US Army’s Aviation and Missile Research, Development and Engineering Center

(AMRDEC) in Huntsville, AL. While currently an Air Force-centric application, the database structure is versatile and adaptable to new domains. The easy to use and flexible software allows organizations and security professionals to:

- Systematically, efficiently and comprehensively study and understand security risks
- Balance risk with mission and competing priorities
- Place security problems in context
- Make an effective business case for security policies, procedures and investments

RISK ASSESSMENT

Security risk assessment is the systematic process of identifying assets you care about, potential threats to those assets, and vulnerabilities that permit loss or damage to those assets. When rolled together in a quantified fashion, these elements define and measure the risk associated with an unwanted event. For risks deemed unacceptable, countermeasures can be implemented to reduce risk in a cost-effective manner. Figure 2 shows a flowchart of this process (Air Force Security Forces Center, 2009).

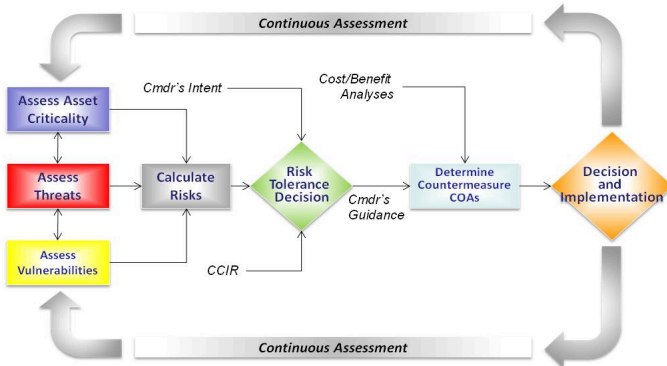


Figure 2. ForcePRO risk assessment flowchart (AFI 31-101).

ForcePRO methodology and approach. The risk model used by ForcePRO is a very conventional security risk model:

$$\text{Risk} = \text{Asset Criticality} \times (\text{Threat} \times \text{Vulnerability})$$

Consequence of loss Probability of loss

In this model, *Asset Criticality* evaluates the consequence of loss by measuring the value of assets to the organization. This step identifies and prioritizes those critical assets that are worthy of protection, whose loss or damage would have a negative impact on the organization. Fundamental to this evaluation are the criteria

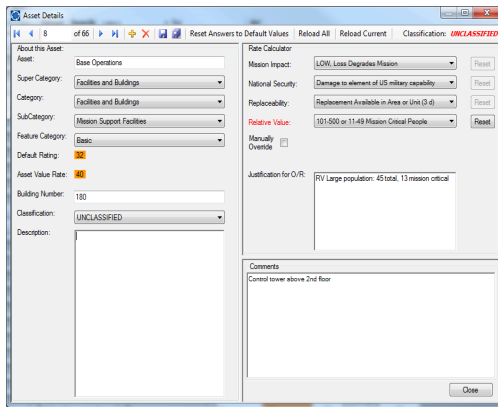


Figure 3. Asset rating detail screen.

used to measure asset value. Typical criteria for military domains include mission criticality, impact on national defense, replaceability, and relative or intrinsic value.

Threat x Vulnerability is a measure of the *probability* of loss or damage to the asset. Malevolent threats are generally considered in terms of adversaries and their tactics (e.g., hackers, terrorists, criminals, etc.). The Air Force version of ForcePRO considers 16 physical security tactics (Table 1) in its assessment. Vulnerabilities are weaknesses that can be exploited by an adversary, caused by lack of adequate security, lax or improper personal behavior, vulnerable software or hardware, and insufficient security policies or procedures. Using the **ForcePRO Vulnerability Assessment Tool (FVAT)**, the expertise of security Subject Matter Experts (SMEs) are captured to assist analysts in evaluating and scoring their organization’s security weaknesses.

Table 1. Current ForcePRO tactics.

Ballistic Tactics	Anti-Personnel Tactics
	Direct Fire Weapons
Contamination Tactics	Airborne CBRN Contamination
	Food Supply Contamination
	Waterborne CBRN Contamination
Eavesdropping Tactics	Acoustic and Electronic Eavesdropping
	Visual Eavesdropping
Explosives Tactics	Indirect Fire Standoff Weapons
	Man-Portable Bombs and Devices
	Package / Mail Bomb
	Vehicle-Borne IED
	Waterfront Attack
Property Tactics	Anti-Aircraft Tactics
	Anti-Property Tactics
	Covert Entry
	Forced Entry

The *Risk Assessment* is the step when all of the earlier assessments (Asset Criticality, Threat, and Vulnerability) are combined and studied together to give a complete picture of the risks to an asset or group of assets. When standard scales are used for measuring the various risk elements, a quantitative measurement of risk can be determined, enabling discrete scenario comparisons and cost-benefit analyses (Figure 4).

The risk assessment results enable security specialists to identify specific unwanted events requiring additional security protection. Using the FVAT, they can

identify candidate countermeasures (e.g., tactics, training, procedures, manpower, sensors, equipment, construction, etc.) to prevent or mitigate these events. These countermeasure Courses of Action (COAs) *measure* the risk reduction (or *benefit*) of the COAs. With a clear and consistent measure of benefit, coupled with the costs of various COAs, the organization leadership can make good and informed decisions to mitigate security risks and manage their security program.



Figure 4. ForcePRO Risk Summary

CONCLUSION

The ForcePRO risk assessment methodology and software uses a structured and repeatable process to organize a large amount of available information (e.g., asset lists, threat data, vulnerability assessments, etc.) and place them in context. Using ForcePRO, the security professional can *visualize* the organization's security issues and *quickly identify* solutions. A thorough risk assessment allows decision makers to effectively evaluate the security risks to their organizations, and to make defensible and cost-effective risk reduction decisions. Today ForcePRO is an USAF application, but the concepts and approach can be readily adapted to any domain with assets you care about, security threats to those assets, and weaknesses in security that might allow the threats to successfully damage or destroy your assets.

The immediate next steps in ForcePRO's development are an improved ForcePRO Vulnerability Assessment Tool (FVAT) and implementing ForcePRO for US Navy ashore installations. Future capabilities envisioned for ForcePRO include:

- Global Information Grid web-based capability

- Interface with other management systems (e.g., CVAMP)
- Geographic Information Systems (GIS) capabilities for map visualization and proximity consequence calculations
- All hazards risk analysis (natural hazards, HAZMAT, cyber, insider threats)
- COA modeling and simulation
- Automated reports and briefings

REFERENCES

Air Force Security Forces Center. (2009). *AFI 31-101, Integrated Defense*. Lackland AFB, TX: Air Force Security Forces Center.

Joint Chiefs of Staff. (2006). *JP 3-0, Joint Operations*. Washington, DC: US Department of Defense.

Risk-Based Cost-Benefit Analysis for Security Assessment Problems

Gregory D. Wyss^a, John P. Hinton^b, Katherine Dunphy-Guzman^b, John Clem^a,
John Darby^a, Consuelo Silva^a, and Kim Mitchiner^a

^aSandia National Laboratories, Albuquerque, New Mexico, 87185-0757,

PH: 505-844-5893, email: gdwyss@sandia.gov

^bSandia National Laboratories, Livermore, California, 94551-0969

ABSTRACT

Decision-makers want to perform risk-based cost-benefit prioritization of security investments. However, strong nonlinearities in the most common physical security performance metric make it difficult to use for cost-benefit analysis. This paper extends the definition of risk for security applications and embodies this definition in a new but related security risk metric based on the degree of difficulty an adversary will encounter to successfully execute the most advantageous attack scenario. This metric is compatible with traditional cost-benefit optimization algorithms, and can lead to an objective risk-based cost-benefit method for security investment option prioritization. It also enables decision-makers to more effectively communicate the justification for their investment decisions with stakeholders and funding authorities.

INTRODUCTION

For many years, safety investment decisions have been made using risk-based cost-benefit analysis in which the benefit metric is heavily based on a quantitative estimate of risk reduction. Many seek to perform similar analyses to prioritize security investments, but this has met with limited success, in part because the “attack likelihood” component of risk is often extremely uncertain and not considered when conditional security risk is assessed. Therefore, Sandia National Laboratories has undertaken a Laboratory Directed Research and Development project to develop a risk-based cost-benefit analysis method to prioritize security investments that overcomes some of these obstacles. The goal of this work was to enable security analysts to describe the benefits of security risk reduction measures based on the degree to which they increase the difficulty for an adversary to successfully prepare and execute an attack that can produce a given level of consequences. The resulting method is highly scalable and enables robust risk-based cost-benefit security investment prioritization to be performed at levels of granularity ranging from a single target up to multiple targets or facilities across an enterprise.

SECURITY RISK ANALYSIS

Kaplan and Garrick’s definition of risk [1] is stated as, “Fundamentally... a risk analysis consists of an answer to the following three questions:

1. What can happen?
2. How likely is it that [it] will happen? and
3. If it does happen, what are the consequences?”

“To answer these questions we would make a list of outcomes or ‘scenarios’ [where each line in the list] can be thought of as a triplet $\langle s_i, p_i, c_i \rangle$ where s_i is a scenario identification or description; p_i is the probability of that scenario; and c_i is the

consequence or evaluation measure of that scenario, i.e., the measure of damage. If this table contains all the scenarios we can think of, we can then say that it (the table) is the answer to the question and therefore is the risk.” Security risk frequently considers three basic components: threat, vulnerability, and consequence. [2] These components map into the risk definition as follows. A scenario s_i represents a specific threat exploiting particular vulnerabilities to produce consequences. The scenario likelihood has two parts: (i) the likelihood for a threat T with particular characteristics (e.g., number of attackers, weapons, tools, etc.) to attempt an attack (P_T), and (ii) the conditional likelihood that the attack by this threat will be successful ($P_{S|T} = 1 - P_{E|T}$). The consequences of an attack are represented by c_i . For high-consequence facilities, attacks are so rare that statistical estimates of P_T are highly uncertain. As a result, analysts often neglect P_T and assess *conditional* risk, i.e. the risk that would exist given that the attack were to occur, on the basis of $P_{S|T}$ or $P_{E|T}$, or, for a design basis threat, $P_{E|DBT}$. [3] Conditional risk has a key drawback that limits its use in cost-benefit analyses: aggregated security risk cannot be computed because *conditional* probabilities $P_{S|T}$ or $P_{E|T}$ cannot be aggregated. [4]

To overcome the obstacles related to the use of probabilities with malevolent adversaries, we have developed a modified definition of risk where, instead of considering the highly uncertain likelihood or probability of an attack, one considers its difficulty for an adversary to successfully accomplish against the target(s) under consideration. Thus, security risk analysis considers the following revised questions:

1. What can happen?
2. How difficult is it for an adversary to make this event happen? and
3. If an adversary causes this event to happen, what are the consequences?

The triplet for security risk then becomes $\langle s_i, d_i, c_i \rangle$ where d_i is the degree of difficulty for an adversary to successfully accomplish attack scenario s_i at a specific target in order to cause consequence c_i .^{*} This definition explicitly acknowledges the observed adversary attack planning behaviors described above and addresses the problems associated with using probabilities to describe the intentional actions of both known and unknown intelligent actors. Risk evaluations using this definition do not require revision as adversary motivations change because this risk definition characterizes scenarios and targets rather than estimating the adversary’s probability of attack. For each target, a number of scenarios can be posed, each correlating to a risk triplet. For a given consequence, there is a “threshold threat” (TT) that is the lowest difficulty (highest risk) scenario for an adversary to be successful.

Security risk analysis seeks to estimate the minimum threat capabilities (TT characteristics) and degree of difficulty required for an adversary to accomplish a specific attack scenario that exploits a target’s vulnerabilities and induces specific consequences with a reasonably high likelihood of adversary success $P_{S|TT} = 1 -$

* This definition of risk, and specifically d_i , is a characteristic of scenario s_i for the specific target. The reader should not assume that d_i characterizes any specific adversary group or DBT. Rather, d_i incorporates the minimum threat capabilities needed for any adversary to have a high likelihood of success when attempting to execute scenario s_i at the specific target. It also incorporates the characteristics and complexities of the scenario that might make the scenario difficult for an adversary to accomplish successfully even if they had the requisite minimum threat capabilities.

$P_{E|TT}$. Adversary attack preparation activities are viewed as a project planning exercise, wherein a planner has success criteria (e.g., adequate or desired consequences and thresholds for likelihood of success), and chooses among alternative strategies that meet these criteria (e.g., achievable resources and plausible attack scenarios), while considering the degree of difficulty to achieve a successful attack. Investments reduce security risk as they either (a) increase the difficulty for an adversary to successfully execute the most advantageous attack scenario, or (b) reduce the severity of the scenario's expected consequences. The latter can be measured using existing consequence metrics, but measuring the former requires development of a metric to characterize the adversary's degree of difficulty in achieving a "successful" attack. Building this metric is not straightforward, as it requires one to compare and aggregate the relative degree of difficulty for disparate adversaries to successfully prepare for (e.g., acquire the requisite resources) and execute an attack (employ those resources in specific ways against specific targets). However, with such a metric, this definition of risk can form the basis of an objective risk-based cost-benefit analysis method to enable security investment prioritization using traditional cost-benefit optimization algorithms.

Using a measure of scenario difficulty, an analyst can compare security risks by comparing attack scenarios' levels of difficulty and consequences. The insights from such comparisons can provide important and useful security risk management insights for a broad range of applications. The objective of a security decision maker might be thought of as follows: to make the easiest attack path as difficult as possible within the constraints imposed by cost, operational and programmatic considerations. Consider a decision maker who is responsible for several sites where each attack leads to similar consequences. Figure 1 shows how this method can be applied to security decision making. Each light-colored bar represents the difficulty of the easiest attack scenario at a notional site in its original (2007) configuration. Note how it was much easier for an adversary to achieve a successful attack at Site D than at any other site. Note also how security at Site B was already significantly better than the original (2008) goal level. The decision maker focused on improving security at Site D, and in 2010, security is much more balanced across the enterprise as the difficulty of the easiest attack is now roughly comparable across all sites (the top of the dark bar in the graph). The decision maker can justify why particular security investments were made and describe the specific benefits that the investments produced. Further, if policy changes cause the security goal to change, the decision maker can explain why additional security investments are needed. Prioritizing investments is straightforward, and the method is compatible with computerized optimization programs.

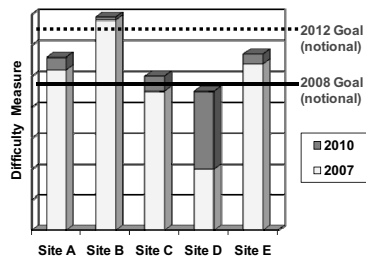


Figure 1. Comparing the relative difficulty of the easiest attack scenarios at five notional facilities where each attack leads to similar consequences.

If a variety of consequences are possible within an enterprise, consider Figure 2. Each attack path or scenario is represented as a dot on the scatter plot, with coordinates that represent the scenario's difficulty d_i and consequences c_i . Those that produce higher consequences *and* are easier to accomplish are more attractive to an adversary because they represent a more efficient use of resources. Thus, they pose a greater risk and should be a higher priority for remediation. A scenario's risk can be reduced by reducing its consequence potential (moving the dot down), increasing its difficulty (moving it to the right), or a combination of these actions. Also, if one reduces the risk of a scenario s_j that is near the center of the pack of dots without also addressing scenarios that are more attractive (those that produce greater consequences *and* are easier to accomplish, whose dots are above and to the left of s_j), then overall security risk may be unaffected by the investment because the most attractive scenarios remain available for adversary exploitation. Thus, security investments should address those scenarios that are non-dominated (i.e., that represent the easiest way to produce consequences greater than or equal to c_j). This approach has strong parallels to game theory. [4]

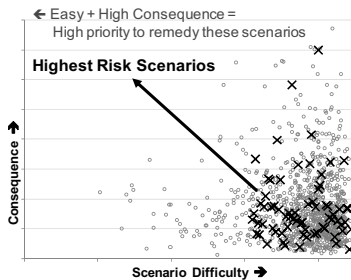


Figure 2. Relative difficulty and consequences of attack scenarios at a notional facility (X symbols) compared with scenarios at other facilities within the enterprise (circles).

Consider Figure 2 from the perspective of the security decision maker for an enterprise. The X symbols represent the attack scenarios available at one facility, and that facility's manager wishes to mitigate the scenarios that are most attractive at that facility. The enterprise decision maker might use this graph, with circles representing attack scenarios available at other facilities within the enterprise, to inform the facility manager that only minimal security improvements will be supported because the enterprise has greater security risks that must be addressed first. Or, if it is known from intelligence sources that the facility is specifically targeted by credible threats, the enterprise decision maker may decide to support security upgrades at the facility anyway, believing that the easiest attack at that facility is not yet difficult enough.

CHARACTERIZING THE DIFFICULTY OF A SUCCESSFUL ATTACK

The method for security risk assessment described above hinges on developing a metric for simply characterizing targets in terms of the overall difficulty for the generalized set of disparate potential adversaries to conduct successful attacks. While it is easy for an analyst to *describe* the difficulties inherent in a specific attack scenario, these difficulties are hard to express as a single metric – either qualitative or quantitative – because of the large number of disparate factors that may cause difficulty to an attacker. To date, our research has not uncovered any generally accepted system of metrics to answer the question, “How difficult is it for an adversary to accomplish this scenario?” or the related question, “How much more capable is one adversary compared to another?” However, a few broadly applicable

and unclassified methods have been proposed for other purposes that may be applicable to this problem. These have been described in various publications [3, 5, 6, 7, 8], and summarized by the authors in previous papers. [4, 9] This section describes a system of metrics designed to describe and summarize the levels of difficulty that adversaries would face in successfully executing attack scenarios.

The proposed approach starts by identifying a scenario that would offer an adversary a reasonable expectation of success (inducing specific consequences) against the target(s) under consideration, as described previously. Such scenarios can be developed by any available means that is used by vulnerability assessment community. Specific to each scenario, either explicitly or implicitly, are the resources (personnel, materiel, and knowledge) that an adversary would need to have, and the manner in which they would need to be employed, in order for the adversary to have a reasonable likelihood of success when executing the scenario against the target(s) under consideration.

Considerations of the difficulty for an adversary to mount this scenario are partitioned into the two essential phases of adversary efforts for any attack scenario - Preparation and Execution. Since adversary success in the scenario requires successful completion of both phases, they are viewed with comparable significance. The primary factors that are generally key to adversary success in each phase of attack have been identified through discussions with subject matter experts, review of various ranking schemes for adversaries or threats or scenarios, and analysis of a diverse set of specific scenarios. Since we require a metric that characterizes the relative difficulty of successfully (inducing and) exploiting target vulnerabilities, we express scenario success factors in terms of their manifestation at the interface between target and threat. For example, while level of funding can be important to adversary success, this is manifested at the target in other factors, such as quality and size of the toolkit used in the scenario. We have developed these factors so that they can be considered as roughly independent dimensions of generally equivalent importance.

The dominant scenario preparation challenges for adversaries are in developing, acquiring, and preparing the resources required for the scenario (personnel, materiel, and knowledge) without being detected or interdicted. The dominant scenario preparation resource attributes include the required number, training and expertise of both outsider attack and insider participants, and the security controls that an insider participant would be required to subvert; the size, complexity, capability and commitment of the attackers' support structure (e.g., intelligence, safe haven, training or staging facilities, finances, R&D); and the characteristics and availability of the tools and weapons that would be required to successfully execute a scenario.

The manner in which adversaries employ their resources during attack execution can also be critically important to their ability to succeed. The dominant execution success factor attributes include the ingenuity or inventiveness (e.g., attacks that reflect unique, imaginative approaches that are more likely to surprise and befuddle even very well prepared defenses); the level of task complexity and precision of coordination required; situational understanding required (acuity to recognize the occurrence of exploitable conditions and the flexibility required to leverage those

opportunities); stealth and covertness (concealment of attack execution activities to delay the point of initial detection and recognition by authorities); and the degree of dedication or commitment required of insider and outsider participants (significance, persistence and certainty of consequences at risk for the attack participants, their support base, and/or their cause).

The Preparation and Execution success factors are represented in 13 dimensions. Five discrete levels of difficulty have been defined for each success factor dimension. The levels of difficulty have been calibrated so that a particular level for one dimension roughly correlates to an equivalent level of difficulty for any other dimension, as shown in Table 1. Levels of difficulty generally correlate with the size of the portion of the spectrum of potential adversaries that could reasonably expect to achieve or acquire the associated level characteristics. Level 1 characteristics are easily accessible or achievable by the general population, while Level 5 characteristics would typically be accessible or achievable only by elite forces or state supported operations. Guidelines are being developed for analysts to consistently assign the appropriate levels to each success factor dimension in order to reflect the relative difficulty that an adversary would encounter to successfully achieve or acquire the characteristics required in that dimension for the scenario to succeed. It is important to note that this process does not assign *adversaries* to a particular level, nor imply that all dimensions of a scenario are at the same level. Rather, the process dissects a successful scenario into the minimum levels of difficulty associated with each of the key factors that generally underlie adversary success.

A numerical value is associated with each of the five levels of difficulty. Since the dimensions are roughly independent and span the most significant challenges that are key to adversary success, the metric for overall difficulty of that scenario for the target(s) under consideration can be calculated as the length of the vector described by the values along each of the phase's dimensions (an L_2 norm). Other aggregation methods are also under consideration. A dimension's values could also be weighted to reflect that dimension's relative general significance to adversary success, although research to date has not indicated a rationale for other than uniform weighting. Because of the qualitative and discrete nature of the assessments, and the diversity of attributes underlying the metric's value, the values are most appropriately interpreted as indicating cohorts of scenarios of similar levels of difficulty required for adversary success in achieving a given level of consequence against the target(s) under consideration. A set of similarly valued conditions (scenario-target pairs) can be considered as a cohort of attack scenarios of comparable difficulty, with differences in values providing a reasonable basis for rank-ordering by level of difficulty. Since the scale for metric values is non-linear, one should not place undue emphasis on ratios of values between cohorts.

While this approach is still under development, the utility of the metric has been demonstrated by evaluating a diverse set of scenarios with widely varying levels of difficulty and consequences. Evaluated scenarios include physical assaults against high security, high consequence facilities, the use of vehicle-borne improvised explosive devices against both mobile targets and government buildings, pathogenic attacks against food chain targets, and cyber attacks against sensitive databases. The

metrics produced for these scenarios have been fully consistent with analysts' and subject matter experts' intuitions regarding relative levels of adversary difficulty. For this reason, we are confident that the method described here embodies the desired characteristics necessary to redress important shortfalls of common security risk assessment methods in providing a sound basis for prioritizing investments to mitigate security risk and for communicating the justifications for investment decisions. However, before this method can be brought to fruition, additional work is needed in the areas of mathematics for metric aggregation, testing for reproducibility and utility of results, and uncertainty analysis.

Table 1. General characteristics used to establish levels of difficulty for dimensions.

Level 1	Level 2	Level 3	Level 4	Level 5
Easy to get/do	Moderately easy to get/do	Difficult	Very difficult	Extremely difficult to get/do
Capability available by legal means	Requires capability similar to criminal activity	Requires capability similar to organized criminal activity	Requires sophisticated capability similar to large corporation	Requires state-supported capability
Requires no special skills	Requires low-level skills (~days of training)	Requires moderate-level skills (~months of training)	Requires high-level skills (~many months of training)	Requires highly specialized skills (~multiple years of training)
Achievable in very short time (~days)	May require ~weeks to achieve	May require ~months to achieve	May require ~many months to achieve	May require very long time to achieve (~multiple yrs)
Easily accessible by general public	Accessible to public that has moderate-level knowledge	Accessible to specialized groups		Accessible only by elites.
Essentially no early warning signatures - little risk to adversary of disruption	Some early warning signatures – some risk of disruption			Very large early warning signatures – great risk of disruption
Rudimentary				Very sophisticated

CONCLUSION

Existing security cost-benefit analysis methods have had limited success in providing robust investment prioritization insights for decision makers, especially for rare and high-consequence events, because the risk insights on which they depend require estimation of an attack probability. Such probabilities are highly uncertain and can change rapidly with adversary capabilities and intentions. This work provides an enhanced definition of risk in which scenario *likelihood* is replaced with scenario

difficulty. The non-statistical nature of observed adversary planning behavior is modeled by treating scenario consequences and difficulty as distinct dimensions of risk. This enables risk-based cost-benefit security investment prioritization using traditional optimization algorithms. To implement this approach, we have developed a metric to quantify vulnerability of targets in terms of scenario threshold threats, which represent minimum levels of difficulty for adversaries to succeed in achieving various levels of consequences. This metric characterizes the scenario and target, and is independent of the specific adversary. Thus, it is less sensitive to the uncertainties of changing threat assumptions. When used with imaginative exploration of potential attack scenarios, these advances enable decision makers to achieve better balance among competing security interests. The method is useful for supporting security risk mitigation decisions at a variety of scales, ranging from individual targets to an enterprise consisting of multiple facilities. Results from this method will provide greater objectivity and unbiased justification for investment decisions; reduce second guessing of investment decisions by funding authorities; leading to more robust and cost-effective security systems.

Acknowledgements. The authors are grateful for support from the Laboratory Directed Research and Development Program at Sandia National Laboratories. Sandia is a multiprogram laboratory operated by Sandia Corporation, a wholly owned subsidiary of Lockheed Martin Corporation, for the United States Department of Energy's National Nuclear Security Administration under contract DE-AC04-94AL85000. This paper has been approved for unlimited release as SAND2010-8652C.

References

- [1] S. Kaplan, and B.J. Garrick, "On the Quantitative Definition of Risk," *Risk Analysis*, 1:1(11), 1981.
- [2] U.S. Department of Homeland Security Risk Steering Committee, "Risk Lexicon," U.S. Department of Homeland Security, Washington, DC., September 2008.
- [3] Garcia, M.L., *The Design and Evaluation of Physical Protection Systems*, Butterworth-Heinemann (Elsevier), Burlington, MA, 2001.
- [4] G. Wyss, J. Darby, C. Silva, and A. Walter, "Risk-Based Cost-Benefit Analysis for Security Assessment Problems," 44th Annual International Carnahan Conference on Security Technology, San Jose, CA, October 5-8, 2010.
- [5] D.P. Duggan, "Generic Threat Profiles," SAND2005-5411, Sandia National Laboratories, Albuquerque, NM, July 2005.
- [6] D.P. Duggan, S.R. Thomas, C.K.K. Veitch, and L. Woodard, "Categorizing Threat: Building and Using a Generic Threat Matrix," SAND2007-5791, Sandia National Laboratories, Albuquerque, NM, September 2007.
- [7] US Department of Energy, "DOE Standard: Vulnerability Assessment," Chapter VII, Adversary Mission Analysis, DOE-STD-0005-2008 (Draft), Official Use Only, US Department of Energy, Washington, DC, September 2008.
- [8] U.S. Department of the Army, *The Military Decision-Making Process*, FM101-5, Washington, DC, 31 May 1997.
- [9] G. Wyss, J. Darby, C. Silva, and A. Walter, "Risk-Based Cost-Benefit Analysis for Security Assessment Problems," Presented at PSAM-10 International Meetings on Probabilistic Safety Assessment and Management, Seattle, WA, June 7-10, 2010.

Assessing vulnerability to floods of the built environment - integrating urban networks and buildings

Damien Serre¹ Serge Lhomme¹, Kristina Heilemann², Leif Sigurd Hafskjold², Andrew Tagg³, Nicholas Walliman⁴, Youssef Diab¹

¹Université Paris-Est, Ecole des Ingénieurs de la Ville de Paris, 15 rue Fénélon, 75010, Paris, Tél: +33 1 56 02 11 05; damien.serre@eivp-paris.fr; serge.lhomme@eivp-paris.fr; youssef.diab@eivp-paris.fr

²SINTEF Building and Infrastructure, Klæbuveien 153, 7465 Trondheim, Norway, Tel.: +47 73 59 82 32; Leif.S.Hafskjold@sintef.no; kristina.heilemann@sintef.no

³HR Wallingford Ltd, Howbery Park, Wallingford, Oxfordshire OX10 8BA, United Kingdom, Tel. +44 1491 822332; a.tagg@hrwallingford.co.uk

⁴Oxford Brookes University, Department of Architecture, School of the Built Environment, Headington Campus, Gypsy Lane, Oxford, UK, OX3 0BP, UK, Tel. +44 1865 483200; nwalliman@brookes.ac.uk

ABSTRACT

The EU is very concerned by flood risk. The effects of floods on urban areas are substantial in terms of damage and economic loss. It is expected, taking into account climate change and urban growth, that this particular risk will be more frequent and will cause more and more damage; the built environment has become very vulnerable to floods.

There is a need to develop methods and tools to assess urban vulnerability to floods. Indeed, some solutions are already available to assess vulnerability of buildings or infrastructure such as networks. But, the city is a complex system and not just a sum of its components. Our purpose is about developing techniques to assess the vulnerability of the city using a systematic approach and integrating existing tools which assess the vulnerability of particular components of the city system.

INTRODUCTION

Floods are considered the major natural hazard in the EU in terms of risk to people and assets. Currently, more than 40 bn € per year are spent on flood mitigation and recovery (incl. compensation of flood damage) in the EU. More than 75 % of the damage caused by floods occurs in urban areas (COST22, 2008). Climate change and concentration of population and assets in urban areas are significant trends likely to affect these numbers in the near future. Global warming is expected to lead to more severe storm and rainfall events as well as to increasing river discharges and sea level rise (Cf. Xynthia in France, 1.5 billion euros). This means that flood risk is likely to increase significantly. Furthermore, 80 % of the population will live in urban areas by 2020 and the economic values in these areas are constantly growing. Therefore flood risk in urban areas will increase disproportionately: flood damage figures could rise to 100 bn € per year by the end of the century (European Environment Agency, 2008).

Urban systems contain assets of high value and complex and interdependent infrastructure networks (i.e. power supplies, communications, water, transport etc.). The infrastructure networks are critical for the continuity of economic activities as well as for people's basic living needs. Their availability is also required for fast and effective recovery after flood disasters. The severity of flood damage therefore largely depends on the degree to which both high value assets and critical urban infrastructure are affected, either directly or indirectly.

Current flood risk management and research mainly use the susceptibility and value of the protected assets (expected damage to buildings and inventory) to assess their vulnerability, i.e. the potential direct damage. Improving the assessment of potential indirect damage to the

entire urban system caused by flood-induced failure of particular important components is of great value. It will allow decision-makers to focus their investments on such "risk hotspots", i.e. particular vulnerable elements of the urban system. This will considerably increase the cost-effectiveness of their investments and improve the overall resilience of our cities.

The principal aim of our research is to improve methods for assessing the vulnerability of the urban environment related to floods, especially by extending conventional methods with the ability to assess indirect impacts of damage to networks and assets with a high value. In this way, the first part of our article will focus on the current methods to assess urban environment vulnerability and we will point out the limits of these existing approaches. The second part will describe the methodologies we are using to assess the vulnerability of cities, where cities are considered as complex and integrated systems. The last part of the paper presents the results of vulnerability assessment of urban technical networks and critical infrastructure buildings (risk hotspots).

EXISTING METHODS OF INFRASTRUCTURE BUILDING VULNERABILITY ESTIMATION

The likelihood that a particular building will be flooded and the frequency and severity of the inundation is calculated as part of the general flood predictions for urban and other areas. However, in order to estimate its individual vulnerability, it is necessary to examine the possible types of flood damage that the building will suffer. As the range of possible damages is so large and difficult to estimate, it is necessary to be selective in any method devised to estimate flood damage to buildings and limit the factors to those that can be realistically calculated.

Calculations are normally limited to tangible costs expressed in financial terms. The direct costs, particularly the structural costs, should be the focus of the predictions, they being directly related to the physical fabric of the buildings and to the structure, construction and materials employed. These are relatively easy to survey and record accurately at various levels of detail by building specialists such as architects and surveyors. The contents of the building and their value, vulnerability to flood damage is more likely to be known by the building occupant, and can also feature strongly in the calculations. This is likely to be the case also for external items and contents. As indirect costs, the clean-up costs are also likely to be possible to estimate with reference to the likely effects on the building and its contents, though the amount of flood debris will depend on the type of flood and surrounding buildings, objects and vegetation. The other indirect costs can only be estimated by the building users according to the severity of the flood effects on the building and with reference to the services they provide and nature of business and employment. This should not form part of the damage estimation with regard to the buildings, but we can use this estimate to help to calculate indirect costs.

Flood damage to buildings and contents are dependent on a number of variables in relation to the flood events. The variables according to Gissing and Blong (2004) are given as: over-floor depth, velocity, rate of rise, debris, contaminant, frequency and duration of inundation and timing. Although depth is the most common variable used in the calculation of flood damage, the importance of velocity is likely to have been undervalued in countries where high water velocity is relatively rare. A small increase in velocity can have a significant impact, particularly at greater depths, particularly for transporting debris.

Other variables relating to the building characteristics are also mentioned, such as the materials that the building is constructed from, the drying characteristics of the materials and the condition of the building prior to being flooded (Soetanto and Proverbs, 2004, p95). To this can be added the planning of the spaces within the building (basements, level of ground

floor above ground etc.), the services and their positions within the building (air conditioning equipment, circuit boards, boilers etc.), as well as the contents and their locations.

The result is that a model that can deal with all these variables is likely to be very complex and difficult to manage, though oversimplification of the variables is likely to lead to inaccurate estimations. A balance must therefore be drawn between excessive complexity and acceptable accuracy.

The function of a damage estimation model is to predict the extent of damage to a building and its contents depending on the severity of the flooding. The output of the model should express the damage in cost form. This will enable calculations to be made in order to assess the cost/benefit analysis of installing flood mitigation measures to the building and/or its surroundings. The output of such models devised for damage estimation in many scenarios (floods, earthquakes, landslides, tsunamis etc) at a variety of scales, are graphs that present stage damage curves.

According to Smith (1994) the basic methodology for the assessment of flood damage for both rural and urban sectors is dependent on the development and use of stage-damage curves, alternatively called loss functions. A curve can relate to a particular class of building and presents information on the relationship between the depth of flooding (stage) and resultant damage.

The initial method when devised some 60 years ago was to base the stage damage curves on the experience of previous flood incidents (actual). However, Smith points out that the specific conditions of each flood event made general predictions unreliable, due to differences in warning time, building types and contents, and on the lack of reliable information about the actual extent of the damages. This led to the development, twenty years later, of synthetic stage-damage curves for different building types and uses based on hypothetical analysis (potential). These are of two types depending on the data on which they are based – existing data bases, or surveys by valuers and loss adjusters. Different stage damage curves in both cases need to be devised for different classes of buildings.

Among available methods we can make references to:

- ANUFLOOD (State of Victoria, 2000, p19);
- HOWAS21 (Bavarian Water Management Agency);
- HAZUS-MH Flood Model – adaptation of earthquake model (Scawthorn et al., 2006);
- New stochastic methodology (Nadal et al., 2010);
- Engineering evaluation (Schwarz and Maiwald 2008)
- Economic assessment of flood mitigation measures - average annual damages (AAD).

These methods are well adapted to assess building vulnerability. But, these approaches are not integrated enough into city functions. These existing methods have some limitations for use in an urban context, especially because cities are complex systems that we cannot assume to be simply the sum of buildings located in flood prone areas. Furthermore, assessing vulnerability with a final criterion based only on the costs of the effects of floods is no longer sufficient as the sole aid for flood risk management in the built environment. Methods taking into account a systemic dimension of the city seem to be more appropriate for understanding how urban systems may react to emergencies such as floods.

Risk and vulnerability assessment should support authorities and infrastructure owners by identifying people, property, buildings and critical infrastructure that are at risk from hazardous events. Vulnerability analyses have been traditionally carried out using empirical methods based on damage vulnerability matrices (Kappos et al. 1998). Probabilistic Safety Analyses (PSA) and Quantitative Risk Analyses (QRV) have been implemented in the safety management of nuclear power plants and in other industrial installations for decades. These

analyses, conducted by specialist consultancy companies, and requiring the knowledge of experts, were therefore rather cost-intensive. The public sector and small and medium enterprises were mostly not able to offer such comprehensive analyses. Therefore a much simpler risk and vulnerability analysis was developed in the early nineties in Norway under the acronym ROS (“Risiko- og Sårbarhetsanalyse”) (Utne et. Al, 2008). Based on the initiative of the Directorate for Civil Protection and Emergency Planning the ROS analysis was conducted in numerous municipalities in Norway during the past decade and is today a part of the Norwegian planning and building act.

The purpose of a ROS-analysis is to avoid the risk of loss of life and harm to health, the environment, important infrastructures and property and to increase the reliability off the social and area planning processes (Norwegian Ministry of Environment). In expert interviews about undesired events, their likelihood and the consequences in the case of an incident are discussed and registered in a risk matrix. The analysis provides a first risk picture on a coarse scale. In most cases more detailed standard risk analyses and model-based risk analyses have to follow. The method is a reliable mapping tool providing an overview about possible causes of risk. The analyses can be carried out during the planning process, during the construction process or for the evaluation of the risk to existing infrastructure. The main purpose is to support the authorities and infrastructure owner within decision making processes. ROS- analyses can provide fundamental knowledge for promoting safety and analyzing costs (Aven, 2008).

A computerized tool for a risk and vulnerability analyses (RVA) was developed within the framework of the Norwegian Research program SAMRISK (Societal Security and Risk). According to a ROS-analysis the method supports an “all hazards” approach across sectors and includes beside others electricity supply, water supply, transport (road/rail), information and communication systems (ICT). The tool InfraRisk focuses on serious events and emphasises dependencies between the sectors. The risk is directly assessed by specifying frequencies and consequences. One severe challenge is the estimation of consequences where either the “average consequences” or the severe “worst consequences” can be highlighted. The choice of the consequences will influence the way assessing the undesired events. In emergency preparedness planning processes the “worst case” approach is most relevant (Utne et. Al, 2008, Vatn, 2007).

The InfraRisk tool considers a large spectrum of different events such as medical, biological and technical catastrophes, dysfunctional human behaviour, crime and terrorism and natural catastrophes. The objective of another research activity within the SAMRISK program was to develop a risk and vulnerability analyses with the focus on climate change and natural hazards. A case study in the Oslo Municipality demonstrated that InfraRisk is a sufficient tool to analyses the risk and vulnerability for critical infrastructure. For this reason it was suggested to modify InfraRisk on a way that the analysis is focused on natural catastrophes.

InfraRisk was modified in so doing that the main events were replaced by natural events which cause floods in urban areas. In that way a new method to analyze the risk of floods and the vulnerability of a specific network due to floods became available (FloodRisk). The starting point for the analysis is the identification of undesired natural events, in this case floods due to intensive precipitation, melting snow, storm surges and higher sea levels and technical events like breaking of dams and water pipes and breakdown of pumping stations. For each main event it is possible to link societal critical functions (SCFs) that are relevant for the main event. Societal critical functions are functions that if they fail to deliver the required output will reduce the function of the specific network. In a further step the various main events get qualified by one or more vulnerability factors (VIFs). The probabilities for the main events are distributed in five categories from “very unlikely” to “frequent”. The last step

of the analyses is the assessment of consequences. The results of the analyses are presented in a risk matrix (Vatn, 2007)

Testing the tools *InfraRisk* and *FloodRisk* in different case areas showed that there are dependencies between undesired events. It also pointed out the need to analyze the infrastructures and the undesired events collectively, and not separately as most often are done in similar analyses (Vatn, 2007). Events like floods can be sufficient to include in the computerised analyses and the modified version is suitable for assessing the risk and vulnerability for a specific sector. The risk matrices provide a time effective overview about weak points and draw a risk picture for urban networks.

VULNERABILITY ASSESSMENT OF A COMPLEX SYSTEM: CITY

Urban growth and climate change oblige us to manage flood risk by integrating new concepts like urban resilience (Ashley et al., 2007, Nie et al., 2009) and developing a systematic approach. In this context, a first analysis of the needs of city governors for decision making tools shows they don't have tools available to help them to prioritize recovery actions but of course, they are interested to have them. Such tool should assist urban planners in assessing the built environment vulnerability. Thus it should allow them to set priorities and to speed up city reconstruction after a flood event and, of course, help to prepare protection systems in case of alert. For this, there is an important need to understand failure mechanisms that lead to disruption of the city.

Here, there is a big issue because the city is a complex entity. For instance, the idea of a city seems perfectly clear to everyone, but defining this system is complex. Thus the definition of a city has been approached in a number of distinct ways. Among the more important viewpoints that have been adopted are the economic, the sociological, the cultural, and the historical. Moreover, until very recently, the city has been assessed by very analytical methods and was characterized by fragmented studies concentrated on very particular aspects (transportation, urban planning, urban sociology, environmental aspects) with few cross-cutting studies. Therefore, each discipline offers its models and theories on urban areas. Yet, for understanding the city as a whole, these analytical and fragmented approaches are not appropriate, in particular because models become more and more complex. So nowadays, the principle is to study the city like a system, especially a complex one (such systems are not fully predictable, due to the inherent uncertainty in how these systems evolve). Indeed, a system is an "autonomous entity with regard to its environment, organized in a stable structure (identifiable in the course of time), constituted by interdependent elements, whose interactions contribute in maintaining the system structure and making it evolve" (Pumain, 1982). As illustrated in the literature (Pumain et al., 1995), (Sanders, 1992), (Beaujeu-Garnier, 1997) a city appears as a set of components interconnected by networks with some critical infrastructure.

Using a safety method approach, composed by functions analysis, and a Failure Modes and Effects Analysis (FMEA), a city model has been built allowing the identification of critical infrastructure and its interdependencies (Lhomme et al., 2011).

PRELIMINARY RESULTS: CRITICAL INFRASTRUCTURE IDENTIFICATION

As civilizations have become more complex and engineered solutions more sophisticated, the public has come to rely on the integrity of built projects for safety and well-being. When those projects fail, the consequences have become commensurately more devastating. Notable infrastructure disasters that have occurred over the past century serve as a stark reminder of the importance of critical infrastructure to public safety, health, and

welfare. Critical infrastructure systems often cross geographic, political, cultural, and organizational boundaries and may be built, natural, or virtual. Built critical infrastructure includes energy; water and wastewater treatment, distribution, and collection; transportation; and communications systems. Natural critical infrastructure systems include lakes, rivers, and streams that are used for navigation, water supply, or flood water storage, as well as coastal wetlands that provide a buffer for storm surges. Virtual critical infrastructure includes cyber, electronic, and information systems (ASCE, 2009).

Today, the term “critical infrastructure” has become central in the emergency preparedness work of many nations, but there is yet no universally accepted definition of the term. Most definitions point toward systems that are of vital importance to the society. An infrastructure is a set of basic facilities, services, and installations that are necessary for the functioning of a community or society, such as transportation and communications systems, water and power supplies, employment centers, medical facilities, and public institutions, including schools, post offices, and prisons. They are critical in that a disruption would threaten the security, economy, public health, safety, and way of life of a community or society. The degree of criticality is bound to differ across systems and cultures but it is widely thought that a breakdown of one or more of these critical systems has the potential to cause very serious disruption.

Usually, critical infrastructures are: Agriculture and Food; Water; Public Health; Emergency Services; Government; Defense Industrial Base; Information and Telecommunications; Energy; Transportation; Banking and Finance; Chemical Industry and Hazardous Materials; Post; National Monuments and icons; Critical Manufacturing.

For a critical infrastructure, becoming dysfunctional is a phenomenon that transcends by far the failure of any, even major, single component. The often incomprehensible cause of system crashes stems from the inherent features of the critical infrastructures: they are multi component systems, prone to cooperative behavior, and typically responding in a non-linear fashion to stimuli and perturbations. Indeed critical infrastructures can be considered as complex systems. A critical infrastructure system is an assemblage of functional objects that provides a certain essential good or service. For instance, a power supply system provides electrical service through the synergistic interactions among its components (the power plant, substations, transformers, and transmission and distribution lines). Commonly in water management studies, an infrastructure must be impacted by flood to be considered as a critical infrastructure

Through direct connectivity, policies and procedures, or geospatial proximity, most critical infrastructure systems interact. These interactions often create complex relationships, dependencies, and interdependencies that cross infrastructure boundaries. The modeling and analysis of interdependencies between critical infrastructure elements is a relatively new and very important field of study. There is an urgent need for appropriate and credible solutions to address such interdependent systems in the areas of vulnerability and risk assessment, as a substantial, and indeed critical, component of the contemporary policy making. We know relatively little about the causes of infrastructural breakdown. It is commonly agreed that complexity and tight coupling allow relatively small disturbances to rapidly escalate into major, compound crises. So there is a need to produce failure scenarios of interdependent critical infrastructures in order to understand their failure modes.

For instance, the utility of traffic control in a municipality is provided by a system of three critical infrastructures: power grid, telecommunication network, and traffic control boxes. However, the proper functioning of the three CI system components is only a necessary condition for the normal operation of the traffic control system. That is why in water management, an infrastructure must be impacted by flood event within be impacted by

the flood hazard (see figure 1). Flood management policies have to take into account these interdependencies and not just focus only on flood hazard areas.

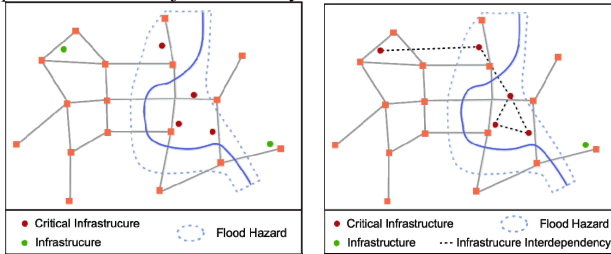


Figure 1. Left: a simple modeling of critical infrastructure in flood risk management: Right: a complex modeling of critical infrastructures integrating infrastructure interdependency.

CONCLUSION

Networks affect the well-being of the people and the smooth functioning of services and, more generally, of economic activities within urban areas. For instance, over 19 billion tons of freight valued at \$13 trillion dollars was moved through the U.S. multimodal transportation system during 2002. In fact, the economy of a nation or regions depends heavily upon an efficient and reliable transportation system to provide accessibility and promote the safe and efficient movement of people and good. The transportation system has been identified as the most important lifeline in the event of natural disasters such as flood. Yet, this is not so evident, because all networks are interconnected and it is difficult to identify the one that is most important or vulnerable. This is equally true for other networked systems such as electricity, water and telecommunication supply. For instance, the August 2003 electrical blackout in North America, began with the loss of a single electricity generation plant in Cleveland, Ohio, followed by a cascading failure of interconnected electrical systems, eventually generating a blackout encompassing eight U.S. states, two Canadian provinces, and nearly 50 million people. In fact, the most important factor in a networked system disturbance is the potential domino effects on the other systems.

Evaluating network infrastructures for potential vulnerabilities is an important component of strategic planning, particularly in the context of managing and mitigating service disruptions. Yet, multiple networks that serve the city are particularly sensitive to flooding, through their structures and geographic constraints. Because social functions are highly dependent on networked systems and the operability of these systems can be vulnerable to disasters, there is a need to understand how networked systems can be made resilient.

At least, these methods and tools for critical infrastructure definition and location, coupled with specific methods to assess vulnerability of particular infrastructure buildings could produce a powerful decision aid in term of flood mitigation prioritization actions.

REFERENCES

- ASCE, 2009, Guiding Principles for the Nation's Critical Infrastructure, p. 42
 Ashley, R., Blanksby, J., Chapman, J., Zhou J. J., 2007, "Towards Integrated Approaches to Reduced Flood Risk in Urban Areas". In: Ashley, R., Garvin, S., Pasche, E.,

- Vassilopoulos, A., Zevenbergen, C. *Advances in Urban Flood Management*, pp. 415-432.
- Aven, T. (2008): *Risk Analyses - Assessing Uncertainties Beyond Expected Values and Probabilities*. Wiley, ISBN 978-0-470-52736-9.
- Beaujeu-Garnier J., 1997, *Géographie urbaine*, cinquième édition, édition Armand Collin.
- European Environment Agency, 2008, *Impacts of Europe's changing climate - 2008 indicator-based assessment*.
- Gissing, A. Blong, R. (2004) *Accounting for Variability in Commercial Flood Damage Estimation*, *Australian Geographer*, vol. 35, no. 2, 209-222.
- Kappos, A.J.; Stylianidis, K.C., Ptilakis, K. (1998) *Development of Seismic Risk Scenarios Based on a Hybrid Method of Vulnerability Assessment*, *Natural Hazards* 17: 177–192, 1998. Kluwer Academic Publishers. Printed in the Netherlands.
- Lhomme S., Serre D., Diab Y., Laganier R. 2011, *A methodology to produce interdependent networks disturbance scenarios*, 10 p. *International Conference on Vulnerability and Risk Analysis and Management*, American Society of Civil Engineers, University of Maryland, Hyattsville, MD, USA.
- Nadal, N., Zapata, R., Pagán, I., López, R and Agudelo, J. (2010) *Building Damage due to Riverine and Coastal Floods*, *Journal of Water Resources, Planning and Management* 136.3 327-336.
- Nie, L.M., Lindholm, O. and Braskerud B.C., 2009, *Urban flood management in a changing climate*. *J. of Water by Norwegian Water Association*, Vol. 2, pp. 203-213.
- Norwegian Ministry of Environment, <http://www.regjeringen.no/en/dep/md.html?id=668>
- Pumain D., 1982, *La dynamique des villes*, Editions Economica.
- Pumain D., Sanders L., Saint-Julien T., 1995, *Villes et auto-organisation*, Economica, 191 p.
- Sanders L., 1992 , « *Système de Villes et synergie* », col. *Villes Ed. Anthropos-Economica*, 274 p.
- Scawthorn, C., et al. (2006) *HAZUS-MH Flood Loss Estimation Methodology. II. Damage and Loss Assessment*, *Natural Hazard Review*, vol. 7, no. 2.
- Schwarz, J., Maiwald, H. (2008) *Damage and loss prediction model based on the vulnerability of building types*, 4th International Symposium on Flood Defence: *Managing Flood Risk, Reliability and Vulnerability*, Toronto, Ontario, Canada.
- Smith, D.I. (1994) *Flood damage estimation – A review of urban stage-damage curves and loss functions*, *Water SA* vol. 20, no. 3.
- Soetanto, R. Proverbs, D.G. (2004) *Impact of flood characteristics on damage caused to UK domestic properties: the perceptions of building surveyors*, *Structural Survey* vol. 22, no. 2, 95-104.
- State Government of Victoria (2000) *Rapid appraisal method (RAM) for floodplain management*. State of Victoria: National Resources and Environment
- Utne, B., Hokstad, P., Kjølle, G., Vatn, J., Tøndel, I.A., Bertelsen, D., Fridheim, H., Røstum, J. (2008) *Risk and Vulnerability Analysis of Critical Infrastructures - The DECRIIS Approach*, SAMRISK conference Sept. 1-2, 2008 in Oslo, <http://www.sintef.no/Projectweb/SAMRISK/DECRIIS/Documents/>
- Vatn, Jørn (2007): *DECRIIS –Description of InfraRisk*, *Arbejtsnotat* 3, 35 pages., Norwegian University of Science and Technology

AKNOWLEDGEMENT

Co-authors would like to thank the EU for funding this research led in the framework of the FloodProBE project (www.floodprobe.eu).

Quantifying System Vulnerability as a Performance Measure for Systems Investment Evaluation and Decision-making

S. Labi¹, Q. Bai¹, I. Kumar¹, A. Ahmed¹, P. Anastasopoulos¹.

¹School of Civil Engineering, Purdue University, 550 Stadium Mall Drive, W. Lafayette, IN 47907

PH (765)494-2204, email: labi@purdue.edu, bai@purdue.edu; ikumar@purdue.edu, anwaar@purdue.edu; panast@purdue.edu.

ABSTRACT

Civil engineering systems are vulnerable to natural and man-made threats. In recent years, agencies are paying increased attention to investments that are geared towards reducing system vulnerability. For purposes of analyzing the effectiveness of such investments and also for vulnerability monitoring, a procedure is needed to quantify the level of system vulnerability at any time. This paper identifies vulnerability types and presents a general procedure for establishing system vulnerability. The procedure quantitatively assesses the threat likelihood and consequence. Threat likelihood is expressed as a function of the system environment (threat type); and consequence, is expressed as a function of the system attributes. Specifically, the consequence of failure due to the threat is evaluated on the basis of possible failure modes and the extent of public exposure in the event of failure. Public exposure, a function of the occupancy (or traffic) and the class of the system, reflects the effect of system failure on users and the surrounding community.

INTRODUCTION

Civil engineering systems are vulnerable to natural and man-made threats that arise from the environment in which they are located. Natural threats include floods, landslides, earthquakes, and hurricanes; man-made threats include overloading due to excessive traffic or occupancy, and accidental or malicious collisions between man-made objects (such as land, sea, or airborne vehicles) and the civil structure. In recent years, agencies are paying increased attention to continuous monitoring of imminent threats and also to evaluation and implementation of investments that reduce system vulnerability. Highly-publicized disaster events such as the 1994 Northridge Earthquake, the 2005 Hurricanes Katrina and Rita, and the 2007 I-35W Mississippi River bridge collapse, underscored the vital importance of monitoring the vulnerability to civil engineering systems to external or internal threats and to assess the effectiveness of actions intended to reduce their vulnerability to such disaster events. The looming specter of global warming (IPCC, 1994) and the subsequent change in sea and groundwater levels, wind speeds, and other environmental changes are expected to cause potentially widespread and deleterious impact on civil structures (ASCE, 2007;

Lenkei, 2007) and thus constitute a serious natural threat that engineers will need to contend with. At the current time, however, there are few or no consistent and objective methodologies that civil engineers can use to assess, and hence constantly monitor, the vulnerability of their systems to natural and man-made threats. Thus, agencies continue to seek methodologies irrespective of civil system type and the nature of the threat, to quantify the vulnerability and to analyze the effectiveness of investments that directly or indirectly address vulnerability.

This paper presents a vulnerability rating procedure synthesized from various procedures from the literature and based on the likelihood and consequence of a threat. The threat likelihood, assessed on the basis of threat type, and is a function of the system environment and not of the system itself. The threat consequence, or impact of failure, is based on the possible failure scope and the extent to which the facility is exposed to the threat – both of these are specific to the facility in question and not to the threat type. The exposure to the threat is a measure of the effect that a failure of the facility will have on its users – this is related to the occupancy of traffic volume of the facility and the importance of the facility in the area socio-economic development or national defense.

REVIEW OF EXISTING LITERATURE

The essential elements of risk assessment (Ezell et al. 2000) are consistent with systems vulnerability analysis: what could go wrong, what is the likelihood that it will go wrong, and what are the consequences? With regard to what could go wrong, a number of studies have identified or quantified the types of threats to civil systems. These threats, which are related to environmental factors or to system characteristics (Hawk, 2003), include hydraulic factors, overload, steel or concrete structural details, collision, and earthquake, condition-related reduction in load capacity (Shirole and Loftus, 1992; Kuprenas et al., 1998; Stein et al., 1999); Small, 1999; Monti and Nistico (2002). Some of these studies developed methods to assess civil structure vulnerability and to select those in need of improvement to guard against imminent threats. Vulnerability assessments have also been carried out in other disciplines besides civil engineering, and offer valuable lessons. Luers et al. (2003) developed a framework to assess the vulnerability of agricultural systems in Mexico's Yaqui Valley. Phillips and Swiler (1998) presented a flexible graph-based approach to security network vulnerability analysis, and used probability theory and various graph algorithms to identify attack paths that have maximum probability of success. Eakin and Luers (2006) investigated the vulnerability of social-environmental systems, and Moy et al. (1986) investigated the reliability in water supply reservoir operation by exploring system vulnerability and system resilience. Ezell (2007) presented a model for quantifying the vulnerability of critical infrastructure, using vulnerability density functions derived from value functions and weights.

DESCRIPTION OF THREAT TYPES

Flooding. Throughout the course of history, increases in the levels of rivers, lakes, and oceans have threatened the stability or functionality of civil structures and facilities

located near these features. These facilities include not only riverports, harbors and seaports, but also highways and hydraulic structures such as levees, weirs, and dams. The rise in water levels may be a cyclical or random event (during tsunamis caused by offshore-epicentered earthquakes, cyclones, and hurricanes) or part of a long-term global warming trend that is causing the polar ice caps to melt and thus increase in sea water levels. The Intergovernmental Panel on Climate Change (IPCC, 2007) reported that since 1961, global average sea level had risen at an average rate of 1.3-2.3 mm/yr; between 1993 and 2003, the rate increased above the previous period to 2.4-3.8 mm/yr.

Erosion, Scour, and Sedimentation. The foundations of civil engineering structures situated near water bodies or at areas of strong wind are vulnerable to erosive forces of water and wind. Also affected are hydraulic and other civil structures downstream where sedimentation of eroded material impairs hydraulic and other functional efficiencies. Features of the environment that increase such vulnerability include the type and nature of the water body (river, lake, or sea) and the erodibility of the residual soils. In the case of rivers, important factors include water volume, velocity, river slope, the shape and nature of the river bed. Also, engineers can obtain clues of erosion and sedimentation vulnerability by measuring the proximity to river confluence, whether the system is affected by backwater, historic scour depth, historic maximum flood depth, and the availability of overflow/relief hydraulic structures. In the case of scour vulnerability, the frequency of floating debris and ice are factors, and the vulnerability of foundations of bridges, culverts, and other hydraulic civil structures can be measured on the basis of the existence of scour countermeasures such as, whether the abutment is located at a river bend, angle of inclination, and embankment encroachment. For piers, vulnerability to scour is influenced by the skew-angle, pier/pile bottom below streambed, and pier width, among other considerations. The elements of erosion and scour vulnerability were established by Shirolé and Holt (1991) and Shirolé and Loftus (1992) for bridge structures but could be easily adapted for other civil structures founded near water bodies. In the current era of incipient climate change, it is expected that increased tropical storm frequencies and strengths will cause increased erosion of soil around civil structures and deposition of the eroded material at other civil structures downstream. These and other similar considerations could be used to derive a measure that describes the existing threat from erosion and scour.

Landslides. Landslides, geological phenomena that include rock falls, slope failure, and shallow debris flows, occurs due to gravity but is triggered or facilitated by a number of contributing factors such as slope stability. Landslides can impair the structural integrity or operational functions of civil engineering structures, and have jeopardized safety at highways and bridges at mountainous areas. General long-term changes in general climatic conditions worldwide are expected to translate into increased geotechnical activity such as rockfalls and landslides in mountainous areas, particularly due to increased rates of groundwater seepage through rock joints and increased groundwater pressure (Beniston, 2004). Also, the trigger mechanisms for landslides are associated with pressure-release joints following glaciations. In assessing the vulnerability of civil systems to landslides, it is needed to address slope instabilities.

Fatigue Failure of Concrete Structures. Concrete, a primary material type used for civil structures, is prone to a variety of failure modes. The most surreptitious of these is fatigue, a progressive and localized structural damage that occurs when a material is subjected to repeated loading and unloading, until the structural element fails with little or no warning. NYSDOT (1997) provided a methodology for assessing the fatigue failure of concrete and steel bridges. With some modification, this could be extended to other types of civil structures. For bridges, this procedure consists of evaluating the superstructure, the substructure and a general assessment of the entire structure. Superstructure assessment considerations include skew, curvature, redundancy, flagging history, deterioration of beams, reinforcement corrosion, concrete deterioration, unreinforced concrete members, deflection conditions, prestressed concrete members, and post-tensioned concrete members. Substructure assessment includes elements such as deterioration of components, stress related cracking at joints, stress related condition of pier capbeams cracking due to differential settlement, punching shear condition, hammerhead pier, solid pier, concrete rigid frame, pier bents with concrete piles, concrete pier caps. General assessment includes bridge location, year of construction, wearing surface condition ratings, debris accumulation on concrete.

Fatigue Failure of Steel Structures. Like concrete structures, steel structural elements are prone to sudden failure due to material fatigue. The procedure to assess the steel-detail vulnerability class consists of evaluating the superstructure and the substructure (NYSDOT, 1999). The vulnerability of steel structural components is assessed on the basis of three elements: (i) primary member (redundancy, fatigue resistance, occupancy level and fatigue design, material toughness, distortion-induced cracking, truss, (ii) external connections (that is whether the connection type is bearing, framed, or suspended or hinged support), (iii) accumulated damage (ever flagged, reason flagged, painted steel, deterioration factors, condition rating factors).

Seismic Events. Earthquakes can be caused by rupture of geological faults, volcanic activity, or nuclear tests. Of the several hundreds of thousands of earthquakes that occur worldwide each year, 15-25% can be felt and a fraction of these are severe enough to pose a threat to civil infrastructure. The failure of civil structures during seismic events is due to: ground movements; local amplification of movement due to transfer of seismic energy from deep harder soils to superficial softer soils; and rupture which is a visible break and displacement of the Earth's surface along the fault line. The vulnerability of a structure to earthquake damage or failure can be assessed as the product of the structural vulnerability and seismic hazard rating for the location of the structure (NYSDOT, 2002). The structural vulnerability is based on (i) the vulnerability of connections, bearings and seat widths (which is influenced by the bearing types, support lengths, support skew), (ii) the pier vulnerability (which considers the pier design, and shear failure), and flexural failure), (iii) abutment vulnerability, and (iv) liquefaction vulnerability. The seismic hazard rating is a function of design seismic acceleration coefficient and also soil profile type to allow for soil amplification effects.

Collision. Civil engineering structures are always prone to accidental damage from its users or nearby activity. Such vulnerability is influenced by the type of occupancy (traffic), nature of occupancy (example, for traffic, number of large trucks and their average speeds), height of the structure, location (for example, in a navigation channel), etc. For bridge structures, the NYSDOT (1996b) developed a collision vulnerability rating that is based on superstructure vulnerability to truck under bridge collision, pier vulnerability to truck under bridge collision, superstructure vulnerability to water vessel collision, pier vulnerability to water vessel collision, superstructure vulnerability to train under bridge collision, and pier vulnerability to train under bridge collision.

Man-made Threats. The vulnerability of a civil engineering system to malicious man-made threats could be assessed on the basis of a number of criteria including: commerce (average and maximum daily truck traffic), detour length, contribution of the facility to overall system operations (such as overall network connectivity or accessibility), navigational access, international access (whether the facility borders on a neighboring country), and designation of the facility in military operations or movement. Rummel et al. (2002) developed a similar set of criteria to develop a criticality index for assessing the vulnerability of bridge structures specifically to man-made threats.

Other Threats. Other threats to civil systems include high wind speed, wind impulses, and variations in wind profile (Lenkei, 2007): these can render tall buildings vulnerable to unsafe occupancy. Occupancy overload can be considered a man-made threat. The overload vulnerability of a civil structure can be measured on the basis of load expectancy (the likelihood that a load heavy enough to cause a failure will ever use the facility), structural capacity, resistance (capacity of a structure to resist applied loads), and condition (the effect of structural deterioration based on condition ratings) (NYSDOT 1996c). Also, the stability of the foundations of existing structures can be threatened by cyclical variations or long-term increases in subsoil pore water pressures due to rises in sea level or local groundwater level. For example, at certain locations and circumstances, the water table could rise due to deglaciation resulting from water accumulation behind unstable moraines of isolated blocks of ice that broke off from the leading edges of retreating glaciers (Beniston, 2004).

A GENERALIZED PROCEDURE TO QUANTIFY SYSTEM VULNERABILITY

Figure 1, synthesized from vulnerability procedures of NYSDOT and other literature, presents a general procedure followed for various types of vulnerability assessments like erosion, scour, fatigue/fracture, earthquake, and collision. The procedure to assign a vulnerability class is specific to threat type (these are discussed in subsequent sections).

Step 1. Computation of Vulnerability Likelihood Level. For a given facility, the vulnerability likelihood level is generally independent of the system (facility) type and rather depends on the environment: the greater the threat from the environment,

generally, the higher the likelihood level. Thus, generally, the vulnerability likelihood level, L , can be expressed as a function of the vulnerability, E , as follows:

$$L = f_L(E) \dots\dots\dots (1)$$

$f_L(E)$ could be obtained using direct assignment of scores by experts (as done by the New York State DOT in its vulnerability manuals) or utility functions. A more objective measurement of $f_L(E)$ could be the use of geographical maps that indicate the variation of the threat level at each location.

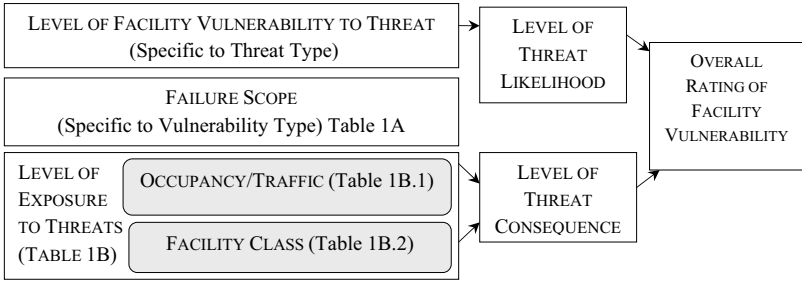


FIGURE 1 Procedure for Rating the Vulnerability of Civil Systems

Step 2. Computation of Vulnerability Consequence Level. Unlike the vulnerability likelihood, the vulnerability consequence is specific to the civil engineering facility and not the threat. The vulnerability consequence is a function of the exposure of the facility to the threat and the domain of possible failure scopes of the facility, as presented in the lower left part of Figure 1, elucidated in Table, 1, and explained below.

(a) Exposure Level

For a facility, the vulnerability exposure level, EL , is defined as a function of the occupancy (or traffic volume), O , and facility class (or importance level), FC , follows:

$$EL = f_{EL}(O, FC) \dots\dots\dots (2)$$

O and FC can be determined from $f_O(\gamma_i)$ and $f_{FC}(\pi_i)$, respectively. Examples include:

$$EL = \Phi_1 O^\alpha + \Phi_2 FC^\beta \dots\dots\dots (3)$$

$$EL = \chi_1 O^\alpha * \chi_2 FC^\beta \dots\dots\dots (4)$$

The New York State DOT, in its vulnerability rating procedure (NYSDOT, 2002-2006) used the simple weighted linear additive form by setting $\Phi_1 = \Phi_2 = 1$, and $\alpha = \beta = 1$, as follows: Vulnerability Exposure Level = Occupancy Score + Facility Class Score.

(b) Consequence Level

For any given facility, the vulnerability consequence level, C , is defined as a function of the exposure level and failure scope as follows:

$$C = f_C(EL, FS) \dots\dots\dots (5)$$

The failure scope, FS, can be determined from $f_{FS}(\delta_i)$. Examples of Eqn (5) include:

$$C = \Omega_1 EL^\omega + \Omega_2 FS^\nu \dots\dots\dots (6)$$

$$C = \Psi_1 EL^\omega * \Psi_2 FS^\nu \dots\dots\dots (7)$$

For example, in the New York State DOT, the vulnerability rating procedure (NYSDOT, 2002-2006) uses a simple weighted linear additive form by setting $\Omega_1 = \Psi_2 = 1$, and $\omega = \nu = 1$. Thus, in that state's procedure, Vulnerability Consequence = exposure level + failure scope.

TABLE 1 Facility-Specific Vulnerability Parameters

FAILURE SCOPE		
A. Failure Scope (Possible Failure Severity)	Failure Scope, FS	Failure Type Level
	Level 1, Very severe damage (δ_1)	$f_{FS}(\delta_1)$
	Level 2, Severe damage (δ_2)	$f_{FS}(\delta_2)$
	...	
	Level N_{FT} , Very little or no damage ($\delta_{N,FS}$)	$f_{FS}(\delta_{N,FS})$
LEVEL OF EXPOSURE		
B.1 Occupancy or Traffic	Occupancy, O	Occupancy Level
	Level 1, Very high occupancy, (γ_1)	$f_{EL}(\gamma_1)$
	Level 2, High occupancy, (γ_2)	$f_{EL}(\gamma_2)$
	...	
	Level N_{OT} , Very low or no occupancy ($\gamma_{N,O}$)	$f_{EL}(\gamma_{N,O})$
B.2 Facility Class (Level of Importance)	Facility Class, FC	Class Level
	Level 1, Very high class (π_1)	$f_{FC}(\pi_1)$
	Level 2, High Class (π_2)	$f_{FC}(\pi_2)$
	...	
	Level N_C , Very low class ($\pi_{N,FC}$)	$f_{FC}(\pi_{N,FC})$

Adapted from (NYSDOT, 1992-1997)

Step 3. Computation of Overall Vulnerability Rating of the Facility. For each vulnerability type, a vulnerability rating level, VR , is defined as a function of the likelihood level (L) and consequence level (C) as follows:

$$VR = f_{VR}(L, C) \dots\dots\dots (8)$$

Examples of this function could include:

$$VR = \Lambda_1 L^\eta + \Lambda_2 C^\tau \dots\dots\dots (9)$$

$$VR = \Theta_1 L^\eta * \Theta_2 C^\tau \dots\dots\dots (10)$$

The New York State DOT, in its vulnerability rating procedure (NYSDOT, 2002-2006) used the simple weighted linear additive form by setting $\Lambda_1 = \Theta_2 = 1$, and $\eta = \tau = 1$; Vulnerability Rating = Likelihood Score + Consequence Score.

In general, vulnerability rating can be calculated using the appropriate functional form for Eqn (8), scaled on a 0-100 scale, and then interpreted in Step 4.

Step 4. Interpretation of the Overall Vulnerability Rating. Figure 2 and Table 2 provide a possible interpretation of the overall vulnerability rating calculated using the above procedure. In Figure 2, the boundaries between the vulnerability descriptions are

based on expert judgments. The authors of this paper are currently carrying out research to determine the appropriate boundaries in a more objective manner.

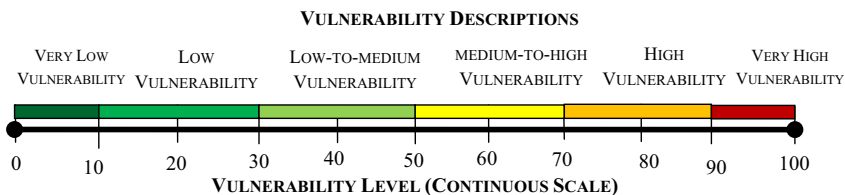


FIGURE 2 Scale for Vulnerability Interpretation

TABLE 2: Interpretation of 0-100 Vulnerability Rating

Vulnerability Rating	Interpretation
0-9.9	Indicates little or no vulnerability.
10-29.9	Indicates low vulnerability. Often reflective of the vulnerability of a civil engineering system that is built to the current design standards.
30-49.9	Indicates low-to-medium vulnerability. Unexpected failure can be avoided during the remaining service life of the facility by performing standard scheduled inspections with due attention to factors that influence the system vulnerability.
50-69.9	Indicates medium-to-high vulnerability. Facilities within this range can be monitored at a frequency slightly exceeding standard frequency. The risk of failure can be tolerated until a normal capital project (that reduces vulnerability, among other benefits) is carried out.
70-89.9	Indicates high vulnerability of the system. The agency should be ready to undertake actions to reduce the vulnerability of the system.
90-100	Indicates very high vulnerability. Immediate action should be undertaken to reduce the vulnerability of the system.

Adapted from NYSDOT (1996-2002) and O'Connor (2000).

CONCLUSION

Civil engineers always face the challenge of protecting their systems from natural or man-made threats. This challenge has gained prominence in recent years and civil systems agencies are increasing the levels of investments to reduce system vulnerability or to enhance system resilience to disasters. Often, there is a need to ascertain the feasibility of such investments or to evaluate and compare alternative investment options, and thus a systematic procedure is needed to quantify the level of system vulnerability before and after investment actions. This paper identifies a number of threat types and presents a general procedure for establishing system vulnerability to these threats. The procedure assesses the threat likelihood and consequence quantitatively. The threat likelihood is a function of the system environment (threat type); and threat consequence is a function of the system attributes. The consequence of system failure due to the threat is described on the basis of possible failure modes and

the extent of public exposure to the event. The exposure, in turn, is a function of the system occupancy (or traffic) and the importance (class) of the system to the society; this reflects the effect of system failure on users and the surrounding community.

REFERENCES

- ASCE (2007). "Impact of Global Climate Change," *ASCE Policy Statement 360*, Energy, Environment, and Water Policy Committee of ASCE, Reston, VA.
- Beniston, M. (2004). *Climatic Change and its Impacts*, Springer.
- Eakin, H., Luers, A.L. (2006). "Assessing the Vulnerability of Social-Environmental Systems," *Annual Review of Environment and Resources* (31), 365-394.
- Ezell, B.C., Farr, J.V., Wiese, I. (2000). "Infrastructure Risk Analysis Model," *J. Infrastructure Systems*, ASCE (6)3, 114-117.
- Ezell, B.C. (2007). "Infrastructure Vulnerability Assessment Model," *Risk Analysis* 27(3), 571-583.
- Hawk, H. (2003). *NCHRP Report 483: Bridge Life-Cycle Cost Analysis*, Transportation Research Board, Washington, DC.
- IPCC (1994) *Climate Change*. Cambridge University Press, Cambridge.
- IPCC (2007). *Climate Change 2007: The Physical Science Basis. Contribution of Working Group I to the Fourth Assessment*, Report of the Intergovernmental Panel on Climate Change, Solomon, S. et al. (eds.). Cambridge University Press, Cambridge, U.K.
- Kuprenas, J. A., Madjidi, F., Vidaurrazaga, A, Lim, C. L. (1998). "Seismic Retrofit Program for Los Angeles Bridges," *J. Infrastructure Systems*, ASCE (4)4, 185-191.
- Lenkei, P. (2007). "Climate change and structural engineering," *Periodica Polytechnica*. 47-50.
- Luers, A.L., Lobell, D.B., Sklar, L.S., Addams, C.L., Matson, P.A. (2003). "A method for quantifying vulnerability, applied to the agricultural system of the Yaqui Valley, Mexico," *Global Environmental Change*, 13(4), 255-267.
- Moy, W.-S., Cohon, J.L., ReVelle, C.S. (1986). "A Programming Model for Analysis of the Reliability, Resilience, and Vulnerability of a Water Supply Reservoir," *Water Resources Research* 22(4), 489-498.
- NYSDOT (1996-2002). *Vulnerability Manuals*, Dept. of Transp., Albany, NY.
- Monti, G. and Nistico, N. (2002). "Simple Probability-based Assessment of Bridges under Scenario Earthquakes," *Journal of Bridge Engineering*, ASCE (7)2, 104-114.
- O'Connor, J. S. (2000). "Bridge Safety Assurance Measures Taken in New York State," *Transportation Research Record 1696*, 187-192.
- Phillips, C., Swiler, L.P., 1998. "A graph-based system for network-vulnerability Analysis," *Proceedings of the New Security Paradigms Workshop*, 22-25, September 1998.
- Rummel, T., Hyzak, M., Ralls, M. L. (2002). "Transportation Security Activities in Texas," *Procs., 19th International Bridge Conference*, Pittsburgh, PA.
- Shirole, A. M., Loftus, M. J. (1992). "Assessment of Bridge Vulnerability to Hydraulic Failures," *Transportation Research Record 1347*, 18-24.

- Shirole, A. (1995). "Seismic Vulnerability Evaluation of New York State Bridges," presented to ASCE Structures Congress, Boston, MA.
- Shirole, A., Holt, R.C. (1991). "Planning for a Comprehensive Bridge Safety Assurance Program," *Transportation Research Record 1290*, 39–50.
- Small, E. P. (1999). "Examination of Alternative Strategies for Integration of Seismic Risk Considerations in Bridge Management Systems," *8th International Bridge Management Conference*.
- Sivakumar, B., Minervino C, M., Edberg, W. (2003). "New Bridge Performance Measures for Prioritizing Bridges," *Procs., 9th International Bridge Management Conference*, Orlando, FL.
- Stein, S. M., Young, G. K., Trent, R. E. Pearson, D. R. (1999). "Prioritizing Scour Vulnerable Bridges Using Risk," *J. Infrastructure Systems*, ASCE (5)3, 95-101.

Resilience and Preparedness of Critical Infrastructures

S. A. Timashev

Science and Engng Center “Reliability and Safety of Large Systems and Machines”,
Ural Branch, Russian Academy of Sciences, Yekaterinburg, Russia, 620049,
PH/FAX (834) 374-16-82; e-mail: timashevs@cox.net

Abstract

Verbally, resilience may be defined as a multi-attribute measure that describes the ability of a system of interdependent CIs to withstand a disaster shock, and its ability to recover within an acceptable envelope of time and cost. As of now, there is no quantitative definition of resilience and strategic preparedness. In this paper an attempt is made to give a generalized quantitative definition of resilience and preparedness as functions of time, taking into account that most of the multiple parameters on which resilience/preparedness is dependent, are random variables or random functions. The overall flow chart for assessing the dynamic integral territorial risk as defined by the "from bottom up" approach is given. The paper describes a new concept in territorial risk analysis and management based on the entropy principle and the territorial life quality index (TLQI). The entropy principle is used to convolute the risk analysis problems, which may contain tens of thousands of variables, into a problem with only one variable - information entropy. The TLQI, which is composed by the regional GDP, regional life expectancy at birth, and the time that a statistically average person living in this region spends during his/her lifetime to provide for her/his well being, is used to account for the human factor in territorial risk analysis.

Introduction

The paper considers an important and complex interdisciplinary integration problem – providing, supporting and controlling (managing) safety of a critical infrastructure (CI) of a large municipal area or territory, embedded into the context and realities of modern society of risk [Crowther Timashev 2008]. In order to describe and analyze resilience and preparedness of CIs it is necessary to first introduce some definitions, and give some

basics of risk analysis as applied to CI, which usually span across a specific territory. Critical infrastructure is any large distributed multicomponent geotechnical man-machine system (which consists of many objects and groups of people, who operate these objects, which are located on the territory in consideration). The CI is designed for providing safety and well being of the population and sustainable development of the territory, and also for supporting effective operation of a PDO, or a whole industry. Risk can always be diminished, but it requires additional expenditures. A demand for zero risk can yield more harm than bring benefit. If the cost of downsizing of risk is larger than the obtained through it benefit, then decreasing risk siphons off resources from critical problems of health care, education, housing, pensions, and some other social services, which also improve the longevity and quality of life. Therefore, the central problem of CIs risk management becomes optimization of the distribution of the limited resources to improve the safety of systems.

The formulated above problem can be solved only through interdisciplinary approach, and by convoluting the plethora of the heterogeneous parameters, which define the operation of the CI, into few integral parameters, which should be simple to understand and use. Due to the fact that the initial statistical data is substantially non-homogeneous, the problem itself is poorly formalized. The main conceptual problem of assessing, monitoring, and managing resilience of interconnected CIs is defined by following three factors: 1) the dimension of the problem is huge (could be tens of thousands of interdependent parameters); 2) the problem is multi-disciplinary, and the parameters involved when solving the problem are from different sciences and branches of engineering, and currently are, as a rule, non-convolutable; 3) the ICI resilience, preparedness and sustainability cannot be adequately described without explicitly accounting for the Human Factor (HF). Hence, before attempting to solve the problem in consideration, two measures have to be introduced, namely: 1) a universal measure of safety/risk; 2) a universal parameter, which allows accounting for the human factor. Proceed to achieve these goals.

Entropy as a universal measure of risk/safety

Modern physics has a useful tool, namely, the entropy concept, for convolution of all significant parameters of a problem into one. Entropy is a universal physical/information parameter, which allows uniting various displays of the physical world into one single parameter, and ideally fits for solving the problem in consideration. The modern informational concept of entropy is flexible and permits accurate and precise interpretation in terms of that section of science where it is applied. It is increasingly widely used in modern science for description of structural disorganization; degree of destruction of connections between elements of a system, and generally, for description of the degree of degradation of any closed system, including territorial CIs [Wilson 1970], [Borge 2001], [King 2001]. In this paper the entropy principle is used [Timashev 2007 2008 2008a] to analyze the level of CI risk.

Life quality index (LQI) as a generalized criterion for territorial risk management

In order to account for the HF, in this paper the concept of "Willingness to Pay" will be used, as it allows seamlessly introducing into consideration the cost of life/limb, without performing the assessment of the cost itself. When analyzing risk it is necessary to answer three mutually dependent questions: 1) Is the considered CI safe enough? 2) What is the size of risk? 3) At what level of expenditures and efforts it is worthwhile to spend to save lives?

In this context it is expedient to turn to the territorial LQI [TLQI, introduced in (Timashev 2007)], which is the generalized form of the LQI. TLQI can serve as an instrument for assessing the expediency and effectiveness of managing risk as related to life, health and safety of the *population of a territory (part of a country), municipality, a system of interdependent CIs, or a potentially dangerous object*. TLQI is a *local* social indicator which reflects the life expectancy of a healthy statistically average person and the quality of her/his life, bettered by accumulated wealth. TLQI permits assessing how well this problem is being solved by offering a consistent structure of sieving off trivial risks. Several mathematical models of LQI are known. One of the most validated is the model proposed by (Nathwany et al 1997):

$$LQI = G^q E, \quad (1)$$

where G is the specific national GDP (\$/person/yr), $q = w/(1-w)$ is the ratio of the average number of work hours to the leisure hours in this country, E is the life expectancy in the country (depending on age). The model (1) is based on the following four social principles of risk and utility management: 1) *The responsibility principle*: decisions made in the interests of the society as related to its collective health and safety should be open, quantitative, defensible, consistent and applicable to all types of life hazards; 2) *The maximal net utility principle*: risks should be managed in a way which maximizes the societal utility; 3) *The compensation principle*: policy is considered socially useful if its beneficiaries receive such a benefit, that after extracting from it the compensation for the victims, they still have some amount of profit; 4) *Life measurement principle*: the measure of utility with respect to health and safety is the life expectancy of healthy and happy life.

Probabilistic definition of regional resilience and strategic preparedness

Resilience has been defined in the literature as an emergent property of systems. There are more than a hundred definitions of resilience, but most of them describe resilience verbally, or explain the term using multiple marginal notions. As of now there is no quantitative definition of the notion of resilience and strategic preparedness. Below these definitions are given (Timashev 2008a). Resilience is dependent on multiple parameters, most of which are random variables (RV) or random functions or random fields (RF). It

also is an explicit function of time. Therefore, resilience has to be also a time dependent RV or RF. Hence, it is possible to quantitatively define resilience (RSL) as follows:

$$RSL(t) = P(P(N_t < N_*(0); E < E_*; \Delta RDP \leq \Delta RDP_*; \Delta t_r < \Delta t_*; C \leq C_*, 0 < \tau < t) \quad (2)$$

Where $P(N_t < N_*(0))$ is the probability that the number of injuries/lethalities during mitigating the catastrophe will not exceed a specific number during the time t ; $P(E < E_*)$ is the probability that the volume of the environmental damage during mitigating the catastrophe will not exceed a specific value during the time t ; $P(\Delta RDP \leq \Delta RDP_*)$ is the probability that the decrease of the regional domestic product will not be larger that a specific value during the time t ; $P(\Delta t_r < \Delta t_*)$ is the probability that the acceptable recovery envelope time will not exceed a specific time; $P(C \leq C_*)$ is the probability that the cost of recovery of the region will not exceed the prescribed value. Now the *strategic preparedness* would be defined as a complex characteristic of a region, which resilience parameters [see formula (2)] are not less than some benchmark values. The overall flow chart for assessing the dynamic integral territorial risk for decision-based data integration for regional response and preparedness (Timashev 2008a) is given in Fig.1.

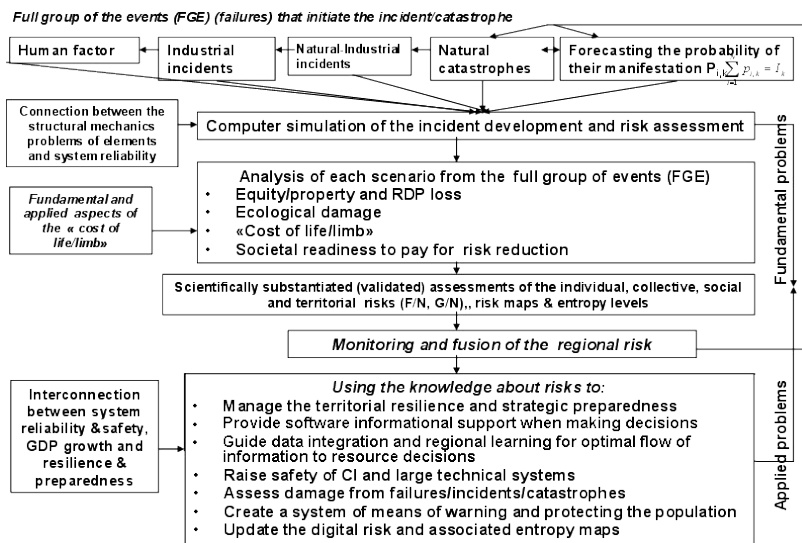


Figure 1. Flow Chart for assessing the dynamic integral territorial risk

Entropy of a pipeline which degradation is described as a Markov pure death process (MPDP)

In this paragraph an implementation of the entropy principle to risk and resilience assessment is given, using the MPDP model (Bushinskaya Timashev 2010) for describing the degradation of the system (in this case, a pipeline). Consider a cross section of a gas/oil pipeline with a defect. The failure pressure of this section at any fixed moment of time t is a random variable $P_f(t) \geq P_{op}$, where P_{op} is the operating pressure in the considered pipeline. The failure pressure $P_f(t)$ can be assessed using one of the internationally recognized codes: B31G, B31Gmod, DNV, Battelle, and Shell 92. The last interval, the smallest values of the failure pressures (the limit state), I_M , take equal to $(0; P_{op}]$. Divide the range of change of failure pressure for the pipe cross section $(P_{op}; P_f(0)]$ into $M-1$ unequal not overlapping intervals $I_i (i = M-1, \dots, 1)$. Here $P_f(0)$ is the failure pressure at time $t = 0$. The P_f (failure pressure FP) of the pipe cross section can only decrease in time, and pass at random moments of time from the i -th state only to the $(i+1)$ -th state, where state I is one of the intervals $I_i (i = 1, \dots, M)$. The solution of the differential equation (DE) which describes the transition of the FP from state to state has the form:

$$\begin{cases} P_1(t) = \exp\{-\rho(t)\} \\ P_i(t) = \frac{\rho^{i-1}(t)}{(i-1)(i-2)\dots 1} \cdot \exp\{-\rho(t)\}, i = 2, \dots, M-1 \\ P_M(t) = 1 - \left[\exp\{-\rho(t)\} + \sum_{i=2}^{M-1} \frac{\rho^{i-1}(t)}{(i-1)\dots 1} \cdot \exp\{-\rho(t)\} \right] \end{cases} \quad (3)$$

Where $P_i(t)$ is the probability that FP of the cross section with a defect is in the i -th state $I_i (i = M, \dots, 1)$ at time t , function $\rho(t)$ is connected with the FP and is defined by formula:

$$\rho(t) = \int_0^t \mu(\tau) d\tau = - \int_0^t \frac{P_f'(\tau)}{\Delta I} d\tau = \frac{P_f(t) - P_f(0)}{\Delta I} \quad (4)$$

Where ΔI is the interval width; $P_f(t)$ is the FP at time t , as given by one of the international codes. Obviously, at the initial time $t = 0$ the RV $P_f(0) \in I_1$, hence, the

initial conditions for the system of DE, which solution is defined by Eqns.(1), have the form:

$$P_1(0) = 1, P_i(0) = 0, (i = 2, \dots, M) \tag{5}$$

The entropy of the RV of FP for the pipeline cross section with defect for the moment of time t is calculated using formula:

$$H_d(t) = -\sum_{j=1}^M P_j(t) \ln [P_j(t)] \tag{6}$$

Where $P_j(t)$ is the probability that FP is in the j -th state I_j ($j = M, \dots, 1$) at moment of time t , as calculated using formulas (3).

If the defects are independent, their FPs will also be independent. Therefore according to the property of the entropy for independent RVs, the entropy of the FP for the whole pipeline system can be assessed using the formula:

$$H_p(t) = \sum_{i=1}^n H_{d_i}(t) = -\sum_{i=1}^n \sum_{j=1}^M P_{ij}(t) \ln [P_{ij}(t)] \tag{7}$$

Where n is the number of defects found in the pipeline; $P_{ij}(t)$ is the probability that the FP of the i -th pipe cross section is in the j -th state I_j ($j = M, \dots, 1$) at moment of time t , as calculated using formulas (3).

As the entropy is a measure of uncertainty, it is obvious that it is equal to zero, when one of the probabilities is equal unity (and others are zeroes), i.e., when the information is totally predictable and does not carry anything new. This is happening at the initial moment of time $t = 0$ (see initial conditions (6)), and when $P_M(t) = 1$ (100% probability that FP is in the last state – limit state).

The entropy is taking maximal value for the even distribution, when all probabilities $P_i(t)$ are equal, i.e., when the uncertainty is maximal. It is obvious, that after reaching the maximum the entropy starts decreasing down to zero value, i. e. till the moment when $P_M(t)=1$. The entropy maximum can be found by solving following equation with respect to t :

$$\frac{dH_d(t)}{dt} = -\sum_{i=1}^M \left[\frac{dP_i(t)}{dt} \ln [P_i(t)] + \frac{dP_i(t)}{dt} \right] = 0 \tag{8}$$

Functions $P_i(t)$ are continuous and differentiable for any moment of time t : $d(t) < wt$, w is the pipe wall thickness, $d(t)$ is the defect depth at time t .

Real life case. Consider now implementation of this procedure on a real life case. Assess the entropy of a segment of a specific pipeline using the limit state ‘‘rupture’’, with following parameters: OD=325 mm; web thickness $w=9$ mm; specific yield strength $SMYS = 245.0$ MPa; ultimate strength $UTS= 410$ MPa; design operating pressure $P_{op} = 6.4$ MPa. The pipeline segment has six dangerous defects (all 100 mm long) with following depths: #1 – 10% wt; #2 – 20% wt; #3 – 30% wt; #4 – 40% wt; #5 – 50% wt; #6 – 60% wt.

Assume that the defect depth growth a_d is 0.5 mm/yr, and defect length growth rate a_l is 5 mm/yr. In order to construct the FP degradation process for the pipeline cross sections which contain defects using the Markov pure death process MPDP and the B31Gmod code. Assuming a linear dependency of the defect size from time t , define for each defect the t_{lim} at which $d(t)=wt$: $t_{lim} = wt - d_0 / a_d$, where a_d is the rate of defect depth growth; d_0 is the initial defect depth at $t = 0$. Assess the entropy of FP as a RV for each cross section with defect. for the above mentioned five design codes and moments of time $t = 0, \dots, t_{lim} - 0.000001$. Results of calculations are shown in Figure 2.

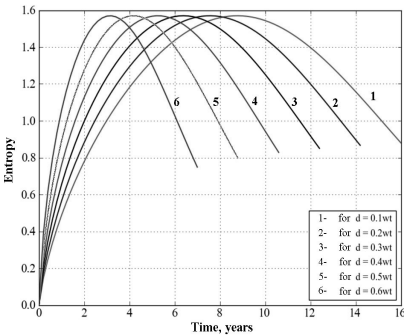


Figure 2. Entropy of six dangerous defects obtained using the B31Gmod code

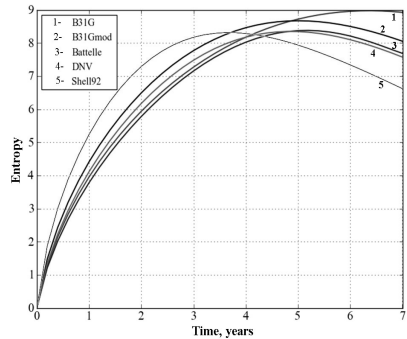


Figure 3. Entropy for the whole pipeline segment as a system of defects, obtained using five international codes

According Figure 2 the maximal value of the entropy for all defects is invariant with respect to the defect and the design code used, but the time needed for reaching the maximal value differs from code to code. According to assessments not shown in this paper due to lack of space, the extreme point for entropy can be used as a signal/symptom of reaching the limit state, because the time for reaching the limit state

is larger than for reaching the extreme point for entropy. The entropy for the whole pipeline assessed using formula (7) for all the five design codes is shown in Figure 3. According to the calculations, the maximum entropy of the whole pipeline segment is much larger than the entropy of the most dangerous defect (defect depth=0.6wt). This is an indication that using formula (7) for assessing the FP entropy for the whole pipeline segment in this case should be coupled with the maximal specific entropies which characterize limit states of each of the defects.

Conclusion

A novel approach was presented for assessing Critical Infrastructures resilience and preparedness in probabilistic terms based on using two universal parameters: the system entropy and the territorial life quality index TLQI.

References

1. Borge, D. (2001). *The Book of Risk*. John Wiley & Sons, Inc.
2. Bushinskaya A.V. Timashev, S.A. (2010) "Description of the Degradation Process for Defective Pipeline Systems by the Markovian Model of Pure Destruction." *Journal of Machinery Manufacture and Reliability*. Volume 39, Number 5, 504-510.
3. Crowther, K. G., Timashev, S.A. (2008). "Risk-Based Systems-Driven Evaluation of Emergency Resource Management for Regional Resilience and Strategic Preparedness." *II All Russia Science and Technology Conference ((Safety of critical infrastructures and territories)) /Abstracts of Papers*, Yekaterinburg, 260.
4. King, J. (2001). *Operational Risk: Measurement and Modeling*. Wiley, Chichester, UK.
5. Nathwany J. S, Lind N. C, Pandey M. D. (1997). "Affordable safety by choice: the life quality method," *Institute for Risk Research, University of Waterloo*, Waterloo.
6. Timashev, S. A. (2008). "Management of risk of interdependent systems of critical infrastructures and territories." *I Safety of Critical Infrastructures and Territories: II All Russia Conference. Abstracts of Papers*. Yekaterinburg, Ural Branch Russian Academy of Sciences, ISBN 5-7691-2016-9, 7-9, in Russian.
7. Timashev, S.A. (2008a). "Risk and Entropy Based Quantitative Definition and Solution of Regional Resilience and Strategic Preparedness." In: *Ibid*, 261-265.
8. Timashev, S. A. (2007). "Management of Territorial Critical Infrastructures using the Life Quality Index." *Safety of Critical Infrastructures and Territories: I All Russia Conference. Yekaterinburg, Ural Branch Russian Academy of Sciences* (in Russian).
9. Wilson, A.G. (1970). "Entropy in Urban and Regional Modeling." *Pion Limited*. London.

DEVELOPMENT OF SPATIAL RISK PROFILES RESULTING FROM SEA LEVEL RISE: WHAT PREDICTIONS OF FUTURE SEA LEVEL RISE MEAN FOR THE BUILT COAST

Michael S. Kearney¹ and Bilal M. Ayyub²

¹Professor, Department of Geography, University of Maryland College Park, MD 20742, USA; PH (301) 405-4057; email: kearney@m@umd.edu

²Professor and Director, Center for Technology and Systems Management, Department of Civil and Environmental Engineering, University of Maryland College Park, MD 20742, USA; PH (301) 405-4057; email: ba@umd.edu

Abstract : Predictions for changes in future sea level rise vary on spatial scales from global perspectives to a few miles of coastline and also from temporal scales of a few decades to almost a century. This wide array of forecasts is challenging enough; however, when confronted by the various ways the predictions are derived (linear extrapolations of individual tide gauges to global numerical models), attempts to navigate through to what is appropriate for risk assessment purposes can be confusing. We will present how concepts of spatial and temporal variability in sea level forecasts, data detrending and assimilation, and other aspects can be understood within the framework of vulnerability and risk. We also discuss how tide gauges can provide a baseline trend for forecasting future sea level change, and how these data can provide insights into intra-annual to decadal oscillations that often are of greater magnitude than the global trends predicted.

Key words : Sea level rise, tide gauge records, Sea level forecasting, IPCC, Satellite altimetry, El Niño, North Atlantic Oscillation

BACKGROUND

The impacts of Anthropogenic Greenhouse Warming (AGW) span phenomena that will have affects from global through continental scales down to regional scales. In many instances, the changes forecast for “regional” scales (e.g., the U.S. middle Atlantic Coast), the finest spatial scales allowable by the global circulation models, appear to be at odds with what might be expected from a warming world. Future trends predicted for regional precipitation are a case in point. Some regions may actually become wetter than present, though generally areas that are now arid can be expected to become even drier. All this reflects the complex nature of seasonal and inter-annual changes in continental pressure systems and winds, where yearly shifts in position or intensity can produce wetter or drier years relative to the normal thirty-year average. Accounting for such variability in climate models is a major challenge, and it should not be surprising that predictions still are unable to provide definitive numbers.

Sea level rise, in comparison, will touch every coast and, thus, is the one truly universal impact of global warming. Unless tectonics at a regional scale or human activities at a very local scale determine otherwise, sea levels everywhere will be higher at the century’s end than now. From this standpoint, the assessment of risk would appear to be simpler: every coastal area will be at risk. But the level of risk is another matter. A survey of the literature since 1983, the year James Hansen and colleagues at the Goddard Institute of Space Sciences (GISS) published their seminal paper on the global sea level record of the 20th century,

demonstrates that only within the last decade or so has there been a consensus about the global rate of sea level rise during the latter half of the last century (See Douglas, 2001). The reasons for such a late emergence of this relative agreement some twenty years after Hansen et al.'s paper are tied to an appreciation – hard won after much research – of the problems embedded in tide gauge records. These records are the basis most of what we know about sea level rise over the last 100 years or so, and are anything but perfect recorders of sea level change. Only since the advent of satellite altimeters like Topex-Poseidon in the early 1990s, revealing the actual complexity of the surface of the oceans, has it become evident how peculiar the distribution of long tide gauge records really is with respect to deducing information on global sea level. And not least in the growing sophistication in determining past sea level changes, has been the recognition that sea level is likely characterized by decadal oscillations, possibly misleading the researcher into conclusions about possible future accelerations or decelerations if the records consulted are too short.

As with any prediction of future events, the predictions for sea level rise show a widening envelope of possibilities with time, while the likelihood (probability) of any particular scenario occurring becomes less. Few people pay much attention to predictions if they lack any real immediacy – i.e., if whatever will occur (even if disastrous) is far off in the future. Unfortunately, the prospect of a dramatic jump in the global sea level trend looms uncomfortably close, possibly only 30 years away according to the best models (IPCC 2007). This is very short time for which to begin for planning what to do, and it can be assumed that any plans made will have to incorporate an integral risk component for weighing the options. Extrapolations made from global models for sea level rise scaled at coast-wide levels, though expedient, nonetheless are not appropriate for adequate risk assessment as the actual change in sea levels and their impact tend to be very site specific. This is especially true when considering flood risks from coastal storms. This paper will describe how the issue of the sea level rise might be considered with respect to risk engineering in coastal infrastructure and development. It will highlight, in particular, new information on processes generally not accounted for in previous sea level rise/storm flood risk studies.

STERIC VERSUS MASS CHANGE IN FUTURE SEA LEVEL CHANGE

The first critical step in assessing the sea level risk is definition of the basic *raison d'être* underlying the need for evaluation – in this case, the question of future sea level rise. Most people in the environmental science and civil engineering community are familiar with the concept of AGW and its proposed major impacts including sea level rise. Many are also familiar with the predictions for sea level rise in the Fourth Assessment Report of the IPCC (IPCC 2007), which forecast a global rise of 41 to 66 cm by 2100 CE. Lastly, it is likely that the controversy surrounding the latest IPCC predictions – virtually identical to those of the Third Assessment – is well known, and the reasons for it (i.e., it underestimates substantially what might happen in massive polar melting occurs).

Over long time scales, in the range of 10^4 – 10^5 years, large changes in sea level occur principally by *mass* change, i.e., the addition of new water principally glacial sources. During the 20th Century, volume changes (*steric*, in this case, thermosteric expansion as opposed halosteric changes (due to salinity variations)) nonetheless appears to be the largest single factor, though it is exceeded collectively by mountain glacier melting and wasting of the Antarctic icesheets (mainly the West Antarctic Icesheet) (Church et al. 2001). Cazenave and Nerem (2004) caution that the causes of recent sea level change remain undecided, particularly with respect to the actual contributions of various components like polar melting. This absence of fundamental understanding of the drivers of global thermosteric sea level variation is a serious impediment to reliable forecasting of future sea level rise, and as such,

affects the risk assessments for coastal change and flooding.

One basic reason for the uncertainties surrounding the suite of factors affecting thermosteric sea level change is the gathering evidence of substantial spatial variation in the steric response. A series of papers over the last decade (e.g., Levitus et al. 2000a,b) document large steric fluctuations (“anomalies”) in world’s oceans since 1950. Depth profiles down to 500 m demonstrate that both warm and cold anomalies were not strictly surface phenomena – though there appears to be differences in depth range between the Atlantic and Pacific Oceans – and they have been related to the El Niño Southern Oscillation (ENSO) and Pacific Decadal Oscillation (PDO) using satellite altimetry data (Lombard et al. 2005). Quasi-decadal patterns have also shown up in an analysis of tide gauge data (Houston and Dean in press), although whether these particular trends are a response to the same large scale oceanic forcings (as those shown in the satellite altimetry analyses) is not certain.

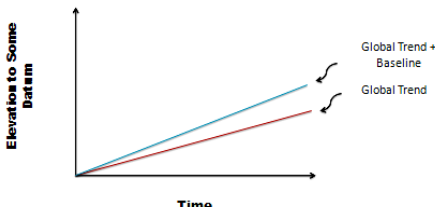


Fig. 1. Detrending to determine the baseline sea level rise for a region.

satellite altimeters (Topex-Poseidon and Jason) is robust enough to enable forecasting, Lombard et al. (2005) suggest that the patterns deduced may have not hold for the future, or even for hindcasting of past trends.

The uncertainties about sources of steric changes in sea level during latter 20th century and the possibility that variability in sea surface elevation shown in satellite altimetry since the early 1990s may be atypical (and not capable of extrapolation for predictions of future change) is not a solid foundation for risk assessment. Within the scope of this general quandary are: 1) recent findings (Miller and Douglas 2004) that sea level rise estimates based on tide gauges and regional averages based on thermosteric expansion vary considerably; and 2) the continuing question of whether considerable storage of heat in the middle layers of the oceans (500-1500 m) – particularly in the Atlantic Ocean – has translated into proportional thermosteric adjustments.

The welter of unknowns confronting expectations that some reasonable assessment of future sea level rise will be attained can be better understood if the evidence for sea level changes is examined. From such an examination, it may be possible to grasp where risk analysis might fit in.

TIDE GAUGES: THEIR ADVANTAGES FOR DETERMINING A LONG TERM BASELINE SEA LEVEL RISE AND RISK

It is not over stating the case to observe that our present understanding of sea level rise over the last 150 years derives principally from tide gauge records. The first real empirical study of where future sea level changes might be headed that gained worldwide attention was the analysis of gauge records by Hansen et al. (1983). Many studies have since superseded

Nonetheless, this variability in steric ocean basin response to factors of global reach like ENSO – whose dimensions are just being outlined – are linkages to late 20th Century sea level trends made by statistical analytical techniques like least squares and empirical orthogonal function analyses, not a numerical model connection. Moreover, though some researchers have asserted that the decade or so of ocean surface altimetry afforded by the

Morever, though some researchers have asserted that the decade or so of ocean surface altimetry afforded by the

Hansen et al.'s work, and have highlighted inherent errors and possible distortions in tide gauge data, but such records still remain the only way of delineating recent sea level history. They have certainly have limitations, however. For one, though tide gauges record regional and even global fluctuations in sea level, they are equally likely to record mainly changes at the site. There are have been many papers addressing this problem, particularly where in the case of Tokyo harbor post World War II construction dramatically changed harbor hydrography (Aubrey and Emery 1986). Douglas (2001) developed a method to "detrend" tide gauge records and account for regional and *in situ* factors relative to more global changes. Nevertheless, there still remains the inevitable problem of extracting information about large scale spatial changes in ocean elevations from point data, and the allied problem that the geographic distribution of reliable, long records tends to be concentrated in the north Atlantic Ocean (Europe and North America); whereas, large areas of the Pacific Ocean (especially the southern Pacific) have few records, and those often of insufficient length to extract long term trends. The northern European and North American records have particular problems in many instances with land surface movements associated with postglacial rebound (uplift in more northerly regions that were under ice or subsidence from forebulge collapse south of former ice margins). Poor spatial distribution is perhaps a major reason that tide gauge records indicate a higher rate of global sea level rise over the past forty years than what is shown in satellite altimetry (Cabanes et al. 2001).

Even as we now appreciate their liabilities, however, the limitations of tide gauges for reconstructing global changes in sea level do have a particular relevance to risk assessment for a coast since they record exactly what occurred. Understanding the general worldwide signal as derived from satellite altimetry is clearly important to global climate research, despite the limitation of short records, but tide gauges shed light on local and regional factors in sea level variations that can be used to derive a baseline forecast for future changes. This capability involves turning the "detrrending" of Douglas (2001) on its head to determine those factors, local and regional, that will occur at the same rate well into the future. Phenomena such as postglacial rebound, tectonism, or deltaic subsidence generally are the common very long range (temporal) factors that contribute to baseline sea level

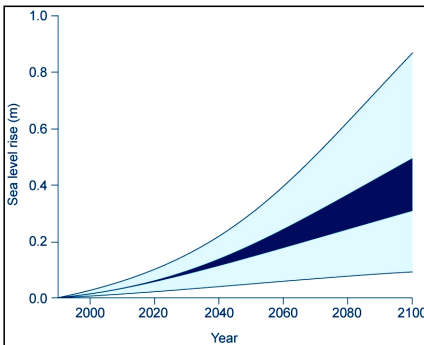


Fig. 2. Simplified figure of the Intergovernmental Panel on Climate Change (IPCC) model forecasts for sea level rise in the 21st Century (after IPCC 2007).

rise of coastal areas. For example, in the U.S. mid-Atlantic region, baseline sea level rise, largely from subsidence due from forebulge collapse, is near 2mm yr^{-1} (Kearney 1996), essentially the same as the rate determined for global sea level rise for the 20th century (Douglas 2001). Hence, regardless of the IPCC scenario considered, it is assured that sea levels will be at least 20 cm higher by 2100 AD in the U.S. middle Atlantic Coast (Fig.1). For the lower end of the IPCC predictions (41 – 50 cm), as much half the risk of whatever trend may occur is already known (Fig. 2).

For the Louisiana coast, tide gauges show not only long term rates of deltaic subsidence (which comprise up to 80% of the relative sea level trend), but also locally effects of shallow

subsidence down to several hundred meters from groundwater pumping and peat collapse (Davis 1985). In fact, without tide gauges it would be difficult to quantify readily the effects of land sinking from anthropogenic fluid on local rates of submergence. Areas of Tidewater Virginia are a case in point. Geodetic surveys (Holdahl and Morrison 1974) reveal that rates of deleaving (subsidence) from deep ground water pumping in this area are much higher than of Chesapeake Bay overall. However, tide gauge records show that the net result of these higher rates of subsidence are a relative sea level rate almost twice the mean trend for the Chesapeake Bay. In summary, while tide gauge records clearly have problems for reconstructing global sea level rise, they are indispensable for ascertaining sea level vulnerability and risk for a particular coast.

INTRA-ANNUAL TO DECADEAL OSCILLATIONS IN SEA LEVEL RISE AND WHAT THEY MEAN FOR VULNERABILITY

The advent of reliable satellite altimetry with the launch of the French-American satellite Topex-Poseidon in the early 1990s was in many respects a revelation for sea level researchers. Not only were global changes in the surface elevations of the world's oceans first portrayed with high accuracy, but also for the first time there was graphic evidence of spatial precision heretofore unobtainable for temporal variability in ocean surface elevations. For forecasting future vulnerability and risk from sea level rise, the elucidation that the magnitude of seasonal sea surface fluctuations often exceeded yearly global variations was a particularly valuable finding. Despite the short record of the Topex-Poseidon (and that of its successor, Jason) and the concern that this raises for whether observed phenomena are transient or more long term features, the documented amplitude of the changes in the altimetry data certainly demonstrate that storm flood risks associated with sea level rise can vary significantly for a low lying coast within a year. Hence, storm surge inundation models could underestimate the extent of coastal flooding if such seasonal fluctuations were not taken into account.

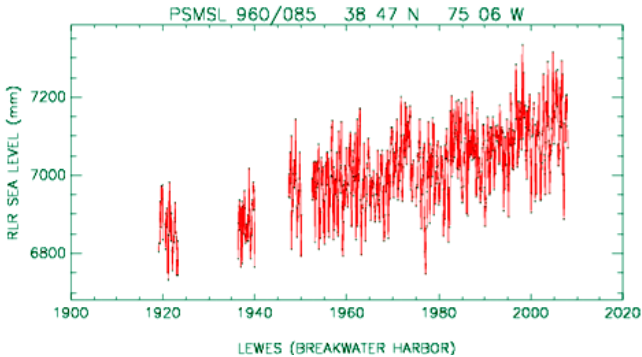


Fig. 3 Monthly sea level record for Lewes, Delaware. Data courtesy the Permanent Service for Mean Sea Level.

Typically, storm surge models for coastal flooding account for changes in the tidal cycle, using spring high tide as the worst case scenario for coastal inundation. Even for a microtidal coast (<2 m mean tidal range), monthly tidal variations could be critical towards predicting

ultimate flood levels. For example, much the U.S. middle Atlantic Coast, where mean tidal ranges are often less than 2 m, is characterized by very low coastal profile, with slopes of 1:2500 or lower. In this region, where just small changes in tidal height can result in widespread inundation, monthly tidal variations are fundamental to understanding coastal vulnerability. Consider the Lewes, Delaware tidal record (Fig. 3), where intra-annual monthly average sea levels can span a range of 0.2 m between the highest (reflecting summer heating) and lowest departures (reflecting winter cooling) from the mean – in exceptional years this range could exceed 0.4 m. Putting this in perspective, this degree of intra-annual tidal fluctuation approaches the low end scenarios for global sea level rise at the end of this century outlined in the IPCC 2007 Assessment Report (IPCC 2007). In fact, the highest annual sea levels in this record can exceed the mean global sea level trend by greater than 15 cm, with a more typical rise of 6 cm. This is close to the top of the envelope of scenarios that the IPCC forecasts for the rise world sea levels from 2010 to 2030. The highest positive departures, within this record and others in open ocean tide gauge records for the U.S. middle Atlantic Coast, appear to terminate periods of rapid sea level acceleration as discussed below.

The reasons for these sharp intra-annual departures in the sea level along the U.S. mid-Atlantic coast appear to be linked with findings from Topex-Poseidon for a distinct annual sea level anomaly with a amplitude of 10 cm in the summer heating phase (Knudsen et al. 1994).

El Niño Southern Oscillation: California Coast

The impact of the El Niño Southern Oscillation (ENSO) on the world's climate is well known. Perhaps less well known is the effect of ENSO events on sea levels. Due to uplift from plate boundary interactions, sea levels along much of southern California are rising slowly if not failing. Figure 4 shows a comparison between satellite data for monthly sea surface temperatures (SST) for the Pacific Ocean from 2° N to 2° S latitude compared to monthly tide gauge record for the pier at the Scripps Institute of Oceanography. Very high sea levels (≥ 20 cm) in the Scripps record for the period covered by the satellite data (c. late 1980s to 2002) can be seen to coincide with significant episodes of Pacific Ocean warming indicate by peaks in SSTs, which mark ENSO periods. The most striking short term sea level high stand in fact straddles the main phase of perhaps the strongest ENSO of the late 20th century. If not for ENSO events, the Scripps tide gauge record is otherwise unremarkable for the last decades of the previous century, arguably displaying a rather flat overall trend. Demonstrating that this particular data set is not anomalous is the tide gauge record for San Diego – though theoretically a less ideal resource for sea level change because of possible influences on the tidal frame from harbor construction (Fig. 5).

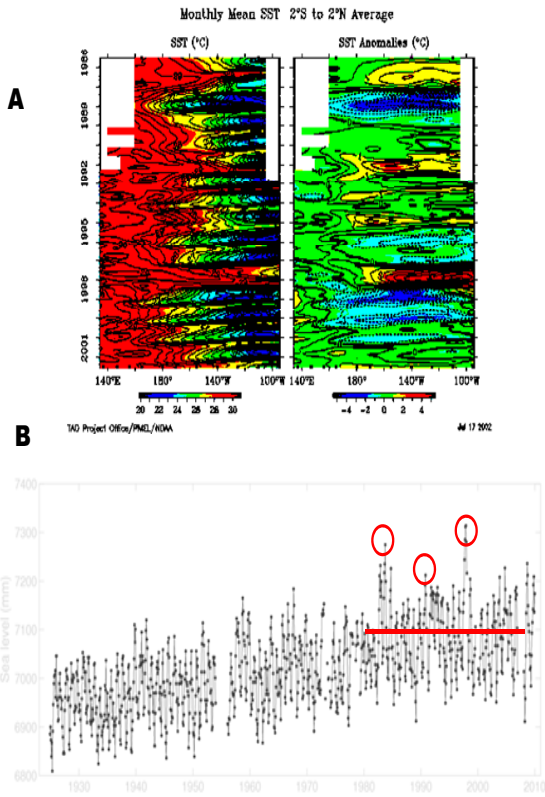


Fig. 4. Comparison of surface temperature changes and anomalies in the equatorial Pacific Ocean with the tide gauge record at the Scripps Institute of Oceanography. Sources: SST figure, TAD Project Office/PMEL/NOAA; figure for Scripps tide gauge record, Permanent Service for Mean Sea Level (PSMSL).

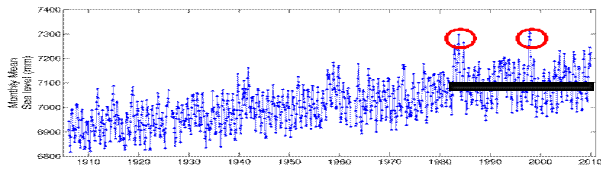


Fig. 5. Tide gauge record for San Diego, CA, showing 1992 and 1998 ENSO events (red circles and the apparent sea level trend since 1980 (thick black line). Source of figure PSMSL.

DECADAL OSCILLATIONS IN SEA LEVEL

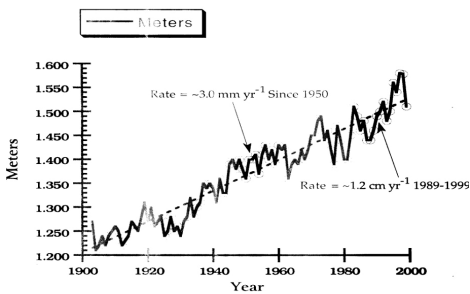


Fig. 6. Smoothed version of the Baltimore tide gauge record. From Kearney et al. (2002).

A pronounced feature of many tide gauges records of U.S. Atlantic coast is the increasing degree of inter-annual variability over the last forty years. Also evident are apparent quasi-decadal oscillations in sea level, with episodes of very high rates of rise lasting almost a decade. A smooth version (by use of a running mean) of the Baltimore tide gauge record, one of the older records for the U.S. middle Atlantic Coast, illustrates this phenomenon well (Fig. 6).

The climatic forcings behind these variations are not clear, but comparison with data for the North Atlantic Oscillation (NAO) reported in Alix et al. (2005) suggests some rough correspondence; however, considerable work needs to be undertaken to account for lagging effects and scale problems. Nevertheless, what is important for this discussion, are the duration and strength of the major sea level accelerations since 1960, the first beginning in the early 1960s and ending about 1976-1977, and the second beginning about 1988-1989 and ending about 1999. Both accelerations witnessed rates of sea level rise well above the local average for this period of about 3-4 mm yr⁻¹. The most recent one, which terminated around 1999, was characterized by an average rate of sea level of rise of 1.2 cm yr⁻¹ in Baltimore gauge, though some tide gauge records elsewhere in the region show rates even higher, up to 1.4 cm yr⁻¹. This exceptionally high rate of sea level rise was accompanied by considerable marsh loss and shore erosion, which had become evident even before the end of episode (cf. Stevenson and Kearney 1996). It is far from clear whether these sharp and sustained jumps in rates of sea level rise will continue; nonetheless, if they do and increase in frequency (let alone intensity) they could prove very damaging if left

unconsidered as an important risk factor.

CONCLUSION

The future course of global sea level change has uncertainties that derive from the Global Circulation Models (GCMs) that underpin the IPCC forecasts, the paucity of sufficient information concerning ocean heat storage versus steric response, the very short time range that whole ocean elevation data have been available from satellite altimetry, and the need for a better understanding of the impact of such phenomena as ENSO, NAO, the Pacific Decadal Oscillation (PDO). It should also be noted that massive polar melting is a "wildcard" that cannot be dismissed. Rapid progress is being made on all these fronts, but whether the uncertainties will be reduced to a level of probabilities amenable to a standard risk analysis is doubtful. Time is not on our side. If the IPCC forecasts for global sea level rise (with all their problems) have ascertained what the general outlines of the global sea level will be, it is only a matter of a few decades, generation or so in human terms, before major effects will be seen.

The sea level rise risk can still be accommodated despite the very short timeline. Baseline scenario for local and regional changes can be developed for existing tidal records, regardless of what eventually transpires globally. The risks presented by the potential range of inter-annual variations are waiting deciphering from extant tide gauge records; the same might be said (with somewhat less confidence) of decadal oscillations. The usefulness of such exercises are clear: the damage of coastal flooding and erosion from any storm is more likely to be greater if it occurs during a high tide coinciding with an inter-annual high stand, or even more so during the terminal high stand of a decadal oscillation (e.g., ENSO or U.S. middle Atlantic sea level accelerations). In fact, analysis of tide gauge records, as noted here, reveal that these high stands often dwarf even decadal changes in the global sea level trend. The tools are thus available to reduce the sea level risk to a level more tractable dimensions for coastal planning and development.

REFERENCES

- Lombard, A., Cazenave, A. Le Traon, P., and Ishii, M. (2005). "Contribution of thermal expansion to present day sea-level change revisited." *Glob. Planet. Change*, 47, 1-16.
- Aubrey, D.G, and Emery, K.O. (1986). "Relative sealevels of Japan from tide-gauge records." *Geological Society of America Bulletin*, 97, 194-205.
- Cabanes, C., Cazenave, A., and Le Provost, C. (2001). "Sea level rise during past 40 years determined from satellite and in situ observations." *Science*, 294, 840-842.
- Church, J.A. *et al.* (2001). *Climate Change 2001: The Scientific Basis* (ed. Houghton, J.T.). Chapter 11. New York: Cambridge University Press.
- Davis, G.H. (198). "Land subsidence and sea level rise on the Atlantic Coastal Plain of the United States." *Environ. Geol. Water Sci.*, 10, 67-80.
- Douglas, B.C. (2001). "An introduction to sea level." In Douglas, B.C., Kearney, M.S. and Leatherman, S.P. (eds.), *Sea Level Rise: History and Consequences*. San Diego: Academic Press, pp. 1-10.

Hansen, J. Gornitz, V., Lebedeff, S., and Moore, E. (1983). "Global mean sea level: indicator of climate change?" *Science*, 219, 996-997.

Holdahl, S.R., and Morrison, N.L. (1974). "Regional investigations of vertical crustal in the U.S., using precise relevelings and mareograph data." *Tectonophysics*, 23, 373-390.

Houston, J.R. and Dean, R.G. (in press). "Is the rate of sea level rise increasing? An analysis based on U.S. tide gauges. In Ayyub, B., and Kearney, M. (eds.), ACSE Monograph on Coastal Infrastructure and Engineering.

IPCC. (2007). *Climate Change 2007: Synthesis Report. Contribution of Working Groups I, II and III to the Fourth Assessment Report of the Intergovernmental Panel on Climate Change* [Core Writing Team, Pachauri, R.K and Reisinger, A.(eds.)]. IPCC, Geneva, Switzerland, 104 pp

Kearney, M. S. (1996). "Sea-level change during the last thousand years in Chesapeake Bay." *J. Coastal Res*, 12, 977-983.

Knudsen, P. (2004). "Global low harmonic degree models of the seasonal variability and residual ocean tides from TOPEX/POSEIDON altimeter data." *J. Geophys. Res.* 99, 24643-24655.

Levitus, S., Stephens, C., Antonov, J.I., and Boyer, T.P. (2000a). "Yearly and year-season upper ocean temperature anomaly fields, 1948-1998." U.S. Gov. Printing Office, Washington, DC, p. 23.

Levitus, S., Antonov, J.I., Boyer, T.P., and Stephens, C. (2000b). "Warming of the world ocean." *Science*, 287, 2225- 2229.

Miller, L., and Douglas, B.C. (2004). "Mass and volume contributions to twentieth-century global sea level." *Nature*, 425, 406-409.

Stevenson, J. C., and Kearney, M. S. (1996). "Shoreline dynamics on the windward and leeward shores of a large temperate estuary." In Nordstrom, K. F., and Roman, C. T. (eds.), *Estuarine Shores: Hydrological, Geomorphological and Ecological Interactions*. New York: John Wiley & Sons, pp. 233-259.

Defining and Assessing Vulnerability of Infrastructure to Terrorist Attack

Geoffrey S. French and David Gootzit¹

Abstract

The Homeland Infrastructure Threat and Risk Analysis Center (HITRAC) of the U.S. Department of Homeland Security (DHS) provides threat, vulnerability, and consequence assessments of terrorist attacks on infrastructure in support of security risk assessments. This paper will describe the components of vulnerability that HITRAC considers and how it integrates those components into an overall vulnerability assessment. The assessment relies on an approach to target selection and preliminary vulnerability identification drawn from observed terrorist methods of operation. The attack methods used as the basis for scenario generation are taken from the 2008 Joint Special Assessment on Potential Terrorist Attack Methods. These are filtered to identify the attack methods most applicable to the facility, asset, or system being assessed. The vulnerability assessment can be used as a stand-alone analysis or feed into a risk model for national or regional assessments.

Introduction

One of the fundamental missions of the U.S. Department of Homeland Security (DHS) is to secure the nation from terrorist attacks, and protecting critical infrastructure in particular is one of the primary goals of the Department. The National Infrastructure Protection Plan (NIPP) provides the overall structure for infrastructure protection efforts and makes security risk the basis for prioritization of resources and efforts. Vulnerability assessment plays a large role in the NIPP. Not only is assessing vulnerability a necessary factor for assessing risk, but it also often the focus of risk mitigation efforts. The need to make comparisons across sectors of infrastructure that have very different features, characteristics, and purposes poses a significant challenge. The Homeland Infrastructure Threat and Risk Analysis Center (HITRAC) provides threat, vulnerability, and consequence assessments of terrorist attacks on infrastructure in support of security risk assessments, and has taken on that challenge. This paper discusses the definition of vulnerability, a conceptual approach to vulnerability assessment, and a simple approach to considering vulnerability at the strategic level that allows a simple assessment of infrastructure and comparison to other infrastructure assets, facilities, and systems.

¹ CENTRA Technology, Inc., 4121 Wilson Blvd., Suite 800, Arlington, Virginia 22203.

Defining Vulnerability

DHS defines vulnerability as “a physical feature or operational attribute that renders an entity, asset, system, network, or geographic area open to exploitation or susceptible to a given hazard” (DHS, 2010). The key to assessing vulnerability properly is in the last phrase of that definition. Although vulnerability assessments can be stand-alone documents, vulnerability is best understood within a risk context, specifically the interaction between the threat and the consequence. This interaction is the reason that vulnerability is sometimes defined as the probability of success given an attack or the probability of the consequences occurring given an event (Paté-Cornell and Guikema, 2002; Ayyub, 2008). In either case vulnerability is the collective influence of physical features or operations that reduce the effectiveness of the adversary’s attack or that make the target better able to sustain the attack. Analysis is highly dependent, therefore, on the method of attack and strength of the attack expected. A building’s vulnerability to an improvised explosive device (IED) will differ from the vulnerability to a vehicle-borne IED (VBIED), for example, depending on the assumptions in the definitions of those attacks, such as amount or type of explosives, entry points, and stand-off distance. Even within the category of VBIED, vulnerability will differ based on terrorist tactics, such as leaving the vehicle on the street adjacent to the building or ramming the vehicle into the building or its defensive perimeter. The more specific the context, the more accurate the vulnerability assessment for any particular target can be.

For security risk, vulnerability is also influenced by the terrorist adversary. Terrorist groups have different levels of competence and expertise. This can affect not only target selection but also their knowledge of countermeasures and their determination to overcome those countermeasures through technology or effort (Little and Rogova, 2006). These aspects of the threat can influence judgments of degree of accessibility or strength of countermeasures. Opportunity to attack, in other words, reflects the interaction of threat and vulnerability; the characteristics of potential attackers help provide further context for high-quality vulnerability assessments. With all of these variables, it is easy to see why some argue that vulnerability is not a static characteristic but a dynamic state and, in the extreme, a combination of the various states of all the aspects of the asset, facility, or system, which is in constant flux (Haimes, 2006). Although this insight is true, it is not particularly helpful for arriving at a mechanism for assessing vulnerability. Given all the complexity, there is still a need for a simple way to generate a repeatable and comparable vulnerability level that is useful for the government and private sector partners for infrastructure protection.

A Conceptual Approach to Vulnerability Assessment

Based on the DHS definition, a vulnerability assessment begins by defining a hazard and then must evaluate the physical features or operational attributes that render an entity, asset, system, network, or geographic area open to exploitation. There are many ways to assess vulnerability, ranging from a checklist of countermeasures to a single judgment of whether an entity is vulnerable or not. There are clearly geographic and temporal elements to vulnerability and it is difficult to create a single approach

that addresses each element appropriately for all attack types and target types. There is a set of considerations, however, that if taken together can form the foundation for almost any vulnerability assessment. These are:

1. Characteristics of the asset itself;
2. The protective measures that prevent access for attack;
3. Access allowed to outsiders and insiders; and
4. The functional dependencies on internal and external entities.

In the field of infrastructure protection, an asset may be a physical item, a facility, a system, or a function. An asset may be physically strong or weak, be part of a highly adaptive network, or a single point of failure. Regardless, within the context of the hazard, its inherent characteristics will make it likely to fail or likely to withstand an attack. The asset's environment provides protections against some hazards, and in some cases the environment is specifically designed to prevent access or provide other protections for the asset. The environment may itself be multi-layered, and there are different approaches to defining and assessing these protections. The Federal Protective Service, for examples, defines the environment as the envelope around the interior of a building, the perimeter around the envelope, and the buffer zone around the perimeter, each with protective characteristics (Harvey, 2010).

It is possible to provide thorough protection to an asset, but for assets to be useful in a broad sense, they must be accessible. For infrastructure in particular, access is often fundamental to the asset's utility. Protective measures, therefore, grant exceptions to both insiders and outsiders to allow access. (These can include signs, advertising, or publications that disclose location, functions, or importance.) A vulnerability assessment should examine these to determine if they pose operational weaknesses or can be exploited by an adversary to gain insight into the protective measures.

Similarly, assets often have functional dependencies, such as on electric power, water, services, or supplies. These may also cause operational weaknesses or be exploited. Thorough vulnerability assessments should also consider the protective measures around the asset's dependencies, as well as the access allowed to them, to get a comprehensive view of an asset's environment. Collectively, the asset, its protections and the exceptions made to grant access, and the asset's functional dependencies make up the asset's vulnerability environment. Figure 1 illustrates this concept.

Although there is no definitive list of vulnerability attributes that should be considered in an assessment, there are three ways that an organization can affect an attack from a defensive perspective. Obviously, an organization can implement countermeasures to detect and stop an attack in progress, and many vulnerability assessments focus on this component of vulnerability. However, an organization can also limit an adversary's opportunity to launch an attack at all. This can include efforts to keep a facility or system's location or criticality unknown to the public, limiting technical information that would allow an adversary to exploit operational or physical vulnerabilities, or other efforts to conceal the asset from an adversary (such as by altering its physical appearance). Finally, an organization can work to limit the effects of an attack by strengthening physical structures, engineering fail-safes that prevent cascad-

ing consequences, or automating operational changes that minimize or negate the intended consequences.

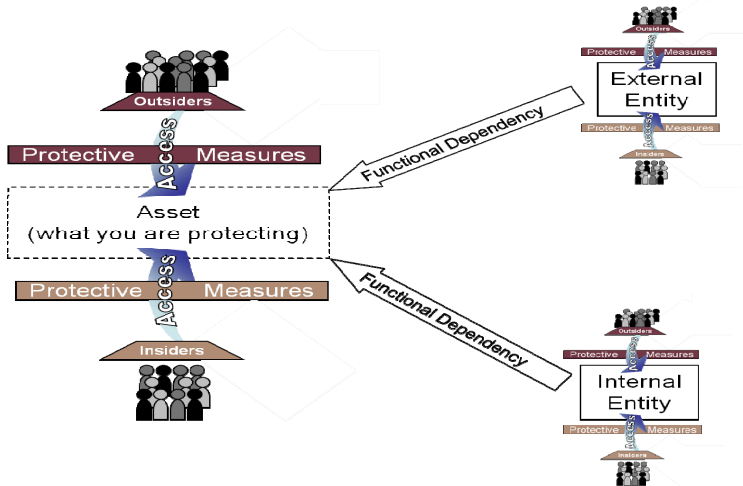


Figure 1: The Vulnerability Environment

The Vulnerability Assessment Process

Given the conceptual approach as defined, a terrorism vulnerability assessment must at a minimum focus on an identifiable asset, facility, or system, and—for a specific attack method—evaluate the efforts or other factors that limit adversary knowledge that would enable an attack, the countermeasures to the attack, and the inherent robustness or resistance to attack. The following sections describe an approach to generate scenarios and measure these three components of vulnerability, and create a vulnerability level for infrastructure security risk.

Generation of Scenarios. A good vulnerability assessment will strike a balance between considering a very large number of possible events and focusing on a single scenario. There are a number of possible attack methods that are feasible, but where there are no indications of adversaries with the capability or intent to carry out certain attacks. One approach that limits the range of attack scenarios while still providing a comprehensive review of possible attacks is using an authoritative list of categories of attacks, such as the DHS–Federal Bureau of Investigation publication “Potential Terrorist Attack Methods – Joint Special Assessment.” Released in April 2008, this document contains a description of a range of potential terrorist attack methods that could be used against critical infrastructure (see Box 1). This joint assessment provides a short description of the tactics, techniques, and procedures that could be used by a terrorist group in an attack. The list of potential attack methods is based on known terrorist capabilities and intelligence reporting on assessed, implied, or stated intent to conduct an attack. By using this joint assessment, analysts conducting a vulnerability

assessment can consider a common set of assumptions when reviewing and ranking the vulnerability for various risk scenarios.

Box 1: Terrorist Attack Methods Used for an Infrastructure Vulnerability Assessment	
Aircraft as a Weapon	Improvised Explosive Device (IED)
Biological Attack - Contagious Diseases	Maritime Vessel as a Weapon
Biological Attack - Non-contagious Diseases	Nuclear Detonation
Chemical	Radiological Dispersal Device (RDD)
Cyber Attack	Stand-off Weapon - Guided
Food or Water Contamination	Stand-off Weapon - Unguided
Hostage-Taking / Assault	Vehicle-Borne IED (VBIED)

Attack Method Filtering. Not all attack methods will apply to a specific asset. To focus on the attack methods that represent the best fit with an attack on the asset, infrastructure analysts can use three filters to screen out inappropriate attack methods: applicability, potency, and proportionality. First, the analyst eliminates any attack methods that would have no effect or could not be used in an attack on the entity, asset, system, network, or geographic area. For example, cyber attacks could not be used to affect national monuments, so there is no need to create a scenario for analysis. Second, some attack methods would not be sufficiently potent to cause a regionally or nationally significant effect. An IED would be ineffective, for example, against a robust concrete dam. Finally, the analyst considers the proportionality of the attack. If a terrorist were to have a nuclear device, for example, it is unlikely that the terrorist would attack an isolated target or an asset of minor consequence.

Event Tree Analysis. A target's vulnerability is, of course, dependent on more than the adversary's selected attack method. Once an adversary decides to attack and the attack method they will use, they must overcome a series of operational hurdles. First, the target must be located, which requires recognizing the asset and its significance. Next, if a target is identified, the attack must overcome the countermeasures and protections in place. Finally, the success of the attack is ultimately determined by whether the asset is robust or resistant enough to sustain damage. From this perspective, a vulnerability assessment must answer three fundamental questions:

1. Can an adversary identify the asset and its criticality?
2. Will the countermeasures in place prevent the attack from succeeding?
3. If the countermeasures fail, will the attack have the desired effect?

A complete assessment of the vulnerability of infrastructure to a terrorist attack is composed of three independent components: the recognizability of the asset, system, or facility, the level of effectiveness of the countermeasures protecting the asset (specifically in the areas of denial, detection, and interdiction), and the level of intrinsic robustness or resistance of the asset or system against an attack. The following sections describe these components in more detail with Table 1, below, detailing the ranking levels and criteria for each.

Recognizability. To estimate Recognizability, the security analyst should examine the potential for an adversary to identify and target an asset, facility, system, or the people present. In most cases, Recognizability takes into consideration labeling or

signage, press, uniqueness, and public knowledge of the asset. For example, an attack on a public facility or system, such as mass transit, ranks “high” because of clear signage, public knowledge, extensive press, and available information. For attacks that require specific technical knowledge, Recognizability takes into account the likelihood an adversary can recognize or locate a specific critical location if necessary; a lower Recognizability ranking reflects the more obscure role of the critical parts. Another example would be a cyber attack. In these cases, the variable separates the Recognizability of a facility’s or asset’s network (the target of the attack described in the scenario) from the Recognizability of the facility or organization itself.

In assessing Recognizability, the analyst should give appropriate consideration to open source information about the asset or facility in question. Terrorist training manuals captured in recent years underscore the use of open sources for intelligence, stating that public sources can provide the vast majority of required information. Moreover, past plots and attacks have demonstrated the use of Internet research to provide information prior to the attack. The most famous example is the casing reports of Dhiren Barot, which included web site information which included explicit references to tactical information drawn from publicly accessible web sites for multiple targets in New York, New Jersey, and Washington D.C. and contained information suggesting more extensive Internet use. Recent incidents demonstrate the continued use of Internet research for target selection and reconnaissance.

Countermeasure Effectiveness. To estimate the level of Countermeasure Effectiveness, an analyst must consider the ability of the protective measures to prevent the successful execution of an attack. Countermeasures can be characterized as three types of intervention: denial, detection, and interdiction. Denial countermeasures typically prohibit access to the target to prevent an attack from succeeding. Detection systems increase the likelihood that the attack is identified quickly prior to or during an attack. Finally, interdiction countermeasures interdict, remove, or neutralize the attack just prior to or during an attack.

There are several considerations for estimating Countermeasure Effectiveness. First, attacks that require very little time to be successful tend to lead to low rankings for countermeasure effectiveness. In these sorts of scenarios although intrusion detection systems and CCTV systems can be part of an effective defensive posture, if no response personnel are present or if they cannot effectively interdict the attack, the ranking reflects the likelihood of effectiveness. Second, cyber attacks have their own considerations separate from physical attacks. For example, some countermeasures actively address any anomalous activity, whereas others only react to known past attack types. Additionally, systems that do not have encryption or authentication of commands would not prevent an attack to manipulate a system and produce unsafe conditions. Finally, wide-area attacks are generally intended to affect the population as a whole or a locality, rather than a specific asset. For these types of attacks, no countermeasures exist to protect against these attacks that target the inherent vulnerability of the general public and are ranked as “low.”

Robustness or Resistance. In a vulnerability assessment, the level of Robustness or Resistance represents the ability of the asset or system to resist, withstand, or

contain damage. This approach addresses whether there are mechanisms in place or inherent characteristics of the facility or system attacked which prevent or reduce the likelihood of damage.

Similar to Recognizability, Robustness is evaluated in the context of the intended target and intended consequences. For example, if the intention is to destroy a facility, several characteristics increase an asset's or system's robustness to a specific scenario, including material strength, structural strength, and redundancies. For attacks that target the public or employees, the Robustness of the system or asset is influenced by a different set of considerations. For example, shatter-proof glass with reinforced window frames can increase a physical system's robustness. Attacks that cripple a workforce, rather than a physical infrastructure, consider worker criticality, worker proximity, and worker substitutability.

Table 1. Ranking Table for Vulnerability Components

Component	Ranking Level				
	Low	Medium-Low	Medium	Medium-High	High
<i>Recognizability</i>	Asset is very unlikely to be recognized; adversary would require a highly trained expert or access to classified or highly sensitive information.	Asset is unlikely to be recognized; an adversary would require some special knowledge or training.	Asset is somewhat likely to be recognized; an adversary would require a moderate amount of research.	Asset is likely to be recognized; an adversary could identify this asset with minimal effort.	Asset is very likely to be recognized; any adversary could easily identify this asset; attack method requires little to no direct targeting.
<i>Counter-measure Effectiveness</i>	The existing countermeasures are very likely to defeat the attack.	The existing countermeasures are likely to defeat the attack.	The existing countermeasures are somewhat likely to defeat the attack.	The existing countermeasures are unlikely to defeat the attack.	The existing countermeasures are very unlikely to defeat the attack.
<i>Robustness / Resistance</i>	The asset is very likely to resist, withstand, or contain the damage from the attack.	The asset is likely to resist, withstand, or contain the damage from the attack.	The asset is somewhat likely to resist, withstand, or contain the damage from the attack.	The asset is unlikely to resist, withstand, or contain the damage from the attack.	The asset is very unlikely to resist, withstand, or contain the damage from the attack.

Combining the Components. For the purposes of the vulnerability approach described in this paper, logical combinations of recognizability, countermeasure effectiveness, and robustness can be combined to create a single index for the general vulnerability of a scenario to provide a qualitative assessment of vulnerability. The general logic for the combination of the five rankings (High, Medium-high, Medium, Medium-low, Low) is illustrated in Figure 3. These judgments serve as the basis for the vulnerability rankings for each scenario, guiding the key judgments in a vulnerability assessment.

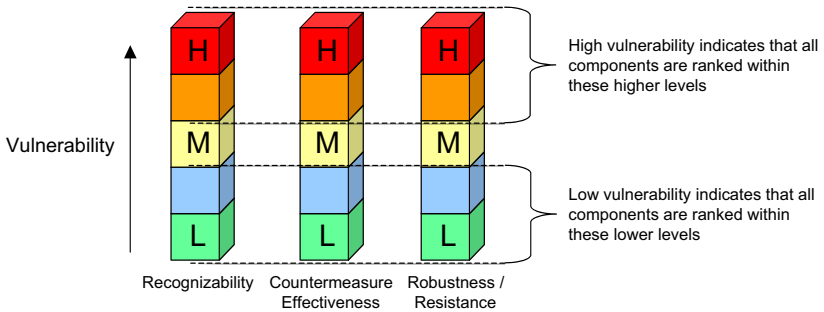


Figure 3. Vulnerability Level – Logic Combinations

Conclusion

There are multiple methods of assessing vulnerability. The advantages of this approach is that it is sufficiently flexible to apply to asset-based and system-based sectors of infrastructure, it provides a simple mental model that allows rapid consideration of vulnerability, it considers dimensions of vulnerability beyond technical countermeasures, and it builds on analysis performed by the counterterrorism community to describe terrorist tactics and preparations for attack. If properly implemented, it can lead to consistent judgments of vulnerability that allow comparison within an organization, across a sector, or for cross-sector analyses. Finally, it was designed to be compatible for risk assessments and can be easily utilized as a module within a larger risk management process.

References

- Ayyub, B.M. (2008). "Terrorism risk: Characteristics and features." *Wiley Handbook of Science and Technology for Homeland Security*, Wiley, London, 59–74.
- Haimes, Y.Y. (2006). "On the definition of vulnerabilities in measuring risks to infrastructures." *Risk Analysis*, 26(2): 293–296.
- Harvey, M. (2010). "Federal Protective Service Risk Assessment and Management Program." Presentation at the 4th Annual Conference on Security Analysis and Risk Management, Arlington, Virginia.
- Little, E.G., and Rogova, G.L. (2006). "An ontological analysis of threat and vulnerability." Proceedings of the 9th International Conference on Information Fusion, Florence, Italy.
- Elisabeth Paté-Cornell and Seth Guikema. (2002). "Probabilistic modeling of terrorist threats: a systems analysis approach to setting priorities among countermeasures." *Military Operations Research*, 7(4): 5–20.
- U.S. Department of Homeland Security. (2010). *Risk Lexicon*.
- U.S. Department of Homeland Security –Federal Bureau of Investigation, "Potential Terrorist Attack Methods," 2008.

Integrating flood defence fragility to measure built environment vulnerability – a GIS based approach

Damien Serre¹ Serge Lhomme¹, Bruno Barroca², Youssef Diab^{1,2}

¹Université Paris-Est, Ecole des Ingénieurs de la Ville de Paris, 15 rue Fénélon, 75010, Paris, Tél: +33 1 56 02 11 05; damien.serre@civp-paris.fr; serge.lhomme@civp-paris.fr; youssef.diab@civp-paris.fr

²University Paris-Est – Department of Urban Engineering, Bâtiment Lavoisier, Boulevard Descartes 77454 Marne la Vallée Cedex 2, France, Bruno.barroca@univ-mlv.fr, ydiab@univ-mlv.fr

ABSTRACT

More and more floods occurred over the last decade in the world, causing important damages. Moreover, levees are often not well maintained, so they hardly resist to major floods and can break easily. At French national scale, the length of levees, estimated to 7500 kilometers, and the lack of data all along these infrastructures complicates their management. In this frame, levee managers need approaches and tools in order to be helped in their maintenance decision. The goal of our research is to develop methods modeling levee failure mechanisms and allowing performance levee assessment. These methods integrated in an existing GIS dedicated to levee management will contribute to obtain a spatial decision support system aiding levee managers in their maintenance decision. Finally we made some tests in a specific area to integrate in the SDSS the level of vulnerability behind dikes to improve the levee manager decision process.

INTRODUCTION

More and more floods have occurred over the last decade in France, leading to important damages. These floods have significant costs, especially because of increasing development in dry river beds. Moreover, embankments are not often well maintained, so they cannot resist to major floods and can breach quite easily.

Embankments ageing and a poor management from their many owners, lead to considerable loss of information, like repairs, reinforcements... Furthermore, their length, estimated to about ten thousands kilometers in France, complicates their management. Local defence managers and French State services are aware that they have to develop management plans to improve and maintain flood defence safety and behavior. But the huge length of these linear infrastructures brings up the following issue: which section must be first taken care of (Diab 2002)?

To answer this question, flood defence managers need specific tools and methods to give them priorities in their interventions. The aim of our research is to provide such tools and methods. Our approach consists in three main steps:

- analyzing and modeling embankments failure mechanisms: this is a fundamental step allowing recognizing, understanding and model physical mechanisms affecting embankments and leading to their failure. For that purpose we use safety methods;
- embankments performance assessment: for this step, we combined data collected on flood defences with failure scenarios constructed in the first step of our approach. Embankment performance is evaluated with a decision aid method;
- integrating the embankment performance assessment model into a specific GIS (Geographic Information System) dedicated to flood defence management: the aim is to use a powerful computer tool to take advantage of embankment performance assessment. The GIS will provide a synthetic vision of the embankment segment performance level.

The application of these three steps allows levee managers to visualize and to locate levee sections classified according to their performance level, so they can better prioritize their maintenance operations.

In the same time, current flood risk management and research mainly use the susceptibility and value of the protected assets (expected damage to buildings and inventory) to assess their vulnerability, i.e. the potential direct damage. Improving the vulnerability assessment taking into account the flood defence fragility is a significant challenge in order to improve vulnerability assessment of cities located behind dikes. This is also the only way to allow flood defence managers taking appropriate decisions based on one hand on the fragility of the flood defences, on the other hand on the vulnerability of the protected area.

Our communication focuses first on describing dike fragility assessment. On the second part present the method we used to assess vulnerability behind flood defences based on spatial analysis through GIS.

A SPATIAL DECISION SUPPORT SYSTEM FOR FLOOD DEFENCE MANAGERS

Since 1995, several engineering offices have been asked by levee managers to develop and to test levee diagnosis and monitoring methods. Studies results allowed to design field observation protocols for levee diagnosis and to describe and follow-up the maintenance or repair works carried out on the levees through a GIS (called Levee SIRS).

Next step, started in 1999 and completed in 2000, was to assess, from a technical and a practical point of view, the interest of local managers for such a GIS. With the support of the Ministry of Environment, a generic demonstration prototype was developed.

In 2001, two local levee managers, each of them managing approximately 250 kilometers of levees located respectively in Camargue and in Isère, joined the project to adopt this modern and innovative management tool.

On the basis of detailed terms of reference for a national call for tenders, a first version of the "Levee SIRS" application was developed and is now fully functional. This application is based on ArcGIS (© ESRI) and Access (© Microsoft) software. It intensively uses ArcGIS© dynamic segmentation capabilities to manage, analyze and represent punctual and linear levee information. Moreover, feeding the SIRS with good quality and complete data was considered as one of the key conditions to make this tool usable by levees managers. A very detailed attention was granted to the field observation cards dedicated to the levee guards who are the main data providers. Our approach consisted in elaborating field survey cards as ergonomic as possible for an operational use in the field, independently from the software application, then to develop on this basis graphic user interfaces for data capture.

This GIS tool is now operational and constitutes a significant progress within the framework of levee sustainable management. However the "Levee SIRS", at this time, does not really allow levee managers optimizing their maintenance actions. For that, new GIS functionalities have to be developed, in particular, to provide a synthetic vision of levees conditions and performance all along their length (Gervais 2010).

Starting from the 1970's numerous Decision Support Systems (DSS) have been developed to support decision-making with expert knowledge. The most generally accepted definition of a DSS is the one articulated by Sprague (1986): "Interactive computer based systems, which help decision-makers utilize data and models to solve unstructured problems". A more detailed definition is the one provided by Turban (1990): "an interactive system, flexible and adaptable, which uses decision rules, models, databases and suitable formal representations of the decision-makers' requests to indicate specific and applicable actions to

solve problems which cannot be solved by the optimization model of Classical Operational Research. It thus assists complex decision processes and increases their efficiency.”

It is usually recognized that a DSS is based on three components:

- a database management system which provides all the functionalities relating to data entry, storage, processing, results editing and exchange with other databases;
- a management system of analytical model database which provides a set of analytical relevant tools, necessary for interpretation and recommendations relating to data, and responding to decision maker needs;
- convivial and interactive user interfaces, which facilitate interactions between decision makers and the DSS.

But, because of the specificity of spatial issues relating to geographical localization, a Spatial DSS (SDSS) needs additional capacities and functionalities Densham (1991) for spatial data entry, spatial analysis and spatial editing in various forms, like maps and charts Laaribi (2000).

Thus, although innovative in the levee management context, the “Levee SIRS”, in its current version, still needs to be enriched with spatial analysis functionalities, allowing levee performance charting, to become a real SDSS.

Our goal was to develop models able to assess levee performance. The first step consisted in modeling levee failure mechanisms in the form of scenarios in order to obtain the information needed for assessing levee performance (Gervais 2010). The model shall include all the failure mechanisms relevant to all types of levees.

We used tools developed in the field of Operational Safety for modeling complex systems and representing the organic links between the sequences of failures in the structures Zwingelstein (1996). The functional model representing the mechanisms is built up with the use of functional analysis and Failure Mode and Effect Analysis (FMEA) methods (Gervais 2010).

We constructed levee failure scenarios by linking failure causes to failure modes, and then to failure effects. In this way, the failure mechanisms are modeled as series of functional failures representing the relevant physical processes (Pilarczyk 1998) taking place within the system and leading to loss or deterioration of function. The scenarios are drawn as causal graphs; each mechanism is modeled in a directed graph describing the functional deterioration processes and sequence of corresponding variables.

The functional model representing scenarios includes three categories of variable: function variables corresponding to failure modes, process variables accounting for failure mode causes and effects, and indicator variables corresponding to the outward evidence of processes.

This kind of model offers multiple advantages. It provides a framework of expert knowledge in the form of functional scenarios; it organizes information on mechanisms around three categories of variable (function, process, and indicator) and can account for partial and progressive deterioration in the variables and non-chronological mechanisms.

We focus now on the multicriteria method used to assess levee performance. We have chosen methods that allowed us, on the basis of the modeled failure scenario, to transform the information collected on the levees into scores reflecting the levee performance level.

The first stage of our work consisted in finding a method able to provide a levee performance assessment based on several criteria. Then, we determined indicators used to support the evaluation of each criterion, and to combine these indicators to give an assessment of each criterion.

We decided to use an interactive multicriteria method, named “assignment by rules establishment” Azibi (2003), which alternates stages of calculations and stages of dialogue

with the decision maker. This kind of method is well fitted to our complex context of aggregation. Rule-based aggregation consists of a set of "if ... then" rules, close to natural language, to express the principles of aggregation.

The condition part (if) concerns the levee assessments on a set of criteria and the conclusion part (then) indicates the total aggregate assessment. This method allows incorporating the preferences of field experts and explaining the synergies and compensations between criteria

To integrate our models into the "Levee SIRS", we upgraded the SIRS database model to include all the indicators and criteria needed for each failure mechanism model, and we coded a performance calculation module Prévot (2005). Then, we assessed the quality of the prototype from two perspectives: first, its ability to reproduce hydraulic infrastructure expert reasoning to assess levee performance as. Second, its ability to provide useful decision support to levee managers.

The prototype was tested on a 2 km levee located in the south of France, near Montpellier. We assessed the levee performance relating to internal erosion failure mechanism.

This operation consisted first in collecting field data on this levee. One day was necessary to gather data needed for performance calculation. The second phase consisted in entering data in the prototype and finally in executing the performance model calculation. A map of the levee performance was produced at the end of the procedure (see figure 1).

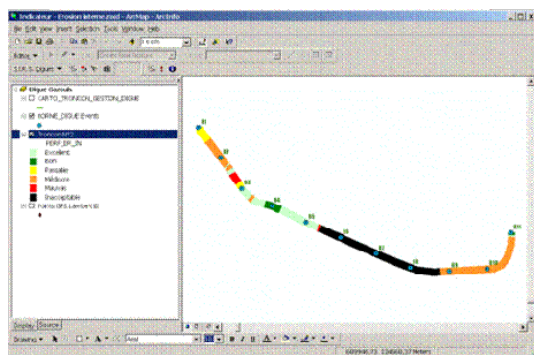


Figure 1. Levee performance map relating to internal erosion failure mechanism (Gervais 2010)

This levee section was well known by several levee experts and reports describing levee performances relating to all failure mechanisms were available. The post comparison of the results obtained with these three approaches (SIRS model, existing reports, and expert analysis) led to very similar conclusions. Even if these results are encouraging, it is too early to generalize them for all kinds of levees yet. Additional tests have to be performed on other kinds of levees and other kinds of failure mechanisms.

About decision aid supplied to levee managers, the contribution of such a tool seems very promising. First of all, performance indicators values can be mapped in a very visual way in the GIS. Furthermore, the prototype allows users to retrieve all indicators and criteria which contributed to each section performance value. Our test also shown that the levee segments, homogeneous in term of performance level, were long enough from operational maintenance perspectives.

Nevertheless, even with this possibility to prioritize maintenance actions based on levee performance, this is not enough to guide the choices. Indeed, vulnerability behind levees has to be assessed to make levee managers able to choose where to start.

CITY VULNERABILITY ASSESSMENT INTEGRATING LEVEE PERFORMANCE

Cazouls-d'Hérault is a small town in the Hérault department in southern France. The city belongs to a Region (Languedoc-roussillon) which is frequently impacted by flood. Indeed 97% of cities of this region have been impacted by natural hazard since 1982: flooding is a major issue in this area. There are two main rivers surrounded the city: river Hérault and river Boyne. These two rivers can flood the city. It is a less than 1000 inhabitant city. So, taking into account of the city size, it is easy to define area with common characteristics (density, road network...).

Data required for this study, comes from "Institut Géographique National" (IGN). IGN is a French public state administrative establishment founded in 1940 to produce and maintain geographical information for France and its overseas departments and territories. We use data from a specific database so called "BD TOPO" because this is a topographic and land-use database. BD TOPO contains a description of the landscape elements in the form of metric accuracy vectors, filed according to a suitable theme. The description of most three-dimensional objects results in a photogrammetric production process.

Thanks to this these data, we study two types of vulnerability in our approach: geographic vulnerability and structural vulnerability (see figure 2). Moreover we divided structural vulnerability in two different approaches: a classical approach based on the study of building vulnerability and a second approach based on the vulnerability of flood defence. At the end, territory vulnerability is assessed thanks to three main indicators (see figure 2).

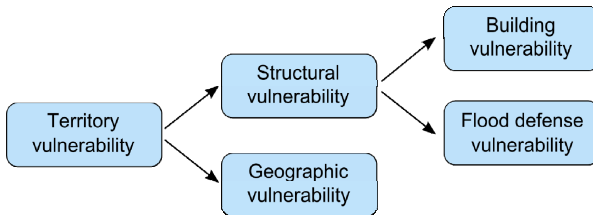


Figure 2. Types of vulnerability analysis

Geographic vulnerability corresponds to the exposure of the territory to flood hazard. Thus, thanks to hydraulic modeling, it is possible to determine territory which can be flooding by a specific flood hazard. In our case, this specific flood hazard corresponds to an historic flood. The situation is very simple to understand because almost all the urban territory is exposed to this hazard (92% of the buildings and 86% of the building surface). So, at our scale, it's important to make the difference between different areas which are not at the same level of exposure. In fact, some areas are located in lower parts of the city than others and impact of flooding is more important due to this geographic location. Here, geographic vulnerability refers to the physical characteristics of the territory in particularly topographic characteristics. In our study a digital elevation model (DEM) has been used for assessing geographic vulnerability (see figure 3).

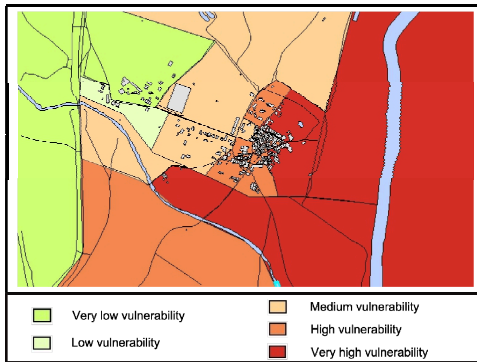


Figure 3. Geographic vulnerability

Structural vulnerability corresponds to the safety level of the population and goods due to facilities against flood. Indeed, population is protected against flood particularly thanks to flood proofing building and flood defences. So we have two main objectives: assessing the building vulnerability and flood defence vulnerability.

For determining the building vulnerability of each area, four indicators have been used. First indicator is the building density. Indeed high building density increase probability that population can be reached by a flood event. Second indicator is the number of less than 4 meters height buildings. Less than 4 meters height buildings cannot ensure security of the population. Third indicator takes into account the building nature because some buildings are not resistant to flooding (mobile homes, cabins...). Fourth indicator deals with public buildings that are considered vulnerable because population gathering increase probability that population can be impacted by flood. Each indicator has been calculated (score between 1 and 5) and thanks to two aggregation functions building vulnerability has been assessed (see figure 4).

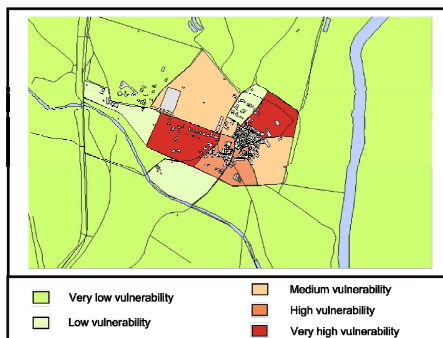


Figure 4. Buildings vulnerability

Flood defence vulnerability has been assessed thanks to safety method. Areas are exposed to this vulnerability at different level. Each area in touch with flood defence is considered at the same level of vulnerability that the flood defence. Areas which are not directly in touch with flood defence are considered at a lower level of vulnerability because

flood defence failures are less problematic. Thanks to the use of this contiguity methodology we can assess flood defence vulnerability (see figure 5).

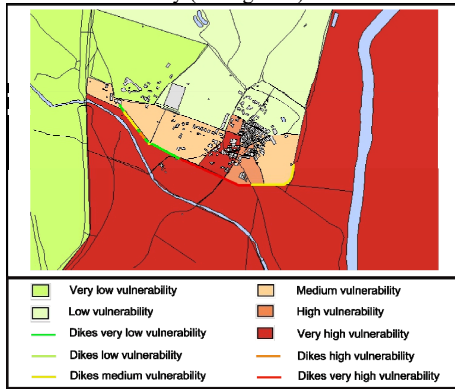


Figure 5. Flood defence vulnerability

Three main indicators have been assessed. Thanks to this assessment, it's possible to cluster the area with common vulnerability characteristics. Indicators aggregation has not been chosen taking into account their heterogeneity. Moreover, automatic clustering gives some incoherence. So we determined different cluster studying result one by one. For instance, we can identify areas with no building vulnerability and areas with high building, flood defence and geographic vulnerability (see figure 6).

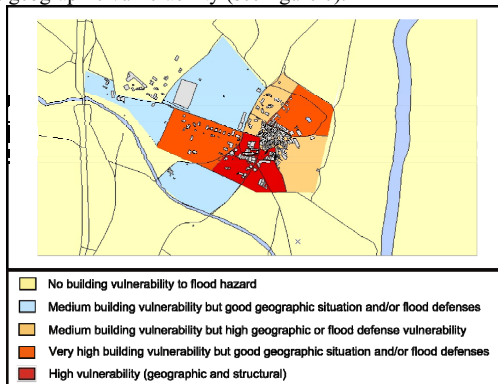


Figure 6. Vulnerability of the territory

CONCLUSION

Our research aimed to produce a method for analyzing levee performance and to integrate it into an existing GIS levee application. The work led to several results which made it possible to build up a SDSS prototype for levee managers.

The first stage of the work made use of Operational Safety methods: functional analysis, failure mode and effects analysis, and fault trees. These methods allowed to model

levee structures, to understand the design functions of levees and their components, to identify failure modes, and to determine causes and effects. Taking into account all these information as well as expert knowledge, we modeled as scenarios the most important levee failure mechanisms. In this way, we obtained for each mechanism the indicators and criteria needed for levee performance evaluation. In terms of results, we modeled the principal mechanisms leading to levee failure and determined, for each mechanism, the criteria needed to evaluate levee performance.

The next stage consisted of aggregating the indicators and criteria to evaluate levee performance. The approach used is a rule-based multi-criteria assignment method, combining discussions with a panel of experts and computational activities. In terms of results, this approach led to a set of criteria evaluation and aggregation rules for each failure mechanisms, ultimately leading to a synthetic evaluation of levee performance.

In order to provide levee managers with a practical working tool, we improved an existing GIS, the "Levee SIRS", in which we incorporated the levee failure mechanisms model and the levee performance multicriteria evaluation model. The prototype is now operational and has been tested on a real levee, producing conclusive performance assessment results for that particular levee. In term of decision-making aid, such tool seems to be very promising for levee managers to determine levee performance and so to optimize their maintenance and repair scheduling. The "Levee SIRS" tends towards a real SDSS as defined by Densham (1991).

The next step related to the development of this SDSS will be to integrate the vulnerability dimension (critical facilities at stake in area protected by levee) and to match it with levee performance to better prioritize management actions. This is what we have been started in developing indicators and spatial analysis to be able to cross levee performance and city vulnerability.

REFERENCES

- Azibi R., (2003) "Construction de critères en aide à la décision : aspects méthodologiques, techniques et pratiques", PhD. Diss., Operational Research, Paris Dauphine University.
- Densham P. J., (1991) "Spatial Decision Support System", In: Maguire D. J., Goodchild M. F. and Rhind D., "Geographical Information System: Principles and Applications", Longman, London, pp.403-412.
- Diab Y., (2002) "La gestion du patrimoine enterré: approche multi-critère d'analyse des risques." In: INFRA 2002, Montréal, Québec, 7 pp.
- Gervais R., Peyras L., Serre D., Chouinard L., Diab Y., 2010. Condition evaluation of water retaining structures by a functional approach: comparative practices in France and Canada, In European Journal of Environmental and Civil Engineering (In press).
- Laaribi A., (2000) "SIG et analyse multicritère", Hermès Editions, Paris, France.
- Pilarczyk K. W., (1998) "Dikes and revetments. Design, maintenance and safety assessment", A.A. Balkema, Rotterdam, The Netherlands.
- Prévoit C., (2005) "Evaluation de l'état des digues. Couplage d'une méthode multicritère avec un SIG." Report, Cemagref, France.
- Sprague R., (1986) "A framework for the Development of Decision Support Systems", In: Sprague R., and Watson. H., "Decision Support Systems: Putting Theory into Practice", London, Prentice-Hall, pp. 7-32.
- Turban E., (1990) "Decision Support and Expert Systems", New York, Macmillan.
- Zwinglestein, G., (1996) "La maintenance basée sur la fiabilité Guide pratique d'application de la RCM", Hermès Editions, Paris, France.

Many-objective Risk-based Planning within Complex Engineering Systems: An Urban Water Planning Example

Patrick M. Reed¹, Joseph R. Kasprzyk², and Gregory W. Characklis³

¹Associate Professor, Department of Civil and Environmental Engineering, Pennsylvania State University, 212 Sackett Building, University Park, PA 16802-1408, phone: (814) 863-2940, fax: (814) 863-7304, email: preed@engr.psu.edu

²Doctoral Candidate, Department of Civil and Environmental Engineering, Pennsylvania State University, 212 Sackett Building, University Park, PA 16802-1408, phone: (814) 865-5673, fax: (814) 863-7304, email: jrk301@psu.edu

³Associate Professor, Department of Environmental Sciences & Engineering, University of North Carolina at Chapel Hill, Rosenau Hall CB# 7431, Chapel Hill, NC 27599, phone: (919) 843-5545, fax: (814) 863-7304, email: charack@unc.edu

ABSTRACT

This paper proposes and demonstrates a new interactive framework for sensitivity-informed *de Novo* planning to confront the severe uncertainties and risks within water management problems. The framework couples global sensitivity analysis using Sobol' variance decomposition with multiobjective evolutionary algorithms (MOEAs) to generate planning alternatives and test their robustness to new modeling assumptions and scenarios. We explore these issues within the context of a risk-based water supply management problem, where a city seeks the most efficient use of a water market. The case study examines a single city's water supply in the Lower Rio Grande Valley (LRGV) in Texas, using both a 10-year planning horizon and an extreme single-year drought scenario.

INTRODUCTION

This paper uses a case study of a single city's use of market-based transfers to augment its water supply in the Lower Rio Grande Valley (LRGV) of Texas, USA [Characklis *et al.*, 2006]. The case study is used to demonstrate a new sensitivity-informed *de Novo* planning framework to promote improved problem understanding of water marketing within the LRGV. Figure 1 presents the framework. Step 1 begins with an *a priori* problem formulation that represents planners' initial conception of the problem through a quantitative model, decision variables that control strategies within the model, and objectives and constraints that measure strategies' performance. In step 2, the framework diagnoses the effect of decision variables and model parameters using Sobol' variance decomposition [Sobol, 2001]. The illustration in figure 1 shows that different variables can have a wide range of sensitivity performance across different evaluative metrics. Step 3 uses insights from the sensitivity analysis to construct a new many-objective planning problem. Objectives and constraints can be removed or added depending on their sensitivity structure or insights learned from previous iterations of the framework. Additionally,

a suite of decision variable formulations of increasing complexity are used to explore the implications of the sensitivity analysis results. This framework seeks a balance between the complexity and effectiveness of a planning formulation. Step 4 solves the *de Novo* formulations using a multi-objective evolutionary algorithm (MOEA) [Coello Coello et al., 2007; Nicklow et al., 2010]. These tradeoffs are discovered using an MOEA using the concept of Pareto optimality; a solution is Pareto optimal if it is better than any other solution in at least one objective. After a quantitative tradeoff comparing performance across decision variable formulations is developed, step 5 uses interactive visual analytics to view the tradeoffs interactively when evaluating the competing decision variable formulations.

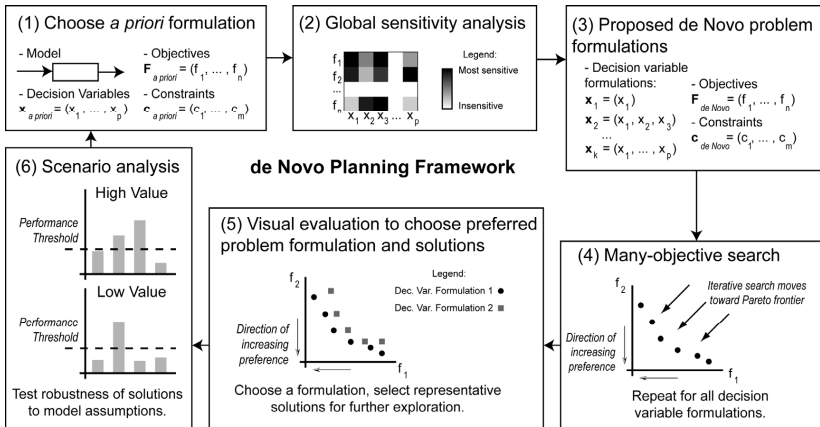


Figure 1. Overview of *de Novo* planning framework components

Use of interactive analytics represents *a posteriori* decision making, where decision makers explore our approximate Pareto-optimal sets to negotiate a choice of alternative as a final decision [Kollat and Reed, 2007]. A major benefit to this approach is that it allows the decision makers to modify their preferences and perform experiments through setting thresholds on objective function values and adding unmodeled objectives [Loughlin et al., 2001] to their analysis. Within step 5, the planners can choose the decision variable formulation that provides preferred performance compared to the other formulations. This focus on finding the non-dominated problem formulation (as compared to the classical focus on non-dominated solutions within a single static formulation) is a unique contribution of this work. Selected solutions within this preferred formulation are also used to further interrogate the effect of deeply uncertain model assumptions on the solutions' performance. Step 6 shows how deviations in model assumptions can change the performance of the selected solutions. For our case study, we use modifications of model assumptions within a drought scenario.

GLOBAL SENSITIVITY ANALYSIS

We are interested in the full multivariate controls that our permanent rights, leases, and options decisions have on a range of objectives. Are they all important? Necessary? We evaluated these questions using Sobol global sensitivity analysis [Sobol, 2001]. The approach can be classified as a variance decomposition technique which can provide insights into the 1st order single parameter effects and interactive parameter effects [Saltelli, 2002; Tang *et al.*, 2007]. In our analysis, we have divided LRGV water portfolio performance criteria into efficiency and risk metrics. Figure 2 on the subsequent page provides a summary the sensitivity rankings. In the figures total order effects represents the full sensitivity of a decision variable in terms of its individual impacts and its interactions with other decisions. First order effects represent the contribution to the model's ensemble variance by a single decision. The difference between total and first order effects provides a sense of the interactive multi-decision sensitivities. It should be noted that a high-degree of interactive effects causes search problems to be more difficult because multiple decision variables impact performance in component objectives. The results of Figure 2 show a fair level of insensitivity for many of the decision variables used by Kasprzyk *et al.* [2009] in the CASE D formulation. The permanent rights and alpha variables impacting leasing provide the strongest sensitivities across the range of metrics tested. The variables for options contracts and the Beta controls on the magnitude of transfers are shown to have a limited impact. The risk indicator metrics show a very strong degree of interaction relative to the efficiency metrics.

WHAT IS THE NON-DOMINATED PROBLEM?

The sensitivity results from Figure 2 motivate the potential to explore simplifications of the CASE D formulation from Kasprzyk *et al.* [2009]. Figure 3 provides a synopsis of 4 problem instances analyzed to determine structural changes in our many-objective water portfolio analysis. The figure shows alternative formulations of the problem from the simplest variant focused on permanent rights and the use of a single alpha trigger for options/leases to the full CASE D formulation (designated formulation IV). The second formulation uses a winter and summer risk threshold for leasing or optioning water. The third formulation adds the beta decision that provides a factor of safety by providing a percentage increase in the alpha purchasing decisions. The fourth formulation includes the full adaptive options contract, multi-period alphas, and betas. In evaluating these problems, we sorted them based on their resultant optimized many-objective tradeoffs to yield a the sorted color-coded results in Figure 4. Figure 4 provides a multiobjective evaluation of the problem formulations where a portfolio solution for any given formulation has to be nondominated in the application's six objectives (i.e., they cannot be exceeded in performance in all six objectives and have to be better in at least one objective).

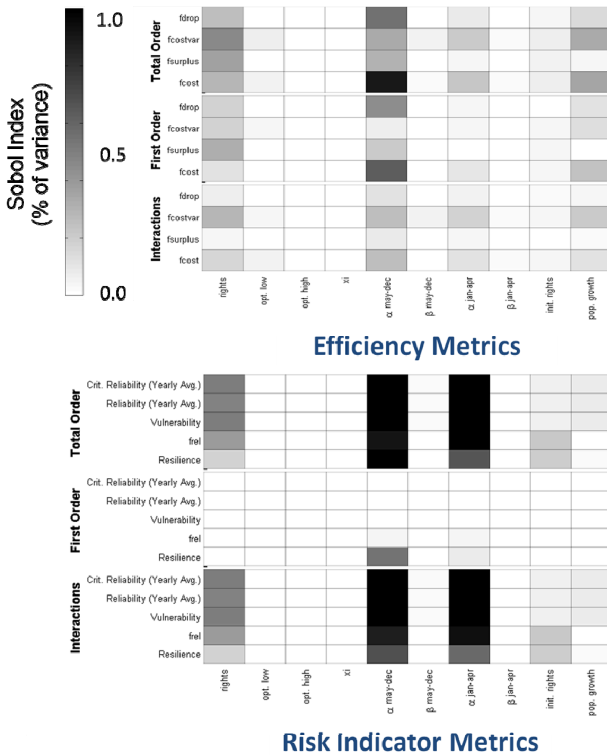


Figure 2. Metrics of interest are shown in rows while variables are shown in columns, with darker shades of gray indicating higher Sobol indices, and more sensitive parameters.

Figure 4 shows that the simplest formulation generally minimizes dropped transfers, maintains lower costs, and attains high reliabilities by using leases. Overall the results demonstrate that the more complex formulations serve to identify solution near the bounding the values of each of the six-objectives considered. In general the simplest formulation dominates the other problem instances in the compromise region of the LRGV planning problem’s tradeoffs. This has the computational benefit of potentially reducing the computational demands posed by the application while enhancing its solution.

	Volumetric Decisions	Strategy Decisions	Percent of Set
I	Permanent Rights, Static Options Contract (single-volume)	Alpha: "when / how much water to acquire"	36%
II		Alpha (Jan-Apr), Alpha (May-Dec)	20%
III		Alpha (Jan-Apr), (May-Dec): "when" Beta (Jan-Apr), (May-Dec): "how much"	18%
IV	Permanent Rights, Adaptive Options		26%

Figure 3. Decision variable sets of increasing complexity used from the simplest formulation to the full adaptive options, leasing, and permanent rights approach of formulation IV. Also shown in the percentage of solutions each formulation contributes to the best overall nondominated solutions across all formulations.

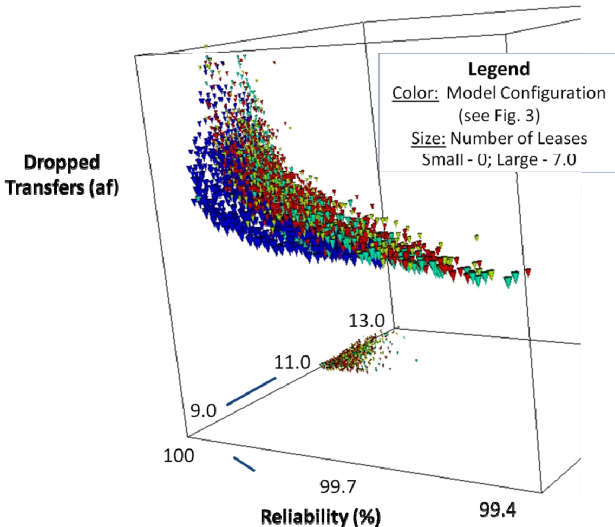


Figure 4. Reference set combining each formulation analyzed where Blue = I, Aqua = II, Yellow = III, and Red = IV from prior figure.

CONCLUSIONS

Risk-based management strategies for water systems often require the consideration of a broad range of performance metrics (cost, risk, reliability, adaptability, etc.). This increase in the complexity of the problems must be accompanied with methodological advances that allow decision makers to better understand the benefits, limits, and controls in how they represent systems with their problem formulations. This paper demonstrates a formalized de novo framework that has the potential to provide more informed, evolving representations of water management problems. The case study builds on prior results for the LRGV water market and demonstrates that a strongly simplified policy and decision representation of water portfolio planning problem can provide enhanced results. This work moves beyond classical multiobjective analysis by shifting the focus from optimal solutions towards improved problem formulations.

ACKNOWLEDGMENTS

The authors of this paper were partially supported by the United States National Science Foundation (NSF) Career grant CBET-0640443. Any opinions, findings, and conclusions or recommendations in this paper are those of the authors and do not reflect the views of the NSF.

REFERENCES

- Characklis, G., B. Kirsch, J. Ramsey, K. Dillard, and C. T. Kelley (2006), Developing portfolios of water supply transfers, *Water Resources Research*, 42(W05403), doi:10.1029/2005WR004424.
- Coello Coello, C., G. B. Lamont, and D. A. Van Veldhuizen (2007), *Evolutionary Algorithms for Solving Multi-Objective Problems*, 2 ed., Springer, New York, NY.
- Kasprzyk, J. R., P. M. Reed, B. Kirsch, and G. Characklis (2009), Managing population and drought risks using many-objective water portfolio planning under uncertainty, *Water Resources Research*, 45(W12401), doi:10.1029/2009WR008121.
- Kollat, J. B., and P. Reed (2007), A Framework for Visually Interactive Decision-making and Design using Evolutionary Multiobjective Optimization (VIDEO), *Environmental Modelling & Software*, 22(12), 1691-1704.
- Loughlin, D. H., S. R. Ranjithan, E. D. Brill Jr., and J. W. Baugh Jr. (2001), Genetic algorithm approaches for addressing unmodeled objectives in optimization problems, *Engineering Optimization*, 33, 549-569.
- Nicklow, J. W., et al. (2010), State of the Art for Genetic Algorithms and Beyond in Water Resources Planning and Management, *Journal of Water Resources Planning and Management*, 136(4), 412-432.

- Saltelli, A. (2002), Making best use of model evaluations to compute sensitivity indices, *Computer Physics Communications*, 145, 280-297.
- Sobol, I. M. (2001), Global sensitivity indices for nonlinear mathematical models and their Monte Carlo estimates, *Mathematics and Computers in Simulation*, 55, 271-280.
- Tang, Y., P. Reed, T. Wagener, and K. van Werkhoven (2007), Comparing sensitivity analysis methods to advance lumped watershed model identification and evaluation, *Hydrology and Earth System Sciences* 11, 793-817.

Risk Management of Asalouye Desalination Project

Meghdad Attarzadeh, David Kim Huat Chua, Michael Beer

Department of Civil Engineering, National University of Singapore, Block E1A #07-03, 1 Engineering Drive 2, Singapore, 117576, Tel (DID): 65-65164643

Email: Meghdad@nus.edu.sg

Abstract:

Nowadays, in the areas that are encountered with drinking water shortage, contiguity of sea with land create a facility to change salty water to drinking water using desalination plant and reverse osmosis method. The first desalination project of Iran has been completed in south of Iran in Asalouye. The project contract was registered between Noor Vijeh Company (special joint stock) and Pars Special Economic Energy Zone (PSEEZ) dependent to Oil Ministry of Iran. By this contract, Noor Vijeh Company must deliver 10000 m³/day of drinking water to PSEEZ from the lines of water delivery pipe. Type of the project contract is Build, Operate and Transfer (BOT) scheme within 21 years concession period. Delivered water price is 0.48 euro/m³ in 7 years duration from the beginning of the project and 0.375 euro/m³ for next 13 years. In this paper, the risks of the project are studied and scrutiny and risk management are performed by offering a matrix model.

Keyword: Desalination, Build Operate Transfer (BOT), risk management, Project Company, pars special economic energy zone (PSEEZ)

1. Introduction

Existence of salts and dangerous materials in the shore of Persian Gulf have created many problems for inhabitants and practitioners of Pars Special Economic Energy Zone (PSEEZ) and surrounding cities. This important problem led managers to produce drink water from sea water using reverse osmosis method. The mentioned project is a BOT project in Asalouye and now is under operation. The project contract was registered between Noor Vijeh Company and Pars Special Economic Energy Zone (PSEEZ) dependent to Oil Ministry of Iran. It has been registered in March, 2003 and has been started in April, 2004. Noor vijeh is an Iranian company that imports the equipments of salt infiltration of salty water from two European companies. Sea water is supplied from 7 shafts in shore and after the stage of filter plica, adding chemical materials and omission of particles, under pressure of 70 bars, the water is entered to sweeten water plant and after taking the salts of water the drinking water is obtained. Main parts of devices included 6 sending filters, 5 micro filters, 5 high pressure pumps, 5 SWRO units, a concrete reservoir of filtered water, a PLC system and post-treatment system. The mentioned technology has been made by two German companies, Linde and B2A. The produced desalinated water is in accordance with WHO standards. After diverging, the produced waters of Noor Vijeh Company are transferred to PSEEZ using polyethylene pipes. Project construction period is 16 months and operation period of equipments and plants is 20 years. All the builds and site operations are done by Noor Vijeh Company in 1 year duration and European company of plants and equipments guarantees installation, operation

and maintenance of the project. By an agreement, PSEEZ guarantees to supply fuel and electricity of the project. At this moment, around 5 years of project operation have been gone and capacity of drinking water production has reached 12500 m³/day [1]. This paper presents the analysis and study of risks and also assesses the existence risks of the project by offering a matrix model.

2. Overview of the consortium, finance model and the project structure

The Noor Vijeh Company obtained the project concession after participating in an international tender. This company started preparation of financial sources, formal planning and codifying steps of the plan after selection and signing the BOT contract in March, 2002. The Export Development Bank of Iran supplied the required currency convenience in order to finance partnership after economic analysis of the plan and experiences of the company in implementation. Project construction processes were finished by Noor Vijeh Company in 8 months duration. Drinking water system was tested and opened after ending the implementing operation and utilization have been started from May 11, 2005 [1]. Main contracts of this project are:

- Contract with PSEEZ (Concession Agreement)
- Financial contract
- Plan and build contract
- O&M contract
- Insurance contract

Project finance structure:

The investment that has been brought in the project is 100 billion Rials (Iran currency). 60 billion Rials of the mentioned value has been supplied by Noor Vijeh Company and 3400 Euros, as a loan, has been supplied by Export Development Bank of Iran. Reimbursement of the loan is as 2 years civic communion, 6 months interval as breathing period and 7 years payment.

- Noor Vijeh Company 60%
- Export development bank 40%

Regarding the transitive water price operated from PSEEZ to Noor Vijeh Company, 0.48 euro/m³ for 7 years from beginning and 0.375 euro/m³ for 13 years, the project IRR and NPV have been calculated 16% and 50 millions Rials, respectively [1].

Construction agreement:

Plan and construction are a type of EPC with Turnkey model. The Noor Vijeh Company is as the EPC contractor and responsible for development, plan and construction engineering, construction operation, supplying and delivery, control, supplying of the sources except energy sources and transportation and test of water infiltration equipments in according with the estimated prices and performed agreements.

O&M agreement (the operative and maintenance contract):

The O&M contract is between Noor Vijeh Company and O&M contractor including [1]: Linde company 50%, B2A company 50%

The O&M Company scopes of work are:

- Operation and maintenance of water infiltration plant except of supplying the energy sources
- Delivery of guaranteed quality water at the delivery point treated water in accordance with the provision of the BOT agreement.

Insurance agreement [2]:

The insurance policies obtained by Noor Vijeh Company include:

- All risks of construction;
- All risks of marine transit;
- All risks of Inland transportation;
- All risks of machinery;
- Business interruption;
- Salary of Workers and employer insurance;
- Third one insurance;

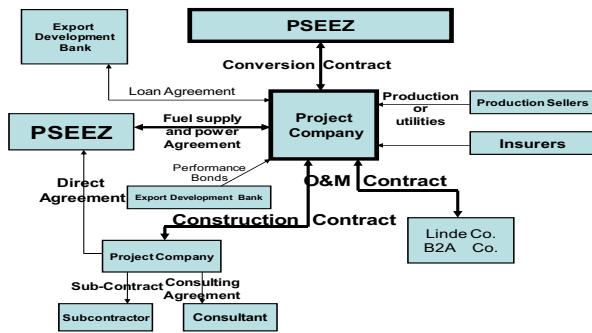


Fig.1. Project Contract Structure [2,3]

3. Risk management

Recognition, allocation and risk management are the only way for reaching to success in implementation of Asalouye desalination project that has different potentials, complex technology and huge investment. Incorrect management causes the loss of the project and waste of all investment. Success in this project is obtained when all of the project components have been satisfied at the end. The risks of the Asalouye desalination project are classified in 4 phases including political, commercial, construction and operation.

3.1. *Political risks*

These risks are caused by the government of host country and they are usually under the control of government. The risks are related to laws, tax rates, government permissions and all of things that are under government authority. These are the most important items for attraction of investors in country. Many problems in Iran related to expropriation, change in law and etc have been solved by recording the law for appreciating and support the foreign investors (FIPPA). The risk of state authorizations is under the power of government of Iran. Noor Vijeh Company must receive necessary authorizations from government for ownership, development, construction and operation of a drastic project. in the project The PSEEZ has performed all the required assistances for taking the necessary authorizations of company as the start, construction and operation of the project were performed in the scheduled dates. Political force major including war, involvement, strike, revolt, change in government, expropriation and etc should be supported by government, PSEEZ and political risk insurance. With respect to the contract duration and dangers that exist in Middle East, government must support the project company in the case of payoff, constant operation costs and required profit of company at occurrence political force major [5]. Unfortunately a problem this project is unsupported political force major by PSEEZ. problem of including installation import limitation and equipment have been solved into country by PSEEZ and custom of Iran has ordained suitable duty rate and the way has opened for equipment entrée and desalination plant to the Iran and particular zone. Perhaps during the project with change in Iran country laws engenders the risks. Important problem of change in laws are returned to the change in taxation rate than duration agreement by parties atone the all of changes including increase and or taxation rate decrease. In total, loss and damage accomplished from change in laws that it is behalf a party contract, it must repair by the other party of contract. A development security was given that it has value 1 million euro by Noor Vijeh Company to the PSEEZ. After giving concession to the project company, Development security will perform, whenever Project Company can't continue the project in during project. In this agreement described topic of judgment between party of state and party of private in case of don dispute, they should refer to internal court in Iran [2]. Maybe This problem don't product a difficult for project company that it is a Iranian company, but in total it is better for increase private sector trust, judgment will refer to laws of Outrish and laws of Newyork that they have international laws and nonpartisan.

3.2. *Commercial risks*

Every event come backing to the pecuniary problem, money rotate, profit rate, project profitable, it is historic to commercial risks. Such risks are from important problem for the project investment and finance institutes. There are some commercial risks, in this project, that PSEEZ solved their with giving fix profit rate 3% because this project is in the bereaved zone and also giving water price with hard currency (Euro) [2]. For stoppage from problem of dept payment was governed from project company to finance institutes has been water price payment in 7 years of first operation is 0.48 euro that it doesn't face with loan reimbursement problems and construction costs.

3.3. *Construction risks*

This time is including all of risks that it comes up in during construction periods and results to author increase cost and time in project. These risks are in construction contractor control and they need assistance by PSEEZ. Delays in construction complete is delay in start of operation and result to unsuccessful in dept payment that it will have a lot of risks for project. In this project attempted with closing construction contract with method Turnkey and lump sum by construction contractor and construction risk insurance, the problem of delay in construction complete and construction cost insurance minimized. Construction contractor prevents construction materials price increase and inaccessibility to them with closing long term contractors with construction materials and raw materials producers in during project. Within construction contractor must provide all of terminal Streets to project site, that nothing problem doesn't in transport. The project company must for stopping from delays, a security got from European companies of desalination equipment and plant producer for equipment installation. Producer companies of equipment must give credible birth certificate for plant ownership to project company. Plant and equipment enter from a long path from European into the Iran, an agreement done between Project Company and insurance company because prevented from plant robbery in marine transit and inland and c equipment probably damages [2].

3.4. *Operation risks*

Operation period risks happen from start of water supply and delivery and they are in operation contractor control. Delay in start of operation or suspension contains is result to costs increase and dept will become for project company and inaccessibility drink water for PSEEZ. According to agreements accomplished each delay or excessive suspension accomplished by project factors, it must repair with detriments payment. In agreement between parties stipulated that Excessive delay can result to contract revocation [2]. All necessary materials supported by Project Company in operation period as cartridge filters are for installation. The project company guarantees replacement and filter installation for 2 years after project delivery to government [1]. The text of agreement between Project Company and PSEEZ coalesced; it is include good quality and desalination plant and equipment efficiency and standard equipment about international in during project period. Project Company must get all quality guarantees on behalf of plant companies' procedure and given to PSEEZ. Also duration an agreement must install plant module system in deferent location that if error was more than 5%, plant maintenance and regulation does for problems solution and stoppage water produce decrease. Private party and plant Producer Company are responsibility all probable damage quality production water and quantity.

Table 1: Risk allocation of the Asalouye SWRO desalination plant project [2], [4]

No	Risk	Who Bear the Risk	Risk management	No	Risk	Who Bear the Risk	Risk management
1	governmental authorization	PSEEZ	The PSEEZ has performed all the required assistances for taking the necessary authorizations	13	Delay in construction finish	Project company	Closing construction contract with method Turnkey
2	Political force major	PSEEZ	Unfortunately a problem this project is unsupported political force major by PSEEZ	14	Site convenience	Project company	Preparation the all of terminal Street to project site
3	Plant import limitation	PSEEZ	custom of Iran has ordained suitable duty rate and the way has opened for equipment entrée and desalination plant to the Iran	15	Operation suspension	Project company	Each delay or excessive suspension accomplished by project factors, it must repair with detriments payment
4	Changes in law	PSEEZ / Project company	loss and damage accomplished from change in laws that it is behalf a party contract, it must repair by the other party of contract	16	Raw materials supply	Project company	The project company guarantees replacement and filter installation for 2 years after project delivery to government
5	project abandonment	Project company	A development security was given that it has value 1 million euro by Noor Vijeh Company to the PSEEZ	17	Equipment quality and efficiency	Project company	Project Company must get all quality guarantees on behalf of plant companies' procedure and given to PSEEZ
6	Dispute resolution	PSEEZ	Referring the dispute resolution to international judgship	18	Produce decrease	Project company	Water module system installation and damage payment on behalf of Project company
7	Foreign currency convertibility	PSEEZ	Water price payment with hard currency(euro)	19	Water price non payment	PSEEZ	Giving payment guarantee that supported on behalf of ministry of economical
8	The transfer of money	PSEEZ	Water price payment with hard currency(euro)	20	Unsuccessful in dept payment	Project company	On half to project company opened an offshore account that if pecuniary not to be, in during project use from said account for dept payment
9	foreign currency exchange rate	PSEEZ	Water price payment with hard currency(euro)	21	Fuel shortage and power	PSEEZ	Construction contractor and operation must give a schedule of fuel supply from operation start for store and timely energy delivery
10	Delay in plant installation	Project company	The project company must a get a security from European companies of desalination plant producer for equipment installation	22	Plant ownership	Project company	Producer companies of equipment must give credible birth certificate for plant ownership to project company
11	Construction price increase	Project company	Lump sum	23	Natural force major	Project company	Insurance companies
12	Construction materials price increase	Project company	Closing long term contractors with construction materials and raw materials producers in during project	24	Environmental damage	Project company	Company has been vast study about environmental laws in Iran and it specified government position about laws performance in during project

Table.2. Management of Political risks, commercial, construction and operation risks [2]

Risk	Government	Noor Vijeh Co (O&M Contractors)	Lender	Insurer
1. Political risks				
Revoke, expropriation, sequestration	×			
Governmental authorization	×			
Project abandonment		×		
Changes in law	×	×		
Increase in taxes				
Plant import limitation	×			
Political force major	×			×
2. Commercial risks				
Interest rate	×		×	
Foreign currency exchange rate	×		×	
Foreign currency convertibility	×			
Water price non payment	×		×	
Unsuccessful in dept payment		×		
3. Construction risks				
Construction materials supply		×		
Construction materials price increase		×		
Fuel shortage	×			
Damage on the plant		×		×
Delay in plant installation		×		
Site convenience		×		
Plant thievery		×		×
Construction price increase				
Environmental damage		×		
Natural force major		×		×
4. Operating risks				
Delay in operation		×		
Operator inability		×		
Operation suspension by means of company	×			
Equipment quality and efficiency		×		
Raw materials supply		×		
Fuel shortage	×			
Power outage	×			
Produce decrease		×		
Operation stops by means of Government	×			
Technology risk		×		
Equipment quality while transfer to Government		×		
Operating unforeseen costs		×	×	
Environmental damage		×		
Natural force major		×		×

The Produced water nonpayment on behalf to PSEEZ results to delay in project company payment to finance institute and costs increase for Project Company. In agreement discussed that all delays in the produced water payment in specific time is comeback to PSEEZ and this party is responsible dept to the export development bank of Iran and company torts. On half to noor vijeh company opened an offshore account that if pecuniary not to be, in during project use from said account for dept payment. It is for stoppage from crisis of dept payment in during project [2].

3.5. Operation and Construction risks

There are Occurrence probability some risks in both construction period and operation that it is noteworthy construction contractor and operation. They are including energy supply, natural force major and environmental. Necessary power and fuel of project was supplied by PSEEZ. PSEEZ is liable for the all probably damage timely fuel unsupplied and power. For stoppage of this problem, construction contractor and operation must give a schedule of fuel supply from operation start for store and timely energy delivery. The project company is liable all delay in energy delivery that resulted to operation suspension and dept increase. The force major happens in duration project to tow forms natural and political. If the force major happens, private party is liable all project damages. The insurance done for force major is construction insurance and plant insurance. Changes in environmental laws can result to again investment costs become that it is new system and equipment situation lieu old convenience for protection of environmental. This problem is to include operator salary and operation costs that it is attentive private party. The Noor Vijeh Company has been vast study about environmental laws in Iran and comparison its with plant and desalination technology and it specified government position about laws performance in during project [2].

4. Conclusions

The risks of this project must give to those parties has risk management ability. This problem had been done with standard agreement regulation between parties. In during operation and implementation period, three general tools for risk mitigation are used:

- Contractual undertakings, including guarantees and diaphanous agreement
- Contingency reserve fund, for extra costs cover and unforeseen in during project
- Insurance for preservation from properties and unforeseen damages cover in during project

With studies done about agreement between contract parties, shown from guarantee and insurance used for risk management during project.

Reference:

- [1]. Interview with Dr.Nasiri; juridical sector Manager of Noor Vijeh Co. (2008)
- [2]. Agreement terms and conditions among PSEEZ & Noor Vijeh Co. (2004)
- [3]. Lee. S. a. "Entry Decision for Unsolicited Build-Operate-Transfer (BOT) Highway Projects: Real options Approach", Ph.D. dissertation, Department of civil, Environmental Engineering: university of Colorado, (2007)
- [4]. S. Q. Wang, 1 L. K. Tiong 2, "Case study of government initiatives for PRC's BOT power plant project",pp. 69-78 , (2000)
- [5]. Benjamin C, Esty. "Modern Project Finance a Case Book", John Willy& sons.Inc, pp. 67-74, (2004)

Forecasting of Erosion and Debris Flow Processes Forthe Energy Supply and Transport Corridors of GeorgiaUsing the Theory of Reliability and Risk

G.V. Gavardashvili

Georgian Water Management Institute, 60, I. Chavchavadze Avenue, 0162, Tbilisi, Georgia. PH (00995 32) 234 094, FAX (00995 32) 217 300; email: givi_gava@yahoo.com

ABSTRACT

To provide forecasting of erosion and debris flow processes for the energy supply and transport corridors of Georgia using the theory of reliability and risk, we have developed a methodology on basis of the theoretical analysis and long-term field surveys (1980-2010) regarding the intensity of rains and solar radiation. At the following stage this methodology will allow us to design new safe measures against erosion and debris flow processes.

To provide study of development dynamics concerning the geometrical dimensions of ditches and gullies – characterizing values of erosion processes in the power supply corridors of oil pipelines (Baku-Tbilisi-Supsa, Baku-Tbilisi-Erzurum) and gas pipelines (Baku-Tbilisi-Shakdeniz), we have determined density distribution law on the basis of the intensity of rains and slope gradients for the case of separate and simultaneous events.

For the forecasting of erosion and debris flow processes in the transport corridors (Transport Corridor Europe-Caucasus –Asia (TRACECA) and Georgian Military Road), we have studied the types of density distribution function for the erosive and accumulating areas of the slopes and debris-flow riverbeds, which will provide safe operation of the energy supply and transport corridors.

INTRODUCTION

The Baku-Supsa Oil Pipeline enters the territory of Georgia in Gardabani district at the height of 250m a.s.l. It runs through the Kartli, Inner-Kartli, Likhi and Meskheti ridges, whose height above sea level varies from 250 to 1500m. Within Georgia's borders the length of the oil pipeline totals 273 km.

As to the Baku-Tbilisi-Ceyhan Pipeline and the Baku-Tbilisi-Shahdeniz gas pipelines, they are placed in Georgian boundaries in a single corridor of the length of 246 km, whose geography is the following: the pipeline enters in Marnauli district (220 m a.s.l.), then it crosses Gardabani, Tetrtsqaro, Tsalka, Borjomi districts (220 m a.s.l.), ending in Akhaltsikhe district at the Turkish border (see Figure 1.).



Figure 1. Diagram of the Gas and Oil Pipelines of Georgia.

For a complex assessment of the energy- and transport corridors of Georgia attention was paid to the geological, climatic landscape characteristics, as well as the state of the soil and erosional processes.

TOWARDS ASSESSING THE VULNERABILITY OF GEORGIA'S ENERGY CORRIDORS. FORECASTING THE EROSIONAL-DEBRIS-FLOW PROCESSES

In order to study the erosional process along the route of the old Baku-Supsa Oil Pipeline and the corridor of the new gas- oil pipeline of Baku-Tbilisi-Shahdeniz and Baku-Tbilisi-Ceyhan field investigations were conducted in 2000-2010.

Expeditionary field investigations were conducted along the route of the pipelines where the angle of slope of the mountain varies within $\alpha = 5^{\circ} - 37^{\circ}$ reaching greater values at some places (Gavardashvili G.V., Topuridze Z.R. (2002)).

One of the important questions in predicting erosional processes on mountain slopes is assessment of the intensity of the origin of gullies and determination of the dynamics of reformation of gullies in the ravine.

The field investigations have shown that sections of slopes adjoining gullies are usually characterized by wash-outs and ravines, the network of the latter increasing at some sections. Identification of the degree of equilibrium on mountain slopes necessitated the study of the dynamics of gullies, taking into account their geometrical dimensions. To determine the depth of gullies it was necessary to identify the runoff feeding the erosional processes, with a view to later elimination of these processes.

As is known, one of the major factors of development of these processes, along with vegetation and soil geology, is the intensity of precipitation, resulting in the formation of showers and snow cover.

In order to attain the goal formulated above the data of meteorological stations of the respective region were used, in particular, the intensity of rainfall (σ_0) of 10% provision. The values of these natural factors on the mountain routes of gas- and oil pipelines, where especially active erosional processes occur, change within: $\sigma_0 = 3,8 - 5,0(mm/min)$. Following the treatment of statistical data (390 points) the

functional link between the depth of gullies (H) and the angle of mountain slope (α), see figure 1.2 has the following form (Gavardashvili G.V., Topuridze Z.R. (2002)):

$$H = (\sigma_0 - 3,8/1,04)^{0,35} \cdot \alpha^{1,13}, \text{ (M)} \quad (1)$$

where, $\sigma_0 > 3,8(\text{mm}/\text{min})$, $\alpha = 5^\circ - 42^\circ$.

Having determined the depth of gullies (H), one must know their width (B) as well; using these parameters, at the next stage the volume of the material undergoing erosion and made part of surface runoff is calculated.

The investigation enabled to derive the dependence for (B), having the form:

$$B = \frac{9,31H^{0,94}}{\alpha^{0,6}} \text{ (M)} \quad (2)$$

where, $2^\circ \leq \alpha \leq 42^\circ$, $H > 2(\text{cm})$.

ASSESSMENT OF THE RELIABILITY AND RISK OF MOUNTAIN SLOPES

Statistical data (790 dots) allow assessment of the ecological situation of slopes, with application of reliability theory and risk.

The relative values of gullies (H/B) will be calculated according to the normal law of distribution, with account of the so-called modulus of precision (h), which is equal to (Ayyub B.M. (2003)): $h^2 = 6,2$, where σ is the mean square deviation of the relative values (H/B) of gullies, equal to $\sigma = 0,284$.

The density of distribution function has the following form (Veksler A.B., Ivashintsov D.A., Stefanishin D.V (2002)):

$$f(H/B) = 0.564 \cdot \exp\{-6.2[(H/B) - 0.724]^2\} \quad (3)$$

The probable state of the ecological situation of slopes at the emergence of gullies following water erosion is $P(H/B) = 0.421$.

The risk of break-down of gas and oil pipelines under erosional sections of mountain slopes at the emergence of gullies equals (Gavardashvili G.V., Topuridze Z.R. (2002)): $R(H/B) = 1 - P(H/B) = 0.579$.

The field investigations along the route of gas- oil pipelines in the TRACECA corridor have shown that at the end sections of gullies in most cases where the slope gradient increases ravines originate, enhancing the risk of the rise of breakdown conditions.

In order to study this problem the regularity of emergence of ravines above gas- and oil pipelines and the TRACECA corridor was investigated. The number of statistical data totaled 225 dots.

The processing of random data shows that the values (H_1/B_1) of ravines obey the normal law of distribution density:

$$f(H_1/B_1) = 0.544 \cdot \exp\{-4.249[(H_1/B_1) - 0.847]^2\} \quad (4)$$

where the modulus of precision (h_1^2) equals: $h_1^2 = 4.249$.

The probability of mountain slope at the emergence of a ravine is calculated:

$$P_1(H_1/B_1) = \int_0^2 0.544 \cdot \exp\{-4.249[(H_1/B_1) - 0.847]^2\} d(H_1/B_1) = 0.414 \quad (5)$$

The risk of break-down of gas- and oil pipelines at the emergence of ravines equals:

$$R_1(H_1 / B_1) = 1 - P_1(H_1 / B_1) = 0.586 \quad (6)$$

Carrying out an analysis and comparing the risk of break-down of gas- and oil pipelines at the emergence of gullies and ravines, we obtain $R_1(H_1 / B_1) > R(H / B)$, $0.586 > 0.579$ which corresponds to the actual development of the event.

At the emergence of water erosion in nature, on mountain slopes there occurs so-called joint negative work of gullies and ravines. In this case, the full probability of a mountain slope under the joint occurrence of gullies and ravines equals:

$$P_0 = P(H / B) \cdot P_1(B_1 / H_1) = 0.421 \cdot 0.414 = 0.174 \quad (7)$$

The risk of break-down of a gas- oil pipeline on a mountain slope at joint emergence of gullies and ravines close to the pipeline is equal to: $R_0 = 1 - P_0 = 0.826$.

On the basis of field investigations, the result obtained points to a considerable value of the risk of break-sown of gas- and oil pipelines.

ASSESSMENT OF THE EROSIONAL RISK OF MOUNTAIN SLOPES

In the Baku-Tbilisi-Supsa Oil Pipeline the loss of soil through erosional processes was estimated with the use of a universal equation (Wischmaier, Smith equation) for 56 selected sections of the corridor (Morgan R.P.C., Hann M.J. (2001)).

In order to assess the erosion risk of mountain slopes in the corridor of gas- and oil pipelines on the territory of Georgia, and on the basis of field investigations carried out in 2001-2010, with account of the specialist literature (Gavardashvili G.V. (2007)). The results of field expedition work along the route of gas- and oil pipelines allowed to make a large sample (the number of statistical data $N = 252$, with corresponding intervals and frequencies m_i) to assess the erosional level objectively.

The mathematical expectation (m_*) was calculated according to the dependence (Ayyub B.M. (2003)): $m_* = \sum_{i=1}^n f(E) \cdot \bar{E} = 3.853$. The mean value of the erosional class (\bar{E}) in the gas- and oil pipelines under study was equal to (Gavardashvili G.V. (2003)): (\bar{E}) = 4.05.

The value of deviation of the erosional class from the mean value of erosion is totaled: $\sum_{i=1}^n (E_i - \bar{E})^2 = 187.053$. The values $f(E) = m_i / N$; the root-mean-square deviation of erosion was calculated from the known relationship of the histogram and theoretical curve of level of erosion $\sigma = 0.862$.

$$f(E) = \frac{1}{\pi} \exp[-h^2 - (E - m_*)^2], \quad (8)$$

where: h is the modulus of precision, which equals: $h^2 = 0.673$.

In our case the dependence (2.5) will assume the following form:

$$f(E) = 0.564 \exp[-0.673(E - 3.853)^2] \quad (9)$$

The equation (2.7) corresponds to the normal distribution law, with account of the so-called modulus of precision (h).

The probability of the state of erosional situation of the mountain landscape in the corridor of gas and oil pipelines equals:

$$P(E) = \int_0^6 0.564 \exp[-0.673(E - 3.853)^2] dE \quad (10)$$

The integral given in the dependence (2.8) was solved by the method proposed by the French mathematician J.V. Poncelet and is equal to $P(E) = 0.523$, while the erosional risk $R(E)$. Of the mountain landscapes in the corridor of gas- and oil pipelines equals:

$$R(E) = 1 - \int_0^6 0.564 \exp[-0.673(E - 3.853)^2] = 1 - 0.523 = 0.447 \quad (11)$$

The results obtained - $R(E) = 0.477$ points to a rather considerable risk of erosion in the mountain landscapes of Georgia in the corridor of gas- and oil pipelines. Therefore, reliable work of this type of gas- and oil pipelines calls for carrying out engineering-ecological, phytoameliorative and complex measures.

FORECAST OF EROSIONAL-MUDFLOW PROCESSES IN THE TRANSPORT CORRIDORS OF GEORGIA

At present two international transport corridors are functioning in Georgia. One of them is the Georgian Military Road, being one of the shortest highways between Georgia and Russia and the second is TRACECA: Transport corridor Europe-Caucasus-Asia (Gavardashvili G.V., King L., Schaifer M. (2007)).

The scientific analysis of the investigation is based on the field expedition conducted by the author in 1981-2010 (Gavardashvili G.V. (2002)).

The purpose of the present study is investigation, using the methods of reliability theory and risk, of the regularity of natural erosional-mudflow processes, including the accumulation and transport of mud-flow debris at mountain sections of water courses.

The main factor in designing regulation structures on mudflow water courses, causing the development of river-bed erosion and determining the necessity of building hydrotechnical structures, is assessment of the sections of mudflow water courses (Gavardashvili G.V., Ayyub B. M., Sobota J., Bournaski E., Arabidze V. (2009)). The experience of conducting field investigations has shown that erosional-mudflows of various intensity occur practically annually. Analogous processes are recorded in the TRACECA corridor too (Gavardashvili G.V. (2007)).

The basic question in studying erosional processes on mudflow water courses is determination of maximum discharge of mudflows during which river-bed deformation takes place. These equations have the following form (Gavardashvili G.V. (2002)):

$$Q_{\max} = A(34 + 400i)F^{0.61} \quad (m^3 / \text{sec}) \quad (12)$$

where: i is the slope of the mudflow channel, F is the area of the catchment basin (km^2), A the empirical coefficient, whose relation to the percentage provision of mudflow discharges ($P_{\%}$) is, e.g. $P_{\%} = 0,1\%$ $A = 2,40$; $P_{\%} = 1,0\%$ $A = 1,0$.

Statistical data ($n=202$) enable the assessment of the state of ecological situation of the erosional sections of a bed of mudflow character.

The mathematical expectation (m) of the depth of erosion equals:

$$m = \sum_{i=1}^n h_i \cdot f(h) = 0.575$$

The value of the depth of erosion obeys the following distribution (Ayyub B.M. (2003), Gavardashvili G.V. (2002)):

$$f(E) = \frac{A_0}{e^h} = \frac{0.3564}{e^h} \quad (13)$$

where: A_0 is the coefficient of distribution and equals $A_0 = 0.3564$.

The probability of the ecological state of the longitudinal profile of mudflow channel at erosion of water course following the passage of a mudflow total: $P(h) = 0.264$.

The risk of a break-down of the equilibrium of the ecological situation of a longitudinal profile of mudflow channel is equal to: $R = 1 - P(h) = 0.736$.

The result obtained shows that in order to preserve the ecological situation of the longitudinal profile of a mudflow channel adjoining a transport corridor or motorway crossing a bridge it is necessary to build antierosional and anti-mudflow trapping structures.

INVESTIGATION OF THE ECOLOGICAL STATE OF A MUDFLOW CHANNEL AT DEPOSITION OF MUDFLOW DEBRIS ON A WATER COURSE

Accumulation of mudflow-debris in the channel results from the diminishment of the gradient of the water course profile. Reduction (in comparison with the original state) of the longitudinal slope facilitates the stabilization of the erosional slope of the erosional activity at the section of the checking of mudflow discharges, at transit sections of the channel or at debris cone (Gavardashvili G.V. (2007))

In order to determine the effect of the river sections just cited on the attenuation of the activity of a mudflow bed the state of the channel should be assessed qualitatively with the aid of reliability theory and risk (Gavardashvili G.V., King L., Schaifer M. (2007))

Full-size investigations carried out on the river Chadistsikhis Khevi enable the assessment of the ecological state of the mudflow channel, taking into account the accumulation of mudflow debris (the number of statistical data: 110 dots).

The mean value of the height of accumulation of mudflow debris (h_1) on the

River Chadistsikhis – Khevi equals: $\bar{h}_1 = \sum_{i=1}^n h_i / N = 87.75 / 110 = 0.79$

The value of deviation of the depth of accumulation from the mean value of accumulation depth equals: $\sum_{i=1}^n (h_1 - \bar{h}_1)^2 = 45.56$. The deviation of the height of

mudflow debris totals: $\sigma_1 = \sqrt{\sum_{i=1}^n (h_1 - \bar{h}_1)^2 / N} = 0.645$. The theoretical curve corresponds to

the Cauchy distribution law (Gavardashvili G.V. (2002)), whose formula has the following form:

$$f(h_1) = \frac{1}{\pi(1+h_1^2)} \quad (14)$$

The probable stability of the longitudinal profile at the section of the mudflow bed, where mudflow debris accumulates, equals:

$$P_1(h_1) = \int_0^{3.2} \frac{dh_1}{\pi(1+h_1^2)} \quad (15)$$

The integral given in the dependence (15) was solved by the method proposed by G.V. Poncelet (Gavardashvili G.V. (2002)) and is equal to: $P_1(h_1) \approx 0.51$. The risk of the breakdown of the stability of the longitudinal profile of the bed, with account of the accumulation of mudflow debris at the section of equilibrium, totals: $R_1(h_1) = 0.49$.

The analysis, carried out, shows that the probability of the stability of the longitudinal profile, with account of the erosion of the river bed following the passage of the mudflow, is lesser than in the bed of accumulation of mudflow debris ($0.265 < 0.51$).

Naturally, the risk of deformation of the longitudinal profile of a mudflow channel at erosion is greater than in the case of accumulation of mudflow debris, i.e. $0.736 > 0.490$, conforming to channel deformation in full-scale conditions.

In the nature of channel deformation, including in water courses of mudflow character, erosion and accumulation in the channel occur synchronously. In this case, the full probability of the stability of the longitudinal profile of the mudflow bed, at simultaneous occurrence of erosion and accumulation, will equal:

$$P_0 = P(h) \times P_1(h_1) = \left(\int_0^{2.3} \frac{0.3564}{e^h} dh \right) \times \left(\int_0^{3.2} \frac{1}{\pi(1+h_1^2)} dh_1 \right) = 0.264 \times 0.51 \approx 0.14 \quad (16)$$

The risk of preservation of the stability of the longitudinal profile of a mudflow bed at synchronous occurrence of erosion and accumulation in the bed amounts to:

$$R_0 = 1 - P_0 = 0.86 \quad (17)$$

The result obtained - $R_0 = 0.86$ points to a great risk of breakdown of the stability of the longitudinal profile of the natural water course of the River Chadistsikhskhevi. Therefore, in order to render the river invulnerable antierosional or antimudflow hydrotechnical structures should be built to regulate the channel.

CONCLUSIONS

- On the basis of field investigations, carried out in 2000-2010 along the route of the Baku-Tbilisi-Supsa oil pipeline, the erosional processes on mountain slopes were studied, in particular the peculiarities and statistics of the origin of gullies and ravines. In order to assess the vulnerability of mountain slopes the quantitative indices of the reliability of slopes and the risk of breakdown of oil pipelines were determined. The distribution density of gullies and ravines was determined for the assessment of mountain slopes. Taking the above said into account, the results of the investigation point to the need for a remission of anti-

- erosional measures, worked out earlier, for mountain slopes, and creation of reliable and cost-effective hydrotechnical antierosional structures.
- An analysis of the field work carried out in the gas- and oil pipeline corridors: Baku-Tbilisi-Shahdeniz (gas pipeline), Baku-Tbilisi-Ceyhan (oil pipeline), and on the basis of reliability theory and risk, the function of distribution of the erosional class of mountain slopes was identified, obeying the law of normal distribution, with the so-called modulus of precision.
 - Using the reliability theory, the density of the distribution of the depth of washout and height of accumulation of mudflow debris in the case of the passage of a mudflow of catastrophic force has been determined in the transport corridors of international significance. To assess the vulnerability of the transport corridors of Georgia, the deformation processes in water course channels have been determined, with account of climate change. Therefore, the investigations carried out have given ground to recommend use of the proposed method. This will allow to implement engineering-ecological measures effectively, not only in the basin of the water course under study but in other mudflow water courses of Georgia, lying in transport corridors of the South Caucasus region as well.

References

- Ayyub B.M. (2003). Risk Analysis Engineering and Economics – A CRC Press Company. Boca Raton, London, New York, Washington, D.C. , 571 .
- Gavardashvili G.V., King L., Schaifer M. (2007). Debris Flows at the river Mletis-khevi (Greater Caucasus Mountains, Georgia) and its Assessment. Methods. Center for International Development and Environmental Research. Giessen University. № 32, Giessen, Germany. 15. (in English). www.unigiessen.de.
- Gavardashvili G.V., Ayyub B. M., Sobota J., Bournaski E., Arabidze V. (2009). Simulation Of Flood And Mudflow Scenarios In Case Of Failure Of The Zhinvali Earth Dam. International Symposium (With The Support Of Unesco) On Floods And Modern Methods Of Control Measures. 23-28 September, Tbilisi, Georgia, 148-163.
- Gavardashvili G.V. (2008). New designs of spring-board type drift-trapper and the methodology for their calculation. Materials of the 14th International Conference on Transport and Sedimentation. June 23-27. St. Petersburg, Russia, 128-136 (in English).
- Gavardashvili G.V. (2002). Estimation of Ecological Equilibrium of Debris-Flow River-beds Along Georgian Military Road Using the Theory of Reliability and Theory of Risk.//Engineering Ecology, Moscow, #2, 11-17(in Russian).
- Gavardashvili G.V. , Topuridze Z.R. (2002). Reliability of Mountain slopes within the corridor of Baku-Supsa oil export pipeline in Georgia.//Engineering Ecology, Moscow, #5, 39-47(in Russian).
- Gavardashvili G.V.(2003).Estimation of Erosion Situation of Georgian Mountain Landscapes in the Gas and Oil Pipeline corridor .//Engineering Ecology, Moscow, #6, 51-57(in Russian).
- Morgan R.P.C., Hann M.J. (2001). Shah Deniz Gas Export :erosion risk assessment.//Interim Report to PB Kvaerner. Grandfield University, UK, Silsoe, , 25.

Probabilistic Dominance Application to the Sacramento-San Joaquin Delta

Jay R. Lund

Director, Center for Watershed Sciences
Professor, Department of Civil and Environmental Engineering
University of California - Davis

jrlund@ucdavis.edu

Abstract

The concept of probabilistic dominance is developed for making multi-objective decisions where there is uncertainty regarding the performance of alternatives. This approach combines traditional the ideas of Pareto optimality and stochastic dominance for comparison of alternatives with both multiple criteria and uncertainty. A simple application is made for the strategic decision of an approach for continuing or ending water exports from the Sacramento-San Joaquin Delta in California.

Introduction

Most decision-making involves both multiple objective and uncertainty. These two aspects of real decisions often make decision analysis one heck of a mess. Many approaches are available for such problems (Arrow and Lind 1970; de Neufville 1990; ReVelle, et al. 1997). A simple approach to this problem is probabilistic dominance, which evaluates the Pareto-optimality of decision alternatives in a probabilistic framework. The performance of each alternative in multi-objective space is first quantified as a probability distribution. The probability that each alternative dominates all other alternatives (or specific alternatives) is then evaluated, in a Pareto-optimal sense.

This paper develops the mathematics of probabilistic dominance for a simple case of uniformly distributed performance on two objectives. This method is then applied to strategic water supply alternatives for water exports from California's Sacramento-San Joaquin Delta, summarizing earlier work (Lund, et al., 2008, 2010). Some conclusions follow.

Probabilities of Superior Performance

Consider a decision problem involving four alternatives (A, B, C, and D) with two objectives (fish viability and economic cost) and uncertain, but uniformly distributed performance. If the boxed areas in Figure 1 represents evenly distributed likelihood of cost and environmental performance for each alternative, then we can calculate the probability of each alternative having superior performance for each objective, separately and together. This indicates the probability of Pareto-optimality for each alternative (Cohon 1978). Others have explored similar ideas in application to multi-objective optimization using evolutionary algorithms (Teich 2001; Fieldsend and Everson 2005) and surgical decisions (Hudgins 1994).

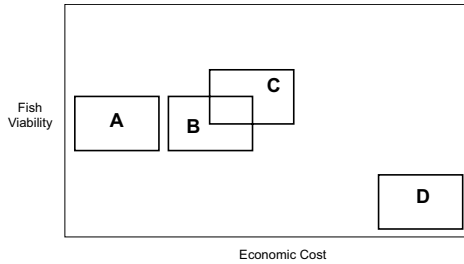


Figure 1 - Performance and Superiority

Figure 1 illustrates this concept. For this case, alternative D is clearly inferior to alternatives A, B, and C, never having a possibility of performing better than A, B, or C on either fish or economic objective. Let $P(A \geq B)$ be the probability that alternative A is superior to alternative B. Then, from Figure 2, $P(A \geq D) = P(B \geq D) = P(C \geq D) = 1$ for either objective and for both objectives taken together.

Alternative A is always superior to B in terms of cost. Half the time A will be superior to B in terms of fish viability, with an equal probability that B will be superior to A for fish. Overall, there is a 50% chance that A is superior to B for both fish and cost.

If C overlaps area B by 25%, as shown with the southwest corner of C at the centroid of B, there is a 87.5% chance that C is better for fish than B (or A) ($=0.5 + 0.5(0.5+0.25)$), with a 12.5% chance that B (or A) is better for fish ($=0.5*0.5*0.5$). For cost, there is a 87.5% chance that B is superior to C, and 12.5% chance that C is better than B. Overall, there is a 10.9% chance that B is superior to C for both objectives, and a 10.9% chance that C is superior to B for both objectives. C will never be superior to A for both objectives, but there is a 12.5% chance that A is superior to C for both objectives. For the remaining probability, each alternative would be better on a different objective, indicating a performance trade-off requiring a value judgment. These calculations are more fully explained in the following section.

Assuming that performance is equally likely over the entire region and not more concentrated near the middle of each area probably means that these calculations are, for the overlapping comparisons, somewhat skewed for overlaps of corners far from the centroid of an alternative's performance region.

A More Formal Derivation

Given two alternatives, each with uncertain and probabilistic performance on two objectives, what is the probability that the actual (point) performance of each alternative will be superior (non-dominated or Pareto-optimal) relative to the other? Consider the problem as in Figure 2, with the assumption that more of Z1 is inferior and more of Z2 is superior, so ideal performance is in the Northwest corner of the diagram.

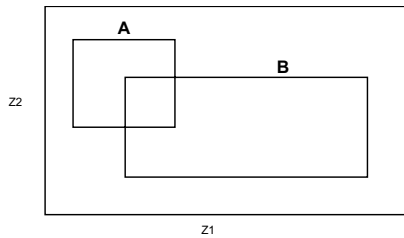


Figure 2 - Performance and Superiority for Two Overlapping Alternatives

Let actual performance of alternatives A and B be points in this multi-objective space, but our knowledge of their future performance is only given by probability distributions $P_A(Z1, Z2)$ and $P_B(Z1, Z2)$. What is the probability that alternative A will be superior to B in terms of each objective and what is the probability that the performance of A will be superior to B for both objectives (i.e., B is a dominated solution)?

Let $P(AsB)$ be the probability that A is superior to B for both objectives, and let $PZi(AsB)$ be the probability that A is superior to B with respect to objective i.

To define overall probabilistic dominance or superiority of A over B,

$$P(AsB) = \int_{-\infty}^{\infty} \int_{-\infty}^{\infty} \left(P_A(Z_1, Z_2) \int_{Z_1}^{\infty} \int_{-\infty}^{Z_2} P_B(z_1, z_2) dz_2 dz_1 \right) dZ_1 dZ_2,$$

where the probabilistic performance of each alternative is independent. If the probabilistic performance of alternative B is a joint probability with alternative A, then

$$P(AsB) = \int_{-\infty}^{\infty} \int_{-\infty}^{\infty} \left(P_A(Z_1, Z_2) \int_{Z_1}^{\infty} \int_{-\infty}^{Z_2} P_B(z_1, z_2 | A(Z_1, Z_2)) dz_2 dz_1 \right) dZ_1 dZ_2,$$

where $P_B(z_1, z_2 | A(Z_1, Z_2))$ is the probability distribution of B's performance given A's performance at Z_1, Z_2 .

For a single objective, the probability that A is superior to B is

$$PZ1(AsB) = \int_{-\infty}^{\infty} \left(P_A(Z_1) \int_{Z_1}^{\infty} P_B(z_1) dz_1 \right) dZ_1$$

for independent probabilistic performance, where less of objective Z1 is better. Where more of objective Z2 is better,

$$PZ2(AsB) = \int_{-\infty}^{\infty} \left(P_A(Z_2) \int_{-\infty}^{Z_2} P_B(z_2) dz_2 \right) dZ_2$$

This should apply to any two alternatives in a two-dimensional performance space. Higher dimensional objective spaces can be incorporated with the suitable additional integrals.

Consider special conditions where the point performance of A and B are independent probability distributions, each of which is uniform between different ranges of performance on each objective, with some overlap of these distributions as in Figure 2. Overlapping and partially overlapping sub-areas of each distribution can be defined as in Figure 3.

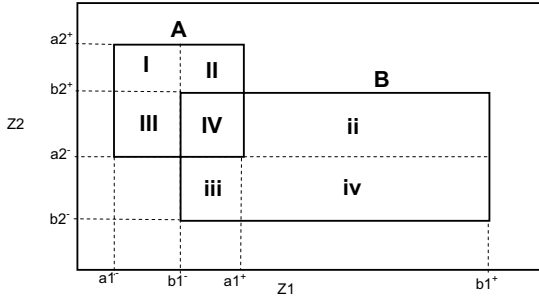


Figure 3 - Performance and Superiority for Two Overlapping Objectives - Detailed

$$P(AsB) = \frac{I}{A} + \frac{II}{A} \left(\frac{ii + iv}{B} + 0.5 \frac{IV + iii}{B} \right) + \frac{III}{A} \left(\frac{iii + iv}{B} + 0.5 \frac{IV + ii}{B} \right) + \frac{IV}{A} \left(\frac{iv}{B} + 0.5 \frac{ii + iii}{B} + 0.25 \frac{IV}{B} \right)$$

where A is the total area of A, B is the total area of B, each Roman number represents a different quadrant area, as shown in Figure 3. If A falls in area I, there is 100% chance that A is superior to B for both objectives. If A falls in area II, there is 100% chance of A being superior for both objectives if B falls in areas ii or iv, and a 50% chance of A being superior if B falls in areas IV or iii. If both A and B fall in area IV, there is a 25% chance of A being superior to B and an identical chance of B being superior to A for both objectives. With complete overlap for both objectives, there is a 25% change of dominance. With an overlap for one objective, there is a 50% chance of dominance for that objective. When there is no overlap for any individual objective dimension, one solution will completely dominate the other.

The area-based equation above can be expanded to the coordinate-based equation:

$$P(AsB) = \frac{(a2^+ - b2^+)(b1^- - a1^-)}{A} + \frac{(a2^+ - b2^-)(a1^+ - b1^-)}{AB} \left((b2^+ - a2^-)(b1^+ - a1^+) + (a2^- - b2^-)(b1^+ - a1^+) + \frac{(b2^- - a2^-)(a1^+ - b1^-) + (a2^- - b2^-)(a1^+ - b1^-)}{2} \right) + \frac{(b2^- - a2^-)(b1^- - a1^-)}{AB} \left((a2^- - b2^-)(a1^+ - b1^-) + (a2^- - b2^-)(b1^+ - a1^+) + \frac{(b2^- - a2^-)(a1^+ - b1^-) + (b2^- - a2^-)(b1^+ - a1^+)}{2} \right) + \frac{(b2^+ - a2^-)(a1^+ - b1^-)}{AB} \left((a2^- - b2^-)(b1^+ - a1^+) + \frac{(a2^- - b2^-)(b1^+ - a1^+) + (a2^- - b2^-)(a1^+ - b1^-)}{2} \right)$$

$$+0.25 \frac{((b2^+ - a2^-)(a1^+ - b1^-))^2}{AB}$$

If terms are given values of zero when they become negative, this equation should be generalizable without foreknowledge of the geometric arrangement of alternatives in objective space. The calculations are much simpler when the alternatives overlap on only one objective, or if they do not overlap at all. Where probabilities of performance are independent, the product of the probabilities of dominance for each single objective is the probability that an alternative is superior for all objectives.

Application – Water Exports from California’s Sacramento-San Joaquin Delta

Much of California’s water supplies currently relies on exports of water from the Sacramento-San Joaquin Delta. About 15% of all water used for urban and agricultural purposes in California comes through the Delta. With sea level rise, land subsidence, earthquakes, and climate change, it becomes more likely that the subsided lands of the Delta will again become inundated and salty enough to either eliminate or greatly reduce these water exports (Lund et al. 2010).

Four strategic approaches are available to address this problem. Water exports can be:

- a) continued through the Delta, with repairs and damage incurred when islands fail,
- b) diverted upstream from the Delta through a peripheral canal or tunnel,
- c) taken both through the Delta and around the Delta (dual conveyance), or
- d) ended completely, probably being phased out over time.

These four approaches are compared on two types of objectives: maintaining the viability of native fish populations and economic cost to California. The details of this analysis can be found in Lund et al. (2008, 2010) and related technical appendices.

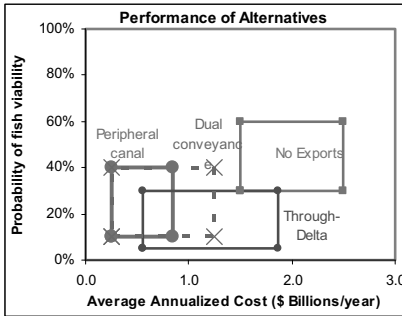
Summary of Results

Results are prepared for three objectives: (1) statewide economic costs, (2) the probability of viable delta smelt populations (sufficiently healthy to remove ESA restrictions on water exports), and (3) the probability of a viable fall run Chinook salmon fishery. Table 1 summarizes the performance of the four strategic alternatives, given the ranges of costs and performance and analysis detailed and justified by Lund et al. (2008). These results illustrate the use of the spreadsheet to compare the performance of the four strategic alternatives with more than one environmental objective. This is done by varying the fish viability probabilities for different spreadsheet “runs.”

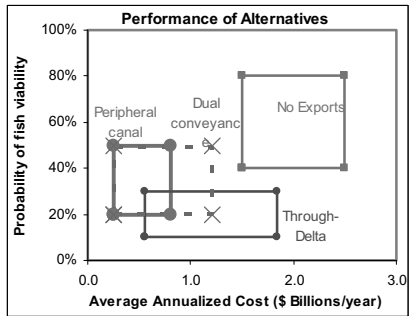
Figure 4 depicts these results in multi-objective graphics. There is clearly uncertainty in the ranges of environmental and economic performance for each strategic Delta alternative. For ending exports, costs are likely to range from \$1.5 billion per year to \$2.5 billion per year, with the probability of viable delta smelt populations ranging from 30 percent to 60 percent. While this represents considerable uncertainty, these results offer some insights for comparing these strategic alternatives.

Table 1 - Estimated range of annual economic cost and fish viability for Delta export alternatives, 2050

	Low Estimate	High Estimate
Continuing through-Delta exports		
Average annualized cost (\$ billions/year)	0.55	1.86
Probability of viable delta smelt population (%)	5	30
Probability of viable Chinook salmon fishery (%)	10	30
Peripheral canal		
Average annualized cost (\$ billions/year)	0.25	0.85
Probability of viable delta smelt population (%)	10	40
Probability of viable Chinook salmon fishery (%)	20	50
Dual conveyance		
Average annualized cost (\$ billions/year)	0.25	1.25
Probability of viable delta smelt population (%)	10	40
Probability of viable Chinook salmon fishery (%)	20	50
Ending Delta exports		
Average annualized cost (\$ billions/year)	1.50	2.50
Probability of viable delta smelt population (%)	30	60
Probability of viable Chinook salmon fishery (%)	40	80



(a) Delta smelt fishery



(b) Fall-run Chinook salmon

Figure 4 - Range of costs and fish population viability for Delta export alternatives, 2050

The results reveal some clear distinctions along both the environmental and economic criteria (Table 1 and Figure 4). The no exports alternative presents some of the best potential outcomes for fish, but also the highest likely costs to the economy, given the need to reduce water use and draw on more costly sources. Continuing through-Delta exports has an intermediate range of economic costs and the lowest range of likely outcomes for both fish species. The peripheral canal, followed by dual conveyance,

has the lowest range of costs, and these alternatives present medium-range opportunities for fish (Figure 4).

However, given the levels of overlap among alternatives for both fish and economic outcomes, the question arises: How likely is it that each alternative will outperform the others? If the likelihood of performance is assumed to be spread evenly and independently over the ranges in Figure 4, we can calculate the probability that each alternative performs better than any other alternative for any single objective or combination of objectives (fish viability and statewide economic cost). Results of these calculations appear in Table 2, with delta smelt viability as the environmental objective

“No exports” appears to be strongly superior to the other alternatives for the fish (probabilities of 94 to 100 percent). These numbers are reversed for economic performance (where ending exports has a 5 percent chance of outperforming through-Delta exports, and no chance of outperforming a peripheral canal or dual conveyance). Even though there is significant overlap between the ranges for the peripheral canal/dual conveyance alternatives and the through-Delta alternative, the through-Delta alternative is clearly inferior when considered over the entire range of potential outcomes. It has a 73 percent chance of performing less well for the fish and a 94 percent change of performing less well from the standpoint of statewide economic costs. Taking both objectives together, the odds of through-Delta performing better than a peripheral canal round up to 2 in 100.

Table 2 - Probabilities That Each Export Alternative is Superior to Others, With Delta Smelt Viability as the Environmental Objective (%)

Alternatives	Delta Smelt	Statewide Cost	Both Objectives*
Through-Delta better than peripheral canal	27	6	1
Through-Delta better than dual conveyance	27	19	5
Through-Delta better than no exports	0	95	0
Peripheral canal better than no exports	6	100	6
Peripheral canal better than through-Delta	73	94	69
Dual conveyance better than no exports	6	100	6
Dual conveyance better than through-Delta	73	81	60
No Exports better than peripheral canal	94	0	0
No Exports better than through-Delta	100	5	5

Notes: * If probabilities of performance are independent, then the probability of superiority for both objectives is the product of superiority on the individual objectives.

Expansions

This simple application illustrates how much can be known for multi-objective decision analysis, even when there is considerable uncertainty in performance. While the approach is fairly simple, it is also likely to be fairly robust and support the communication of analytical insights and uncertainties to decision-makers.

Some extensions of this approach are certainly possible. Some non-uniform probability distributions of performance might be examined analytically, and more general and even odd probability distributions of performance might be analyzed for probabilistic dominance numerically. Similarly, probabilistic dominance in more than two dimensions of performance also can be examined analytically for simple cases and numerically for more complex cases.

Conclusions

Despite years of fascinating scholarship and applications of multi-objective methods, we have not yet finished with the development and application of fairly simple methods for providing insight to decision-makers on multi-objective problems. Probabilistic dominance has potential for developing and communicating useful insights from probabilistic decision analyses for policy-makers.

References

- Arrow, K.J. and R.C. Lind (1970), "Uncertainty and the evaluation of public investment decisions," *American Economic Review*, Vol. 60, No. 3, June, pp. 364-378.
- Cohon, J.L. (1978), *Multiobjective Programming and Planning*, Academic Press, NY.
- de Neufville, R. (1990), *Applied Systems Analysis*, McGraw-Hill, NY.
- Fieldsend, J.E. and R.M. Everson (2005), "Multiobjective optimisation in the presence of uncertainty," *2005 IEEE Congress on Evolutionary Computing*, proceedings.
- Hudgins, W.R. (1994), "Patients' Attitude about Outcomes and the Role of Gamma Knife Radiosurgery in the Treatment of Vestibular Schwannomas," *Neurosurgery*, Vol. 34(3), March, p 459-465.
- Lund, J., E. Hanak, W. Fleenor, W. Bennett, R. Howitt, J. Mount, and P. Moyle, *Comparing Futures for the Sacramento-San Joaquin Delta*, University of California Press, Berkeley, CA, February 2010.
- Lund, J., E. Hanak, W. Fleenor, W. Bennett, R. Howitt, J. Mount, and P. Moyle, "Decision Analysis of Delta Strategies," Appendix J to *Comparing Futures for the Sacramento-San Joaquin Delta*, Public Policy Institute of California, San Francisco, CA, July 2008.
- ReVelle, C.S., E.E. Whitlach, and J.R. Wright (1997), *Civil and Environmental Systems Engineering*, Prentice-Hall, Upper Saddle River, NJ.
- Teich, J. (2001), "Pareto-front exploration with uncertain objectives," in E. Zitzler, et al, (eds.), *Evolutionary Multi-Criterion Optimization*, First International Conference, EMO 2001 Zurich, Switzerland, March 7-9, 2001 Proceedings, Springer-Verlag, Berlin, pp. 314-328.

Capacity Planning Under Nonstationary Uncertainties

Neela P. Babu, Jan Kuakkel, Daniel P. Loucks, Warren E. Walker

Abstract

A typical problem facing engineers when designing infrastructure to serve future demands is that those future demands are unknown, or at best uncertain. With respect to water supply systems, not only are future demands uncertain, so are the supplies that will be available to meet those demands. Traditionally engineers have based their design capacity estimates based in part on the statistical characteristics of past hydrological records. Today we recognize we can no longer make such assumptions. The past does not necessarily reflect what will happen in the future given the impacts of changes in climate and land cover and use. These changes together with changes in human populations, their age and spatial distributions, their standards of living, and their activities alter the demand for water along with the spatial and temporal distributions and amounts of runoff. Hence we face both demand and supply uncertainty where even the probability distributions of those possible values are unknown. Whatever those distributions will be, increased variability of supply is almost certain, and this in turn strengthens the argument for increased infrastructure capacities in advance of when they are needed. Some of this infrastructure, such as reservoirs and major water supply diversions, will be designed to last for the next 100 years or longer. The capacities of such projects are not easily expanded or reduced as the changes in stochastic nature of demand requirements and available supplies become more certain. One cannot monitor and then alter capacities accordingly in some adaptive framework as might be possible with respect to operating policies. How do we decide what capacities to build now that will affect our ability to serve those living in the next 100 years or so? Do we just apply engineering 'safety factors'? This paper attempts to address this question.

Introduction

If uncertainty affects our ability to adequately predict even the probability distributions of possible future water demands and supplies, this in turn makes it difficult to predict even the probability distributions of the future impacts of any existing or proposed water resource system of interest. Such problems are sometimes referred to as decision-making under deep uncertainty (Lempert et al., 2002), or severe uncertainty (Ben-Haim, 2006). Available modeling techniques struggle to offer useful decision support for such decision-making problems. Perhaps this problem can be overcome by using the available modeling techniques not to attempt to predict a future, but in an exploratory way to define the degree of system robustness to many possible futures, using a lot of sensitivity analyses and judgment. We will illustrate this argument with an example later in this paper.

Uncertainties surrounding changes in climate, technological developments, and human populations and their activities, as well as changes in the cost of materials, the discount rates on borrowed money, and impacts of water management on the natural and built environment, all make it difficult to predict the expected consequences of the different options that are considered in any long-run decision-making problem involving the selection of capacities that cannot easily be changed over time. Uncertainty has always been a problem, specifically when the future is involved. Throughout history farmers who count on rain to grow crops must make planting and harvesting decisions in the face of uncertainty about the weather. These decisions can

change from one growing period to another. All of us, we assume, are making decisions on how to invest our savings for long-term growth, not just for short-term income. This is again an example of decision-making under considerable uncertainty, as we all know too well. Given that decision-making under uncertainty pervades many areas of human activity, it is not surprising that a wide variety of analytical tools and techniques have emerged that offer decision support. Mathematical models form the core of many such decision support methods. Many of the model-based decision support methods applied to water resource systems rely on some historical hydrological data together with an assumption that past hydrological events are at least somewhat relevant for thinking about the future.

Exploratory Modeling and Analysis

Exploratory Modeling and Analysis (EMA) can be used to address questions such as “Under what circumstances would a particular decision do well? Under what circumstances would it likely fail?” The basic steps in EMA are: (i) develop a relatively fast and simple model of the system of interest; (ii) generate an ensemble of possible, but not necessarily likely, future worlds; (iii) specify a variety of policy options; (iv) calculate and compare the performance of the various options across the ensemble of future worlds; all in an effort to come to some conclusion about what to do. Obviously there are other well-established techniques, such as optimization modelling, Monte Carlo sampling and the use of artificial neural networks that can be usefully and successfully employed in the context of EMA (Walker, 2000).

An Illustration

There are two specific water system design questions one can try to answer using EMA. First, given the ranges of uncertainties that impact the performance of a water resource system, what is the range of design (capacity) decisions that should be considered? Second, given a particular design decision, how well does it perform over a range of possible future conditions? One can then see where, if any, the system performance becomes unsatisfactory, and from this, what measures might be taken to avoid such adverse events.

Consider the water resource system shown in Figure 1. It is based on an ongoing planning and design study taking place in the Middle East. A reservoir near the border of two countries is being proposed to provide irrigation water to local farmers, to increase the reliability of meeting the agreed quantity of water to be released to the neighboring country, and importantly, to transfer water to a natural lake to help replenish its volume and restore its ecosystem. Over the past decade the lake volume has been substantially reduced due to decreased inflows resulting from upstream diversions of water for agriculture. This man-made drought has degraded the natural ecosystem of the lake.

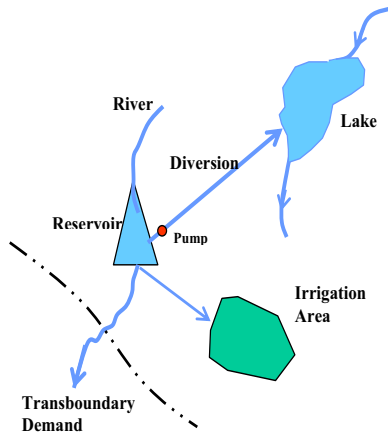


Figure 1. Water Resource System in which the active storage capacity of the reservoir is to be determined.

This proposed reservoir will likely operate over the next 100 years or so, and hence the issue is just how much active storage capacity should be provided given assumed diversion demands but an uncertain inflow probability distribution and associated statistical characteristics. Similarly we do not know what the changes in demands may be over this period either, but for this example we will assume they are specified and fixed. Once the reservoir is built, altering its capacity becomes difficult because of an unacceptably high political as well as economic cost. Hence the reservoir capacity decision made now must apply for subsequent century.

We begin with a set of models for generating a sequence of possible inflows. Each model contains parameters, such as the mean, standard deviation and serial correlation of flows, whose values are typically based on historical data. Then we alter the models by multiplying the mean flow by a factor that either increases or decreases that value. We call this parameter α . Next we introduce an exaggeration factor, that increases the difference between the actual generated flow and the new mean. This we call β . We also alter the standard deviation and correlation coefficients. For various 'reasonable' values of each of those four parameters we obtain time series of flow sequences that seem to be reasonable in a new climate regime, where the extremes are more severe, and longer in duration. Figure 2 shows the impact of various values of α and β on the sequences of flows from a particular flow generation model.

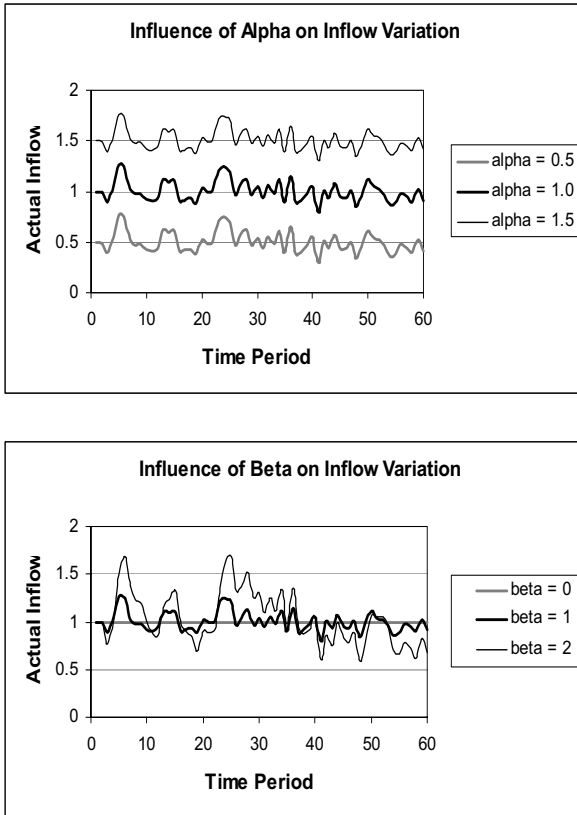


Figure 2 Plots showing impact on reservoir inflows associated with changes in α assuming $\beta = 1$, and associated with β , assuming $\alpha = 1$. The historical mean inflow is 1 and the new mean is therefore α .

We can then use these generated sequences of flows in an optimization or simulation model to estimate the reservoir capacity that is required to meet the demand targets and, gives us a tradeoff between the reliability of meeting those targets and the maximum deviation or vulnerability when a failure occurs (see for example Loucks and van Beek, 2005). Of interest in this paper is the influence of changes in some of those parameters on the active storage reservoir capacity needed to meet the specified demands. The percent of the flow scenarios that satisfy the demand given a particular reservoir capacity is what we call the robustness of that capacity. In this example the reservoir release demand equals the historical mean flow. The relative reservoir capacity is actual capacity divided by historical mean flow.

Figure 3 illustrates the impact of various ranges of α on the robustness of any particular value of relative reservoir capacity. The relative reservoir capacity is the actual capacity divided by mean flow. In this figure the serial correlation is assumed no less than 0, and the parameter β ranges from 1 to 1.9.

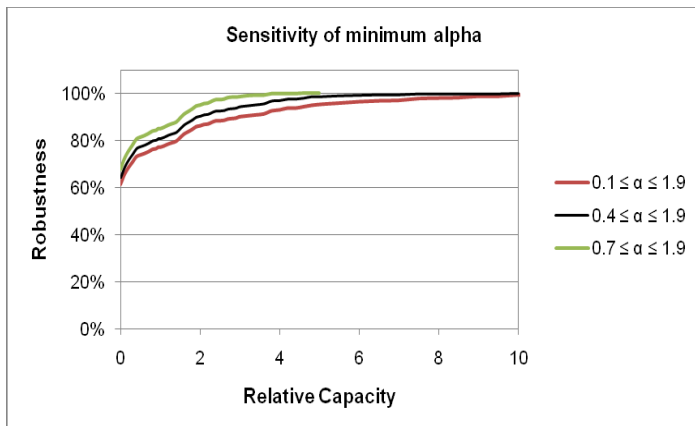


Figure 3. Sensitivity of reservoir capacity robustness values to various ranges of the mean flow multiplier, α . For this illustration the serial correlation ranges from 0 to 1, and beta ranges from 1 to 1.9.

The robustness of any particular reservoir capacity is only one performance measure that can be considered when deciding on how much capacity to build. Cost is another. Clearly there is a tradeoff between cost and robustness. The larger the capacity the more robust it is, but it also costs more. Figure 4 shows this tradeoff. Just as for life or health insurance, we can chose to accept more risks and incur a lower cost of construction, or we can spend more for more insurance, even though we are not sure we will ever need it.

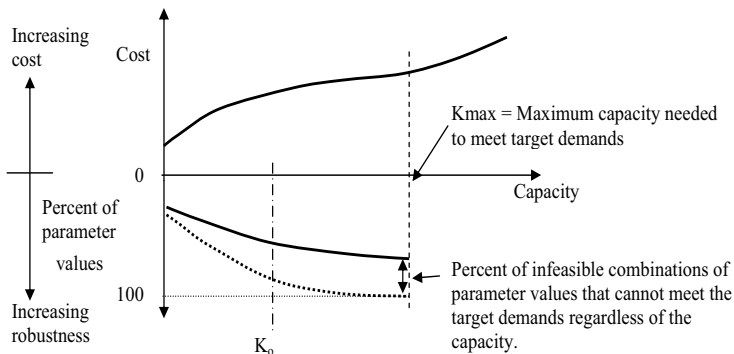


Figure 4. Cost function for reservoir capacity and percentage combinations of discrete (σ , ρ , α , β) values that permit meeting the demand for given capacity, or for which the capacity permits the smallest possible target deficit obtainable when there is insufficient water to meet the demand.

Perhaps to make Figure 4 a little clearer, for any particular capacity, say K_0 , the solid curve immediately below the horizontal axis indicates the percentage of combinations of parameter values that will result in meeting the target demand if the capacity available is K_0 . The dotted curve below the solid curve indicates the total percentage of additional infeasible combinations of parameter values for which the minimum target deficit deviation can be achieved with a capacity equal to or less than K_0 .

Note that when providing sufficient water is available, more capacity is needed to meet a demand target when the variation in supply over time increases. The greater the standard deviation the greater the capacity needed; decreasing α results in less water, and less water leads to less storage capacity requirements and higher failure vulnerabilities with respect to meeting the target demands. Yet the upper bound on the reservoir capacity needed to insure against any reasonable surprises in the next 100 years is not necessarily found by assuming the limits of the ranges of each of those parameters.

Having identified the tradeoffs between cost and robustness, in some sense, does not tell us just which design value to pick, in this example. Just as in all multi-objective decision-making projects, judgment is required, not only in deciding what decision is 'best', but before that, in picking what might be considered reasonable ranges of the parameter values. Again, the purpose is to find out just what the envelope of solutions might be under conditions of change, to determine which parameters most affect the outcome, i.e., the reservoir capacity in our example, and for those situations in which target demands cannot be met, just what options are available to adjust or adapt to smaller targets should in fact such measures are needed in the future.

Determining needed reservoir capacities

Given the large number of combinations of discrete values of the four parameters we varied to generate each flow sequence, each of which was used in an optimization model to determine the needed reservoir capacity, we explored the use of a quicker way to obtain this data. Instead of using the optimization model requiring say 50 periods of inflows to determine the needed reservoir capacity, or if the demand cannot be met, the minimum capacity needed to minimize the demand deficit, and doing this for all discrete combinations of parameter values, we developed an artificial neural network (ANN) model. Once that model was calibrated (or trained) it could give us these capacities just based on the input values of the four flow parameters, i.e., α , β , the serial correlation and standard deviation.

The accuracy of the ANN results can be summarized by the use of a confusion matrix. Table 1 shows the confusion matrix for the reservoir capacity value. As this confusion shows, out of 3200 runs, the trained network only generated 6 false positives, and no false negatives.

Table 1 : Confusion matrix for the capacity variable.

		predicted	
		0	1
actual	0	676	6
	1	0	2518

Conclusion

Here we have argued that there is a class of decision-making problems for which few techniques are available. Following the classic distinction between decision-making under risk and decision-making under uncertainty, such decision-making problems could be called decision-making under deep uncertainty. This is formally defined as a situation in which decision-makers do not know or cannot agree on a system model, the prior probabilities for the uncertain parameters of the system model, and/or how to value the outcomes.

When facing decision-making problems under deep uncertainty, analysts currently struggle to offer valid, credible model-based decision support, among other reasons because their toolkit is not adequate under these conditions. The existing toolkit comes from a predictive modeling paradigm. That is, known facts and information is condensed into a single 'best estimate' model that is used for predictive purposes. Under conditions of deep uncertainty this is problematic, both because facts and information might be contested and because there might not be enough information of adequate quality to allow for such an approach. Therefore, there is a need for an alternate way of providing model-based decision advice under conditions of deep uncertainty. One such approach is known as Exploratory Modeling and Analysis (EMA) or Robust Decision Making (RDM).

EMA/RDM is a method for analyzing complex and uncertain systems through a series of computational experiments. In decision-making under deep uncertainty, there is still a wealth of information, knowledge, and data available. The method capitalizes on this by specifying an ensemble of models that is consistent with this. A single model run drawn from this set of models is not a "prediction," rather it provides a computational experiment that reveals how the world would behave if the various guesses any particular model makes about the various uncertainties were correct. Through conducting a series of computational experiments and analyzing the results, analysts can draw valid inferences that can be used for decision-making, without falling into the pitfall of trying to predict what is unpredictable. This paper provided an example of this approach applied to the determination of the capacity of a water supply reservoir.

BEN-HAIM, Y. (2006) *Information-Gap Decision Theory: Decisions under Severe Uncertainty*, New York, Wiley.

LEMPERT, R. J. (2002) A New Decision Sciences for Complex Systems. *Proceedings of the National Academy of Sciences of the United States of America*, vol. 99, no. 3, pp. 7309-7313.

LOUCKS, D.P. and VAN BEEK, E., (2005), *Water Resources Systems Planning and Management: Methods, Models and Applications*. UNESCO, Paris, France

<http://www.wldelft.nl/md/intro/fields/water-management/book.html>

<http://ecommons.cornell.edu/handle/1813/2798>

WALKER, W. E. (2000) *Uncertainty: The Challenge For Policy Analysis in the 21st Century*. P8051, Santa Monica, RAND pdf obtained from:

<http://www.rand.org/pubs/papers/2009/P8051.pdf>.

A Hybrid Approach of Uncertainty Analysis for Performance Measurement of Water Distribution System

Krishna Khatri¹ and Kalanithy Vairavamoorthy²

¹Research Fellow, Department of Urban Water and Sanitation, UNESCO-IHE, Delft; Delft University of Technology; TU Delft, the Netherlands; University of Birmingham, UK; k.khatri@unesco-ihe.org; k.b.khatri@bhm.ac.uk

²Professor, University of South Florida, School of Global Sustainability, 4202 E. Fowler Avenue, BEH 304, Tampa FL, 33620, USA; vairavk@grad.usf.edu

ABSTRACT

Performance analysis of a water distribution systems involves hydraulic analysis to ensure that designed nodal demand in each node is maintained at a desired level of pressure and velocity over a design period. Those calculated performance values are mostly used as important surrogates while optimizing a systems design. However, input parameters used for the performance analysis are uncertain and both quantitative and semi-quantitative types. This paper presents a hybrid approach of uncertainty analysis to capture the both types of uncertainty associated in a water distribution systems. The uncertainty associated with nodal demands has been described by probability distribution functions and pipes roughness coefficient by fuzzy membership functions. The technique has been illustrated by a simple water distribution networks. The results from the hybrid approaches are consistent with the deterministic and stochastic approach.

Keywords: Performance; uncertainty analysis; fuzzy set; random sampling, a hybrid technique; Monte Carlo simulation; water distribution networks

INTRODUCTION

One of the main objectives of a water distribution networks optimization problem is to achieve the required level of performances throughout its design period. Performance criteria that has been mostly considered for the analysis are reliability, redundancy and resiliency that ensures sufficient water quantity, quality, pressure and velocity. However, input parameters used for the performance analysis, for example nodal demand and pipes roughness, are always uncertain. Moreover, the system is planned and designed for a far future. Thus, the degree of uncertainty will be further aggravated due to multiple sources of uncertainty associated with future change pressures that include climate change, economical development, deterioration of underground pipes, changes in public behavior and advancement in technology. Consequently, an optimized design proposed for the future without through analysis of uncertainty in input parameters could be less representative of a real case. Thus, a proper description, representation and propagation of uncertainty associated to the input

parameters of water distribution system could be the first step of a analysis to produce a trustworthy performance result.

A performance analysis in a water distribution system need to deal with a mixed nature of data base. For example, as a precise or "crisp" variable such as the length, diameter and elevation of a pipe; statistical information such as water demand in a node; imprecise information such as roughness of pipes and decay rate of chlorine residual. Therefore, it consists of both types of uncertainty: randomness due to inherent variability in the system behavior and imprecision due to lack of knowledge and information on the system. The former type of uncertainty is often referred to as objective, aleatory, stochastic whereas the latter is often referred to as subjective, epistemic state of knowledge (Apostolakis, 1990). A probabilistic representation of uncertainty may be possible when sufficient data are available for statistical analysis, for example for a nodal demand. However, to the elicitation of expert knowledge that is often of ambiguous, qualitative nature, a number of alternative representation frameworks have been proposed (Ferson et al., 2004), for example, fuzzy set theory (Zadeh, 1965), evidence theory (Shafer, 1976), possibility theory (Dubois & Prade, 1982, probability bounds, and interval analysis (Moore, 1979). Therefore, uncertainty associated to a pipe roughness may not be represented by the probabilistic approach.

The contribution of the present paper is the adaptation of a hybrid approach of uncertainty to analyze the performances of a water distribution system and a comparison of the results with the deterministic and the stochastic approach that can be applicable for a complex Engineering problems. Next section presents hybrid approaches of uncertainty analysis.

THEORY OF UNCERTAINTY ANALYSIS

Different types of uncertainty require distinct methods for its characterization, description, propagation, and interpretation (Baudrit et al., 2006). Two well established theories: probability and fuzzy set has been employed here to describe the information regarding variability and imprecision, respectively. A detail information on probability, possibility, fuzzy set, fuzzy α -cut, Dempster-Shafer theories can be find in previous work (Baudrit et al., 2006; Dubois & Prade, 1982; Geer & Klir, 1992;; Klir & Yuan, 1995; see, Zadeh, 1978) and that has not been presented here.

A hybrid approach employed here to handle and process the mixed information through a model that consists of either by converting one form of information into the other or joint propagation of both. There are several transformation techniques to transform one form of information into the other. Most of the transformation techniques are based on several principles including Zadeh consistency principle (Zadeh, 1978), Dubois and Prade's consistency and the preference preservation principles (Dubois and Prade, 1982), Delgado and Moral's maximal specificity principle (Delgado and Moral,

1987), Geer and Klir's information-preservation principle (Geer and Klir, 1992), and other techniques (Yamada, 2001). Moreover, other techniques for processing joint probability and possibility distributions are presented by many researchers (Guyonnet et al., 2003; Baudrit et al., 2006).

A simplified algorithm has been presented here based on the evidence theory and further extension of the techniques discussed by Geer and Klir (1992) and proposed by Yamada (2001). It converts a fuzzy membership function into a probability distribution function and converted probability information is then propagated through the model (i.e., hybrid conversion and homogenous propagation). The conversion, is applicable for fuzzy sets with triangular or trapezoidal form, which is commonly applied in most of the Engineering problems. For the simplicity, the probability distribution functions considered are unimodal and fuzzy number are convex and normal. To compare the results, a joint propagation technique developed by Guyonnet et al., (2003) is also presented and analyzed.

Possibility to probability transformation

To characterize the Dempster Shafer Theory (DST), let $X = \{x_1, \dots, x_n\}$ be a finite set of discrete events, $p(A)$ and $\pi(A)$ are probability and possibility respectively. Any function $m: 2^X \rightarrow [0,1]$ satisfying $m(\emptyset) = 0$ and $\sum_{A \subseteq X} m(A) = 1$ is the basic probability assignment (bpa or m). The bpa expresses the degree of belief committed exactly to set A . Every subset A for which $m(A) \neq 0$, is a focal element. If, F be the set of all focal elements, then the pair (F, m) is called body of evidence. In this method, $E_p = (F^p, m_p)$ and $E_\pi = (F^\pi, m_\pi)$ are the bodies of evidence defining the probability and possibility distribution (fuzzy), respectively. Thus, the transformation between probability $p(A)$ and possibility $\pi(A)$ can be replaced by the transformation between E_p and E_π , where $m_p(\{A\}) = p(A)$, $F^p = \{\{x_i\} | x_i \in X_1 \cup \dots \cup X_{k_p}\}$ and $F^\pi = \{F_1, \dots, F_{k_\pi}\}$. For the further detail, see Geer and Klir (1992) and Yamada (2001). Major steps for the conversion is given by:

- i) Represent the uncertainty associated to fuzzy event by a membership function.
- ii) Perform a fuzzy α -cut operation by selecting a value of α_i at random in $[0, 1]$. Determine the lower bound and upper bound for all α_i ($i = 1, \dots, n$) and cardinality of each α -cut. If, the values of α -cut are limited to the finite set $\{0, 0.1, 0.2, \dots, 0.9, 1\}$ and ordered in a nested structure then the nested set will be $A_{\alpha=1} \subset A_{\alpha=0.9} \subset A_{\alpha=0.80} \subset \dots \subset A_{\alpha=0} \equiv X$
- iii) Order the possibility distribution obtained from the α -cut such that $\pi(A_i) = 1 \geq \dots \geq \pi(A_j) \geq \dots \geq \pi(A_{n+1}) = 0$.

- iv) Calculate the probability value based on the evidence theory (Yamada, 2001) such that $p(A_i) = m_p(\{A_i\}) = \sum_{h=k, K} m_\pi(F_h^\pi) / |F_h^\pi|$, where $\forall A_i \in G_k = F_k^\pi - F_{k-1}^\pi$.
- v) Plot the probability distribution functions calculated from the above Equation (from the step iv).

Joint propagation of probabilistic and possibilistic uncertainty

If any model output, $f(\cdot) = f(P_1, P_2, \dots, P_n, F_1, F_2, \dots, F_m)$ with corresponding input probability variables, (P_1, P_2, \dots, P_n) and possibilistic variables, (F_1, F_2, \dots, F_m) is given then the hybrid procedure consists of the following steps (Guyonnet et al., 2003):

- i) Generate i^{th} realization of n probabilistic variables vectors: P_1, P_2, \dots, P_n .
- ii) Select a value α of the membership functions and corresponding cuts of the membership functions.
- iii) Calculate the *inf* (smallest) and *sup* (largest) values of the α -cut.
- iv) Assign these *inf* and *sup* values to the lower and upper limits of the α -cut of $f(\cdot) = f(P_1, P_2, \dots, P_n, F_1, F_2, \dots, F_m)$.
- v) Return to step (ii) and repeat steps (iii) and (iv) for another α -cut. The fuzzy result of $f(P_1, P_2, \dots, P_n, F_1, F_2, \dots, F_m)$ is obtained from the *inf* and *sup* values of $f(P_1, P_2, \dots, P_n, F_1, F_2, \dots, F_m)$.
- vi) Repeat to step (i) to generate a new realization of the random variables.

After 'N' times simulation, a family of 'N' fuzzy interval values is thus obtained. The final *inf* and *sup* values of $f(P_1, P_2, \dots, P_n, F_1, F_2, \dots, F_m)$ is developed after extracting a certain percentage of confidence level for each level of α . For each α cut of random fuzzy set, all the left side and right side of sets is arranged in an increasing order. The set $[F \inf_d^\alpha, F \sup_d^\alpha]$ is considered such that $P(\text{leftside} \leq F \inf_d^\alpha) = 1 - d\%$ and $P(\text{rightside} \leq F \sup_d^\alpha) = d\%$. A fuzzy interval F_d is formed within $\alpha \in [0,1]$. The standard value for $d=95$ is chosen.

APPLICATION AND RESULTS

A simple distribution networks of water mains (Figure 1) has been presented for the uncertainty analysis based on the information given in Table 1. The performance of a system (pressure and velocity) for critical nodes and links has been analyzed for the following four cases.

Deterministic Analysis

The nodal demands and the coefficient of pipes roughness were considered as crisp values for the hydraulic analysis. The deterministic results of EPANET (Rossman, 2000) analysis for critical nodes and links is shown in Figure 2.

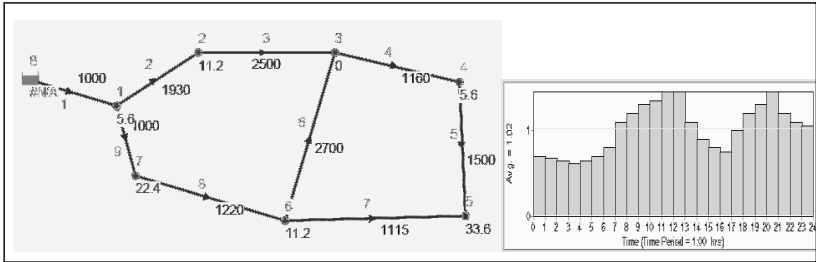


Figure 1: A water distribution network (shown pipe length (m), base demand (LPS) and daily demand patterns)

Table 1: Input parameters for a water distribution system

Link	Start Node	End Node	Elevation of start Node (m)	Length (m)	Diameter (mm)	Coefficient Roughness Values for CI pipes			Remarks
						Min.	Likely	Max.	
1	8	1	80	1000	500	90	100	110	C=150 for 0 year age;
2	1	2	18	1930	457	95	110	125	C=110 for 10 years
3	2	3	18	2500	305	90	100	110	age; C=100 for 20
4	3	4	14	1160	305	90	100	110	years age; C= 90 for 30
5	4	5	12	1500	152	100	110	120	years age (Stephenson, 1979)
6	3	6	-	2700	152	80	90	100	
7	5	6	14	1115	152	80	90	100	
8	6	7	14	1220	381	100	110	120	
9	7	1	14	1000	381	90	100	110	

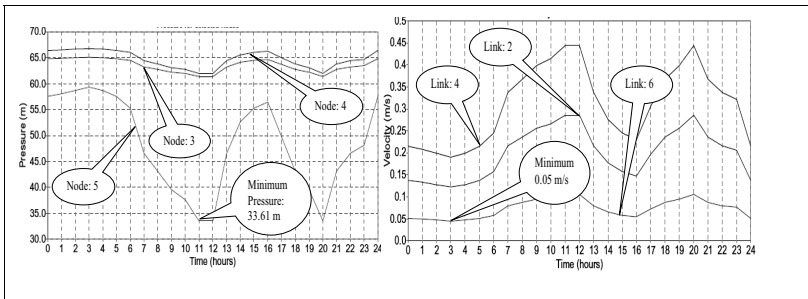


Figure 2: Pressures in critical nodes 3, 4 & 5 and velocity in critical links 2, 4 & 6

Probabilistic Analysis

The nodal demands was considered to be following Gaussian PDFs with means equal to the deterministic demand values and standard deviations equal to 10% of the

corresponding mean values. The uncertainty in the friction coefficient in all pipes was assumed to be uniformly distributed stochastic variables on the interval of deterministic value (Figure 3). The Monte Carlo simulation (1000 runs) was performed for the probabilistic analysis to propagate the defined uncertain variables. The results after the analysis has been presented in Figure 4, which are closer to the deterministic results.

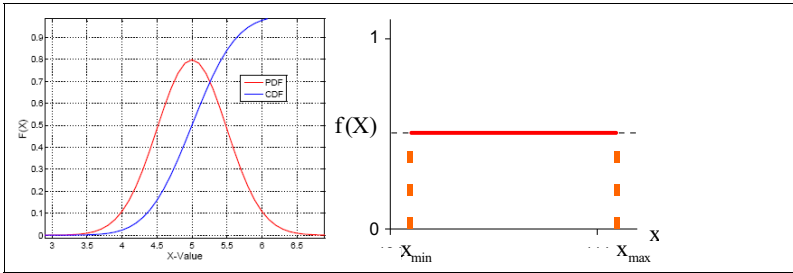


Figure 3: Inputs parameters consisting of nodal demand as a Gaussian PDF (first Figure) and coefficient of pipe roughness as an uniform PDF (second Figure)

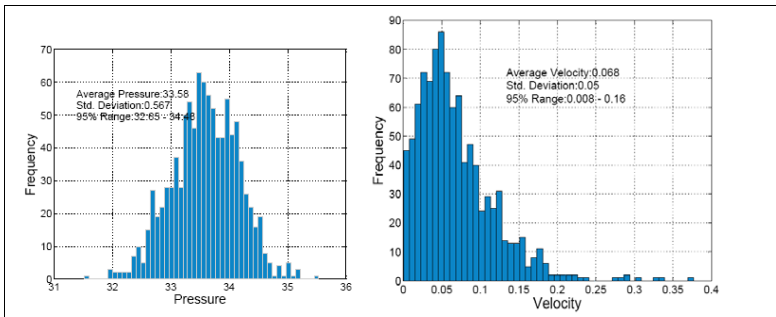


Figure 3: Pressure distribution for the node 5 at 11 hrs and velocity distribution for the link 6 at 3 hrs

Hybrid Analysis by Conversion and Homogeneous Propagation

The nodal demands has been described by Gaussian PDFs and the coefficient of roughness in each pipe by a triangular fuzzy membership functions based on Table 1. The fuzzy membership functions has been converted into the probability distribution functions employing the developed algorithm. The fuzzy interval analysis by α -cuts (@ 0.10 intervals) and PDFs thus obtained is shown in Figure 4. The uncertainty has been propagated by Monte Carlo simulations (1000 runs) and the results are presented in

Figure 5. The results are slightly different than the deterministic approach and with a higher degree of uncertainty.

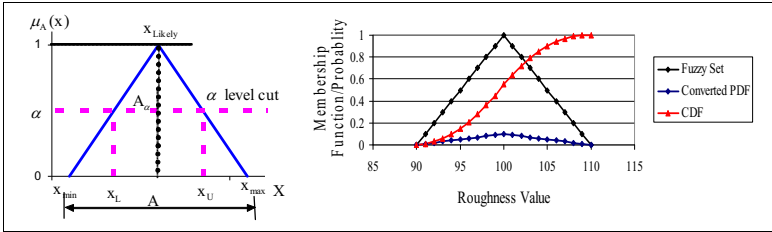


Figure 4: Fuzzy α -cut (left Figure) and conversion of a fuzzy membership function into the probability distribution (right Figure) for the pipes roughness

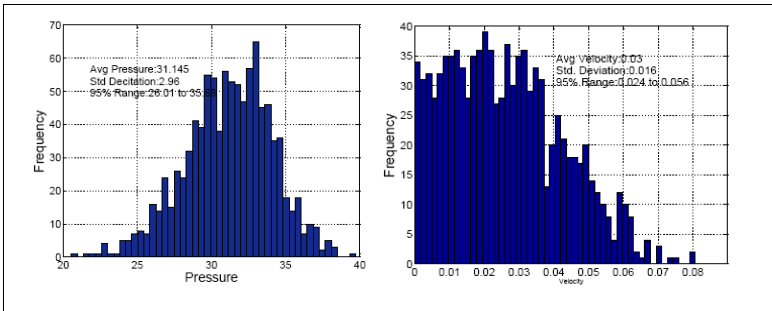


Figure 5: Pressure distribution for the node 5 at 11 hrs and velocity distribution for the link 6 at 3 hrs after Monte Carlo simulation

Hybrid Analysis by Joint Propagation

The hybrid approach developed by Guyonnet et al. (2003) has been employed in this case. The nodal demands and pipe roughness are described by Gaussian PDFs and triangular fuzzy membership functions respectively. The uncertain variables was propagated with α -cuts (@ 0.10 intervals) and Monte Carlo simulation (1000 runs). The output of the simulation is random fuzzy numbers. The results of propagation and aggregation for nodal pressure and velocity are shown in Figures 6 & 7. This aggregation is undertaken according to the representation theorem which formulates a fuzzy set from its α -cuts. The most likely pressure at the node 5 during 11 hrs ranges from 29.75 to 33.01 (shown in the dotted lines in Figure). Similarly, the velocity at the link 6 ranges around 0.033 to 0.36 m/s. Both the results are calculated for the 95% confidence interval.

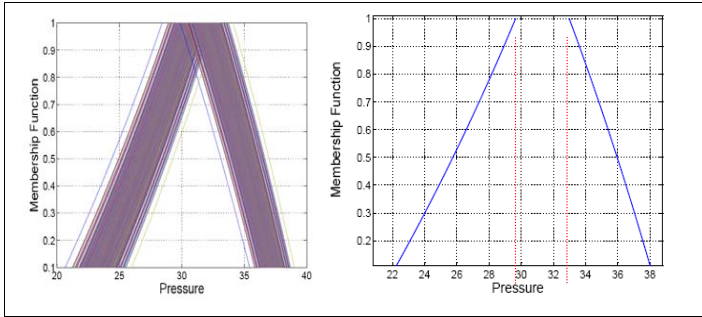


Figure 6: Pressure distribution for the node 5 at 11 hrs after the hybrid propagation (A random fuzzy results of N-simulation & synthesized output)

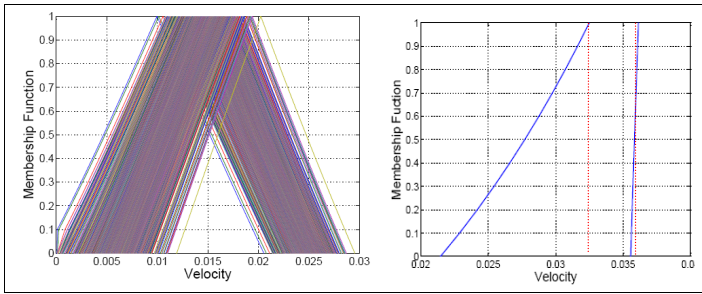


Figure 7: The velocity distribution for the link 6 at 3 hrs after the hybrid propagation (A random fuzzy results of N-simulation & synthesized output)

DISCUSSION AND CONCLUSION

This paper presented the hybrid approaches of uncertainty analysis to analyze the performances of a water distribution network. The comparative results of the analysis has been presented in Table 2. The performances results obtained from the three techniques are consistent with the deterministic approach. The results obtained from the hybrid techniques show a greater degree of uncertainty compared to the probability approach. Computationally, the hybrid conversion and homogenous propagation technique is simpler than the hybrid propagation proposed by Guyonnet et al.(2003). Selection of any techniques will depend on information available in the real case problem. The hybrid approach could be a better approach for propagating the uncertainty while we have to deal with the both aleatory and epistemic state of knowledge. This may be more applicable in many cases where the data are limited. However, application of a

hybrid approach in a complex problem (e.g., very big water distribution networks of hundreds of nodes) could be computationally expensive.

Table 2 : Results of the performance analysis

Analysis Approach	Pressure at node 5 at 11 hrs	Velocity at pipe 6 at 3 hr
1) Deterministic	33.61	0.05
2) Probabilistic	Mean: 33.58, std. deviation: 0.567, Range: 32.65 to 34.48 (95% confidence interval)	Mean: 0.068, std. deviation: 0.05, Range: 0.008 to 0.16 (95% confidence interval)
3) Hybrid analysis by conversion and homogenous propagation	Mean: 31.14, std. deviation: 2.96, Range: 26.01 to 35.88 (95% confidence interval)	Mean: 0.03, std. deviation: 0.016, Range: 0.024 to 0.058 (95% confidence interval)
4) Hybrid propagation	Range: 29.75 to 33.01 (95% confidence interval)	Range: 0.033 to 0.036 (95% confidence interval)

Although having significant research on transformation of one form of information into the another, none of the techniques are free from criticism either in their theoretical perspective or computational burdens during the application. It is not sure yet that different conversions methods give similar results after the conversion or hybrid propagation. The possibility is a ordinal and epistemic scale of uncertainty whereas the probability is of a quantitative type and highly sensitive to the small noise and errors. Evidently the value of possibility is less precise than those of probability. Conversion of one form into the another may be required for simplification of a modeling task, however a conversion technique must ensure that any information should not be lost or added after the conversion. For a water distribution case, it has complex interdependencies among the nodal demand, pressure and velocity, which requires further investigation both from the theoretical and practical points of view.

ACKNOWLEDGEMENTS

The authors would like to acknowledge the financial support of the Delft Cluster, Delft and the SWITCH project UNESCO-IHE, Delft of the Netherlands for conducting this research.

REFERENCES

- Apostolakis, G. (1990). The concept of probability in safety assessments of technological systems. *Science* 250(4986), 1359 - 1364.
- Baudrit, C., Dubois, D., & Guyonnet, D. (2006). Joint propagation and exploitation of probabilistic and possibilistic information in risk assessment. *IEEE Transactions On Fuzzy Systems*, 14(5), 593-608.
- Delgado, M., & Moral, S. (1987). On the concept of possibility-probability consistency *Fuzzy Sets and Systems*, 21(3), 311-318

- Dubois, D., & Prade, H. (1982). On several representations of uncertain body of evidence. In M. M. Gupta & E. Sanchez (Eds.), *Fuzzy information and decision making* (pp. 167-181). Amsterdam: North Holland Publishing.
- Ferson, S., Joslyn, C. A., Helton, J. C., Oberkampf, W. L., & Sentz, K. (2004). Summary from the epistemic uncertainty workshop: consensus amid diversity *Reliability Engineering & System Safety*, 85(1-3), 355-369
- Geer, J. F., & Klir, G. J. (1992). A mathematical analysis of information-preserving transformations between probabilistic and possibilistic formulations of uncertainty. *International Journal of General Systems*, 20(2), 143-176.
- Guyonnet, D., Bourguin, B., Dubois, D., Fargier, H., Côme, B., & Chilès, J.-P. (2003). Hybrid approach for addressing uncertainty in risk assessments. *Journal of Environmental Engineering*, 129(1), 68-78.
- Klir, G., & Yuan, B. (1995). *Fuzzy sets and fuzzy logic theory and applications*. New Jersey: Prentice Hall P T R.
- Moore, R. E. (1979). *Methods and Applications of Interval Analysis*. Philadelphia, PA: SIAM.
- Shafer, G. (1976). *A Mathematical Theory of Evidence*. Princeton, NJ: Princeton University Press.
- Revelli, R., & Ridolfi, L. (2005). Fuzzy Approach for Analysis of Pipe Networks. *Journal of Hydraulic Engineering*, 128(1), 93-101.
- Rossman, L. A. (2000). EPANET 2 users manual, USEPA, Washington, D.C.
- Yamada, K. (2001). *Probability -possibility transformation based on evidence theory*. Paper presented at the IFSA World Cong. and 20th NAFIPS International Conference.
- Zadeh, L. A. (1965). Fuzzy sets. *Inf. Control*, 8, 338-353.
- Zadeh, L. A. (1978). Fuzzy sets as a basis for a theory of possibility. *Fuzzy Sets and Systems* 100(1), 9-34.

A New Approach of Risk Analysis for Complex Infrastructure Systems under Future Uncertainties: A Case of Urban Water Systems

Krishna Khatri¹ and Kalanithy Vairavamoorthy²

¹Research Fellow, Department of Urban Water and Sanitation, UNESCO-IHE, Delft; Delft University of Technology, TU Delft, the Netherlands; and University of Birmingham, UK; k.khatri@unesco-ihe.org

² Professor, University of South Florida, School of Global Sustainability, 4202 E. Fowler Avenue, BEH 304, Tampa FL, 33620, USA; vairavk@grad.usf.edu

ABSTRACT

This paper presents a new hybrid hierarchical integrated risk assessment framework (H-HIRA) developed for analyzing integrated risks and uncertainties in urban water systems due to future change pressures, such as climate change, population growth, urbanization and deterioration of infrastructure systems. It is based on several key concepts that include application of a system of systems approach to decompose a complex system into a hierarchical order; DPSIR framework to analyze the likely impacts of future change pressures; a hybrid approach for description and propagation of uncertainties; integrated system modeling to analyze the risk and vulnerability in a system; and a fuzzy set based multi-criteria analysis to select a robust risk management strategy. The framework can be applied for analyzing risks in any complex infrastructure system, and most importantly for risk informed decision making during the strategic planning of infrastructure systems.

Keywords: Urban water systems; future change pressures; a system of systems; uncertainties; risks assessment; fuzzy set; multi-criteria analysis; risk management.

INTRODUCTION

Since the last decade, the intensity and magnitude of risk events in an urban area such as floods, drought and water contamination have increased dramatically. Dealing with the future and developing sustainable urban water systems (UWS) has been further challenging due to uncertain and dynamic future change pressures. Risk informed decision making techniques have been recognized as important aids when planning for the future (Hall and Solomatine, 2008). This process requires through assessment on a system's performance, its likelihood of failure and consequences - if the system goes wrong due to threats and opportunities created by developments within the sector, and by forces from outside the water sector. In addition, it identify a strategy that is "least regrettable" or "not regrettable" while meeting the other overall goals of a system. Thus, it involves analyzing the likely impacts of future change pressures (e.g., climate change, population growth and urbanization) under a very wide range of future scenarios. However, one of the main challenges of a risk based decision making process is to

identify a complete risk assessment framework that can be applied readily while planning an UWS for a city of the future.

Despite the many innovations embedded within previous works on risk assessment and risk management studies (such as Haimes, 1981; White et al., 1999; Ezell et al., 2000; Kleiner et al., 2004; Ayyub et al., 2007; Lindhe et al., 2009; Ashley et al., 2007) what seems to be missing is a single integrated framework that can sufficiently handle the issue of a system complexity, its dynamism, multiple sources of hazards and vulnerabilities as well as uncertainties in an UWS. This paper presents a new risk assessment framework based on a hybrid approach. It applies probability, possibility, fuzzy set and Dempster-Shafer theory for uncertainty analysis and multi-criteria analysis for a strategy selection. Detailed information with respect to these theories can be found in previous work (see, Zadeh, 1978; Dubois and Prade, 1982; Geer and Klir, 1992; Klir and Yuan, 1995; Baudrit et al., 2006; Khatri and Vairavamorthy, 2009) and has not been presented in this paper. The framework is presented in the next section.

A HYBRID HIERARCHICAL RISK ASSESSMENT FRAMEWORK (H-HIRA)

A new Hybrid Hierarchical Risk Assessment framework (H-HIRA) proposed to analyze and manage risks in UWS is presented in Figure 1. The main features of the H-HIRA are described in the following sections.

A hierarchical decomposition of a system based on system approach

The UWS system is decomposed into different systems, sub-systems and components in a hierarchical order based on a system of systems approach (SOS) that helps to simplify the complexities of a system. An advantage of a systems analysis is that all the elements of the system can be modeled either analytically or conceptually (Keating et al., 2003). Figure 2 depicts an UWS that has been decomposed into a system, sub-systems and components of each system. Each element in the hierarchy is referred to as a "node." The top-most node is called the root node that represents a system of systems level. Any node coming from the root node is a parent node, and node decomposed further from the parent node is called child node to that parent node. Any nodes that terminate in the hierarchy and they have no further nodes (i.e., no children) are called leaf nodes. Based on the systems approach, the integrated risk in any level will be the compounded risk up to that level.

Application of DPSIR framework

Impacts of various sources of global change pressures in an UWS for the future has been analyzed applying DPSIR (Driver-Pressure-State-Impact-Response) framework. The DPSIR framework allows to analyze cause and effect relationships between interacting components of a complex social, economic and environmental system. It provides a base for identifying preliminary sources of hazards, vulnerability, risks and responses in any infrastructure systems.

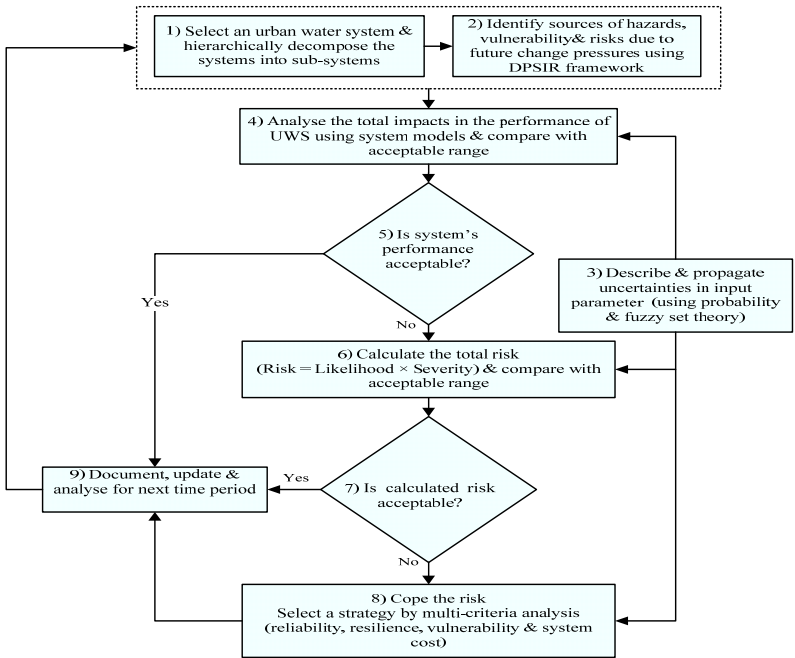


Figure 1. A Hybrid Hierarchical Risk Assessment framework for UWS (H-HIRA)

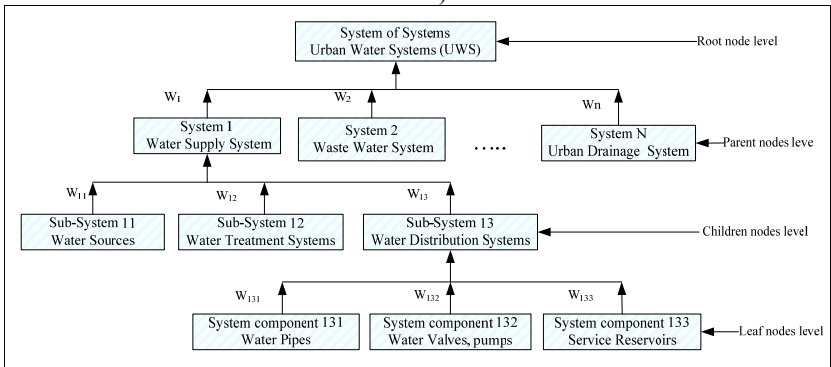


Figure 2. A hierarchical decomposition of UWS in a system of systems approach

Further details and application on the DPSIR framework is available in Carr et al., (2007) and Maxim et al. (2009). The application of the DPSIR in this work has been illustrated by Figure 3.

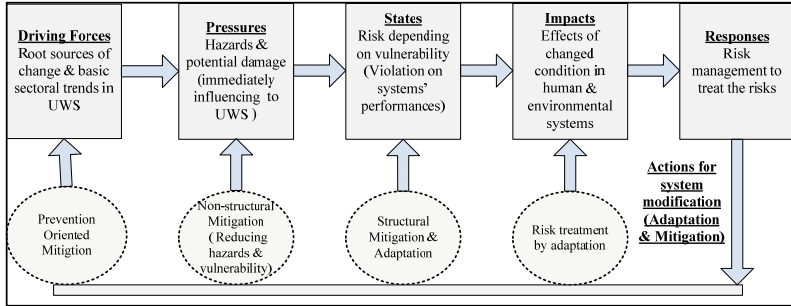


Figure 3. The DPSIR framework for preliminary analysis for sources of hazards, types of risk, sources of uncertainty & risk management options in an UWS

Uncertainty analysis

Risk assessment for an UWS system inevitably involves many uncertainties. The uncertainties arise due to natural variability, social interactions in a built system, and technological complexities in a system model and processing. Two well established theories: probability and fuzzy set has been employed here to describe the information regarding variability and imprecision respectively. This framework applies Monte Carlo and Latin hypercube sampling for propagation of probabilistic information, and fuzzy α -cut operation for fuzzy information.

In this framework, a new algorithm has been proposed based on evidence theory and the further extension of the techniques discussed by Geer and Klir (1992) and proposed by Yamada (2001) that simplify the conversion process. The algorithm converts the probability information into the fuzzy number. The conversion, is applicable for fuzzy sets with triangular or trapezoidal form, which is commonly applied in most of the Engineering problems. For the simplicity and to reduce the computational complexity, the probability distribution functions considered are unimodal type and fuzzy number are convex and normal.

To characterize the Dempster Shafer Theory (DST), let $X = \{x_1, \dots, x_n\}$ be a finite set of discrete events, $p(A)$ and $\pi(A)$ are probability and possibility respectively. Any function $m: 2^X \rightarrow [0,1]$ satisfying $m(\emptyset) = 0$ and $\sum_{A \in X} m(A) = 1$ is the basic probability assignment (bpa or m). The bpa expresses the degree of belief committed

exactly to set A . Every subset A for which $m(A) \neq 0$, is a focal element. If, F be the set of all focal elements, then the pair (F, m) is called body of evidence. In this method, $E_p = (F^p, m_p)$ and $E_\pi = (F^\pi, m_\pi)$ are the bodies of evidence defining the probability and possibility distribution (fuzzy), respectively. Thus, the transformation between probability $p(A)$ and possibility $\pi(A)$ can be replaced by the transformation between E_p and E_π , where $m_p(\{A\}) = p(A)$, $F^p = \{\{x_i\} | x_i \in X_1 \cup \dots \cup X_{k_p}\}$ and $F^\pi = \{F_1, \dots, F_{k_\pi}\}$. For the further detail, see Geer and Klir (1992) and Yamada (2001).

Probability to possibility transformation

- i) Represent the uncertainty due to random event by a probability distribution function (PDF), $\int_{\mathbb{R}} p_x dx = 1$.
- ii) Considering a unimodal PDF, identify an interval $[X_L, X_R]$ in a PDF so that $\int_{X_L}^{X_R} p(x) dx = 1$. The $[X_L, X_R]$ level will be selected such that it will be within the 99.7% confidence interval. For example, if $p(x)$ is a Gaussian function with standard deviation σ , the interval $[3\sigma, +3\sigma]$ around the mean value will be chosen. The probability function that decreased asymptotically to zero will be neglected for the simplicity.
- iii) Determine the peak level $[X_p, X_p]$ of the PDF such that $\int_{X_p}^{X_p} p(x) dx = 0$.
- iv) The base interval $[X_L, X_R]$ of the PDF will be considered as the support of the possibility distribution function $\pi(x)$ (which is a fuzzy number $\mu(x)$). It will represent the α -cut at level $\alpha = 0$ of the membership function. The top level will correspond to the α -cut, at level $\alpha = 1$.
- v) Within the base interval $[X_L, X_R]$ and the peak $[X_p, X_p]$ of the PDF, undertake n numbers of finite divisions of nested intervals $[X_{L_i}, X_{R_i}]$ and calculate the corresponding probability values. Order the calculated values such that $p(A_1) \geq p(A_2) \geq \dots \geq p(A_n)$.
- vi) Calculate the possibility distribution (membership value) based on evidence theory (Yamada, 2001) such that $\pi(A_i) = i * p(A_i) + \sum_{j=i+1}^n p(A_j)$ (1)
- vii) Plot the fuzzy membership functions calculated from Equation (1).

Possibility to probability transformation

- i) Represent the uncertainty associated to the fuzzy event by a membership function.
- ii) Perform a fuzzy α -cut operation by selecting a value of α_i at random in $[0, 1]$; determine the lower bound and upper bound for all $\alpha_i (i=1, \dots, n)$ and cardinality of each α -cut. If, the values of α -cut are limited to the finite set $\{0, 0.1, 0.2, \dots, 0.9, 1\}$ and ordered in a nested structure then the nested set will be $A_{\alpha=1} \subset A_{\alpha=0.9} \subset A_{\alpha=0.80} \subset \dots \subset A_{\alpha=0} \equiv X$
- iii) Order the possibility distribution obtained from the α -cut such that $\pi(A_i) = 1 \geq \dots \geq \pi(A_i) \geq \dots \geq \pi(A_{n+1}) = 0$.
- iv) Calculate the probability value based on evidence theory (Yamada, 2001) such that :

$$p(A_i) = m_p(\{A_i\}) = \sum_{h=k, K} m_x(F_h^\pi) / |F_h^\pi| \tag{2}$$
 where $\forall A_i \in G_k^\pi = F_k^\pi - F_{k-1}^\pi$.
- v) Plot the probability distribution functions calculated from Equation (2).

Risk assessment

The performance of an UWS is analyzed by using system models considering various future scenarios and input uncertainties. The output of the analysis (model) is compared with predefined acceptable performance levels to identify the existence of risks in a system. As shown in Figure 1, a risk in a system is perceived, only if the performances of a system has been violated. The magnitude of a risk is calculated by:

$$Risk = f\{Likelihood\ of\ risk(L), Severity(S), Vulnerability(v)\} \tag{3}$$

The likelihood (L) and severity (S) component are represented by fuzzy numbers as shown in Figures 4(a) and (b). The likelihood is the model output in the probabilistic form that needs to be converted into the fuzzy number using Equation (2). The seven fuzzy membership functions (triangular fuzzy number) that represents the likelihood and consequences are defined as extremely low: $[0, 1/6]$, very low: $[0, 1/3]$, slightly low: $[1/6, 1/2]$, medium: $[1/3, 2/3]$, slightly high: $[1/2, 5/6]$, very high: $[2/3, 1]$ and extremely high: $[5/6, 1]$ respectively. Any value from 0 to 1 will represent the relative magnitude of impacts and consequence, for example '0' means no presence of risk/impact and '1' means full possibility of presence and impact.

The vulnerability represents the criticality of a system that has been represented by weights as shown in Figure 2. For a single component, vulnerability is assumed to be unity as it will be reflected by severity components. The weights for the different components and systems of UWS has been assigned by the AHP technique involves the following three steps that include i) pairwise comparison of the different components and development of a judgment matrix, ii) the synthesis of the matrix to compute the

priority vector, and iii) checking the consistency of the judgment matrix (see Saaty, 1988).

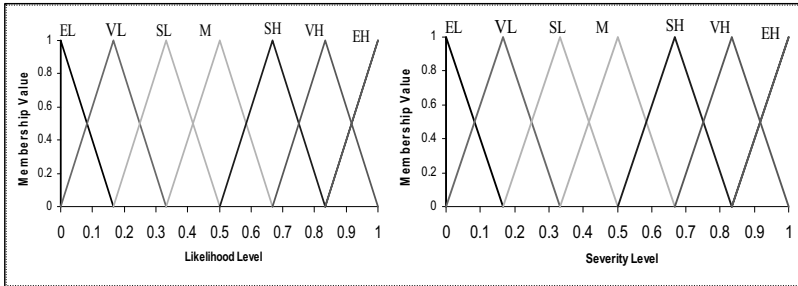


Figure 4. (a) Likelihood of risk, and (b) severity level of risk

The application of Equation (3) needs a α -cut operation as shown in Figure 5(a). The resulting risk has been represented by five fuzzy numbers: very low, low, medium, high, and very high as shown in Figure 5(b).

Risk at a sub-system and a system level (see Figure 2) is aggregated considering the degree of vulnerability and weights assigned to each system and is given by:

$$R_j = \sum_{i=1}^n W_{ji} (L_{ji} \otimes S_{ji}) \tag{4}$$

where R_j is the integrated risk at level j of a system; L_{ji} and S_{ji} are the likelihood and consequences of the risk. The risk acceptance level will depend on the types of risk and the cost associated to its reduction.

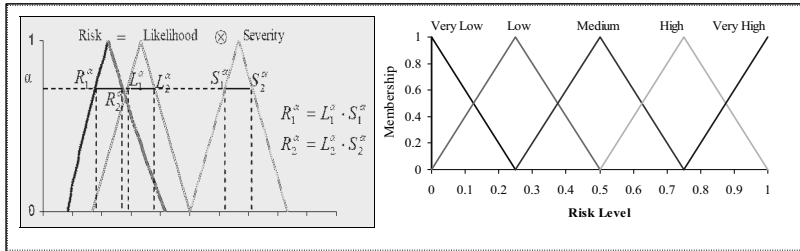


Figure 5. (a) Calculation of risk at component level and (b) representation of risk

Risk management

Reliability, resilience, and vulnerability are the widely used risk measures in water resource planning (Hashimoto et al., 1982; Moy et al., 1986; Jain and Bhunya, 2008). In this work, an additional risk measure ‘economic rate of return’ during the appraisal period has also been included to check the economic and financial viability of the investment. Considering the uncertainties contained by the selected risk measures, a fuzzy set theory based multi-criteria technique has been formulated that calculates the risk index (see Roy, 2005; Wang et al., 2009).

A risk index is taken as a surrogate for a strategy selection. It is formulated as a linear weighted function of the risk of failure $(1 - \lambda)$, the risk of non-recovery from failure $(1 - \gamma)$, the level of vulnerability (ν) and relative internal rate of return $(1 - IRR)$ for the various options available. The risk index is computed by

$$RI = w_1(1 - \lambda) + w_2(1 - \gamma) + w_3\nu + w_4(1 - IRR) \tag{5}$$

The relative importance of the measures is computed by the AHP technique . The algorithm applied for this framework is given in Figure 6. In the Equation (5), the reliability is interpreted as the probability of no failure to a system within a planning period. It is the probability that the system state lies in the set of satisfactory states, $\lambda = P[x(t) \in S]$. It is taken as the ratio of the number of satisfactory days (Ns) to the total operation period T as given by $\lambda = Ns / T$.

The resiliency states the ability of a system to recover from failure to an ‘acceptable state’ once a failure has occurred. We adopt a simple relation developed by

Moy *et al.*, (1986) as given by $\gamma = \left\{ \frac{1}{M} \sum_{j=1}^M d(j) \right\}^{-1}$, where $d(j)$ is the duration of the j^{th} failure event, and M is the total number of failure events.

Vulnerability is a measure of a system’s unacceptable status once it has passed into that status and refers to the likely magnitude of a failure. A metric for overall system vulnerability is the expected maximum severity of a sojourn, S_j into the set of unsatisfactory states, e_j and is given by $\nu = \sum S_j e_j$. For example, the ratio of the average water deficit to the average water demand during the operation period, T will be considered as vulnerability.

The IRR is computed simply by equating the net present value equal to zero and given by $PV = \sum_{t=1}^T \frac{C_t}{(1 + IRR)^t} - C_o$ where C_o is the initial investment outlay, C_t is net cash flow in period t .

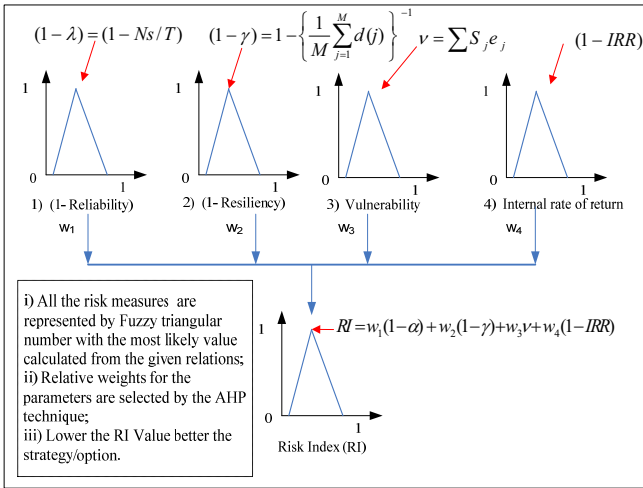


Figure 6. Flow chart for risk index calculation

DISCUSSION AND CONCLUSIONS

We have presented a Hybrid Quantitative Risk Assessment Framework (H-HIRA) that can be applied to analyze the risk in an UWS due to future change pressures. The framework can addresses most of the major issues of risk assessment in a single framework, such as dealing with system's complexities, analyzing and integrating the multiple sources of hazards, appropriate description and propagation of different types of uncertainties, responding to a dynamic system, and selection of a robust strategy based on the risk measures.

The framework recognizes a system of systems approach to simplify a complex system, incorporates the DPSIR framework to analyze the multiple sources of hazards and risks (causes and consequences). It develops a new algorithm for converting one form of information into another ensuring the consistency, preference preservation and maximal specificity principles. The possibility is an ordinal and epistemic scale of uncertainty whereas the probability is of a quantitative type and highly sensitive to the small noise and errors. Evidently the value of possibility is less precise than those of probability. Therefore, the conversion from the probability into the fuzzy form has been undertaken during risk assessment.

The risk in a system is perceived only if the system's performances are less than planned. The aggregated risk at any level of a system is analyzed considering both risk

and vulnerability. The fuzzy set based multi-criteria analysis assesses the reliability, resilience, vulnerability and internal rate of return and produces a risk index. The weights associated to the risk measures are computed by the AHP technique utilizing the experts' knowledge and relative criticality results. The strategy having a least index is preferred over the higher one. The framework has been already demonstrated on analyzing the major risk in UWS, such as the risk of water availability, the risk of water pipe failures, the risk of urban flooding and this has not been presented in this paper. This framework is flexible enough to be applied to other infrastructure systems. It can also be applied for a risk informed decision making, particularly during the strategic planning of infrastructure systems.

ACKNOWLEDGEMENTS

The authors would like to acknowledge the financial support of the Delft Cluster, Delft and the SWITCH project UNESCO-IHE, Delft of the Netherlands for conducting this research.

REFERENCES

- Ashley, R., Blanksby, J., Cashman, A., Jack, L., Wright, G., Packman, J., Fewtrell, L., Poole, T. and Maksimovic, C. (2007). Adaptable urban drainage: Addressing change in intensity, occurrence and uncertainty of stormwater (AUDACIOUS). *Built Environment*, 33(1), pp. 70-84.
- Ayyub, B.M., McGill, W.L. and Kaminskiy, M. (2007). Critical Asset and Portfolio Risk Analysis: An All-Hazards Framework. *Risk analysis*, 27(4), pp. 789-801.
- Baudrit, C., Dubois, D. and Guyonnet, D. (2006). Joint propagation and exploitation of probabilistic and possibilistic information in risk assessment. *IEEE Transactions On Fuzzy Systems*, 14(5), pp. 593-608.
- Carr, E.R., M.Wingard, P., Yorty, S.C., Thompson, M.C., Jensen, N.K. and Roberson, J. (2007). Applying DPSIR to sustainable development. *International Journal of Sustainable Development & World Ecology* 14.
- Dubois, D. and Prade, H. (1982). On several representations of uncertain body of evidence. In: M.M. Gupta and E.Sacnchez (eds.), *Fuzzy information and decision making*, North Holland Publishing, Amsterdam, pp. 167-181.
- Ezell, B.C., Farr, J.V. and Wiese, I. (2000). Infrastructure risk analysis of municipal water distribution system. *Journal of Infrastructure Systems*, 6(3), pp. 118-122.
- Graham, J. and Harvey, C. (2002). How do CFOs make capital budgeting and capital structure decisions? *Journal of Applied Corporate Finance*, 15.1.
- Hall, J. and Solomatine, D. (2008). A framework for uncertainty analysis in flood risk management decisions. *Intl. J. River Basin Management*, 6(2), pp. 85-98.
- Hashimoto, T., Stedinger, J.R. and Loucks, D.P. (1982). "Reliability, resiliency, and vulnerability criteria for water resource system performance evaluation." *Water Resources Research*, 18, pp. 14-20.

- Jain, S.K. and Bhunya, P.K. (2008). Reliability, resilience and vulnerability of a multipurpose storage reservoir. *Hydrological Sciences*, 52(2), pp. 434-447.
- Khatri, K. and Vairavamoorthy, K. (2009). Water demand forecasting for the city of the future against the uncertainties and the global change pressures: case of Birmingham, UK, Proc. of EWRI/ASCE: 2009, Kansas, USA
- Kleiner, Y., Sadiq, R. and Rajani, B. (2004). Modeling failure risk in buried pipes using fuzzy Markov deterioration process. NRCC-46739, pp. 1-13.
- Klir, G. and Yuan, B. (1995). *Fuzzy sets and fuzzy logic theory and applications*. Prentice Hall P T R, New Jersey.
- Lindhe, A., Rosén, L., Norberg, T. and Bergstedt, O. (2009). Fault tree analysis for integrated and probabilistic risk analysis of drinking water systems. *Water Research*, 43(6), pp. 1641-1653
- Maxim, L., Spangenberg, J.H. and O'Connor, M. (2009). An analysis of risks for biodiversity under the DPSIR framework. *Ecological Economics*, 69, pp. 12–23.
- Moy, W.S., Cohon, J.L. and C. S. ReVelle (1986). A programming model for analysis of the reliability, resiliency, and vulnerability of a water supply reservoir. *Water Resources Research*, 22(4), pp. 489–498.
- Roy, B. (2005). Paradigms and Challenges. In: J.Figueira, S. Greco and M. Ehrgott (eds.), *An overview of MCDA techniques today, multiple criteria decision analysis: state of the art surveys*, Springer Science, Boston.
- Saaty, T.L. (1988). *Multicriteria decision-making: The analytic hierarchy process*. University of Pittsburgh, Pittsburgh.
- Wang, J.J., Jing, Y.Y., Zhang, C.F. and Zhao, J.H. (2009). Review on multi-criteria decision analysis aid in sustainable energy decision-making. *Renewable and Sustainable Energy Reviews*, doi:10.1016/j.rser.2009.06.021.
- White, C., Victory, T.F. and Mulhern, L. (1999). Using hierarchical organization to reduce complexity in water distribution system simulation models, Proc. of WRPMD 1999 — Preparing for the 21st Century, Proceedings of 29th Annual Water Resources Planning and Management Conference ASCE.
- Yamada, K. (2001). Probability -possibility transformation based on evidence theory, Proc. of IFSA World Cong. and 20th NAFIPS International Conferenc IEE Xplore, pp. 70-75.
- Zadeh, L.A. (1978). Fuzzy sets as a basis for a theory of possibility. *Fuzzy Sets and Systems* 100(1), pp. 9-34.

Toward Guidance for Identifying and Measuring Structural Damage Following a Blast Event

Andrew D. Sorensen Ph.D.¹ and William McGill Ph.D.²

¹Postdoctoral Research Scholar, College of Information Sciences and Technology, The Pennsylvania State University, 3127 Research Drive, State College, PA 16801; PH (806) 401-4845; Email: asorensen@ist.psu.edu.

²Assistant Professor, College of Information Sciences and Technology, The Pennsylvania State University, 102L IST Building, University Park, PA 16802; PH (814) 867-0270; Email: wmcgill@ist.psu.edu.

Abstract

Careful study of the patterns and extent of structural damage in the vicinity of a suspected blast event can be useful for identifying characteristics about the nature of the blast insult such as charge weight and directional properties. However, the lack of focused research in this area, as well as the lack of evidence collections standards, prevents post blast investigators from fully utilizing this data. This paper will discuss some preliminary steps taken toward developing guidance for documenting structural damage at a blast scene. A variety of structural materials and configurations are considered in terms of the ways they can fail when subjected to a blast insult and the existing literature is leveraged to develop guidance on how to identify and measure the corresponding structural damage. Once collected, such information can be used to back-calculate the properties of the initiating blast event.

Introduction

According to the Global Terrorism Database (GTD), the majority of terroristic acts involved the use of explosives employed against targets (GTD, 2010). When these events occur, post blast investigation is used to determine the type of explosive that is used, the container the explosive is housed in, and the detonation device. The current investigative procedure utilizes a variety of methods including chemical analysis, crater measurements, and other site observables such as witness testimony. The structural damage incurred by the surrounding buildings due to the blast load is not usually taken into account, and in fact is not typically part of modern post blast investigative guidance. While the currently employed methods are very adept at determining the explosive material, container, construction and detonation design, and even the blast epicenter, utilizing the observed structural damage at the blast scene can provide vital additional information such as charge weight and blast directional properties.

It is widely understood that the blast environment is characterized by the pressure-time history at various points in the neighborhood of the blast (Wesevich *et. Al.*, 2005). The *neighborhood* of the blast is defined as the region for which the blast causes a positive pressure differential above ambient pressure. The *pressure-time history* for an explosive event depends on: the position of the explosive charge relative to the point of measurement in three-dimensional space, the specific explosive material composition, the manner in which the explosive was detonated, the efficiency of detonation, the container of the explosive, the presence of obstacles and reflection surfaces, and the amount of energy absorbed by other objects.

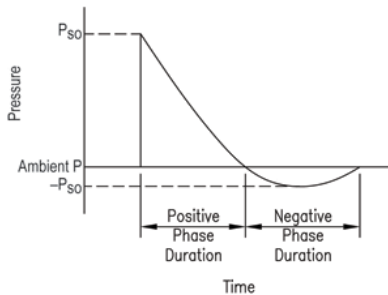


Figure 1: Typical Pressure-Time History Due to an Explosion

The investigative method that is required to use structural damage to determine blast characteristics is by necessity a hybrid of techniques used by forensic engineers, forensic chemists, and criminal investigators. Each discipline has their own set of professional standards and methods (Noon, 1995; Beveridge, 1998; Thurman, 2006; Harmon, 2008; NFPA, 2008). A number of texts concerning forensic engineering exist that are concerned with determining the cause of a structural member failure (Lewis, 2003; Carper, 2000). However, these texts do not prescribe a set investigative method for collecting structural damage observables.

This paper seeks to begin to develop a set of criteria and procedures that can be used by post blast investigators to utilize structural damage observables at a blast scene to back calculate the charge weight of the explosive and blast directional properties. The method utilize to carry out this objective is to review the existing literature on forensic analysis of blast scenes as well as research on the behavior of structural materials exposed to blast loading. The literature is reviewed to determine what how the structural damage observables should be evaluated and any potential areas where the evaluation of these observables may provide faulty conclusions. The paper concludes by providing a brief summary of a procedure that can be used to identify and collect these observables by taking into account the knowledge gleaned from the existing literature.

Material Response to Blast Loading

Observed structural damage is a useful, but by no means precise, indicator of the strength of an explosion. Given exposure to a blast wave, a material will respond in such a way that results in observable damage or not. It is the observable damage that is of interest to the post-blast investigator. If damage is observed, the post-blast investigator can say with certainty that the force at the location of damage was sufficiently high to damage the material. If the damage pattern is a function of load, then a careful description of the pattern will assist in back-calculating the incident pressure or impulse. If the damage is binary or not easily sized with load, then at a minimum one can say that the limit state separating damage from non-damage was exceeded.

There are four building materials whose response to blast loads that have received attention in the existing literature: reinforced concrete, masonry, steel, and glass. The distress observables for these materials vary and correspond to the innate behavior of the materials themselves. Concrete and masonry are brittle materials that behave differently under varying levels of damage. As such, the damage levels can be used to calculate the loads or pressures that caused the damage. These two materials can therefore be analyzed. Conversely, steel is a ductile material, and in its plastic region, a constant load or pressure causes strain and permanent deformation in the material. Therefore, the resulting deformation or strains cannot be used to accurately predict the exact applied loads. All that is known is that the elastic loading limit state has been exceeded. Furthermore, if a steel member exhibits rupture or tearing, it can be deduced that the plastic loading limit state has been exceeded. Similarly, although glass is a brittle material, once a certain load is met the glass crack and/or shatters. Once again, from this all that can be deduced is that a load or pressure large enough to crack and/or shatter was experienced by the glass. This information is still quite useful however, as it can be used to determine blast centers and pressure distributions.

It should be noted that there are many examples of post blast structural engineering analysis in the existing literature (Luccioni *et. Al.*, 2004). These papers usually deal with the catastrophic and widely publicized events such as the first attack on the World Trade Center (Ramabhushanam *et. Al.*, 1994) and the Alfred P. Murrah building in Oklahoma City (Corley *et. Al.*, 1998; Mlakar *et. Al.*, 1998; Sozen *et. Al.*, 1998; Tagel-Din *et. Al.*, 2006). However, these papers analyze the entire affected

structure and begin with knowledge of the blast loads. Furthermore they rely on highly developed numerical models for their analysis. Recently a number of published papers have attempted to determine the location and mass of the explosive device based on the resulting structural damage, but once again these papers have relied on the results of complex numerical analysis to compare against observed damage (Vaidogas, 2005; Ambrosini *et. Al.*, 2005). It should also be noted that once again, no prescribed method for obtaining and evaluating structural damage observables are presented in any of these papers.

There is one publication however that acknowledges that the structural damage caused by an explosion is readily available for study and is permanent (Yallop, 1980). The permanency of the structural damage has advantages over chemical analysis and other investigative techniques where the timeliness of the acquiring of samples or the loss of evidence at a site can distort the true nature of the insult. This book published in 1980 predates most chemical analysis currently in use and instead relies more on deriving inferences from the location and distortion of an object. As such, it provides a framework that can be expanded upon to suit the purposes of this paper. Yallop identifies three different types of observable damage: permanent distortion of objects, the displacement of objects, and flame and heat effects. The most relevant of these damage types, permanent distortion of objects, includes the plastic deformation of materials, fracture of surfaces and containers, and fragment attack or what is commonly referred to as projectile impact. Permanently distorted objects are on the whole reliable sources of information.

The blast site is analyzed by employing a direction/damage diagram which consists of a plan of the scene of the explosion, on which is marked the location of any damage which can be confidently ascribed to the explosion and which indicates the direction of travel of the blast or resulting fragments. The greater the number of such observations that can be put on the diagram the greater the reliability of the deductions that can be made from it. The diagram should also include observations where no damage appears to be present. This helps to determine the boundaries of the blast scene as well as the directional properties of the insult. Yallop suggests that a minimum of ten observations should be used to make any deductions, but many more observations are desirable.

As discussed by Yallop, one of the challenges when using structural damage observables to determine blast loads and directional characteristics is differentiating between the damage done by the blast wave and damage done by subsequent fires that result from the blast. Two examples where failure to make this differentiation can lead to faulty conclusions is in the analysis of concrete spallation and cracked window glazing. Spall due to fire is characterized by char around the location of spall. Additionally the cause can be determined by observing whether the spall is located on the side of the slab exposed to fire or on the opposite side (Nash *et. Al.*, 1995). In window glazing, Loughran (2003) points out that care must be taken when identifying the cause of failure in glass as it possible that the failure is due to thermal changes. A thermal break in glass can be identified as the crack occurs at a right angle (90°) to the surface of the glass. This distinction is important because equations relating to the pressure at which glass breaks should not be applied to breaks caused by thermal expansion.

Another area where caution must be exerted is to identify the extents of the negative blast pressure of the blast area as shown in Figure 1. Structural damage in this zone can be difficult to analyze because the structural members have experienced bi-directional loading. One method useful in identifying the negative blast pressure area is by examining the location of window glazing fragments. Glazing fragments in the negative pressure zone may be located on both sides of the original window panes (Krauthammer *et. Al.*, 2000). A similar issue can occur to structural damage observables that have experienced reflected pressures from other surfaces. Ideally structural damage observables used for analysis should be those where a direct pressure is the most likely force that the structural member experienced. These observables can be located by looking at the line of sight between the observable and the blast center if it is known. It is also likely that those observables that are located on the exterior, or furthest away from the blast center, experience the true blast pressure. By collecting a large number of these observables, the amount of error in determining the blast load decreases. Additionally, by identifying, as Yallop prescribes, the failure direction of the structural damage observable, the direction of the blast pressure wave can normally be ascertained.

The literature on material behavior also includes a number of analytical methods that can be used to calculate the blast load by measuring or observing certain damage levels to the structure. As previously mentioned, because steel is a ductile material, its damage levels can be evaluated using stress analysis or other equations provided for the design of steel structures as long as the safety factors in those design equations can be identified and removed (AISC, 2005). For reinforced concrete the following methods are available:

- The level of spall resulting from a blast can be identified and corresponding equations provide a range of blast loads (McVay, 1998; Nash *et. Al.*, 1995; Xu and Lu, 2006).
- If the explosive is detonated directly above a reinforced concrete slab, the geometry of the resulting crater can be utilized (Luccioni *et. Al.*, 2004).
- For slabs and walls, yield line analysis can be used by observing the crack patterns (Biggs, 1964; Mays *et. Al.*, 1996).
- For shear walls, the damaged shape can be correlated to failure modes of a single degree of freedom model where resistance functions were developed for four different failure modes (Naito *et. Al.*, 2006).

For masonry structures the following methods are available:

- For unreinforced masonry walls that demonstrate out of plane bending, the residual deflection in the wall can be measured and utilized (Moradi *et. Al.*, 2008).
- For masonry infill walls that are framed by reinforced concrete or steel, the in-plane failure modes or crack lines can be identified and corresponding equations utilized (Garbin *et Al.*, 2005).

For glazing products the following methods are available:

- If a glass pane is only cracked, then a series of graphical diagrams can be utilized (Mainstone, 1976).

- If an idea of the flexural strength of shattered window glass is known then a ASTM charts can be utilized by applying a procedure demonstrated by Norville and Conrath (2001, 2006).

From this literature a number of reoccurring factors or observables were shown to have an effect on the materials behavior under blast loading. These include the boundary conditions of the structure, the geometry of the structure, material strength, identification of crack-lines and crack widths, identification of any residual deflection, and the three dimensional distance of the material from the blast center. As such for all structural damage observables these items should be evaluated and noted. By identifying a number of these damage observables, and utilizing the analytical techniques available, post blast investigators can back-calculate a range of blast loads that can be correlated to the charge weight.

Conclusion

All structural damage observables, if actually observed at a blast scene, constitutes a portion of the corpus of evidence available to the post-blast investigator as he seeks to understand and ascertain the details of an explosion event. The following outlines the general collection guidelines that can be used to collect post blast structural damage observables. It should be noted that many of these items may already be part of the post blast investigative process while others may need to be integrated into existing procedures.

- 1) Identify the boundary of blast damage. The entire blast damaged area does not need to be sectioned off, however the extents of the blast boundary should be located. If possible the extents of the negative pressure area should also be identified and spatially located.
- 2) If an obvious blast center is apparent, this location should be spatially located.
- 3) Within the blast damage boundary, numerous structural blast damage observables should be located and their spatial position marked. The greater the number of observables, the more accurate the resulting conclusion will be. If a blast center has been identified the distance from the observable to the blast center should be determined.
- 4) For each structural blast damage observable a sketch of the structure should be made identifying the: material, geometry and dimensions, boundary conditions, location and size of any cracks, the location and amount of any permanent deformation, any spalling, any fire damage or charring, and anything else that seems unusual or out place. Pictures should also be taken to help document the observable.
- 5) If possible samples of the damaged structure should be collected for later testing to determine material properties.
- 6) For each structural blast damage observable a description of the line of site between the observable and the blast center should be noted (i.e. there are no obstructions between the two, or multiple structures are located between the two). This will help determine the load experienced by the observable is a direct pressure or a reflected pressure.

As previously mentioned, by collecting multiple specimens the range of possible blast loads is reduced and those specimens whose results lie far outside the range of the majority of specimens can be discounted. Because of the number of unknowns in this process however, it appears that statistical processes such as reliability analysis should be utilized in this procedure in order to be able to account for variations in material strength and geometry.

Acknowledgement

Funding for this research is provided by the Department of National Intelligence's (DNI) Intelligence Community Postdoctoral Fellowship Program.

References

- AISC (2005) *Steel Construction Manual, Thirteenth Edition*. American Institute of Steel Construction, Chicago, IL.
- Ambrosini, D., Luccioni, B., Jacinto, A., and Danesi, R. (2005) "Location and Mass of Explosive from Structural Damage." *Engineering Structures* (27), 167-176.
- Beveridge, A. Ed. (1998). *Forensic Investigation of Explosives*. CRC Press, Boca Raton, FL.
- Biggs, J. M. (1964) *Introduction to Structural Dynamics*. McGraw-Hill, New York, NY.
- Carper, K. (2000) *Forensic Engineering, 2nd Edition*. CRC Press, Boca Raton, FL.
- Corley, W., Mlakar, P., Sozen, M., and Thornton, C. (1998) "The Oklahoma City Bombing: Summary and Recommendations for Multihazard Mitigation." *Journal of Performance of Constructed Facilities*, ASCE 12(3), 100-112.
- Garbin E., Galati N., and A. Nanni, (2005) "Design Guidelines for the Strengthening of Unreinforced Masonry Structures Using Glass Grid Reinforced Polymers (GGRP) Systems," Technical Report Prepared for Bondo Inc. & TechFab LLC., University of Missouri-Rolla, Rolla, Missouri, March 2005.
- Global Terrorism Database, START, accessed on January 14, 2010.
- Harmon, D. E. (2008). *Careers in Explosives and Arson Investigation*. Rosen Central, New York, NY.
- Krauthammer, T., and Altenberg, A. (2000) "Negative Phase Blast Effects on Glass." *International Journal of Impact Engineering*, 24, 1-17.
- Lewis, G. (2003) *Guidelines for Forensic Engineers*. American Society of Civil Engineers, Reston, VA.
- Loughran, P. (2003) *Falling Glass*. Birkhäuser, Berlin, Germany.
- Luccioni, B., Ambrosini, R., and Danesi, R. (2004) "Analysis of Building Collapse Under Blast Loads." *Engineering Structures* (26), 63-71.
- Mainstone, R. (1976) "The Response of Buildings to Accidental Explosions." *Garston, Eng.: Building Research Establishment, Current paper - Building Research Establishment*; CP 24/76.
- Mays, G., Hetherington, J., and Rose, T. (1996) "Resistance-Deflection Functions for Concrete Wall Panels with Openings." *Journal of Structural Engineering* 124(5), 579-587.

McVay, M. (1988) *Spall Damage of Concrete Structures*. Technical Report SL 88-22. US Army Corps of Engineers Waterways Experiment Station.

Mlakar, P., Corley, W., Sozen, M., and Thornton C. (1998) "The Oklahoma City Bombing: Analysis of Blast Damage to the Murrah Building." *Journal of Performance of Constructed Facilities*, ASCE 12(3), 113-119.

Moradi, L., Davidson, J., and Dinan, R. (2008) "Resistance of Membrane Retrofit Concrete Masonry Walls to Lateral Pressure." *Journal of Performance of Constructed Facilities*, ASCE 22(3), 131-142.

Naito, C., and Wheaton, K. (2006) "Blast Assessment of Load-Bearing Reinforced Concrete Shear Walls." *Practice Periodical on Structural Design and Construction*, ASCE 11(2), 112-121.

Nash, P., Vallabhan, C., and Knight, T. (1995) "Spall Damage to Concrete Walls from Close-In Cased and Uncased Explosions in Air." *ACI Structural Journal* 92(6), 680-687.

National Fire Protection Association (2008). *NFPA 921 Fire & Explosion Investigations 2008 Edition*. NFPA Press, Quincy, MA.

Noon, R. (1995). *Engineering Analysis of Fires and Explosions*. CRC Press, Boca Raton, FL.

Norville, H., and Conrath, E. (2001). "Considerations for Blast Resistant Glazing Design." *Journal of Architectural Engineering*, ASCE 7(3), 80-86.

Norville, H., and Conrath, E. (2006). "Blast-Resistant Glazing Design." *Journal of Performance of Constructed Facilities*, ASCE 12(3), 129-136.

Ramabhushanam, E., and Lynch M. (1994) "Structural Assessment of Bomb Damage for World Trade Center." *Journal of Performance of Constructed Facilities*, ASCE 8(4), 229-242.

Sozen, M., Thornton, C., Corley, W., and Mlakar, P. (1998) "The Oklahoma City Bombing: Structure and Mechanisms of the Murrah Building." *Journal of Performance of Constructed Facilities*, ASCE 12(3), 120-136.

Tagel-Din, H., and Rahman, N. (2006) "Simulation of the Alfred P. Murrah Federal Building Collapse due to Blast Loads." *Proceedings of the 2006 AEI Conference, Omaha, Nebraska*, ASCE 190(40798), 32-47.

Thurman, J. T. (2006). *Practical Bomb Scene Investigation*. CRC Press, Boca Raton, FL.

Vaidogas, E. (2005) "Explosive Damage to Industrial Buildings: Assessment by Resampling Limited Experimental Data on Blast Loading." *Journal of Civil Engineering and Management* 11(4), 251-266.

Wesovich, J., and Olson D. (2005) "Forensic Explosion Analysis." *Metropolis & Beyond Proceedings of the 2005 Structures Congress and the 2005 Forensic Engineering Symposium*, ASCE, Reston, VA.

Xu, K. and Lu, Y. (2006) "Numerical Simulation Study of Spallation in Reinforced Concrete Plates Subject to Blast Loading." *Computers and Structures* (84), 431-438.

Yallop, H. G. (1980). *Explosion Investigation*. Forensic Science Society and Scottish Academic Press, Edinburgh, Scotland.

Expected Building Damage using Stratified Systematic Sampling of Failure triggering Events

Stefan T. Szyniszewski, Ph.D.¹

¹ Structural Engineer, Bechtel Power Corporation, 5275 Westview Drive, Frederick, MD 21702; PH (352) 328 5434; email: s.szyniszewski@gmail.com

ABSTRACT

Expected building damage is proposed as a measure of building performance against structural collapse. The proposed novel concept is illustrated with a case study of a typical steel framed building subjected to a bomb explosion and the resulting column removal. Stratified approach to systematic sampling was used to assign appropriate weights to sampled damage scenarios. Finally, an overall expected building damage resulting from randomly located explosions was analytically derived.

The analytical expected damage gives a mean building failure as a function of the explosion reach. The presented expected damage is a scalar performance measure and thus it lends itself to a comparison of alternative designs. Expected damage function is a collapse signature of a given building that takes into account copiousness of explosion locations and feasible detonation magnitudes.

INTRODUCTION

Progressive collapse is a structural failure that results from a localized damage, such as a column failure, that propagates all the way through the building and leads to the total or partial collapse that is well beyond the initial damage reach. Thus, a building can be potentially destroyed by a relatively small explosion due to structural instabilities resulting from the initial explosion as well as dynamic load amplifications and building inability to redistribute the increased tributary loads to the survivor members. Bombing of the Murrah Federal building is the most prominent example of the disproportionate collapse (Osteraas, 2006).

PROBABILISTIC LOAD APPLICATION - SYSTEMATIC SAMPLING

Two primary sources of variability are multiple locations of feasible explosions and various TNT charges that can be detonated. Even when considering just a single explosion around the building perimeter, it becomes apparent that an abundant number of events need to be considered. Spatial variability and explosion magnitudes must be taken into account in order to explore the building resistance to a localized damage.

The systematic sampling procedure can be outlined as:

- A. Pick a location of explosion
- B. Select a charge weight (explosive reach)

- C. Estimate effects on the building
- D. Analyze building response to the sudden column(s) removal
- E. Pick a larger TNT, repeat the above procedure at the same location,
- F. Move to the next sampling location, repeat the assessment for the number of prescribed explosive charges,
- G. Obtain multiple results from analyses
- H. Assign damage metrics to each outcome such as an area of damaged floors normalized by the total floor area
- I. Average results for each TNT weight to generate a damage signature curve that characterizes the building damage as a function of explosion reach. Note, that such measure is independent of explosive locations. It is clearly a probabilistic quantity in the holistic sense that characterizes the investigated structure.

Each collapse simulation requires evaluation of the explosive damage and subsequent effects of column(s) removal, should column damage occur. Assessment of susceptibility to progressive collapse requires large displacements, large strains, contact, advanced material models and dynamic solver capabilities. A relatively crude systematic sampling scheme for a typical 6x4 bays building (Figure 1) has 56 spatial sampling locations. If only 5 detonation charges at each location are considered, the total sample size reaches 280. Each run typically takes significant time to run on a modern personal computer. In short, analyzing even a simple building by means of the brute force systematic sampling approach poses serious computational challenges that can be dealt with only by use of large and very powerful computers.

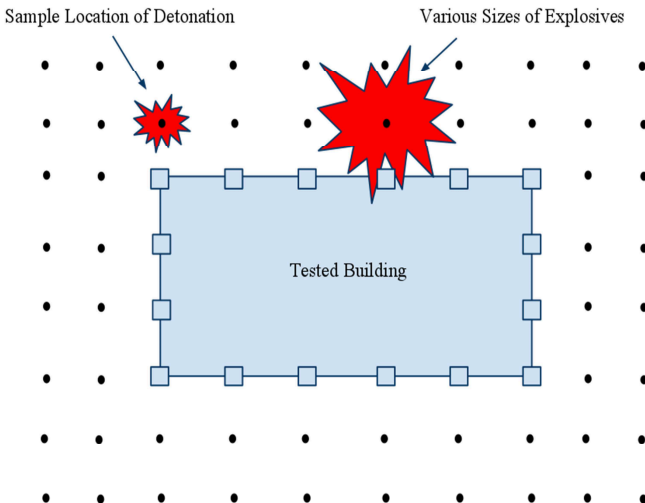


Figure 1. Systematic Sampling of Local Damage Events.

ANALYTICAL STRATIFICATION OF EXPLOSION LOCATIONS

Systematic sampling can be stratified by closed form calculations rooted in understanding of blast characteristics in conjunction with targeted structural simulations of only unique column removal cases. The proposed analytical formulation is based on the following premises: A) blast effects have spherical reach (Osteraas, 2003) and B) structural effects can be considered as a sudden column(s) removal (Szyniszewski, 2009). The herein introduced stratification framework can however be generalized by inclusion of more accurate blast and damage representations. Yet, major drivers need to be understood and explained first, before secondary effects are taken into account. It is postulated that each detonation can be uniquely characterized by its explosion reach, namely R (Figure 2). Should a column be within the damage reach, it will fail. Conversely, columns beyond the damage reach retain sufficient load carrying capacity to support their share of tributary loads. Obviously the larger the explosive, the bigger are structural consequences and more columns can be potentially damaged.

Whereas, traditional damage characterization is focused on explosive reach, structural engineers are interested in the damage inflicted to the building. Thus, column vulnerability range is introduced such that an explosion within the vulnerability range results in the column's destruction (Figure 3). On the other hand, detonations of a given magnitude that are beyond the vulnerability range have no structural effect on the investigated column. Column vulnerability range is exactly equal to the explosive reach for each considered explosive. Each column has its vulnerability range that is a function of the given explosion reach.

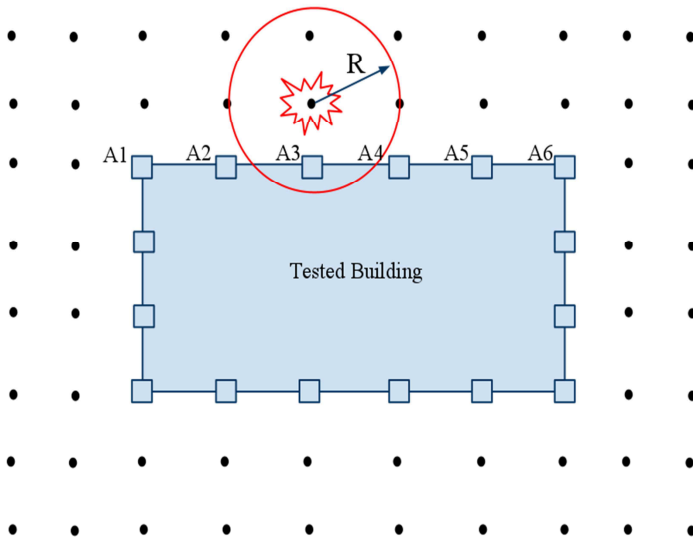


Figure 2. Explosion Reach R .

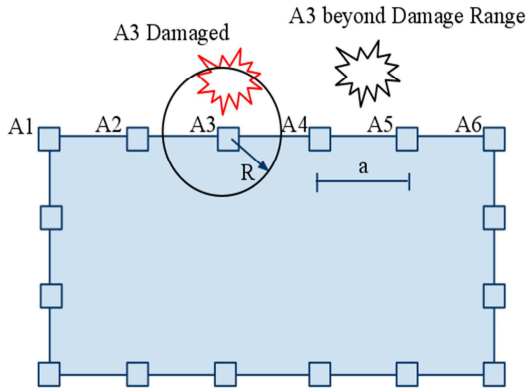


Figure 3. Column Damage Vulnerability Range.

Each blast will inevitably cause some damage to the building (Figure 4). The minimum expected damage can be estimated as a common area of the explosive range and the building interior area. A number of detonation locations within each column vulnerability range are possible. An explosion at the geometric center is taken as the expected location. Thus the proportional damage inflicted to the building is the shaded area shown in Figure 4.

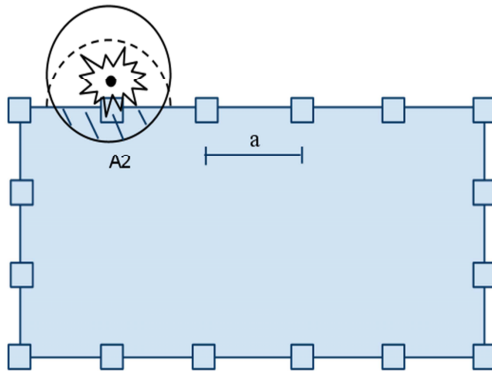


Figure 4. Building Damage without Progressive Collapse.

The explosive reach is normalized by the span between the columns to provide a non-dimensional parameter describing the initial damage intensity, $\eta \equiv \frac{R}{a}$. Thus the minimum building damage expressed in units of [a] is

$$A_{min} = \frac{3}{4} \eta^2 a^2, \quad \eta \in (0, 1)$$

However, should progressive collapse be triggered by the sudden column removal, then collapse extent will be greater than the minimum failure characterized by the quadratic function of the explosive reach defined above (Figure 4). In such a case, progressive collapse will cause partial or total collapse of the building (Figure 5). The collapse extent is quantified with the number of collapsed bays. A collapsed bay is defined as a region with final displacements greater than the half of the story height. A partial collapse is typically cut-off by shear connection failures (Szyniszewski, 2009) so that the extent of the collapse zone can be easily identified by inspection of numerical simulation results. The sample results for the investigated columns A1 thru A6 are listed in Table 1. Lastly, a reasonable sampling region must be selected for the investigated array of explosive scenarios. It is not realistic to expect a very small explosive to be planted far away from the building. However, as the effectiveness of the charge increases, the feasible detonation region should proportionally increase as well. The sampling region is expressed by: $A_{sampl} = (n_{cases} - 1) \cdot \eta + 2\eta^2$

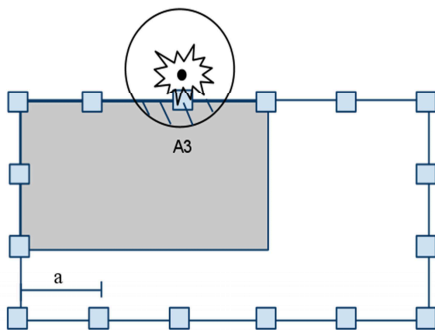


Figure 5. Damage resulting from Progressive Collapse

Table 1. Damage Assessment Matrix

Removed Column	A1	A2	A3	A4	A5	A6
Collapsed Bays	0	0	6	4	0	0

Therefore, the expected damage, expressed as a function of the explosive reach, η :

$$E[D] \left(\eta \in \left(0, \frac{1}{2} \right) \right) = \frac{\left(\frac{4 \cdot 3}{4} \eta^2 + 6 + 4 \right) \cdot \frac{\pi \eta^2}{2}}{(n_{cases} - 1) \cdot \eta + 2\eta^2}$$

**SPATIAL INTERACTIONS BETWEEN COLUMN VULNERABILITIES
MULTIPLE COLUMN REMOVALS**

Once explosive reach exceeds $\eta/2$, two columns can be damaged by a single explosion (Figure 6). All the points of explosions that lie within the shaded region will destroy two columns. This region can be decomposed into: the triangular portion (Figure 7) and two complementary arch regions (Figure 8).

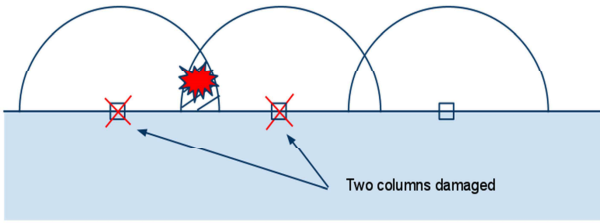


Figure 6. Two columns damaged

Thus the area based, relative weight of two columns removal:

$$A_{II} = A_{tri} + 2 \cdot A_{arch}$$

$$A_{tri} = \frac{1}{2} \cdot (2\eta - 1) \cdot \sqrt{\eta^2 - \left(\frac{1}{2}\right)^2}$$

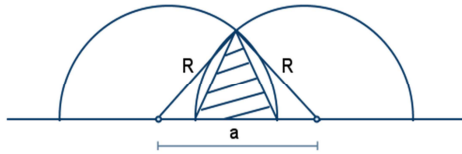


Figure 7. Common Area of Two Triangles. Triangular Portion.

$$A_{arch} = \frac{1}{2} \cdot \eta \cdot (\alpha - \sin \alpha)$$

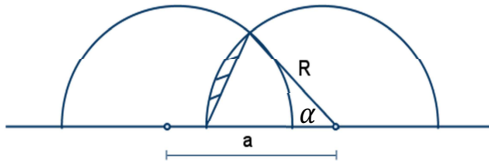


Figure 8. Common Area of Two Triangles. Arch Portion.

The area corresponding to only one column failure (Figure 9):

$$A_I = \frac{\pi \cdot \eta^2}{2} - 2 \cdot A_{II}$$

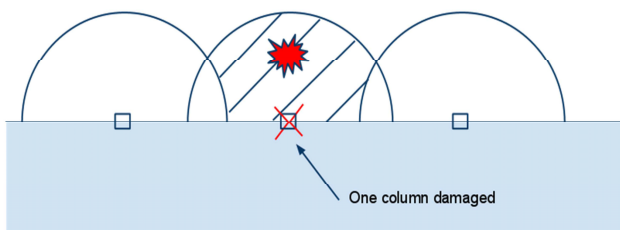


Figure 9. Only one column damaged.

Cases corresponding to the single column removal will obviously yield the same results as previously calculated. Only cases with the two columns removal need to be furthermore analyzed. Non-linear, large displacement, dynamic analysis should be employed to correctly assessed the damage extent (Szyniszewski, 2009). Building damage quantified as the number of collapsed bays for $\eta \in (\frac{1}{2}, 1)$ is given in Table 2.

Table 2. Damage Assessment Matrix

Removed Column	A1	A2	A3	A4	A5	A6
Collapsed Bays	0	0	6	4	0	0
Removed Columns	A1-A2	A2-A3	A3-A4	A4-A5	A5-A6	
Collapsed Bays	0	8	24	12	0	

Sampling region encompasses an area with feasible detonation locations. Thus, the expected damage as a function (Figure 10) of the non-dimensional explosive reach, η :

$$E[D] \left(\eta \in \left(\frac{1}{2}, 1 \right) \right) = \frac{\left(\frac{2 \cdot 3/4 \eta^2 + 6 + 4}{n_{\text{allbays}}} \right) \cdot \left(\frac{\pi \eta^2}{2} - 2A_{II} \right) + \left(\frac{2 \cdot 3/4 \eta^2}{n_{\text{allbays}}} \right) \cdot \left(\frac{\pi \eta^2}{2} - A_{II} \right)}{(n_{\text{cases}} - 1) \cdot \eta + 2\eta^2} + \frac{\left(\frac{2 \cdot 3/4 \eta^2 + 8 + 24 + 12}{n_{\text{allbays}}} \right) \cdot A_{II}}{(n_{\text{cases}} - 1) \cdot \eta + 2\eta^2}$$

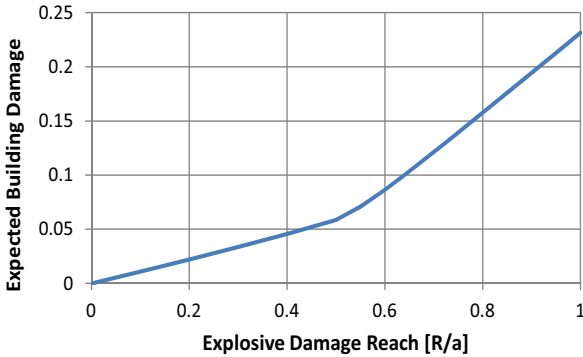


Figure 10. Expected Building Damage. Function of Explosive Damage Reach

SUMMARY

Progressive collapse is a serious threat to structural safety, especially in countries prone to terrorist attacks. An explosion and the associated localized building damage may lead to the total building collapse. Assessment of the building vulnerability requires consideration of multiple damage scenarios in order to ensure satisfactory safety. The number of possible explosion locations and their magnitudes quickly leads to copious collapse analyses. Such numerical, non-linear, large displacement, dynamic simulations are computationally very expensive.

Analytical organization of failure triggering events was introduced in this paper. Closed-form stratification that is based on the explosion characteristics was derived. The novel method provides expressions for the expected building damage as the function of the explosive reach. It requires running the absolute minimum of time consuming, complex nonlinear simulations to assess the structural damage ensuing from a sudden column removal.

REFERENCES

- Osteraas, J. (2006). "Murrah building bombing revisited: A qualitative assessment of blast damage and collapse patterns." *Journal of Performance of Constructed Facilities*, 20(4), 330-335.
- Szyniszewski, S. (2009). "Dynamic energy based method for progressive collapse analysis." *2009 Structures Congress - Don't Mess with Structural Engineers: Expanding Our Role, April 30, 2009 - May 2, 2009*, Proceedings of the 2009 Structures Congress, American Society of Civil Engineers, Austin, TX, United States, 1259-1268.

Design of supplemental dampers for seismic risk reduction of isolated bridges

Alexandros A. Taflanidis¹

¹University of Notre Dame, Department of Civil Engineering and Geological Sciences, Notre Dame, IN, 46556, USA, email: a.taflanidis@nd.edu

ABSTRACT

In this work the probabilistically-robust design of supplemental dampers for multi-span bridge systems is investigated. The adopted bridge model explicitly addresses nonlinear characteristics of the isolators and the dampers, the dynamic behavior of the abutments and pounding effects. A probabilistic framework is used to address the various sources of structural and excitation uncertainties and characterize seismic risk. Stochastic simulation is used to evaluate this risk and perform the associated design optimization for the dampers.

INTRODUCTION

Applications of seismic isolation techniques to bridges have gained significant attention over last decade (Makris and Zhang 2004). Lead-rubber bearings are typically selected for this purpose in order to isolate the bridge deck from its support, at the abutments and potentially at the locations of intermediate piers. This configuration provides with enhanced capabilities for energy dissipation during earthquake events while also accommodating thermal movements during the life-cycle of operation of the bridge. It is associated, though, with large displacement for the bridge deck relative to its supports, especially under near fault earthquake ground motions. Such large displacements may lead to (i) large inelastic deformations and plastic hinging at the piers and abutments or to (ii) pounding of the deck between adjacent spans or to intermediate seismic stoppers or to the abutments supporting the ends of the bridge. Such excessive vibrations will ultimately lead to significant damages that affect not only the serviceability but also the structural integrity of the bridge system. For controlling such vibrations, application of seismic dampers has been proposed and applied to isolated bridges (Makris and Zhang 2004). One of the main challenges in the design of such dampers has been the explicit consideration of the nonlinear behavior of the isolators and the dampers in the design process. Another challenge has been the efficient control of the dynamic response under future near-field ground motions considering their potential variability. This work investigates an approach that addresses all these challenges. A probabilistic framework is used to address the various sources of uncertainty and characterize seismic risk, and stochastic simulation is then used to evaluate this risk. In this setting, consideration of complex nonlinear models for the system is feasible and all important sources of nonlinearity may be incorporated into the model used.

BRIDGE MODEL

For simplicity of the analysis, we will assume a two-span, straight bridge, whose fundamental behavior in the longitudinal direction can be adequately characterized with a planar model. Each span of the bridge is modeled as a rigid body. The interaction with the abutment and the dynamic characteristics of the latter are incorporated in the analysis by modeling the abutment as a mass connected to the ground by a spring and a dashpot, with stiffness and damping properties that are related to the local soil conditions. A schematic of the bridge model with two spans is illustrated in Figure 1. The two spans and abutments are distinguished by using the convention *right* and *left* for each of them. The gap between the two spans is denoted by x_o and the gap between the left or right span and the corresponding abutment by x_{ol} or x_{or} , respectively. Let also x_p , x_{sl} , x_{sr} , x_{al} , x_{ar} , denote, respectively, the displacement relative to the ground of the pier, the left and right span of the bridge and the left and right abutment. The total mass for the pier, the left and right span of the bridge and the left and right abutment are denoted, respectively, by m_p , m_{sl} , m_{sr} , m_{al} , m_{ar} . This leads to equation of motion:

$$\begin{aligned} m_{sl}\ddot{x}_{sl} + (f_{ial} + f_{cl} + f_{dl}) + f_{ipl} + f_c &= 0 \\ m_{sr}\ddot{x}_{sr} + (f_{iar} + f_{cr} + f_{dr}) + f_{ipr} - f_c &= 0 \\ m_p\ddot{x}_p + C_p\dot{x}_p + f_p - f_{ipl} - f_{ipr} &= -m_p\ddot{x}_g \\ m_{al}\ddot{x}_{al} + C_{al}\dot{x}_{al} + f_{al} - (f_{ial} + f_{cl} + f_{dl}) &= -m_{al}\ddot{x}_g \\ m_{ar}\ddot{x}_{ar} + C_{ar}\dot{x}_{ar} + f_{ar} - (f_{iar} + f_{cr} + f_{dr}) &= -m_{ar}\ddot{x}_g \end{aligned}$$

where \ddot{x}_g is the ground acceleration; C_p , C_{al} , C_{ar} denote, respectively, the damping coefficient for the pier and the left and right abutment; f_c , f_{cl} and f_{cr} are the impact forces due to pounding between the two spans or between the spans and the left or right, respectively, abutments; f_{dl} and f_{dr} are the left and right damper forces; and f_{ial} , f_{ipl} or f_{iar} , f_{ipr} are the forces of the isolators that support the left or right span of the bridge to the abutment and the pier, respectively; f_p corresponds to the restoring force for the pier which is modeled as hysteretic bilinear force with ultimate strength as depicted in Figure 1. All these forces are discussed in more detail next.

The hysteretic behavior of each isolator is described by a Bouc-Wen model:

$$\delta_{yi}\dot{z} = \alpha_{is}\dot{x}_b - z^2(\gamma_{is}\operatorname{sgn}(\dot{x}_bz) + \beta_{is})\dot{x}_b$$

where x_b is the displacement of the isolator, which corresponds to the relative displacement of the span relative to its support; z is a dimensionless hysteretic state-variable that is constrained by values ± 1 ; δ_{yi} is the yield displacement; and α_{is} , β_{is} , and γ_{is} are dimensionless quantities that characterize the properties of the hysteretic behavior. Typical values for these parameters are used here, taken as $\alpha_{is}=1$, $\beta_{is}=0.1$, and $\gamma_{is}=0.9$. The isolator forces f_i may be then described based on the state-variable z and the relative isolator displacement x_b . For lead-rubber bearings, these forces are:

$$f_i = k_p x_b + (k_e - k_p)\delta_{yi}z \quad (1)$$

where k_p is the post yield stiffness and k_e the pre-yield stiffness.

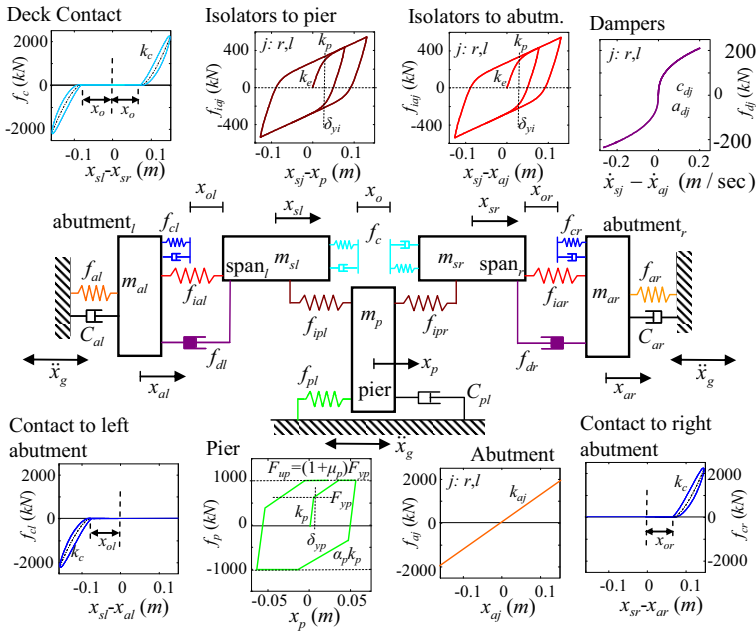


Figure 1: Schematic model for two-span bridge system

The force due to pounding between the adjacent spans is modeled as a double-sided Hertz contact force with an additional damper that incorporates in the analysis the energy dissipated during the contact (Muthukumar and DesRoches 2006)

$$f_c = \begin{cases} 0 & ; \text{if } |x_{sl} - x_{sr}| \leq x_o \\ k_c \operatorname{sgn}(x_{sl} - x_{sr}) |x_{sl} - x_{sr}|^{\beta_c} + c_c (\dot{x}_{sl} - \dot{x}_{sr}) & ; \text{if } |x_{sl} - x_{sr}| \geq x_o \end{cases}$$

where $\operatorname{sgn}(\cdot)$ is the sign function, k_c the contact stiffness, c_c the non-linear damper coefficient and β_c the contact exponent, taken here with the nominal value for Hertz type of impact, i.e. $\beta_c=1.5$ (Muthukumar and DesRoches 2006). The damper coefficient may be expressed in terms of the ratio of relative velocities of the pounding bodies before and after the contact, called coefficient of restitution e_c , as :

$$c_c = k_c 0.75 |x_{sl} - x_{sr}|^{\beta_c} (1 - e_c^2) / |v_{con}|$$

where v_c is the relative velocity at the beginning of contact. The force due to pounding of the left (or right) span to the left (or right) abutment are modeled similarly as left (or right)-sided contact forces.

For viscous damper connecting the left span to the corresponding abutment (Makris and Zhang 2004) the force is described

$$f_{dl} = c_d \operatorname{sgn}(\dot{x}_{sl} - \dot{x}_{al}) |\dot{x}_{sl} - \dot{x}_{al}|^{\alpha_d} \quad (2)$$

where c_d is the damping coefficient and α_d an exponent parameter. These adjustable characteristics are the controllable damper parameters to be selected at the design stage. Maximum forcing capabilities for the damper, related to cost constraints, may be incorporated into the model as a saturation of the damper force to f_{\max} . Similar modelling holds for the dampers connecting the light span to the abutment.

NEAR FAULT EXCITATION MODEL

The analysis and design of any seismic system needs to be performed considering potential damaging future ground motions. For base-isolated bridges this translates to consideration of near-fault ground motions and a stochastic model for such excitations is discussed next. According to it the high-frequency and long-period components of the motion are independently modeled and then combined to form the acceleration time history. The fairly general, point source stochastic method is selected for modeling the higher-frequency ($>0.1\text{--}0.2$ Hz) component. This method is based on a parametric description of the ground motion’s radiation spectrum $A(f;M,r)$, which is expressed as a function of the frequency, f , for specific values of the earthquake magnitude, M , and epicentral distance, r . The duration of the ground motion is addressed through an envelope function $e(t;M,r)$, which again depends on M and r . More details on $A(f;M,r)$ and $e(t;M,r)$, are provided in (Taflanidis et al. 2008). The time-history (output) for a specific event magnitude, M , and source distance, r , is obtained according to this model by modulating a normalized white-noise sequence $\mathbf{Z}_w=[Z_w(i\Delta t): i=1,2,\dots, N_T]$ by $e(t;M,r)$ and subsequently by $A(f;M,r)$.

For describing the pulse characteristic of near-fault ground motions, the simple analytical model developed by Mavroeidis and Papageorgiou (2003) is selected. According to it, the pulse component of near-fault motions is described through the following expression for velocity pulse:

$$V = \frac{A_p}{2} \left[1 + \cos \left(\frac{2\pi f_p}{\gamma_p} (t - t_o) \right) \right] \cos [2\pi f_p (t - t_o) + \nu_p]; t \in [t_o - \frac{\gamma_p}{2f_p}, t_o + \frac{\gamma_p}{2f_p}] \quad (3)$$

= 0; otherwise

where $A_p, f_p, \nu_p, \gamma_p$, and t_o describe the signal amplitude, prevailing frequency, phase angle, oscillatory character (i.e., number of half cycles), and time shift to specify the epoch of the envelope’s peak, respectively. A number of studies (Mavroeidis and Papageorgiou 2003; Bray and Rodriguez-Marek 2004) have been directed towards developing relationships that connect these pulse characteristics to the seismic hazard of a site. These studies link the amplitude and frequency of near-fault pulses to the moment magnitude and epicentral distance of seismic events. For the rest of the pulse parameters no clear link has been yet established. They need to be considered as independent model parameters. The *stochastic model* for near-fault motions is finally established by combining the above two components (Taflanidis et al. 2008). The model parameters consist of the seismological parameters M and r , the additional parameters for the velocity pulse, $A_p, f_p, \nu_p, \gamma_p$, and the white noise sequence \mathbf{Z}_w .

PROBABILISTICALLY ROBUST DESIGN

The characteristics of the models for the seismically isolated bridge and for future earthquake excitations, are not known with absolute certainty. For explicitly incorporating all uncertainties in the modeling process, let $\theta \in \Theta \subset \mathcal{R}^{n_\theta}$, denote the augmented vector of model parameters for the structural system, θ_s , and the excitation, θ_q , models, where Θ represents the space of possible model parameter values. The uncertainty in these model parameters is then quantified by assigning a probability model $p(\theta)$ to them, which incorporates our available prior knowledge about the system and its environment into the model. Also, let the vector of controllable damper parameters, referred to herein as *design variables*, be $\varphi \in \Phi \subset \mathcal{R}^{n_\varphi}$, where Φ denotes the admissible design space.

Finally, the seismic performance of the bridge, for specific design φ and model description θ , is characterized by the performance measure $h(\varphi, \theta)$, which ultimately quantifies performance according to the designer criteria (an example is discussed in the illustrative application considered later). In this stochastic setting, the overall performance is then described by the following *stochastic integral* that corresponds to the expected value of $h(\varphi, \theta)$ and ultimately quantifies seismic risk

$$C(\varphi) = \int_{\Theta} h(\varphi, \theta) p(\theta) d\theta \quad (4)$$

Since the models adopted for the bridge and the excitation are complex and include a large number of uncertain model parameters this multi-dimensional integral (4) cannot be calculated, or even accurately approximated, analytically. An efficient alternative approach is to estimate the integral by *stochastic simulation*. Using a finite number, N , of samples of θ drawn from some importance sampling density $p_{is}(\theta)$, an estimate for (4) is given by

$$\hat{C}(\varphi) = 1/N \sum_{i=1}^N h(\varphi, \theta_i) p(\theta_i) / p_{is}(\theta_i) \quad (5)$$

where vector θ_i denotes the sample of the uncertain parameters used in the i^{th} simulation. The importance sampling density $p_{is}(\theta)$ may be used to improve the efficiency of this estimation. This is established by focusing on regions of the Θ space that contribute more to the integrand of the stochastic integral in (4). If $p_{is}(\theta) = p(\theta)$ then the evaluation in (5) corresponds to direct Monte Carlo. The robust stochastic design is finally established by selecting the design variables that minimize $C(\varphi)$, and is expressed through the *stochastic optimization*

$$\varphi^* = \arg \min_{\varphi \in \Phi} \hat{C}(\varphi)$$

where any additional deterministic constraints, related, for example, to location or space constraints for the dampers are incorporated into the definition of admissible design space Φ . The estimate of the objective function for this optimization involves an unavoidable estimation error and significant computational cost, features that make the optimization problem challenging. The novel two-stage optimization approach (Taflanidis and Beck 2008), based on the innovative Stochastic Subset Optimization (SSO) algorithm, is used in this study to efficiently perform this optimization.

TWO-SPAN BRIDGE EXAMPLE

Models and uncertainty description. The design of nonlinear viscous dampers for a two-span seismically isolated bridge is considered. The mass of the pier is taken as $m_p=100$ ton. For the pier restoring force f_p as illustrated in Figure 1, the initial stiffness k_p , post-yield stiffness coefficient α_p , over-strength factor μ_p , yield displacement δ_{yp} , have mean values 70 kN/mm, 10%, 30% and 0.04 m, respectively. All these parameters are treated as independent Gaussian variables with coefficient of variation 10%. The damping coefficient C_p is selected based on modal damping assumption, using the initial period of the pier. The damping ratio ζ_p is treated as uncertain variable following a log-normal distribution with median 3% and coefficient of variation 25%. The mass of the left and right abutments are taken, respectively, as $m_{al}=400$ ton, $m_{ar}=500$ ton. For the right and left abutment restoring forces f_{ar} , f_{al} the stiffness's k_{ar} and k_{al} , respectively, are modeled as correlated Gaussian variables with mean value 2500 kN/mm, coefficient of variation 15%, and correlation coefficient 50%. The damping ratios for each abutment ζ_{al} , ζ_{ar} are treated as correlated uncertain variables following a log-normal distribution with median 8%, coefficient of variation 20% and correlation coefficient 50%.

For the left and right span of the bridge the self-weight of the deck is taken as 1000 and 1200 ton respectively. Vehicle traffic is modeled as additional loads m_{il} and m_{ir} for the left and right span, respectively, that follow independent exponential distributions with mean value 20 ton. The isolators connecting each span to its supports are lead-rubber bearings modeled by Equation (1). All isolators have same properties; post-yield stiffness $k_e=3.0$ kN/mm, pre-yield stiffness $k_p=30.0$ kN/mm, and yield displacement $\delta_{yp}=2.5$ cm. The contact stiffness for all Hertz impact forces, between the two spans or between each of the spans and the respective abutment, is taken as $800 \text{ kN/mm}^{1.5}$ (Muthukumar and DesRoches 2006). The respective gap dimensions x_o , x_{ol} , x_{or} , whose potential variability is influenced by common weather conditions, are modeled as correlated log-normal variables with median 10 cm, coefficient of variation 20%, and large correlation coefficient, 70%. The coefficient for restitution for the energy dissipated during contact is modeled as a truncated [0 1] Gaussian variable with mean value 0.7 and coefficient of variation 15%.

The uncertainty in moment magnitude for seismic events, M , is modeled by the Gutenberg-Richter relationship truncated to the interval $[M_{min}, M_{max}]=[6, 8]$, which leads to a PDF $p(M)=b \exp(-bM)/[\exp(-bM_{min})-\exp(-bM_{max})]$ with b representing a regional seismicity factor, chosen in this study as $b=0.9 \log_e(10)$. For the uncertainty in the event location, the epicentral distance, r , is assumed to follow a log-normal distribution with median 8 km and coefficient of variation 0.5. For the near-field pulse, the pulse frequency f_p (rad/sec) and the peak ground velocity A_v (cm/sec) are selected (Bray and Rodriguez-Marek 2004) to be log-normally distributed with median value

$$\ln \tilde{f}_p = 8.60 - 1.32M \quad \ln \tilde{A}_v = 4.46 + 0.34M - 0.58 \ln(r^2 + 7^2)$$

and coefficient of variation 0.39 and 0.4, respectively. The probability models for the number of half cycles and phase are chosen, respectively, as Gaussian with mean 2 and coefficient of variation 15%, and uniform in the range $[-\pi/2, \pi/2]$.

Damper configuration and performance. Nonlinear viscous dampers are applied to the connection of each of the two spans to its corresponding abutment, as illustrated in Figure 1. They are modeled by Equation (2) with maximum force capability for each damper, selected as 4000 kN. Coefficients a_d and c_d correspond to the design variables for the problem and for cost reduction (bulk ordering) are chosen the same for all dampers. The initial design space for each of them is defined as $a_d \in [0.3, 2]$ and $c_d \in [0.1, 30]$ MN (sec/m) a_d . A simplified design problem is also considered where a_d is set to 1, corresponding to a linear viscous damper. The bridge performance measure assumed in this study addresses potential seismic damages for all components of the bridge: the pier, the abutments, and the deck. The failure criteria used are: (i) the maximum pier shear V_p , associated with yielding and inelastic deformations for the pier, (ii) the maximum displacement for the left and right abutment x_r and x_l , respectively, associated with permanent deformations for the ground, and (iii) the maximum velocity for impact between the two spans v_o or between each of the spans and the left or right abutment v_l and v_r , respectively, associated with the damages that occur during pounding. The performance measure is the average of the fragilities for each of these components. The fragilities are assumed to have a lognormal distribution with median μ and coefficient of variation β , so

$$h(\boldsymbol{\varphi}, \boldsymbol{\theta}) = 1 / 6 \sum_{i=1}^6 \Phi_g(\ln(z_i / \mu_i) / \beta_i)$$

where Φ_g is the standard Gaussian cumulative distribution function and $\mathbf{z} = \{V_p, x_r, x_l, v_o, v_l, v_r\}$ is the performance variable vector. The characteristics for the median of the fragility curves are $\mu_p = 2000$ kN for the pier shear, $\mu_x = 8$ mm for the abutment displacement and $\mu_v = 10$ cm/sec for the impact velocity, whereas the coefficient of variation is set for all of them equal to $\beta_p = \beta_x = \beta_v = 0.5$.

Results and discussion Results are presented in Table 1 for the optimal design, which includes the optimal design configuration for both nonlinear (NLD) and linear damper implementation, the overall objective function $C(\boldsymbol{\varphi})$ as well as the expected fragility for each of the components. The performance of the bridge with no dampers (NoD) is also reported. The results illustrate that the addition of the viscous dampers leads to significant reduction of seismic risk for the bridge; there is a big deference between the optimal $C(\boldsymbol{\varphi}^*)$ and the uncontrolled performance $C(\boldsymbol{\theta})$. All six components contributing to the overall fragility are characterized by a considerable reduction, with the maximum pounding velocities having the largest one. This illustrates that the viscous dampers can significantly reduce the undesirable impact between the different spans, which can have devastating effects for the serviceability of the bridge, while simultaneously efficiently controlling other modes of failure for the bridge, as the pier shear or the abutment displacements. It should be also pointed out that the optimal linear damper configuration provides still a significant improvement over the uncontrolled bridge performance. Implementation, though, of nonlinear dampers provides a further reduction in the bridge fragility, especially with respect to the pier and abutment failure criteria. The exponent coefficient for the dampers under optimal design is 0.72, which corresponds to a significant degree of nonlinearity. This illustrates the importance of a design methodology that can efficiently address damper nonlinearities, so that a truly optimal design is identified

Table 1: Optimization results; units for c_d are MN (sec/m)^{ad}.

Case	Φ^*		$C(\Phi^*)$	Expected fragility for each component					
				V_p	z_l	z_r	v_o	v_l	v_r
NLD	c_d	12.9	0.045	0.109	0.030	0.058	0.067	0.033	0.012
	a_d	0.72							
LD	c_d	26.7	0.056	0.125	0.047	0.083	0.007	0.032	0.011
	a_d	1.00							
NoD	c_d	0	0.279	0.367	0.152	0.231	0.287	0.374	0.261
	a_d	-							

CONCLUSIONS

The robust design of supplemental dampers for seismically isolated multi-span bridge systems was discussed in this study. The basis of the suggested approach is a probabilistic framework that explicitly addresses all sources of uncertainty, related either to future excitations or to the structural configuration, by appropriate probability models. Seismic risk is then expressed by a multidimensional integral over the space of the uncertain model parameters. Stochastic simulation was suggested for evaluation of this stochastic performance which allowed for consideration of complex nonlinear models for the bridge system and its excitation. An example was presented that considered the design of nonlinear viscous dampers for a two-span bridge protection.

REFERENCES

- Bray, J. D., and Rodriguez-Marek, A. (2004). "Characterization of forward-directivity ground motions in the near-fault region." *Soil Dynamics and Earthquake Engineering*, 24, 815-828.
- Makris, N., and Zhang, J. (2004). "Seismic response analysis of a highway overcrossing equipped with elastomeric bearings and fluid dampers." *Journal of Structural Engineering*, 130(6), 830-845.
- Mavroeidis, G. P., and Papageorgiou, A. P. (2003). "A mathematical representation of near-fault ground motions." *Bulletin of the Seismological Society of America*, 93(3), 1099-1131.
- Muthukumar, S., and DesRoches, R. (2006). "A Hertz contact model with non-linear damping for pounding simulation." *Earthquake Engineering & Structural Dynamics*, 35, 811-828.
- Taflanidis, A. A., and Beck, J. L. (2008). "An efficient framework for optimal robust stochastic system design using stochastic simulation." *Computer Methods in Applied Mechanics and Engineering*, 198(1), 88-101.
- Taflanidis, A. A., Scruggs, J. T., and Beck, J. L. (2008). "Probabilistically robust nonlinear design of control systems for base-isolated structures." *Journal of Structural Control and Health Monitoring*, 15(3), 697-719.

Evaluating the Efficiency of Current Nonlinear Static Pushover Procedures on Estimating Torsion effect for asymmetric High-rise Buildings

Q.W. Zhang*, Kusnowidjaja Megawati, L.P. Huang, T. C. Pan

1 School of Civil & Environmental Engineering, Nanyang Technological University, N1.1-B3-03d, 50 Nanyang Avenue, Singapore, P.O. Box 639798, Tel: (65) 6592-7548, Fax: (65) 6790-1585, Email: qwzhang@ntu.edu.sg

ABSTRACT:

In present paper, the capability of current nonlinear static pushover methods on estimating the torsion effects of existing buildings has been studied. One real high-rise building with dominant torsion mode has been performed pushover analysis using two classic nonlinear static pushover procedures. Time history analysis has also been performed using tremor monitoring ground acceleration records. According to the comparison between the results of pushover analysis and time history analysis, the efficiency of MPA procedures and N2 method on estimating torsion effect for asymmetric high-rise buildings have been evaluated.

KEYWORDS:

Nonlinear Static Pushover Procedures, Torsion Effects, N2 Method, MPA Method

1. INTRODUCTION

The nonlinear static procedure (NSP) is an analysis which using an incremental iterative solution of static equilibrium equation to obtain the response of structure to increasing lateral load pattern. NSP can easily provide valuable information about the locations of structural weaknesses and failure mechanisms in the inelastic range. The NSP is now widely used by the structural engineers as a standard tool for estimating seismic demands for buildings. The earlier NSP method can be divided to three stages which are: (i) the Capacity Spectrum Method (CSM), adopted by ATC-40 [1996]; (ii) the Displacement Coefficient Method (DCM), presented in FEMA-273 [1997] and then further developed in FEMA 356 [2000];(iii) the N2 method, adopted by EC 8[2004]. Lots of earthquake field investigations show that irregular structures were suffered more damage than regular buildings. Elevation irregularities may cause weak story failures along the height of building. Plan irregularities, on the other hand, may cause non-uniform damage among the structural elements of the same story due to non-uniform displacement demands [2007]. As an approximate method, the early stage NSP has certain shortcomings on well considering the torsion effects of the buildings. Starting in 1997, many researchers put significant efforts into extending pushover analysis to

asymmetric-plan buildings. By applying a height-wise distribution of lateral forces at the floor centers of mass, an approximate non-linear static analysis procedure was developed by Kilar V and Fajfar P. [1996]. De Stefano M and Rutenberg A. focused on special considerations necessary to consider interaction between walls and frames in pushover analysis of wall-frame structures [1998]. Faella G and Kilar V. investigated the accuracy of applying lateral forces at different locations in the plan of asymmetric buildings [1998]. A classic method, modal pushover analysis (MPA), in which combining 'modal' demands due to the first two or three terms of expansion was extended to asymmetric-plan buildings by Chopra A.K. and Goel R.K. (2004). N2 method, another simplified nonlinear methods based on pushover analysis and inelastic response spectrum has also been extended to considering torsion effects of the buildings by Peter Fajfar, Damjan, Maru Sic and Iztok Perus[2005]. Four real buildings subjected to inelastic response-history analyses and pushover analyses were performed by Kosmopoulos A.J. and M. N. Fardis[2007] in order to estimating inelastic seismic deformations in asymmetric multi-storey RC buildings. Emrah Erduran(2008) use two idealized building to evaluate the capability of current nonlinear static procedures in capturing torsion effects.

Present study will concentrated in evaluating the efficiency and applicability of two classic nonlinear static pushover methods on estimating seismic performance for existing high-rise buildings with irregular plan. One existing building with 19 stories, irregularities in plan and little engineered earthquake resistance is chosen to perform the analysis. Results of the response history analyses (RHA) using the tremor monitoring records will be compared with the estimates obtained from the NSP.

2. DESCRIPTION OF THE PROCEDURES

Modal Pushover Analysis Procedure Modal pushover analysis (MPA) was developed by Chopra A.K. and Goel R.K. (2002). In MPA procedure, the seismic demand due to individual terms in the modal expansion of the effective earthquake forces is determined by non-linear static analysis using the inertia force distribution for each mode. These 'modal' demands due to the first few terms of the modal expansion are then combined by the CQC rule to obtain an estimate of the total seismic demand for inelastic systems. When applied to elastic systems, the MPA procedure is equivalent to standard response spectrum analysis (RSA). MPA was originally used for analyzing planar structures. Chopra A.K. and Goel R.K.[2004] extended the concept to estimate seismic demands of plan-asymmetric buildings. The basic procedure of the MPA to estimate the seismic demands for an asymmetric plan multi-storey building can be summarized as a sequence of following steps:

- 1) Compute the natural frequencies and modes of the building.
- 2) For the n th mode, develop the base shear-roof displacement pushover curve by non-linear static analysis of the building. Between the two pushover curves obtained

corresponding to two lateral directions, x and y , preferably choose the pushover curve in the dominant direction of motion of the mode.

3) Idealize the pushover curve as a bilinear curve. Convert the idealized pushover curve to the force–displacement relation for the n th mode inelastic SDF system.

4) Compute the peak deformation of the n th mode inelastic single-degree-of-freedom (SDF) system defined by the force–deformation relation and damping Ratio.

5) Calculate peak roof displacement in the direction of the selected pushover curve associated with the n th mode inelastic SDF system.

6) Repeat Steps 3–5 steps for as many modes as required for sufficient accuracy. Compute the dynamic response due to the n th mode.

7) Determine the total response (demand) by combining gravity response and the peak modal responses using the CQC rule.

N2 Method The original N2 Method was developed by Fajfar P. [2000] for the nonlinear static analysis of planar structures. The method combines the pushover analysis of multi-degree-of-freedom (MDOF) models with the response spectrum analysis of an equivalent single-degree-of-freedom system. Fajfar and his co-workers find that any favorable torsional effect on the stiff side, which may arise from elastic analysis, may disappear in the inelastic range. It means that the results obtained by pushover analysis of a 3D structural model could be combined with the results of a linear dynamic (spectral) analysis. The former results control the target displacements and the distribution of deformations along the height of the building, whereas the latter results define the torsional amplifications. Based on this assumption Fajfar and his co-workers developed the extension of the N2 method to plan asymmetric buildings[2005]. The basic steps of the extended N2 method are as below:

1) Perform pushover analyses by using a 3D mathematical model. Loading is applied at the centers of mass, independently in two horizontal directions. Determine the target displacement (displacement demand at CM at roof level) for each of two horizontal directions.

2) Perform a linear modal analysis of the 3D mathematical model, independently for excitation in two horizontal directions and combine the results according to the SRSS rule.

3) Determine the correction factors to be applied to the relevant results of pushover analyses. The correction factor is defined as the ratio between the normalized roof displacements obtained by elastic modal analysis and by pushover analysis. The normalized roof displacement is the roof displacement at an arbitrary location divided by the roof displacement at the CM. If the normalized roof displacement obtained by elastic modal analysis is smaller than 1.0, take 1.0. Correction factors are defined for each horizontal direction separately. The correction factor depends on the location of the plan.

4) Multiply all relevant quantities obtained by pushover analyses with appropriate correction factors. For example, in a perimeter frame parallel to the X-axis, all quantities are multiplied with the correction factor determined with pushover results obtained for loading in the transverse direction and for the location of this frame.

3. DESCRIPTION OF BUILDING

Singapore, an island state located at latitude 1.3° N and longitude 103.8° E with an area of about 700 km^2 , is relatively far from earthquake zones in Sumatra. It is, however, frequently shaken by large-magnitude earthquakes along the Sumatran subduction zone and the Sumatran fault. In order to evaluate the seismic capacity of existing buildings in Singapore, some tri-axial seismic sensors were installed at the selected buildings. One of these buildings with asymmetric plan is selected as the example building to perform the evaluating analysis.

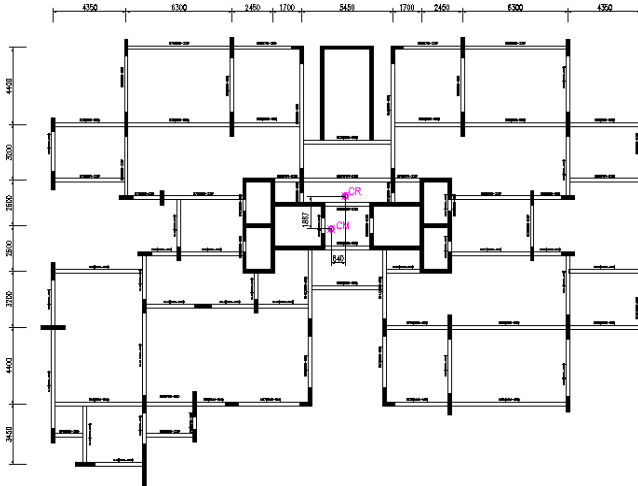


Figure 1 Typical Storey Structural Plan

Selected building was built in the 1990s and located in east part of Singapore. It is a 19th-storey building with irregular in plan. The structure plan of typical floor is shown in figure 1 and a 3D FEM model view is shown in figure 2. The length of the building is 35.05m and width of the building is 23.85m. The structure system of the building is RC beam-column frame & shear wall structure.

To qualify the asymmetry of each building, the following two points were established and shown in figure 1:

Centre of rigidity, CR, is determined as the location of the centroid of the stiffness of single-story lateral resisting elements (typically planar) arbitrarily located in plan.

Center of mass, CM, is the mean location of all the mass in a system.

The center of mass was shifted in the longitudinal direction by 1.87 m, about 8% of the plan dimension and was shifted in the transverse direction by 0.84 m, about 3% of the plan dimension. Therefore, the present building can be regarded as a bi-directional eccentricity structure.

Ground motion The magnitude 7.6 southern Sumatra earthquake of September 30, 2009 occurred as a result of oblique-thrust faulting near the subduction interface plate boundary between the Australian and Sunda plates. Figure 3 shows the ground motion of example building recorded during the magnitude 7.6 earthquake on 30 September 2009.

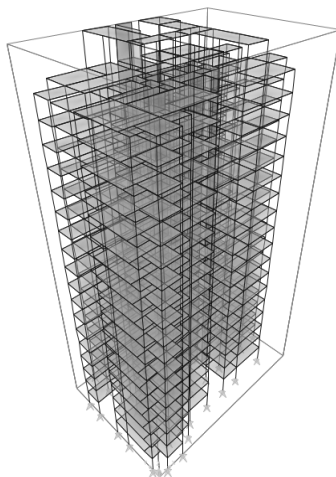


Figure 2 FEM model

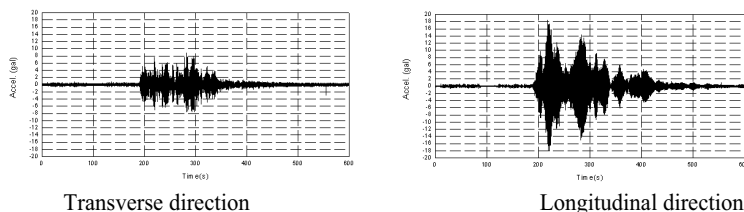


Figure 3 Ground Motion Records

4. ANALYSIS RESULTS COMPARISON

Nonlinear static analysis procedures

The pushover analyses of the bi-directionally eccentric system under modal type lateral force and uniform lateral loads distribution have been performed. The capacity curve under first three modal shape lateral loads distribution and uniform lateral load distribution are shown in figure 4 and figure 5 respectively. For modal pushover analyses, the contribution of the first three modes pairs was included in analysis. For N2 method, considering the dominant displacement of first mode is torsion, the pushover analysis under the uniform force distribution was performed. All of these analyses are performed by SAP 2000.

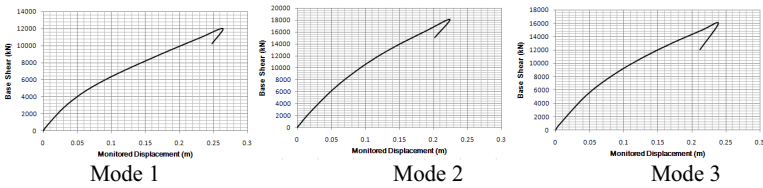


Figure 4 Pushover curve (mode shape load)

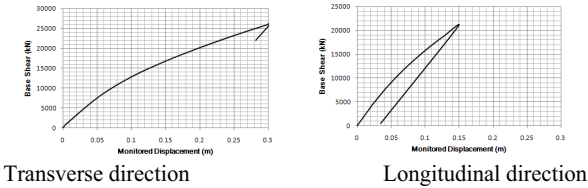


Figure 5 Pushover curve (uniform load)

Time history analysis

The conclusions carried out by Peter Fajfar et. al. (2005) show that any favorable torsion effect which may arise from elastic analysis may disappear in the inelastic range. Therefore, in order to simplify the analysis without losing precision, one bi-directional THA is presently performed. The displacement response time histories obtained by THA are shown in figure 6.

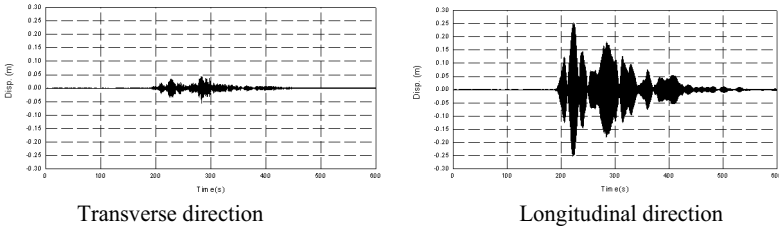


Figure 6 Displace response time history curve

Results comparison

In order to compare the torsion components, the results of NSP and THA are presented in terms of displacements normalized by the displacement at the mass centre (u/u_{CM}). In mass-eccentric systems, the flexible edge is the edge nearer to the mass centre CM, and stiff edge is the other edge. Displacements are plotted separately for transverse and longitudinal direction. Schematic plots of the floor-plan and of normalized displacements in Figure 7.

From figure 7, the following conclusions can be carried out:

1. Excellent agreement of the N2 method and MPA procedure results with the results of THA procedure can be observed for the building on the transverse direction.
2. On the longitudinal direction, the results obtained by N2 method are still very close to the results obtained by THA method. But for MPA method, torsion effects are over-estimated. The reasons of differences may due to the basic

assumption of the MPA method. For MPA procedure, ‘modal’ demands due to the first few terms of the modal expansion are combined by the CQC rule to obtain an estimate of the total seismic demand for inelastic systems. For the buildings with dominant torsional mode shape, the lateral load distribution will affect final combining results significantly. Actually, when earthquake occur, the building is impossibly subjected to pure torsional type lateral load distribution. Therefore, for the buildings with dominant torsional mode shape, the MPA procedure may over-estimate the torsion effects on the building.

3. In general, both MPA method and N2 method can provide a relative precise estimation of torsion effect on the building.

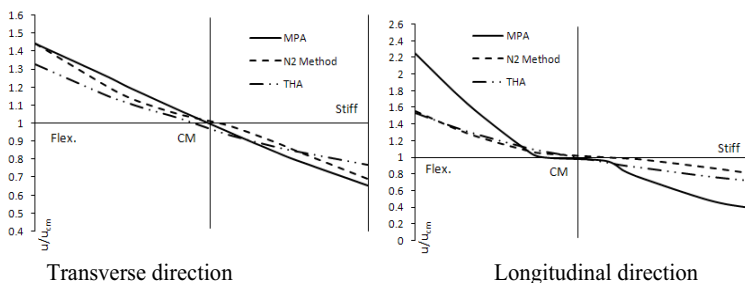


Figure 7 Torsion effects obtained by different analyses

5. CONCLUSION

Present study evaluated the efficiency and applicability of two current nonlinear static pushover methods on estimating seismic performance for asymmetric high-rise buildings with irregular plan. The comparisons between results of nonlinear pushover analyses and time history analyses of one existing building show that both N2 and MPA method can provide a well estimating for the torsion effect on transverse direction. Nevertheless, on the longitudinal direction, errors from MPA procedure are increasing due to overestimate torsional effects when using CQC rule combining ‘modal’ demands obtained from the first few terms of the modal expansion. In general, both MPA method and N2 method can provide a relative precise estimation of torsion effect on the building.

REFERENCES

- ATC(Applied Technology Council) (1996). *Seismic Evaluation and Retrofit of Concrete Buildings, Volume 1. ATC-40 Report*, Redwood City, California.
- CEN(European Committee for Standardisation) (2004). “*European (draft) Standard EN 1998-1: Eurocode 8 – Design of Structures for Earthquake Resistance – Part 3: Assessment and Retrofitting of Buildings – Stage 49.*” CEN, Brussels.

- Chopra A.K., Goel R.K. (2002). "A modal pushover analysis procedure for estimating seismic demands for buildings." *Earthquake Engineering and Structural Dynamics* , 31(3),561 - 582.
- Chopra, A.K. and Goel, R.K. (2004). "A modal pushover analysis procedure to estimate seismic demands for unsymmetric-plan buildings." *Earthquake Engineering and Structural Dynamics* ,33(8), 903 - 927.
- De Stefano M., Rutenberg A. (1998). "Predicting the dynamic response of asymmetric multistorey wall-frame structures by pushover analysis: two case studies." *Proceedings of the 11th European Conference on Earthquake Engineering*, Balkema, Rotterdam.
- Erduran E.(2008). "Assessment of current nonlinear static procedures on the estimation of torsional effects in low-rise frame buildings ." *Engineering Structures*, 30 2548–2558
- Faella G., Kilar V. (1998). "Asymmetric multi-storey R/C frame structures: push-over versus nonlinear dynamic analysis." *Proceedings of the 11th European Conference on Earthquake Engineering*, Balkema, Rotterdam.
- Fajfar P. (2000). "A nonlinear analysis method for performance-based seismic design." *Earthquake Spectra*,16(3), 573 - 592.
- Fajfar P., Marusic D., Peruc I. (2004). "Torsional effects in the pushover-based seismic analysis of buildings." *Journal of Earthquake Engineering*, 9(6), 831–54.
- FEMA (Federal Emergency Management Agency) (1997). *NEHRP Guidelines for the Seismic Rehabilitation of Buildings, Developed by the Building Seismic Safety Council for the Federal Emergency Management Agency (Report No. FEMA 273)*. Washington, D.C.
- FEMA (Federal Emergency Management Agency) (2000). *Pre-standard and commentary for the seismic rehabilitation of buildings (Report No. FEMA 356)*. Washington, D.C.
- Kosmopoulos A.J., Fardis M.N. (2007). "Estimation of inelastic deformations in asymmetric multistory RC buildings." *Earthquake Engineering and Structural Dynamics*, 36(9), 1209–34.
- Kilar V., Fajfar P. (1997). "Simple push-over analysis of asymmetric buildings." *Earthquake Engineering and Structural Dynamic* , 26(2),233–249.

Analysis of Bridge Performance under the Combined Effect of Earthquake and Flood-induced Scour

Swagata Banerjee¹ and Gautham G. Prasad²

¹Department of Civil and Environmental Engineering, Pennsylvania State University, State College, PA 16802; PH (814) 863-2936; email: swagata@engr.psu.edu

²Department of Civil and Environmental Engineering, Pennsylvania State University, State College, PA 16802; PH (510) 366-6690; email: gug124@psu.edu

ABSTRACT

The study evaluates the combined effect of earthquake and flood-induced scour on the performance of bridges located in regions having moderate to high seismic and flood hazards. For the analysis California is chosen as the bridge site where the probabilities of having these two natural hazards are reasonably high. Two example reinforced concrete (RC) bridges are considered. A 100-year flood event with discharge rate of 158.6 m³/s, velocity of 0.8 m/s and upstream depth of 11.9 m is chosen to represent regional flood hazard. Finite element analyses are performed to evaluate performance of these bridges under regional seismic events in presence of scour resulted from the scenario flood event. Result shows that in presence of flood-induced scour bridges become more vulnerable under seismic excitations.

INTRODUCTION

Bridges are important components of highway and railway transportation systems. Failure of bridges due to natural or manmade hazards may cause significant disruption of transportation system performance, and thus may result in major economic losses to the society. Therefore, safety and serviceability of bridges have always been great concerns to the civil engineering profession.

A large population of bridges (nearly 70% according to the National Bridge Inventory, or NBI) in US is located in moderate to high seismically active, flood-prone regions. Flood-induced soil erosion, commonly known as scour, causes loss of lateral support at bridge foundations (Bennett et al, 2009). This can impose additional flexibility to bridges which in turn may amplify the effect of seismic ground motions. Hence, earthquake in presence of flood-induced scour is a critical multi-hazard for bridges located in seismically active, flood-prone regions. Although the joint probability of occurrence of earthquake and flood within the service life of a bridge is relatively small, one event can occur just after another (even before the aftermath of the previous event is taken care of). For example, an earthquake of magnitude 4.5 struck the state of Washington on January 30, 2009. This seismic event occurred within three weeks after the occurrence of a major flood event in that region. Such successive occurrences of extreme events can significantly increase structural vulnerability from that under discrete events.

The importance of consideration of possible multi-hazard events for the reliable performance evaluation of structures is well understood; however, the availability of relevant literature is very limited. NCHRP Report 489 (Ghosn *et al.* 2003) documented reliability indices of bridges subjected to various combinations of extreme natural hazards. Ghosn *et al.* (2003) assumed each extreme event to be a sequence of independent load effects, each lasting for equal duration of time. The service life of a bridge was also divided into several time intervals with durations equal to that of loads. Occurrence probabilities of independent natural events within each time interval were calculated and combined to obtain joint load effects. This methodology, however, cannot be applied for load combinations involving bridge scour. This is because scour itself does not represent any load; rather it is a consequence of flood hazard. Therefore, load combination or load factor design, as proposed in NCHRP Report 489, may not provide a reliable estimation of bridge performance under a natural hazard in presence of flood-induced bridge scour. Rigorous numerical study is required for this purpose.

In the present study, the combined effect of earthquake and flood-induced scour on bridge performance is studied. Two example reinforced concrete bridges, one 2-span and another 3-span, are considered for this purpose. It is assumed that the example bridges are located in California where the annual probabilities of occurring earthquake and flood are reasonably high. A 100-year flood with a discharge rate of $158.6 \text{ m}^3/\text{s}$, velocity of 0.8 m/s and upstream depth of 11.9 m is considered here. This scenario flood is used by the Federal Emergency Management Agency (FEMA) for a flood insurance study (FIS) in Sutter County, California (FIS 2008). Total scour depths for the two example bridges are calculated as the summation of local and contraction scour following HEC-18 (Richardson and Davis 2001) guidelines. These two scour components are the expected outcome from accelerated flow due to flood or similar events. Finite element model of these example bridges with and without flood-induced scour are developed using SAP2000 Nonlinear (Computer and Structures, Inc. Version 14.1.0) and analyzed under several ground motions that represent the regional seismicity.

EXAMPLE REINFORCED CONCRETE BRIDGES

Schematics of two example reinforced concrete bridges are shown in Fig. 1 and Fig. 2. Bridge deck is composed of 2.1 m deep and 12.9 m wide hollow box-girder. Diameter (D) and length (L) of bridge pier are 2.4 m and 19.7 m , respectively. Bridge piers are supported on pile foundations, each consisting of 40 similar piles with 0.38 m diameter and 18.2 m length.

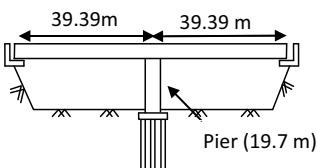


Fig.1: Schematic of 2 span bridge

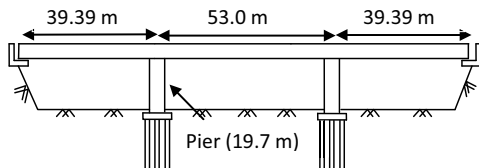


Fig.2: Schematic of 3 span bridge

Group Equivalent Pile

For analytical purpose, pile foundations (or pile groups) are represented with equivalent piles. Properties of equivalent pile are estimated so that equivalent pile has the same bending stiffness as of the pile group. Under seismic loading the pile groups may have sway and/or rocking motions. Depending on motion type, properties of equivalent piles differ. The bending stiffness for rocking and sway motion is calculated using the Eq. 1 and Eq. 2 (Yin and Konagai, 2001). For rocking motion, bending stiffness of the equivalent pile EI^G is calculated as

$$EI^G = \Sigma \{ (E_p I_p) + E_p A_p (x_p - x_0)^2 \} \quad (1)$$

where A_p , E_p and $E_p I_p$ are respectively the cross-sectional area, elastic modulus and bending stiffness of a single pile in the group, and x_p and x_0 respectively represent coordinate of a pile and centroidal coordinate of the cross-section of group pile. Once EI^G is evaluated using the properties of the pile group, corresponding diameter of the equivalent pile d_{eq} is calculated. In the present study, d_{eq} for rocking motion is estimated to be 4.2 m.

Similarly, bending stiffness of the equivalent pile EI_p for the sway motion is calculated as

$$EI_p = n_p \times E_p I_p \quad (2)$$

where $E_p I_p$ represents bending stiffness of single pile while n_p is the number of piles in a pile group. The d_{eq} of the equivalent pile is calculated so that it has a bending stiffness equal to the bending stiffness calculated from Eq. 2. In the present study, d_{eq} for sway motion is estimated to be 1.0 m.

Calculation of Scour Depth (S)

A 100-year flood with a discharge rate of 158.6 m³/s, velocity of 0.8 m/s and upstream depth of 11.9 m (FIS 2008) is considered herein. The scour depth of the two example bridges are calculated as the summation of local and contraction scour. These two scour components are the expected outcome from accelerated flow due to flood or similar events. Thus total scour depths (S) are calculated using HEC-18 (Richardson and Davis 2001) guidelines.

Finite Element Model

Two dimensional finite element models of the example bridges are developed in SAP2000. Bridge piers are modeled as double column bents. Hence plastic hinges are expected to form at pier ends (i.e., at top and bottom) when the bridges are excited under seismic ground motions. This is modeled by introducing nonlinear hinges at top and bottom of bridge piers. Bridge girders are modeled so that the lateral translation in vertical direction is completely restrained and the girder is free to move in the longitudinal direction. In reality, the horizontal movement of bridge superstructure in the longitudinal direction is limited to the initial gap provided between girder-abutment connections.

The soil-foundation-structure interaction is modeled by applying nonlinear springs, known as P-y springs, along the length of the equivalent pile (Fig. 3a). Stiffness of these springs is calculated using API recommendation (API 2000). Load-deflection curves of these nonlinear springs (P-y) are developed for every 0.3 m depth of the equivalent pile. The loss of lateral support due to scour is modeled by removing P-y springs from scour depth as shown in Fig. 3b. Ends of the equivalent piles are considered to have hinge connections.

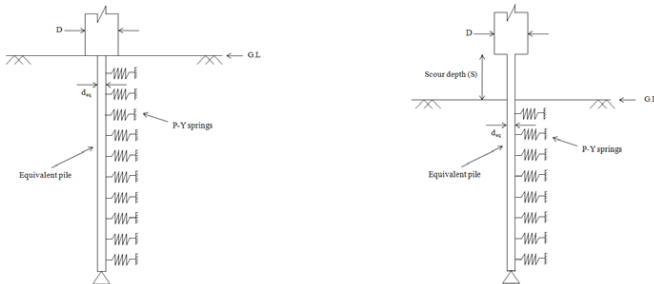


Fig 3a: Soil-pile interaction (without scour) Fig3b: Soil-pile interaction (with scour)

TIME HISTORY ANALYSIS

Earthquake Ground Motions

Nonlinear time history analyses of these bridges are performed under three sets of earthquake ground motions having annual exceedance probabilities as 2%, 10% and 50% in 50 years. These motions were originally generated for FEMA/SAC project (http://nisee.berkeley.edu/data/strong_motion/sacsteel/ground_motions.html) for the area of Los Angeles in California. Each set consist of 20 records. Among these three sets, 3 representative earthquakes are shown in Table 1.

Table 1: Representative earthquakes (among 60 LA earthquakes) with different probabilities of exceedance

Probability of exceedance	Ground motion ID	Representative earthquake	Magnitude	Duration (sec)	PGA (cm/sec ²)
2% in 50 years (strong earthquake)	LA 21 - LA 40	LA 40	7.1	59.98	613.28
10% in 50 years (moderate earthquake)	LA 01 - LA 20	LA 06	6.5	39.08	230.08
50% in 50 years (weak earthquake)	LA 41 - LA 60	LA 43	6.5	39.08	140.67

Parametric Study

Parametric study is performed to determine the effect of number of span, scour depth (S), diameter of equivalent pile (d_{eq}) and the combined effect of earthquake and flood-induced scour on the seismic performance of concrete bridges. For this, finite element analyses are performed taking combinations of (i) number of bridge spans: two and three, (ii) scour depths as 0 m, 0.6 m, 1.5 m and 3.0 m so that the ratio of scour depth to pier diameter (S/D) becomes 0, 0.25, 0.625, and 1.25, (iii) d_{eq} as 1.0 m (for sway motion), 1.2 m, 1.6 m, 2.4 m and 4.2 m (for rocking motion) that yield D/d_{eq} to be 2.5, 2.0, 1.5, 1.0, and 0.57, and (iv) earthquake ground motions with varying hazard levels.

Displacement Ductility

During seismic excitation, axial force develops at girder-abutment interfaces when the horizontal translation of bridge girder exceeds the initially provided gap at those locations. This may eventually result in bridge failure. The likelihood of occurring such failure increases as the bridge loses its base support due to scour. However, not much information is available in current literature on this issue, and thus, analytical modeling is required to realistically characterize the behavior of bridge abutments under seismic events. This is beyond the scope of the current paper. Thus, for analytical purpose, the present study represents bridge seismic damage by tracking the displacement of bridge girder when the lateral restrains at abutments in the longitudinal direction are removed. The seismic response of the example bridges is thus expressed in terms of displacement ductility (μ_{Δ}) which can be defined as the ratio of displacement of the bridge girder to the yield displacement. The mathematical expression of μ_{Δ} is given in Eq. 3 (Caltrans, 2006),

$$\mu_{\Delta} = \Delta_D / \Delta_y \quad (3)$$

where Δ_D and Δ_y are the estimated global displacement and yield displacement of bridge girder from its initial (undeformed) position.

Seismic damage states of the example bridges are decided according to their displacement ductility under various ground motions. It should be noted here that the longitudinal displacements of bridge girder and the top of the pier are the same as the example bridges have monolithic connections at pier girder joint. Threshold values of μ_{Δ} for different damage states are calculated when the threshold rotation ductility values (obtained from Banerjee and Shinozuka 2008) are achieved. For this calculation, a cantilever pier with a plastic hinge assigned at the bottom of pier is modeled separately in SAP2000. Push over analysis is performed to determine the yield and plastic displacements at the top of the pier which correspond to the yield and plastic rotations of pier bottom (at the location of plastic hinge), respectively. Ultimate displacement is estimated as the sum of yield displacement and plastic displacement (Priestley *et al.*, 1996). Thus the threshold values of displacement ductility for various damage states are obtained as 2.16, 2.83 and 4.6 respectively for minor, moderate and major damage of the bridge.

Analysis Result

Effect of span number and S/D: Fig. 4(a) and 4(b) show the displacement at the top of bridge pier obtained under strong ground motion LA40 and moderate ground motion LA06 (for $D/d_{eq} = 2.00$), respectively. It is found that, for all values of S/D, the displacement at top of pier is always higher for the 2-span bridge than that for the 3-span bridge. These figures indicate that in presence of scour, the effect of seismic events on bridges can amplify to a great extent. Hence, presence of flood-induced scour makes bridges more vulnerable to seismic hazard.

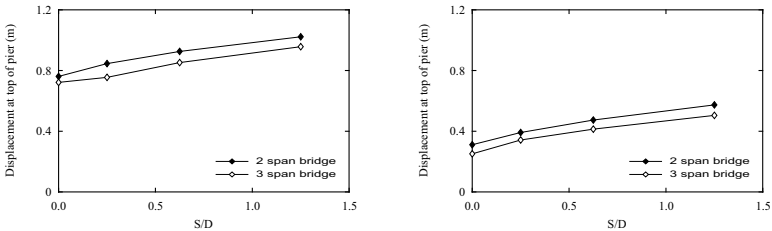


Fig. 4: Variation of displacement at top of bridge pier with S/D (for $D/d_{eq} = 2.0$); (a) under strong earthquake LA40 and (b) under moderate earthquake LA06

Effect of D/d_{eq} : Fig. 5 shows the pier-top displacement of the 2-span bridge under LA40 and LA06. Results reported in this figure are obtained from analyses performed with a constant value of S/D ($= 0.625$) and with various values of D/d_{eq} ratio. It can be observed with increase in D/d_{eq} ratio, the bridge response increases. Similar trends are observed for other values of S/D and for the 3-span bridge, as well.

For the two-span bridge, Fig. 6 represents the variation of displacement at top of pier (Δ_T) with various D/d_{eq} and S/D under LA40. It is found that for higher D/d_{eq} , the rate of increase of Δ_T with scour depth is higher than that for lower D/d_{eq} . This result indicates that bridges with higher D/d_{eq} are more sensitive to the combined effect of earthquake and flood-induced scour. It is interesting to note here that when pier diameter (D) is less than the diameter of equivalent pile (d_{eq}), i.e., $D/d_{eq} < 1.0$, seismic response of the bridge becomes insensitive to scour depth.

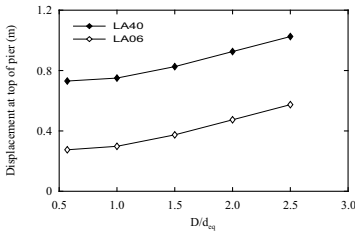


Fig. 5: Variation of displacement at pier top with D/d_{eq} under LA40 and LA06 (for 2-span bridge and $S/D = 0.625$)

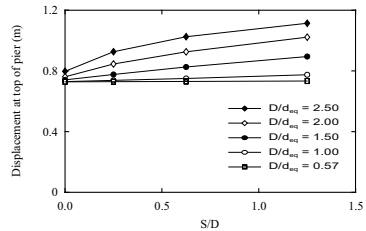


Fig. 6: Variation of displacement at pier top with various D/d_{eq} and S/D under LA40 (2-span bridge)

Effect of ground motion hazard level: Fig. 7 shows the observed displacement at bridge pier top under 60 LAZ earthquakes in presence ($S/D = 0.625$) and absence ($S/D = 0$) of flood-induced scour. For obvious reason, bridge response is at the highest level under strong motions (i.e., for LA21 to LA 40), at the moderate level under moderate motions (i.e., for LA01 to LA 20), and at the lower level under weak motions (i.e., for LA41 to LA 60). It is important to note here that in presence of scour, bridge seismic response may get amplified to a large extent. The integrated effect of scour and a moderate earthquake can produce bridge damage at the same level of a strong earthquake occurring in absence of scour (i.e., as a discrete event). Likewise, weak earthquakes in presence of scour can produce similar level of bridge damage that can be expected under moderate earthquakes.

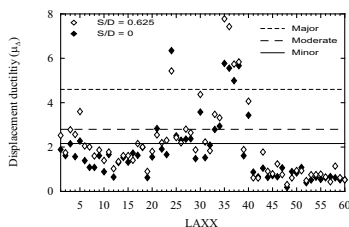


Fig 7: Variation of displacement ductility of the pier (for 2-span bridge and $D/d_{cq} = 2.0$) under different ground motions

BRIDGE PERFORMANCE UNDER MULTHAZARD

Bridge response presented in Fig. 7 is categorized under different bridge performance levels such as minor, moderate and major damage using the threshold limits for these damage states as stated before. This literature provides the damage limits in terms of displacement ductility which, by definition, is the ratio of observed to yield displacement at the top of bridge piers. As found in Fig. 7, the bridge is expected to suffer from major damage under 5 earthquakes among 60 (displacement ductility is equal or more than the threshold limit for that damage states). Such information will further be analyzed to generate fragility curves that will represent the probability of bridge failure in a damage state under certain ground motion intensity. Difference between median fragility parameters will quantitatively represent the impact of considering multihazard events over discrete events.

CONCLUSIONS AND NEED FOR FUTURE RESEARCH

The study reflects on the importance of considering earthquake in presence of flood-induced scour to be a critical multihazard scenario for bridge performance analysis. Bridge vulnerability may increase to a large extent under such multihazard from that under discrete hazards. It also indicates some important aspects that require further attention; (i) 3D modeling of bridges to identify all possible failure modes that have potential to govern global nature of bridge failure under seismic events in presence of flood-induced scour, and (ii) reliability and uncertainty analysis.

Moreover, various regions of United States having moderate to high seismic and flood hazards need to be studied to develop a comprehensive knowledgebase on the performance of regional bridges under multiple natural hazards.

REFERENCES

- Banerjee, S., and Shinozuka, M. (2008). "Mechanistic quantification of RC bridge damage states under earthquake through fragility analysis", *Probabilistic Engineering Mechanics*, Vol.23, No.1, pp. 12-22.
- Bennett, C. R., Lin, C., Parsons, R., Han, J. (2009). "Evaluation of behavior of a laterally loaded bridge pile group under scour conditions", *Proceedings of SEI 2009 Structures Congress*, Texas, pp. 290-299.
- California Department of Transportation (CALTRANS), Seismic design criteria, Version 1.4, 2006.
- Computer and Structures, Inc., (1995), SAP2000 (Structural Analysis Program), Berkley, CA, Version 14.1.0.
- Flood Insurance Study for Sutter County, California, Federal Emergency Management Agency (FEMA), Flood Insurance Study Number 060394V000A, 2008.
- Ghosn, M., Moses, F., Wang, J., "Design of highway bridge for extreme events", *NCHRP Report 489*, Transportation Research Board, Washington, D.C., 2003.
- National Bridge Inventory, Federal Highway Administration (FHWA), U.S. Department of Transportation, <http://www.fhwa.dot.gov/bridge/nbi.htm> (Mar .11, 2010)
- Priestley, M.J.N., Seible, F., and Calvi, G.M. (1996). *Seismic Design and Retrofit of Bridges*. John Wiley & Sons, Inc., New York, N.Y
- American Petroleum Institute (API), Recommended practice for planning, designing and constructing fixed offshore platforms." (2000). *21st Ed., API Recommended Pract. 2A-WSD (RP 2A)*.
- Richardson, E.V., and Davis, S. R., "Evaluating Scour at Bridges", *Publication No. FHWA NHI 01-001, Hydraulic Engineering Circular No – 18*, Federal Highway Administration, U.S. Department of Transportation, Washington, D.C., 2001.
- Yin, Y., and Konagai, K. (2001). "A simplified method for expression of the dynamic stiffness of large-scaled grouped piles in sway and rocking motions", *Journal of Applied Mechanics*, JSCE, Vol. 4: 415-422.

Uncertainty Modeling in Bridge Network Maintenance Optimization

Paolo Bocchini¹ M.ASCE and Dan M. Frangopol² Dist.M.ASCE

¹Advanced Technology for Large Structural Systems (ATLSS) Engineering Research Center, Department of Civil and Environmental Engineering, Lehigh University, 117 ATLSS Drive, Bethlehem, PA 18015, USA; PH (610) 758 3066; FAX (610) 738 5553; email: paolo.bocchini@lehigh.edu

²Advanced Technology for Large Structural Systems (ATLSS) Engineering Research Center, Department of Civil and Environmental Engineering, Lehigh University, 117 ATLSS Drive, Bethlehem, PA 18015, USA; PH (610) 758 6103; FAX (610) 768 4115; email: dan.frangopol@lehigh.edu

ABSTRACT

The present paper collects a series of tools, methods, and convenient solutions used to model and handle efficiently the huge amount of random variables associated with techniques for the life-cycle simulation and maintenance optimization of bridge networks. The randomness in the deteriorating reliability of individual bridges is modeled by means of time-dependent models with random parameters. The uncertain effects of the preventive maintenance actions are represented by numerical superposition of four contributions and characterized by up to six random parameters. The complete rehabilitation of a bridge is supposed not to restore perfectly the original reliability level, and also in this case the extent of the imperfection (i.e. difference between original reliability and reliability after the intervention) is treated as a random parameter. Finally, the in/out of service state of the individual bridges along the life cycle of the bridge network is modeled by means of either a multivariate (i.e. correlated) Bernoulli random variable or a random field.

INTRODUCTION

Due to the dramatic shortage in funding for civil infrastructure development and replacement, the problem of maintenance optimization for existing bridges is of paramount importance. Indeed, several studies have addressed this issue both at the individual bridge level and at the transportation network level. For instance, Frangopol (2010) reported the state-of-the-art and state-of-practice on maintenance optimization for individual bridges. Augusti *et al.* (1998) pioneered the problem of maintenance optimization at the network level proposing a technique for the comparison and ranking of several maintenance plans. More recently, Peeta *et al.* (2010) proposed an efficient technique for the optimal allocation of limited funding among the bridges of a highway network, considering also the effect of uncertainty, but disregarding correlations and aging. Gao *et al.* (2010) presented a remarkable framework for the optimization of the maintenance interventions on pavements of a

transportation network. Bocchini and Frangopol (2011) proposed a methodology for the optimal scheduling of the maintenance interventions at the bridge network level, including uncertainty, correlation, and deterioration. The present paper illustrates and discusses some of the techniques that have been used to model realistically the most significant uncertainties involved in this kind of analysis. In fact, when dealing with the forecast of future degradation processes, future maintenance actions and future damages due to extreme events, a large amount of uncertainty must be included in the model, especially if the study focuses on the bridge network level.

A first source of both epistemic and aleatory uncertainty is the time-dependent reliability profile of the individual bridges. Usually, when an entire network is considered, the degradation details are unknown for several bridges. Moreover, the deterioration process is always affected by uncertain factors. Therefore, the time-dependent bridge reliability can be described by means of probabilistic models as functions of random parameters.

The actual effects of the maintenance and rehabilitation interventions are uncertain too. In fact, even if most of the interventions types (such as repainting) are relatively standard, their effects on the reliability profile are aleatory in terms of duration and magnitude. Therefore, these effects can be also modeled with random parameters.

Finally, the synthetic in/out of service state of the bridges of a transportation network, often due to the occurrence of an extreme event, can be modeled either as a set of correlated random variables or as a random field.

The large amount of uncertainty that affects the problem is presented herein in the perspective of a holistic framework for the maintenance optimization at the network level.

UNCERTAINTY IN THE TIME-DEPENDENT RELIABILITY OF BRIDGES

Due to environmental aggressive agents, material aging, fatigue, and other stressors, all the structural components are subject to deterioration along their life-cycle. Some studies have developed techniques for the accurate computation of the reliability index $\beta(t)$ along the life-cycle of the structure (Akgül and Frangopol 2004a, b, 2005a, b). However, when dealing with an entire transportation network, available data are limited and these studies cannot be carried out without several assumptions and approximations. In this situation, probabilistic models of the time-dependent profile of the reliability index are an effective alternative. These models are actually random processes, since they are characterized by random parameters. The choice of the model depends on the limit state and on the major structural characteristics of the bridge. Bocchini and Frangopol (2011) summarized three of these models and proposed a new one:

$$\text{bilinear: } \beta(t) = \beta^0 - \mathcal{H}(t - T^I) \cdot R^L(t - T^I) \quad (1)$$

$$\text{quadratic: } \beta(t) = \beta^0 - \mathcal{H}(t - T^I) \cdot R^Q(t - T^I)^2 \quad (2)$$

$$\text{square root: } \beta(t) = \beta^0 - \mathcal{H}(t - T^I) \cdot R^S \sqrt{t - T^I} \quad (3)$$

$$\text{exponential: } \beta(t) = \beta^0 - \mathcal{H}(t - T^I) \cdot \left\{ R^E(t - T^I) + Q - Q \exp \left[- \left(\frac{t - T^I}{S} \right)^2 \right] \right\} \quad (4)$$

where β^0 is the initial value of the reliability; $\mathcal{H}(\cdot)$ is the Heaviside step function; T^l is the initiation time when the deterioration starts to affect the structural reliability; R^l , R^Q , R^S , and R^E are reliability degradation rates; Q is a parameter that tunes the shape of the exponential model during the first years after T^l ; and S is a shape parameter associated with the position of the inflection point in the exponential model. In general, all the parameters are assumed to be random variables. Therefore, for every model there are three to five random parameters. Frangopol *et al.* (2001a, b) provided the probability distribution associated with bending and shear limit states for some of these parameters. Similarly, for other cases the probability distributions can be assessed by analytical computations and engineering judgment. Because of the large number of random parameters, the use of Latin Hypercube sampling can dramatically enhance the computational efficiency (Bocchini *et al.* 2011).

All the models in Equations (1)-(4) capture the propagation of the uncertainty along the life-cycle, as Figure 1 shows.

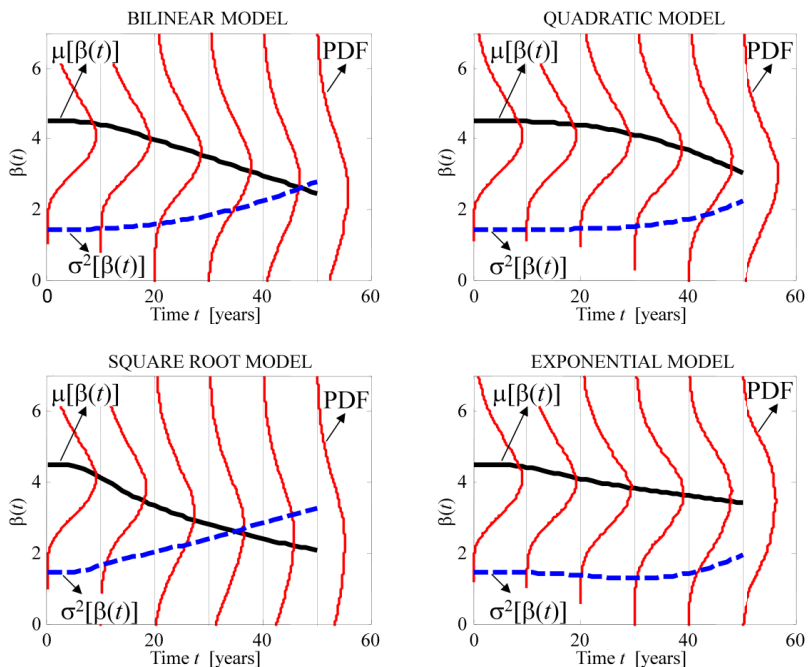


Figure 1. Four reliability index $\beta(t)$ models as described by Equations (1)-(4). The thick solid lines represent the mean values of $\beta(t)$ denoted as $\mu[\beta(t)]$; the thick dashed lines represent the variance of $\beta(t)$ denoted as $\sigma^2[\beta(t)]$; the thin continuous lines are the probability density functions (PDF) of $\beta(t)$ at some representative years.

UNCERTAINTY IN THE EFFECT OF PREVENTIVE MAINTENANCE

To maintain or improve the reliability of the structures, preventive maintenance actions are applied at predefined times along the life-cycle. The actual improvement due to these interventions is uncertain and should be modeled by random parameters. Bocchini and Frangopol (2011) proposed to describe the improvement in β as the superposition of up to four components: (i) a constant improvement, (ii) a linear improvement for a limited time that eventually becomes constant, (iii) a quadratic improvement for a limited time that eventually becomes constant, (iv) a delay in the deterioration process. The analytical definition of the four components is:

$$\text{constant: } \hat{\beta}(t > t_a) = \beta(t > t_a) + M_0 \tag{5}$$

$$\text{linear: } \hat{\beta}(t > t_a) = \beta(t > t_a) + \min [M_1(t - t_a), M_1D_1] \tag{6}$$

$$\text{quadratic: } \hat{\beta}(t > t_a) = \beta(t > t_a) + \min [M_2(t - t_a)^{0.5}, M_2D_2^{0.5}] \tag{7}$$

$$\text{delay: } \hat{\beta}(t > t_a) = \mathcal{H}(t - t_a)\mathcal{H}(t_a + D_0 - t)\beta(t_a) + \mathcal{H}(t - t_a - D_0)\beta(t - D_0) \tag{8}$$

where $\hat{\beta}$ is the modified reliability index that includes the effect of the preventive maintenance actions; t_a is the time of application of preventive maintenance; M_0 is an uncertain parameter that determines the magnitude of the constant improvement; M_1 and M_2 are the rates of improvement for the linear and quadratic components, respectively; D_1 and D_2 are the time intervals after which the linear and quadratic components become constant, respectively; $\mathcal{H}(\cdot)$ is the Heaviside step function; and D_0 is the time interval during which the deterioration is suppressed.

As mentioned previously, parameters $M_0, M_1, M_2, D_0, D_1,$ and D_2 in Equations (5)-(8) are affected by uncertainty and are modeled as random variables. Therefore, depending on the components that are considered, each maintenance intervention can involve up to six random parameters. Therefore, also in this case, Latin Hypercube sampling can be proficiently applied.

UNCERTAINTY IN THE EFFECT OF REHABILITATION

Even though preventive maintenance is applied to maintain or improve the reliability of the structure, the serviceability limit state can be reached along the life-cycle and rehabilitation interventions could be required to bring the bridge back in service. This type of intervention is usually modeled as a complete rehabilitation of the initial bridge reliability index profile $\beta(t)$. However, rehabilitation are never perfect, therefore also in this case a random parameter $\Delta \in [0, 1] \subset \mathbb{R}$ is introduced to model the uncertain level of imperfection of the repair:

$$\tilde{\beta}(t > t_r) = \beta(t - t_r) - \Delta \cdot [\beta(0) - \beta(t_r)] \tag{9}$$

where $\tilde{\beta}$ is the reliability index profile that takes into account also the rehabilitation and t_r is the time of application of the intervention. As a result, the original reliability index is reduced by the random quantity $\Delta \cdot [\beta(0) - \beta(t_r)]$.

Along the life-cycle of a bridge, several preventive maintenance actions and rehabilitation can be combined. Therefore, Equations (5)-(9) are used repeatedly to modify the value of $\beta(t)$.

UNCERTAINTY IN THE BRIDGE SERVICE STATE

For a life-cycle maintenance optimization of a bridge network, all the mentioned uncertainty must be combined to obtain a probabilistic characterization of the in/out of service state of the bridges along their service lives. Two different approaches to accomplish this task have been proposed in Bocchini and Frangopol (2011) and in Bocchini *et al.* (2011). Both the approaches account for the fact that the service state of bridges belonging to the same transportation network are correlated, since they can share similar traffic loads, environmental conditions, age, design, and building techniques. Moreover, both approaches are based on the assessment of a correlation distance among the damage levels of the individual bridges, when subject to extreme events. Bocchini and Frangopol (2010) proposed a simple technique to fit a correlation model for the damage level of the bridges of a network subject to an extreme event, such as an earthquake. The analytical formulation of the proposed model is:

$$\rho(\xi) = A \exp\left(-\frac{\xi^2}{\lambda^2}\right) + K \quad (10)$$

where ρ is the correlation coefficient between the damage levels of two bridges subject to an extreme event; ξ is the distance between the two bridges; A , K , and λ are parameters of the model that can be assessed using the least square method over the results of a series of fragility analyses (see Bocchini and Frangopol 2010 for details). In particular, the value of the correlation distance λ provides a measure of the degree of correlation in the network. The correlation coefficient in Equation (10) is an explicit function only of the distance between the bridges, but the process for the assessment of the parameters takes into account also the structural characteristics of each individual bridge.

Dichotomized Gaussian simulation. The approach proposed in Bocchini and Frangopol (2011) is based on the Dichotomized Gaussian simulation technique (Emrich and Piedmonte 1991). The bridge in/out of service state is modeled as a multivariate binary random variable $s_{bi}(t)$:

$$s_{bi}(t) = \begin{cases} 1 & \text{if bridge } b \text{ of sample } i \text{ is in service at time } t \\ 0 & \text{if bridge } b \text{ of sample } i \text{ is out of service at time } t \end{cases} \quad (11)$$

The marginal distribution of $s_{bi}(t)$ is a Bernoulli distribution with expected value computed from the reliability index as: $\Phi[\beta_{bi}(t)]$, where Φ is the standard Gaussian cumulative distribution function. The covariance, instead, is obtained from Equation (10), since it is assumed that the same parameters are valid also for the correlation among the bridge service states.

Bocchini and Frangopol (2011) proposed a modified version of the Dichotomized Gaussian technique to overcome the issue of incompatibility that can arise when the marginal distribution and the covariance matrix are assigned arbitrarily. This technique provides also a fine tuning of the correlation, since it updates the covariance matrix based on the time-dependent values of the reliability indices $\beta_{bi}(t)$ (i.e. based on the structural characteristics of the bridges).

Random fields simulation. An alternative approach for the simulation of the bridge in/out of service states (Bocchini *et al.* 2011) is based on random fields. In this case, Equation (10) is used to generate samples of a field with Uniform distribution that represents synthetically the demand of the external stressors. The value of the field at the location of each bridge is compared to the time dependent reliability to determine whether the bridge is in service or not:

$$s_{bi}(t) = \mathcal{H}\{\Phi[\beta_{bi}(t)] - d_i(\mathbf{x}_b, t)\} \quad (12)$$

where $s_{bi}(t)$ is the bridge service state defined as in Equation (11); $\mathcal{H}\{\cdot\}$ is the Heaviside step function; Φ is the standard Gaussian cumulative distribution function; and $d_i(\mathbf{x}_b, t) \in [0, 1] \subset \mathbb{R}$ is the value of the i -th sample of the demand at the location \mathbf{x}_b of bridge b and at time t .

With respect to the Dichotomized Gaussian technique, the simulation of random fields is much more computationally efficient, especially in the case of complex problems. Therefore, random field simulation is strongly preferable when dealing with large bridge networks.

CONCLUDING REMARKS

Several techniques and convenient solutions to model the uncertainties involved in the life-cycle bridge assessment and maintenance optimization have been presented. They all collect the physical and epistemic uncertainties involved in the problems at hand (e.g. the time of initiation of the degradation process, the rate of deterioration, the impact of the maintenance applications on the reliability of the bridge, the degree of correlation between the bridge service states) and combine them to build a probabilistic, time-dependent model of the bridge service states s_{bi} .

This probabilistic model of the random variables s_{bi} can be used within different frameworks, but given the complexity, strong non-linearity, and high number of random parameters, Monte Carlo simulation appears the most reasonable choice, from a probabilistic point of view.

Different preventive maintenance schedules and strategies can be compared and ranked at the network level. Moreover, an automated numerical optimization technique, such as Genetic Algorithms (Goldberg 1989), can be used to find the optimal solution or the optimal set of solutions (Bocchini and Frangopol 2011).

The list of uncertainties that have been addressed is not exhaustive, but the most important ones have been considered. In fact, in the perspective of a holistic framework, only the parameters that most significantly affect the final result must be included. Furthermore, in such a framework all the choices associated with a correct

stochastic representation of the problem should be made compatible with the need of keeping the computational cost of the analysis feasible also for realistically large applications. Therefore, this topic is extremely challenging and worth of further investigations.

ACKNOWLEDGMENTS

The support from (a) the National Science Foundation through grant CMS-0639428, (b) the Commonwealth of Pennsylvania, Department of Community and Economic Development, through the Pennsylvania Infrastructure Technology Alliance (PITA), (c) the U.S. Federal Highway Administration Cooperative Agreement Award DTFH61-07-H-00040, and (d) the U.S. Office of Naval Research Contract Number N-00014-08-0188 is gratefully acknowledged.

The opinions and conclusions presented in this paper are those of the writers and do not necessarily reflect the views of the sponsoring organizations.

REFERENCES

- Akgül, F., and Frangopol, D. M. (2004a). "Lifetime performance analysis of existing steel girder bridge superstructures." *Journal of Structural Engineering*, ASCE, 130(12), 1875-1888.
- Akgül, F., and Frangopol, D. M. (2004b). "Lifetime performance analysis of existing prestressed concrete bridge superstructures." *Journal of Structural Engineering*, ASCE, 130(12), 1889-1903.
- Akgül, F., and Frangopol, D. M. (2005a). "Lifetime performance analysis of existing reinforced concrete bridges. I: Theory." *Journal of Infrastructure Systems*, ASCE, 11(2), 122-128.
- Akgül, F., and Frangopol, D. M. (2005b). "Lifetime performance analysis of existing reinforced concrete bridges. II: Application." *Journal of Infrastructure Systems*, ASCE, 11(2), 129-141.
- Augusti, G., Ciampoli, M., and Frangopol, D. M. (1998). "Optimal planning of retrofitting interventions on bridges in a highway network." *Engineering Structures*, Elsevier, 20 (11), 933-939.
- Bocchini, P., and Frangopol, D. M. (2010). "On the applicability of random field theory to transportation network analysis." In *Bridge Maintenance, Safety, Management and Life-Cycle Optimization (Frangopol, Sause & Kusko eds.)*, CRC Press, Taylor and Francis, UK, 3018-3026.
- Bocchini, P., and Frangopol, D. M. (2011). "A probabilistic computational framework for bridge network optimal maintenance scheduling." *Reliability Engineering and System Safety*, Elsevier, doi: 10.1016/j.ress.2010.09.001 (in press and available on line).
- Bocchini, P., Frangopol, D. M., and Deodatis, G. (2011). "Computationally efficient simulation techniques for bridge network maintenance optimization under uncertainty." In *Computational Stochastic Mechanics (Deodatis & Spanos eds.)*, Research Publishing Services (in press).

- Emrich, L. J., and Piedmonte, R. P. (1991). "A method for generating high-dimensional multivariate binary outcomes." *The American Statistician*, ASA, 45(4), 302-304.
- Frangopol, D. M. (2010). "Life-cycle performance, management, and optimization of structural systems under uncertainty: accomplishments and challenges." *Structure and Infrastructure Engineering*, Taylor & Francis, doi:10.1080/15732471003594427 (in press and available on line).
- Frangopol, D. M., Kong, J. S., and Gharaibeh, E. S. (2001a). "Reliability-based life-cycle management of highway bridges." *Journal of Computing in Civil Engineering*, ASCE, 15(1), 27-34.
- Frangopol, D. M., Gharaibeh, E. S., Kong, J. S., and Miyake, M. (2001b). "Reliability-based evaluation of rehabilitation rates of bridge groups." In *Proceedings of the international conference on safety, risk, and reliability trends in engineering*, IABSE, Malta.
- Gao, L., Xie, C., and Zhang, Z. (2010). "Network-level multi-objective optimal maintenance and rehabilitation scheduling." In *Proceedings of the 89th Annual Meeting of the Transportation Research Board of the National Academies*, TRB, Washington, DC, USA.
- Goldberg, D. E. (1989). *Genetic Algorithms in Search, Optimization, and Machine Learning*. Addison-Wesley Professional.
- Peeta, S., Salman, F. S., Gunnec, D., and Viswanath, K. (2010). Pre-disaster investment decisions for strengthening a highway network, *Computers and Operations Research*, Elsevier, 37(10), 1708-1719.

Overcoming the limitations of traditional model-updating approaches

James-A. Goulet¹, Ian F.C. Smith²

¹Swiss Federal Institute of Technology (EPFL), IMAC Laboratory, EPFL ENAC IS IMAC, Station 18, CH-1015, Lausanne, Switzerland; James.A.Goulet@gmail.com

²Swiss Federal Institute of Technology (EPFL), IMAC Laboratory, EPFL ENAC IS IMAC, Station 18, CH-1015, Lausanne, Switzerland; Ian.Smith@epfl.ch

ABSTRACT

Model updating is useful for improving structural performance assessments. This paper examines an important assumption of traditional model-updating approaches. This assumption requires the error independence between points where predictions and measurements are compared. Simulations performed on a full-scale bridge show that uncertainties are correlated for both static and dynamic predictions. Therefore, traditional model-updating techniques are not appropriate in such situations. Model updating limitations related to randomness and independence of uncertainties may be overcome by an interpretation strategy called Candidate Model Search for System Identification (CMS4SI). Instead of judging a model by its ability to fit measured data, the approach falsifies models using threshold values that are based upon uncertainties. Uncertainties may be correlated, systematic, independent or random.

KEYWORDS

Uncertainties, Correlation, Systematic errors, Performance assessment, Model Updating, Model Calibration, System Identification, CMS4SI

Structural performance assessment tasks such as reliability analyses, remaining fatigue life evaluations, and earthquake response predictions require behavior models of structures. The quality of such performance assessments is thus determined by the accuracy of model predictions. To improve accuracy, engineers take measurements and then perform model-updating (also known as model-calibration, model-tuning and curve fitting) in order to reduce uncertainties related to models.

There are two types of traditional model updating. The first type aims to minimize the discrepancy (residual) between predicted and measured values (for example (Bakir et

al. 2008; Bell et al. 2007; Ka-Veng Yuen 2006; Sanayei et al. 1997; Schlune et al. 2009; Teughels and De Roeck 2004). In the presence of several *comparison points* (measurements and predictions), it is often not possible to obtain a residual of zero. Therefore, there are procedures to minimize the overall residual over comparison points. All proposals have the same goal; adjust the parameter values to get the best overall fit between predicted and measured values (residual minimization).

The second group of model-updating approaches involves maximizing the likelihood of a model (Beck and Katafygiotis 1998; Cheung and Beck 2009; Hadidi and Gucunski 2008; Tarantola 2005; Yuen et al. 2006). This approach usually accounts for uncertainties which come from both measurements and modeling. Posterior probability (sometimes called likelihood) for possible model parameter values (model instances) are computed according to uncertainty sources. The goal is to select the model instance(s) which maximizes the posterior probability. More than one model instance may be selected if they reveal an equivalent likelihood.

This paper discusses the reasons why such traditional model updating approaches may not be reliable for the identification of full-scale structures. The first section presents the limitations associated with traditional model-updating approaches. The second section then describes the candidate model search for system identification algorithm (CMS4SI) which overcomes the limitations of traditional model-updating.

LIMITATIONS OF TRADITIONAL MODEL-UPDATING

Several successful model-updating applications can be found among the methodologies reported above. However, most of these examples employed simulated data and they either implicitly or explicitly include the assumption that uncertainties at different comparison points are independent. When independence is present and with a large amount of comparison points, either minimizing the residual or maximizing the likelihood may lead to valid results since the average errors are likely to cancel. Results from such processes lead to best estimates analogously to what is done in linear regression based on the Gauss-Markov theorem (Plackett 1972). This theorem says that for a linear regression, if errors can be represented as Gaussian, uncorrelated and equally distributed random variables, the best unbiased estimate is obtained from least-square regression. If the assumption of uncertainty independence of comparison points does not hold, the premise behind least-square regression as well as the assumption of traditional model updating is no longer valid.

Is the hypothesis of independence valid for the identification full-scale structures? For measurement uncertainties such as sensor resolution and repeatability, it is reasonable to assume such independence. However, modeling uncertainties, such as model simplifications, geometry variations and some values for constant, are usually

affected by bias. Model simplification errors reflect the accuracy with which the model is representative of the full-scale structure. Such uncertainty is always present in models and in most cases; one can rely only upon experience to quantify its extent. In this paper, the correlation between prediction quantities and their locations is studied for the model of a full-scale bridge. The structure studied is the Langensand Bridge (Switzerland).

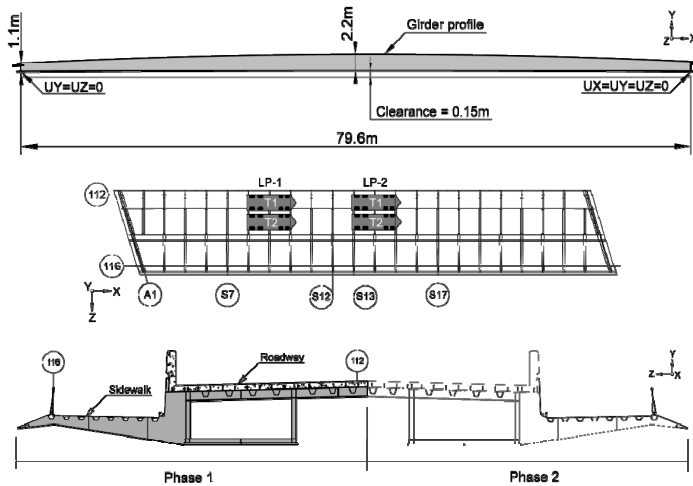
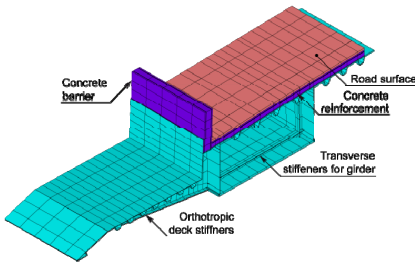


Figure 1 – Langensand Bridge elevation, top view and cross section, reproduced with permission from ASCE (Goulet et al. 2010)

This structure is an 80m long single span bridge. Only half of the structure (Phase 1) is studied. Figure 1 shows the elevation, the top view and cross section of the structure. Key reference axes, describing the sensor and load configuration layout, are also presented. In this study, six displacement sensors were used along with seven rotations and three strain measurements. Details of sensor placement and load configuration may be found in a publication by Goulet et al. (Goulet et al. 2010). Dynamic modal frequencies are simulated for 15 modes. The cross section of the finite element model used for the analysis is shown in Figure 2 along with the uncertainties associated with the FE model. Every uncertainty source presented in Figure 2 is a parameter of the model. Stochastic sampling is performed using the Monte-Carlo method in order to combine uncertainty sources.



Uncertainty source	unit	Mean	STD
Δv concrete	-	0	0.025
Truck weight	Ton	35	0.125
Δt steel plates	%	0	1
Δt pavement	%	0	5
Δt concrete	%	0	2.5
Strain sensor positioning	mm	0	5

Figure 2 – Finite element model of the bridge, reproduced with permission from ASCE (Goulet et al. 2010) and uncertainty data associated with the FE model

For each instance, predictions are computed for quantities such as displacement, rotation, strain and modal frequencies. The objective is to examine the correlation between the prediction quantities and their locations.

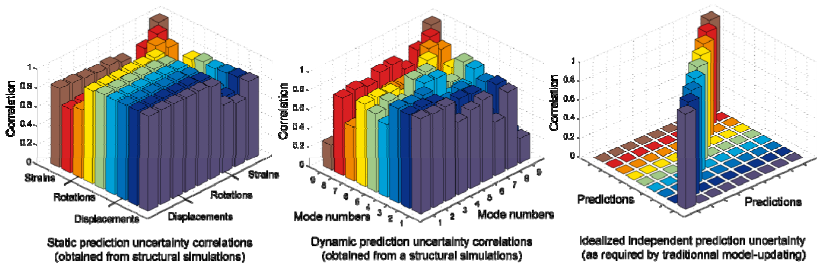


Figure 3 – Correlations between prediction quantities using a full-scale bridge simulation

Figure 3 shows a three-dimensional representation of the correlation matrices for model-dependent prediction uncertainties. In this figure, the horizontal planes are prediction quantities and locations and the height of vertical bars is the correlation between two predictions. The left graph shows results obtained from the stochastic combination of uncertainties for static prediction. Correlations between static predictions (displacement, rotations and strains) are high. Table 1 summarizes the average correlation between static prediction types. Displacement and rotations are almost perfectly correlated. Strains show a less correlated dependency due to the local character of these predictions. The correlation between load cases is also tested. On average, the uncertainty correlation between static-load cases is 0.98.

The center graph shows the correlation between prediction uncertainties for dynamic frequencies. In this case, correlations are lower than for static predictions and tend to decrease as the modes are significantly different (i.e. modes close to each other are highly correlated). However, the correlation still remains generally high. For instance

the correlation between the first and second mode is of 0.98 and 0.6 between the first and the tenth.

Table 1 – Average uncertainty correlation between static prediction quantities

Prediction quantities	Displacement	Rotations	Strains
Displacement	0.99	0.98	0.74
Rotations	0.98	0.97	0.75
Strains	0.74	0.75	0.59

The right graph represents the idealized case of independent prediction uncertainty as required in traditional model-updating. Prediction uncertainties in both cases (for static and dynamic) do not satisfy the independence requirements. Therefore, traditional model-updating is not appropriate for such a structure. Either the best-fit model or the most probable model(s) are likely to be biased due to correlated modeling errors and therefore, results may not be representative of the real structure behavior. This underlines the need for a methodology which is not limited to cases where uncertainties are independent.

CANDIDATE MODEL SEARCH FOR SYSTEM IDENTIFICATION (CMS4SI)

In many scientific communities, it has been acknowledged for centuries that it is not possible to fully validate a hypothesis (model); it is only possible to falsify it. Tarantola (2006) explicitly acknowledged that fact and suggested that inverse tasks such as structural identification may only be solved by falsifying model instances. Therefore the challenge is to separate, in a rigorous and systematic way, candidate and rejected models. Several attempts have been made (Goulet et al. 2010; Ravindran et al. 2007; Robert-Nicoud et al. 2005) without fully succeeding in capturing the complexity of uncertainty combination, especially for multiple measurements.

Candidate model search for system identification is proposed to overcome the limitations mentioned in the previous section and to account for uncertainties and their correlations. This algorithm does not find a best match between predictions and measurements and it does not find the most likely model instance. Starting from an initial population of models, the approach filters out the models instances for which the discrepancy between predicted and measured values is sufficient to be sure that the right model will remain in the set according to a desired target reliability. The limits separating accepted and rejected models are called the thresholds (one for each comparison point). Threshold values are maximal plausible errors that occur through combining uncertainties from modeling and measuring. The algorithm defining the threshold values is summarized in the graph presented in Figure 4.

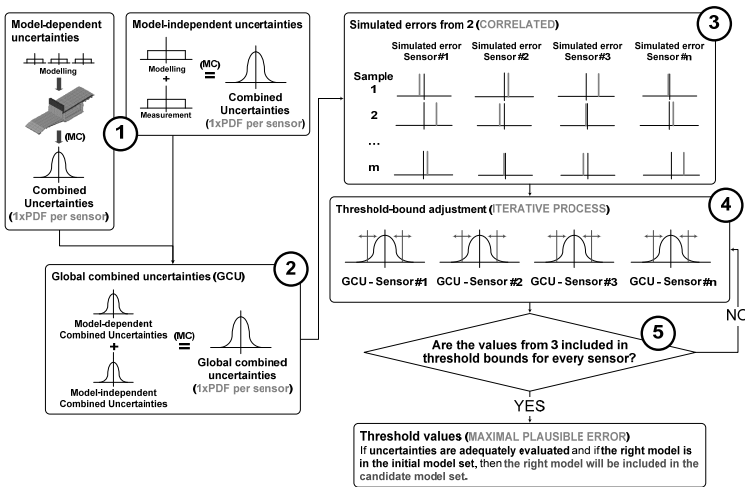


Figure 4 – Steps of Threshold Computation (PDF = Probability density function; MC= Monte-Carlo combination)

In step one, uncertainties are combined using Monte-Carlo (MC) stochastic sampling into two separate processes. Model-dependent uncertainties have to be combined through the finite element template model used for generation of model instances. The output is a matrix containing the predicted values for an instance of input parameter on each line (model-dependent errors). Each column is a comparison point used in the analysis. In Figure 4, this number is referred as a sensor for the purpose of simplification. Several thousand input parameter instances are used to obtain an uncertainty distribution for each comparison point. The mean of each distribution is subtracted from each of its samples in order to obtain the variation compared to a mean model. This result is named model-dependent combined uncertainties. Separately, model-independent uncertainties are combined in a MC process which does not involve the template model. Several million model instances are generated in order to obtain representative probability density functions (PDFs) of model independent uncertainties. For each instance, a sample is drawn in each uncertainty distribution and then summed to obtain a combined distribution.

Due to computational limitations, much fewer model-dependent uncertainties can be managed compared with model-independent uncertainties. Therefore, the data in the matrix has to be copied several times and concatenate in order to have the same size as the second. In step two, both model independent and dependent errors are summed. This results in global combined uncertainties, presented as a matrix having several million rows and as many columns as there are comparison points. Next, we define

the global uncertainty coverage interval that ensures that the right model is in the candidate model set with a probability of Ψ . For common identification purposes, Ψ is set to 95%. By definition, the right model should be able to predict every observation; only one observation is sufficient to discard a model instance. The uncertainty between different comparison points is not always perfectly correlated. Therefore, the use of several comparison points requires a larger coverage interval than that defined for one measurement. Each time a comparison point is added to filter model instances, threshold values increase to account for the additional chance of wrongly rejecting the right model. The amount of increase is dependent upon the error independence between comparison points. Threshold values are defined in the third to fifth steps.

In the third step, correlated samples are drawn from each global uncertainty distribution and then added to a randomly chosen instance of model-dependent combined error. In the fourth and fifth steps, correlated simulated errors are used to define the coverage interval required in order to include the simulated errors simultaneously for each sensor. The validity of Ψ is verified and the coverage interval is adjusted for every comparison point in order to be sure that simulated errors are within the threshold bounds. Under the assumption that the uncertainties have been adequately evaluated, this procedure ensures that the right model is not wrongly discarded according to Ψ , the desired target reliability. The outcome obtained from filtering corresponds to the set of models that are able to explain the measured behavior while accounting for uncertainties and their correlations.

The system identification methodology explained here for the case of structural identification can be generalized to be applicable to any inverse problem where models and observations are compared.

CONCLUSIONS

Traditional model-updating approaches are only valid for situations where uncertainties are random and independent. Other situations are often called biased uncertainty. For most complex structures (for example, full scale bridges, buildings and dams) the uncertainties related to models do not fulfill such requirements.

Simulations performed on a full-scale bridge showed that uncertainties are correlated for both static and dynamic predictions. Therefore traditional model-updating techniques are not appropriate in such situations.

Model updating limitations related to randomness and independence of uncertainties may be overcome by an interpretation strategy called Candidate Model Search for System Identification (CMS4SI). Instead of judging a model by its ability to fit

measured data, the approach is based on the principle that it is only possible to falsify a model. Therefore, a threshold which accounts for systematic and random uncertainties along with correlations is appropriate discarding models from the initial model set. This strategy is scientifically sound and further work is evaluating its universal applicability.

ACKNOWLEDGEMENTS

This research is funded by the Swiss National Science Foundation under contract no. 200020-117670/1.

REFERENCES

- Bakir, P. G., Reynnders, E., and Roeck, G. D. (2008). "An improved finite element model updating method by the global optimization technique [']Coupled Local Minimizers'." *Computers & Structures*, 86(11-12), 1339-1352.
- Beck, J. L., and Katafygiotis, L. S. (1998). "Updating Models and Their Uncertainties. I: Bayesian Statistical Framework." *Journal of Engineering Mechanics*, 124(4), 455-461.
- Bell, E. S., Sanayei, M., Javdekar, C. N., and Slavsky, E. (2007). "Multiresponse parameter estimation for finite-element model updating using nondestructive test data." *Journal of Structural Engineering-Asce*, 133(8), 1067-1079.
- Cheung, S. H., and Beck, J. L. (2009). "Bayesian Model Updating Using Hybrid Monte Carlo Simulation with Application to Structural Dynamic Models with Many Uncertain Parameters." *Journal of Engineering Mechanics*, 135(4), 243-255.
- Goulet, J.-A., Kripakaran, P., and Smith, I. F. C. (2010). "Multimodel Structural Performance Monitoring." *Journal of Structural Engineering*, 136(10), 1309-1318.
- Hadidi, R., and Gucunski, N. (2008). "Probabilistic Approach to the Solution of Inverse Problems in Civil Engineering." *Journal of Computing in Civil Engineering*, 22(6), 338-347.
- Ka-Veng Yuen, J. L. B., Lambros S. Katafygiotis., (2006). "Efficient model updating and health monitoring methodology using incomplete modal data without mode matching." *Structural Control and Health Monitoring*, 13(1), 91-107.
- Plackett, R. L. (1972). "Studies in the History of Probability and Statistics. XXIX: The Discovery of the Method of Least Squares." *Biometrika*, 59(2), 239-251.
- Ravindran, S., Kripakaran, P., and Smith, I. F. C. (2007). "Evaluation reliability of multiple-model system identification." 14th EG-ICE Workshop, Maribor, Slovenia.
- Robert-Nicoud, Y., Raphael, B., Burdet, O., and Smith, I. F. C. (2005). "Model identification of bridges using measurement data." *Computer-Aided Civil and Infrastructure Engineering*, 20(2), 118-131.
- Sanayei, M., Imbaro, G. R., McClain, J. A. S., and Brown, L. C. (1997). "Structural model updating using experimental static measurements." *Journal of Structural Engineering-Asce*, 123(6), 792-798.

- Schlune, H., Plos, M., and Gylltoft, K. (2009). "Improved bridge evaluation through finite element model updating using static and dynamic measurements." *Engineering Structures*, 31(7), 1477-1485.
- Tarantola, A. (2005). "Inverse Problem Theory and Methods for Model Parameter Estimation." SIAM, ed., Philadelphia.
- Tarantola, A. (2006). "Popper, Bayes and the inverse problem." *Nat Phys*, 2(8), 492-494.
- Teughels, A., and De Roeck, G. (2004). "Structural damage identification of the highway bridge Z24 by FE model updating." *Journal of Sound and Vibration*, 278(3), 589-610.
- Yuen, K.-V., Beck, J. L., and Katafygiotis, L. S. (2006). "Unified Probabilistic Approach for Model Updating and Damage Detection." *Journal of Applied Mechanics*, 73(4), 555-564.

Reliability Analysis of Mooring Dolphin Structures

Reda Farag¹, Mahmoud El-Meligy² and Achintya Haldar³

¹Structures & Metallic Construction Dept, Housing & Building Research Center, PO Box 1770, Cairo, 87 Tahrir St., Ph: 37617057, Fax: 33351564, red_bordany@yahoo.com

²Structural Eng. Dept, Mansoura University, Mansoura, Gomhoria St., Ph: 22759971, Fax: 2244690, egroup_egypt@yahoo.com

³Dept of Civil Eng. & Eng. Mech, The University of Arizona, PO Box 210072, Tucson, 1209 E. 2nd St., Ph: 5206212142, Fax: 5206212550, haldar@u.arizona.edu

ABSTRACT

A mooring dolphin structures (MDS), consisting of steel-pipe-piles and soil around them, are important elements of marine structures. The reliability analysis of such complicated systems is very challenging. The limit state functions for them are implicit in nature. Reliability evaluation using the classical Monte Carlo simulation technique may not be practical since each deterministic evaluation will require several hours of computer time. A new hybrid method is presented in this paper. The system is represented by finite elements and its reliability is estimated by intelligently integrating the stochastic finite element, response surface methods, and advanced factorial schemes. The procedure is verified with the help of an example.

INTRODUCTION

Steel pipe piles embedded in soil are an integral part of offshore foundation structures to carry mooring loads. The behavior of such complicated structural system is highly affected by the inherent uncertainties in the design variables related to the loading conditions, soil, pile material properties and the pile-soil interaction behavior. Considering the presence of large amount of uncertainties, deterministic design of steel-pile-soil system may not be desirable. The reliability evaluation of such complex systems is extremely challenging. A novel procedure is suggested in this paper for this purpose.

A typical layout of mooring dolphin structure (MDS) is shown in Figure 1. The basic elements common to mooring system include: mooring and breasting structures, mooring lines, deck fittings, separators and access trestles and catwalks (BS 6349-4). The mooring loads are generally caused by wind and currents producing longitudinal and lateral forces on the system. The longitudinal forces are generally conservatively assumed to be resisted by the spring lines while the lateral loads are resisted by MDS. The flexible dolphins are designed to absorb the kinetic energy of a berthing vessel by horizontal displacements of pile head.

MOORING DOLPHIN STRUCTURE

Suppose the reliability analysis of any one of the MDS system shown in Figure 1 is under consideration. A conceptual representation of the system, in the form of finite elements (FE), is shown in Figure 2. In this representation, the steel is represented by beam elements, the soil is represented by 8 noded solid elements, the soil boundaries are represented as spring elements, and the soil-pile contact is represented by contact elements.

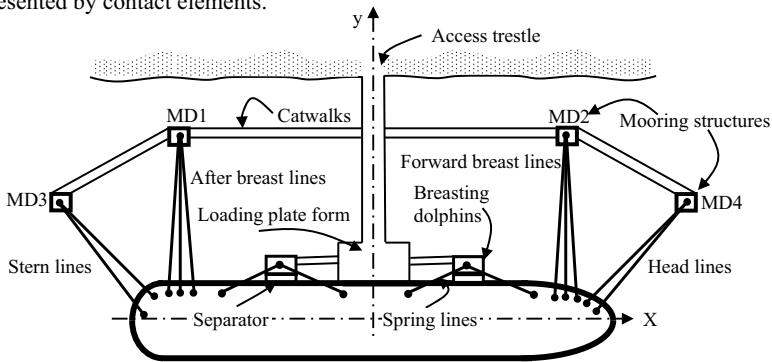


Figure 1. Typical mooring pattern

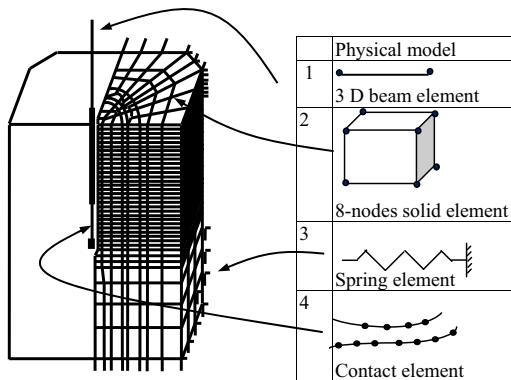


Figure 2. Finite element representation of a typical MDS

In this representation, the volume of soil to be considered is an important modeling variable. It is determined using a trial and error approach. The responses of the steel-pile-soil system are plotted as a function of the soil domain. For the mathematical modeling, the soil domain is selected when the responses did not change significantly with the increase in the size of the soil domain. Then, the far boundaries of soil are represented using spring elements. The selected soil domain is

represented physically using 8-noded solid elements with Drucker-Prager material nonlinearity. Initially, the steel–pipe-pile was presented by shell elements to consider the effect of the pile size. However this representation dramatically increases the time of FE analyses. To improve the efficiency, the soil-pile contact is physically represented by node to curve contact elements and the pile is represented by 3-D beam element, as shown in Figure 2. The Hook's law is found to be acceptable to represent the behavior of pile material under the considered working load.

For the pile-soil contact problem, various contacts constitutive laws can be used including the Lagrange multiplier and penalty function. The penalty function method introduces large numerical values into the stiffness matrix of the system to simulate the rigidity between the two contacted nodes. It introduces a major difficulty in selecting the proper penalty values. The Lagrange multiplier method introduces new variables (Lagrange multipliers) causing increase in the bandwidth of the stiffness matrix. A hybrid technique is used in COSMOS/M (2000); it does not require assigning penalty values and the sizes of the matrices remain unchanged. This hybrid approach is used in this study.

A NOVEL RELIABILITY EVALUATION METHOD

In any reliability-based design, appropriate limit states must be defined in terms of basic design variables. For the system shown in Figure 2, they cannot be defined explicitly. For implicit limit states, Haldar and Mahadevan (2000) suggested to approximately generate them using the response surface method (RSM). However, the basic RSM cannot incorporate distributional information of the design variables and becomes very inefficient if the limit state functions are not generated in the failure region. Since the first- or second-order reliability method (FORM/SORM) is iterative in nature and can address both the issues discussed above, in the proposed method, they are integrated with RSM. In this study, a commercial computer program STATISTICA (2008) is used to formulate the implicit limit state functions. Using SORM in COMREL (1997), the reliability information is extracted. For efficient presentation, additional discussions on RSM are required at this stage.

RESPONSE SURFACE METHODOLOGY

The primary purpose of applying RSM in reliability analysis is to approximate the original complex and implicit limit state function using a simple and explicit polynomial Bucher and Bourgand (1990). In implementing any RSM-based scheme, three issues need consideration are (1) the degree of polynomial to be used to generate the response surface, (2) the location of center points, and (3) experimental sampling points. For the complicated MDS system, the research team proposed to use second-order polynomial, without and with crosses terms. They can be expressed as:

$$\hat{g}(X) = b_0 + \sum_{i=1}^n b_i X_i + \sum_{i=1}^n b_{ii} X_i^2 \quad (1)$$

$$\hat{g}(X) = b_0 + \sum_{i=1}^n b_i X_i + \sum_{i=1}^n b_{ii} X_i^2 + \sum_{i \neq j} \sum b_{ij} X_i X_j \quad (2)$$

where X_i ($i = 1, 2, \dots, k$) is the i th random variable, and b_0, b_i, b_{ii} , and b_{ij} are unknown coefficients to be determined. The numbers of coefficient that is necessary to define the above two equations are $p_1 = 2k+1$ and $p_2 = (k+1)(k+2)/2$, respectively. Considering only 10 basic design variables in the analytical model, i.e., $k = 10$, it will take 21 and 66 deterministic evaluations to develop the above two equations, respectively, indicating significant differences in the computational efficiency. This issue needs further attention.

The selection of these sampling points is called experimental design. Commonly used methods for selecting sampling points are saturated design (SD), central composite design (CCD), and saturated design with edge points. SD is less accurate but more efficient since it requires only as many sampling points as the total number of unknown coefficients to define the response surface. CCD is more accurate but less efficient since a regression analysis needs to be carried out to evaluate the unknown coefficients for the response surface. The sampling points should be selected as close as possible to the failure point or center point. The integration of FORM/SORM with RSM enables to iteratively locate the center point. The first iteration will start at the mean values of all random variables and the corresponding response surface can be generated. So, the mean value of the random variables is used as an initial center point. A new center point \mathbf{x}_{c_2} then can be generated to develop an explicit performance function for the next iteration following the linear interpolation scheme as:

$$\mathbf{x}_{c_2} = \mathbf{x}_{c_1} + (\mathbf{x}_{D_1} - \mathbf{x}_{c_1}) \frac{g(\mathbf{x}_{c_1})}{g(\mathbf{x}_{c_1}) - g(\mathbf{x}_{D_1})} \quad \text{if } g(\mathbf{x}_{D_1}) \geq g(\mathbf{x}_{c_1}) \quad (3)$$

$$\mathbf{x}_{c_2} = \mathbf{x}_{D_1} + (\mathbf{x}_{c_1} - \mathbf{x}_{D_1}) \frac{g(\mathbf{x}_{D_1})}{g(\mathbf{x}_{D_1}) - g(\mathbf{x}_{c_1})} \quad \text{if } g(\mathbf{x}_{D_1}) < g(\mathbf{x}_{c_1}) \quad (4)$$

where, $x_{c_1}, x_{D_1}, x_{c_2}, x_{D_2}$ are the center and checking points in the first and second iteration respectively, and $g(x_{c_1}), g(x_{D_1})$ are the response values at the center and checking points respectively. These iterations can be repeated until a pre-selected convergence criterion of $(\mathbf{x}_{c_{i+1}} - \mathbf{x}_{c_i}) / \mathbf{x}_{c_i} \leq \varepsilon$ is satisfied. ε is considered to be $|0.05|$ in this study.

EFFICIENCY CONSIDERATION

A nonlinear finite element (NLFE) analysis of a typical full size MDS considered in this study may require up to 6 hours. Obviously, conducting only one hundred of such analyses will require about 25 days ($6 \times 100 / 24$) of continuous running of the computer. This may not be practical. This leads to the conclusion that the required response surfaces need to be generated with as few deterministic analyses as possible. Since the proposed algorithm is iterative and the basic SD and CCD require different amount of computational effort, the first attempt was to use SD

and CCD in intelligent ways improving efficiency without compromising accuracy. Huh and Haldar (1999) proposed few schemes. Some of the schemes of interest to this study are:

Scheme 0: SD using 2^{nd} order polynomial without the cross terms throughout all the iterations. This scheme is the most efficient but least accurate in estimating the probability of failure among all the schemes considered in this study.

Scheme 1: SD using 2^{nd} order polynomial without the cross terms in intermediate iterations and SD with edge points and full 2^{nd} order polynomial in the final iteration.

Scheme 2: SD using 2^{nd} order polynomial without the cross terms in intermediate iterations and CCD using full 2^{nd} order polynomial in the final iteration.

Considering the above three schemes, the total number of FE analyses required to generate the necessary response surface are $2k+1$, $(k+1)(k+2)/2$ and 2^k+2k+1 , respectively. To demonstrate the computational effort needed to implement the three schemes, for $k = 10$, the total number of required FE analyses will be 21, 66, and 1045, respectively, for the above three schemes.

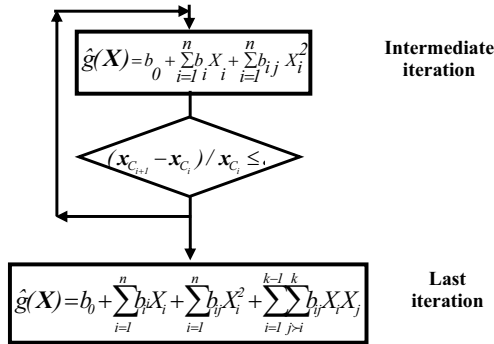


Figure 3. Schemes 0, 1 and 2

The above schemes lead to the proper direction, however, for large complicated systems may require further improvement in the efficiency. Two such improvements considered in this study are:

Scheme M1: To improve the efficiency of Scheme 1, it is suggested to add the cross terms (edge points), $k(k-1)$, only for the most important variables in the last iteration. For an example, suppose the total number of basic variables is k and the total number of most sensitive random variable is m , the total number of FE analyses required for Scheme 1 and M1 are $(k+1)(k+2)/2$ and $2k+1+m(2k-m-1)/2$, respectively. For $k = 10$ and $m = 3$, the total number of FE analyses will be 66 and 45, respectively. Obviously, Scheme M1 improves the efficiency further.

Scheme M2: Instead of using full factorial plan in CCD, Myers and Montgomery (2009) recently proposed using quarter the factorial plan. The required number of sampling points for Scheme 2 and M2 will be 2^k+2k+1 and $2^{k-2}+2k+1$, respectively.

For $k = 10$, the required number of FE analyses will be 1045 and 277, for the two schemes.

LIMIT STATES FOR MDS

As mentioned earlier, reliability is always estimated for specific limit states. The limit states can be defined to satisfy serviceability and ultimate strength requirements. For MDS, the serviceability limit state of drift at the top and the flexural strength limit state of the yield strength are considered. They can be expressed as:

$$G_{fb}(\mathbf{X}) = F_y - \hat{g}_{fb}(\mathbf{X}) \quad (5)$$

$$G_{ux}(\mathbf{X}) = X_{all} - \hat{g}_{ux}(\mathbf{X}) \quad (6)$$

where, $G_{fb}(\mathbf{X})$, $G_{ux}(\mathbf{X})$ are the flexural and drift limit state functions, respectively, $\hat{g}_{fb}(\mathbf{X})$, $\hat{g}_{ux}(\mathbf{X})$ are the flexural and drift response surface functions, respectively, F_y , X_{all} are the allowable flexural yield strength and drift, respectively. X_{all} is considered to be 1.5 m, as suggested in (BS 3649-2). The above method needs to be verified at this stage.

EXAMPLE

A 117 m long MDS, as shown in Figure 4, is considered to elaborate the procedure. The pile is embedded in a homogenous elastic soil that has lateral subgrade reaction $K_h = 150 \text{ t/m}^2$. The pile has unsupported free length of 17.3 m and has a circular cross section with outside radius $r = 0.95 \text{ m}$ and thickness $t = 2.8 \text{ cm}$.

STATISTICAL PROPERTIES OF ALL DESIGN VARIABLES

For the reliability analysis, it is important now to quantify uncertainty in all the design variables. The flexural capacity and deformation behaviour of steel-pipe-pile soil system depends on the structural system as well as the load, material and geometric statistical properties. For the steel pile, the steel-modulus of elasticity, the cross sectional area expressed in terms of the internal and external radii of the pile and the unit weight of steel are considered to be random variables. For soil, the soil-elastic modulus, the cohesion, friction angle and the unit weight are assumed to uncertain design variables (JCSS, 2006). The mooring force H is assumed to follow Gumbel/EV-I distribution, the assumption made for wind loading. The information of uncertainty associated with all these random variables is obtained from the literature and is summarized in Table 1. The bias factor is defined as the ratio of mean/nominal.

RELIABILITY EVALUATION

Before conducting the actual reliability analysis, to simplify the problem, the response surface was generated using first order polynomial. The sensitivity indexes of the random variables H , r , α_{lv} , K_h , E_s , and t are found to be -0.90154, 0.32687, -0.26842, 0.05921, 0.05436 and 0.04327, respectively. Since the sensitivity index for the thickness of the pipe is less than 0.05, it is considered to be deterministic variable

at its mean value of 2.8 cm in the subsequent reliability analysis. The reliability indexes β are estimated using the proposed method using all the schemes are summarized in Table 2. The reliability indexes according to Schemes 0, 1, and 2 are found to 1.671, 1.815, and 1.744, respectively. The corresponding required FE analyses are 9, 15, and 25, respectively. Scheme M1 is considered next by adding cross terms for the most significant variables in the final iteration. Initially, 3 cross terms of the most significant variable H , followed by 2 cross terms of r , and finally 1 cross term of k_h were added requiring 12, 14 and 15 FE analyses, respectively. The corresponding reliability indexes are found to be very similar; close to 1.816, as shown in Figure 5. The β -index using Scheme M2 requires 12 FE analyses. Scheme M2 is more efficient than Scheme 2 without compromising accuracy.

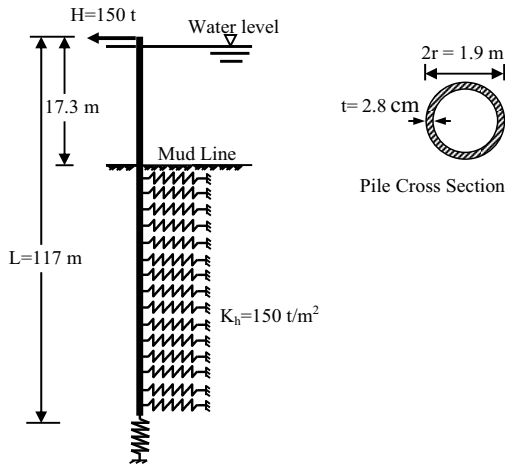


Figure 4. An idealized MDS

Table 1. Uncertainty in the design variables

Random variables	Distribution	Nominal	Mean	Bias	COV	Ref.
Lateral load, H	EV-I	150 t	117	0.78	0.37	[NBS]
Radius, r	Lognormal	0.95 m	0.95	1.00	0.10	Bender
Thickness, t	Lognormal	2.8 cm	2.8	1.00	0.05	Bender
Steel E-modulus, E_s	Lognormal	2.01E7 t/m ²	2.01E7	1.00	0.06	[NBS]
Lateral sub grade reaction, K_h	Lognormal	150 t/m ²	172.5	1.15*	0.21*	---
Model coefficient, α_u	Normal	1.0	1.0	1.0	0.10*	----

* Data not available. Assumed parameters are based on judgment.

CONCLUSION

A new reliability analysis method is developed by intelligently integrating the stochastic finite element and response surface methods and advanced factorial

schemes. It is specifically developed for large complicated structural systems where each deterministic finite element analysis may require several hours of computer time. The method is clarified by estimating reliability of complicated mooring dolphin structures used for offshore structures.

Table 2. Summary of reliability indexes for different schemes

Scheme	0	1	M1		2	M2
			H	H & r		
β	1.67	1.82	1.82	1.82	1.74	1.74
No. of Analyses	9	15	12	14	25	13

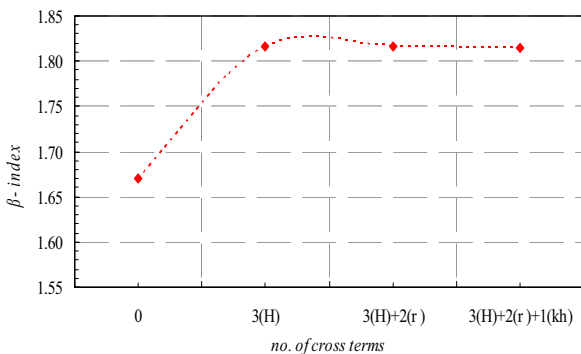


Figure 5. Improvement in β -index

REFERENCES

Bendar, H. (1981). "Pressure Vessel Design Handbook" Van Nostrand Reinhold company, N.Y.

Bucher, C. and Bourgund, U. (1990). "Fast and Efficient Response Surface Approach for Structural Reliability Problem". *Structural Safety* 7:57-66.

British Standard, BS 6349-2:1988, Code of practice for "Marine Structures".

COMREL, User's Manual, R.C.P., (1996), Munich, Germany.

COSMOS/M 2.6, (2000), Structural Research & Analysis Corp., Los Angeles, California.

Huh, J., and Haldar, A. (2002). "Seismic Reliability of Nonlinear Frames with PR connections using Systematic RSM," *Probabilistic Eng. Mechanics*, 17(2), 177-190.

Myers, R. H., and Montgomery, D.C. (2009). *Response Surface Methodology: Process and Product Optimization Using Designed Experiments*, John Wiley & Sons, N.Y.

National Bureau of Standards (NBS) (1982), special publication 577.

Poulos, H. and Davis, E. (1980). "Pile Foundation Analysis and Design", John Wiley & Sons.

STATISTICA Trial V. 8, 1984-2008, Statsoft Inc.

Adaptive Reliability Analysis of Reinforced Concrete Bridges using Nondestructive Testing

Q. Huang¹, P. Gardoni², and S. Hurllebaus³

¹Zachry Dept. of Civil Engineering, Texas A&M University, College Station, TX, 77843, PH (614) 595-6115; FAX (979) 845-6156; email: qindan_h@tamu.edu

²Zachry Dept. of Civil Engineering, Texas A&M University, College Station, TX, 77843, PH (979) 845-4340; FAX (979) 845-6156; email: pgardoni@civil.tamu.edu

³Zachry Dept. of Civil Engineering, Texas A&M University, College Station, TX, 77843, PH (979) 845-9570; FAX (979) 845-6156; email: shurlebaus@civil.tamu.edu

ABSTRACT

Seismic fragility reflects the ability of a structure to withstand future seismic demands. To obtain an accurate assessment of seismic fragility, it is critical to incorporate information about the current structural properties. This paper describes a probabilistic framework to incorporate information from nondestructive testing (NDT) in the estimates of the seismic fragility of a reinforced concrete (RC) bridge. The proposed framework combines global and local damage detection methods to incorporate information from nondestructive testing (NDT) on the properties of an existing bridge. As an illustration, the proposed probabilistic framework is used to assess the seismic fragility of an example reinforced concrete bridge.

INTRODUCTION

Seismic fragility (the conditional probability that the structural demand(s) attains or exceeds a corresponding capacity for given earthquake intensity measures, \mathbf{s}) is often used to evaluate the performance of existing bridges in seismic zones. The fragility estimates reflect the current state of the bridge and can be used in optimizing the allocation of resources for maintenance, repair, and/or rehabilitation of bridge networks. Efforts have been made in estimating seismic fragilities for reinforced concrete (RC) bridges (e.g., Mander and Basoz 1999, Gardoni et al. 2003, Zhong et al. 2008, Padgett and DesRoches 2009, Huang et al. 2010a). In these studies the structural properties and/or other inputs are assumed based on as-designed values. However, the as-designed values might not be representative of the actual in-field values because the actual construction might differ from the design or because the original structural properties might have changed over time due to deterioration. Therefore, the fragilities in these studies might not accurately reflect the actual bridge performance.

This paper describes a probabilistic framework to incorporate information from nondestructive testing (NDT) in the seismic fragility estimates of RC bridges. The actual conditions of an existing RC bridge are identified using global and local damage detection methods. Damage detection methods using nondestructive testing (NDT) that can be applied during the operation of structures are an effective way to evaluate the in-place structural properties and detect potential damages. A combination of global and local damage detection methods is usually helpful: global damage detection can be used to identify the structural properties at the global level and also to detect potential damage locations, and local damage detection can be used in the suspected damaged area to

determine the structural properties at the local level.

FRAGILITY ESTIMATE

Following Gardoni et al. (2002, 2003), the seismic fragility of a bridge is expressed as

$$F(\mathbf{s}, \Theta) = P \left\{ \bigcup_{k=1}^p \left[C_k(\mathbf{x}, \Theta_{C,k}) - D_k(\mathbf{x}, \Theta_{D,k}, \mathbf{s}) \leq 0 \right] \mid \mathbf{s} \right\} \tag{1}$$

where $\Theta = (\Theta_{C,k}, \Theta_{D,k})$, in which $\Theta_{C,k}$ and $\Theta_{D,k}$ respectively denote the parameters in the capacity model (C_k) and the demand model (D_k) for the k^{th} failure mode, and \mathbf{x} = a vector of basic variables (e.g., material properties and member dimensions). Two typical failure modes are considered: the deformation ($k = \delta$) and shear ($k = \nu$) failure modes in the column(s). The probabilistic capacity and demand models adopted in this paper are formulated following Gardoni et al. (2002, 2003) as:

$$C_k(\mathbf{x}, \Theta_{C,k}) = \hat{c}_k(\mathbf{x}) + \gamma_{C,k}(\Theta_{C,k}, \mathbf{x}) + \sigma_{C,k} \varepsilon_{C,k} \tag{2}$$

$$D_k(\mathbf{x}, \Theta_{D,k}) = \hat{d}_k(\mathbf{x}) + \gamma_{D,k}(\Theta_{D,k}, \mathbf{x}) + \sigma_{D,k} \varepsilon_{D,k} \tag{3}$$

where $\Theta_{C,k} = (\theta_{C,k}, \sigma_{C,k})$, $\Theta_{D,k} = (\theta_{D,k}, \sigma_{D,k})$, $\hat{c}_k(\mathbf{x})$ and $\hat{d}_k(\mathbf{x})$ = selected deterministic models, $\gamma_{C,k}(\theta_{C,k}, \mathbf{x})$ and $\gamma_{D,k}(\theta_{D,k}, \mathbf{x})$ = correction terms, $\sigma_{C,k} \varepsilon_{C,k}$ and $\sigma_{D,k} \varepsilon_{D,k}$ = model errors in which $\sigma_{C,k}$ and $\sigma_{D,k}$ = constant standard deviations of the model errors, and $\varepsilon_{C,k}$ and $\varepsilon_{D,k}$ = random variables with the standard normal distribution.

In particular, in this paper, we adopt the probabilistic capacity model proposed by Huang et al. (2009), which is developed based on the formulation of Eq. (2). The probabilistic capacity model is built for a circular RC bridge column with non-uniform flexural stiffness over the column height to account for the effects of non-uniform deterioration. We use the probabilistic seismic demand models for RC bridges with one single-column bent proposed by Huang et al. (2010a), which is constructed based on the formulation of Eq. (3). This demand model accounts for the randomness in the seismic excitations and uses two earthquake intensity measures: the peak ground velocity, PGV , and the pseudo-spectral acceleration, PSA , at the first mode period of the bridge, T_1 . Therefore, $\mathbf{s} = \{PSA / g, PGV \cdot T_1 / H_c\}$ in which g = standard gravity ($= 9.8129 \text{ m/s}^2$), and H_c = height of the bridge column. The adopted probabilistic capacity and demand models consider the prevailing uncertainties including uncertainties in the structural properties, statistical uncertainties, and model errors. Choe et al. (2007) and Huang et al. (2010a) provide the formulations of the capacity and demand models including the statistics information of $\Theta_{C,k}$ and $\Theta_{D,k}$.

GLOBAL AND LOCAL DAMAGE DETECTION

Global damage detection. Following the framework proposed by Huang et al. (2010b), the procedure for the global damage detection method adopted in this study is summarized as follows:

- a) conduct a vibration test on an existing bridge to record the time-history responses;

- b) extract modal frequencies and mode shapes from the time-history responses using the time domain decomposition method (TDD) (Kim et al. 2005);
- c) build a preliminary finite element model (FEM) based on the structure design drawings, field measurements, and engineering knowledge;
- d) use Bayesian model updating to update the preliminary FEM into a baseline by matching the extracted modal frequencies from Step (b);
- e) identify possible damage locations through the Damage Index Method (DIM) (Stubbs and Kim 1996) using the mode shapes of the damaged structure extracted from Step (b) and the mode shapes of the baseline built in Step (d).

Note that the errors associated with each step of the global damage detection should be considered. The details of how to simulate and propagate the errors can be found in Huang et al. (2010d).

Local damage detection. In the proposed approach, the local assess of the structural properties is carried out following Huang et al. (2010c). Huang et al. (2010c) focused on the assessment of the concrete strength f'_c and proposed a regression model to predict f'_c based on SonReb measurements (rebound number, RN, and ultrasonic pulse velocity, UPV (m/s)), water-cement ratio, w/c , and the age of the concrete, t (days). The regression model is written as

$$\sqrt{f'_c} = \theta_{s0} + \theta_{s1} \cdot RN^{2.0} + \theta_{s2} \cdot UPV^{3.0} + \theta_{s3} \cdot (w/c)^{-0.5} + \theta_{s4} \cdot \ln t + \sigma_s \varepsilon_s \quad (4)$$

where $\theta_s = \{\theta_{sj}\}$ = model parameters, $\sigma_s \varepsilon_s$ = model error, σ_s = standard deviation of the model error, and ε_s = random variable with the standard normal distribution.

ILLUSTRATION

This section uses a three dimensional (3-D) finite element model (FEM) of an example bridge built in OpenSees (McKenna and Fenves 2000) to illustrate the proposed framework. The numerical model simulates a typical box-girder RC highway bridge with one single-column bent with a pile foundation. In the FEM, the box-girder superstructure is modeled by elastic beam elements with a total of 72 elements. The column is modeled by non-linear beam-column elements using fiber cross sections with a total of 20 elements. The soil is assumed to be in Class C according to the soil classification of the U.S. Geological Survey (USGS). The stiffness properties for the springs that are used to model the interaction between the soil and the pile are provided by Mackie and Stojadinović (2003).

Tables 1 and 2 give the design parameters for the bridge FEM. For the purpose of the illustration, the values of $f'_{c,d}$, $f'_{c,c}$, and $K_{abut,t}$ are assumed to be unknown and will be determined by the global damage detection. A local damage is introduced into the target baseline by reducing 20% value of f'_c in column Elements 15 and 16 shown in Figure 1a. The reduced concrete strength is denoted as $f'_{c,dam}$. The value of $f'_{c,dam}$ will be determined by the local damage detection. The FEM with the damaged column elements is considered as the damaged bridge.

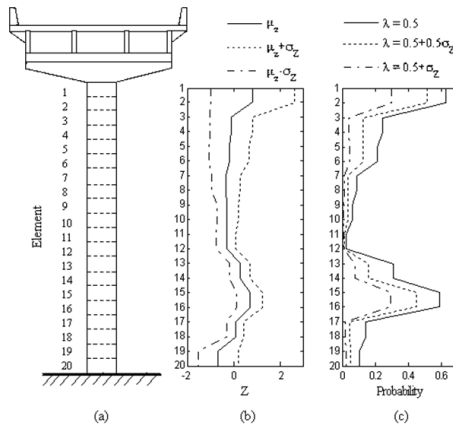


Figure 1. (a) Bridge column configuration, (b) Z values for the column elements, and (c) probability of damage detection under 1% measurement error

Table 1. Assumed values for the design parameters in the FEM of the example bridge

Design parameter	Assumed values and distributions		
	Mean	Coefficient of variation	Distribution
Span (the shorter one), L_1	30.480 m	1%	Lognormal
Two-span ratio, L_2 / L_1	1.25	—	—
Column height, H_c	6.706 m	1%	Lognormal
Column concrete cover, <i>cover</i>	0.038 m	10%	Lognormal
Reinforcement nominal yield strength, f_y	344.74 MPa	5%	Lognormal
Transverse reinf. nominal yield strength, f_{yt}	275.79 MPa	5%	Lognormal
Longitudinal reinf. ratio (column), ρ_l	3.59%	—	—
Transverse reinf. ratio (column), ρ_s	1.06%	—	—
Pile soil stiffness, K_{soil}	(USGS) C	—	—
Additional bridge dead load, $w_{i,s}$ of self-weight	10%	25%	Normal

Table 2. Target and identified values for the design parameters in the FEM of the example bridge

Design parameter	Target value	Identified value		
		Mean	Distribution	COV
Concrete compressive strength of column, $f'_{c,c}$	41.38 MPa	43.41 MPa [†]	Lognormal	21.4% [†]
Concrete compressive strength of deck, $f'_{c,d}$	41.38 MPa	39.86 MPa [†]	Lognormal	7.7% [†]
Abutment stiffness in trans. direction, $K_{abut,t}$	127.94 kN/mm	128.53 kN/mm [†]	Normal	3.4% [†]
Square root of concrete compressive strength of column Elements 15 and 16, $\sqrt{f'_{c,dam}}$	5.75 MPa	5.75 MPa [‡]	Normal	0.9% [‡]

[†]Identified using global damage detection; [‡]Identified using local damage detection.

Application of global damage detection

Vibration test. A vibration test is conducted first on the damaged bridge by applying a pulse force on the bridge deck in X (longitudinal), Y (transverse), and Z (vertical) directions. The acceleration responses are recorded every 6 nodes on the deck and every other node on the column. This simulates 13 and 10 records obtained from accelerometers evenly distributed along the deck and along the column, respectively. We use 10s and 0.005s as the recording time and the sampling time, respectively. Since the measured time history responses in this example are the numerical acceleration responses at the nodes, they are noise-free. To simulate the measurement error, a Gaussian white noise with zero mean and standard deviation equal to 1% of the amplitude of the acceleration response is added to the noise-free time history responses. If the vibration test is repeated m times, then m sets of responses are recorded. Each set of responses are different because the measurement error is random.

Identification of the baseline. A preliminary FEM is constructed in the same way as the target baseline, but with different values of $f'_{c,d}$, $f'_{c,c}$, and $K_{abut,t}$. Table 3 shows the ratios between the preliminary values, $(f'_{c,d})_p$, $(f'_{c,c})_p$, and $(K_{abut,t})_p$, and the values in the target/identified baseline, $(f'_{c,d})_b$, $(f'_{c,c})_b$, and $(K_{abut,t})_b$. Table 4 compares the mode frequencies of the preliminary FEM, the target baseline, the identified baseline, and the damaged bridge. The differences between the frequencies in the preliminary FEM and the ones in the damaged bridge indicate that the preliminary FEM needs to be updated. The posterior probability of density function (PDF) of the unknown parameters $\mathbf{x}_m = \{f_{c,d}, f_{c,c}, K_{abut,t}\}$, $p'(\mathbf{x}_m)$, can be obtained by a Bayesian model updating as $p'(\mathbf{x}_m) = \kappa L(\mathbf{F} | \mathbf{x}_m) p(\mathbf{x}_m)$, where κ =normalizing factor, $p(\mathbf{x}_m)$ =prior probability density function of \mathbf{x}_m , $L(\mathbf{F} | \mathbf{x}_m)$ =likelihood function, and \mathbf{F} =frequency data obtained from the vibration test. As a result of the Bayesian model updating, the parameter ratios in the identified baseline come to an agreement with the ratios in the target baseline shown in Table 3. Accordingly, the mode frequencies in the identified baseline agree well with the frequencies in the target baseline as found in Table 4, indicating that the preliminary FEM has been updated successfully.

Table 3. Parameter ratios between the baseline and the preliminary values

Parameters	Preliminary FEM	Target baseline	Identified baselines	
			Mean	St. Dev.
$(f'_{c,d})_b / (f'_{c,d})_p$	1.0	1.2	1.259	0.269
$(f'_{c,c})_b / (f'_{c,c})_p$	1.0	1.2	1.156	0.089
$(K_{abut,t})_b / (K_{abut,t})_p$	1.0	1.5	1.507	0.051

Identification of damage locations by DIM. With the mode shapes from the identified baseline and the mode shapes extracted from the vibration data obtained from the vibration test, the DIM is then applied to identify the damage locations in the column. If the column is divided into small segments along the height (in this case, we use 20

segments with the same length), for the q th segment, the DIM calculates a damage index, DI_q . Then, a corresponding normalized damage index is calculated as $Z_q = (DI_q - \mu_{DI}) / \sigma_{DI}$, where μ_{DI} and σ_{DI} refer to the mean and standard deviation of DI_q . To identify the damage location, a threshold value needs to be selected. When a threshold λ_q is chosen, the probabilities that the DIM indicates damage (ID_q) and does not indicate damage (NID_q) in the q th segment can be defined as $P(ID_q) = P(Z_q \geq \lambda_q) \approx (\# \text{ of cases of } Z_q \geq \lambda_q) / n$ and $P(NID_q) = P(Z_q < \lambda_q) \approx (\# \text{ of cases of } Z_q < \lambda_q) / n$, where n = number sets of mode shapes that are extracted from vibration records.

Table 4. Comparison of modal frequencies (Hz)

Mode	Preliminary [†] FEM	Target [†] baseline	Identified baseline		Damaged FEM [‡]
			Mean	St. Dev.	
z_1	2.4752	2.5009	2.5049	0.0221	2.5415
z_2	3.2977	3.4484	3.4309	0.0566	3.4213
z_3	4.7685	4.9970	4.9673	0.0886	4.9853
y_1	2.3623	2.7673	2.7759	0.0393	2.7370
y_2	3.8474	4.6464	4.6517	0.0616	4.6921

[†] frequencies obtained from modal analysis; [‡] frequencies obtained from TDD

Figure 1b shows the damage index of the column elements in the damaged bridge under a measurement noise level of 1%. The variability of the damage index shown in Figure 1b indicates the influences of the modeling and measurement errors on the DIM. To determine the probability of damage detection, three different threshold values are used as shown in Figure 1c. A lower value of the threshold gives a higher probability of correct detection for the damaged elements but also a higher probability of false detection for the undamaged elements. Furthermore, the probability of false detection for the undamaged element adjacent to the end of the column is relatively high, which is partially due to the spline interpolation in the DIM applied in those elements (Huang et al. 2010b).

Application of local damage detection. In the suspected damage area that is identified by the global damage detection, the local damage detection can be applied in order to detect the damage severity. In this numerical study, following the regression model of Eq. (4), we assume the estimate of $\sqrt{f'_{c,dam}}$ for damaged Elements 15 and 16 has a mean of $5.753\sqrt{\text{MPa}}$ and a standard deviation of $0.5192\sqrt{\text{MPa}}$.

Estimation of fragilities. To account for the inherent randomness of the structural properties in the fragility estimate for the damaged bridge, some quantities are considered as random variables, as shown in Tables 1 and 2. Different ways to treat the uncertainties give different fragility estimates. Therefore, it is worthy to first look at the contributions of each random variable to the variability in the limit state functions. This can be done by examining the important measures of the random variables (Der Kiureghian and Ke 1985). Through important measure analysis, it is found that $\theta_{C,k}$, $\theta_{D,k}$, $\varepsilon_{C,k}$ and $\varepsilon_{D,k}$ are

the most important random variables while the variability in the other random variables can be ignored so they are fixed at their mean values. Furthermore, the distributions of $\theta_{C,k}$ and $\theta_{D,k}$ in Eqs. (2) and (3) are multi-variate t distributions, which can be approximately considered as normal distributions since the number of data used to assess $\theta_{C,k}$ and $\theta_{D,k}$ is large. Therefore, the difference $C_k(\mathbf{x}, \theta_{C,k}) - D_k(\mathbf{x}, \theta_{D,k}, \mathbf{s})$ has approximately a normal distribution since both $C_k(\mathbf{x}, \theta_{C,k})$ and $D_k(\mathbf{x}, \theta_{D,k}, \mathbf{s})$ are linear functions of approximately normal random variables. Thus, the fragilities can be estimated by a simple approximate form proposed by Huang et al. (2010a) without using any specialized reliability software.

Figure 3 shows the fragility estimates for deformation, shear, and bi-variate failure modes. Each contour line represents a fragility level in the range of 0.1-0.9 for a given pair of PSA/g and $PGV \cdot T_1 / H_c$. The solid lines denote the actual fragilities of the target damaged bridge assuming all the properties are known and the dotted lines denote the fragility based on the identified structural properties using the proposed framework. The discontinuities in fragility contour lines in shear and bi-variate fragilities are due to the fact that $\sigma_{D,v}$ is not a constant (Huang et al. 2010a). As shown in Figure 3, the solid lines and the dotted lines are consistently close to each other indicating that the fragilities using the identified structural properties obtained from the proposed framework are accurate enough to reflect the true performance of the bridge.

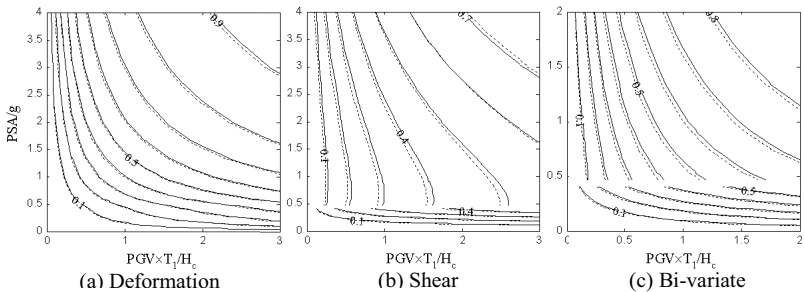


Figure 3. Fragilities of the target damaged FEM (solid lines) and the identified damaged FEM (dotted lines)

CONCLUSIONS

This paper describes a probabilistic framework to incorporate information from nondestructive testing (NDT) in the estimates of the seismic fragility of a reinforced concrete (RC) bridge. The proposed framework combines global and local damage detection methods. Global damage detection uses the dynamic responses of a structure obtained from a vibration NDT to assess its global/equivalent structural properties and detect potential damage locations. Local damage detection method uses local measurements from a NDT technique to identify the local characteristics of the structure at selected area. This study considers the measurement and modeling errors in the application of the damage detection methods. Then, the bridge reliability is evaluated

through probabilistic capacity and demand models calculated using the structural properties obtained from the damage detection. Finally, the result of the case study shows that the proposed framework can successfully provide the up-to-date structural properties and accurate fragility estimates of reinforced concrete bridges.

REFERENCES

- Der Kiureghian, A. and Ke, J.-B. (1985). "Finite-element based reliability analysis of frame structures." *The 4th International Conference on Structural Safety and Reliability*: 395-404, Kobe, Japan.
- Gardoni, P., Der Kiureghian, A. and Mosalam, K.M. (2002). "Probabilistic capacity models and fragility estimates for reinforced concrete columns based on experimental observations." *ASCE Journal of Engineering Mechanics* 128(10): 1024-1038.
- Gardoni, P., Mosalam, K.M. and Der Kiureghian, A. (2003). "Probabilistic seismic demand models and fragility estimates for RC bridges." *Journal of Earthquake Engineering* 7, 79-106.
- Huang, Q., Gardoni, P. and Hurlebaus, S. (2009). "Probabilistic Capacity Models and Fragility Estimates for Reinforced Concrete Columns Incorporating NDT Data." *ASCE Journal of Engineering Mechanics* 135(12): 1384-1392.
- Huang, Q., Gardoni, P. and Hurlebaus, S. (2010a). "Probabilistic Seismic Demand Models and Fragility Estimates for Reinforced Concrete Highway Bridges with One Single-Column Bent." *ASCE Journal of Engineering Mechanics*, 136(11).
- Huang, Q., Gardoni, P. and Hurlebaus, S. (2010b). "A Probabilistic Damage Detection Approach Using Vibration-based Nondestructive Testing." *Structural Safety* (in review).
- Huang, Q., Gardoni, P. and Hurlebaus, S. (2010c). "Predicting Concrete Compressive Strength Using Ultrasonic Pulse Velocity and Rebound Number Data." *ACI Materials Journal* (in review).
- Huang, Q., Gardoni, P. and Hurlebaus, S. (2010d). "Extracting Modal Parameters Considering Measurement and Modeling Errors." *Reliability Engineering & System Safety* (in review).
- Kim, B.H., Stubbs, N. and Park, T. (2005). "A new method to extract modal parameters using output-only responses." *Journal of Sound and Vibration*, 282(1-2): 215-230.
- Mackie, K. and Stojadinović, B. (2003). "Seismic Demands for Performance-Based Design of Bridges." Pacific Engineering Earthquake Research Center, University of California.
- Mander, J. B. and Basoz, N. (1999). "Seismic fragility curve theory for highway bridges." *Optimizing Post-Earthquake Lifeline System Reliability* 16: 31-40.
- McKenna, F. and Fenves, G. L. (2000). "An object-oriented software design for parallel structural analysis." *Proceedings of the Advanced Technology in Structural Engineering*, ASCE Structures Congress 2000, Washington D.C.
- Padgett, J.E. and DesRoches, R. (2009). "Retrofitted Bridge Fragility Analysis for Typical Classes of Multi-Span Bridges." *Earthquake Spectra* 25(1): 117-141.
- Stubbs, N. and Kim, J.T. (1996). "Damage localization in structures without baseline modal parameters." *AIAA Journal* 34(8), 1644-1649.
- Zhong, J., Gardoni, P., Rosowsky, D. and Haukaas, T. (2008). "Probabilistic seismic demand models and fragility estimates for reinforced concrete bridges with two-column bents." *ASCE Journal of Engineering Mechanics* 134(6), 495-504.

MODELING LONG-TERM RELIABILITY OF VERTICAL BARRIERS

Arthur S. Kurzydlo¹ and Jamshid Mohammadi²

¹ Dearborn Engineering Corporation, 1170 S. Plymouth Ct., Chicago, Illinois 60605; PH (312) 341-0037; email: akurzydlo@dearbornengineering.com

² Civil, Architectural and Environmental Engineering Department, Illinois Institute of Technology, IIT Center, Chicago, Illinois 60616; PH (312) 567-3540; email: mohammadi@iit.edu

ABSTRACT

The concept of containment is often employed at existing and planned landfills, at sites contaminated with dense nonaqueous phase liquids (DNAPLs) and at sites where a physical barrier is required. A vertical cutoff wall is one of the critical elements of the containment system. This physical barrier can provide hydraulic control and prevent migration of contaminants from the area of impacts. Several types of vertical cutoff walls are currently available and include steel or plastic sheet pile walls, geomembrane walls, slurry walls, deep soil mixing type walls or grouted walls. The other components of the containment system include surface water control and capping or liners. Ideally, a properly designed, constructed and operated containment system would create a totally impervious site encapsulation.

Realistically, since the design, construction and operation are performed under conditions of uncertainty, containment system performance should be measured in terms of probability. Whether the containment system is in the design phase or in operation, the reliability of the vertical barrier should be assessed.

The reliability of the vertical cutoff wall is a function of several variables. These variables are associated with uncertainties and are evaluated through a probabilistic analysis. The performance function is intended as a means to evaluate a component's dependence on design and control variables. These variables are selected based on engineering design principles, historical field data collected by the authors and data published by others.

Assessment of long-term reliability of steel sheet pile wall with sealant is presented and a design equation is derived based on probability and field data. Similarly, reliability of each containment system component can be evaluated. The proposed model provides a means for comparison between different technologies and at the same time allows assessment of the reliability of multi-component systems. Additionally, this model can provide important information that can be used in risk analyses.

INTRODUCTION

The vertical barrier is one of the critical elements within the containment system employed to address groundwater and soil pollution. A typical containment system is a combination of several measures like vertical barrier wall, interceptor drain, extraction well and impermeable cap. Each element of this system is designed to perform a certain function. It is of great interest to know how well this function is performed. This knowledge is necessary during feasibility studies to compare various alternatives and to select the most suitable technology. This will also aid in the analysis of the effectiveness of various alternatives, reliability of the system, and in-site risk assessment evaluation.

Reliability of the containment system is a function of each component's reliability. The proposed model evaluates this reliability through the performance function and compares that with long-term performance data. The reliability of the vertical barrier is a function of several variables. These variables are subject to uncertainties and are evaluated through a probabilistic analysis.

DESIGN AND CONTROL VARIABLES

The design and control variables are related to the material properties, design methods, construction methods, and functional requirements (future use of the site). It is necessary to recognize and analyze these variables.

Several different types of vertical barriers are currently used. Among the most popular barriers are slurry walls, steel sheet pile walls, vibrating beam walls, deep soil mixing type walls, jet grouted walls, and composite walls. Design variables for vertical barriers include, (i) common and (ii) specific variables. Common variables are wall permeability, longevity, and deformability. Those variables, in turn, are functions of soil characteristics, key-in requirements, associated remedial measures, construction methods, quality control, compatibility with contaminants and/or contaminated groundwater, performance monitoring, and laboratory techniques. Specific variables for steel sheet pile wall with sealant include steel sheet and sealant material characteristics like steel corrosion and sealant's (waterstop) compatibility and durability.

ANALYSIS OF UNCERTAINTIES

Evaluation of engineering reliability requires information on uncertainty in terms of standard deviation or coefficient of variation. Uncertainties may be associated with physical phenomena that are inherently random or with predictions and estimations that are made with inadequate information. In the case of the containment system, each element such as vertical barrier or cap represents a function of several random variables. Random variable uncertainty is associated with i) inherent variability, ii) prediction error.

Inherent Variability

Inherent variability stems from natural uncertainty associated with random phenomena. Each variable may be described in terms of a range of possibilities, with their respective likelihood of occurrence, which is a probability density function. Quite often, a random variable is defined with the mean or median and standard deviation or coefficient of variation.

Prediction Error

Errors of prediction include estimation error (such as statistical sampling error) as well as the imperfection of the prediction model. Such prediction error may include a systematic component (bias) and random component (random error). Systematic component may arrive from factors not accounted for in the prediction model that tend to consistently bias the estimate in some direction. Random error is involved whenever there is a range of possible errors due to sampling.

In practice, each variable can be presented as an estimate of the mean value (\bar{x}) and estimate of the standard deviation (s_x). When, for practical purposes, errors of prediction are limited to the errors in estimation of the respective mean values, the systematic error can be adjusted by a bias correction factor v , and the random error in mean value (\bar{x}) is expressed in terms of coefficient of variation (C.O.V.) and is treated statistically.

ASSESSMENT OF RELIABILITY

Reliability of the containment systems can be evaluated the same way the reliability of many other engineering systems are evaluated by formulating the system performance in terms of a capacity and a demand function. Capacity or demand of each measure is a function of several variables as described in the preceding section. The reliability formulation is as follows: A performance function describing the level of performance of a system is represented as (Ang and Tang, 1980).

$$g(x) = g(x_1, x_2, \dots, x_n) \quad 1$$

where $X=(x_1, x_2, \dots, x_n)$ is a vector of basic state variables, and the function $g(x)$ determines the performance or state of the system.

A design variable can be represented by a probability density function (PDF). Estimation of the probability of no failure requires the knowledge of the PDF. When the distribution is unknown the second-moment formulation can be used (Cornell, 1969; Ang and Cornell, 1974).

With the second-moment formulation, the reliability may be measured entirely with a function of the first and second moments of the design variables. This function is a reliability index, β . It is a convenient approach when no information on the probability distribution is available. The method will result in a reasonable accuracy especially when the level of uncertainties in the random variables is low and the random variables are statistically independent of each other. Reliability of each containment system component can be determined through the probability of the safe state. Alternatively, the method based on the Hasofer-Lind index can be used to assess the reliability (Hasofer and Lind, 1974). The second moment method based on the Hasofer-Lind computes the safety index by transferring the failure surface into a space of reduced variables. The safety index β is then the shortest distance of the transformed failure surface from the origin of the reduced random variables. This method can especially be used when random variables are correlated.

Based on this probability, a safe design can be selected. For example when choosing a barrier wall for the project, the reliability model will allow one to select the most reliable design.

In today's practice, several types of vertical cutoff walls are in use. They include slurry walls, steel sheet pile walls, geomembrane walls, deep soil mixing type walls and grouted walls. Reliability of steel sheet pile walls was previously evaluated by the authors (Kurzydlo and Mohammadi, 1994) as was the reliability of the slurry wall (Kurzydlo and Mohammadi, 1995).

The performance function used in the wall reliability analysis is simplified as a linear function, i.e.:

$$g(x) = D - E \quad 2$$

where D = demanded permeability
 E = expected permeability

The usual requirement for the demanded permeability (D) is 10^{-7} cm/sec.

The expected permeability of the steel sheet pile wall with sealant is a function of permeability of the steel sheet pile and permeability of the sealant.

$$\log E = \alpha (\log W + \log S) \quad 3$$

where W = wall permeability
 S = sealant permeability
 α = correction coefficient

The correction coefficient depends on a bond between the sealant and the wall. It is a function of construction methods, quality assurance and quality control (QA/QC), contractors' experience, as well as temperature and humidity.

Permeability of the sealant is a function of groundwater quality, contaminants type and concentration, as well as QA/QC and contractors experience. Permeability of the wall depends on how well the wall is constructed. This, in turn is a function of soil conditions, type and size of the sheet, contractors experience and QA/QC.

The performance of vertical barriers in containment systems is monitored and evaluated with time. As more information becomes available, the long-term reliability may be modeled.

For the last 15 years, the performance of the sheet pile wall evaluated by authors in 1994 was observed and recorded (Kurzydło, 2010). Based on that performance the authors assessed the permeability of the wall to be 5×10^{-8} cm/sec with (C.O.V.) $\Omega_E = 0.10$. Also, by examination of the mean permeability values, as previously presented, the relationship between the wall permeability (logarithmic function) and sealant permeability (logarithmic function) can be approximated as $\log S = \frac{1}{2} * \log W$.

The best method to present or model the long-term performance of the vertical barrier is to use design criteria that engineers are familiar with and can use to verify the reliability of the proposed barrier. Thus, we utilize the most general and versatile form of criteria which are design factors for each design variable. We use the second-moment approach in which the required criteria are formulated on the basis of information for the first and second moments of the design variables.

The previously obtained mean values and C.O.V.'s of wall permeability and sealant permeability are

wall: $\mu_W = 5.17 \times 10^{-6}$ cm/sec with (C.O.V.) $\Omega_W = 0.81$

sealant: $\mu_S = 1.00 \times 10^{-10}$ cm/sec with (C.O.V.) $\Omega_S = 0.35$

The corresponding demanded permeability D is based on regulatory requirements and its assessed C.O.V. is $\Omega_D = 0.10$

To arrive at long-term model design factors the authors first used an iterative process to calculate the design factors based on original project data with higher safety index and then used the 15-year wall permeability to calibrate the model through iterations using a decreasing safety index.

For the original project phase (Phase I) first iteration, the required safety index (target reliability) β was taken as 2.5, i.e. $\beta = 2.5$ and the total wall permeability E was

taken from the original project data. For simplicity, when symbol E is used it means the logarithm of the mean value of E. Also, the correction $\alpha = 1.0$. Since, the logarithm of total wall permeability is equal to the sum of logarithms of wall and sealant permeability, $E = W + S$, the mean design factors for the expected total wall permeability (logarithm of) and the demanded permeability (logarithm of) can be calculated.

Using the second-moment formulation (Ang and Tang, 1990):

$$\text{mean value of } E = \log \mu_E = \log \mu_W + \log \mu_S = \log \mu_W + \frac{1}{2} \log \mu_W = 1 \frac{1}{2} \log \mu_W$$

To simplify the process, in the subsequent calculations we use the symbol μ_E , μ_W , μ_S with the understanding that it represents the logarithm of the mean value of permeability

$$\sigma_E = \sqrt{(\sigma_W^2 + \sigma_S^2)}$$

$$\sigma_S \Omega_W / \Omega_S \sigma_W = (\sigma_S / \sigma_W) \times (0.81 / 0.35) = 1 / 2$$

$$\sigma_S = 0.22 \sigma_W$$

$$\sigma_E = \sqrt{(\sigma_W^2 + (0.22 \sigma_W)^2)} = \sqrt{(1.05)} \times \sigma_W$$

$$\begin{aligned} \Omega_E = \sigma_E / \mu_E &= (\sqrt{(1.05)} \times \sigma_W) / (1 \frac{1}{2} \mu_W) = (\sqrt{(1.05)} / 1 \frac{1}{2}) \Omega_W \\ &= 0.68 * 0.81 = 0.55 \end{aligned}$$

At the failure surface $D = E$, then first iteration

$$\alpha_D = (\Omega_D) / \sqrt{(\Omega_D^2 + \Omega_E^2)} = (0.10) / \sqrt{(0.10^2 + 0.55^2)} = 0.179$$

$$\alpha_E = -(\Omega_E) / \sqrt{(\Omega_D^2 + \Omega_E^2)} = (-0.55) / \sqrt{(0.10^2 + 0.55^2)} = -0.984$$

$$\text{Thus, } D = \mu_D (1 - \alpha_D \times \beta \times \Omega_D) = 0.955 \mu_D$$

$$E = \mu_E (1 + \alpha_E \times \beta \times \Omega_E) = 2.353 \mu_E$$

The second iteration yielded the following results

$$D = \mu_D (1 - \alpha_D \times \beta \times \Omega_D) = 0.8 \mu_D$$

$$E = \mu_E (1 + \alpha_E \times \beta \times \Omega_E) = 2.1 \mu_E$$

The third iteration yielded the following results

$$D = \mu_D (1 - \alpha_D \times \beta \times \Omega_D) = 0.9 \mu_D$$

$$E = \mu_E (1 + \alpha_E \times \beta \times \Omega_E) = 2.25 \mu_E$$

Thus, the first phase (original design) requirement is represented by

$$g(x) = D - E = 0.9 \mu_D - 2.25 \mu_E \geq 0 \quad 4$$

For the calibration phase (Phase II) we performed iterations with the required safety index (target reliability) β progressively decreasing from 2.5 to 1.2.

The following is the calibrated design equation (requirement) derived using safety index β assumed equal to 1.2, i.e. $\beta = 1.2$ and the total wall permeability E (logarithm of mean value) equal to the 15-year value from the project data.

$$g(x) = D - E = 1.0 \mu_D - 1.5 \mu_E \geq 0 \quad 5$$

Incorporating 15-year value (log of mean permeability), the requirement yields

$$1.0 \mu_D \geq 1.5 \mu_E$$

$$1.0 (\log 1.00 \times 10^{-7} \text{ cm/sec}) \geq 1.5 (\log 5.00 \times 10^{-8} \text{ cm/sec})$$

$$-7 \geq 1.5 (-7.3)$$

$$-7 \geq -10.95 \quad \text{Which satisfies the design requirements}$$

Using the original design values the requirement yields

$$1.0 \mu_D \geq 1.5 \mu_E$$

$$1.0 (\log 1.00 \times 10^{-7} \text{ cm/sec}) \geq 1.5 (\log 5.17 \times 10^{-6} \text{ cm/sec})$$

$$-7 \geq 1.5 (-5.3)$$

$$-7 \geq -7.95 \quad \text{Again, this satisfies the design requirements.}$$

Thus, the above presented design requirement can be used to model and design a steel sheet pile wall with a sealer (vertical barrier) with the reliability $\beta = 1.2$ and the corresponding safety factor of 1.5.

CONCLUSIONS

Assessment of long-term reliability of steel sheet pile wall with sealant is presented and a design equation is derived based on probability and field data. The reliability analysis is shown to be an important tool during the wall feasibility and technology selection studies. This analysis allows for comparison of different technologies and highlights the weak and strong components within the selected technology. Containment system reliability gives sufficient information for risk analysis and should lead to the future reliability based design of vertical barriers.

REFERENCES

- Ang A. H-S. and Cornell C.A. (1974) Reliability Bases of Structural Safety and Design. J. of Structural Division, ASCE, Vol.100, No. ST9, pp. 1755-1769.
- Ang A.H-S. and Tang W.H.(1980) Probability Concepts in Engineering Planning and Design, Volume II Decision, Risk and Reliability. John Wiley and Sons, New York, NY.
- Cornell C.A. (1969) Structural Safety Specification Based on Second-Moment Reliability. Sym. Int. Assoc. of Bridge and Struct. Engr., London, UK.
- Hasofer, A.M., and Lind, N. (1974). "An exact and invariant first-order reliability format," Journal of Engineering Mechanics Division, ASCE, 100(1), 111-121.
- Kurzydlo, A. S. (2010), Private communication with operator of containment system installed in Wisconsin in 1994.
- Kurzydlo A.S. and Mohammadi J. (1994) Reliability Model for the Analysis of Hazardous Waste Containment Systems. Proceedings of the Second International Symposium and Exhibition on Environmental Contamination in Central and Eastern Europe, Budapest, Hungary.
- Kurzydlo A.S. and Mohammadi J. (1995) Vertical Cutoff Walls -- Reliability Analysis. Proceedings of the 5th International Landfill Symposium, Sardinia.

Managing Biological Invasions Under Severe Uncertainty: Light Brown Apple Moth in California

Craig D. Osteen¹ and L. Joe Moffitt²

¹Economic Research Service, United States Department of Agriculture, N4055, 1800 M Street NW, Washington, D.C. 20036-5831; PH (202) 694-5547; FAX (202) 694-5775; email: costeen@ers.usda.gov

²Department of Resource Economics, 212B Stockbridge Hall, University of Massachusetts, 80 Campus Center Way, Amherst, MA 01003-9246; PH (413) 545-5719; FAX (413) 545-5853; email: moffitt@rescon.umass.edu

The views expressed in the paper are the authors' and do not necessarily represent those of United States Department of Agriculture or any other State or Federal agency.

ABSTRACT

Managing biological invasions often necessitates decision making by public officials facing severe uncertainty about many important factors influencing eventual outcomes. Use of relatively sparse decision models is typically necessary and significant lead time for analysis is unfortunately an uncommon luxury. Moreover, development of relevant information to reduce uncertainty and promote more informed decisions in a timely manner is only rarely feasible. Such an uncertain decision making environment can often engender strategies that are simplistic, highly inefficient, and hard to justify in a rigorous manner. In this paper, info-gap decision theory is leveraged to examine a management strategy for light brown apple moth (*Epiphyas postvittana*) which was discovered in California during 2007. The guiding principle of the analysis is that robustness to uncertainty is an appropriate management objective when facing the severe uncertainty associated with biological invasions. The info-gap strategy is contrasted with strategies following from other popular decision criteria under uncertainty.

INTRODUCTION

The scenario with which this paper is concerned is as follows. An invasive species is newly detected in a geographic area. The presence of the invader in the area is worrisome to at least some of the area's stakeholders. Public officials must respond rapidly to the invasion with little and/or contradictory information. With this information gap, official decisions are often flawed. For example, in the United States, invasive species detections are often met initially with eradication programs that are abandoned subsequently.

When information is sparse and perhaps contradictory, is there a branch of decision theory especially suited to enabling better decisions? The scenario with which this paper is concerned is typical of biological invasions. Nearly all of the information that officials must base policy decisions on is highly subjective and often, as in the case of the invasion considered in this paper, highly controversial. In fact, decision criteria which are closed computational methodologies can provide interested stakeholders with a virtual invitation for hyperbole and even distortion when the scant information available for decision is being assimilated initially. As is demonstrated subsequently, policy formulation based on robust satisficing offers officials some flexibility not available under traditional criteria.

TRADITIONAL DECISION CRITERIA UNDER UNCERTAINTY

Traditional decision criteria under uncertainty include the maximin, maximax, and equally likely criteria (see e.g., Render et al., 2009). The first two are cast as polar extremes in terms of pessimism and optimism while the latter presumes uncertain events are equally likely. Some newer alternatives to these traditional decision criteria under uncertainty often assume mappings similar in character to the equally likely criterion.

Each of these traditional decision criteria can be interpreted in the context of the classic decision problem (Table 1) where A_i and E_j are acts and events, respectively, and outcomes are denoted by $V(A_i, E_j)$ with larger values of V preferred. The maximin optimal decision is found as the solution to Maximize $\min_{(E_j)} V(A_i, E_j)$; the maximax optimal decision is found as the solution to Maximize $\max_{(A_i)} \max_{(E_j)} V(A_i, E_j)$; and the equally likely optimal decision is found as the solution to Maximize $\sum_j V(A_i, E_j)$.

It bears noting that each of these traditional decision criteria lead to an optimal decision, often unique, once the information contained in Table 1 is specified. In particular, the magnitudes of all or perhaps just some of the $V(A_i, E_j)$ in the body of the table will turn out to be the drivers of the optimal decision under the closed computational methodologies associated with these traditional criteria.

Table 1. Decision Table Under Uncertainty.

Event	E_1	E_2	...	E_m
Probability	?	?	...	?
Act				
A_1	$V(A_1, E_1)$	$V(A_1, E_2)$...	$V(A_1, E_m)$
A_2	$V(A_2, E_1)$	$V(A_2, E_2)$...	$V(A_2, E_m)$
.
.
.
A_n	$V(A_n, E_1)$	$V(A_n, E_2)$...	$V(A_n, E_m)$

INFO-GAP

Info-gap decision theory (Ben-Haim 2006) is primarily a prescriptive theory providing support to decision makers under uncertainty. Distinct from traditional alternatives, the info-gap approach is not a closed computational methodology but rather a flexible perspective on decision analysis whose assessments assist decision makers in evaluating options, developing strategies, and evolving preferences. Both the flexibility and method of any relatively new decision theory, such as info-gap, in addressing the classic decision problem of Table 1 is of significant interest to researchers and practitioners alike.

A bird's-eye view of info-gap decision theory is as follows. An info-gap is a disparity between what is known, referred to as the nominal model, and what needs to be known in order to make a comprehensive decision. The theory is based on a model of uncertainty, a model of the system that generates outcomes, and a performance requirement.

Specific formulation of an info-gap model of uncertainty depends on the type of initial information available which is then invested in determining the structure of a family of nested sets of uncertain events. Nesting imposes the property of "clustering" which is the defining characteristic and unifying feature of a wide range of info-gap models of uncertainty; e.g., convex, non-convex, continuous, discrete, bounded, unbounded, hybrid, as well as others employing various measures of deviation. There is also a

wide range of successful applications of info-gap attesting to the theory's adaptable structure in modeling real-world decisions.

The uncertainty model, system model, and performance requirement are combined in formulating a robustness function which supports the choice of action. From an info-gap perspective, a decision which achieves an acceptable outcome over a large range of uncertain realizations is preferable to a decision which fails to achieve an acceptable outcome even under small error. Info-gap theory takes the position that the best strategy is the one that satisfies the decision maker with an outcome that is both "good enough" and that makes the decision maker as immune as possible from an unacceptable outcome. In brief, an info-gap robust optimal decision maximizes the reliability of an adequate outcome. In this way a robustness function generates preferences on available decisions.

An info-gap model of the classic decision problem associated with Table 1 can be formulated as follows. Let $|\cdot|$ and $\mathcal{P}(\cdot)$ denote cardinality (number of elements) and power set (the set of all subsets), respectively. An info-gap uncertainty model, $\mathcal{U}(\alpha)$ with elements denoted by u , can be defined as

$$\mathcal{U}(\alpha) = \{h \in \mathcal{P}(\{E_1, E_2, \dots, E_m\}) : |h| \leq \alpha\}; \alpha = 0, 1, 2, \dots$$

i.e., $\mathcal{U}(\alpha)$ is the set of all subsets of $\{E_1, E_2, \dots, E_m\}$ with cardinality no greater than α . The uncertainty model exhibits the key, defining info-gap property of being a family of nested sets since $\alpha < \alpha'$ implies that $\mathcal{U}(\alpha) \subseteq \mathcal{U}(\alpha')$. The nominal model is the empty set; i.e., existing information does not point toward any observable event. The system model is reflected in the evaluation of $V(A_i, E_j)$ which is compared to a performance requirement, V^* .

Preferences over acts generated by a robustness function, $\hat{\alpha}(A_i)$, enable identification of the act which achieves an acceptable outcome over the largest range of uncertain realizations; i.e., the act which provides as much immunity as possible from an unacceptable outcome. Since the nominal model is not an observable event, a measure of robustness is global in nature. The info-gap robustness function is

$$\hat{\alpha}(A_i) = \max \{ \alpha : (\min_{(E_j \in u, u \in \mathcal{U}(\alpha))} V(A_i, E_j)) \geq V^* \}$$

The robust optimal decision is

$$\hat{A} = \underset{(A_i)}{\operatorname{argmax}} \hat{\alpha}(A_i)$$

An important feature of the info-gap theory, which contributes significantly to its flexibility in modeling, is that the precise interpretation/nuance and evaluation of the notion of robustness is a user-defined combination of the uncertainty model, system model, and performance requirement. The specific definition of robustness embodied in the right hand side of the expression immediately above means the robustness associated with act A_i is the largest value of α such that there exists an element $u \in \mathcal{U}(\alpha)$ with $V(A_i, E_j) \geq V^*$ for all events $E_j \in u$. Hence, robustness at uncertainty level α means that at that level, there is at least one element in the uncertainty model which meets the performance requirement and which was not an element in the uncertainty model at uncertainty level $\alpha - 1$. Hence, this is manner in which the robust optimal decision will maximize the reliability of an adequate outcome in this classic decision problem.

Info-gap generalizes the maximin (maximax) criterion in this classic decision problem in the sense that the maximin (maximax) optimal decision is a special case of info-gap's optimal robust decision whenever $V^* \leq (\max_{(A_i)} (\min_{(E_j)} V(A_i, E_j)))$ ($V^* = (\max_{(A_i)} (\max_{(E_j)} V(A_i, E_j)))$). The optimal robust decision can be evaluated as the solution to $\underset{(A_i)}{\operatorname{Maximize}} |u|$ Subject to $u \in \mathcal{P}(\{E_1, E_2, \dots, E_m\}); V(A_i, E_j) \geq V^* \forall E_j \in u$ whenever this might offer a more convenient evaluation method.

MANAGEMENT OF THE LIGHT BROWN APPLE MOTH (*EPIPHYAS POSTVITTANA*) IN CALIFORNIA

The presence of the light brown apple moth (*Epiphyas postvittana*), referred to subsequently as LBAM, in California was first detected by a retired University of California entomologist in the yard of his Berkeley, California home during 2007. Although LBAM was already established in Hawaii, it had never been previously identified, nor apparently ever been the subject of detection efforts, in the continental United States. Evaluation of unrelated-to-LBAM trapping evidence at the time indicated that it might have been present in California during 2006. Information contained in this section is based on United States Department of Agriculture (2008) and United States Department of Agriculture (2010).

Following discovery of LBAM in Berkeley in Alameda county, officials launched an eradication program for LBAM and claimed success in Napa county (approximately 30 miles to the north) and Los Angeles county (approximately 375 miles to the south) as well as in the city of Oakley in Contra Costa county (approximately 30 miles to the east). A quarantine was maintained initially in 10 other counties. Additionally, a comprehensive eradication program that involved delimiting surveys, trapping, pesticide applications (aerial release of LBAM pheromones), and development of integrated pest management (IPM) methods was developed with anticipated eradication by 2011 to be followed by control maintenance activities. The presence of the program allowed Canada, Mexico, and other states to relax trade restrictions and accept LBAM-host crops from non-infested California counties with no restriction.

By late 2007, some projections of LBAM economic impacts began to emerge into public view. Initial projected impacts of LBAM, if not controlled, were estimated to be up to \$2.6 billion annually should LBAM enter the San Joaquin Valley. In 2007 and 2008, the United States Department of Agriculture (USDA) allocated about \$90 million in emergency funding to the LBAM program. At the same time, substantial disagreement about the status of LBAM among experts was also becoming apparent. Dissenters from the official view maintained that the geographical dispersion of LBAM over hundreds of miles indicated that it had been present in California for decades, could not be eradicated, and was causing no crop damage. Public distaste for the aerial eradication efforts in many affluent areas of the state led to multiple filings of petitions with the Secretary of Agriculture to declassify LBAM as an "actionable" pest. Additionally, legal challenges to officials led to a state court ruling in the spring of 2008 suspending/terminating the aerial spray program.

Despite controversy, eradication efforts continued without aerial spraying. Officials conducted statewide and national (47 states) surveys, evaluated biological control (parasitic wasps), and accelerated development of sterile insect technology (SIT) – mass rearing of sterile insects. Mating disruption (ground-based application of LBAM pheromone) and insecticidal control (targeted ground-based application of organic pesticides, spinosad and Bt, in areas with high larval populations). By 2009, LBAM was considered to be present in 15 California counties but regarded as eradicated in Los Angeles and San Luis Obispo counties. Officials contracted with the National Academy of Sciences (NAS) to evaluate their official responses to petitioners. In the response to the NAS evaluation, the USDA estimated that if uncontrolled, LBAM would cause nationwide annual production losses of \$694 million to \$1.597 billion, and annual losses of \$219 million to \$503 million in California. Following the NAS evaluation, officials determined that LBAM eradication was no longer feasible due to continuing spread; however, the "actionable" status was maintained and a control/containment program continues at the present time. As of 2010, 17 counties in California are quarantined.

Policy officials at the time of discovery were concerned with how best to respond, in a broad sense, to the presence of this (alleged) invader. The key policy question was whether an eradication program should be undertaken. Table 2 depicts the decision problem summarizing the information that officials had available when a decision to eradicate LBAM was reached during 2007.

Table 2. Decision Table for Light Brown Apple Moth Under Uncertainty.

Event	LBAM an Eradicable, Serious Pest	LBAM a Serious Pest, Not Eradicable	LBAM Harmless
Probability	?	?	?
Act			
Eradication Program	-\$.09 b	-\$.64 b	-\$.09 b
No Eradication Program	-\$1 .1 b	-\$1 .1 b	\$0

Policy definitions in Table 2 correspond to the notation in Table 1 as follows: A_1 refers to implementation of an eradication program; A_2 refers to no public agency programming. Definitions of uncontrolled events are as follows: E_1 refers to LBAM being a devastating pest which is eradicable, E_2 refers to LBAM being a devastating pest which is not eradicable, and E_3 refers to LBAM being a harmless organism.

Numbers in the body of Table 2 and corresponding to the $V(A_i, E_j)$ in Table 1, show an estimate of the present value of net benefits corresponding to each act/event pair. In particular, the outcome associated with A_1, E_1 is the outcome associated with $A_1, E_3 = -\$0.09$ billion (all Commodity Credit Corporation (CCC) funds allocated to LBAM, assuming all funds are spent, eradication works (or LBAM causes no damage), and there is no LBAM damage). The outcome associated with $A_1, E_2 = -\$0.64$ billion (half of the outcome associated with A_2, E_1 (-\$0.55 billion) plus eradication cost (-\$0.09 billion). The outcome associated with A_2, E_1 is the outcome associated with $A_2, E_2 = -\$1.1$ billion (no eradication program). The outcome associated with $A_2, E_3 = \$0$ (no eradication program and no LBAM damage).

The magnitude of the outcomes shown in the body of Table 2 are not atypical of those associated with biological invasions; viz., catastrophic consequences are forecasted to accrue to inaction while the status quo is preserved by action at what appears to be relatively modest cost. The LBAM case is somewhat distinctive in that experts were so very much more divided than usual in forecasting both events and conditional outcomes.

Table 3 shows optimal decisions associated with the maximin, maximax, equally likely, and info-gap decision criteria. A graph of the info-gap robustness function is shown in Figure 1. While the maximax criterion favored no eradication effort, both the maximin and equally likely criteria supported eradication of LBAM.

Table 3. Optimal Management of Light Brown Apple Moth Under Severe Uncertainty.

Decision Criterion	Optimal Act
Maximin	A_1
Maximax	A_2
Equally Likely	A_1
Info - Gap	A_1 , if $V^* < -\$.09 b$; A_2 , otherwise

The LBAM control program remains controversial, and the desired decision depends on one's perspective on potential damages and the effectiveness of the control program. As of October 2010, the USDA maintains that LBAM has the potential to cause serious damages in terms of agricultural production losses and quarantines that prevent sales and exports of crops. Part of the USDA's mission is to protect agricultural and resource values from the damages of invasive species or exotic pests and diseases. The USDA often tries to respond quickly to new pest threats or infestations to minimize spread, damage, or control costs, while grower interests may pressure the Department to use Government funds to exclude or control them. While the USDA now considers eradication of LBAM to be infeasible, a control program continues. The USDA decision to control LBAM corresponds to those suggested by the max-

imin and equally likely criteria, as well as the info-gap criterion with a performance requirement of production losses and control costs greater than \$90 million (which assumes pest damage).

Alternatively, the opponents and petitioners, with the support of some well known scientists, argue that LBAM is not damaging or spreading, and that the eradication or control program is unnecessary. From the USDA's viewpoint, not controlling LBAM would correspond to the optimal choice under the maximax criterion or the info-gap criterion with a performance requirement of production losses and control costs less than \$90 million (no pest damage). Many opponents are residential or non-agricultural landowners, who would receive little or no benefit from the program, but could be directly affected by the negative effects of the control program, as well as contributing taxes to pay for the program. For these opponents, no control would be optimal.

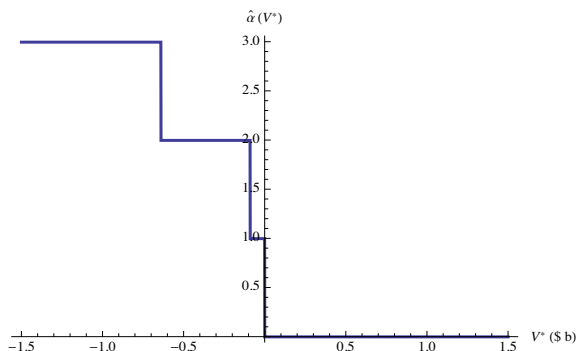


Figure 1. Robustness-performance trade-off

The info-gap optimal robust decision and associated robustness depends on the performance requirement as shown in Table 3 and Figure 1, respectively. Info-gap counsels action based on maximizing the range of uncertainty over which performance can be achieved. In this case, making no response to a backyard discovery of LBAM in the absence of any observed damages due to its presence, could have been justified according to the info-gap criterion, in contrast to the maximin optimal decision as well as the equally likely optimal decision.

As is often the case with the discovery of new pests, the uncertainty in the LBAM decision derives from two important sources: 1) the uncertain spread and damage of LBAM, and 2) the uncertain effectiveness of potential control methods. Based on economic decision criteria, the eradication or control program should be implemented if prevented or reduced damages exceeded costs. So, even if the pest is very damaging, an ineffective program would not be justified if damage prevention or reduction was less than costs. Alternatively, a program that would successfully eradicate the organism would not be worth implementing if the organism caused insufficient damage to warrant the cost. Obtaining more information to address these two sources of uncertainty influences the decisions to control the pest or not and what methods to use. As a result, USDA's response program included LBAM monitoring and the development or refinement of control methods.

CONCLUDING REMARKS

As the case of LBAM illustrates well, experts' forecasts of future events and future consequences of actions can be impacted by many considerations and can differ greatly. Some traditional decision criteria under uncertainty, interpreted in modern renditions as closed computational methodologies, may be more vulnerable to sparse, subjective information than a robust satisficing approach such as info-gap.

The latter ultimately reaches an optimal decision under uncertainty using not only a given database but also by valuing robustness in conjunction with other important subjective information from the decision maker as well; viz., a performance requirement. The latter enables policy officials extra flexibility in evaluating exceptionally controversial choices.

REFERENCES

- Ben-Haim, Y. 2006. *Info-Gap Decision Theory: Decisions Under Severe Uncertainty*, Second Edition, Academic Press, Amsterdam.
- Render, B., Stair, R. M., Jr., and Hanna, M. E. 2009. *Quantitative Analysis for Management*, Tenth Edition, Pearson Education, Inc., Upper Saddle River, New Jersey.
- United States Department of Agriculture. 2008. "USDA Budget Explanatory Notes for the Committee on Agriculture" for FY 2009, FY 2010, and FY 2011.
- United States Department of Agriculture. 2010. "APHIS Draft Response to Petitions for the Reclassification of Light Brown Apple Moth [*Epiphyas postvittana* (Walker)] as a Non-Quarantine Pest." Revision 2. January 14, 2010.

Robust Conservation Decision-Making

Eve McDonald-Madden^{1,2*}, Peter W.J. Baxter^{1,3}, and Hugh P. Possingham¹

¹ Centre for Applied Environmental Decision Analysis, School of Integrative Biology, University of Queensland, St. Lucia QLD 4072 Australia.

² CSIRO Sustainable Ecosystems and Climate Adaptation Flagship, St Lucia QLD 4072 Australia

³ Australian Centre of Excellence for Risk Analysis, School of Botany, University of Melbourne, Parkville VIC 3010 Australia.

Abstract

Decision-making for conservation is conducted within the margins of limited funding. Furthermore, to allocate these scarce resources we make assumptions about the relationship between management impact and expenditure. The structure of these relationships, however, is rarely known with certainty. We present a summary of work investigating the impact of model uncertainty on robust decision-making in conservation and how this is affected by available conservation funding. We show that achieving robustness in conservation decisions can require a triage approach, and emphasize the need for managers to consider triage not as surrendering but as rational decision making to ensure species persistence in light of the urgency of the conservation problems, uncertainty, and the poor state of conservation funding. We illustrate this theory by a specific application to allocation of funding to reduce poaching impact on the Sumatran tiger *Panthera tigris sumatrae* in Kerinci Seblat National Park, Indonesia.

To conserve our environment, conservation managers must make decisions in the face of substantial uncertainty. Further, they must deal with the fact that limitations in budgets and temporal constraints have led to a lack of knowledge on the systems we are trying to preserve and on the benefits of the actions we have available (Balmford & Cowling 2006). Given this paucity of decision-informing data there is a considerable need to assess the impact of uncertainty on the benefit of management options (Regan *et al.* 2005). Although models of management impact can improve decision making (e.g. Tenhumberg *et al.* 2004), they typically rely on assumptions around which there is substantial uncertainty. Ignoring this 'model uncertainty', can lead to inferior decision-making (Regan *et al.* 2005), and potentially, the loss of the species we are trying to protect.

Current methods used in ecology allow model uncertainty to be incorporated into the model selection process (Burnham & Anderson 2002; Link & Barker 2006), but do not enable decision-makers to assess how this uncertainty would change a decision. This is the basis of information-gap decision theory (info-gap); finding

strategies most robust to model uncertainty (Ben-Haim 2006). Info-gap has permitted conservation biology to make the leap from recognizing uncertainty to explicitly incorporating severe uncertainty into decision-making. In this paper we present a summary of McDonald-Madden *et al* (2008a) who use an info-gap framework to address the impact of uncertainty in the functional representations of biological systems on conservation decision-making. Furthermore, we highlight the importance of two key elements limiting conservation decision-making – funding and knowledge – and how they interact to influence the best management strategy for a threatened species.

Methods

Case study – Managing the Sumatran tiger in Kerinci Seblat National Park.

In Kerinci Seblat National Park the Sumatran tiger is threatened by a reduction in prey abundance, habitat destruction, and illegal poaching (Linkie *et al.* 2006). Management activities include implementing antipoaching patrols. Funds used to implement antipoaching patrols in this region must be allocated across four core subpopulations and each year managers must decide how many subpopulations to manage given the overall budget available. McDonald-Madden *et al* (2008b) investigated the optimal management of these subpopulations by estimating a relationship between the resources spent on antipoaching patrols in a subpopulation and the annual probability of extinction of a subpopulation. While this relationship was based on information from a recent study on population viability and conservation management options for Sumatran tigers in this area (Linkie *et al.* 2006), the functional form of this relationship is highly uncertain. In McDonald-Madden *et al* (2008a) we extend this work to look at how to make robust decisions regarding the number of subpopulations of Sumatran tiger to manage given uncertainty in the relationship between resources (or the number of subpopulations, n , over which resources, x , are divided) and probability of a subpopulation extinction. Here, the probability of extinction of a single subpopulation in one year is a function of n :

$$P\left(\frac{x}{n}\right) = P_0 \left(1 - \frac{1}{\left(\frac{kn}{x}\right)^\theta + 1} \right) \quad \text{where } n \in \{0, \dots, N\}.$$

The value of k specifies what budget is required to halve the initial annual probability of extinction (when unmanaged), whilst θ alters the shape of the function. For a given value of k , large values of θ indicate that the initial benefit of increasing the budget allocated to the subpopulation is small, while small values of θ mean that there is a large initial benefit to budget increase. Varying k and θ changes the relationship between probability of extinction and resources, thus altering the specified model of the system (see Fig. 1).

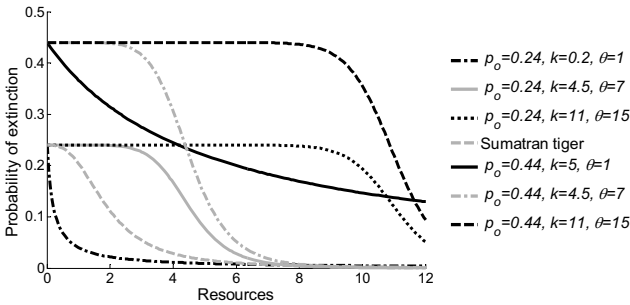


Figure 1: Possible models of the change in probability of extinction given increasing investment. All curves are derived from the assumed mathematical representation of our theoretical ecological system with varying shape parameters, θ , half-saturation points, k , and probabilities of extinction when unmanaged, P_0 . All representations are feasible extinction risk models. The representation initially assumed for the Sumatran tiger is shown.

To investigate robust decision-making for the Sumatran tiger given our uncertainty in this assumed relationship we use an info-gap approach. An info-gap model requires three main elements (Regan *et al.* 2005):

1. a mathematical process model that delivers a measure of performance as a result of management, in this case anti-poaching patrols,
2. a performance requirement, below which we consider our performance unacceptable, and
3. a model describing uncertainty.

Below we outline each element for the optimal management of the Sumatran tiger in Kerinci Seblat National Park (for more details see McDonald-Madden *et al.* 2008a).

Measure of performance

There are five potential management actions based on the number of subpopulations that are managed, including no subpopulations being managed, management of one subpopulation, up to all four existing subpopulations, N , being managed. This management decision is implemented over the entire period over which extinction is considered, t . We base the performance of a management action on the number of extant subpopulations that remain at the end of the management horizon. The expected number of extant subpopulations (E) in the next time step is the sum of the number of subpopulations that are managed that persist, and the number of subpopulations that are not managed that persist:

$$E = n \left(1 - P \left(\frac{x}{n} \right) \right)^t + (N - n)(1 - P_0)^t,$$

where P_0 is the probability of extinction of a subpopulation if it is not managed. We assumed that all subpopulations are the same (but see Chauvenet *et al.* 2010), and as such P_0 and $P(x/n)$ are equal for all subpopulations.

Performance requirement

Using info-gap a manager can specify a ‘performance requirement’ they wish to achieve and thus choose the strategy that attains this goal under the highest level of (unknown) uncertainty. In info-gap theory this approach is known as robust satisficing (Ben-Haim 2006). In conservation, an idealistic performance requirement would be to save all subpopulations of our threatened species, however, this may often be unrealistic due to limitations in funding and the need to distribute resources between subpopulations. Here we consider the minimum acceptable requirement or critical performance requirement (E_c) of keeping at least one population, $E_c \geq 1$, as well as a more risk-averse requirement of ensuring at least two remaining subpopulations, $E_c \geq 2$. Both are commonly considered notions in conservation theory (Bascombe *et al.* 2002; McCarthy *et al.* 2005).

Uncertainty model

The relationship between extinction risk and management investment assumed in this study is not likely to be correct. Indeed there are a range of potential values of k , θ and P_0 that will lead to a multitude of different functional forms (see Fig. 1). The ranges of possible values around the best estimate values of k , θ and P_0 , \tilde{k} , $\tilde{\theta}$ and \tilde{P}_0 respectively, are a function of our uncertainty, α , known as the horizon of uncertainty.

We use an ellipsoid bound info-gap model of uncertainty for vectors of our variables k , θ and P_0 (Ben-Haim 2006):

$$U(\alpha) = \left\{ k, \theta, P_0 : \left[\frac{k - \tilde{k}}{\tilde{k}} \right]^2 + \left[\frac{\theta - \tilde{\theta}}{\tilde{\theta}} \right]^2 + \left[\frac{P_0 - \tilde{P}_0}{\tilde{P}_0} \right]^2 \leq \alpha^2 \right\}, \alpha \geq 0.$$

The ellipsoid-bound model enables us to consider overall uncertainty in the model specification by varying k , θ and P_0 at different rates around the ellipsoid. The distribution of uncertainty between k , θ and P_0 can be described using azimuthal ($0 \leq \omega \leq 2\pi$) and polar ($0 \leq \tau \leq \pi$) angles:

$$\begin{aligned} \tilde{\theta} &= \theta + \theta\alpha \sin \omega \sin \tau \text{ where } \tilde{\theta}, \theta, \alpha \geq 0, \\ \tilde{k} &= k + k\alpha \cos \omega \sin \tau \text{ where } \tilde{k}, k, \alpha \geq 0, \text{ and} \\ \tilde{P}_0 &= P_0 + P_0\alpha \cos \tau \text{ where } \tilde{P}_0, P_0, \alpha \geq 0, \tilde{P}_0, P \leq 1. \end{aligned}$$

The true value of α is unknown (Ben-Haim 2006), as we do not know how uncertain we are of the best estimates of k , θ and P_0 . The greater our uncertainty, the higher the value of α and the larger our ellipsoid of uncertainty. Thus the set $U(\alpha)$ of possible values for k , θ and P_0 becomes more inclusive as α increases.

Using info-gap we are not trying to find the strategy that maximizes the expected number of extant subpopulations but rather determine a robust management

strategy that guarantees a minimally satisfactory level of performance, E_c . To ensure we find this minimal point of satisfaction we calculate the minimum number of extant subpopulations within the ellipsoid for each value of α . We do this numerically by systematically sampling angles ω and τ and calculating the points \tilde{k} , $\tilde{\theta}$ and \tilde{P}_0 around (and within) the ellipsoid. We then use these values to calculate our performances and thus identify the minimum performance for that horizon of uncertainty. Hence for each management strategy we assess how wrong we can be about our assumed model of the system (how large α can be) whilst still satisfying our performance requirement.

We investigate the effect of budget, x , and time over which extinction is considered, t , on the choice of the most robust management strategy.

Results

When our uncertainty in the functional form of the relationship between resources and extinction risk increases then the values of $\tilde{\theta}$, \tilde{k} and \tilde{P}_0 that give the worst performance increase. In essence, this means that the initial benefit of increased funding invested in a subpopulation is reduced, the budget required to halve the unmanaged risk of extinction increases and the probability of extinction when unmanaged increases as our uncertainty, α , increases. Further, more funding and increased uncertainty increases the disparity among management strategies.

An increase in funding available to manage the Sumatran tiger changes which is the most robust strategy and also enables better performance levels (expected number of extant subpopulations, E) to be met (Figure 2a and b). With a relatively low budget ($x=6$) we can ensure one subpopulation is saved from extinction by managing two subpopulations, although the robustness of this strategy to model uncertainty ($\alpha \approx 0.25$) is minimal (Fig. 2a). If we double the budget, our ability to attain the higher performance criteria ($E_c = 2$) increases and the management of more subpopulations becomes a more robust strategy (Fig. 2b). However, this risk-averse criterion can only be achieved with limited robustness to uncertainty, irrespective of what strategy is implemented. A less risk-averse manager can reach their aim ($E_c = 1$) with greater robustness to uncertainty in the extinction-investment curve (Fig. 2b).

The time horizon, t , over which we consider extinction, also influences the most robust strategy and the decision based on the performance criterion (Fig. 2c and d). If extinction risk is considered over one year then any strategy will enable us to attain either performance criteria with a reasonable level of model uncertainty (Fig. 2c). If we increase the time horizon, however, the expected number of extant populations decreases (Fig. 2d). When we consider extinction over 10-year horizon a less risk-averse manager can retain at least one subpopulation for all strategies but only under relatively low levels of uncertainty; however, if the manager is risk-averse, wishing to conserve two subpopulations, then their goal can only be achieved under minimal uncertainty (Fig. 2d). Thus for longer-term management objectives one should focus resources on fewer subpopulations to reach performance requirements whilst staying immune to uncertainty.

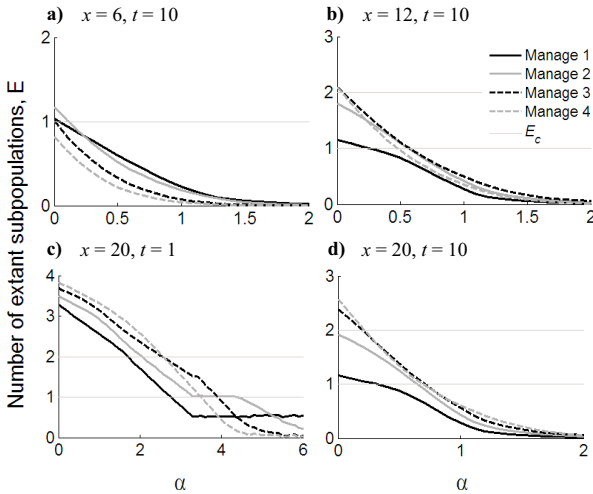


Figure 2: The performance measure, the number of extant subpopulations, E , as a function of increasing uncertainty, α , for each strategy from manage one subpopulation to managing all four subpopulations of Sumatran tiger in the Kerinci Seblat National Park. The robustness of the strategies are investigated for varying budgets, x and time over which extinction is considered, t : a) $x=6, t=10$, b) $x=12, t=10$, c) $t=1, x=20$, and d) $t=10, x=20$. Two possible thresholds for the performance level, $E_c = 1$, and $E_c = 2$ are shown. In all cases budget, x , is 20. Note different scales of horizon of uncertainty axis, α .

Managing all tiger subpopulations is only robust for large budgets and under minimal model uncertainty (Fig. 2a). The most robust option over a variety of budgets and reasonable levels of model uncertainty is to manage fewer subpopulations (two or three subpopulations). If precise understanding of the system is limited and thus model uncertainty around the extinction-investment curve is high and the budget available for management is small, then the optimal approach is to concentrate efforts in one subpopulation. Similarly, when we investigate robust decision-making for different time horizons over which we consider extinction, that is we consider a short-term or long-term approach to management, we see that again the most robust management involves triage (Fig. 2c,d). In both these scenarios, the minimum performance obtained varies depending on uncertainty, budget and time. The greatest performance is achieved for low uncertainty in combination with well-funded projects or short management horizons (Fig. 3).

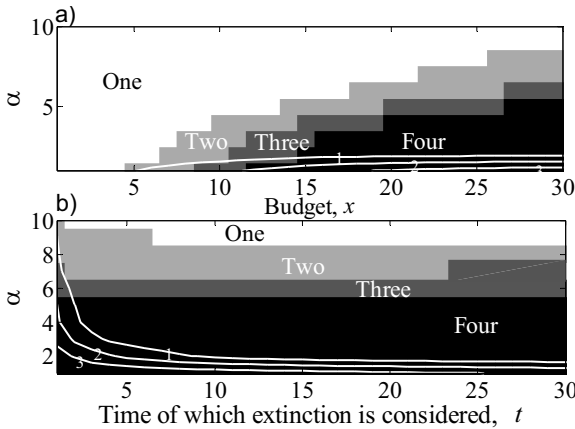


Figure 3: The most robust management decision for the Sumatran tiger in the Kerinci Seblat National Park under uncertainty, α , for a) varying budgets, x (time horizon for extinction here is 10 years), and b) varying time of which extinction is considered, t (budget here is 30 units). Possible decisions are to manage four, three, two, or one subpopulation (shaded areas). The contour lines represent bounds of performance of one, two and three subpopulations extant at the end of the management period.

Discussion

The funding available to conservation programs is a major factor limiting the effectiveness of such programs. Here we discover that it also reduces a management strategy's robustness to our incomplete understanding of the systems we are trying to save. As budgets increase, more inclusive policies (i.e. managing more subpopulations of the Sumatran tiger) become robust, which in turn leads to an increase in performance of our conservation program. The benefit gained from higher resources, however, is only apparent for marginal levels of uncertainty. If our uncertainty is immense, high levels of performance remain elusive even if funding levels are commensurately large. In these situations the most robust strategies are those that take a triage approach (see Bottrill *et al.* 2008) and distribute financial resources towards fewer subpopulations rather than attempt to manage all or even most of our remaining subpopulations. We also show that the time horizon over which a conservation program is designed impacts on the management strategy that gives the most robust performance under model uncertainty. If our objectives are myopic, the highest performance can be expected from the most inclusive management actions. However, as we extend the horizon over which performance is evaluated, triage is an inevitable feature of robust strategies - allocating money towards fewer subpopulations.

Conscience has meant that the default management strategy in many conservation programs is to attempt management of all known subpopulations of a threatened species. Given these same programs are likely to be making decisions under severe budgetary and knowledge constraints, this is unlikely to be the most robust strategy. Indeed inclusive management may only be tenable for species known

to respond decisively to intervention and for whom substantial funding is available. Such species are unlikely to be "critically threatened". Under current levels of funding and knowledge, subpopulation triage will be required to prevent the global extinction of many species. As unpalatable as the recommendation might be, our investigation of the impact of model uncertainty on robust decision-making in conservation, shows that triage will commonly be the most robust approach to preventing the extinction of threatened species.

Acknowledgements

Information on the Sumatran tiger was provided by M. Linkie, University of Kent, Canterbury. We thank E. Game for commenting on this manuscript.

References

- Balmford A. & Cowling R.M. (2006) "Fusion or Failure? The Future of Conservation Biology". *Conserv Biol*, 20, 692-695
- Bascompte J., Possingham H. & Roughgarden J. (2002) "Patchy populations in stochastic environments: Critical number of patches for persistence". *Am Nat*, 159, 128-137
- Ben-Haim Y. (2006) *Info-gap decision theory: decisions under severe uncertainty*. second edn. Academic Press, Sydney.
- Bottrill M., Joseph L.N., Carwardine J., Bode M., Cook C., Game E.T., Grantham H., Kark S., Linke S., McDonald-Madden E., Pressey R.L., Walker S., Wilson K.A. & Possingham H.P. (2008) "Is conservation triage just smart decision-making?" *Trends Ecol Evol*, 23, 649-654
- Burnham K.P. & Anderson D.R. (2002) *Model Selection and Multimodel Inference*. Second Edition edn. Springer, New York.
- Chauvenet A.L.M., Baxter P.W.J., McDonald-Madden E. & Possingham H.P. (2010) "Optimal allocation of conservation resources among subpopulations of a threatened species: how important is patch quality?" *Ecol Appl*, 20, 789-797
- Link W.A. & Barker R.J. (2006) "Model weights and the foundations of multimodel inference". *Ecology*, 87, 2626-2635
- Linkie M., Chapron G., Martyr D.J., Holden J. & Leader-Williams N. (2006) "Assessing the viability of tiger subpopulations in a fragmented landscape". *J Appl Ecol*, 43, 576-586
- McCarthy M.A., Thompson C.J. & Possingham H.P. (2005) "Theory for designing nature reserves for single species". *Am Nat*, 165, 250-257
- McDonald-Madden E., Baxter P.W.J. & Possingham H.P. (2008a) "Making robust decisions for conservation with restricted money and knowledge". *J Appl Ecol*, 45, 1630-1638
- McDonald-Madden E., Baxter P.W.J. & Possingham H.P. (2008b) "Subpopulation triage: How to allocate conservation effort among populations". *Conserv Biol*, 22, 656-665
- Regan H.M., Ben-Haim Y., Langford B., Wilson W.G., Lundberg P., Andelman S.J. & Burgman M.A. (2005) "Robust decision-making under severe uncertainty for conservation management". *Ecol Appl*, 15, 1471-1477
- Tenhumberg B., Tyre A.J., Shea K. & Possingham H.P. (2004) "Linking wild and captive populations to maximize species persistence: optimal translocation strategies". *Conserv Biol*, 18, 1-11

A New Approach of Decision Making Under Uncertainty for Selecting a Robust Strategy: A Case of Water Pipes Failure

Krishna Khatri¹ and Kalanithy Vairavamoorthy²

¹Research Fellow, Department of Urban Water and Sanitation, UNESCO-IHE, Delft; Delft University of Technology; TU Delft, the Netherlands; and University of Birmingham, UK; k.khatri@unesco-ihe.org

²Professor, University of South Florida, School of Global Sustainability, 4202 E. Fowler Avenue, BEH 304, Tampa FL, 33620, USA; vairavk@grad.usf.edu

ABSTRACT

Planning is a crucial part of delivering policies on sustainable development of urban infrastructure systems. However, strategic planning has been plagued due to future uncertainties. This paper presents a new technique based on information gap theory to analyze the failure rate of underground pipes under uncertainty and situations of scarce data. It predicts pipe failure based on a simple regression based model and Monte Carlo simulation technique. Once the failure rate is calculated, it analyses the robustness of failure using an information gap robustness function. The information gap robustness function ensures the robustness of the decision under maximum uncertainty without violating the minimum acceptable failure rate of the pipes. The methodology has been demonstrated on a case of water pipes failure in Birmingham UK. The trade-off between uncertainty and failure rate will be helpful for decision making while preparing a sustainable water pipes rehabilitation plan.

Keywords: Uncertainty; pipe deterioration; failure rate; information gap; robustness; decision making; urban water systems; Monte Carlo simulation.

INTRODUCTION

Urban areas have been served by the urban water systems developed during the last century and expanded with large and complex pipes. While getting older, the systems begin a deterioration process that eventually leads to consecutive pipe failure. An accurate quantitative picture of failure rate will allow utilities to implement efficient proactive pipe failure management strategies thus minimizing the overall operation costs (economic, social and environmental) of urban water systems. For a through analysis of pipe breakage and failure prediction requires detailed information on physical and environmental factors. However, one of the main issues mostly cited in published literature is the lack of data on both the network of water pipes and also pipe breakage history. This is even more critical in cities of the developing countries where little information exists in both. Therefore, the problem of predicting the future failure rate of underground pipes due to the deterioration and ageing process is particularly important within these data scarce situations.

There are many factors that can affect the deterioration and breakage rate of urban water pipes, such as static or dynamic or multiple in nature. The static factors include the pipe characteristics such as pipe material, diameter, wall thickness and backfilled soil. The dynamic factors are age, temperature, soil moisture, soil electrical receptivity, bedding condition, dynamic loading, and operational factors (Kleiner and Rajani, 2001). These multitude of factors quite often exhibit a combined effect, for example, corrosion may have weakened a pipeline and excessive pressure (internal or external) will cause a pipe break (Seica and Packer, 2004). These factors cause water pipes deterioration in two ways. Firstly, the structural deterioration diminishes the water pipes strength to withstand the various types of stress. Secondly, the deterioration of the inner surface of the water pipes due to the internal corrosion. Due to the continuous deterioration process, the water pipes follow the three general phases of failure that can be described by a Bathtub curve. Generally, the first phase appears during the early life of the pipe installation. This is predominantly due to design errors or manufacturing and assembly problems. The second phase is a random failure of relatively constant but at a lower rate that will be observed after all the components are settled. Finally, the third phase usually begins after some years of operation and accumulation of damages. In this phase, the deterioration rate increases exponentially until the pipe fails (see further in Kleiner and Rajani (2002) and Sægrov et al (1999)).

In order to model the pipes failure process, three categories of analysis: physical, descriptive, and predictive are available (Kleiner and Rajani, 2001). The main models that are used to model pipe failure processes are classified as aggregate, regression and probabilistic types. The aggregate models are exponential or linear models of the number of breaks versus the age of pipes. The regression models consider the major factors that influence pipe degradation analysis. The probabilistic models apply the survival analysis. Further description of any particular models, its limitations and application examples can be found elsewhere (Rajani and Makar, 2000; Pelletier et al., 2003; Yan and Vairavamoothy, 2003; Sadiq et al., 2004; Kleiner and Rajani, 2010).

The modeling process for calculating the failure rate of an entire water network is extremely difficult due to the presence of a large number of variables responsible for the water pipe failure. As a city grows and pipe histories change, the set of variables becomes more complex. This is even becomes more challenging in a case of limited data and prevalence of associated uncertainties. This paper presents a new approach to help in a decision making process based on the information gap theory (hereafter, info-gap) (Ben-Haim, 2006). It utilizes a simple regression model proposed by Shamir and Howard (1979) coupled with Monte Carlo random simulation technique to predict the failure rate. It analyses the robustness of pipes failure rate using an info-gap robustness function. The data used for the analysis is based on data from Severn Trent water company, UK. The next section presents the robustness analysis and the info-gap theory.

ROBUSTNESS ANALYSIS AND INFORMATION GAP THEORY

Robust decision methods are appropriate for many problems involving decision making under severe uncertainty. It is a technique for handling uncertainty that influences the future decisions. It seeks robust rather than optimal strategies that perform “well enough” by meeting or exceeding selected criteria across a broad range of plausible futures. There are a variety of techniques for responding the effects of uncertainty into decision making. These include the use of probability theory, possibilities theory, fuzzy set theory, imprecise probabilities, and evidence theory (see Klir and Smith, 2001; Baudrit et al., 2006). A framework for dealing with uncertainty that is more related to urban water systems can be found in Hall and Solomatine (2008).

Despite the multiple techniques available for uncertainty analysis, all of the techniques and combined approaches rely on either multiple data samples or subjectively defined distributions or intervals based on expert belief. An info-gap theory is a new approach for decision making under the sparse information and deep uncertainty (Ben-Haim, 2006). It assists decision making where the gap between what is known and what needs to be known is quite often substantial and where some approaches of modeling may not be possible. Info-gap theory and robustness analysis has been widely applied in many disciplines including water resources planning (Hipel and Ben-Haim, 1999); flood model analysis (Hine and Hall, 2010); life cycle analysis (Duncan et al., 2008); conservation management (Regan et al., 2005); power and sample size calculations (Fox et al., 2007); and structural analysis (Takewaki and Ben-Haim, 2005).

An info-gap robustness analysis requires three main elements: a system model, an info-gap uncertainty model, and a performance measure. The system model describes the structure and behavior of the system. This may be in the form of a set of differential equations, a network model or probabilistic model. The info-gap model of uncertainty consists of a family of nested, convex sets centered on a nominal value. The discrepancy between the available information for the analysis (known as nominal value) and the unknown value formulated by an info-gap model (may be input parameters used for the analysis or a model and its result). The performance requirement is a vector of parameters such as time, design variables, and model parameters that need to be maintained or achieved by the systems.

For example, a pipes failure model developed by Shamir and Haward (1979) is a process model which is given by, $B_t = B_{t_0} e^{\delta(t-t_0)}$ (1)

where, t_0 is the base period of the pipe failure analysis; B_{t_0} is the number of pipes burst/year/km for the i^{th} group of pipes at time t_0 ; δ is the growth rate coefficient (1/year) with the range for the i^{th} group of pipes that vary around 0.05 to 0.15 depending on the pipe materials and diameters (Shamir and Haward, 1979).

The info-gap models are defined based on information about how the bounds, on the uncertain variable grow, even if those bounds are unknown. Info-gap bounds can assume the form of various envelope types, such as uniform bound, energy bound models, envelop bound models, slope bound models, and hybrid type models (see Ben-Haim, 2006). Since the model results from Equation (1) is uncertain due to uncertainty in the growth rate coefficient, which is a simple uniformly bounded info-gap model and is given by,

$$\delta = U(\lambda, \bar{\delta}) = \{\delta : |\delta - \bar{\delta}| \leq \lambda, \lambda \geq 0\} \tag{2}$$

Let the minimum pipe failure rate that has been observed for most of the time in a system represent a performance criteria, B_c . Then the robustness function $\bar{\lambda}(B_c)$ is the immunity against failure, and therefore a large value of $\bar{\lambda}(B_c)$ is desirable. The opportunity function is immunity against sweeping success, so a small value of failure, $\bar{\beta}(B_w)$ is desirable. A robustness function maximizes the size that the uncertainty parameters can take but still satisfy the minimum constraints. This implies that any predicted values larger than those observed will be considered as robust for the future planning time period (t). For the cases where a higher performance value is desirable (i.e., the bigger the better), the robustness and opportunity functions are expressed as:

Robustness: $\bar{\lambda}(B_c) = \max \{ \lambda : \text{minimal requirements are satisfied} \}$ (3)

Opportunity: $\bar{\beta}(B_w) = \min \{ \lambda : \text{sweepings success is obtained} \}$ (4)

$$\bar{\lambda}(t, B_c) = \max \left\{ \lambda : \left(\min_{\delta \in \Delta(\lambda, \bar{\delta})} B_f(t, \delta) \right) \geq B_c \right\} \tag{5}$$

$$\bar{\beta}(t, B_w) = \min \left\{ \lambda : \left(\max_{\delta \in \Delta(\lambda, \bar{\delta})} B_f(t, \delta) \right) \geq B_w \right\} \tag{6}$$

On the other hand, when smaller performance is better, such as cost and environmental impacts, a minimization should be replace with the inner maximization (see Ben-Haim, 2004).

PROBLEM FORMULATION AND APPLICATION

As mentioned, water pipe failure analysis requires a large amount of data on the static, dynamic and operational conditions. In this analysis, we assume a decision problem where the data is limited and as a result the available advanced models can not be applied. In addition, available data is not recorded precisely as such the information about the failure condition of the pipes is uncertain. For this analysis, we utilize a simple regression model as shown in Equation (1) supplemented by Monte Carlo simulation and info-gap robustness analysis. The reasons for selection of Shamir and Howard’s (1979) model are its simplicity and wide application in the field. The algorithm developed for this analysis is given below:

- i) Prepare the pipe failure data for the different groups of pipes (i.e., considering pipe types, diameter, length, and ages) such that Shamir and Howed (1979) Equation (1) can be readily applied.
- ii) Consider Equation (1) as a process model for the info-gap robustness analysis.
- iii) Develop a uniform bound info-gap model (Equation 2) assuming that all the uncertainties are captured by the growth coefficient, such that $(\bar{\delta} - \lambda) \leq \delta \leq (\bar{\delta} + \lambda)$. The approximate likely variation of the value is assumed to be around 0.05 and 0.15, and the variation of λ for the upper level is $(\bar{\delta} + \lambda)$ which starts from $\bar{\delta} = 0.05$ and with an incremental fraction of uncertainty @ 0.01 (i.e., (i.e., $\lambda(1) = 0.01$). The reason for selecting this fraction is considering the available maximum range of $\bar{\delta} = 0.15$.
- iv) Using Equation (1) and considering the range of values for δ , run sufficient numbers of Monte Carlo simulation for the uniform distribution of δ (with minimum and maximum value of δ). The reason for considering a uniform distribution function is the condition of ignorance which depends on the field condition.
- v) Calculate the minimum, median and maximum values of the failures with 99% confidence interval. The minimum failure level for each year will be considered as the critical threshold failure level of the pipes for the info-gap robustness analysis.
- vi) Analyze the info-gap robustness, employing Equation (5) and plot the uncertainties versus pipe failure results.

The pipe failure data used for this analysis are 3" CI pipes of water mains from Staffordshire managed by Severn Trent Water, UK. The data has been analyzed without any further training and testing. Figure (1-a) presents the proportion of different age groups of 3" CI pipes from the total length of 68.35 km that were rehabilitated/installed during the last few decades. Figure (1-b) illustrates the failure rate of the different group of the pipes based on the observed data.

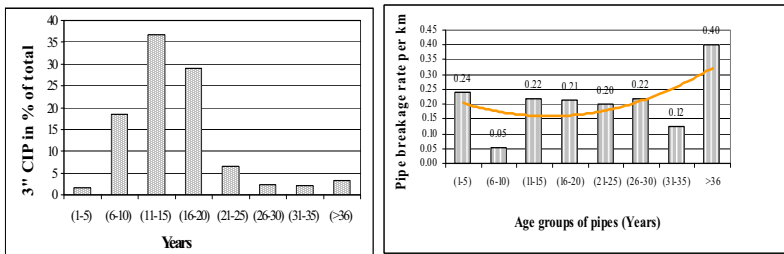


Figure 1 a) Proportion of 3" CI pipes in different age groups; b) observed breakage rate of 3" CI pipes in different age groups

RESULTS AND DISCUSSION

The aforementioned algorithm was applied to analyze the robustness of pipe failure rate prediction (for 3" CI) against the uncertainties. The average failure rate for the first age group (1-5 years) pipes is 0.244 number/km (Figure 1b). This value was considered as the critical threshold, B_c for the analysis. The failure rate for the future, B_t was predicted by Shamir and Howard's (1979) model coupled with Monte Carlo simulation (10000 samples) as shown in Figure 2. The critical failure rate, B_c for the other years (t) has been taken as the lower values of the 99% confidence interval of Monte Carlo simulation results (Table 1). This is considered only for the situation where no failure data is available for the different age group of pipes. However, if pipe failure data is available for different age groups, B_c should be selected after comparing with the field results as in the case of Birmingham (Figure 1b).

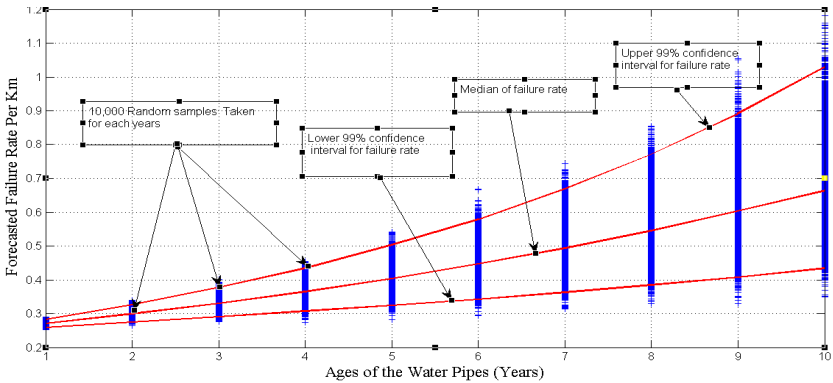


Figure 2. Variation of the pipe breakage rate based on the Sahrir and Howard (1979) Equation (1)

Table 1: Predicted failure rate of pipes after Monte Carlo simulation based on 1 to 5 years failure data

Failure rate prediction with 99% confidence interval for different Years										
Level/Year	2011	2012	2013	2014	2015	2016	2017	2018	2019	2020
Lower	0.258	0.275	0.290	0.307	0.324	0.341	0.362	0.384	0.407	0.434
Median	0.270	0.299	0.330	0.365	0.403	0.446	0.493	0.544	0.603	0.663
Upper	0.282	0.326	0.377	0.434	0.503	0.578	0.670	0.771	0.891	1.029

The trend lines show the future failure rate of the water pipes but the results available are not completely consistent with the actual failure rate. The reason may be due to application of raw data without any training and higher failure rate of the water pipes during the early time of their installation (which is the first phase of a pipe

deterioration based on the Bathtub trends). The next year group pipes (6 to 11 years) was analyzed (taking failure rate of 0.05), the results are more consistent and near to the observation (see Table 2).

Table 2: Predicted failure rate of pipes after Monte Carlo simulation based on 6 to 11 years failure data

	Failure rate prediction with 99% confidence interval for different Years									
Level/Year	2011	2012	2013	2014	2015	2016	2017	2018	2019	2020
Lower	0.084	0.089	0.094	0.100	0.106	0.111	0.118	0.125	0.133	0.141
Median	0.088	0.097	0.107	0.119	0.131	0.145	0.161	0.177	0.197	0.216
Upper	0.092	0.106	0.123	0.141	0.164	0.189	0.218	0.251	0.291	0.336

Figure 3 presents the info-gap based robustness curve derived for the first phase of pipes failure ($B_c = 0.244$) using Equation 5. As mentioned in the algorithm, the lower level of growth rate was considered from, $\bar{\delta} = 0.05$ with a horizon of uncertainty, $(\bar{\delta} + \lambda)$ starting from $\lambda(1) = 0.01$. This is because any failure rate cannot be lower than the lowest limit of calculation without any significant changes in the internal and external condition of pipes. The computed results of the critical failure rate, B_c on the y-axis and the robustness level, $\bar{\lambda}(t, B_c)$ on the x-axis shows on how the failure rate changes with the future time horizon (i.e., 2, 4, 6, 8, 10 year) and with the levels of uncertainty. As a result, the failure rate of the pipe for the year 2 (bottom line) is lower than that for years 4, 6, 8, and 10. The failure rate of the pipes can be selected within the envelope based on the field condition and associated uncertainties.

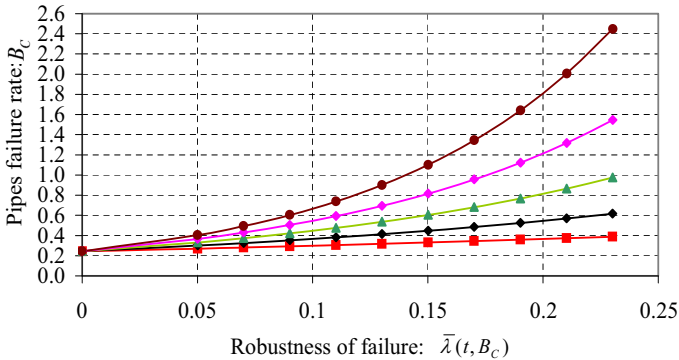


Figure 3. The robustness curve, $\bar{\lambda}(t, B_c)$ vs critical failure rate, B_c for the years 2, 4, 6, 8 & 10 from the bottom to the top respectively. The horizontal axis denotes the maximum uncertainty allowed to guarantee the expected critical failure rate.

The failure rate predicted from the robustness analysis is higher than the actual observation (compared to Figure 1-b). This is reasonable as robustness analysis is based on the higher degree of uncertainty. The results are also consistent when compared with the Monte Carlo simulation (Figure 2). However, this methodology has been developed for data scarce situations. If there is a lesser degree of uncertainty than expected, that will lead to sweeping success as shown in Equation (6) (see Ben-Haim (2006) for the detail analysis). It means, the observed failure rate will be lower than the predicted. Different prior information will be a guide for selecting particular pipe failure rates which is similar to a risk taking and risk aversion situation of decision making.

CONCLUSIONS

We have presented an info-gap theory based approach for decision making while predicting a failure rate water pipes under data scarce situations and/or during associated uncertainties. The info-gap robustness was analyzed using the regression based pipes failure prediction model, a critical threshold level of pipe failure calculated by Monte Carlo simulation, and a uniform bound info-gap uncertainty model. The robustness curve derived from the analysis allows us to analyze the rate of pipe failure in the future at various degrees of uncertainties and various local conditions. The methodology was demonstrated by analyzing a real case of 3" diameter CI pipes of water mains in UK. The preliminary results are consistent with field observation.

Currently, considerable progress has been made towards developing advanced pipe failures prediction models for the sustainable management of urban water systems. Most of them are based on the advanced soft computing and optimization techniques that apply the GIS tool to handle the huge and complex database. However, the real hurdle for their application is the scarcity of the data and associated uncertainties. As a matter of fact, model results may be misleading for real cases. The presented info-gap analysis methodology holds a higher potential for application within urban water systems that consist of multiple sources of uncertainties and the complexities. However, the proposed methodology also need to be further analyzed addressing the multiple sources of uncertainties that exists in a real case. The application of info-gap theory in urban water systems is very limited and requires further research in the future.

ACKNOWLEDGEMENTS

The authors would like to acknowledge the financial support of the Delft Cluster, Delft and the SWITCH project UNESCO-IHE, Delft of the Netherlands for conducting this research.

REFERENCES

- Baudrit, C., Dubois, D. and Guyonnet, D. (2006). Joint propagation and exploitation of probabilistic and possibilistic information in risk assessment. *IEEE Transactions On Fuzzy Systems*, 14(5), pp. 593-608.

- Ben-Haim, Y. (2004). Uncertainty, probability and information-gaps. *Reliability Engineering & System Safety*, 85(1-3), pp. 294-266.
- Ben-Haim, Y. (2006). *Info-gap decision theory, Decisions under severe uncertainty*. Academic Press, Oxford.
- Duncan, S.J., Bras, B. and Paredis, C.J.J. (2008). An approach to robust decision making under severe uncertainty in life cycle design. *Int. J. Sustainable Design*, 1(1), pp. 45-59.
- Fox, D.R., Ben-Haim, Y., Hayes, K.R., McCarthy, M.A., Wintle, B. and Dunstan, P. (2007). An info-gap approach to power and sample size calculations. *Environmetrics* 18(18), pp. 189-203.
- Hall, J. and Solomatine, D. (2008). A framework for uncertainty analysis in flood risk management decisions. *Intl. J. River Basin Management*, 6(2), pp. 85-98.
- Hine, D. and Hall, J.W. (2010). Information gap analysis of flood model uncertainties and regional frequency analysis. *Water Resources Research*, 46, pp. doi:10.1029/2008WR007620.
- Hipel, K.W. and Ben-Haim, Y. (1999). Decision making in an uncertain world: information-gap modeling in water resources management. *IEEE Transactions on Systems, Man, and Cybernetics, Part C: Applications and Reviews*, 29(4), pp. 506-517.
- Kleiner, Y. and Rajani, B. (2001). Comprehensive review of structural deterioration of water mains: statistical models. 3(3), pp. 131-150.
- Kleiner, Y. and Rajani, B. (2002). Forecasting variations and trends in water-main breaks. *Journal of Infrastructure Systems*, 8(4), pp. 122-131.
- Kleiner, Y. and Rajani, B. (2010). I-WARP: Individual water main renewal planner. *Drinking Water Engineering and Science*, 3, pp. 71-77.
- Klir, G.J. and Smith, R.M. (2001). On measuring uncertainty and uncertainty-based information: Recent developments. *Annals of Mathematics and Artificial Intelligence* 32, pp. 5-33.
- Pelletier, G.v., Mailhot, A. and Villeneuve, J.-P. (2003). Modeling water [pipe breaks—three case studies. *Journal of Water Resources Planning and Management*, 129(2), pp. 115-123.
- Rajani, B. and Makar, J. (2000). A methodology to estimate remaining service life of grey cast iron water mains. *Can. J. Civ. Eng.*, 27, pp. 1259-1272.
- Regan, H.M., Ben-Haim, Y., Langford, B., Wilson, W.G., lundberg, P., Andelman, S.J. and Burgman, M.A. (2005). Robust decision-making under severe uncertainty for conservation management. *Ecological Applications*, 15(4), pp. 1471-1477.
- Sadiq, R., Rajani, B. and Kleiner, Y. (2004). Probabilistic risk analysis of corrosion associated failures in cast iron water mains. *Reliability Engineering and System Safety* 86, pp. 1-10.
- Sægrov, S., Baptista, J.F.M., Conroy, P., Herz, R.K., LeGau re, P., Moss, G., Oddevald, J.E., Rajani, B. and Schiatti, M. (1999). Rehabilitation of water networks survey of research needs and on-going efforts. *Urban Water*, 1, pp. 15-22.

- Seica, M.V. and Packer, J.A. (2004). Mechanical properties and strength of aged cast iron water pipes. *Journal of Materials in Civil Engineering*, 16(1), pp. 69-77.
- Shamir, U. and Howard, C.D.D. (1979). An analytic approach to scheduling pipe replacement. *Journal of AWWA*, 71(5), pp. 248-258.
- Takewaki, I. and Ben-Haim, Y. (2005). Info-gap robust design with load and model uncertainties. *Journal of Sound and Vibration* 288, pp. 551-570.
- Yan, J.M. and Vairavamoorthy, K. (2003). Fuzzy approach for the pipe condition assessment, New Pipeline Technologies, Security, and Safety, *Proc. of Proceeding of ASCE international conference on pipeline engineering and construction*, Baltimore, Maryland, USA, American Society of Civil Engineers pp. 1817.

Robust Satisficing and the Probability of Survival

Yakov Ben-Haim

Yitzhak Moda'i Chair in Technology and Economics, Faculty of Mechanical Engineering, Technion—Israel Institute of Technology, Haifa 32000 Israel, +972-4-829-3262, yakov@technion.ac.il

ABSTRACT

Concepts of robustness are often employed when decisions under uncertainty are made without probabilistic information. We present a theorem which establishes necessary and sufficient conditions for non-probabilistic robustness to be equivalent to probability of success. When this “proxy property” holds, probability of success is enhanced (or maximized) by enhancing (or maximizing) robustness. Applications to investment in risky assets and forecasting are discussed.

INTRODUCTION

Robustness to severe uncertainty is often evaluated without probabilistic models, for instance when uncertainty is specified by a set of possibilities with no measure function on that set. When is a robust decision likely to succeed? What can we say about the probability of success of a decision when we have no probabilistic information about the uncertainties? If robustness is used as a criterion to select a decision, when is this criterion equivalent to selection according to the probability of successful outcome? In short, when is (non-probabilistic) robustness a good (probabilistic) bet?

We present a proposition, based on info-gap decision theory, which identifies conditions in which the probability of success is maximized by an agent who robustly satisfices the outcome without using probabilistic information. We show that this strategy may differ from the outcome-optimizing strategy indicated by the best available data and models. We refer to this as a “proxy theorem” since it establishes conditions in which robustness is a proxy for probability. An info-gap robust-satisficing strategy attempts to attain an adequate or necessary (but not necessarily extremal) outcome while maximizing the agent’s immunity to deficient information. The robust-satisficing approach requires no knowledge of probability distributions. This proposition provides insight into the prevalence of decision-making behavior which is inconsistent with outcome-optimization based on the best-available (but faulty) models and data. Best-model strategies are vulnerable to error, and other—robust-satisficing—strategies will be shown to have higher probability for survival by the agent in commonly occurring situations. We will consider examples of risky investment and of forecasting.

PRELIMINARY DISCUSSION of the PROXY THEOREM

Before embarking on the technical details, we describe the essence of the proxy theorem and its significance.

The agent chooses an action r which results in outcome $G(r, q)$ where q is an uncertain parameter, vector, function or a set of such entities. The discussion in this section assumes that $G(r, q)$ is a loss, but, with minor modifications, it applies to rewards as well. We will refer to $G(r, q)$ as the ‘performance function’. For instance, q might be an uncertain estimate of a critical parameter such as a rate of return, or q could be a vector of uncertain returns, or q could be a probability density function (pdf) for uncertain returns, or q could be a set of such pdf’s, or q could be uncertain constitutive relations such as supply and demand curves.

The agent’s knowledge and beliefs about q are represented by a family of sets, $\mathcal{Q}(h)$, called an info-gap model of uncertainty, where h is a non-negative real number. $\mathcal{Q}(h)$ is a set of values of q , so if q is a vector, function, or set, then $\mathcal{Q}(h)$ is a set of vectors, functions or sets. As h increases, the range of possibilities grows, so $h' < h$ implies $\mathcal{Q}(h') \subseteq \mathcal{Q}(h)$. This is the property of *nesting*, and it endows h with its meaning as an *horizon of uncertainty*. All info-gap models have the property of nesting. Sometimes the agent may have a specific estimate of q , denoted \tilde{q} . In this case, in the absence of uncertainty (that is, $h = 0$), \tilde{q} is the only possibility so $\mathcal{Q}(0) = \{\tilde{q}\}$. This is the property of *contraction*, which is common among info-gap models (Ben-Haim, 2006), though our proxy theorem does not depend on the contraction property. An info-gap model is a quantification of Knightian uncertainty (Knight, 1921; Ben-Haim, 2006, sections 11.5.6 and 13.5).

The agent “survives” if the loss does not exceed a critical value G_c . The robustness of action r is the greatest horizon of uncertainty, h , up to which $G(r, q) \leq G_c$ for all $q \in \mathcal{Q}(h, \tilde{q})$. Denote the robustness by $\hat{h}(r, G_c)$. More robustness is preferable to less robustness, so the robustness generates a preference ranking of the actions (denoted \succ_r), namely, $r \succ_r r'$ if $\hat{h}(r, G_c) > \hat{h}(r', G_c)$.

Now consider the probability of survival for decision r , namely, the probability that q will take a value so that $G(r, q) \leq G_c$. Let $p(q|r)$ denote the pdf for q , noting that it may depend on the decision r . We do not know this pdf, and q itself may be a probability density or a set of functions, so $p(q|r)$ could be quite complicated. Nonetheless, we can define the probability of survival as $P_s(r, G_c) \equiv \text{Prob}[G(r, q) \leq G_c]$. We cannot evaluate $P_s(r, G_c)$ because the pdf $p(q|r)$ is unknown, but if we did know it, then it would generate preferences \succ_p over decisions, defined as $r \succ_p r'$ if $P_s(r, G_c) > P_s(r', G_c)$.

A proxy theorem establishes conditions in which \succ_r and \succ_p are equivalent.

INFO-GAP ROBUST-SATISFICING: A PRÉCIS

This paper employs info-gap decision theory (Ben-Haim, 2006), which has been applied in a large array of decision problems under severe uncertainty in engineering (Ben-Haim, 2005), biological conservation (Burgman, 2005), economics (Ben-Haim, 2010) and other areas (see <http://info-gap.com>).

The agent must make a decision by choosing a value for r , which may be a scalar, vector, function, or linguistic variable such as “go” or “no-go”. The outcome of the decision is expressed as a loss (or reward), quantified by a scalar performance function $G(r, q)$, which depends on the decision r and on an uncertain quantity q . q is an uncertain parameter, vector, function, or a set of such entities. The uncertainty in q is represented by an info-gap model, whose two properties—contraction and nesting—were defined earlier. The info-gap model may depend on the decision.

We now define the robustness function:

$$\hat{h}(r, G_c) \equiv \max \left\{ h : \left(\max_{q \in \mathcal{Q}_r(h)} G(r, q) \right) \leq G_c \right\} \tag{1}$$

We define $\hat{h}(r, G_c) \equiv 0$ if the set of h 's in eq.(1) is empty. We can “read” this equation from left to right as follows. The robustness, \hat{h} , of decision r with aspiration for loss no greater than G_c , is the maximal horizon of uncertainty h up to which all realizations of $q \in \mathcal{Q}(h)$ result in loss $G(r, q)$ no greater than G_c .

A critical question is: when does the robust preference ranking, \succ_r , agree with the probability of survival preference rank, \succ_p ?

If \succ_r and \succ_p agree then robustness is a proxy for the probability of survival. By choosing r to enlarge or maximize robustness we would also enlarge or maximize the probability of survival. We are not able to *evaluate* the probability of survival, but we would be able to *enlarge* or *maximize* it.

We first define a concept of coherence, we then present a proxy theorem, and conclude with two examples.

COHERENCE: DEFINITION

We are considering performance functions $G(r, q)$ which are scalar and depend on the decision r and on q which is an uncertain parameter, vector, function or set. Without loss of generality we may consider $G(r, q)$ itself to be the uncertain entity, whose info-gap model is generated by the info-gap model for a more complex underlying uncertainty q . It is, however, more convenient to retain the distinction between $G(r, q)$ (the performance function) and q (the uncertainty) and to assume that $G(r, q)$ is monotonic in q which is a scalar. This includes the case that q is itself the performance function which depends on more complex underlying uncertainties.

In summary, q is an uncertain scalar variable (which may depend on more complex underlying uncertainties), r is a decision variable, and $G(r, q)$ is a scalar performance function. An info-gap model for uncertainty in q is $\mathcal{Q}_r(h)$, which may depend on the decision, r . The corresponding robustness function, eq.(1), is $\hat{h}(r, G_c)$. The cumulative probability distribution (cpd) of q is $P(q|r)$.

For any $h \geq 0$, define $q^*(h, r)$ and $q_*(h, r)$, respectively, as the least upper bound and greatest lower bound of q -values in the set $\mathcal{Q}_r(h)$. Define $\mu(h)$ as the

inner maximum in the definition of the robustness in eq.(1):

$$q^*(h, r) \equiv \max_{q \in \mathcal{Q}_r(h)} q, \quad q_*(h, r) \equiv \min_{q \in \mathcal{Q}_r(h)} q, \quad \mu(h) \equiv \max_{q \in \mathcal{Q}_r(h)} G(r, q) \tag{2}$$

We will consider performance functions $G(r, q)$ which are monotonic (though not necessarily strictly monotonic) in q at fixed r . We define the inverse of such functions, at fixed r , as follows. If $G(r, q)$ *increases* as q increases then its inverse is defined as:

$$G^{-1}(r, G_c) \equiv \max \{q : G(r, q) \leq G_c\} \tag{3}$$

If $G(r, q)$ *decreases* as q increases then its inverse is defined as:

$$G^{-1}(r, G_c) \equiv \min \{q : G(r, q) \leq G_c\} \tag{4}$$

$G(r, q)$ is assumed to be monotonic but we do not assume that $G(r, q)$ is continuous in q , which is why we need the inequalities rather than equality.

Definition 1 . $\mathcal{Q}_r(h)$ and $P(q|r)$ are **upper coherent** at decisions r_1 and r_2 and critical value G_c , with performance function $G(r, q)$, if the following two relations hold for $i = 1$ or $i = 2$, and $j = 3 - i$:

$$P[G^{-1}(r_i, G_c)|r_i] > P[G^{-1}(r_j, G_c)|r_j] \tag{5}$$

$$G^{-1}(r_i, G_c) - q^*(h, r_i) > G^{-1}(r_j, G_c) - q^*(h, r_j) \tag{6}$$

for $h = \hat{h}(r_j, G_c)$ and $h = \hat{h}(r_i, G_c)$

$\mathcal{Q}_r(h)$ and $P(q|r)$ are **lower coherent** if eqs.(5) and (6) hold when $q^*(h, r)$ is replaced by $q_*(h, r)$.

Roughly speaking, coherence implies some “information overlap” between the info-gap model, $\mathcal{Q}_r(h)$, and the probability distribution, $P(q|r)$. Eq.(5) depends on $P(q|r)$ but not on h or $\mathcal{Q}_r(h)$, while eq.(6) depends on h and $\mathcal{Q}_r(h)$ but not on $P(q|r)$. Both relations depend on G_c, r_i, r_j and the performance function $G(r, q)$. $\mathcal{Q}_r(h)$ and $P(q|r)$ are coherent if each of these relations holds. Coherence does not imply that either function, $\mathcal{Q}_r(h)$ or $P(q|r)$, can be deduced from the other. Coherence does imply that knowledge of one function reveals something about the other.

If the cpd $P(q|r)$ does not depend on r then eq.(5) is equivalent to:

$$G^{-1}(r_i, G_c) > G^{-1}(r_j, G_c) \tag{7}$$

Likewise, if the info-gap model $\mathcal{Q}_r(h)$ does not depend on r then $q^*(h, r)$ and $q_*(h, r)$ also do not depend on r and eq.(6) is identical to eq.(7). In other words $P(q|r)$ and $\mathcal{Q}_r(h)$ are always upper and lower coherent if neither of them depends on the decision, r .

Upper coherence becomes interesting if the uncertainty models, $P(q|r)$ and $\mathcal{Q}_r(h)$, *do* depend on the decision. Now eq.(5) does not imply eq.(7) because the

cpd may change as r changes. However, if the info-gap model is coherent with the probability distribution then $q^*(h, r)$ “compensates” for the change in the cpd and eq.(6) is the resulting “correction” of eq.(7).

Proposition 1, to be presented shortly, asserts, roughly, that coherence is necessary and sufficient for the proxy property to hold. But how does an agent choose a coherent info-gap model without knowing the pdf? The answer derives from the adaptive survival implications of the proxy property. An agent who chooses an info-gap model which is coherent with the pdf has a survival advantage over an agent who chooses a non-coherent info-gap model because of the proxy property. This is true even if the agent was unaware of the coherence when choosing. The learning or adaptation which takes place—even if it is non-volitional as in animals—leads to the identification of coherent info-gap models.

PROXY THEOREM: MONOTONICITY and COHERENCE

Definition 2 $Q_r(h)$ and $P(q|r)$ have the **proxy property** at decisions r_1 and r_2 and critical value G_c , with performance function $G(r, q)$, when:

$$\hat{h}(r_1, G_c) > \hat{h}(r_2, G_c) \quad \text{if and only if} \quad P_s(r_1, G_c) > P_s(r_2, G_c) \quad (8)$$

The proxy property is symmetric between robustness and probability of success. However, we are particularly interested in the implication from robustness to probability. Thus, when the proxy property holds we will sometimes say that robustness is a proxy for probability of success.

Nesting of the sets $Q_r(h)$ implies that $q^*(h, r)$ and $q_*(h, r)$, defined in eq.(2), are monotonic increasing and decreasing functions, respectively. They are continuous if the following additional properties hold.

Definition 3 An info-gap model, $Q_r(h)$, **expands upward continuously** at h if, for any $\varepsilon > 0$, there is a $\delta > 0$ such that:

$$|q^*(h', r) - q^*(h, r)| < \varepsilon \quad \text{if} \quad |h' - h| < \delta \quad (9)$$

Continuous downward expansion is defined similarly with $q_*(\cdot)$ instead of $q^*(\cdot)$.

We now state a proposition whose proof is not presented due to lack of space.

Proposition 1 Info-gap robustness to an uncertain scalar variable, with a loss function which is monotonic in the uncertain variable, is a proxy for probability of survival if and only if the info-gap model $Q_r(h)$ and the probability distribution $P(q|r)$ are coherent.

Given:

- At any fixed decision r , the performance function, $G(r, q)$, is monotonic (though not necessarily strictly monotonic) in the scalar q .

- $\mathcal{Q}_r(h)$ is an info-gap model with the property of nesting.
- r_1 and r_2 are decisions with positive, finite robustnesses at critical value G_c .
- $\mathcal{Q}_r(h)$ is continuously upward (downward) expanding at $\hat{h}(r_1, G_c)$ and at $\hat{h}(r_2, G_c)$ if $G(r, q)$ increases (decreases) with increasing q .

Then: The **proxy property** holds for $\mathcal{Q}_r(h)$ and $P(q|r)$ at r_1, r_2 and G_c with performance function $G(r, q)$.

If and only if: $\mathcal{Q}_r(h)$ and $P(q|r)$ are **upper (lower) coherent** at r_1, r_2 and G_c with performance function $G(r, q)$ which increases (decreases) in q .

This proposition establishes that coherence is both necessary and sufficient (together with some other conditions) for the proxy property to hold.

EXAMPLE: RISKY ASSETS

Formulation. Consider N risky assets in a 2-period investment.

The investor purchases amount r_i of asset i in the first period, at price p_i ; no purchases are made in the second period. In the second period, the payoff of asset i is $q_i = p_i + d_i$ where d_i is the uncertain dividend. The initial wealth is w and the consumptions in the two periods, c_1 and c_2 , are:

$$c_1 = w - p^T r, \quad c_2 = q^T r \tag{10}$$

where superscript T implies matrix transposition.

The utility from consumption c_j is $u(c_j)$ which we assume to be strictly increasing in c_j : positive marginal utility. The discounted utility for the two periods is $u(c_1) + \beta u(c_2)$ where β is a positive discount factor. This is the “natural” reward function for this problem, but it is not consistent with our formal definitions and results which assume the performance function is a loss. We define the performance function as:

$$G(r, q) = -u(c_1) - \beta u(c_2) \tag{11}$$

Uncertainty and Robustness. The uncertainty derives from the unknown payoff vector of the risky assets in the 2nd period, q . We do not know a probability distribution for q and we cannot reliably evaluate moments. There are many types of info-gap models which could be used (Ben-Haim, 2006). We will consider a specific example subsequently.

Now note from eqs.(10)–(11) that the performance function, $G(r, q)$, depends on the uncertain payoffs only through the consumption in the second period, c_2 , which is a scalar uncertainty. To emphasize that the performance function depends on the uncertain payoff vector only through c_2 we write $G(r, c_2)$. Thus c_2 is the scalar uncertainty required by the proxy theorem, and that c_2 derives from an uncertain vector, q . In this way the N -dimensional uncertain vector, q , is “aggregated” into a single scalar uncertainty, c_2 . Note that $G(r, c_2)$ decreases monotonically in the scalar uncertainty c_2 , thus satisfying the monotonicity requirement of proposition 1.

Whatever info-gap model is adopted for q , denoted $\mathcal{Q}(h)$, an info-gap model for c_2 is:

$$\mathcal{C}_r(h) = \{c_2 : c_2 = r^T q, q \in \mathcal{Q}(h)\}, \quad h \geq 0 \quad (12)$$

The investor prefers less negative utility $G(r, c_2)$ rather than more, and G_c is the greatest value of discounted 2-period negative utility which is acceptable. If G_c cannot be attained (or reasonably anticipated) then the investment is rejected. G_c is a “reservation price” on the negative utility.

For given investments r , the robustness to uncertainty in the consumption in the second period, c_2 , is the greatest horizon of uncertainty h up to which all realizations of c_2 result in discounted negative utility no more than G_c . More robustness is preferable to less, at the same level G_c at which the negative utility is satisfied.

The conditions of proposition 1 hold if the info-gap model, $\mathcal{C}_r(h)$, and the pdf of c_2 are coherent. When coherence holds, any change in the investment, r , which augments the robustness also augments (or at least does not reduce) the probability that the performance requirement, $G \leq G_c$, will be satisfied. The probability of success can be maximized by maximizing the robustness, without knowing the probability distribution of the vector of returns on the risky asset.

Because of the proxy property, coherence of an agent’s info-gap model is a re-enforcing attribute: the survival value is greater for coherent than for non-coherent models. This suggests the possibility of an evolutionary process by which coherent info-gap models are selected (though the agent may be unaware of this selection process). This process works because very simple info-gap models can be coherent with the corresponding pdf even though their information-content is much less than the pdf itself. For example, Gigerenzer and Selten (2001) have demonstrated the efficacy of simple, satisficing heuristics in human and animal decision making.

ONE-SIDED FORECASTING

In this example we consider one-sided forecasting, in which forecast error in one direction (either under- or over-estimate) must not be too large. See also Ben-Haim (2009). Here are some examples. (1) You must catch a plane at the airport on the other side of the metropolis. Being too early is inconvenient but being late is terrible. How long will it take to get to the airport? (2) You must allocate funding for a new project. Under-allocation might mean some problems later on, but over-allocation means other important projects will not be funded at all. How much is needed for the project? (3) You must estimate enemy fire-power and under-estimation can have severe consequences for your forces in the field. (4) Major fiscal programs will increase the rate of inflation unless monetary counter measures are implemented. It is necessary to forecast the amount by which inflation could rise. One-sided objectives like these are quite common and can reflect contextual understanding of the dominant type of failure. They can also arise due to asymmetric utility.

A forecaster's prediction of the scalar quantity of interest is r , while the true future value, q , is unknown. That is, r is a forecast model developed by the analyst while q is reality. Thus r is the decision and q is the uncertainty. The performance function is the error, $G(r, q) = r - q$. If over-prediction must be no larger than G_c then the performance requirement is: $G(r, q) \leq G_c$, where G_c will usually be positive.

One can show that the coherence and monotonicity assumptions of proposition 1 always hold. Thus the robustness is a proxy for success in the one-sided forecast requirement. Any change in the forecasting model, r , which enhances the robustness also increases the probability of one-sided forecast success. The forecasting model may be very different from a statistically estimated or scientifically realistic model. Nonetheless, if r 's robustness exceeds the robustness of the statistically estimated model (due to crossing of their robustness curves) then r has higher probability of successful one-sided forecasting. Since "success" means "acceptable one-sided error", a model whose robustness at acceptable forecast error is large (or maximal) will be preferred, even if that model is "sub-optimal" as a representation of reality.

SUMMARY

This paper presents an approach to economic rationality, linking Knightian uncertainty, robustness and satisficing behavior in a coherent quantitative theory. The paper identifies general conditions for the competitive advantage of robust-satisficing, facilitating an understanding of satisficing behavior under uncertain competition.

REFERENCES

- Ben-Haim, Y., 2005. Info-gap Decision Theory For Engineering Design. Or: Why 'Good' is Preferable to 'Best', chapter 11 in *Engineering Design Reliability Handbook*, E. Nikolaidis, D. Ghiocel and Surendra Singhal, eds., CRC Press.
- Ben-Haim, Y., 2006. *Info-Gap Decision Theory: Decisions Under Severe Uncertainty*, 2nd edition, Academic Press, London.
- Ben-Haim, Y., 2009. Info-gap forecasting and the advantage of sub-optimal models, *European Journal of Operational Research*, 197: 203–213.
- Ben-Haim, Y., 2010. *Info-Gap Economics: An Operational Introduction*, Palgrave.
- Burgman, M., 2005. *Risks and Decisions for Conservation and Environmental Management*, Cambridge University Press, Cambridge.
- Gigerenzer, G., Selten, R., eds., 2001. *Bounded Rationality: The Adaptive Toolbox*, MIT Press.
- Knight, F.H., 1921. *Risk, Uncertainty and Profit*, Hart, Schaffner and Marx. Re-issued by Harper Torchbooks, New York, 1965.

An Info-Gap Model to Examine the Robustness of Cost-Efficient Budget Allocations

Vanessa M Adams¹ and Robert L Pressey¹

1. Australian Research Council Centre of Excellence for Coral Reef Studies, James Cook University, Townsville, QLD 4811, Australia; PH +61 7 4781 4000; FAX +61 7 4781 6722; email: vanessa.adams@jcu.edu.au (VM Adams) and bob.pressey@jcu.edu.au (RL Pressey)

ABSTRACT

Benefit cost ratios (BCR) have been applied to conservation decisions for two reasons: cost-efficiency and transparency in decision making. Because BCRs are ratios of benefits to costs, the uncertainties associated with the two components (benefits and costs) are compounded. Therefore, BCRs can potentially involve more uncertainty than allocation strategies based solely on maximizing benefits. The robustness of decisions, defined here as the inverse of the number of misallocations due to uncertainties in benefits and costs of projects, is an unexplored component of applying BCRs to conservation decision making. To investigate the robustness to uncertainty of conservation investment with BCRs, we developed an information-gap model (info-gap) for using BCRs in selecting “portfolios” of conservation projects. Our model allows us to explore how uncertain we can be in our estimates of benefit and cost parameters while still selecting a portfolio that performs better than a critical threshold of misallocations perceived to be unacceptable. We first give a full theoretical description of our info-gap model formulation and then explore applications of the model to several hypothetical data sets.

INTRODUCTION

The simultaneous consideration of costs and benefits has resulted in substantial gains for the allocation of conservation budgets (Ando et al. 1998; Ferraro 2003). Benefit-cost ratios (BCRs) have been utilized to allocate conservation budgets more transparently and cost-efficiently (Bottrill et al. 2008; Fuller et al. 2010). However, if estimates of the benefits and costs of conservation actions are highly uncertain, then the selection of conservation projects for funding could result in neglecting projects that should receive immediate funding while investing in projects that would not have been selected given better data. Because BCRs are a ratio of benefits to costs, the uncertainties associated with the two components (benefits and costs) are compounded and therefore BCRs can potentially be more uncertain than allocation strategies based solely on maximising benefits.

If decision makers are using BCRs to be more transparent in their decisions, then it is important to also be transparent about the uncertainties associated with those decisions and the potential to misallocate scarce funds. When allocating scarce resources, managers accept the need for cost-efficiency to maximize the return for a specific financial budget; but they might also want to ensure that their decisions are

robust by minimizing the misallocation of investment at any level of uncertainty in estimates of key parameters. An important unanswered question is therefore: how do we account for uncertainties in a decision making process that relies on both costs and benefits?

To explore the robustness of cost-efficient budget allocations we develop an information-gap model (info-gap) for use of BCRs in selecting conservation “portfolios”, or sets of conservation projects. We define conservation projects to be discrete conservation investments under consideration by an agency. Examples are sets of threatened species requiring management or land parcels under consideration for protection. Info-gap is a decision-theory framework that evaluates how robust each decision is by testing how far a parameter or function can deviate from the estimated value while still giving an acceptable outcome (Ben-Haim 2006).

A unique feature of info-gap theory is that the horizon of uncertainty is unbounded and unknown, and the approach can therefore be applied when probabilistic models of uncertainty are either unavailable or unreliable. Thus, for BCRs as a decision making tool, we assume that managers will often not be able to develop reliable probabilistic models of estimated benefits and costs of conservation actions. We develop an info-gap model that allows us to explore how uncertain we can be in our estimates of benefits and costs while still selecting a conservation portfolio that performs better than a critical threshold of misallocations perceived to be unacceptable. Our model and analyses are meant to be general and descriptive rather than prescriptive. While our application of the info-gap model is focused on conservation budget allocations, the steps that we implement can be applied to any decision making process. Because correlations of benefits and costs are important in determining the advantages of considering costs (Babcock et al. 1997), we apply our model to two types of data - correlated and uncorrelated - to provide general rules of thumb for managers.

METHODS

Info-gap model for parameter uncertainty in conservation decision making

Info-gap theory has three model requirements: a process model to measure performance, an uncertainty model, and a performance requirement (Ben-Haim 2006). The uncertainty model is a mathematical equation describing the error involved in our best estimates of the data. The performance requirement is the critical threshold at which our decisions must perform.

For our process model, we will consider allocation over a set S of i conservation projects for $i=1\dots N$. Each conservation project, s_i , has an associated benefit b_i and associated cost c_i . We will discuss different conservation projects and their associated benefits and costs in more depth in the case studies. For now, we assume a generic conservation project with benefit b_i constrained between 0 and 1. We define c_i to be the cost of the conservation project and we represent this as a fraction between 0 and 1 of units in dollars, for example in millions.

We select a set of conservation projects using a cost-efficient allocation by including a project in our set $S(\tilde{\gamma}, \theta) = \{s : \gamma_i \geq \theta\}$ where $\gamma_i = \frac{b_i}{c_i}$ and we chose θ such that any project with a BCR which is greater than or equal to θ is selected and any project with a BCR less than θ is excluded from our conservation portfolio. We consider only complete inclusion or exclusion of conservation projects, s_i , in the set. Thus, conservation projects are fully funded in our portfolio, and there are no partial benefits or costs associated with partial selection of projects. It is worth noting that, in the conventional application of BCRs, the critical value for accepting or rejecting a project would be θ equal to one, indicating that the benefits are equal to or greater than the costs. However, in the application of BCRs to conservation budget allocations, θ is budget-driven and derived by ranking projects based on BCRs from highest to lowest and selecting projects until the budget is exhausted.

We use the fractional-error info-gap model (Regan et al. 2005; Ben-Haim 2006) to describe the error of our best estimates of b_i and c_i , \tilde{b}_i and \tilde{c}_i :

$$U(\alpha, \tilde{b}, \tilde{c}) = \left\{ \begin{array}{l} b : \left| \frac{b_i - \tilde{b}_i}{\tilde{b}_i} \right| \leq \alpha \\ c : \left| \frac{c_i - \tilde{c}_i}{\tilde{c}_i} \right| \leq \alpha \end{array} \right\}, \alpha > 0$$

where α is the ‘‘horizon of uncertainty’’ and is unbounded and unknown (Ben-Haim 2006). The greater our uncertainty, the higher the value of α . In this case α is the same for both b and c .

To measure the performance of our process model we define the set of $D(\gamma)$ to be the number of conservation projects that are excluded or included in error. To define $D(\gamma)$, we first consider the union of the sets of projects selected assuming our best estimates of b_i and c_i , $S(\tilde{\gamma})$, and the set of projects assuming complete knowledge of b_i and c_i , $S(\gamma)$. The union is the set of all projects selected regardless of uncertainty. We then consider the intersection between the two sets. The intersection gives us the set of projects that is included both with and without uncertainty. If we then remove the intersection from the union, we are left with only those projects that were included or excluded in error. So, for a given θ , $D(\gamma) = [S(\gamma) \cup S(\tilde{\gamma})] - [S(\gamma) \cap S(\tilde{\gamma})]$. We would like the value of $D(\gamma)$ to be as small as possible, but we select a critical value D_c as the acceptable performance threshold. Values of $D(\gamma)$ larger than this critical value are unacceptable.

The robustness function for our set $S(\gamma)$ is given by:

$$\hat{\alpha}(\theta, D_c) = \max \left\{ \alpha : \left(\max_{b, c \in U(\alpha)} D(\gamma, \theta) \right) \leq D_c \right\}.$$

Thus, the equation addresses the question of how wrong, or uncertain, we can be in our estimates of b and c while still achieving an acceptable outcome, or minimizing

the number of misallocations. The system of equations can be solved to explore the robustness of conservation budget allocations for a combination of values of the variables θ and D_c .

Data

We consider two categories of data, uncorrelated and correlated, to demonstrate the issues associated with different types of data. For each category of data we draw upon an example from the literature in which BCRs have been used for budget allocations. First we consider the example of allocating a budget to a set of conservation projects where each project is the discrete management of a threatened species (Bottrill et al. 2008; Joseph et al. 2009). For each species, s_i , a common definition of the benefit b_i is $b_i = t_i * p_i$ where t_i is the probability of threat for conservation feature i and p_i is the probability of success, or the likelihood of the project neutralizing the threat (Bottrill et al. 2008; Joseph et al. 2009). We define c_i to be the cost of a conservation project for species i and we represent this as a fraction between 0 and 1 of units in millions. Management of different species can have variable costs and probability of success which could result in uncorrelated benefits and costs of projects. To reflect this, for 50 hypothetical threatened species projects, we draw values of the associated benefit b_i and associated cost c_i from the normal distribution with no correlation (Figure 1A).

Second, we consider the example of selecting land parcels for protection. One recent definition of the benefit b_i for each land parcel, s_i , is $b_i = \sum_{j=1}^m a_{ji} / r_j$ where m is the number of vegetation types, a_{ji} is the area of vegetation type j in parcel i and r_j is the proportion of vegetation type j remaining since clearing has occurred (Fuller et al. 2010). The cost of a parcel can be based on different components of conservation costs such as acquisition to protect the parcel or management to maintain its conservation values. Several studies have found that areas of high conservation value, such as species-rich sites or rare vegetation types, are more costly to acquire (Ando et al. 1998; Ferraro 2003; Adams et al. 2010), leading to positively correlated benefits and costs. Although we are not aware of studies that have demonstrated negatively correlated benefits and costs, we propose this situation here for illustrative purposes: pristine areas with high conservation value tend to have low management costs while areas that are moderately degraded have lower conservation value but require more expensive management for invasive species or disturbances such as fire. Therefore, we consider positively correlated data drawn from the normal distribution (correlation coefficient of 0.5) to represent the case where acquisition costs are considered (Figure 1B) and negatively correlated data drawn from the normal distribution (correlation coefficient of -0.5) to represent the case where management costs are considered (Figure 1C).

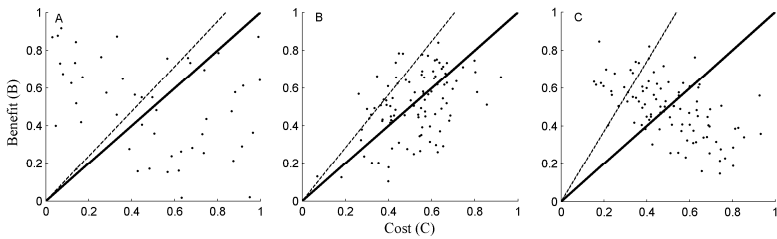


Figure 1. Plots of projects considered for conservation funding. Projects are plotted based on their associated benefits and costs. The $\theta=1$ line, representing benefits equal to costs and used conventionally in complete accounting of benefits and costs, is drawn for reference (solid line). In a budget-driven selection process, typical of the hypothetical case studies presented here, θ is defined by the budget and all points above the corresponding budget-driven θ reference line (associated with \$5,000,000 budget, also shown in each graph as a dashed line) are selected for funding. A) Benefits and costs associated with discrete management actions for 50 species are drawn from the normal distribution with a correlation coefficient of 0. B) Benefits and costs of acquisition of 100 land parcels for protection are drawn from the normal distribution and have a correlation coefficient of 0.5. C) Benefits and costs of management of 100 land parcels are drawn from the normal distribution and have a correlation coefficient of - 0.5.

Model analysis

For all three data sets we plot the conservation projects' benefits against costs and consider this to be the decision state-space (Figure 1). Before formal analysis, visual inspection of the decision state-space can provide important information about the sensitivity of funding decisions to particular values of θ . We can examine natural clustering of the data around various values of θ , plotted as lines with slope equal to θ (Figure 1). Based on the structure of our info-gap model, robustness is a measure of the number of points within a particular envelope around the selected θ line. Those points closest to the θ line are most likely to result in misallocations either from mis-inclusion (moving below the θ line when we consider the true values of \tilde{b}_i and \tilde{c}_i as compared to our best estimates b_i and c_i) or mis-exclusion (moving above the θ line). In our examples each θ also has an associated budget so it is important to realize that selecting a lower θ will allow a manager to engage in more conservation projects but will also require a higher budget.

We assume a fixed budget of \$5,000,000, set θ accordingly, and select our portfolio $S(\gamma, \theta)$ for each of the three data sets. We use the term "budget-driven θ " for the θ value based on the budget of \$5,000,000 to indicate the situation in which a department is given a non-negotiable budget to allocate to projects. The actual value of θ is given as a slope in the analysis. We explore the sensitivity of funding decisions to our budget-driven θ by looking at two other values of θ (± 0.5). A higher value of θ ($\theta + 0.5$) represents a smaller budget which will therefore select fewer conservation projects. As stated above, robustness is a measure of the number of

points within a particular envelope of the selected θ threshold line. In the case of lower budgets, and therefore higher values of θ , the θ threshold line will be steeper and therefore will have fewer points above it. This means that there is a smaller set of potential mis-inclusions (points just above the threshold line). However the converse of this is that more projects might be inadvertently excluded (potential mis-exclusions are just below the threshold line). Similarly, a lower value of θ ($\theta - 0.5$) will be associated with a larger budget and will have a smaller set of potential mis-exclusions, but could lead to more projects being inadvertently included.

We solve the system of equations for $\hat{\alpha}(\theta, D_c)$ and plot $\hat{\alpha}(\theta, D_c)$ against D_c , which is considered the robustness curve associated with a selected value of θ . For a selected value of D_c the robustness of a selected value of θ is given by the x -value, or conversely we can interpret robustness as the y -value (D_c) for a selected value of α . Therefore, for different values of θ the curve that is furthest to the right represents the most robust selection. If robustness curves cross it indicates that, for a given critical value D_c , if the manager wishes to select the most robust strategy, then their selection of θ would change. Thus, whether θ is selected a priori or based on a budget, if the critical value D_c selected is near a cross in robustness curves, then selection of θ should be considered carefully.

RESULTS

For the uncorrelated data (Figure 2), the largest value of θ (1.692, corresponding to the smallest budget) is most robust, i.e. it has the smallest number of misallocations for any level of uncertainty. The other two values of θ have similar robustness. Misallocations at different values of θ vary greatly. For example, at an uncertainty level of 0.2, we find that D_c varies from 7 to 13 depending on the selection of θ . The robustness curves for $\theta = 1.192$ and 0.692 cross several times. While $\theta = 1.692$ is the most robust for all values of D_c , this corresponds to only a portion of the budget of \$5,000,000 being spent, which might be politically unacceptable. An agency might therefore be mainly interested in decisions based on $\theta = 1.192$ (representing the nominated budget) or $\theta = 0.692$ (a larger budget). In this case, the agency would want to be particularly attentive to points in which the robustness curves cross because this indicates that selecting a different value of θ could result in a more robust portfolio. For example, the robustness curves for $\theta = 0.692$ and $\theta = 1.192$ cross at our threshold of 5 misallocations ($D_c = 5$). For values of D_c less than 5, a selection of $\theta = 1.192$ results in higher robustness. However at $D_c = 5$ we find that $\theta = 0.692$ is more robust with $\hat{\alpha}(\theta, D_c)$ equal to 0.08 compared to $\hat{\alpha}(\theta, D_c)$ equal to 0.06 for $\theta = 1.192$. For managing agencies, this means that if a maximum of 5 misallocations is acceptable and the budget driven θ is 1.192, then uncertainty in estimates of b and c can be at most 6% ($\hat{\alpha}(\theta, D_c) = 0.06$).

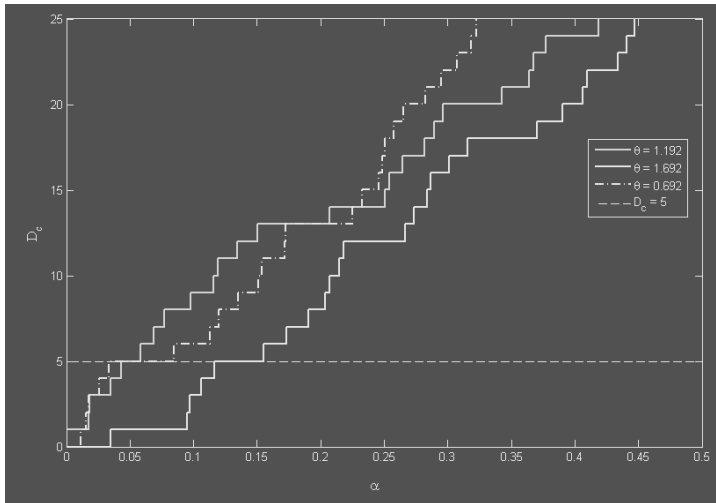


Figure 2. Robustness curves for uncorrelated data. The budget-driven value of $\theta = 1.192$ is shown as the grey robustness curve. Also shown are $\theta + 0.5$ (the black robustness curve) and $\theta - 0.5$ (the dashed robustness curve). The selected critical threshold D_c (horizontal dashed line) is 5 misallocations. The points at which the critical threshold line intersects the robustness curves gives the levels of uncertainty (α) that can exist in our parameters while still giving an acceptable number of misallocations. For the budget-driven θ (grey) and $D_c = 5$, $\alpha = 0.06$.

For both the positively and negatively correlated data, the robustness curves are close together at low values of D_c but splay out for higher values of D_c (Figure 3). The curves cross below values of D_c of 15. This indicates that, depending on our selection of D_c , our selection of θ might need to change if we wish to select the more robust allocation (Figure 3). For most values of D_c , the larger values of θ are more robust (have larger values of $\hat{\alpha}(\theta, D_c)$ for any given D_c) (Figure 3).

When we compare the robustness of the positively and negatively correlated data based on budget-driven θ , the negatively correlated data are much more robust (Figure 3). For example, for θ values corresponding to the nominal budgets (grey robustness curves) and accepting 5 misallocations, $\hat{\alpha}(\theta, D_c)$ for the positively correlated data is about 0.015 compared to 0.04 for the negatively correlated data.

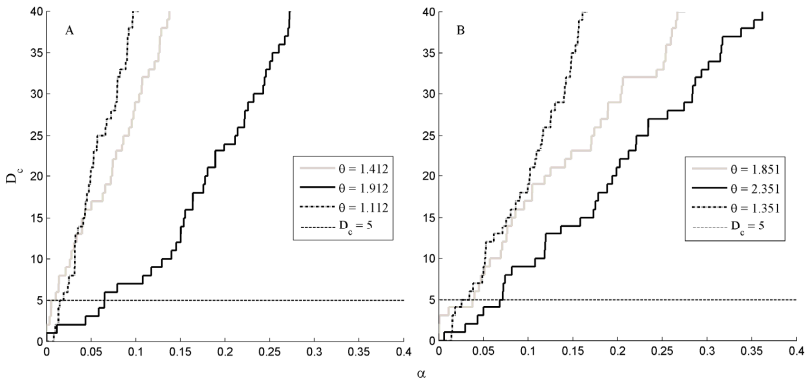


Figure 3. Robustness curves for positively and negatively correlated data for budget-driven values of θ (grey robustness curves), $\theta + 0.5$ (black robustness curves) and $\theta - 0.5$ (dashed robustness curves). The selected critical threshold $D_c = 5$ is plotted as horizontal dashed lines. The point in which the critical threshold line intersects the robustness curves gives the levels of uncertainty that can exist in our parameters while still resulting in an acceptable number of misallocations. A) Robustness of positively correlated data. The budget-driven θ is 1.412 and 14 conservation projects are funded. B) Robustness of negatively correlated data. The budget driven θ is 1.851 and 18 conservation projects are funded.

DISCUSSION

BCRs provide a systematic approach to budget allocation that is transparent and accountable. Yet, uncertainties in our estimates can cause actual outcomes of projects to differ from expected outcomes. If we wish to be accountable with our spending we must understand the uncertainties in our decisions. The info-gap model presented here provides one way of calculating the robustness of decisions under uncertainty. While our model was developed to assess the robustness of BCRs for allocating conservation budgets, it can be applied to any problem that uses BCRs. Our model demonstrates that selecting a value of θ a priori, such as $\theta = 1$ in conventional applications of BCRs or selecting θ based on a budget, can compromise robustness. Instead, if several values of θ are explored based on the info-gap model presented here, a strong argument can be presented for changing θ (and therefore perhaps arguing for a larger budget) to ensure more robust budget allocation.

We examine the effects of correlations in data on the robustness of prioritization strategies. Negatively correlated benefits and costs will, in general, lead to more robust decisions than positively correlated benefits and costs, so managers might consider this when deciding how to allocate budgets. A feature of our info-gap model is that values of θ with clusters of projects within a close envelope will be less robust. This feature of the model can be used to examine how correlations in data affect robustness of different values of θ . Visual inspection of the decision space and

the plotted values of θ help us to interpret the robustness of the different values of θ considered.

In our model, we aggregate the misallocated conservation projects by summing incorrect inclusions and exclusions. These could be analysed separately. In general, lower values of θ (larger budgets) will be more robust to incorrect exclusions because higher percentages of all projects are selected. Similarly, higher values of θ (lower budgets) will be more robust to incorrect inclusions because smaller percentages of all projects are selected. An argument for larger budgets is therefore that their associated lower θ values can reduce incorrect exclusions.

The method presented here can be generalized to the following steps: 1. compile data on benefits and costs of projects and consider the “decision-space”; 2. test for correlations between benefits and costs; 3. check for clumping of data points around critical threshold values of θ ; and 4. test the robustness of different strategies. Managers must make trade-offs between budget selection (and therefore selection of θ) and robustness in decisions. These trade-offs represent value judgements, but a transparent and thorough analysis, such as the one applied here, will guide and support these decisions.

REFERENCES

- Adams, V. M., R. L. Pressey and R. Naidoo. (2010). “Opportunity costs: who really pays for conservation.” *Biological Conservation* 143:439–448.
- Ando, A., J. Camm, S. Polasky, and A. Solow. (1998). “Species distributions, land values, and efficient conservation.” *Science* 279:2126–2128.
- Babcock, B. A., P. G. Lakshminarayan, J. Wu, and D. Zilberman. (1997). “Targeting tools for the purchase of environmental amenities.” *Land Economics* 73:325–339.
- Ben-Haim, Y. (2006). *Info-Gap theory: Decisions under severe uncertainty*. Academic Press, London.
- Bottrill, M., L. N. Joseph, J. Carwardine, M. Bode, C. Cook, E. T. Game, H. Grantham, S. Kark, S. Linke, E. McDonald-Madden, R. L. Pressey, S. Walker, K. A. Wilson, and H. Possingham. (2008). “Is conservation triage just smart decision-making?” *Trends in Ecology and Evolution* 23:649–654.
- Ferraro, P. J. (2003). “Assigning priority to environmental policy interventions in a heterogeneous world.” *Journal of Policy Analysis and Management* 22:27–43.
- Fuller, R. A., E. McDonald-Madden, K. A. Wilson, J. Carwardine, H. S. Grantham, J. E. M. Watson, C. J. Klein, D. C. Green, and H. P. Possingham. (2010). “Replacing underperforming protected areas achieves better conservation outcomes.” *Nature* 466:365–367.
- Joseph, L. N., R. F. Maloney, and H. P. Possingham. (2009). “Optimal allocation of resources among threatened species: a project prioritization protocol.” *Conservation Biology* 23:328–338.
- Regan, H. M., Y. Ben-Haim, B. Langford, W. G. Wilson, P. Lundberg, S. J. Andelman, and M. A. Burgman. (2005). “Robust decision-making under severe uncertainty for conservation management.” *Ecological Applications* 15:1471–1477.

Info-gap approach to regression

Miriam Zacksenhouse, and Simona Nemets

Faculty of Mechanical Engineering, Technion, Haifa, Israel, 32000; email: mermz@tx.technion.ac.il

Abstract

The problem of determining the coefficients of a linear model from experimental data has been the subject of scientific research since the beginning of the 19th century. The standard technique, which minimizes the residual error, is sensitive to uncertainties and becomes ill-posed when the data is redundant. Regularization techniques replace the original ill-posed problem with a well-posed problem, but are sensitive to the proper selection of the regularization parameter, which controls the fidelity to the original problem.

We have recently applied info-gap techniques to derive a robust-satisficing linear regression. The method is based on satisficing a level of residual error that is consistent with the data. Here we demonstrate the performance of this method and compare it to existing regularization methods including L-curve and generalized cross-validation. It is shown that the proposed method yields superior results in the presence of (i) significant noise, (ii) correlated noise, and (iii) model uncertainties.

INTRODUCTION

Using Info-gap techniques, we have previously developed a Robust satisficing (RS) linear regression, which provides the highest level of robustness to uncertainties in the data for a given required limit on the residual error (Zacksenhouse et al. 2009, Nemets, 2010). When the uncertainty in the data is modeled by an absolute info-gap model, the robust satisficing linear regression has the form of Tikhonov regularization (Tikhonov and Arsenin, 1997), with a regularization parameter that depends on the level of required performance (Zacksenhouse et. Al. 2009, Nemets, 2010). Thus, the proper regularization parameter is directly determined by the required level of performance. However, when the level of required performance is not dictated by external constraints, the issue of proper selection of the required performance remains.

Given the inherent trade-off between performance and robustness, we further suggested to use the consistency between the observations and the linear model to determine a unique, parameter free regression. In particular, we showed that the *best* possible residual error that the robust-satisficing regression can achieve has a unique minimum with respect to the regularization parameter. The RS regression, which minimizes this function is termed the model consistent RS (MCRS), and provides a parameter free regression (Zacksenhouse et. al. 2009, Nemets, 2010).

In this paper we demonstrate the performance of this method and compare it to existing regularization methods including L-curve (Hansen, 1992, Hansen and O'Leary, 1993) and generalized cross-validation (GCV, Golub et. al., 1979). It is shown that the proposed method yields superior results in the presence of (i) significant noise, (ii) correlated noise, and (iii) model uncertainties.

METHODS

Let $\tilde{A} \in R^{m \times n}$ ($m > n$), and $\tilde{b} \in R^m$ denote uncertain measurements of variables that are expected to be related by the linear model: $\tilde{A}x = \tilde{b}$, where x is the vector of regression coefficients. Tikhonov regression, with regularization parameter μ , is given by (Tikhonov and Arsenin, 1997), $x_\mu = (\tilde{A}^T \tilde{A} + \mu I)^{-1} \tilde{A}^T \tilde{b}$. For absolute Info-gap model (see Appendix A, and Ben-Haim, 2006) the RS regression has the form of the Tikhonov regression with a regularization parameter that depends on the level of required performance (Zacksenhouse et. Al., 2009, Nemets, 2010). The MCRS method selects the regularization parameter which minimizes the consistent windfall performance (CWP), defined in Appendix A and in Zacksenhouse et. al., 2009, Nemets, 2010), versus the regularization parameter μ .

The Consistent windfall performance curve is a powerful tool both for selecting the regularization parameter and for evaluating the accuracy of the solution. We differentiate between three cases: (i) The CWP curve crosses: this indicates that the solution can be computed accurately with some level regularization, and the regularization parameter is selected as the minimal parameter for which CWP is below zero; (ii) The CWP curve does not cross zero: this indicates that there is no regularization solution that may provide zero residual error, and the regularization parameter that minimizes the CWP is selected.

The Info-gap based MCRS method for selecting the regularization parameter μ , is compared with two existing regularization methods: (i) The L-curve method (Hansen, 1992, Hansen and O’Leary, 1993), which selects the regularization parameter at the corner of the curve depicting the log of the solution norm $\log(\hat{x}_\mu)$ versus the log of the residual norm $\log(\|\tilde{A}\hat{x}_\mu - \tilde{b}\|)$ for different regularization parameters, and (ii) The GCV method (Golub et al., 1979), which selects the regularization parameter that

minimizes the GCV function defined by:
$$GCV \text{ function} = \frac{\|\tilde{A}\hat{x}_\mu - \tilde{b}\|^2}{\text{trace}(I - \tilde{A}\tilde{A}^\#)^2}$$

Performance evaluation and comparison is based on five data sets, which were generated as follows:

1. An Arbitrary matrix A (62×32) is multiplied by arbitrary column vector x^{exact} to obtain b^{exact} .
2. Vector b is generated by $b = b^{exact} + e_\perp$, where e_\perp is chosen to be orthogonal to Image(A) in order to ensure that b is not at the column span of A. Size of e_\perp controls the degree of consistency in the relation between A, b.
3. A and b are degraded by additive white noise with zero mean and standard deviation σ_A, σ_b .
4. A and b are degraded by correlated noise, which are produced by applying circular averaging filter with radius r.

Thus, each of the five data sets is characterized by three features:

1. Measure of consistency, which is controlled by a ratio $r_{orth} = \frac{\|e_{\perp}\|}{\|x_{exact}\|}$.
Increasing this ratio increases the portion of b , which is orthogonal to Image(A).
2. Measure of white noise, which is controlled by $rwA = \frac{\|e_{nA}\|}{\|A\|}$ and $rwB = \frac{\|e_{nB}\|}{\|b\|}$
3. Measure of correlation, which is controlled by radius r of the circular averaging filter.

In order to evaluate the performance of the methods, residual norm as function of the regularization parameter was computed for the testing data. This enables us to see which method yields smaller residual error on the testing data.

RESULTS

The results for each scenario are summarized in three plots, which depict the relevant decision curve for each method, and a fourth plot, which presents performance comparison for the testing data:

- Top left plot: L-curve with parameter selected by `l_corner` function from Hansen, 1994.
- Top right plot: GCV function with minimum found by `gcv` function from Hansen, 1994.
- Bottom right plot: CWP versus regularization parameter with parameter selected by MCRS method.
- Bottom left plot: Residual norm of the testing data as function of the regularization parameter, compare the residual errors obtained by the three methods.

SCENARIO 1: ALMOST IDEAL DATA

The first data set depicts a scenario in which the data is almost ideal: $r_{orth} = 0.0001$; $rwA = 1.6e-4$; $rwB = 3.3e-8$; $r = 1$ (circular averaging with radius 1). Figure 1 demonstrates that for this data set, all three methods select very small regularization parameters, and achieve similar, close to optimal performance (resulting residual errors are close to zero). L-curve has a distinct corner, GCV function has an easy detectible minimum. The CWP function is negative for almost all valid regularization parameters, suggesting that the problem can be accurately solved.

SCENARIO 2: SIGNIFICANT WHITE NOISE

The second data set depicts a scenario in which the data is corrupted with white noise: $r_{orth} = 0.0001$; $rwA = 0.5$; $rwB = 3.5e-4$; $r = 0$ (no correlation). Figure 2 indicates that significant white noise causes L-curve to lose its usual L-shape, and thus L-curve method produces meaningless parameter. However, GCV and MCRS methods can overcome the noise and produce sensible solutions. For this scenario, GCV and MCRS achieve close to optimal residual error, though this level is not close to zero.

The CWP function is positive for small regularization parameters, suggesting that certain regularization is needed to solve the problem accurately.

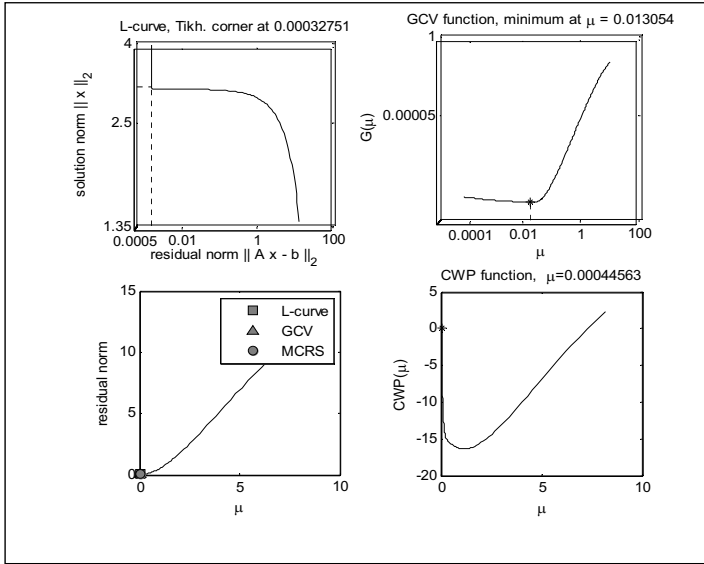


Figure 1: Analysis plots and performance comparison for scenario 1

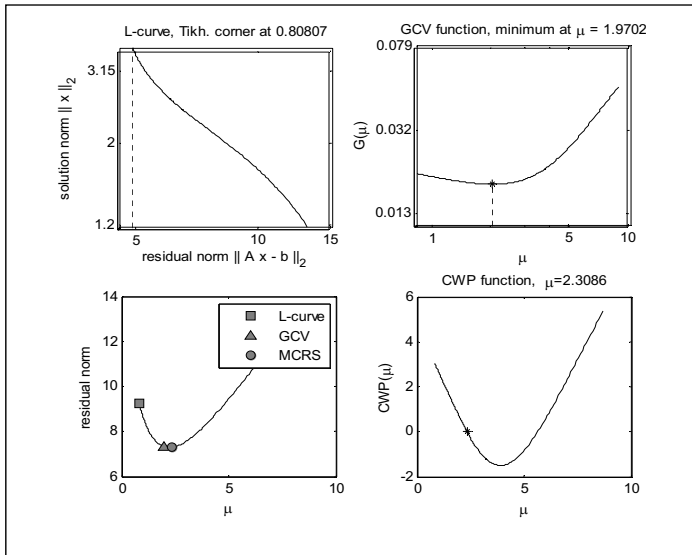


Figure 2: Analysis plots and performance comparison for scenario 2

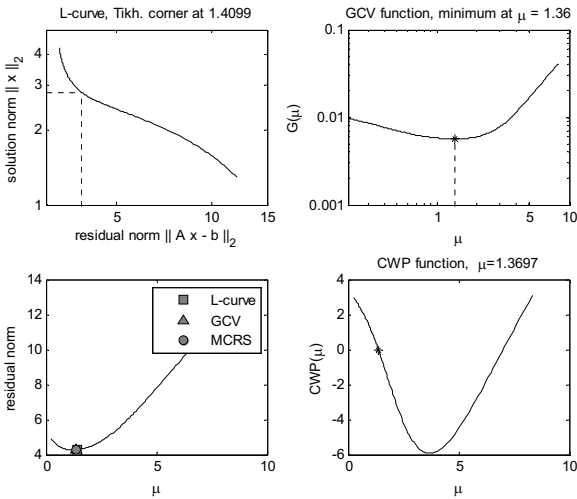


Figure 3: Analysis plots and performance comparison for scenario 3

SCENARIO 3: SMALL INCONSISTENCY

The third data set depicts a scenario in which the data is slightly inconsistent with the model: $r_{orth}=1$, $rwA=0.1$, $rwB=3.6e-5$, $r=0$ (no correlation). Small inconsistency results in L-curve whose corner is not easily detected; yet, the L-curve method results in an acceptable parameter. GCV and MCRCs select similar parameters. All three methods achieve residual error, close to minimal possible residual error. CWP function again is positive for small regularization parameters, suggesting that certain regularization is needed to solve the problem accurately.

SCENARIO 4: SIGNIFICANT INCONSISTENCY

The fourth data set depicts a scenario in which the data is significantly inconsistent with the model: $r_{orth}=2.8$; $rwA=0.5$; $rwB=3.1e-5$; $r=0.1$ (very small correlation). In this scenario the L-curve fails, GCV produces acceptable parameter, but its performance is inferior to that of MCRCs. CWP function is above zero for all regularization parameters, indicating that there is no regularization parameter that may result in zero residual error, properly reflecting the inconsistency in the model. Indeed, the minimal possible residual norm for this scenario is large, compared to other scenarios.

SCENARIO 5: CORRELATED NOISE

The last data set includes correlated noise: $r_{orth}=2.8$, $rwA=0.5$, $rwB=3e-5$, $r=3$ (circular averaging with radius 3). Adding correlation to the data causes the GCV method to fail, in agreement with (Hansen and O’Leary, 1993; Thompson, 1991). L-curve and MCRCs method select similar regularization parameters, and achieve close to optimum residual error.

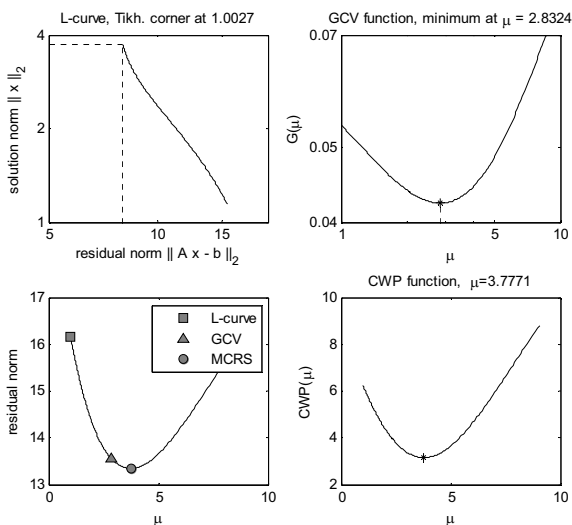


Figure 4: Analysis plots and performance comparison for scenario 4

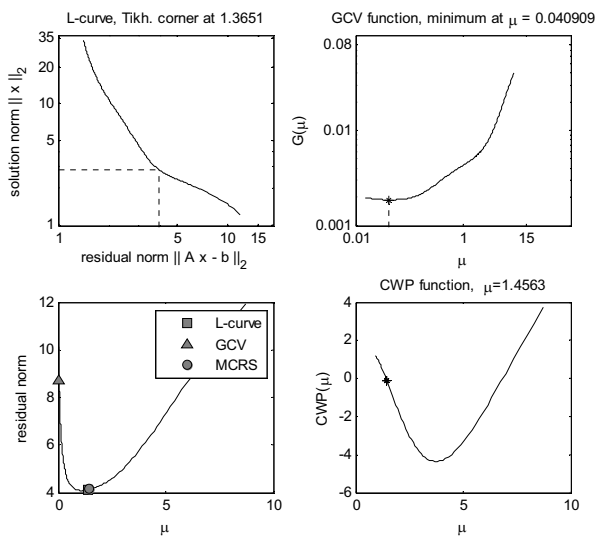


Figure 1: Analysis plots and performance comparison for scenario 5

SUMMARY AND DISCUSSION

When the data is consistent or only slightly inconsistent with the linear model (scenarios 1,3), the MCRS achieves residual errors which are similar to those achieved by existing methods. However, the MCRS clearly outperforms the existing methods for more challenging scenarios (2,4,5): Scenarios 2 and 4 demonstrate that MCRS outperforms the L-curve when the data is corrupted with significant noise or significantly inconsistent with the linear model, respectively. The limitations of the L-curve method in these cases are in agreement with Hanke (1996). Scenario 5 demonstrates that MCRS outperforms GCV method in the presence of correlated noise. The limitation of the GCV method in this case is in agreement with Thompson (1997).

Moreover, the results demonstrate that the plot of consistent windfall performance versus regularization parameter incorporates important information about the features of the data set. The minimal values of the CWP functions in Figure 1-4 demonstrate the relation between minimal possible residual error and minimal value of CWP function. Particularly, as the minimal value of CWP function decreases, minimal possible residual error decreases also, implying that the solution becomes more accurate.

Acknowledgments

This work was supported by the Abramson Center for the Future of Health, the Bernstein Research Fund and by the fund for the promotion of research at the Technion. The authors thank Yakov Ben-Haim, for introducing the authors to Info-gap theory and for for numerous helpful suggestions.

Appendix A: Consistent Windfall Performance

The Appendix defines the robust satisficing (RS) regression, the windfall performance, and the consistent Windfall Performance (CWP). Info-gap theory is detailed in [1] and the RS regression was developed in [2].

Let $\tilde{A} \in R^{m \times n}$ ($m > n$), and $\tilde{b} \in R^m$ denote uncertain measurements of variables that are expected to be related by the linear model: $\tilde{A}x = \tilde{b}$, where x is the vector of regression coefficients. Uncertainty is represented by the Info-gap model:

$$U(\alpha, \tilde{A}, \tilde{b}) = \{ \tilde{A} \in R^{m \times n}, \tilde{b} \in R^m : \|A - \tilde{A}\| \leq \alpha, \|b - \tilde{b}\| \leq \nu \alpha \} \quad \alpha > 0$$

Here α is the unknown level of uncertainty in the coefficients matrix A, and ν is the relative level of uncertainty in b. Herein, we assume that ν is known and describes the uncertainty with single parameter α .

Given a candidate solution $\hat{x} \in R^n$, its performance is quantified by the residual error with the ideal observations: $r = \|A\hat{x} - b\|$

Definition – Robustness: *The robustness of the regression \hat{x} to uncertainties in the observations is the largest level of uncertainty α up to which all possible ideal observations result in residual norms that are smaller than the required performance*

$$\rho : \hat{\alpha}(\hat{x}, \rho) \equiv \max_{\alpha} \left\{ \alpha : \left(\max_{A, b \in U(\alpha, \tilde{A}, \tilde{b})} \|A\hat{x} - b\| \right) \leq \rho \right\}$$

Definition – Opportuneness: *The opportuneness of the regression \hat{x} given uncertainties in the observations is the smallest level of uncertainty α for which the*

info-gap model includes an ideal observation with a residual error that is better than the performance (referred to as the windfall performance) φ :

$$\hat{\beta}(\hat{x}, \varphi) \equiv \min_{\alpha} \left(\alpha : \min_{A, b \in U(\alpha; A, b)} \|A\hat{x} - b\|_2 \leq \varphi \right)$$

Definition – Robust Satisficing Regression: *Given a sub-optimal critical performance ρ , the robust satisficing regression is the regression that maximizes the robustness for satisficing ρ : $\hat{x}_{RS}(\rho) = \arg \max_{\hat{x}} \hat{\alpha}(\hat{x}, \rho)$*

Definition – Consistent Windfall Performance: *The windfall performance consistent with the RS regression $\hat{x}_{RS}(\rho)$, is a windfall performance whose opportuneness $\hat{\beta}(\hat{x}_{RS}(\rho), \varphi_{RS})$ is equal to the robustness $\hat{\alpha}(\hat{x}_{RS}(\rho), \rho)$.*

References:

- Ben-Haim, Y., (2006), "Info-gap decision theory: decisions under severe uncertainty", 2nd Edition, Academic Press, London.
- Engl H.W., Hanke M., Neubauer A., (1996), "Regularization of inverse problems", Kluwer, Dordrecht.
- Golub, G.H. et al, (1979) "Generalized cross-validation as a method for choosing a good ridge parameter", *Technometrics*, 21(2):215-223.
- Hanke M., (1996), "Limitations of the L-curve method in ill-posed problems", *BIT*, 36:287-301.
- Hansen P.C., (1992), "Analysis of discrete ill-posed problems by means of the L-Curve", *SIAM Review*, 34(4): 561-580.
- Hansen P.C., O'Leary D.P., (1993), "The use of the L-curve in the regularization of discrete ill-posed problems", *SIAM J. Sci. Comput.*, 14:1487-1505.
- Hansen P.C., "Rank-deficient and discrete ill-posed problems", *SIAM*, 1997.
- Hansen P.C. (1990) "The discrete Picard condition for discrete ill-posed problems", *BIT*, 30:658-672.
- Hansen P.C., (1994) "Regularization Tools: A Matlab package for analysis and solution of discrete ill-posed problems", *Numerical Algorithms*, 6:1-35.
- Hanson R.J., Lawson C.L., (1974) "Solving least squares problems", Prentice-Hall Englewood Cliffs.
- Nemets S., (2010) *Info-gap approach to regularization*, MSc Thesis, Faculty of Mechanical Engineering, Technion, Israel.
- Thompson A.M, et al. (1991), "A study of methods for choosing of smoothing parameter in image restoration by regularization", *IEEE Trans. Pattern Anal. Machine Intell.*, 13: 3326-3339.
- Tikonov A.N., Arsenin V.Y. (1997), "Solution to ill-posed problems" Washington.
- Zacksenhouse M., Nemets S., Lebedev M.A., Nicolesiu M.A.L. (2009), "Robust Satisficing Linear Regression: performance/ robustness trade-off and consistency criterion", *Mechanical Systems and Signal Processing*, 23(6): 1954-1964.

Robust Resource Allocation: An Info-Gap Approach

Lior Davidovitch¹ and Yakov Ben-Haim²

¹Faculty of Mechanical Engineering, Technion – Israel Institute of Technology, Haifa 32000 Israel; email: liordav@technion.ac.il

²Yitzhak Moda'i Chair in Technology and Economics, Faculty of Mechanical Engineering, Technion –Israel Institute of Technology, Haifa 32000 Israel; PH 972-4-8293262; FAX 972-4-8295711; email: yakov@technion.ac.il

ABSTRACT

A decision maker wishes to distribute a fixed amount of resources between several alternatives. Each alternative responds differently to allocation, as expressed by its responsiveness. The alternatives' different responsiveness to investment can be exploited for efficient allocation of resources. However, the responsiveness is highly uncertain, so prediction is difficult and uncertainty must be accounted for in designing an allocation. We use info-gap theory for satisficing (not minimizing) accumulated loss from several alternatives. We demonstrate the trade-off between robustness to uncertainty and total loss, and show the tight connection between the decision maker's notion of adequacy and the resulting allocation.

INTRODUCTION

Resource allocation is a fundamental managerial action. The benefit from a given amount of resource varies between the different groups which receive allocations, and a policy maker would like to enhance the total benefit from the resource. Examples are ample: How should a limited stock of influenza vaccinations be distributed between young patients and elderly patients? How should the budget of a company be distributed between R&D and advertising? Or even, how should an investor distribute his or her portfolio?

Such decisions are almost always made under severe uncertainty considering the correlation between assigned resources and the yield of the different investment alternatives. In other words, in the responsiveness of the different alternatives. Various approaches have been used to tackle the problem of resource allocation under uncertainty.

Markowitz (1952) argued that a portfolio should be chosen from the set of efficient portfolios. That is, the set of portfolios that yields the optimal weighted average between expected utility and variance, for some given weights. This concept is the

basis of modern portfolio theory. Arrow (1964) considers the allocation of securities in uncertain markets (such as stock markets) is in fact an optimal—that is, equilibrial—resource allocation in the presence of risk.

Starr (1973) notes that an Arrow optimum is in fact *ex ante* optimal, and once uncertainty is removed (the actual state of the world is revealed) the allocation may not be *ex post* optimal. Starr considers the conditions for which an *ex ante* optimum is also an *ex post* optimum, and thus there is no necessity for additional information. Rothenberg and Smith (1985) consider the impact of uncertainty on the equilibrium of allocated resources. They investigate the conditions under which uncertainty in some underlying parameters (such as the production output function) will increase or decrease the social welfare or the wage rate, and how it would influence the resource allocation with respect to uncertainty-free equilibrium. Batra (1974) extends the analysis under the assumption that firms are risk-averse. The extent of research is extremely wide, and almost all researchers—and all of the noted above—assume probabilistic uncertainty.

In this paper we suggest the use of info-gap decision theory (Ben-Haim 2006) for formulating an allocation strategy, whereby one tries to *satisfice* the total gain (or loss), rather than to *optimize* it. By “satisficing” we mean keeping the value of a loss function below an acceptable level. Satisficing is to be distinguished from optimizing which entails minimizing the loss. The motivation for satisficing (rather than optimizing) derives from the great uncertainty associated with estimates of the responsiveness to resource allocation.

Info-gap decision theory has been applied to robustly allocate resources in a variety of problems. Berleant *et al.* (2008) use info-gap analysis, alongside second order stochastic dominance, to select an investment portfolio which is both lucrative and robust. Davidovitch *et al.* (2009) consider the most robust mix of structured sampling and workers motivational programs for the detection of invasive species. Davidovitch and Ben-Haim (2010) aim for a robust profiling strategy to satisfice the rate of drivers running red lights. Davidovitch (2009) generalizes the concept of profiling to a general resource allocation problem.

We will demonstrate the irrevocable trade-off between robustness to this uncertainty on the one hand, and reduction of the loss on the other. An allocation which attempts to minimize loss is an allocation with zero robustness to uncertainty in the responsiveness function. We will also show that satisficing is a somewhat demanding process, as it requires the decision maker to commit to a benchmark: in the general case, different definitions of what is adequate will result in different resource allocations.

RESOURCE ALLOCATION MODEL

We will denote by $C_i(b_i)$ the loss function for alternative i given that a fraction b_i of the resources are allocated to this alternative. The goal of the decision maker is to divide the resources between n groups, $\sum_{i=1}^n b_i = 1$, in a way that will satisfactorily manage the total loss: $L(b) = \sum_{i=1}^n C_i(b_i)$. We will assume that $C_i(b_i) \geq 0$.

Unfortunately, there is considerable uncertainty surrounding the responsiveness functions $C_i(b_i)$. All we have is an estimate, $\tilde{C}_i(b_i)$, which may be quite erroneous. We will model the uncertainty with the following info-gap model:

$$(1) \quad U(\alpha, \tilde{C}) = \{C: C_i(b_i) \geq 0, |C_i(b_i) - \tilde{C}_i(b_i)| \leq \omega_i(b_i)\alpha\}, \alpha \geq 0$$

At any horizon of uncertainty α , the set $U(\alpha, \tilde{C})$ contains all non-negative responsiveness functions $C_i(b_i)$ which deviate from the nominal function by no more than $\omega(b_i)\alpha$. Since α is unbounded, this is an unbounded family of nested sets of responsiveness functions.

The weight on the horizon of uncertainty, $\omega(b_i)$, can be used to modulate the horizon of uncertainty as a function of the allocation, b . For instance, if $\omega(b_i) = \tilde{C}_i(b_i)$, then the uncertainty is proportional to the estimate $\tilde{C}_i(b_i)$. However, if $\omega_i(b_i) = 1$, then the uncertainty is independent of the allocation, b_i .

INFO-GAP ANALYSIS

A fundamental tool of the info-gap analysis is the robustness function. The robustness of an alternative is the greatest level of uncertainty which still guarantees an acceptable loss. In our case, the robustness of an allocation b is the greatest level of uncertainty for which the total loss is no greater than L_c :

$$\hat{\alpha}(b, L_c) = \max \left\{ \alpha : \left(\max_{C \in U(\alpha, \tilde{C})} \sum_{i=1}^n C_i(b_i) \right) \leq L_c \right\}$$

From eq.(1) it is easily derived, using basic algebra, that:

$$(2) \quad \hat{\alpha}(b, L_c) = \begin{cases} 0 & , L_c \leq \xi(b) \\ \frac{L_c - \xi(b)}{\zeta(b)} & , L_c > \xi(b) \end{cases}$$

where $\xi(b) = \sum_{i=1}^n \tilde{C}_i(b_i)$, $\zeta(b) = \sum_{i=1}^n \omega_i(b_i)$.

Eq.(2) implies that robustness curves are linear, where the crossing of the x -axis is the nominal loss, $\xi(b)$, and the slope is a function of the cumulative uncertainty weight, $\zeta(b)$.

RESULTS

Figure 1 illustrates the robustness curves for four typical allocation alternatives (the underlying responsiveness functions and info-gap model are detailed in Appendix B. The *nominal optimal* (curve *a*) is the allocation that yields the minimal loss under the nominal assumption (minimal $\xi(b)$). Since the robustness curves cross the x -axis at the nominal loss, this allocation has the lowest crossing-point of the x -axis. The robustness for the nominal optimal is zero. That is, a decision maker aiming for the optimization value has no immunity to uncertainty. Note that the nominal optimal robustness curve is crossed by other robustness curves. The crossing of the robustness curve of the nominal optimal allocation means that it is *not* the most robust allocation for all choices of the critical value.

The *uncertainty-free* allocation (curve *b*) is an allocation for which there is no uncertainty surrounding the outcome ($\zeta(b) = 0$). In other words, when $\omega_i(b_i) = 0$ for all i . This means that the info-gap model does not become more inclusive as the horizon of uncertainty increases, and therefore the worst case for any horizon of uncertainty is equal to the nominal loss. As a result, the robustness is either zero if the nominal result is higher than the critical value, or infinity if the nominal result is smaller than the critical value. Hence the vertical robustness curve.

Another allocation is *robust-dominated* (curve *c*): for every critical loss there is some other allocation with greater robustness. This is important, since robust-dominated allocations should never be chosen. Sufficient conditions for an allocation to be robust-dominated are derived in Davidovitch (2009), but will not be elaborated here.

The fourth allocation is *non robust-dominated* (curve *d*): it is not optimal nor uncertainty-free, but it is not robust-dominated which means that there are values for the critical loss for which it is the most robust allocation.

Is there a single most robust allocation? Is there an allocation which is most robust for a wide range of values of the critical loss? These alternatives would appeal to many decision makers. We will claim that in the general case there is no such alternative, and every value for the critical loss derives a different choice for the robust-satisficing decision maker. This is the "no free meals law" of info-gap.

Consider, for simplicity, a decision maker who wishes to allocate resources between two groups. The decision maker is a robust-satisficer, and thus wishes to find an allocation which will maximize the robustness for a given critical value L_c :

$$\hat{b}(L_c) = \arg \max_b \hat{\alpha}(b, L_c)$$

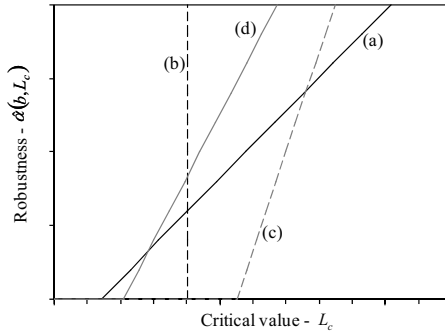


Figure 1: Robustness curves of four typical allocations: the optimal allocation (a), an uncertainty-free allocation (b), a robust-dominated allocation (c), and a non robust-dominated allocation (d).

The following proposition states that in the general case, an allocation will be most robust for at most one critical value. In other words, except for special cases, different critical values will yield different choices.

Proposition 1 Given $n = 2$, allocation b , such that $b_1 \neq 0$, $b_2 \neq 0$, $\xi(b)$ is differentiable, $\zeta(b)$ is differentiable, $\zeta(b) > 0$, $\tilde{C}_i(b_i)$ is convex, if b is not nominal optimal, then b is the most robust allocation for at most one critical value.

The importance of the above observation to the decision maker is that there is no single "robust-dominant" decision, an allocation which is more robust than any other allocation for all critical values. The most robust allocation is a function of the satisficing criterion, namely, of the goal the decision maker seeks to achieve. In other words, the robust-satisficing allocation, $\hat{b}(L_c)$, depends on the decision maker's choice of the critical value, L_c .

CONCLUSION

Under a set budget, a manager is expected to utilize differences in the responsiveness functions of investment alternatives to augment profits or decrease loss. However, the responsiveness functions are often rough estimates, subject to severe uncertainty. Since estimation errors may lead to adverse results, it is preferred that an allocation be as robust as possible.

This paper has developed a robust-satisficing methodology for allocation of resources when the responsiveness functions are highly uncertain. We have used info-gap decision theory for satisficing (not minimizing) the total loss. We have demonstrated the trade-off between robustness to uncertainty on the one hand, and reduction of total loss on the other hand. Attempting to minimize the total loss has zero robustness to

uncertainty in the responsiveness functions. Since the responsiveness functions are often uncertain, low robustness is undesirable. Positive robustness is obtained only by aiming at a loss which is larger than the estimated minimum. The robust-satisficing strategy chooses an allocation which guarantees an acceptable loss (which usually will not be the estimated minimum), for the largest possible range of error in the estimated responsiveness. The robustness analysis enables the decision maker to evaluate allocation options in terms of whether they promise adequate results, at plausible levels of immunity to error in the responsiveness functions.

We have shown that the allocation chosen by a robust-satisficing decision maker is intimately linked with the criterion for adequacy, the critical loss. Since each choice of critical loss would result in a different allocation, the decision maker must carefully choose a critical value.

APPENDIX A: PROOF TO PROPOSITON

Proof to Proposition 1: If b is most robust, then shifting an infinitesimal amount of resources between group 1 and group 2 should not change the robustness. In other words:

$$\left(\frac{\partial}{\partial b_1} - \frac{\partial}{\partial b_2}\right)\hat{\alpha}(b, L_c) = 0$$

We will denote:

$$\xi'(b) = \left(\frac{\partial}{\partial b_1} - \frac{\partial}{\partial b_2}\right)\xi(b), \quad \zeta'(b) = \left(\frac{\partial}{\partial b_1} - \frac{\partial}{\partial b_2}\right)\zeta(b)$$

And now:

$$\begin{aligned} (3) \quad \left(\frac{\partial}{\partial b_1} - \frac{\partial}{\partial b_2}\right)\hat{\alpha}(b, L_c) &= \left(\frac{\partial}{\partial b_1} - \frac{\partial}{\partial b_2}\right)\frac{L_c - \xi(b)}{\zeta(b)} \\ &= \frac{-\xi'(b)\zeta(b) - L_c\zeta'(b) + \xi(b)\zeta'(b)}{\zeta(b)^2} \\ &= 0 \end{aligned}$$

Eq. (3) is linear in L_c . Therefore, if eq. (3) holds for more than one value of L_c , then $\zeta'(b) = 0$. But if $\zeta'(b) = 0$ then eq. (3) can be reduced to $\frac{\xi'(b)}{\zeta(b)} = 0$. Since $\zeta(b) > 0$ then the above implies $\xi'(b) = 0$.

$\xi(b)$ is a sum of two convex functions, and therefore convex in itself. This means that $\xi'(b) = 0$ only if b is the nominal optimal allocation. ■

APPENDIX B: NUMERICAL EXAMPLE

In this appendix we will detail the assumptions that result in Figure 1. The assumptions are a result of an analysis by Davidovitch and Ben-Haim (2010), which estimates the responsiveness to policing of “young” drivers (ages 17-30) versus older drivers, and utilizes this estimation (along with a corresponding info-gap model) to satisfy the crime rate.

We will denote the two groups by y (“young”) and \bar{y} (the complementary group). b_i will denote the fraction of the policing resources allocated to group i . Then according to Davidovitch and Ben-Haim (2010):

$$\tilde{C}_i(b_i) = \exp\left(-\gamma_i \frac{b_y}{\pi_i} - \delta_i\right)$$

where π_i is the fraction of group i within the population, and γ_i and δ_i are both parameters of the responsiveness of group i .

The info-gap model used by Davidovitch and Ben-Haim (2010) is as follows:

$$U(\alpha, \tilde{C}) = \left\{ C: C_i(b_i) \geq 0, \left| \frac{C_i(b_i) - \tilde{C}_i(b_i)}{\tilde{C}_i(b_i)} \right| \leq \alpha \left| \frac{b_i - b_i^0}{b_i^0} \right| \right\}, \quad \alpha \geq 0$$

where b_i^0 is the fraction of policing resources that were allocated to group i when the crime rate of group i was measured. That is, there is zero uncertainty surrounding the responsiveness for allocation b_i^0 , and the uncertainty grows as the allocation differs from b_i^0 .

The parameters used by Davidovitch and Ben-Haim (2010) are given in Table 1. The allocations resulting in the curves in Figure 1 are given in Table 2.

Table1: Parameters for Numerical Example

Group	π_i	γ_i	δ_i	b_i^0
Age 17-30 (y)	0.145	1.31	1.57	0.145
Age 31+ (\bar{y})	0.855	0.47	2.54	0.855

NOTE.—Parameters for the responsiveness functions and info-gap model underlying Figure 1 (Davidovitch and Ben-Haim, 2010).

Table2: Allocations for Numerical Example

Curve	b_y	$b_{\bar{y}}$
a	0.268	0.732
b	0.145	0.855
c	0.120	0.880
d	0.200	0.800

NOTE.—Parameters for the allocations resulting the robustness curves of Figure 1 (Davidovitch and Ben-Haim, 2010).

REFERENCES

- Arrow, K. J. (1964). The role of securities in the optimal allocation of risk-bearing, *The Review of Economic Studies*, 31(2):91–96.
- Berleant, D., Andrieu, L., Argaud, J. P., Barjon, F., Cheong, M. P., Dancre, M., Sheble, G. and Teoh, C. C. (2008). Portfolio management under epistemic uncertainty using stochastic dominance and information-gap theory, *International Journal of Approximate Reasoning*, 49(1):101–116.
- Batra, R. (1974). Resource allocation in a general equilibrium model of production under uncertainty, *Journal of Economic Theory*, 8(1):50–63.
- Davidovitch, L. (2009). *Strategic interactions under severe uncertainty*, PhD Thesis, Technion–Israel Institute of Technology.
- Davidovitch, L., Stoklosa, R., Majer, J., Nietrzeba, A., Whittle, P., Mengersen, K., and Ben-Haim, Y. (2009). Info-gap theory and robust design of surveillance for invasive species: The case study of Barrow Island, *Journal of Environmental Management*, 90:2785–2793.
- Davidovitch, L., and Ben-Haim, Y. (2010). Is your profiling strategy robust?, working paper.
- Markowitz, H. (1952). Portfolio selection. *The Journal of Finance*, 7(1):77–91.
- Rothenberg, T. J., and Smith, K. R. (1985). The effect of uncertainty on resource allocation in a general equilibrium model, *The Quarterly Journal of Economics*, 85(3):440–459.
- Snizek, J., May, D., and Sawyer, J. (1990). Social uncertainty and interdependence: A study of resource allocation decisions in groups, *Organizational Behavior and Human Decision Processes*, 46(2):155–180.
- Starr, R. M. (1973). Optimal production and allocation under uncertainty, *The Quarterly Journal of Economics*, 87(1):81–95.

This page intentionally left blank

Author Index

Page number refers to the first page of paper

- Achenie, L. E. K., 276
Adams, Vanessa M., 971
Agarwal, Jitendra, 230
Agdas, Duzgun, 86
Ahmed, A., 754
Aktas, M., 683
Aly, Aly Mousaad, 352
Anastasopoulos, P., 754
Aslan, H., 683
Attarzadeh, Meghdad, 360, 805
Ayyub, Bilal M., 113, 197, 334, 708,
772
- Babu, Neela P., 829
Bai, Q., 754
Banerjee, Swagata, 667, 889
Barroca, Bruno, 425, 790
Baxter, Peter W. J., 945
Beer, Michael, 53, 360, 805
Beisner, Keith E., 659
Ben-Haim, Yakov, 963, 988
Bensi, M., 541
Bent, Russell, 180
Beraud, H el ene, 425
Biscontin, G., 533
Bitsuamlak, Girma, 352
Blockley, David, 230
Bocchini, Paolo, 897
Broglia, S., 561
Brown, Colin B., 222
Bruhn, Ronald L., 659
Buckley, Cody M., 268
Buritic a, J., 214
- Cather, Ross, 477
Cavdaroglu, Burak, 171
Chang, Che-Yu, 113, 197, 334
- Characklis, Gregory W., 798
Chen, C. C., 129
Chen, Liang, 284, 316, 374
Cheng, Hu, 316, 326
Cheung, Kwok F., 610
Ching, Jianye, 675
Chowdhury, Arindam Gan, 352
Chua, David Kim Huat, 360, 805
Clem, John, 738
Coate, A. R., 578
Coffrin, Carleton, 180
Corotis, Ross B., 485
Cui, Qingbin, 284
- Darby, John, 738
Das, Ajoy Kumar, 518
Datskov, I. V., 276
Davidovitch, Lior, 988
Davidson, Michael T., 86
Diab, Youssef, 724, 746, 790
Due nas-Osorio, Leonardo, 205, 214
Dunphy-Guzman, Katherine, 738
Duthinh, Dat, 501
- Ellis, Ralph D., 86
El-Meligy, Mahmoud, 914
Erdogmus, Ece, 268
- Farag, Reda, 914
Feng, Ye, 316
Ferson, Scott, 29, 53, 70, 526
Francis, R., 468
Frangopol, Dan M., 897
French, Geoffrey S., 782
Furuta, Hitoshi, 1, 300

- Gardoni, Paolo, 342, 417, 450, 533,
 633, 922
 Gastaldi, M., 138
 Gavardashvili, G. V., 813
 Gecchele, G., 138
 Gómez, C., 214
 Goode, J., 526
 Gootzit, David, 782
 Goulet, James A., 78, 905
 Graf, William, 246
 Grimson, R., 526
 Guikema, Seth D., 155, 468, 594
 Gurley, Kurt, 602, 618
 Guryev, E., 716

 Hafskjold, Leif Sigurd, 746
 Haldar, Achintya, 518, 914
 Harris, C. E., Jr., 417
 Hayashi, I., 45
 Heilemann, Kristina, 746
 Hernandez-Fajardo, Isaac, 205
 Hinton, John P., 738
 Hirokane, Michiyuki, 96
 Hope, Mark, 610
 Hou, Weihong, 699
 Hryniewicz, Olgierd, 21
 Hu, Zhenghui, 246
 Huang, L. P., 881
 Huang, Q., 922
 Huang, Youliang, 326, 374
 Hubert, Gilles, 425
 Hurlebaus, S., 922
 Huyck, Charles, 246

 Inoue, Yuhei, 96
 Irias, X. J., 493, 578
 Irish, J. L., 587
 Ishibashi, Ken, 300
 Ishiguro, Yukako, 104

 Javanpour, Mohsen, 252
 Jha, M. K., 129
 Jiang, Y., 45
 Johnson, Peggy A., 570

 Kagaya, Seiichi, 104
 Kamal, H. A., 708
 Kang, M. W., 129
 Kang, Won-Hee, 549
 Kasama, K., 691
 Kasprzyk, Joseph R., 798
 Katona, Tamas J., 260
 Kaulzarich, Kyle, 268
 Kearney, Michael S., 334, 772
 Kennedy, Andrew B., 610
 Khatri, Krishna, 836, 846, 953
 Kikuchi, Shinya, 121
 Kim, Byung-Cheol, 292
 Kiureghian, A. Der, 541, 561
 Knox, Kenneth J., 732
 Krohns, H., 188
 Kronprasert, Nopadon, 121
 Kuakkal, Jan, 829
 Kuklin, Alexander A., 163
 Kumar, I., 754
 Kumar, Ramesh, 450
 Kurzydlo, Arthur S., 930
 Kuyuk, H. S., 683

 Labi, S., 754
 Laganier, Richard, 724
 LaRocca, Sarah, 155
 Lee, Yajie (Jerry), 246
 Lee, Young-Joo, 238
 Lhomme, Serge, 724, 746, 790
 Lin, Ning, 11
 Liu, Mei, 230
 Liu, Z., 468
 Loucks, Daniel P., 829
 Lounis, Z., 433
 Lowrie, Robert, 477
 Lu, Yujie, 284
 Lund, Jay R., 821

 Mao, Longquan, 284, 316, 326, 374
 Maravas, A., 62
 Mardfekri, M., 633
 Maria-Sanchez, Pedro, 477
 Markham, Kristen, 197, 334

- Martins, Marcelo Ramos, 394
 McDonald-Madden, Eve, 945
 McGill, William, 70, 857
 Megawati, Kusnowidjaja, 881
 Melendez, Lou, 477
 Mickley, James, 70
 Mitchell, John E., 171
 Mitchiner, Kim, 738
 Mitrani-Reiser, J., 468, 618
 Miyawaki, Yusuke, 96
 Modares, M., 510
 Moffitt, L. Joe, 938
 Mohammadi, Jamshid, 510, 930
 Molarius, R., 188
 Moskvichev, V. V., 442
 Mousa, Mohammed A., 458
 Mujumdar, Vilas, 308
 Murphy, C., 342, 417
- Nakatsu, Koichiro, 1, 300
 Nateghi, Roshanak, 594
 Naydenov, A. S., 410
 Nemets, Simona, 980
 Nguyen, Lan, 485
 Nicheporchuk, V. V., 442
 Norton, Terri, 268
 Nurre, Sarah G., 171
- Osteen, Craig D., 938
 Ostrovsky, G. M., 276
- Pan, T. C., 881
 Pantouvakis, J. P., 62
 Park, J. K., 533
 Petersen, Brad, 268
 Phoon, Kok-Kwang, 675
 Pinelli, Jean-Paul, 468, 602, 618
 Pita, G. L., 468, 618
 Poluyan, L., 716
 Possingham, Hugh P., 945
 Potra, Florian, 501
 Prasad, Gautham G., 889
 Pressey, Robert L., 971
- Ramirez, Josue, 334
 Reed, Patrick M., 798
 Rodriguez, C. E. Patiño, 385
 Rodriguez-Nikl, Tonatiuh, 222
 Roesset, J. M., 633
 Rossi, R., 138
- Sánchez-Silva, M., 214
 Saassouh, B., 433
 Sarsama, J., 188
 Schleder, Adriana Miralles, 394
 Schonfeld, P., 129
 Serre, Damien, 425, 724, 746, 790
 Sharkey, Thomas C., 171
 Shubin, Alexander V., 163
 Shibina, Julia L., 163
 Shokin, Yu I., 442
 Siegrist, Jack, 29, 368, 526
 Silva, Consuelo, 738
 Simiu, E., 626
 Smith, Ian F. C., 78, 905
 Smith, Jane, 610
 Song, Junho, 238, 549
 Sorensen, Andrew D., 857
 Souza, Gilberto Francisco Martha,
 385, 394
 Strandén, J., 188
 Sznyszewski, Stefan T., 865
- Taflanidis, Alexandros A., 402, 610,
 873
 Tagg, Andrew, 746
 Tanaka, Seizo, 610
 Taylor, Craig, 246
 Timashev, S. A., 147, 716, 764
 Torkian, Boback Bob, 602
 Trandafir, Aurelian C., 659
 Tyrnin, A. N., 147
- Uchida, Ken-etsu, 104
 Uddin, Nasim, 458
 Udoh, I. E., 587

Vairavamoorthy, Kalanithy, 836, 846,
953

Van Hentenryck, Pascal, 180

Vanmarcke, Erik, 11

Verho, P., 188

Walker, Warren E., 829

Wallace, William A., 171

Walliman, Nicholas, 746

Wang, Jingchun, 699

Wang, S., 45, 129

Wang, Yan, 37

Weekes, J., 618

Westerink, Joannes J., 610

Wyss, Gregory D., 738

Xu, Pengfei, 699

Yang, Wu, 374

Yeo, DongHun, 641, 650

Zacksenhouse, Miriam, 980

Zarfam, Panam, 252

Zen, K., 691

Zhang, Q. W., 881

Zhao, Xin, 326

Subject Index

Page number refers to the first page of paper

- Aerodynamics, 641
Algorithms, 129, 300, 493
Assessment, 374
Attenuation, 667
- Barriers, 930
Bayesian analysis, 121, 533, 541, 561
Benefit cost ratios, 738, 971
Best management practice, 284
Biological processes, 938
Blasting, 857
Bridge maintenance, 897
Bridges, 873, 889, 971
Build/operate/transfer, 805
Buildings, 326, 374, 602, 746
- Calibration, 905
California, 821, 889, 938
Caribbean, 485
Case studies, 477, 493
Cavitation, 708
Chile, 485
China, 326, 374
Chloride, 433
Classification, 417, 602
Climate change, 578
Closed form solutions, 450
Commercial buildings, 618
Computation, 1
Computational fluid dynamics
 technique, 626
Computer software, 70
Concrete bridges, 922
Concrete structures, 433, 641
Conservation, 945
Construction materials, 352
Containment, 930
- Corrosion, 433
Costs, 458
- Damage, 549, 857
Damping, 873
Data analysis, 29, 138, 368, 468, 526,
 980
Databases, 626, 641, 650
Debris, 813
Decision making, 21, 222, 308, 385,
 561, 754, 945, 953, 971, 988
Decomposition, 171, 214
Deformation, 533
Deltas, 821
Desalination, 805
Design, 222, 626, 873
Deterioration, 953
Disasters, 188, 526
Displacement, 659
Drinking water, 805
Dynamic analysis, 659
- Earthquakes, 1, 104, 246, 485, 501,
 561, 667, 683, 889
Economic factors, 163, 410, 485
Electric power, 180, 188
Electric transmission, 594
Electric transmission structures, 594
Entropy methods, 147
Environmental issues, 938
Erosion, 813
Evacuation, 45, 533, 699
Experimentation, 138
Explosions, 865
- Failures, 205, 238, 450, 708, 953
Fatigue, 238

- Finite element method, 633, 675
- Floods, 96, 425, 724, 746, 790, 889
- Florida, 352, 618
- Forecasting, 813
- France, 724, 790
- Freight transportation, 197
- Fuzzy sets, 21, 53, 62, 138

- Geographic information systems, 790
- Georgia, 813
- Government policies, 326
- Ground motion, 533, 667

- Hawaii, 610
- High-rise buildings, 641, 881
- Hurricanes, 180, 352, 587, 602, 610, 618
- Hybrid methods, 510, 836

- Indonesia, 945
- Infrastructure, 147, 155, 163, 171, 214, 222, 230, 238, 246, 284, 292, 300, 308, 334, 360, 402, 410, 417, 450, 518, 764, 782, 829, 846
- Investments, 738, 754, 963
- Isotopes, 675

- Japan, 1, 96, 104

- Landfills, 930
- Landslides, 659
- Life cycles, 458
- Lifeline systems, 205
- Low-rise buildings, 618

- Man-made disasters, 442, 541, 716, 754
- Mapping, 442, 716
- Markov process, 86
- Measurement, 836, 857, 881
- Models, 29, 417
- Monitoring, 510
- Monte Carlo method, 86, 691, 836, 914

- Mooring, 914

- Natural disasters, 1, 45, 96, 342, 458, 468, 541, 602, 716, 754
- Natural gas, 394
- Networks, 155, 214
- Noise pollution, 518
- Nondestructive tests, 922
- Nuclear power, 260

- Offshore structures, 385, 394, 633, 914
- Optimization, 276, 501, 897

- Parameters, 78, 276
- Parks, 945
- Planning, 121, 300, 798, 829
- Policies, 308, 342
- Power plants, 260
- Predictions, 113
- Probability, 37, 53, 121, 205, 252, 260, 292, 360, 385, 450, 501, 633, 683, 821, 963
- Probability density functions, 78
- Probability distribution, 70, 86
- Project delivery, 477
- Project management, 62
- Public buildings, 316, 352, 561
- Public transportation, 121

- Rail transportation, 197
- Reconstruction, 268
- Regression analysis, 980
- Regulations, 222
- Rehabilitation, 402
- Reinforced concrete, 922
- Reliability, 699
- Religious buildings, 268
- Research, 316
- Residential buildings, 618
- Resource allocation, 988
- Restoration, 171, 180, 570
- Retaining walls, 699
- Rivers and streams, 570

- Russia (after 1991), 410, 716
- Safety, 45, 316, 326, 374
- Sampling, 246, 865
- Satellites, 772
- Scheduling, 62
- Scour, 889
- Sea level, 334, 587, 772
- Sea water, 113
- Security, 214, 732, 738, 764, 782
- Seismic effects, 252, 260, 268, 402, 873, 922
- Sensitivity analysis, 402
- Shear strength, 675
- Simulation, 86, 96, 104, 129, 138, 246, 610
- Sinkholes, 708
- Slope stability, 691
- Social factors, 163, 410
- Soil properties, 675, 691
- Solar power, 501
- Solids flow, 813
- Spacecraft, 129
- Spatial analysis, 691, 708
- Spectral analysis, 45, 113
- Statistics, 21, 29, 113, 368, 468, 526, 594
- Steel pipes, 914
- Stochastic processes, 360
- Storm surges, 587, 610
- Structural analysis, 905
- Structural design, 458, 641
- Structural failures, 865
- Structural reliability, 11, 53, 238, 510, 518, 549
- Structural systems, 238, 252
- Suspension bridges, 683
- Sustainable development, 222
- Terrorism, 782
- Torsion, 881
- Transportation management, 121, 477
- Transportation networks, 230
- Turbines, 633
- Turkey, 268, 683
- United States Air Force, 732
- Urban areas, 205, 425, 716, 746, 798, 846
- Urban development, 724
- Utah, 659
- Waste management, 425
- Water distribution systems, 549, 836, 846
- Water management, 798
- Water pipelines, 953
- Water supply, 578, 821
- Watersheds, 570, 578
- Waves, 113
- Wind forces, 11, 641
- Wind loads, 501, 594
- Wind speed, 650